SEDHYD 2019

Proceedings of SEDHYD 2019: Conferences on Sedimentation and Hydrologic Modeling

Volume 2

Hydraulic and Sediment Transport Modeling, Hydroecological Modeling, Infrastructure in the Stream Environment, International Opportunities - Brazil

Proceedings of SEDHYD 2019: Conferences on Sedimentation and Hydrologic Modeling, 24-28 June 2019 in Reno, NV.

These engineering and scientific proceedings provide much of the latest information on sedimentation and hydrologic modeling (applied research and state of-the-practice) from Federal agencies, universities, and consultants. SEDHYD is the successor to the Federal Interagency Conferences on Sedimentation and Hydrologic Modeling. The Subcommittee on Sedimentation convened the first Federal Interagency Sedimentation Conference (FISC) in 1947. Subsequent FISC conferences were convened in 1963, 1976, 1986, 1991, 1996, and 2001. The Subcommittee on Hydrology convened their first Federal Interagency Workshop, "Hydrologic Modeling Demands for the 90s," in 1993. Subsequent to that workshop, the Subcommittee on Hydrology convened the Federal Interagency Hydrologic Modeling Conferences (FIHMC) in 1998 and 2002. Subsequently, the Subcommittees on Sedimentation and Hydrology began convening the Federal interagency conferences together in 2006 and again in 2010, and 2015. Beginning in 2019, the SEDHYD Conference was hosted by SEDHYD, Inc., a non-profit organization.

Since 1947, the Sedimentation and Hydrologic Modeling Conferences have provided over 3,000 technical papers and extended abstracts and provided engineers and scientists with the opportunity to learn and exchange information about the latest developments and research related to sedimentation and hydrologic modeling. As a continuation of these conferences, SEDHYD provides an interdisciplinary mix of scientists and managers from government agencies, universities, and consultants to present recent accomplishments and progress in research and on technical developments related to sedimentation processes, hydrologic modeling, and the impact of sediment on the environment.

The SEDHYD conference provides a mixed set of formats that include formal technical presentations, poster sessions, field trips, workshops, computer model demonstrations, and a student paper competition. The SEDHYD conference also provides excellent networking opportunities.

The SEDHYD 2019 Conference site was at the Peppermill Hotel and Resort in Reno, Nevada. Reno is situated in a high desert just east of the beautiful Sierra Nevada Mountains. The city lies on the western edge of the Great Basin, at an elevation of 4,400 feet (1,300 meters) above sea level. The Reno downtown area (along with Sparks) occupies a valley informally known as Truckee Meadows. The area offers spectacular desert landscapes and ecosystems, as well as numerous indoor and outdoor recreational opportunities.

SEDHYD 2019 Planning Committee

Planning Committee Position	Volunteer	Organization
SEDHYD Conference Chair	Jerry Webb	West Consultants
SEDHYD Operations Chair	Jennifer Bountry	Reclamation
SEDHYD Technical Program Chair	Chandra Pathak	USACE
SEDHYD Technical Program Chair (YP)	Will Farmer	USGS
SEDHYD Technical Program	Jerry Bernard	NRCS, retired
Sedimentation Conference Chair	Tim Randle	Reclamation
Sedimentation Program Chair	Eddy Langendoen	ARS
Sedimentation Program Chair (YP)	Joel Sholtes	Mesa State
Hydrologic Modeling Conference Chair	Claudia Hoeft	NRCS
Hydrologic Modeling Program Chair	Jim Barton	USACE, retired
Hydrologic Modeling Program Chair (YP)	Jessica Driscoll	USGS
Student Program Coordinator	Amanda Cox	MWRRC
Proceedings Coordinator	Bob Boyd	BLM
Proceedings Coordinator	Peter Doran	BLM
Poster & Computer Model Demonstration Coordinator	Eddie Brauer	USACE
Short Course Coordinator	Jeff Bradley	ASCE, West Consultants
Short Course Coordinator (YP)	Kevin Denn	USACE, St. Paul Dist.
Field Trip Coordinator	Steve Berris	USGS
Field Trip Coordinator (YP)	Jena Huntington	USGS
Web site Coordinator	Darren Nezamfar	USACE
Registration Coordinator	Penni Baker	USACE
Registration Volunteer	Kathy Randle	
Young Professionals Coordinator	Caroline Ubing	Reclamation
Young Professionals Coordinator	Sara Horgen	Reclamation
Exhibit Coordinator	Molly Wood	USGS
Exhibit Coordinator	Tim Straub	USGS
AV Equipment Coordinator	Jeff Harris	West Consultants
Planning Committee	Jo Johnson	NRCS
Planning Committee	Jon Fripp	NRCS
Planning Committee	Paul Boyd	USACE
Planning Committee	Meg Jonas	USACOE, retired
Planning Committee	Robert R Mason	USGS
Planning Committee	Victor Hom	NOAA

SEDHYD, Inc.

SEDHYD, Inc. Position	Volunteer
SEDHYD President & Board Chair	Jerry Webb
SEDHYD Vice President & Board Member	Jerry Bernard
SEDHYD Treasurer & Board Member	Don Frevert
SEDHYD Secretary & Board Member	Matt Romkens
SEDHYD Board Member	Doug Glysson

Table of Contents

Table of Contents

Hydraulic and Sediment Transport Modeling (continued)

Table of Contents

Hydraulic and Sediment Transport Modeling (continued)

Table of Contents

Table of Contents

Table of Contents

Infrastructure in the Stream Environment (continued)

International Opportunities - Brazil

Hydraulic & Sediment Transport Modeling

2-D Modeling of Sediment Transport in Arkansas River at W.D. Mayo Lock and Dam

Andrey Shvidchenko, Senior Engineer, Northwest Hydraulic Consultants, Sacramento, CA, ashvidchenko@nhcweb.com

Brad Hall, Principal, Northwest Hydraulic Consultants, Sacramento, CA, bhall@nhcweb.com

Abstract

This paper presents results from a sediment modeling study undertaken by Northwest Hydraulic Consultants (NHC) to support the design of a proposed hydroelectric generating facility at the W.D. Mayo Lock and Dam on the Arkansas River. The sediment modeling was conducted using a 2-d AdH model of the 2.8-mile study reach of the river. The input parameters for the model were developed using available flow records, measured sediment data, and bathymetric surveys. The model was run for a range of flows for the existing and project conditions. The modeling results were used to assess the potential project impacts on sediment transport processes and to identify operational conditions for minimizing adverse sediment deposition in the vicinity of the lock and dam.

Introduction

The W.D. Mayo Lock and Dam is located at River Mile (RM) 319.6 on the Arkansas River (Figure 1). The lock and dam facilities were constructed in 1970's as part of the McClellan-Kerr Arkansas River Navigation System and are owned and operated by the U.S. Army Corps of Engineers (USACE). The existing structure consists of a navigation lock and a gated spillway adjacent to the lock. The gates are operated to maintain navigable depths upstream of the dam during low flow conditions. At high flows exceeding approximately 125,000 cubic feet per second (cfs), the gates are fully opened to provide "open river" conditions.

Figure 1. W.D. Mayo Lock and Dam on Arkansas River at flow 110,000 cfs (aerial image from Google Earth).

The proposed hydroelectric facility includes the addition of a powerhouse adjacent to the dam's left descending abutment. The powerhouse approach and tailrace channels will be excavated in the river channel to provide efficient flow passage through the powerhouse and satisfactory channeling of the power plant discharges back into the main river. The powerhouse will generate power for all river flows up to approximately 105,000 cfs.

The primary objective of the numerical movable bed sediment modeling was to assess the potential impacts of the proposed hydropower project on sediment erosion and deposition patterns in the vicinity of the lock and dam facility, particularly in the lower lock approach (which is subject to chronic sedimentation and periodic maintenance dredging). This paper briefly describes the development of a numerical sediment model, derivation of model input parameters, key assumption, and main results from sediment transport simulations. For more detailed description and analysis see NHC (2012, 2018).

Model Development

The sediment modeling was conducted using the two-dimensional (2-d) Adaptive Hydraulics (AdH) computer program developed by the USACE. The 2-d model extended approximately 1.5 miles upstream and 1.3 miles downstream of the dam. The input parameters for the numerical model were developed using available bathymetric data, Light Detection and Ranging (LiDAR) surveys, project design drawings, flow records, and measured sediment data.

Separate models were developed for the existing and project conditions. The existing conditions model topography was developed by merging the bathymetric and LiDAR survey data collected in 2011. The project condition topography was developed by adding the project channel to the existing condition topography. The existing and project conditions topography in the vicinity of the lock and dam are shown in Figure 2.

Mesh spacing within the computational domain was developed from a series of preliminary runs to reasonably represent most topographic features and structures, and at the same time provide manageable model run times. Mesh spacing ranged from 20 feet (ft) near structures such as the dam spillway, gates, locks, and training dikes to 100 ft in relatively uniform channel areas to 300 ft in floodplain areas.

Given that sediment deposits in the study area are primarily composed of sand, a single sediment size of 1.5 millimeters, corresponding to the average median bed material size in the area, was used in the sediment models developed in this study. Available data suggest that significant portions of the channel in the vicinity of the dam are apparently scored to bedrock, with localized alluvial deposits, mostly along the banks. Therefore, the thickness of sediment layer in the models was set to 1.6 ft to initiate sediment transport computations and, at the same time, to prevent excessive bed scour (which is controlled by bedrock). After testing various upstream sediment inflow scenarios, equilibrium transport condition was specified at the upstream model boundary.

The model was calibrated to measured stages, velocity distributions, and sediment loads. The calibrated model was then used to simulate morphological changes in the study reach of the Arkansas River for a range of flows under existing and project conditions. The model hydraulic boundary conditions are summarized in Table 1. The comparison between the project and existing conditions modeling results was used to assess the potential project impacts on sediment transport processes in the vicinity of the lock and dam.
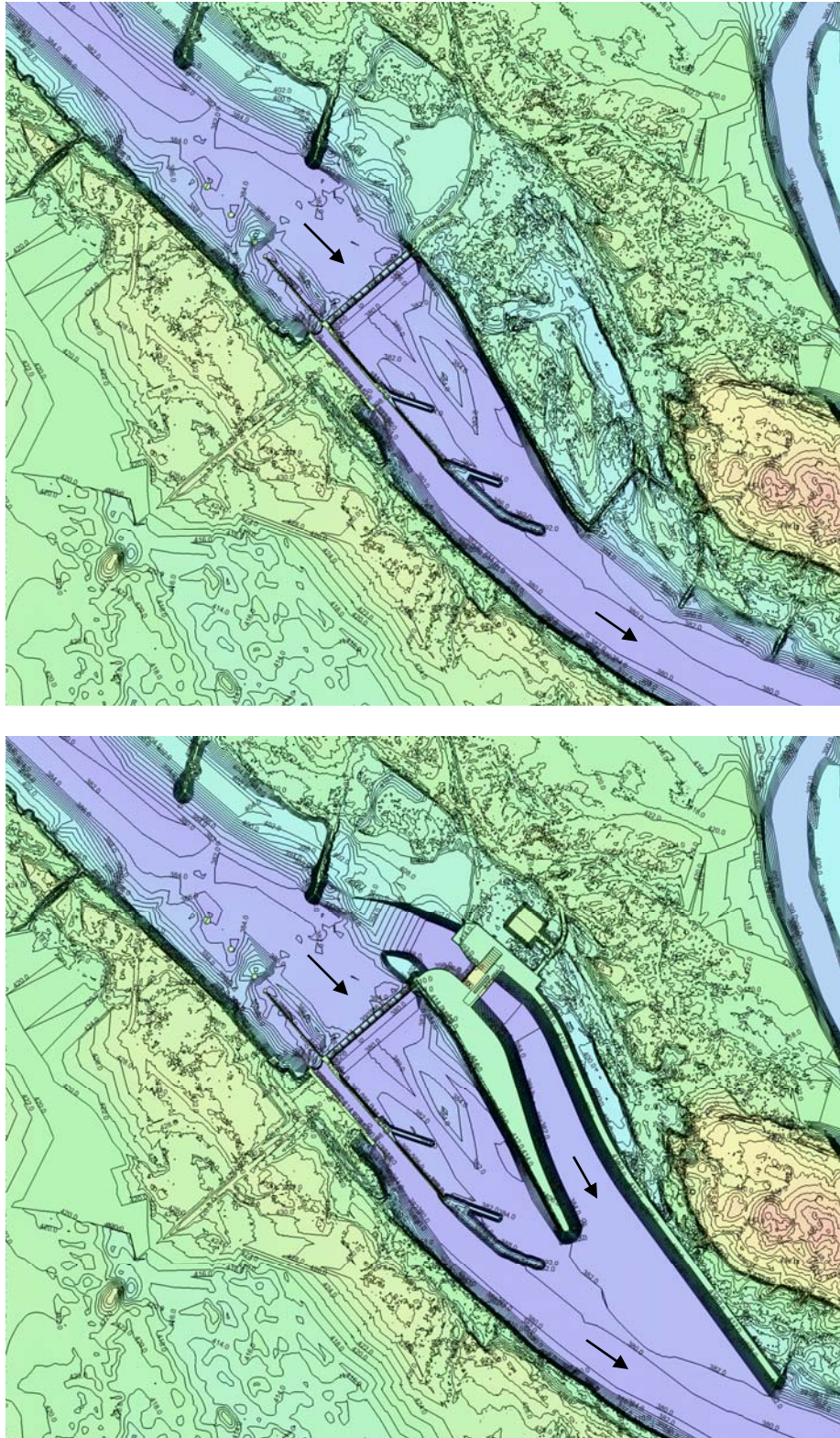
Figure 2. Existing (top) and project (bottom) conditions topography.

Table 1. Hydraulic boundary conditions.

Flow (cfs)		Water surface elevation (ft NGVD29*)		Flow duration (USACE data)	
Total	Powerhouse	Above dam gates (RM 319.6)	Downstream boundary (RM 318.3)	Days in a year	% time
30,000	30,000	412.0	394.8	281.2	77.00
60,000	30,000	412.0	399.8	38.9	10.7
105,000	30,000	412.0	405.9	23.1	6.3
150,000	0	412.8 (gates open)	410.8	19.3	5.3
200,000	0	418.1 (gates open)	415.4	1.6	0.4
250,000	0	421.2 (gates open)	419.4	0.5	0.1
300,000	0	424.8 (gates open)	423.2	0.6	0.2

*NGVD29 = National Geodetic Vertical Datum of 1929.

Results

The existing condition and project condition models were run for a range of constant flows with the same starting channel topography and the same initial thickness of movable bed material. The Van Rijn function was used to simulate sediment transport processes. All the simulations showed initially high sediment transport rates which then gradually reduced and approached a relatively stable value. Each simulation continued until an approximate equilibrium sediment condition (stable solution) was achieved in the model. The model runtime ranged from about 10 days (prototype time) at 60,000 cfs to 3 days at 300,000 cfs.

The modeling results included flow velocity distributions, depths, sediment loads, and bed changes (relative to the initial bed topography). Flow velocities and corresponding bed aggradation and degradation computed in the vicinity of the lower lock (which is of main concern for navigation) under the existing and project conditions are compared for selected flows in Figures 3-8. The main modeling results are briefly discussed below.

Existing Conditions

The movable bed simulations indicated significant sediment transport in the vicinity of the W.D. Mayo Lock and Dam at flows 60,000 cfs and greater. According to the historical flow record, this threshold flow is exceeded (and hence bed material is transported) on average about 23% of the time (or 84 days) in a year. The computed total sediment load at the dam ranged from less than 1 ton/day at 60,000 cfs to 120,000 tons/day at 150,000 cfs and 280,000 tons/day at 300,000 cfs. Suspended sediment load constituted about 94-96% and bed load constituted about 4-6% of the total sediment load. Computed sediment loads were in reasonable agreement with available measured sediment transport data.

The model results indicated active bed degradation along the central portion of the channel both upstream and downstream of the dam. The existing training dikes concentrate the flow along the central part of the river (particularly downstream of the dam), which resulted in the erosion of bed material at these areas in the model. Such model behavior indicated that significant portions of the prototype channel in the vicinity of the dam are likely degraded to bedrock, which agrees with the field observations.
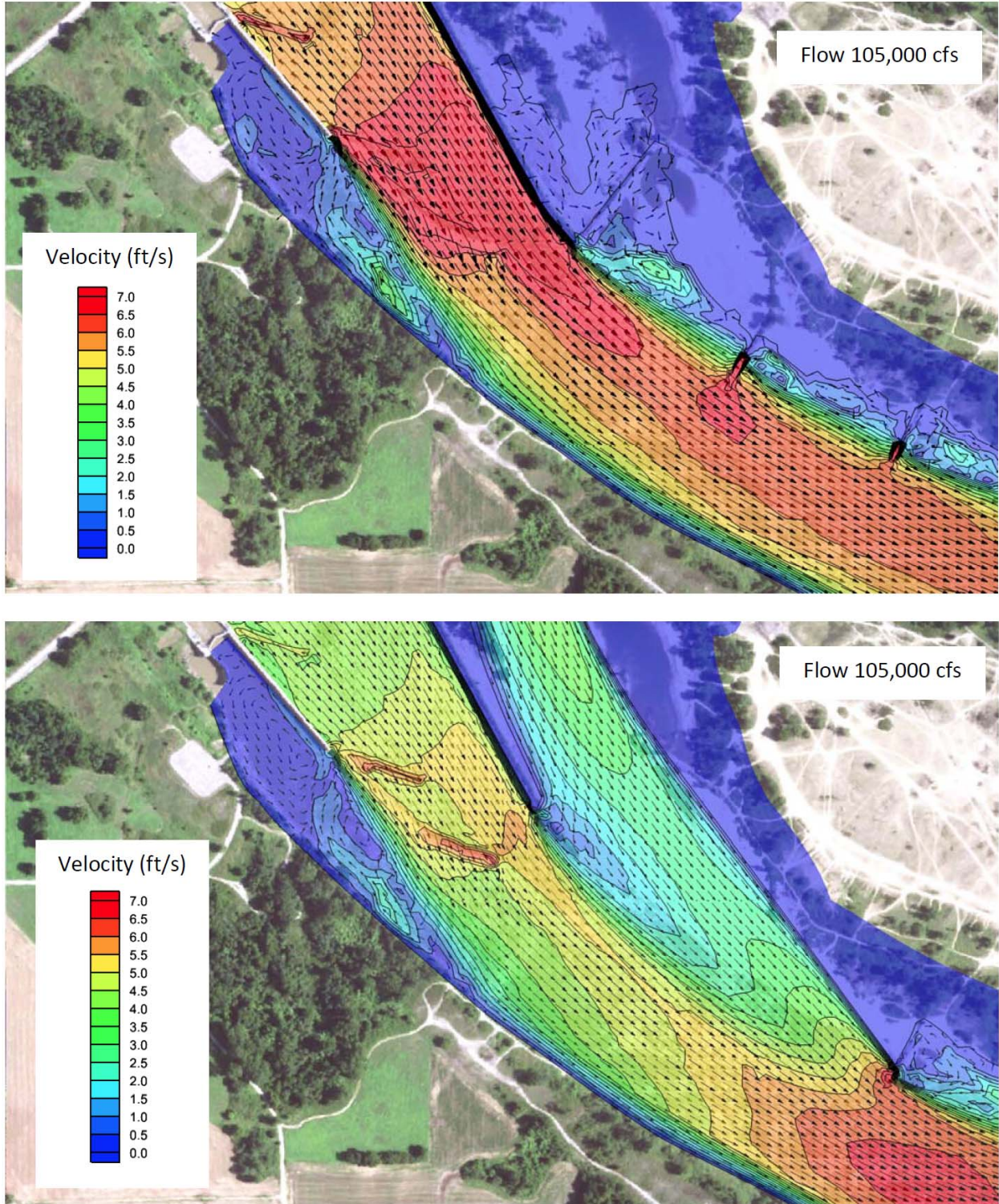
Figure 3. Velocities computed near downstream lock approach for flow of 105,000 cfs for existing (top) and project (bottom) conditions.
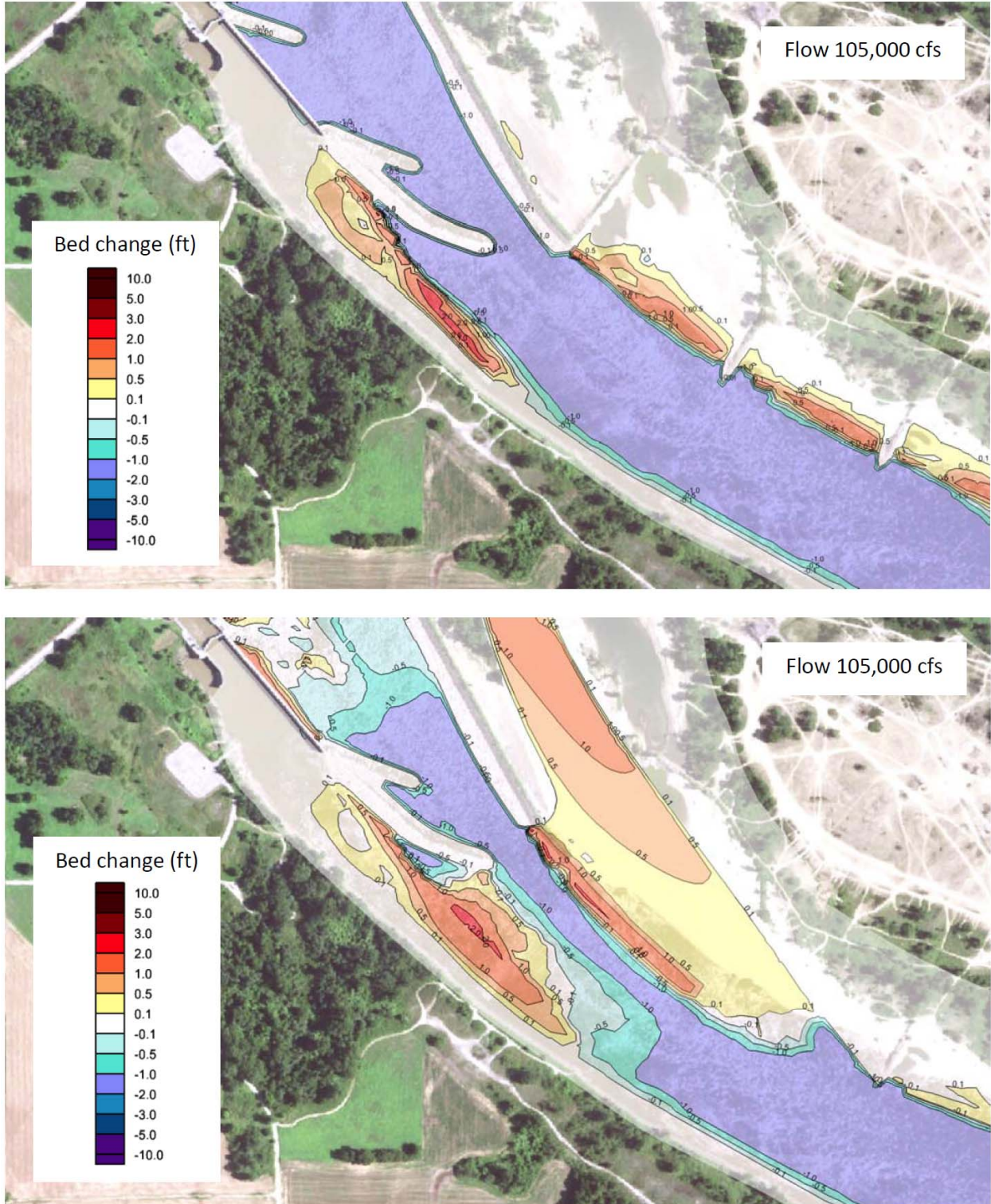
Figure 4. Bed aggradation and degradation computed near downstream lock approach for flow of 105,000 cfs for existing (top) and project (bottom) conditions.
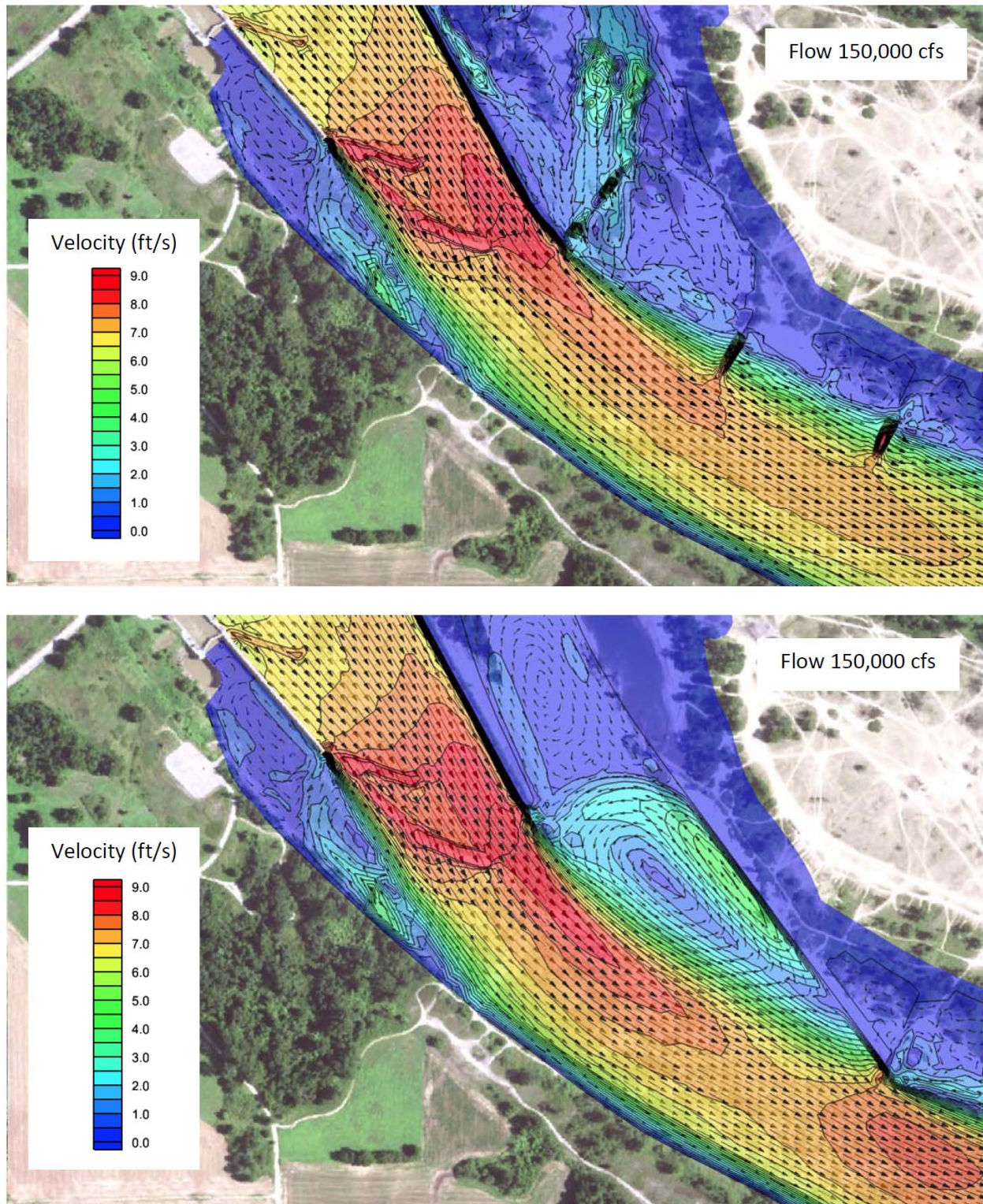
Figure 5. Velocities computed near downstream lock approach for flow of 150,000 cfs for existing (top) and project (bottom) conditions.
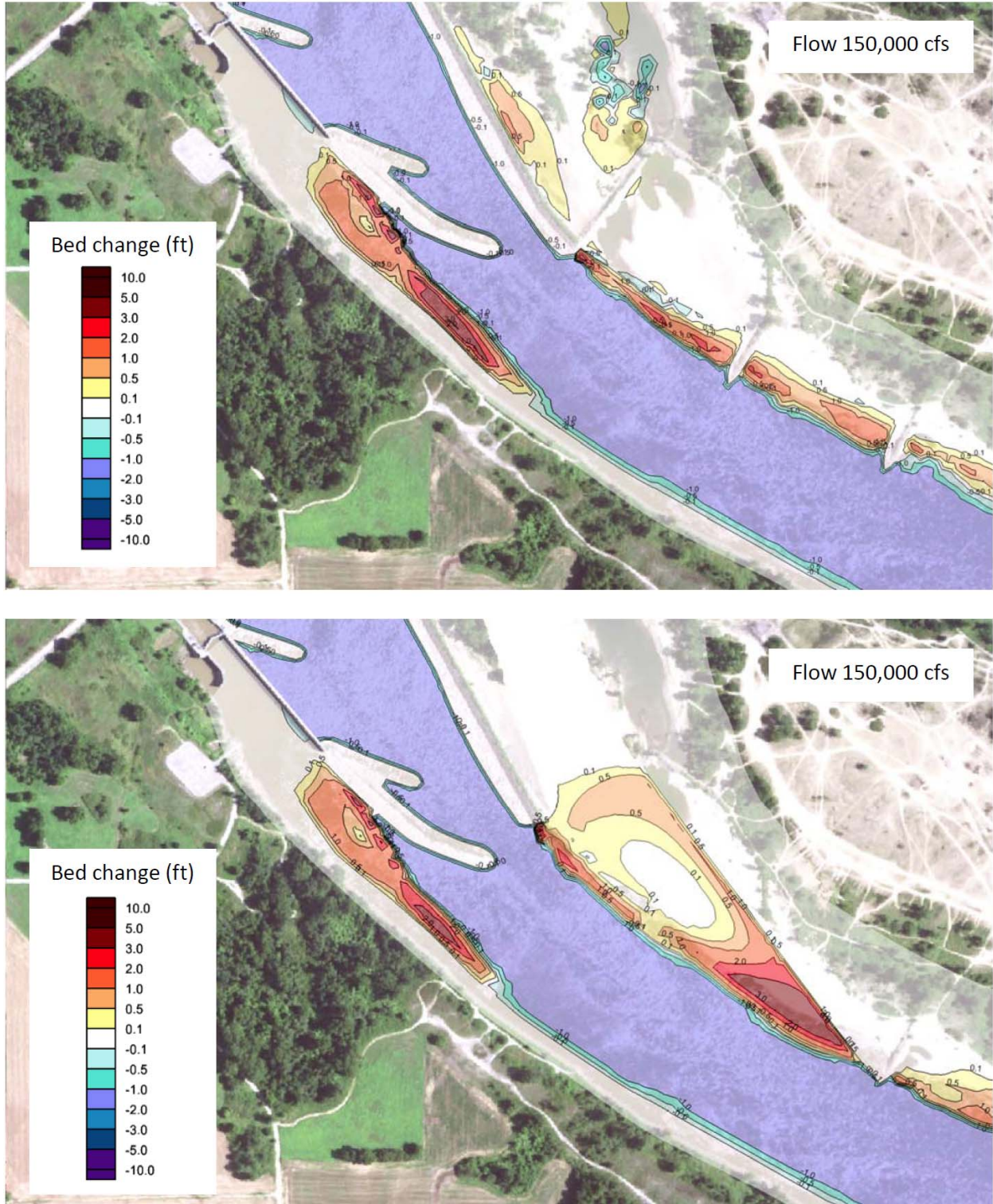
Figure 6. Bed aggradation and degradation computed near downstream lock approach for flow of 150,000 cfs for existing (top) and project (bottom) conditions.
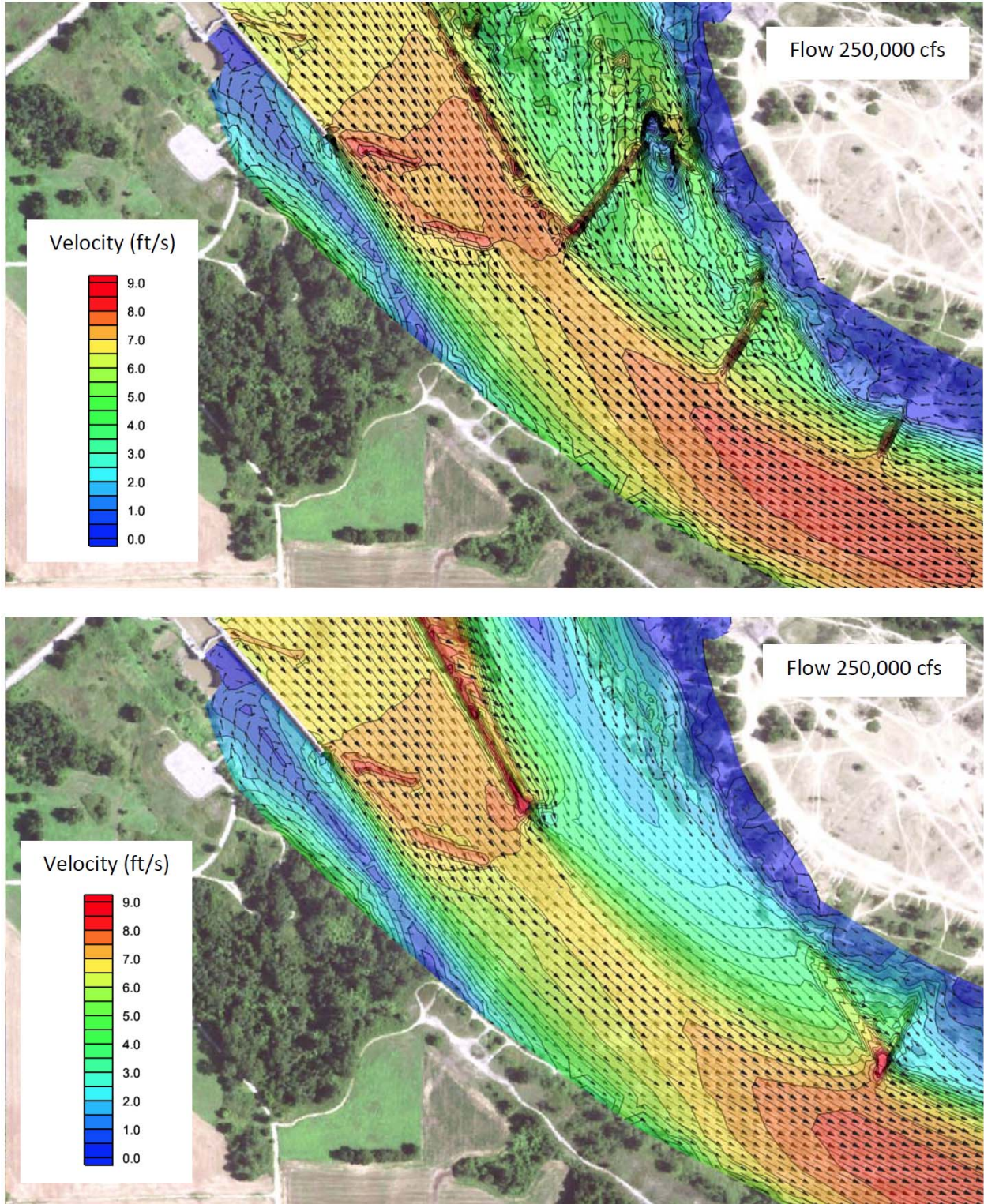
Figure 7. Velocities computed near downstream lock approach for flow of 250,000 cfs for existing (top) and project (bottom) conditions.
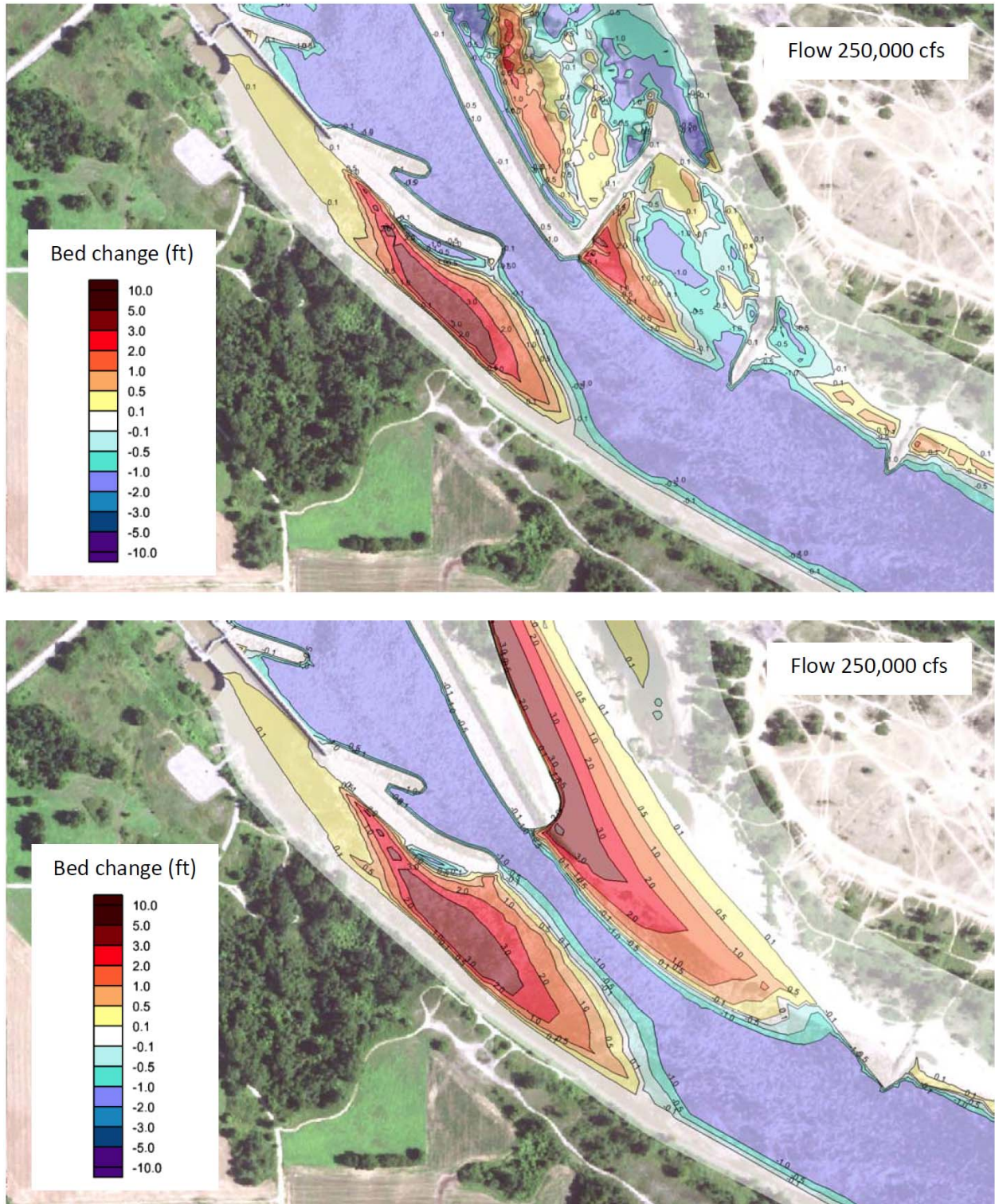
Figure 8. Bed aggradation and degradation computed near downstream lock approach for flow of 250,000 cfs for existing (top) and project (bottom) conditions.

The simulated bed changes demonstrated sediment deposition in the ineffective flow areas at the upper and lower lock approaches, which is consistent with the field observations and dredging records. The computed sediment deposition in the upper lock approach ranged from about 1-2 ft at 105,000 cfs to 2-3 ft at 150,000 cfs and 3-5 ft at 200,000 cfs and greater flows. The depositional area extended about 2,000-3,000 ft upstream of the lock. The computed deposition in the lower lock approach ranged from 0.5-1 ft at 60,000 cfs to 2-3 ft at 105,000 cfs and 3-5 ft at 150,000 cfs and greater flows. The depositional area extended about 1,500-2,000 ft downstream of the lock.

The model also showed potential sediment accumulation in the slow flow areas between the training dikes. Sediment was brought in and deposited between the dikes by eddy action of currents from the main channel. The maximum computed deposition between the dikes ranged from 0.5-1 ft at 60,000 cfs to 2-3 ft at 105,000 cfs and 5-7 ft at 200,000 cfs and the greater flows.

Project Conditions

The total sediment load computed at the W.D. Mayo Lock and Dam for the project conditions was similar to the existing conditions load. However, the powerhouse operation changed the lateral distribution of the sediment load. During powerhouse operations, from 80% (at 60,000 cfs) to 30% (at 105,000 cfs) of the total sediment load was conveyed through the powerhouse, which altered the sediment transport pattern in the downstream reach. During high flows, when the powerhouse was closed, sediment load over the spillway was similar to the existing conditions load.

Channel morphological patterns computed for the project conditions upstream of the dam were similar to the existing conditions results. However, the project significantly altered sediment transport, erosion, and deposition patterns in the reach extending about 3,500-4,000 ft downstream of the dam.

During powerhouse operations, sediments were conveyed through the powerhouse and deposited in the lower part of the tailrace channel. The model computed about 0.5-1 ft of deposition in the tailrace channel for 60,000 cfs and 1-2 ft of deposition for 105,000 cfs. During open river flows (when the powerhouse was closed), sediment was brought from the main channel into the recirculating flow area that formed at the downstream end of the tailrace channel, as well as with overtopping flows over the northeast embankment at the dam. The computed maximum sediment deposition in the tailrace channel was about 2-4 ft for 150,000 cfs and 3-5 ft for 200,000 cfs and 300,000 cfs. The depositional area in the tailrace channel progressively increased for higher flows, which indicated there may be a need for periodic dredging within the tailrace channel.

The project did not affect computed sediment deposition upstream of the lock, while its effect on deposition downstream of the lock varied with the river discharge. For 60,000 cfs, the diversion through the powerhouse reduced the flow in the main channel to below the threshold conditions for bed material movement and, as a result, the model showed no changes in bed elevations downstream of the lock. For 105,000 cfs, the diversion through the powerhouse reduced flow velocities in the main channel downstream of the dam (see Figure 3), which reduced sediment transport capacity and significantly increased the depositional area downstream of the lock compared to the existing conditions (see Figure 4). For the open river flows of 150,000 cfs and 200,000 cfs, the powerhouse was closed and most of the flow was conveyed through the main channel. As a result, the flow velocity pattern and magnitude downstream of the dam were

similar to the existing conditions (see Figure 5) and there was no significant impact on sediment deposition in the lower lock approach under the project conditions (see Figure 6). The range of flows 150,000-200,000 cfs represents an approximate bankfull (or channel forming) discharge and therefore has a dominant long-term effect on shaping the overall channel morphology. For the flows of 250,000 cfs and 300,000 cfs, the powerhouse was closed, but the tailrace channel effectively intercepted and conveyed overbank flows into the river, which reduced flow velocities in the main channel (see Figure 7) and increased depositional area at the lower lock approach under the project conditions compared to the existing conditions (see Figure 8).

The flow of 250,000 cfs is equaled or exceeded only for about 0.3 % of the time (or about 1 day) in a year. Sediment deposits formed by these high flows will likely be re-worked during receding stages by subsequent bankfull flows (150,000-200,000 cfs), which will re-shape the channel and eliminate the project effect on sedimentation at the lower lock approach. Since navigation through the lock is feasible up to 150,000 cfs, sediment deposited during the rare flow events will likely pose no significant problem for navigation. However, the modeling results indicated that sediment deposited at the lower lock during powerhouse operations at flows around 105,000 cfs will unlikely be re-worked by subsequent lower flows and, therefore, may have implications to navigation and could lead to additional dredging.

Sensitivity Analysis

A series of sensitivity tests were conducted to ascertain that the computed morphological trends are reasonable. The sensitivity tests were performed with different sediment size and thickness of sediment layer. The test simulations indicated that while the computed magnitude of bed changes was affected by the sediment size and initial thickness of the sediment layer in the model, the effects of the project on the sediment transport and morphological processes were comparable.

Additional test simulations were conducted to evaluate the combined morphological effects of changing flow conditions (selected high flows followed by lower flows). The test simulations demonstrated that morphological processes in the study reach depended on a particular combination of flows. For river flows up to the bankfull flow (150,000-200,000 cfs), the main project effect on sediment deposition in the lower lock approach was produced by the higher flows in a flow sequence, especially by river flows around 105,000 cfs with the powerhouse in operation. Sediment deposited at the lock by very high, rare flow events was generally re-worked by subsequent bankfull flows.

An additional sensitivity test was conducted to evaluate the possibility of reducing sediment deposition at the lower lock approach during powerhouse operations. The test demonstrated that periodic closures of the powerhouse would be an effective means of flushing sediment below the dam and reducing the project impact on sediment deposition at the lower lock approach.

Summary and Conclusion

The main objective of this sediment modeling study was to evaluate the potential long-term impacts of the proposed hydropower project on sediment erosion and deposition in the vicinity of the W.D. Mayo Lock and Dam on the Arkansas River. The sediment modeling was conducted using a 2-d AdH model of the 2.8-mile study reach of the river. The model was developed using available bathymetric and topographic surveys, flow records, and measured sediment data. The model was calibrated to measured stages, velocity distributions, and sediment loads. The

calibrated model was run for a range of flows for the existing and project conditions. The comparison between these conditions was used to assess the potential project impacts on sediment transport processes in the vicinity of the lock and dam.

The numerical modeling results obtained for the existing conditions demonstrated sediment deposition at the upper and lower lock approaches, which is consistent with the field observations. The computed annual sediment deposition ranged from about 1-3 ft at low to moderate gated flows to 2-5 ft at high open river flows. The depositional areas in the model extended several thousand feet both upstream and downstream of the lock.

The addition of the powerhouse in the model changed the lateral flow distribution, which altered sediment transport, erosion, and deposition patterns, particularly downstream of the dam. Sediments tended to deposit in the powerhouse tailrace channel for most of the flows evaluated. The computed annual deposition in the tailrace channel ranged from about 1-2 ft during powerhouse operations to 2-5 ft during open river flows.

The project did not affect computed sediment deposition upstream of the lock, while its effect on deposition downstream of the lock varied with the river discharge. The project did not increase sediment deposition at the lower lock approach for relatively low sediment moving flows (around 60,000 cfs) and for bankfull flows (150,000-200,000 cfs). However, the project increased the depositional area at the lower lock approach for high gated flows with the powerhouse in operation (around 105,000 cfs) and very high open river flows with the powerhouse closed (250,000 cfs and greater). The observed flow statistics were used to evaluate the long-term contribution of the computed flow-specific project impacts. Based on the numerical modeling results, operational conditions were identified to minimize adverse deposition in the lower lock approach and reduce dredging requirements.

References

NHC 2012. W.D. Mayo Lock & Dam Hydropower Project: Preliminary Phase Mathematical Model Study, Two-Dimensional Mathematical Modeling. Report prepared for Cherokee Nation Businesses and SAIC Energy, Environment and Infrastructure, LLC, Tulsa, OK by Northwest Hydraulic Consultants Ltd., Vancouver, British Columbia. 7 September 2012.

NHC 2018. W.D. Mayo Lock and Dam Hydroelectric Project: Numerical Sediment Modeling. Report prepared for Benham Design, LLC, Tulsa, OK and U.S. Army Corps of Engineers, Tulsa District, Tulsa, OK by Northwest Hydraulic Consultants Inc., Sacramento, CA. 14 May 2018.

A New Modeling Tool for the Fate and Transport of Oil-Particle-Aggregates in Rivers After an Oil Spill

David Soong, Research Hydrologist, U.S. Geological Survey, Central Midwest Water Science Center, Urbana, Illinois, dsoong@usgs.gov

Zhenduo Zhu, Assistant Professor, Department of Civil, Structural, and Environmental Engineering, University at Buffalo, Buffalo, New York, zhenduoz@buffalo.edu

Faith Fitzpatrick, Research Geomorphologist, USGS, Upper Midwest Water Science Center, Middleton, Wisconsin, fafitzpa@usgs.gov

Jared Vegrzyn, Student employee, U.S. Geological Survey, Central Midwest Water Science Center, Urbana, Illinois, jvegrzyn@contractor.usgs.gov

John Berens, Graduate student, V.T. Chow Hydrosystems, Department of Civil and Environmental Engineering, University of Illinois at Urbana-Champaign, Urbana, Illinois, jberens2@illinois.edu

Tatiana Garcia, AquaINTEL Inc., Champaign, Illinois, tgarcia@aquaintel.co

Marcelo Garcia, Professor and Director of V.T. Chow Hydrosystems, Department of Civil and Environmental Engineering, University of Illinois at Urbana-Champaign, Urbana, Illinois, mhgarcia@illinois.edu

Introduction

The 2010 Enbridge pipeline rupture and spill of diluted bitumen near Marshall, Michigan, resulted in a 4-year cleanup of lingering sheen and sludge related to the submerged oil-particle-aggregates (OPAs) along a 60-km stretch of the Kalamazoo River (Federal On Scene Coordinator, 2016). Modeling river hydrodynamics for projecting OPA depositional areas along the Kalamazoo River was a major effort in the coordination of emergency responses and was led by the U.S. Geological Survey (USGS) (Fitzpatrick et al., 2015b). This modeling helped determine if dredging was necessary for the largest remaining deposits. Through this experience, on-scene coordinators and task teams became aware of the challenges in locating OPAs in inland waterways for planning recovery operations. A transport model to assist oil-spill responders in identifying contaminated areas and prioritizing cleanup options would be needed in the case of future spills in other inland freshwater environments.

Spilled oil typically enters a waterbody as a floating slick, which then transforms through complex physical, chemical, and biological processes and breaks down to oil droplets. Oil droplets within the water column aggregate with river sediment to form OPAs. OPAs may be slightly heavier than the water and they transport in suspension or sink to the bed, depending on the turbulent state of the river; settled OPAs can be re-suspended and transported by differing river flows. An OPA tracking model was developed in 2018 with support from the USGS Midwest Region. The model, FluOil, adopted the transport mechanisms of an existing Asian carp egg-tracking model FluEgg (Garcia et al., 2013), replaced the egg characteristics with OPA transport properties, and added mechanisms for the deposition and resuspension of OPAs. For assessing its functionality with the aim of it serving as a decision-support tool, the study team applied FluOil to the Illinois River to review OPA transport scenarios using hypothetical oil-spill incidents during high and low flows. These hypothetical test scenarios led the study team to outline the following four tasks for continued model development: (1) gather existing OPA transport properties, (2) add an OPA

formation module, (3) verify FluOil through a case study, and (4) refine FluOil's graphic user interface (GUI) and prepare a user's manual.

The FluOil Model

FluOil simulates the time-dependent movement of an OPA plume in suspension and deposition along a river. Outputs are in text and graphic formats, where the graphic outputs also can be projected into map products for visualizing the location and spatial extent of OPAs in a realistic background environment. Users can use the model to estimate the travel times of the OPA plume and the vertical distribution of OPAs at a given location in addition to the depositional area. Although FluOil performs its computations in three dimensions, it currently is limited to a main-channel transport to achieve an objective for rapid assessment. It can be used in the early stages of response and assessment or later with recovery and mitigation of an inland oil spill incidence.

FluOil is intended for responders operating on site to generate information for timely evaluations. It reads inputs specified by users including: river hydraulics, OPA transport properties, spill location, and simulation period. Figure 1 shows the homepage of the FluOil GUI where users specify the OPA transport properties and load the river hydraulics. The model is flexible in using steady or unsteady hydraulics (U.S. Army Corps of Engineers, 2016; HEC-RAS V 5.0.3 is used in the study), depending on which fulfills the purpose of the assessment.

FluOil Applications on the Illinois River: The scenarios tested on the Illinois River showed that the model is capable of simulating OPA movements and predicted heavy depositions upstream of locks and dams and Peoria Lake; these are the known depositional areas along the river. Figure 2 shows screen shot captures from FluOil of OPA movements near the two depositional area.

OPA Transport Properties

Transport properties for modeled OPAs are currently specified by the user through the following parameters: diameter, settling velocity, and critical shear stress. Particular attention is needed to assist less-experienced users in specifying appropriate values; also, challenges may exist even for experienced users because different types of crude oil will lead to different types of OPAs, or the same type of crude oil can result in different types of OPAs in the presence of different sediments or temperature. It is planned to use results from an ongoing literature review to create a tabulation of OPA transport properties for users to select in the specific fresh-water environment as part of FluOil's GUI. The OPA transport properties in inland waters have been described for Cold Lake Blend weathered diluted bitumen (Waterman and Garcia, 2015). For application in OPA transport models, Fitzpatrick et al. (2015b) categorized three common OPA types by diameter, oil to sediment proportions, settling rate, and resuspension potential (Waterman and Garcia, 2015; Hayter et al., 2015). Guidance for selecting which type of OPA to simulate in a practical event is not well established. Furthermore, much of the research done to date on OPA

formation and behavior is in a marine environment; OPA transport properties in rivers pertinent to other common types of crude oil is lacking (Fitzpatrick et al., 2015a).

The two oil types with readily available literture on OPA transport properties are conventional crude (CC) and diluted bitumen (DB). CC is further categorized into light, medium, and heavy crudes, according to density. Most heavy crude is found in Canada and Venezuela, and most bitumen deposits are found in Canada. Three main types of OPAs that can form are: droplet, solid, and flake aggregates; the formation is influenced by the type of sediment available, water temperature, turbulence energy, and biological and chemical properties.

Model Verification

A phased approach was implemented during the Kalamazoo River spill to investigate the presence and relative distribution of submerged oil in the Kalamazoo River and Morrow Lake. A qualitative assessment of depositional areas with the presence of submerged oil were performed using repeated in-channel sediment poling (Federal On Scene Coordinator, 2016). The georeferenced results were converted to maps showing areas with none, light, moderate, and heavy oiled sediment deposit (Figure 4). The first sets of poling data (i.e., data from inserting a graduated metal pole equipped with a disk into the sediment and then recoding observations) collected in the fall of 2010 present an opportunity for validating FluOil.

An unsteady HEC-RAS model is under development for this spill. The model domain covers the reach of the Kalamazoo River from Marshall to Comstock, Michigan, a 60-km reach impacted by the 2010 Enbridge spill. Figure 3 illustrates the preliminary results of the Kalamazoo River HEC-RAS model under calibration. After the calibration and verification are complete, the hydrodynamic characteristics for the periods in Fall of 2010 will be prepared as the inputs to FluOil to simulate the depositional areas, which will be compared to the poling results. Figure 4 illustrates the results of the poling conducted in Fall of 2010 in one segment of the Kalamazoo River. The sensitivity of parameters for the current OPA properties will be summarized and documented.

OPA Formation Module

Specifying the OPA transport properties implies that OPAs are already formed when entering the river. In the 2010 Enbridge spill, DB entered the Kalamazoo River after having contacted floodplain soils and sediment in wetlands. However, oil spills can enter the river directly as oil slicks through rail freights or storage tanks. The time and distance for oil droplets in transport, collision, and aggregation with sediment particles to form OPAs comprise a portion of the processes that need to be included in such cases. The study team is interested in assessing how the predicted OPA plumes and depositional areas might vary if the formation processes are considered. Based on oil droplet formation and oil to OPA formation numerical models developed by Zhao et al. (2014a; 2014b; 2016), Jones and Garcia (2018) developed a one-dimensional simplified particle tracking algorithm, 1DHydroOPA, for the formation, transport, and fate of

OPAs in the riverine environment. The study team is converting the algorithms as a new module in FluOil that utilizes the transport and re-entrainment mechanisms of FluOil. The study team plans to develop hypothetical oil spill cases based on flow and sediment characteristics of the Illinois River for evaluating the module, for illustrating the with- and without OPA formation scenarios, and for illustrating the uncertainty in the predicted locations of the OPA plume and the depositional areas.

Model Refinement and Access

After completion the FluOil code and executable files will be available for public access and use. Currently (spring, 2019) the study team is developing a user's manual, guidelines for selecting appropriate OPA transport properties, the collision and aggregation module, and is working on improving the GUI.
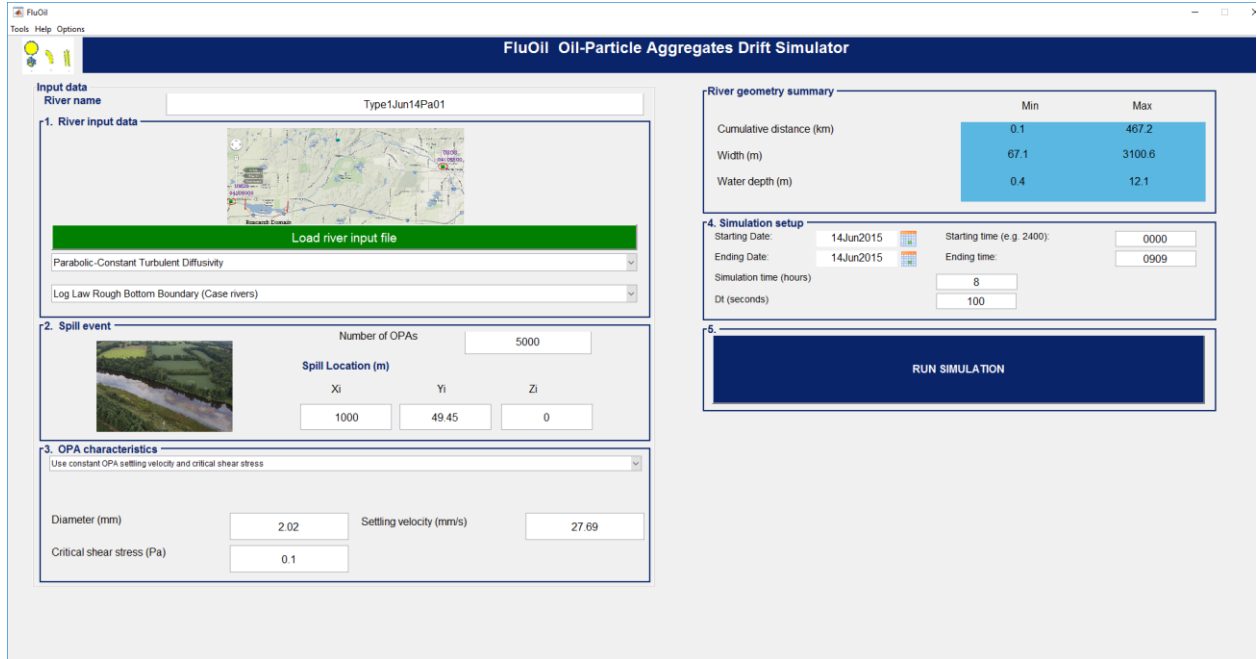
Figure 1. Homepage of the FluOil GUI.
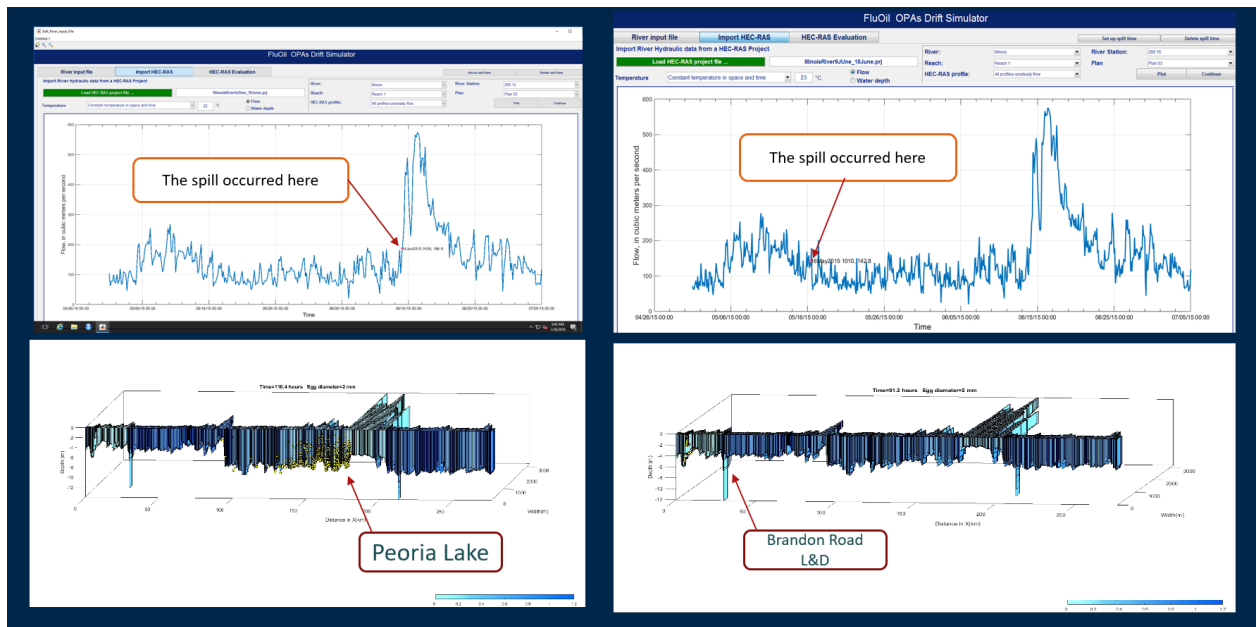
Figure 2. Simulated movements and potential deposition areas of oil-particle aggregates (OPAs) under high and low flow conditions for hypothetical oil spill incidents on the Illinois River. Yellow dots represent the OPAs.
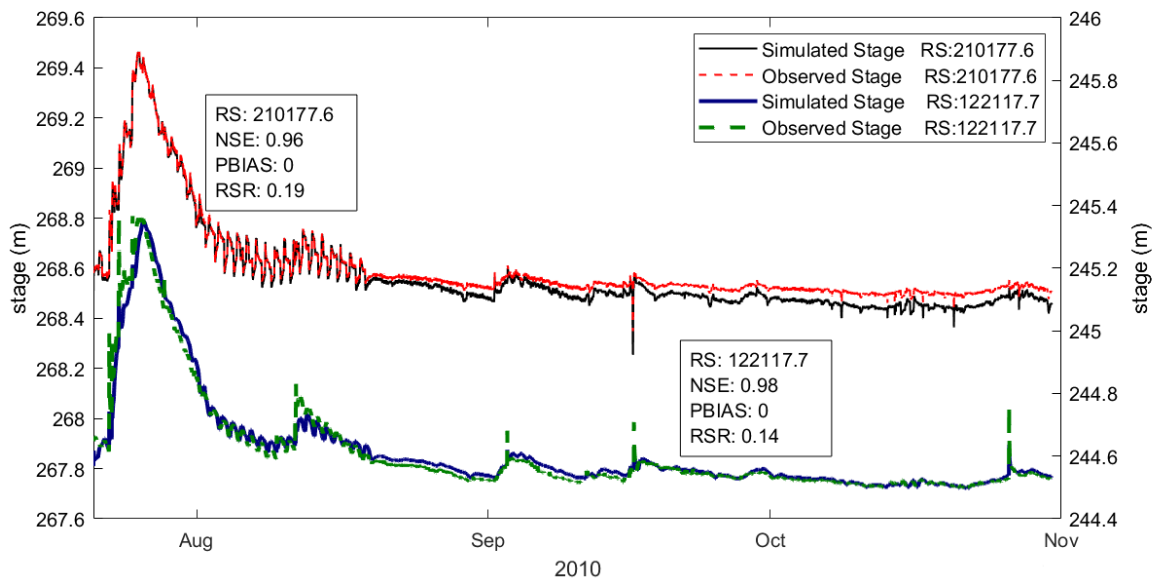
Figure 3. Simulated and observed water-surface elevations at USGS gaging stations Kalamazoo River at Marshall (station number 04103500; River Station (RS) 210177.6) and Kalamazoo River near Battle Creek (station number 04105500; RS 122117.7). NSE: Nash-Sutcliffe efficiency, PBIAS: percent bias, RSR: ratio of the root-mean-square error to the standard deviation of measured data.
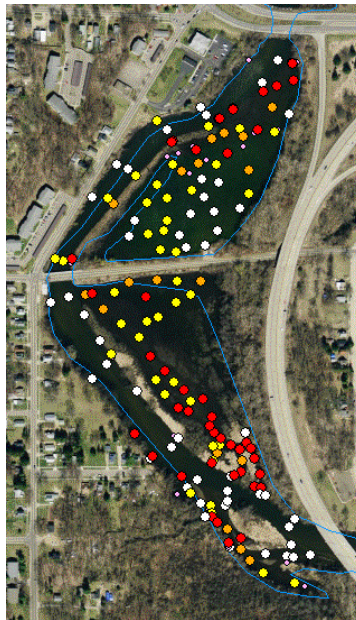
Figure 4. An example of the Fall 2010 pre-dredging poling results (source: Enbridge Line 6B Oil-Spill On-Scene-Coordination Team, slide provided by Fitzpatrick). The red dots represent where poling results are classified as heavy, the orange dots are for moderate oil-particle aggregate (OPA) content, yellow dots represent light OPA content, and white dots indicate that no OPAs were found.

References

Federal On Scene Coordinator (FOSC), 2016, FOSC desk report for the Enbridge oil spill in Marshall, Michigan, U.S. Environmental Protection Agency, 241 pp., url: https://www.epa.gov/enbridge-spill-michigan/fosc-desk-report-enbridge-oil-spill, accessed December, 2018.

Fitzpatrick, F.A., Boufadel, M.C., Johnson, Rex, Lee, Kenneth, Graan, T.P., and others, 2015a, Oil-particle interactions and submergence from crude oil spills in marine and freshwater environments—review of the science and future science needs: U.S. Geological Survey Open-File Report 2015-1076, 33 p.

Fitzpatrick, F. A., Johnson, R., Zhu, Z., Waterman, D., McCulloch, R. D., Hayter, E. J., Garcia, M. H., Boufadel, M., Dekker, T., Soong, D. T., Hoard, C. J., and Lee, K., 2015b, Integrated Modeling Approach for Fate and Transport of Submerged Oil and Oil-Particle Aggregates in a Freshwater Riverine Environment. In *Proceedings, Federal Interagency Sedimentation Program Conference:* pp. 1–12.

Garcia, T., Jackson, P. R., Murphy, E. A., Valocchi, A. J., and Garcia, M. H., 2013, Development of a Fluvial Egg Drift Simulator to evaluate the transport and dispersion of Asian carp eggs in rivers. *Ecological Modelling*, *263*, pp. 211–222.

Garcia, T., Murphy, E.A., Jackson, P.R. and Garcia, M.H., 2015, Application of the FluEgg model to predict transport of Asian carp eggs in the Saint Joseph River (Great Lakes tributary). *Journal of Great Lakes Research*, 41(2), pp. 374-386.

Hayter, E., McCulloch R., Redder, T., Boufadel, M., Johnson, R., Fitzpatrick, F., 2015, Modeling the transport of oil particle aggregates ad mixed sediment in surface waters, The US Army Engineer Research and Development Center (ERDC) Letter Report, prepared for US Environmental Protection Agency, Region 5, Chicago, IL, 44 p., url: https://archive.epa.gov/region5/enbridgespill/data/web/pdf/enbridge-spill-kalamazoo-river-letter-report-opa-201502-50pp.pdf, accessed December 2018.

Jones, L., & Garcia, M. H., 2018, Development of a Rapid Response Riverine Oil–Particle Aggregate Formation, Transport, and Fate Model. *Journal of Environmental Engineering*, *144*(12), 04018125.

U.S. Army Corps of Engineers, 2016, HEC-RAS, River Analysis System User's Manual, version 5.0: Davis, Calif., U.S. Army Corps of Engineers Institute for Water Resources, Hydrologic Engineering Center, available at https://www.hec.usace.army.mil/software/hec-ras/documentation.aspx

Waterman, D.M., & Garcia, M.H., 2015, Laboratory tests of oil-particle interactions in a freshwater riverine environment with Cold Lake Blend weathered bitumen. Civil Engineering Studies, Hydraulic Engineering Series No 106.

Zhao, L*.,* Torlapati, J., Boufadel, M*.,* King, T.*,* Robinson, B*.,* and Lee, K., 2014a, VDROP: a numerical model for the simulation of droplet formation from oils of various viscosities: *Chemical Engineering Journal*, 253, pp. 93–106.

Zhao, L., Torlapati, J., King, B. Davidson, T., Boufadel, M., and Lee, K., 2014b, A numerical model to simulate the droplet formation process resulting from the release of diluted bitumen products in marine environment: Proceedings, 2014 International Oil Spill Conference, Savannah, GA, pp. 449–462.

Zhao, L., Boufadel, M. C., Geng, X., Lee, K., King, T., Robinson, B., and Fitzpatrick, F., 2016, A-DROP: A predictive model for the formation of oil particle aggregates (OPAs). *Marine Pollution Bulletin*, *106*(1–2), pp. 245–259.

Assessing the Applicability of the Wilcock 2-Fraction Bedload Transport Model at the Caspar Creek Experimental Watersheds, CA

Extended Abstract

Paul Richardson, Postdoctoral Fellow, USDA Forest Service, Arcata, CA,
paul.richardson@usda.gov
Joe Wagenbrenner, Research Hydrologist, USDA Forest Service, Arcata, CA,
jwagenbrenner@fs.fed.us

Introduction

Predicting bedload transport rates is useful for many reasons, but accurate predictions are difficult to make. At the Caspar Creek Experimental Watersheds, a long-term monitoring site in a coast redwood forest in northern California, we wish to know how bedload transport responds to logging and sediment input such as landslides. To complete such analysis requires being able to accurately measure and predict bedload transport yields. Here, we focus on developing an approach to reconstruct an 18-year record of annual bedload yields for the North Fork of Caspar Creek (Figure 1) and compare the reconstructed yields to predictions from the Wilcock 2-faction bedload transport model (Wilcock, 2001).
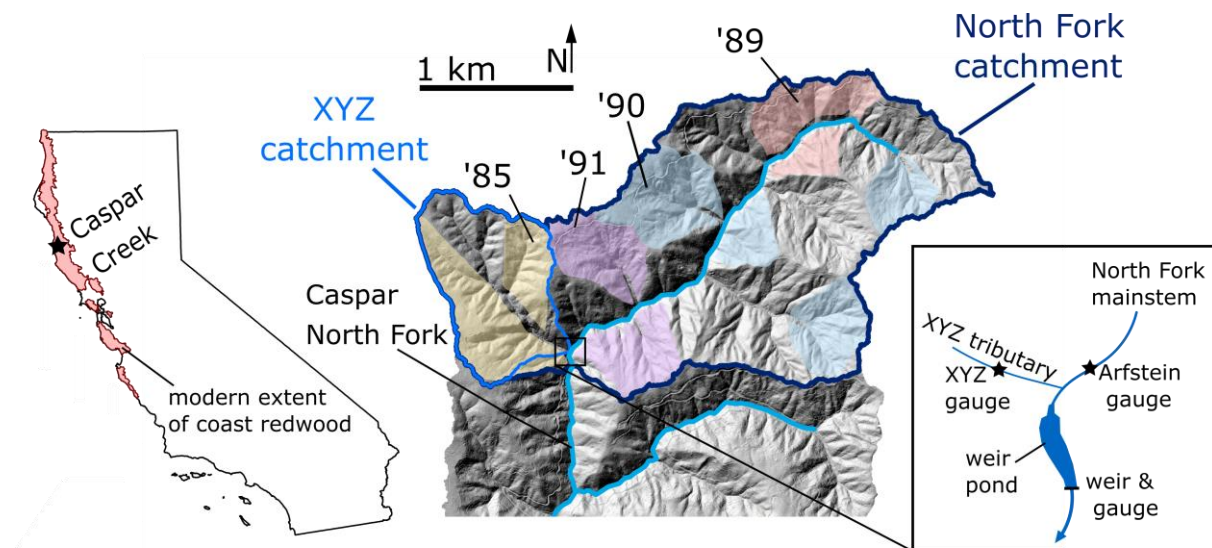
Figure 1. Shaded relief map of the Caspar Creek Experimental Watersheds created from LiDAR data gridded to 1 m. Colored overlay marks boundaries of previously logged catchments and the year the catchment was logged. Inset of California shows location of study site and modern extent of coast redwood (kindly supplied by Save the Redwoods League). Boxed inset shows additional detail near the North Fork weir pond.

Methods

A weir pond is located at the North Fork catchment outlet (Figure 1) and traps bedload, suspended load, and organic material. For hydrologic year (HY) 2000, an automated sampler

was installed to monitor suspended sediment yields from the XYZ tributary. This sampler complemented the pre-existing suspended sediment samplers at the pond outlet and on the main stem of the North Fork and made it possible to estimate the mass of suspended sediment that settles in the weir pond.

A delta composed primarily of sand and gravel exists at the upstream end of the weir pond. The remainder of the pond sediment is a mixture of settled suspended sediment and organic matter. The weir pond is cleaned of sediment and organic material every 5-10 years. During the North Fork cleanout in 2018, sediment samples were collected along 10 approximately evenly-spaced transects perpendicular to the long axis of the pond. The samples were collected and analyzed for the fraction of organic matter (f_o). In addition, a topographic survey is completed each year, which enables us to estimate the annual captured volume of sediment and organic debris in the pond (V_p). The pond volume can be subdivided into individual components according to

$$V_p = V_b + V_s + V_o, \tag{1}$$

where V is annual volume and the subscript denotes the pond (p), bedload (b), settled suspended sediment (s) or organic matter (o). V_s and V_o can be approximated as

$$V_s + V_o = \frac{M_s + M_o}{\rho_{s,o}}, \tag{2}$$

where M_s is the annual settled suspended sediment mass, M_o is the annual organic mass, and $\rho_{s,o}$ is the density of mixed organic matter and settled suspended sediment. We calculated M_s as the difference in measured suspended sediment storm loads calculated upstream and downstream of the weir pond. The mass of each weir pond can also be subdivided into individual components according to

$$M_p = M_b + M_s + M_o, \tag{3}$$

where M_p is the pond mass and M_b is the bedload mass. We estimated the organic mass (M_o) according to

$$M_o = f_o \rho_p V_p, \tag{4}$$

where ρ_p is the pond density. The pond and bedload mass are calculated according to

$$M_i = \rho_i V_i, \tag{5}$$

where i is either p (pond) or b (bedload). By combining equation (1)-(5), we can solve for M_b,

$$M_b = \frac{\rho_b V_p - \frac{\rho_b}{\rho_{s,o}}\left(1 + \frac{f_o}{1 - f_o}\right) M_s}{1 + \frac{\rho_b}{\rho_{s,o}}\left(\frac{f_o}{1 - f_o}\right)}. \tag{6}$$

All values in equation (6) were determined from field measurements or samples collected from the North Fork weir pond. We also collected bulk samples from the North Fork delta during summer 2018 to determine the gravel fraction (≥ 2 mm) of the delta.

We compared the reconstructed gravel yields from HY2000-2017 against predicted gravel yields using the 2-fraction bedload transport model described in Wilcock (2001). We focused on modeling bedload transport through the Arfstein reach and used HEC-RAS 5.0.6 to reconstruct flow velocity through a cross-section ~16 m upstream of the Arfstein gauging site from 10-minute discharge measurements made at the Arfstein gauge. We calibrated all model parameters from field measurements along the Arfstein reach of the North Fork except the reference shear stress for gravel (τ_{rg}), which is the shear stress at which a small but observable amount of gravel transport occurs. We calibrated τ_{rg} by minimizing the root mean square error (RMSE) between the predicted and reconstructed annual bedload yields.

Results

Analysis of the pond cores suggests that the organic fraction (f_o) is 0.09. Using previously collected data from the North Fork weir pond (Napolitano, 1996), we calculated a bedload density (ρ_b) of 1.83 kg/cm³ and a density of mixed organic and settled suspended sediment ($\rho_{s,o}$) of 1.18 kg/cm³. Analysis of the bulk sediment samples collected from the delta suggests that the gravel fraction of the delta is 0.68. We summarize the remaining pond analysis results in Figure 2.
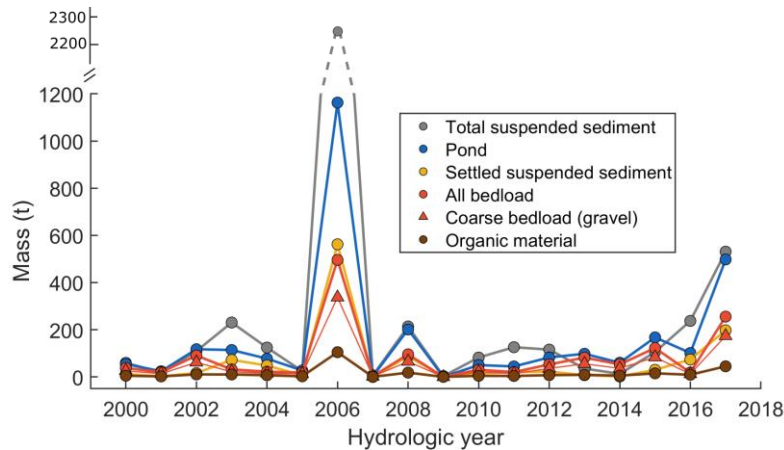
Figure 2. North Fork pond results for HY2000-HY2017. During HY2006, a large landslide contributed to higher than usual suspended sediment yields.

Minimizing the RMSE for the yields required a τ_{rg} of 9.1 Pa. Alternatively, τ_{rg} can be estimated from

$$\tau_{rg}^* = \frac{\tau_{rg}}{(\rho_s - \rho)gD_{50}}, \qquad (7)$$

where ρ is fluid density, ρ_s is sediment density, g is gravitational acceleration, τ_{rg}^* is the dimensionless reference shear stress, and D_{50} is the median grainsize of the gravel fraction. Flume experiments suggest that $\tau_{rg}^* \sim 0.04$ when the surface sediment is mostly gravel (Wilcock,

2001). Results from previous pebble counts show that $D_{50} \sim 1.8$ cm for the gravel fraction through the Arfstein reach, which suggests that $\tau_{rg} \sim 11.3$ Pa from equation (7). The calibrated τ_{rg} from the RMSE analysis resulted in an estimate of τ_{rg} that is slightly lower. Reconstructed annual bedload yields and predicted yields compare reasonably well (Figure 3). However, the model did not always predict low yields accurately. This analysis will be benefited by consideration of additional annual bedload measurements that include intermediate (100-300 t) and high (>300 t) bedload yields.
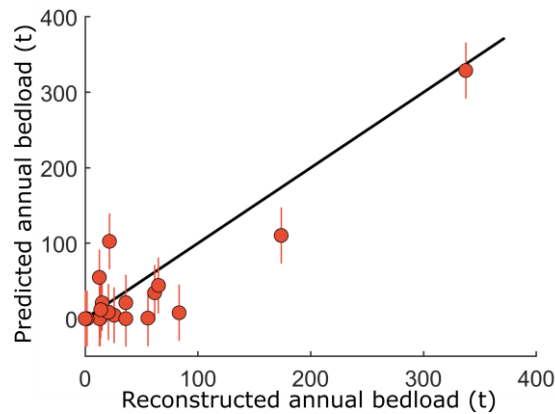
Figure 3. Comparison of reconstructed annual bedload yields and predicted annual bedload yields for the gravel fraction (≥ 2 mm). Uncertainty shown as 1 RMSE between the predicted and reconstructed yields. 1-to-1 reference line shown in black.

Summary

We presented an approach for reconstructing annual bedload yields deposited in the North Fork weir pond at the Caspar Creek Experimental Watersheds. This approach may also be suitable for estimating bedload yields for other weir ponds. We compared reconstructed annual gravel yields from the North Fork of Caspar Creek for HY2000-HY2017 to results of gravel yields predicted by the Wilcock 2-fraction bedload transport model. We calibrated the reference shear stress by minimizing the RMSE between the predicted and reconstructed bedload yields. We find that the calibrated reference shear stress is similar to the value predicted from bedload transport theory and flume experiments. We conclude that the accuracy of the bedload reconstruction approach and the bedload transport model are likely sufficient for addressing questions regarding catchment disturbance when large differences are expected between measured bedload yields and bedload predictions made for an undisturbed condition.

References

Napolitano, M. B. (1996). Sediment transport and storage in North Fork Caspar Creek, Mendocino County, California: water years 1980-1988. MS thesis, Humboldt State University, Arcata, California. 148 p.

Wilcock, P. R. (2001). Toward a practical method for estimating sediment-transport rates in gravel-bed rivers. Earth Surface Processes and Landforms, 26(13), 1395-1408.

Automating the Classification of Hysteresis in Event Concentration-Discharge Relationships

Scott D. Hamshaw, Post-doctoral Associate, Vermont EPSCoR, University of Vermont, Burlington, VT, Scott.Hamshaw@uvm.edu

Doug Denu, Research Assistant, Vermont EPSCoR, University of Vermont, Burlington, VT, Douglas.Denu@uvm.edu

Maike Holthuijzen, Research Assistant, Vermont EPSCoR, University of Vermont, Burlington, VT, Maike.Holthuijzen@uvm.edu

Safwan Wshah, Assistant Professor, Department of Computer Science, University of Vermont, Burlington, VT, Safwan.Wshah@uvm.edu

Donna M. Rizzo, Professor, Department of Civil & Environmental Engineering University of Vermont, Burlington, VT, Donna.Rizzo@uvm.edu

Abstract

The response of in-stream sediment concentration and discharge during rainfall-runoff events provides information about dominant watershed processes as it represents the amalgamation of the connectivity, erodibility, and the spatial location of sediment sources. A common way to collapse the sediment and streamflow response into a readily interpretable visualization is to utilize an event concentration-discharge (C-Q) plots which frequently exhibit patterns of hysteresis. However, challenges exist given the subjective nature of visual classifications and when scaling to large data sets. Hysteresis indices have been used to facilitate an automated and objective analysis method. In this study, we present an alternative method for automating hysteresis classification utilizing all the information present in the event C-Q plots. Thus, avoiding the loss of information that may occur when collapsing data into metrics and enabling the local sediment dynamics to be interpreted to a greater extent.

We developed an automated machine learning tool using images of event C-Q plots to classify storm events into pre-defined hysteresis pattern types. The classifier utilizes a convolutional neural network, a machine learning method that has achieved excellent predictive accuracy in image classification tasks. We then applied this tool using surrogate suspended sediment data from turbidity monitoring in eight watersheds within the Lake Champlain Basin in Vermont encompassing 760 individual storm events. The tool accurately and efficiently classifies events and represents an advancement over manual visual classification.

Background

Event Sediment Dynamics

The various mechanisms controlling suspended sediment transport in watersheds during hydrological events are complex. Efforts to gain insight into the watershed processes that result in soil erosion, sediment loading of rivers, and transport to downstream ecosystems has resulted in detailed study of watershed streamflow and sediment responses to rainfall events. The coupling between the streamflow and sediment responses to rainfall events is apparent in the relationship between streamflow and suspended sediment concentration (SSC) (Lefrançois *et*

al., 2007; Lloyd *et al.*, 2016). This relationship can change as a function of the sediment source availability, sediment storage, and hydrological pathways (connectivity) present in the watershed (Asselman, 1999; Duvert *et al.*, 2010; Sherriff *et al.*, 2016; Hamshaw *et al.*, 2018). A characteristic of this complex coupling is that the SSC response during a hydrological event is not in phase with the associated streamflow response (Gao and Josefson, 2012), which results in hysteretic behavior in the streamflow–SSC relationship. For decades, hydrological scientists have studied this hysteretic behavior to understand the origin and transport of sediments in watersheds using an approach commonly referred to as hysteresis analysis (Williams, 1989; Seeger *et al.*, 2004; Lawler *et al.*, 2006; Smith and Dragovich, 2009; Gellis, 2013; Sherriff *et al.*, 2016; Hamshaw *et al.*, 2018).

Hysteresis in Event Concentration-Discharge Relationships

The shape and direction of hysteresis loops highlight the temporal offset between SSC and streamflow. Hysteresis patterns can be used to understand the physical processes in watersheds. For example, clockwise loops have been recognized to be broadly characteristic of sediment sources being located near the watershed outlet, whereas counter-clockwise loops indicate that sediment sources are primarily located in the headwaters of the watershed (Gellis, 2013; Sherriff *et al.*, 2016). Additional physical processes have been connected with categories of hysteresis resulting in a number of interpretations for each general type (Williams, 1989; Lefrançois *et al.*, 2007; Smith and Dragovich, 2009; Gellis, 2013; Hamshaw *et al.*, 2018).

The most common hysteresis analysis is to classify plots into a general set of five classes (i.e. linear/no hysteresis, clockwise, counter-clockwise, figure-eight, and complex). These general categories, first identified by Williams of USGS (1989), continue to be used to this day by researchers. The manual, visual categorization of hysteresis loops is human resource intensive and has critical computational drawbacks. There has been progress toward automatic categorization of hysteresis using hysteresis indices from event C-Q data (Lawler *et al.*, 2006; Lloyd *et al.*, 2016; Zuecco *et al.*, 2016; Vaughan *et al.*, 2017). This approach is computationally efficient, and to some extent, effective. However, the hysteresis indices are not unique (i.e., individual storm events with different hysteresis patterns can have the same index value), and, therefore, often require additional metrics such as loop area or direction to preserve information lost during data compression (Zuecco *et al.*, 2016). An approach that utilizes the full information of the hysteresis plot is therefore necessary.

Machine Learning for Pattern Recognition

Machine learning methods can help identify patterns in hydrological data. For example, feed-forward backpropagation algorithms have long been used in rainfall-runoff modeling and streamflow prediction (Abrahart *et al.*, 2012). More recently, a new family of machine learning methods called deep learning that excel at classification applications such as hand-written character recognition (O'Connor *et al.*, 2013) have been developed, sparking extensive research into deep learning over the last decade. One of the earliest and most successful deep networks for image classification is the convolutional neural network (CNN) (LeCun *et al.*, 2015). These networks were introduced in the early 1990s (LeCun *et al.*, 1989) and have exhibited excellent performance for tasks such as hand-written digit and face recognition, image classification competitions (Simonyan and Zisserman, 2014), and speech recognition (Sainath *et al.*, 2015). CNNs can be conceptualized as a series of feature detectors (i.e. edges, corners, shape, color pattern, etc.) connected to a classifier.

The true potential of CNN networks was only fully understood when applied to large datasets (e.g. ImageNet dataset containing over 14 million labeled images) using high performance

computing. Several high-performance CNN architectures have been established including LeNet-5 (LeCun *et al.*, 1990), AlexNet (Krizhevsky *et al.*, 2012), VGGNet (Simonyan and Zisserman, 2014), GoogleNet (Szegedy *et al.*, 2015), and ResNet50 (He *et al.*, 2016). With the increase in computing power including GPU processing on standard desktop computers, CNNs are becoming more widespread in disciplines outside of computer vision, especially in biology and ecology (Dyrmann *et al.*, 2016; Xu *et al.*, 2017). Thus, due to the wide applicability of CNNs for a variety of tasks, they present a promising method for classifying hysteresis plots.

This project aims to demonstrate the performance of an advanced deep learning architecture (the ResNet50 CNN) to classifying hysteresis patterns in suspended sediment data. As efforts are made to collect and provide access to ever more high-frequency monitoring data, analysis methods such as those demonstrated here highlight the potential of continuous monitoring data and machine learning approaches to understand our watersheds.

Methods

Study Area & Dataset

We obtained streamflow and suspended sediment data from eight watersheds within the Lake Champlain Basin in Vermont between 2013 and 2016 (Figure 1). These included the Mad River watershed and five of its subwatersheds as well as Hungerford Brook and Wade Brook. Suspended sediment data was determined using surrogate monitoring of turbidity. In the case of the Mad River watersheds turbidity was measured using FTS DTS-12 sensors and YSI EXO2 sondes for Hungerford Brook and Wade Brook. Turbidity monitoring was paired with event sampling of total suspended solids (TSS) at each site for developing TSS-turbidity relationships. See Hamshaw et al. (2018) and Vaughan et al. (2017) for further details on streamflow and turbidity monitoring studies.
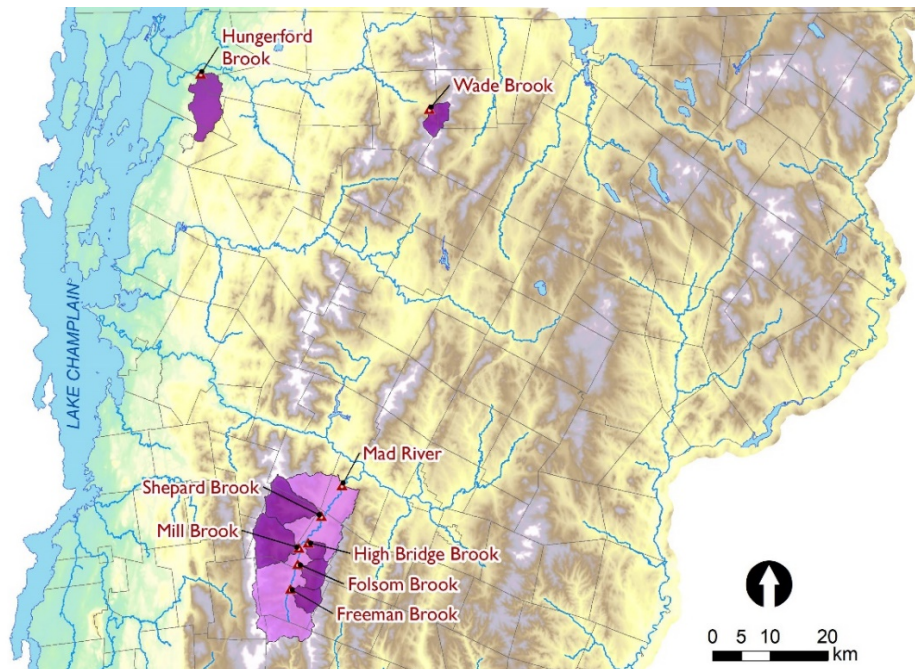
Figure 1. Map of study watersheds in the Lake Champlain basin in Vermont.

Event Concentration-Discharge Analysis

Hydrological events analyzed in this were previously extracted from continuous records of streamflow and turbidity as part of event-based analysis of nutrient dynamics in Hungerford Brook and Wade Brook (Vaughan *et al.*, 2017) and sediment dynamics in the Mad River watershed (Hamshaw *et al.*, 2018). Both studies utilized an approach of identifying an event start as a threshold increase in streamflow and concentration and event end as the inflection point in the falling limb of the hydrograph (Figure 2a). We constructed individual event concentration-discharge plots ("hysteresis plots") from the extracted time series segments (Figure 2b).
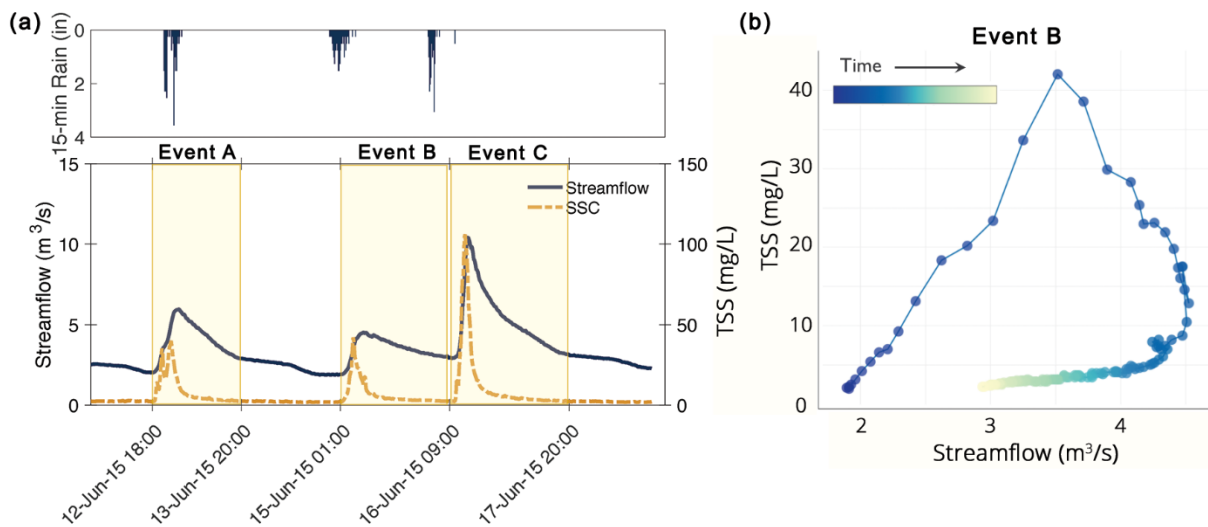
Figure 2. (a) Example segmentation of individual events in streamflow and sediment time series and (b) example (event C) concentration-discharge plot.

To assist with development and evaluation of automated hysteresis classification models all individual storm events were manually labeled based on the type of hysteresis observed in the event concentration-discharge plot. The categories (classes) of hysteresis patterns (Figure 3) used for classification of individual storm events are based on those identified in the Mad River watershed monitoring project (Hamshaw et al. 2018). These categories are an expansion of the typical categories (e.g. linear, clockwise, counter-clockwise, figure-eight).
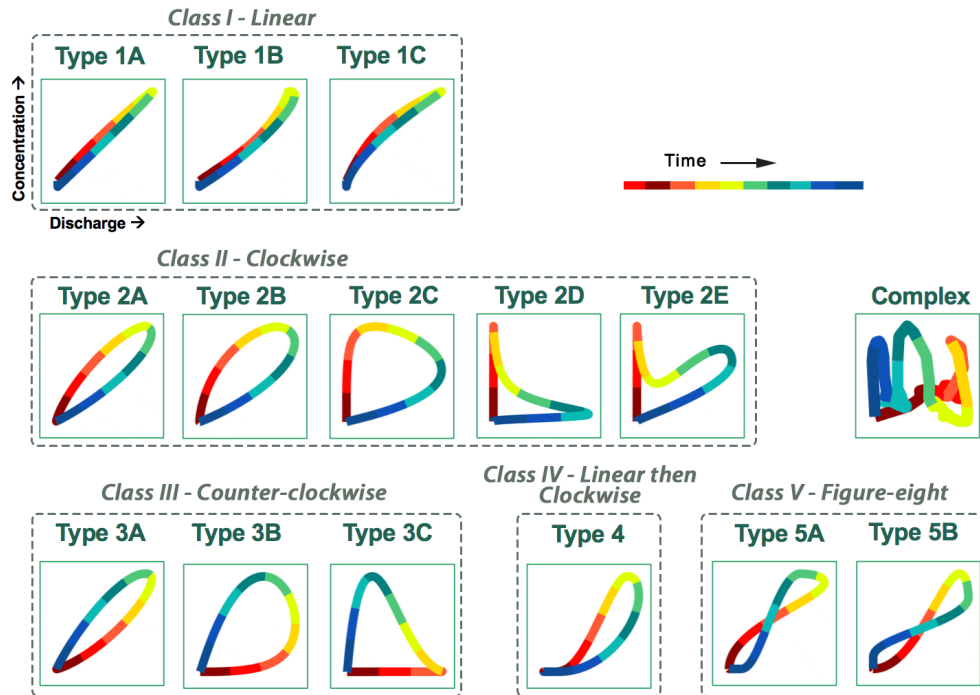
Figure 3. Types of hysteresis patterns as originally described by Hamshaw et al. (2018).

Hysteresis Classification Convolutional Neural Network

Individual storm event hysteresis plots were converted to images for input to the deep learning model. This allowed for use of existing, open source deep learning architectures designed for image classification. We note this method of classification based on images of hysteresis plots was also previously developed in a proof-of-concept study by Hamshaw et al. (2018). Processing of events was automated in MATLAB (Version 9.2) where each hysteresis plot was converted to a grayscale image (256 pixels x 256 pixels) and time was preserved in the shading of the data with white representing storm start and darker grey, the end of event (Figure 4). The images were randomly divided into training and testing subsets based on their manually labeled hysteresis type (Figure 5). For the training data set, event sampling was done by hysteresis type in order to achieve as equal representation of hysteresis types as possible.

We used the model weights and architecture of ResNet50, a residual convolutional neural network (CNN), as our base model to classify the image data. Residual networks (ResNets), a type of CNN developed by (He *et al.*, 2016), have achieved excellent predictive accuracies in image classification competitions. We decided to use the ResNet50 as our base model for hysteresis image classification because it is one of the more efficient (in terms of computing resources), yet highly accurate classification models for images. The ResNet architecture is a very deep neural network characterized by skipped connections and batch normalization (He *et al.*, 2016). As the name suggests, ResNet50 is composed of 50 weight layers that are tuned during model training. Readers are referred to He et al. (2016) and Sze et al. (2017) for in depth discussion of model architecture and training methods. We used the Python (version 3.6) implementation available in the Keras deep learning package (Chollet and others, 2015), which utilizes TensorFlow (Abadi *et al.*, 2015) as its computational engine. We utilized an NVIDIA DGX-1 deep learning server to train and test the model.
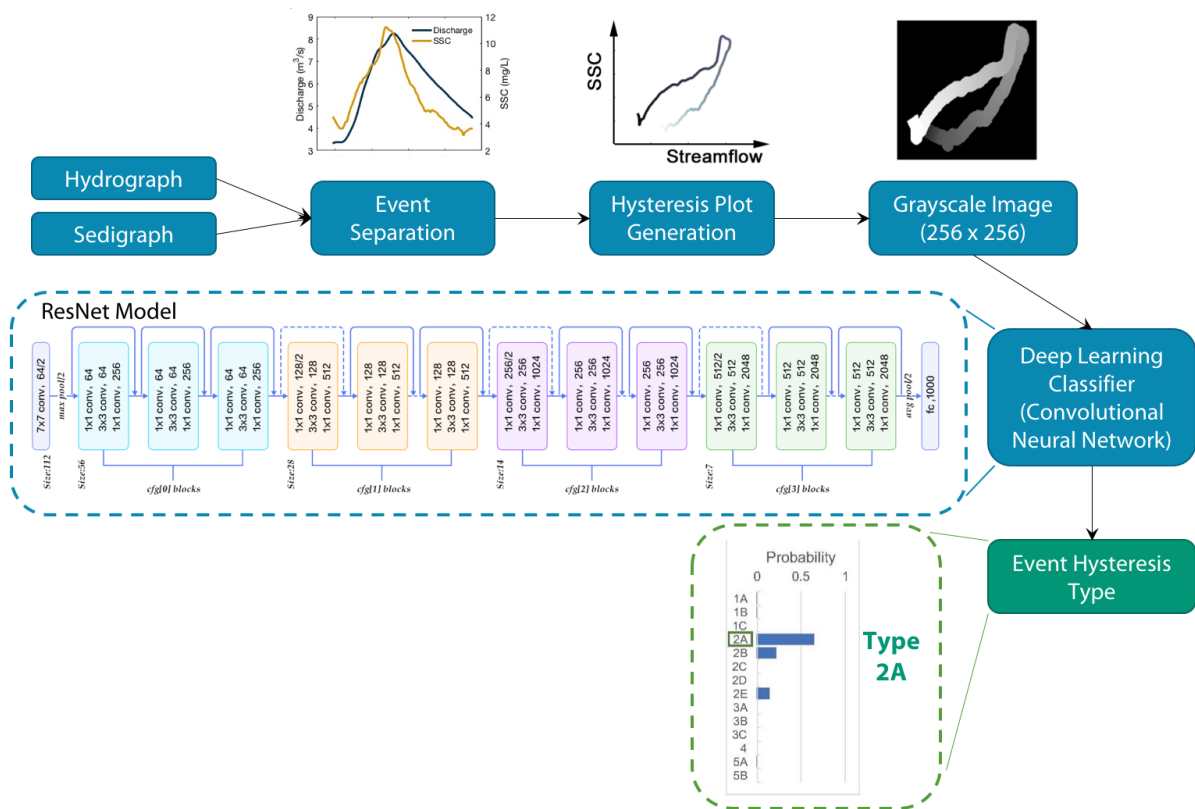
Figure 4. Model workflow for classification of hydrological events based on image of hysteresis plot using a deep learning classifier.
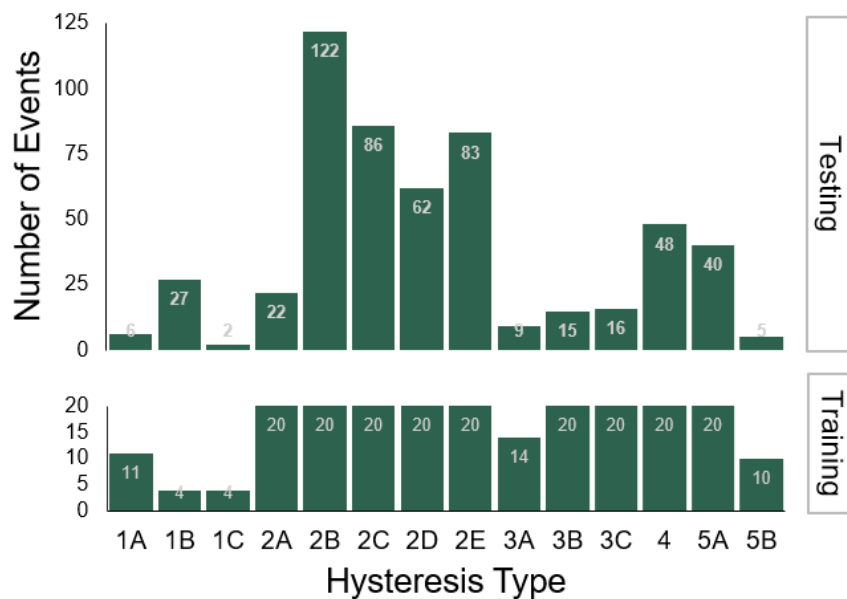
Figure 5. Training and testing data set by type of hysteresis.

Input data to the CNN was represented as 256x256 pixel grayscale image data of a hysteresis pattern. Due to the small size of the training dataset (223 images) compared to those typical of deep learning applications, we performed data augmentation prior to training the model to increase the training data set size. Data augmentation consisted of creating "new" storm events where hysteresis plots were slightly shifted and perturbed from the original sample. The built-in data augmentation tool in the Keras package was used to perform all data augmentation. After applying the augmentation methods, we obtained a total of 1115 hysteresis plot images. The CNN model was trained using 20% of the training data for validation. In Keras, when a validation split of the data is specified within the fit method, the validation set is chosen randomly prior to each epoch. Thus, for each epoch, a different validation set is used to estimate the validation loss.

We performed a parameter sweep over several values of learning rates and batch sizes to determine optimal values for these parameters. Models in the parameter sweep were run for 1000 epochs. We chose not to include the number of epochs in the parameter sweep and instead chose to set the number of epochs very high and assess the optimal number of epochs by inspecting graphs of loss vs. epochs. We used categorical cross-entropy as the loss function and the Adam optimizer (Kingma and Ba, 2014) for all models. After training the model, we chose the model in which the loss function decreased to the greatest degree over 1000 epochs and used that model to predict onto the test data (543 images). Accuracy was assessed as the percentage of 543 test events classified by the CNN model as the same as the manual labels.

Results and Discussion

Hysteresis types of storm events

The manual classification of the 765 storm events observed across the eight study watersheds showed variations in distribution of hysteresis types across watersheds. Across all watersheds Class II (Clockwise) patterns were most common (Figure 6). The exception to this was the larger Mad River watershed and low-gradient, agricultural land use dominated Hungerford Brook where Class III (counter-clockwise) and Class V (Figure-eight) patterns occurred frequently. Attributing to the predominance of smaller, steep forested watersheds in the dataset (six of eight watersheds) the representation of hysteresis types was not especially well balanced. A study area that features watersheds with more balanced variation of land use and drainage area would likely result in a more balanced distribution of observed hysteresis types. For data-driven modeling approaches such as machine learning, access to a wide variety of training and testing data can be significant for successful model development.
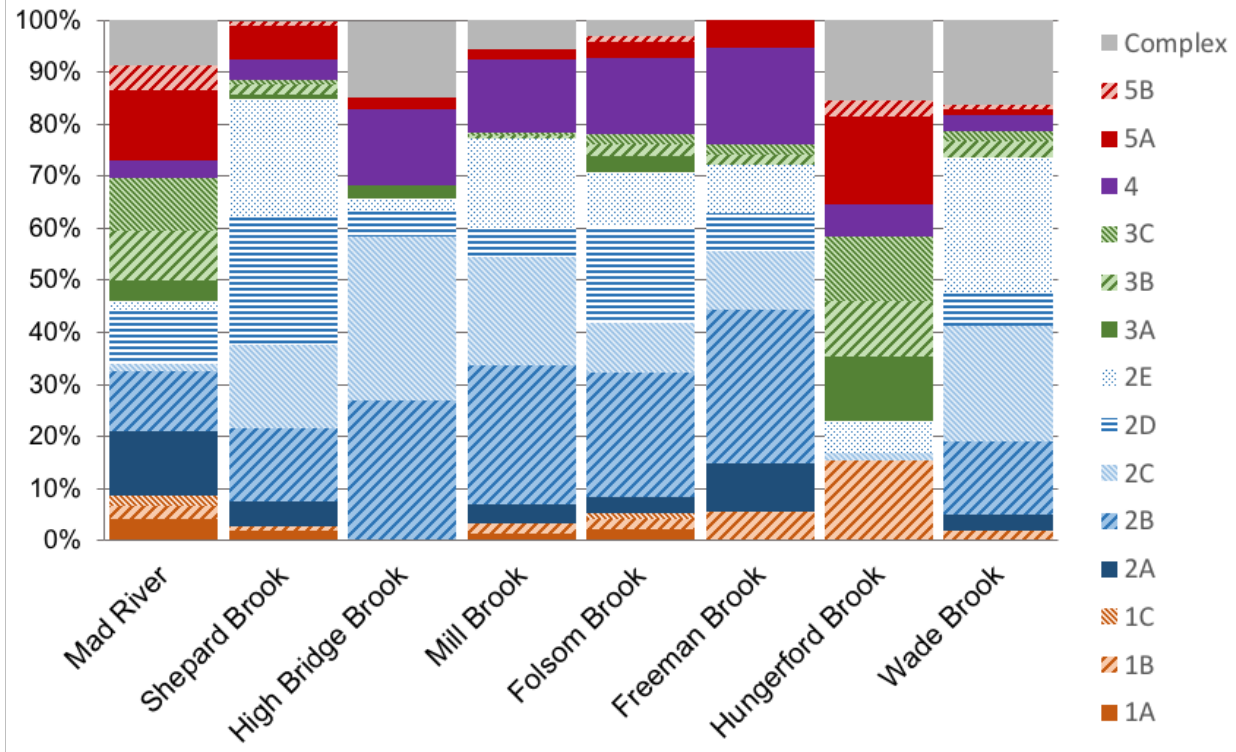
Figure 6. Observed hysteresis patterns of 760 storm events used in training and testing CNN model

CNN Model Performance

The CNN classifier achieved an overall accuracy of 69% on the test dataset. This improves over automated classification using the more basic neural network classifier previously demonstrated by Hamshaw et al. (2018). The classification accuracy of our CNN model approaches manual, visual classification of hysteresis patterns (Romero *et al.*, 2018). We found that when the CNN model mis-classified an event, it often was placed into one of the most visually similar categories. For example, while 78% of Type 2C were classified correctly, 21% of the misclassifications were into the similar Type 2D and 2E classes. The confusion matrix (Figure 7) shows classification accuracies for each hysteresis type. Values along the diagonal show the classification accuracy for each particular type of hysteresis whereas values on the off-diagonals are considered mis-classifications. While hysteresis type is not a true ordinal variable, in a general sense mis-classifications on the 1-off diagonal can be considered "near-misses."

PREDICTED Hysteresis Type

	1A	1B	1C	2A	2B	2C	2D	2E	3A	3B	3C	4	5A	5B
1A	83%	7%	0%	0%	0%	0%	0%	0%	0%	0%	0%	0%	5%	0%
1B	0%	30%	0%	0%	0%	0%	0%	0%	0%	0%	0%	0%	0%	0%
1C	0%	0%	0%	0%	1%	0%	0%	0%	0%	0%	0%	0%	0%	0%
2A	0%	7%	0%	45%	2%	0%	0%	1%	0%	0%	0%	2%	5%	20%
2B	0%	0%	0%	32%	67%	9%	0%	4%	0%	0%	0%	10%	8%	20%
2C	0%	0%	0%	0%	7%	78%	3%	20%	0%	0%	0%	0%	2%	0%
2D	0%	0%	0%	0%	1%	0%	85%	4%	0%	0%	0%	6%	12%	0%
2E	0%	0%	0%	5%	11%	12%	5%	63%	0%	0%	0%	0%	0%	0%
3A	0%	4%	0%	0%	0%	0%	0%	0%	67%	0%	6%	0%	0%	0%
3B	0%	0%	0%	0%	1%	0%	0%	1%	11%	73%	6%	0%	10%	0%
3C	0%	4%	0%	0%	0%	0%	2%	0%	0%	20%	88%	0%	2%	0%
4	0%	30%	50%	18%	8%	1%	5%	5%	11%	0%	0%	77%	5%	2%
5A	17%	11%	50%	0%	2%	0%	0%	2%	11%	7%	0%	4%	50%	0%
5B	0%	7%	0%	0%	0%	0%	0%	0%	0%	0%	0%	0%	0%	40%

(ACTUAL Hysteresis Type — row labels)

Figure 7. Confusion Matrix of Testing Data Classification

Dataset Challenges

Although we achieved a reasonable overall accuracy of 69%, we speculate that our inability to achieve a greater overall classification accuracy was primarily due to inherent complexity of hysteresis patterns present in event C-Q relationships. In a related study using a subset of the Mad River storm events, manual visual classification at best was 85% accurate (Romero *et al.*, 2018). However, we speculate three additional factors also contributed to inability to achieve higher classification accuracies: 1) the sparsity of data, 2) imbalanced class representation, 3) and similarity among classes. Due to the substantial number of parameters that need to be estimated during training, deep learning techniques are best suited to large datasets (Najafabadi *et al.*, 2015), and deep learning techniques tend to overfit on smaller datasets (LeCun *et al.*, 2015) like ours. We attempted to resolve the issues associated with small datasets by conducting a simple data augmentation. Furthermore, a small training dataset size and class imbalance are two attributes that, when combined, can have a substantial, negative impact on the performance of deep learning methods. Since our data exhibited these characteristics, it is not surprising that our classification accuracy plateaued at 69%. Expansion of the training data set to encompass additional storm events from more watersheds and monitoring periods would likely improve CNN model performance.

Finally, the hysteresis data were characterized by poor distinction among several of the 14 different hysteresis types. We chose to test the methodology on the expanded hysteresis classification scheme developed by Hamshaw et al. (2018). However, the model could be just as easily trained and tested on storm events using a simplified classification scheme, such as the more traditional clockwise, counter-clockwise, and figure eight patterns (Williams, 1989). For example, if we aggregated our results to the four commonly used categories of no hysteresis, clockwise, counter-clockwise, and figure-eight hysteresis, then the classification accuracy would improve to 89.7%. Our results would suggest that approach may be more appropriate on datasets smaller than ours. However, we believe our initial results show that a CNN classifier is a promising method to automate the classification of hysteresis types.

Modeling Environment

In this study, the pre-processing routines were developed in MATLAB (version 9.2) and the CNN model implementation in Python. This approach clearly requires programming knowledge, and therefore, presents a challenge over simpler methods such as hysteresis indices. However,

we believe the availability of deep learning models are more accessible than ever; given the variety of algorithms available off the shelf ready to use or to provide a starting point. The CNN used as proof-of-concept here (ResNet50) is now available in a variety of common programming languages (e.g., MATLAB, R, Python) and can be implemented in very few lines of code as a result of wrapper packages (e.g. Keras) or included functions (MATLAB). While efficient training of a CNN often requires high-performance GPU hardware and therefore may not be practical for all applications, once trained CNNs operate fast and may be used directly on more basic computing hardware (e.g. typical desktop and laptop computers) without requiring additional network training required. Finally, because this approach is analogous to machine learning applications used for handwritten character recognition, a number of tutorials are now available based on the similar MNIST benchmark data set (e.g. Pedregosa et al., 2011; Eclipse Deeplearning4j Development Team, 2017).

Summary

The deep learning tool for automating visual pattern recognition from hydrological data presented here represents a novel application of machine learning in hydrology. As illustrated in this study, the automation of analysis of hysteresis patterns allows for rapid application to data sets containing hundreds of storm events. While further research is warranted on developing consistent, automated methods for extracting storm events from continuous streamflow and sediment monitoring data, the potential to generate datasets containing thousands of storm events exists. As these datasets begin to reflect a variety of watersheds with different land use, climate, geology, topography, and drainage area, the application of deep learning methods offer an opportunity for building a greater understanding of drivers of sediment loading during storms across both time and space

Acknowledgements

References

Abadi M, Agarwal A, Barham P, Brevdo E, Chen Z, Citro C, Corrado GS, Davis A, Dean J, Devin M, et al. 2015. TensorFlow: large-scale machine learning on heterogeneous systems. Software available from tensorflow. org. 2015. *URL https://www. tensorflow. org*

Abrahart RJ, Anctil F, Coulibaly P, Dawson CW, Mount NJ, See LM, Shamseldin AY, Solomatine DP, Toth E, Wilby RL. 2012. Two decades of anarchy? Emerging themes and outstanding challenges for neural network river forecasting. *Progress in Physical Geography* **36** (4): 480–513 DOI: 10.1177/0309133312444943

Asselman NEM. 1999. Suspended sediment dynamics in a large drainage basin: the River Rhine. *Hydrological Processes* **13** (10): 1437–1450 DOI: 10.1002/(SICI)1099-1085(199907)13:10<1437::AID-HYP821>3.0.CO;2-J

Chollet F, others. 2015. *Keras*. Available at: https://keras.io

Duvert C, Gratiot N, Evrard O, Navratil O, Némery J, Prat C, Esteves M. 2010. Drivers of erosion and suspended sediment transport in three headwater catchments of the Mexican Central Highlands. *Geomorphology* **123** (3–4): 243–256 DOI: 10.1016/j.geomorph.2010.07.016

Dyrmann M, Karstoft H, Midtiby HS. 2016. Plant species classification using deep convolutional neural network. *Biosystems Engineering* **151**: 72–80 DOI: 10.1016/j.biosystemseng.2016.08.024

Gao P, Josefson M. 2012. Event-based suspended sediment dynamics in a central New York watershed. *Geomorphology* **139**–**140**: 425–437 DOI: 10.1016/j.geomorph.2011.11.007

Gellis AC. 2013. Factors influencing storm-generated suspended-sediment concentrations and loads in four basins of contrasting land use, humid-tropical Puerto Rico. *CATENA* **104**: 39–57 DOI: 10.1016/j.catena.2012.10.018

Hamshaw SD, Dewoolkar MM, Schroth AW, Wemple BC, Rizzo DM. 2018. A New Machine-Learning Approach for Classifying Hysteresis in Suspended-Sediment Discharge Relationships Using High-Frequency Monitoring Data. *Water Resources Research* **54** (6): 4040–4058 DOI: 10.1029/2017WR022238

He K, Zhang X, Ren S, Sun J. 2016. Deep residual learning for image recognition. In *Proceedings of the IEEE Conference on Computer Vision and Pattern Recognition* 770–778.

Kingma DP, Ba J. 2014. Adam: A Method for Stochastic Optimization. *arXiv:1412.6980 [cs]* Available at: http://arxiv.org/abs/1412.6980 [Accessed 14 January 2019]

Krizhevsky A, Sutskever I, Hinton GE. 2012. Imagenet classification with deep convolutional neural networks. In *Advances in Neural Information Processing Systems* 1097–1105.

Lawler DM, Petts GE, Foster IDL, Harper S. 2006. Turbidity dynamics during spring storm events in an urban headwater river system: The Upper Tame, West Midlands, UK. *Science of The Total Environment* **360** (1–3): 109–126 DOI: 10.1016/j.scitotenv.2005.08.032

LeCun Y, Bengio Y, Hinton GE. 2015. Deep learning. *Nature* **521** (7553): 436–444 DOI: 10.1038/nature14539

LeCun Y, Boser B, Denker JS, Henderson D, Howard RE, Hubbard W, Jackel LD. 1989. Backpropagation applied to handwritten zip code recognition. *Neural computation* **1** (4): 541–551

LeCun Y, Boser BE, Denker JS, Henderson D, Howard RE, Hubbard WE, Jackel LD. 1990. Handwritten digit recognition with a back-propagation network. In *Advances in Neural Information Processing Systems* 396–404.

Lefrançois J, Grimaldi C, Gascuel-Odoux C, Gilliet N. 2007. Suspended sediment and discharge relationships to identify bank degradation as a main sediment source on small agricultural catchments. *Hydrological Processes* **21** (21): 2923–2933 DOI: 10.1002/hyp.6509

Lloyd CEM, Freer JE, Johnes PJ, Collins AL. 2016. Technical Note: Testing an improved index for analysing storm discharge-concentration hysteresis. *Hydrology and Earth System Sciences* **20** (2): 625–632 DOI: 10.5194/hess-20-625-2016

Najafabadi MM, Villanustre F, Khoshgoftaar TM, Seliya N, Wald R, Muharemagic E. 2015. Deep learning applications and challenges in big data analytics. *Journal of Big Data* **2** (1): 1

O'Connor P, Neil D, Liu S-C, Delbruck T, Pfeiffer M. 2013. Real-time classification and sensor fusion with a spiking deep belief network. *Frontiers in Neuroscience* **7** DOI: 10.3389/fnins.2013.00178

Romero ET, Davila Torres NM, Hamshaw SD, Denu D, Rizzo DM, Dewoolkar MM. 2018. Evaluating the Visual Classification of Suspended Sediment – Discharge Hysteresis via Crowd-sourcing and In- stream Monitoring

Sainath TN, Kingsbury B, Saon G, Soltau H, Mohamed A, Dahl G, Ramabhadran B. 2015. Deep Convolutional Neural Networks for Large-scale Speech Tasks. *Neural Networks* **64**: 39–48 DOI: 10.1016/j.neunet.2014.08.005

Seeger M, Errea M-P, Beguerı́a S, Arnáez J, Martı́ C, Garcı́a-Ruiz J. 2004. Catchment soil moisture and rainfall characteristics as determinant factors for discharge/suspended

sediment hysteretic loops in a small headwater catchment in the Spanish pyrenees. *Journal of Hydrology* **288** (3–4): 299–311 DOI: 10.1016/j.jhydrol.2003.10.012

Sherriff SC, Rowan JS, Fenton O, Jordan P, Melland AR, Mellander P-E, hUallacháin DÓ. 2016. Storm Event Suspended Sediment-Discharge Hysteresis and Controls in Agricultural Watersheds: Implications for Watershed Scale Sediment Management. *Environmental Science & Technology* **50** (4): 1769–1778 DOI: 10.1021/acs.est.5b04573

Simonyan K, Zisserman A. 2014. Very Deep Convolutional Networks for Large-Scale Image Recognition. *arXiv:1409.1556 [cs]* Available at: http://arxiv.org/abs/1409.1556 [Accessed 13 January 2019]

Smith HG, Dragovich D. 2009. Interpreting sediment delivery processes using suspended sediment-discharge hysteresis patterns from nested upland catchments, south-eastern Australia. *Hydrological Processes* **23** (17): 2415–2426 DOI: 10.1002/hyp.7357

Sze V, Chen Y, Yang T, Emer JS. 2017. Efficient Processing of Deep Neural Networks: A Tutorial and Survey. *Proceedings of the IEEE* **105** (12): 2295–2329 DOI: 10.1109/JPROC.2017.2761740

Szegedy C, Wei Liu, Yangqing Jia, Sermanet P, Reed S, Anguelov D, Erhan D, Vanhoucke V, Rabinovich A. 2015. Going deeper with convolutions. In *2015 IEEE Conference on Computer Vision and Pattern Recognition (CVPR)*IEEE: Boston, MA, USA; 1–9. DOI: 10.1109/CVPR.2015.7298594

Vaughan MCH, Bowden WB, Shanley JB, Vermilyea A, Sleeper R, Gold AJ, Pradhanang SM, Inamdar SP, Levia DF, Andres AS, et al. 2017. High-frequency dissolved organic carbon and nitrate measurements reveal differences in storm hysteresis and loading in relation to land cover and seasonality: high-resolution doc and nitrate dynamics. *Water Resources Research* **53** (7) DOI: 10.1002/2017WR020491

Williams GP. 1989. Sediment concentration versus water discharge during single hydrologic events in rivers. *Journal of Hydrology* **111** (1): 89–106

Xu M, Papageorgiou DP, Abidi SZ, Dao M, Zhao H, Karniadakis GE. 2017. A deep convolutional neural network for classification of red blood cells in sickle cell anemia (Q Nie, ed.). *PLOS Computational Biology* **13** (10): e1005746 DOI: 10.1371/journal.pcbi.1005746

Zuecco G, Penna D, Borga M, van Meerveld HJ. 2016. A versatile index to characterize hysteresis between hydrological variables at the runoff event timescale. *Hydrological Processes* **30** (9): 1449–1466 DOI: 10.1002/hyp.10681

Blue River Fish Barrier: 2D Numerical Hydraulic and Sediment Transport Modeling

Caroline Ubing, MS, PE, Hydraulic Engineer, U.S. Bureau of Reclamation, Denver, CO, cubing@usbr.gov
Michael Sixta, MS, PE, Hydraulic Engineer, U.S. Bureau of Reclamation, Denver, CO, msixta@usbr.gov

Abstract

Steady-state two-dimensional (2D) numerical hydraulic and sediment transport modeling simulations were performed on a fish barrier located on the Blue River, approximately 0.5 miles upstream of its confluence with the San Francisco River in east central Arizona. The fish barrier structure and downstream jetty were constructed in 2012 to prevent upstream movement of non-native fish. In September of 2013, a large storm event deposited approximately 2.3 feet (ft) of sediment on the structure's apron on river left, potentially allowing upstream migration of non-native species. To prevent upstream passage and the impact of future sediment deposition, four alternatives were analyzed: 1) no action, 2) remove jetty, 3) increase the entire barrier height by 4 ft, and 4) increase a portion of barrier height upstream of the current depositional area by 4 ft. The objective of the numerical modeling was to evaluate if the hydraulic conditions at the structure prevent upstream movement of non-native fish species and the sediment aggradation and degradation upstream, at, and downstream of the structure. The numerical model applied to this study was SRH-2D, a two-dimensional (2D) mobile bed hydraulics and sediment transport model for river systems (Lai, 2008).

Each alternative was analyzed to determine if it is a physical barrier (drop in bed elevation of 4 ft or depths < 0.25 ft) or a velocity barrier (magnitude > 6 ft/s across the barrier). Assuming a stationary bed, upstream fish passage is possible under the "no action" alternative during the 2-yr and 5-yr flood events. Removing the jetty (Alternative 2) only allowed upstream movement during the 2-yr flow event. The mobile bed analysis evaluated structure stability and depositional potential downstream and at the structure. Model results show a depositional feature forms downstream of the structure along the right bank for all alternatives, with the greatest deposition occurring during the 2-yr event. The hydraulic conditions surrounding the fish barrier were again analyzed to determine if there is a physical/velocity barrier to prevent upstream movement of non-native fish species after maximum deposition. Model results show that Alternative 3, a 4-ft increase over the entire barrier length, was the only alternative that maintained a physical or velocity barrier for all flow events.

Introduction

A fish barrier and downstream scour-preventing jetty were constructed on the Blue River, approximately 0.5 miles upstream of its confluence with the San Francisco River in east central Arizona to prevent upstream movement of non-native fish. In September of 2013, a large storm event peaking at roughly 6,000 cubic feet per second (cfs) deposited approximately 2.3 ft of sediment on the structure's river left apron, potentially allowing upstream migration of non-native species (Figure 1). To prevent upstream passage and the impact of future sediment deposition, four alternatives were proposed: 1) no action, 2) remove jetty, 3) increase the entire barrier height by 4 ft, and 4) increase the barrier height only on the portion of weir upstream of the current depositional area by 4 ft. The objective of the numerical modeling was to evaluate if the hydraulic conditions at the structure prevent upstream movement of non-native fish species and the sediment aggradation and degradation upstream, at, and downstream of the structure for eight flow events ranging from low flow to the 100-year flood.

Figure 1. Blue River Fish Barrier (4/13/2014). The depositional bar that formed on river left has buried the structure apron.

Design Analysis

Hydrology

A previous Hydrology and Hydraulics study determined peak discharge events (2-, 5-, 10-, 25, and 100-year events; Reclamation, 2002). Flow estimates were developed by applying the Arizona Department of Transportation (ADOT) Method utilizing data from the USGS gage 09444200, located on the Blue River roughly 7.5 miles upstream of the project site. A scaling factor was applied to the gage data to compensate for the additional drainage area. To evaluate sediment aggradation and degradation during a flood, 24-hr flood hydrographs were developed utilizing National Streamflow Statistics (NSS) Program and peak discharge values.

Upstream fish movement is a concern during both high and low flow events; therefore, the 09444200 USGS gage data were analyzed to determine a low flow (average daily discharge during June, July, and August, the driest months of the year), 95% non-exceedance, and 99% non-exceedance flow values. No scaling factors were applied as the scaling at low flows is unknown. The 2013 storm event that deposited roughly 2.3 feet of sediment on the left bank structure apron peaked at an approximate 3.5-year event. With a peak scaled discharge of 6,060 cfs, the storm contained three peaks within an approximate 40 hour time window. A 135-hour hydrograph was used to represent this event and model validation, which included the rising limb, peaks, and recessional limb.

Model Selection and Input Data

SRH-2D is a two-dimensional (2D) mobile-bed hydraulics and sediment transport model for river systems developed by Reclamation at the Technical Service Center (Lai, 2008). SRH-2D solves the depth-averaged dynamic wave equations with a depth-averaged parabolic turbulence model using a finite-volume numerical scheme. The model adopts a zonal approach for coupled modeling of channels and floodplains; a river system is broken down into modeling zones (delineated based on natural features such as topography, vegetation, and bed roughness), each with unique parameters such as flow resistance. One of the major features of SRH-2D is the adoption of an unstructured hybrid mixed element mesh, which is based on the arbitrarily shaped element method of Lai (2000) for geometric representation. This meshing strategy is flexible enough to facilitate the implementation of the zonal modeling concept, allowing for greater modeling detail in areas of interest that ultimately leads to increased modeling efficiency through a compromise between solution accuracy and computing demand.

Model Topography: Five topographic surfaces were utilized for this study: existing conditions, as-built conditions, and three proposed alternative surfaces. Existing conditions topography was developed by combining three datasets utilizing the nearest neighbor algorithm: topographic survey data provided by Reclamation's Phoenix Area Office (PXAO), interpolated cross sections based on the survey data, and a digital elevation model (DEM) obtained from Intermap. The survey was conducted in April of 2017 using the NAD 1983 (2011) State Plane Arizona East Coordinate System and North American Vertical Datum 1988 (NAVD 88). Interpolated cross sections (XS) were added in-between surveyed cross sections to smooth transitions in the modeled channel. Intermap data was acquired from airborne Interferometric Synthetic Aperture Radar (IFSAR) technology. IFSAR produces data with a vertical accuracy of 1.64 feet and a horizontal accuracy of 3.28 feet (www.intermap.com). The resultant raster surface was used to assign elevations to the 2D model mesh from which the numerical modeling computations were performed.

All alternative topography was based on the existing condition topography. Alternative 2 conditions were created by removing the jetty, leaving the sediment deposition and scour holes. Alternative 3 involved increasing the height of the entire barrier 4 feet (to a final barrier height of 8 ft), while Alternative 4 increased the height of the barrier 4 ft in the portion directly upstream of the current sediment deposition. The wall increase for Alternative 4 is approximately 82 ft in length beginning on the left bank.

Model Mesh and Materials: A 2D mesh is what defines the SRH-2D model topography and solution spacing. The mesh (nodes) stores ground elevation information from the model surface and consists of quadrilateral and triangular shaped elements. The mesh was developed using Aquaveo's Surface-Water Modeling System (SMS) v 12.1.11. The same computation mesh of roughly 40,000 elements was used for all modeling conditions. The mesh consisted of primarily quadrilateral elements in the channel and triangular elements in the floodplain and overbanks; the fish barrier was comprised of quadrilateral elements. The mesh element density was also refined around the fish barrier for greater topographic representation (Figure 2).

Material data distributes sediment characteristics spatially across the model domain. Five different material zones were implemented to represent both the hydraulic roughness as well as different thicknesses of the erodible sediment layer. The thickness of the channel and erodible floodplain were both set to 32 ft, which is an arbitrary value to represent an effectively infinite erodible layer. The non-erodible floodplain represented in the upper bluffs do not get inundated

during the 100-yr event. The concrete was also set to be non-erodible to prevent erosion on the structure and jetty. Finally, the sill sediment, deposited on the apron, was set to an erodible depth of 2 ft to allow that sediment to mobilize when appropriate until it reached the concrete material beneath.

The roughness was set to a constant value of 0.028 for the entire model domain. A single value was applied for model stability. No calibration data was available; therefore an average of multiple forms of the Strickler's equation was applied.

Model BoundaryConditions:

Boundary conditions for the SRH-2D model were specified at the upstream and downstream model domain. The upstream boundary condition

Figure 2. Model mesh at the fish barrier structure.

required both hydrologic (flow) and sediment data as inputs. Five storm hydrographs were used for the flow input, while a sediment capacity rating curve was applied for the sediment input. The curve was developed with SRH-Capacity (Huang and Bountry, 2009), a numerical model whose purpose is to compute sediment transport capacity using sediment transport equations for a given set of hydraulic parameters. Another rating curve assigning a water surface elevation to the full range of flows from all hydrographs was used for the downstream boundary condition.

Particle size gradation data was derived from two geologic test pits (TP) collected on September 14, 2000 and two pebble counts (PC) collected on September 14, 2009. All samples were collected at/around the proposed fish barrier site. The average of the four grain size distributions was used in the model (Figure 3). The average distribution was binned into seven different sediment size classes for the mobile bed modeling.
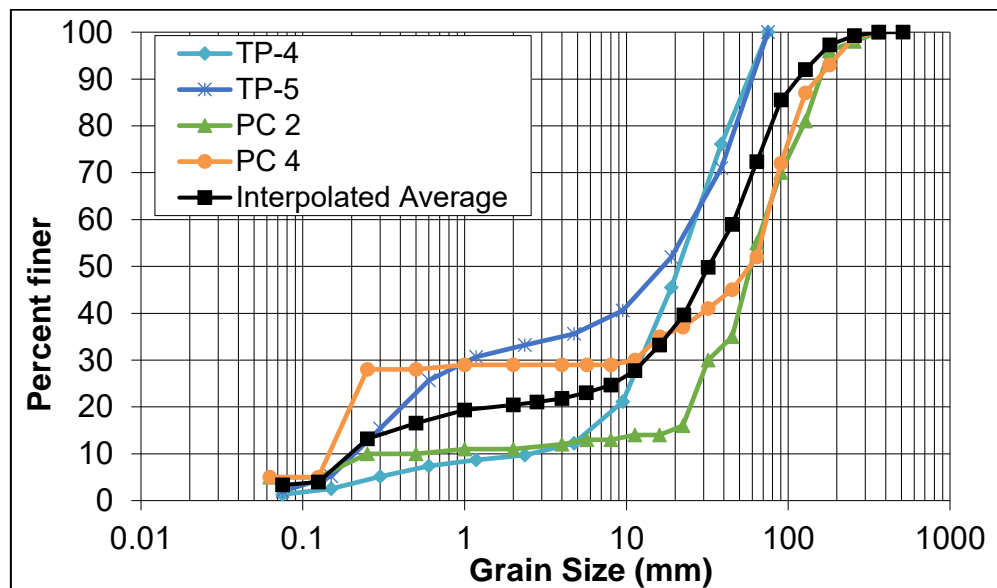
Figure 3. Input sediment gradation distribution.

Model Sensitivity Analysis

Numerical models are often calibrated to best reflect project conditions. If data are available, the surface roughness and sediment equation parameters are adjusted to best represent measured data. Neither a water surface profile nor an associated discharge measurement was collected for this modeling effort; therefore, no data were available for which to calibrate surface roughness.

In lieu of a model calibration, a sensitivity analysis was performed on the sediment equation parameters by running a series of SRH-2D mobile-bed simulations with the as-built conditions surface using the 2013 storm hydrograph to attempt to replicate the deposition that resulted. Twelve simulations varying the sediment transport equation (Parker, Wilcock, Meyer-Peter and Muller, Wu, and Parker coupled with Engelund & Hansen), Shield's parameter, hiding factor, suspended load erosion/deposition adaptation coefficients, and adaptation length were run. The five sediment transport equations were selected as they are commonly used for rivers with both sand and gravel beds. No sensitivity was performed on the incoming sediment load. Model results were assessed at five distinct (monitoring) points located on the depositional bar (Figure 2). The resultant run with the smallest difference between the existing surface and model results (Figure 5) utilized the parameters below and was subsequently used for evaluating all design alternatives:
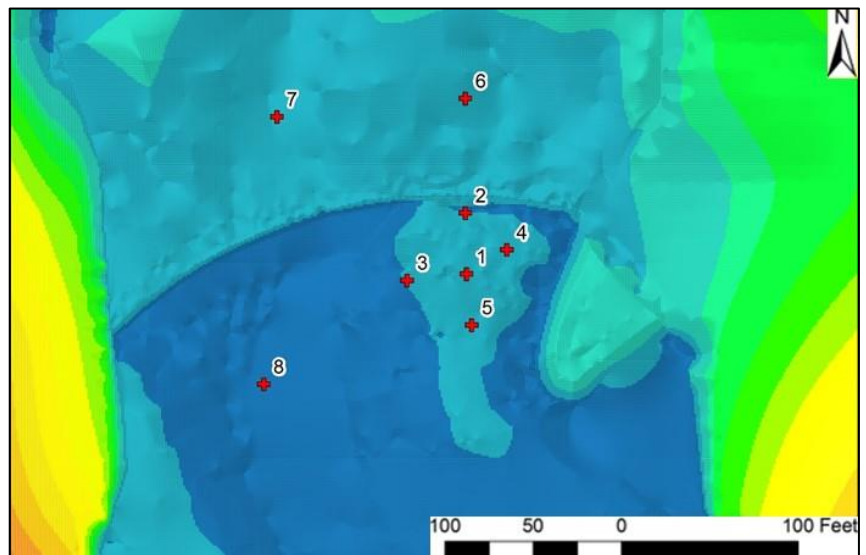
Figure 4. Model sensitivity results were primarily assessed on the depositional bar feature (at monitoring points 1-5).

- Equation: Parker combined with Engelund and Hansen
- Shield's parameter: 0.04 (model default)
- Hiding Factor (H.F.): 0.65 (model default)
- Deposition Adaptation Coefficient (DEP): 0.25 (model default)
- Erosion Adaptation Coefficient (ERO): 1.0 (model default)
- Adaptation Length (A.L.): 10 meters
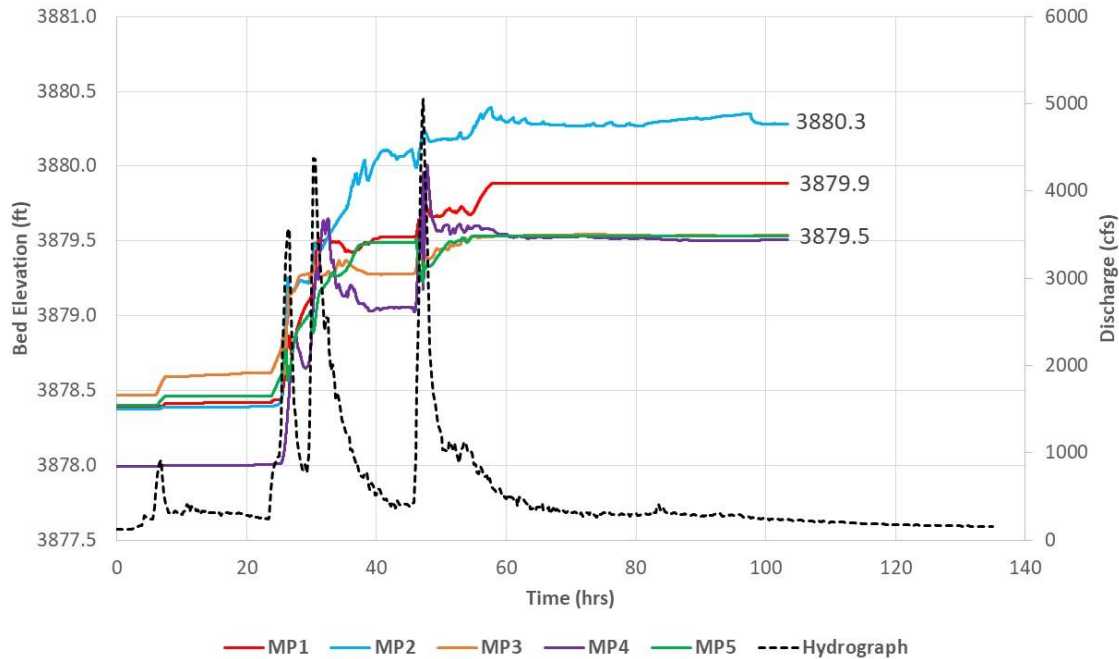
Figure 5. Results from selected sensitivity analysis sediment run. Existing bed elevation values (ft) at each monitoring point (MP) are noted on right side of chart.

Model Results Discussion

The primary objective of the Blue River Fish Barrier hydraulics and sediment transport modeling was to determine if the hydraulic conditions allow upstream movement of non-native fish species and evaluate the structure stability and depositional potential downstream under four alternatives.

The criteria, identified by team biologists, to impede upstream migration was categorized as either a physical or velocity barrier; only one (either/or) of the barrier types needs to be established to prevent fish passage. The physical barrier was defined as a change in bed elevation of 4 ft or water depth values of less than 0.25 ft. The velocity barrier was defined as velocity magnitude values greater than 6 ft/s at the barrier crest. The two criteria were first analyzed with the no action alternative and then again under all proposed alternative conditions.

Stationary Bed Conditions

A stationary bed analysis was performed assuming no sediment transport (no aggradation or degradation) to evaluate whether or not a fish passage barrier (physical and/or velocity) is present. The results show that upstream fish movement is possible for the No Action alternative during the 2-yr and 5-yr flood events (Table 1). A physical barrier exists during the low flow, 95% and 99% non-exceedance events because all flow is concentrated within the main channel where no sediment has deposited on the sill and a 4 ft drop is maintained. The existing depositional bar is not inundated until the 2-yr and 5-yr flood events. During these events velocity values dip below 6 ft/s over the bar. Beginning at the 10-yr flood event, velocity values on the barrier crest are consistently above 6 ft/s. The No Action alternative was further analyzed to determine the average time per year that upstream migration is possible. Model results show that the existing depositional bar becomes inundated at a flow of approximately 1,700 cfs. According to USGS

instantaneous gage records (09444200), a flow discharge of 1,700 cfs is exceeded 1% of the time, which amounts to approximately 12 hours (0.5 days) each year over the 19-year record.

Assuming a stationary bed, upstream passage is possible under Alternative 2 conditions, but a wall increase (both whole and partial) created a barrier for all analyzed flow events. Removing the jetty (Alternative 2) had a minimal impact on the hydraulic performance of the barrier. Furthermore, it does not meet the barrier criteria at the 2-yr food event. For these reasons, it was eliminated as a viable solution and was not analyzed further, under mobile bed conditions. Both Alternatives 3 and 4 do not allow upstream passage for all flow events analyzed, assuming a stationary bed. A physical barrier is present for all flow events while a velocity barrier, due to flow concentration, is present beginning at the 2-yr flood event and extending through the 100-yr flood event.

Table 1. Barrier type assuming stationary bed conditions (no aggradation or degradation).

	No Action	Alternative 2	Alternative 3	Alternative 4
Low Flow	Physical	Physical	Physical	Physical
95% Non-exceedance Flow	Physical	Physical	Physical	Physical
99% Non-exceedance Flow	Physical	Physical	Physical	Physical
2-yr Flood	None	None	Velocity + Physical	Velocity + Physical
5-yr Flood	None	Velocity	Velocity + Physical	Velocity + Physical
10-yr Flood	Velocity	Velocity	Velocity + Physical	Velocity + Physical
25-yr Flood	Velocity	Velocity	Velocity + Physical	Velocity + Physical
100-yr Flood	Velocity	Velocity	Velocity + Physical	Velocity + Physical

Mobile Bed Conditions

The mobile bed analysis evaluated structure stability and depositional potential downstream and at the structure for the 2-, 5-, 10-, 25-, and 100-yr events. In general, the model results show predominant aggradation along the project reach. There is a contraction approximately 550 ft downstream of the fish barrier that causes a backwater effect downstream of the barrier up to the 5-yr flood event (Figure 4). The backwater effect increases water depths and decreases velocities,

which can lead to sediment deposition. A depositional feature near the right bank was indeed observed in the sediment model results for the no action alternative and Alternatives 3 and 4 during the 2-, 5-, 10-yr events. Under existing conditions, erosion was observed along the main channel, near the lowest point in the structure where flow concentrates. The most deposition occurred during the 2-yr event downstream of the structure (Figure 5). Therefore, sediment deposition for each alternative was analyzed for this event. Under Alternative 3 conditions, a high volume of sediment deposited upstream of the fish barrier with lower deposits observed downstream of the structure. Finally, under Alternative 4 conditions, deposition is observed upstream of the wall increase, and the downstream sediment bar on river right continues to form to a similar size and magnitude as was seen in the existing conditions.
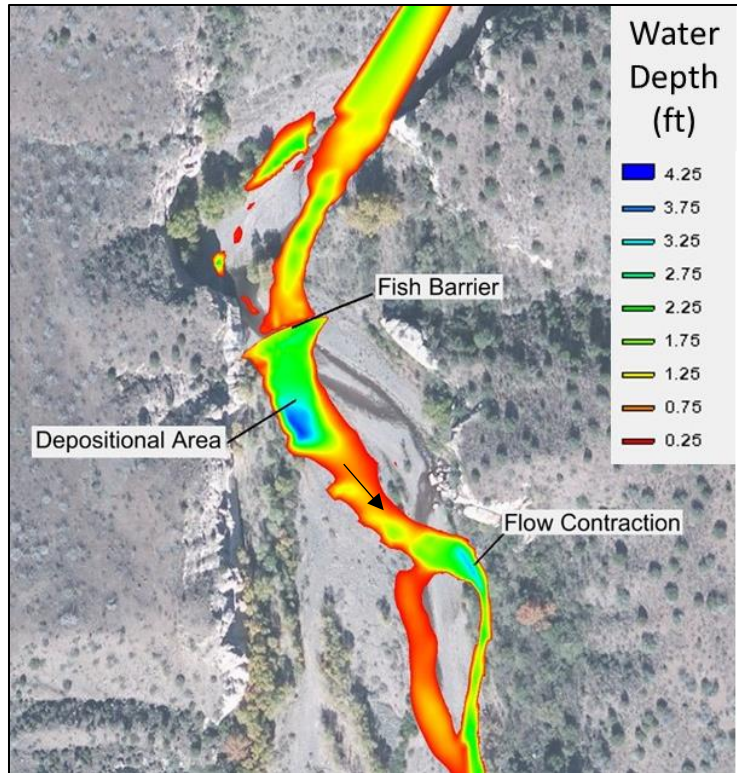
Figure 6. Flow contraction downstream of the fish barrier. Figure shows flow depth results for the 95% exceedance flow event.

The fish barrier was again analyzed to determine if there is a physical and/or velocity barrier to prevent upstream movement of non-native fish species using the resultant topography after one 2-yr storm hydrograph (Table 2). The 2-yr storm was selected as it produced the largest observed depositional volume. Results show that the depositional bar that forms downstream of the barrier near the right bank could remove the physical barrier for the no action and Alternative 4 conditions for two flow events: 95% and 99% non-exceedance flows for both. There is no barrier for the no action alternative during the 2-yr flood event. Alternative 4 appears to concentrate enough flow to create a velocity barrier at the 2-yr event.
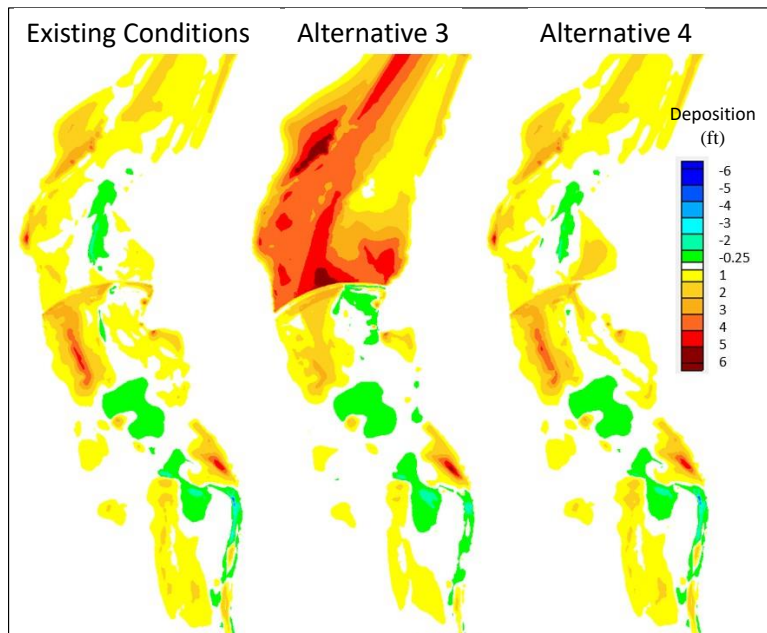
Figure 7. Erosion and deposition results after the 2-yr peak flow hydrograph (56.4 hours). Negative (-) values (green through blue) show erosion, while positive (+) values (yellow through red) show deposition (ft).

Alternative 3 conditions produced the least deposition downstream of the structure after one 2-yr storm hydrograph (Figure 5). Model results predict that deposition did not exceed 4 ft; therefore, the physical barrier remains intact for all flood events. Given that a barrier of one type or another is in place over the full suite of modeled flows for Alternative 3 (whole wall), this was selected as the preferred alternative.

Table 2. Barrier type assuming mobile bed conditions (aggradation and degradation after one 2-yr storm event).

	No Action	Alternative 3	Alternative 4
Low Flow	Physical	Physical	Physical
95% Non-exceedance Flow	**None**	Physical	**None**
99% Non-exceedance Flow	**None**	Physical	**None**
2-yr Flood	**None**	Velocity + Physical	Velocity
5-yr Flood	Velocity	Velocity + Physical	Velocity + Physical
10-yr Flood	Velocity	Velocity + Physical	Velocity + Physical
25-yr Flood	Velocity	Velocity + Physical	Velocity + Physical
100-yr Flood	Velocity	Velocity + Physical	Velocity + Physical

Model Limitations

All numerical models require simplifying assumptions and thus have limitations that manifests itself in uncertainty. Every model makes certain simplifying assumptions that must be considered while viewing and evaluating model results. The accuracy of model results depend on the quality of input data, which in this case included topographic data, bed sediment gradations, flow hydrographs, sediment supply rates, and downstream water surface elevation fluctuations with flow. The absolute values of erosion and deposition are less accurate and should instead be evaluated according to trends and on a basis relative to other model simulations.

Mobile-bed sediment transport modeling is subject to a number of uncertainties, the biggest of which being the incoming sediment supply. Incoming sediment loads can produce large changes in the bed elevation (less sediment causing more erosion, more sediment causing more deposition). Despite these uncertainties, Reclamation is confident about the major findings and conclusions made regarding the project based on the model results.

Model Uncertainty Analysis

To gain a better understanding of how particular uncertainties affect the possible range of erosion/deposition results, a model uncertainty analysis was performed by using four differing sediment transport formulas with various parameters and roughness under the preferred alternative (Alternative 3) conditions, all of which should be considered when evaluating model results.

The evaluated sediment transport methods included the following:
1. Parker's (1990) bed load transport capacity equation.
2. Wilcock and Crowe's (W/C; 2003) bed load transport capacity equation.
3. Wu (2000) total load sediment transport equation.

4. Parker's (1990) bed load transport capacity equation combined with Engelund and Hansen (E/H; 1967), where the transport capacity of particle sizes greater than 2 mm (gravel) are computed with Parker, and the transport capacity of particle sizes less than 2 mm (sand) are computed with E/H.

Results from this uncertainty analysis were primarily quantified by averaging the results over a series of roughly 325 mesh elements located approximately 50 feet downstream of the concrete apron spanning both the main channel and sediment deposition areas. Results indicated that erosion can range from 0.1-2.8 ft, while the deposition can range from 0.1-2.0 ft. The sediment transport methods that showed the greatest amount of erosion and deposition were Wu and E/H with Parker (using a Shield's value of 0.05), respectively. The sediment transport methods that showed the least amount of erosion and deposition were E/H with Parker (using a Shield's value of 0.05; n = 0.028) and Wilcock & Crowe, respectively. Comparing the results against the preferred representative sediment transport formula and parameter set as determined from the sensitivity analysis yields a variance of +2.5/-0.2 ft and +0.3/-1.6 ft for erosion and deposition, respectively.

Summary and Conclusions

Due to a large depositional feature, the Blue River Fish Barrier is potentially no longer a barrier to the upstream passage of non-native fish species for the 2-yr and 5-yr flood events. To address this concern, four alternatives were analyzed 1) No Action, 2) remove jetty, 3) increase the entire barrier height by 4 ft, and 4) increase the barrier height only upstream of the current deposition by 4 ft. Each of these alternatives were analyzed to determine if they met either the physical barrier (drop in bed elevation of 4 ft or depths less than 0.25 ft) or velocity barrier (magnitude greater than 6 ft/s across the barrier) criteria. Each alternative was assessed given the existing bed surface and the bed surface after a 2-yr storm hydrograph where a depositional bar formed on the right bank. Model results showed that that both Alternatives 3 and 4 were a barrier for all flows analyzed assuming only hydraulic conditions with a stationary bed. However, after incorporating the sediment deposition associated with a 2-yr storm event, a no-barrier condition exists for Alternative 4 during the 95% and 99% non-exceedance flow events. A barrier remains for all evaluated flow events under Alternative 3. Therefore, a 4 ft wall increase across the entire barrier is recommended to reduce the risk of upstream fish migration. However, it is also recommended that a No Action alternative be considered given the infrequent amount of time that the flows that prevent the barrier from being a barrier exist. Based on local hydrologic data, the range of flows where this happens occurs approximately 12 hours each year.

References

Bureau of Reclamation 2002. Hydrology and Hydraulics, Blue River Fish

Engelund, F. and Hansen, E. 1967. A Monograph on Sediment Transport in Alluvial Streams. Teknisk Forlag, Copenhagen.

Huang, J.V., and J. Bountry. (2009). SRH-Capacity User Manual, Version 1.37. U.S. Department of Interior, Bureau of Reclamation, Technical Service Center, Denver, CO.

Lai, Y.G. (2000). Unstructured grid arbitrarily shaped element method for fluid flow simulation. AIAA Journal. 38(12), 2246-2252.

Lai, Y.G. (2008). SRH-2D version 2: Theory and User's Manual. Sedimentation and River Hydraulics – Two-Dimensional River Flow Modeling. U.S. Department of the Interior, Bureau of Reclamation, Technical Service Center, Denver, CO.

Meyer-Peter, E. and Muller, R. 1948. Formulas for bed-load transport. Proc. 2d Meeting IAHR, Stockholm. pp. 39-64.

Parker, G. 1990. "Surface based bedload transport relationship for gravel rivers," Journal of Hydraulic Research, Vol. 28(4), 417–436.

Wilcock, P.R. and Crowe J.C. 2003. "Surface-Based Transport Model for Mixed-Size Sediment," Journal of Hydraulic Engineering, ASCE, 129(2):120-128.

Wu, W., Wang, S.S., and Jia, Y. 2000. "Nonuniform sediment transport in alluvial rivers," Journal of Hydraulic Research, Vol. 38(6):427-434.

Dam-Break Flows of Water-Granular Mixtures: A Numerical Study

Nuttita Pophet, Research Assistant, NCCHE, Oxford, MS, nuttita@ncche.olemiss.edu
Mustafa Altinakar, Director and Research Professor, NCCHE, Oxford, MS, altinakar@ncche.olemiss.edu
Yavuz Ozeren, Research Assistant Professor, NCCHE, Oxford, MS, yozeren@ncche.olemiss.edu

Abstract

Dam-break flows of water-granular mixtures such as landslides, debris flows and tailings-dam break flows, are often catastrophic events. These types of flows can cause loss of life, property damage and environmental problems. Understanding the dynamic behavior of these types of flows and developing reliable predictive mathematical and numerical models for solving real-life problems are therefore necessary. In this study, dam-break flows of water-granular mixtures are investigated numerically by taking into account the presence of porous flow in the deforming granular mass. The numerical model is solved by coupling two solvers in the open source finite-volume platform OpenFOAM. The *interFoam* solver simulates the movement of a water-granular mixture by solving the Navier-Stokes equations. The free surface is captured using the volume of fluid (VOF) method. Shear stresses due to inter-particle contacts in the mixture are modeled by making use of a pressure-dependent, effective shear viscosity. This effective viscosity is calculated by using the instantaneous pore water pressure field provided by the *porousInterFoam* solver. The *porousInterFoam* solver is a modified version of *interFoam* to simulate porous flow in the granular matrix by including a sink term in the momentum equation to account for the pressure drop when porous medium is present in the domain. The coupled model is validated against laboratory experiments of dam-break flows of water-granular mixtures conducted in the dam-break facility of NCCHE at the USDA-ARS National Sedimentation Laboratory in Oxford, Mississippi.

Introduction

Granular flows, driven by gravity force, are mass movements of mixtures of solid particles and interstitial fluid. Examples include landslides, debris flows, and tailings dam-break flows, for which the interstitial fluids are water and/or air. These types of flows can be extremely destructive for human lives, properties and infrastructure, and the environment. Understanding the dynamic behavior of these types of flows and developing reliable predictive models are important. The development of numerical models for granular flows centers around three main issues: choice of a level of approximation of the flow field and pressure field in the model, choice of coupling between the solid and fluid phases, and choice of a rheological model or a constitutive equation. Granular flows have been extensively studied using numerical models based on depth-averaged shallow water equations. The experimental data suggests that replacement of the vertical distribution of velocity by a depth-averaged velocity and the omission of vertical velocities does not reflect true flow behavior and may lead to incorrect predictions in the region of strong vertical velocity gradient. Moreover, because such models ignore the velocity component normal to the bed, they account for solid-solid and solid-fluid interaction effects only in a rudimentary way (Iverson, 1997).

Based on the level of coupling between solid and fluid phases, theoretical models can be categorized into: single-phase flow, and two-phase mixture models. Single-phase flow models treat the mixture as a homogeneous material and employ a non-Newtonian rheological model to incorporate the effect of grain-grain interaction (Berzi et al., 2010). The rheologies adopted range from visco-plastic (Bingham, 1922) to collisional regime (Bagnold, 1954). However, as emphasized by Meng and Wang (2016), although such simple models can describe the dynamic behavior of the mixture to some extent, they are unable to account for complex interactive coupling between the fluid and granular phases or the dynamic behavior of each phase.

The two-phase mixture models can be classified as two-phase and mixture models. In the two-phase model, the momentum and continuity equations of each phase are solved separately (e.g., Armanini, 2013). Coupling is achieved through the pressure and inter-phase exchange coefficients. When there is a wide distribution of the particulate phase or when the interphase laws are unknown or their reliability becomes questionable, however, the mixture model is a good substitute for the two-phase approach in many cases (Ansys Fluent, 2009). In the mixture model, the continuity and momentum equations for the mixture are solved together with algebraic expressions for the relative velocities (Savage et al., 2014). This model can be used to simulate grain-fluid flows where the phases move at different velocities, but assume a local equilibrium over short spatial length scale. In this way, the model can incorporate a separate response from the interstitial fluid and the solid phase.

Choice of a constitutive equation is an important consideration when modeling granular flows. Unlike Newtonian fluids, which are well described by the Navier-Stokes equations, no constitutive law can reproduce the diversity of behavior observed with a cohesionless granular material (Forterre and Pouliquen, 2008). This difficulty originates from fundamental characteristics of granular matter such as negligible thermal fluctuation, highly dissipative interactions, and a lack of separation between the microscopic grain scale and the macroscopic scale of the flow (Goldhirsch, 2003). As a result, granular flows are often divided into three regimes and the appropriate constitutive equation is chosen based on the flow regime. In a quasi-static regime, the deformations are very slow and the particles interact by frictional contacts. The most frequently adopted constitutive relation for the quasi-static regime is the shear rate-independent models based on Mohr-Coulomb (M-C) theory. A grain-inertia regime is the regime where the flow is very rapid and dilute, and the particles interact by collisions. The shear rate-dependent relationships are mostly based on extension of the kinetic theory. In an intermediate regime, the material is dense but still flows like a liquid, with the particles interacting with each other both by collision and friction. The so-called μ(I)-rheology has been developed for this regime (GDR MiDi, 2004).

In this study, a 3-D numerical model for mixture flows is developed by coupling the model of grain-fluid mixture flow with the model of flow in porous media. The coupled model is built on the open-source finite-volume platform OpenFOAM, which provides a library of numerical schemes necessary for the discretizations. The *interFoam* and *porousInterFoam* solvers with some modifications are employed for flows of mixture and flows in porous media, respectively. To investigate the efficiency and accuracy of the coupling technique, the developed model is verified by experimental data of granular dam-break flows.

Materials and Methods

Governing Equations

Mixture Flows (*interFoam*)**:** Granular/debris flows are usually treated as a motion of continuum despite the fact that they contain solid particles. This approximation makes the

equations of mass and momentum conservation for granular flows similar to those for the motion of a generic fluid (Lorenzini and Mazza, 2004). The governing equations can be written in the differential form as:

$$\nabla \cdot \boldsymbol{u} = 0 \tag{1}$$

$$\frac{\partial \rho_m \boldsymbol{u}}{\partial t} + \nabla \cdot (\rho_m \boldsymbol{u}\boldsymbol{u}) = \rho_m \boldsymbol{g} + \nabla \cdot \boldsymbol{\sigma} \tag{2}$$

where:

$\boldsymbol{u}$ is the velocity vector;

$\boldsymbol{g}$ is the gravitational acceleration vector;

ρ_m is the density of the mixture with $\rho_m = (1 - n)\rho_s + n\rho_f$, where n is the porosity, and ρ_s and ρ_f are the density of the solid particles and the interstitial fluid, respectively;

$\boldsymbol{\sigma}$ is the stress tensor, generally expressed as $\boldsymbol{\sigma} = -p\mathbf{I} + \boldsymbol{\tau}$; where p is pressure, $\mathbf{I}$ is the unit tensor and $\boldsymbol{\tau}$ is the shear stress tensor,

$$\boldsymbol{\tau} = 2\mu_{eff}(\|\boldsymbol{D}\|, p)\boldsymbol{D} \tag{3}$$

where $\boldsymbol{D} = \boldsymbol{D}(\boldsymbol{u}) = (\nabla\boldsymbol{u} + (\nabla\boldsymbol{u})^T)/2$ is the strain rate tensor, and $\|\boldsymbol{D}\|$ is second invariant of the strain rate tensor: $\|\boldsymbol{D}\| = \sqrt{2\boldsymbol{D}_{ij}\boldsymbol{D}_{ij}}$. In the case of a dry granular flow, an interstitial fluid plays no significant role in the dynamics of the flow. The effective viscosity can be defined as

$$\mu_{eff} = (\|\boldsymbol{D}\|, p) = \frac{\mu p}{\|\boldsymbol{D}\|} \tag{4}$$

where μ is analogous to a coefficient of friction. Within this description, the granular mixture is then described as an incompressible non-Newtonian fluid, with an effective viscosity (μ_{eff}) depending on both the shear rate and the pressure, a signature of the underlying frictional nature of the medium (Forterre and Pouliquen, 2008). This description is similar to the one developed in other viscoplastic materials like mud. A flow threshold is given by a frictional Drucker-Prager criterion (Drucker and Prager, 1952) for which $|\boldsymbol{\tau}| > \mu p$ is recovered when $\|\boldsymbol{D}\|$ goes to zero and the viscosity diverges as can be seen in Eq. (3) and (4).

In the case of an initially saturated grain-fluid mixture, the total mixture pressure (p) is replaced by the effective inter-particle normal stress (p_{eff}) which is approximated by subtracting the pore water pressure (p_f) from the total mixture pressure. This definition of effective stress correspond to Terzeghi's effective stress. The effective viscosity can be defined as:

$$\mu_{eff}\left(\|\boldsymbol{D}\|, p_{eff}\right) = \frac{\mu(p - p_f)}{\|\boldsymbol{D}\|} + k(\|\boldsymbol{D}\|)^{n-1} \tag{5}$$

where k is the consistency index and n is the flow index. The effective viscosity is then the sum of a frictional term and a viscous term. The consistency index (k) and the flow index (n) are model calibration parameters. In this study, $k = 0.3$ and $n = 0.33$ give the most promising results. The pore water pressure (p_f) is obtained by solving porous media flows through the mixture as described in detail in the next subsection.

Porous Media Flows (*porousInterFoam*)**:** In this study, the macroscopic governing equations for the fluid flow in porous media derived by Wang et al., 2015 are employed. The macroscopic equations is obtained by the technique of volume averaging of the microscopic continuity and momentum equations over a representative elementary volume (REV). The intrinsic phase average is used in the derivation and defined by

$$\langle \varphi_f \rangle^f \; = \; \frac{1}{V_f} \int_{V_v} \varphi_v \, dV \tag{6}$$

where the subscript f means fluid quantity which refers to the portion of fluid existing within the gaps of the solid skeleton, V_f represents the volume of the fluid phase within the representative elementary volume V, and φ_f is a quantity associated with the fluid phase. The intrinsic phase average can be related to the phase average (also called Darcy's quantities) with $\langle \varphi_f \rangle = \; n \langle \varphi_f \rangle^f$, where n is the porosity. As concluded by Wang et al., 2015, the macroscopic conservation equations derived using the intrinsic phase average velocity are Galilean invariant. The following macroscopic equations can be obtained

$$\nabla \cdot \boldsymbol{u_f} \; = \; 0 \tag{7}$$

$$\frac{\partial \rho_f \boldsymbol{u_f}}{\partial t} + \nabla \cdot \left(\rho_f \boldsymbol{u_f} \boldsymbol{u_f} \right) = \; -\nabla p_f + \mu_f \nabla \cdot \left[\nabla \boldsymbol{u_f} + (\nabla \boldsymbol{u_f})^T \right] + \boldsymbol{F} \tag{8}$$

where ρ_f is the fluid density, $\boldsymbol{u_f}$ is the intrinsic phase average velocity, p_f is the pore pressure, μ_f is the fluid dynamic viscosity and $\boldsymbol{F}$ is the total body force including the resistance from the porous medium and other external forces and defined by

$$\boldsymbol{F} = \; -\frac{\mu_f n}{K} \left(\boldsymbol{u_f} - \boldsymbol{u_p} \right) - \rho_f \frac{n^2 F_n}{\sqrt{K}} \left(\boldsymbol{u_f} - \boldsymbol{u_p} \right) \left| \boldsymbol{u_f} - \boldsymbol{u_p} \right| + \rho_f \boldsymbol{g} \tag{9}$$

where K is the permeability, $\boldsymbol{g}$ is the gravitational acceleration, $F_n = 1.75/\sqrt{150n^3}$ is the geometric function of the porous medium, and $\boldsymbol{u_p}$ is the velocity of the moving porous medium. In the case as $n = 1$ (i.e., in the absence of porous media) the value of K will become infinite, and the above equations reduces to the Navier-Stokes equations for pure fluid flows. By modeling porous media flows in this way, the flows inside and outside the porous medium are solved with the same set of equations. This approach avoids the need to specify matching conditions at the pure fluid and porous medium interface, at which interface jump conditions were defined for velocity and shear stresses (del Jesus et al., 2012). Further details of the derivation can be found in Wang et al., 2015.

The Coupling Algorithm

In order to couple *interFoam* and *porousInterFoam*, a python library is developed to wrap the two solvers into a main program. A flowchart of the coupled algorithm is presented in Figure 1. In the flowchart, after the main program starts, geometry, parameters, constants and coefficients are initialized. At half time step of the mixture solver (*interFoam*), the porous flow model (*porousInterFoam*) is solved. At this stage, pore water pressure (p_f) is obtained and sent to the mixture model to calculated the viscous shear stress. Then, the mixture model is solved for grain-

fluid mixture flow. At this stage, geometry of the porous medium and mixture velocity are obtained and sent back to the porous flow model. These steps continue until the simulation ends.
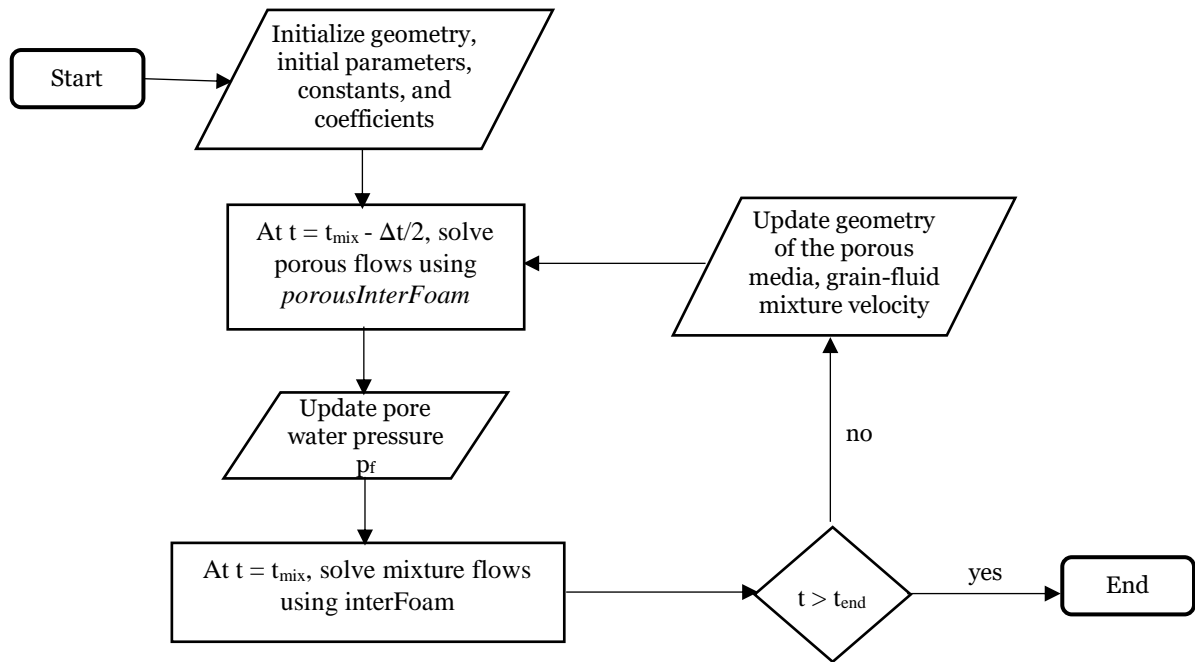
Figure 1. Detailed relationship of *porousMixtureInterFoam* algorithm.

Experimental Setup

Figure 2. PET pellets.

An experiment (Rebillout et al., 2017) conducted in the dam-break facility of National Center for Computational Hydroscience and Engineering (NCCHE) at the USDA-ARS National Sedimentation Laboratory in Oxford, Mississippi is used to validate the coupled model. In this experiment, the channel with a 7.6 m long flume having a width of 0.5 m and a height of 0.6 m was divided by a sliding gate into: (i) a 3.24 m length of upstream reservoir, and (ii) a 4.36 m length of dam-break channel. The PET pellets used in the experiment and the experimental setup are shown in Figure 2 and Figure 3. Some of the intrinsic and bulk properties of the material are summarized in Table 1. In the table, D_m is the mean nominal diameter, *Sf* is the shape factor, n is the porosity, ρ_{PET} is the density of the PET pellets, K the (packed) hydraulic conductivity, and ϕ is the friction angle. At the beginning of the experiments, the sliding gate is pulled upward with a speed of about 8 m/s to release the mixture of PET pellets and water to the downstream channel. Blue dye was added to the water in order to facilitate the tracking of the phreatic surface by imaging techniques. The flow fields in the upstream reservoir and the downstream channel were recorded using two and four high-speed cameras, respectively.

Table 1. Properties of the PET pellets (Ozeren et al., 2014).

d_{10} (mm)	d_{50} (mm)	d_{90}(mm)	D_m (mm)	*Sf*	n (packed)	ρ_{PET} (kg/m³)	K (mm/s)	ϕ (°)
2.812	2.867	2.920	2.861	0.832	0.34	1422	16.6	30
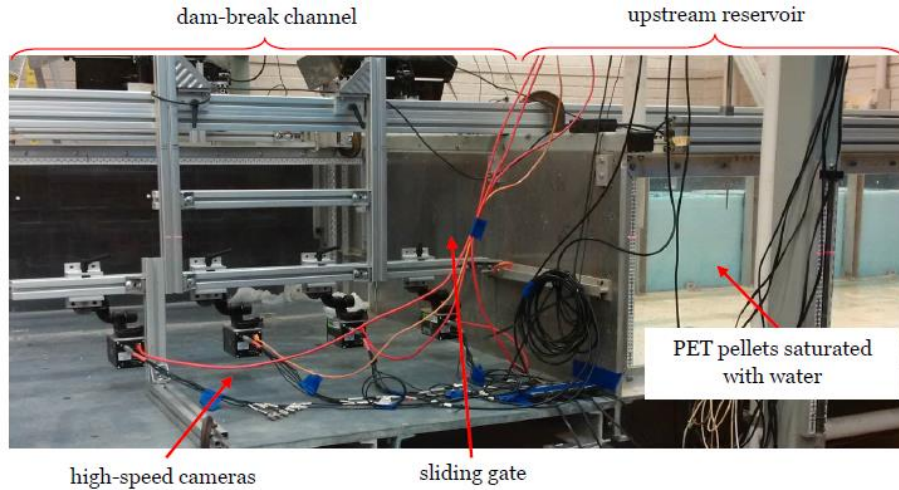
Figure 3. Experimental setup (Rebillout et al., 2017).

Simulation Setup

In the numerical simulation, the 3.93 m-long and 0.5 m-high computational domain (Figure 4) is initialized as two zones with different initial properties: (i) the mixture zone containing PET pellets saturated with water, and (ii) the empty cell zone. This domain is used for both the *interFoam* solver for mixture flow and the *porousInterFoam* solver for flow in porous media. In the mixture flow model, the wall boundary condition is used for the left boundary while atmosphere and open boundary conditions are used for the top and right boundaries, respectively. At the bottom, the Coulomb slip boundary condition is employed. For the porous flow model, boundary conditions are the same as the mixture model except at the bottom where the slip boundary condition is used. For both solvers, the time step is set to 0.001 s while the cell size is 0.01 m.

Simulation Results

Mixture Profiles and Velocity Fields

Figure 5 shows the mixture profiles of the simulation and the experiment and velocity magnitude for the simulation at time 0.25, 0.5, 1.25, 1.5, 2.0 and 2.25 s. At time t = 0.25 s, the mixture column starts falling and the front starts moving in both the simulation and the experiment. The maximum velocity is concentrated at the front of the mixture profile with the magnitude of about 0.5 m/s. At time t = 0.5 s, the velocity magnitude develops at the front to the maximum of about 0.75 m/s. The front in the simulation is almost at the same location as the experiment which is at about x = 0.24 m. However, there is discrepancy between the shapes of the mixture in the simulation and the experiment. This may be due to the expansion (change in porosity and volume fraction of grains) of the densely-packed grain column while shearing. Since the model does not consider this effect, no expansion is allowed in the simulation. However, even neglecting this effect, the model can still reproduce the experiment from the initial falling stage, the flowing stage to the stopping stage. The front in the simulation propagates at almost the same speed as the experiment. At time t = 2.25 s, the velocity magnitude of almost zero is observed in the simulation which indicates that the model can predict the stopping stage.
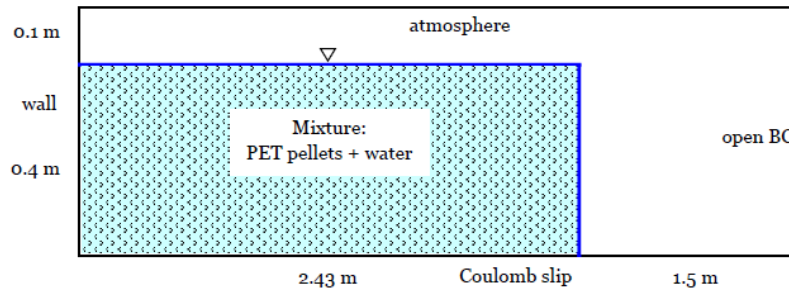
Figure 4. Computational domain.
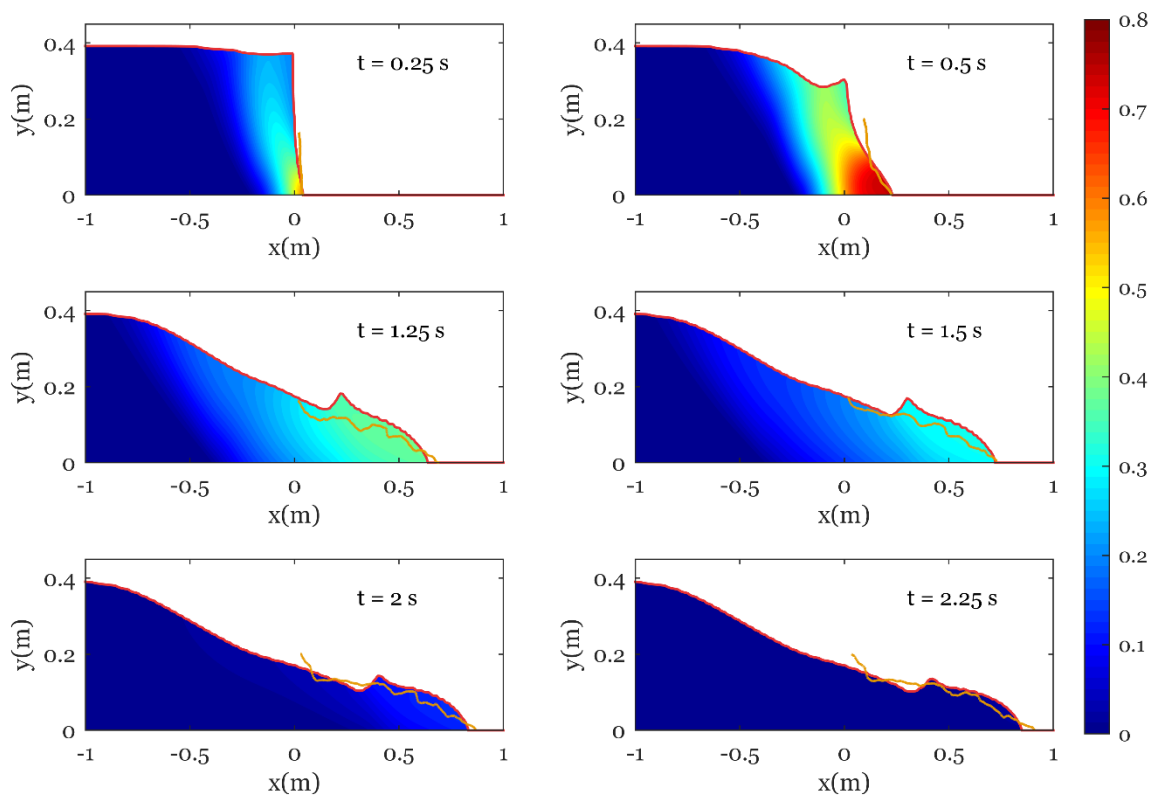
Figure 5. Comparison of the mixture profiles between the simulation (red line) and the experiment (yellow line), and velocity magnitude for the simulation at different times.

Pressure Distribution and Strain Rate

Figure 6 shows pressure distribution and shear rate of the mixture obtained from the simulation at time t = 0.25, 0.5 and 1.25 s. The figure shows that pressure varies from 0 at the interface to about 4000 Pa near the bed in the non-flowing region where the mixture velocity is almost zero (see Figure 5 for the velocity field). At time t = 0.25 s, the strain rate is concentrated near the bottom front of the mixture profile with the maximum of about 7 s^{-1} while at time t = 1.25 s the maximum of about 1.5 s^{-1} is observed near x = -0.4 m.
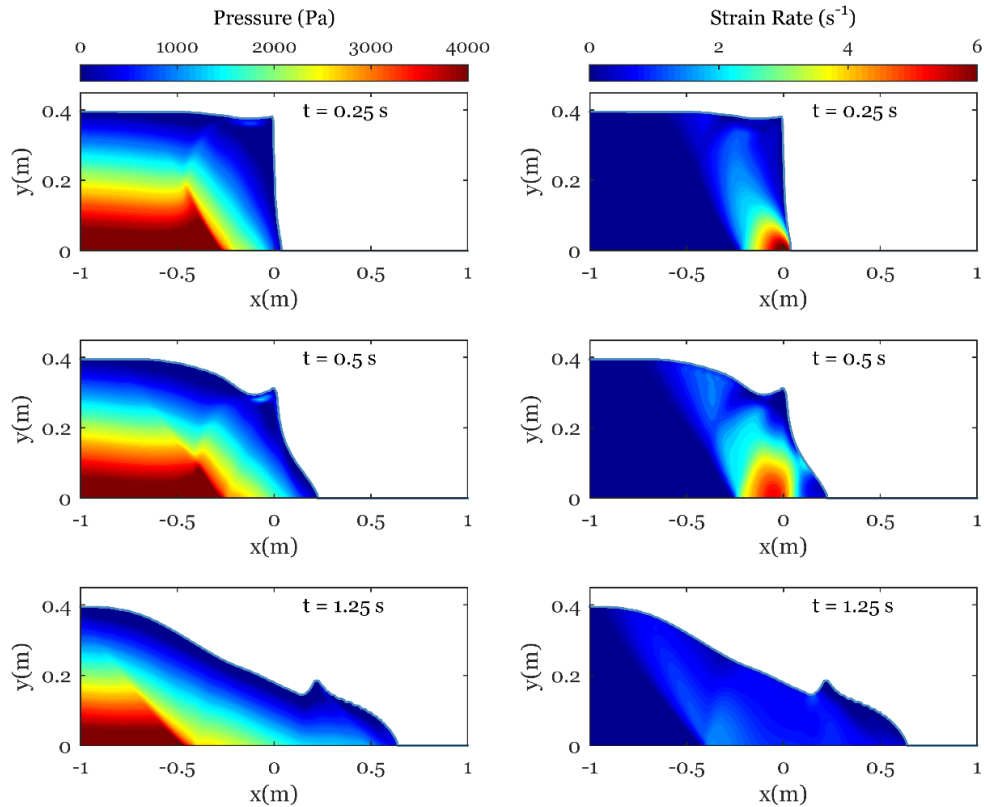
Figure 6. Pressure distribution and shear rate obtained from the simulation at different times.

Comparison of Simulated and Experimental Mixture Profiles

Figure 7 shows the mixture profiles obtained from the simulation and extracted from the experiment over a snapshot of the experiment at the final deposit (t = 2.25 s). It can be seen that the extracted profile (yellow line) follows the surface near the glass wall. However, the profile inside is different in some locations and the flow is not 2D. As a result, it is difficult to define the surface in the experiment. This may be one of the reasons for the difference between the profiles observed in Figure 5. The other issue is the front deposit. The mixture stops somewhat sooner in the simulation than in the experiment. This may be due to the bed friction coefficient used in the Coulomb slip boundary condition in which the value is set to the same value as an internal friction coefficient.
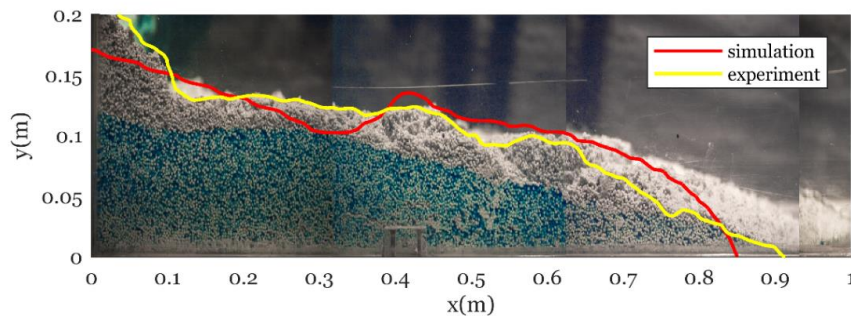
Figure 7. Plots of the mixture profiles obtained from the simulation (red) and extracted from the experiment (yellow) over a snapshot of the experiment at the final deposit (t = 2.25 s).

Conclusion

A numerical model is developed by coupling the mixture model with the porous model using OpenFOAM software. The two main solvers used are the *interFoam* for grain-fluid mixture flows and the *porousInterFoam* for flows in porous media. These two solvers solve the governing equation analogous to the Navier-Stokes equation but with additional terms or different physical interpretation of an existing term. The coupled model is validated using experimental data. The comparison shows good agreement between the simulated and measured granular profiles and the front evolution.

References

Ansys Fluent. 2009. Theory Guide. Ansys Inc 5.5.

Armanini, A. 2013. "Granular flows driven by gravity," Journal of Hydraulic Research, 51(2):111–120.

Bagnold, R.A. 1954. "Experiments on a gravity-free dispersion of large solid spheres in a Newtonian fluid under shear," Proceedings of the Royal Society of London. Series A, 225(1160):49–63.

Berzi, D., Jenkins, J.T., and Larcher, M. 2010. "Debris flows: Recent advances in experiments and modeling," Advances in Geophysics, 52:103–138.

Bingham, E.C. 1922. Fluidity and plastic (Vol. 2). McGraw-Hill.

Del Jesus, M., Lara, J.L., and Losada, I.J. 2012. "Three-dimensional interaction of waves and porous coastal structures: Part I: Numerical model formulation," Coastal Engineering, 64:57–72.

Drucker, D.C., and Prager, W. 1952. "Soil mechanics and plastic analysis or limit design," Quarterly of Applied Mathematics, 10(2):157–165.

Forterre, Y., and Pouliquen, O. 2008. "Flows of dense granular media," Annual Review of Fluid Mechanics, 40:1–24.

GDR MiDi. 2004. "On dense granular flows," The European Physical Journal, 14(4):341–365.

Goldhirsch, I. 2003. "Rapid granular flows," Annual Review of Fluid Mechanics, 35(1):267–293.

Iverson, R.M. 1997. "The physics of debris flows," Review of Geophysics, 35(3):245–296.

Lorenzini, G., and Mazza, N. 2004. Debris flow: Phenomenology and rheological modeling. Wit Press, Boston.

Meng, X., and Wang, Y. 2016. "Modelling and numerical simulation of two-phase debris flows," Acta Geotechnica, 11(5):1027–1045.

Ozeren, Y., Aleixo, R., Marsooli, R., and Altinakar, M. 2014. Physical properties of artificial sediment.

Rebillout, L., Ozeren, Y., and Altinakar, M. 2017. Dam break experiments with granular material.

Savage, S.B., Babael, M.H., and Dabros, T. 2014. "Modeling gravitational collapse of rectangular granular piles in air and water," Mechanics Research Communications, 56:1–10.

Wang, L., Wang, L.P., Guo, Z., and Mi, J. 2015. "Volume-averaged macroscopic equation for fluid flow in moving porous media," International Journal of Heat and Mass Transfer, 82:357–368.

Determination of Sediment Transport Pathways from Dredged Material Placement Sites within Pool 11 of the Upper Mississippi River System

Lucie M. Sawyer, Civil-Hydraulic Engineer, USACE, Rock Island, IL,
Lucie.M.Sawyer@usace.army.mil
Tahirih C. Lackey, Research Hydraulic Engineer, ERDC, Vicksburg, MS,
Tahirih.C.Lackey@usace.army.mil
Anton Stork, Civil-Hydraulic Engineer, USACE, Rock Island, IL,
Anton.J.Stork@usace.army.mil

Introduction

The Rock Island District Corps of Engineers has multiple dredge cuts within Pool 11 of the Upper Mississippi River. Existing placement sites have become unavailable for use due to regulatory concerns, requiring the District to identify new placement sites and revise the Dredged Material Management Plan (DMMP) for this reach. During the planning process to identify new dredged material placement sites, state regulatory agencies identified a significant concern regarding the fate of the dredged material placed along banklines and within historic island footprints, and whether this material could migrate to biologically sensitive areas.

In the past, the Rock Island District has used physical hydraulic sediment response (HSR) models to provide a qualitative analysis of material movement in response to channel maintenance actions. However, given the resource constraints of maintaining a physical model laboratory, new techniques are needed. The objective of this study is to evaluate potential pathways of sediment originating from dredged material placement sites within Pool 11 based on a numerical model, the Particle Tracking Model (PTM).

Background and Objective

The three potential sources of dredged material evaluated were Hurricane Island, Finley's Landing, and the Bathtub site (Figure 1). Hurricane Island bankline (RM 599) has historically been used for dredged material placement for both the Hurricane and Finley's dredge cuts. Finley's Landing (RM 596) bankline site is also a historic placement site immediately upstream of the Finley's Landing Dredge Cut. The newly proposed Bathtub placement site (RM 594) would be created within an existing side-channel island footprint. Seven sensitive areas were also identified for this project (Figure 1). These areas were chosen due to both their proximity to the source locations and interests of concern such as existing dredge cuts, mussel beds, aquatic vegetation, wetlands, side channel border and backwater habitat.
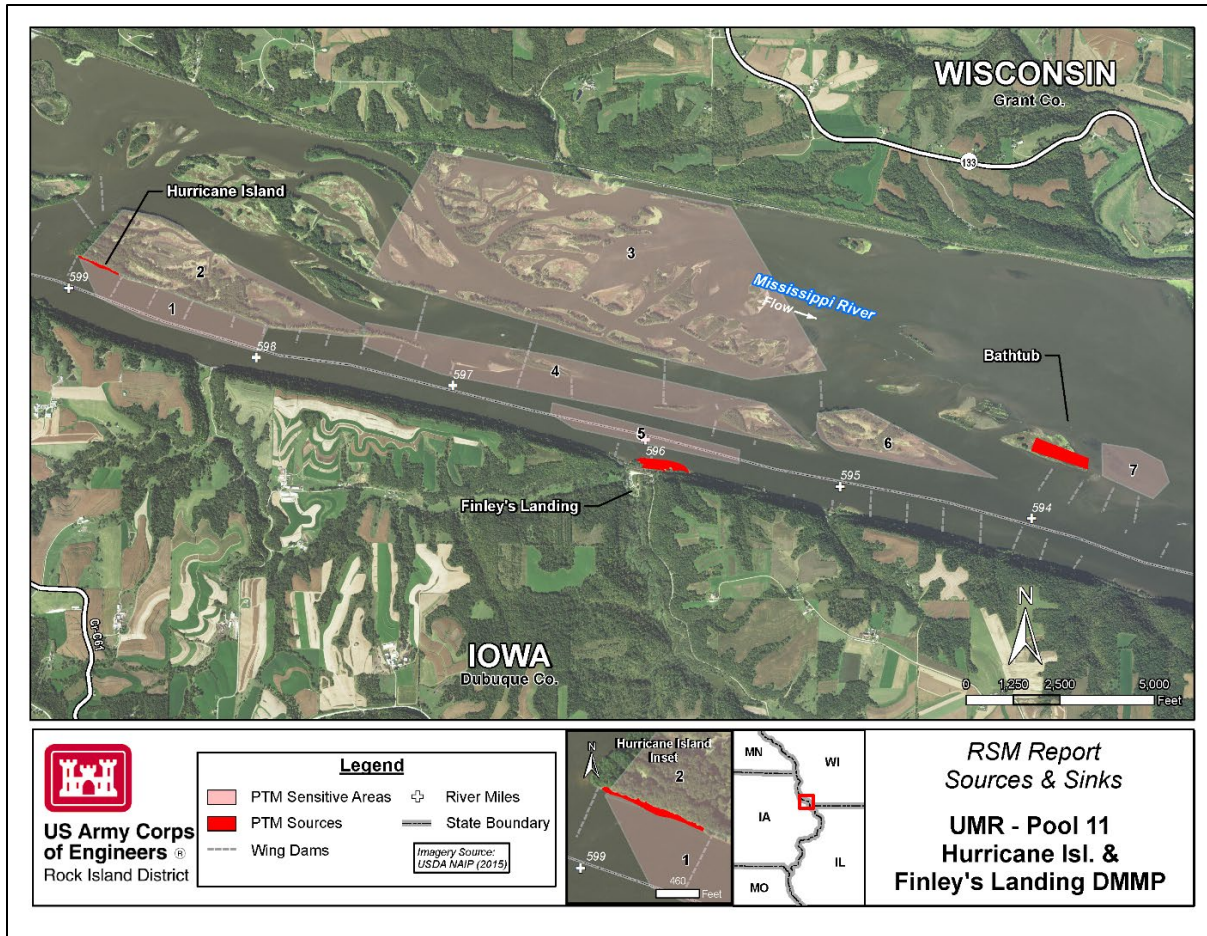
Figure 1. Pool 11 sediment sources and sensitive areas.

The primary objective of this analysis was to evaluate potential pathways of sediment originating from the Hurricane Island and Finley's Landing bankline placement sites as well as potential pathways of dredged material placed during initial construction of the Bathtub site using the PTM. The specific questions of interest included:

(1) What is the fate of dredged material from bankline placement sites?

(2) Is material from these sites building habitat in areas of interest?

(3) Is material from these sites negatively impacting sensitive areas?

(4) What are the potential pathways of material migration during construction of the Bathtub site?

Methods

An assessment of the potential pathways of dredged material placed within Pool 11 using the PTM was conducted to assist in communicating potential risks and benefits of material migration with project partners. A PTM's straight forward pathways analysis, utilizing oftentimes existing hydrodynamic output, offers significant efficiencies over physical modeling for the purposes of particle pathways analysis and visualization. The PTM is a Lagrangian model

designed to simulate potential transport pathways of sediment particles released from a source such as dredges, placement sites, etc. in a simulated wave and hydrodynamic environment.

To best address the regulatory agencies' concerns, a "conservative" analysis was used to evaluate potential pathways using the PTM. The model can simulate advection, diffusion, deposition, as well as particle bed interactions which predict resuspension. However, simplifications in the bottom boundary physics computed by the PTM and the frequency of particle bed interactions for sand-sized particles make the model best-suited to simulate qualitative analysis of sand transport, as is demonstrated herein. A conservative approach focuses the analysis on less frequent hydrodynamic conditions when significant transport is most likely to occur, rather than average or long term conditions. The conservative analysis was limited to generally high flows, when flow paths show greater potential for transport to areas of concern.

Hydrodynamic Modeling - AdH

The 2D hydrodynamic code Adaptive Hydraulics (AdH) was used to simulate hydrodynamics within the reach of interest to be used for input to the PTM. Significant effort was placed on the mesh development in order to provide adequate resolution for hydraulically significant features such as river training structures, and sensitive areas within the existing bathymetry as well as for alternative bathymetries including potential features of interest, identified by stakeholders. Mesh convergence criteria focused on changes in computed discharge (<1%) throughout the area of interest. Final node spacing near the outer boundary of the mesh was 100-200 feet and 50 feet within the main channel. Calibration of the AdH model was based on ADCP transect data collected during a discharge of 156,750 cfs, slightly less than the 20% annual chance exceedance discharge (169,000 cfs).

A 5-year hydrodynamic simulation period from 1/1/1989 – 12/31/1993 was initially chosen for simulation in AdH due to the variability and the presence of significant high flow events within the hydrologic record. In order to identify a shorter period for analysis using the PTM, AdH-computed shear stresses near the sources were evaluated relative to the critical shear stress for medium-sized sand to further screen the hydrograph for periods of maximum transport potential for this "conservative" PTM analysis. The AdH mesh, bathymetry and hydrodynamic output were used as input to the PTM in addition to native bed sediment and sediment source characterizations.

Particle Pathways – PTM

Based on evaluation of the 5-year hydrodynamic simulation as described above, for the PTM simulation, a 1-year hydrodynamic period (1/1/1991-12/31/1992) and a 6-month period (4/1/1993-10/1/1993) were selected as sufficient to understand maximum transport from the three potential dredged material sources: Hurricane Island; Finley's Landing; and the Bathtub site. These two hydrodynamic periods were chosen due to the number of high flow events present (1-yr) and the magnitude of the high flow event present (6-month). Each simulated dredged material placement "source" was placed at the bed and defined using 5,000 particles available for transport throughout the entire simulation (instantaneous source). Sensitivity analyses varying the sediment source release rates and number of particles were conducted, with the most diverse range of particle pathways resulting from an instantaneous source with 5,000 particles.

Grain size distribution information from Pool 11 dredge cut samples were used to characterize each source. The native sediment file was defined based on available sediment gradations to distinguish existing channel, backwater and island sediment types. Results from the 6-month analysis are discussed below.

Results

Particles originating from the Hurricane Island source (red) showed transport pathways along, through, and onto Hurricane Island and within the channel border area, all of which have been identified as sensitive areas (Figure 2). Particle position plots from the Hurricane Island source illustrated that many of the particles remained at the placement site. Qualitatively, this demonstrated that while there are pathways away from the placement site, there is a strong possibility that some sediment may remain deposited when placed. Results showed movement of some particles onto the island and across the island via the interior bisecting channel. This on-island deposition is supported by observations made by the State of Wisconsin. Figure 2 showed some of the particles were deposited within the channel border area creating shallow islands, a desirable habitat identified by resource managers. Sediment originating from the Finley's Landing source either remained at the placement site or was drawn downstream and transported close to the shoreline. Bed shear stresses remained too low at the Bathtub source to transport any particles. Particle pathways results from the 1-year simulation for each of the three sources are very similar to those from the 6-month simulation.
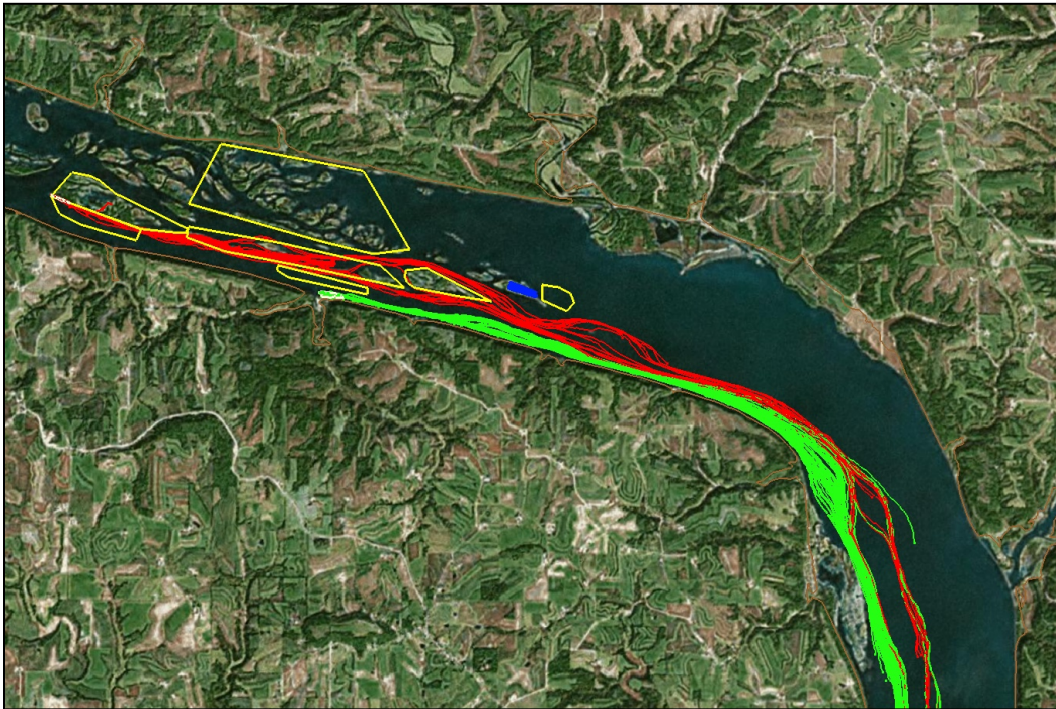
Figure 2. PTM one-year simulation sediment pathways.

Conclusions

Results from this work indicate the possibility of material from the Hurricane Island placement site migrating to areas of concern, corroborating anecdotal observations made by regulatory agencies and project partners. The ability to visualize potential pathways of material movement is a valuable assessment and communication tool for interagency planning teams to better understand the potential benefits and impacts of dredged material placed within the river system. The PTM has demonstrated its strength in providing these tools herein.

References

MacDonald, N.J., Davies, M.H., Zundel, A.K., Howlett, J.C., Demirbilek, Z., Gailani, J.Z., Lackey, T.C., Smith, J., 2006. PTM: Particle Tracking Model: Model theory, implementation, and example applications. In: Technical Report TR-06-20. U.S. Army Engineer Research and Development Center, Vicksburg, MS.

USACE, Engineer Research and Development Center (2015). Adaptive Hydraulics (AdH) Version 4.5 Hydrodynamic User Manual.

Development of a Fully Unsteady Flow Sediment Transport Model for the Mississippi River below Tarbert Landing

Travis Dahl, Research Hydraulic Engineer, USACE ERDC-CHL, Vicksburg, MS, Travis.A.Dahl@usace.army.mil
Stanford Gibson, Research Hydraulic Engineer, USACE IWR-HEC, Davis, CA, Stanford.Gibson@usace.army.mil
Christopher Nygaard, Hydraulic Engineer, USACE Portland District, Portland, OR, Christopher.J.Nygaard@usace.army.mil
Ronald Heath, Research Hydraulic Engineer, USACE ERDC-CHL, Vicksburg, MS, Ronald.E.Heath@usace.army.mil

Abstract

The U.S. Army Corps of Engineers developed an unsteady sediment model for the lower Mississippi River. This model was developed with the goal of providing an initial demonstration of the unsteady, movable bed features of HEC-RAS 5.0.3 on the Mississippi River. The model simulated flow and bed change along the lower 323 miles of the Mississippi, from Tarbert Landing, to a downstream Gulf of Mexico boundary condition, 18 miles downstream of Head of Passes. This is the largest fully-unsteady sediment transport model developed in HEC-RAS to date. The modeling domain included thirteen sub-reaches, simulating overbank inundation by diverting high flows over numerical lateral weirs into simulated floodplain channels. The unsteady hydraulic model was calibrated to water surface elevation at four internal gages and sediment transport was calibrated to bed volume change between 2004 and 2012. The sediment calibration was also checked against internal concentration data and specific gage analyses at four gages. The model performed well, reproducing the bed volume change trend and concentrations. In this paper we discuss the development process and lessons learned.

Introduction

Sedimentation in the Lower Mississippi River directly affects commercial navigation, ecosystem services, and flood damage reduction. Additionally, sediment diversions out of the river and into the delta are being designed and constructed to build land in sensitive ecotones. Therefore, the U.S. Army Corps of Engineers (USACE) districts, the U.S. Army Engineer Research and Development Center (ERDC), Coastal and Hydraulics Laboratory (CHL), and their partners are investigating the flow of sediment through the Lower Mississippi River system, including the effects of natural and engineered sediment diversions from the river to the delta and in-channel dredging. Sediment models that can simulate flow and sediment diversions, as well as dredging and potential impacts to riverine sediment processes, can help design and assess these alternatives.

The USACE and their partners have developed several sediment models of the Lower Mississippi River with the HEC-6T sediment model. The release of HEC-RAS 5.0 included the capability to couple sediment transport with the unsteady flow capabilities, making fully unsteady, sediment transport available for the first time in a single, publicly released, 1D, USACE model. A

fundamental limitation of using a quasi-unsteady model, such as HEC-6T or older versions of HEC-RAS, for regional systems is that the timing of flood peaks, tributary inflows, and diversion operations must be altered so events are synchronized to the correct flow in the river. Moving to an unsteady hydraulic framework allows models to calculate more accurate timing of events, structure operations, tidal influences.

The Lower Mississippi River includes several particularly unsteady hydraulic processes. We developed a fully unsteady hydraulic and sediment transport model of the lower 323 miles of the Mississippi (Figure 1), from Red River Landing to the Gulf of Mexico, to support studies and operations in this area. This paper summarizes the creation and validation of the fully unsteady hydraulic and sediment model of the Mississippi River. We also outline the next steps in the development and extension of the model.
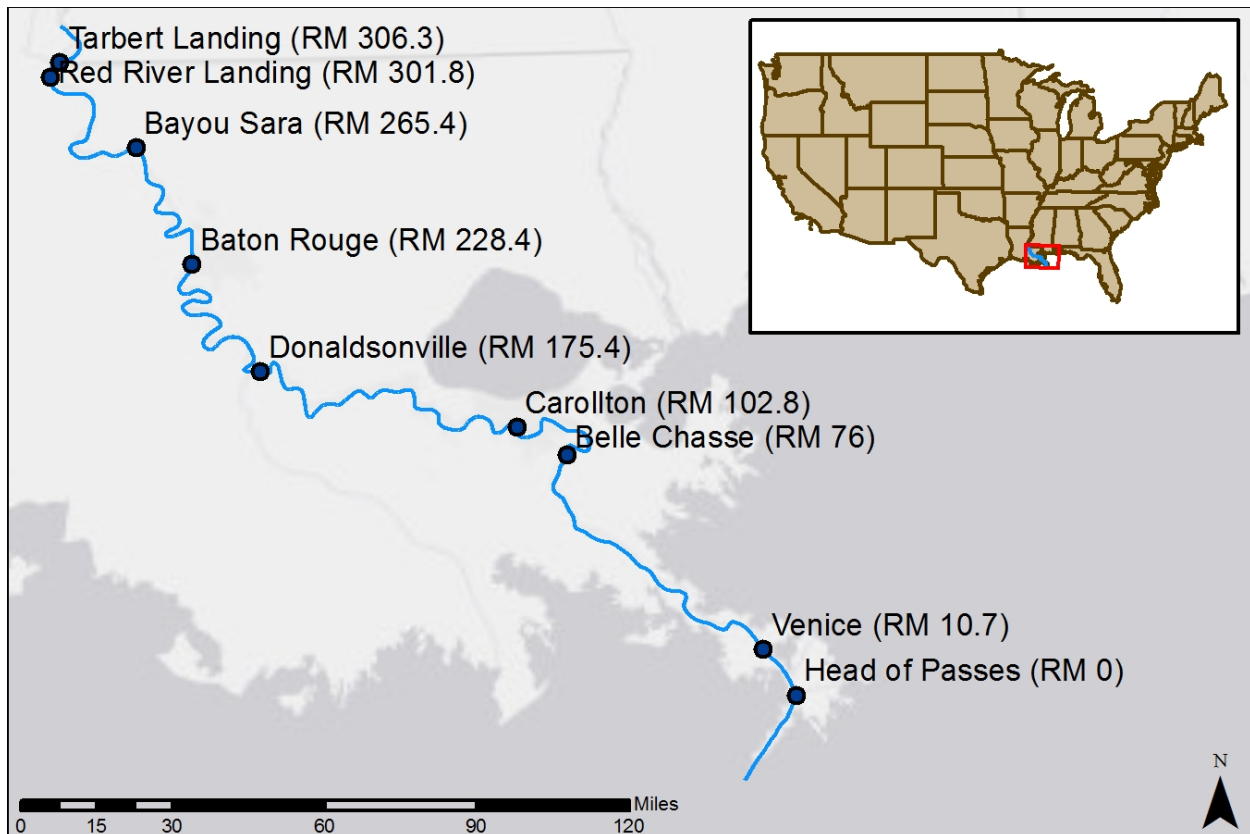
Figure 1. Location map of the study area and calibration points.

Model Development

Unsteady Hydraulic Model Development

A series of HEC-6T models of the Lower Mississippi River were developed in the past by the USACE. The USACE used these models to examine the effect of diversions at Myrtle Grove (Thomas 2012) and West Bay (Sharp et al. 2013), as well as long-term sedimentation trends in

support of the Flowline assessment. Hereafter, when the HEC-6T model is referred to, unless otherwise specified, the reference is to the model modified for the Delta Management Study.

We obtained bathymetry data from the USACE New Orleans District for two different years, 2004 and 2012. We supplemented the in-channel data with lidar data provided by the Louisiana Oil Spill Coordinator's Office. Upstream flows and sediment loads at Tarbert Landing (RM 306.3) were obtained from the U.S. Geological Survey (USGS) (USGS Gage#07295100). The New Orleans District also provided flows for the Morganza floodway and Bonnet Carré Spillway. Within the 2004 to 2012 calibration window, the Morganza Control Structure only operated during the 2011 flood while the Bonnet Carré Spillway diverted flow in 2008 and 2011. Water levels at Pilots Station in Southwest Pass (National Oceanic and Atmospheric Administration [NOAA] Gage #8760922) were used to develop a downstream boundary condition for the model.

The mainline levees downstream of Baton Rouge are very close to the main channel, but the distance between the levees above that point can be over ten miles in some cases (Biedenharn et al., 2018). The unsteady-sediment geometry models all large floodplain areas as reaches. Each of these floodplain reaches is connected to the main river reach with numerical lateral structures on the upstream end, which simulate the natural levees, and junctions at the downstream end, where water surface elevations in the river and floodplain are assumed to be equal (Figure 2). Modeling the floodplains as reaches allows the model to simulate sediment transport through the overbank areas and the impact of these floodplain diversions on the sediment continuity in the river channel.

Bathymetry and overbanks were cut separately in HEC-GeoRAS for ArcMap 10.1 and combined into a single model geometry. We modified the geometry within HEC-RAS to improve stability in several ways. Modeling the downstream end of floodplain reaches with inline structures improved model stability when the floodplain reach became perched above the mainstem during low flows while still allowing the passage of sediment. The inline structures were placed at the ground elevation so that they did not affect outflows. Pilot channels were added to floodplain reaches where thalweg inflection points forced the solution to critical depth. Levees and ineffective flow areas focused the sub-cross-section conveyance distribution to calculate appropriate shear stresses in the Mississippi River mainstem.

The upstream hydraulic boundary is a daily flow record from the USACE gage at Tarbert Landing, which reports the instantaneous flow each morning. The downstream stage boundary condition is located at the Pilots Station gage location but is populated with long-term average monthly elevations (Table 2)

Bonnet Carré flows were modeled using the same flow-flow rating curve as the HEC-6T model. Distributary hydrology downstream of the Bonnet Carré Spillway at RM 130 is much more complex and uncertain, however. In the post-2006 diversion development period, only 40% of water passing Tarbert Landing continues into the Gulf through Southwest Pass during low flow. The Unsteady HEC-RAS model includes 12 modeled diversions between Bonnet Carré and the Gulf. We simulated these diversions with flow-flow diversion rating curves.
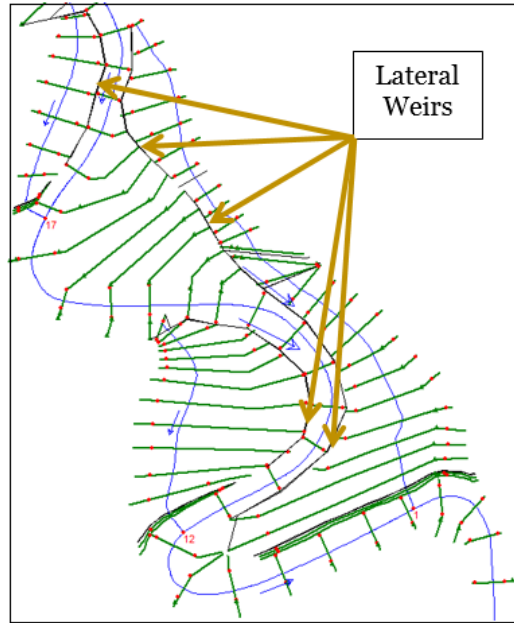
Figure 2. Model geometry approach to floodplain flow.

Table 1. Downstream boundary condition used in Unsteady HEC-RAS model.

Month	Jan	Feb	Mar	Apr	May	Jun	Jul	Aug	Sep	Oct	Nov	Dec
Average Elevation NAVD88	-0.4	-0.4	-0.2	0	0	0.1	-0.1	0.2	0.5	0.4	0	-0.3

Sediment Model Development

The project reach included excellent, synoptic, bed gradation data (Nordin and Queen 1992). The 323-mile study reach included 161 bed samples, a sample every 2 miles. Despite the inherent noise in this data, the sample density was sufficient for us treat the initial bed gradation—often a source of significant uncertainty—as a fixed model parameter.

The initial upstream sediment boundary condition came from the HEC-6T model. The HEC-6T boundary condition defines sediment load with a flow-load rating curve. The rating curve is convex, indicating the system may be supply limited at high flows (Gibson and Cai 2017). A standard power function defines the flow-load relationship up to 600,000 ft3/s. However, the curve has a hard inflection point at 600,000 ft3/s. Above this flow, the flow-load relationship is nearly linear, with a power of less than 1.

During the model development and validation process, we updated the upstream boundary condition to leverage the careful analysis of the rating curve from the previous studies while accommodating the lower measured wash load. The sand mass (fine sand [FS] to very fine gravel [VFG]) was fixed from the HEC 6T rating curve by multiplying the percent of sand by the total load at each point on the flow-load curve. The team then fit a new total load rating curve to

the Old River data. The bed sand fractions (FS to VFG) were prorated (retaining their relative proportion) to maintain the same sand mass as the HEC-6T curve for each flow. Then the very fine sand (VFS) load was estimated and the balance of the total load mass was distributed evenly between the five silt and clay grain classes. This produced a rating curve that conserved the sand fractions from previous analysis but generated computed wash loads (defined as clay to VFS) at the model boundary consistent with the more recent measurements. Bringing boundary condition wash load into line with the measurements aligned the concentration calibrations downstream.

After determining that the model was insensitive to the placement of the movable bed limits, we placed them at approximately a bank full discharge. No deposition was allowed outside of these limits.

The HEC-RAS model leveraged the unsteady flow hydraulics to simulate flow and sediment diversions. We used the following sediment diversion rules to specify the grain size classes diverted: (1) Diversions upstream of RM 120, except Bonnet Carré, diverted all fine grain classes (<VFS) in proportion to the diverted flow, but kept sand in the channel, (2) Bonnet Carré diverted very fine sand and smaller particles in proportion to flow, (3) downstream of RM 120, flow-weighted diversions pulled out clay to medium silt while coarser material transported downstream. The exceptions to this were Ft. St. Philips, where coarse silt was also diverted, and the major diversions at Baptiste Collette, Grand Pass, West Bay, Cubits Gap, Pass A Loutre, and South Pass, which all diverted sands in addition to silts and clays.

The rates of subsidence, or sinking of the land, vary spatially, with rates generally increasing with proximity to the Gulf. The primary and secondary causes of this subsidence are active areas of research. The study team added subsidence capabilities to HEC-RAS as a precursor to this study. This model introduced subsidence downstream of RM 185.6, increasing subsidence rates gradually downstream, reaching a maximum rate of 18.5 millimeters per year (mm/yr) at Head of Passes.

The Unsteady Sediment HEC-RAS model cohesive parameters were adopted directly from the HEC-6T model. The HEC-6T model varied the deposition thresholds for clay and silt longitudinally to better match observed dredging and deposition. This rate was set to 0.01 lb/ft2 above RM 11.5 (near Venice, LA), increased to 0.02 lb/ft2 between RM 11.5 and Head of Passes, and increased further to 0.035 lb/ft2 downstream of Head of Passes. While HEC-RAS can use different cohesive parameters at individual cross sections, this iteration of the model used one threshold for all cohesive grain classes throughout the domain.

The model uses the Copeland (labeled Exner 7 in HEC-RAS; Copeland, 1993) method for bed mixing and armoring because it was developed for large, sand-bed rivers and had been used previously on the Mississippi River.

Historical water temperature data, taken from the HEC-6T model, were grouped and averaged by month. These monthly average temperatures were converted into a recurring monthly time series.

Dredging on the Lower Mississippi River focused on the lower 250 river miles during the simulated time window. The model used dredging templates from the HEC-6T model and

updated them based on the cross sections in the new model. The dredge algorithm in HEC-RAS cut each cross section down to the dredge template elevation each year.

Dredging operations in the Mississippi River re-entrain dredge material, allowing the river to transport it downstream. HEC-RAS can re-introduce sediment but discharges sediment from each dredge event into one cross section. Therefore, the modeling team divided dredging each year into 12 local dredge reaches. Dredged sediment was reintroduced downstream of the reach for all sites above Venice, LA. Dredged material below Venice was removed from the model, to reflect the practice of placing this material outside of the active channel near Head of Passes or an offshore disposal area.

Model Validation

Unsteady Hydraulic Validation

We used the flows from 6 February through 3 August 2008, which included a moderate flood, for the initial hydraulic calibration of the Unsteady HEC-RAS model. All of the flow diversions constructed before 2005 were included in the calibration geometry. Water surface elevations in the unsteady flow model were calibrated to the 2008 dataset by adjusting channel Manning's n roughness values.

To further improve the calibration throughout the full flow range, we included flow-roughness variation in the model. The final calibration values are listed in Table 5 and Table 6. Channel roughness varies between a maximum of 0.035 and a minimum of 0.018 and is considered reasonable for a mobile sand bed river. Overall, roughness increases with flow at the upstream end of the model and decreases with flow at the downstream end of the model. Direct relationships between flow and roughness are common in sand bed rivers as bed form amplitude increases with flow (at least until the river reaches a plane bed regime and n-values drop). The inverse relationship between flow and n-value downstream may be compensating for error in the floodplain diversion hydrology. The difference may also be influenced by the variation in batture width, the area between the river at low stage, and the levees. At the upstream end of the model, the batture is several miles wide while the levees are typically adjacent to the river downstream of Baton Rouge. At high flows, this may have the effect of focusing the flow in the channel and reducing bed-form roughness.

Overall model calibration is good throughout the range of flows and stages for the extended timeframe (Figure 3). Additional information on the calibration is available in Dahl et al. (2018). Given the high quality of bathymetric and topographic data available, flow measurements appear to be the most significant data uncertainty affecting stage calibrations. In particular, the magnitude and timing of flow diversions is the primary data uncertainty in the hydraulic model.
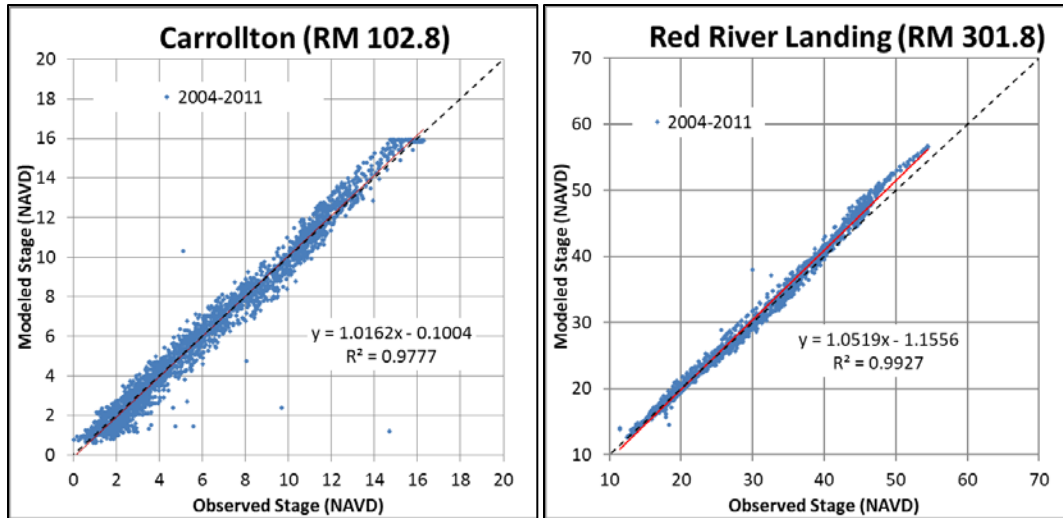
Figure 3. Representative hydraulic calibration locations. The line of perfect agreement between the observed and modeled flows is indicated by the dashed line.

Sediment Calibration

The primary result that we used for sediment calibration were longitudinal cumulative volume change. We also compared the model results to observed suspended sediment concentrations. The calibration period was a net depositional period in the river, with some erosion in the upstream end of the model reach. However, the recent history of this reach includes both depositional and degradational periods.

Longitudinal Cumulative Volume Change: There are a number of sediment transport functions which should be applicable to this system, including Toffaleti, Toffaleti-MPM, and Laursen-Copeland. After initially testing of these and other functions, we decided to use Laursen-Copeland, because it was the best fit to the longitudinal cumulative volume change. The Laursen-Copeland method accommodated the upstream boundary conditions, limiting scour through the upstream 130 miles of the model to approximately 1,000 million ft³, similar to the upstream scour observed in the data.

The HEC-6T model uses three different cohesive deposition thresholds, ranging from 0.010 to 0.035 lb/ft². By default, HEC-RAS only allows a single cohesive deposition threshold for the entire model, although it is possible to alter it for different cross sections. The modeling team used the default value of 0.020 lb/ft².

We calculated the longitudinal cumulative volume change for the model domain between 2004 and 2012 using the USACE Kansas City District (NWK) Cross Section Viewer (Shelley and Bailey 2017). The longitudinal cumulative volume curve accumulates volume change from upstream to downstream. It smoothes noise from individual cross-section perturbations into discernable regional trends and, more importantly, allows modelers to compare volume change between surveys and model results with different cross-section resolutions and locations. The longitudinal cumulative volume curve computed from the 2004 and 2012 cross sections is shown in Figure 4 along with the calculated longitudinal cumulative volume change produced by the calibrated model. The model captures the overall trend of deposition and erosion. Note that

there are some uncertainties in the calculation of the measured volume change; bed elevation change can vary laterally, longitudinally, and temporally, especially in the presence of moving bed forms. The use of volume change, especially longitudinal cumulative volume change, can help to mitigate these factors.
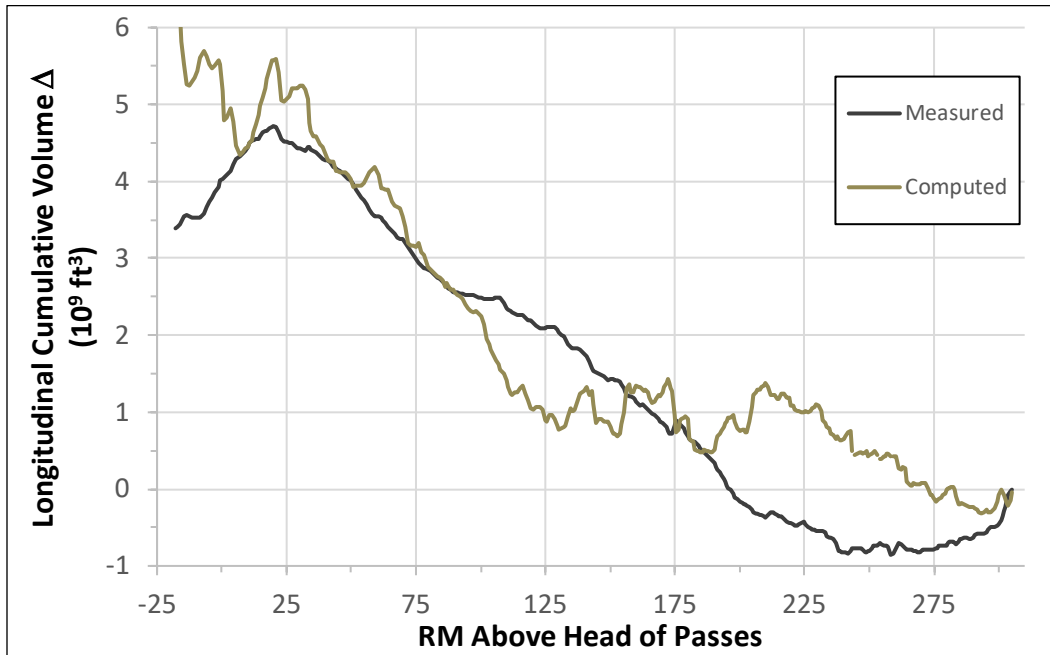
Figure 4. Comparison of computed and measured longitudinal cumulative volume change. Note that the large upward trend in computed volume below Head of Passes is due, at least in part, to subsidence, which is not reported separately in HEC-RAS.

The model performed well with the best estimate parameters and the Laursen-Copeland equation with one substantial divergence. The model reproduced the total sediment volume change of the entire reach and the local erosion or deposition trends in most sub-reaches. However, the model deposited too much sediment in the tight channel bends near and through New Orleans. The modeling team could not disperse this deposition downstream by changing any of the sediment parameters within reasonable ranges. Other sediment modelers with experience in this reach suggested that other current sediment models deposit more sediment in these tight river bends than observed, regardless of the dimensionality of the model. In particular, the 1D model does not reproduce the multi-dimensional dynamics that keep these pools deep. Therefore, the bathymetric cross sections were modified through this reach to reduce them to their equivalent 1D cross sectional area.

Suspended Sediment Concentrations: A sediment transport model should be evaluated against all available physical evidence. Therefore, we also compared the model concentrations to observed sediment concentrations at Belle Chasse, near RM 76, downstream of New Orleans.

In the total load plot (Figure 5-bottom), the model captured the concave quality of the flow-concentration curve and performed well in the moderate-to-high flow range, tracking the central tendency of the data.
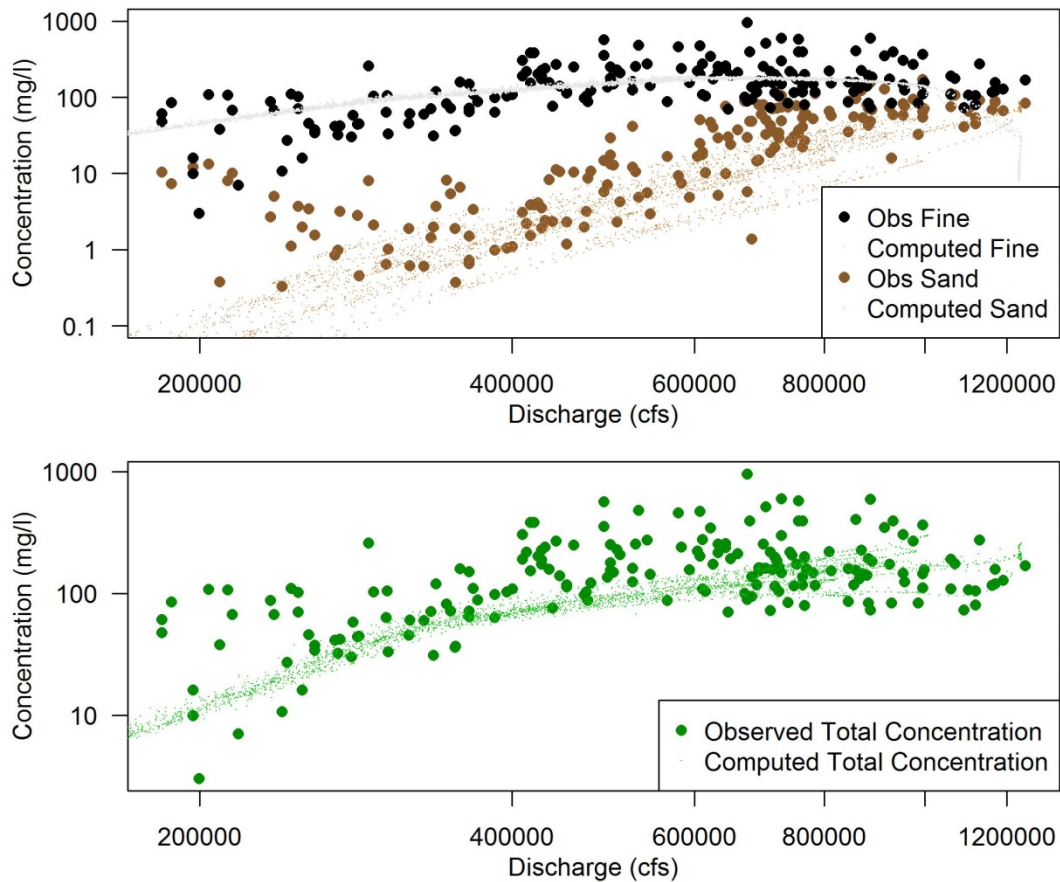
Figure 5. Measured and computed concentrations at Belle Chasse between 2004 and 2012, for the total sediment load (bottom) and portioned at 63 microns, for a sand/fine split (top).

The sand-fine split (Figure 5-top) offers additional insight. Generally, concentrations of sand in the model were towards the low end of the observed concentrations. Concentrations of fines in the model fell in the middle of the observed data. The computed concentrations qualitatively match the inflection point in the observed data near 600,000 ft3/s.

Further information on the sediment validation, including comparison to specific gage analysis, can be found in Dahl et al. (2018).

Conclusions

This study demonstrated that HEC-RAS is an effective tool to simulate sediment transport on the complicated Lower Mississippi River system. The model was able to capture the general trends in sediment deposition through the study reach as well as sediment concentrations at Belle Chasse. The model also captured the stage and flow dynamics, as evidenced by both the hydrographs at Baton Rouge and comparison with specific gage data.

If districts within MVD would like to leverage the advanced capabilities in HEC-RAS, to save effort by building a sediment model on an existing HEC-RAS hydraulic model, or to simply work

faster in an HEC-RAS interface and workflow because of its continuity with their experience and education, the HEC-RAS sediment capabilities are a viable option.

The efforts during this study also identified a number of opportunities for improved understanding of the Lower Mississippi River system and improvements to the modeling capabilities of HEC-RAS. General understanding of the sediment transport in the Mississippi River could be greatly enhanced by continued study and monitoring of the effects of flow diversions on sediment. It may be possible to see additional improvements in the Unsteady Sediment HEC-RAS model results by leveraging the lessons learned from the ongoing Adaptive Hydraulics (AdH) models being conducted at the ERDC-CHL. Similarly, ongoing work at the ERDC-CHL on flocculation of cohesive sediment should help to inform future iterations of the model. The differences in observed flows at Tarbert Landing and Baton Rouge may be addressed by implementing the recommendations in Lewis et al. (2017). Including the Old River Control Complex and extending the model boundary upstream to Natchez, MS, may also help to compensate for the discrepancies in observed flows. Finally, one of the problem areas during the development of the Unsteady Sediment HEC-RAS model was the tendency of the model to deposit in deep holes in the lower river. These deep holes tend to occur at tight bends in the river such as Carrolton Bend (~RM 104-105) and Algiers Point (~RM 94-95) and where the river encounters confining material (Gibson et al. 2019). This behavior is not unique to 1D sediment models and has been observed in both two-dimensional and three-dimensional (3D) sediment models of the area, warranting further investigation.

References

Biedenharn, D. S., Killgore, K. J., Little, C. D., Murphy, C. E., Kleiss, B. A. 2018. Attributes of Lower Mississippi River batture. MRG&P Technical Note No. 4. Vicksburg, MS: US Army the Corps of Engineers, Mississippi Valley Division.

Copeland, R. R. 1993. Numerical Modeling of Hydraulic Sorting and Armoring in Alluvial Rivers. PhD dissertation. Available from ProQuest Dissertations & Theses Global. (304045475). https://search-proquest-com.erdclibrary.idm.oclc.org/docview/304045475

Dahl, T. A., Heath, R. E., Gibson, S. A., Nygaard, C. J. 2018. HEC-RAS unsteady flow and sediment model of the Mississippi River: Tarbert Landing to the Gulf. MRG&P Report No. 25. Vicksburg, MS: US Army Corps of Engineers, Mississippi Valley Division.

Gibson, S. A., and C. Cai. 2017. Flow dependence of suspended sediment gradations. Water Resources Research 53(11):9546–9563.

Gibson, S., Osorio, A., Creech, C., Amorim, R., Dircksen, M., Dahl, T. and Koohafkan, M. 2019. Two pool-to-pool spacing periods on large sand-bed rivers: Mega-pools on the Madeira and Mississippi. Geomorphology, 328, pp.196-210.

Lewis, J., G. Brown, and S. Ayres. 2017. Investigation of Discharge Measurements of the Lower Mississippi River below Natchez, MS. MRG&P Tech Note No. 3. Vicksburg, MS: U.S. Army Engineer Research and Development Center.

Nordin, C. F., and B. S. Queen. 1992. Particle Size Distribution of Bed Sediments along the Thalweg of the Mississippi River, Cairo, Illinois, to Head of Passes, September, 1989. Potamology Program (P-1); Report 7. Vicksburg, MS: U.S. Army Engineer Waterways Experiment Station.

Sharp, J. A., C. D. Little, G. L. Brown, R. E. Heath, L. C. Hubbard, F. Pinkard, K. S. Martin, N. D. Clifton, D. W. Perkey, and N. B. Ganesh. 2013. West Bay Sediment Diversion Effects. ERDC/CHL TR-13-15. Vicksburg, MS: U.S. Army Engineer Research and Development Center.

Shelley, J., and P. Bailey. 2017. The Cross Section Viewer: A Tool for Automating Geomorphic Analysis Using Cross Section Data. ERDC/TN RSM-18-3. Vicksburg, MS: U.S. Army Engineer Research and Development Center.

Thomas, W. A. 2012. HEC-6T Sediment Study, Allocation of Water and Sediment Resources, Myrtle Grove Diversion for Land Building. Clinton, MS: Mobile Boundary Hydraulics.

Development of 'Debris Library' and 1D HEC-RAS and 2D Adaptive Hydraulics Linkage-Architecture for Predicting Post-Wildfire Non-Newtonian Flows

Ian E. Floyd, Research Physical Scientist, US Army Engineer Research and Development Center, Vicksburg, MS, ian.e.floyd@usace.army.mil

Stanford Gibson, Research Hydraulic Engineer, Hydrologic Engineering Center, Davis, CA, standford.gibson@usace.army.mil

Ronald E. Heath, Research Hydraulic Engineer, US Army Engineer Research and Development Center, Vicksburg, MS, ronald.e.heath@usace.army.mil

Marielys Ramos-Villanueva, Research Hydraulic Engineer, US Army Engineer Research and Development Center, Vicksburg, MS, marielys.ramos-villanueva@usace.army.mil

Nawa Pradhan, Research Hydraulic Engineer, US Army Engineer Research and Development Center, Vicksburg, MS, nawa.pradhan@usace.army.mil

Abstract

The assumption of Newtonian fluid flow conditions, linear stress-strain relationships, fails for sediment laden fluids with volumetric concentrations more that $5-10\%$. As sediment concentrations increase, they begin to affect the fluid properties which alter the stress-strain relationship. Debris-flows, mud-flows and hyperconcentrated flows depart from linear, zero intercept stress-strain assumptions embedded in the clear water flow equations. The 'Debris Library' assigns a stress-strain relationship under non-Newtonian sediment laden fluid flow conditions. The 1D Hydrologic Engineering Center River Analysis System (HEC-RAS), 2D Adaptive Hydraulics (AdH), and Sediment Transport Library (SEDLIB) are fully coupled shallow-water and sediment transport models. This study identified the physical non-Newtonian processes needed then developed the linkage-architecture to pass HEC-RAS, AdH, and SEDLIB computed flow velocity, depth, concentration, and grain-size to the non-Newtonian 'Debris Library'. The Library then computes the non-Newtonian friction slope, shear stresses (boundary and internal), and sediment transport capacity back to the parent hydraulic code and sediment transport library.

Introduction

The amount and intensity of large wildfires in the U.S. has become a major concern, especially in the arid and semi-arid western U.S. where over the past decade every state has experienced an increase in the number of large fires according to the National Interagency Fire Center (NSTC, 2015). Immediately following a wildfire, vegetation is removed, organic soil horizons are reduced to ash, and development of hydrophobic soils combine to result in increased water and sediment runoff. Post-wildfire environments can experience a spectrum of hydrologic and sedimentological responses ranging from no response to catastrophic floods, deadly debris flows, and damaging sedimentation has been documented in locations around the world (Rowe et al., 1954; Lane et al., 2006; Shin, 2010; Shakesby, 2011; Moody et al., 2013). In the years following a wildfire, ecotone shifts, gully formation, and channel incision alter the hydrologic system response, resulting in dramatic changes in hydraulic and sediment impacts down system.

In most of the western U.S. post-wildfire recovery can take decades, posing potential long-term operation and management concerns for U.S. Army Corps of Engineers (USACE) and other federal, state and local agencies. These flows often carry large boulders, trees, and even automobiles. Soil fragmentation due to mass wasting processes deliver sediment to the valley bottoms and are subsequently available for sediment mobilization. Large wildfires, specifically in geomorphically sensitive arid regions, represent a significant perturbation to the environments; with fires and debris flows are natural processes in many parts of the western U.S. that dramatically alters the geomorphology, hydrology and sedimentation regimes. Additionally, wildfires impact hydrology by removing the vegetation inception canopy, production of ash and charred material, reduction of organic binding materials in soils, increases in hydrophobic soils, and modifying the intrinsic and hydraulic properties of soils and sediments (Certini, 2005; Moody et al., 2009; Ebel et al., 2012). Hydrologic and hydraulic models can be used tools for assessing wildfire impacts to flood risk management, with an increasing need to develop and improve non-Newtonian numerical modeling capabilities within operational models. This research aims to improve understanding of effects on flood risk management and enhancement of prediction capabilities to assist with planning, management, and mitigation in post-wildfire environments using practical science-based approaches and smart integrated numerical approaches. This paper documents the numerical model development, enhancements, and architecture necessary for predicting post-wildfire non-Newtonian flows within USACE numerical models. This is accomplished by modifying the shallow-water conservation of mass and momentum equations; modification of erosional and depositional processes; and utilizing intense hyperconcentrated non-equilibrium sediment transport function.

Numerical Modeling Approach

Post-wildfire flood response can range from no response to destructive debris flows and debris floods. Debris flows are unsteady gravity driven events that involve complex mixtures of sediment, water and entrained material (i.e., organics, woody debris, unconsolidated substrate) and are commonly modeled using shallow-water equations with non-Newtonian approximations (e.g. Iverson, 1997; Jin and Fread, 1997; Imran et al., 2001). These types of flows are dominantly influenced by grain-size distribution, sediment concentration, and flow stress state (as a function of slope). The stress state is typically used to describe the dominant form of physical and numerical turbulent dissipation within the fluid flow. These stress states generally represent the processes of; cohesion, internal friction between fluid and sediment, turbulence, and the inertial impact between particles. Typically hydraulic and sediment transport models assume that the flow behaves as a Newtonian fluid. In Newtonian fluids the viscosity is constant and is independent of shear rate (or strain) with a linear relationship between shear stress and shear rate. Viscosity is a fluid's ability to resist flow (or shear deformation) and is traditionally expressed as kinematic or dynamic viscosity. Increasing the sediment solids concentration in relationship to water leads to non-Newtonian behavior which results in a non-linear relationships between shear stress and shear rate.

Non-Newtonian Model Library 'Debris Library'

Post-fire floods represent a range of geophysical flows that are non-Newtonian unsteady gravity driven events. A variety of methods are appropriate for dynamically predicting debris flow events and are commonly grouped into the following categories.

- Linear (Bingham 1922) and non-linear viscoplastic models (Jin and Fread 1997; Imran et al. 2001)
  - Most commonly used to describe the rheology of laminar mud flows.
  - Bingham rheology model is the most mature method, with applications quantifying fluid mud in estuaries and density currents in reservoirs.
- Dispersive fluid models (Bagnold 1954; Takahashi 1978)
  - Describes the particle-to-particle interaction between granular-clastic (i.e., silt, sand or gravel) particles, commonly applied to sediment-water mixtures containing mostly sand and gravel with lower quantities of fine sediment ($\leq$ 5%–10% by volume).
- Dispersive-turbulent stress models (O'Brien et al. 1993)
  - Incorporates the dispersive model with a turbulent stress model to describe the mechanics of particle-to-particle interactions within a clay, silt, and organic matrix. Commonly applied to sediment mixtures containing cohesive sediment in quantities greater than 10% by volume.
- Coulomb-based frictional models (Iverson 1997; Iverson and Denlinger 2001).
  - Commonly used to describe the non-Newtonian mechanics of poorly sorted (i.e., wide range of sediment grain sizes) heterogeneous clastic debris flows.

Increasing the solid content increases the viscosity of flow, generating internal dissipative forces within the fluid. At higher concentrations, particularly with coarse particles, particle collision and friction introduce additional internal forces. Therefore, applying the momentum equation to non-Newtonian flows requires additional terms to capture these resisting forces. To account for the increased sediment concentrations modifications will be made to the shallow-water equations, application including drag coefficient using Bingham-based assumptions (Happel and Brenner, 1965; Julien 2010), addressing hindered settling (Richardson and Zaki, 1954), accounting for increased viscosities (Einstein and Chien, 1955; Dabak and Yucel, 1986), and incorporation of non-Newtonian bedload (sheet flow) and suspended load transport functions (Rickenmann, 1991; Abrahams, 2003; Yang et al., 1996).
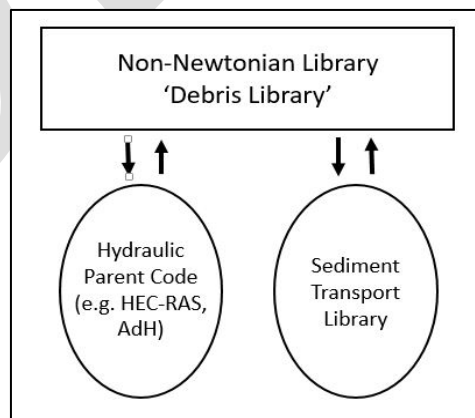
Figure 1. Debris Library' linkages to the hydraulic parent code and sediment transport model.

The Quadratic Model: The quadratic model combines the following stress components of non-Newtonian sediment mixtures (1) cohesion between particles, (2) internal friction between fluid and sediment particles, (3) turbulence, and (4) inertial impact between particles. The O'Brien et al. (1993) quadratic model decomposes the stress-strain relationships into the above four components, such that the shear stress is.

$$\tau_{MD} = \tau_{yield} + \tau_{viscous} + \tau_{turbulent} + \tau_{dispersive}$$

Where, τ_{MD} = mud-and-debris shear stress (Pa), τ_{yield} = yield stress (Pa), $\tau_{viscous}$ = viscous shear stress (Pa), and $\tau_{dispersive}$ = dispersive shear stress (Pa). Numerically these terms are additive and as concentration increases and as the sediment component coarsens, the Library adds terms. This section steps through the cumulative components of each model and is summarized in Figure 1.
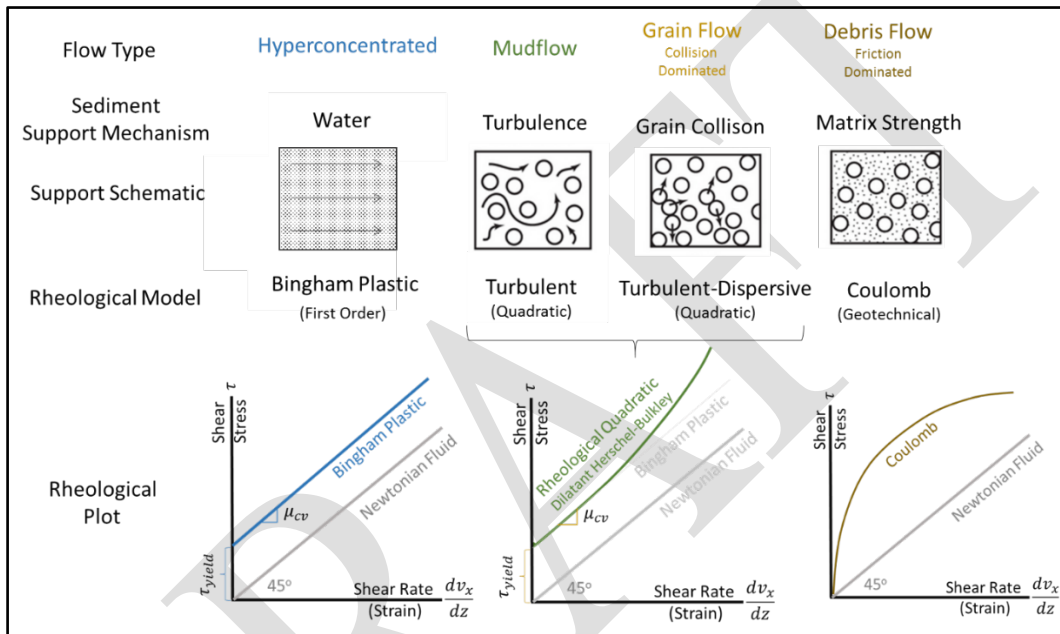
Figure 2 Classification, processes, conceptual model, and rheological model of the four non-Newtonian flow types in the Debris Library.

The Quadratic model is defined as

$$\tau_{MD} = \tau_y + \mu_m \left(\frac{dv_x}{dz}\right) + \rho_m l_m^2 \left(\frac{dv_x}{dz}\right)^2 + c_{Bd}\rho_s \left(\left(\frac{C_*}{C_v}\right)^{1/3} - 1\right)^{-2} d_s^2 \left(\frac{dv_x}{dz}\right)^2 \qquad (1)$$

where, dv_x/dz is the shear rate (1/s) computed as a function of depth averaged velocity and flow depth ($dv_x/dz = 3\bar{u}/h$), μ_m = mixture dynamic viscosity (Pa s), ρ_m = sediment mixture mass density (kg/m³), l_m = mixing length (m), c_{Bd} = Bagnold empirical parameter ($c_{Bd} \cong 0.01$), ρ_s = sediment particle density (kg/m³), C_*= maximum volumetric sediment concentration (-), C_v = volumetric sediment concentration (-), and d_s = sediment grain size (m). After substitution the Quadratic model is defined as

$$\tau_{MD} = \tau_y + \mu_m \left(\frac{3\bar{u}}{h}\right) + \rho_m l_m^2 \left(\frac{3\bar{u}}{h}\right)^2 + 0.01\rho_s \left(\left(\frac{0.615}{C_v}\right)^{1/3} - 1\right)^{-2} d_s^2 \left(\frac{3\bar{u}}{h}\right)^2 \qquad (2)$$

where, $\bar{u}$ = depth averaged velocity (m/s), and h = flow depth (m). The Library allows the user and/or parent program to select a specific non-Newtonian model.

Non-Dimensional Parameters: The Library can also select the appropriate closure model, which is particularly useful if the flow type changes over time or space, making a single model inappropriate. The classifications stated above have included approximate concentration thresholds for a range of non-Newtonian flow conditions. However, physically representing the flow classification involves additional variables to include concentration grain size and other considerations. Therefore, the Library computes four dimensionless numbers to determine the non-Newtonian flow type is:

1. The Viscous Parameter (Julien and Lan, 1991; Julien 2010)

$$\Pi_{viscous} = \frac{\tau - \tau_{yield}}{\mu_m \left(\frac{3\overline{u}}{h}\right)} \tag{3}$$

2. The Turbulent Parameter (Julien and Lan, 1991; Julien 2010)

$$\Pi_{turbulent} = \frac{l_m^2 \rho_m}{0.01 d_s^2 \rho_s} \left(\left(\frac{0.615}{C_v}\right)^{1/3} - 1\right)^2 \tag{4}$$

3. The Bagnold number (or dispersive parameter) is very similar to the dispersion shear, except that the sediment laden viscosity is included in the denominator and the strain is not squared, to make the parameter dimensionless (Bagnold, 1954; Hill, 1966; O'Brien et al., 1993).

$$\Pi_{dispersive} = \frac{0.01 \rho_s d_s^2}{\mu_m} \left(\left(\frac{0.615}{C_v}\right)^{1/3} - 1\right)^{-2} \left(\frac{3\overline{u}}{h}\right) \tag{5}$$

4. The Savage Number (Iverson and LaHusen, 1993) determines the difference between collision dominated and friction dominated flows in coarse material:

$$\Pi_{Savage} = \frac{\rho_s \left(\frac{3\overline{u}}{h}\right)^2 d_s}{(\rho_s - \rho) g h} \tag{6}$$

The library uses these numbers to classify flow for each control volume and determine which components of the internal shear equation it should include. The classifications are summarized in Table 2 below.

Table 1 Dimensionless thresholds between flow classifications.

Flow Type	Thresholds
Newtonian	$\Pi_{viscous} < 1$
Hyperconcentrated	$1 < \Pi_{viscous} < 5$
Mudflow	$\Pi_{viscous} > 5$; $\Pi_{turbulent} > 1$
Grain Flow	$\Pi_{viscous} > 5$; $\Pi_{dispersive} > 4$
Debris Flow	$\Pi_{Savage} < 0.1$

Hydraulic Numerical Modeling

The shallow water flow equations solve the continuity and momentum equations simultaneously to compute water stage and velocity. The momentum equation sums the forces that act on a hydraulic control volume. The frictional forces that are between the fluid and the solid boundary

($F_{friction}$) are the primary resisting forces in the standard Newtonian clear-water hydraulic equations. Mud and debris flows must account for additional resisting forces. Increasing the solid content increases the viscosity of non-Newtonian flows generating internal resisting forces within the fluid. At higher concentrations, particularly with coarse particles, particle collision and friction introduce additional internal resisting forces. Most of the theoretical and numerical modifications involve integrating the new internal fluid forces in the momentum equation.
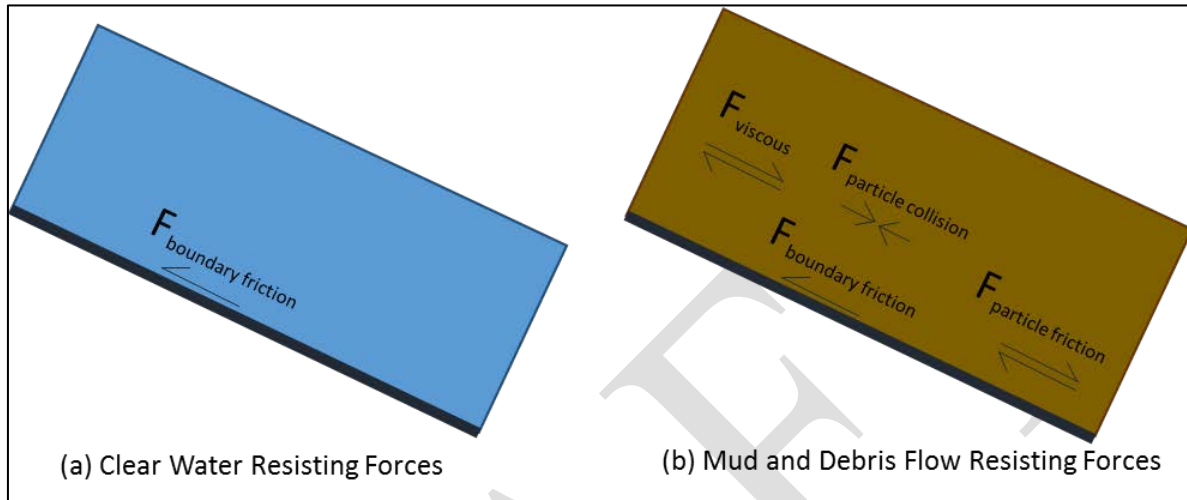
Figure 2: Schematic comparing the resisting forces in clear water flow and mud and debris flows.

The 1D Saint-Venant unsteady flow equations can be applied to non-Newtonian flows by including an additional friction slope term in the conservation of momentum equation. In this effort the conservation of mass and momentum are defined as

$$\frac{\partial Q}{\partial x} + \frac{\partial A}{\partial t} - q = 0 \tag{7}$$

$$\frac{\partial Q}{\partial t} + \frac{\partial Q\bar{u}}{\partial x} + gA\left(\frac{\partial z}{\partial x} + S_f + S_{MD}\right) = 0 \tag{8}$$

Where, Q = volumetric flow discharge (m³/s), x = downstream distance in channel (m), t = time (s), A = cross sectional area of channel (m²), q = lateral inflow or outflow (m²/s), z = distance from bed (m), S_f = Newtonian friction slope (m/m), and S_{MD} = non-Newtonian friction slope (m/m). The non-Newtonian friction slope is computed from

$$S_{MD} = \frac{\tau_{MD}}{\rho_m g h} \tag{9}$$

Sediment Transport Modeling

For this study the HEC-RAS sediment transport library with Bank Stability and Toe Erosion Model (BSTEM) and the Sediment Transport Library (SEDLIB) will be used for the mobile bed calculations in conjunction with the non-Newtonian library and hydraulic parent code. The BSTEM develop by National Sediment Laboratory, United States Department of Agriculture (USDA), Agricultural Research Station (ARS) is a physics-based model that accounts for the geotechnical and hydraulic processes leading to channel and bank erosion (Simon et al., 2000; Langendoen and Simon, 2008; Simon et al., 2010). The SEDLIB is capable of solving problems of multiple grain sized, cohesive and non-cohesive sediment types, and multiple discrete bed layers. It estimates erosion and deposition processes simultaneously, and simulates such bed

processes as armoring, consolidation, and discrete depositional strata evolution. Currently, additional research and development is needed to verify and validate mobile-bed applications with BSTEM and SEDLIB, therefore only a mathematical representation will be provided.

A fixed bed model will not compute the concentration dynamically or consider dynamic feedbacks between transport, scour, deposition and the flow regime. Coupling the Debris Library with a mobile bed model will augment sediment routing algorithms and erosion or deposition calculations based on the non-Newtonian stress states. It will also adjust the stress states and flow conditions based on dynamic concentration and grain size feedbacks. Presumably a mobile bed model can simulate changes between flow types (e.g. from mudflow to hyperconcentrated flow as sediment deposits – or vice versa) either temporally or spatially. However, a mobile bed model requires much more information from the Debris Library. Not only does the hydrodynamic engine require flow bulking and an augmented friction slope (computed from the non-Newtonian shear equation), but the transport equations require several updated parameters. The Debris Library must pass a mobile bed model a sediment laden viscosity, a hindered fall velocity, and the augmented unit weight of the flow-sediment mixture. The shear stress used to adjust the friction slope will also affect the transport function. However, this assumes that the standard transport functions will work reasonably well with these non-Newtonian parameters. While there are a few examples of this approach (Yang et al., 1996), the Library provides customized bed load and suspended load functions, respectively, designed specifically for high concentration simulations (Rickenmann, 1991).

Non-Newtonian Sediment Transport: As the shear stress increases, particles either go into suspension or the particles will move as bedload in several layers, called sheet flow. We consider this an analogous processes that mechanically describes intense sediment transport during post-wildfire non-Newtonian flow events. For sheet flow, we have coarser particles whose settling velocity is of the same order as the turbulent fluctuations. In this case, the turbulence cannot move a particle into suspension and the sediment is transported in several layers as bedload. The vertical turbulent fluctuation near the bed is in order of shear velocity (u_*), so commonly the criterion for a particle to be moved in suspension is

$$\frac{w_s}{u_*} < 0.8 \; to \; 1 \tag{10}$$

where, w_s = clear water particle settling velocity (m/s), and u_* = shear velocity (m/s) (Fredsoe and Deigaard 1992). Another unique aspect of high concentrated sediment events is an increased bed load layer thickness between 10 and 50 times d_{90} sediment grain size (Wilson, 1987). Rickenmann (1991) developed a dimensionless intense bed load transport function from 252 flume experiments at Eidgenossische Technische Hochschule (ETH) in Zurich, defined as

$$\Phi_B = \frac{3.1}{(s-1)^{1/2}} \left(\frac{d_{90}}{d_{30}}\right)^{0.2} \theta_m^{1/2} (\theta_m - \theta_c) Fr^{1.1} \tag{11}$$

where,

$$s = \frac{\rho_s}{\rho} \tag{12}$$

$$\theta_m = \frac{u_{*,m}^2}{g(s-1)d_s} \tag{13}$$

$$u_{*,m} = \sqrt{\frac{\tau_{MD}}{\rho_m}} \tag{14}$$

$$\theta_c = \frac{0.24}{D_*} + 0.055[1 - e^{-0.02D_*}] \tag{15}$$

$$D_* = d_s \left[\frac{(s-1)g}{v_m^2} \right]^{1/3} \tag{16}$$

$$Fr = \frac{u_m}{\sqrt{gh_m}} \tag{17}$$

where, Φ_B = dimensionless bedload transport rate (-), s = specific gravity (-), d_{30} = the 30th and 90th percentile particle sizes (m), θ_m = sediment mixture Shields parameter (-), θ_c = critical threshold parameter from Soulsby and Whitehouse (1997) (-), $u_{*,m}$ = non-Newtonian mixture shear velocity (m/s), D_* = dimensionless grain diameter (-), v_m = mixture kinematic viscosity (m²/s), Fr = mixture Froude Number (-), u_m = non-Newtonian mixture velocity (m/s), and h_m = flow depth (m). The Rickenmann 1991 approach will be combined with a non-equilibrium suspended sediment transport function currently in SEDLIB developed by Brown (2008). Alternatively, Yang et al., 1996 developed bedload and suspended load transport approaches for predicting hyperconcentrated flows from the Yellow River - a modification of Yang (1979) unit stream power formulations. The Yang et al. (1996) modified equation for predicting total bed material load is defined as,

$$\log C_t = 5.165 - 0.153 \log \frac{w_m d_s}{v_m} - 0.297 \frac{u_*}{w_m} + \left(1.780 - 0.360 \log \frac{w_m d_s}{v_m} - 0.480 \log \frac{u_*}{w_m} \right) \log \left(\frac{\gamma_m}{\gamma_s - \gamma_m} - \frac{\bar{u} S_f}{w_m} \right) \tag{18}$$

where, C_t = the total bed-material concentration (ppm), w_m = hindered settling velocity (m/s), v_m = kinematic viscosity (m²/s), γ_m = specific weight of sediment mixture (N/m³), and γ_s = specific weight of sediment particle (N/m³). Yang and Simões (2005) developed an approach to estimate the wash load component of total load to supplement Yang et al., 1996. The wash load is determined from

$$C_{wv} = (\alpha - 1) C_{tv} \tag{19}$$

where, C_{wv} = the wash load concentration by volume (-), α = empirical coefficient ($\alpha = C_v / C_{tv}$) determined iteratively, and C_{tv} = the total bed-material load by volume (-). The total bed-material load by volume is computed from

$$C_{tv} = \frac{C_t \times 10^{-6}}{s - (s-1) C_t \times 10^{-6}} \tag{20}$$

Hindered Settling: When sediment slurry volumetric concentration increases above 0.15, the sediment particles start to hinder each other, resulting in decreased particle settling velocity compared to the same particle in clear water (Tomkins et al. 2005). In non-Newtonian mechanics, this phenomena is referred to as *hindered settling*. A variety of explanations have been proposed to explain the physical processes responsible for hindered settling. A complete review is outside the scope of this document, but additional background and theory on hindered settling can be found in Cheng (1997), Winterwerp and Van Kesteren (2004), Tomkins et al. (2005), and Cuthbertson et al. (2008). Most hindered settling expressions for non-cohesive and cohesive sediments are based on the formulation by Richardson and Zaki (1954) where return flow, wake formation, and buoyancy are accounted for empirically, and defined as

$$w_m = w_s (1 - C_v)^m \tag{21}$$

where, w_m = the hindered settling velocity (m/s), and m = an empirical coefficient (-) and has been shown to vary with particle Reynolds number between approximately 2.5 and 7 (Yang 2003; Baldock et al., 2004). The effects of hindered settling are commonly observed in post-fire floods via very large sediment clast being transported considerable distances from the source location.

Conclusion

High intensity wildfires remove vegetation, including alteration of soils and subsurface root structures, purge organic soil, and create widespread hydrophobic soils, resulting in increased flooding, sediment transport and extreme flood events. Post-wildfire floods generate gravity driven surface runoff and erosion events that involve complex mixtures of water, ash, sediment, and entrained debris (i.e., destroyed upstream infrastructure, woody debris, and very large sediment clasts). This work will set the stage for developing a national framework for addressing post-fire sediment movement and related debris and mud flows within USACE numerical models.

References

Abrahams, A.D. 2003. "Bed-Load transport equation for sheet flow," Journal of Hydraulics Engineering 153: 159-163.

Bagnold, R.A. 1954. "Experiment on gravity-free dispersion of a large solid sphere in a Newtonian fluid under shear," Proceeding of the Royal Society of London, Series A, 224:49-63.

Baldock, T.E., Tomkins, M.R., Nielson, P., Hughes, M.G. 2004. "Settling velocity of sediments at high concentrations," Coastal Engineering 51(1):91-100.

Bingham, E.C. 1922. "Fluidity and plasticity," v. 2, McGraw-Hill.

Brown, G.L., 2008. "Approximate profile for nonequilibrium suspended sediment," Journal of Hydraulic Engineering 134(7): 1010 – 1014.

Certini, G. 2005. "Effects of fire on properties of forest soils: a review," Oecologia 143:1-10.

Cheng, N.S. 1997. "Effect of concentration on settling velocity of sediment particles," Journal of Hydraulic Engineering 123(8):728–731.

Cuthbertson, Dong, A.P., King, S., and Davies, P. 2008. "Hindered settling velocity of cohesive/non-cohesive sediment mixtures," Coastal Engineering 55(12):1197–1208.

Dabak, T., and Yucel, O. 1986. "Shear viscosity behavior of highly concentrated suspensions at low and high shear-rates," Rheologica Acta 25:527-533.

Ebel, B.A., Moody, J.A., and Martin, D.A. 2012. "Hydrologic conditions controlling runoff generation immediately after wildfire," Water Resources Research, 48:1-13.

Einstein, H.A., and Chien, N. 1955. "Effects of heavy sediment concentration near the bed on velocity and sediment distribution," MRD Series, no. 8. Berkeley: University of California: Institute of Engineering Research; Omaha, Nebraska: U.S. Army Engineering Division, Missouri River, U.S. Army Corps of Engineers.

Fredsoe, J., and Deigaard, R. 1992. "Mechanics of Coastal Sediment Transport," Advance Series on Ocean Engineering – Volume 3, World Scientific Publishing Company.

Happel, J., and Brenner, H. 1965. "Low Reynolds Number hydrodynamics," Englewood Cliffs, N.J., Prentice-Hall.

Hill, H.M. 1966. "Bedforms due to fluid stream," Journal of the Hydraulics Division, ASCE, 92:127-143.

Iverson, R.M. 1997. "The physics of debris-flows," Reviews of Geophysics, American Geophysical Union 35(3):245-296.

Iverson, R.M., and LaHusen, R.G. 1993. "Friction in debris flows: inferences from large-scale flume experiments," American Society of Civil Engineers (Ed.), Hydraulic Engineering, 93:1604-1609.

Iverson, R.M., and Denlinger, R.P. 2001. "Flow of variably fluized granular masses across three-dimensional terrain: 1. Coulomb mixture theory," Journal of Geophysical Research 106(B1):537-552.

Imran, J., Parker, G., Locat, J., and Lee, H. 2001. "1D numerical model of muddy subaqueous and subaerial debris flows," Journal of Hydraulic Engineering, 127:959-968.

Jin, M., and Fread, D.L. 1997. "1D Modeling of Mud/Debris unsteady flows," Journal of Hydraulic Engineering, 125(8):827-834.

Julien, P.Y., and Lan, Y. 1991. "Rheology of Hyperconcentrations," Journal of Hydraulic Engineering 115, (3):346-353.

Julien, P.Y. 2010. "Erosion and Sedimentation," Cambridge University Press 2nd Eds.

Langendoen, E.J., and Simon, A. 2008. "Modeling the evolution of incised streams, II: Streambank erosion," Journal of Hydraulics Engineering 134(7): 905-915.

Lane, P.N.J., Sheridan, G.J., Noske, P.J. 2006. "Changes in sediment loads and discharge from small mountain catchments following wildfire in south eastern Australia," Journal of Hydrology 331:495-510.

Moody, J.A., Kinner, D.A., and Ubeda, X. 2009. "Linking hydraulic properties of fire affected soils to infiltration and water repellency," Journal of Hydrology, 379: 291-303.

Moody, J.A., Shakesby, R.A., Robichaud, P.K., Cannon, S.H., Martin, D.A. 2013. "Current research issues related to post-wildfire runoff and erosion processes," Earth-Science Reviews 122:10-37.

NSTC, 2015. Wildland fire science and technology task force final report. Committee on Environment, Natural Resources, and Sustainability Subsommittee on Disaster Reduction, National Science and Technology Council, November 2015, 28 pp.

O'Brien, J.S., Julien, P.Y., and Fullerton, W.T. 1993. "Two dimensional water flood and mudflow simulation," Journal of Hydraulic Engineering 119(2):244-261.

Richardson, J.F., and Zaki, W.N. 1954. "Sedimentation and fluidization: part 1," Transactions of Institution of Chemical Engineers 32:35-53.

Rickenmann, D. 1991. "Hyperconcentrated flow and sediment transport at steep slopes," Journal of Hydraulic Engineering 117:1419-1439.

Rowe, P.B., Countryman, C.M., Storey, H.C. 1954. "Hydrologic analysis used to determine effects of fire on peak discharge and erosion rates in southern California watersheds," USDA Forest Service, California Forest and Range Experimental Station, pp. 49.

Shakesby, R.A. 2011. "Post-wildfire soil erosion in the Mediterranean: review and future research directions," Earth-Science Reviews 105:71-100.

Simon, A., Curini, A., Darby, S.E., and Langendoen, E.M. 2000. "Bank and near-bank processes in an incised channel," Geomorphology 35: 193-217.

Simon, A., Thomas, R.E., and Klimetz, L. 2010. "Comparison and experiences with Field Techniques to Measure Critical Shear Stress and Erodibility of Cohesive Deposits," 2nd Joint Federal Interagency Conference, Las Vegas, NV, June 27 – July 1, 2010.

Shin, S.S. 2010. "Response of runoff and erosion with vegetation recovery in differently treated hillslopes after forest fire," Korea. 8th International Symposium on Ecohydraulics, Seoul, Korea, September 2010.

Takahashi, T. 1978. "Mechanical characteristics of debris-flows," Journal of Hydraulic Engineering 104:381-396.

Tomkins, M. R., Baldock, T.E., and Nielson, P. 2005. "Hindered settling of sand grains," Sedimentology 52(6):1425–1432.

Wilson, K.C. 1987. "Analysis of bed-load motion at high shear stress," Journal of Hyraulic Engineering 113(1): 97-103.

Winterwerp, J. C., and Van Kesteren, W.G.M. 2004. "Introduction to the physics of cohesive sediment in the marine environment," Developments in Sedimentology 56, Elsevier.

Yang, C.T., 1979. Unit stream power equations for total load. Journal of Hydrology 40(1-2):123-138.

Yang, C.T. 2003. Sediment transport: theory and practice. Krieger Publishing Company, Florida.

Yang, C.T., and Simões, F.J. 2005. Wash load and bed-material load transport in the Yellow River. Journal of Hydraulic Engineering 131(5):413-418.

Yang, C.T., Molinas, A., and Wu, B. 1996. "Sediment transport in the Yellow River," Journal of Hydraulic Engineering 122(5):237-244.

Development of SRH-COAST: A General Wave-Flow Model for Coastal Environment

Han Sang "Hans" Kim, Hydraulic Engineer, Bureau of Reclamation, Denver, CO, hskim@usbr.gov
Yong G. Lai, Hydraulic Engineer, Bureau of Reclamation, Denver, CO, ylai@usbr.gov

Extended Abstract

The estuary and coastal environment is characterized by very complex natural processes. A prominent feature is the wind-generated waves, which transfer energy and lead to various phenomena not observed where the hydrodynamics is dictated only by currents. Tides are also an important factor, raising and lowering the water level and causing tidal waves. With the rising sea level due to global warming and shortage of natural resources following population expansion, proper coastal engineering and management are becoming more important for many parts of the world.

Over the past several decades, many numerical models have been developed to predict the sea state in a given environment, beginning with assumptions of simple flow and wave conditions (Cardone et al., 1975; Fleming and Hunt, 1976). More recent efforts utilize depth-integrated two-dimensional (2D) or quasi-three-dimensional (3D) flow equations with the so-called third-generation wave models. Some of today's widely used models include CCHE2D-COAST (Ding and Wang, 2008), which combines the finite element solver CCHE2D (Jia and Wang, 2001) with a wave module; FVCOM (Chen et al., 2013), a 3D finite volume coastal model; and Delft3d (Deltares, 2019), a 2D/3D finite difference hydrodynamics solver coupled with SWAN (SWAN Team, 2018).

In this paper, the authors present a new estuary and coastal model, SRH-COAST, which is currently in development at the U.S. Bureau of Reclamation. It is a coupled model that combines SRH-2D, the two-dimensional hydraulic and sediment model for river systems (Lai, 2008), with a third-generation wave model. With the capability to model wave propagation and flow in general wave-current environments, including depth- and current- induced mechanisms such as refraction and shoaling, SRH-COAST will be particularly suitable for estuary modeling where river and ocean meet.

SRH-2D, which functions as the flow module, solves the depth- and Reynolds-averaged Navier-Stokes equations using a finite volume discretization. This discretization scheme has the benefit of satisfying the conservation laws and achieving solution stability. The 2D solution domain is represented by a network of mesh cells that can assume any shape. Primarily, a mixture of triangles and quadrilaterals is used, as shown in Figure 1. Such meshes are easily generated using a number of popularly used 2D mesh generators. In the course of the model development, a number of mesh shapes will be tested and compared to understand whether certain mesh types are superior to other types. The reader is referred to Lai (2008) for more detail.

The wave module is based on the approaches found in the third-generation wave models (e.g., SWAN). That is, the wave action balance equation is solved, where the spectrum shape is not pre-imposed and the non-linear effects are not parameterized (Holthuijsen, 2007). This makes
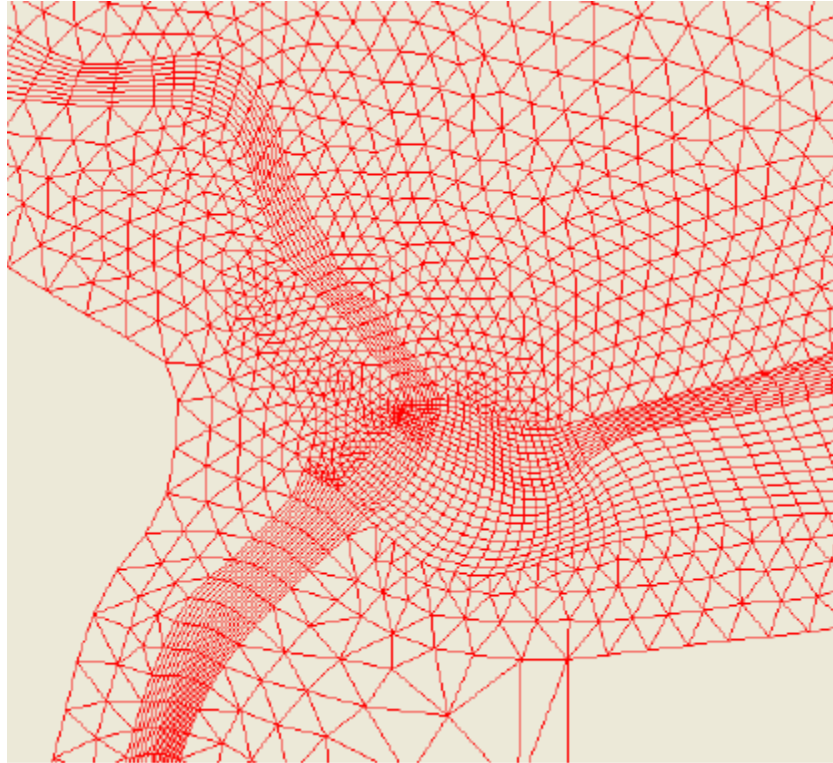
Figure 1. Example of a mesh utilizing both triangular and quadrilateral cells

SRH-COAST a general-purpose tool, which can simulate wave propagation, generation, and dissipation in a wide array of sea states. The wave action balance equation is given as:

$$\frac{\partial N}{\partial t} + \frac{\partial \left(c_{g,x} + U\right)N}{\partial x} + \frac{\partial \left(c_{g,y} + V\right)N}{\partial y} + \frac{\partial c_\theta N}{\partial \theta} + \frac{\partial c_\sigma N}{\partial \sigma} = \frac{S}{\sigma}$$

where N = wave action; t = time; $c_{g,x} = c_g \cos \theta$ and $c_{g,y} = c_g \sin \theta$ are group velocities in x- and y- directions, respectively; U and V = depth-averaged ambient flow velocities in x- and y- directions, respectively; θ = wave propagation direction measured counter-clockwise from positive x-axis; σ = wave angular frequency; c_θ = turning rate of the wave direction; c_σ = frequency shifting; and S = sum of the source and sink terms associated with wave generation and dissipation processes. To solve for N, the operator-splitting technique of Hsu et al. (2005) is adopted.

It is critical that the solutions obtained from the flow and wave modules are shared between them in a consistent manner. With the velocity field computed from the flow module, the effects due to the ambient currents can be accounted for in the wave module. In turn, the wave module is responsible for providing variables that quantify wave characteristics and wave-induced mechanisms, to be used by the flow module for the source/sink terms (and turbulence closure and boundary conditions, if applicable methods are employed). Both modules use an identical mesh, thus information can be transferred directly without spatial interpolation. The coupling between the flow and wave modules is depicted in Figure 2.
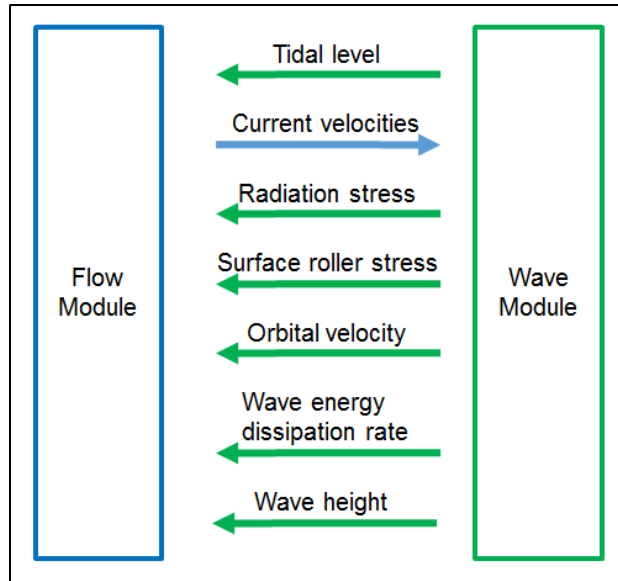
Figure 2. Coupling between the flow and wave modules

In a preliminary study, the wave module was validated by simulating depth-induced shoaling (change in the wave height due to change in the water depth). It utilized a square mesh measuring 4,000 m by 2,000 m with 50 cells in the direction of the wave propagation and 20 cells in the transverse direction. The depth decreases linearly towards the shoreline from 20 m to 0.5 m. As presented in Figure 3, the computed wave height and the analytical solution show a good agreement.
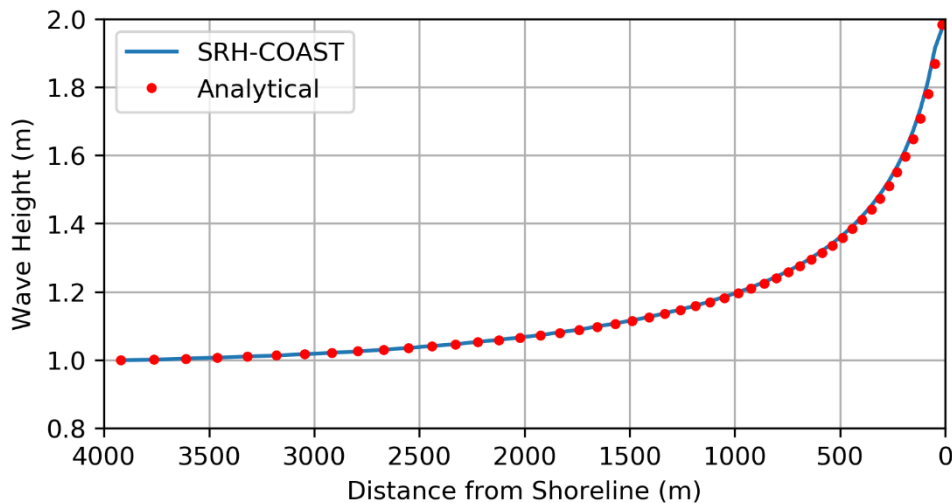
Figure 3. Change in wave height over a sloping bed

In the next stages of the model development, SRH-COAST will continue to be validated with cases that involve wave-current interactions and have known solutions. The various approaches for computing the source terms will also be explored.

References

Cardone, V.J. and Pierson, W.J. 1975. "Hindcasting the directional spectra of hurricane generated waves," Proceedings of the Offshore Technology Conference.

Chen, C., Beardsley, R.C., Cowles, G., Qi, J., Lai, Z., Gao, G., Stuebe, D., Xu, Q., Xue, P., Ge, J., Hu, S., Ji, R., Tian, R., Huang, H., Wu, L., Lin, H., Sun, Y., and Zhao, L. 2013. "An unstructured grid, finite volume coastal ocean model: FVCOM," User Manual, third ed. SMAST/UMASSD Technical Report-13-1701.

Deltares. 2019. "Delft3D-FLOW," User Manual, Version 3.15.59206, Deltares, The Netherlands.

Ding, Y. and Wang, S.S.Y. 2008. "Development and application of a coastal and estuarine morphological process modeling system," Journal of Coastal Research, Special Issue No. 52, 127-140.

Fleming, C.A. and Hunt, J.N. 1976. "Application of a sediment transport model," Proceedings of the 15th International Conference on Coastal Engineering, 1194-1202.

Holthuijsen, L.H. 2007. Waves in Oceanic and Coastal Waters. Cambridge University Press, UK.

Hsu, T.W., Ou, S.H., and Liau, J.M. 2005. "Hindcasting nearshore wind waves using a FEM code for SWAN," Coastal Engineering 52, 177-195.

Jia, Y. and Wang, S.S.Y. 2001. "CCHE2d: Two-dimensional hydrodynamics and sediment transport model for unsteady open channel flows over loose bed," Technical Report, No. NCCHE-TR-2001-1, National Center for Computational Hydroscience and Engineering.

Lai, Y.G. 2008. "SRH-2D version 2: Theory and User's Manual," Technical Service Center, Bureau of Reclamation, Denver, CO 80225.

SWAN Team. 2018. "SWAN – Scientific and technical documentation," Delft University of Technology, available from *http://www.swan.tudelft.nl*.

Dynamic Dam Breaches: Predicting Sediment Laden Dam Breach Flood Wave Propagation for Future Conditions Using FLO-2D

Michael Gerlach, Project Manager, WEST Consultants, Tempe, AZ,
mgerlach@WESTconsultants.com
Brent Travis, Director of Applied Research, WEST Consultants, Tempe, AZ,
btravis@WESTconsultants.com
Brian Wahlin, Vice-President, WEST Consultants, Tempe, AZ,
bwahlin@WESTconsultants.com

Abstract

Dam breaches are a critical factor in floodplain, emergency, and reservoir management but rarely account for the impact of sediment storage within the reservoir on the flood wave propagation. Moreover, the volume of the impounded sediment typically increases over time; thus, influencing the potential for dam failure, the water level behind the dam, and the failure characteristics of a breach, should it occur. This aspect is particularly important for predictions of tailings dam failures, wherein both the sediment storage and the physical characteristics of the dam structure itself are in constant flux. To account for this dynamic influence of sediment inflow and dam characteristics on flood wave propagation, a dynamic modeling system was developed that utilizes the dam breach and subsequent downstream 2D flood routing capabilities of FLO-2D. This unique model provides a methodology wherein the user can specify how the impounded sediment and water storage volumes and the dam / levee bank height and width change over time. The user then selects any future time scenario and executes the FLO-2D breach model for the corresponding predicted dam and sediment characteristics. This paper describes this model and provides an example of its application to a hypothetical tailings facility. The modeled implications of floodplain changes over time are discussed, and suggestions for future applications of the model to other, related facilities such as coastal levees and sediment basins are provided.

Introduction

A breach can occur at any point during the life of a tailings storage facility (TSF), whether by overtopping given a significant enough hydrologic event [i.e., probable maximum flood (PMF)], a piping failure, foundation failure, or earthquake (O'Brien, 2015). Because the tailings facility is dynamic, growing both from incoming sediment load as well as from periodic structural improvements (Figure 1), the likelihood of these hydrologic and piping failure modes, in particular, changes over time, as does the progression and severity of the ensuing breach. It can, thus, be useful for tailings facility management and design to understand this dynamic relationship and the corresponding downstream consequences of failure. To assist in that regard, a new modeling approach was developed. This approach utilizes the dam breach and subsequent downstream 2D flood routing capabilities of FLO-2D in conjunction with a "Tailings Dam Tool", or TDT, wherein the user can specify how the impounded sediment and water storage volumes and the dam / levee bank height and width are changing over time. This allows

the user to identify the worst-case failure scenarios over a time period of interest. The TDT, thus, allows mine engineers/planners to identify an optimum program for expanding the TSF that accommodates mine operations and costs and, simultaneously, minimizes downstream consequences of failure.
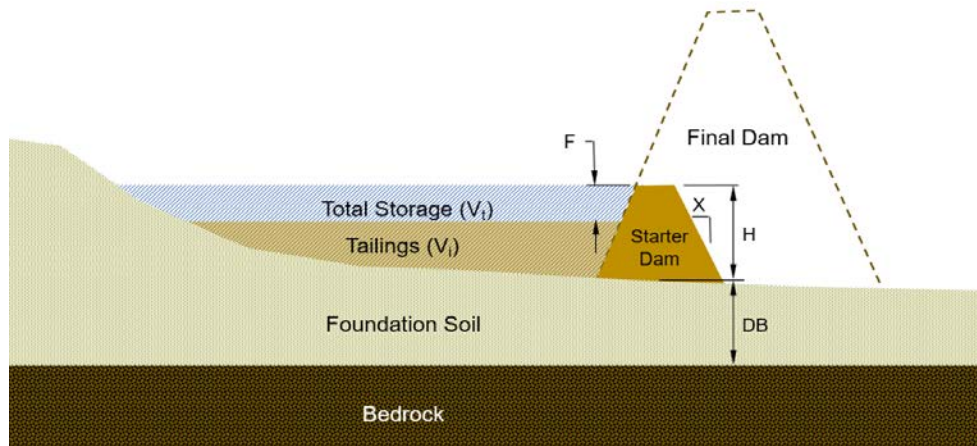
Figure 1. Tailings dam definition sketch.

Approach

The overarching approach to executing the combined TDT / FLO-2D model within the context of TSF operation and / or design is as follows:

1. Couple the developed TDT with FLO-2D to route the breach hydrograph at any given point in time for any given condition of tailings volume and TSF embankment due to a PMF inflow.
2. Run the TDT at a specified time interval over the desired duration of operation. Inputs to the Tailings Dam Tool are varied according to operational inputs (annual tailings production rate, total tailings storage volume, and TSF embankment raises). Geotechnical properties for the embankment along with hydrologic data for the PMF are used to determine the failure mode and the corresponding breach hydrograph and volume of tailings material released.
3. Import the resulting breach hydrograph into FLO-2D for computation of the downstream inundation area and corresponding depths, velocities and travel times at critical facilities.
4. Use the results to refine the TSF operation plan, if necessary, to minimize the adverse downstream consequences based on an understanding of the corresponding risk of failure.

At present the particular tailings factors must be relayed to FLO-2D directly, but development is currently underway (expected completion in spring, 2019) to allow general project input via a single GUI (Figure 2).

Physical/Site Data:	Initial	Final	
Tailings Dam Height (H):	50	270	feet
Total Impoundment Volume (V_t):	7,783,951	51,772,000	cubic yards
Tailings Volume (V_i):	0	46,720,000	cubic yards
Freeboard (F):	100	280	feet
Tailings Dam Slope (X:1):	2	2	
Hydrologic Data:			
Probable Maximum Precipitation:	14		inches
Watershed Area:	3		sq. miles
Runoff Volume:	3,613,867		cubic yards
Geotechnical Data:			
Depth to Bedrock (DB):	40		feet
Foundation Soil Character:	Granular		
SPT Blow Count:	3		
Unit Weight of Foundation Soil (γ_b):	120		pcf
Unit Weight of Dam Material (γ_D):	110		pcf
Cohesion of Dam Material:	100		pcf
Friction Angle of Dam Material (Φ):	25		degrees

Figure 2. Proposed Tailings Dam Tool (TDT) GUI interface. (Currently under development.)

With the overall project information entered into the TDT, variable dam construction conditions can be considered (e.g., how high to build the dam and when to do so). The program then automatically executes FLO-2D with this information, and provides critical results including peak hydrograph flowrate, total volume released, and total sediment released.

Example

As an example of how the proposed TDT could be used, consider a hypothetical tailings facility with the soils, hydrologic, and geometric data, as specified in Figure 2. Assuming a continuous production rate of 1 cfs, then a 50-foot height increase of the dam every six years results in the failure scenarios shown in Figure 3.
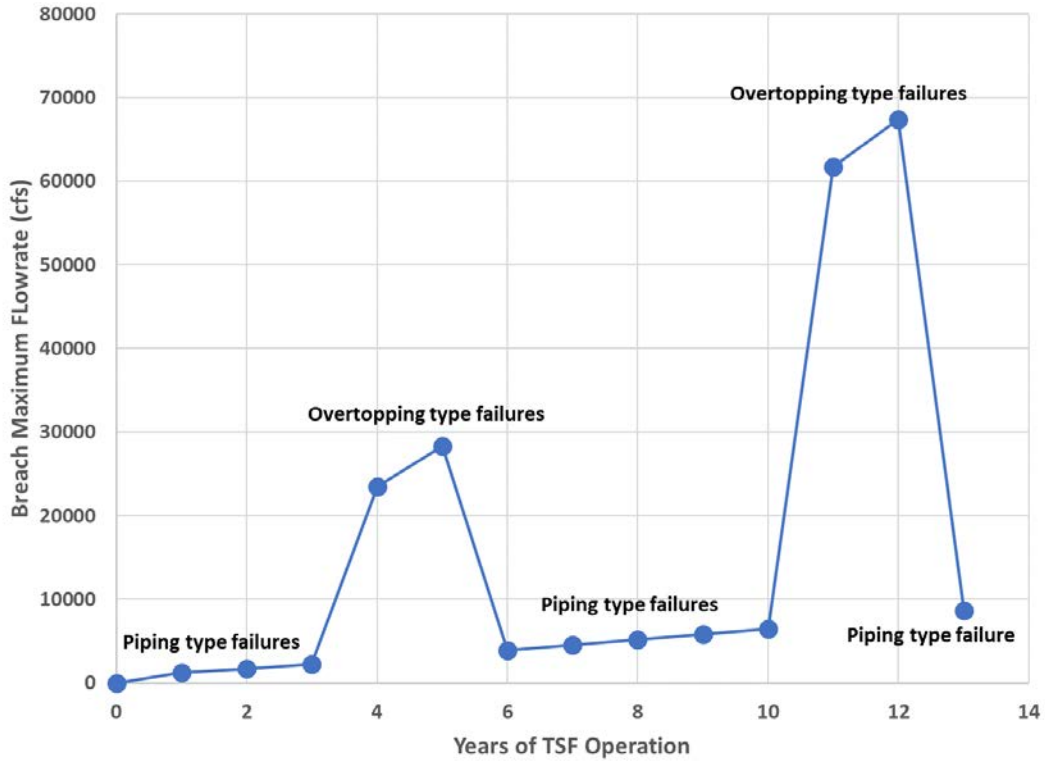
Figure 3. Breach Maximum Flowrate versus Years of TSF Operation

The transition between piping type failures and overtopping type failures is considerable, with overtopping resulting in much higher maximum breach flowrates. The difference in overall sediment outflow is also substantial.
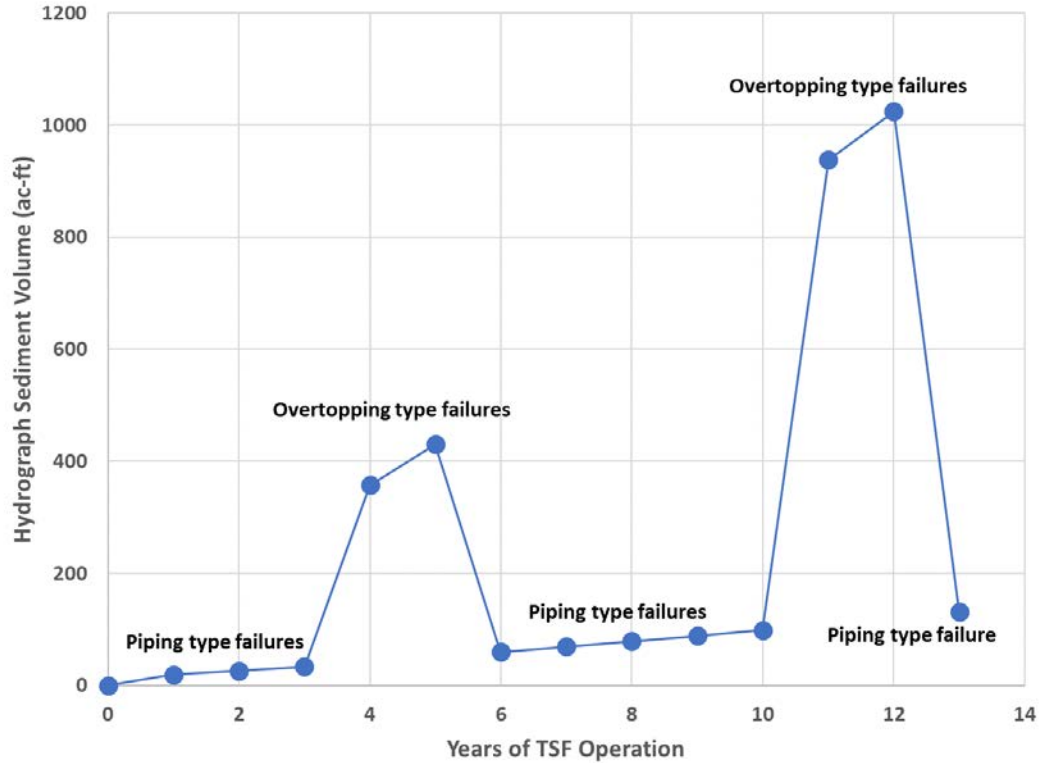
Figure 4. Breach Maximum Flowrate versus Hydrograph Sediment Volume

Conclusion

The TDT is a useful tool for tailings management, operations, and design. By combining the disparate aspects of breach failure (geotechnical, hydrologic, geometric) into one integrated algorithm, the consequences for operations and design decision making becomes immediately apparent. Here, the example shows that an overtopping-type failure is of much greater consequence compared with the piping failure, suggesting that the original construction plan (a 50-foot increase every 6 years) be revisited. Of course, other TSF may have different outcomes. A facility with weaker material and a more aggressive construction schedule may experience greater piping failure consequences compared with overtopping. Indeed, it is the nonlinearity of this process that justifies application of the TDT and its continued development.

Reference

O'Brien, J.S., Gonzalez-Ramirez, N., Tocher, R.J., Chao, K.C., and Overton D.D. (2015). "Predicting Tailings Dams Breach Release Volumes for Flood Hazard Delineation," Proc. of the Association of State Dam Safety Officials Conference, New Orleans.

Evaluating Uncertainty in Manning's Roughness Coefficients in One-Dimensional Steady HEC-RAS Modeling

Nam Jeong Choi, Hydrologist, U. S. Geological Survey, San Antonio, TX, nchoi@usgs.gov
Frank L. Engel, Geographer, U. S. Geological Survey, San Antonio, TX, fengel@usgs.gov
J. Ryan Banta, Hydrologic Studies Chief, U. S. Geological Survey, San Antonio, TX, jbanta@usgs.gov

Abstract

The step-backwater solution of the one-dimensional shallow water equations has been a popular approach to model water-surface elevations for flood-inundation mapping. U.S. Army Corps of Engineering Hydrologic Engineering Center River Analysis System (HEC-RAS) is a nationally accepted hydraulic model used to simulate flood inundation. Model simulation results will vary depending on selection of the Manning's roughness coefficients. In this study, the effects of uncertainty in Manning's roughness coefficients were investigated for a 23-mile reach of the Medina River near Bandera, Texas. One-parameter (uniform), two-parameter (main channel and floodplain), and three-parameter (main channel, left floodplain, and right floodplain) scenarios are being tested to see how multiple roughness coefficients affect the uncertainty in the model for the study area that is being developed. Model performance will be evaluated using the root-mean-square-error of water-surface elevation differences between the model result and the stage-discharge rating curve at the U.S. Geological Survey streamflow gaging station at the Medina River at Bandera, Texas (station number 08178880). Uncertainty in Manning's roughness coefficients will be determined through Monte Carlo simulation of randomly distributed roughness coefficient values for each parameter test from 0.001 to 0.3 for 10,000 runs.

Introduction

The step-backwater solution of the one-dimensional energy equation has been a popular approach to model water-surface elevations for flood-inundation mapping owing to its simplicity and stability. One of the most widely used models is U.S. Army Corps of Engineers Hydrologic Engineering Center's River Analysis System (HEC-RAS) (U.S. Army Corps of Engineers Hydrologic Engineering Center, 2016). HEC-RAS is a nationally accepted hydraulic model for the National Flood Insurance Program of Federal Emergency Management Agency (Federal Emergency Management Agency, 2019), and U.S. Geological Survey (USGS) Flood Inundation Maps are often produced using HEC-RAS (U.S. Geological Survey, 2019).

HEC-RAS is used to solve the one-dimensional energy equation to get the backwater water-surface elevations of steady uniform flow. To solve these equations, the HEC-RAS model requires input datasets about the surface elevation topography (including cross sectional surveys), streamflow in the reach of interest, and the roughness of the stream channel.

One of the largest sources of uncertainty in one-dimensional hydraulic models involves the selection of values for Manning's roughness coefficient, commonly referred to as "n" values. The

uncertainty of n values has been studied by many including Pappenberger et al. (2005, 2008), Warmink et al. (2010), and Yang et al. (2014). The n values are often selected as a model calibration parameter because of its critical impact on water-surface elevations. By calibrating Manning's roughness coefficients to measured water-surface elevation data, one-dimensional models like HEC-RAS can often produce accurate maps of flood inundation.

For HEC-RAS modeling, an n value is assigned to each model cross-section which reflects various channel conditions at that location—vegetation, obstacles, and surface irregularities for example. There are many different methods to estimate n values from available data such as photographs, tables, composite formulae, or measurement programs (Arcement and Schneider, 1989)). A single realization of a HEC-RAS model geometry can have as many n values as the number of modeled cross-section points, which makes determining realistic n values a challenge. This paper provides an overview of ongoing research to assess the uncertainty in simulated water-surface elevations resulting from using multiple n value representations of cross-section roughness in a HEC-RAS model for a reach of the Medina River in Texas.

Model Development

The study area includes a 23-mile reach of the Medina River near Bandera, Tex. from the confluence of the Medina River and Winans Creek downstream to English Crossing Road near Pipe Creek, Tex. (Figure 1). Bandera is between two meander bends of the Medina River near the intersection of State Highways 16 and 173 in the Texas Hill Country. A USGS streamflow-gaging station on the Medina River at Bandera, Tex. (station number 08178880, hereinafter referred to as the Bandera station) is downstream from the Main Street bridge that is part of Highway 173. Land cover in the study area consists of patches of ashe-juniper, live oaks, and mesquite trees intermingled with grass-covered rangeland; steep and rocky areas of exposed limestone dot the landscape. The climate in the area is semi-arid, and many tributaries to the Medina River are dry most time of the year (Bomar, 1983). The combination of steeply sloping terrain and the tendency for tropical cyclones from the Gulf of Mexico to move inland across the area during summer and fall contribute to frequent episodes of flash flooding (Caran and Baker, 1986).

Modeled channel cross-sections were extracted from a digital elevation model (DEM) derived from light detection and ranging (lidar) data collected during historically low-flow conditions in December 2013 (Texas Natural Resources Information System, 2014). Field measurements of the depth of water in the channel near the Bandera station and English Crossing Road during low-flow conditions were used to adjust elevations of cross-section points that were submerged when the lidar data were collected.

Streamflow discharges at the Bandera station are being modeled and calibrated by using the USGS Bandera Station stage-discharge rating curve. The model-targeted streamflows range from 2,370 cubic-feet-per-second (ft^3/s, 67.1 cubic-meter-per-second [m^3/s]) to 248,000 ft^3/s (7,040 m^3/s) corresponding to gage heights of 10 feet (ft, 3.05 meter [m]) to 38 ft (11.59 m). The rating curve at the Bandera station (fig. 2; solid black line) and 29 flow stages (gage heights) (fig. 2; red circles) ranging from 10 ft to 38 ft in one-foot increments that are being modeled using HEC-RAS. The HEC-RAS model calibration will be considered "acceptable" when the computed root-mean-square-error (RMSE) between the modeled and observed water-surface elevations are less than one foot.

Uncertainty Analyses

The model performance will be tested with three different scenarios of n values: one-parameter (uniform n value), two-parameter (two n values, one for the main channel and one for the floodplains), and three-parameter (three n values, one for the main channel, one for the left floodplain, and one for the right floodplain). Uncertainty in Manning's roughness coefficients will be determined through Monte Carlo simulation of randomly distributed values of n for each parameter test from 0.001 to 0.3 for 10,000 runs. The tested n value range will cover the normal range of expected n values of natural streams. Natural streams and associated floodplains exhibit n values from 0.025 to 0.2 (Chow, 1959). This roughly matches with the "observed" n value range of 0.016–0.213 from Conyers and Fonstad (2005) for their work in the Texas Hill Country. The model fit for each Monte Carlo simulation is being evaluated by computing the root-mean-square-error (RMSE).
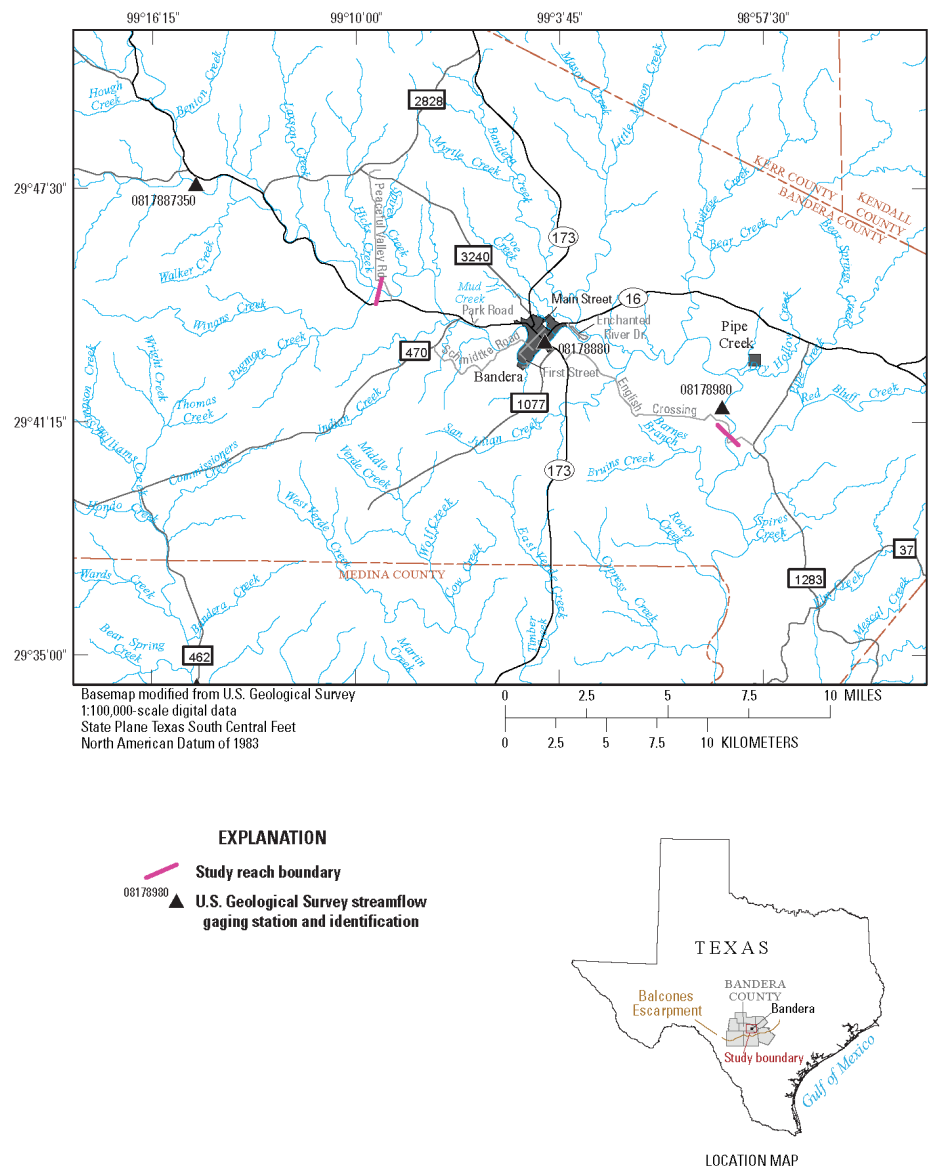
Figure 1 Study site map of the study area, which includes a 23-mile reach of the Medina River near Bandera, Texas.
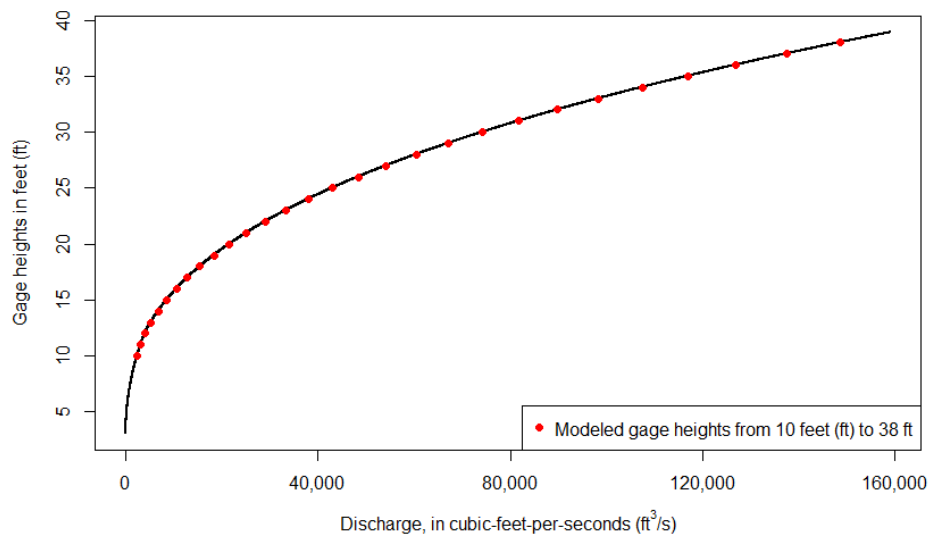
Figure 2 Stage-discharge rating curve at the U.S. Geological Streamflow gaging station 08178880 at Medina River at Bandera, Texas, with 29 modeled flow stages (gage heights) ranging from 10 feet to 38 feet.

References

Arcement, G.J., and Schneider, V.R. 1989. "Guide for selecting Manning's roughness coefficients for natural channels and flood plains," U.S. Geological Survey Water-Supply Paper 2339, 38 p. accessed February 27, 2019, at https://pubs.er.usgs.gov/publication/wsp2339.

Bomar, G.W. 1983. Texas Weather. pp. 54–58. ISBN 0-292-78053-2.

Caran, S.C., and Baker, V.R. 1986. "Flooding along the Balcones Escarpment, central Texas," in Abbott, P.L., and Woodruff, C.M., eds., The Balcones Escarpment—Geology, Hydrology, Ecology and Social Development in Central Texas, Geological Society of America, pp 1–14.

Conyers, M., and Fonstad, M. 2005. "The unusual channel resistance of the Texas Hill Country and its effect on flood flow predictions," Physical Geography, 26(5):379–395. Accessed February 27, 2019, at http://doi.org/10.2747/0272-3646.26.5.379.

Chow, V.T. 1959. Open-Channel Hydraulics: New York, McGraw-Hill, 680 p.

Federal Emergency Management Agency. 2019. "Hydraulic numerical models meeting the minimum requirement of National Flood Insurance Program," accessed February 11, 2019, at https://www.fema.gov/hydraulic-numerical-models-meeting-minimum-requirement-national-flood-insurance-program.

Pappenberger, F., Beven, K., Horritt, M., and Blazkova, S. 2005. "Uncertainty in the calibration of effective roughness parameters in HEC-RAS using inundation and downstream level observations," *Journal of Hydrology* 302(1–4):46–69, accessed February 27, 2019, at http://doi.org/10.1016/j.jhydrol.2004.06.036.

Texas Natural Resources Information System. 2014. "StratMap 2014 50cm Bandera & Lampasas Lidar," accessed February 29, 2019, at https://tnris.org/data-catalog/entry/stratmap-2014-50cm-bandera-lampasas/.

U.S. Army Corps of Engineers Hydrologic Engineering Center. 2016. "HEC-RAS River Analysis System User's Manual, Version 5.0," accessed February 12, 2019, at www.hec.usace.army.mil.

U.S. Geological Survey. 2019. "USGS Flood Inundation Mapping (FIM) Program," accessed February 12, 2019, at https://water.usgs.gov/osw/flood_inundation/.

Warmink, J.J., Booij, M.J., van der Klis, H., and Hulscher, S.J.M.H. 2010. "Uncertainty in design water levels due to uncertain bed form roughness in the river Rhine," proceedings of River Flow 2010, Braunschweig, Germany, pp 359–366.

Yang, T.-H., Wang, Y.-C., Tsung, S.-C., and Guo, W.-D. 2014. "Applying micro-genetic algorithm in the one-dimensional unsteady hydraulic model for parameter optimization," Journal of Hydroinformatics, 16(4): 772–783, accessed February 29, 2019, at http://doi.org/10.2166/hydro.2013.030.

HEC-RAS2D and SRH-2D: A Comparison Using an Equivalent Computational Mesh Developed for Analysis of the SR 107 Bridge

Keelan Jensen, Senior Hydraulic Engineer, WEST Consultants, Inc., Bellevue, WA, kjensen@westconsultants.com
Julie Heilman, State Hydraulic Engineer, Washington Department of Transportation, Olympia, WA, HeilmaJ@wsdot.wa.gov
Henry Hu, Vice President, WEST Consultants, Inc., Bellevue, WA, hhu@westconsultants.com

Abstract

The State Route 107 (SR107) Bridge crosses the Chehalis River just downstream of the City of Montesano, in Grays Harbor County, WA. Currently, the Chehalis River takes a very sharp bend to the right (viewed downstream) just upstream of the bridge. In an effort to determine what risk the river poses to the bridge and its approaches, several hydraulic models have been developed along this reach and the hydraulic characteristics of the river in this location have been thoroughly investigated.

WEST Consultants, Inc. (WEST) previously developed a calibrated SRH-2D hydrodynamic model of the Chehalis River in the vicinity of the SR107 bridge, extending from upstream of the meander bend to just upstream of the confluence of the Chehalis and Wynoochee Rivers. At the request of Washington Department of Transportation (WSDOT), WEST developed an HEC-RAS two-dimensional model mirroring the existing SRH-2D model to evaluate the similarities and differences in results generated by the two model programs. This paper documents the methods used to develop a two-dimensional RAS model from a mesh previously developed for the SRH-2D model, as well as the adjustments that needed to be taken to allow the model to run. The paper also presents and compares the results of the two models, and discusses possible explanations for any differences in the results. Finally, the paper presents results of sensitivity analyses performed on computational parameters such as time step, model mesh layout, and model computation method.

This comparison is not intended to determine model superiority, and it does not account for different advantages inherent in each model design. The purpose of this comparison is to determine how results from the two models compare when the same computational mesh is used for each model. Additional testing is recommended to take advantage of model features in each model and to determine in which scenarios specific model features would be most useful.

Introduction

The SR 107 Bridge crosses the Chehalis River just downstream of the City of Montesano, in Grays Harbor County, Washington (Figure 1). Currently, the Chehalis River takes a very sharp bend to the right (viewed downstream) just upstream of the bridge. Also upstream of the bridge, a meander bend threatens to cut off, which could significantly change the river hydraulics around and through the bridge . While the hydraulics of the Chehalis River currently pose a threat to the SR 107 Bridge and its south approach, the river is relatively stable and the bridge is inspected after

major flood events. A prior study was performed by WEST for WSDOT to investigate how an avulsion through the meander bend would affect the hydraulic conditions and scour potential at the SR 107 bridge crossing. For that study, WEST developed a calibrated SRH-2D hydrodynamic model of the Chehalis River in the vicinity of the SR107 bridge, extending from upstream of the meander bend to just upstream of the confluence of the Chehalis and Wynoochee Rivers (WEST, 2015). Figure 1 shows the model extents and vicinity.

For this study, WSDOT has asked WEST to create an HEC-RAS two-dimensional model mirroring the SRH-2D model to evaluate the similarities and differences in results generated by the two models. While the previous study included several different scenarios, for this comparison we only looked at the existing condition of the river. This report addresses only the initial comparison phase, which consisted of importing the SRH-2D mesh into the HEC-RAS model, with a few adjustments to meet the model needs. We could then compare how the two models compute results using the same mesh, even if the mesh is probably not the most efficient or correct for HEC-RAS modeling. If funding is available, future phases will potentially include adjusting the mesh and other model settings to take full advantage of the HEC-RAS 2-dimensional features. The discussion of results includes recommendations for future work.
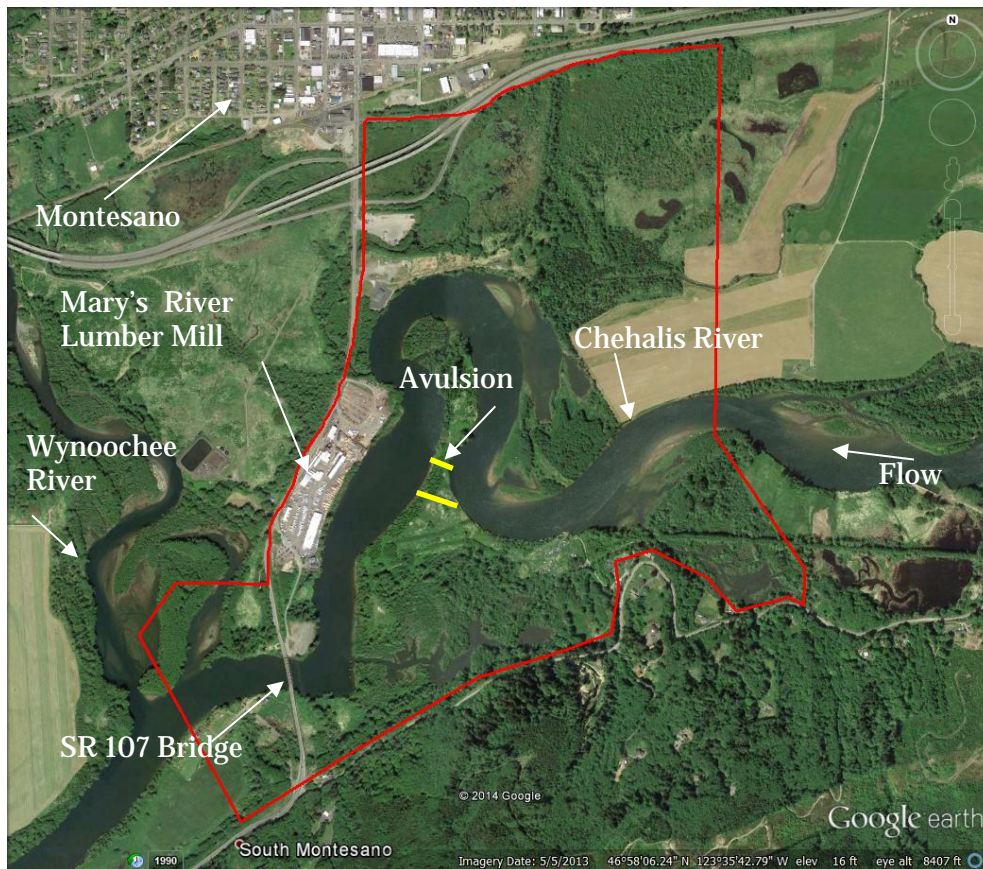
Figure 1. Project Location and Overview (background image courtesy of Google). The red line delineates the study area.

Model Development

The original SRH-2D model developed by WEST modeled approximately 2 miles of river and covered the entire 100-year floodplain. In developing the 2D model grid for the study area, WEST tried to provide sufficient horizontal grid resolution to allow testing of several different morphological scenarios with the same computational grid. Grid cell spacing varied from 25 feet in the channel to 100 feet in the overbank regions. Model elevations were obtained from a recent channel survey combined with 1-meter LiDAR data in the overbanks. Aerial imagery was used to determine land use types, which were then assigned roughness values using the WSDOT Hydraulics Manual (WSDOT 2010). These roughness values were calibrated by comparing water surface elevations and in-channel flow at four locations in the model domain that corresponded approximately to cross section locations in an existing calibrated 1D HEC-RAS model. This 1D HEC-RAS model was also used to develop inflow hydrographs for the upstream boundary and stage hydrographs for the downstream boundary. The final grid and roughness zones are shown in Figure 2. The roughness values used in the modeling are shown in Table 1.
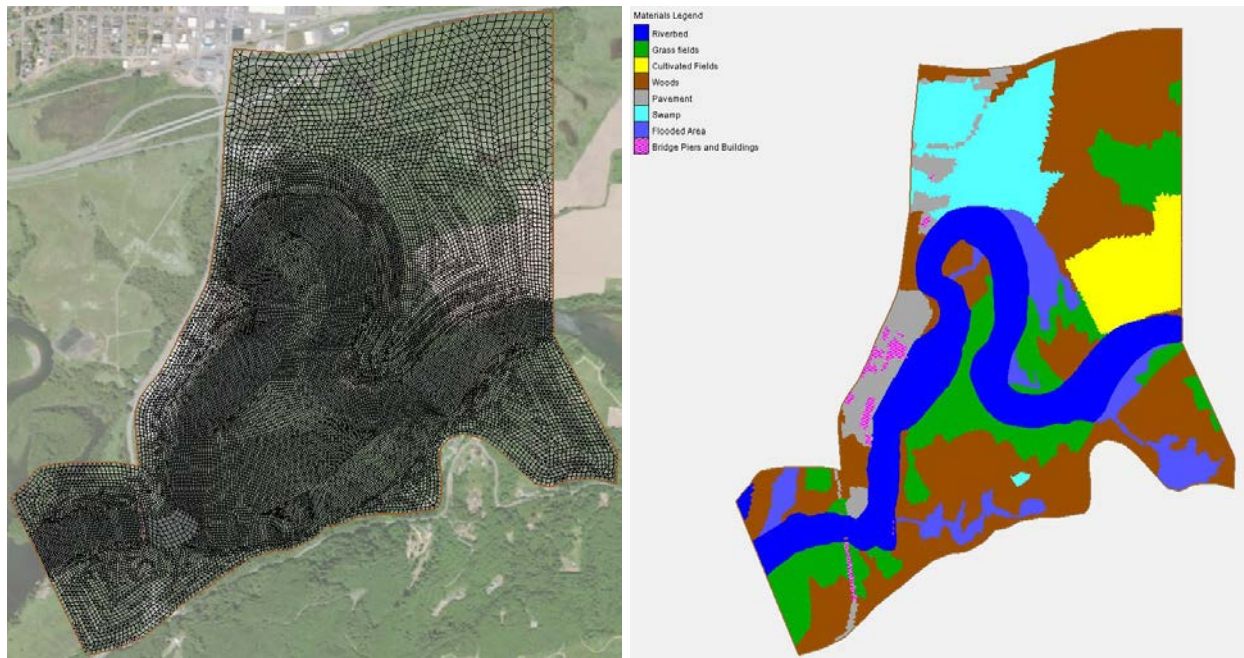
Figure 2. Final model grid (left) and assigned roughness (right)

Table 1. Roughness Values used in Modeling

Land Cover Classification	Manning's N Value
Riverbed	0.0225
Grass Fields	0.045
Cultivated Fields	0.03
Woods	0.075
Pavement	0.012
Swamp	0.0525
Flooded Area	0.03
Bridge Piers and Buildings	0.2

The existing SRH-2D model was used as the template for developing the HEC-RAS model, and where possible all parameters were left the same. We used the SRH-2D mesh extents to define the 2D flow area in the HEC-RAS model, and used the cell centers from the SRH-2D mesh to define the HEC-RAS cell centers. While this created approximately the same mesh as was used in the SRH-2D model, there are some differences in the cell shape and size due to the different techniques each model uses to create the mesh. The SRH-2D model sets the node points at the corner of each cell, and the cell faces connect each node while the cell centers are calculated based on node locations. The SRH-2D model elements are also limited to quadrilateral and triangular shapes. The HEC-RAS model sets the center point of each cell, and then creates cell faces based on perpendicular distance between cell centers. The cells in the HEC-RAS model can also have up to eight cell faces, resulting in a wider variety of cell shapes. We did have to adjust the HEC-RAS mesh slightly in two or three instances to meet the HEC-RAS mesh requirements, but the two meshes are as close to being identical as possible. We also used the same background terrain for both models, which allowed RAS to take advantage of the subgrid scale modeling in its calculations.

In the SRH-2D model, we followed standard practices methodology and simulated the bridge piers using holes in the mesh at each pier location. For the HEC-RAS model, we represented the piers using internal weir structures. We created structures bounding the extents of each pier, and set the weir elevation of each structure to 45 feet, which is approximately equal to the top of bridge elevation, and ensures that the piers will not be overtopped. We then forced the cell faces to snap to the internal structure extent. We created a land cover layer for the HEC-RAS model based on the roughness coverage we used in the SRH-2D development, and we assigned the same Manning's n-values used for the SRH-2D model.

We added boundary condition lines to the HEC-RAS 2D area to match the locations of boundary condition lines in SRH-2D. We used the same upstream flow hydrographs and downstream stage hydrographs that were used in the SRH-2D model. We simulated the 2007 flood event, a 2-year synthetic event, and a 100-year synthetic event. Because the area is tidally influenced, all three events were run using unsteady flow with varying discharge and stage. The HEC-RAS model requires a slope to calculate normal depth for flow distribution at the upstream inflow boundary, and we used the approximate upstream channel slope of 0.000493 (measured in HEC-RAS) for this value.

In the SRH model, the default parabolic turbulence model was used with a turbulence coefficient of 0.7 (default). In the RAS model, the Eddy Viscosity Transverse Mixing Coefficient

was left blank, which is also the default. The HEC-RAS model was run for the same time period as the SRH-2D model, with a computation interval of one second to match the SRH-2D model time step. The output was recorded every hour, the computation method in the HEC-RAS model was set to Full Momentum, and all other model parameters were kept at the model default.

Results Comparison

After running the HEC-RAS model, we compared the maximum water surface elevation (WSE), velocity, and bed shear stress at six locations for all three events. We chose the six locations based on areas of interest in the original SRH-2D model run, and attempted to select locations with importance to the bridge hydraulics. Unfortunately, there was no available observed data in the study area for the simulated events. The names and descriptions of the six locations chosen are shown in Table 2, and the locations are shown in Figure 3. We also compared the computational run time of the HEC-RAS model to the SRH-2D model for all three events. These results comparisons are shown in Table 3 through Table 6.

Table 2. Locations used for model comparisons.

Location	Description
Left Pier	Located just upstream of the first bridge pier located on the left (looking downstream) side of the main span
Right Pier	Located just upstream of the first bridge pier located on the right (looking downstream) side of the main span
US Bridge	Located upstream of the bridge in the middle of the channel, near the midpoint of the bend.
Right Bank	Located in the right overbank on the inside of the bend. This location is in a parking area that experienced the highest velocities in the SRH-2D simulation.
US Bend	Located upstream of the bend, at the upstream end of a likely avulsion location
Near Mill	Located in the middle of the channel, at the downstream end of the mill.
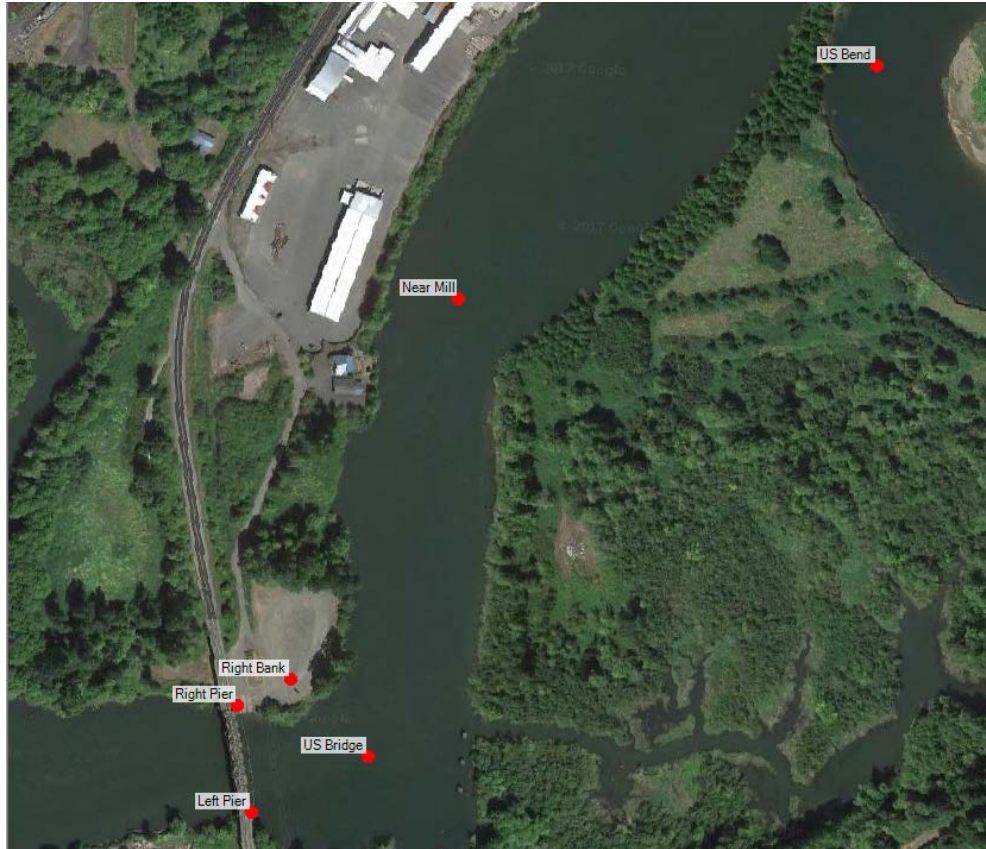
Figure 3. Locations used for comparisons.

Looking at the maximum WSE results shown in Table 3, we see that the HEC-RAS WSEs are generally higher than the SRH-2D WSEs. The higher flow events produced larger differences between the two models. Differences between the model results were less than 1 foot at all locations for all three events. The largest difference occurred at the Near Mill location during the 2007 event.

Table 3. Comparison of Maximum Water Surface Elevations (ft), SRH-2D vs. HEC-RAS

Location	2007 Event			2-year Event			100-year Event		
	SRH	**RAS**	**Diff.**	**SRH**	**RAS**	**Diff.**	**SRH**	**RAS**	**Diff.**
Left Pier	18.21	18.50	0.29	11.76	11.81	0.05	20.14	20.55	0.41
Right Pier	16.88	17.31	0.43	11.55	11.57	0.02	18.46	18.98	0.52
US Bridge	18.54	18.92	0.38	11.82	11.90	0.08	20.53	20.99	0.46
Right Bank	17.04	17.27	0.23	N/A	N/A	N/A	18.94	19.27	0.33
US Bend	20.35	20.99	0.64	13.53	13.97	0.44	22.20	22.43	0.23
Near Mill	19.39	20.21	0.82	12.04	12.18	0.14	21.46	21.79	0.33

Results were more varied for the maximum velocity magnitudes, shown in Table 4. While there was not a general trend in the differences, there were some patterns that emerged. The HEC-RAS velocities were lower than SRH-2D velocities at the Left Pier location, but were higher at

the Right Bank Location. Velocities for the larger events were lower at the US Bridge location, but were the same for the 2-year event, which is an in channel event. The difference in velocity was less than 1 ft/s at all locations except the US Bend location. This location is upstream of a significant meander bend, and at higher flows a significant amount of flow leaves the channel and flows in the overbank. This could cause larger variations in computed velocities.

Table 4. Comparison of Maximum Velocity Magnitudes (ft/s), SRH-2D vs. HEC-RAS

Location	2007 Event			2-year Event			100-year Event		
	SRH	RAS	Diff.	SRH	RAS	Diff.	SRH	RAS	Diff.
Left Pier	7.26	6.82	-0.44	4.69	4.54	-0.15	7.73	7.03	-0.70
Right Pier	5.02	4.25	-0.77	0.85	1.10	0.25	7.25	7.42	0.17
US Bridge	5.56	4.66	-0.90	4.31	4.31	0.00	5.68	4.87	-0.81
Right Bank	10.36	11.31	0.95	N/A	N/A	N/A	11.21	11.97	0.76
US Bend	4.70	2.94	-1.76	5.11	4.06	-1.05	4.99	6.23	1.24
Near Mill	5.66	4.77	-0.89	5.25	5.87	0.62	5.68	5.99	0.31

Velocity vectors and magnitudes near the peak velocity for each event are shown in Figures 4 through 9. For the higher flow events (2007 and 100-year) both models calculated higher flow velocities on the inside of the bend upstream of the bridge and on the left overbank downstream of the bridge. For the lower flow 2-year event, again both models show increased velocity on the inside of the bend and also near the left bridge pier.

Near the bridge, both the 2007 event and the 100-year event have very similar flow paths and velocity distributions between the two models. The 2-year event had similar velocity distribution also, but an analysis of the flow paths shows that the RAS model has more flow towards the center of the channel, while the SRH results show more flow pushed towards the inside of the bend. The SRH model also shows a large eddy on the outside of the bend which is not nearly as pronounced in the RAS model.

Upstream of the bend, during the 100-year event, both models show that a majority of the flow leaves the main channel and flows overland towards the bridge. However, the RAS model shows a more even distribution of flow both leaving the channel and flowing across the floodplain, whereas the SRH model has a large portion of flow leaving the channel further upstream of the bend, and then flowing through a depression on the south side of the flood plain. This could explain why the RAS velocity was much higher at the US Bend location, since the majority of flow would have left the main channel before reaching the comparison point in the SRH model. For the 2 year event, the RAS model had more flow on the right side of the channel compared to the SRH modeling results, which could also explain why the velocity was so much lower at the US Bend location (near the left side of the channel) in the RAS model.

Table 5 shows a comparison of the maximum shear stress computed in each model. HEC-RAS results show generally lower shear stress than SRH-2D for most locations. At the Near Mill location, HEC-RAS and SRH-2D results are essentially the same, while at the US Bend location the HEC-RAS model results are higher than the SRH-2D results for both the 2007 and 100-year events.

Table 5. Comparison of Maximum Shear Stress (lb/ft²), SRH-2D vs. HEC-RAS

Location	2007 Event			2-year Event			100-year Event		
	SRH	RAS	Diff.	SRH	RAS	Diff.	SRH	RAS	Diff.
Left Pier	0.29	0.27	-0.02	0.15	0.11	-0.04	0.31	0.22	-0.09
Right Pier	0.55	0.44	-0.11	0.04	0.05	0.01	1.04	0.93	-0.11
US Bridge	0.13	0.07	-0.06	0.08	0.06	-0.02	0.14	0.07	-0.07
Right Bank	0.32	0.29	-0.03	N/A	N/A	N/A	0.32	0.29	-0.03
US Bend	0.10	0.17	0.07	0.13	0.05	-0.08	0.11	0.17	0.06
Near Mill	0.15	0.15	0.00	0.14	0.16	0.02	0.15	0.16	0.01

Both models were run on the same computer to ensure that runtimes could be reasonably compared. The HEC-RAS model took less time to run than the SRH-2D model for all three simulations, as shown in Table 6.

Table 6. Comparison of Computation Times (hours), SRH-2D vs. HEC-RAS

	SRH	RAS	Diff.
2007 Event	11.5	7.2	-4.3
2-year Event	12.7	7.3	-5.4
100-year Event	13.3	9.1	-4.2

We also ran the 2007 event in the HEC-RAS model with a 3 second time step to test if changing the time step would have any significant impact on the model results. Table 7 shows the results using a 3 second time step compared to the SRH-2D results. We found that the WSE was within half a foot of the SRH-2D results at all locations, and the shear stress was lower in the RAS model at the locations near the bridge, and higher and the two more upstream locations. However, there was more variability in the velocity comparisons. The HEC-RAS velocity model results were lower at both pier locations and at the US Bridge location, but were higher at the other three locations. Velocities at all locations were within one foot per second of the SRH-2D model results, except at the US Bend location.

Table 7. Comparison of WSE, Velocity, and Shear Stress for the 2007 Event
Using a 3-second timestep

Location	WSE			Velocity			Shear		
	SRH	RAS	Diff.	SRH	RAS	Diff.	SRH	RAS	Diff.
Left Pier	18.21	18.49	0.28	7.26	6.90	-0.36	0.29	0.22	-0.07
Right Pier	16.88	17.32	0.44	5.02	4.18	-0.84	0.55	0.45	-0.10
US Bridge	18.54	18.90	0.36	5.56	4.65	-0.91	0.13	0.07	-0.06
Right Bank	17.04	17.32	0.28	10.36	11.16	0.80	0.32	0.28	-0.04
US Bend	20.35	20.58	0.23	4.70	6.18	1.48	0.10	0.17	0.07
Near Mill	19.39	19.64	0.25	5.66	6.01	0.35	0.15	0.16	0.01

Table 8 shows the comparison of the HEC-RAS results using both the 1-second and 3-second time steps. We found that the HEC-RAS results are not sensitive to the computational time step near the bridge, but there is some variation in the WSE and Velocity at the two more upstream locations. At both locations the 1-second run had higher WSE and lower velocities than the 3-second run. The shear values were similar at all locations except the left pier.

Table 8. Comparison of HEC-RAS results using 1-second and 3-second time steps.

Location	WSE			Velocity			Shear		
	1 sec	3 sec	Diff.	1 sec	3 sec	Diff.	1 sec	3 sec	Diff.
Left Pier	18.50	18.49	-0.01	6.82	6.90	0.07	0.27	0.22	-0.05
Right Pier	17.31	17.32	0.01	4.25	4.18	-0.07	0.44	0.45	0.01
US Bridge	18.92	18.90	-0.02	4.66	4.65	-0.01	0.07	0.07	0.00
Right Bank	17.27	17.32	0.05	11.31	11.16	-0.16	0.29	0.28	-0.01
US Bend	20.99	20.58	-0.41	2.94	6.18	3.23	0.17	0.17	0.00
Near Mill	20.21	19.64	-0.57	4.77	6.01	1.24	0.15	0.16	0.01

Summary and Recommendations

Overall, the HEC-RAS model and SRH-2D model produced similar results at all six locations of interest, and the flow paths and flow distribution were similar between the two models as well. The HEC-RAS model generally showed slightly higher water surface elevations and lower shear stress, but there was not a general pattern for the velocity differences between the two models.

While this phase of work did not include a thorough investigation and explanation of why the model results are different, there are several simple reasons for the minor differences. One possible reason for the difference in results is that the HEC-RAS model was not specifically calibrated, but all roughness values were taken from the existing SRH-2D model. We understand that the SRH-2D model and HEC-RAS model apply roughness to the computational mesh differently. The SRH-2D model applies the roughness value to the cell itself while the HEC-RAS model applies it at the cell faces. This could require an adjustment of HEC-RAS parameters to account for the differences. In future phases, we also recommend we investigate if the two models apply roughness in different ways in the equations. Other possible reasons include the ability of HEC-RAS to use underlying terrain to apply subgrid calculations, different applications of eddy viscosity, or difference in the numerical schemes of the two models.

We found that the HEC-RAS model took less time to run than the SRH-2D model for all three events. In the HEC-RAS model simulations for this study, we set the computation interval in the HEC-RAS model to 1-second in an effort to match the SRH-2D model runs. However, the HEC-RAS model may be able to run with larger computational intervals without negatively affecting the results. Because of this, as part of future work we recommend performing full sensitivity tests on the HEC-RAS model computation interval.

As was stated in the introduction, this study is only the first step in a comparison of SRH-2D and HEC-RAS 2D. The purpose of this comparison was to see how the results of the two models

compare when the same computational mesh is used. The purpose was not to determine whether one model is better than the other. We did not adjust the mesh to account for the different computational methods used in HEC-RAS vs. SRH, nor did we make adjustments to the mesh where it seemed the initial mesh was not set up in the most optimal way. However, we recommend making these adjustments in subsequent phases. Some of these adjustments would include adding break lines in the HEC-RAS model to account for elevation features; adjusting the upstream boundary condition to better represent high flows; and performing sensitivity analyses on model parameters such as roughness, inflow boundary slope, and time step to determine how the results are affected.

References

Washington Department of Transportation (WSDOT). 2010. "Hydraulics Manual", Publication Number M 23-03.03.

WEST Consultants, Inc. 2015. "SR 107/4 Bridge and Chehalis River Flood Authority Flood and Scour Mitigation Analysis", Unpublished Report prepared for WSDOT.
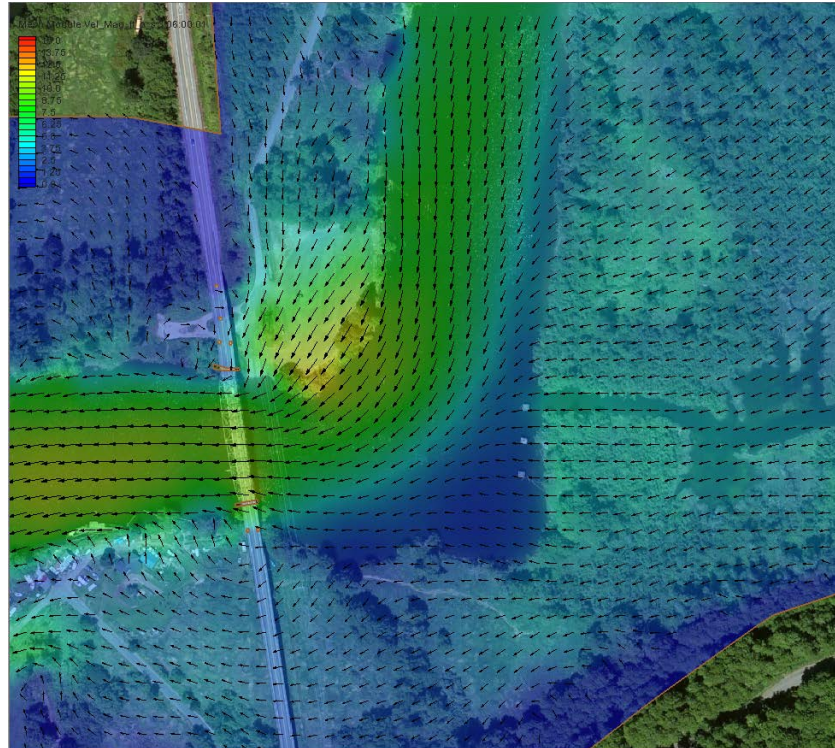
Figure 4. SRH-2D Velocity Magnitude and Vectors – 2007 Event.
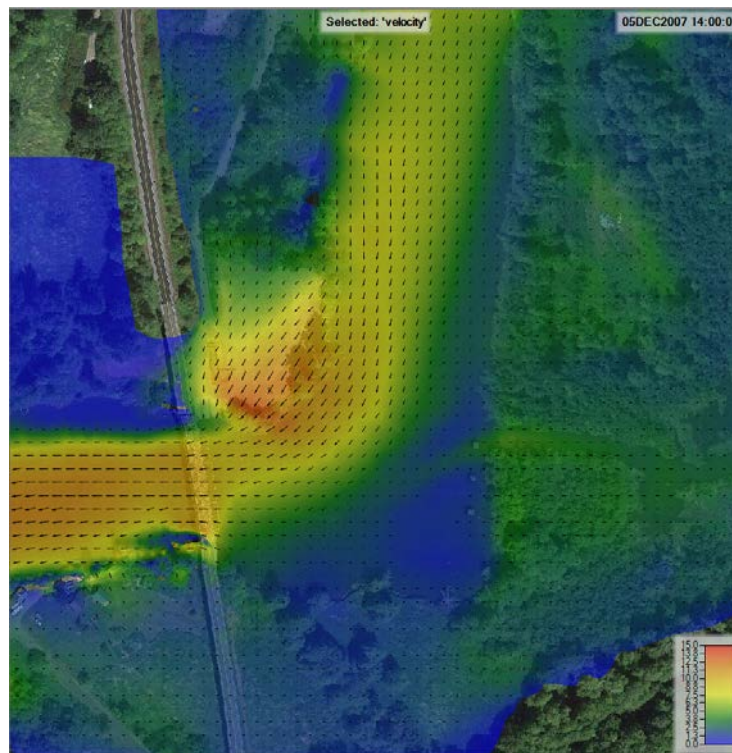
Figure 5. HEC-RAS Velocity Magnitude and Vectors – 2007 Event.
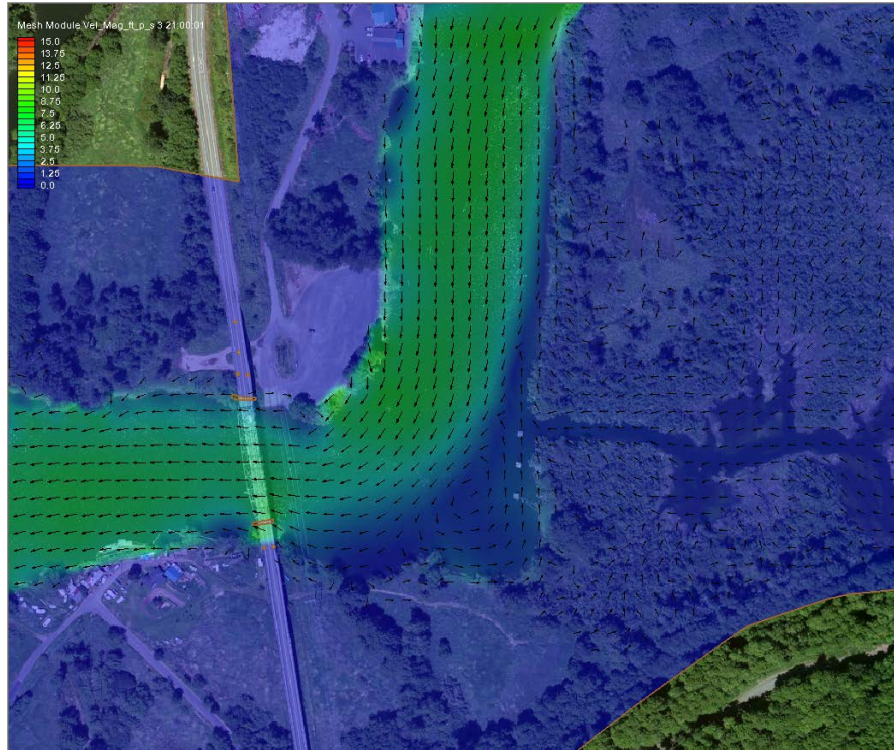
Figure 6. SRH-2D Velocity Magnitude and Vectors – 2-year Event.
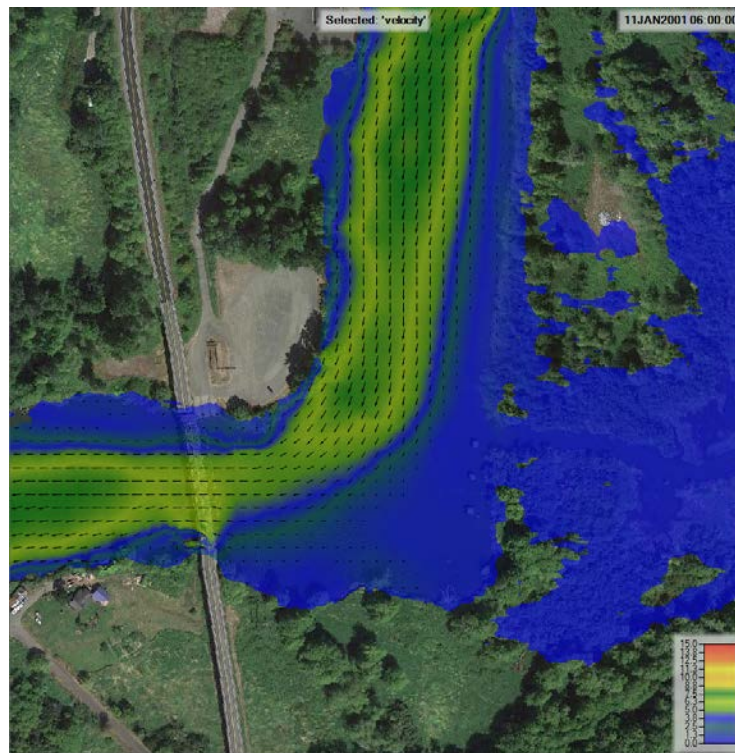
Figure 7. HEC-RAS Velocity Magnitude and Vectors – 2-year Event.
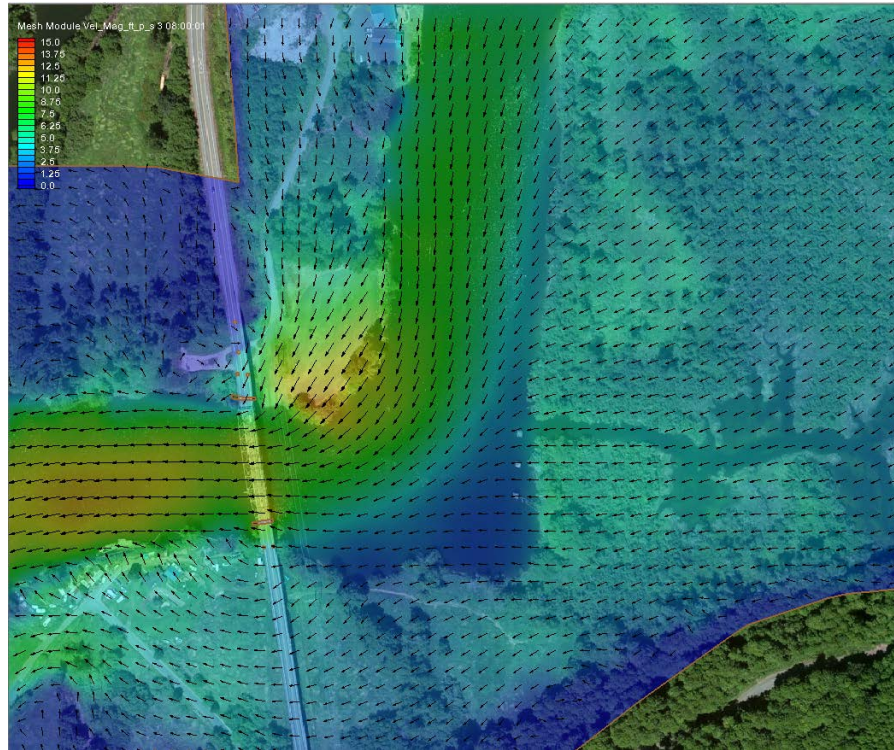
Figure 8. SRH-2D Velocity Magnitude and Vectors – 100-year Event.
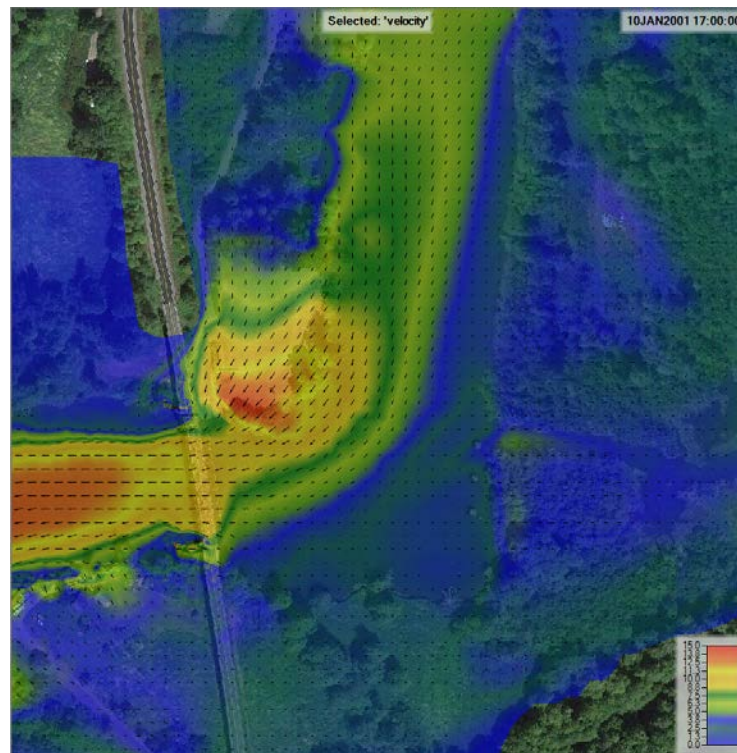
Figure 9. HEC-RAS Velocity Magnitude and Vectors – 100-year Event.

Hydraulic Assessment of Notched River Training Structures Near Island 63

Edmund M. Howe, P.E., CFM, Chief, Hydrology & Hydraulics, United States Army Corps of Engineers, Little Rock, AR, Edmund.M.Howe@usace.army.mil
Roger A. Gaines, P.E., Ph.D., Hydraulic Engineer, United States Army Corps of Engineers, Vicksburg, MS, Roger.A.Gaines@usace.army.mil

Abstract

Historically, the flows in the Mississippi River carved multiple pathways to the Gulf of Mexico by creating cut-offs and secondary channels. The stabilization of the Mississippi River through the use of river training structures and revetments has impaired this natural process; consequently, it has turned secondary channels into a finite resource (Killgore, Hoover, Lewis, & Nassar, 2012). As environmental legislation gained momentum in the 1970s, the United States Army Corps of Engineers (USACE) utilized different design and construction methods to aid and restore biological and ecological diversity without causing impediments to navigation on the Mississippi River. Notching dike structures is one method employed by the USACE to sustain, restore, or create these secondary channels. Notching is the process of removing a section from the crown of the dike to alter flow, scour, and depositional patterns for environmental improvement. More research on notched dikes exists on the Missouri River and the Upper and Middle reaches of the Mississippi River than on the Lower Mississippi River (LMR). One potential reason for this imbalance of research on notched dikes is that the LMR generally has a less developed floodplain than do the other systems. Ease of access to collect sufficient amounts of pertinent data for research on notched dikes can be more difficult and more expensive on the LMR than on the Missouri River and the Upper and Middle Mississippi River reaches. The LMR is also uncontrolled –meaning there are no reservoirs. The lack of control results in potentially wider variations in not only flow rate but also sediment transport. Designing a notched dike for these wide variations can be challenging, especially without the availability of ample data and research. This increases the need for alternative methods such as numerical models for assessing the performance of the notched training structures. The Island 63 reach in the LMR contains multiple notched dikes suitable for study and detailed investigation.

Classifying existing notched structures and determining optimal designs for new notches without the use of detailed, multi-dimensional, hydrodynamic and sediment transport models is possible. Limitations to this approach include documentation of the notch geometry, location type, reach type, upstream and downstream controlling features and elevations. Classification requires enough data to correlate and differentiate between objects or in this case seven notched dike structures. However, the performance of the seven structures in this study can be used as references for design. It can also be used as the beginnings of classification to construct a more comprehensive database to develop correlations between hydraulic performance and environmental variables. The use of multi-dimensional hydrodynamic models without sediment transport is becoming faster and more accessible which would provide additional variables such as velocity and flow rates to draw even better correlations with aquatic wildlife habitat field surveys.

A quasi-three-dimensional Adaptive Hydraulics/SEDLIB model (hydrodynamic model with sediment transport) was assembled and used to provide a hydraulic assessment of seven notched river training structures in the Lower Mississippi River The ADH model was simulated in version 4.5 utilizing Surface-water Modeling System (SMS) software version 11.1 for terrain processing and mesh development. Various text editors such as Notepad ++ ©, Notepad 2 ©, and WinMerge © were used to aid in model development. MatLab © was also essential for post-processing much of the output datasets. Due to the intensive computational nature of such an extensive ADH model, simulations were performed on Topaz, the High Performance Computer housed at the Engineering Research and Development Center in Vicksburg, MS. The model domain extends approximately 15 to 20 river miles upstream and downstream of Island 63 with a total reach length of 36 river miles. The base mesh consists of 105,981 nodes and 210,861 elements. The model extends the width of the floodplain (levee to levee) for approximately 32 river miles. Model mesh elevation data were a composite of several survey sources from the years 2004 and 2005 including bathymetric surveys of the river channel and Light Detection and Ranging (LiDAR) surveys of the floodplain (Figure 1). River training structure elevations were obtained from original design drawings or from latest available surveys where applicable. River training structures may have settled or may have sustained slight damage during high water events, but no notable changes or damages that would impact the integrity of the structures were known from any inspection trip at the time of this analysis. The 2013 channel sediment particle distributions were available from Gaines and Priestas (2015).
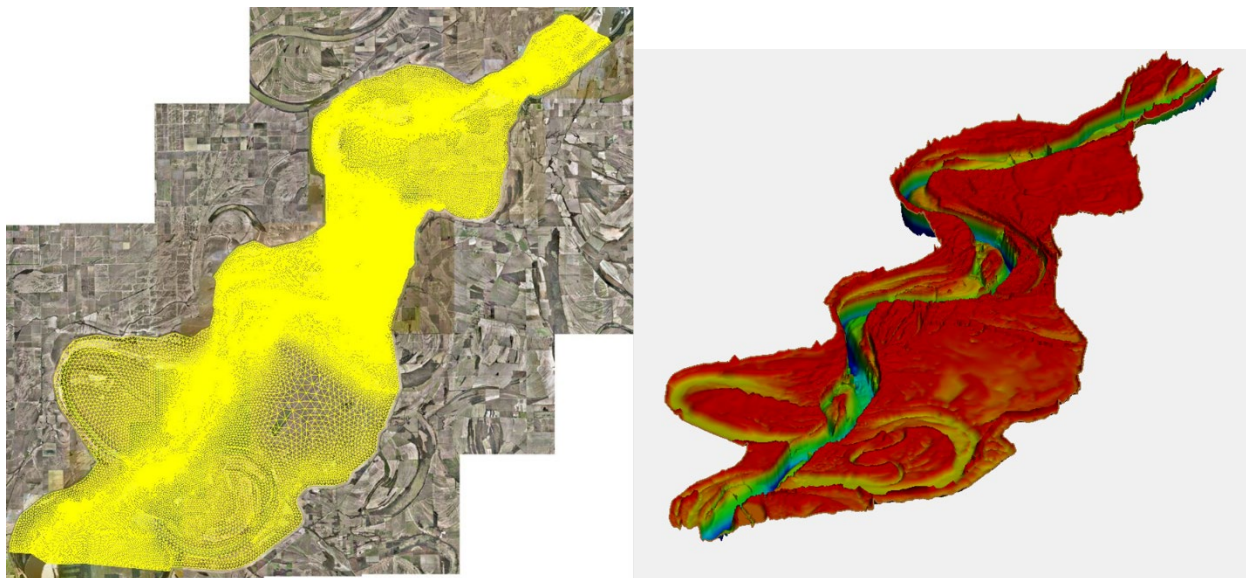
Figure 1. Model Mesh and Elevations

The hydraulic assessment of the seven notches (Figure 2) included assessing the impacts to navigation, the long-term trends, and the potential for increasing aquatic wildlife habitat diversity. The impacts to navigation due to diverting flow through the notched structures are minimal. In the long-term, the restored areas in the proximity of the notches appear to be sustainable with the exception of one structure. However expectations regarding what constitutes "restored" should be clearly understood and communicated. It is nevertheless possible to determine a design for a notch that can achieve a reasonable restoration goal. Restoration goals can range from simply improving connectivity to the river from existing conditions to fully developing a sustainable secondary channel. An understanding of the minimum and maximum expectations for an existing dike notch or a new dike notch is essential

in defining a reasonable restoration goal. Additional aquatic habitat research is needed to correlate particular habitats with the associated favorable hydraulic conditions that produce that habitat. This additional research would help to refine a notch design that is within reasonably defined restoration goals (typically physical limitations of the existing site) for a target type of habitat.
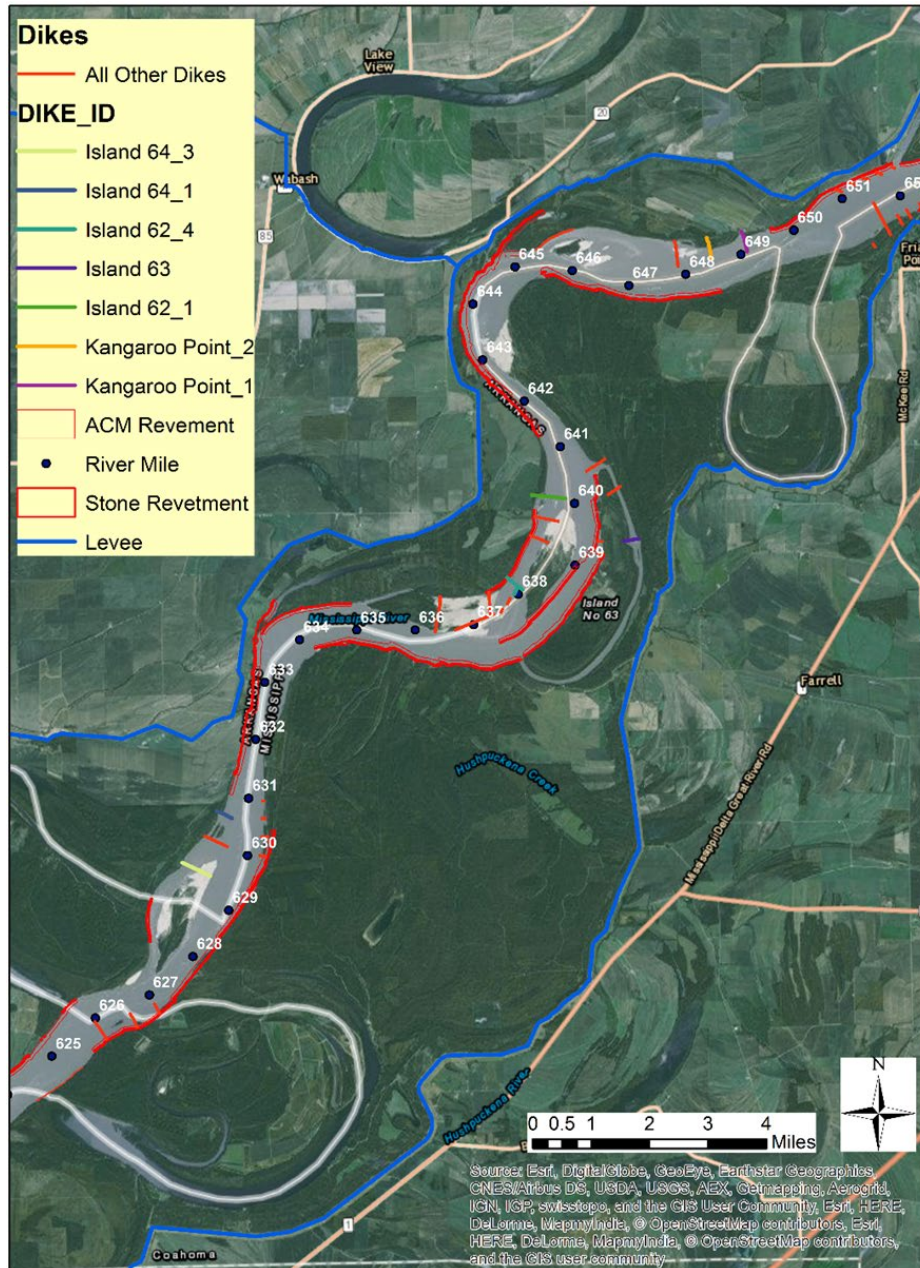
Figure 2. Plan View of River Training Structures

Significant Findings

From the hydraulics assessment of seven notched dike structures within the Island 63 reach some conclusions were drawn about them specifically and other recommendations inferred or extrapolated that can assist in developing a comprehensive evaluation process of existing notched structures and provide insights to design of new notched structures.

1) Overall, the main channel flow for the purposes of navigation do not appear to be negatively impacted by notching. A low percentage of flow compared to the main channel flow gets diverted through the notch (Table 1).

Table 1. Percentages of main channel flow rate

Simulated Flow Rate, kcfs	300	400	500	600	700	800	900	1,000
Exceedance Frequency, %	74%	58%	45%	34%	25%	19%	13%	9%
Structure	Percentage of Main Channel Flow							
Kangaroo Point Dike 1	0.0%	0.2%	0.7%	1.3%	1.9%	2.5%	3.0%	3.4%
Kangaroo Point Dike 2	0.0%	0.0%	-0.1%	-0.3%	0.1%	0.6%	1.1%	1.6%
Island 62 Dike 1	0.0%	0.1%	0.4%	1.4%	2.5%	3.6%	4.1%	4.5%
Island 62 Dike 4	0.0%	0.0%	0.1%	0.3%	0.3%	1.0%	1.5%	1.8%
Island 63 Dike 6	0.0%	0.5%	1.4%	2.0%	2.2%	2.0%	2.1%	2.2%
Island 64 Dike 1	0.0%	0.2%	0.5%	0.7%	0.9%	0.9%	1.0%	1.0%
Island 64 Dike 3	0.0%	0.1%	1.0%	1.2%	1.2%	1.2%	1.1%	1.1%

2) Five of the seven structures fluctuated about an equilibrium in the long-term assessment indicating that their connectivity to the river in terms of flow is neither increasing nor decreasing significantly. These are listed below:
   a) Island 62 Dike 1
   b) Island 62 Dike 4
   c) Island 64 Dike 1
   d) Kangaroo Point Dike 1
   e) Island 63 Dike 6

3) The analysis of Island 64 Dike 3 structure indicated a decreasing connectivity to the river in terms of flow. This structure has a significant deposition upstream of it that is approximately 4 feet higher than the notch invert. Island 64 Dike 2 is just upstream and is not notched which restricts flow to the notch in Dike 3. Notching of Dike 2 could help alleviate the decreasing connectivity (Figure 3).
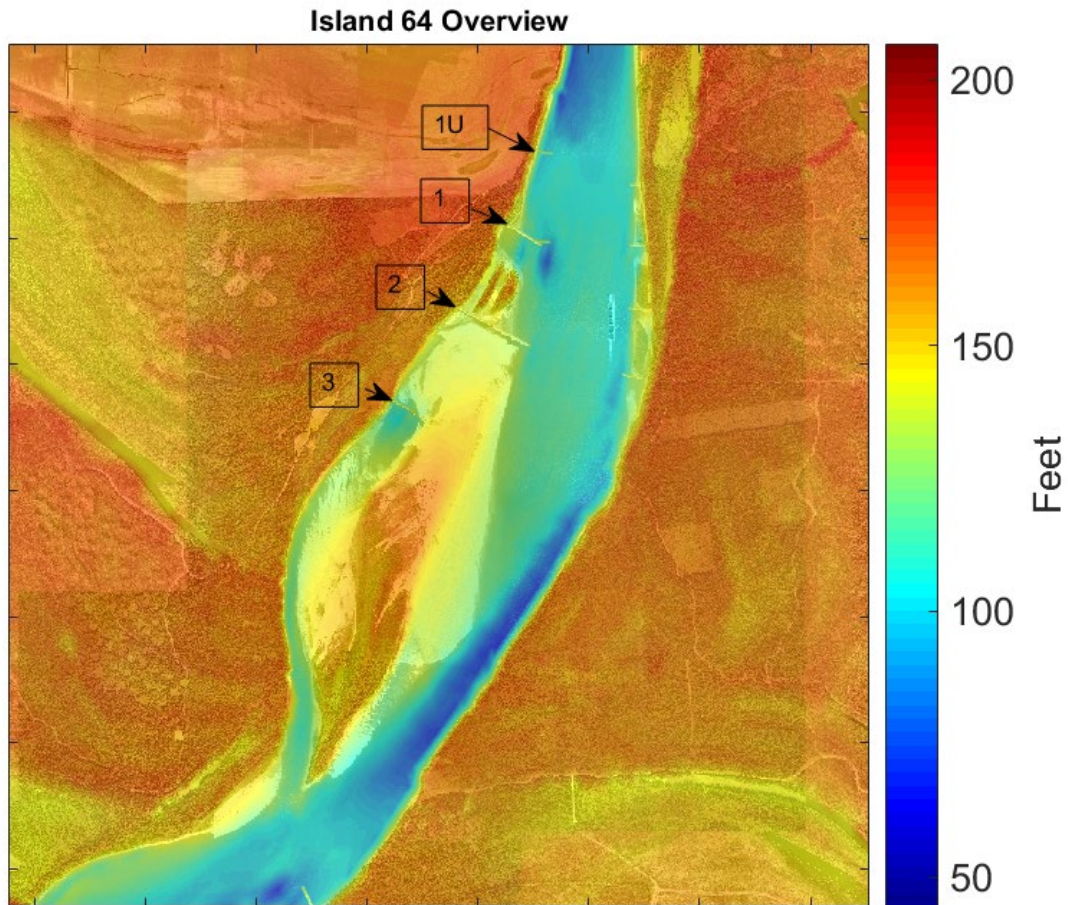
Figure 3. Island 64 Overview

4) The analysis of Kangaroo Point Dike 2 indicated an increasing flow connectivity to the river. This structure can see concentrated flows from the notched dike just upstream, and it can have flow through its notch through a lateral connection to the river (in between the dike field). Having multiple possible paths for flow to access the notch in tandem with lower elevations of deposits downstream indicated a higher likelihood of a more defined channel forming Figure 4.
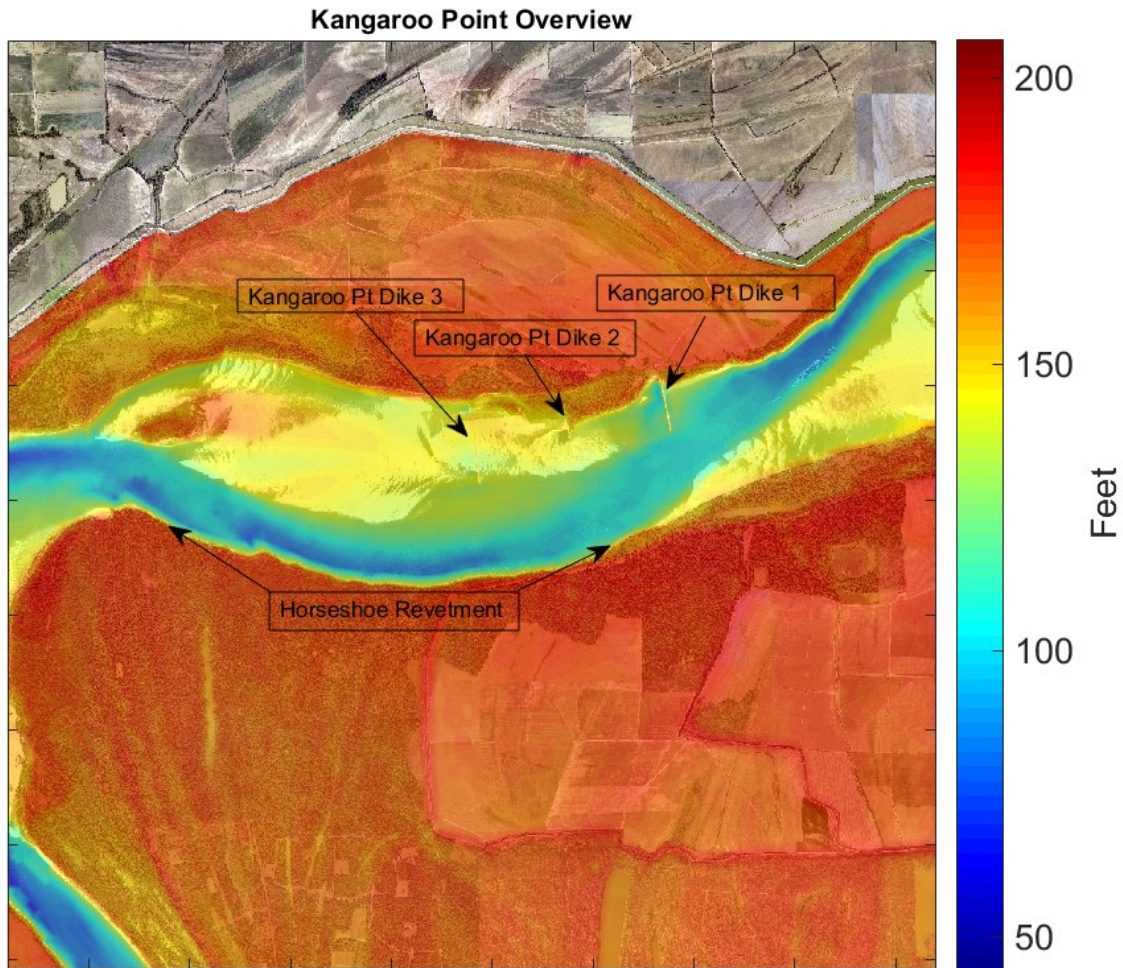
Figure 4. Kangaroo Point Overview

5) Evaluating notched structures should follow a process which identifies key variables that can eventually be used to make more refined correlations with aquatic habitat research, document negative impacts to navigation, and assist with assessing long-term sustainability. Key variables are given as a through m below. Variables a-h can be readily obtained without complex, multi-dimensional modeling. Variables i through m require more complex modeling efforts but could be used to target specific habitats.

    a) Completion date of the training structure
    b) Completion date of the training structure notch
    c) Reach type
    d) Location type
    e) Notch invert
    f) Notch area
    g) Upstream and downstream controlling features and elevations
    h) Flow and frequency of the Mississippi River to achieve notch flow
        (1) This can be approximated using gage relationships or the Mississippi River one-dimensional HEC-RAS model previously developed by Mississippi Valley Division District Offices.

i)   Notch flow rates for different Mississippi River flow rates
j)   Notch and habitat velocities for different Mississippi River flow rates
k)   Habitat depths for different Mississippi River flow rates
l)   The presence of eddies for different Mississippi River flow rates
m) Trends in downstream scour as a result of notching

Each of these variables should be stored in a database that could then be utilized to help categorize and classify potential dike notching locations. Including a correlation with the type of aquatic habitat in the database would greatly aid in ranking sites for potential construction of notches.

References

Berger, R. C., Tate, J. N., Brown, G. L., & Savant, G. (2015). Guidelines for solving two-dimensional shallow water problems with the adaptive hydraulics modeling system. Retrieved from https://adh.usace.army.mil/new_webpage/main/main_page.htm.

Bernard, R.S., Schneider, M.L. (1992). Depth-averaged numerical modeling for curved channels. (Technical Report HL-92-9). Vicksburg, MS: US Army Engineer Waterways Experiment Station.

Brown, G. L., Trahan, C., J. N. Tate, & G. Savant. (2014). SEDLIB multiple grain sized mixed sediment library: technical manual. Retrieved from https://adh.usace.army.mil/new_webpage/main/main_page.htm.

Brunner, G.W. (2016). HEC-RAS river analysis system user's manual. Retrieved from http://www.hec.usace.army.mil/software/hec-ras/documentation.aspx

Burch, C. W., Abell P. R., Steven, M. A., Dolan, R., & Dawson, B. (1984). Environmental guidelines for dike fields. (Technical Report E-84-4). Vicksburg, Mississippi: US Army Engineer Waterways Experiment Station.

Chow, V.T. (1959). Open-Channel Hydraulics. New York, New York: McGraw-Hill.

Gaines, R.A., & Priestas, A.M. (2015). Particle size distributions of bed sediments along the Mississippi River, Grafton, Illinois, to Head of Passes, Louisiana, November 2013). (MRG&P Report No. 7). Vicksburg, Mississippi: U.S. Army Corps of Engineers Mississippi Valley Division.

Garcia, M. & G. Parker. (1991). Entrainment of bed sediment into suspension. Journal of Hydraulic Engineering ASCE, 117(4), 414-435.

Jordan, J. W., (2012). River training structures and secondary channel modifications, Upper Mississippi River restoration environmental management program environmental design handbook (7-1–7-78). Rock Island, IL: U.S. Army Corps of Engineers.

Killgore, K. J., J. J. Hoover, B. R. Lewis, & R. Nassar. (2012). Ranking secondary channels for restoration using an index approach. (EMRRP Technical Notes Collection. ERDC TN-EMRRP-ER-15). Vicksburg, MS: U.S. Army Engineer Research and Development Center. Retrieved from http://el.erdc.usace.army.mil/emrrp/techran.html

Lane, E. W. (1947). Report on the subcommittee on sediment terminology. Transactions, American Geophysical Union. 28(6):936–938.

Martin, J.L. & McCutcheon, S.C. (1999). Hydrodynamics and Transport for Water Quality Modeling. Boca Raton, Florida: CRC Press.

McNutt, D. L. (1977). Stabilizing the island 63 reach, Mississippi River. ASCE Spring Convention and Exhibit. American Society of Civil Engineers: Dallas, TX.

Radspinner, R. R., Diplas, P., Lightbody, A. F., & Sotiropoulos, F. (2010). River training and ecological enhancement potential using in-stream structures. Journal of Hydraulic Engineering, 136(12), 967-980. doi: 10.1061/(ASCE)HY.1943-7900.0000260

Shields, F. D. (1995), Fate of lower Mississippi river habitats associated with river training dikes. Aquatic Conservation Marine and Freshwater Ecosystems, 97–108. doi:10.1002/aqc.3270050203

Simon, A., Doyle, M., Kondolf, M., Shields, F.D., Rhoads, B. and McPhillips, M. (2007), Critical evaluation of how the Rosgen classification and associated natural channel design methods fail to integrate and quantify fluvial processes and channel response. Journal of the American Water Resources Association, 43: 1117–1131. doi:10.1111/j.1752-1688.2007.00091.x

Spasojevic, M., & F. Holly, Jr. (1994) Three-dimensional numerical simulation of mobile-bed hydrodynamics. (Technical Report HL-94-2). Vicksburg, MS: U.S. Army Engineer Waterways Experiment Station.

Tate, J.N. & Berger, R.C. (2006). ADH Sediment Module Testing. (ERDC TN-SWWRP-06-6). Vicksburg, MS: Engineering Research and Development Center.

Hydrodynamic Modeling of Extreme Flood Levels in an Estuary Due to Climate Change

JK Vonkeman, PhD Student, Department of Civil Engineering, University of Stellenbosch, Stellenbosch, South Africa
O Sawadogo, Hydraulic Modeler & Researcher, Department of Civil Engineering, University of Stellenbosch, Stellenbosch, South Africa
DE Bosman, Senior Coastal Engineer, Department of Civil Engineering, University of Stellenbosch, Stellenbosch, South Africa
GR Basson, Professor, Head: Water Division, Department of Civil Engineering, University of Stellenbosch, Stellenbosch, South Africa, grbasson@sun.ac.za

Abstract

The determination of extreme flood levels in an estuary should consider river floods and waves penetrating the estuary. The Breede River estuary in South Africa, 50 km in length, is discussed as case study in this paper. A two-dimensional hydrodynamic model Mike21C of the DHI Group of the 50km estuary (including the estuary mouth) was set up and calibrated against historical flood levels (1906 and 2008), and field data (tidal level, flow velocities and sediment transport) obtained during 2017. The model was then used to route the 100-year flood with a peak of 3789 m³/s through the entire estuary. The flood included an increase of 15% for future climate change. Open and initially closed estuary mouth conditions were investigated with the movable bed model. For future climate change scenarios the initial closed estuary mouth berm crest level was selected as 3.5 masl and the hydrodynamic model simulated the breaching of the berm as the flood hydrograph was routed through the estuary. Based on the 2013 AR5 report of the IPCC sea level rise predictions due to climate change, sea level rise values of 0.5 m and 1.0 m in 50 and 100 years' time respectively, were assumed for the study. The initial estuary bed levels were also raised correspondingly along the full length of the estuary for the future scenarios due to expected sediment deposition.

The tidal boundary in the hydrodynamic model was set constant at the respective recurrence interval maximum tidal levels (based on observed data) and a long wave with a height of 0.7 m and a period of 180 s was also specified at the open boundary to include the effect of infragravity waves associated with wave grouping of shorter period stormy waves. (The penetration of the shorter period stormy waves into the estuary and associated wave runup were treated separately). From the output of the MIKE21C model the maximum simulated water levels in the model domain were obtained, and the velocity heads were added, to obtain the energy levels which account for turbulent flow wave action. In order to determine the floodline levels for the Breede River Estuary, the runup of the shorter period stormy waves on the estuary banks were also obtained by modelling the penetration of the shorter period stormy waves with SWAN and the consequent wave runup was then determined with empirical methods. The final floodline levels were determined by adding the wave runup heights of the shorter period stormy waves to the maximum routed flood levels.

Short period waves originating from deep sea (swell) in combination with locally generated wind waves can penetrate an open estuary mouth and therefore can contribute to more extensive flood

levels when its consequent wave runup is superimposed on a concurrent river flood level. For this purpose, waves from the most critical direction causing maximum penetration into the lower estuary (i.e. waves from the east-southeasterly direction) were transferred from deep sea through an open mouth into the estuary by means of the nearshore wave model, SWAN. The transfer of the east-southeasterly swell from deep sea was done concurrently with a local wind blowing from the same sector over the entire SWAN model area. The resultant wave penetration into the estuary was therefore a combination of deep sea swell and locally wind generated waves. The 100-year wave and wind conditions were used to determine the spatial distribution of the penetrated wave conditions in the estuary and its consequent wave runup at eight locations in the lower estuary. The highest flood line level (flood energy level plus wave runup height) of 8.1 masl was calculated near the mouth for the future climate change scenario, 100 years from the present.

Keywords

Extreme flood, climate change, flood routing; estuary, wave penetration; wave runup

Introduction

The determination of extreme flood levels in an estuary should consider river floods and waves penetrating the estuary. Floodlines were determined for the Breede River estuary in the Western Cape, South Africa, from about 10 km upstream of Malgas to the mouth at Witsand, which is discussed as a case study in this paper (Figure 1). The scope of work includes flood hydrology determination, field work for hydrodynamic model setup and calibration, hydrodynamic modelling of flood levels caused by extreme floods, but also considering wave penetration through an open mouth during storms. Climate change was accounted for in future scenarios by modelling the sea level raised by 0.5 m and 1.0 m in 50 and 100 years' time respectively.

Figure 1. Location of the study area in Africa

Field Measurements

Three different aspects of field work were done for the setup and calibration of the hydrodynamic modelling:
1. Local residents and representatives of the Malgas and Witsand communities identified reliable historical flood markers along the Breede River Estuary which were surveyed by a Trimble GPS. A total of nine markers were measured for the 2008 flood with one

additional marker for the 1906 flood at the Malagas Church. The surveyed flood levels were also checked against the LiDAR survey data. The aerial photograph in Figure 2, provided by Mr Peter Müller illustrates the extent of the 2008 flood in the Breede River Estuary.

2. An underwater bathymetric survey of the 50km extent of the Breede River Estuary was done because no sufficiently reliable historical underwater survey data was available. The bathymetric survey was carried out from a small boat with Sontek Rivercat Acoustic Doppler Current Profiler (ADCP) equipment followed by post-processing on HYPACK software.

3. Sediment transport near the mouth of the river (bedload and suspended sediment sampling), was carried out using standard USGS equipment. Flow velocity and discharge was also measured at these five sites by the ADCP, while a Department of Water and Sanitation (DWS) pressure gauge and logger was used to record the water levels in the estuary. Finally, 25 bed sediment grab samples were collected along the full length of the estuary for grading analysis. The average median sediment size was found to be 0.35 mm, while near the mouth the marine sediment has an average median size of about 0.50 mm.

Figure 2. Aerial photograph of 2008 flood along the Breede River Estuary

Flood Hydrology and Risk

The probability of a flood peak that has a 1% chance of being exceeded in any year is described as a 100-year flood event. However, the Annual Exceedance Probability (AEP) avoids the common misconception that, for example, a 100-year flood can only occur once every 100 years. The actual risk of experiencing different flood events is summarized in Table 1. A conservative approach in the study has been assumed whereby the same recurrence interval for the flood, wave, wind and tidal level occurred simultaneously. This is not an unrealistic approach since the values for the recurrence intervals do not differ significantly. However, the joint probability of an extreme flood occurring simultaneously with an extreme wind velocity will of course be less than the selected individual probabilities of a flood and a wind velocity.

The flood hydrology was calculated by using probabilistic methods (average of the Log-Normal and Log-Pearson Type 3) of observed historical flood records. The annual recurrence interval floods used in this study for the future 50- and 100-year floods are 3196 and 3789 m³/s at the mouth, and include 15% increase for future climate change impacts and 10% for flow measurement inaccuracy. For the current scenario these floods are 2779 and 3295 m³/s, for the 50- and 100-year floods respectively.

Table 1. Probabilities of experiencing a given size flood once or more in a lifetime

Size of flood (chance of occurrence in any year) ARI/AEP	Probability of experiencing the given flood in a period of 70 years	
	At least once (%)	At least twice (%)
1 in 10 (10 %)	99.9	99.3
1 in 20 (5 %)	97.0	86.4
1 in 50 (2 %)	75.3	40.8
1 in 100 (1 %)	50.3	15.6
1 in 200 (0.5 %)	29.5	4.9

Based on field work and hydrodynamic modelling, the 1906 flood was calibrated against the flood mark at the Malagas Church and found to be 2700 m³/s. Compared to the historical flood peak data, this 1906 corresponds to about a historical 1:80 year flood event. The 2008 flood peak is estimated to be 1546 m³/s, based on the extrapolated DWS gauging station stage-discharge rating, and has an annual recurrence interval of minimum 25 years based on the historical data.

The Effect of Climate Change

Sea Level Rise

The International Panel for Climate Change (IPCC) has issued five Assessment Reports (AR) since its establishment in 1988. The projected sea level rise for the South African south coast presented in Table 2 was based on the Fifth Assessment Report (AR5) of the IPCC in 2013/14. The sea level rise projections of the IPCC are based on the 5 – 95% projection ranges of 21 CMIP5 (Coupled Model Intercomparison Project Phase 5) climate models for the 2046-2065 and 2081−2100 periods under different RCP (Representative Concentration Pathway) scenarios. It is recommended that the maximum rise in sea level due to climate change should be taken as 0.5 m and 1.0 m in 50 and 100 years' time respectively.

Table 2. Estimation of projections of sea level rise for the South African south coast

	2046 - 2065				2081 - 2100			
Scenario	Mean	Likely range			Mean	Likely range		
RCP2.6	0.28	0.20	to	0.37	0.46	0.30	to	0.64
RCP4.5	0.30	0.22	to	0.38	0.54	0.37	to	0.73
RCP6.0	0.29	0.21	to	0.37	0.56	0.38	to	0.73
RCP8.5	0.35	0.25	to	**0.44**	0.73	0.52	to	**0.95**

Change in Wind Conditions Due to Climate Change

According to the information on projected change in wind velocity due to climate change from the IPCC AR5, it is evident that the projected change in wind velocity (both for the daily averaged and 99th percentile of the daily averaged velocities) is very small on the SA south coast. However, the projected change in wind velocity in the southern ocean close to the polar zone shows an increase of about 10% for daily averaged and 5% for the 99th percentile of the daily

averaged velocities – this is probably due to the shifting of the pathways of the southern extra-tropical cyclones further south to the polar area and probable increase in wind velocity there. Based on the above information, the projected local wind velocities for the Breede River Estuary study was assumed, for the purpose of this study, not to be affected.

Change in Wave Conditions Due to Climate Change

The projected change in wave conditions due to climate change in the IPCC AR5 (Figure 13.26) indicates a very small change in the projected annual mean significant wave height (SWH) on the SA south coast – an increase of about 1%. The change in projected mean wave period is very small on the SA south coast and the change in projected wave direction is more from the south (a change of about 5° anticlockwise). Subsequent to the publishing of IPCC AR5 (2013), Wang et al. (2014) of the Climate Research Division, Science and Technology, Environment Canada, published work on projected wave height change due to climate change. This study made statistical projections of changes in ocean wave heights using sea level pressure information from 20 CMIP5 (Coupled Model Inter-comparison Project Phase 5) global climate models for the 21st century. From the information in Wang et al. (2014) it can be concluded that although the 1:10 year significant wave height is projected to increase over large portions of the globe (including the southern ocean area close to Antarctica), the projected change close to the SA south coast is very small. From the information in Mentaschi et al. (2017), [which agrees with the predictions of Wang et al. (2014)], it can be stated that the projected 1:100 year wave energy flux shows for the SA south coast a slight increase for 2050 (in the order of 2-3%) and no change for 2100. Based on the above research on projected change in wave height conditions for the period 2070 to 2099, it was assumed for the purpose of this study that the wave conditions are not altered by climate change.

Hydrodynamic Modelling of Floods

Model Setup

The 2D fully hydrodynamic model Mike 21C of DHI was used to simulate the flood levels in the Breede River Estuary. In addition, the sediment transport, erosion and deposition were modelled by a movable bed. The model bathymetry was set up by using the LiDAR data as well as the underwater survey as shown in Figure 3. The bathymetry includes the river reach extending 3km upstream of Malgas to 3km into the sea, a total length of approximately 47km. Sea bed levels were obtained from the General Bathymetric Chart of the Oceans (GEBCO). The model used a curvilinear grid 15m wide by 30m long in the flow direction and simulation time steps in the order of 1 second. The runtime for each simulation was approximately 26 hours.

Model Calibration Against Field Data

Based on the bed sediment grab samples and spring tide measurements, the hydrodynamic model was calibrated with a Manning n-value of 0.045 as representative bed roughness in the main channel. A bed roughness of 0.060 was selected for the floodplains based on the vegetation heights from the LiDAR ground and non-ground level data, which was also calibrated against the 2008 flood levels.
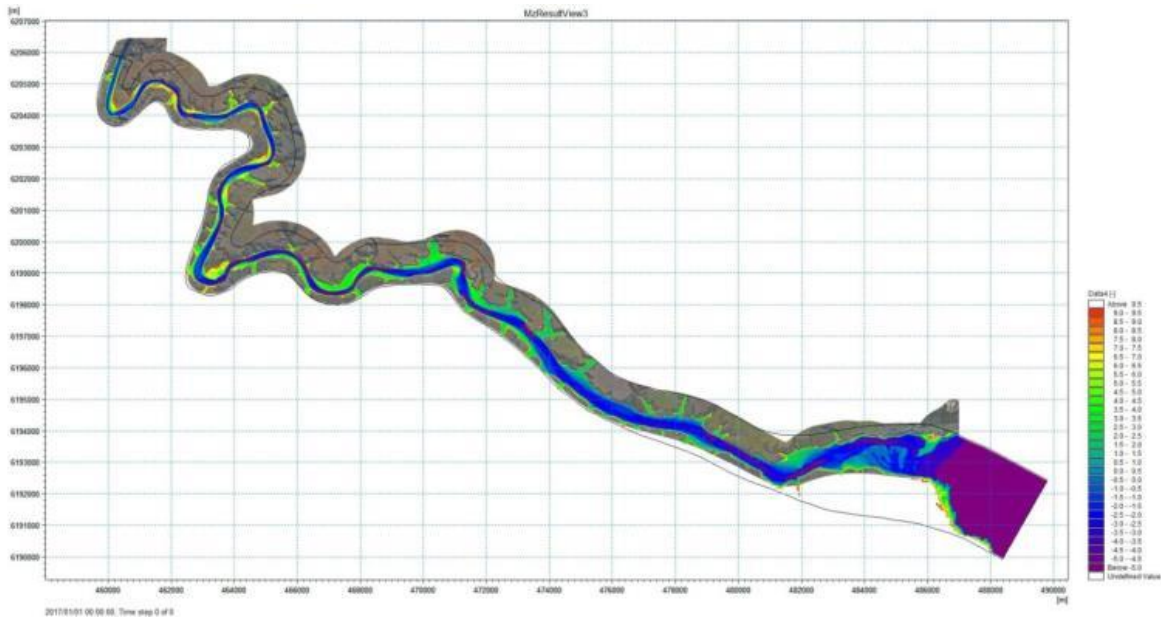
Figure 3. Bathymetry of the Breede River Estuary (masl**)**

Figure 4 shows the simulated versus observed tidal water levels in the estuary at Witsand tide gauge of DWS (H7T014). Table 3 shows the simulated bed sediment loads, flow velocities and flow depths at the flow measurement transect in the Lower Breede River Estuary, which compare reasonably well with the observed values when one compares the average values of flow depth and of bed load. The simulated flood levels in the Upper Breede River Estuary were also compared with the surveyed flood marks near Malgas for the 2008 flood as indicated in Table 4. On average the simulated flood levels are 0.26 m higher than the observed water levels and are considered acceptable. The 1906 flood was also simulated whereby an inflow discharge of 2 700 m³/s replicated the observed flood level at the Malgas church (Table 5) which could be used in the probabilistic flood analysis. There is of course some uncertainty with the 1906 simulated flood peak due to the assumption that the estuary bed was similar as in the more recent survey.
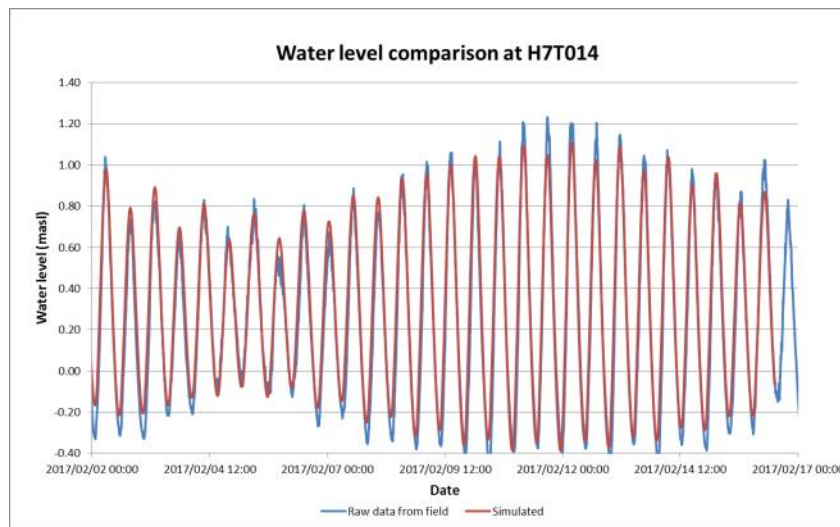
Figure 4. Calibrated water levels in the Breede River Estuary at the DWS tidal gauge H7T014

Table 3. Calibrated flow velocities, depth and bedload in the Lower Breede River Estuary

Sample sites	Flow velocity (m/s)		Flow depth (m)		Bed load (kg/s.m)	
	Observed	Simulated	Observed	Simulated	Observed	Simulated
20;21	0.73	0.49	5.20	5.74	0.0065	0.0070
22	0.75	0.51	6.40	5.82	0.0016	0.0102
23,24	0.76	0.44	5.55	4.37	0.0170	0.0087
Average	**0.75**	**0.48**	**5.72**	**5.31**	**0.0084**	**0.0086**

Table 4. Simulated 2008 flood levels compared with the surveyed flood marks

GPS Waypoint	Description	Latitude	Longitude	Observed maximum water level (masl)	Simulated maximum water level (masl)
27	De Kock Patio	34°17'50.19"S	20°34'39.32"E	7.56	8.13
28	Malagas Church	34°17'47.61"S	20°35'03.65"E	8.37	7.86
29	Malagas Hotel	34°18'01.69"S	20°35'16.79"E	7.96	7.71
30	Lemoentuin Steps	34°19'07.98"S	20°36'42.64"E	6.61	6.86
31	Rob's House	34°20'27.98"S	20°35'54.94"E	5.97	6.15
32	Diepkloof Gardens	34°21'12.16"S	20°36'03.90"E	5.17	6.04
33	Riverine Marker	34°20'49.75"S	20°36'53.11"E	5.01	5.76

Table 5. Simulated 1906 flood level compared with the surveyed flood mark

GPS Waypoint	Latitude	Longitude	Observed maximum water level (masl)	Simulated maximum water level (masl)	Simulated flood peak (m³/s)
28	34°17'47.61"S	20°35'03.65"E	10.05	10.15	2700

Model Boundary Conditions and Scenarios

A total of 18 simulation scenarios with different flood peaks and berm heights were considered as indicated in Figure 5. Climate change was accounted for in future scenarios by modelling the sea level raised by 0.5 m and 1.0 m in 50 and 100 years' time respectively. At the upstream end of the estuary, a 17 day flood hydrograph (with a shape based on the 2008 observed flood) was specified at the model boundary. While at the downstream boundary in the ocean, a constant tidal level was specified as well as a long wave with a height of 0.7 m and a period of 180 s. Maximum tidal levels of 2.07 masl and 2.16 masl were obtained for the 50-year and 100-year return intervals respectively (based on recorded tidal data at Mossel Bay from UHSLC).

Open and closed initial condition estuary mouths were simulated. While the mouth has never closed in the past, it is possible that future land use changes with climate change in the catchment could decrease the drought flow of the Breede River to such an extent and duration, that the mouth could close. The LiDAR survey indicates that the wave over wash builds the beach berm up to 2.5 masl and this is probably realistic for the current scenario. As a sensitivity test a berm crest level of 3.5 masl was, however, also simulated. The hydrodynamic model routes the flood hydrograph through the estuary, fills the lower estuary upstream of a closed initial berm, and eventually spills over the berm, eroding the sandy berm until the berm ultimately breaches. The lowest elevation of the berm crest of the closed initial mouth determines where the mouth will breach first. These lowest levels on the berm are determined by wave over wash events. For future climate change scenarios the initial closed berm crest levels will be higher. It is assumed that the sea level will rise by 0.5 m and 1.0 m in 50 and 100 years' time respectively, due to climate change. The initial estuary bed levels were also raised correspondingly for the future scenarios along the full length of the estuary.
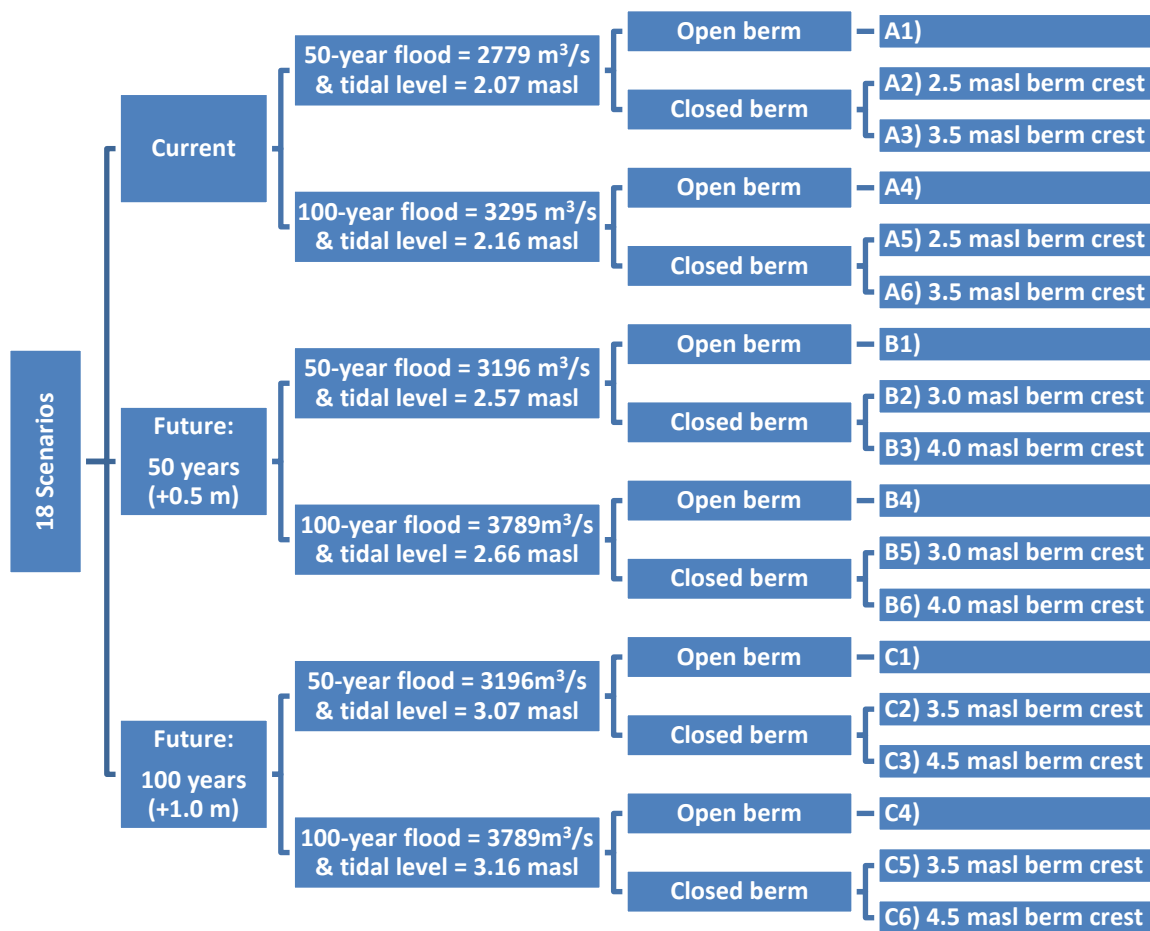
Figure 5. Hydrodynamic model scenarios

Simulated Maximum Flood Levels along the Estuary

From the output of the model simulations, the maximum water levels were obtained and the velocity head added to obtain the energy levels (to account for turbulent wave action). Figure 6 shows a long section of the simulated maximum water levels for scenario C. Note that the bed

levels are indicated for the current scenario and the berm crest is shown schematically only. The key findings from the simulation results are as follows: In the upper estuary the difference between the current and 100-year flood levels is approximately 0.9 m for Scenarios A and C. In the upper estuary the 100-year flood levels could rise by approximately 1.5 m, 100 years from now. In the lower estuary the difference between the 50- and 100-year flood levels with an initially closed berm is very small over approximately 6 km upstream of the mouth, for the current and future scenarios, and for both berm heights. In the lower estuary near the mouth the flood level can rise by approximately 1.2 m due to climate change and closed berm initial conditions, 100 years from now, for the highest berm scenario (similar to what could happen in the upper estuary). The initial crest level of an initial closed mouth condition plays an important role in the flood levels at the lower estuary. The berm breaches on the northern side near Witsand during the 50- and 100-year floods, while the southern berm remains generally intact after the flood. The simulated maximum flow velocities, as well as well as the breaching of the berm after a flood are shown in Figures 7 and 8, respectively.
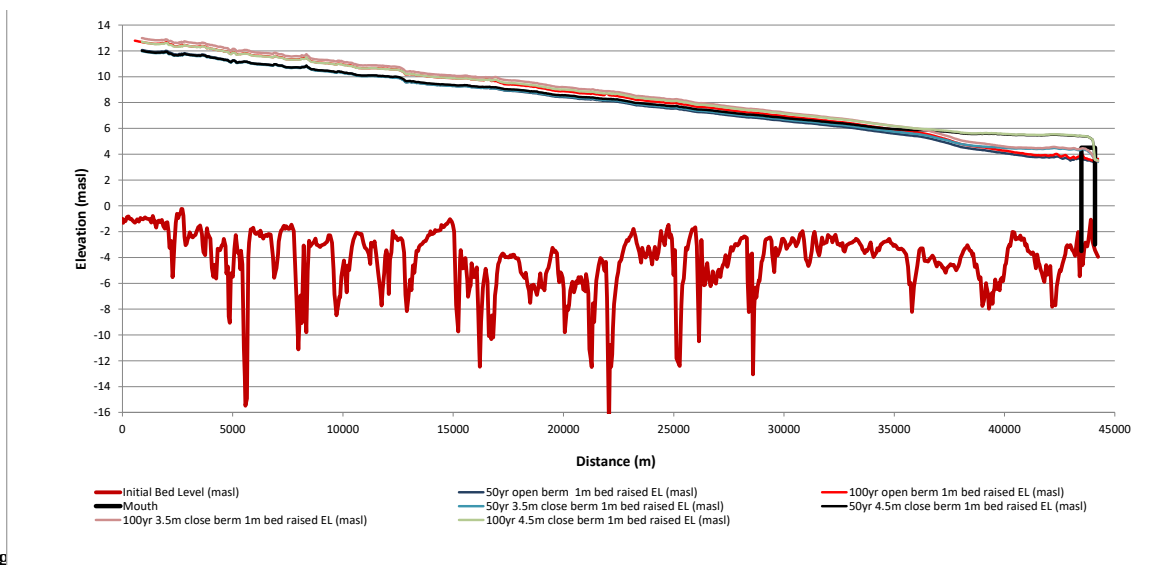
Fig ... ow)
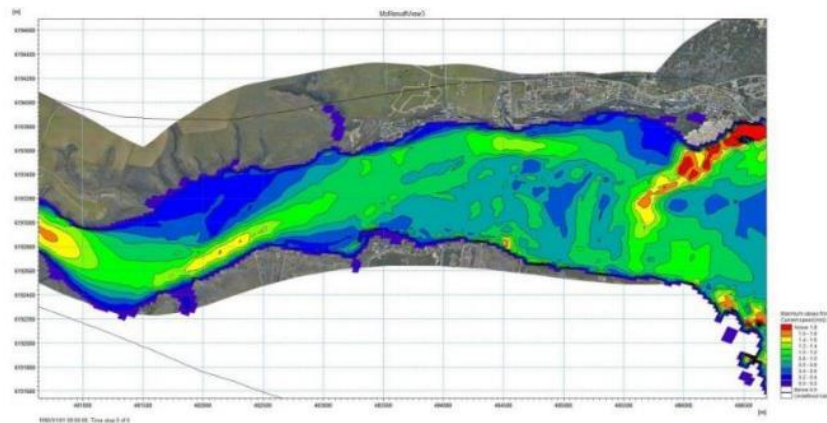
Figure 7. Simulated maximum flow velocities for current Scenario A1 in the lower estuary
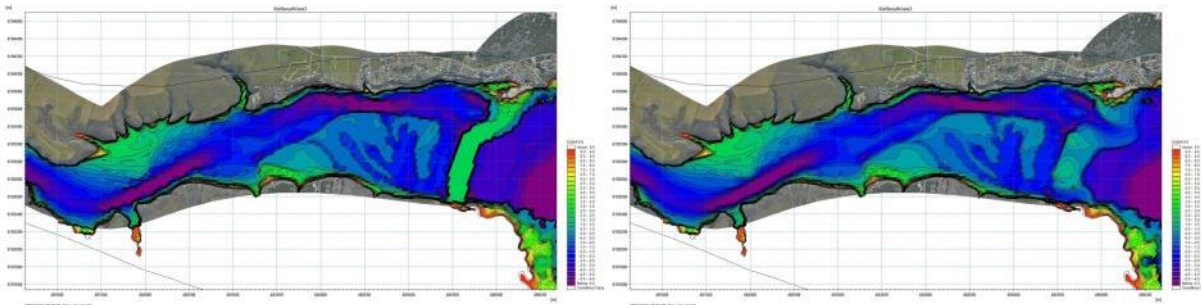
Figure 8. Simulated bed levels in the lower estuary for Scenario A5 before (left) and after (right) the flood

Simulation of Wave Heights

Background

Short waves originating from deep sea (swell) can penetrate an open estuary mouth and therefore can contribute to more extensive flood levels when its consequent wave runup is superimposed on a concurrent river flood level. For this purpose, the most critical swell direction causing maximum penetration into the lower estuary was found to be the East-southeasterly swell, which was transferred from deep sea through an open mouth into the estuary by means of the nearshore wave model, SWAN. The transfer of deep sea swell was simulated concurrently with a local wind blowing from the same sector over the entire SWAN model area. The resultant wave penetration into the estuary was therefore a combination of deep sea swell and locally wind generated waves. The 50- and 100-year wave and wind conditions were used to determine the spatial distribution of the penetrated wave conditions in the estuary and its consequent wave runup at eight locations in the lower estuary for the following flood line scenarios - (wave runup was derived with empirical methods with SWAN derived wave parameters and bank slopes):

- Scenario B1: 50-year ARI event, 50 years in the future with open estuary mouth
- Scenario B2: 50-year ARI event, 50 years in the future with closed initial estuary mouth
- Scenario C4: 100-year ARI event, 100 years in the future with open estuary mouth
- Scenario C6: 100-year ARI event, 100 years in the future with closed initial estuary mouth

Model Setup and Boundary Conditions

The main input data required by SWAN included the bathymetry and estuary water levels as per the hydrodynamic model Mike21C for the different scenarios. A nesting approach was implemented whereby the waves were first computed on a coarse grid with a 500 m resolution, covering a larger seabed region (see Figure 9). The waves were then computed on a finer grid with a 50m resolution over the smaller region of interest (nested in the larger region) by employing the boundary conditions that were generated by the coarse grid computation. This approach was deemed necessary to ensure the mesh nearshore was sufficiently refined and to ensure the boundaries were distanced sufficiently far from the area of interest in the mouth.
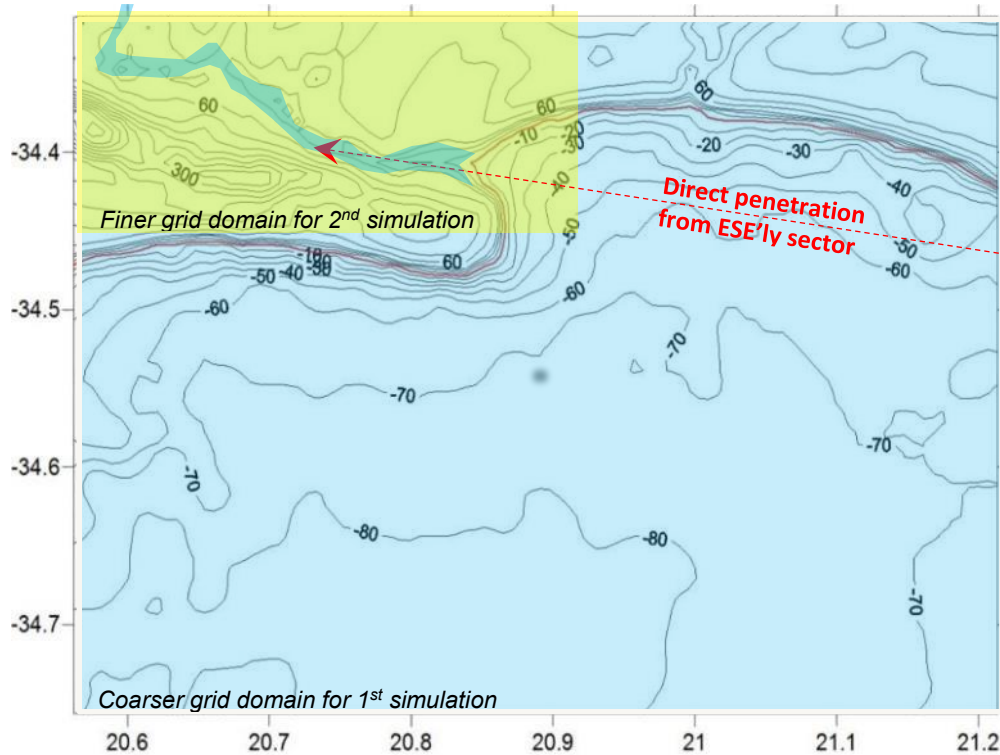
Figure 9. Seabed bathymetry from GEBCO data indicating the SWAN model domain

The following assumptions were made based on hindcast wave and wind data (ERA-Interim) from the ECMWF (European Centre for Medium-Range Weather Forecasts):

- The mouth was assumed to be completely washed open after the flood as shown in Figure 7. A Joint North Sea Wave Project (JONSWAP) spectrum with a peak enhancement factor (or wave spectrum gamma) of 1.75 and wave direction spreading of 30° specified the shape of the spectra at the computational grid boundaries.
- A significant deep sea swell wave height and mean wave period as per Table 6 with a wave direction of 110° specified the wave conditions at the wet boundaries of the coarse grid. This condition was identified as the critical swell condition for penetration into the estuary.
- Simulations were performed with a local wind blowing over the modelled area with a speed as per Table 6, with a nautical wind direction of 95°. This wind condition was initially identified as the critical locally generated condition which could be generated in the nearshore and penetrate into the estuary.

Table 6. Wind and wave conditions for the 50- and 100-year Annual Recurrence Interval (ARI) events

Annual Recurrence Interval or ARI (years)	50	100
Flood event	Q_{50}	Q_{100}
Extreme tidal levels (m)	2.07	2.16
Significant wave height (m)*	5.9	6.2
Mean wave period (sec)*	11	12
Wind speed (m/s)*	19.1	20

parameters assumed unaffected by climate change for the study area for future Scenarios B and C

Simulation Results of Lower Estuary

The resulting significant wave heights and wave direction vectors, as well as the mean wave periods, for Scenario C4 are shown in Figures 10 and 11 respectively. Similar results with a maximum significant wave height of approximately 1.5 m were generated in the estuary for all scenarios. The critical point in the estuary is located on the left bank (north) at the Breede River Lodge where the largest wave heights and periods reach the estuary banks (Location 6 in Figure 12). The increased wave heights at the small bays (Locations 6, 7 and 8) are due to the wave shoaling effect at shallow river beds. The significant wave heights and peak wave periods yielded by the SWAN simulations are summarized for the four floodline scenarios and different locations in Table 7. Locations 2 and 4 have a flat slope and shallow slope with a large period while Locations 7 and 8 have a steep slope. Note the decreased wave heights at Locations 3 and 4 which imply that the wave effects are diminished further inward towards the river. Generally, Scenario B2 yields the largest wave heights.

Table 7. Significant wave heights and peak wave periods simulated by SWAN

Scenario	Location	1	2	3	4	5	6	7	8
B1	Hs (m)	0.92	0.86	0.55	0.73	1.14	1.70	0.91	1.08
	Tp (sec)	8.80	5.87	2.84	7.44	9.10	11.12	7.53	9.47
B2	Hs (m)	1.06	1.00	0.69	1.01	1.34	2.08	1.23	1.48
	Tp (sec)	7.76	5.72	3.69	7.13	8.75	11.66	9.08	11.03
C4	Hs (m)	1.01	1.02	0.61	0.92	1.48	2.31	1.39	1.63
	Tp (s)	8.01	6.93	3.37	7.81	12.52	14.24	11.89	13.52
C6	Hs (m)	0.58	0.79	0.66	0.91	1.24	1.92	0.95	1.22
	Tp (s)	4.01	3.98	2.96	5.26	7.89	11.88	6.36	9.09
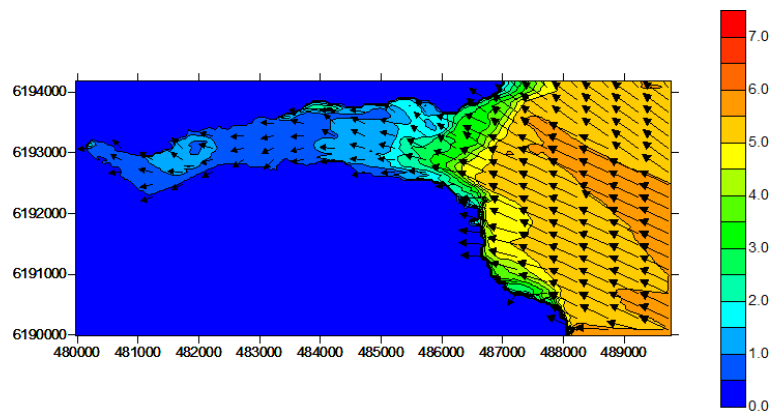
Figure 10. Contour map showing significant wave height with peak wave direction vectors for Scenario C4 (Hs in m)
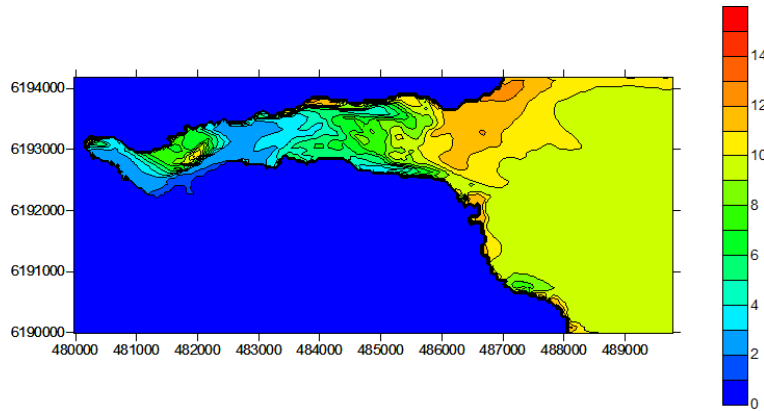
Figure 11. Contour map showing mean wave period for Scenario C4 (Tm in s)

Figure 12. Eight critical locations selected for wave runup calculations in the lower estuary

Runup Calculations

Wave runup is the extreme levels reached by oscillating waves on a slope, which is a function of wave height, wave period and bank slope, and could be more or less than the incident wave height. Wave runup for the wave height which is exceeded by 2% of the waves in the irregular wave train was derived with empirical methods at the eight critical locations. Three different empirical methods, namely EM as described in EurOtop II (2016), TAW (2002a), and Ahrens (1981), were considered to determine the wave runup for smooth slopes based on the significant wave height Hs and peak wave periods Tp simulated by SWAN. Refer to The Rock Manual (2007) (pages 487 to 517) for explanations of the methods used. The EM (2016) method is described in the EurOtop II Manual (2016) (pages 100 to 107) which states that this method may replace the other methods outlined in The Rock Manual. Therefore, for the purpose of this study the EM (2016) method took precedence over the other three methods. However, in cases where the EM (2016) method was not applicable, the average of the TWA (2002a) and Ahrens (1981) was used. The different methods produced very similar results. In addition, a reduction factor used to account for oblique wave attack at an approach angle. Table 8 gives the slope and reduction factors employed in the wave runup equations. Note that the significant wave heights yielded by SWAN account for the reduction in wave height caused by waves breaking on a shallow foreshore. Therefore, the equations for a shallow foreshore outlined in the EurOtop II Manual (2016) are not applicable.

Table 8. Slope and oblique wave attack parameters at different locations

Location	1	2	3	4	5	6	7	8
Slope tan α (%)	12.0	3.2	6.3	2.8	12.9	9.0	15.0	14.4
Wave approach direction	90°	60°	75°	10°	80°	85°	85°	80°
Reduction factor	0.82	0.87	0.84	0.98	0.82	0.82	0.82	0.82

The runup heights for the different scenarios and locations are summarized in Table 9 and are defined as the vertical height above the concurrent flood level, i.e. the flood level obtained from the Mike21C model simulations. Scenario C4 experiences the highest wave runup of up to 4.12 m, particularly at Location 8, owing to its steepness. Despite this extreme value, the runup levels diminish from an average of 2 m at the river mouth to approximately 0.5 m inland. For the upper estuary, average runup heights of 0.75 m for the 100-year flood and 0.5 m for the 50-year flood were used.

Table 9. Wave runup heights above the concurrent flood levels for the selected floodline scenarios and locations (m)

Location	1	2	3	4	5	6	7	8
Scenario B1	1.66	0.30	0.22	0.35	2.05	2.14	1.76	2.33
Scenario B2	1.57	0.32	0.32	0.39	2.14	2.48	2.47	3.17
Scenario C4	1.58	0.39	0.27	0.41	3.22	3.20	3.50	4.12
Scenario C6	0.60	0.20	0.25	0.27	1.85	2.43	1.52	2.37

Combined Flood Levels

Table 10 summarizes the Mike21C flood levels combined with the short wave runup results at the different locations in the lower estuary. The maximum water level at each location, between Scenarios B1 and B2, should be used to determine the proposed Breede River floodline for a 50-year flood. For future development, the 100-year flood is proposed, based on the maximum water levels at each location for Scenarios C4 and C6. Table 10 indicates the following: there is a relatively large range of maximum water levels depending how exposed the location is to waves; the initially closed mouth gives higher combined flood levels than the open mouth scenario; and Scenario B has higher water levels than some of the Scenario C values.

Table 10. Simulated combined river flood routed energy levels and wave runup at eight locations in the lower estuary (masl)

Location:	1	2	3	4	5	6	7	8
Scenario B1	4.38	3.38	3.66	3.90	5.31	5.35	4.86	5.36
Scenario B2	5.76	4.79	4.87	4.96	6.63	6.93	6.93	7.60
Maximum of B:	**5.76**	**4.79**	**4.87**	**4.96**	**6.63**	**6.93**	**6.93**	**7.60**
Scenario C4	4.90	4.26	4.51	4.73	7.20	7.10	7.46	8.12
Scenario C6	5.84	5.71	5.79	5.79	7.35	7.90	7.06	7.87
Maximum of C:	**5.84**	**5.71**	**5.79**	**5.79**	**7.35**	**7.90**	**7.46**	**8.12**

For existing properties and infrastructure, the maximum 50-year floodline is proposed. The floor levels of existing dwellings should be above the floodline. For any new future infrastructure development or alterations/extensions to existing properties near the estuary, it is proposed that the maximum 100-year with climate change 100 years from now floodline is implemented.

Conclusions and Recommendations

The extreme flood levels in the Breede River Estuary were determined by modelling river floods and waves penetrating the estuary. A two dimensional hydrodynamic model was set up and calibrated against 1906 and 2008 historical flood levels and field data collected in 2017. Open and initially closed estuary mouth conditions were investigated with the movable bed model. Probabilistic hydrological methods were used to calculate the 50- and 100-year floods (i.e. 3196 and 3789 m^3/s, respectively) which included a 15% increase for future climate change. The effect of climate change was further included in future scenarios 50 and 100 years from the present by raising the sea level 0.5 and 1.0 m, respectively. The initial estuary bed levels were also raised correspondingly for the future scenarios. However, the wind and wave conditions were assumed to remain unaffected by future climate change for the study site. The tidal boundary in the hydrodynamic model was set constant at the respective recurrence interval maximum tidal levels (based on observed data) and a long wave with a height of 0.7 m and a period of 180 s was also specified at the open boundary. The model simulated maximum water levels were increased with their respective velocity heads to obtain the energy levels, to account for turbulent flow wave action. In order to finally determine the floodlines for the Breede River Estuary, the short wave runup heights on the estuary banks were also determined and then added to the routed energy levels. Short waves originating from deep sea (swell) can penetrate an open estuary mouth and therefore can contribute to more extensive flood levels when its consequent wave runup is superimposed on a concurrent river flood level. For this purpose, the most critical swell direction causing maximum penetration into the lower estuary (i.e. swell from the east-southeasterly direction) was considered. The transfer of the east-southeasterly swell from deep sea into the estuary was done concurrently with a local wind blowing from the same sector over the entire SWAN model area. The resultant wave penetration into the estuary was therefore a combination of deep sea swell and locally wind generated waves. It was found that the swell and wind conditions for the 50- and 100-year recurrence intervals do not differ significantly. The 50- and 100-year wave and wind conditions were used to determine the spatial distribution of the penetrated wave conditions in the estuary and its consequent wave runup at eight locations in the lower estuary. The highest flood line level (flood energy level plus wave runup) of 8.1 masl was calculated near the mouth for the future climate change scenario, 100 years from the present.
For existing residential and other properties and infrastructure the maximum floodline levels of Scenarios B1 and B2 in Table 10 are proposed. The scenarios are based on the 50-year flood with 50-year future climate change considered, as well as an open mouth or a low closed mouth berm crest level as initial condition in order to obtain conservatively high flood levels in the lower Breede River estuary. For any new future infrastructure or development near the estuary, the maximum floodline levels of Scenarios C4 and C6 in Table 10 is implemented are proposed.

Acknowledgements

References

CIRIA, CUR, CETMEF (2013) .The Rock Manual. The use of rock in hydraulic engineering, 2nd Edition. Delft University of Technology.

ECMWF Data centre. http://www.ecmwf.int/en/research/climate-reanalysis/browse-reanalysis-datasets.

EurOtop (2016). Manual on wave overtopping of sea defences and related structures. An overtopping manual largely based on European research, but for worldwide application. Van der Meer, J.W., Allsop, N.W.H., Bruce, T., De Rouck, J., Kortenhaus, A., Pullen, T., Schüttrumpf, H., Troch, P. and Zanuttigh, B., www.overtopping-manual.com

GEBCO 30 arc-second global grid of elevations, GEBCO_2014 Grid (2014). http://www.gebco.net/data_and_products/gridded_bathymetry_data/gebco_30_second_grid/

IPCC Intergovernmental Panel on Climate Change (2013). The Physical Science Basis. Working Group I. Contribution to the Fifth Assessment Report of the Intergovernmental Panel on Climate Change. http://ipcc.ch/report/ar5/

Mentaschi, L., M. I. Vousdoukas, E. Voukouvalas, A. Dosio, and L. Feyen (2017). Global changes of extreme coastal wave energy fluxes triggered by intensified teleconnection patterns,

University of Hawaii, Seal Level Centre (UHSLC). Recorded tidal data at http://uhslc.soest.hawaii.edu/

Wang L W et al (2014). Changes in global ocean wave heights as projected using multi-model CMIP5 simulations. Climate Research Division, Science and Technology Branch, Environment Canada, Toronto, Ontario, Canada.

Isleta Island Removal Project: Interpretation of Four Years of Post-Construction Monitoring Observations Compared to Design-Phase 2D Hydraulic and Sediment Transport Model Results and Lessons Learned

Walt Kuhn, Project Manager, Tetra Tech, Albuquerque, NM, walt.kuhn@tetratech.com
Jessica Tracy, Director, Water Resources, Pueblo of Isleta, NM, poi36001@isletapueblo.com
Cody Walker, Water Rights Protection Specialist, Water Resources, Pueblo of Isleta, NM, poi36004@isletapueblo.com

Abstract

In 2011 the Pueblo of Isleta (POI) obtained a grant from the New Mexico Water Trust Board (NMWTB) to remove islands from the Rio Grande below the Isleta Diversion Dam (IDD). The IDD is one of three major irrigation works spanning the Middle Rio Grande (MRG) in Central New Mexico. Operations of the IDD and reach-scale geomorphic changes resulted in the formation of perennially-vegetated islands in the 2,000 feet downstream of the dam, impacting (1) the POI's cultural practices, and (2) habitats for federally-listed species such as the Rio Grande Silvery Minnow (RGSM) and the Southwestern Willow Flycatcher (SWFL). A primary design consideration for the Isleta Island Removal Project (IIRP) was how to create a naturally-sustained channel in a stable morphology with minimal maintenance required from the POI.

The POI selected Tetra Tech to design the IIRP, develop construction plans and specifications, prepare bid documents, and oversee construction. During the design phase of the project Tetra Tech worked with the POI to develop existing conditions and design conditions SRH-2D models, and Tetra Tech performed fixed- and mobile-boundary simulations to evaluate design alternatives.

The POI constructed the IIRP in 2014 with the goal of modifying the channel geometry on the Rio Grande in the 2,000 feet downstream of the IDD to (1) benefit the federally-listed species, specifically the RGSM, (2) remove as many islands and bars and as much sedimentation within the project site as was sustainable, and (3) maintain flow against the west bank throughout the year.

Since 2014, the POI and U.S. Bureau of Reclamation (USBR) have completed (1) geomorphic monitoring using repeat cross section surveys (most recently in 2018), (2) a 2017 high-resolution topographic-bathymetric survey, and (3) a Monitoring and Adaptive Management Plan. Currently, the POI is investigating alternatives to mitigate sedimentation around the IDD and in the canal headworks and is working with the USBR and the Middle Rio Grande Conservancy District to provide fish passage around the IDD. The efforts contribute to the sustainable operation of the IDD. The extensive monitoring, data collection, and on-going work presents a unique opportunity to evaluate how well Tetra Tech's design conditions model predicted the geomorphic change that has occurred in the 4 years following the IIRP construction.

This paper will (1) provide a history of the IIRP and follow-on projects led by the POI, including ongoing work, (2) quantitatively compare modeled geomorphic change with actual geomorphic change, and (3) discuss lessons learned.

Introduction

In 2011 the Pueblo of Isleta (POI) obtained a watershed restoration and management grant from the New Mexico Water Trust Fund (NMWTF) to remove islands from the Rio Grande below the Isleta Diversion Dam (IDD). Sedimentation downstream of the IDD is forming islands that impact (1) the POI's cultural practices and (2) habitats for federally listed species such as the Rio Grande Silvery Minnow (RGSM) and the Southwestern Willow Flycatcher (SWFL). The NMWTF recommended the IIRP for construction.

The IIRP is located within the Pueblo of Isleta in Valencia County, New Mexico (Figure 1). The boundaries of the project site (i.e., the area to be modified) begin approximately three hundred feet downstream of the IDD and extend approximately two thousand feet downstream.

The goals of the IRP were to (1) provide a benefit for the federally listed RGSM; (2) remove as many islands, river bars, and as much sedimentation as is sustainable within the project site; and (3) provide flow against the west bank throughout the year. The project design considered the accumulated sediment trapped by the IDD upstream of the project site and, as much as possible, provided for efficient transport of this material through the project site to minimize deposition through the project site. The POI contracted Tetra Tech to design the modification of the MRG that would meet the goals of the IIRP defined above while also minimizing potential future sedimentation impacts through the IIRP (Tetra Tech 2013).

Since construction was completed in 2014, several surveys have been performed. This post-construction data collection provides a unique opportunity to compare the actual geomorphic change with what was simulated in the design conditions model.

Design

The design consisted of a three-tier channel (Figure 2). The low flow channel was designed to contain flows less than 1,200 cfs. The lower bench was designed to convey flows from 1,200 to 3,000 cfs, and the upper bench was designed to convey flows over 3,000 cfs. The benches were constructed by excavating two existing bank attached bars. A rip rap spur dike was designed at the upstream end of the east terrace to force flows towards the west bank and maintain the terrace. The top of the spur dike was set at the same elevation as the top of the terraces.
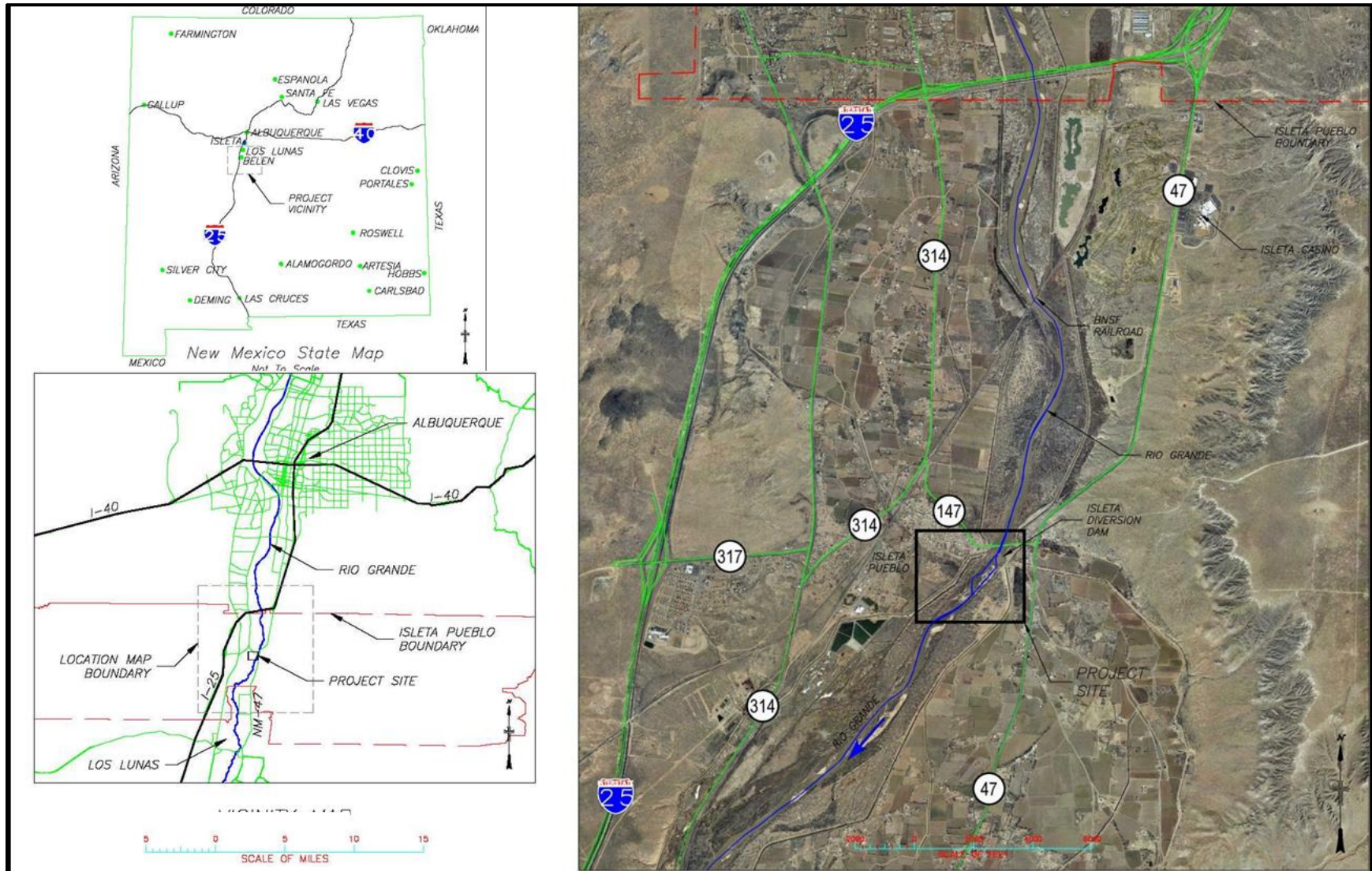
Figure 1. Study Area

Model Development

Because design involved iteratively testing different channel geometries to determine when sedimentation issues were minimized and reduced relative to existing (i.e., pre-construction) conditions, numerical modeling was used to develop the designed channel geometry. Because of the complex hydraulics in the contraction zone downstream of the IDD and because alternate and mid-channel bars were likely to form, Tetra Tech determined that a 2D, depth-averaged numerical model was necessary. The primary tool used to evaluate existing conditions and evaluate alterative design terrains was SRH-2D version 30 (Lai 2008) developed and maintained by the U.S. Bureau of Reclamation's (Reclamation) Technical Service Center's Sedimentation and River Hydraulics (SRH) Group. Existing and design conditions meshes were developed using SMS version 11.0 (Aquaveo 2012).

First, constant flow fixed-bed simulations were performed on the existing conditions model to calibrate the Manning's n-values. One single n-value for the bed sufficiently predicted water surface elevations across a range of flows (Tetra Tech 2013). Downstream boundary conditions for all simulations were defined as a rating curve based on a previous HEC-RAS model (Ayres Associates 2006). Both existing and design conditions models used the same n-values. Initial design conditions geometry was determined by (1) picking a low-flow channel width based on stable channel widths upstream and downstream of the site; (2) running the model to determine the elevation of the lower benches; and (3) running the model again to determine the elevation of the upper benches. Next, constant flow fixed-bed simulations were performed on both existing and design conditions models and resulting hydraulic parameters were compared. Unsurprisingly, the design conditions model simulated velocities that were more uniform in the lateral and longitudinal directions relative to the existing conditions model. The degree of longitudinal hydraulic uniformity was deemed sufficient to move into mobile-bed simulations where minor changes to the river geometry were considered and sedimentation potential was evaluated.
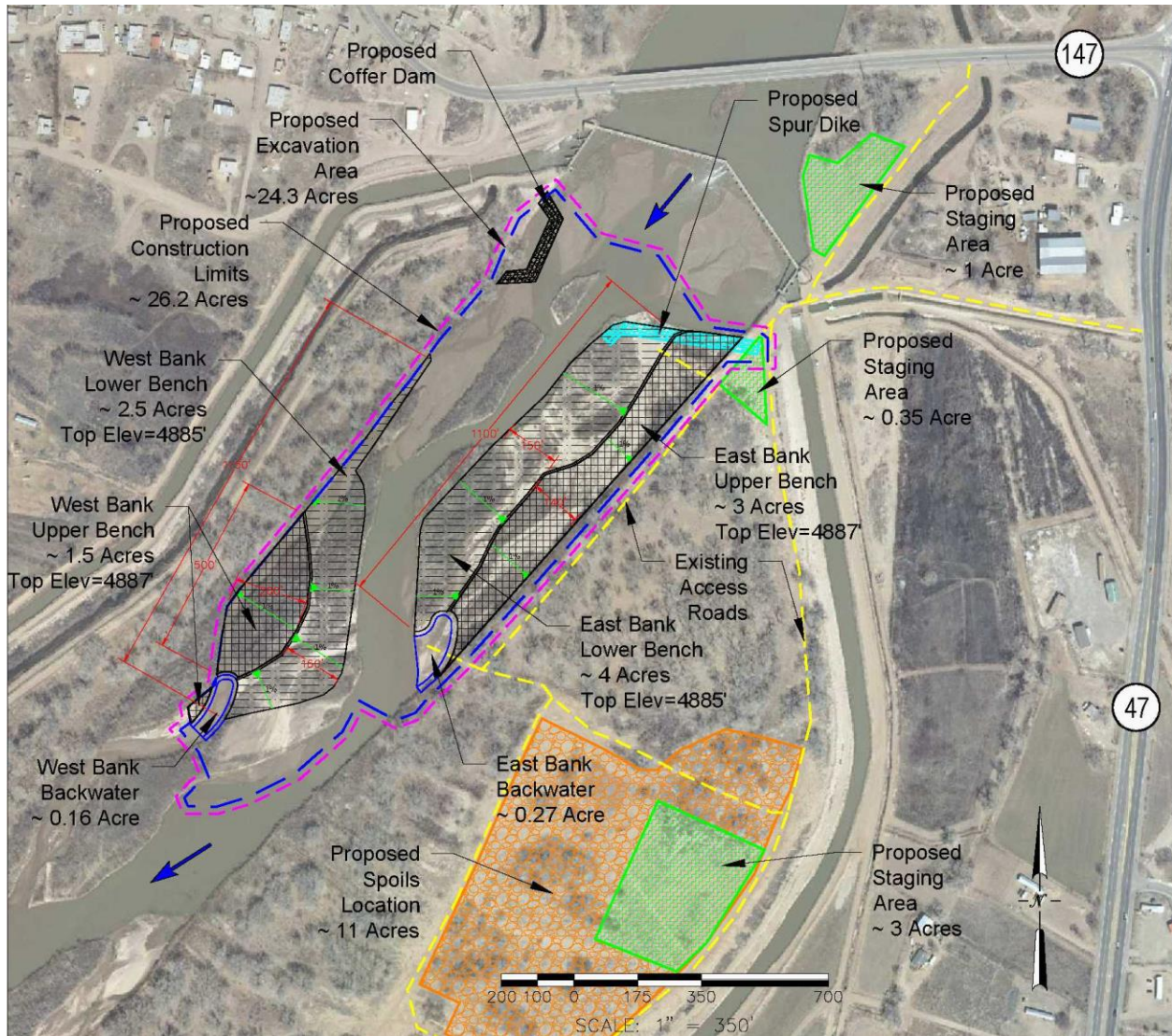
Figure 2. Plan View of the IIRP Design

The mobile bed simulations required an upstream inflow hydrograph and corresponding sediment discharge. The inflow hydrograph was synthesized such that flows increased from 1,000 cfs to 1,700 cfs before decreasing again to 1,000 cfs. This represents a spring runoff hydrograph has an annual chance exceedance (ACE) of approximately 85 percent (Tetra Tech 2009). A constant 500 cfs diversion was defined as the combined diversion from both sluiceways of the IDD, resulting in a peak flow of 1,200 cfs through the IIRP site (**Figure 3**). Because the bed of the Rio Grande has been relatively stable in recent decades, it was assumed that the upstream boundary of the model had a transport capacity that was in equilibrium with its supply. Therefore, SRH-Capacity (Huang and Bountry 2009) was used to develop a sediment transport capacity rating curve. The bed material in the modeled reach was predominately sand with a D_{16}, D_{50}, and D_{84} of 0.23, 0.42, and 1.00 mm, respectively (Tetra Tech 2009). Ultimately, the Englund-Hansen (1967) equation was selected for modeling because it was appropriate for the sand-dominate bed and because of its numerical simplicity. The Yang (1979) equation was also considered, but it caused numerical instability and model crashes. The sediment transport rating curve produced by SRH-Capacity caused the Rio Grande to aggrade at the upstream end

of the model. This was likely because uniform flow did not exist at the upstream boundary. The rating curve was scaled iteratively until the upstream boundary was stable (Figure 4).
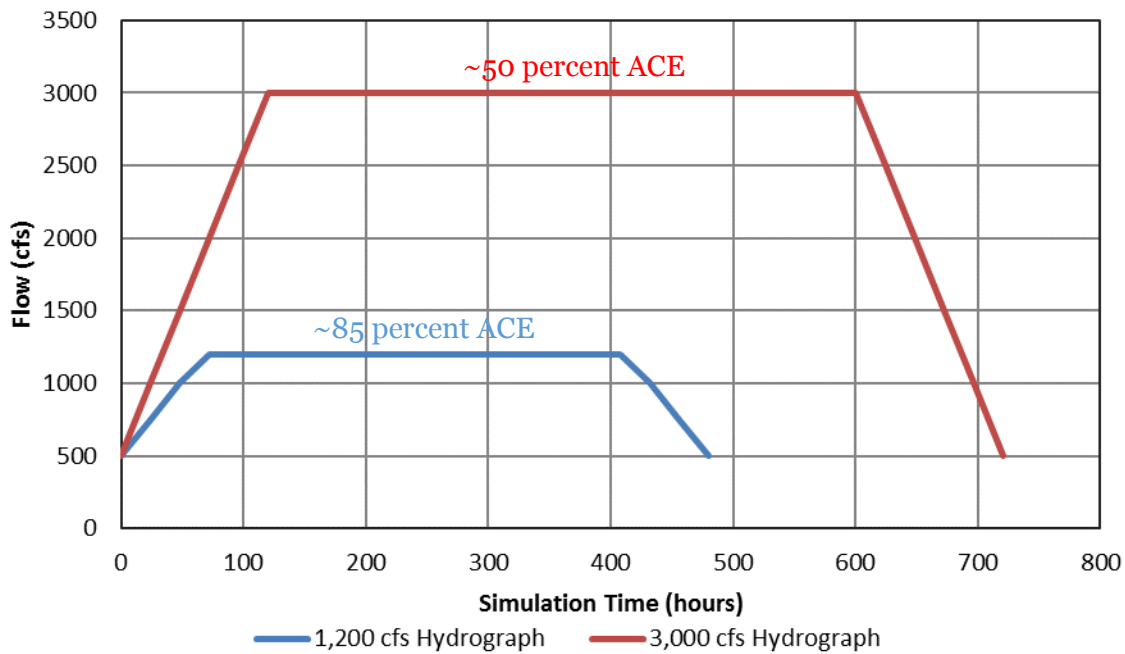
Figure 3. Simulated Spring Runoff Hydrograph through the IDD
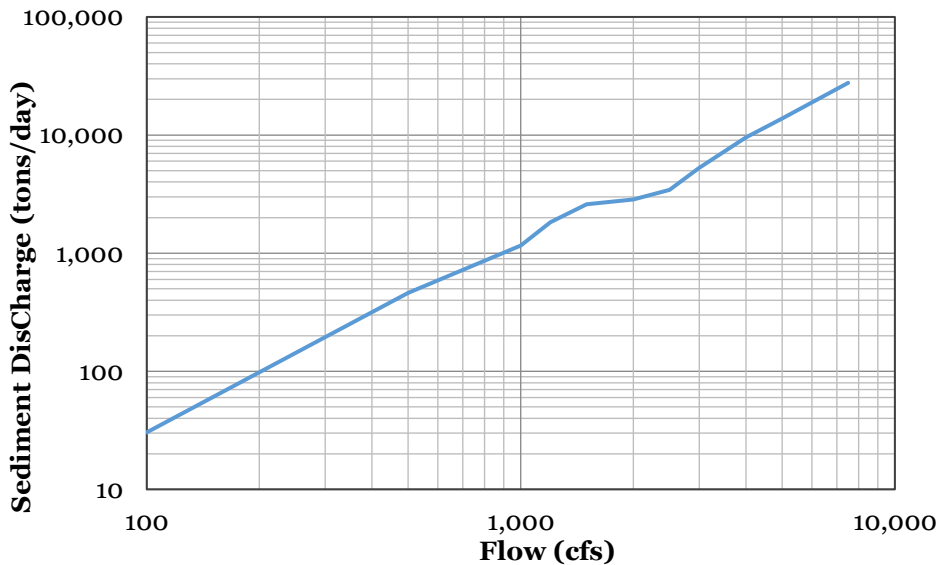
Figure 4. Scaled Upstream Sediment Inflow Rating Curve

SRH-2D did not include an algorithm to simulate radial gate operations. Gates were simulated as completely open or completely closed. Different gate operations were iteratively simulated to identify which operations reduced deposition along the west bank immediately downstream of the IDD. The gate operations that best achieve these objectives are presented in Table 1. The

same gate openings and closures were simulated in both existing and design conditions. The number of open gates at different flows was based on the findings of Tetra Tech (2009).

The mobile bed model was used to simulate three consecutive hydrographs to represent three runoff events (i.e., the final bed mesh elevations simulated from the first simulation were used as the input to the simulation of the second hydrograph). The model indicated that the IIRP would reach equilibrium at around three years based on average change in channel elevation. Minor changes to channel geometry were considered and the geometry that produced the least sedimentation after three years was selected for design (Figure 5). The absolute change simulated by modeling different hydrographs would differ (e.g., the number of years required to reach equilibrium) from the selected hydrographs. However, the relative response is expected to be similar (i.e., the geometry selected for design would still reach equilibrium more quickly than non-selected geometries).

Table 1. Description of IDD Gate Operations

Flow (cfs)	No. of Open Gates	Open Gate Locations
100	30	All gates open
1,200	2	3rd gate from right bank diversion, and 1st gate left of center
3,000	4	3rd - 5th gate from right bank diversion, and 1st gate left of center
5,000	8	3rd - 8th gate from right bank diversion, and 1st and 2nd gate left of center
7,000	30	All gates open
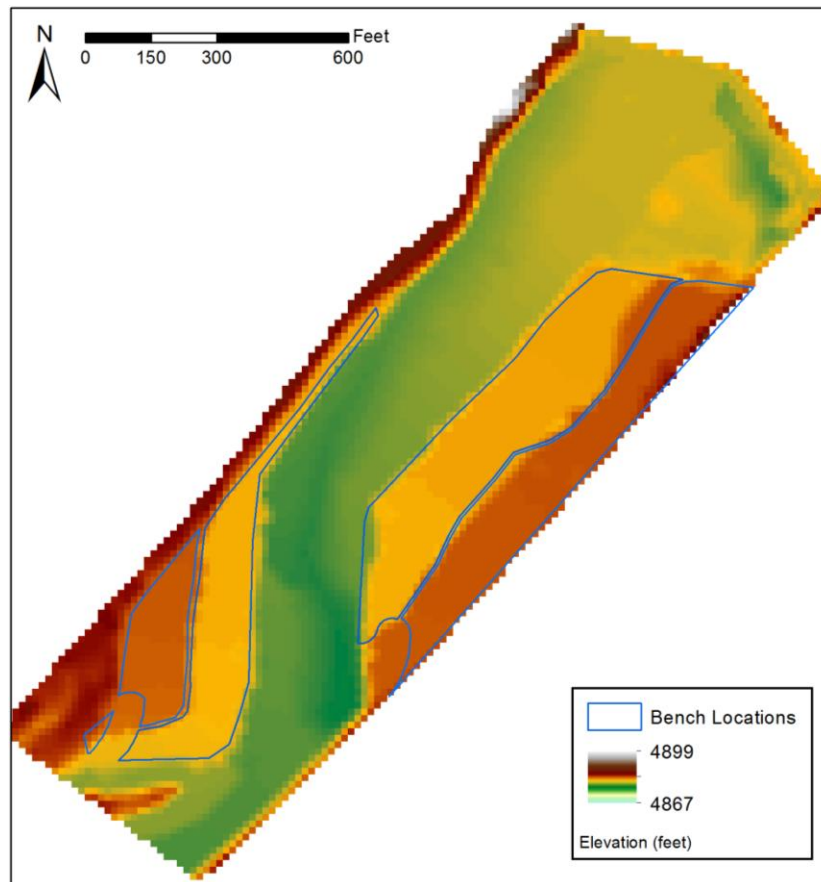
Figure 5. IIRP Designed Topography and Bathymetry

Results

The end of simulation topography and bathymetry were exported from SMS for three consecutive 1,200 cfs hydrograph simulations (Figure 6) and two consecutive 3,000 cfs hydrograph simulations (Figure 7).

After the third 1,200 cfs hydrograph is simulated, large portions of both lower benches were laterally eroded. Natural levees formed on what remains of the lower benches. One low flow channel consolidated, and four large bars formed: two mid-channel bars extending downstream of the IDD, one west bank-attached bar, and one nearly bank-attached bar to the east.
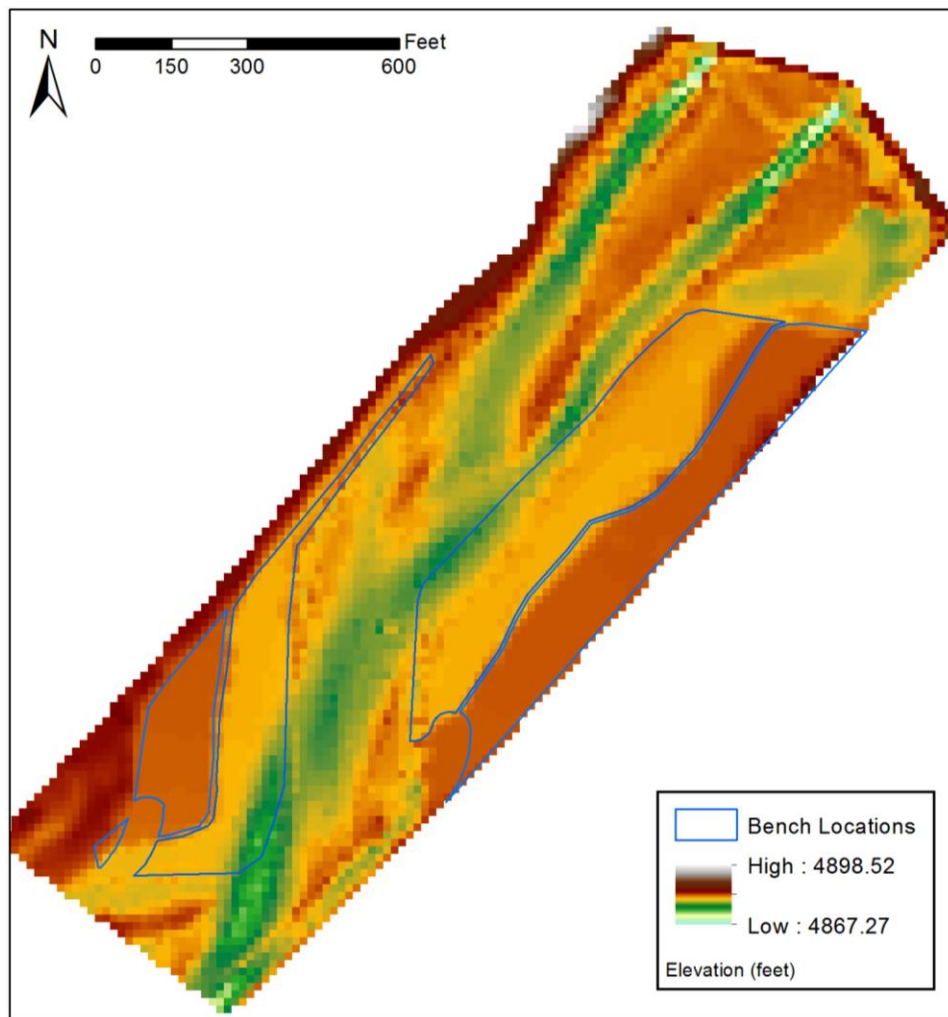
Figure 6. Simulated IIRP Topography and Bathymetry after the Third 1,200 cfs Hydrograph

After the two 3,000 cfs hydrographs are simulated, large portions of the eastern lower bench had eroded laterally, while the western lower bench had been protected from lateral erosion by the formation of a west bank-attached bar immediately upstream of the bench. What remains of the eastern lower bench aggraded. While most of the eastern upper bench degraded, the bed of the Rio Grande aggraded substantially between the IDD and the eastern terrace feature against the east bank. Unlike the 1,200 cfs hydrograph simulations, no bar formed near the east bank downstream of the east terrace feature.
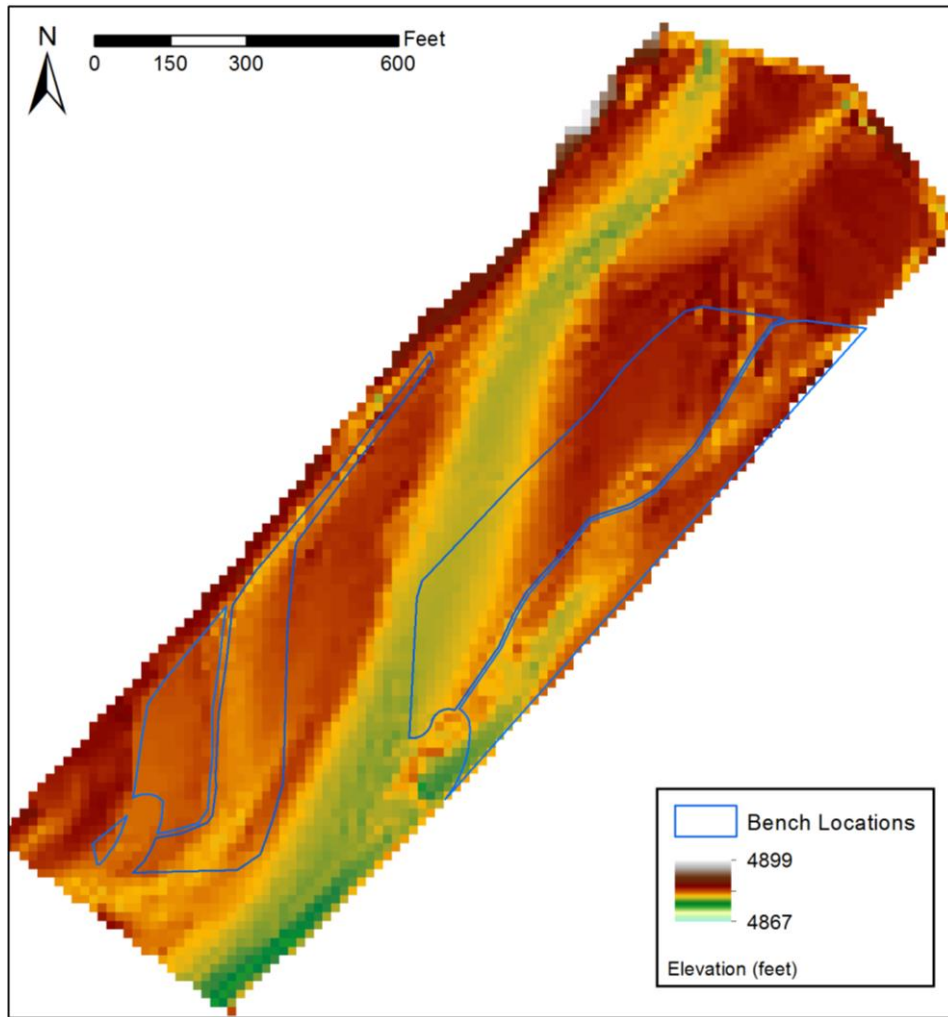
Figure 7. Simulated IIRP Topography and Bathymetry after the Second 3,000 cfs Hydrograph

Post-Construction Activities

Since construction was completed, yearly surveys have been conducted to monitor changes to river geometry. Flow records from nearby gages have been used to compare actual flows to synthesized flows and assess how well the model performed. The original design for the project included mechanical destabilization of both lower benches to prevent perennial vegetation formation (vegetation formation was not modeled). However, as the bar revegetated, the POI was pleased with the type and variety of vegetation. Few invasive species have been located during post-construction monitoring, and native cottonwood-coyote willow including a large percentage of tree willow species, which are less common is this reach of the Rio Grande, have become established. It was decided to keep the desirable vegetation. Thus, the evolution of the lower benches was substantially different than modeled and comparisons are only useful in a limited way.

Data Collection

In 2017 Reclamation contracted Tetra Tech to develop a high-resolution (Occam Engineers and Tetra Tech 2018) digital terrain model of the Rio Grande and its floodplain for one mile upstream and downstream of the IDD (Figure 8). Data was collected during low flows in July and August, following the spring runoff. While other surveys have been conducted, this survey is used for the basis of analysis because it provides the most comprehensive data set of the topography and bathymetry of the IIRP.
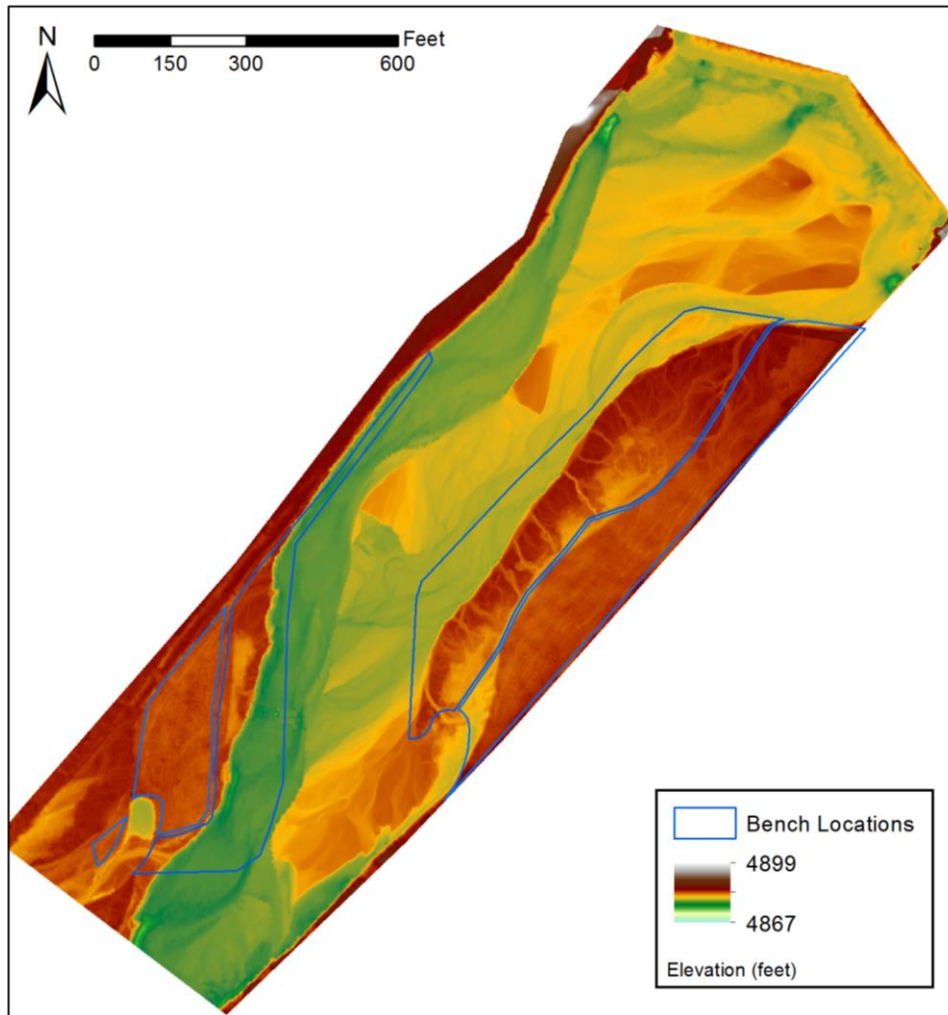
Figure 8: Topography and Bathymetry Based on 2017 Survey

Hydrology

The U.S. Geological Survey's (USGS) Rio Grande near Bosque Farms gage (No. 08331160) is located 3.2 river miles downstream of the IIRP site. The flow at this gage represents a good estimate for flows at the site during spring runoff (Figure 9). The 2014 runoff produced similar volumes and peak flows to the simulated 1,200 cfs peak flow hydrograph. The 2015 and 2016 runoff hydrographs were between the 1,200 cfs and 3,000 cfs peak flow hydrographs from a volume perspective and peak near 3,000 cfs. The 2017 runoff hydrograph was above average and had greater peak flows and volumes than any hydrograph simulated. Differences in

synthetic and measured flows are partially responsible for differences between simulated and surveyed river geometries. This is as especially the case with the 2017 runoff; however, 2016 surveys were not performed. Because of this, absolute comparisons and lessons learned will be discussed with professional judgement.
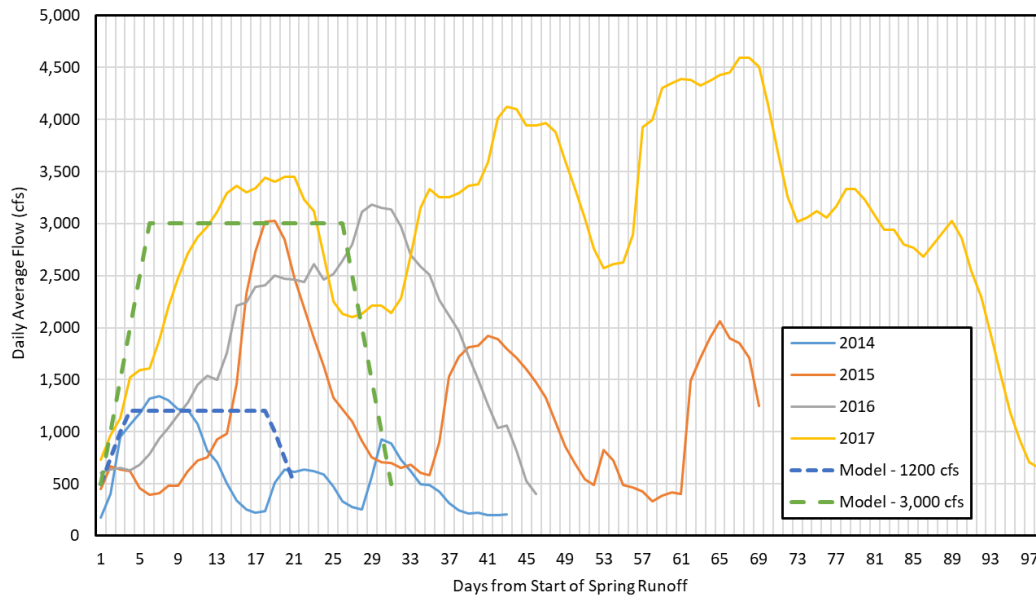
Figure 9. Actual and Modeled Hydrographs

Model Results versus Actual Change

Digital terrain models of the designed geometry, 2017 topographic and bathymetric survey, and the 1,200 cfs and 3,000 cfs hydrograph model results were created. ArcGIS's raster calculator was used to evaluate aggradation and degradation (simulated and actual) that occurred post-construction (Figure 10 through Figure 12). Table 2 through Table 2. Summary of Changes to Channel through the IIRP (2017 versus Design)

Feature	Comparison	Description of Change
IDD to start of East Terrace	2017 vs. design	Most of the bed aggraded by up to 2 feet. The influence of gate operations is apparent; degradation immediately downstream of some gates is as much as 3 feet.
	Three 1,200 cfs hydrographs vs. design	Most of the bed aggraded by up to 2.5 feet. 6 feet of scour were simulated. This is the result of limitations in simulating gate operations.
	Two 3,000 cfs hydrographs vs. design	Much of the bed aggraded by 1 to 6 feet. The number of open gates and bed material supply through the dam increased, leading to scour of up to 1.5 feet.
Next to East Terrace	2017 vs. design	Most of the bed aggraded (up to 3.7 feet where mid-channel bars formed). A few areas degraded by less than 0.5 feet.
	Three 1,200 cfs hydrographs vs. design	Most of the bed aggraded (up to 5 feet where mid-channel bars formed). A few areas were stable.
	Two 3,000 cfs hydrographs vs. design	Much of the bed is stable. With alternate bars of up to 5.5 feet forming.

Next to West Terrace	2017 vs. design	A large bar formed near the east bank. Aggradation is wide spread and up to 5.6 feet. 2018 cross section survey shows that much of this bar has eroded.
	Three 1,200 cfs hydrographs vs. design	A 5-foot high bar formed near the east bank. Up to 4 feet of scour is predicted adjacent to the bench. The rest of the channel aggrades by 0 to 1.5 feet.
	Two 3,000 cfs hydrographs vs. design	Much of the channel aggrades by 1 to 4 feet with up to 3 feet of erosion occurring against the east bank.

Table 3. Summary of Changes to East Terrace in the IIRP (Simulation of Three 1,200 cfs Hydrographs versus Design)

Feature	Comparison	Description of Change
East Terrace – Upper Bench	2017 vs. design	Largely stable with some natural levees (up to 2.5 feet high) forming at the upstream end. The degradation is artificial—the result of an embayment added post-modeling.
	Three 1,200 cfs hydrographs vs. design	Stable. Flows were not large enough to inundate bench.
	Two 3,000 cfs hydrographs vs. design	Much of the bench degrades by 0.5 to 4 feet.
East Terrace – Lower Bench	2017 vs. design	Half of the east bench, next to the channel was laterally eroded, while the other half aggraded by 1.5 to 2.5 feet as perennial vegetation establish.
	Three 1,200 cfs hydrographs vs. design	A small portion of the bench is laterally eroded. 0.5 to 1.0-foot high natural levees form on upstream end. Much of the bench is stable.
	Two 3,000 cfs hydrographs vs. design	The upstream half aggrades by 2.5 feet, while the downstream half laterally erodes.

Table 4 describes the aggradational or degradation changes (simulated and actual) presented in Figure 10 through Figure 12.
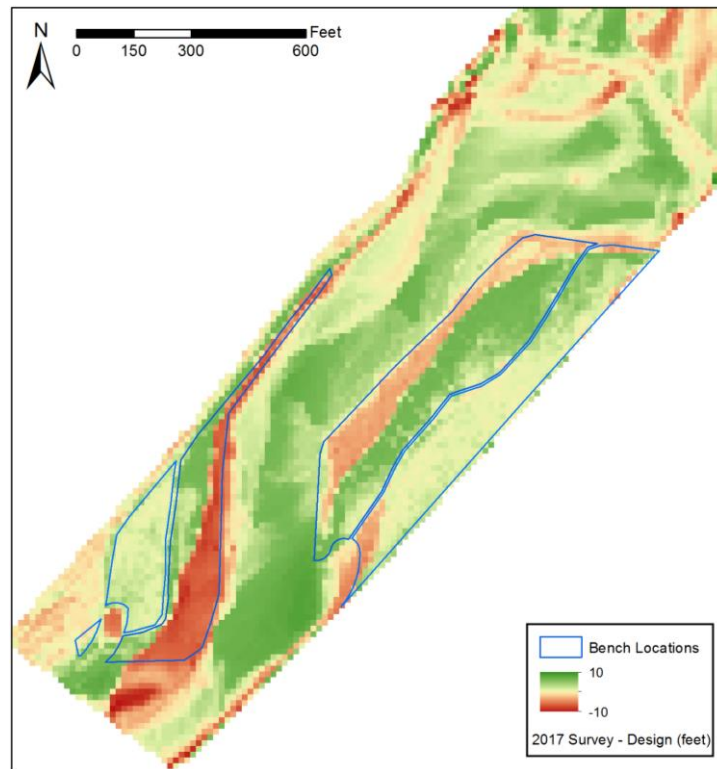
Figure 10. Bed Elevations Changes (2017 minus Design)
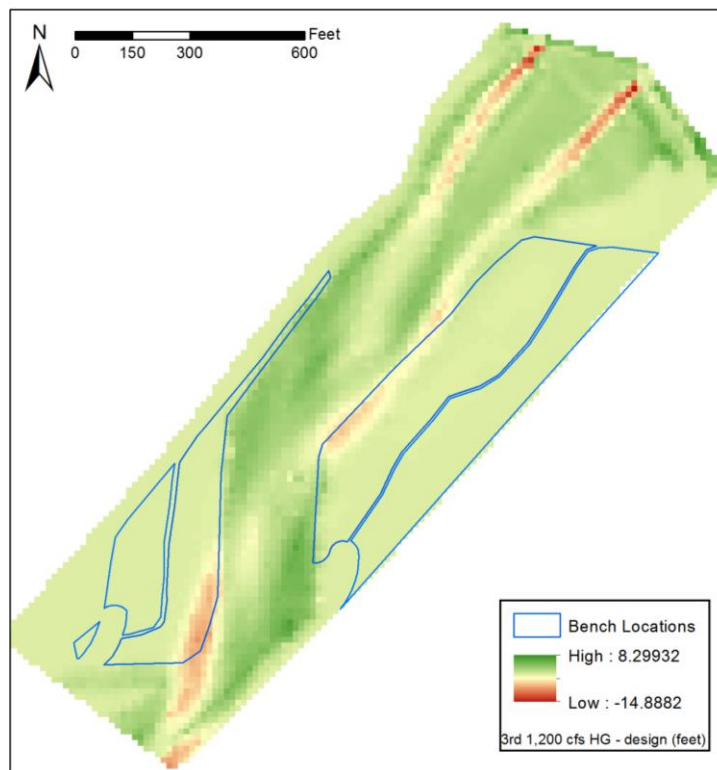
Figure 11. Bed Elevations Changes (After Third 1,200 cfs Hydrograph Simulation minus Design)
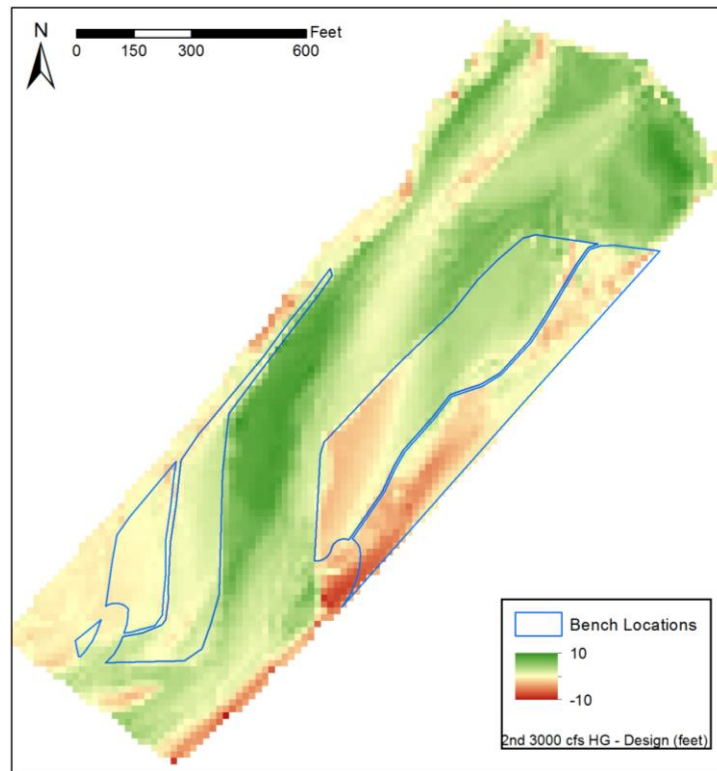
Figure 12. Bed Elevations Changes (Second 3,000 cfs Hydrograph Simulation minus Design)

Table 2. Summary of Changes to Channel through the IIRP (2017 versus Design)

Feature	Comparison	Description of Change
IDD to start of East Terrace	2017 vs. design	Most of the bed aggraded by up to 2 feet. The influence of gate operations is apparent; degradation immediately downstream of some gates is as much as 3 feet.
	Three 1,200 cfs hydrographs vs. design	Most of the bed aggraded by up to 2.5 feet. 6 feet of scour were simulated. This is the result of limitations in simulating gate operations.
	Two 3,000 cfs hydrographs vs. design	Much of the bed aggraded by 1 to 6 feet. The number of open gates and bed material supply through the dam increased, leading to scour of up to 1.5 feet.
Next to East Terrace	2017 vs. design	Most of the bed aggraded (up to 3.7 feet where mid-channel bars formed). A few areas degraded by less than 0.5 feet.
	Three 1,200 cfs hydrographs vs. design	Most of the bed aggraded (up to 5 feet where mid-channel bars formed). A few areas were stable.
	Two 3,000 cfs hydrographs vs. design	Much of the bed is stable. With alternate bars of up to 5.5 feet forming.
Next to West Terrace	2017 vs. design	A large bar formed near the east bank. Aggradation is wide spread and up to 5.6 feet. 2018 cross section survey shows that much of this bar has eroded.
	Three 1,200 cfs hydrographs vs. design	A 5-foot high bar formed near the east bank. Up to 4 feet of scour is predicted adjacent to the bench. The rest of the channel aggrades by 0 to 1.5 feet.
	Two 3,000 cfs hydrographs vs. design	Much of the channel aggrades by 1 to 4 feet with up to 3 feet of erosion occurring against the east bank.

Table 3. Summary of Changes to East Terrace in the IIRP (Simulation of Three 1,200 cfs Hydrographs versus Design)

Feature	Comparison	Description of Change
East Terrace – Upper Bench	2017 vs. design	Largely stable with some natural levees (up to 2.5 feet high) forming at the upstream end. The degradation is artificial—the result of an embayment added post-modeling.
	Three 1,200 cfs hydrographs vs. design	Stable. Flows were not large enough to inundate bench.
	Two 3,000 cfs hydrographs vs. design	Much of the bench degrades by 0.5 to 4 feet.
East Terrace – Lower Bench	2017 vs. design	Half of the east bench, next to the channel was laterally eroded, while the other half aggraded by 1.5 to 2.5 feet as perennial vegetation establish.
	Three 1,200 cfs hydrographs vs. design	A small portion of the bench is laterally eroded. 0.5 to 1.0-foot high natural levees form on upstream end. Much of the bench is stable.
	Two 3,000 cfs hydrographs vs. design	The upstream half aggrades by 2.5 feet, while the downstream half laterally erodes.

Table 4. Summary of Changes to West Terrace in the IIRP (Simulation of Two 3,000 cfs Hydrographs versus Design)

Feature	Comparison	Description of Change
West Terrace – Upper Bench	2017 vs. design	Stable to 0.5 feet of aggradation.
	Three 1,200 cfs hydrographs vs. design	Stable. Flows were not large enough to inundate bench.
	Two 3,000 cfs hydrographs vs. design	Relatively stable.
West Terrace - Lower Bench	2017 vs. design	Most of this feature was laterally eroded. What little remains aggraded by 0.5 to 2.5 feet as perennial vegetation established.
	Three 1,200 cfs hydrographs vs. design	A small portion of the bench is laterally eroded. Much of the bench is stable.
	Two 3,000 cfs hydrographs vs. design	0.5 to 1.5 feet of aggradation. No lateral erosion.

Lessons Learned

Results that the model simulated reasonably well include: (1) prediction of lateral erosion of the lower benches; (2) prediction of overall aggradation trends in the channel; (3) model predicts natural levee formation but a lesser magnitude and extent than occurred. The simulation of the 1,200 cfs hydrographs better predicted the location of the lateral erosion, while the 3,000 cfs model better predicted the erosion magnitude. While both simulations reasonably predicted the magnitude of aggradation and degradation, the location of the low flow channel was off to some extent in both models; though the 1,200 cfs hydrograph simulation performed better. The differences in channel location are in part tied to differences in gate operations near the west side of the river. The underprediction of natural levee extents is related to the model being developed to simulate conditions in which perennial vegetation was routinely destabilized, which differs from what occurred.

Results that the model captured poorly include (1) bed change magnitudes immediately downstream of the IDD and (2) stability of the upper benches, (3) magnitude of aggradation on lower benches. The first issue is directly linked to the lack of a radial gate operations algorithm in SRH-2D in 2013. Additionally, the MRGCD routinely changes gate operations to maintain

correct upstream water surface heads and manage downstream aggradation and scour. The second and third issues were tied to the fact that vegetation formation differed from what was planned. Though not important for this study, it is worth noting that movement of macro forms was not predicted. The model tended to consolidate and straighten a low flow channel while adjacent bar elevations increased or decreased.

Overall, SRH-2D performed well at predicting the general magnitude of aggradation and degradation and even lateral erosion trends. However, for certain applications SRH-2D has limitations that should be understood when applying the model or interpreting the results. First, gate operation hydraulics do affect model results. Second, the exact location of bars, the low flow channel, and lateral erosion are not accurately predicted and are influenced by a tendency for the low flow channel to consolidate and straighten. Finally, the future management of any restoration design is shrouded in uncertainty. Time and budget permitting, sensitivity analysis where channel parameters such as roughness, or infrastructure operations, are changed may provide useful insights into future adaptive management needs. Simulation of a range of flow scenarios can also give modelers a sense of the level of uncertainty associated with the model results.

Acknowledgements

References

Aquaveo, LLC. 2012. Surface Water Modeling System. Build Date November 5, 2012.

Ayres Associates, Inc. 2006. Pueblo of Isleta Rio Grande Flow Characterization. Report Prepared for the Pueblo of Isleta, Water Resources Development and Protection. Isleta, Nm. March 2006.

Engelund, F. and Hansen, H. 1967. A Monograph on Sediment Transport in Alluvial Streams. Teknish Forlag, Technical Press. Copenhagen, Denmark.

Huang, J.V. and Bountry, J. 2009. SRH-Capacity User Manual: Version 1.37. U.S. Bureau of Reclamation, Technical Service Center, Sedimentation and River Hydraulics Group. Denver, Co. October.

Lai, Y. 2008. Theory and User's Manual. U.S. Bureau of Reclamation, Technical Service Center, Sedimentation and River Hydraulics Group. Denver, Co. November 2008.

Occam Engineers and Tetra Tech. 2018. Field Data Collection Report – Bathymetric and Topographic Surveys: Isleta Diversion Dam and San Acacia Diversion Dam. Prepared for the U.S. Bureau of Reclamation, June.

Tetra Tech. 2009. Hydraulic and Sediment-transport Models for Rio Grande Restoration Projects within Isleta Pueblo, NM: Baseline Model Development. Draft Technical Memorandum, November.

Tetra Tech. 2013. Isleta Island Removal Project (IRP) Design Analysis Report. Prepared for the Pueblo of Isleta, October.

Yang, C.T. (1979). "Unit stream power equations for total load," Journal of Hydrology, Vol. 40, 123-128.

Kansas River HEC-RAS Sediment Transport Model

Aaron Williams P.E., Hydraulic Engineer, U.S. Army Corps of Engineers
Kansas City District, Kansas City, MO, Aaron.R.Williams@usace.army.mil

John Shelley Ph.D. P.E., Hydraulic Engineer, U.S. Army Corps of Engineers
Kansas City District, Kansas City, MO, John.Shelley@usace.army.mil

Abstract

The Kansas River Basin includes nine federal reservoirs. Sedimentation in these reservoirs is an emerging problem that must be addressed so that benefits provided by the reservoirs for water quality, water supply, fish and wildlife, recreation, and flood control can be realized into the future. Many strategies for managing reservoir sediment include passing the sediment to the downstream channel. However, state agencies and downstream users of the Kansas River have concerns about how an increase in sediment load may affect the river. To answer these and other questions, this 1-dimensional HEC-RAS sediment transport model for the Kansas River was developed.

Introduction

The model domain spans approximately 357 miles, making it one of the largest HEC-RAS sediment models ever built. It commences immediately downstream of Kannapolis Reservoir, continuing down the Smokey Hill River though the Kansas River, concluding at the confluence of the Kansas River and Missouri River. Model calibration begins in 2007 and ends in 2018. Model parameters are calibrated based on bed change from multiple sets of repeated cross section measurements, stage trends at USGS gages, channel mining records, and other available information.

Kansas River Basin Overview

The Kansas River Basin has a total of 18 Federal reservoir projects, including nine major reservoirs within the lower end of the drainage basin. These reservoirs regulate stream flow in approximately 85 percent of the drainage basin (IWR). Each of the nine major reservoirs share common operational principles among their multipurpose, flood control and surcharge pools. The storage and release of water from these pools is accomplished by adherence to project specific Water Control Manuals. Following the guidance in each Water Control Manual ensures project compliance with congressionally approved operating purposes. Figure 1 shows a map of the Kansas River basin and its reservoirs.
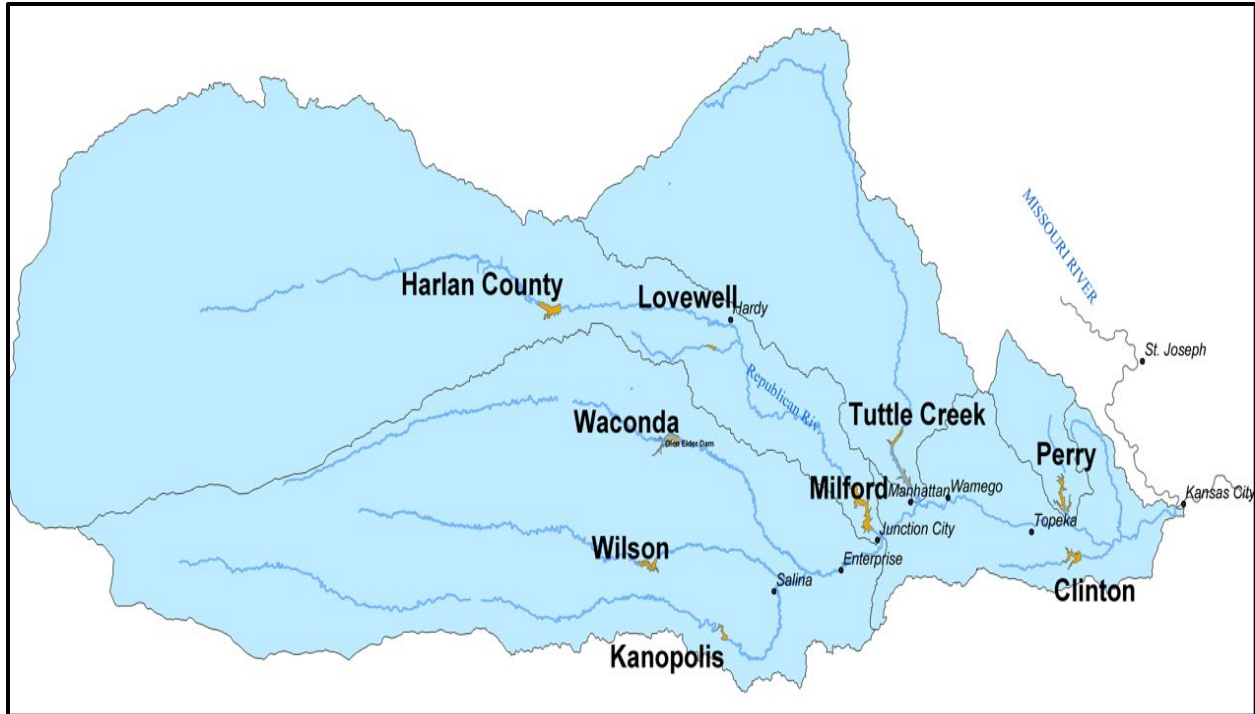
Figure1. Kansas River Basin map.

The Kansas River begins at the confluence of the Republican and Smoky Hill Rivers near Junction City and flows 173 miles to Kansas City, where it joins the Missouri River. The Kansas River Basin drains almost the entire northern half of Kansas, as well as part of Nebraska and Colorado (53,000 square miles in all). It is the longest prairie based river in the world. It serves as a critical drinking water supply for more than 600,000 people in addition to being used for irrigation, municipal wastewater and industrial discharges, cooling water for three coal-fired power plants, and a source of commercial sand and gravel. In addition to the reservoirs, there are several Federal levee projects located on the banks of the Kansas River that provide flood risk reduction benefits, mainly to larger urban areas such as Topeka and Kansas City, Kansas. The Kansas River is an important resource for the State of Kansas.

Reservoir Sedimentation Issues

Approximately 13 M yd³of sediment per year are deposited in Tuttle Creek, Milford, Kanopolis, Wilson, Harlan County, and Waconda reservoirs (Shelley 2017). Traditional dredging methods typically employ the use of hydraulic or mechanical excavation to remove sediment from reservoirs and discharge to upland disposal areas. A recent dredging project, using hydraulic dredging and upland disposal, was conducted at John Redmond Reservoir in 2016. The project removed 3 M yd³ of deposited sediment at a cost of $20 M, or $6.67 / yd³ (KWO 2016). Alternative dredging techniques such as Hydrosuction and Water-Injection Dredging are currently being analyzed to determine their effectiveness on reservoirs within the Kansas River Basin. Both techniques would significantly reduce the cost to remove sediment once deposited in reservoirs (Shelley 2017), however a significant portion of the cost reduction is realized due to the passing of sediment to downstream rivers.

Sediment on the main stem of the Kansas River affects infrastructure, such as water supply intakes, irrigation diversion structures, and other uses such as recreation and ecological resources. Sediment loads on the Kansas River have been greatly reduced since the construction of reservoirs in the basin. The current strategies being studied would pass fine material entering reservoirs into the downstream rivers. Benefits of passing this fine material include increased storage capacity of reservoirs as well as enhanced habitat for native species in the Kansas River (Shelley et al. 2016). Conversely, the increased fine sediment load could have negative impacts on water supply and irrigation.

Model Development

Hydraulic Model Development

To develop the sediment transport model a robust steady-state 1-Dimensional HEC-RAS hydraulic model was first created using available bathymetric and LIDAR data along with available flow and stage data. Initial condition bathymetric data was collected in 2007 and final condition bathymetric data was collected in 2018. Five (5) hydraulic grade control structures exist within the model domain. Information for four (4) of the structures was obtained from a previously developed HEC-RAS model. Information for the final structure was collected in 2018 in conjunction with the bathymetric survey. Bathymetric survey data is only available for the lower half of the model domain. Model geometry where bathymetric data is not available is supplemented with high resolution LIDAR data collected during low flow leaf off conditions in 2018.

Sediment Data

Sediment data used for the development of this model was obtained from the USGS and supplemented by bed gradation samples collected specifically for this model. Suspended sediment and flow data from the USGS (https://cida.usgs.gov/sediment/) were used to determine incoming sediment loads and balance sediment budgets. Bed sediment samples were collected at strategic locations in 2018 and analyzed for particle grain size. The bed gradation information was used to populate the initial model bed sediment conditions as well as supplement the coarse fraction of the incoming suspended load. No bed load measurements are available so bed load was estimated to be 5% of the total suspended sediment load (Einstein 1950). Annual dredging tonnages at approximate locations were entered into the model as well.

Sediment Budget

To satisfy the conservation of mass and balance the sediment budget, an unmeasured quantity of sediment entering the control volume was calculated. Comparing sediment sources and sinks in the sediment budget control volume, a significant quantity of bed material load and wash load was unaccounted for. Bed material load was assumed to be material courser than 0.125 mm based on measured bed gradations collected in 2018 (Biedenharn 2006). Bank erosion, estimated using repeat aerial imagery, accounts for a majority of the unmeasured incoming sediment load. A summary of the sediment budget is included in Table 1. Due to data availability, the sediment budget domain begins at the Kansas River Wamego USGS gage (#06887500) and ends at the Kansas River Desoto USGS gage (#06892350).

Table 1. Sediment Budget Summary

Sediment Source/Sink	Bed Material Load (million ton)	Wash Load (million ton)	Total Load (million tons)
Wamego (Upstream of Control Volume)	9.79	19.14	28.93
Tributaries (Measured)	3.18	7.47	10.65
Inflows (Unmeasured)	4.21	11.98	16.19
Channel Mining	4.51	N/A	4.51
Bed Change	9.04	N/A	9.04
Desoto (Downstream Control Volume)	5.51	39.22	44.73

The model is being calibrated to observed bed changes measured by repeat hydrographic surveys collected in 2007 and 2018. Measured bed changes in the form of longitudinal cumulative mass change is shown in Figure 2. The model will also be calibrated to stage trends at USGS gages. Annual channel mining information was entered into the model during calibration. Detailed timing for the dredging is unavailable, so the annual quantity of sand removed was assumed to be removed equally from March to November of each year in the approximate locations provided by the channel miners.
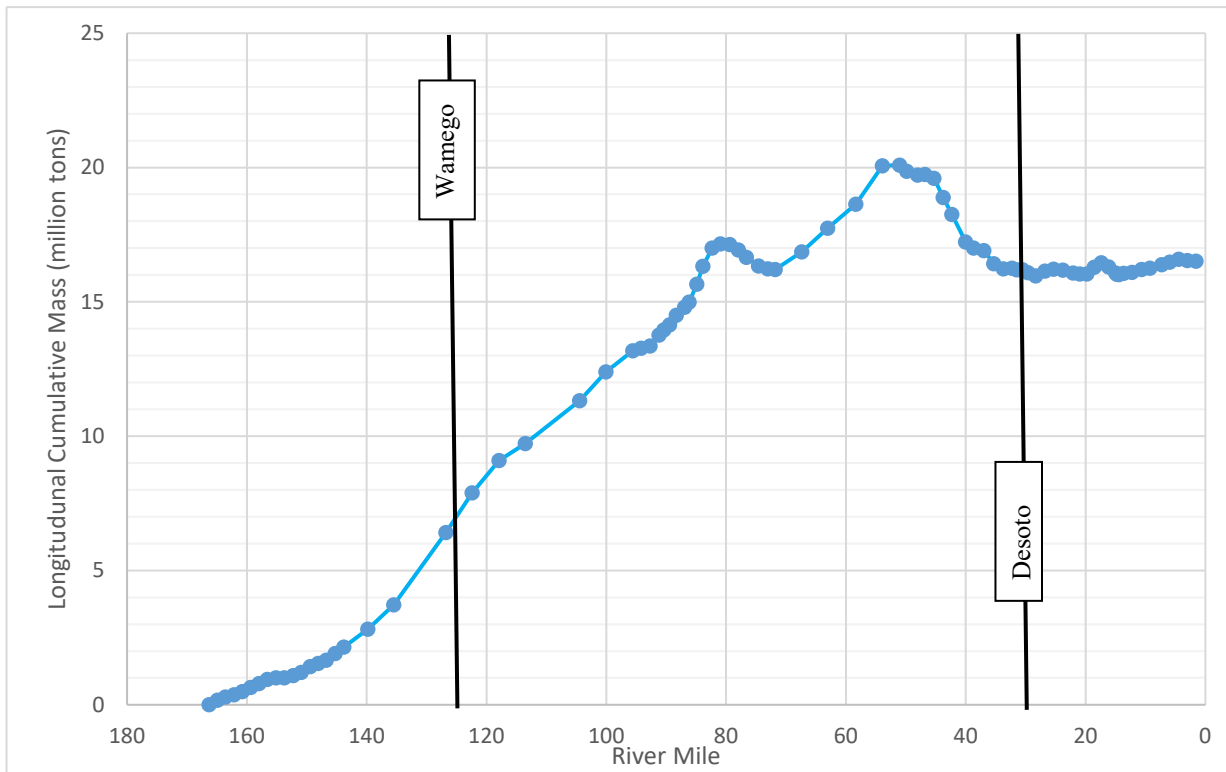
Figure2. Longitudinal Cumulative Mass Change

Future Model Use

Several innovative strategies to manage sediment accumulation in reservoirs within the Kansas River Basin are currently being studied, including strategies which pass sediment to the downstream channel. State agencies and major users of the Kansas River have questions about how an increase in sediment load may affect the river. This calibrated sediment transport model will aid decision makers as to the effects an increase in sediment load will have on the Kansas River and its stakeholders. After calibration, the next step is to develop and run future project scenarios. Results of this model will then help inform decision makers of the impacts of management actions.

References

Biedenharn, S., Thorne, C., Watson, C. 2006. Wash Load/Bed Material Load Concept in Regional Sediment Management. Proceedings of the Eighth Federal Interagency Sedimentation Conference (8thFISC), April2-6, 2006, Reno, NV, USA

Einstein, H.A., (1950), The bed-load function for sediment transportation in open-channel flows. U.S. Department of Agriculture, Soil Conservation Service, Technical Bulletin No. 1026.

IWR. 2019. US Army Corps of Engineers – Institute of Water Resources Kansas River Summary Page. https://www.iwr.usace.army.mil/sustainablerivers/sites/kansas/

KWO. 2016. John Redmond Reservoir Dredging Fact Sheet. Kansas Water Office. http://www.kwo.org/Projects/JRDredging/JRRD%20Fact%20Sheet.pdf

Shelley, J., Boyer, M., Granet, J., and Williams, A. 2016. Environmental Benefits of Restoring Sediment Continuity to the Kansas River. ERDC/CHL CHETN-XIV-50. June 2016.

Shelley, J. E. 2017. Analysis for a Hydrosuction Sediment Removal System at Tuttle Creek Lake, KS. ERDC/TN RSM-17-XX, U.S. Army Engineer Research and Development Center, Vicksburg, MS.

USACE 2011. Kansas River Basin Regional Sediment Management Section 204 Stream and River Channel Assessment. Prepared by Gulf South Research Corporation and The Watershed Institute for the U.S. Army Corps of Engineers, Kansas City District. January, 2011.

Linking GSSHA to SEDLIB: Improvements to In-Stream Sediment Modeling

Gary L. Brown, Research Hydraulic Engineer, USACE Engineer Research and Development Center, Vicksburg, MS, gary.l.brown@erdc.dren.mil

Dr. Nawa Raj Pradhan, Research Hydraulic Engineer, USACE Engineer Research and Development Center, Vicksburg, MS, nawa.pradhan@erdc.dren.mil

Dr. Charles Downer, Research Hydraulic Engineer, USACE Engineer Research and Development Center, Vicksburg, MS, charles.W.Downer@erdc.dren.mil

Dr. Joseph Gutenson, Research Hydraulic Engineer, USACE Engineer Research and Development Center, Vicksburg, MS, Joseph.Gutenson@erdc.dren.mil

Extended Abstract

The Gridded Surface Subsurface Hydrologic Analysis (GSSHA) model is a watershed analysis and management tool with the ability to simulate the movement of water, sediment, and associated constituents at the watershed-scale (Downer and Ogden, 2004). GSSHA provides the ability to explicitly simulate important watershed features such as streams, hydraulic structures, embankments, subsurface drainage systems, as well as reservoirs, lakes and detention basins, storm and tile drains.

When simulating a watershed, GSSHA utilizes an orthogonal mesh of 2D finite volumes to discretize the full domain. This mesh is used to compute all overland and groundwater flow and transport processes. Superimposed on this mesh, a link-node network of 1d finite volumes is used to describe the stream flow and transport processes. These two separate computational domains are linked dynamically at the time-step level, with fluxes that pass between them.

Heretofore, much of the development of sediment transport capability within GSSHA has focused on watershed processes, e.g.: raindrop and rill erosion, sheet flow transport processes, etc. (Downer et al., 2014). By contrast, the sediment transport processes developed for the stream flow network have been less rigorous. The stream flow network has been utilized primarily as a passive mechanism; whereby silt and clay sized sediment are represented as wash load emanating from the overland flow, and cannot interact with the sediment bed. The 1d channel network was developed to transport sand, but the sand transport model is an Exner-type equilibrium model, and is not capable of simulating any sand sorting or armoring processes within the streambed.

To introduce the ability to simulate dynamic sediment processes within the channel network, the in-stream module of GSSHA has been linked to the SEDLIB sediment transport library (Brown 2012). SEDLIB was developed at the Coastal and Hydraulics Laboratory (CHL) under the System Wide Water Resources Program (SWWRP) and Flood and Coastal (F&C) research program. SEDLIB is a fully generalized, multi-grain class, multi-bed layer, cohesive and cohesionless sediment transport module. It passes fluxes of sediment to and from the bed to the parent model (GSSHA), which then transports the sediments using the transport capabilities native to the parent model. SEDLIB was developed as a general in-stream sediment process library. In theory, SEDLIB can be linked to any H&H source code. SEDLIB has already been

linked with another ERDC H&H model, AdH (Adaptive Hydraulics). In this form, SEDLIB has been used broadly by many USACE engineers throughout the United States to simulate sediment transport processes at a variety of scales, from small watershed-scale streams to the largest rivers and estuaries.

The linkage between GSSHA and SEDLIB required a replacement of the existing in-stream sediment transport processes within GSSHA. The primary change that resulted was the introduction of a detailed description of the initial bed conditions within the channel network, which must be provided by the user. This initial condition describes the initial bed layers, and the grain class distribution of sediment within each layer.

When GSSHA is run with SEDLIB, the sediment bed in the 1d channel network becomes an additional source and/or sink of silt and clay sized sediment. Also, sediments that are buried at depth in the sediment bed can be exposed to erosion under very high shear stresses, and be introduced into the watershed. This capability can be used, for example, to investigate the likelihood of exposing buried contaminated sediments. The SEDLIB module also simulates the bed dynamics associated with sand and gravel sized sediments, including armoring, sorting and fining processes. Hence, SEDLIB provides a full suite of sediment bed dynamics that can be simulated in the channel network.

The linked GSSHA/SEDLIB model has been applied to simulate hydrodynamics and sediment transport for the USDA-ARS Goodwin Creek Experimental Watershed (GCEW). The GCEW is a rural 21.1 km² watershed near Batesville, Mississippi. The USDA-ARS has collected rainfall, runoff, and suspended sediment data in the watershed since 1986 at the basin outlet and the outlet of 12 sub-watersheds ranging in size from 0.17 to 17 km². A similarly dense precipitation data set has also been collected. Previous studies of this watershed using GSSHA (Downer et al., 2014) have revealed some deficiencies in the ability of the model to simulate peak sediment discharge, especially for the initial event, during storm events. These deficiencies were hypothesized to be associated with in-stream erosion of fines, which were not being simulated within the original GSSHA model. Hence, these results were revisited with the coupled GSSHA-SEDLIB model, to investigate this hypothesis numerically.

The new results confirm the plausibility of the hypothesis. The introduction of erodible fines with the numerical channel network increases the peak sediment discharges in a manner consistent with the observed discharges. Since there is insufficient data available to directly characterize the erosion rate of these fines, it is necessary to utilize a set of discharge data as a calibration data set, and then compare these concentrations to other events where no calibration adjustments are made, to validate the modeling quantitatively. The results of this modeling exercise demonstrate the added capability that is afforded to GSSHA with the introduction of SEDLIB to the model.

References

Brown, G.L. 2012. Modification of the Bed Sediment Equations of Spasojevic and Holly (1993) to Account for Variable Porosity, Variable Grain Specific Gravity, and Nonerodable Boundaries, IIHR Third International Symposium on Shallow Flows, Iowa City, IA, June 4-6 2012.

Downer, C., Pradhan, N., Ogden, F., and Byrd, A. 2014.Testing the Effects of Detachment Limits and Transport Capacity Formulation on Sediment Runoff Predictions Using the U.S. Army Corps of Engineers GSSHA Model, Journal of Hydrologic Engineering.

Downer, C. W., and F. L. Ogden. 2004. GSSHA: A model for simulating diverse streamflow generating processes. Journal of Hydrologic Engineering 9(3): 161-174.
Yang, C. T. (1973). "Incipient motion and sediment transport." J. Hydraul. Div., 99(HY10), 10067.

Middle Rio Grande and Tributaries Numerical Sediment Routing Study, Cochiti Dam to Elephant Butte Reservoir

Miles Yaw, PE, Hydraulic Engineer, Tetra Tech, Ft. Collins, CO, miles.yaw@tetratech.com
David Pizzi, PE, Hydraulic Engineer, Tetra Tech, Ft. Collins, CO, david.pizzi@tetratech.com
Jonathan AuBuchon, PE, Regional Sediment Specialist, USACE, Albuquerque, NM, Jonathan.Aubuchon@usace.army.mil
Ryan Gronewold, PE, Chief, Planning Branch, USACE, Albuquerque, NM, ryan.p.gronewold@usace.army.mil
Stanford Gibson, Ph.D., Research Hydraulic Engineer, USACE, Davis, CA, Stanford.gibson@usace.army.mil

Abstract

The U.S. Army Corps of Engineers (USACE) Albuquerque District and Tetra Tech have partnered to develop a numerical sediment routing study to assess the impacts of anthropogenic influences and climatic changes on the fluvial geomorphology of the Middle Rio Grande (MRG). The study, consisting of four HEC-RAS sediment routing models of the approximately 170-mile reach of the MRG between Cochiti Dam and the headwaters of Elephant Butte Reservoir (EBR), was developed to evaluate the sediment balance of the MRG and the geomorphic influence of various drivers and controls of channel evolution. The four models were designed to evaluate the MRG as a single inter-dependent system, rather than a set of discrete, independent reaches. Because it employs a single modeling framework to evaluate the entire MRG between Cochiti Dam and EBR, the study provides a unique opportunity to look at the inter-connectivity of the river reaches. The models were developed using available physical and hydrologic data and were calibrated and validated to provide the best fit to observed morphological changes and suspended sediment measurements at selected USGS gages. Using the validated models, various scenarios designed to isolate different influences on the sediment balance and the resulting geomorphology, such as infrastructure modification, diversion dam removals, changes in long-term hydrology, and tributary loading uncertainty, were evaluated and compared with a baseline scenario to provide insight into potential future changes. These relative changes were found to be useful in understanding the magnitude of changes caused by possible future actions or events, providing insight into potential long-term morphological adjustments on the MRG. This paper will provide an overview of the methods and challenges associated with development, calibration, and application of the model, and will summarize the results obtained for various scenarios.

Background

The USACE Albuquerque District is leading a geomorphic characterization study to aid in the environmental stewardship of vital resources along the MRG through New Mexico. More specifically, the USACE is conducting the study to better understand the impacts associated with MRG water resource facilities on the geomorphology and sedimentation of the mainstem channel. Influences of dams, such as Cochiti Dam on the mainstem and Jemez and Galisteo Dams on major tributaries, irrigation diversion structures, channel improvements and protection measures, water deliveries and diversions, and sediment delivery from contributing drainage areas were all evaluated and expected to have some effect on the physical evolution of the channel.

Two previous components of this work (Tetra Tech 2012; Tetra Tech 2013a) have been completed. Tetra Tech (2012) includes (1) a records and literature search related to changes in mainstem geomorphology and sedimentation in response to the construction and operation of USACE dams, (2) an analysis of sediment stored in the Kellner Jetty jack fields, (3) the compilation in a geodatabase of historical sedimentary and morphologic parameters, and (4) a recommended bed material sampling plan to supplement available bed material gradations. Tetra Tech (2013a) was conducted to quantify flood event-

based and mean annual sediment yields from contributing tributary drainage areas to the MRG, as well as the sediment delivery into the mainstem channel. While the findings and results from these two reports are beneficial as stand-alone products, their values can be more fully recognized when considered as building blocks for numerical sediment routing modeling of the MRG.

Various reaches of the MRG have been the subject of other geomorphic studies and sediment routing models conducted by numerous entities over the last several decades, but these analyses have generally had a more limited scope (MEI 2002; Tetra Tech 2010; Makar and AuBuchon 2012; Varyu 2011; Varyu 2013a; Fox and Varyu 2014). Many of these previous studies therefore provide a limited, albeit locally detailed evaluation of the contemporary and historical drivers of geomorphic change along the MRG. This study is unique and powerful in that it assimilates data and resources collected by many different governmental and private stakeholders along the MRG over several decades into a single, unified numerical platform for evaluating the historical and future impact of these drivers of geomorphic change on the entire MRG, from Cochiti Dam to EBR.

This study is composed of four interdependent HEC-RAS one-dimensional sediment routing models, which together cover the entire MRG from the outlet works of Cochiti Dam to the headwaters of EBR at RM 60, approximately 170 river miles. Each of the four models represents a different subreach of the MRG, with the three primary diversion structures (Angostura Diversion Dam [ADD], Isleta Diversion Dam [IDD], and San Acacia Diversion Dam [SADD]) serving as the boundaries between the models (**Figure 1**). A unified modeling strategy was incorporated across all four subreaches so that the models act as subcomponents of a larger integrated model with water and sediment fluxes captured at the boundary conditions, facilitating propagation of geomorphic changes downstream. The modeling provides a quantitative basis for characterizing the following influences on the geomorphology of the MRG:

- Flow regulation and reduction of sediment supply caused by Cochiti Dam
- Flow diversions and grade control at diversion structures
- Uncertainty in the magnitude of sediment loading from contributing tributary drainage areas
- Uncertainty in the future Upper Rio Grande basin snowpack and associated spring runoff,
- Fluctuating pool elevation in EBR, and uncertainty associated with future storage conditions, and
- The proposed realignment of the Rio Grande near Bosque del Apache NWR.
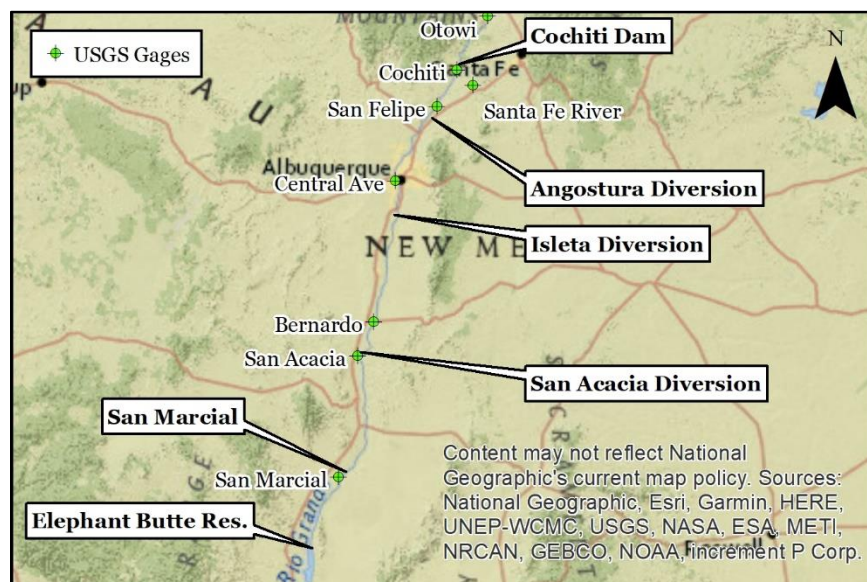
Figure 1. Study area of the MRG numerical model, showing features marking the boundary of each subreach

Modeling of the Cochiti Reach began with HEC-RAS 4.2 beta and was continued with each successive release of HEC-RAS, with final modeling of all reaches conducted using HEC-RAS v. 5.0.6. Tetra Tech assisted HEC in the testing and development of each version of HEC-RAS, and one of the direct results of

this arrangement was the incorporation of a Rouse-based transport limiter for the MPM-Toffaleti function, presented below in the section titled "Selection of Transport Functions".

Modeling Framework

Fixed-Bed Modeling

HEC-RAS models of the four reaches were constructed from various data sources reflecting the 2012 bed configuration. Where possible, bathymetric survey data from U.S. Bureau of Reclamation (BOR) repeat rangeline surveys were used. This bathymetric data was supplemented as necessary with the 2012 BOR Aggradation/Degradation rangeline survey (Varyu 2013b), which uses a backwater calculation to estimate the mean elevation of subaqueous channel at the time of a LiDAR survey. The model hydraulics were calibrated to available historical water surface observations collected during high-flows: 2010 aerial photography (Cochiti Reach), 2005 flood surveyed water surfaces (Tetra Tech 2005, Isleta Reach), 2008 flood surveyed water surfaces (Tetra Tech 2008, Albuquerque, Isleta, and San Acacia Reaches). The flow in the MRG at the time of the observations (which exceeded 3,000 cfs during the 2010 event, exceeded 4,000 cfs in 2008, and exceeded 5,000 in 2005) provide an ideal basis for calibration of hydraulics since higher flows are greater stimulants of geomorphic change.

Bed Material Sampling

Sediment models can be highly sensitive to the starting bed material gradation, and accurate representation of the current conditions of the bed material was critical to ensuring accurate predictive simulations. Therefore, an extensive program of bed material sampling was conducted, in which 133 bed material samples were collected between Cochiti Dam and EBR. Selected quantiles (D_{84}, D_{50}, and D_{16}) from the bed material samples are shown in **Figure 2**.
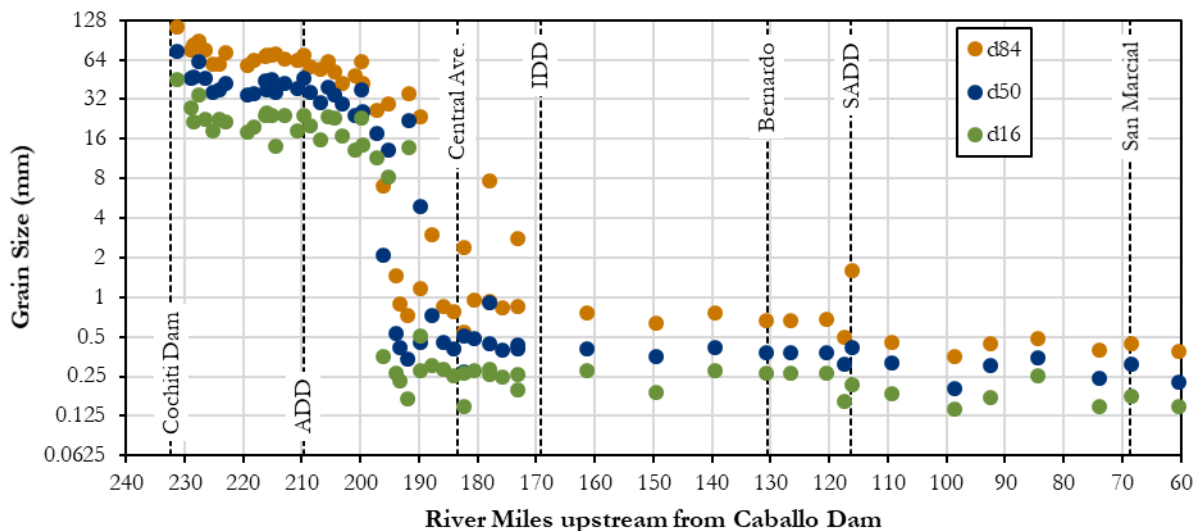
Figure 2. Selected quantiles of sampled surface bed material, Cochiti Dam to EBR

The channel bed downstream from Cochiti Dam is characterized by a coarse armor layer, with small cobbles and very coarse gravels overlaying a substrate of fine to coarse gravels. As shown in Figure 2, the armor layer persists with very little change until the channel begins to transition to a sand-dominated bed in the vicinity of the Bernalillo Bridge (RM 204). The transition zone from a gravel-cobble bed to a sand-dominated channel spans about 12 river miles from the Bernalillo Bridge to the Alameda Bridge (RM 192). The transition zone is characterized by transitory deposits of sand moving over a coarse substrate. Downstream from the transition zone, the channel is dominated by sand-size material, progressively fining downstream. The median grain size near the Central Avenue bridge (RM 183.4) was about 0.4-mm,

and the median grain size near the headwaters of EBR (RM 60) was about 0.23-mm. The bed slope ranges from more than 8 feet per mile near Cochiti Dam to about 3.5 feet per mile at San Marcial.

Prototype Development

The prototype is the model of observed changes in mainstem MRG geomorphology against which the calibration and validation simulations are compared. Prototypes are necessary for calibrating and validating the numerical sediment routing model to evaluate the reliability of predictive modeling. The prototype of geomorphic change along the MRG has two primary components: (1) the observed historical geometric channel change, as estimated from the BOR Agg/Deg datasets, and (2) the observed mass flux at the USGS gaging stations between Cochiti Dam and EBR.

The BOR has collected Agg/Deg datasets every ten years since 1962. The three most recent surveys (1992, 2002, and 2012) were used to develop a prototype of observed vertical bed change for a calibration period (1992-2002) and a validation period (2002-2012). Because HEC-RAS performs the sediment routing and bed change calculations based on mass accounting, the prototype of vertical bed change was also used to derive a channel mass change prototype. Due to differences in the methods of data collection between the datasets and uncertainty and error associated with the underwater prism of the Agg/Deg data, a prototype accuracy of ± 0.5-feet was assumed, and error bands on the mass prototype derived from the vertical change were calculated based on the assumed accuracy.

Ongoing sampling by the USGS at San Felipe (gage no. 08319000), Albuquerque (08330000), Bernardo (08332010), San Acacia (08354900), and San Marcial (08358400) was used to develop a prototype of observed mass flux at each location in the models. At each of the five gaging stations, the USGS has collected total suspended sediment discharge measurements with reported percent finer than 0.0625-mm. The washload fraction (the proportion of each measurement finer than 0.0625-mm) was removed from the observations to allow for calibration of the suspended mass in transport simulated by HEC-RAS to the observed suspended bed material discharge.

Mobile-Bed Modeling

The four fixed-bed hydraulic models were converted to moveable-boundary models using a unified modeling strategy, using the same parameters and modeling assumptions in each reach. The models were calibrated and validated by adjusting model parameters, initial conditions, and boundary conditions until an acceptable level of agreement was reached between the simulated results and the prototypes. The models were then used to simulate 13 predictive scenarios – a baseline scenario representing the current state of the channel and incorporating all current major geomorphic influences and 12 scenarios designed to test the influence of each major geomorphic control and source of uncertainty in the model.

Hydrology: The calibration and validation period were simulated using historical observations from 1992-2002 (calibration) and 2002-2012 (validation). Observed mainstem flows at the USGS gages were supplemented with MRGCD irrigation diversion and return data. The historical pool elevations in EBR provided the downstream boundary. The predictive scenarios were simulated by using the historical hydrology of WY1976-2012, which includes a representation of recent hydrologic scenarios spanning both wet and dry water years, as a proxy for baseline future hydrology of WY2013-2049. This is neither expected nor intended to be an accurate prediction of future hydrology, but only to provide a baseline for evaluation of the current geomorphic influences of the Rio Grande.

Tetra Tech (2013a) detailed 130 tributaries to the MRG, 35 of which were considered significant enough contributors of sediment to include in this study. Of the 35 contributing tributaries, 30 are ungaged, leaving a large data gap in the hydrologic boundary. In the calibration and validation periods, tributaries were assumed to flood once each year with a volume equal to the average annual monsoon season flood for that tributary, based on the results of Tetra Tech (2013a), and scaled to reflect drier or wetter periods. Tributary flood series for the predictive scenarios were synthesized using a probabilistic method, wherein an inverted Gumbel distribution (Gumbel 1958) cumulative distribution function was used to calculate precipitation depths in each tributary basin associated with randomly generated non-exceedance probabilities for each of the 37 simulation years. A goodness of fit test (Anderson and Darling 1954) was

applied to evaluate discrepancies between the distribution of randomly generated events and the theoretical distribution fit to the location and scale parameters of the Gumbel distribution derived from a sample of historical storms at Cochiti Dam. The location and scale parameters were estimated from the sample using maximum likelihood estimates as described in Stephens (1979).

Sediment supply: Of the five gaged tributaries, only one (Rio Puerco) has reliable sediment discharge measurements. The suspended sediment discharge measurements collected on the Rio Puerco by the USGS were scaled by 140-percent to incorporate an estimate of bedload (Graf 1994). A sediment capacity calculation was performed for the Rio Jemez to estimate a Q-Q$_s$ relationship that was then applied to the gaged flows to compute the sediment delivery.

For all other tributaries, during the calibration and validation simulations, annual tributary sediment delivery was estimated to be the average annual flood based on modeled delivery results and areal bed material delivery regression equations provided in Tetra Tech (2013a). For the predictive scenarios, annual tributary delivery was computed based on the runoff volumes of the probabilistic flood series developed for each tributary. Both bed material load and the sand component of the MUSLE load were included. Daily sediment output from the downstream end of each model provided the upstream sediment supply to the downstream reaches.

Selection of Transport Function: There are eight transport functions available in HEC-RAS v. 5.0.6 and each was evaluated for use in the models. Two critical constraints on the selected function are apparent from the prototype development and the sampled bed material: (1) a total load function was necessary to allow calibration to the observed mass flux at the USGS gages, and (2) the selected function must be able to adequately calculate transport of both sand and gravel sized material. From the two constraints, six transport functions were immediately disqualified, and the coupled MPM-Toffaleti function was selected because it has one key advantage over the Copeland function as they are implemented in HEC-RAS: the output from the MPM-Toffaleti function allows for parsing of suspended load and bedload, and so the model results could be directly compared to the USGS observations of suspended bed material that composed the prototype of mass transport.

However, application of the coupled MPM-Toffaleti function on the MRG and contemporaneously on the Middle Susitna River (Tetra Tech 2015) generated sediment discharge rating curves with sharp discontinuities (**Figure 3**). The MPM-Toffaleti function, which was developed to compute total bed material load in large rivers with coarse substrate, can predict unrealistic transport rates under certain conditions for coarse grain classes at relatively high energy. The problem is intrinsic to the Toffaleti equation itself, rather than the coupling.
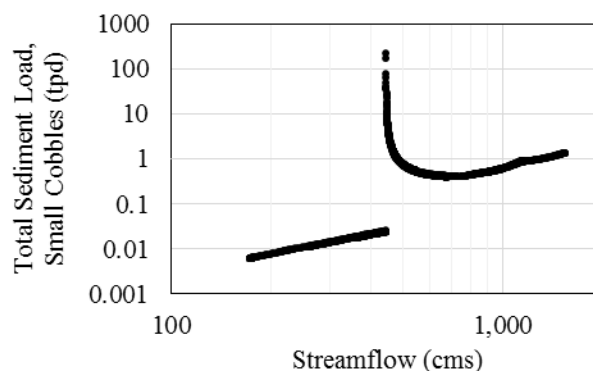
Figure 3. Total load of small cobbles (64-128 mm) computed by HEC-RAS at Susitna RM 107.1 using the coupled Toffaleti-MPM function

The problem arises in the denominator of the reference unit sediment discharge, M$_i$ (as adapted from Vanoni 1975):

$$M_i = \frac{g_{SSLi}(1+n_v-0.756z_i)}{\left(\frac{R_h}{11.24}\right)^{1+n_v-0.756z_i}-(2d_{si})^{1+n_v-0.756z_i}} \tag{1}$$

where $t$he variables g_{ssLi}, n_v, and z_i are sediment transport variables, R_h is the hydraulic radius, and d_s are the nominal transported grain classes.

The quantity $1 + n_v − 0.756z_i$, in equation (1) is almost always negative, making the numerator of Equation 1 negative for most practical applications. Therefore, if the denominator of Equation 1 is ever positive, M_i computes a negative mass flux. For the smallest grain classes, $2d_{si}$ is much smaller than $R_h/11.24$. Since both quantities are raised to the same negative exponent, the denominator is typically also negative, resulting in a positive flux for smaller grain sizes. However, as the grain size increases and $2d_{si}$ approaches $R_h/11.24$, the denominator of Equation 1 approaches and passes through zero. In these cases:

$$\lim_{\left(2d_{si}\to\frac{R_h}{11.24}\right)^-} M_i = \infty \tag{2}$$

This explains the discontinuity in Figure 1, which is characteristic of the asymptotic behavior of a function in the form $y = 1/x$. As $2d_{si}$ exceeds $R_h/11.24$, M_i becomes negative, and the function no longer makes physical sense.

Because the original, and particularly, the hybrid versions of Toffaleti are useful and widely applied in large river systems with coarse bedload components, the function was modified to account for the numerical discontinuity as a direct result of the MRG modeling. The Rouse number is commonly used to distinguish between bedload and suspended load conditions (Cheng and Chiew 1999; van Niekerk et al 1992; Shah-Fairbank et al. 2011; Gibson and Cai 2017), and to partition load mechanisms in other transport functions that separate the bed and suspended load computations (Bagnold 1977; Van Rijn 1984). Julien (2002) suggests that bedload is dominant in situations where the ratio of total shear velocity, u_*, to fall velocity, ω, is less than about 0.4, and above this ratio flow turbulence is sufficient to move the sediment as mixed or suspended load. For $u^*/\omega = 0.4$, the dimensionless Rouse number (Ro) is:

$$Ro = \frac{\omega}{\beta\kappa u_*} = 6.25 \tag{3}$$

where β is the ratio of the turbulent mixing coefficient to the momentum exchange coefficient, assumed for most practical purposes to equal one; and κ is the von Kármán constant, 0.4. A Rouse number greater than about 2.5 often indicates that sediment moves primarily as bedload, with mixed load still an important component of total transport. As the Rouse number increases, the tendency for material to move as bedload increases.

A feature was added to HEC-RAS v. 5.0 and later which limits Toffaleti transport capacity for any size class where $u_*/\omega \leq 0.4$. This feature checks the Rouse number associated with each grain class to filter illegitimate suspended transport calculations of large particles, which tend to invoke the negative flux condition. This check sets the Toffaleti transport capacity to zero in all zones for all size classes that do not meet the Rouse suspension threshold, and sets the bed load transport capacity to the value calculated by MPM if the hybrid MPM-Toffaleti function is chosen.

It can be demonstrated that the ratio u^*/ω can be expressed as a function of R_h only, assuming a drag coefficient of 1.5 and a water temperature of 20°C, and using a form of fall velocity found in Julien (2010):

$$\frac{u_*}{\omega} = \frac{\sqrt{gR_hS}}{\left(\frac{9.76e-5}{d_S}\right)\left(\sqrt{1+0.139d_*^3}-1\right)} \tag{4}$$

From Equation 4, it is possible to approximate the lower zone threshold or hydraulic radius at which $u_*/\omega = 0.4$. **Figure 4** shows this result for a range of slopes and hydraulic radii and demonstrates that the transport limiter will become active at hydraulic radii exceeding $2d_{si}$, thus preventing the numerical

artifact for slopes up to about 1%. As a provision for rare cases not eliminated by the Rouse-based limiter, a separate logical flag has also been included to exclude suspended load if $R_h/11.24 \leq 2d_{si}$.
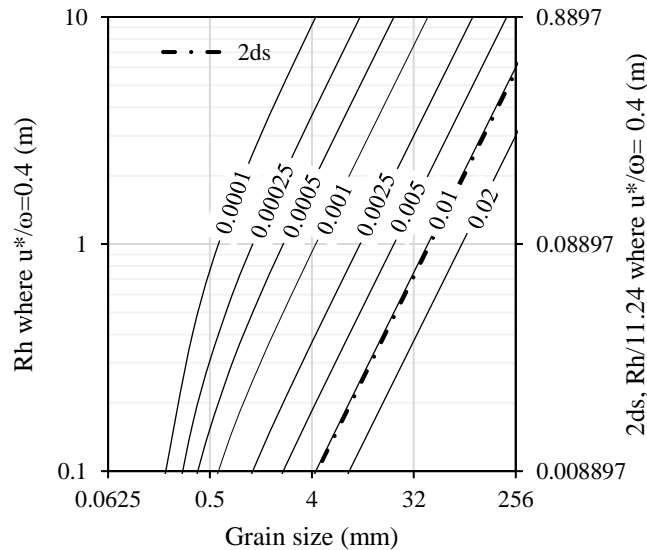
Figure 4. For a given slope, the hydraulic radius (left-axis) and corresponding lower zone threshold ($R_h/11.24$, right-axis) at which the ratio of shear velocity to fall velocity will be equal to 0.4. The Rouse-based limiter is effective above and left of the 2ds line, while the logical flag is effective below and right of the 2ds line.

Figure 5 shows results from the MRG and whether or not the Rouse-based limiter prevented sediment transport for a given grain size at various hydraulic radii. The described limiter filtered out suspended transport for all size classes larger than coarse sand. Coarse sand was filtered out at the lowest hydraulic radii. The result is in general agreement with the estimated activation threshold for slopes between 0.025% and 0.08%, similar to the range of slopes observed in the model (perfect agreement is impossible due to variations in slope, water temperature, and calculation method for fall velocity).
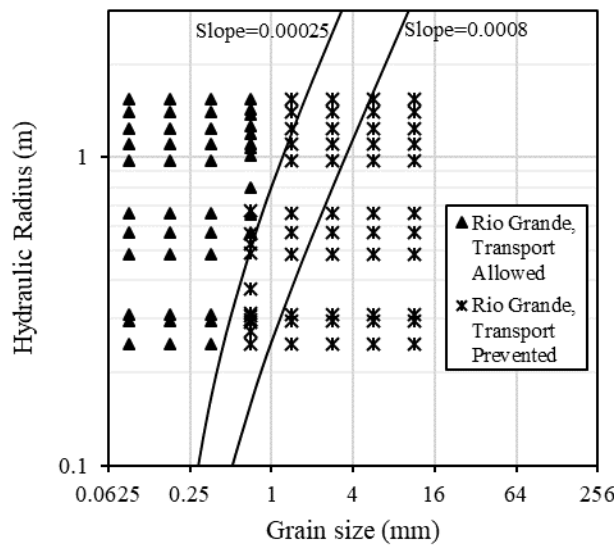
Figure 5. Model results for the Rio Grande before and after the Rouse based limiter was activated. Shown are maximum, minimum, and decile results for hydraulic radii that were filtered and unfiltered, and the approximate activation thresholds (the hydraulic radius at which $u_*/\omega=0.4$) for slopes similar to those in the model.

Modeling Scenarios: In addition to the *Baseline Scenario*, a suite of 12 predictive scenarios was designed to quantify the estimated future impact of changes in the geomorphic drivers and controls along the MRG. *Scenarios 1 through 5* test the removal of each of the major in-stream dams (Cochiti, Angostura, Albuquerque Drinking Water, Isleta, and San Acacia). *Scenario 6* was designed to test the removal of irrigation diversions, but not the structure, at San Acacia. *Scenarios 7 and 8* test sensitivity of the Baseline results to higher and lower tributary loads, quantifying the effect of uncertainty in the tributary bed material delivery. *Scenario 9* simulates a reduced future snowpack to test the influence of a reduced water flux, a common predicted result from climate change models for rivers with a snow-pack runoff in the arid southwest (Mote et al. 2005; Elias et al 2015). *Scenarios 10 and 11* test the influence of pool elevations (persistent high pool and persistent low pool) in EBR. And finally, *scenario 12* tests the influence of the proposed channel realignment in the Bosque del Apache NWR.

Model Results

Calibration and Validation

Modeling parameters were adjusted until there was reasonable agreement between the simulation and prototype bed profiles and rating curves. The calibration model of the Cochiti and Isleta Reaches simulated median bed change within 0.4-feet of the prototype, and the Albuquerque Reach was within 0.7-feet[1]. Each of the three models replicated local trends of aggradation and degradation reasonably well, and the model was able to successfully replicate the suspended bed material rating curves at the USGS gages.

The models were then tested for their ability to replicate an independent dataset during the validation period (2002-2012) without adjustment of the modeling approach or parameters. As demonstrated by **Figure 6**, with only local divergences the model was able to replicate the historical bed change.
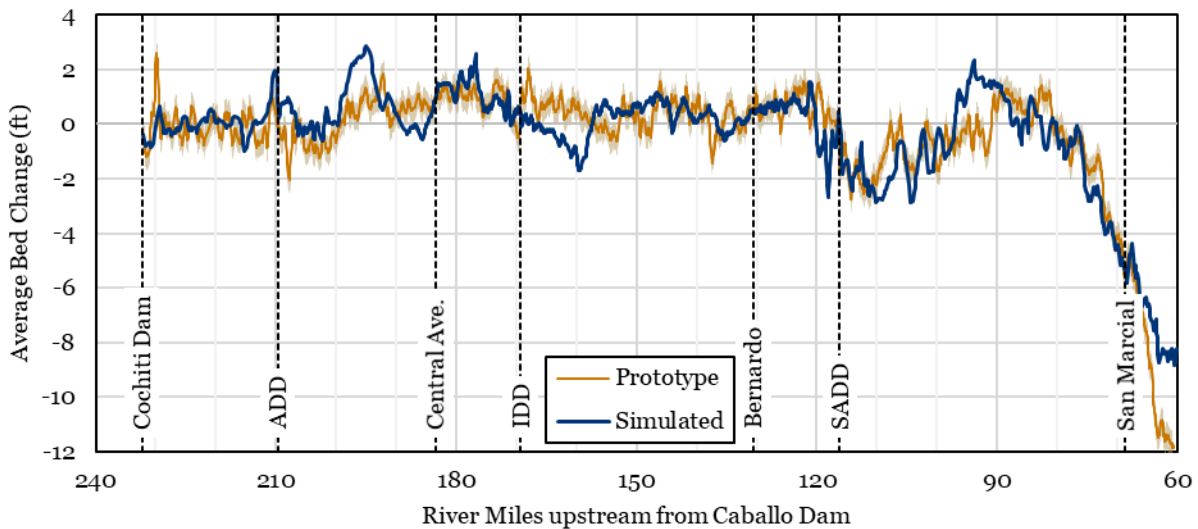
Figure 6. Model results from the validation period (2002-2012) showing simulated average bed change versus the prototype (±0.5' error bands also shown)

The importance of the local divergences between the simulated bed profile and the prototype were evaluated by comparing the simulated cumulative longitudinal channel mass change (net aggradation or degradation) with the prototype and the range of cumulative aggradation or degradation associated with the assumed prototype error of ±0.5 feet, as shown in **Figure 7**. The model shows reasonable agreement with the mass prototype throughout the entire reach.

---

[1] A calibration model for the San Acacia Reach was not simulated because the amount of geomorphic change caused by fluctuations in the pool elevation in EBR since 1992 made it impossible to use 2012 geometry to reproduce bed changes between 1992 and 2002.
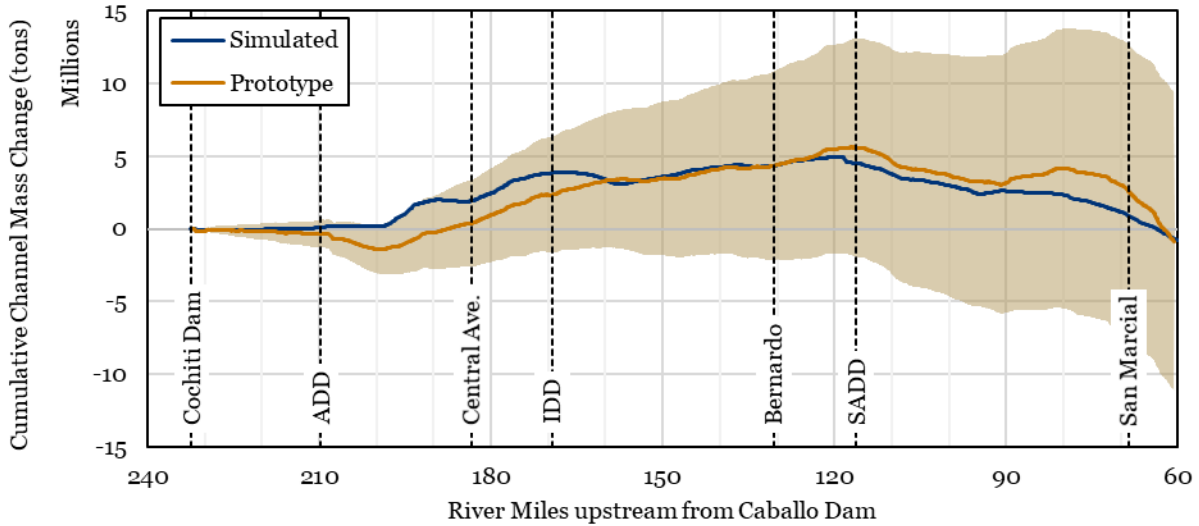
Figure 7. Model results from the validation period (2002-2012) showing simulated longitudinal channel mass change versus the prototype (shading represents mass change associated with ±0.5' error in the prototype)
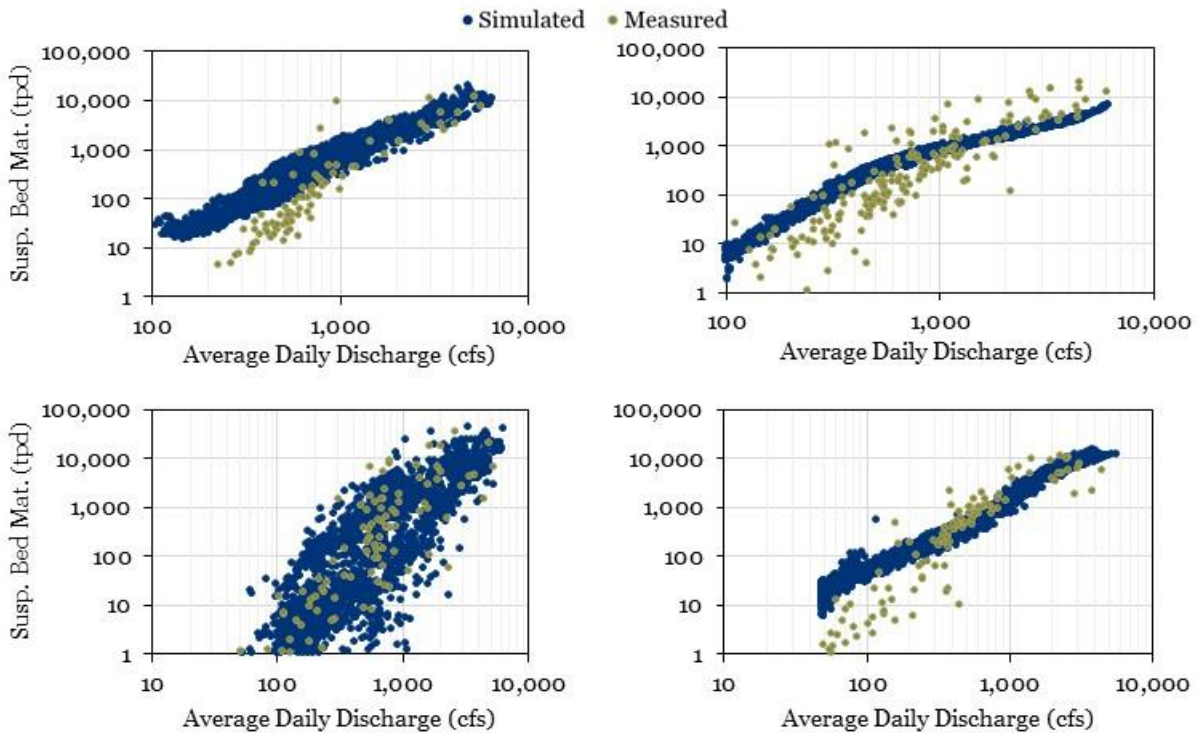
Figure 8. Model results of suspended bed material discharge, compared to USGS measurements at (clockwise from top left) Central Ave., Bernardo, San Marcial, and San Acacia

Simulated suspended bed material discharge was compared to USGS observations at each of the gaging stations in the reach (**Figure 8**). The model reproduced the observed suspended bed material measurements at each gaging station. There was a slight bias towards over-predicting suspended bed material transport at discharges below about 500 cfs. The bias is perhaps most pronounced at San Marcial, but only about 2-percent of the suspended load is transported at flows less than 300 cfs, thus the bias does not introduce a significant modeling error.

Predictive Scenarios

The calibrated and validated sediment routing models were used to predict future changes to the morphology of the MRG. A baseline model was simulated for 37 years using the 2012 bed configuration with current geomorphic driver conditions and controls in place. Several scenarios were designed to isolate and test the influence of one geomorphic driver or control and results were compared to the baseline. Due to the volume of results that were produced by the modeling, results for the scenarios have been summarized here in the form of subreach scale sediment budgets, with notable results discussed. **Table 1** shows the sediment balance from the baseline scenario. All four subreaches are aggradational in terms of total mass storage, with more than half of the aggradation occurring in the Albuquerque Reach.

Table 1. Sediment budget results for *Baseline Scenario*. All units in millions of tons.

Reach	Upstream Supply	Tributary Supply	Diversion	Downstream Delivery	Sediment Storage
Cochiti	0.079	26.1	-1.22	22.3	2.67
Albuquerque	22.3	27.7	-1.09	14.0	34.9
Isleta	14.0	47.8	-0.459	57.1	4.33
San Acacia	57.1	4.06	0	37.2	23.9
Combined	0.079	105.7	-2.77	37.2	65.8

Removal of Cochiti Dam: Cochiti Dam is the largest mainstem dam on the MRG upstream of Albuquerque, NM. Removal of Cochiti Dam was simulated by combining the observed flow series on the Rio Grande at Otowi (USGS 08313000) and on the Santa Fe River above Cochiti Lake (USGS 08317200) to remove the effect of flow regulation. The sediment rating curve resulting from removal of the dam was estimated by combining the USGS suspended sediment discharge measurements at Otowi with an estimate of bedload developed by Tetra Tech (2013b). Results from the Removal of Cochiti Dam scenario (**Table 2**) indicate that removing the dam increases the upstream sediment load from essentially zero to about 42M tons, and that this increase in sediment supply is nearly all deposited upstream from IDD. Positive values in the sediment budget tables reflect increased sediment storage compared to the baseline.

Table 2. Sediment budget results for *Removal of Cochiti Dam Scenario*. All units in millions of tons.

Reach	Upstream Supply	Tributary Supply	Diversion	Downstream Delivery	Sediment Storage	Change in Storage vs. Baseline
Cochiti	42.3	26.1	-2.38	53.0	13.1	10.4
Albuquerque	53.0	27.7	-1.14	15.6	64.0	29.1
Isleta	15.6	47.8	-0.434	57.6	5.43	1.10
San Acacia	57.6	4.06	0	39.9	21.7	-2.23
Combined	42.3	105.7	-3.95	39.9	104.2	38.4

Removal of Diversion Dams: There are four diversion dams along the MRG, and each provides grade control and abstracts flow for agricultural or municipal uses. Removal of each of the diversion dams was evaluated by removing the structure and associated sediment and flow diversions from the model. These models were only simulated in the reach in which the dam is located, with sediment and water flux effects propagated downstream. Results from the diversion dam removal scenarios are shown in **Tables 3 through 6**. Removing any of the three primary irrigation diversions (ADD, IDD, SADD) results in less storage upstream as the impounded sediments are removed, and more storage downstream as they are deposited. Removal of the Albuquerque Drinking Water Diversion (ABCWUA; Table 4) increases the flow rate in the river slightly, which in turn causes small reductions in sediment storage as there is a marginal increase in sediment transport capacity of the river.

Table 3. Sediment budget results for *Removal of Angostura Diversion Dam Scenario*. All units in millions of tons.

Reach	Upstream Supply	Tributary Supply	Diversion	Downstream Delivery	Sediment Storage	Change in Storage vs. Baseline
Cochiti	0.079	26.1	0	23.9	2.29	-0.384
Albuquerque	23.9	27.7	-1.18	14.8	35.6	0.675
Isleta	14.8	47.8	-0.458	57.1	5.12	0.788
San Acacia	57.1	4.06	0	37.2	23.9	-0.021

Table 4. Sediment budget results for *Removal of Albuquerque Drinking Water Diversion Dam Scenario*. All units in millions of tons.

Reach	Upstream Supply	Tributary Supply	Diversion	Downstream Delivery	Sediment Storage	Change in Storage vs. Baseline
Albuquerque	22.3	27.7	-1.13	14.7	34.2	-0.720
Isleta	14.7	47.8	-0.447	58.0	4.11	-0.216
San Acacia	58.0	4.06	0	38.7	23.3	-0.638

Table 5. Sediment budget results for *Removal of Isleta Diversion Dam Scenario*. All units in millions of tons.

Reach	Upstream Supply	Tributary Supply	Diversion	Downstream Delivery	Sediment Storage	Change in Storage vs. Baseline
Albuquerque	22.3	27.7	0	25.1	25.0	-10.0
Isleta	25.1	47.8	-0.418	61.6	11.0	6.64
San Acacia	61.6	4.06	0	41.0	24.6	0.632

Table 6. Sediment budget results for *Removal of San Acacia Diversion Dam Scenario*. All units in millions of tons.

Reach	Upstream Supply	Tributary Supply	Diversion	Downstream Delivery	Sediment Storage	Change in Storage vs. Baseline
Isleta	14.0	47.8	0	59.0	3.06	-1.27
San Acacia	58.9	4.06	0	37.0	25.9	1.99

Tributary Load Sensitivity: There is much uncertainty in the tributary load to the MRG due to both the ephemeral nature of the tributary watersheds and the lack of stream gaging. This uncertainty was evaluated by using the upper and lower 50% prediction intervals on the bed material component of the tributary rating curves. The MUSLE component was not scaled. Results from the higher tributary load test are shown in **Table 7**. Increased tributary loads translate almost directly into increased sediment storage. Results from the lower tributary load scenario are shown in **Table 8**. Decreases in bed material delivery from the tributaries translate almost directly to decreases in sediment storage in the MRG.

Sensitivity to the sediment load from the Rio Jemez and Rio Puerco were not considered in these scenarios because their loads were not estimated in the same way as the ungaged tributaries. Results in the Albuquerque Reach were highly sensitive to the load from the Rio Jemez, therefore two sub-scenarios were simulated that tested sensitivity to the Rio Jemez load, doubling it in one scenario and halving it in the other. Results indicated that the bed profile of the Albuquerque Reach could fluctuate by several feet based on the Rio Jemez load, but that it made very little difference downstream from Central Avenue.

Table 7. Sediment budget results for *Higher Tributary Load Scenario*. All units in millions of tons.

Reach	Upstream Supply	Tributary Supply	Diversion	Downstream Delivery	Sediment Storage	Change in Storage vs. Baseline
Cochiti	0.079	27.5	-1.25	23.0	3.38	0.710
Albuquerque	23.0	28.2	-1.09	14.1	36.0	1.05
Isleta	14.1	48.6	-0.463	57.3	4.92	0.590
San Acacia	57.3	4.37	0	37.1	24.5	0.599
Combined	0.079	108.7	-2.80	37.1	68.8	2.95

Table 8. Sediment budget results for *Lower Tributary Load Scenario*. All units in millions of tons.

Reach	Upstream Supply	Tributary Supply	Diversion	Downstream Delivery	Sediment Storage	Change in Storage vs. Baseline
Cochiti	0.079	25.0	-1.18	21.5	2.41	-0.258
Albuquerque	21.5	27.0	-1.07	13.9	33.5	-1.40
Isleta	13.9	45.3	-0.449	55.2	3.60	-0.731
San Acacia	55.1	3.85	0	37.1	21.9	-2.07
Combined	0.079	101.2	-2.70	37.1	61.4	-4.46

Reduced Snowpack: The future impact of a decreased snowpack (reduction in water flux) was estimated by modifying the boundary flow series at Cochiti Dam, Rio Jemez, and Rio Puerco. The quartile of wettest years during the simulation period were randomly replaced by the quartile of driest years, and the EBR pool was modified to reflect a persistent low pool. The result of the reduced snowpack is shown in **Table 9**. The decreased flow volume and tributary delivery resulting from a reduced snowpack causes less aggradation in the two upstream reaches and more aggradation in the two downstream reaches.

Table 9. Sediment budget results for *Reduced Snowpack Scenario*. All units in millions of tons.

Reach	Upstream Supply	Tributary Supply	Diversion	Downstream Delivery	Sediment Storage	Change in Storage vs. Baseline
Cochiti	0.079	26.1	-1.78	22.3	2.07	-0.598
Albuquerque	22.3	17.9	-0.950	8.05	31.3	-3.64
Isleta	8.05	46.1	-0.562	47.5	6.09	1.76
San Acacia	47.5	4.06	0	26.9	24.7	0.727
Combined	0.079	94.2	-3.29	26.9	64.2	-1.75

Elephant Butte Reservoir Pool Elevation: The San Acacia reach is heavily influenced by the pool elevation in EBR and is known to have fluctuated by several tens of feet historically in response to storage fluctuations. The future impact of EBR pool elevation was evaluated by synthesizing a persistent high pool elevation and a persistent low pool elevation using the Upper Rio Grande Water Operations Model (URGWOM). These scenarios were only evaluated in the San Acacia Reach. Results for the high and low pool scenarios are shown in **Table 10**. The low pool scenario resulted in about 5.9M tons less storage of sediment than the baseline, with generally lower channel elevations everywhere downstream from about RM 96. Likewise, the high pool scenario resulted in generally higher channel elevations downstream from RM 96, and about 6.1M more tons of sediment storage in the San Acacia Reach.

Table 10. Sediment budget results for *High and Low Pool Scenarios*, simulated only in the San Acacia Reach. All units in millions of tons.

Scenario	Upstream Supply	Tributary Supply	Diversion	Downstream Delivery	Sediment Storage	Change in Storage vs. Baseline
High Pool	57.0	4.06	0	31.1	30.0	6.10
Low Pool	57.0	4.06	0	43.1	18.0	-5.92

RM 83 Channel Realignment: The BOR has proposed realigning the channel through BDA by shifting the main flow path to the east and out of its currently perched channel. With guidance from BOR staff, an estimated channel alignment and profile was inserted into the model, together with assumptions about the sectional shape of the designed channel. The realigned channel is expected to be vulnerable to fluctuations in EBR pool elevation, and therefore the realigned channel was simulated under baseline, low, and high pool scenarios. These simulations were only performed in the San Acacia Reach. The results shown in **Table 11** do not represent a final evaluation of the impact of the BOR's proposed design but serve as a conceptual check of the feasibility of channel realignment under varying conditions in EBR.

Table 11. Sediment budget results for *RM 83 Realignment Scenarios*, simulated only in the San Acacia Reach. All units in millions of tons.

Scenario	Upstream Supply	Tributary Supply	Diversion	Downstream Delivery	Sediment Storage	Change in Storage vs. Baseline
Baseline Pool	57.0	4.06	0	35.8	25.3	1.34
High Pool	57.0	4.06	0	31.1	31.0	7.06
Low Pool	57.0	4.06	0	41.5	19.6	-4.33

Vertical channel change: The sediment budget results above reflect the relative influence of each evaluated scenario on the total mass balance (channel and overbanks combined) of the MRG. The Rio Grande has been narrowing in many reaches due to bar accretion and subsequent colonization of the bars by vegetation. As the channel narrows, it is deepening in some locations, and the total mass balance alone may not provide an accurate representation of the geomorphic processes in the reach. **Table 12** presents the median change in mean bed elevation on a subreach scale for each scenario. Downstream from Isleta the main channel tends to be degradational, even while the cumulative mass balances indicate aggradation. This would indicate a tendency for sediment to accumulate in the floodplains.

Table 12. Median change in mean channel bed elevation in each subreach for each scenario.

	Reach			
Scenario	Cochiti	Albuquerque	Isleta	San Acacia
Baseline	0.00	3.02	-3.00	-1.02
Removal of Cochiti Dam	1.19	4.41	-3.53	-1.32
Removal of ADD	-0.33	3.07	-2.83	-0.97
Removal of ABCWUA Dam	---	2.91	-3.05	-1.00
Removal of IDD	---	2.49	-1.44	-0.81
Removal of SADD	---	---	-3.04	-0.66
Higher Tributary Load	0.00	3.10	-2.94	-0.81
Lower Tributary Load	-0.15	2.82	-3.04	-1.17
Reduced Snowpack	0.02	2.26	-2.39	-1.37
EBR High Pool	---	---	---	-0.32
EBR Low Pool	---	---	---	-1.15
Realignment – Baseline Pool	---	---	---	-1.02
Realignment – High Pool	---	---	---	-0.09
Realignment – Low Pool	---	---	---	-1.10

Conclusions

From the modeling results, several conclusions can be drawn about the relative influence of each of the assessed geomorphic drivers and controls along the MRG:

- The river is currently in a generally aggradational state in terms of total mass storage, a result that does not change on the net in any scenario. However, the channel tends to be degradational downstream from Isleta Diversion Dam indicating a continued trend of accretion of the banks and islands and narrowing and deepening of the main channel in these locations.
- The Albuquerque Reach is currently in a state of long-term aggradation, likely caused by delivery of sediments from the Rio Jemez. A sensitivity analysis to the sediment load from the Rio Jemez revealed that downstream reaches are unlikely to be influenced during the simulation horizon by sediments delivered by the Rio Jemez, but the amount of aggradation experienced by the Albuquerque Reach is highly sensitive to the Rio Jemez load.
- Delivery of sediment past RM 60 is generally insensitive to the geomorphic influences on the channel, remaining at about 37 million tons of bed material during the simulation window. However, the high and low pool scenarios do influence the delivery of material past RM 60 (31.1 million and 43.1 million tons, respectively) as the backwater from the reservoir limits transport rates in the high pool scenario and the progressive headcut moving upstream increases transport

rates in the low pool scenario. Reduced flows from a diminished snowpack severely decrease bed material delivery past RM 60 (to 26.9 million tons).

- Removal of Cochiti dam would result in widespread aggradation upstream from SADD, concentrated in the Cochiti and Albuquerque reaches. Upstream from IDD there would be channel aggradation along with widespread overbank aggradation, whereas downstream from IDD, an increase in channel degradation is predicted to occur along with overbank accretion.
- Effects of diversion dam removal are relatively small and local. Isleta Diversion Dam has the largest influence, and impacts all reaches except the Cochiti Reach. Removing IDD is predicted to result in about 10 million tons less sediment stored in the Albuquerque Reach during the simulation window.
- Flow abstractions associated with ABCWUA cause general degradation downstream when returned to the stream, however these adjustments are minor and amount to only about 40,000 tons of degradation per year between the dam and EBR.
- Future anticipated climate change resulting in a reduced snowpack causes comparatively less sediment storage upstream from IDD, and comparatively more storage downstream from IDD.
- EBR pool elevations have a large influence on the morphology and sediment balance of the MRG downstream from SADD.
- The model is sensitive to tributary bed material loading in that increases or decreases in tributary loads result in almost one-to-one increases or decreases in sediment stored in the MRG. However, on the magnitudes tested in this study, differences in tributary loads do not result in substantial changes to bed elevation in the reaches, and do not alter delivery of bed material past RM 60.

Acknowledgements

References

Anderson, T.W., and D.A. Darling, 1954. "A Test of Goodness of Fit." Journal of the American Statistical Association, Vol. 49(268): pp. 765-769.

Bagnold, R. (1977) Bed Load Transport by Natural Rivers, Water Resources Research, 13(2), 303-312.

Cheng, N. and Chiew, Y. (1999) "Analysis of Initiation of Suspended Sediment from Bed Load," ASCE Journal of Hydraulic Engineering, 125(8), 885-861.

Elias, E. H., Rango, A., Steele, C.M., Mejia, J.F., and Smith, R. 2015. "Assessing climate change impacts on water availability of snowmelt-dominated basins of the Upper Rio Grande basin". Journal of Hydrology: Regional Studies **3**:525-546.

Fox, B. and Varyu, D. 2014. Middle Rio Grande Base Level Modeling. Technical Report No. SRH-2014-27. U.S. Department of the Interior, Bureau of Reclamation, Technical Service Center, Denver.

Gibson, S. and Cai, C. (2017) "Flow Dependence of Suspended Sediment Gradations," Water Resources Research, in press.

Graf, W. L., 1994. "Plutonium and the Rio Grande. Oxford University Press. New York.

Gumbel, E.J., 1958. Statistics of Extremes. Columbia University Press. New York.

Julien, P. Y. (2002). River Mechanics. Cambridge University Press, New York.

Julien, P. Y. (2010). Erosion and Sedimentation. 2nd Ed. Cambridge University Press, Cambridge, UK.

Makar, P. and AuBuchon, J. 2012. Channel Conditions and Dynamics of the Middle Rio Grande River. Varyu, D. 2013. 2012 Cross Section Geometry Generation and Validation. U.S. Department of the Interior, Bureau of Reclamation, Albuquerque.

MEI. 2002. Geomorphic and Sedimentologic Investigations of the Middle Rio Grande Between Cochiti Dam and Elephant Butte Reservoir. Mussetter Engineering Inc. for New Mexico Interstate Stream Commission, Albuquerque.

Mote, P. W., Hamlet, A.F., Clark, M.P. and Lettenmaier, D.P. 2005. "Declining mountain snowpack in western North America." Bulletin of the American Meteorological Society **86**:39-49.

Shah-Fairbank, S.C., Julian, P.Y., Baird, D.C., (2011) "Total Sediment Load from SEMEP using Depth-Integrated Concentration Measurements," Journal of Hydraulic Engineering, 137(12), 1606-1614, DOI: 10.1061/(ASCE)HY.1943-7900.0000466.

Stephens, M.A., 1979. "The Anderson-Darling Statistic." Technical Report No. 39. Department of Statistics, Stanford University. Stanford, California.

Tetra Tech, 2010. "River Mile 80 to River Mile 89 Geomorphic Assessment and Hydraulic and Sediment-continuity Analyses." Prepared by Tetra Tech, Inc. for the U.S. Department of the Interior, Bureau of Reclamation, Albuquerque Area Office, Technical Services Division. February 2010. Albuquerque, New Mexico.

Tetra Tech, 2012. "Rio Grande and Tributaries Preliminary Data Collection and Assembly." Prepared for the U.S. Army Corps of Engineers, Albuquerque District. Albuquerque, New Mexico.

Tetra Tech, 2013a. "Rio Grande and Tributaries Tributary Sediment Yield and Delivery Study." Prepared for the U.S. Army Corps of Engineers, Albuquerque District. Albuquerque, New Mexico.

Tetra Tech, 2013b. Geomorphic and Hydraulic Assessment of the Rio Grande from US Highway 550 Bridge to Montaño Bridge – 2004 to 2012. Prepared for the U.S. Department of the Interior, Bureau of Reclamation, Albuquerque Area Office, Environmental Division. Albuquerque, New Mexico.

Tetra Tech (2015). "Fluvial Geomorpholgy Modeling below Watana Dam, Study Plan Section 6.6." Prepared for Alaska Energy Authority.

van Niekerk, A., Vogel, K., Slingerland, R., and Bridge, J. (1992) Routing of Heterogeneous Sediment Over Movable Bed: Model Development, ASCE Journal of Hydraulic Engineering, 118(2), 246-262.

van Rijn, L. C. (1984). "Sediment transport, Part II: Suspended load transport." ASCE Journal of Hydraulic Engineering, 110(11), 1613–1641.

Varyu, D. 2011. One-Dimensional Modeling and Indicator Results for the Middle Rio Grande. Technical Report No. SRH-2-11-25. U.S. Department of the Interior, Bureau of Reclamation, Technical Service Center, Denver.

Varyu, D. 2013a. Aggradation/Degradation Volume Calculations: 2002-2012. Technical Report No. SRH-2013-28. U.S. Department of the Interior, Bureau of Reclamation, Technical Service Center, Denver.

Varyu, D. 2013b. 2012 Cross Section Geometry Generation and Validation. Technical Report No. SRH-2013-21. U.S. Department of the Interior, Bureau of Reclamation, Technical Service Center, Denver.

Vanoni, V.A. (1975). Sedimentation Engineering, ASCE Manual of Practice - 110, New York.

Modeling Bank Migration on the Missouri River with HEC-RAS: A Calibrated HEC-RAS/BSTEM Model

Michael Koohafkan, Department of Water Resources, Sacramento CA/University of California – Davis, koohafkan@ucdavis.edu

Stanford Gibson, PhD, Hydrologic Engineering Center, US Army Corps of Engineers, Davis, CA
Sanford.Gibson@usace.army.mil

Paul M Boyd, PhD, PE, Omaha District, US Army Corps of Engineers, Omaha, NE
Paul.M.Boyd@usace.army.mil

Dan Pridal, PE, Omaha District, US Army Corps of Engineers, Omaha, NE
Daniel.B.Pridal@usace.army.mil

The US Army Corps of Engineers' Hydrologic Engineering Center began to include mobile bed capabilities with Version 4.0 of the River Analysis System (HEC-RAS) software. These capabilities compute vertical bed changes in response to dynamic sediment mass balance and bed processes. However, many riverine sediment problems involve lateral bank erosion. Lateral toe erosion and bank failure processes require models that simulate feedback between bed and bank processes. The Bank Stability and Toe Erosion Model (BSTEM) developed by the National Sediment Laboratory, United States Department of Agriculture (USDA), Agricultural Research Station (ARS) was included in HEC-RAS version 5.0 and updated in subsequent releases. BSTEM couples iterative, planar bank failure analysis based on a fundamental force balance with a toe scour model that allows feedback between the hydraulic dynamics on the bank toe. These feedbacks can exacerbate failure risk (in the case of toe scour) or decrease failure risk (in the case of toe protection).

The Missouri River eroded aggressively, downstream of Gavins Point dam for about 20 years after dam closure (Skalak et al, 2013). The erosion along this reach included both bed degradation and bank migration. The Hydrologic Engineering Center (HEC) and the Omaha District of the US Army Corps of Engineers (NWO) developed an HEC-RAS model of the Missouri River from Gavins Point Dam (RM 811) to Ponca (RM 751) to simulate historical large-scale bank movement and sediment inputs, and to evaluate alternative design impacts on future bank movement. The study team selected the bank erosion parameters in the USDA-ARS BSTEM module to calibrate bank migration against five surveys spanning August 1986 through August 2011.

Model Setup

The study team calibrated the model against computed longitudinal cumulative Planform Area Change (LCPAC) curves, rather than the longitudinal cumulative volume change (LCVC) curves that HEC-RAS automatically generates and modelers typically used to evaluate sediment transport models. Planform area change (PAC) is the lateral migration of the bank toe multiplied by the control volume streamwise length. This metric is analogous to computations of bank area loss based on differencing surveyed bank lines with GIS. LCPAC curves differ from LCVC curves in that they do not consider the bank height in change calculations. LCPAC curves may be more representative of bank losses than LCVC curves when surveys of the floodplain surface are missing or have reduced accuracy relative to channel surveys, and to isolate the

calibration of bank change from uncertainty in bed change calibration. LCPAC curves can be computed from the HEC-RAS BSTEM outputs (and from historic surveys) as the difference in the bank toe location at a cross-section between successive observations multiplied by the cross-section length.

Cross section geometries were compared to aerial photographs to identify potential issues. Three cross sections (1960RM 775.8, 773.76, 768.41) were problematic because channel migration changed the angle between the original cross section and the river, making them diverge from the 1D assumption of orthogonality. These cross sections would severely over-estimate actual bank migration; an example of this issue is shown in Figure 1. The identified cross sections were therefore excluded from the calibration dataset.

Figure 1. An example of the potential for erroneous bank change calculations due to channel migration. Range line labels refer to 1941 river mile markers. The channel has migrated such that the survey range line in the lower-right corner becomes essentially parallel to the channel. Erosion of the river-left bank occurring below range line 810.2 would be erroneously captured in repeated surveys of range line 808.5.

BSTEM requires several additional soil parameters. Many of these parameters have significant spatial variability and can vary by multiple orders of magnitude along a short river reach. Even with extensive field data collection efforts, bank erosion parameters (e.g. soil erodibility and critical shear stress) have high uncertainty. The study team opted to use a single representative soil type for the model for initial values prior to detailed calibration. This decision was consistent with the Oct 2012 Missouri River Jet Erosion Testing Report, which established that virtually all banks in the modeled reach are composed of sand. The average gradation generated from the dataset was used for the representative bank soil type. The properties of the representative soil type are shown in Table 1. The study team selected two of these soil properties calibration parameters; the representative values for the remaining six parameters were used for all cross sections. Critical shear stress was the primary calibration parameter to

account for the uncertainty in the one-dimensional shear stress assumptions. Erodibility was used as a secondary parameter to account for variability in soil characteristics. Both parameters carry a high degree of uncertainty and are difficult to measure in the field, particularly in sandy soils.

Table 1. Representative bank soil parameters.

Parameter	Value
Saturated unit weight	$117.8 \dfrac{\text{lbf}}{\text{ft}^3}$
Friction angle	$28.3°$
Cohesion	$8354 \dfrac{lbf}{ft^2} (*)$
ϕ^b	$15°$
Critical Shear Stress	$0.0106 \dfrac{lbf}{ft^2}$
Erodibility	$8.96 \times 10^{-5} \dfrac{ft^3}{lbf \cdot s}$
Saturated hydraulic conductivity	$300 \dfrac{ft}{day} (*)$
Reservoir width	$1\, ft (*)$

(*) This parameter was assigned a synthetic value to prevent bank failure plane computation.

Calibration

The calibration approach adjusted the global erodibility parameter first and then changed local critical shear stresses at each cross-section bank to generate a strong calibration for the 1960-1986 survey period. Both erodibility and critical shear stresses were the adjusted to improve bank migration results for all 5 survey periods. The calibration results are included in 2 (calibration for total combined bank change) and 3 (calibration of left and right bank change separately). These are LCPAC calibrations that compare the cumulative planform area change from the model and the repeated cross sections from upstream to downstream.

A strong calibration was achieved for both banks for all five survey periods. For some cross sections in the lower third of the model reach, calibrating the later surveys required some over-prediction of bank area change in the 1960-1986 period. In general, error between modeled and simulated toe migration were within 25-50%. This is consistent with the expected uncertainty of sediment transport models. Errors in simulated bank migration are magnified by control volume lengths; larger control volumes have a disproportionately large effect on the LCPAC curves relative to the actual error in toe migration. The calibrated critical shear stresses and erodibility mostly varied from 0.0025 to 0.16 lb/ft² and 0.0003 to 0.0009 ft³/lbf/s respectively.
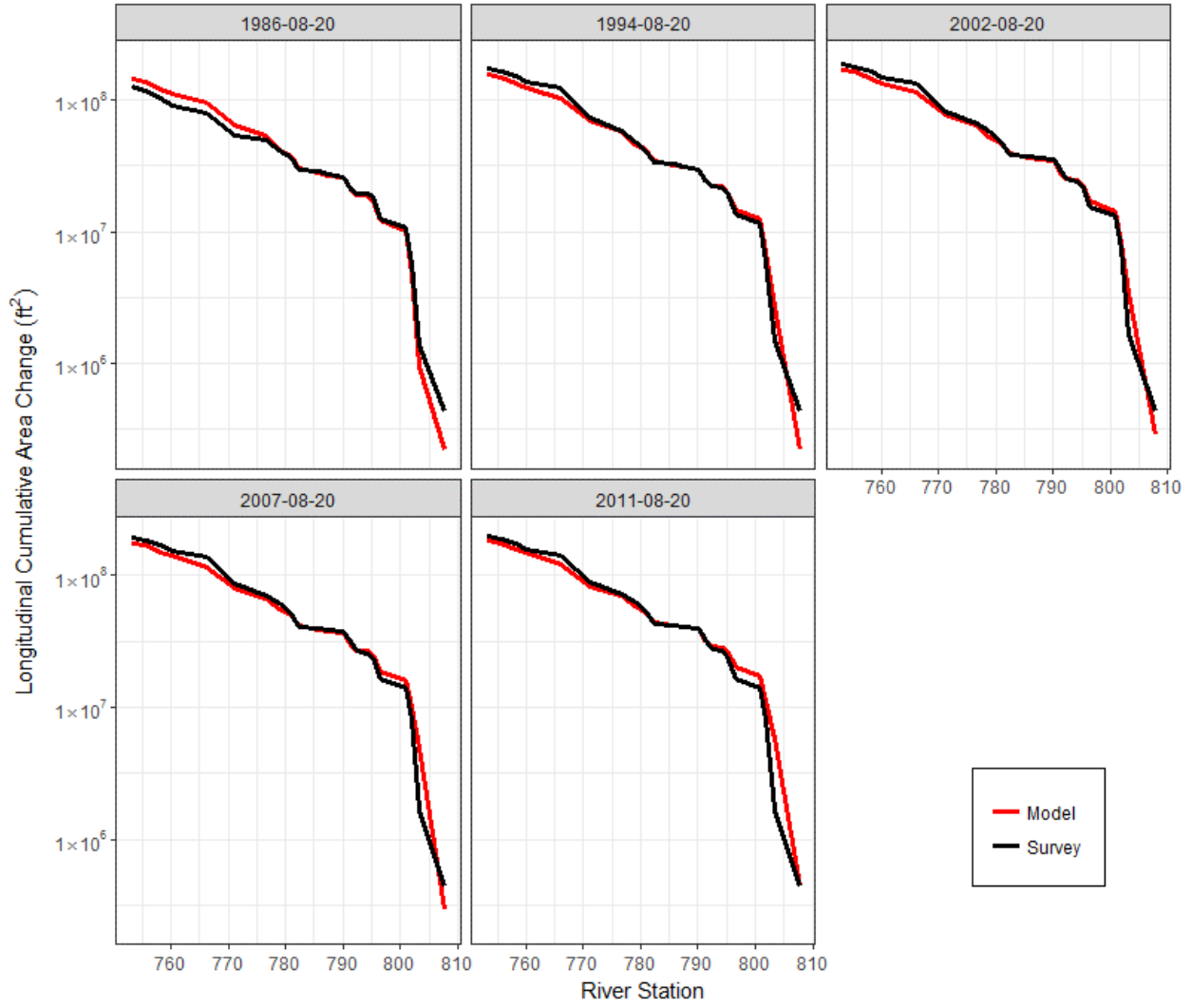
Figure 2. LCPAC calibration results.
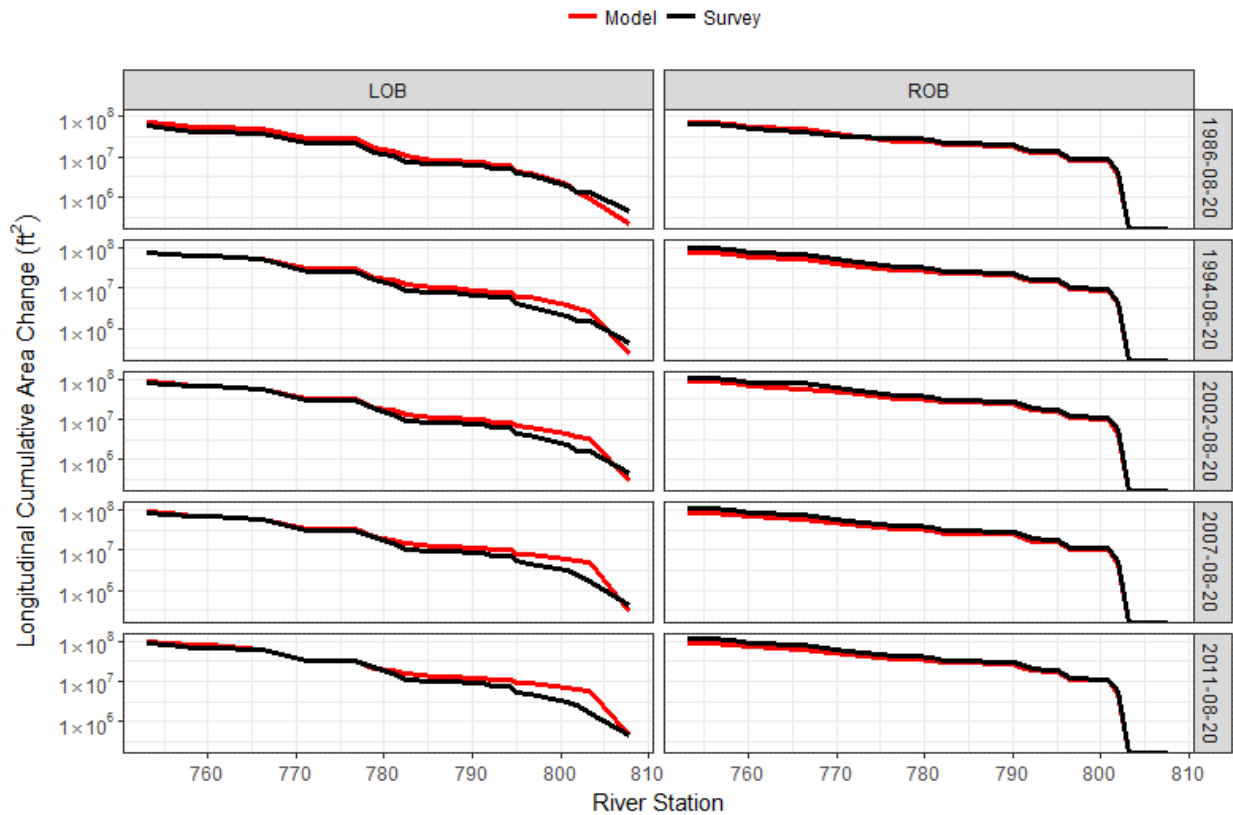
Figure 3. LCPAC calibration results for left and right banks independently.

Modeling Challenges and Lessons Learned

The modeling team encountered several challenges applying the HEC-RAS/BSTEM model on this spatial and temporal scale. These challenges and lessons learned are worth reporting to support future work with this tool.

First, developing an HEC-RAS/BSTEM model requires more careful cross section definition than models that only simulate hydraulics or, even, vertical bed change. Both channel and floodplain geometry contribute to the total volume of computed bank erosion. Therefore, bank erosion analysis requires accurate surveys of both the channel and the floodplain in order to develop accurate estimates of historical bank erosion. The Gavins Reach HEC-RAS/BSTEM model geometry was based on a survey completed in 1960 and compared with five repeat surveys, completed in 1986, 1994, 2002, 2007, and 2011. Some cross sections were not mapped to the same extents in all surveys; for example, the 2007 survey was restricted to the channel and overbank regions were not surveyed. In order to ensure consistency in computations based on the calibration data, missing data for individual cross sections were replaced with data from prior surveys where appropriate.

Second, the BSTEM algorithm is sensitive to the number of cross-section points between the bank toe and top of bank, and to the location of the toe relative to the bank height and adjacent node elevations. The study team found that simplifying BSTEM cross sections by (1) removing

nodes between the bank toe and top of bank and (2) ensuring that the bank toe node was located near the channel bed improved model performance and stability. In some cases, small secondary channels were removed to improve model performance. The study team had to correct for these changes for when comparing simulated bank erosion to historical surveys. These geometry modifications to improve model performance changed the original survey data at several locations. Because of these differences, some of the modeled cross sections could not be compared to the surveyed bank volume change and were excluded from the analysis.

Third, HEC-RAS computes bed change and bank migration volume independently. However, parsing lateral bank migration from bed change contributions to the total sediment volume change at a 1D cross section can pose challenges. This is illustrated in the cross section schematic shown in Figure 4. Sediment eroded near the bank toe reflects both bank erosion and bed erosion, but precisely the model cannot identify these contributions precisely. This uncertainty in processes operating at the bank toe must be considered when assessing model performance and validation from calculations of sediment volume. This computational distinction motivated the decision to use LCPAC curves to evaluate the model results. Planform volume analysis avoids issues with floodplain survey accuracy and discriminating between bed and bank change at the toe regions while still capturing the dominant patterns in bank change. The study team computed plan form volume change from the HEC-RAS, HDF5 output using R, but HEC is developing more robust model analysis tools that automate these analyses.
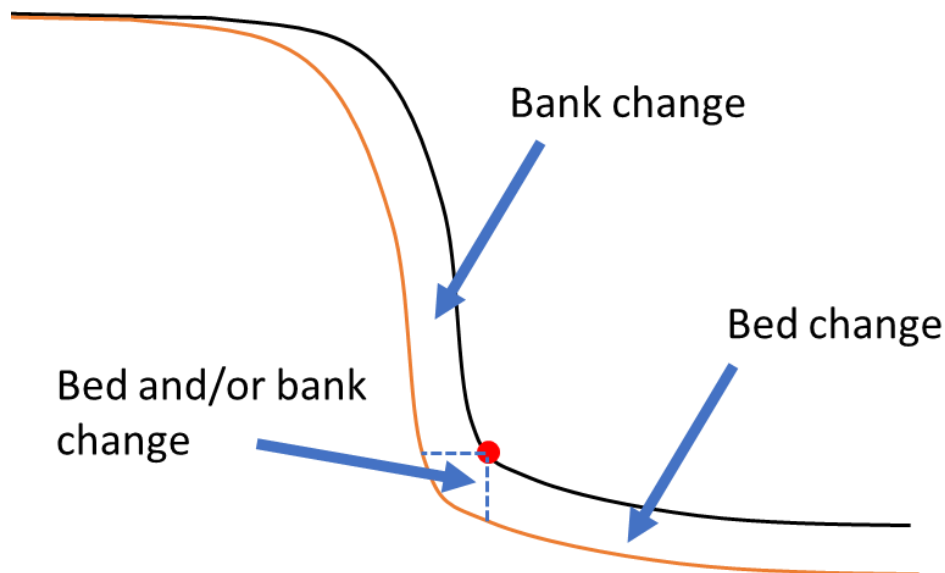
Figure 4. A schematic of cross-section change as computed from survey data. Cross section change in the vicinity of the bank toe can be attributed to bed change, bank change, or some combination of the two.

A fourth challenge arises from simplifications inherent in the cross section-based representation of channels in one-dimensional models. Because bed and bank change computed at cross sections are interpolated upstream and downstream, modeled patterns of cross-section change are significantly simplified and computed bank migration may differ significantly from bank delineations based on aerial or satellite imagery. A schematic of planform area computation at a single cross-section is shown in Figure 5.
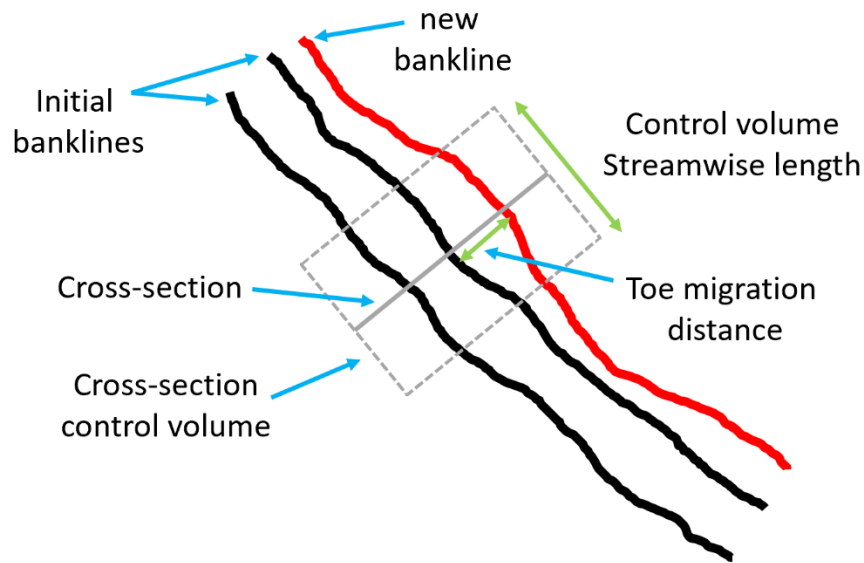
Figure 5. Schematic of bank planform area change computation.

Finally, bank protection complicates long term bank erosion simulations like the one documented above. If agencies or individuals stabilize banks successfully – within a calibration period - a well parameterized model will over-predict bank migration or a modeler might artificially select parameters to match the cumulative erosion assuming the bank eroded over the whole simulation. Both approaches make the model inappropriate for future projections. Therefore, HEC added a bank protection feature to the HEC-RAS/BSTEM module in versions 5.0.3 and later. HEC-RAS can account for bank stabilization by disabling the bank erosion model for any simulation time after a user-specified protection date (Figure 6). Because bank protection was common in the 1970's and 1980's along this reach, the calibration presented in Figure 2 and Figure 3 would not be possible without accounting for it. And without accounting for bank protection, the model would not be useful for projection.

Figure 6: Bank protection tool added to HEC-RAS version 5.0.3 and later.

Conclusion

The USDA-ARS Bank Stability and Toe Erosion Model (BSTEM) incorporated in HEC-RAS simulated bank migration on the Missouri River, downstream of Gavins Point dam. The calibration required critical shear stresses that spanned three orders of magnitude to reproduce longitudinal volume change (per cross section and for each individual bank) over five calibration periods spanning 71 years. The calibrated erodibilities spanned less than two orders of magnitude, with the majority of cross sections requiring an erodibility slightly smaller than the value determined from laboratory analysis.

References

Gibson, S., Brunner, G., Piper, S., and Jensen, M. (2006). "Sediment Transport Computations in   HECRAS." Eighth Federal Interagency Sedimentation Conference (8thFISC), Reno, NV, 57-64.

Gibson, S., Simon, A., Langendoen, E., Bankhead, N., and Shelley, J. (2015) "A Physically-Based Channel-Modeling Framework Integrating HEC-RAS Sediment Transport Capabilities and the USDA-ARS Bank-Stability and Toe-Erosion Model (BSTEM)," Federal Interagency Sediment Conference, SedHyd Proceedings.

Langendoen, E.J. and Simon, A. (2008). Modeling the evolution of incised streams, II: Streambank erosion. Journal of Hydraulic Engineering, 134(7): 905-915.

Skalak KJ, Benthem AJ, Schenk ER, Hupp CR, Galloway JM, Nustad RA, Wiche GJ. 2013. Large dams and alluvial rivers in the Anthropocene: the impacts of the Garrison and Oahe Dams on the Upper Missouri River. Anthropocene 2: 51–64. DOI:10.1016/j.ancene.2013.10.002.

Modeling Dynamic Bank-Erosion Processes to Evaluate Impacts of Flow Regulation and to Develop Flow Metrics Based on Magnitude and Duration of Flows Above Erosion Thresholds

Andrew Simon, Senior Principal, Cardno, Oxford, MS, andrew.simon@cardno.com
Jennifer Hammond, Senior Engineer, Cardno, Fayston, VT, jennifer.hammond@cardno.com
Kimi Artita, Senior Civil Engineer, Sci-Tek Consultants, Inc., Clemson, SC, kartita@scitekanswers.com

Abstract

Process-based modelling of bank processes is crucial to evaluate impacts of flow releases and bulk transfers of water from Dartmouth Dam to the Mitta Mitta River and ultimately to the southern arm of Lake Hume, Victoria, AUS. The river serves as a conduit for water transfers from Dartmouth Reservoir to the lake. Actual and prospective erosion of the banks under historical and alternative flow-release scenarios were modelled at seven sites along the Mitta Mitta River using the dynamic version of the Bank-Stability and Toe-Erosion Model (BSTEM-Dynamic). This approach allowed for identification of erosion-threshold conditions which ranged from about 5,200 megalitres per day (ML/d) to almost 13,000 ML/d, generally decreasing downstream. This variation in erosion thresholds coincided with a general increase in erosion rates downstream. Modelled bank-erosion rates over the period ranged from 0.89 m^3 per meter of channel length (m3/m) to 9.8 m3/m. Erosion did not begin at any site until daily-flow rates were greater than about 5,000 ML/d, indicating that this discharge would be a conservative, erosion-limiting daily-transfer rate. Previously reported recommendations for drawdown rates (5 mm/hr) were found to be slower than the hydraulic conductivity of any of the materials tested.

The magnitude and duration of flows above erosion thresholds exert a strong influence on bank erosion rates. Consequently, these parameters were evaluated for their relative influence on bank erosion during the 19 flow-release periods that occurred during the 2006-2016 period. Significant regression relations show that that a metric, defined as the median ratio of the flows to the erosion threshold, multiplied by the duration of those flows (in days) explains much of the variation in average erosion rates for a given release type. Reversing these regressions can be used to help guide operational-release scenarios to limit bank erosion to a certain, acceptable value.

Introduction

The Mitta Mitta River flows for about 100 kilometers (km) downstream of Dartmouth Dam to the southern arm of Lake Hume (Figure 1). The river serves as a conduit for bulk-water transfers from Dartmouth Reservoir to Lake Hume for the primary purpose of ensuring that water supply in Lake Hume does not become too low, particularly during dry seasons. Completed in 1979, Dartmouth Dam has significantly altered the flow regime downriver by (1) storing inflows to pass of floodwaters over its spillway to mitigate floods downstream, and (2) provide bulk-water transfers during dry periods to supplement storage in Lake Hume. The Murray-Darling Basin

Authority (MDBA) seeks to conduct water transfers to limit bank instability and environmental damage while promoting ecological attributes and ecosystem functions.
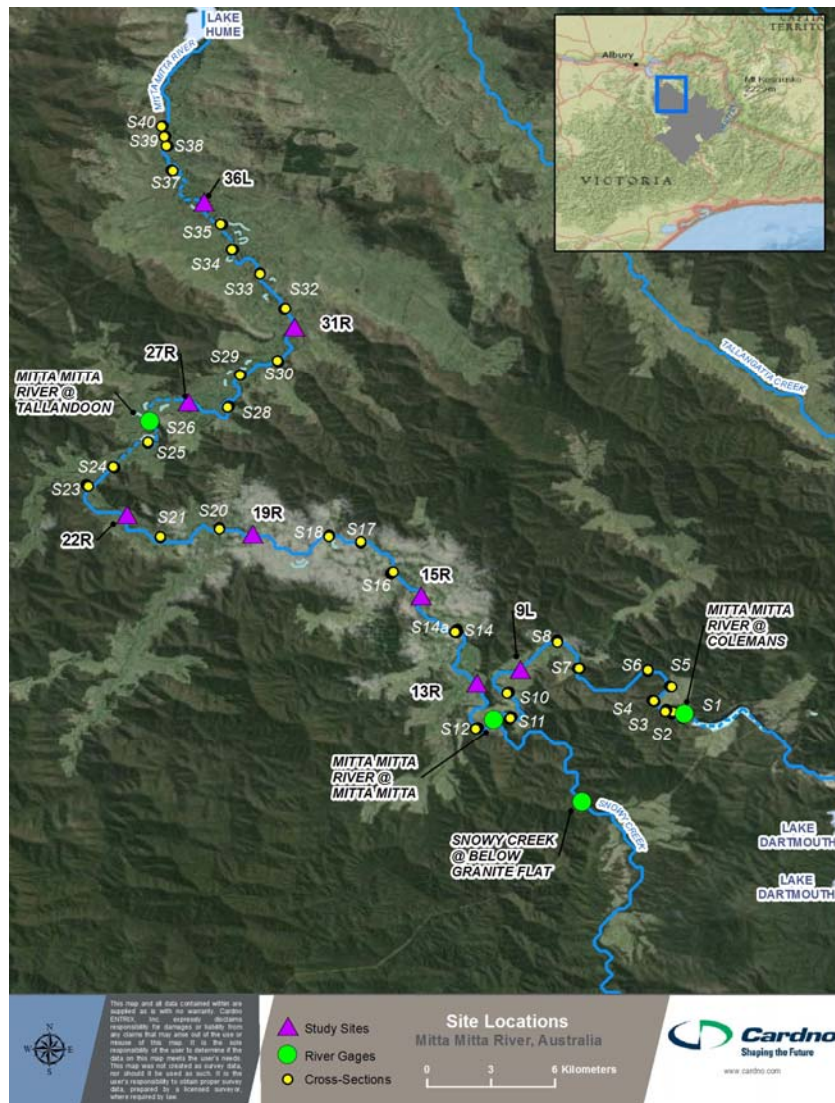
Figure 1. Map of the study reach showing locations of the detailed-study sites and flow gauges.

Bank erosion and lateral migration of meanders has long been an active process along reaches of the Mitta Mitta River. Bank scour, lateral-bank retreat and channel migration are the result of interactions between the hydraulic forces operating at the bank toe and other bank surfaces, and the gravitational (geotechnical) forces operating on the bank mass. MDBA wants a better quantitative understanding of the role of different operational-flow scenarios on bank processes and erosion rates. To quantify the important controls and threshold conditions on bank erosion along the Mitta Mitta River, this study takes a process-based approach to quantify the driving and resisting forces to use a deterministic numerical model: BSTEM-Dynamic.

This study addresses prior uncertainty regarding the role of the magnitude and duration of high-flow events on rates of bank erosion, particularly those flows between 5,000 and 10,000 ML/d. The frequency and duration of these flows have increased compared to pre-regulated conditions

as a result of the bulk transfers to Lake Hume. Current practice is to keep releases below 5,000 ML/d where practical, taking into consideration demand patterns. Compounding this is the issue of the role of drawdown where there is conflicting evidence on the hydraulic conductivity of the banks. Green (1999) indicates that the banks can drain at rates of 0.7 metres per day (m/d), which would be sufficient to minimize large head differences between the ground and surface waters for rates of fall up to 0.35 m/d. A subsequent report (Lawson and Treloar, 2001), however, suggested that banks may drain at rates much slower (i.e., 0.086 m/d).

Objectives and Scope

This study provided for a physically based numerical analysis of bank-erosion processes along the Mitta Mitta River. The investigation focused particularly on determining the factors controlling bank-erosion rates along the Mitta Mitta River downstream from Dartmouth Dam. The primary objective was to determine the most effective way to make bulk transfers of water from Dartmouth Lake to Lake Hume that limits bank erosion. This meant investigating the roles of the magnitude and duration of high flows, rates of rise and particularly fall, and the general pattern of transfers in determining bank-erosion rates. This was accomplished by simulating bank erosion over a range of operational-flow scenarios using BSTEM-Dynamic at seven representative sites. The model provides for dynamic fluctuations of both ground and surface-water levels. Figure 1 shows a map of the study reach with locations of the detailed-study sites and flow gauges.

Boundary Resistance and Hydraulic Conductivity

The erodibility of surficial bank and bank-toe materials by hydraulic forces is important to modelling and predicting bank-erosion rates because it is the hydraulic processes that can cause undercutting of the bank, making it more susceptible to collapse. Based on 30 in situ tests with a submerged jet-test device, the hydraulic resistance (τ_c) of all but about 1% of the materials is equivalent to gravel-sized or finer materials (Figure 2, Right). In fact, about 50% of the materials are only as resistant as sand-sized materials $\tau_c < 2.0$ Pascals (Pa).

Geotechnical data (cohesion and friction angle) obtained in situ with a Borehole Shear Tester are the fundamental measures of bank strength used to simulate and predict bank stability under a range of moisture conditions. Results of 13 individual tests along the Mitta Mitta showed that the cohesive strengths of the banks ranged from 0.0 to 13.9 kPa. The median value of effective cohesion is 0.84 kPa (average = 3.4 kPa), defining generally low strengths, in keeping with the generally silty and sandy bank materials.

Results of falling-head tests of hydraulic conductivity conducted in the field showed a median value of about 1.0 m/d, with an inter-quartile range from 0.4 to 2.3 m/d, indicating that these materials are generally quite conductive. These values should be considered relative to the maximum operational drawdown rates that range from 0.24 m/d (10 mm/h) to 0.48 m/d (20 mm/h) and to 0.7 m/d (30 mm/h), which are overlain in Figure 2 (Left). Thus about 55% of the materials tested drain faster than the maximum drawdown rates. These results further indicate that in some cases and at some sites, conductivity rates are less than recession rates and could, therefore, play a role in increasing bank erosion. Although Lawson and Treloar (2001) report infiltration rates "as low as" 0.086 m/d, the lowest rates measured in this study were 0.16 m/d at site 36L and 0.19 m/d at site 22R. For flows greater than 5,000 ML/d, they suggest drawdown

rates should be < 0.12 m/d (5 mm/h) and possibly slower in the downstream reaches. This would be slower than any of the conductivity values measured in this study and would, therefore, certainly be effective at limiting the drawdown condition.
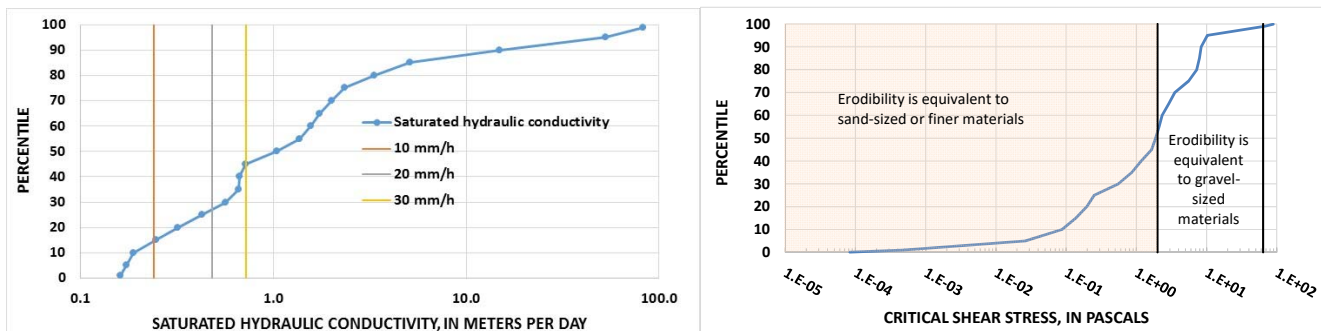
Figure 2. Distribution of measured, saturated hydraulic conductivity compared to the three entitlement rates of fall (Left) and critical shear stress of the surficial bank materials (Right).

Hydrology

BSTEM relies on stage data to generate boundary shear-stress distributions along the wetted part of the bank face for each time step. Thus, a flow series for each of the seven modelling sites was generated from 15-minute discharge data from gauging stations on the Mitta Mitta River and Snowy Creek (Figure 1). These data were first converted to an hourly-maximum discharge record and then to an hourly-stage record using the Manning equation in a normal-depth calculation worksheet. The flow series for all of the Mitta Mitta River gauges reflect releases from Dartmouth Dam as can be seen from some of the broad peaks representing bulk transfers (Figure 3). The ratio of the catchment area at each site to the closest gauge was used to scale the flows.
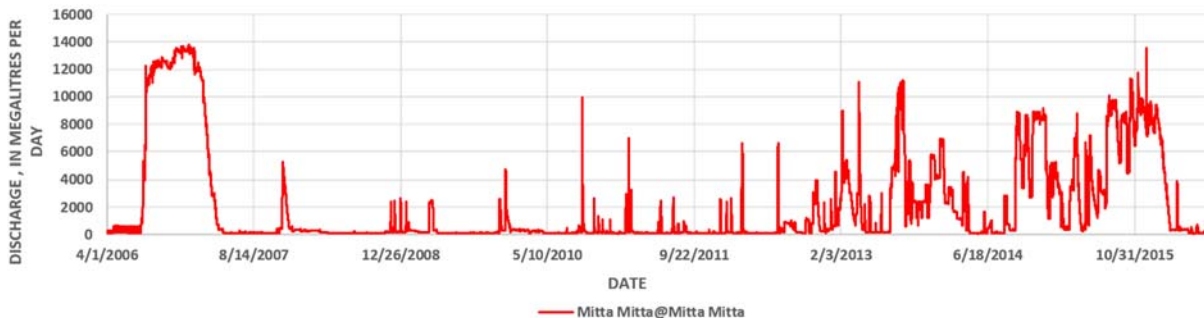
Figure 3. Maximum-hourly flows for a gauging station on the Mitta Mitta River system for the model period.

Bank-Stability Modelling with BSTEM-Dynamic

BSTEM-Dynamic contains both geotechnical-stability and hydraulic-erosion algorithms, thereby allowing for deterministic analysis of bank stability over an unsteady flow series Simon et al. (2011). The time step and period of analysis is selected by the user. As such, flow stage at each time step is read into the model, and the amount and location of hydraulic erosion is calculated. The resulting new bank geometry for that time step is then used in the geotechnical algorithm to determine the stability of the bank by calculating the bank's Factor of Safety (<1.0 = unstable, >1.0 = stable) at that time step. If a geotechnical failure is predicted, the geometry is updated

again to account for the failure before the next flow-stage value is read in at the next time step. In this way BSTEM-Dynamic 2.3 can predict the retreat of a streambank for flow series ranging in length from hours to decades. In addition to being able to account both hydraulic and geotechnical processes, the model has a groundwater component that contributes to the geotechnical-strength algorithm, and can account for the effects of root-reinforcement provided by riparian vegetation, through the RipRoot sub-model.

To calibrate the model for a site, the 2006 surveyed geometry, hourly-flow series and the bank-resistance data for each identified layer were input into BSTEM-Dynamic. In addition, a hydraulic roughness value (n) was assigned to each layer according to the characteristics of the bank surface. The model was then run for the full simulation period until completion (1 April 2006 to 6 July 2016). An example is shown for site 27R (Figure 4, Left). Results of the calibration runs showed bank-erosion volumes ranging over an order of magnitude from about 0.89 m3/m (of channel length) at site 27R to about 9.8 m3/m at site 22R (Figure 4, Right). In general, the largest amount of erosion occurs in the middle reach at sites 19R and 22R with sites (9L, 13R and 27R) having the lowest amounts. Because each of the sites was subjected to the same flow series, differences in bank-erosion rates at individual sites are related to site-specific conditions at that site, including bank height and angle, bank-material strength and, particularly, bank-surface erodibility. This is because in spite of moderate bank-material strengths, a location that has weak bank-toe materials and is subject to scour and undercutting during moderate and high flows can readily lose support for the upper part of the bank and fail. The two sites with the highest amount of erosion over the period, sites 22R and 19R, have the most erodible bank-toe materials, with critical shear stresses of 0.8 and 1.1 Pa, respectively (equivalent to sand-sized materials).
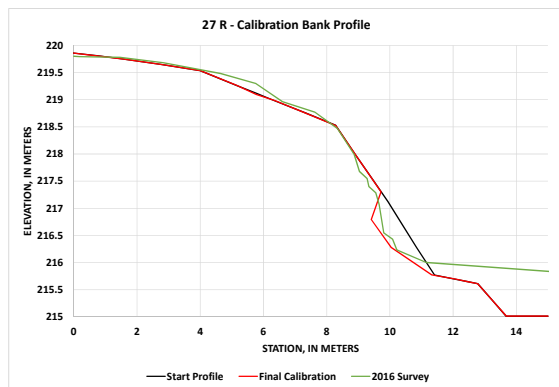
Site	Geotechnical Erosion (m^3/m)	Hydraulic Erosion (m^3/m)	Total Erosion (m^3/m)	Unit Erosion (m^3/m/y)
9L	-	0.978	0.978	0.095
13R	0.149	0.771	0.920	0.090
15R	0.379	1.23	1.61	0.156
19R	0.171	3.48	3.65	0.355
22R	6.25	3.57	9.82	0.957
27R	0.076	0.812	0.888	0.087
36L	0.181	0.978	1.16	0.113

Figure 4. Calibration results for site 27R showing good agreement between the modeled profile (in red) and the 2016 survey in green (Left), and for all sites (Right). Both the 2006 and 206 profiles are from surveys

Bank Erosion during Flow Transfers and Flow-Threshold Conditions:

The relation between flow-transfer periods and bank erosion can be obtained by taking the results from the BSTEM output and summing the hourly bank-erosion data that fall within a given flow-transfer period. This, along with quantifying the actual flow thresholds that initiate erosion, helps provide insight into the pattern of alternative flow scenarios to test which would tend to limit bank erosion. Thus, analyses were conducted to: (1) evaluate any relation between bank erosion and the magnitude and duration of flow events that occurred during the period April 2006 to July 2016; and (2) determine the flow-thresholds for bank erosion.

Erosion amounts during the 19 flow-transfers periods (expressed in ML/mo) were extracted from the model results and processed to determine the total amount of erosion, transfer amount and duration of the transfer (Figure 5). Aside from two relatively low average monthly release periods of 2,763 and 8,470 ML/mo, measurable erosion has occurred at average monthly-transfer rates above 90,000 ML/mo. Total-erosion amounts (sum of erosion at each site) increased for the average monthly bulk-transfer amounts of 131,000 (20 months between August 2014 and March 2016) and 244,000 ML/mo (9 months between August 2006 and April 2007). These represent the three bulk-transfer periods with the greatest average-monthly flows between 2006 and 2016. These flow periods with the highest erosion amounts also have the longest durations, ranging from 9 to 20 months.
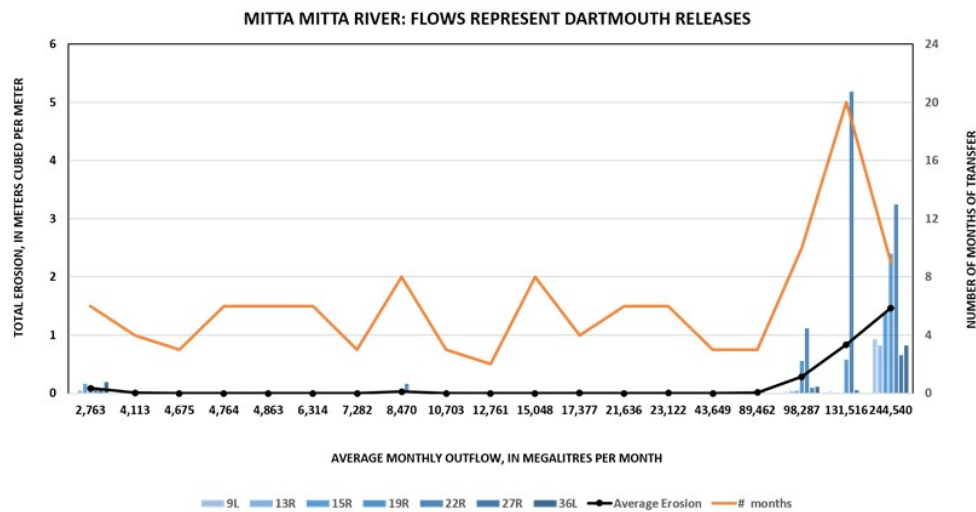
Figure 5. Bank erosion during flow-transfer periods also showing durations of transfers.

Clear operational guidance based on average-monthly values and duration of the flow periods is not appropriate because of the uncertainty surrounding the magnitude of the daily flows represented by a particular average value. To address this, we need to include the resistance of the boundary to quantify the magnitude and duration of flows that exceed that critical condition. For instance, sites with the most erodible materials having the lowest thresholds for erosion. Based on output from BSTEM-Dynamic, the three sites with erosion thresholds near 5,000 ML/d (19R, 22R and 36L) have the three lowest critical shear stress values at the bank toe; 1.1, 0.8 and 0.1 Pa, respectively, equivalent to the resistance of sand-sized materials. The sites in the upper part of the study reach (sites 9L, 13R and 15R) have the highest erosion thresholds, ranging from about 9,500 ML/d at 9L to 13,000 ML/d at 13R (Table 1). From this we would expect that the upper sites will show less erosion between 5,000 and 10,000 ML/d with erosion increasing closer to the 10,000 ML/d threshold.

Table 1. Erosion-threshold values for each of the seven modelled detailed-study sites.

Site	9L	13R	15R	19R	22R	27R	36L
Threshold (ML/d)	9,504	12,960	11,232	5,184	5,184	6,912	5,702

The percent contribution of different discharge classes is compared to contributions expressed as actual volumes of erosion (Figure 6). The left plot places all sites on an equal footing by expressing results as relative contributions, clear differences in the amount of bank erosion at

sites 22R and 15R, or 22R are apparent. Site 22R is shown to be most responsive at lower flows with the bulk of erosion taking place in the range of 6,000 to 10,000 ML/d. The two downstream-most sites (36L and 27R) are also quite responsive at moderate flows, resulting in the bulk of the erosion occurring at about 10,000 ML/d. Aside from site 22R, measureable erosion does not take place until flows of about 10,000 ML/d are being discharged.
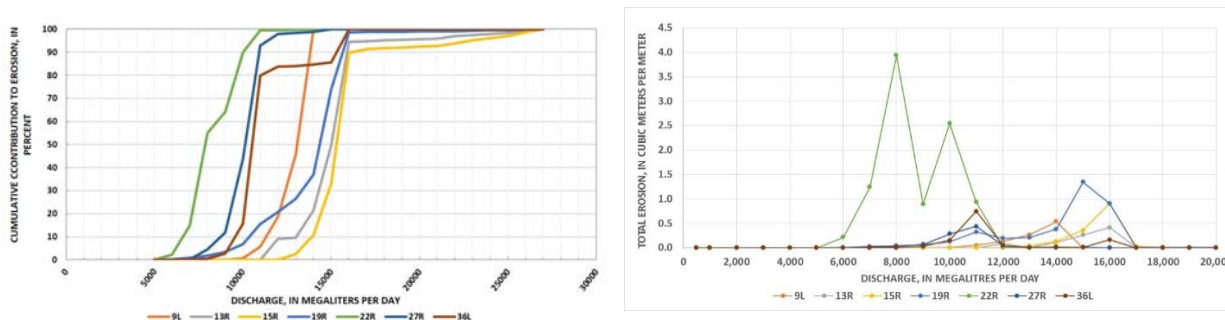
Figure 6. Contribution of discharges to bank erosion. Note the lack of erosion below 5,000 ML/d.

Bank Erosion during Flow Transfers and Flow-Threshold Conditions:

To help determine the most effective way to make bulk transfers of water from Dartmouth Dam downstream to Lake Hume without causing undue environmental damage, a series of alternative-flow scenarios was developed. The basis for the flow scenarios as provided by MDBA was that all of the scenarios would deliver about the same amount (volume) of water over a similar period. Obviously, there is a myriad of potential combinations of these variables that could be tested. Four were selected that deliver about 920,000 ML in a 7-month period (~130,000 Gl/month averaged over 7 months) (Figure 7).

1. *Moderate - Constant* – This flow scenario represents a "constant" release of 5,000ML/d over the entire flow period excluding the time to peak and for recession to 200 ML/d.
2. *Maximum RoF* – The second scenario represents a variable release strategy to approximate a naturally-shaped hydrograph. This scenario uses the maximum permissible RoF of river levels at the Colemans gauge (20 mm/h), the 2nd-highest peak-flow rate of about 7,500 ML/d and the 2nd-shortest duration of peak flows at 30.3 days.
3. *Slower and Smaller* – this scenario is similar to the second, with a variable release except that rates of fall are kept to 5 mm/h, and peak-flow rates are about 6,400 ML/d. The duration of peaks for this scenario is also the shortest, at 25.8 days.
4. *Worst Case / Maximum Flow* – transfers are undertaken as late as possible and at channel capacity rates of approximately 10,000 ML/d. Here a single peak is held for 85.5 days. This was a feature of past operations and such flow patterns were known to exacerbate bank erosion.
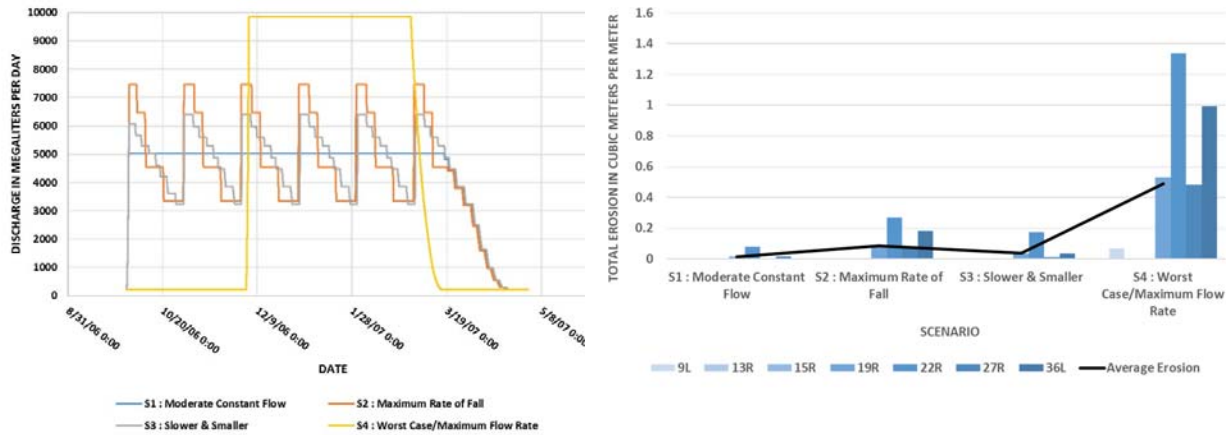
Figure 7. Hydrographs of the four alternative-flow scenarios (Left) and associated bank-erosion (Right).

The Worst Case / Maximum Flow represents the scenario with the highest erosion rates at the sites that had any erosion (Figure 7, Right). This should not be surprising given that this flow scenario has the highest peak flows (about 10,000 ML/d), and the highest magnitudes and durations of flows in excess of threshold conditions (38-51%). At the other end of the spectrum is the Moderate-Constant Flow scenario where we get the lowest erosion rates for all sites with any erosion. This was also to be expected because in spite of the fact that the duration of the peak flow (167 days) was almost twice that of the Worst Case scenario, the peak-flow rate was held to about 5,000 ML/d and only 6% to 11% of the flows were in excess of the threshold flow condition. It should be noted, however, that although the constant-flow scenario produces minimal erosion because it is below erosion-threshold values for all sites, it could produce negative environmental and ecological aspects because of the lack of flow variability. It is unlikely that operational guidelines to limit bank erosion would be developed in isolation of these issues.

A series of relationships using the magnitude and duration of flows above the erosion threshold as the primary metric, were developed. These are useful in interpreting how the same sites respond differently to the different alternative-release schemes as a function of the magnitude and duration of flows. Lack of space here precludes a detailed discussion of their development and the reader is directed to the major Cardno report for MDBA which this is based (Simon et al., 2018). Here we refer to one that is based on the sum of the ratios of the flow rate to the threshold value for each day that it is in excess of the erosion threshold (Figure 8). In effect, this single value then represents both magnitude and duration for each site/scenario. From this we can see that the Constant-Moderate Flow (Scenario 1) can withstand long durations above the erosion threshold because the magnitude of those excess flows is small. The converse is true for the Worst Case / Maximum flow (Scenario 4) scenario where greater flow magnitudes result in shorter acceptable flow durations to limit bank erosion. The Maximum RoF (Scenario 2) also shows a clear and similar increase in bank-erosion rates with increasing duration. For the Smaller and Slower (Scenario 3), bank-erosion rates don't increase appreciably until the index is greater than about 125.
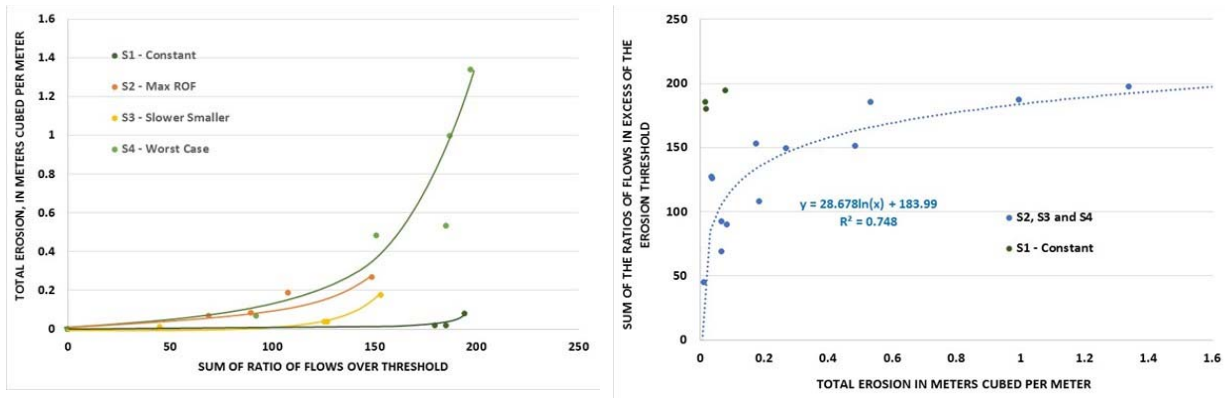
Figure 8. Relations between bank-erosion rates and the sum of the daily ratios of flow-to-erosion threshold over the 216-day simulation period for each flow scenario (Left) and inverted for flow scenarios 2, 3 and 4, which capable of producing significant erosion (Right). The regression equation shown on the right graph can be used to estimate the magnitude and duration of releases that produce certain bank-erosion rates.

As a potential tool for operations managers, the data in Figure 8 (Left) are combined for those flow scenarios that are capable of producing significant erosion (Scenarios 2, 3 and 4) and inverted to solve for the sum of these ratios (Figure 8, Right). Results, which can be easily derived for a proposed flow release, are listed for specified erosion rates:

- 0.05 m³/m, 98.1;
- 0.10 m³/m, 118.0;
- 0.15 m³/m, 129.6;
- 0.20 m³/m, 137.8;
- 0.30 m³/m, 149.5;
- 0.40 m³/m, 157.7; and
- 0.50 m³/m, 164.1.

Summary

Using hourly time steps, a historical flow period from 2006 to 2016 was selected for modelling to coincide with the timing of repeat channel surveys. Surveyed changes in bank geometry over the period were used to calibrate BSTEM-Dynamic over the period between surveys. Erosion rates ranged over an order of magnitude, from 0.89 m3/m (of channel length) at site 27R to 9.8 m3/m at site 22R, located on the outside of a broad meander bend. This deterministic approach allowed for identification of specific erosion-threshold conditions, which ranged from about 5,200 ML/d to almost 13,000 ML/d depending on the resistance of the bank materials and the geometry of the bank. The highest erosion thresholds and, therefore, lowest bank-erosion rates were found in the upstream reaches at sites 13R, 15R and 9L. In general, erosion increased downstream. At all sites, erosion did not begin until daily-flow rates were greater than about 5,200 ML/d, indicating that this discharge would be a conservative, erosion-limiting rate for transferring water.

Field measurements of hydraulic conductivity of the banks disclosed a median value of about 1.0 m/d (~40 mm/h) and an inter-quartile range from 0.4 to 2.3 m/d (17 to 95 mm/h), indicating that the bank materials are generally quite conductive. These values are generally higher than operational drawdown rates, indicating that water can normally drain out of the banks at the rate of recession imposed by releases. Limiting drawdown rates to half or less of the measured

conductivity (i.e., below 15 mm/h, to as low as 5 mm/h) would provide even greater certainty to limit drawdown-associated bank instability.

The Worst Case / Maximum Flow scenario represents the case with the highest erosion rates. This is not surprising, given that this flow scenario has the highest peak flows (about 10,000 ML/d) and the highest magnitudes and durations of flows in excess of threshold conditions. In contrast, the Moderate-Constant Flow scenario had the lowest erosion rates. This too was to be expected because the peak-flow rate was held to about 5,000 ML/d, below the erosion threshold for most sites. Although the Moderate-Constant Flow scenario produces minimal erosion, it could produce other negative environmental and ecological impacts because of an unnatural lack of flow variability. Further, except for site 22R, measurable erosion starts to occur at about 10,000 ML/d, indicating that this may be an important discharge management threshold. Thus, flows between 5,000 and 10,000 ML/d, which produce some erosion, may represent a reasonable range of daily-transfer rates while maintaining general bank stability. This of course is a function of the local erosion thresholds and the duration of the flows above threshold. Establishing various combinations of magnitude and duration that result in acceptable amounts of erosion within this flow range can be estimated using regression relations that were developed from the simulated erosion rates and these flow parameters.

References

Green, S.J., 1999. Drawdown and Riverbank Stability. Unpublished Masters Research Thesis, Department of Civil and Environmental Engineering, University of Melbourne.

Lawson and Treloar, 2001. Geomorphic Investigation of the Influence of Changed Flows on the Mitta Mitta River. Report Submitted by Lawson and Treloar Pty Ltd to North East Catchment Management Authority.

Simon, A., Hammond, J. and Artita, K, 2018. Geotechnical Assessment of River Banks along the Mitta Mitta River. Report submitted by Cardno Inc. to Murray Darling Basin Authority, 146 p.

Modeling Mississippi River Dredging Strategies after the Lock Closure at Upper St. Anthony Falls

Alex Nelson, Hydraulic Engineer, P.E., U.S. Army Corps of Engineers, St. Paul, Minnesota, alexander.g.nelson@usace.army.mil

Abstract

With the closure of the Upper St. Anthony Falls (USAF) lock in 2015, new opportunities have arisen to investigate eliminating channel maintenance in the upper navigation pools of the Mississippi River near Minneapolis and St. Paul, Minnesota. Since lockages through USAF have halted, the current dredging activities that are in place to ensure a nine-foot navigation draft in the pool may no longer be required. Additionally, due to reduced commercial boat traffic traveling to USAF through Lock & Dam No. 1 (LD1), elimination of channel dredging through this reach may also be warranted. The results of this sediment transport modeling study, using HEC-RAS hydraulic modeling software, show the relative differences in dredging quantities between the current channel maintenance practices and proposed alternatives. Modeled impacts for two alternatives, eliminating dredging above USAF and eliminating dredging above LD1, are quantified for the Mississippi River system through Lake Pepin in order to assess the viability of each strategy. In addition, future studies may utilize this model to analyze sediment trends through Lake Pepin and to investigate the feasibility of major operational changes (e.g. water level drawdowns) or physical changes (e.g. dam modification) at the structures in the navigation system.

Introduction

Background

The Water Resources Reform and Development Act of 2014 (WRRDA 2014) required that the Upper St. Anthony Falls Lock and Dam (USAF Lock) be permanently closed. This closure occurred on June 10th, 2015. The closure of the USAF Lock essentially ended the need for annual maintenance dredging in the commercial navigation channel in Pool 1 and the Upper St. Anthony Falls Pool. The decision that has to be made by the St. Paul District of the U. S. Army Corps of Engineers (USACE) is whether to 1) continue channel maintenance as usual, 2) stop channel maintenance in the USAF Pool and in Pool 1, or 3) develop a sediment management strategy based on the beneficial use of dredge material. Because navigation channel dredging can be a large sink for sand-size sediment, reducing dredging in the USAF Pool and Pool 1 may eventually have an effect on downstream reaches.

The St. Paul District of the U.S. Army Corps of Engineers (USACE) is responsible for maintaining a 9-foot navigation channel on the Upper Mississippi River (UMR) between Minneapolis, Minnesota and Guttenburg, Iowa. This includes the lower 14.7 miles of the Minnesota River, and portions of the lower St. Croix and Black Rivers. The Upper St. Anthony Falls Lock is the upstream most navigation dam on the Mississippi River and the head of navigation is just a few miles upstream of the lock. Maintaining the 9- foot channel is done through periodic dredging and through a system of locks and dams. The USACE dredges and disposes of approximately 66,000 cubic yards of sand annually between the Upper St. Anthony Falls Pool (USAF) and Lock and Dam 1, and 160,000 cubic yards annually on the UMR between Lock and Dam 1 and Lake Pepin. The total from both reaches represents over 25-percent of the district- wide dredging. In addition to the cost associated with channel maintenance dredging, other sediment related impacts in this reach include a turbidity impairment (MPCA, 2012), off-

channel sediment deposition affecting habitat and recreational boating, reduced light penetration and aquatic vegetation growth, and accelerated sediment deposition in Lake Pepin. It is estimated that 85 - 90 percent of the sediment deposited in Lake Pepin originates from the Minnesota River watershed (Engstrom et. al., 2009). Figure 1 shows the extent of the study area.

To estimate the effects of navigation channel dredging, off-channel sediment deposition, and tributary sediment loads on sediment transport on the UMR, the USACE developed a district-wide bed material sediment budget in 2003 (USACE, 2003). Bed material refers to sand-size sediment that can be found on the bed of the main channel, but can be transported as bed load or suspended load. This bed material budget was based on interpretation of available sediment transport information at U.S. Geological Survey (USGS) gaging stations, long-term channel dredging data, studies of sediment transport and deposition, and measured hydraulic characteristics on the UMR. Total sediment load measurements obtained on the Minnesota River at Ft. Snelling during the years 2011 to 2015 (Groten et. al., 2016) have improved the sediment budget significantly. However, while the sediment budget has been a valuable tool, it isn't a numerical model and can't predict the temporal and spatial effects of changed sediment transport capacity and sediment loads.

Project Location and Study Area

The study area is on the Mississippi River 9-Foot Navigation Channel between River Mile (RM) 857.6, the upstream limit of the 9 foot channel project, and RM 764, the downstream end of Lake Pepin. For hydraulic modeling purposes, the upstream extent has been extended to RM 866 to include the Anoka gage on the Mississippi River and the downstream extent has been extended to RM 753 to capture the downstream control of the water level for Lake Pepin at Lock and Dam No. 4. This reach includes numerous structures and incoming tributaries, shown in Figure 1.
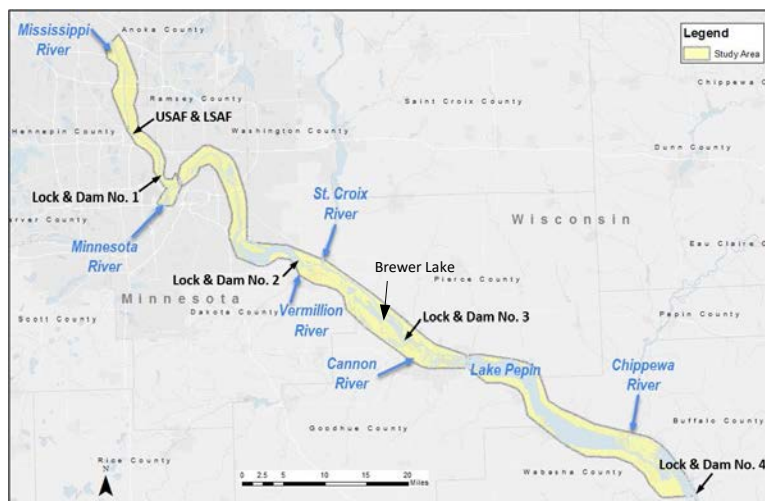
Figure 1. Overview of the Modeling Study Area

Purpose and Need

A numerical model is needed for the reach of the Mississippi River from the USAF Pool to Lake Pepin to simulate the effects of changed dredging in the USAF Pool and Pool 1. The primary purpose of the model is to simulate the spatial and temporal effects of dredging changes in USAF and Pool 1 on downstream dredging and backwater deposition of sand sized sediment in

pools 2, 3, and 4. Other purposes include determining the effects of a secondary channel closure proposed for the Brewer Lake Inlet in Pool 3. The appropriate model must be capable of modeling the complexities of flow exchanges between main channel and backwater areas and advanced operations of multiple lock and dam structures, while also being capable of modeling long reaches of river over 100 miles in length. Advanced two-dimensional and three-dimensional models would be appropriate for capturing complex hydraulic behavior, but would not be efficient over a domain as large as the proposed study area. Conversely, simple spreadsheet models and sediment budgets would be efficient, but incapable of capturing the hydraulic complexities of this system. The HEC-RAS one-dimensional model has been selected for this study as appropriate as it is capable of effectively modeling hydraulics and sediment over large domains as well as capturing smaller scale complexities at flow splits and structures.

Methods

Data Collection

Flow and Stage Gage data: Water surface elevation data, flow records, and sediment measurements are important pieces of data for both the construction and calibration of a hydraulic and sediment model. Water surface elevation data is available through continuous measurements using Data Collection Platform (DCP) instruments and through daily observations of stage data at structures, points of interest, and established gage locations. The U.S. Army Corps of Engineers collects continuous and daily records of water surface elevation for pool and tailwater (TW) levels at each of the operated lock and dam structures as well as at "control point" locations which are used for hinge-point operations of the navigation system. The United States Geological Survey (USGS) collects water surface elevation at established gaging stations which can be converted to a continuous record of discharge or streamflow by maintaining a stage-discharge relationship for each gage location through the periodic measuring of discharge at that location (Olson & Norris, 2007). The most complete shared record for all the gages in the study area is the period from 2007-2015.

Suspended Sediment: In addition to measurements of stage and flow at various gage locations, the USGS collects field samples of suspended sediment concentration and sediment grain size distribution for use in water quality and runoff analyses. This suspended sediment data can also be used as an input to a sediment transport model. The units for the collected concentration values are recorded in mass per volume, or typically milligrams per liter using the International System of Units (SI). The HEC-RAS sediment model requires total sediment load in units of weight per time, or tons per day using English units. To convert the concentration to a total load, the concentration needs to be multiplied by the instantaneous river flow that occurs at the time of the concentration measurement, as well as a coefficient to convert to the appropriate units. The total load, in tons per day, can be calculated by the following equation (Porterfield, 1972):

$Q_s = Q_w * C_s * K$ where

$\quad\quad Q_s \quad = \quad$ Sediment discharge or sediment load, in tons per day (tons/day)
$\quad\quad Q_w \quad = \quad$ Discharge or streamflow, in cubic feet per second (ft3/s or cfs)
$\quad\quad C_s \quad = \quad$ Concentration of suspended sediment, in milligrams per liter (mg/L)
$\quad\quad K \quad = \quad$ 0.00269, the coefficient to convert units

$$K = \left(\frac{86,400\ seconds}{1\ day}\right) * \left(\frac{1\ meter}{3.28\ feet}\right)^3 * \left(\frac{1000\ liters}{1\ cu.meter}\right) * \left(\frac{1\ kilogram}{10^6 milligrams}\right) * \left(\frac{2.2\ pounds}{1\ kilogram}\right) * \left(\frac{1\ ton}{2000\ pounds}\right) = 0.00269$$

Suspsended sediment concentration measurements are available for the three main inflows to the model domain: the Mississippi River, the Minnesota River, and the St. Croix River. The Mississippi River has a total of 7,714 sediment measurements while the Minnesota River has a total of 74 measurements and the St. Croix River has 9 observations that can be used to develop a flow-load curve. A power-fit regression of the log-transformed values of flow and load was developed for each set of data and used as an initial best estimate for the flow-load relationship. The measured data and the best estimate curves are shown in Figure 2.
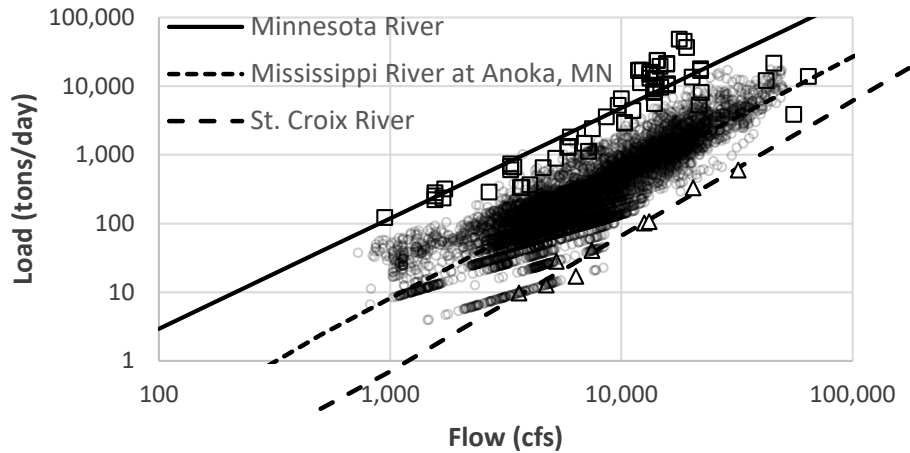
Figure 2. Flow-Load Relationships for three major inflows to the sediment model

The flow-load relationships for these three major inflows show roughly two orders of magnitude difference in total sediment load. For example, at 10,000 cfs the best estimate for the St. Croix River is 77 tons/day, the best estimate for the Mississippi River is almost ten times greater at 486 tons/day, and the best estimate for the Minnesota River is ten-fold greater still at 6061 tons/day. The higher sediment loads that are found within the Minnesota River Basin can help explain why this tributary contributes over 85% of the sediment that makes its way to Lake Pepin (Engstrom, 2009).

Sediment samples collected by the USGS, in addition to obtaining a measurement of concentration, can be analyzed to determine the sediment grain size distribution. The percentage of the suspended sediment that falls into the various grain classes of sands (0.0625-1 mm), silts (0.004-0.0625 mm), and clays (< 0.004 mm) can be determined through sieve and hydrometer tests as described in the American Society for Testing and Materials (ASTM) procedure D422-63(2007)e2 (ASTM, 2007). There is an inherent amount of variability in the testing for particle size distribution which is difficult to capture in a 1D sediment model. For this reason, most of the inflows in the model were assumed to have the same suspended sediment gradation based off of the median values from the numerous samples. The one exception, the Minnesota River, was assumed to have a higher percentage of finer material (coarse silts and fine sands) based on the median values of samples from that collection site.

River Bed Gradations: The sediment model allows for different gradations of bed material to be assigned at each cross-section in the model. Bed samples were found throughout the model domain area, both on the main channel and in backwater areas such as marinas. The various types of bed gradations were sorted in groups based on pool and flow type (i.e. main channel vs. backwater areas or sloughs). The median values were taken for each group and applied to the various reaches as appropriate. For example, the North & Sturgeon Lake area was modeled with bed gradations for "Pool 3 Coulee/Sloughs".

Ultimately, since the system is primarily depositional rather than erosional, the sediment modeling results are not very sensitive to the bed gradations.

Digital Elevation Model (DEM): The modeling domain must extend far enough upstream to encompass the dredge locations above Upper & Lower St. Anthony Falls (USAF & LSAF) and far enough downstream to create a downstream boundary that does not affect the stage and flow calculations at Lake Pepin. The U.S. Army Corps of Engineers St. Paul District has numerous years of extensive bathymetric datasets in each of the pools in the study area through surveys performed by USACE for dredging, navigation, and ecosystem restoration purposes. The St. Paul District GIS Section has merged these datasets with above-low-water Light Detection and Ranging (LiDAR) data collected by the Minnesota Department of Natural Resources (MN DNR) since 2008; providing seamless datasets for pools throughout the study area. These datasets have been merged for this study to create a single Digital Elevation Model (DEM), which is used to attribute elevation data to the hydraulic model features.

Model Construction

The selected software for the modeling effort is HEC-RAS (USACE, 2016). This software, originally developed as a one-dimensional (1D), steady-flow hydraulic modeling software package, now has capabilities for unsteady flow, sediment modeling, and two-dimensional (2D) flow. For this effort, the software is used to construct a 1D, unsteady-flow, hydraulic river model; calibrate the hydraulic model to collected stage and flow data; further develop the model into a 1D, unsteady-flow, *sediment* hydraulic river model; calibrate the sediment model to observed dredging records; and assess sediment impacts for changes to existing system operations. HEC-RAS does not currently have the capabilities to model sediment in 2D. Instead a 1D model, which calculates the water surface profile by solving the 1D Saint-Venant (momentum) equations over successive river "cross-section" features, is used rather than a 2D model capable of solving the 2D Saint-Venant equations or diffusive wave equations across multidirectional cell features. While a 1D model is less detailed in nature, it can provide shorter model run times for added complexities such as sediment, multi-year flow records, and large model domains.

The cross-section location data, river centerline features, Manning's n-values for roughness, and ineffective flow limits were taken from various existing HEC-RAS models developed for the Mississippi River in this area:
- Mississippi River through St. Paul (Pool 2) developed as part of a USGS study (Czuba et. al. 2014)
- Lower Minnesota River from latest Corps Water Management System (CWMS) Modeling by USACE, St. Paul District in 2016
- Mississippi River through Pools 3 & 4, developed as part of a modeling effort for the Nuclear Regulatory Commission in 2015

While the 1D model cannot capture the complexities of two-dimensional flow, the floodway can be modeled as multiple channels to better capture the flow splits near Grey Cloud Island (Baldwin Lake and Spring Lake), Prairie Island (Vermillion River and North & Sturgeon Lakes), and Red Wing (Wisconsin Channel).

The cross-section and "lateral structure" features that connect the various reaches are "cut" from the developed seamless DEM to ensure that model represents the conditions with the best available data. The lock and dam structures are imported from the previously developed models to ensure that the gates, sills, and dam crests were set to the appropriate sizes, elevations, and datum.

All elevations used in the modeling effort and presented in this report are in North American Vertical Datum of 1988 (NAVD 88). The conversion from the National Geodetic Vertical Datum of 1929 (NGVD29) is to add 0.194 feet at the upstream end of study area and 0.036 feet at the downstream end of study area.

Hydraulic Model Calibration and Validation

The hydraulic model was calibrated to water surface elevation data at pool, tailwater, and control point gages and to flow estimates at USGS gage locations. The metric used to assess the calibration to observed flow is the Nash-Sutcliffe model efficiency coefficient (NSE) which is a common metric used to assess the predictive power of hydrologic models (Nash & Sutcliffe, 1970). The model accuracy is high as the NSE values approach a value of 1. The four discharge gages that were compared showed NSE values of 0.95-0.99 indicating that the model is very accurate in terms of flow.

Backwater flow was also validated against periodic backwater measurements collected by the St. Paul District. Various locations throughout Pool 2 and Pool 3 were measured to help estimate the flow conveyance of the main channel compared to backwater or side channel areas. In Pool 2, lower velocity areas such as Baldwin Lake and Spring Lake still convey up to 20% of the total flow on the river. In Pool 3, the Vermillion River and North & Sturgeon Lakes can convey an even greater percentage of the total flow. At Pool 3 in particular, the flow splits to secondary channels and backwater lakes are very complex, with numerous sloughs and breakout areas allowing for interchanging flow. The 1D model is able to capture the flow splits surprisingly well, with strong validation between the modeled flow and the periodic measurements of flow.

The modeled water surface elevation data at the navigation structures and control points was compared to the observed data using the estimator of mean square error (MSE) which is the sum of the squared difference between observed and predicted values (Legates & McCabe, 1999). This is another common metric in statistical modeling for goodness of fit, with values closer to 0 indicating higher accuracy. Values at the various gages generally range from 0.13-0.59 feet with the L&D 3 pool having a higher MSE of 1.77 feet. These values are found to be generally acceptable for sediment modeling purposes.

Sediment and Dredging Model Calibration

Sediment transport in HEC-RAS can be modeled using a variety of different transport functions, fall velocity equations, bed change options, as well as numerous other calibration parameters. For this modeling effort, multiple different transport functions were investigated initially (Yang, Ackers-White, etc.) but ultimately, the Laursen-Copeland transport function equation was selected for use in the model. The Laursen method (Laursen, 1958) is a total

sediment load predictor developed through experiments and qualitative analysis for grain sizes between 0.011 and 29 mm. Copeland (Copeland, 1989) contributed to the development of the equation to extend the applicability to gravel-sized sediments. The Laursen-Copeland equation showed promising initial results and is the recommended transport equation to use in HEC-RAS for modeling fine grained sediments, outperforming other transport functions in the very fine sand and very coarse silt range (USACE Hydraulic Reference Manual, 2016). The bed sorting method was set to 'Active Layer' of roughly 1 meter in thickness. Rather than specify 3 or 5 different layers in HEC-RAS, a simplistic approach was used where the "active layer" is the portion that is actively transporting and depositing material and the "inactive layer" is the layer below, where sediments are mixed into from the active layer. The fall velocity method was set to the equation developed by Dietrich (Dietrich, 1982) as that method has shown strong results in past studies and was recommended by Dr. Gary Parker as a superior method compared to the other options in HEC-RAS. The bed change option was set to the 'Reservoir Option', which deposits more sediment in the deeper part of the cross-section. This method was more realistic for the series of reservoirs present in the lock and dam system, as opposed to the other options of depositing and eroding sediment uniformly within the movable bed limits or allowing deposition across the entire wetted area uniformly.

Dredging in HEC-RAS is modeled by specifying a station, elevation, width, and time & date of a dredging event at each cross-section in the model. The dredging events were set for July 15 of each year in the model, to represent the entire season's worth of dredging typically occurring over mid-to-late summer. The dredged volume is removed from the system to reflect the standard practice in the Upper Mississippi River of storing dredged material at dredge disposal sites rather than redistributing the material back into the river at a different location.

Modeling the dredging in HEC-RAS based on specified rules is imperfect compared to the subjective decisions that are made in the actual dredging of the system. Channel maintenance is required to maintain the nine foot navigation channel below the Levee Control Profile (LCP). The nine foot channel currently requires dredging to 10.5 feet below the LCP to ensure sufficient draft for barge traffic. However, in actual practice, when dredging does occur the invert is brought to 12 feet below the LCP in order to gain efficiencies in the dredging program (i.e. over-dredge by 1.5 feet so that other locations may be prioritized the following year). In addition to the planned over-dredging, subjective decisions will be made to minimize mobilization of the dredging equipment and to utilize sediment storage sites efficiently. For these reasons, the modeled dredging may not always accurately reflect what actually occurred in the system. However, the model should, on average, do a good job of capturing the total sediment removed through channel maintenance.

With the modeling methods and dredging events specified, the main calibration parameter used in the model was adjusting the flow-load relationships of the Mississippi River and Minnesota River. Sediment transport, in the model and in reality, reflects the total load of the system which consists of a suspended sediment portion and a bed-load sediment portion. Because the starting flow-load ratings in this model are based on the suspended sediment concentrations, they lack the bed-load sediment estimate, under-predict the total load, and will be adjusted upward during the calibration process. According to the Channel Maintenance and Management Plan, the Upper Mississippi River and tributaries have bed-loads that are between 0 and 40% of the total load, with 10% being the typical value. To account for the bed-load and to achieve calibration, the loads were incrementally increased in the flow- load rating curves until the modeled dredging quantities matched the measured historic dredging quantities. If modeled dredging quantities were low in the St. Anthony Falls Pool and Pool 1, the Mississippi River flow-load curve was increased. If dredging quantities were low in Pools 2-4, the flow- load curve

for the Minnesota River (as the largest contributor of sediment) was increased. For the final calibration the ultimate flow load curves were adjusted to the final curves.

Results

Existing Channel Maintenance Practices

Sediment modeling is traditionally very difficult to replicate with high precision and accuracy. Often times, results that are within a factor of two of the measured data are found to be sufficient due to the wide range of variability in sediment data and the complex processes that make up sediment transport. The total dredge quantity modeled in the period from 2008 through 2015 from the Upper St. Anthony Falls Pool through Lake Pepin is 11% higher than the measured volume. Annual quantities for each pool show error sometimes as great as a factor of two, but overall the average modeled dredging quantities compare very well with the average measured quantities. A summary of the average annual dredging volume by pool is shown in Figure 3.
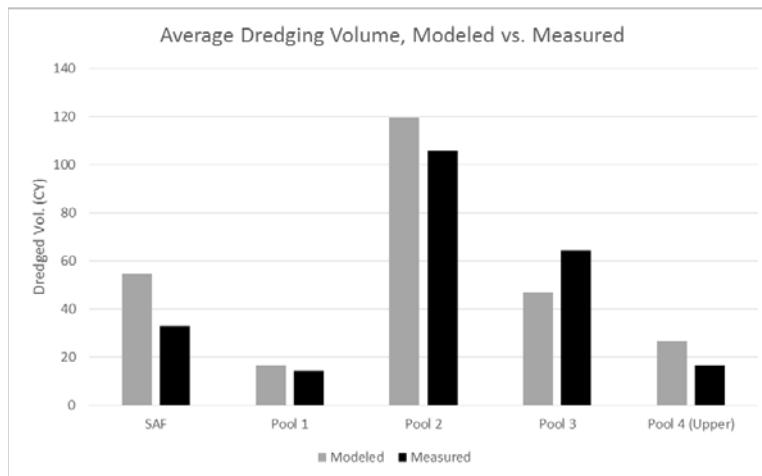
Figure 3. Comparison of modeled and measured average annual dredging quantities by pool

With a calibrated sediment dredging model established, the model can be run with various alternatives to show the relative impact the alternative would have to dredging quantities. This calibrated model will be referred to as the base condition model, or the current dredging model. The following sections describe the results of different alternatives to the current channel maintenance plan. These various alternatives will be compared to the base condition model rather than the measured data so that a direct comparison of relative impacts can be made and the residuals between measured and model data will not influence the results.

Alternative 1 – Eliminate dredging above Upper St. Anthony Falls

The first alternative (Alternative 1) is to eliminate channel maintenance activities above St. Anthony Falls. With the closure of the USAF to navigation that occurred in 2015 as a result of WRRDA 2014, there may no longer be a need to dredge the nine foot channel to boat traffic in the USAF Pool. This alternative is modeled with all dredging activities removed above USAF Lock & Dam. Dredging activities in pools below USAF are modeled using the current dredging plan from the base condition model. The changes in total dredging quantities from the base

condition model of current dredging practices to the Alternative 1 model are shown (summarized by pool and by year) in Figure 4.
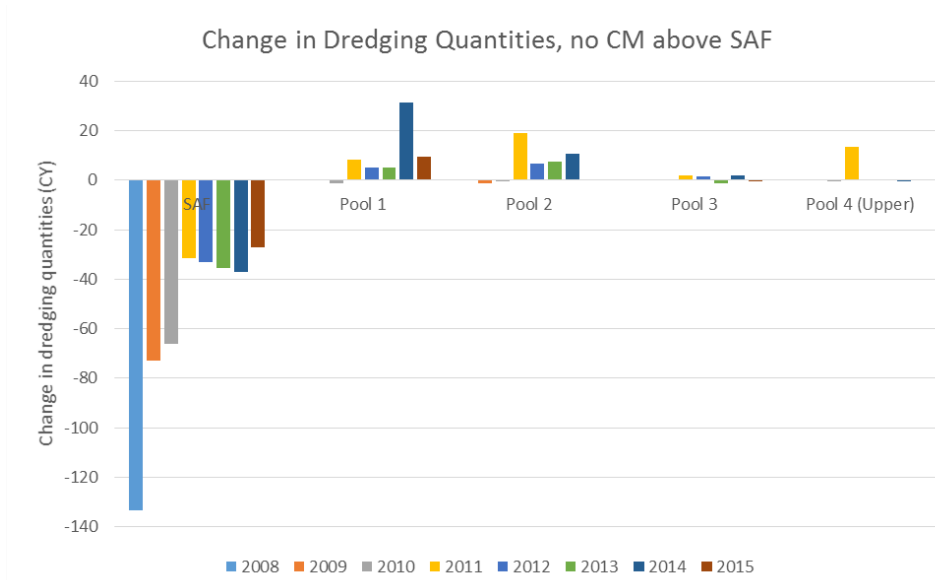
Figure 4. Comparison of change in annual modeled dredging quantities by pool for Alternative 1

The results of Alternative 1 show increases in dredging for each of the downstream pools, with the greatest increases found in Pool 1. Pools 1 and 2 show positive trends in dredging increases, as well, indicating that the sediment may still be working its way downstream over the 8 year period. Overall, however, the downstream increases in dredging are far less than the total reduction in dredging found in the USAF pool. The relative change in dredging is high for Pool 1 with a 123% increase in total dredging for the pool in Year 8 since the change is implemented for Alternative 1. There is also a strong positive trend in Pool 1, indicating that dredging increases in that pool may continue to be high. The relative change in other pools, however is fairly minimal. The average annual increase to Pools 2, 3, & 4 are 4%, 1%, and 6%, respectively.

Alternative 2 – Eliminate dredging above Lock & Dam No. 1

The second alternative (Alternative 2) is to eliminate channel maintenance activities above Lock & Dam No. 1, including the elimination of dredging above Upper & Lower St. Anthony Falls. With the closure of the USAF to navigation in 2015, commercial boat traffic in Pool 1 has been minimal in recent years. Data from the Corps of Engineers Lock Performance Monitoring System (USACE LPMS, 2017), shows the typical total lockages for Lock & Dam No. 1 have been reduced from around 1,500 per year to around 1,000 per year, with commercial lockages decreasing from 600 per year to 100 per year.

To represent a scenario where commercial navigation is closed through LD1, Alternative 2 is modeled with all dredging activities removed in USAF Pool and Pool 1. Dredging activities in pools below Lock & Dam No. 1 are modeled using the current dredging plan from the base condition model. The changes in total dredging quantities from the base condition model of current dredging practices to the Alternative 2 model are shown (summarized by pool and by year) in Figure 5.

The results of Alternative 2 show increases in dredging for each of the downstream pools, with the greatest increases found in Pool 2. Pool 2 shows a positive trend in dredging increases, as well, indicating that the sediment may still be working its way downstream over the 8 year period. Overall, however, the downstream increases in dredging are far less than the total reduction in dredging found in the upper pools.
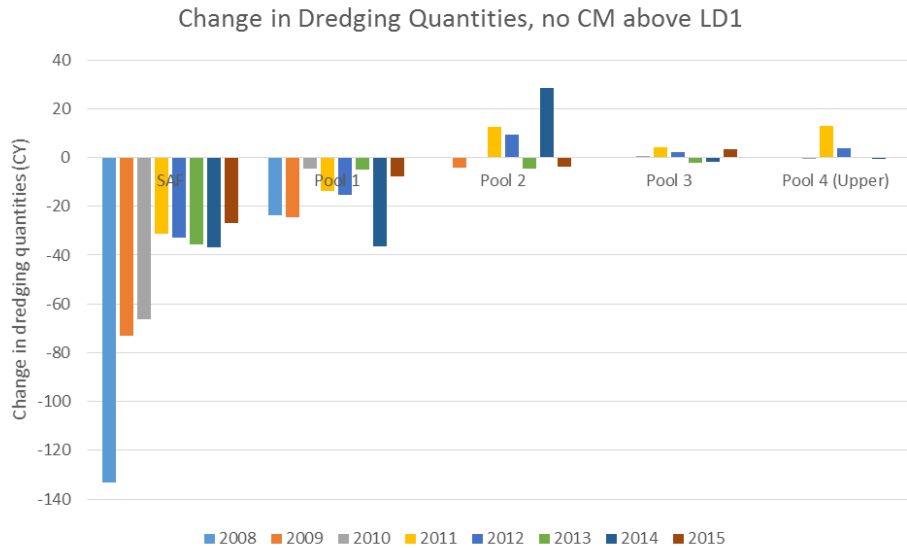
Figure 5. Comparison of change in annual modeled dredging quantities by pool for Alternative 2

The relative change in dredging is minimal for Pool 2 with a maximum increase of 14% in Year 7 since the change is implemented for Alternative 2. There is also an increasing trend in Pool 2, indicating that dredging increases in that pool may continue to be high. The relative change in other pools is also minimal. The average annual increase to Pools 2, 3, & 4 are 4%, 2%, and 8%, respectively.

Conclusions

Comparison of Existing and Proposed Alternatives

Both alternatives, the removal of dredging above Upper St. Anthony Falls and the removal of dredging above Lock & Dam No. 1, result in a net reduction in average dredging volumes over the eight year modeling period. While Alternative 1 results in increased average dredging quantities in Pools 2, 3 & 4 of 4%, 1% and 6%, respectively, the total average dredging for the system shows a net decrease of 15%.

Similarly, Alternative 2 shows increased average dredging in Pools 2, 3 & 4 of 4%, 2%, and 8%, respectively, but a net decrease in average dredging for the system of 24% due to the removal of channel maintenance in Pool 1 and above St. Anthony Falls.

When the total modeled dredging is compared over time (Figure 6), trends in the sediment transport through the system can be identified. In the first 3 years in the model following the implementation of each alternative (2008-2010), the system shows overall reductions in dredging of 29-40% for Alternative 1 and 30-48% for Alternative 2. However, in Year 4 (2011), Alternative 1 shows an increase in total dredging of 3% and Alternative 2 shows only a 4% reduction in dredging quantities compared to the current dredging plan. Toward the end

of the 8 year model period, Alternative 1 again shows a year where dredging quantities exceed the current dredging plan quantities (2014) and both alternatives show less of a reduction in total dredging than in Year 1.
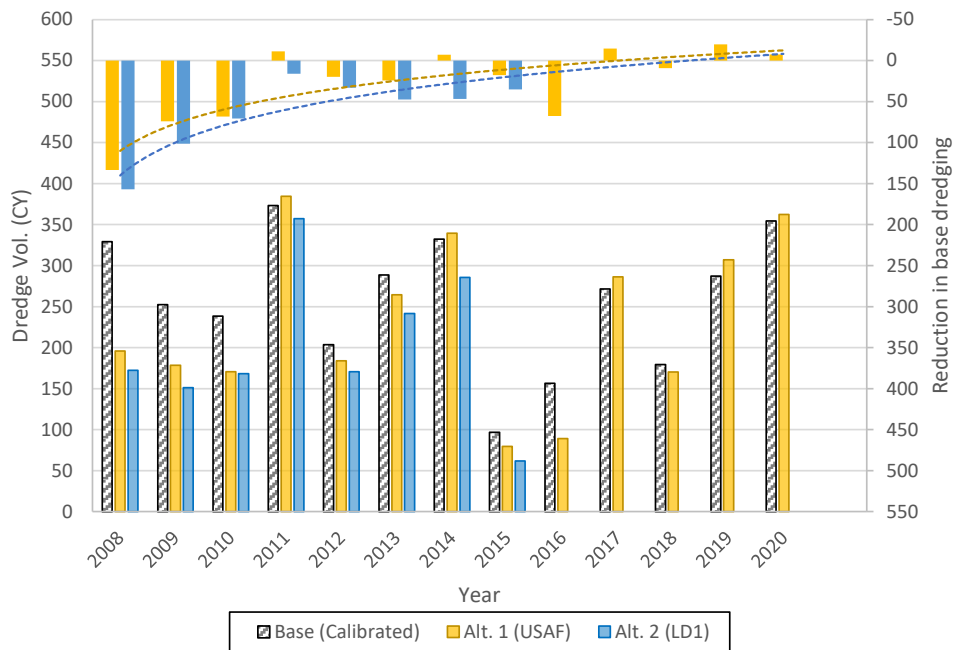
Figure 6. Trend in total change in dredging quantities after channel maintenance change. (The columns extending from the bottom of the plot represent total dredged volume (left y-axis) and the columns at the top of the plot represent reduction in base dredging (right y-axis). Note that the Alternative 2 model run was unstable for the future scenario beyond 2015.)

A trend-line for Alternative 1 shows that the expected change in dredging quantities for the system is close to zero by the end of a 10 year period. This might suggest that the system has reached an equilibrium by the end of 10 years and that the total dredging quantities may be net neutral with the current dredging practices. The downstream pools on average, will have slightly higher required dredging to compensate for the lack of a sediment sink above USAF. Alternative 2 shows a similar trend, although it may take longer than a decade to reach equilibrium. Beyond 10 years, the system may expect to be net neutral with the current dredging practices and additional dredging may be required in the downstream pools, on average.

The sediment transport modeling results indicate that eliminating dredging in Pool 1 and/or the USAF Pool will result in significant net reductions in average dredging between the USAF pool and Lake Pepin in the near term. Dredging in Pools 2, 3, and Upper 4 will increase a small amount, however, the reduction in dredging upstream of Pool 2 more than compensates for the downstream increases. Some of the sand not dredged in the USAF Pool and Pool 1 ends up settling out in off-channel areas. However, in the long term, modeling results indicate that once the new equilibrium is reached with each of the alternatives, it is likely that nearly 100% of the new forgone dredging material will end up in the immediate downstream pool. That is, for Alternative 1 most of the dredging increases after 10 years will occur in Pool 1 and for Alterative 2, most increases will occur in Pool 2.

Changes in downstream sediment transport and dredging won't occur immediately, but rather will take a number of years. The model results indicate that the timescale for these changes to

occur may be a decade or two. Aleatory variability in the future hydrology for the system and epistemic uncertainty in the sediment quantities and characteristics lead to high uncertainty in the estimated timeframe for equilibrium, but the model confirms expected trends in sediment deposition with the introduction of each of these alternatives.

Model as a tool to investigate sediment trends

In addition to using the model to assess different channel maintenance management strategies, the model can also be used as a tool to investigate sediment trends in the Mississippi River through Lake Pepin. Numerous studies in recent decades have looked into water quality (Lung & Larson, 1995), rates of deposition (McHenry et al 1980), and sources of sediment (Engstrom et al 2009) in Lake Pepin. This model could be used as a tool to support each of those areas of concern as well as similar fields throughout the Upper Mississippi River. The modeled longitudinal pattern of sediment deposition and particle size change match the measured sediment properties from other researchers (McHenry 1980, Cumulative Effects Report 2000, Engstrom 2009) and they match main channel borings obtained in this reach by the Corps in 2010. This portion of the river, between RM 785 and RM 780, also defines the delta at the upstream end of Lake Pepin. By having this modeling capability to not only capture the sediment budget but to be able to model and predict the grain sizes and locations of sediments, this tool can help with future studies to forecast future water quality and lake capacity concerns for this part of the river.

Model as a tool to investigate operational changes

Recent interest has been sparked to consider even more drastic changes to the navigation system than channel maintenance strategies The Corps of Engineers has expressed interest in investigating the federal interest in continued operation of the upper three lock & dam structures through a Disposition Study (USACE, 2016). This sediment transport model could be considered, along with numerous other types of models and tools, as one source of information for identifying positive and negative impacts from a change in the operating pools or full removals of dams. The model can coarsely capture the progression of erosion of sediment behind the dam in the case of a removal, but more importantly help to quantify broader impacts to the Mississippi River system through Lake Pepin.

Again, this model would only be one line of evidence in trying to predict the success of such a large scale dam removal project in a highly visible area. With the appropriate amount of additional work and funding, however, this model could prove to be a valuable asset in helping to support or screen-out options to restore the Mississippi River Gorge.

References

ASTM D422-63(2007)e2, Standard Test Method for Particle-Size Analysis of Soils (Withdrawn 2016), ASTM International, West Conshohocken, PA, 2007, www.astm.org

Brunner, Gary W. HEC-RAS River Analysis System. Hydraulic Reference Manual. Version 1.0. HYDROLOGIC ENGINEERING CENTER DAVIS CA, 1995.

Congress, U. S. "Water Resources Reform and Development Act of 2014." Public Law (2014): 113-121.

Copeland, Ronald R., and Thomas, William A. 1989. "Corte Madera Creek Sedimentation Study."

Numerical Model Investigation. US Army Engineer Waterways Experiment Station, Vicksburg,

MS. TR-HL-89-6.

Czuba, Christiana R., et al. Development of flood-inundation maps for the Mississippi River in Saint Paul, Minnesota. No. 2014-5079. US Geological Survey, 2014.

Dietrich, William E. "Settling velocity of natural particles." Water resources research 18.6 (1982): 1615- 1626.

Dorothy, Olivia. "Restore the Gorge!" American Rivers. https://www.americanrivers.org/2015/03/restore-the-gorge/. March 16, 2015.

Engstrom, Daniel R., James E. Almendinger, and Julie A. Wolin. "Historical changes in sediment and phosphorus loading to the upper Mississippi River: mass-balance reconstructions from the sediments of Lake Pepin." Journal of Paleolimnology 41.4 (2009): 563-588.

Laursen, Emmett M., 1958 (Feb). "Total Sediment Load of Streams," Journal of the Hydraulics Division, American Society of Civil Engineers, 84(HY1), 1530-1 to 1530-36.

Legates, David R., and Gregory J. McCabe. "Evaluating the use of "goodness-of-fit" measures in hydrologic and hydroclimatic model validation." Water resources research 35.1 (1999): 233-241.

Lenhart, Christian. "Restoration of the Mississippi River Gorge: Issues and Research Needs." Ecological Restoration 30.3 (2012): 218-227.

Lung, Wu-Seng, and Catherine E. Larson. "Water quality modeling of upper Mississippi River and Lake Pepin." Journal of Environmental Engineering 121.10 (1995): 691-699.

McHenry, J. Roger, Jerry C. Ritchie, and Charles M. Cooper. "Rates of recent sedimentation in Lake Pepin." JAWRA Journal of the American Water Resources Association 16.6 (1980): 1049-1056.

Minnesota Pollution Control Agency (MPCA). "South Metro Mississippi River Total Suspended Solids Total Maximum Daily Load." Draft Report. Minnesota Pollution Control Agency, Saint Paul, Minnesota, 2012.

Nash, J. Eamonn, and Jonh V. Sutcliffe. "River flow forecasting through conceptual models part I—A discussion of principles." Journal of hydrology 10.3 (1970): 282-290.

Olson, Scott A., and J. Michael Norris. US Geological Survey Streamgaging… from the National Streamflow Information Program. No. 2005-3131. Geological Survey (US), 2007.

Porterfield, George. Computation of fluvial-sediment discharge. US Government Printing Office, 1972.

U.S. Army Corps of Engineers (USACE). Bed Material Budget for the St. Paul District Reach of the Upper Mississippi River, Anoka, Minnesota to Guttenburg, Iowa. U.S. Army Corps of Engineers, St. Paul District, 190 East Fifth Street, St. Paul, MN 55101-1638. 2003.

U.S. Army Corps of Engineers (USACE), Hydrologic Engineering Center. HEC-RAS, River Analysis System, Version 5.0.3 [Computer Software]. (2016). Accessed from http://www.hec.usace.army.mil/software/hec-ras/.

U.S. Army Corps of Engineers (USACE), Hydrologic Engineering Center. HEC-RAS, River Analysis System, Hydraulic Reference Manual, Version 5.0. February 2016.

U.S. Army Corps of Engineers (USACE). "Lock Performance Monitoring System", (LPMS). http://corpslocks.usace.army.mil/. Accessed August 2017.

U.S. Army Corps of Engineers (USACE). "Disposition Study, Upper and Lower St. Anthony Falls and Lock and Dam 1." http://www.mvp.usace.army.mil/Home/Projects/Article/692881/disposition-study- upper-and-lower-st-anthony-falls-and-lock-and-dam-1/. March 14, 2016.

WEST Consultants, Inc. "Upper Mississippi River and Illinois Waterway Cumulative Effects Study." Contract No. DACW25-97-R-0012. Prepared by WEST Consultants, Inc. Bellevue, Washington, June 2000.

Modeling Sediment Deposition Effects on Dam Breach Propagation: An HEC-RAS Investigation Using RiskRAS Software

Brent Travis, Director of Applied Research, WEST Consultants, Tempe, AZ,
btravis@WESTconsultants.com
Gyan Basyal, Staff Engineer, WEST Consultants, Tempe, AZ,
gbasyal@WESTconsultants.com
Brian Wahlin, Vice-President, WEST Consultants, Tempe, AZ,
bwahlin@WESTconsultants.com

Abstract

Sediment deposition within dam reservoirs typically increases over time. This affects dam stability, including reduction of freeboard and storage capacity, increased outward pressure along the inner face of the dam, and possible invalidation of dam breach flood wave predictions. This paper addresses the latter possibility by utilizing new, recently-developed software that predicts flood wave arrival times and extents via direct consideration of the probabilistic aspects of the breach parameters. This software, named RiskRAS, is a multipurpose GUI-based HEC-RAS Monte Carlo simulation tool, written in the Python language utilizing reliable and well-tested libraries. Here, RiskRAS was used to generate 1% flood waves for an existing dam considering the original and 10% reservoir capacity sedimentation scenarios. The results are discussed and practical guidelines suggested for how to approach flood wave propagation analysis for dams at risk for significant future sedimentation, and the implications this risk in terms of the necessity, scheduling, and extent of any dredging operations.

Introduction

Reservoirs are dynamic. Not only does their stage change according to meteorological conditions and operations, but the base of the reservoir itself changes over time due to sediment inflow (or outflow). Dams, in particular, tend to trap sediment in the upstream reservoir. However, dam breach studies, which are a critical component of most floodplain, emergency, and reservoir management planning, rarely consider the impact of sediment storage within the reservoir on the flood wave propagation.

Assuming the volume of the impounded sediment increases over time but the inflow hydrograph to the reservoir remains the same, the potential impact on floodwave propagation is threefold, although the net effect (e.g., an increase versus decrease in downstream flooding extents) is not immediately apparent:

1. A higher reservoir base at the same water surface elevation will reduce capacity, thus decreasing the overall volume released and influencing the outflow hydrograph;
2. The failure characteristics of the dam breach will change because the effective upstream dam height decreases with sediment deposition;

3. A partially filled reservoir with increase sediment transport within the floodwave, thus increasing the outflow due to bulking.

A critical factor to dam breach studies in general, and the one considered here in particular, is the inherent uncertainty of the corresponding parameters. Breach initiation, overall extents, propagation speed, and failure type are all factors that are currently the subject of intense research [e.g., Dhiman and Patra (2018); Zhong, Chen, and Deng (2018)] yet inherently stochastic. Research alone will not permit a confident deterministic approach. Risk analysis is needed.

RiskRAS

In recognition of the need to improve flooding risk assessment for dam and levee breach evaluations, WEST has developed new software that directly incorporates probabilistic aspects of all major components consistent with Monte-Carlo type simulations. The resulting product, named RiskRAS, is a multipurpose GUI-based HEC-RAS simulation tool with a simple graphic interface. It allows the user to assign a statistical distribution to one or more key parameters in the chosen HEC-RAS 1D or 2D model. Completely automated, RiskRAS runs the HEC-RAS model multiple times, selecting randomized values of the key parameters for each run (consistent with a Monte Carlo analysis). When complete, the results can be used to determine the risk of a particular event occurring, evaluate parameter sensitivity, and/or determine most likely outcomes. RiskRAS is written in the Python language utilizing reliable and well-tested libraries. Some specific features are as follows:

- Easy to use GUI interface minimizes learning curve, allowing efficient, error-free simulations
- Facilitates statistical distribution type and parameter selection with dynamic plots
- Guided input selection
- Instant results reporting through dynamic tables and figures
- Python-based program allows easy modification for project specific applications
- Live feedback during simulation

Beyond the present application, RiskRAS can also be used for:

- Dam Break Modeling
- Levee Breach Modeling
- River Model Sensitivity Analyses
- Emergency Action Planning
- Uncertainty Analyses
- Risk Analyses
- Design of Simulated Experiments
- Floodplain Delineation

RiskRAS will be made available as freeware to the general public once beta testing is complete in the Summer of 2019.

Bald Eagle Dam and Reservoir Application

Here, RiskRAS was used to evaluate the overall flow distribution downstream of a dam break considering both initial (no sedimentation) conditions and after 10% of the reservoir capacity has filled with sediment. For this project, the Bald Eagle Dam and Reservoir [data files provided by the U.S. Army Corps of Engineers (USACE) Hydrologic Engineering Center (HEC)] was modeled in RiskRAS. Because detailed information about the dam was not available, the breach location was simply assumed to be midway across the dam span as was assumed at the location shown below (Figure 1).
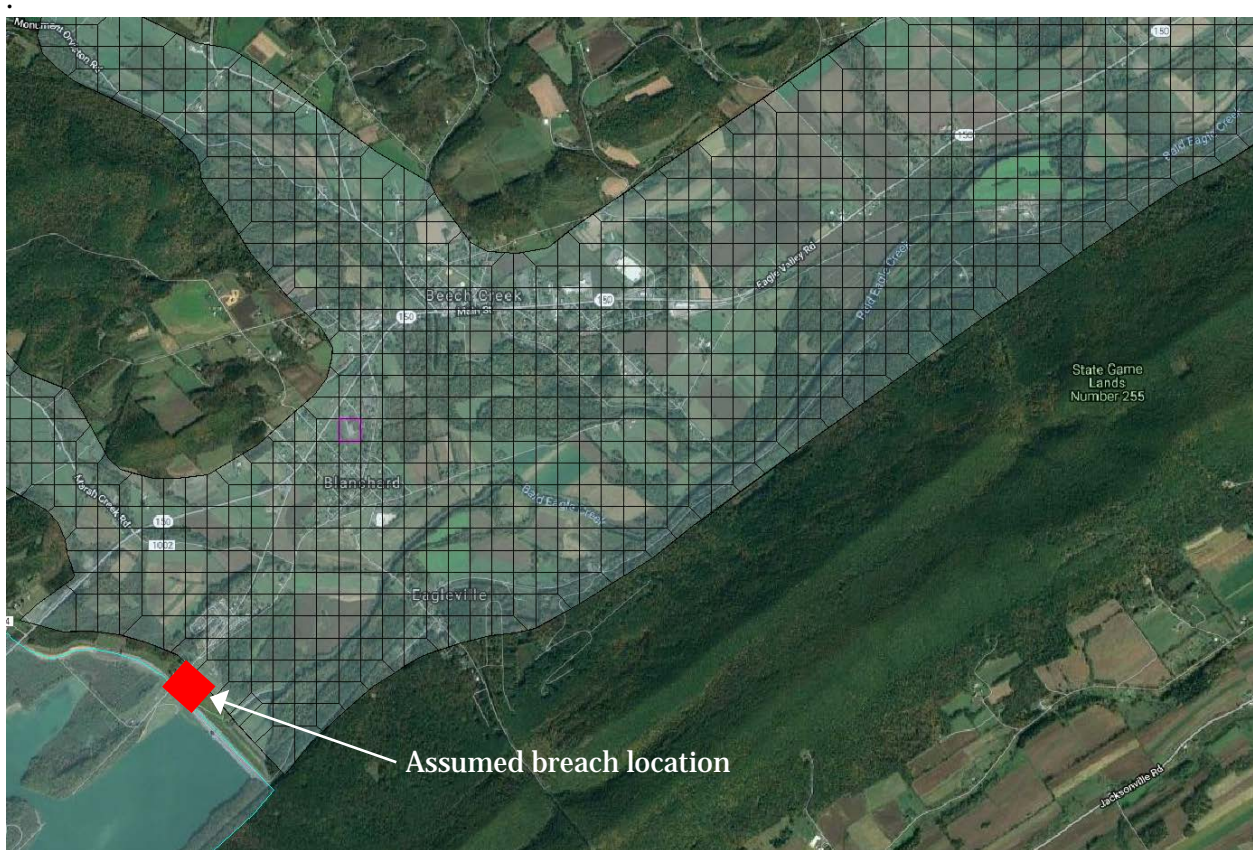
Figure 1. Bald Eagle Dam and Reservoir with theoretical breach location

Overtopping at the breach was assumed to be the breach instigation mechanism. Other breach parameters and their associated statistical distributions are shown in Figure 2 (taken directly from the RiskRAS GUI interface). The left-side and right-side slopes of the breach were assumed to be constant values at 0.5H:1V.

Breach Geometry	Failure	Failure Trigger	Progression					
	Distribution	Median	Sigma	Min	Max	Skewness	Shape Factor
Final Bottom Width	Gaussian ▼	500	50	200	1000		
Final Bottom Elevation	Triangular ▼	625.1		625.1	626		0.2
Left Side Slope	▼	0.5					
Right Side Slope	▼	0.5					
Weir Coefficient	Gaussian ▼	2.6	0.2	2	3		
Formation Time	Skew Normal ▼	2	0.5	1	3	-0.5	
Piping Coefficient	▼	0.5					

Figure 2. Bald Eagle Dam and Reservoir RiskRAS model stochastic parameters

Flow values were evaluated immediately downstream of the breach. A total of 100 separate scenarios were considered in each of two realizations: An empty (no sedimentation) reservoir and a reservoir 10%-filled with sediment.

Note that, generally speaking, thousands of runs are required to account for the expected variability in the input values and provide a corresponding statistical distribution of the results. Hence, the 100 runs used for each realization is unlikely to provide the number of output results needed to provide a complete statistical distribution to fully encompass the likely anticipated respond to the breach. That said, although the 100 runs used for each realization are too small to be taken as completely reliable, they were deemed sufficient here at the alpha testing level and as a proof of concept.

Results

The results of the simulations are shown in Figure 3 below.
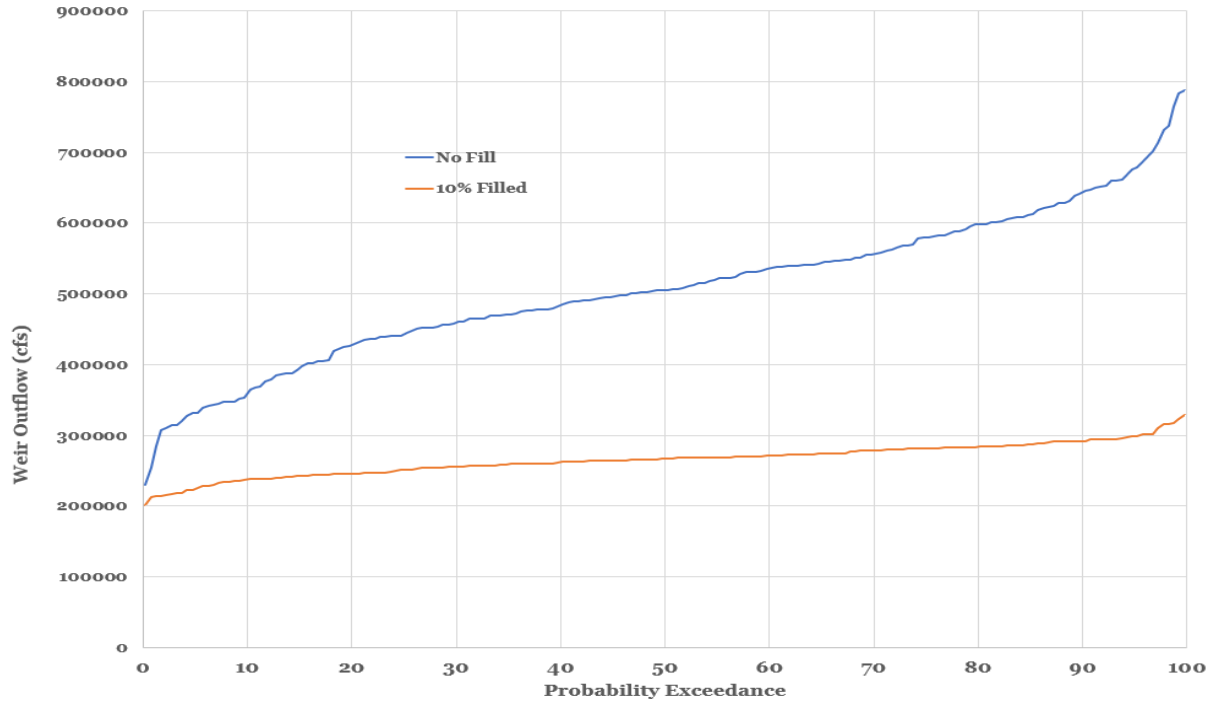
Figure 3. RiskRAS Monte Carlo simulation results

The results are dramatic. The non-filled exceedance probability distribution is significantly different than the 10%-filled distribution. The median value of the "no fill" condition was approximately 500,000 cfs whereas the median condition of the "10% filled" condition was substantially lower at about 250,000 cfs – or approximately half of the "no fill" condition. Furthermore, the 95% probability exceedance values are even more pronounced.

There are several factors that influence the peak outflow from the breach that are likely responsible for the substantial difference between the "no fill" and "10% filled condition":

1. The reservoir base is much narrower than the width at design water surface elevation, and hence the 10% fill condition raised the base elevation of the breach higher than simply 10% of the height (actual value was over 50% of the height).
2. The weir outflow equations are nonlinear and highly sensitive to this height difference;
3. Overtopping at the 10% fill condition distributes the flow early in the hydrograph, providing a mediating influence, much like a detention basin might be expected to operate. The "non filled" condition is less likely to overtop.

Further realizations and closer analysis currently underway may reveal other contributing factors.

Conclusions

The predicted outflows of the study are substantially different between the "no fill" and "10% filled" conditions. If these results can be generalized, then for a reservoir with increasing

sedimentation, the anticipated breach discharge is expected to be much less than would occur under non-filled conditions, and therefore, the overall dam breach floodplain is likely to be much smaller. The magnitude of this difference increases significantly as different exceedance probabilities are considered. Hence, a conservative approach is to assume an empty (dredged) reservoir when it comes to breach modeling, at least if bulked flow is not considered. On the other hand, for conditions where periodic reservoir dredging is not considered, updating the breach analysis may be a warranted effort.

Further applications of RiskRAS allows estimation of floodplain arrival times to places of interest, stage exceedance estimations, re-delineation of floodplains, and provides information for spillway remediation and or design.

References

Dhiman, S. and Patra, K.C. 2018. "Experimental study of embankment breach based on its soil properties", ISH Journal of Hydraulic Engineering, 1—11.

Zhong, Q., Chen, S. and Deng, Z., 2018. "A simplified physically-based model for core dam overtopping breach." Engineering Failure Analysis, 90, pp.141-155.

Sediment Monitoring to Support Modeling a Reservoir Sediment Flush on a Sand-bed River in Northern Nebraska

Nathaniel J. Schaepe, Hydrologist, U.S. Geological Survey, Lincoln, NE,
nschaepe@usgs.gov

Paul M. Boyd, **Ph.D. P.E.** Hydraulic Engineer, U.S. Army Corps of Engineers, Omaha, NE,
Paul.M.Boyd@usace.army.mil

Any use of trade, firm, or product names is for descriptive purposes only and does not imply
endorsement by the U.S. Government.

Abstract

The U.S. Geological Survey (USGS) in cooperation with the U.S. Army Corps of Engineers (USACE), monitored a sediment flush event from Spencer Dam located on the Niobrara River near Spencer, Nebraska, during the fall of 2014. Data collected during the flush were used to validate a one-dimensional sediment transport model developed by the USACE. The USACE surveyed 26 cross sections within the reservoir and as far as 1 kilometer (km) upstream from the reservoir pool to about 10 km downstream from the dam before and after the flushing event to measure erosion and deposition. They also collected surficial sediment samples from sandbars within the reservoir. The USGS assisted USACE in its model validation efforts by collecting sediment data before, during, and after the flush using both traditional sampling techniques and a continuous laser-diffraction particle-size analyzer. From the context of longitudinal volumetric change, the model replicated erosion in the upper half of the reservoir within 4 percent of that observed by survey data and it replicated deposition downstream from the dam within 5 percent. However, the model underpredicted the erosion of the accumulated delta sediments in the reservoir by 43 percent. The timing and magnitude of suspended sediment concentrations produced by the model compared reasonably well to the discrete suspended-sediment sample results. These results indicate cross-sectional survey data and discrete sediment data may be adequate for developing sediment flush models for reservoirs in similar well-sorted sand-bed streams.

The USGS installed a continuous particle-size analyzer immediately downstream from the dam. Although the particle-size analyzer was successful in providing a large dataset during the flushing event, based on discrete point samples, it overestimated the amount of fine particles and underrepresented the amount of coarse material. It also required a significant amount of maintenance during the flushing event because of the large sediment load and the rapid bed aggradation. The maintenance issues with the particle-size analyzer along with uncertainty in the correlation to discrete suspended-sediment samples reduced its value for model validation. However, these issues may have been specific to the flushing event at Spencer Dam, which involved a sand-bed dominated stream and a wide channel. It is foreseeable that other sediment flush models developed for different streams with dissimilar sediment gradations may benefit from similar continuous sediment data, but adequate planning and evaluation should be performed.

Introduction

The Niobrara River in northern Nebraska is a wide and shallow sand-bed river, which drains a large area of the Nebraska Sandhills ecoregion (Figure 1). In its lower reaches, the river is characterized by a sand-bed braided channel, dominated by actively migrating sandbars (Alexander et al., 2010). A hydroelectric dam (referred to as Spencer Dam [Figure 1]) built near Spencer, Nebr. (not shown in Figure 1) was retrofitted in the 1950s to manage for this sediment. Sluicing gates at Spencer Dam are lowered twice a year to allow accumulated sediments to pass downstream. In 2014, the usual spring flush was cancelled because of adverse river conditions, so the 2014 fall flush event consisted of an entire year's worth of accumulated sediment.
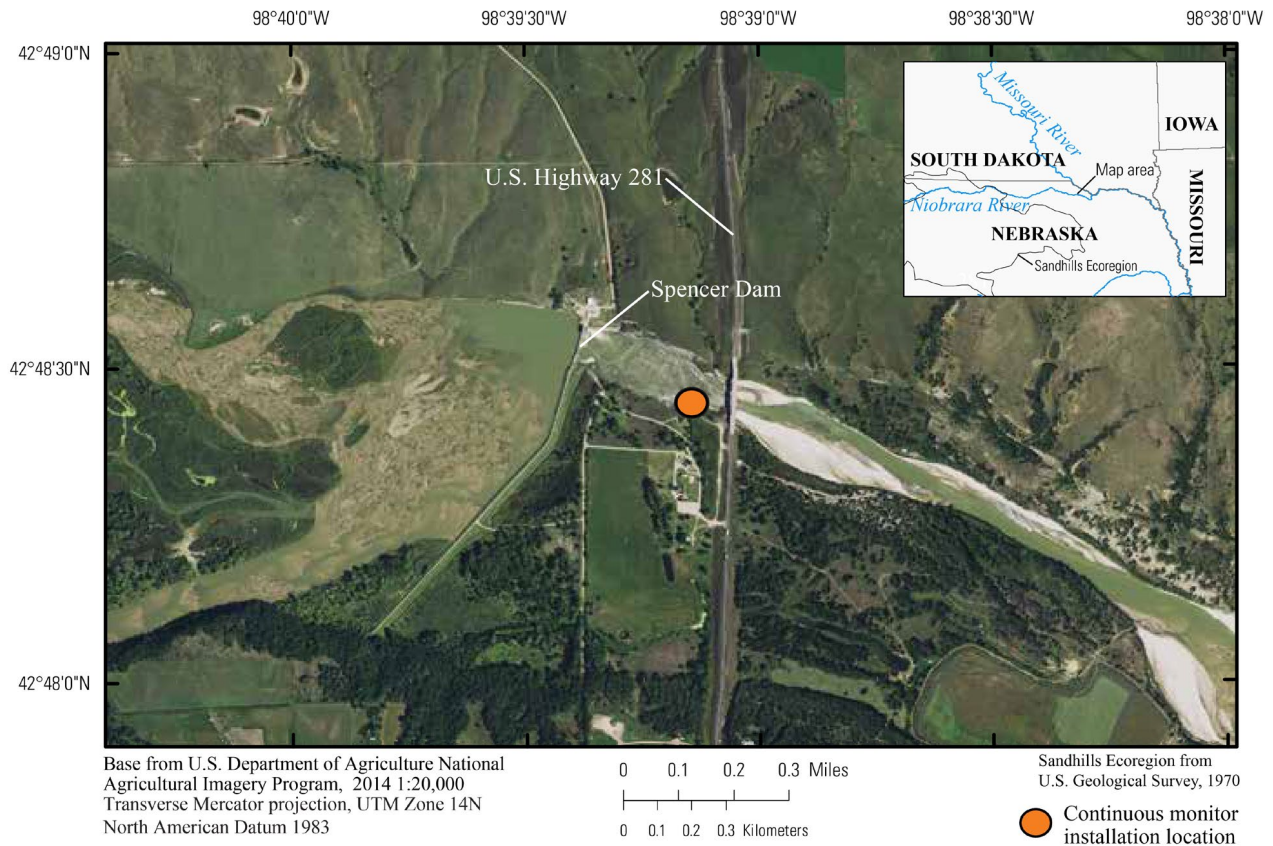
Figure 1. The Niobrara River near Spencer Dam in northern Nebraska

Sedimentation is a common problem for reservoir managers throughout the world. Periodic drawdown flushing is one method for managing the accumulated sediment (Lai and Shen; 1996; Wang and Hu 2009). However, the effectiveness of flushing can vary because the characteristics of each reservoir and dam system are unique. The composition of the sediment in the reservoir, the size of the reservoir, and the design of the dam are only a few of the factors that may influence the success of flushing.

The U.S. Army Corps of Engineers (USACE) has incorporated sediment transport features in HEC-RAS 5.0 (USACE 2016) that can be used to model sediment flushing events. These tools had been used for sediment management studies, but model results had never been compared to

a reservoir flushing event (Gibson and Boyd 2016). In the fall of 2014, USACE identified the Spencer Dam fall sediment flush as an opportunity to evaluate the new model features in HEC-RAS 5.0. The Spencer Dam fall sediment flush also provided a way to test and incorporate the U.S. Department of Agriculture's Bank-Stability and Toe Erosion Model (BSTEM) (Gibson et al. 2015) into HEC-RAS 5.0. Final analysis of BSTEM performance is not yet complete and will not be addressed within this paper.

To validate the HEC-RAS 5.0 model, the U.S. Geological Survey (USGS) in cooperation with USACE, collected data before, during, and after the sediment flush. USACE surveyed cross sections within the reservoir pool and as far as 1 kilometer (km) upstream from the reservoir pool to about 10 km downstream from the dam. The USGS collected discrete sediment samples, as well as continuous suspended-sediment size data using an autonomous particle-size analyzer before, during, and after the flush at a location just downstream from the dam (Figure 1). USACE also collected surficial sediment particle-size samples within the reservoir before the flush.

This paper examines how sediment monitoring was used to assist USACE with model validation for the Spencer Dam sediment flush and discusses the implications for modeling and monitoring similar sediment flush events.

Description of Fall 2014 Reservoir Flush

Spencer Dam operators began lowering gates at midnight October 5, 2014. This initial drawdown was done slowly and resulted in less than 1 meter (m) of lowering in the reservoir. At 8:00 am on the morning of October 6 the operators began raising the four main Tainter gates every hour until they were fully open at about 13:20 in the afternoon. These gates dropped the reservoir pool elevation about an additional 2 m. Once these gates were open, a sluice gate, with an opening 1.5 m lower than the main gates, was opened. All these gates remained open until November 7, 2014 (Gibson and Boyd 2016).

Sediment releases began increasing as the main Tainter gates were lowered but when the sluice gate was opened, it created sudden and impactful morphological changes within the reservoir. A head cut moved rapidly upstream from the sluice gate opening and areas of sandbars left dry by the drawdown began rapidly scouring and slumping into the active channels (Figure 2). Three main channels formed within the reservoir: one along the right bank, one midchannel, and one along the left bank. After 24 hours most of the flow was concentrated in the right channel. Once the right channel became severely incised, the amount of flow and geomorphic activity in the other two channels became comparably insignificant (Gibson and Boyd 2016).

Figure 2. Photograph of the Spencer Dam reservoir during the October 2014 sediment flush looking upstream from right bank. The streamflow is moving towards the bottom right corner.

The channel downstream from the dam became extremely turbulent with moving dunes and antidunes. By the afternoon of the first day, the water appeared to take on characteristics of a slurry. The streambed in the vicinity of the continuous sampler and the Hwy 281 bridge began aggrading within hours after the first lowering of the main Tainter gates. Prior to the sediment release, the bed below the bridge was found to be primarily bedrock, but by the afternoon of the second day the bed had risen about 1.5 m because of the deposited sediment (Gibson and Boyd 2016).

Although suspended-sediment concentrations were highest for the first 48 hours after the flush, suspended-sediment concentrations remained well above pre-flush conditions even 4 weeks after the flush.

Methods

Cross-Sectional Surveys

The USACE surveyed cross sections from approximately 1 km above the reservoir pool to 10 km downstream from the dam. Twenty-six cross sections were surveyed between the reservoir pool and the first kilometer downstream from the dam. The cross sections within the reservoir pool were separated by an average spacing of 75 m. Above and below the reservoir pool, cross section spacing ranged from 0.2 km to 5 km. The cross sections were surveyed prior to the flush and cross sections downstream from the reservoir pool were surveyed immediately after the flush. However, water within the reservoir froze because of an abnormally early extreme cold period and so cross sections within the reservoir were not able to be surveyed after the flush. USACE resurveyed all cross sections during and after the spring flush of 2015 and used the data to assist in filling in the survey data gaps. In areas that were surveyed both after the fall 2014 flush and before and after the spring 2015 flush, the constructed cross sections overlapped reasonably well, which implies the morphological changes during the fall 2014 and spring 2015 flushes were similar downstream from the dam and that pre-flush cross sections were similar in the reservoir

pool. Based on visual observations the morphologic changes that occurred within the reservoir pool were similar as well (Gibson and Boyd 2016).

Discrete Monitoring

USGS collected discrete suspended-sediment samples and bed-sediment samples at the Highway 281 bridge (Figure 1) as well as one site upstream from the reservoir and at two bridge locations downstream from Highway 281 (not shown in Figure 1). The focus of this paper is related to the USACE model, which only estimated suspended sediment concentrations at Hwy 281. Data and associated information for the other discrete suspended-sediment samples and bed-sediment samples collected by the USGS can be found in Schaepe and Zelt (2018) and the data can be downloaded from the USGS National Water Information System Web Interface (USGS 2016). Additionally, USACE collected 17 surficial sediment samples from sandbars along a 1-km segment within the reservoir prior to the flush.

Discrete suspended-sediment samples were collected by the USGS before, during, and after the sediment flush from the Hwy 281 bridge. USACE wanted to quantify the rapid suspended-sediment concentration changes that occurred during the beginning of the flush, so more samples were collected in the first few days of the flush; thereafter the sampling frequency was reduced. Five samples were collected the first day of the flush (October 6, 2014), six samples were collected on the second day, four samples were collected on the third day, and two samples were collected on the fourth and fifth days. Single samples were collected on day 16 and day 33 (the final day) of the sediment flush. One sample was collected before the flush on October 2 to determine background concentrations and one sample was collected on November 13 shortly after the reservoir pool was filled (November 7 through November 10) and the dam resumed regular operations (November 10).

Suspended sediment samples were collected using equal-width-increment (EWI) sampling techniques (Edwards and Glysson 1999), so that the entire stream cross section would be represented in each sample. EWI sampling was utilized over equal-discharge-weighted sampling because the rapidly changing streamflow caused by the flush made equal-discharge-weighted sampling impractical. Replicate samples were collected for 22 of the 25 samples collected at the Highway 281 bridge to quantify sample variability. Quantifying the variability between replicate sets provides information on the precision of the sample result. Replicate samples were collected concurrently meaning that at each station two bottles were filled, one for sample set A and one for sample set B. At the next station the order was switched so that one set was not always collected prior to the other. The median difference between replicate sets was 12.1 percent (Schaepe et al. 2018). Suspended-sediment concentrations were determined by the USGS Iowa sediment laboratory using standard methods (Guy 1969). Additional information about these samples and sample data can be found in Schaepe and Zelt (2018).

Several suspended-sediment point samples were collected near the intake of the continuous particle-size analyzer (see "Continuous Monitoring" section) for quality control. These samples were collected using a USGS DH-81 bottle sampler using standard USGS methods (Edwards and Glysson 1999). The samples were analyzed by laser diffraction using a LISST-Portable (Sequoia Scientific 2011a). Additional information about these samples can be found in Schaepe et al. (2018).

Continuous Monitoring

The USGS installed an on-site laser-diffraction particle-size analyzer (LDPSA)(Sequoia LISST Streamside, Sequoia Scientific 2011b) to collect continuous suspended-sediment particle-size samples during the beginning of the sediment flush when sediment concentrations were expected to change most rapidly. USGS deployed the LDPSA the week prior to the sediment flush to ensure that the instrument was working as expected and to obtain pre-flush baseline data. It was then redeployed the night before the sediment flush at the same location and operated sporadically during the first 4 days of the flush.

The LDPSA instrument collects water by pumping it from the stream and then analyzes it using laser diffraction technology. The results are given volumetrically (microliters/liter) for 32 log-spaced size classes ranging from 1.9 to 386 microns (µm) (Sequoia Scientific 2011b), although only nine of those size classes were quality-assured for this study. The LDPSA measures sediment particles using a 670-nanometer wavelength laser beam. A photodiode measures the light energy from the laser beam that passes through the water-sediment mixture. Particle-size measurements are based on the multiangle scattering pattern. The resolution of the LDPSA is 1 milligram per liter (mg/L) and this resolution can be maintained for concentrations as large as 8,000 mg/L. Additional information about laser diffraction technology can be found in Agrawal and Pottsmith (2000).

The LDPSA was installed approximately 0.4 km downstream from the dam on the right bank. Most of the components were mounted in a storage box on top of the bank, about 7.6 m above the river, and the pump was installed using a sliding rail system and set in the water about 1.2 m from the bank. Additional information on instrument components, instrument settings, and calibration data can be found in Schaepe et al. (2018).

Sediment Transport Model

The Spencer Dam flushing event was modeled using a one-dimensional (1D) HEC-RAS 5.0 unsteady sediment model. Cross-sectional survey data measured before the flush was used to define the spatial parameters of the model. An inline structure was included in the model to represent the dam, and gate operations, which were provided by Nebraska Public Power District, were input to the model as a time series (Gibson and Boyd 2016).

The Yang sediment transport function (Yang, 1973) was selected for the final model. The Copeland algorithm was used to model bed-material mixing. Model outputs of erosion and deposition volumes were not sensitive to the transport function or bed-material mixing algorithm. However, incision rates were sensitive to the transport function and the Yang transport function most effectively reproduced the rates observed during the flush (Gibson and Boyd 2016).

The model was run using 6-second time steps. Larger time steps introduced steep friction slopes, which created high shear stresses causing the bed to be unstable which led to over-prediction of erosion in the model. Larger time steps also created hydraulic instabilities. Smaller time steps did not produce a steep enough energy grade line to initiate scouring (Boyd and Gibson, 2016). Additionally, the timing of the sluice gate opening was reduced in comparison to the flushing event to improve model stability (Gibson and Boyd 2016). Additional evaluation of the model's handling of the sluice gates opening will be needed so that the model results can be considered reliable for various sluicing scenarios.

Surficial sediment samples collected before the flush were used to calibrate bed gradations. Most of these samples consisted of at least 90 percent fine-medium grain-sized sand. Model test runs indicated that it was not sensitive to sediment boundary conditions; thus, a simple equilibrium load boundary was defined at the upstream cross section (Gibson and Boyd 2016).

Performance of Sediment Monitoring Techniques

Logistical Challenges of Discrete Monitoring

Sampling conditions at the Hwy 281 bridge were difficult because of the extreme river conditions, especially during the first day and a half of the sediment flush. The initial surge of stored water and sediment, combined with the bridge constriction, made sampling conditions difficult. Stream velocities consistently exceeded 7 feet per second. The high velocities combined with the additional force from the heavy sediment load routinely dragged the sampler downstream during sampling. Large sand dunes were constantly forming and moving within the sample channel cross section. These sand dunes may have contaminated some of the suspended-sediment samples with bed material.

Logistical Challenges of Continuous Monitoring

Although the monitoring equipment location was well located for capturing the rapid changes in sediment concentrations, because of its close proximity to the dam, the flow and sediment characteristics were problematic for autonomous sampling from a fixed bank-side location. During the flush, bank material was continually eroding and falling into the river near the pump. Streambed aggradation during the first night of the flush was so substantial that the pump became fully buried in sediment and therefore could not operate. It took until early afternoon of the following day to reposition the pump and resume sampling. The stream depth near the bank was limited to around 0.5 m, which made it difficult to maintain enough distance between the pump to the streambed to ensure that bed material was not being sampled. Because of the rapid aggradation and shallow depths, the pump had to be moved several times during the flushing event.

Comparison of Continuous Sediment Sampling versus Discrete Sampling

Comparisons of LDPSA results to the results of discrete point samples collected near the LDPSA pump and discrete suspended sediment samples at the bridge indicated differences in sample composition and magnitude. The differences between the LDPSA and the discrete point samples near the pump are related to the sample intake method (pump compared to nozzled bottle sampler), because they both employ the same method of analysis (laser diffraction). The LDPSA samples had a larger percentage of fine material and lower percentage of coarse material than the discrete point samples collected near the LDPSA pump (Figure 3). Pump samplers are known to underestimate the coarse load (Edwards and Glysson 1999; Roseen et al. 2011) because the pumping force cannot overcome the momentum of the coarser material, especially for particles that are further away from the pump (Edwards and Glysson 1999). The result of this is that the LDPSA's sample had a greater proportion of fine material and a smaller proportion of coarse material than the discrete point samples collected near the pump.
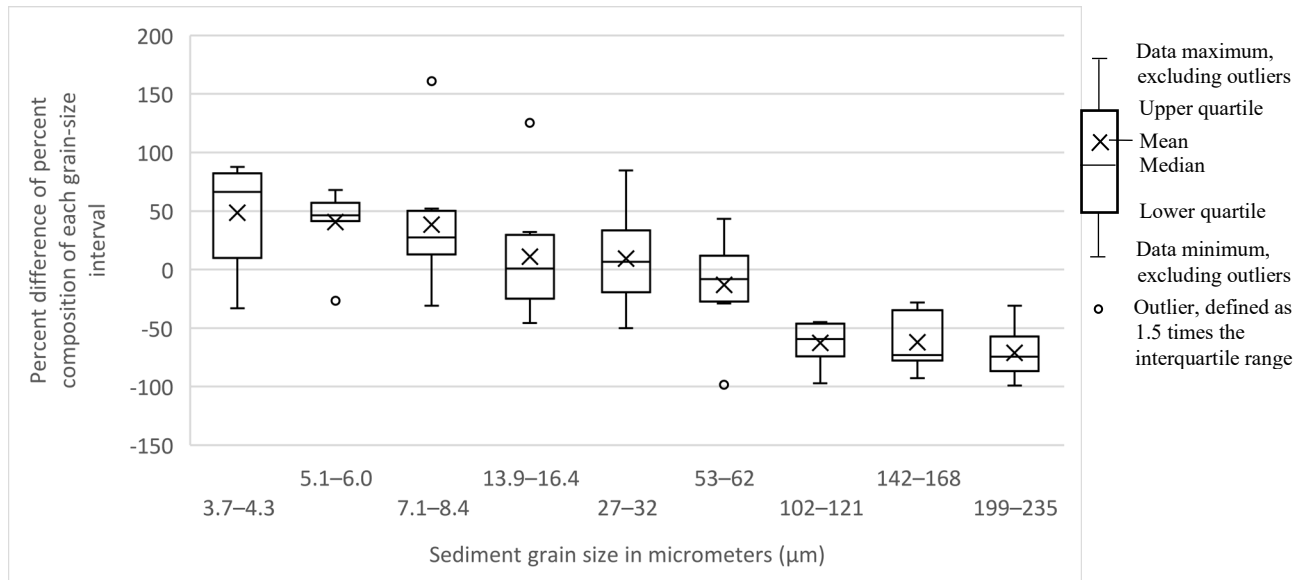
Figure 3. Comparison of measured concentrations for selected sediment grain sizes collected by LISST-Streamside (Sequoia Scientific 2011b) continuous sediment monitor and selected discrete point samples collected near the continuous sediment monitor and analyzed by LISST-Portable (Sequoia Scientific 2011a). Positive differences indicate the LISST-Streamside results were higher than those of the LISST-Portable.

Differences between LDPSA data and bridge sample results indicate that suspended-sediment concentrations near the pump were not representative of the channel cross section as a whole. A complete grain-size distribution was not determined from the LDPSA data (see Schaepe et al. 2018), but if simple interpolation is used to create a full distribution and an effective density of 1.24 grams per milliliter (calculated by Czuba et al. 2015) is assumed, then concurrent (collection times were within 15 minutes of one another) samples from LDPSA data and bridge discrete suspended-sediment sample results have a coefficient of determination of 0.05 which indicates a poor relation of the two datasets.

The concentrations measured at the bridge were substantially higher than those measured by the LDPSA. There are many factors that may have contributed to these differences. The difference in channel configuration was most likely the largest contributing factor. The cross section at the bridge was confined, which created a mostly deep and fast cross section. The channel cross section at the pump was much wider and so velocities were lower, and depths were smaller. This indicates that more sediment would be transported in suspension at the bridge site compared to the cross section at the pump (Edwards and Glysson, 1999).

As with the discrete point samples collected near the pump, the sample intake method used for the bridge sample was different than for the LDPSA samples. The bridge discrete suspended-sediment samples were collected at 10 equally spaced locations within the cross section. As a result, the bridge discrete suspended-sediment samples represented the entire water column whereas LDPSA samples only represented the volume around the pump intake. Also, the discrete suspended-sediment bridge samples were collected with an isokinetic bottle sampler; the LDPSA samples were collected by a pump.

Sediment transport model performance

Bathymetric Comparison

Overall the sediment transport model performed well in estimating scour and deposition within the reservoir and downstream from the dam. The total volume change estimated by the model in the upper half of the reservoir was within 4 percent of the surveyed volume change. The sediment deposition volume estimated by the model for the 500-m stretch of river directly downstream from the dam was within 5 percent of the surveyed volume. However, within the deltaic portion of the reservoir the model underestimated erosion volumes by 43 percent (Gibson and Boyd 2016), although some of the measured erosion may have been associated with the differences between the fall 2014 flush and the 2015 spring flush.

The performance of the model is demonstrated by a plot of a typical reservoir cross section (Figure 4). The plot shows that the model accurately estimated incision depth but failed to accurately represent the lateral erosion. This occurred because dry sediments that the model assumed to be stable became compromised when toe slopes beneath them eroded. This causes sediment in the incising bank to slump off, increasing the rate of channel expansion. Most sediment models underestimate these lateral erosional processes because they estimate erosion only at the channel-bar interface. Additional geotechnical and lateral process models are needed to accurately model these geomorphological processes (Gibson and Boyd 2016).
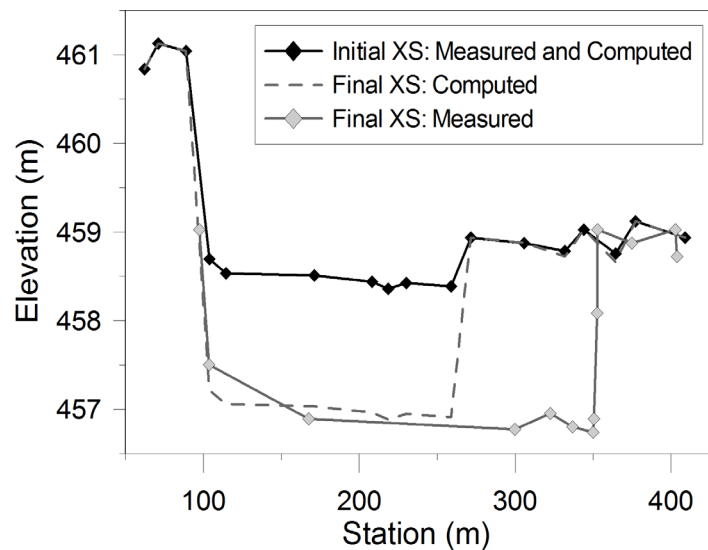
Figure 4. Measured and computed cross sections before the fall 2014 (initial XS) and after the spring 2015 flush (final XS) at a representative, mid-reservoir transect from Gibson and Boyd (2016). Vertical coordinates referenced to the North American Vertical Datum of 1988.

Suspended-Sediment Concentration Comparison

Model results for sediment concentrations were compared to the discrete suspended-sediment sample concentrations collected from the Hwy 281 bridge (Figure 5). The model computed total sediment load concentrations whereas the discrete suspended-sediment samples only included the suspended portion; therefore, the model results were expected to be higher. In a different segment of the Niobrara River, Colby and Hembree (1955) found that the suspended fraction

represented an average of 51 percent of the total load. When suspended sediment concentrations were above 1,000 mg/L the average increased to 0.67. Turowski et. al (2010) summarized studies by Maddock and Borland (1950) and Lane and Borland (1951) and reported that for sand-bed streams the suspended fraction made up 74 to 91 percent of the total load for concentrations between 1,000-7,500 mg/L and 80-95 percent for concentrations greater than 7,500 mg/L. These studies indicate that for higher concentrations of suspended sediments in sand-bed streams, the suspended load should become a larger percentage of the total load. Therefore, Gibson and Boyd (2016) determined that the model estimated the timing and magnitude of the sediment load reasonably well.
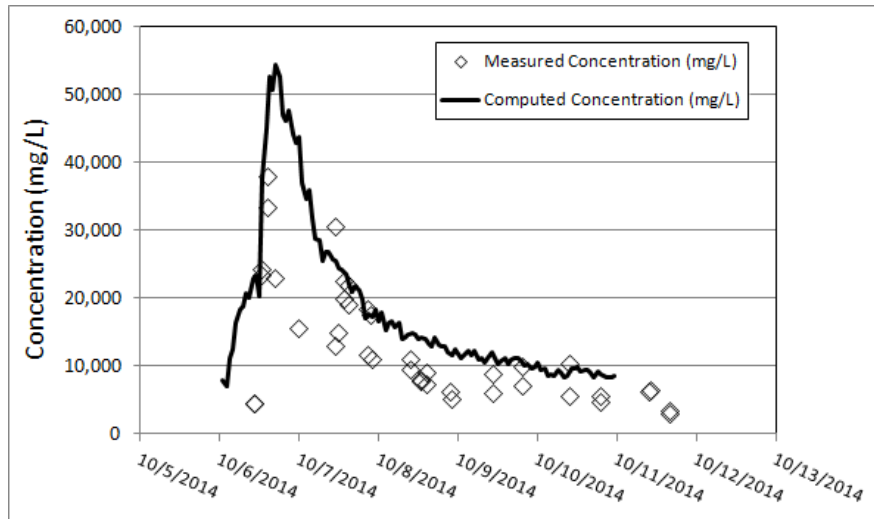
Figure 5. Suspended-sediment concentrations during the flush measured 500 m downstream from the dam and the total-sediment concentration computed at that location by HEC-RAS (Boyd and Gibson 2016)

Discussion

Continuous and discrete sediment monitoring are useful for refining and verifying sediment flush models. However, the type or types of data recommended for collection will depend on the needs of the model, site conditions, and the resources available. Preferably, knowledge about previous flushes can be used to inform monitoring decisions. In cases where no previous flushing events have been monitored, information from existing models developed for other similar flushing events may be used but greater uncertainty should be expected.

At a minimum, cross-sectional information, both upstream and downstream, would provide valuable information for the model. Surficial sediment samples collected upstream from Spencer dam also proved to be a vital component of the Spencer model and such data would provide models with a starting point for estimating the gradations of sediment that will be transported downstream from the dam. The discrete suspended-sediment samples indicated that the model adequately estimated sediment concentrations downstream from the dam. This indicates that for the Niobrara River and possibly other sand-dominated streams, sediment-size gradation information collected within the reservoir may be adequate for model calibration. For streams that have a wider range of sediment sizes, continuous suspended-sediment monitoring may be needed to identify the composition of sediment in suspension during the flush.

If it is determined that continuous suspended-sediment monitoring data will be collected during a sediment flush, it is critical to assess whether the equipment will operate effectively and to determine what type of data are needed. If previous sediment flushes have been observed, those conditions should be used to dictate selection of monitoring equipment. If no prior knowledge is available, preliminary hydrologic and sediment models based on site reconnaissance should be used to guide the monitoring design. Prior background information at a minimum should include identification of possible monitoring locations, estimates of aggradation downstream from the dam, estimation of suspended-sediment sizes, and an understanding of channel geometry.

No matter what conditions are expected, discrete suspended-sediment monitoring is necessary for validation and interpretation of continuous data (Landers et al. 2016; Czuba et al. 2015; Rasmussen et al. 2009). However, because of the extreme conditions that occur during a sediment flush, discrete monitoring may be difficult. For example, during the Spencer Dam sediment flush in fall 2014, the only safe and reasonable location for discrete monitoring was at a bridge location that was not ideal for sample collection. At this bridge location, flow was highly constricted, which introduced velocities that were higher than the maximum velocity recommended for the sampling equipment. In addition, large dunes were constantly migrating on the streambed. In deeper rivers, it may be possible to avoid such situations by using a boat. For other situations, possible alternatives may include temporary cableways, an alternate bridge location, or a wadeable cross section. The quality of discrete sample results is highly dependent on the sampling site (Edwards and Glysson 1999; Landers et al. 2016) and so it is critical a suitable location for discrete sampling is identified. The objective of the investigator should be to collect the best discrete data possible so that any continuous data that are collected can be adequately interpreted and used appropriately.

If an adequate discrete suspended-sediment monitoring site can be identified and continuous monitoring results are required, then conditions at the site should be evaluated to determine the most applicable continuous monitoring technology. For example, aggradation, such as occurred downstream from Spencer Dam, limits how instruments may be installed and used. Some instruments, such as turbidity monitors and the Sequoia LISST-SL, can be cabled from the bridge and moved up or down as necessary. Other instruments that are more fixed must be mounted on some type of sliding rail system such as was used in this study or similar to how the acoustic Doppler velocity meter (ADVM), which was used in the Clearwater and Snake Rivers in Washington and Idaho (Wood and Teasdale 2013), was mounted. However, these moveable units are not free from effects from aggradation, because sediment composition of the sample being analyzed is dependent on proximity to the bed (Edwards and Glysson 1999; Landers et al. 2016), and during times when the equipment is not attended, the distance from the instrument to the bed will change. Other possible alternatives would be to use an intake attached to a floating mount or engineering a constriction near the intake that would prevent deposition.

A determination or estimation of the gradations of sediment in suspension during a flush will help determine the most appropriate continuous monitoring equipment. If it is determined that the sediment in suspension will primarily be fine sediments, then a turbidity monitor may be used as a surrogate for suspended-sediment concentration (Rasmussen et al. 2009; Uhrich and Bragg 2003). However, in a sediment flush, the types of turbidity monitors that can be used may be limited because the concentrations may exceed the upper limits of the equipment's capabilities. ADVMs have also been shown to adequately estimate suspended-sediment

concentrations in fine-sediment dominated streams (Landers et al. 2016) and are still useful during periods of high concentrations.

In streams where sediments in suspension are a mixture of fine and coarse material then multi-frequency ADVMs and laser diffraction technology (such as LISST instruments) are preferable to turbidity monitors for estimating suspended-sediment concentrations (Landers et al. 2016; Topping et al. 2015; Czuba et al. 2015). These technologies also can be used to estimate suspended-sediment size (Landing et al. 2016; Czuba et al. 2015) whereas turbidity monitors cannot.

Variability of suspended-sediment within a cross section has a large effect on the quality of continuously monitored data. This is especially true during a sediment flush when changes are occurring quickly. Channel geometry can either contribute to the variability or limit it. In the case of Spencer Dam, the constriction of the bridge combined with the bedrock bed constrained the initial flush of water so that flow increases were mainly noticeable as an increase in stream velocity. These increases along with the initial pulse of sediment created a cross section dominated by suspended sediment. As the flush went on, the bed aggraded so that the water rose above existing gravel and sandbar constrictions and then widened and began to form bars and side channels. Once this occurred, most of the sediment in suspension was in the center of the channel. Monitoring of a previous flush may have provided information as to the best location to place a continuous monitor that would have accounted for these cross-section deviations, but because of the nature of sand-bed streams it would not necessarily respond the same way during a subsequent flush. Only comparative analysis of continuous data to discrete cross-sectional data could determine how well the data corresponded.

To avoid issues related to changes in cross-sectional suspended-sediment variability, if possible, a cross section should be selected that is relatively narrow with high banks so that the majority of sediment remains in suspension during the flush. If an ADVM is used, the channel should be straight for at least 5 to 10 channel widths both upstream and downstream from the monitoring location, and the ADVM should be adequately placed upstream or downstream from obstructions (such as bridge piers) and be far enough upstream or downstream from the discrete sampling location to avoid acoustic interference (Landing et al. 2016). Even if the grain-size distribution across the cross section remains constant, the distribution of grain sizes may change with time, which can affect acoustic attenuation (Topping and Wright 2016). This will add to the analysis time related to ADVM post-processing.

As is indicated by most of this section, monitoring sediment during a sediment flush presents challenges, especially for continuous monitoring. Because of this, the needs of the study should be carefully weighed against safety, the probability of obtaining quality data, and the resources available. Each sediment flush modeling project is unique and complex, and thus requires careful planning and preparation. It is ultimately the responsibility of the investigators to decide the data needs of their model and determine if those data can be collected, safely, practically, and within cost constraints.

References

Agrawal, Y.C., and Pottsmith, H.C., 2000. "Instruments for particle size and settling velocity observations in sediment transport," Marine Geology, 168:89–114.

Alexander, J.S., Zelt, R.B., and Schaepe, N.J., 2010. "Hydrogeomorphic and hydraulic habitats of the Niobrara River, Nebraska—with special emphasis on the Niobrara National Scenic River," U.S. Geological Survey Scientific Investigations Report 2010–5141, 62 pp, available at https://doi.org/10.3133/sir20105141.

Boyd, P.M. and Gibson, S. 2016. "Applying 1D sediment models to reservoir flushing studies: measuring, monitoring, and modeling the Spencer Dam sediment flush with HEC-RAS," U.S. Army Engineer Research and Development Center Coastal and Hydraulics Laboratory Technical Note XIV-52, 12 pp

Colby, B.R. and Hembree, C.H. 1955. "Computations of total sediment discharge Niobrara River near Cody, Nebraska." U.S. Geological Survey Water-Supply Paper 1357, 187 pp., available at https://doi.org/10.3133/wsp1357.

Czuba, J.A., Straub, T.D., Curran, C.A, Landers, M.N., and Domanski, M.M. 2015. "Comparison of fluvial suspended-sediment concentrations and particle-size distributions measured with in-stream laser diffraction and in physical samples," Water Resources Research 51(1):320-340

Edwards, T.K., and Glysson, G.D., 1999. "Field methods for measurement of fluvial sediment," U.S. Geological Survey Techniques of Water-Resources Investigations, book 3, chap. C2, 89 pp, available at https://doi.org/10.3133/twri03C2.

Gibson, S., Simon, A., and Bankhead, N. 2015. "A physically-based channel-modeling framework integrating HECRAS sediment transport capabilities and the USDA-ARS Bank-Stability and Toe-Erosion Model (BSTEM)," Proceedings of the 10th Federal Interagency Sedimentation Conference, Reno, Nev., pp 1-12

Gibson, S. and Boyd, P.M. 2016. "Monitoring, measuring, and modeling a reservoir flush on the Niobrara River in the Sandhills of Nebraska," U.S. Army Corps of Engineers publication available at http://rsm.usace.army.mil/pubs/pdfs/RiverFlow2016-Gibson-Boyd.pdf

Guy, H.P., 1969. "Laboratory theory and methods for sediment analysis," U.S. Geological Survey Techniques of Water-Resources Investigations, book 5, chap. C1, 58 pp, https://pubs.usgs.gov/twri/twri5c1/

Lai, J.S. and Shen, H.W. 1996. "Flushing sediment through reservoirs," Journal of Hydraulic Research, 34(2):237-255

Landers, M.N., Straub, T.D., Wood, M.S., and Domanski, M.M., 2016. "Sediment acoustic index method for computing continuous suspended-sediment concentrations," U.S. Geological Survey Techniques and Methods, book 3, chap. C5, 63 pp, http://dx.doi.org/10.3133/tm3C5

Lane, E.W. and Borland, W.M. 1951 "Estimating bed load." Transactions of the American Geophysical Union, 32:121–123

Maddock, T. and Borland, W.M. 1950. "Sedimentation Studies for the planning of reservoirs by the Bureau of Reclamation." Technical Report, United States Department of the Interior, Bureau of Reclamation, Branch of Project Planning

Rasmussen, P.P., Gray, J.R., Glysson, G.D., and Ziegler, A.C., 2009, "Guidelines and procedures for computing time-series suspended-sediment concentrations and loads from in-stream turbidity-sensor and streamflow data," U.S. Geological Survey Techniques and Methods book 3, chap. C4, 53 pp, available at https://doi.org/10.3133/tm3C4

Roseen, R.M., Ballestero, T.P., and Fowler, G.D. 2011. "Sediment Monitoring Bias by Automatic Sampler in Comparison with Large Volume Sampling for Parking Lot Runoff," Journal of Irrigation and Drainage Engineering, 137(4):251-257

Schaepe, N.J., Coleman, A.M., and Zelt, R.B., 2018. "Documentation of particle-size analyzer time series, and discrete suspended-sediment and bed-sediment sample data collection, Niobrara River near Spencer, Nebraska, October 2014," U.S. Geological Survey Data Series 1079, 11 pp, https://doi.org/10.3133/ds1079

Schaepe, N.J., and Zelt, R.B., 2018. "Niobrara River suspended-sediment and bed-sediment data collected during hydroelectric dam flush near Spencer, Nebr., October through November, 2014," U.S. Geological Survey Data Release, https://doi.org/10.5066/F74M93RK.

Sequoia Scientific, 2011a. "LISST-Portable, User's guide, version 3.11," Bellevue, Wash., Sequoia Scientific, 45 pp

Sequoia Scientific, 2011b. LISST-StreamSide suspended sediment sensor, Operating manual, version 2.1: Bellevue, Wash., Sequoia Scientific, 89 pp

Topping, D.J., Wright, S.A., Griffiths, R.E., and Dean, D.J., 2015. "Physically based method for measuring suspended-sediment concentration and grain size using multifrequency arrays of single-frequency acoustic-doppler profilers,'" Proceedings of the 10th Federal Interagency Sedimentation Conference, Reno, Nev., pp 833–846

Topping, D.J., and Wright, S.A., 2016. "Long-term continuous acoustical suspended-sediment measurements in rivers—Theory, application, bias, and error," U.S. Geological Survey Professional Paper 1823, 98 pp, available at http://dx.doi.org/10.3133/pp1823

Turowski, J. M., Rickenmann, D., and Dadson, S. J., 2010. "The partitioning of the total sediment load of a river into suspended load and bedload: a review of empirical data," Sedimentology, 57(4): 1126-1146, available at https://doi.org/10.1111/j.1365-3091.2009.01140.x.

U.S. Army Corps of Engineers, 2016. "HEC-RAS river analysis system, hydraulic reference manual, version 5.0," U.S. Army Corps of Engineers Hydrologic Engineering Center User Manual, 547 pp, available at https://www.hec.usace.army.mil/software/hec-ras/documentation/HEC-RAS%205.0%20Reference%20Manual.pdf

U.S. Geological Survey, 1970, "Land resource regions and major land resource areas of the United States," digital data, adapted from U.S. Soil Conservation Service, 1:2,000,000 scale, accessed November 25, 2002, at http://water.usgs.gov/lookup/getspatial?mlra.

U.S. Geological Survey, 2016, National Water Information System—Web interface, accessed September 28, 2016, at https://dx.doi.org/10.5066/F7P55KJN

Uhrich, M.A. and Bragg, H.M., 2003. "Monitoring instream turbidity to estimate continuous suspended-sediment loads and yields and clay-water volumes in the Upper North Santiam River Basin, Oregon, 1998–2000," U.S. Geological Survey Water-Resources Investigations Report 03–4098, 43 pp, available at https://doi.org/10.3133/wri034098

Wang, Z.H. and Hu, C. 2009. "Strategies for managing reservoir sedimentation," International Journal of Sediment Research, 24(4):369-384

Wood, M.S., and Teasdale, G.N., 2013. "Use of surrogate technologies to estimate suspended sediment in the Clearwater River, Idaho, and Snake River, Washington, 2008–10," U.S. Geological Survey Scientific Investigations Report 2013-5052, 30 pp available at https://doi.org/10.3133/sir20135052

Yang, C. T., 1973. "Incipient motion and sediment transport," American Society of Civil Engineers Journal of the Hydraulics Division, 99(10):1679-1704, 197

Newtonian and Non-Newtonian Sediment Fluid Flow Hydrodynamic Runoff Model

Nawa Raj Pradhan, Ph.D., US Army Corps of Engineers, Engineer Research and Development Center, Coastal and Hydraulics Laboratory, Vicksburg, MS, Nawa.Pradhan@erdc.dren.mil

Ian Floyd, US Army Corps of Engineers, Engineer Research and Development Center, Coastal and Hydraulics Laboratory, Vicksburg, MS, Ian.E.Floyd@erdc.dren.mil

Charles Downer, Ph.D., US Army Corps of Engineers, Engineer Research and Development Center, Coastal and Hydraulics Laboratory, Vicksburg, MS, Charles.W.Downer@erdc.dren.mil

Stanford Gibson, Ph.D., US Army Corps of Engineers, Hydrologic Engineering Center, Davis, CA, Stanford.Gibson@erdc.dren.mil

Ronald Heath, US Army Corps of Engineers, Engineer Research and Development Center, Coastal and Hydraulics Laboratory, Vicksburg, MS, Ronald.E.Heath@erdc.dren.mil

Abstract

Assumption of Newtonian fluid flow condition, linear stress-strain relationship, fails for sediment laden fluids with higher volumetric sediment concentrations. As sediment concentrations increase, they begin to affect the fluid properties which alter the stress-strain relationship. In this study we developed the debris library, DebrisLib, that assigns a stress-strain relationship under non-Newtonian sediment-laden fluid flow conditions. This study also developed a linkage architecture to pass the hydrodynamic information to the non-Newtonian sediment dynamic subroutines and then returns the non-Newtonian sediment dynamic information. The Gridded Surface Subsurface Hydrologic Analysis (GSSHA) model is deployed as the hydrodynamic model. GSSHA-computed flow velocity, depth and concentration is passed to non-Newtonian sediment dynamic subroutines where internal shear stresses are computed and returned back to GSSHA. Using the volumetric sediment concentration, the Newtonian and non-Newtonian sediment fluid flow was tested in a 2D hydrodynamic runoff digital flume model. This test case of digital flume model overland simulation showed that mixed density and viscous fluid shear stress is significantly underestimated if a non-Newtonian condition is ignored. This under estimation of shear stress would significantly underestimate the sediment yield.

Introduction

Estimates of sediment graphs associated with hydrographs are essential for producing sediment yield estimates for designing efficient sediment control structures and for water quality

predictions. Physics-based distributed prediction of erosion and deposition of sediment is significant for not only long-term local geomorphological and landform changes point of view but also for better understanding of the land surface process and sediment sourcing and sinking mechanisms and its impact on hydrology, ecosystem, transport system, environment and socio-economy. Land use change and soil physical and chemical properties change also leads to the change in sediment sourcing, sinking and transport mechanism. One of the natural and/or man-made causes that brings about such changes in land use and soil property is wildfires. A rainfall event after a wildfire triggers a hyperconcentrated mud and debris flow. Such events with high concentration of sediment also changes the sediment laden water flow properties. The prime change of such water flow property is a non-linear shift of the viscosity which ultimately makes the water flow condition non-Newtonian.

Assumption of Newtonian fluid flow condition, defined by a linear stress-strain relationship, fails for sediment laden fluids with higher volumetric sediment concentrations. As sediment concentrations increase they begin to affect the fluid properties which alter the stress-strain relationship. Debris flows depart from linear stress-strain with no intercept assumptions embedded in the clear water flow equations. In this study, we developed the debris library, DebrisLib, that assigns a stress-strain relationship under non-Newtonian sediment laden fluid flow conditions (Pradhan et al., 2018; Floyd et al., 2019). This study also developed a general linkage architecture to pass the hydrodynamic information to the non-Newtonian sediment dynamic subroutines and then return non-Newtonian sediment dynamic information. The GSSHA model is deployed as the hydrodynamic model in this study. The GSSHA model is a fully-coupled overland/in-stream sediment transport (Newtonian flow regime) hydrodynamic model (Downer et al., 2015; Pradhan et al., 2018). GSSHA-computed flow velocity, depth and concentration is passed to non-Newtonian sediment dynamic subroutines where internal shear stresses are computed and passed back to GSSHA (Pradhan et al., 2018). Based on the volumetric sediment concentration, the Newtonian and non-Newtonian sediment fluid flow was tested in a 2D hydrodynamic runoff digital flume model.

Methodolody

The following steps were implemented as a method to develop the non-Newtonian sediment fluid flow dynamics capability in the parent hydrodynamic model:
   a) The non-Newtonian processes were identified and coded as subroutines / functions.
   b) The non-Newtonian process functions were arranged in the parent overland hydrodynamic code to align in correct order with other Newtonian and hydrodynamic processes. This arrangement and code development (in the two-dimensional overland sediment hydrodynamic GSSHA model) followed the linkage architecture
   c) A test case, two-dimensional overland flume GSSHA model, was developed to make basic initial non-Newtonian internal shear stress function tests.

Details of the methodology are provided in the following sections.

Overland Sediment Detachment

Soil detachment can occur due to rainfall and overland flow. Total detachment is comprised of the sum of rainfall and overland flow detachment. Detachment by raindrops is considered to be a function of rainfall momentum, which is related to rainfall intensity (Downer et al., 2015). In this study, the analysis of the Newtonian and Non-Newtonian sediment transport mechanism is based on the flow shear stress. Flow shear stress falls under the surface runoff detachment mechanism.

Detachment by Surface Runoff: Surface runoff detaches soil particles by exerting a shear stress that breaks the bonds between soil particles. Erosion in rills is lumped and described as gross rill erosion. Within a grid cell rill erosion and flow within rills are assumed to be uniformly distributed. The detachment capacity rate by surface runoff has the form

$$D_c = a(\tau - \tau_{cr})^b \left(1 - \frac{G}{T_c}\right) \tag{1}$$

where

D_c = detachment capacity rate (kg m$^{-2} \cdot$ s^{-1}),
a,b = empirical coefficients
τ = the flow shear stress (Pa)
τ_{cr} = the critical shear stress (Pa)
G = the sediment load (kg m^{-2} s^{-1})
T_c = the sediment transport capacity of surface runoff (kg m^{-2} s^{-1})

Shear stress in Newtonian Flow: Most hydraulic and sediment transport simulations assume that the transporting fluid has "Newtonian" properties. A Newtonian Fluid has two properties 1) a linear stress-strain relationship (Figure 1), and 2) that has a zero intercept (Figure 1).
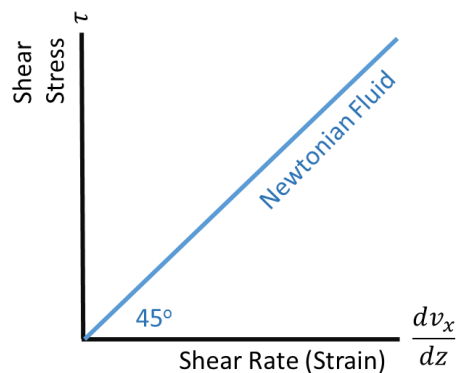
Figure 1. Model of Newtonian Fluids, which have a linear stress strain ratio and a stress-strain intercept of zero.

These Newtonian flow properties are appropriate for most fluids, including sediment laden fluids with lower volumetric concentrations, 16-530 g/l (Costa, 1988; Hessel, 2002).

Clear water flow resisting force is the boundary friction force and the boundary shear stress employed in the Newtonian flow condition is defined as:

$$\tau = \gamma R S_f \tag{2}$$

where

γ = the specific weight of water (Nm^{-3})
R = the hydraulic radius (m)
S_f = the friction slope

As sediment concentrations increase, they begin to affect the fluid properties, which alter the stress-strain relationship. Along with the primary boundary frictional force, these internal forces are resisting force due to viscosity, resisting force due to particle collision, and resisting force due to inter-particle friction. In general, as concentration increases (and the solid component coarsens) and internal shear stresses develop, the fluid crosses the Newtonian flow boundary and go through non-Newtonian flow regimes classified as:

   (a) Hyperconcentrated Flow
   (b) Mudflow
   (c) Grain Flow
   (d) Debris Flow,

The respective component of the total shear stress, τ, are

(a) yield shear stress + viscous shear stress, $\tau_{yield} + \tau_{viscous}$

(b) turbulent shear stress, $\tau_{turbulent}$

(c) dispersion shear stress, $\tau_{dispersive}$ and

(d) internal friction dominated shear stress, $\tau_{Mohr-Coulomb}$

The combination of the shear stress in non-Newtonian flow is defined as (O'Brien, J.S., and Julien, P.Y. 1985):

$$\tau = \tau_{yield} + \tau_{viscous} + \tau_{turbulent} + \tau_{dispersive} + \tau_{Mohr-Coulomb} \tag{3}$$

Figure 2 is the Newtonian fluid rheological plots where Figure 2a is the $\tau_{yield} + \tau_{viscous}$ plot with the shear strain, Figure 2b is the $\tau_{yield} + \tau_{viscous} + (\tau_{turbulent}$ and or $\tau_{dispersive})$ plot with the shear strain. The last term on the right-hand side of equation 3 defines the pseudoplastics fluid which display the opposite properties of dilatant fluid shown in Figure 2c. This study is focused on the shear stress that falls on the rheological plots Figure 2a and Figure 2b.
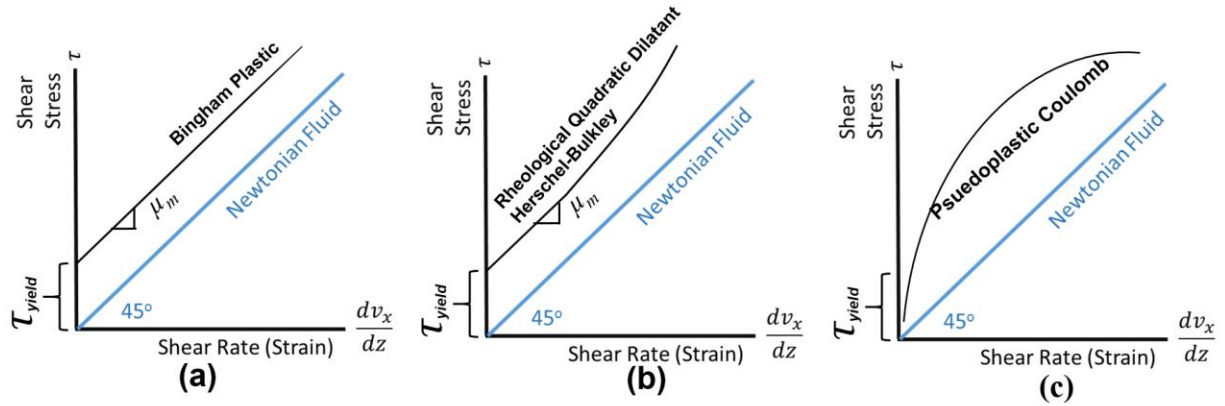
Figure 2. Newtonian fluid rheological plots.

From Equation 3 and Figure 2a, τ_{yield} and $\tau_{viscous}$ represent the intercept and the linear slope times the shear rate respectively in the hyperconcentrated fluid flow condition and the shear stress in this condition is defined as (Julian, 1995):

$$\tau_{hyperconcentrated} = \tau_{yield} + \mu_m \left(\frac{dv_x}{dz} \right) = \tau_{yield} + \mu_m \left(\frac{3\bar{u}}{h} \right) \tag{4}$$

where

μ_m = the viscosity of the mixture (kg m⁻¹S⁻¹)
τ_{yield} = the critical shear stress (Pa)
v_x = fluid layer velocity (ms⁻¹)
z = distance between fluid layers (m)
h = depth of water (m)
$\bar{u}$ = effective flow velocity

The turbulent shear is a second order (quadratic) term, making the stress-strain relationship non-linear as shown in Figure 2b, such that shear increases with the square of strain. From Equation 3 and Figure 2b, at rheological quadratic turbulent dilatant fluid stage, turbulent stress is added to hyperconcentrated stress as (Julian, 1995):

$$\tau_{hyperconcentrated} + \tau_{turbulent} = \tau_{hyperconcentrated} + \rho_m l_m^2 \left(\frac{dv_x}{dz} \right)^2$$

$$= \tau_{hyperconcentrated} + \rho_m l_m^2 \left(\frac{3\bar{u}}{h} \right)^2 \tag{5}$$

where

ρ_m = the density of the mixture (kg m⁻³)
l_m = the Prandtl mixing length (Julien, 1995)

The diffusive shear is also a second order (quadratic) term, which is added to turbulent shear stress at higher concentration stage of sediment in the water. From Equation 3 and Figure 2b, at rheological quadratic diffusive dilatant fluid stage, diffusive stress is added to summation of hyperconcentrated stress and turbulent stress as (Julian, 1995):

$$\tau_{hyperconcentrated} + \tau_{turbulent} + \tau_{diffusive}$$

$$= \tau_{hyperconcentrated} + \tau_{turbulent} + c_{Bd}\rho_s\left(\left(\frac{0.615}{C_v}\right)^{1/3} - 1\right)^{-2} d_s^2 \left(\frac{dv_x}{dz}\right)^2$$

$$= \tau_{hyperconcentrated} + \tau_{turbulent} + 0.01\rho_s\left(\left(\frac{0.615}{C_v}\right)^{1/3} - 1\right)^{-2} d_s^2 \left(\frac{3\bar{u}}{h}\right)^2 \qquad (6)$$

where

C_{Bd} = an empirical parameter
$C_{Bd} \cong 0.01$ (Bagnold, 1954)
d_s = the particle diameter
ρ_s = particle density
C_v = the volumetric sediment concentration ranging from 0 to 1

Non-Newtonian Sediment Dynamics in a Hydrodynamic Model

Figure 3 represents the flow chart for a general linkage architecture of the non-Newtonian sediment laden fluid shear dynamics in a hydrodynamic model. Both for the overland and channel hydrodynamic and sediment dynamic model, first a threshold for non-Newtonian flow regime is identified with the calculation of a dimensionless parameter. Julian (1995) shows that the threshold for non-Newtonian flow regime is identified by the range of a viscous Parameter defined as:

$$\Pi_{viscous} = \frac{\tau - \tau_{yield}}{\mu_m \frac{dv_x}{dz}} = \frac{\tau - \tau_{yield}}{\mu_m\left(\frac{3\bar{u}}{h}\right)} \qquad (7)$$

where
μ_m = the viscosity of the mixture (kg m⁻¹s⁻¹)
τ_{yield} = the critical shear stress (Pa)
v_x = fluid layer velocity (ms⁻¹)
z = distance between fluid layers (m)
h = depth of water (m)
$\bar{u}$ = effective flow velocity

$\Pi_{viscous} > 1$ employs the non-Newtonian flow, $1 < \Pi_{viscous} \le 5 <$ is hyperconcentrated flow and $\Pi_{viscous} > 5$ defines the fluid flow conditions where additional stresses like turbulent and dispersive internal stresses are developed as shown in equation 6 and in Figure 2.

If the dimensionless parameter value falls in the non-Newtonian fluid flow, the fluid internal resistance shear stress is calculated as per equation 3 from the hydrodynamic flow information such as: velocity, depth of water and sediment concentration. The calculated non-Newtonian shear stress is then passed to the hydrodynamic model which estimates the sediment detachment capacity in equation 1. Also, this internal shear stresses of mud and debris flows can be deployed to estimate the hydraulic head slope of the sediment laden flow in equation 2.

Assumption of Newtonian fluid flow condition and a linear stress-strain relationship, fails for sediment laden fluids with higher volumetric sediment concentrations. As sediment concentrations increase they begin to affect the fluid properties which alter the stress-strain relationship. Debris flows depart from linear stress-strain assumptions with no intercept embedded in the clear water flow equations. In this study we developed the debris library that assigns a stress-strain relationship under non-Newtonian sediment-laden fluid flow condition (Pradhan et al., 2018; Floyd et al., 2019).
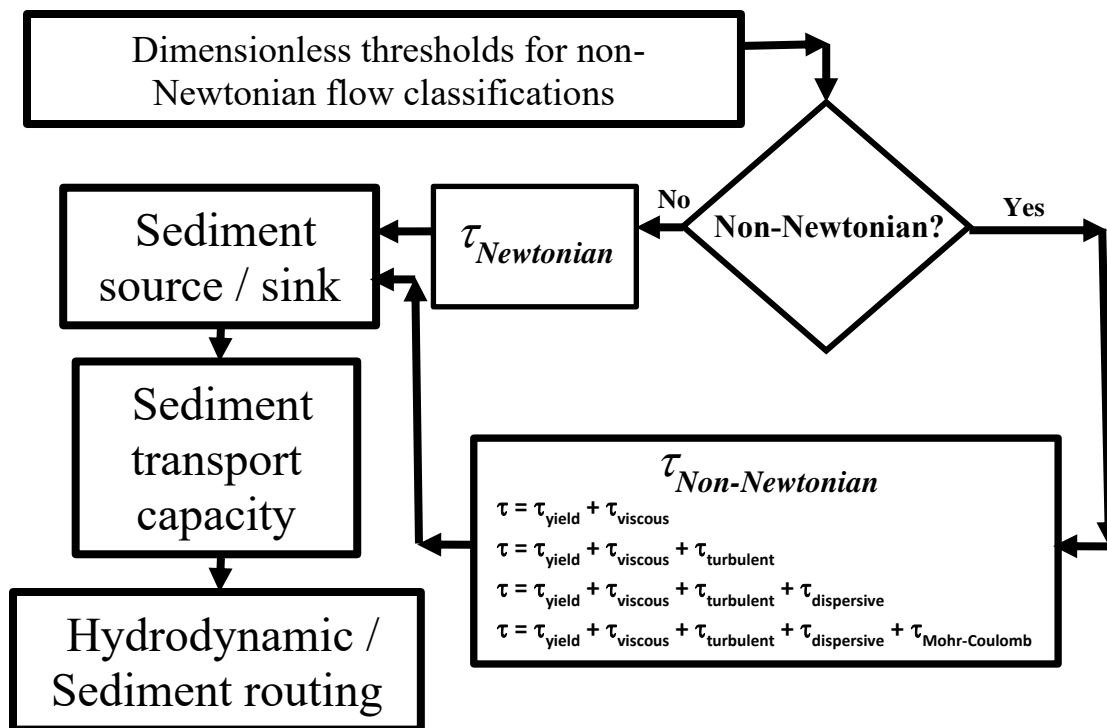
Figure 3. Linking hydrodynamics with non-Newtonian sediment fluid flow dynamics

Figure 4 shows a linkage architecture developed by this study to pass overland and channel hydrodynamic information to the non-Newtonian sediment dynamic subroutines, DebrisLib, and then to return non-Newtonian sediment dynamic information. GSSHA hydrodynamic model was deployed as overland and channel hydrodynamics shown in Figure 4. GSSHA model

is a fully coupled overland/in-stream and lake sediment transport (Newtonian flow regime) hydrodynamic model (Downer et al., 2015; Pradhan et al., 2018). In this study, GSSHA computed flow velocity, depth and concentration is passed to non-Newtonian sediment dynamic subroutines where internal shear stresses are computed and passed back to GSSHA (Pradhan et al., 2018). Although Figure 4 shows both the overland and in-stream non-Newtonian sediment flow dynamics linkage architecture in the hydrodynamics model, this study presents only the overland non-Newtonian sediment laden fluid flow condition.
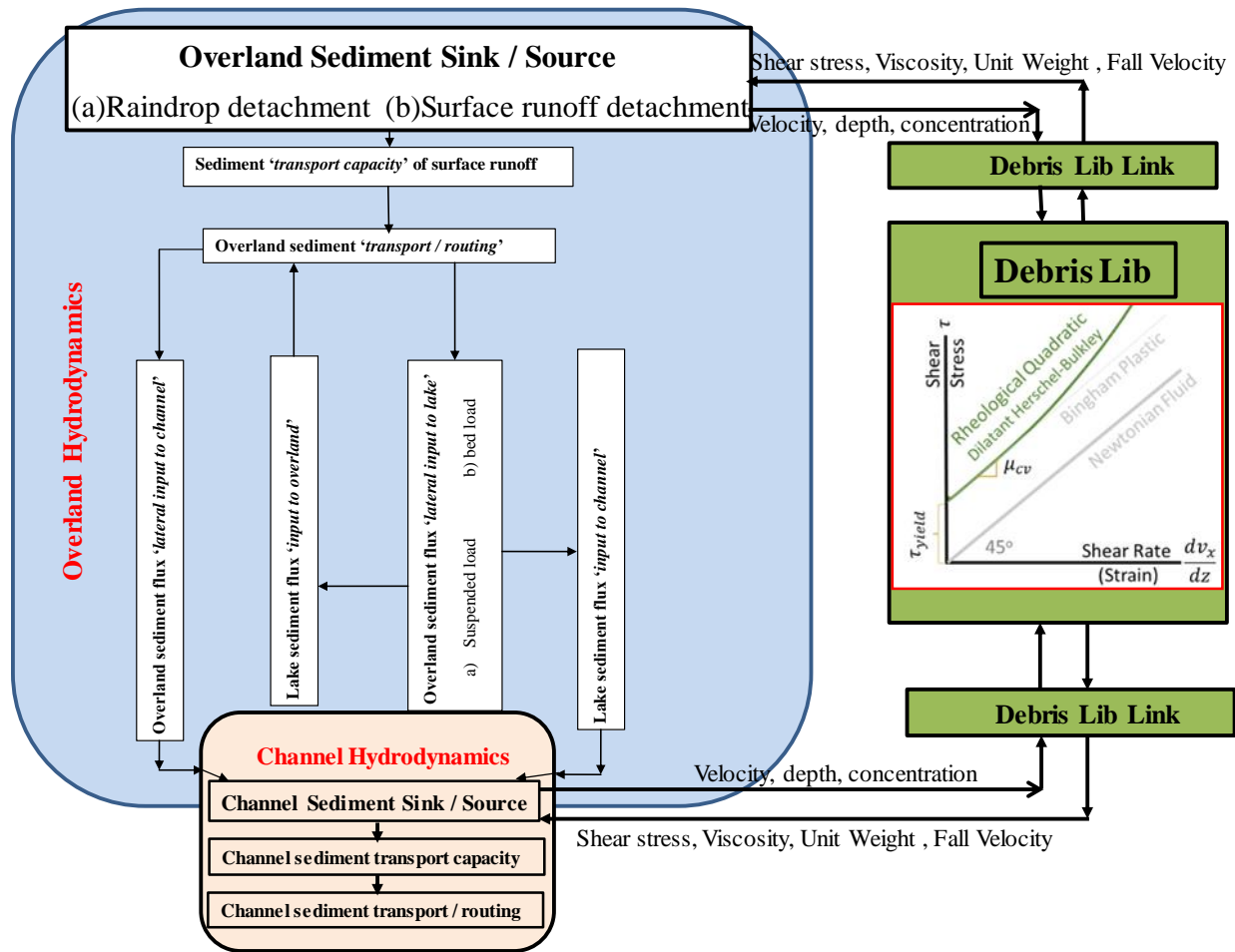
Figure 4. Linking non-Newtonian sediment fluid flow dynamics in a hydrodynamics model.

Test Case Model Development

For this study a simple linkage model was developed which includes:
(a) the non-Newtonian flow regime identification employing equation 7,
(b) passing of flow velocity, flow depth and the sediment concentration to non-Newtonian subroutines from the hydrodynamics model under non-Newtonian condition,

(c) calculation of the respective non-Newtonian shear stress employing equations 3 through equation 6, and

(d) calculation of the detachment capacity in equation 1using the non-Newtonian shear stress for each grid under non-Newtonian condition.

A gridded digital flume model was developed as shown in Figure 5 to test the Newtonian and non-Newtonian shear stress that would develop for sediment sourcing force. The contrived model included a uniform precipitation, two-dimensional overland flow and overland sediment erosion processes (Downer et al., 2015). Figure 5a shows the length and the slope of the flume which is based on the USGS debris flow flume (Iverson, 2010). Figure 5b shows the plan view of the GSSHA flume model where the elevations are hypothetically adjusted to maintain the slope defined by Figure 5a. The grid resolution of the GSSHA flume model in Figure 5b is two meters, which is also the width of the flume. Figure 5c shows the two-dimensional flow vector of the overland flume model.
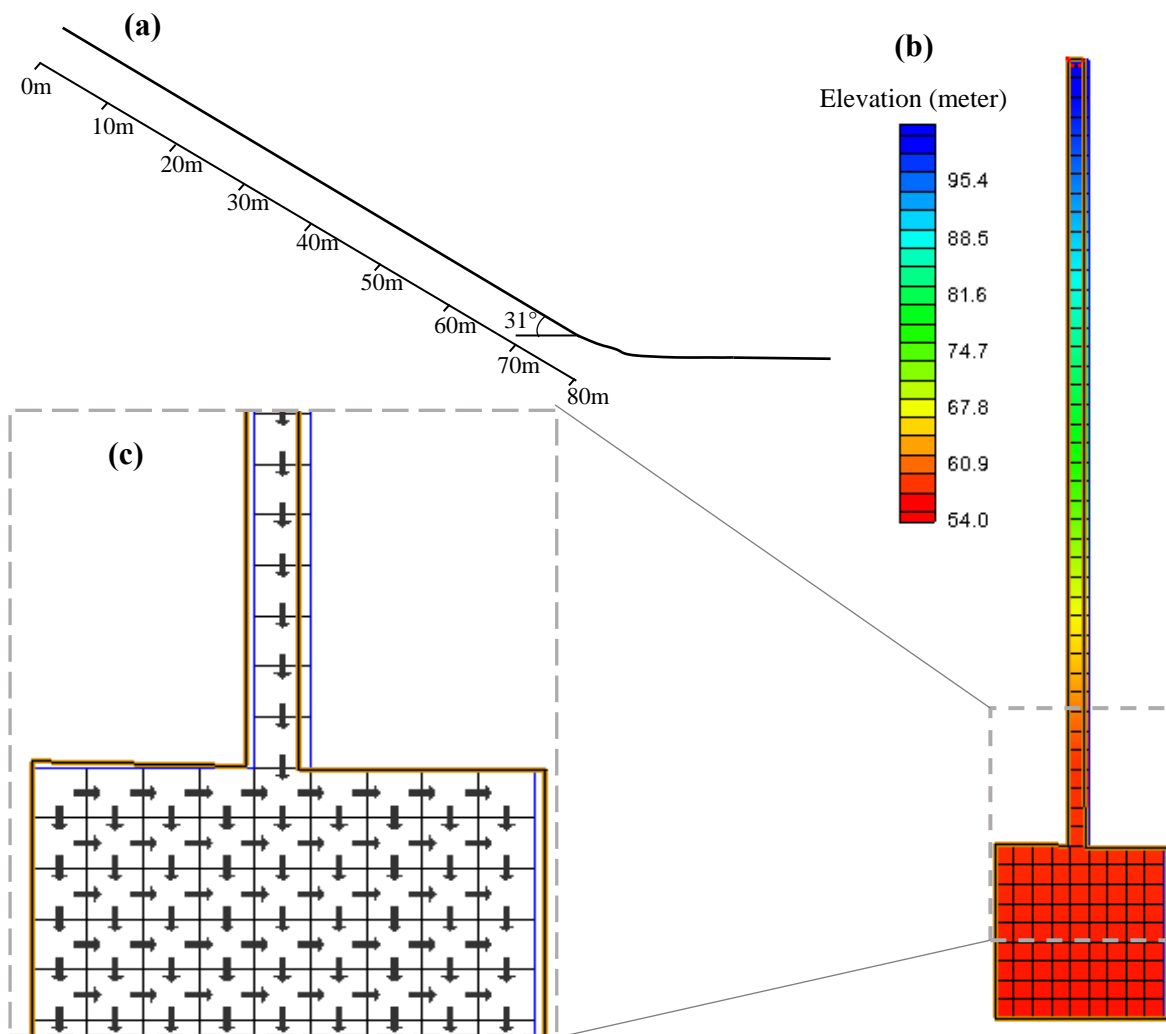
Figure 5. A gridded digital flume model: (a) side view with the length and the slope of the flume (b) Plan view with elevation of the GSSHA flume model (c) two-dimensional overland flow vector.

Results and Discussion

Based on the volumetric sediment concentration, the Newtonian and non-Newtonian sediment fluid flow was tested in 2D hydrodynamic runoff digital model. A sediment concentration boundary condition of 0.05 m³m⁻³ was deployed at the beginning of the flume (0 m of Figure 5a). This sediment concentration was gradually increased until the hyperconcentration stage was reached as shown by equation 4 and Figure 2a. The total shear stress (yield shear stress + viscous shear stress) was calculated employing equation 4. At the hyperconcentrated stage, Newton boundary shear stress, defined by equation 2, was also calculated as to compare the difference in magnitude of shear stress, if the Newtonian assumptions are employed even when the non-Newtonian condition already existed. Figure 6 shows a huge difference in the magnitude of non-Newtonian and Newtonian shear stress. Figure 6 shows that shear stress is significantly underestimated if a non-Newtonian condition is ignored. This underestimation of shear stress would underestimate the sediment yield predictions unless unrealistic parameter values and initial conditions are imposed during the calibration process. The boundary sediment concentration was further increased until a turbulent shear condition was identified with the dimensionless parameter value defined by equation 7. Figure 6 shows this turbulent shear stress added to the hyperconcentrated shear stress in shear thickening fluid or dilatant condition. The result could be different from Figure 6 for shear thinning, pseudo plastic condition, which is yet to be tested.
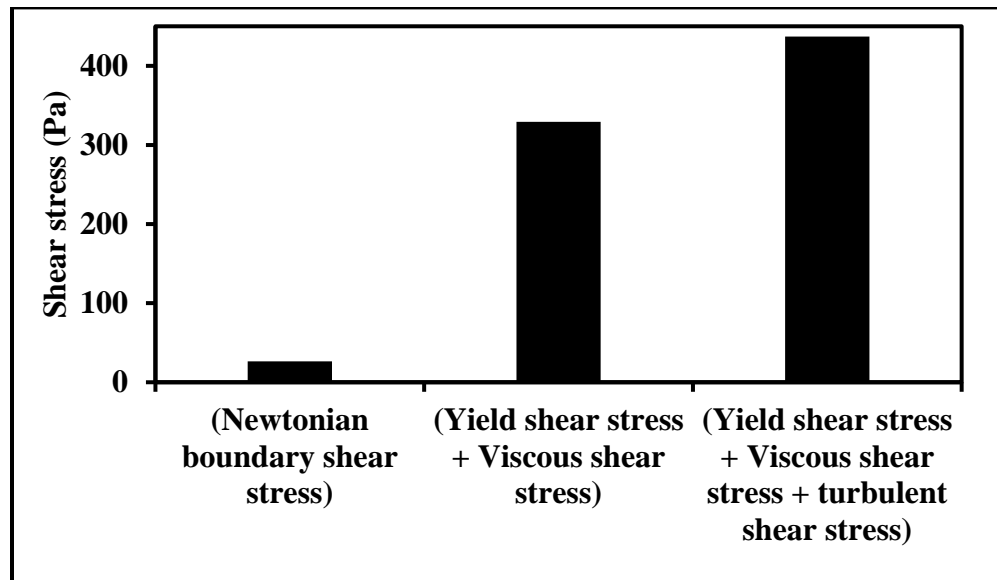
Figure 6. A comparison of simulated non-Newtonian total shear stresses with the Newtonian shear stress under non-Newtonian condition.

In Equation 4, yield stress, τ_{yield} , is empirically defined. Yield stress (O'Brian and Julian, 1985; Julian, 1995) is defined as:

$$\tau_{yield} = ae^{b*C_v} \tag{8}$$

The yield stress equation has two user-specified parameters, a linear coefficient 'a' and exponential multiplier of the concentration 'b'. Julian (1995) provides Table 1 to guide parameter selection:

Table 1. Yield stress parameters from Julian (1995)

Material	a	b
"Typical soil"	0.005	7.5
Kaolinite	0.05	9
Sensitive Clays	0.03	10
Bentonite	0.002	100

Most of these empirical relationships are derived from laboratory scale physical models. Fitting of the 'a' and 'b' parameter values listed in Table 1 was performed in the virtual laboratory digital flume model. Costa (1988) specifies the dirty water concentration for non-Newtonian /Newtonian flows as shown in Table 2.

Table 2. Dirty water concentration (g/l) of different types of flow (based on Costa, 1988; Hessel, 2002)

Normal stream flow concentration (g/l)	Hyperconcentrated flow concentration (g/l)	Debris flow concentration (g/l)
16-530	530-1285	1285-2088

Table 2 shows that approximately 50% or 0.5 m^{3}m^{-3} of concentration would transition the Newtonian flow towards non-Newtonian fluid flow condition. Therefore, 50% concentration was used as a boundary condition in the flume model. 'a' and 'b' parameter values were adjusted by employing this boundary concentration in Equation 8 so that the viscous parameter defined by Equation 8 fell within the flow condition defined in Table 2. This process resulted parameter value of a = 0.03 and that for b = 18.9 for this test case. Figure 6 was analyzed based on this identified values of 'a' and 'b'.

Conclusion

Newtonian fluid flow condition with linear stress-strain relationship are not applicable for sediment-laden fluids with high volumetric sediment concentrations. As sediment concentrations increase, they begin to affect the fluid properties, which alter the stress-strain relationship. In this study, the debris library was developed that calculates a stress-strain relationship under non-Newtonian sediment laden fluid flow conditions. This study also developed a linkage architecture to relate the hydrodynamic information to the non-Newtonian sediment dynamic subroutines and return the non-Newtonian sediment dynamic information to

the hydrodynamic parent code. The Gridded Surface Subsurface Hydrologic Analysis (GSSHA) model is deployed as the hydrodynamic model. GSSHA-computed flow velocity, depth and concentration information is linked to non-Newtonian sediment dynamic subroutines. The non-Newtonian sediment dynamic subroutines computed the internal shear stresses which are returned to GSSHA. Based on the volumetric sediment concentration, the Newtonian and non-Newtonian sediment fluid flows were tested in a 2D hydrodynamic runoff digital flume model. 2D overland simulation of this test case digital flume model showed that mixed density viscous fluid shear stress is significantly underestimated if a non-Newtonian conditions are ignored. This underestimation of shear stress would therefore significantly underestimate the sediment yield. In this initial phase of the coupling and testing research and development effort, the result analysis is limited only to the internal resisting shear stress of the overland flow process. The research and development effort so far includes:

1) Development of the non-Newtonian sediment dynamics subroutines. We define these combined non-Newtonian sediment dynamics subroutines as DebrisLib and is still in progress.
2) Linkage of these non-Newtonian sediment dynamics subroutines with the overland hydrodynamics so that the linkage architecture represents the mathematical model of physically-based sediment and hydrodynamic processes aligned in order to calculate the internal shear stresses.
3) Development and numerical testing of a sediment hydrodynamic digital flume model for internal shear stresses calculations and to identify the parameter value ranges.

Development and coupling of the non-Newtonian overland sediment transport and routing mechanism in the overland hydrodynamic model is in progress. Development of the non-Newtonian fluid flow processes in the 1D instream hydrodynamic model will follow the 2D overland non-Newtonian fluid flow processes.

References

Bagnold, R.A. 1954. "Experiments on a gravity-free dispersion of large solid spheres in a Newtonian fluid under shear", Proc. Roy. Soc. Lond. A225, 49-63.

Costa, J.E. 1988. "Rheologic, geomorphic, and sedimentologic differentiation of water floods, hyperconcentrated flows, and debris flows", Chapter 7 in: Baker, V.R., R.C. Kochel & P.C. Patton (eds.) Flood Geomorphology. New York: Wiley, pp. 113-122

Downer, C.W., Pradhan, N.R., Ogden, F.L., and Byrd, A. 2015. "Testing the effects of detachment limits and transport capacity formulation on sediment runoff predictions using the US Army Corps of Engineers GSSHA model", ASCE J. Hydrol. Eng., 10.1061/(ASCE)HE.1943-5584.0001104

Floyd, I.E., Gibson, S., Heath, R.E., Ramos-Villanueva, M., and Pradhan, N. 2019. "Development of 'Debris Library' and 1D HEC-RAS and 2D Adaptive Hydraulics Linkage-Architecture Post-Wildfire for non-Newtonian Flows", submitted to Proc. SEDHYD 2019, Reno, NV.

Hessel, R. 2002. "Modelling soil erosion in a small catchment on the Chinese Loess Plateau. Applying LISEM in extreme conditions", Netherlands Geographical Studies 307. KNAG: Utrecht, The Netherlands.

Iverson, R. M., Logan, M., LaHusen, R. G., and Berti, M. 2010. "The perfect debris flow? Aggregated results from 28 large-scale experiments", J. Geophys. Res., 115, F03005, doi:10.1029/2009JF001514.

Julien, P.Y. 1995. Erosion and Sedimentation. Second edition, Cambridge University Press, Cambridge, UK.

O'Brien, J.S., and Julien, P.Y. 1985. "Physical properties and mechanics of hyperconcentrated sediment flows", Proc. ASCE Specialty Conference on the Delineation of Landslide, Flashflood and Debris Flow Hazards, Utah Water Research Lab, Series UWRL/G-85/03, 260-79.

Pradhan, N.R., Floyd, I.E., Heath, R., Downer, C.W., and Gibson, Stanford. 2018. "Development of 'Debris Library' and 'GSSHA' linkage-architecture for non-Newtonian sediment fluid flow", 2018 AGU Fall Meeting, Washington D.C., 10-14 December, Paper Number: EP21D-2277.

Long-Term Effects of Dredging Operations in the Lower Mississippi River

Ronald Copeland, Research Hydraulic Engineer, U.S. Army Corps of Engineers, Vicksburg, MS, Ronald.R.Copeland@erdc.dren.mil

James Lewis, Mississippi River Science and Technology Office Director, U.S. Army Corps of Engineers, Vicksburg, MS, James.W.Lewis@usace.army.mil

Justin Giles, Research Hydraulic Engineer, U.S. Army Corps of Engineers, Vicksburg, MS, Justin.S.Giles@usace.army.mil

Abstract

Dredging of the Mississippi River to maintain navigation is an important, ongoing effort which requires significant resource allocation each year. The objective of this effort was to assess the feasibility of using a one-dimensional numerical sedimentation model (HEC-6T) to test the effectiveness and efficiency of alternative dredging approaches to optimize the nation's resource allocation. The HEC-6T model used for this work had been calibrated and externally reviewed in previous studies. Currently, in the Lower Mississippi River above Venice, Louisiana, dredged material is returned back into the channel downstream from the dredging site. This study assessed the impact of removing the dredged material from the channel and disposing of it onto the overbank or over the levees. Over the 50-year simulation period it was determined that dredging quantities could be reduced by about 50 percent. These results suggest that targeting overbank disposal at a few key locations could optimize the dredging impacts. The model was also used to assess the effects that wet and dry hydrologic cycles could have of dredging requirements.

Introduction

Dredging is required to maintain an adequate navigation channel along the Mississippi River. This USACE mission is both necessary and expensive. A research project was conducted to assess the effectiveness and efficiency of alternative dredging approaches in an attempt to optimize resource allocations. The study approach was to utilize a validated and externally reviewed one-dimensional HEC-6T model that was developed for the Mississippi River and Tributaries Flowline Project.

The USACE developed a HEC-6T numerical model of the Mississippi River between East Jetty, at the end of Southwest Pass, and Cairo, Illinois, at the confluence of the Ohio River, to determine the effect of sedimentation on maximum water surface elevations 50 years into the future. The model included dredging activity for the lower portion of the river, below Venice, Louisiana, but it did not include the impacts of dredging activities further upstream. Dredging in the upstream reaches was considered to have a relatively minor influence on long-term sedimentation because dredged materials in upstream reaches are typically removed from the

bed and pumped back into the flowing water downstream of the dredging site, a technique referred to as "in-channel disposal".

The HEC-6T numerical model contains several dredging algorithms that are useful to evaluate alternative dredging operations. One option that can be evaluated is the location of dredge material disposal. Disposal location options include 1) back into the river immediately downstream at the next cross section, 2) back into the river downstream from the specific dredging site, 3) into a permanent holding site on the overbank, or 4) complete removal from the system. Another option that can be evaluated is timing of dredging operations with respect to the rise and fall of the annual hydrograph and the effects of high or low periods of annual runoff. This paper discusses how these dredging approaches were analyzed.

Methodology

The HEC-6T one-dimensional numerical model of the Mississippi River developed to determine the long-term effects of sedimentation on project flood water-surface elevations was used as a starting point for this study. That model had been calibrated using 1991-2013 geometry changes, water-surface elevations and hydrographs.

For this study, annual dredging operations were added at several sites and the numerical model dredging parameters were adjusted to reproduce reported dredging volumes, over the 23-year period between 1991 and 2013. It is recognized that actual dredging operations are subject to several constraints not necessarily simulated in the numerical model. These may include availability of dredges, dredging site priorities, and available funding among others. It is also recognized that uncertainty is associated with reported dredging quantities as with all field data. For purposes of this study, simulation of the actual dredging dates and dredging capacities was not attempted. Dredging volumes calculated in this study should be considered approximate. It was determined during the course of model calibration that detailed modeling would be required to obtain accurate dredging volumes at individual sites. This detailed modeling effort is beyond the scope of this research effort, which is intended to provide relative effects of dredging activities on a system-wide basis.

One of the most significant challenges associated with the dredging simulation was a lack of adequate channel geometry data. This was especially apparent for dredging sites where dikes had been constructed. In some cases, as-built top-of-dike elevations were not available. In all cases, existing top-of-dike elevations were unknown so that dike degradation could not be definitively simulated. There is also uncertainty associated with the actual dredging depth, the timing of dredging, and the capacity of the dredges involved.

In addition to Southwest Pass and upstream of Head of Passes to Venice, fifteen existing dredging sites were included in the numerical model, which were designated the most dredged sites for each district. Of these fifteen, eleven were located in the deep draft navigation channel between New Orleans and Baton Rouge.

Calibration to Reported Dredging Volumes

The HEC-6T numerical model used in this study had been previously calibrated to measured water-surface elevations, specific gage records, measured sediment transport at intermediate gages and dredging in Southwest Pass and between Head of Passes and Venice. The calibration is documented in multiple reports: Copeland and Thomas, 1992; Copeland et al., 2010; and Copeland, 2018. Water surface elevation calibration was accomplished by varying Manning's roughness coefficients with discharge. This was done for the initial hydrographic survey geometry. The model was then run for a 23-year calibration period and calculated water-surface elevations at the end of the calibration period were again compared to measured stages to evaluate the model's ability to predict specific gage changes. Intermediate gages at Union Point, Tarbert Landing, and Belle Chasse were used to evaluate the ability of the model to transport the appropriate volume of each size class through the study reach. Dredging records in Southwest Pass and between Head of Passes and Venice were used to evaluate the ability of the model to correctly account for sediment deposition in the lower reaches of the river where significant distributary flow reduces the sediment transport capacity. For this study the model was additionally calibrated to reported dredging volumes. Upstream from New Orleans, reported annual dredging volumes were available for the period 1991-2013 for the dredging sites used in this study. At and below New Orleans, dredging records were available for 1996-2013. The reported dredging volumes in Southwest Pass and between Head of Passes and Venice were combined in the available reported data. In addition, the reported dredging volumes for Southwest Pass included dredging downstream from the numerical model boundary. Consequently, reported dredging records downstream from Venice could not be used in the calibration study. Calibration parameters for fine sediment properties from previous model studies were therefore used for this study.

In the numerical model, dredging was simulated at the beginning of each year between 1991 and 2013. A dredging depth and advanced maintenance depth was specified at each dredging site. Except in reaches below Venice, dredged material was re-introduced back into the water column at the next downstream cross section, to represent the in-channel disposal method. This handling of the dredged material proved to be significant at dredging sites with more than one cross section. For calibration of the dredging volume, multiple options were used, which include:

1) Distance between dredged cross sections and cross sections upstream and downstream from the dredging reach - The numerical model calculates dredging volumes using a length equal to half the distance between cross sections (as opposed to the fixed-end method). Cross sections were added to the numerical model to achieve a better representation of dredging site lengths at several dredging sites.
2) Depth and width of the dredging template - These parameters naturally affect the calculated dredging volumes. Survey data, especially in the New Orleans District below Baton Rouge, were used to estimate reasonable limits within which these variables could be used as calibration parameters.
3) Width of movable bed - The movable bed width can be set equal to the dredging template width or it can extend beyond the limits of the dredging template in the numerical model. In most cases, the movable bed was confined to the dredging template. This

assignment precludes long-term deposition at the dredging site and assumes that the dredging operation will maintain a relatively constant cross-sectional area. The option to allow deposition outside the dredging template was only used in cases where the calculated dredging exceeded reported dredging.

4) Number of dredging cycles each year - The numerical model dredges cross-sections in the dredging reach to the designated dredging template at the beginning of each calendar year. In the model this occurs "instantaneously" i.e. during the first day. In cases where the dredging site consists of one cross-section or where dredging volumes are minimal, one dredging cycle per year is sufficient. However, in cases where there are more than one cross section and dredged material from an upstream cross section deposits in a downstream cross section, then more than one dredging cycle may be required to obtain appropriate dredging volumes.

5) Dredging capacity – not used in this study as a calibration parameter. Dredging capacity of 100,000 cubic yards per day was assigned to the Southwest Pass and Head of Passes dredging sites, which is consistent with previous studies.

Calibration parameters at each dredging site are shown in Table 1. Results of the calibration study are shown in Table 2 and Figure 1.

Table 1. Calibration Parameters used in Dredging Simulations

SITE	Model Cross Sections River Mile	Number of Cross-Sections	Dredging Template Elevation FT NGVD 29	Advance Maintenance FT	Number of cycles per year	Movable-Bed Width = Dredging Width
Southwest Pass	-18.0 to -0.01	14	-55 to -60	3	2	Yes
Head of Passes	0.72 - 5.5	6	-50	3	2	Yes
New Orleans Harbor	100.2	1	-45	3	1	No
Belmont	153.1 - 153.4	4	-45.5	3	8	Yes
Smoke Bend	175	1	-46	3	1	Yes
Philadelphia	183	1	-45	3	1	Yes
Alhambra	189.5 - 189.8	2	-45	3	90	Yes
Bayou Goula	197.9 - 198.2	2	-45	3	60	Yes
Granada	203.6 - 204.1	2	-45	3	60	Yes
Medora	211.6 - 212	2	-42	3	1	No
Sardine Point	218.9	1	-45	3	1	No
Red Eye	223.5 - 224.4	3	-45	3	80	Yes
Baton Rouge US	230.4 - 232.7	4	-44.5	3	1	Yes
Westover	652.5	1	107	2	1	No
Finley Bar	704.08	1	147	1	1	No
Redman Bar	740 - 741	2	160	3	1	No
Kate Aubrey	788.13	1	186	3	1	Yes

Table 2. Reported and Calculated Dredging between 1991 and 2013.

| SITE	Model Cross Sections River Mile	Reported 1991-2013 Million Cubic Yards	Calculated 1991-2013 Million Cubic Yards
New Orleans Harbor	100.2	19.3	22.1
Belmont	153.1 - 153.4	52.1	53.0
Smoke Bend	175	11.2	11.3
Philadelphia	183	5.1	5.8
Alhambra	189.5 - 189.75	58.4	59.9
Bayou Goula	197.9 - 198.2	25.6	25.8
Granada	203.6 - 204.1	28.0	25.6
Medora	211.6 - 212	29.2	30.3
Sardine Point	218.9	23.2	21.4
Red Eye	223.5 - 224.4	114.7	114.3
Baton Rouge US	230.4 - 232.7	37.1	37.0
Westover	652.5	15.1	16.9
Finley Bar	704.08	14.4	14.9
Redman Bar	740 - 741	22.0	19.2
Kate Aubrey	788.13	9.8	9.5
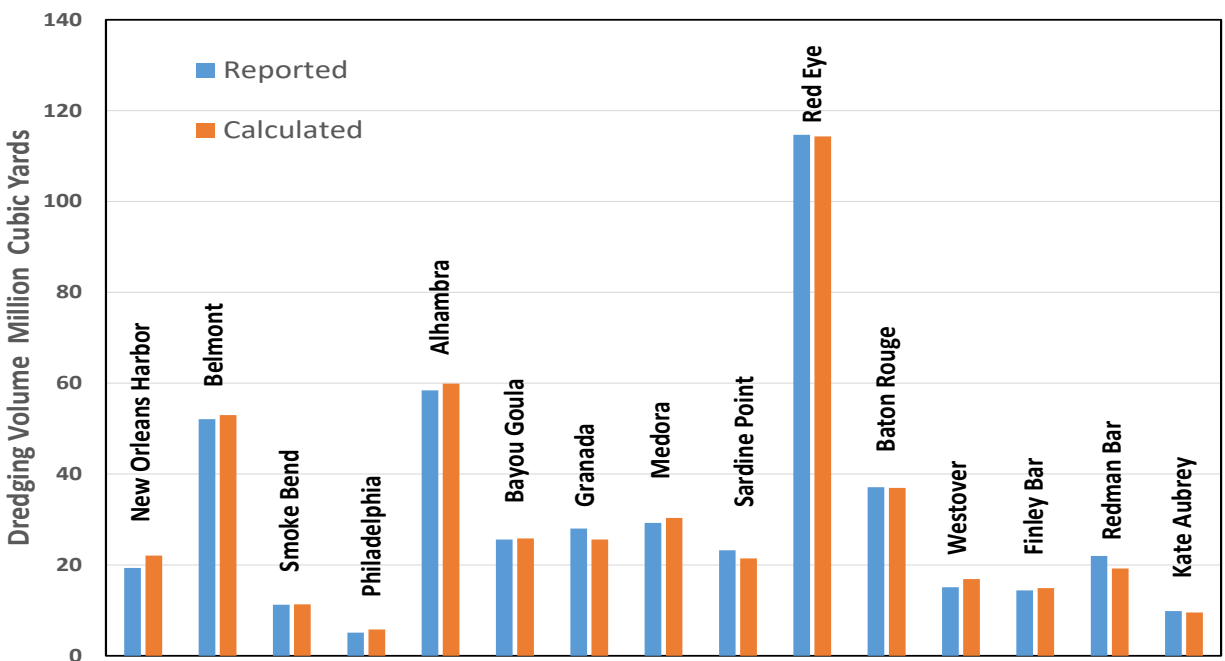
Figure 1. Calculated and Reported Dredging 1991-2013

Results and Discussion

Overbank Disposal

The current practice, in the Lower Mississippi River above Venice, is in-channel disposal. One option evaluated for this study was the disposal of dredged material over the levee (potentially into receding marsh lands). This alternative may be more expensive in terms of a specific dredging site, but could prove cost effective in terms of not having to re-dredge the same material over and over at downstream sites. There is also the potential advantage of marsh replenishment. Marsh replenishment is already being practiced in reaches of the Mississippi River downstream from Venice.

Dredging volumes over a 50-year period at several sites were first calculated by the model assuming current in-channel disposal of dredged material at dredging sites upstream from Venice. Then, dredging volumes over the same 50-year period at the same sites were calculated by the model assuming overbank disposal at all dredging sites. The 50-year dredging volumes at the sites evaluated in this study are shown in Table 3 and Figure 2. As expected, dredging requirements were reduced significantly at sites downstream from sites where in-channel disposal is currently practiced. The HEC-6T results show that overbank disposal would reduce dredging volumes above Venice by about 350 million cubic yards (almost 50 percent) over 50-years.

Table 3 shows little difference in dredging volumes in Southwest Pass and above Head of Passes. In these dredging reaches overbank disposal and physical removal are already practiced. This partially explains why dredging volume differences are insignificant below Venice. However, another factor is the significant distance between Head of Passes and the upstream dredging sites (100 miles to New Orleans Harbor and 150 miles to Belmont). Sediment can be eroded from the channel bed over these many miles to meet some of the sediment deficit created by the removal of sediment from the river by overbank disposal. The numerical model results suggest that the alluvial system response to upstream changes in sediment supply may take decades to affect downstream conditions.

There was no dredging calculated at the dredging sites upstream from River Mile 700 for either of the two disposal options. This is due to the dredging constraints established during the calibration phase of the study and to the degradation trend currently active in this reach of the river.

Table 3. Calculated 50-Year Dredging Volumes Comparing Current and Overbank Disposal Options

SITE	Model Cross Sections River Mile	Current Disposal Operations Million Cubic Yards	Overbank Disposal at All Dredging Sites Million Cubic Yards	Percent Reduction
Southwest Pass	-18.0 to -0.01	171.3	171.8	-0.3%
Head of Passes	0.72 - 5.5	651.3	632.3	2.9%
New Orleans Harbor	100.2	31.0	32.1	-3.4%
Belmont	153.1 - 154	68.2	24.1	64.7%
Smoke Bend	175	8.2	3.2	60.2%
Philadelphia	183	1.1	0.0	100.0%
Alhambra	189.5 - 189.75	78.6	12.9	83.5%
Bayou Goula	197.9 - 198.2	53.3	18.3	65.7%
Granada	203.6 - 204.1	41.4	11.3	72.6%
Medora	211.6 - 212	56.8	34.3	39.5%
Sardine Point	218.9	41.3	28.2	31.8%
Red Eye	223.5 - 224.4	236.1	120.5	49.0%
Baton Rouge US	230.4 - 232.7	78.5	61.2	22.0%
Westover	652.5	30.0	28.6	4.7%
Finley Bar	704.08	0.0	0.0	0.0%
Redman Bar	740 - 741	0.0	0.0	0.0%
Kate Aubrey	788.13	0.0	0.0	0.0%
Total		1547.0	1,178.8	23.8%
Above Venice		724.4	374.8	48.3%
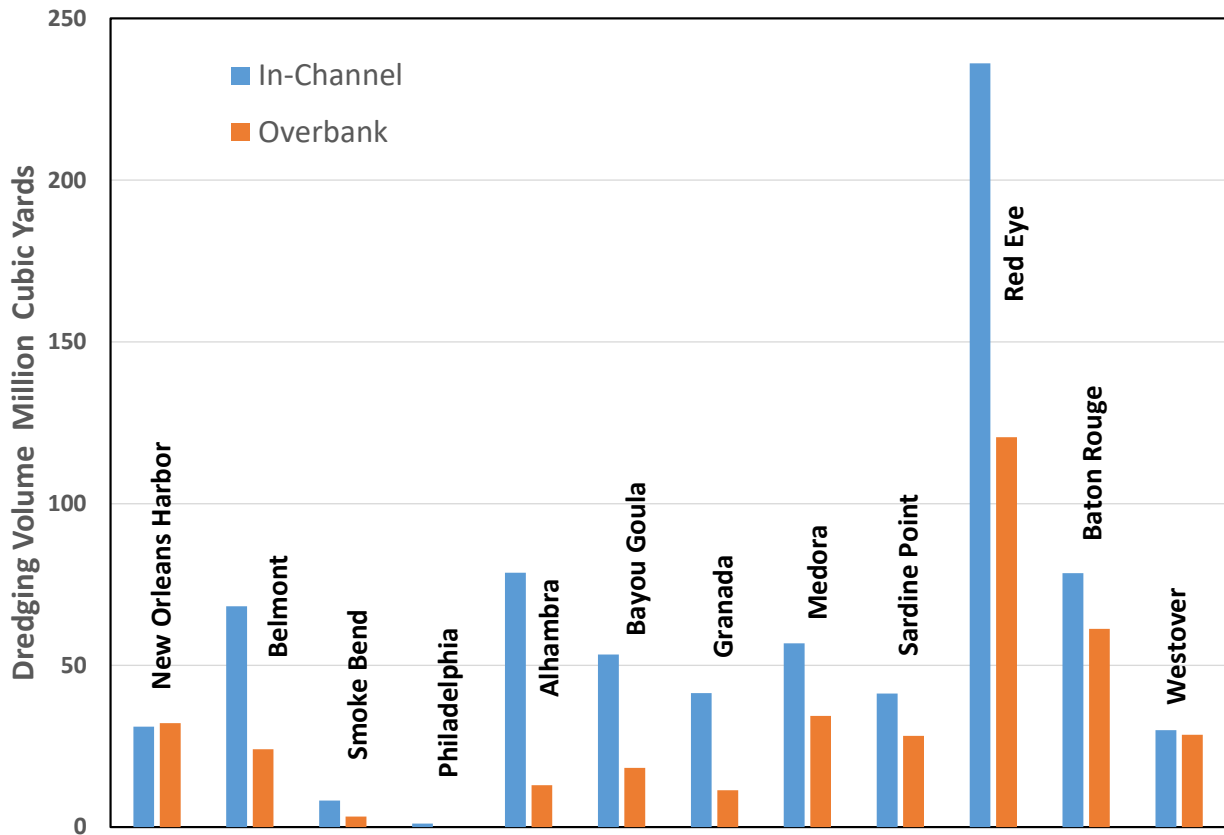
Figure 2. Calculated 50-Year Dredging Volumes Comparing Current and Overbank Disposal Options

Removing dredged sediment from the river also affects conditions upstream from the dredging sites. The numerical model calculated the quantity of sand passing each cross section every day during the 50-year simulation for both the in-channel and overbank disposal options. These daily quantities were accumulated as the simulation progressed. The difference between the sand transported past each cross section with in-channel and overbank disposal is shown in Figure 3. The differences were calculated by subtracting sand passing with overbank disposal from sand passing with in-channel disposal after 10, 30, and 50 years. Upstream differences with the disposal options are best demonstrated at the Westover dredging site (River Mile 652) where sand transport is not complicated by the proximity of other dredging sites. As expected, immediately downstream from the dredging site, sand transport is greater with in-water placement than with overbank disposal because sand is returned to the river. Somewhat surprisingly however, upstream from the dredging site, sand transport is less with in-channel disposal than with overbank disposal. This is attributed to an increase in upstream sediment transport potential that occurs as a result of permanent lowering of the bed downstream. This decrease in bed elevation occurs as a consequence of both the removal of dredged material and increased scour as the river bed seeks to restore the sediment deficit. Thus, it can be concluded that the natural river processes will dampen the expected benefit of reduced dredging requirements associated with overbank disposal (on the order of 50 percent).
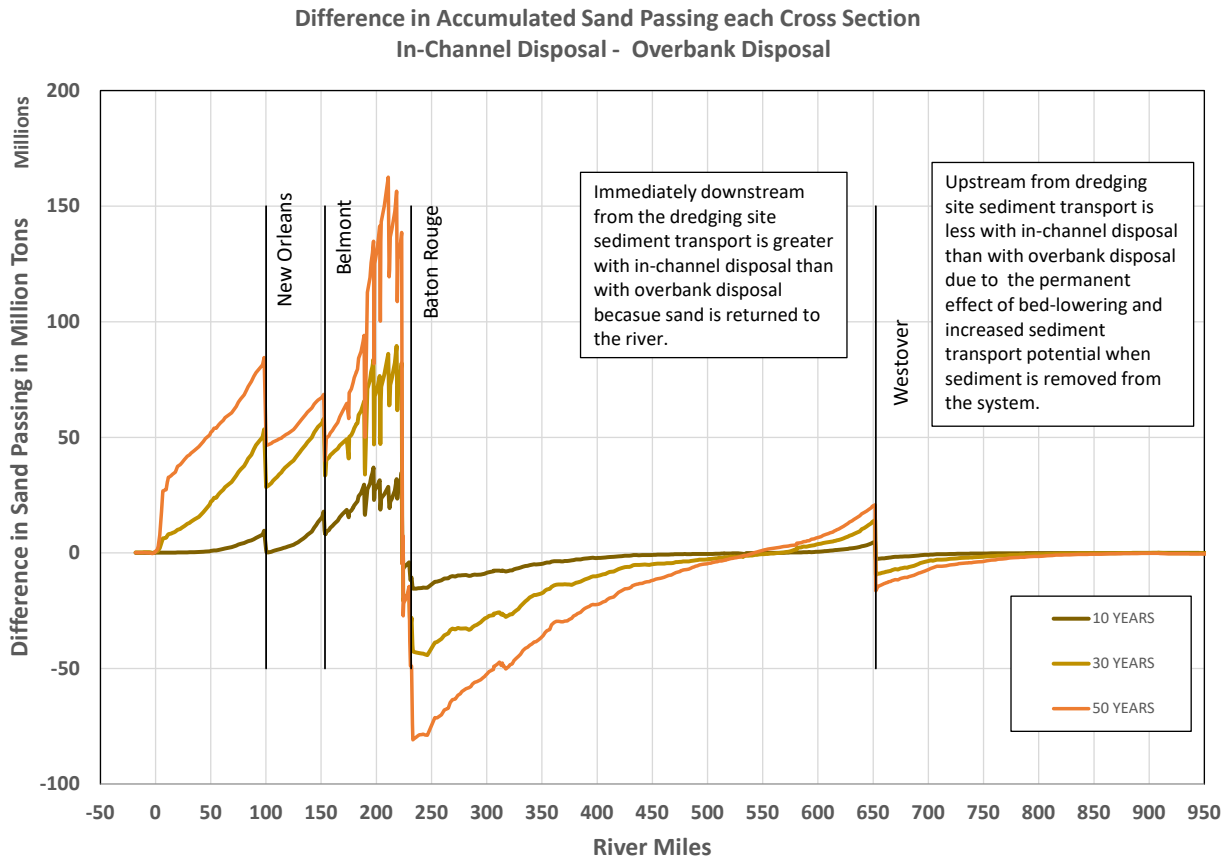
Figure 3. Difference in accumulated sand passing each cross section

It is unlikely that overbank disposal is feasible at all dredging sites along the Lower Mississippi River. Disposal site proximity and pumping costs are factors to be considered. Fifty years of overbank disposal was simulated at two sites while the current practice of dredging disposal was simulated at the other dredging sites. The two sites were Medora Crossing at River Mile 212 and Sardine Point at River Mile 219. These two sites are on opposite sides of Australia Point, which is currently an undeveloped area inside the mainline levee. This is not a proposal, only a demonstration of model capability.

The reduction in the downstream dredging quantities over 50 years with overbank disposal at Medora Crossing and Sardine Point is quantified in Table 4 and Figure 4. The overall reduction in dredging volume for the sites above Venice for the 50-year period was eleven percent or 82.6 million cubic yards. Erosion of channel bed material downstream from Medora Crossing accounts for the reduction in total calculated dredging being slightly less than the combined calculated dredging at Medora and Sardine, which was 89.0 million cubic yards.

Table 4. Calculated 50-Year Dredging Volumes comparing Current Disposal Operations and Overbank Disposal at Medora Crossing and Sardine Point

SITE	Model Cross Sections River Mile	Current Disposal Operations Million Cubic Yards	Overbank Disposal at Medora and Sardine Million Cubic Yards	Percent Reduction
Southwest Pass	-18.0 to -0.01	171.3	171.3	0.0%
Head of Passes	0.72 - 5.5	651.3	649.3	0.3%
New Orleans Harbor	100.2	31.0	31.2	-0.4%
Belmont	153.1 - 154	68.2	62.2	8.8%
Smoke Bend	175	8.2	6.5	20.5%
Philadelphia	183	1.1	0.0	100.0%
Alhambra	189.5 - 189.75	78.6	50.6	35.6%
Bayou Goula	197.9 - 198.2	53.3	34.7	35.0%
Granada	203.6 - 204.1	41.4	18.5	55.4%
Medora	211.6 - 212	56.8	46.4	18.3%
Sardine Point	218.9	41.3	42.6	-3.4%
Red Eye	223.5 - 224.4	236.1	238.3	-0.9%
Baton Rouge	230.4 - 232.7	78.5	80.9	-3.1%
Westover	652.5	30.0	30.0	0.0%
Finley Bar	704.08	0.0	0.0	0.0%
Redman Bar	740 - 741	0.0	0.0	0.0%
Kate Aubrey	788.13	0.0	0.0	0.0%
Total		1547.0	1,462.7	5.4%
Above Venice		724.4	641.8	11.4%
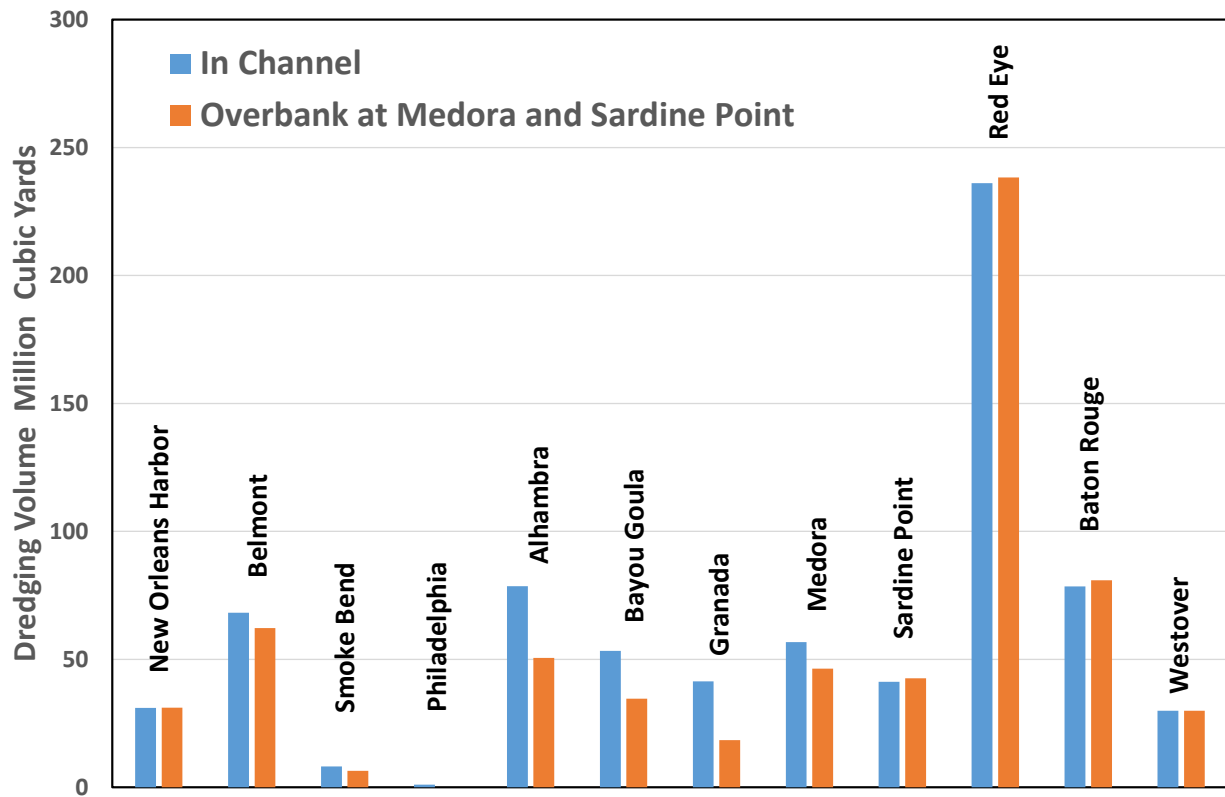
Figure 4. Calculated 50-Year Dredging Volumes comparing Current Disposal Operations and Overbank Disposal at Medora Crossing and Sardine Point Crossing

The calculated progression of downstream sedimentation with overbank disposal at Medora Crossing and Sardine Point is demonstrated by comparing the difference between calculated thalweg elevations for 50-year simulations with overbank disposal and in-channel deposition at the two dredging sites. Figure 5 shows this difference at three cross sections downstream where dredging does not occur. At River Mile 201, which is about eleven miles downstream from Medora Crossing, the effect of overbank disposal at Medora and Sardine is relatively quick and the current dredging practice results in about 2.3 feet more deposition at River Mile 201 after 50 years. At River Mile 188, which is about 24 miles downstream from Medora, the sedimentation effect of overbank disposal at Medora and Sardine is significantly less. At River Mile 188, the 50-year deposition difference is about 1.2 feet, but the effect doesn't get started until about 25 years have passed. At River Mile 169.2, which is about 43 miles downstream from Medora, sedimentation effects are even more muted. The downstream attenuation of sedimentation effects is attributed to erosion of the channel bed in response to the decrease in sediment supply from the overbank disposal. Of significance is the length of time required for the effects of sediment transport disruption to affect downstream reaches.

DIFFERENCE IN THALWEG ELEVATION
In-Channel Disposal - Overbank Disposal at Medora and Sardine
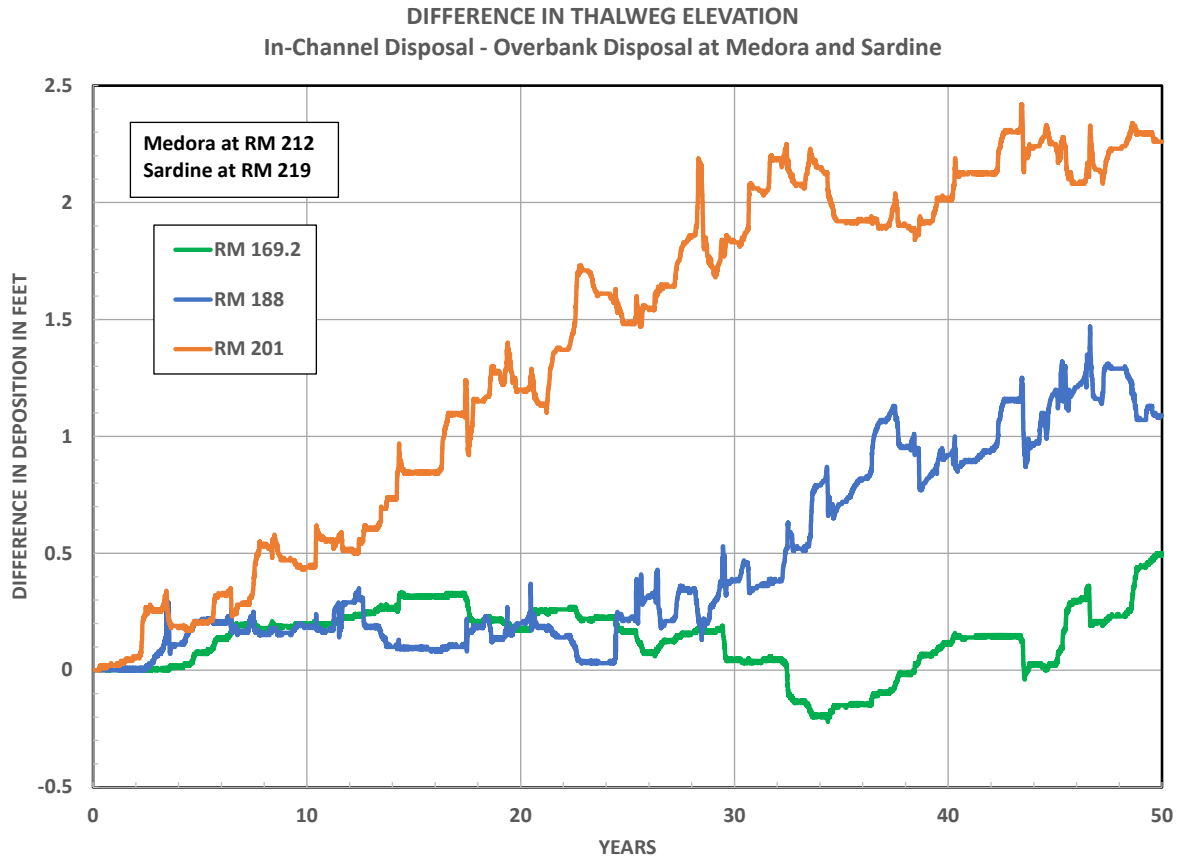
Figure 5. Difference in calculated thalweg elevations during a 50-year simulation with and without overbank disposal at Medora Crossing and Sardine Point

Effect of Wet and Dry Cycles

The model was used to evaluate the effects of long-term wet and dry runoff cycles on dredging quantities. Seven-year wet and dry cycles were extracted from the 1988-2014 hydrograph. The wettest water years during that period were: 1993, 1994, 1997, 1998, 2008, 2010 and 2011. The driest years were 1988, 1992, 2000, 2001, 2006, 2012 and 2014. The seven-year simulations were run using the in-channel deposition base test that models current dredging practice. The same dredging template elevations and dredging widths were used for both the wet and dry years. In actual practice, dredging depths may increase in dry years to insure that the authorized navigation depth is maintained. However, in this study, the same dredging parameters were used for the wet and dry hydrographs in order to isolate the actual effects of the high and low runoff. Calculated dredging quantities are shown in Table 5 and Figure 6. The results indicate significantly higher dredging requirements during wet years.

Table 5. Calculated dredging volumes for wet and dry cycles

SITE	Model Cross Sections River Mile	7 Years of Abundance Million Cubic Yards	7 Years of Drought Million Cubic Yards	Percent Difference (Wet-Dry) / Wet
Southwest Pass	-18.0 to -0.01	38.2	8.9	76.7%
Head of Passes	0.72 - 5.5	107.1	23.5	78.1%
New Orleans Harbor	100.2	8.2	2.1	74.4%
Belmont	153.1 - 154	24.8	2.5	89.7%
Smoke Bend	175	4.2	0.0	100.0%
Philadelphia	183	0.0	0.6	-100.0%
Alhambra	189.5 - 189.75	21.5	7.2	66.5%
Bayou Goula	197.9 - 198.2	10.7	6.4	40.3%
Granada	203.6 - 204.1	9.6	5.9	38.1%
Medora	211.6 - 212	8.9	5.7	36.2%
Sardine Point	218.9	6.9	3.8	45.2%
Red Eye	223.5 - 224.4	46.4	17.6	62.0%
Baton Rouge US	230.4 - 232.7	11.0	17.2	-56.7%
Westover	652.5	4.8	3.8	20.8%
Finley Bar	704.08	0.6	0.0	100.0%
Redman Bar	740 - 741	0.0	0.0	0.0%
Kate Aubrey	788.13	0.0	0.0	0.0%
Average Annual - Total		43.2	15.0	65.3%
Average Annual - Above Venice		22.5	10.4	53.8%
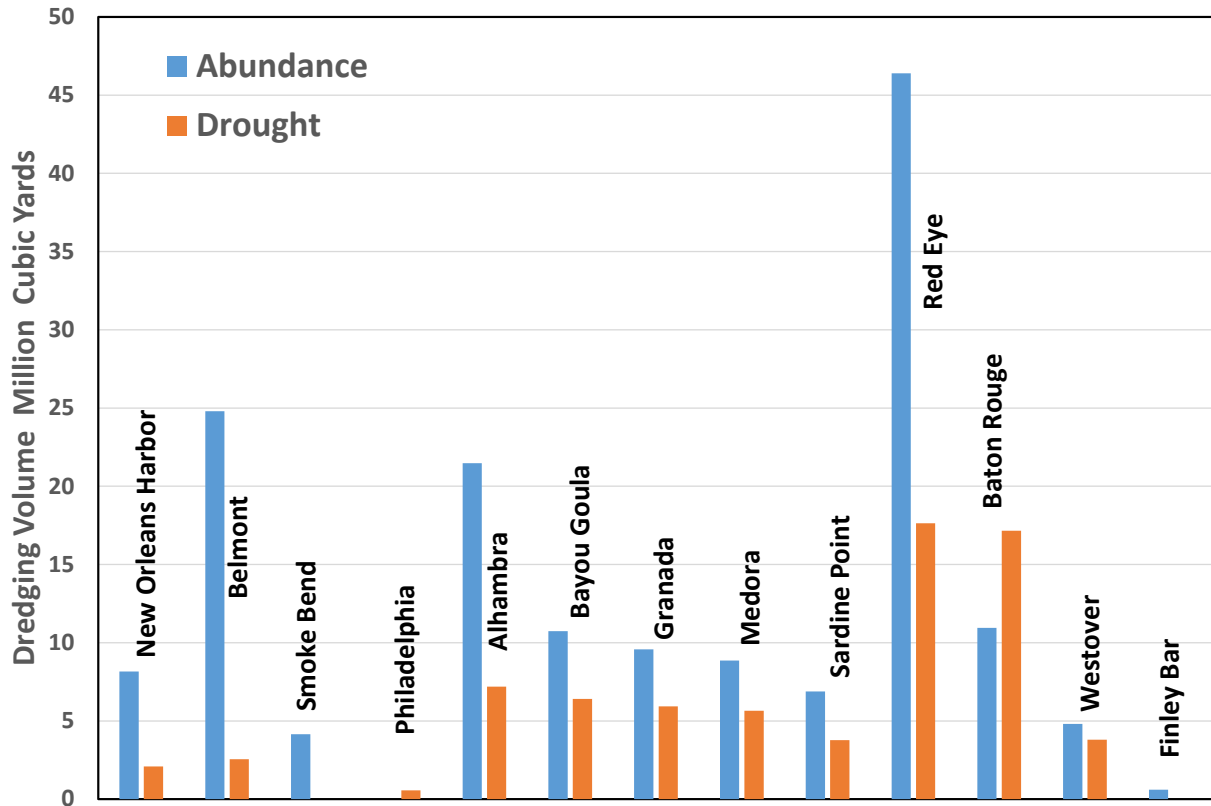
Figure 6. Calculated dredging with in-channel disposal for seven consecutive wet and dry years

Conclusion

The goal of this study was to assess various dredging alternatives to determine methods to optimize the dredging process. Use of the numerical model discussed in this study would supply only one factor, specifically the reduction in dredging volumes, to be considered in the economic feasibility and overall viability of altered dredging operations. Other factors include: disposal site availability and location, equipment required including different dredge types, pumps and transport piping, haul/barge logistics, utility pipelines in the river and navigation impacts. Two main areas were analyzed, disposal options and dredging during wet and dry cycles. The dredging options evaluated in the study have proved to have more impact than originally expected. As stated previously, values represented in this study are merely approximate due to the number of uncertainties dealing with sediment transport and dredging volumes. Regardless of the uncertainty involved, showing nearly 50% reduction (above Venice) between in-channel and overbank disposal is substantial. Also, understanding how wet and dry seasons impact dredging can be very helpful when planning future dredging operations. More studies may be used in the future to determine more long-term benefits for dredging practices.

References

Copeland, Ronald R. and Thomas, William A. 1992. *Lower Mississippi River Tarbert Landing to East Jetty - Sedimentation Study, Numerical Model Investigation.* Technical Report HL-92-6, USACE Waterways Experiment Station, Hydraulics Laboratory, Vicksburg, Mississippi.

Copeland, Arthur, Gaines, Lombard, Stephens, and Thomas 2010. *Issues in Development of a 1000-Mile-Long Numerical Sedimentation Model of the Mississippi River*, Proceedings of the Joint Federal Interagency Sedimentation Conference, Las Vegas, NV.

Copeland, Ronald R. 2018. Mississippi River and Tributaries Flowline Assessment: Mississippi River Sedimentation Report. MRG&P Report No. 24; Volume 4. Vicksburg, MS: U.S. Army Engineer Research and Development Center.

Thomas, William A. 2018. *Sedimentation in Stream Networks – HEC-6T*, Mobile Boundary Hydraulics Inc. Software, Hot Springs, Arkansas.

Physical Changes to Fish Habitat Resulting from River Training Structure Construction

Edward Brauer, P.E., Hydraulic Engineer, United States Army Corps of Engineers, St. Louis, Mo, Edward.j.brauer@usace.army.mil

Background

River Training Structures are used in many rivers around the world to manipulate flow and sediment transport for the purposes of navigation and environmental restoration. As part of the Supplemental Environmental Impact Statement on the Mississippi River between the Ohio and Missouri Rivers (Regulating Works) effort, completed in 2016, the Corps needed to quantify the habitat changes that occurred with continuing dike and revetment construction. It was decided that rather than focus on specific fish species, the focus would be on the physical changes that occurred due to the presence of the structures compared to a condition without structures. It was determined through coordination with environmental partners that two of the most defining attributes of aquatic habitat are velocity and depth. Since there is insufficient field data, particularly velocity data at the flows of interest, it was necessary to use numeric simulations to approximate the velocity fields around the structures. The main purpose of this study was to use the results of the hydraulic model in conjunction with bathymetric data to quantify the volume of different depth and velocity combinations that were created or eliminated by the construction of river training structures on the Middle Mississippi River (MMR).

The physical changes made to rivers by the construction of river training structures is three dimensional; i.e, complex flow separation zones and velocity acceleration and deceleration. Previous analyses of physical aquatic habitat have been conducted using two-dimensional hydraulic models (e.g., Jacobsen et al. 2009, Remo et al. 2013). Such models can provide a good approximation of two-dimensional flow fields around river training structures but are unable to replicate the three dimensional flow patterns around complex innovative structures used extensively on the MMR.

Hydraulic Modeling

Study Reach

Since it was not feasible to model the entire MMR due to budget, time, and technological constraints, the Corps had to select a reach of the 195-mile MMR that would adequately characterize the impacts of future river training structure construction. Factors that were considered include: locations of rated gages, a number of different configurations of river training structures (e.g. traditional dikes, chevron dikes, notched dikes, offset dikes, bendway weirs, point bars, side channels etc.), habitats in the reach (e.g., main channel border, sandbar, side channel, main channel etc.), and available bathymetric datasets.

A 19-mile stretch of the MMR from river mile 110 near Chester, IL, to river mile 92 was selected for analysis (Figure 1). This stretch of river includes a rated gage at the upstream end (allowing the model to be calibrated to observed water surface and velocity data), contains the majority of

structure and habitat types in the MMR, has good coverage of bathymetric data, and is of an appropriate length for maximizing data output and minimizing computation requirements.

The study reach included 15 bendway weirs, 155 traditional dikes (with some modifications), seven chevron structures and three side channels. The Mississippi River within the study reach has an average depth of 32 feet, an average slope of 0.012% (0.6 feet per mile), and an average width of 2,240 feet.
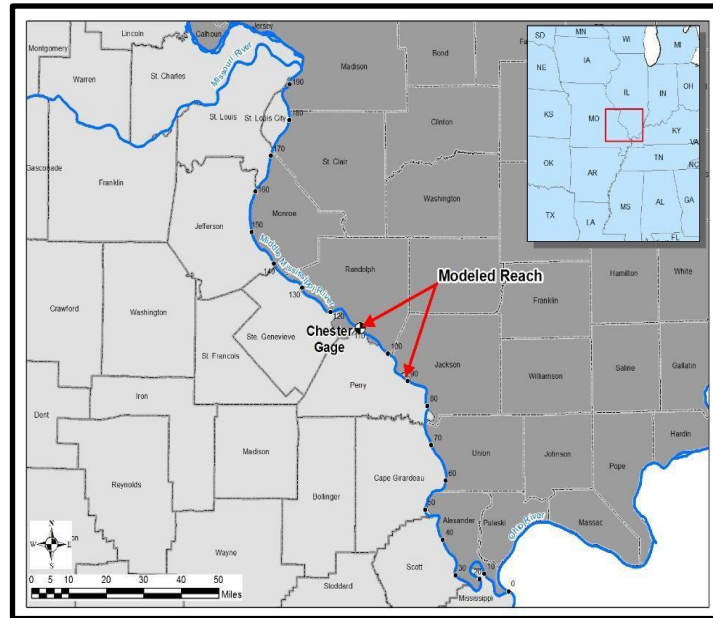
Figure 1. Study Reach

Model Selection and Source Data

The U.S. Army Corps of Engineers, St. Louis District (MVS) contracted with West Consultants to conduct the modeling and develop the post processing scripts (WEST 2014). The numeric model CCHE3D, developed at the National Center for Computational Hydroscience and Engineering (NCCHE), University of Mississippi, was used for the numeric simulations. CCHE3D is three dimensional (3-D) finite element based model for simulating free surface turbulent flows. CCHE3D has been used successfully to simulate turbulent flows around spur dikes.

The elevation data for the mesh was based on a DEM developed using bathymetry and LiDAR data provided by MVS. The bathymetry data was a combination of main channel, and side channel single beam surveys, single beam dredge surveys, and multi beam main channel surveys. All data was converted to the NAD83 Universal Transverse Mercator (UTM), Zone 16 horizontal datum, NAVD88 vertical datum, and metric units.

Analysis Methodology

The model was used to analyze velocities for three separate discharges: average annual low discharge (111,000 cfs), average annual discharge (213,000 cfs), and average annual high discharge (303,000 cfs). These discharges correspond to structures being emerged by 10 feet,

emerged by 2 feet, and submerged by 4 feet, respectively. These discharges were chosen because they cover the full range of flows occurring in a typical year and cover a broad enough range to adequately capture the full range of velocity and depth profiles in the modeled reach. They were also chosen because they correspond to flows for which recent field measurements of water surface and velocity have been collected, thereby increasing model accuracy.

Velocity and depth are the two primary physical characteristics that differentiate regions of riverine fish habitat. In order to quantify fish habitat in a 3D environment, 1-m by 1-m by 1-m volumes were categorized by paired combinations of depth and velocity. For each of the discharges, 6 depth categories and 5 velocity categories were computed. Depth catagories were assigned by the depth of the cube within the water column. In other words, all individual 1 m volumes at a particular point in the river were assigned the same depth category, irrespective of where they fell within the water column at that location. This was done to avoid classifying, for example, surface waters over shallow sandbars the same as surface waters over deep water in the main channel. The depth and velocity classifications were developed with input from natural resource agency partners. The number of depth and velocity categories had to be limited to a reasonable number so that processing of model data did not become exceedingly time consuming. The chosen depth and velocity categories are skewed toward higher resolution at shallower and lower velocity habitat due to the fact that those areas are, in general, considered more likely to provide better fish habitat in the MMR.

Model Results Post Processing

The main purpose of this study was to use the results of the hydraulic model in conjunction with bathymetric data to quantify the volume of different depth and velocity combinations that were created or destroyed by the construction of river training structures on the MMR. To do this, additional tools were developed in the ArcGIS Version 10.1 Toolbox that creates workspace directories, classifies velocity data into ranges and calculates associated area within the model extents or a specified area, computes the area of each velocity zone, defines the volume difference between the CCHE3D water surface elevation and a raster file of the bathymetry data. A VBA program in Excel was created to extract the area of classified velocity zones from the DBF files generated from other tools and summarizes in table form the area, and volume for each velocity zone per 1 meter depth increments, and the total fractional volume for each velocity zone.

Habitat Analysis

Proxy Reaches

It was not possible to do a direct pre- and post- construction comparison since there was not sufficient high density survey data to produce usable results. To compensate for this limitation, proxy impact sites were selected for habitat types of interest. As described in the study reach section, the study reach included a number different habitat types that are representative of the entire MMR. For the pre-construction sites, the impact site was defined as the area that is representative of the habitat characteristics of the feature of interest. For post-construction sites, the impact site was defined as the area that is impacted by the structures of interest. Example of impact sites for selected habitat types can be found in Figure 2.

The velocities calculated by the three dimensional model and the bathymetry data were clipped to the boundaries of the impact sites and the impact sites were evaluated independently and compared to other sites.
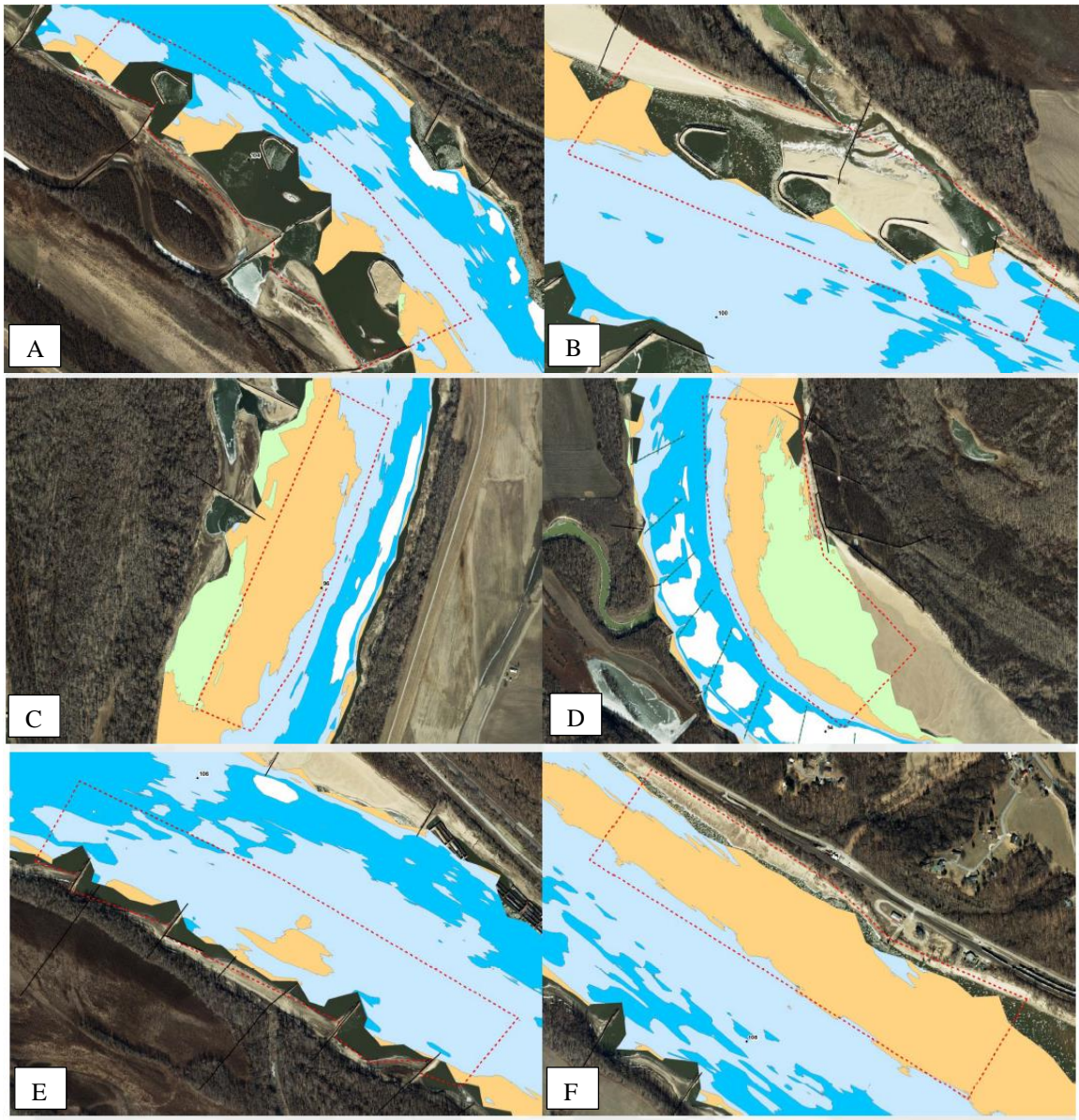
Figure 2. Examples of impact sites. (A,B) chevron Field, (C,D) point bars, (E) sandbar with dikes (F) sandbar without dikes

Eight control sites were evaluated. These sites included point bars, off channel sandbars, and locations with long existing river training structures. These eight control sites were selected to represent the locations where new river training structures would likely be placed. The similar control sites were averaged together to create a general profile for what habitat exists at that site. Nine construction sites were evaluated. These sites included weirs, traditional dikes, offset dikes, notched dikes, and chevron shaped dikes. One objective for the construction sites was to model both traditional configurations and 'innovative' configurations so a direct comparison could be

made between the two. Six other sites of interest were evaluated in the model. These sites represented locations that the environmental partners considered areas of good habitat (i.e., side channels, island tips, etc.).

Data Analysis

The full study reach was evaluated in the three dimensional model for flowrates of 111,000 cfs, 213,000 cfs, and 303,000 cfs (Figure 3). The model data was then clipped to the proxy reach of interest. The clipped model data was then processed using the tools described above to calculate the volume of the selected depth and velocity pairs.
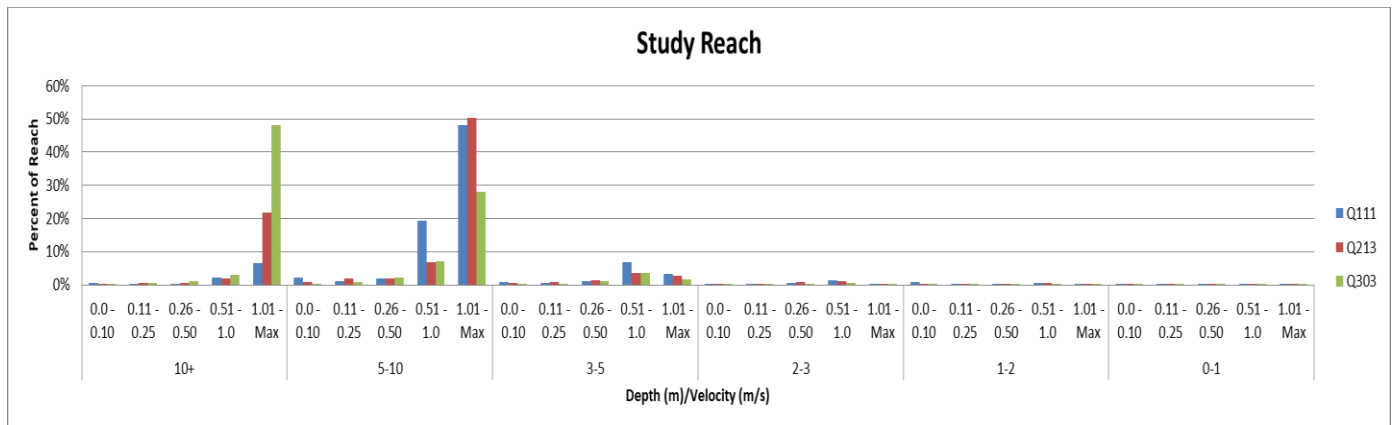
Figure 3. Velocity and Depth Profile of the full study reach.

The majority of the habitat in the full study reach was greater than three meters deep with velocities greater than 0.51 meters per second. This was expected since by volume a majority of the flow is in the main channel which is the deepest part of the channel with the highest velocities.

Site Specific Analysis

Example Site Analysis

As described above, the purpose of this study was to understand the type and quantity of habitat that is changed when different types of river training structures are constructed on the MMR. For example, how the velocity and depth change when a series of chevrons are constructed adjacent to a typical dike field (Figure 4).
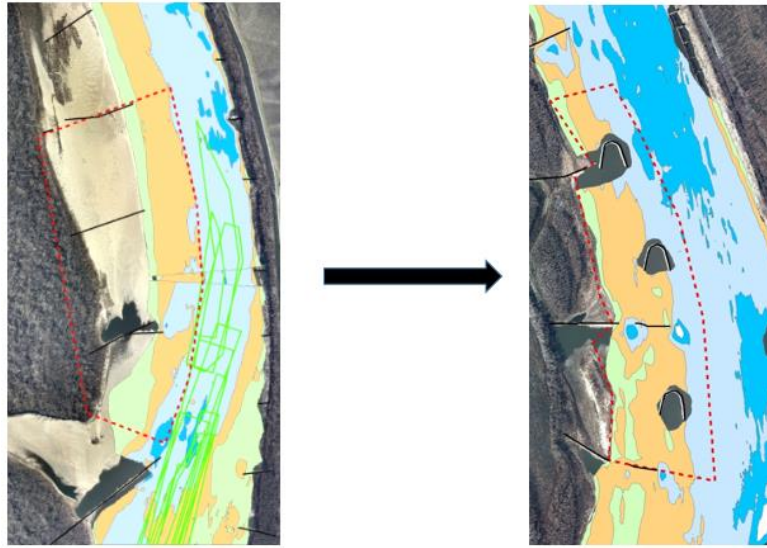
Figure 4. Example of a pre- and post- construction proxy site.

To do this, both the reference site (degraded dike field) and the construction site (chevrons) were clipped from the numerical model results and processed using the method described above. The reference site was used as the pre- construction condition (Figure 5) and the construction site was used as the post- construction condition (Figure 6). Figure 7 shows the habitat change that occurs with river training structures. It is the calculated difference between the two sites.
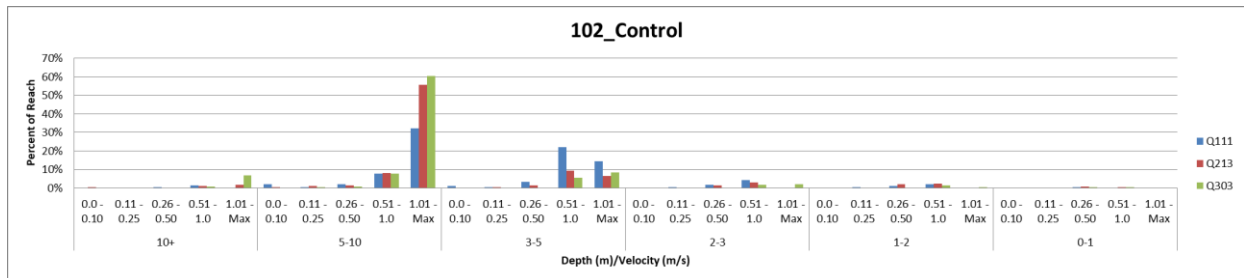
Figure 5. Velocity and Depth Profile of the reference site
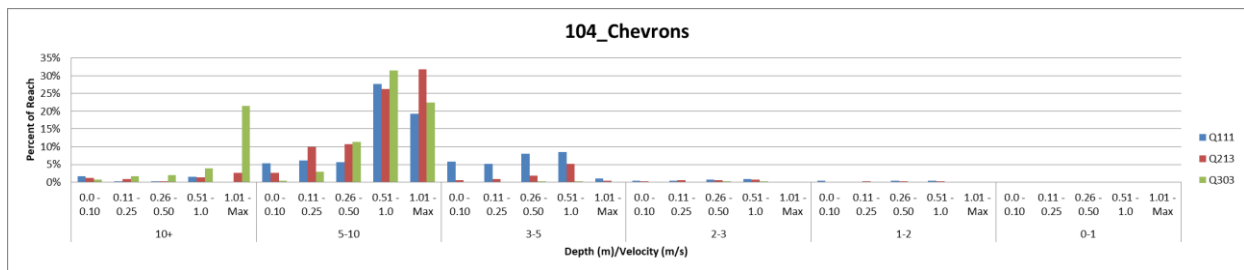
Figure 6. Velocity and Depth Profile of the construction site
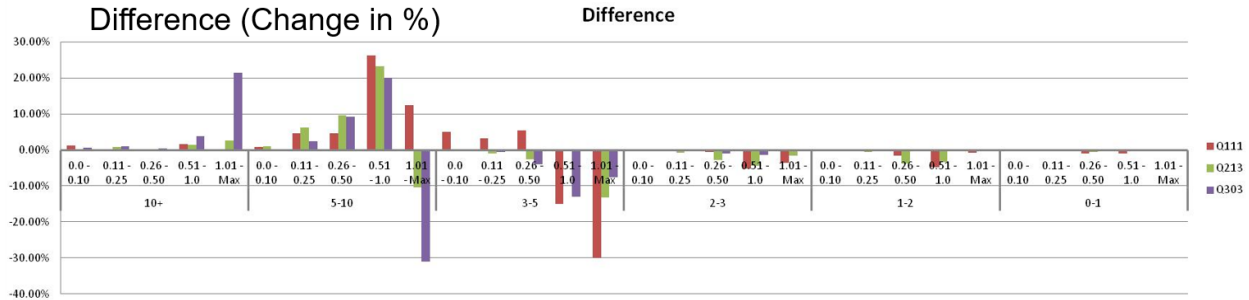
Figure 7. Difference in habitat between the reference and construction site.

As shown in Figure 7, constructing chevrons in the degraded dike field results in a significant loss of moderate depth, high velocity habitat and some small changes in shallower, moderate depth habitat. These results are reasonable give the designed purpose of the chevron structures is to convert main channel and main channel border habitat to shallower moderate depth habitat.

The next question that needed to be answered was if the changes in habitat were significant to the overall study area. This was determined through coordination with our environmental partners. As shown in Figure 3, there exists an abundance of moderate to deep, moderate to high velocity habitat in the study reach. The habitat type that was scarce was the lower depth, lower velocity habitat and the moderate depth, moderate to high velocity habitat. To understand the significance of the change, the percent of habitat from the modeled area that exists in the construction area was calculated (Figure 8). In our example, although the change in shallow water habitat may be a relatively small percentage within the work area, it may represent a large percentage of that habitat type in the entire reach/river. This fact must be considered in the decision on the significance of the impact.
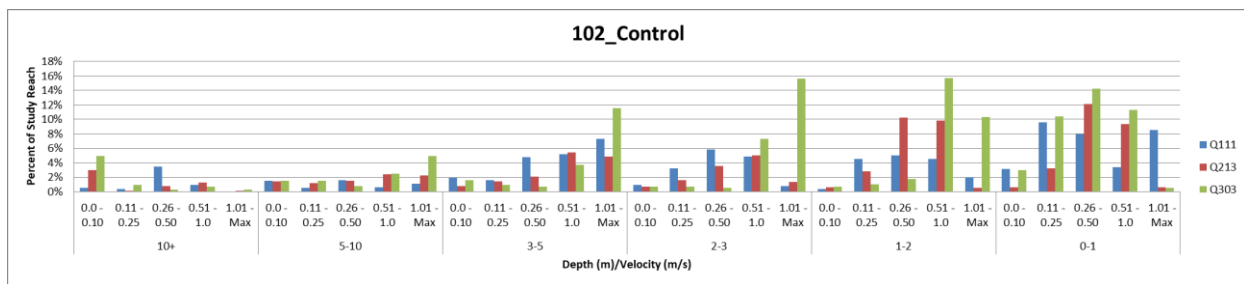
Figure 8. Percent of habitat from the modeled area in construction area

Habitat Changes

Through the process described above, the changes in habitat for different combinations of constructed features and reference sites were quantified. This data was averaged to calculate an average change that would occur with future potential construction (Figure 9). Due to the dynamic nature of the river, and the ongoing nature of the Regulating Works project it is currently unknown exactly where structures will be constructed or what types of structures will be

constructed, therefore only general trends can be addressed. On average, the model showed that river training structure construction will result in an increase in shallow to moderate depth, low to moderate velocity habitat. This is habitat that is generally considered good habitat for many fish species.
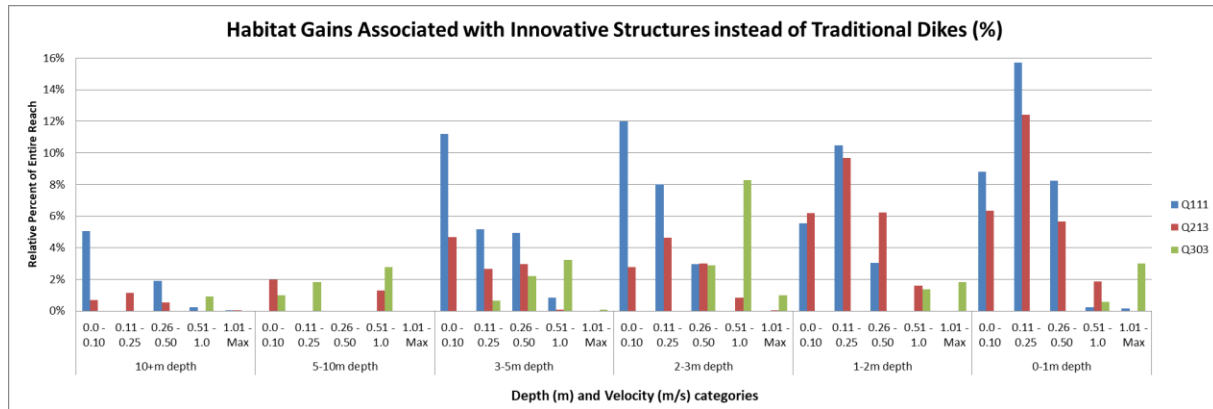
Figure 9. Habitat gains associated with river training structure construction.

The habitat losses associated with river training structure construction are shown in Figure 10. The model showed that generally the construction of river training structures resulted in a loss of moderate to shallow depth, moderate to high velocity habitat. As shown in Figure 3, this habitat type is scarce in the overall study reach. To understand what habitat type was most impacted by structure construction, the different pre-construction habitat types were evaluated and compared with the habitat losses. It was discovered that the losses due to habitat construction matched the habitat profile of main channel border habitat (Figure 11).
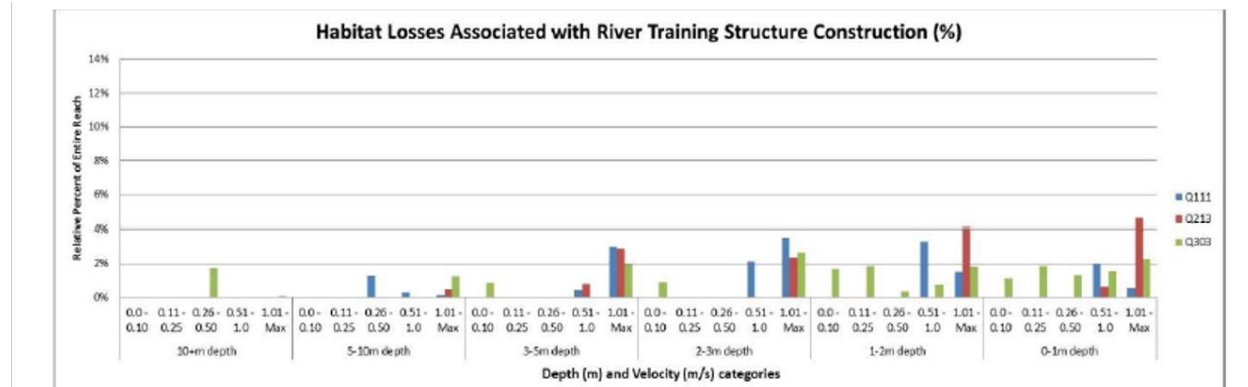
Figure 10. Habitat losses associated with river training structure construction.
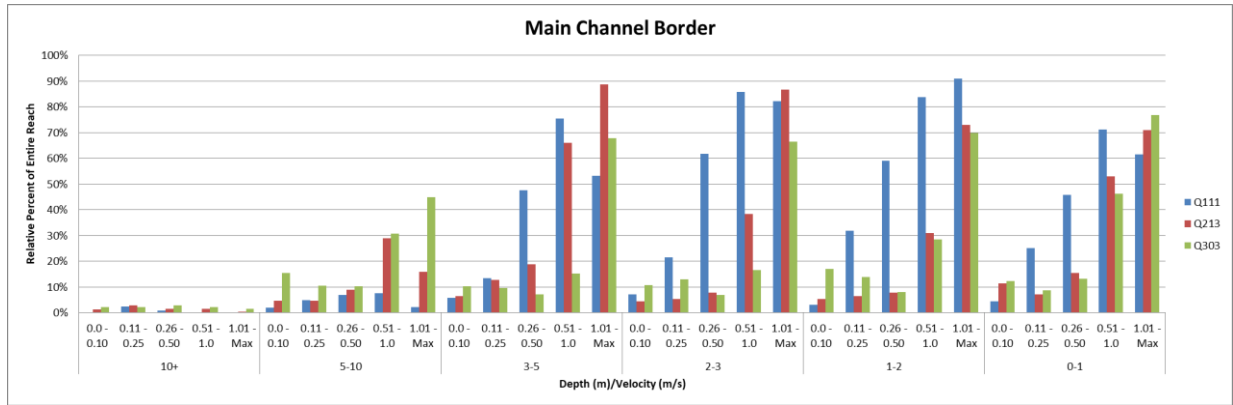
Figure 11. Habitat profile of main channel border habitat.

Main channel border habitat is generally referred to as the habitat that exists at the intersection of the main navigation channel and the river banks in a river crossing (Figure 12). Main channel border habitat generally has a gradually sloped sandbar that creates moderate to shallow depths. The velocity profile of main channel border is moderate to high velocities. Main channel border habitat may contain the presence of a structure.
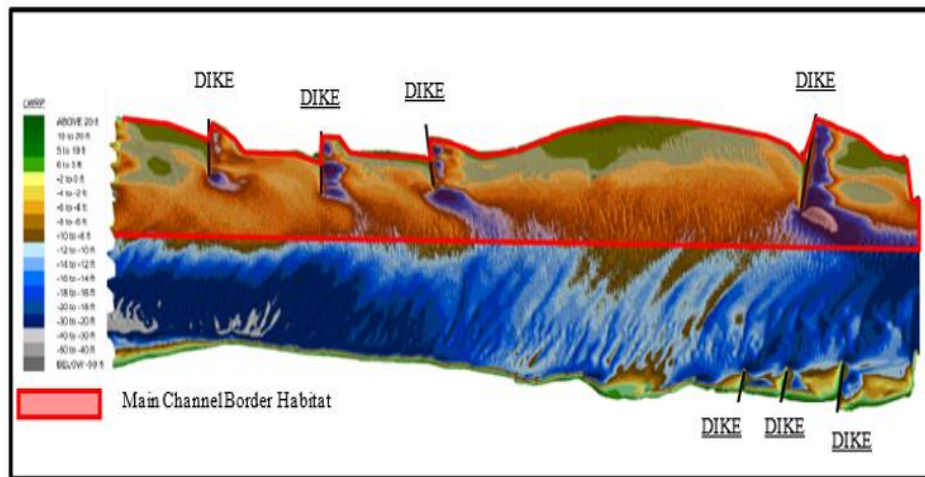
Figure 12. Description of main channel border habitat

"Innovative Structures"

The post- construction data set was separated into traditional river training structures and "innovative river training structures" to evaluate if the intended goal of creating different habitat types with the modification of the size, shape and elevation of traditional structures has been achieved. Innovative river training structures include but are not limited to chevron shaped structures, notched dikes, offset extensions.

The analysis revealed that innovative structure fields had more shallow to moderate depths with more low to moderate velocities than traditional dike fields (Figure 13). This analysis confirmed that the intended benefit of structure design modifications was being achieved.
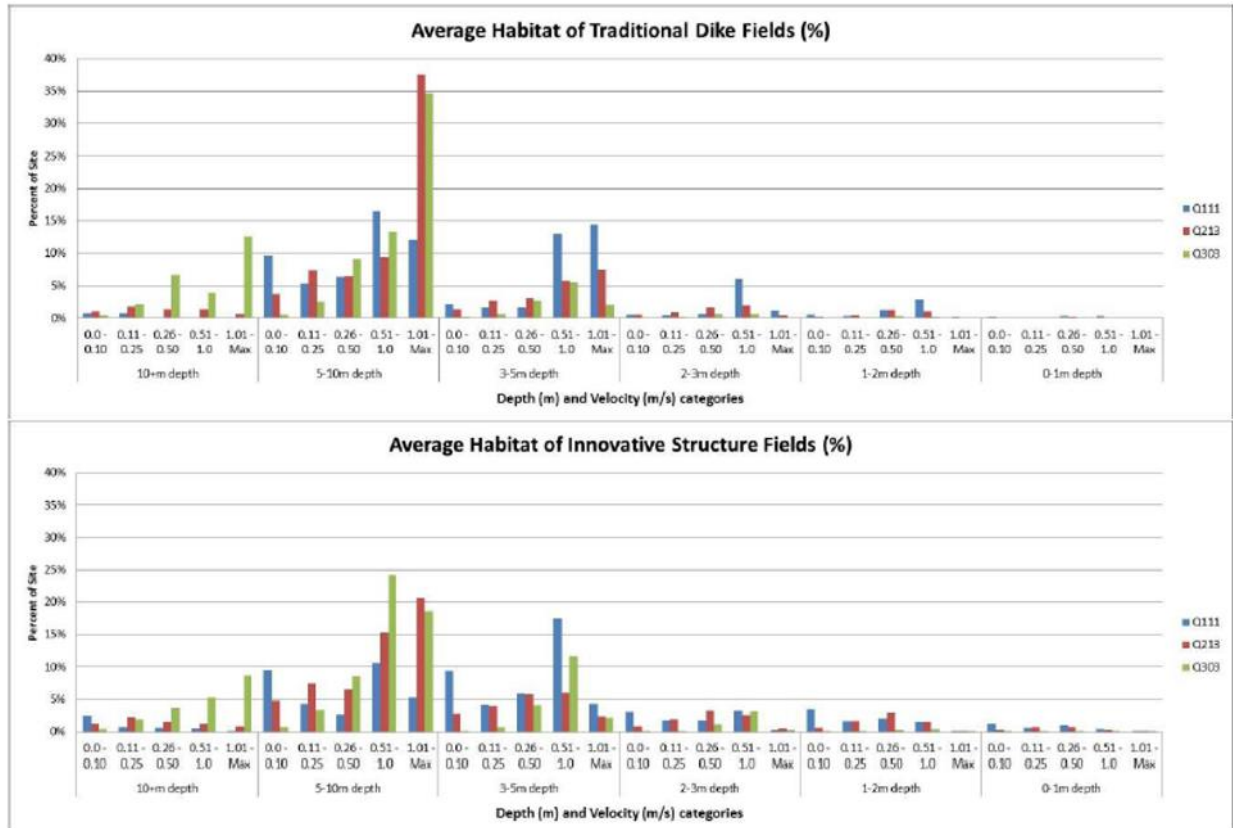
Figure 13 Comparison between traditional and "innovative" river training structures

Results

1. Use of innovative structures is accomplishing the intended goal of avoiding and minimizing habitat impacts by increasing habitat diversity. The analysis of model results for areas with innovative structures compared to areas with traditional dikes showed an increase in diversity of depth and velocity categories. In the modeled reach, innovative structures consist of chevrons, offset dikes, and notched dikes. The innovative structure fields tend to provide a more even distribution of habitat categories, particularly on the shallow end of the habitat scale.

2. Construction of river training structures generally results in an increase in shallow, low-velocity habitat which is generally regarded as important fish habitat. When comparing model results for work sites to control sites, a general increase in the relative percent of low velocity habitat can be seen, particularly in shallow, low-velocity habitat. This is intuitively reasonable given that river training structure construction, whether traditional or innovative, generally results in some sediment accretion downstream of the structures in an area of low current velocity.

3. Construction of river training structures generally results in a decrease in shallow to moderate-depth, moderate- to high-velocity habitat which is important habitat to some MMR fish guilds. While there is a gain in low-velocity habitat as discussed in conclusion 2 above, model results indicate that river training structure construction causes a loss in shallow to moderate-depth, moderate- to high-velocity habitat. The loss appears to be relatively small, but given the limited quantity of habitat of this type in the MMR, the relative loss is more meaningful. The depth and

velocity characteristics of this loss are reasonable given the locations in which river training structures are generally constructed – shallow to moderate-depth unstructured main channel border habitat. This habitat would typically be expected to exhibit moderate to high velocities given its location in the river channel and presumed lack of river training structures to act as current breaks. Indeed, modeled depth and velocity profiles for such unstructured main channel border areas mimic the depth and velocity profiles of this habitat loss.

References

Jacobson, R.B., H.E. Johnson, III, and B.J. Dietsch. 2009. Hydrodynamic simulations of physical aquatic habitat availability for pallid sturgeon in the Lower Missouri River, at Yankton, South Dakota, Kenslers Bend, Nebraska, Little Sioux, Iowa, and Miami, Missouri, 2006– 07: U.S. Geological Survey, Scientific Investigations Report 2009–5058, 67 p.

Remo, J. W. F., A. Khanal, and N. Pinter. 2013. Assessment of chevron dikes for the enhancement of physical-aquatic habitat within the Middle Mississippi River, USA. Journal of Hydrology 501:146-162.

USACE (U.S. Army Corps of Engineers). 2017. Final Supplement I to the Final Environmental Statement, Mississippi River between the Ohio and Missouri Rivers (Regulating Works). U.S. Army Corps of Engineers, St. Louis District, St. Louis, Missouri.

WEST Consultants, Inc. 2014. Evaluation of Aquatic Habitat on the Middle Mississippi River. Prepared by WEST Consultants, Inc. for the U.S. Army Corps of Engineers, St. Louis District, St. Louis, Missouri.

Sediment Transport Predictions for Operations at Nolichucky Dam

Martin J. Teal, Senior Vice President, WEST Consultants, San Diego, CA,
mteal@westconsultants.com
Filippo Bressan, Senior Engineer, WEST Consultants, San Diego, CA,
fbressan@westconsultants.com
Curtis M. Jawdy, Lead Hydrologist, Tennessee Valley Authority, Knoxville, TN,
cmjawdy@tva.gov

Abstract

Nolichucky Dam is owned by the Tennessee Valley Authority (TVA) but predates that agency as the dam was completed in 1913 and acquired during the Second World War. In the 1970s TVA halted power generation and let the reservoir fill in. In order to perform a NEPA review and coordinate with the state environmental agency, TVA needed to activate the controlled spillway gates to lower the pool below the uncontrolled spillway level in order to perform inspections. TVA needed to know if the stored sediment would be expected to move during the spill, and if so, what would be the volume mobilized and resulting concentrations. TVA tasked WEST Consultants (WEST) to evaluate sediment transport through Davy Crockett Reservoir and over Nolichucky Dam during the planned spillway operations. WEST developed a numerical model using the two-dimensional (2D) hydrodynamic and sediment transport model SRH-2D. Several modeling challenges were encountered as described in the paper. Model results indicated that the existing velocities and shear stresses in the reservoir are very low and are not strong enough to move significant amounts of sediment for flow rates expected during operations both for existing conditions with the gate closed and after the gate is opened, although there is a small increase in concentration immediately after gate opening. The predicted volume of sediment scoured was approximately two orders of magnitude less than the amount expected to be moved with the gate closed during an approximately yearly flow.

Introduction

Purpose

WEST Consultants, Inc. (WEST) was tasked by the Tennessee Valley Authority (TVA) to evaluate sediment transport through Nolichucky Reservoir on the Nolichucky River in eastern Tennessee, upstream of Nolichucky Dam. The purpose of the study is to provide scour and sediment loading predictions resulting from planned spillway operations, in support of spillway inspections.

Study Location

Nolichucky Dam is a concrete dam on the Nolichucky River near Greeneville, Greene County, TN. The dam is located about 46 miles upstream from the Nolichucky River mouth and impounds Nolichucky Reservoir (Davey Crockett Reservoir) which extends about 6 miles upstream of the dam. Nolichucky Dam is a concrete gravity overflow type dam that is 94 feet high and 482 feet long. The dam has an ogee-type spillway with a vertical lift gate that is 25 feet

wide and 10 feet high (see Figure 1-1). The elevations of the dam crest and the gated spillway crest are 1,240.9 and 1,230.9, respectively.

Approach

In order to evaluate sediment transport through Nolichucky Reservoir during the planned spillway operations, WEST developed a numerical model using the two-dimensional (2D) hydrodynamic and sediment transport model SRH-2D (USBR, 2017), and the Surface-water Modeling System SMS (Aquaveo, 2014).

SRH-2D solves the 2D dynamic depth-averaged St. Venant equations, and allows for simulation of non-equilibrium sediment transport. SRH-2D is a *coupled model*, that is, at every time step the hydrodynamics is computed first, then sediment transport is computed based on the local and instantaneous values of shear stress, and finally the bed is adjusted to take into account computed erosion or deposition. This cycle is repeated for the following time steps using the updated geometry at the beginning of each new time step.

Non-equilibrium sediment transport is expected to occur during hydraulic transients, such as during the opening of a gate, when unsteady flow conditions are dominant. The numerical model was developed in order to include the area of Nolichucky Reservoir that may be subjected to erosion from the planned spillway operations. The Nolichucky Dam spillway was set as the downstream model boundary and the upstream model boundary was set approximately 1 mile upstream from the dam. The model length of 1 mile was based on the fact that sediment accumulation is principally in the downstream section of the reservoir, in proximity to the gate.

Model development involved the following steps:

1. Acquisition and clean-up of bathymetric data for Nolichucky Reservoir.
2. Development of a stable numerical grid with cell sizes ranging from 3 to 15 feet.
3. Development of appropriate boundary conditions downstream and upstream in order to include inflows of 1,900 cubic feet per second (cfs) and 13,000 cfs.
4. Development of a conceptual *surface model* to characterize the hydraulic roughness of surface materials of the lake bed and bank.
5. Development of a conceptual *subsurface model* to characterize the different sediment types in the lake bed and banks, such as non-cohesive sand and cohesive silt and clay.

Limitations of the present analysis include:

1. Because of safety issues, the bathymetry within 80 feet of the gate could not be collected. This uncertainty is expected to affect sediment transport near the dam. Sediment transport uncertainty was assessed by assuming a constant bathymetry upstream of the gate.
2. 2D modeling focused on the first mile of Nolichucky Reservoir upstream of the dam. The rest of the lake was modeled based on the available Elevation-Storage curve from 1970. This limitation is expected to affect the duration of the transient after the gate is fully open. With the existing Elevation-Storage curve, the transient after the gate is fully open lasts about 24 hours.

Data Availability and Model Development

Nolichucky Reservoir Numerical Grid

A sonar bathymetric survey of Nolichucky Reservoir was conducted by TVA on March 16, 2018 and transmitted electronically to WEST on March 22, 2018. The survey covered the Nolichucky Reservoir bed from just upstream of the dam to a point about one mile upstream (Figure 1). Due to the shallow depths of the lake, the sonar head was maintained near the water surface and this caused air bubbles that led to some noise in the data (TVA, 2018a). In order to obtain a smooth bottom, WEST removed the spikes by averaging the data based on nearby points. The sonar survey revealed that sediment accumulation at an elevation of 1,228 feet exists around 100 feet upstream of the dam.
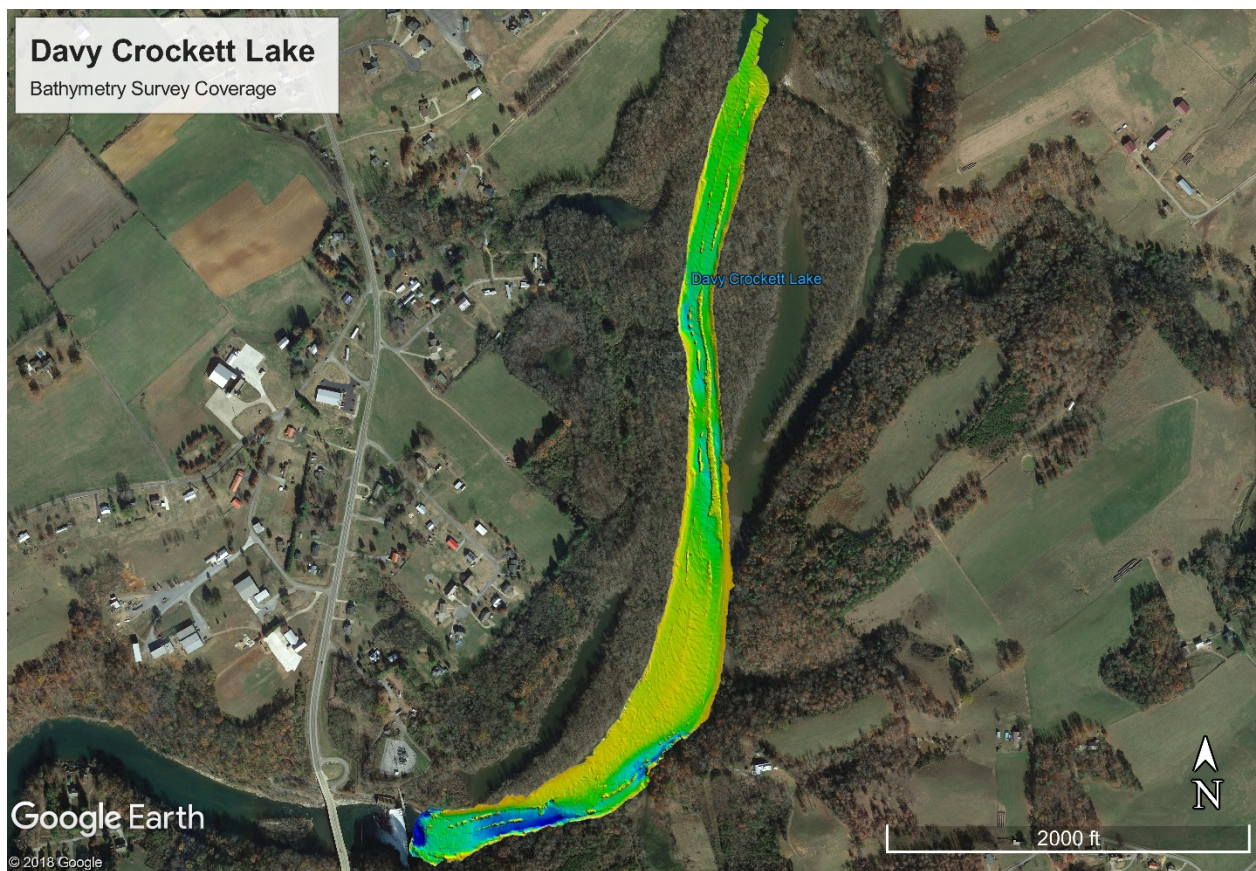
Figure 1. Coverage of bathymetric survey of Nolichucky Reservoir provided by TVA (darker colors represent lower elevations as shown in subsequent figures).

Based on the 2018 and older bathymetry and dam drawings, WEST developed a numerical grid for about 1 mile of Nolichucky Reservoir. After initial tests, the cell size was set to 15 feet and an area with refined 3-foot cells was created near the spillway to account for the strong curvilinear flow. Figure 2 shows the numerical grid close to Nolichucky Dam. Two grids were developed to simulate the different gate conditions: Closed Gate and Open Gate (Figure 3). An additional grid with a flat bathymetry of 1,228 (the elevation of sediment accumulation 100 feet upstream of the dam) was created in order to assess the uncertainty in bathymetry near the dam.
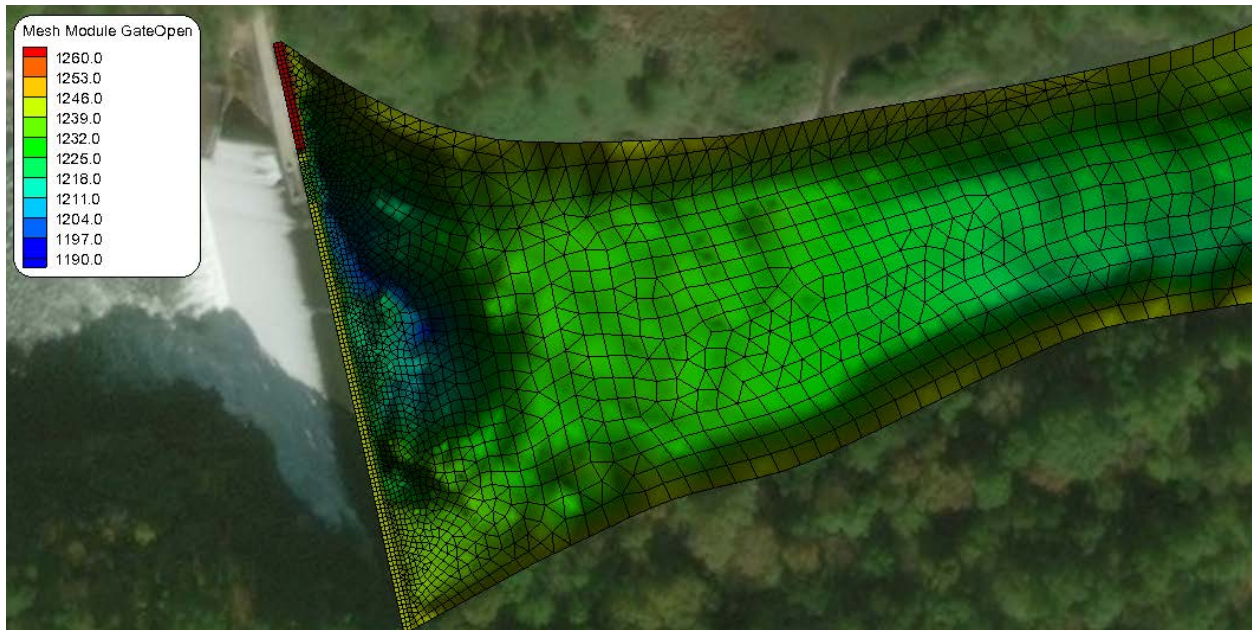
Figure 2. Nolichucky Reservoir numerical grid near Nolichucky Dam
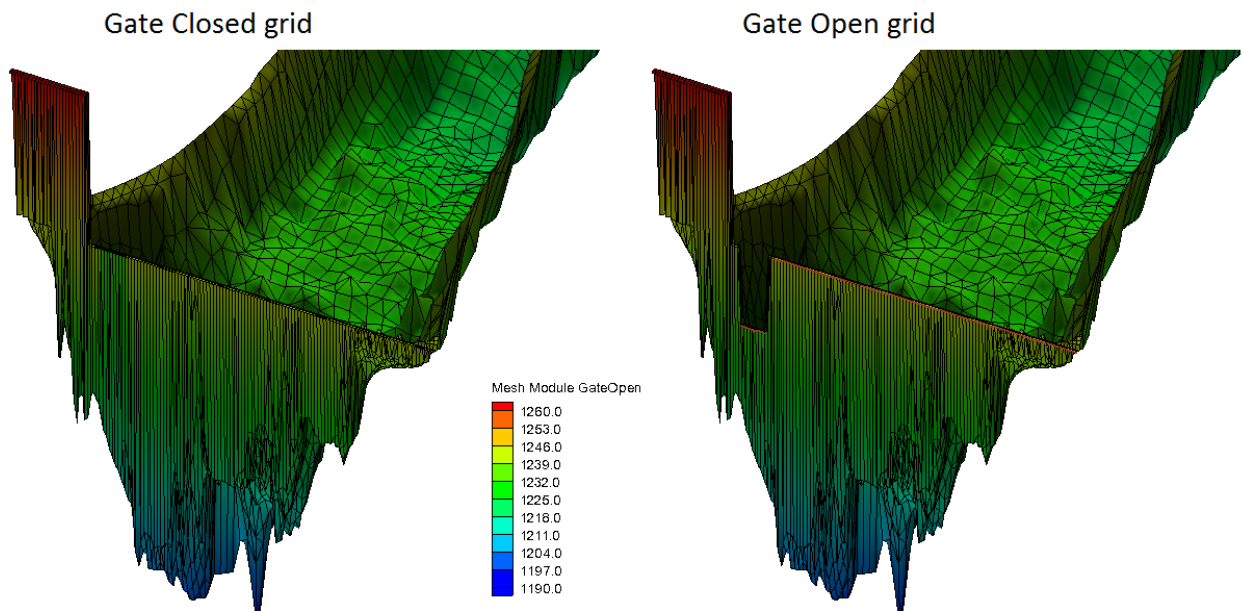
Figure 3. Nolichucky Reservoir numerical grids with gates closed and open

Nolichucky Dam Rating Curves

Rating curves for the Nolichucky Dam spillway and gate were provided by TVA and transmitted electronically to WEST. The available ratings are shown in Figure 4 below and were used develop boundary conditions for the model. Based on discussions with TVA, the upstream boundary condition was set as a constant inflow of 1,900 cfs and two different boundary

conditions were set at the dam: the rating curve with the gate closed and the rating curve with the gate open.
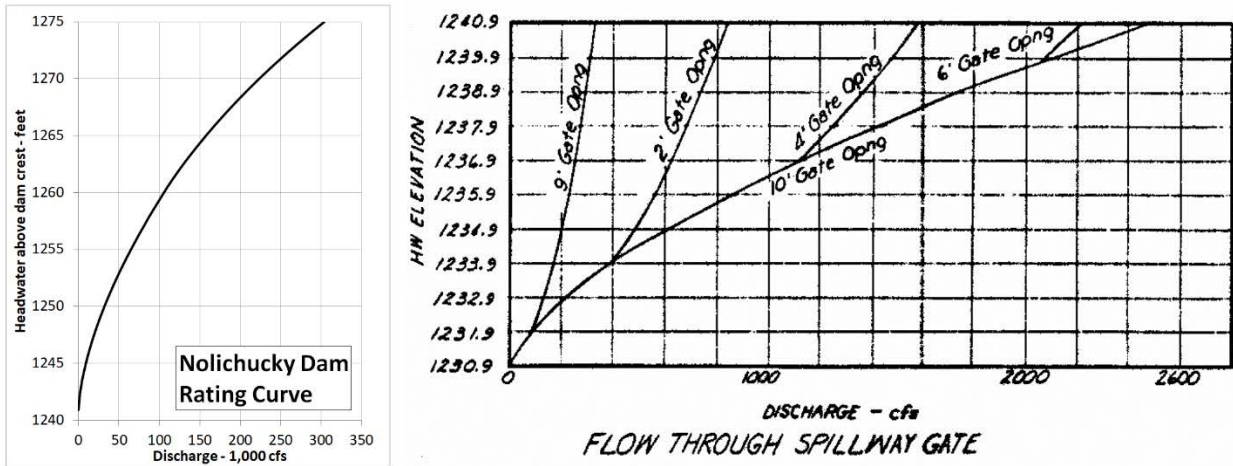
Figure 4. Rating curves for Nolichucky Dam

Nolichucky Reservoir Bed and Bank Sediment

Sediment data from lake bed and bank samples were provided by TVA (2018b) and included Atterberg limits, soil classification and particle size analysis of 16 different sampling locations (12 in the river bed and 4 on the right bank). Figure 5 shows the bed and bank sediment sampling locations.
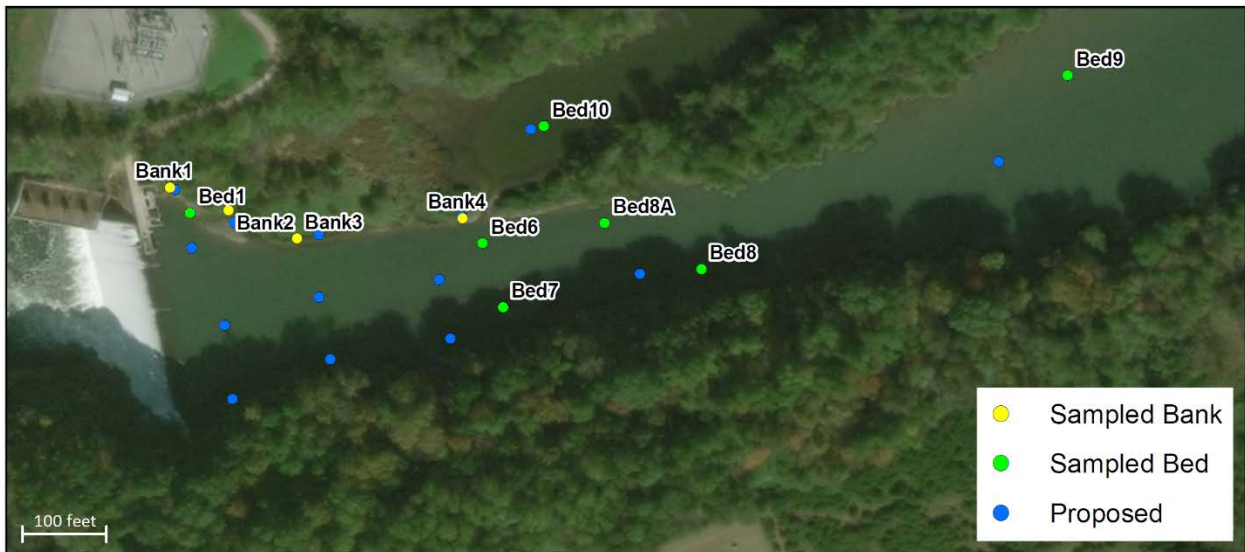
Figure 5. Bed and bank sediment sampling locations

The sediment properties were used to develop different bed zones in SRH-2D and sediment layers up to a depth of 10 feet (Figure 6).

The roughness coefficients were estimated based on Chow (1959) and the sediment grain size distributions. The transport rate of sand and silt was estimated using the total load formula of Engelund-Hansen (1967). The erodibility properties of the fine sediment were based on Briaud et al. (2008) and the soil classification. The fine graded sediment samples (cohesive sediment) were found to be within the high and low plasticity silt range (MH and ML, respectively) and their erodibility properties are shown in Figure 7.

Figure 6. Bed and bank zones included in SRH-2D
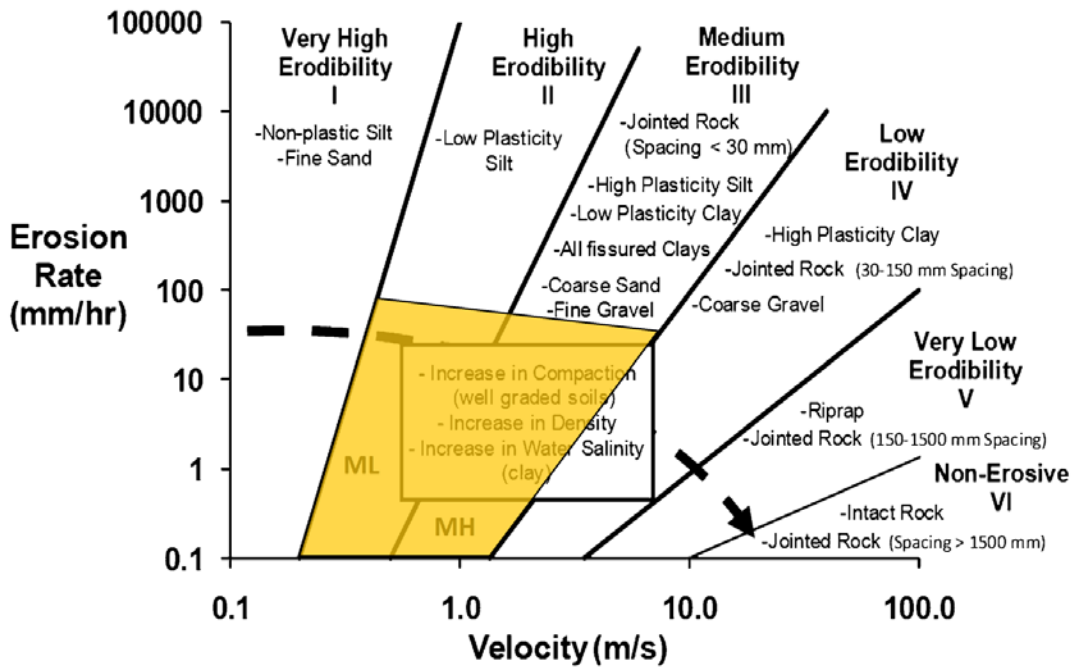
Figure 7. Erodibility categories identified for Nolichucky Reservoir (yellow). Chart after Govindasamy et al., 2013.

Results

General

SRH-2D model results were visualized spatially for the lake area in front of Nolichucky Dam. In addition, results were plotted along the thalweg of the lake (shown in Figure 8). Results included several hydraulic and sediment transport parameters which are discussed in the following sections.
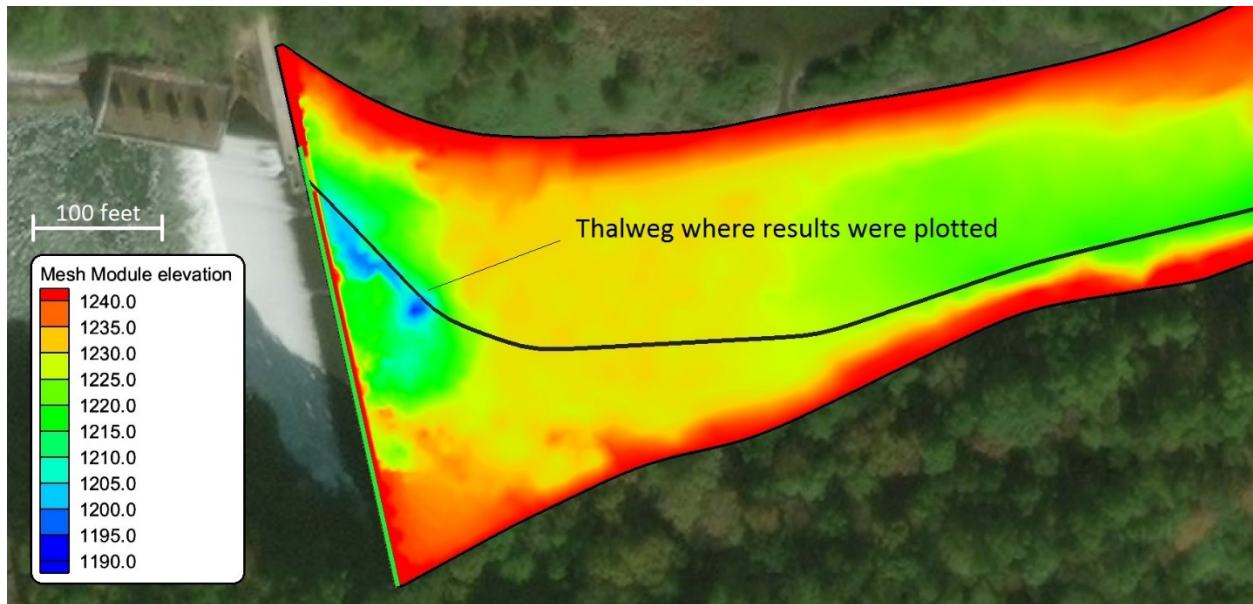
Figure 8. Area in front of Nolichucky Dam and defined thalweg

In the following figures, results from four conditions are compared:

1. *Closed Gate – Q = 1,900 cfs*
   This case represents the existing conditions in Nolichucky Reservoir, with a constant upstream flow of 1,900 cfs and the gate closed.
2. *Closed Gate – Q = 13,000 cfs*
   This case represents the existing conditions in Nolichucky Reservoir, with a constant upstream flow of 13,000 cfs and the gate closed.
3. *Open Gate - Surveyed bathymetry*
   This case represents conditions during spillway operation with the gate fully open and a constant upstream flow of 1,900 cfs. The surveyed bathymetry was used for the entire Nolichucky Reservoir bed.
4. *Open Gate - Flat bathymetry*
   This case represents conditions during spillway operation with the gate fully open, a constant upstream flow of 1,900 cfs and an artificially flat bathymetry in front of Nolichucky Dam. The elevation of the flat bathymetry was set equal to the height of the existing sediment accumulation 100 feet upstream of the dam.

Nolichucky Reservoir Water Surface Elevations and Velocities

Figure 9 shows the water surface elevation along the Nolichucky Reservoir thalweg when the gate is closed and when it is open. The volume of the sediment wedge in front of Nolichucky Dam was estimated to be about 2,600,000 ft³. Figure 10 shows the flow velocity along the Nolichucky Reservoir thalweg when the gate is closed and when it is open. The figure shows that 200 feet away from the dam the velocity approaches a value very close to that obtained with the closed gate. Figure 11 shows a map of velocities for all of the conditions analyzed. The case with the gate closed and a flow of 13,000 cfs indicates that the velocities are much higher than the case with the gate open and surveyed bathymetry (at 1,900 cfs).
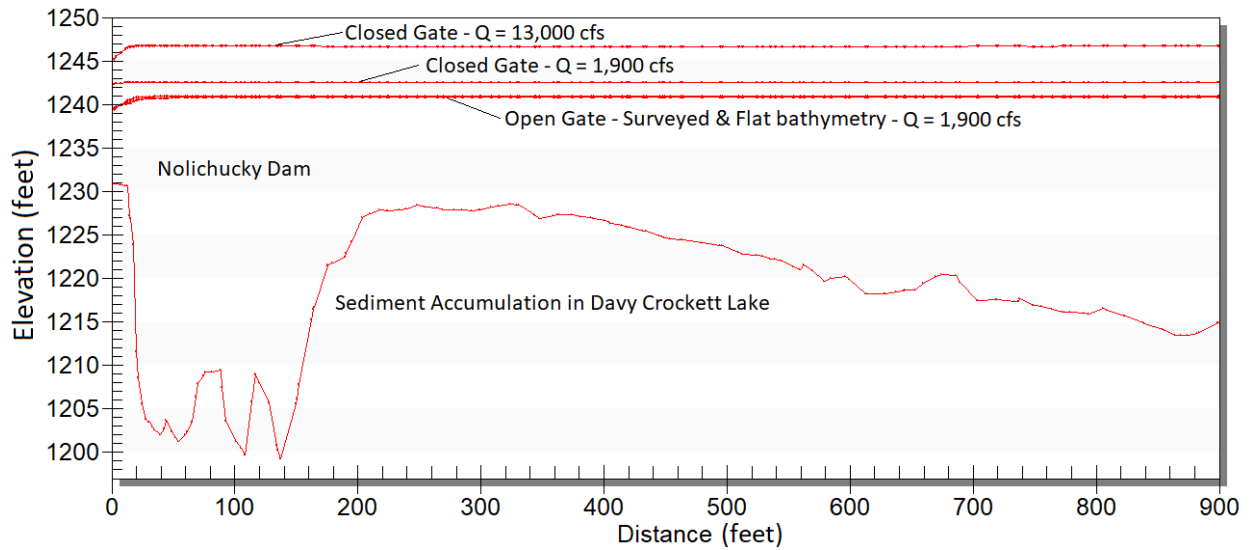
Figure 9. Water surface elevations and bed profile along Nolichucky Reservoir thalweg
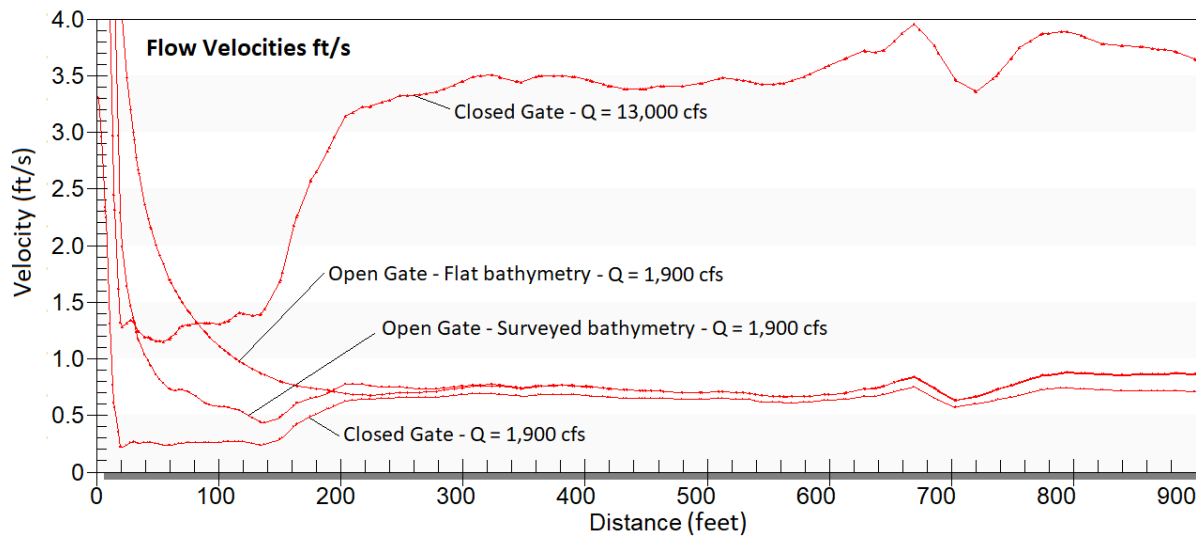
Figure 10. Velocities along Nolichucky Reservoir thalweg
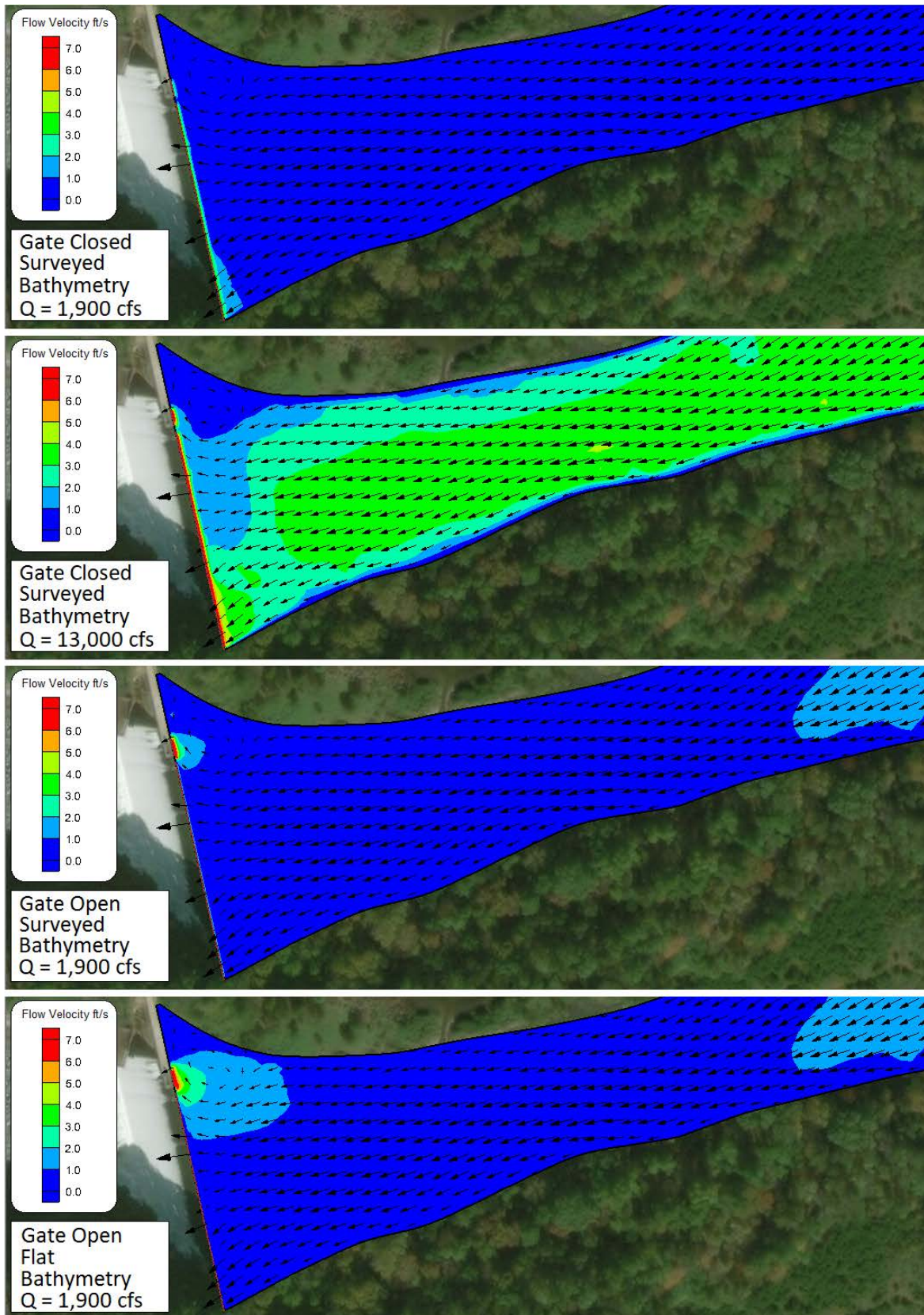
Figure 11. Velocities in Nolichucky Reservoir close to the dam

Nolichucky Reservoir Shear Stress and Sediment Concentration

Figure 12 shows the shear stress along the Nolichucky Reservoir thalweg when the gate is closed and when it is open. Figure 13 shows the shear stress within 300 feet of the dam for the gate closed condition with Q = 13,000 cfs and the gate open condition with surveyed bathymetry (1,900 cfs). Figure 14 shows a map of shear stress for all of the conditions analyzed. As observed for the velocity, the open gate shear stress approaches a value very close to that obtained with the closed gate within 200 feet of the dam. Far away from the dam, the shear stress for the case with a closed gate and a flow of 13,000 cfs is much higher than the case with an open gate and surveyed bathymetry (at a flow of 1,900 cfs). Near the gate the shear stress is higher when the gate is open, but only for the first 30 feet upstream of the dam and right in front of the gate. Figure 14 shows that the only location of significantly increased shear stress is a small area directly upstream of the gate.
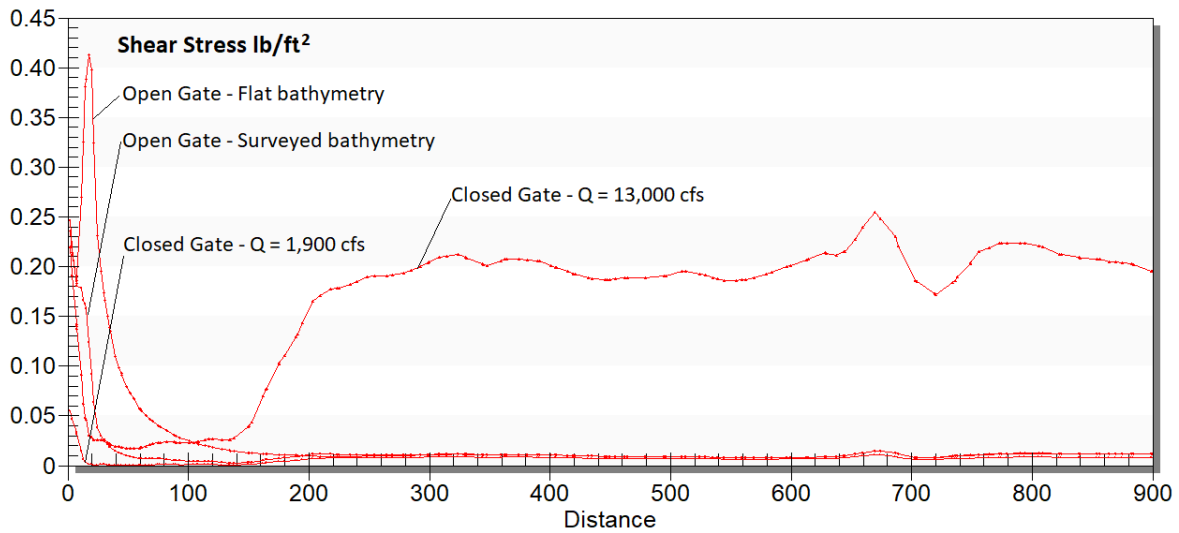
Figure 12. Shear stress along Nolichucky Reservoir thalweg
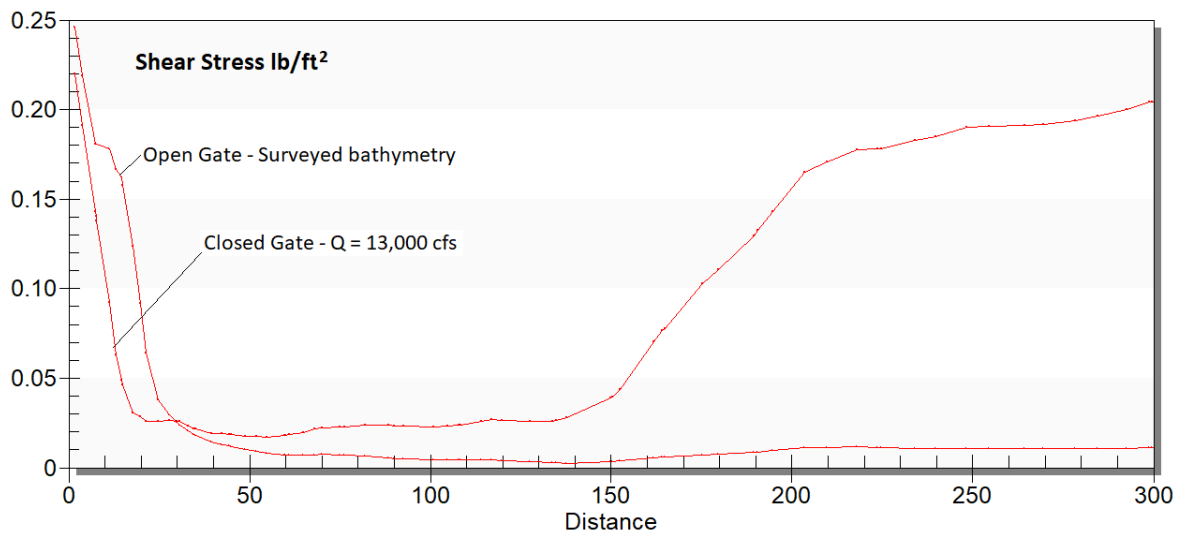
Figure 13. Shear stress within 300 feet of the dam
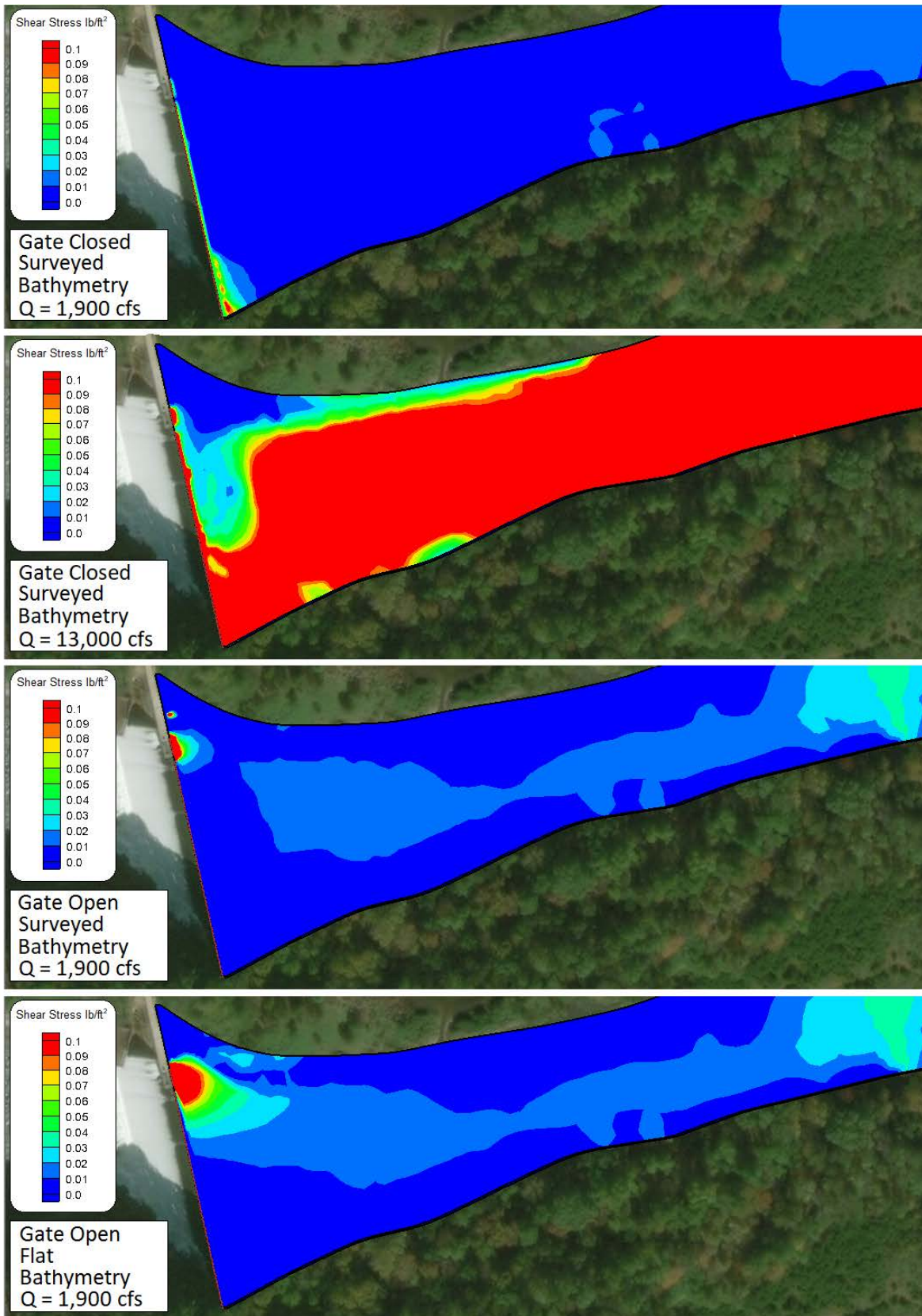
Figure 14. Shear stress in front of the dam for different scenarios

Figure 15 shows the sediment concentration along the Nolichucky Reservoir thalweg when the gate is closed and when it is open. The figure indicates that the sediment concentration during a flood of 13,000 cfs is around 600 mg/L and is much higher than the sediment concentration that would occur with a flow of 1,900 cfs with the gate either closed or open. Figure 16 shows sediment concentration vs. time in front of the open gate with Q = 1,900 cfs. The sediment concentration reaches a peak of about 100 mg/L after the gate is open and reaches a value of about 20 mg/L within 24 hours. These results show that opening of the spill gate during a low flow period would move significantly less sediment than a flood of approximately yearly recurrence with the gate closed.
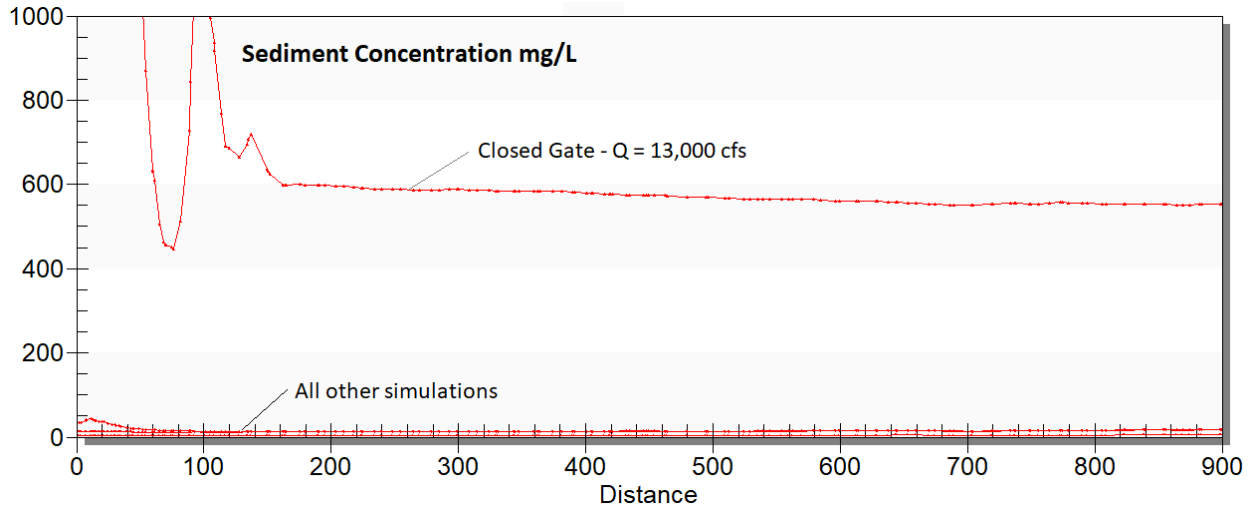
Figure 15. Sediment concentration in front of Nolichucky dam
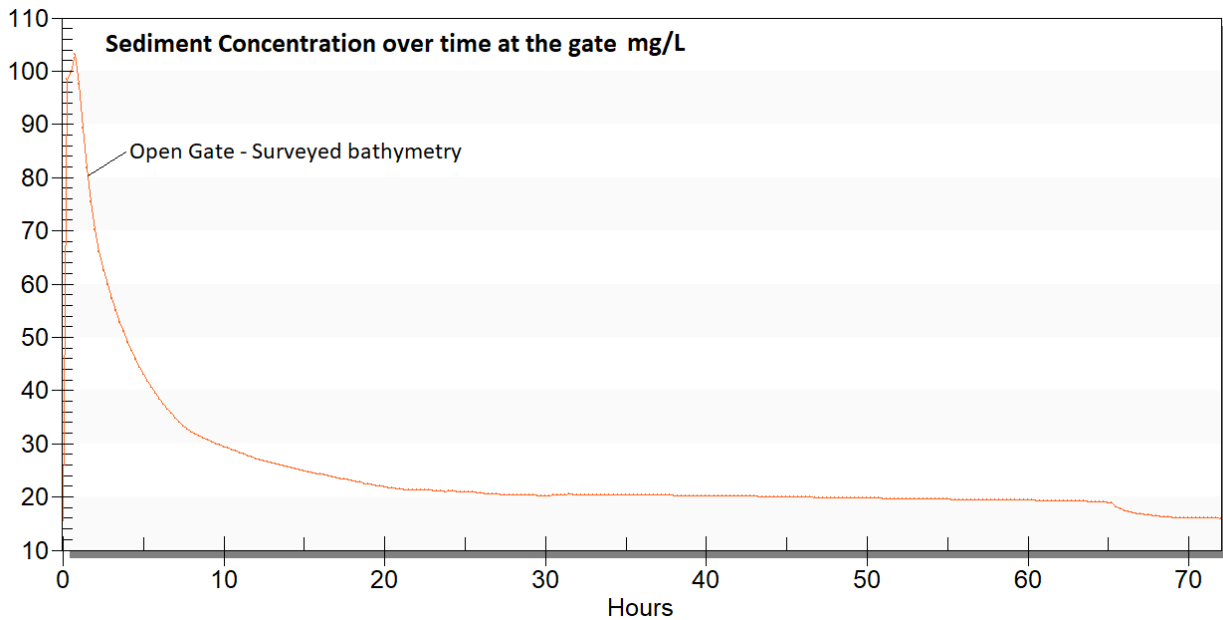
Figure 16. Sediment concentrations at the gate over time

Sediment Erosion and Scour Depths at the Gate

The sediment transport induced by the opening of the gate will tend to scour the area in front of the gate. However, because of the low values of shear stress and sediment concentration, the model results indicate that the amount of scour will be only a few feet. Figure 17 shows the scour depth contours in front of the gate and Figure 18 shows the time evolution of the scour depth. The maximum scour after three days was estimated to be 1.9 feet. The amount of sediment scoured in this area is approximately 11 cubic yards. This volume of sediment is significantly less than the 9,500 cubic yards of sediment that would be moved with the gate closed during a 13,000 cfs flow for 24 hours, which occurs on approximately a yearly interval.

Figure 17. Scour depths near the gate
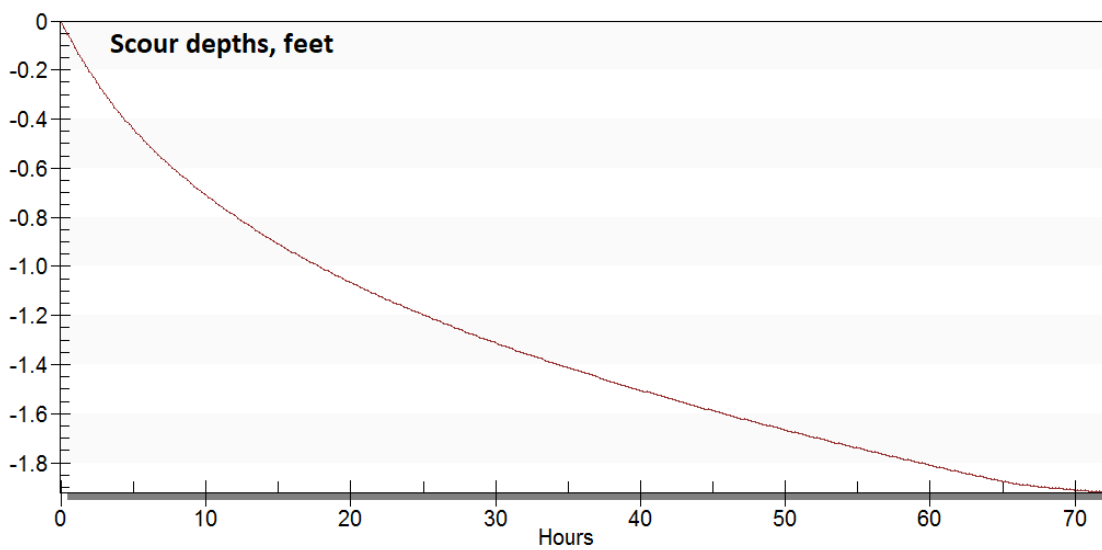
Figure 18. Scour depth evolution in front of the gate

Conclusions

WEST developed a two-dimensional numerical model using SRH-2D (USBR, 2017) to evaluate sediment transport through Nolichucky Reservoir on the Nolichucky River in eastern Tennessee, upstream of Nolichucky Dam. The purpose of this study was to provide scour and sediment loading predictions for spillway operations that TVA is planning for upcoming gate replacement and operation.

The model results indicate that the existing velocities and shear stresses in the reservoir are very low and are not strong enough to move significant amounts of sediment for a flow rate of 1,900 cfs. Sediment concentrations for existing conditions with the gate closed were found to be around 3 mg/L across the lake thalweg. Sediment concentrations were found to reach a peak value of about 100 mg/L after the gate is open and will reach a value of about 20 mg/L after 24 hours. Because of the limited predicted sediment transport, only a small amount of scour was identified, with a maximum scour of about 1.9 feet immediately in front of the gate. The resulting volume of sediment scoured was approximately 11 cubic yards, a significantly lesser volume than the 9,500 cubic yards expected to be moved with the gate closed during a flow of 13,000 cfs, a flowrate that occurs at the site approximately yearly.

Because the bathymetry near Nolichucky Dam (within about 80 feet of the face) was uncertain, a simulation was also performed with an artificial flat bed in this area at an elevation equal to the existing sediment accumulation upstream. In the presence of the flat bathymetry, the resulting sediment concentration at the gate was on average 30 mg/l, with a peak of about 160 mg/l during the initial transient period after the gate is fully open. Because of the increased sediment transport, the maximum scour after a flow duration of 2 days was 6.6 feet in front of the gate. This scour hole is about 33% of the actual scour hole that is currently in front of the gate, indicating that a period longer than 2 days would be necessary to scour the flat bathymetry to match the existing bathymetry.

The flat bathymetry scenario can be considered as representative of a situation in which stratification effects (cold, dense water at the bottom) prevent water from flowing freely in the deepest lake section closest to Nolichucky Dam. The stagnant water at low elevations would have the effect of reducing the flow area, thereby increasing flow velocities. In the model, however, the flat bed consists of sediment which can be mobilized and produces higher concentrations than would be observed if flow were over a stagnant body of water in front of the dam.

An additional simulation representing a flow of 13,000 cfs (an event expected to occur yearly) over the dam with the gate closed was run in order to compare the sediment transport results with the condition of an open gate and a flow of 1,900 cfs. The comparison indicated that a flow of 13,000 cfs would induce a much higher shear stress and the sediment concentration would reach a value of about 600 mg/L along the lake thalweg. Given these results, the small amount of sediment directly above the gate that could potentially move in response to gate operations is inconsequential compared to the larger volume of sediment moved by existing processes at an approximately yearly interval.

Two-Dimensional model, Version 3.2.0, March 2017.

Projecting Floodplain Depositional Patterns Using Long-Term 1D Sediment Modeling Results and Short-Term 2D Hydraulic Model Output

John Shelley, Civil Engineer, U.S. Army Corps of Engineers, Kansas City District, 601 E 12th St., Kansas City, MO, john.shelley@usace.army.mil

Abstract

Locust Creek is a perched channel that flows through Pershing State Park, an ecologically sensitive area in north-central Missouri. Over the past two decades, excessive floodplain deposition from Locust Creek has smothered unique and important habitats in the park. An analysis tool was needed to assess multiple options for reducing the floodplain deposition. A 1D mobile bed model by itself was insufficient, as it could not correctly distribute the sediment laterally in the floodplain. A 2D mobile-bed model for the area was untenable due to the large spatial extent of the system and the long time frame (50 years) for desired projections. In order to model this system, outputs from an HEC-RAS 1D, long-term mobile bed model simulation and an HEC-RAS 2D hydraulic model output from three discreet, synthetic flood hydrographs were combined.

Introduction

Locust Creek is a perched, sand-bed channel that flows through Pershing State Park in north-central Missouri (Figure 1). Over the past two decades cycles of channel aggradation and log jams has caused Locust Creek to abandon its historic channel, cut new channels in the floodplain, and flow into an undersized drainage ditch. This process has deposited tremendous quantities of sediment on sensitive wet prairie habitats in the park. A U.S. Army Corps of Engineers feasibility study is currently assessing potential habitat restoration solutions.
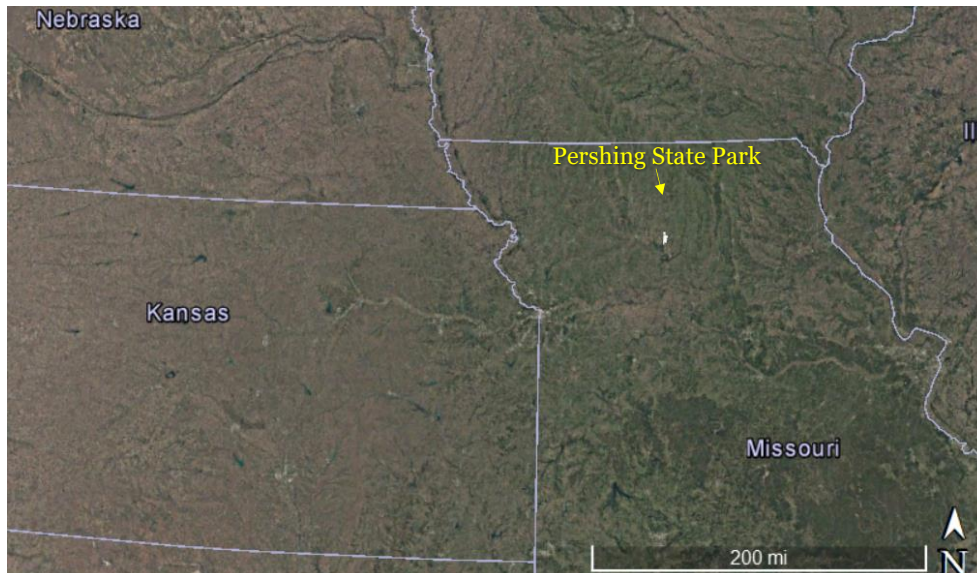
Figure 1. Location of Pershing State Park (Left).

As a part of the study, a modeling tool was needed to assess how potential alternatives would impact floodplain deposition. The complex hydraulics clearly called for a 2D modeling framework. However, the large surface area and desired long-term projections (50 years) made 2D mobile-bed modeling untenable.

For practicality, a modeling framework was developed which includes an uncoupled HEC-RAS 1D sediment model and 2D hydraulic model. The 2D model provides important flow inputs used to develop 1D model boundary conditions. The 2D model was also used as a "post-processor" to more realistically distribute the modeled 1D sediment floodplain deposition volumes.

The graphs and figures presented here are drafts provided to demonstrate the modeling process. The final analyses and results will be documented in the Grand River Basin Ecosystem Restoration Study feasibility report, which may differ from those presented here.

HEC-RAS 2D Hydraulic Model for Flow Boundary Conditions

The model domain begins in a relatively straight channel at a gaged location. Just upstream of Pershing State Park, however, flow bleeds off from the main channel through multiple "pirate channels" into Higgins Ditch (see Figure 2). RAS 2D, by computing hydraulics on sub-grid bathymetry, allowed a workable way to compute the combined effect of many small "pirate channels." The 2D model was used to generate flow-split rating curves that were used to create the upstream boundary condition for the 1D sediment model.
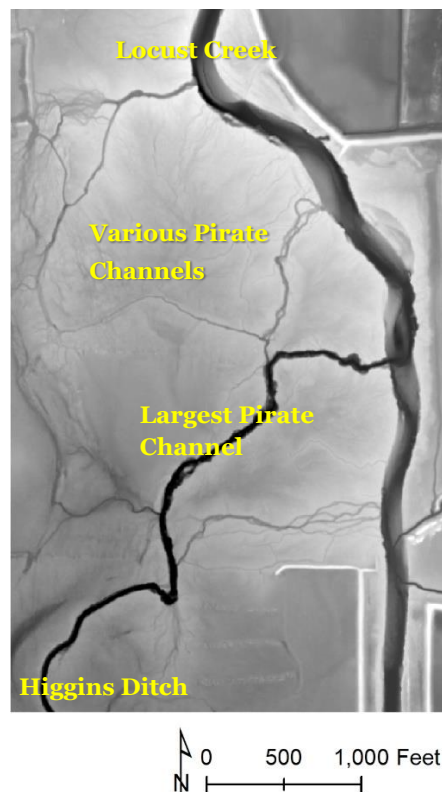
Figure 2. LIDAR indicating pirate channels that steal water from Locust Creek. Flow is from top to bottom.

HEC-RAS 1D Mobile-bed Sediment Model for Long-term Projections

The HEC-RAS 1D sediment model was used to simulate two channels (Higgins Ditch and the old Locust Creek) through Pershing State Park to predict channel change and floodplain sedimentation volumes. The 1D model results in longitudinal cumulative volume change curves, such as in Figure 3.
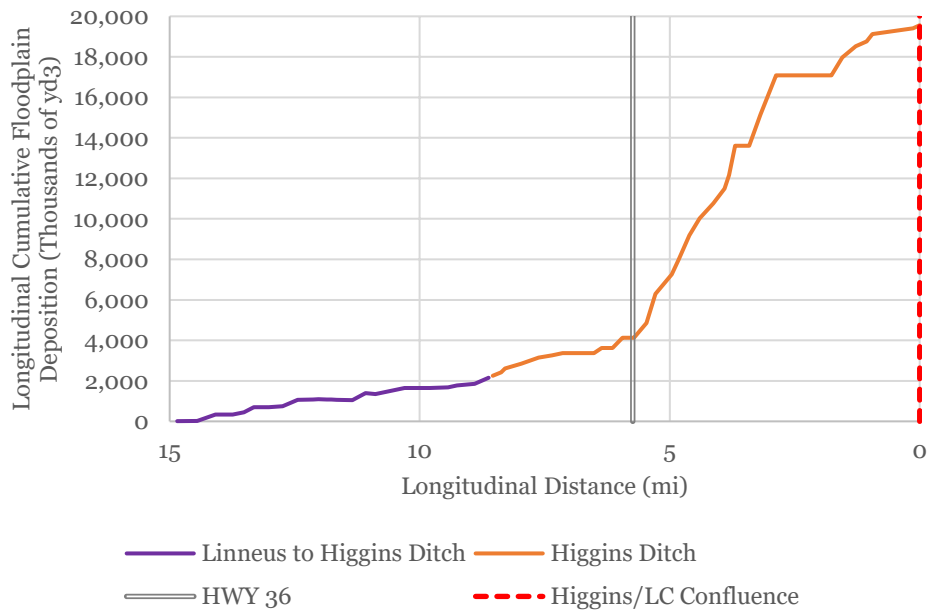
Figure 3. Longitudinal Cumulative Volume Curve

HEC-RAS 2D Hydraulic Model for Lateral Floodplain Deposition

HEC-RAS 1D uses the "veneer method" for distributed floodplain sediment; RAS spreads the deposition volume over all wetted nodes equally, resulting in an even veneer of sediment. Such an approximation can inadequately describe the patterns of overbank sediment deposition in complex floodplains. In order to provide more realistic floodplain deposition locations and amounts, the HEC-RAS 2D model was used to approximate the sediment distribution following these steps:

1. Three representative overbank hydrographs were run through the 2D hydraulic model, with a 10%, 20%, and 50% annual exceedance probability (i.e. a 10 year, 5-year, and 2-year flow, respectively).
2. The 2D model produced raster output for the duration of inundation of at least 0.1 ft and for the maximum depth.
3. A weighting factor was generated in GIS according to the following equation:

$$W = 0.2 * D_{10}t_{10} + 0.2 * D_5 t_5 + 0.6 * D_2 t_2$$

Where W = the weighting factor for an individual cell within a habitat area.

t = the duration of inundation for a given cell for the 10-year, 5-year, or 2-year hydrograph

D = the maximum depth of inundation for a given cell for the 10-year, 5-year, or 2-year hydrograph

This weighting accounts for the relative frequency of each event in a hypothetical 10-year period with one 10-year event, one 5-year event, and three 2-year events. This conforms to the definition of each of these statistically-defined flows (i.e. the 10-year flow has an annual exceedance probability of 0.1, the 5-year has an annual exceedance probability of 0.2, and the 2-year has an annual exceedance probability of 0.5.)

This weighting produces reasonable lateral trends in that areas more frequently inundated will deposit more and that areas inundated to greater depths will deposit more. (See Figure 4.)

4. Sum the weighting factors in each habitat area.
5. Use these summed weighting factors to laterally apportion sediment volume from the 1D sediment model in locations where the model cross section spans more than one habitat area.
6. Divide each weighting factor value by the summed weighting factor for the habitat area to create a raster of normalized weighting factors which define the fraction of the total deposition volume in the habitat area assigned to each cell. (See Figure 4.)
7. Multiply the normalized weighting factor (fractional volume) for each cell by the total deposition volume for the habitat area to create a per-cell deposition volume.
8. Divide by the cell area to create a per-cell deposition depth.
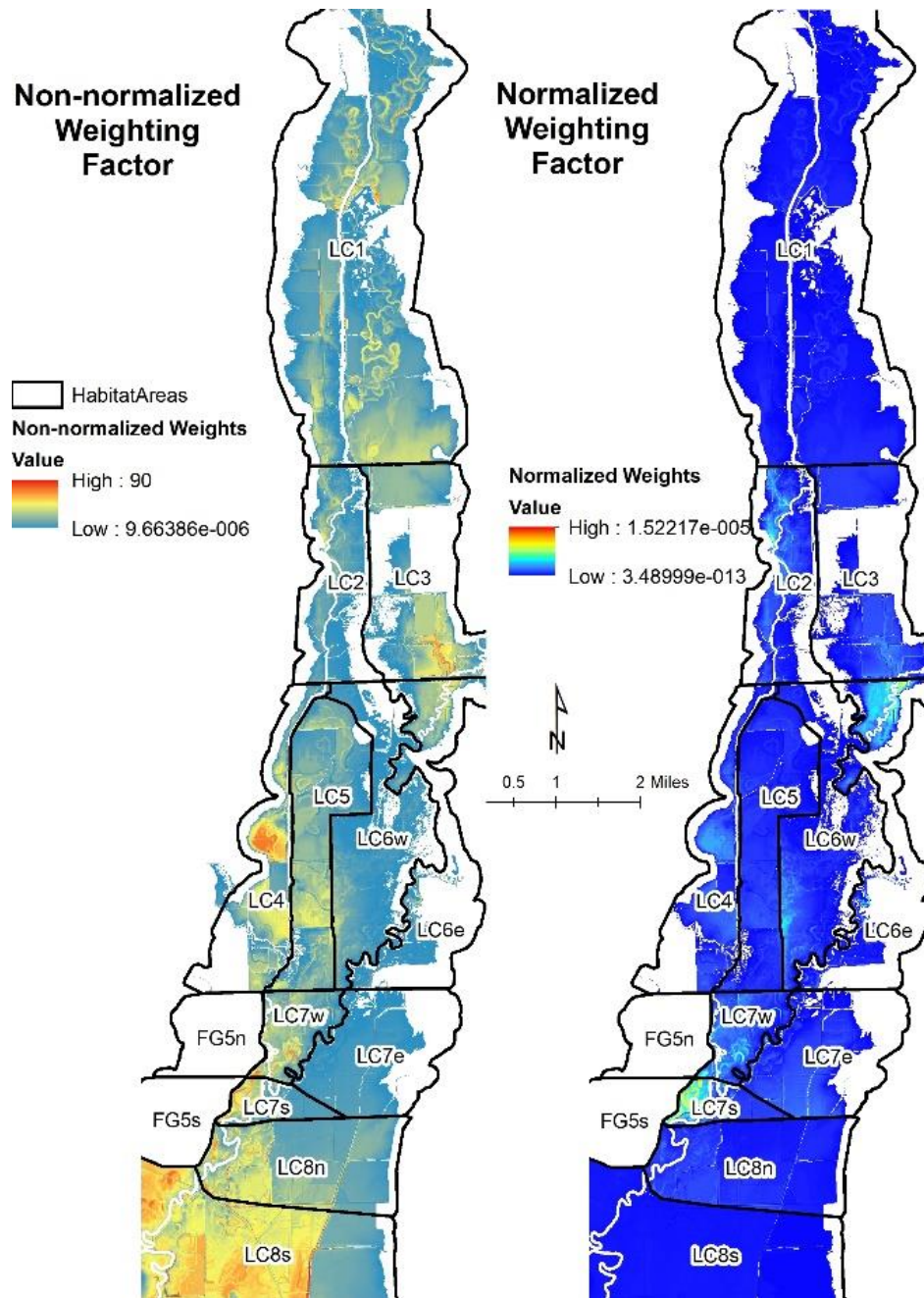
Figure 4. Weighting Factors from Steps 3 and 6

The result of this analysis is that the upstream-to-downstream distribution of sediment is a function of the 1D sediment model. The lateral distribution of sediment is a function of the 2D hydraulic model. The deposition depths (Figure 5) are reasonable estimates for testing alternatives and assessing future habitat values.
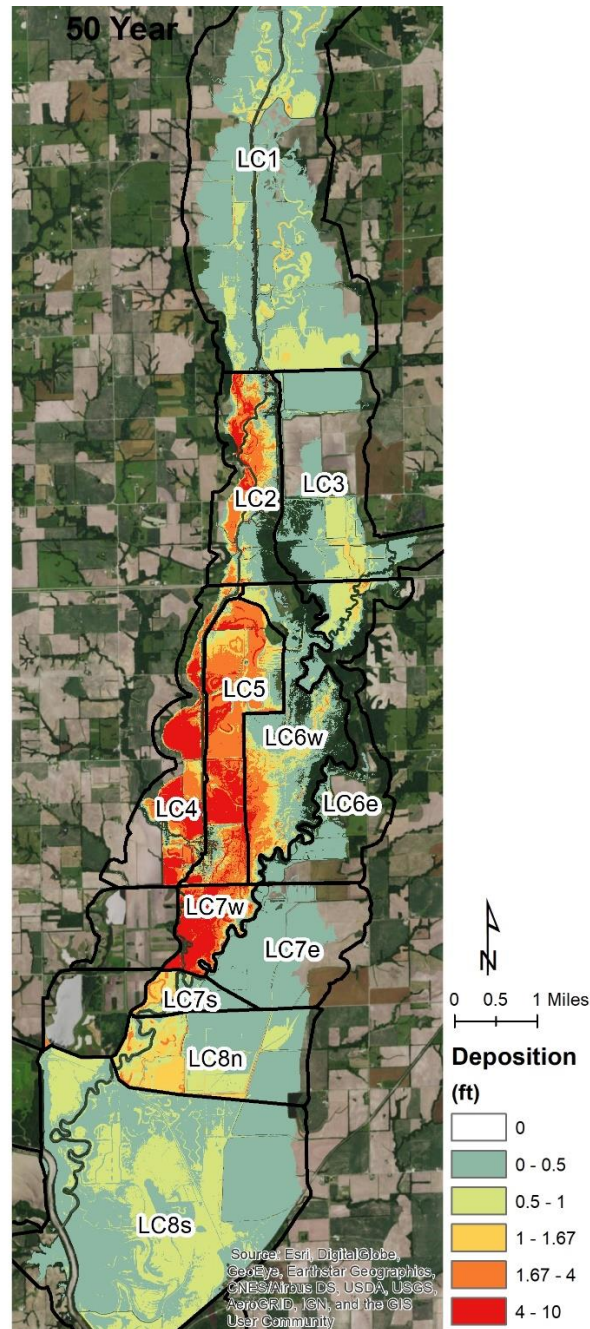
Figure 5. Floodplain Deposition

Conclusions and Limitations

This approach is not as accurate as a fully-coupled 2D flow/sediment model. In addition, it required the extra work of updating two models every time assumptions or alternatives changed. However, the 50-year sediment simulation ran in under three hours on a personal computer, which was faster than running even a single year of fixed-bed hydraulics through the 2D model.

Notwithstanding the limitations, the approach documented in this paper provided more reasonable and actionable results than a 1D modeling approach by itself could provide.

Acknowledgements

Rainfall-Runoff Relationships Complementing Previous Sediment Transport Studies at the Arroyo de Los Piños, Socorro, New Mexico

Madeline Richards, New Mexico Institute of Mining and Technology, Socorro, NM
madeline.richards@student.nmt.edu
Dr. Daniel Cadol, New Mexico Institute of Mining and Technology, Socorro, NM,
daniel.cadol@nmt.edu
Dr. Jonathan B. Laronne, Ben Gurion University of the Negev, Beer Sheva, Israel,
john@bgu.ac.il
David Varyu, United States Bureau of Reclamation, Denver, CO, dvaryu@usbr.gov
Kyle Stark, New Mexico Institute of Mining and Technology, Socorro, NM,
kyle.stark@student.nmt.edu
Stephen Brown, US Army Corps of Engineers, stephen.w.brown@usace.army.mil

Abstract

In semi-arid climates, sediment influx to large rivers, such as the Rio Grande, from small ephemeral streams is challenging to quantify (Bull, 1997). Small ephemeral streams are not studied as often as perennial streams because of their erratic nature and the fact that they are usually located in hard to access, remote deserts where flash floods are common. The Arroyo de los Piños is currently one of very few study sites collecting data on water velocity and discharge, bedload and suspended sediment, as well as other measurements that may be relevant during a flood event. This study site is located close to the confluence of the arroyo and the Rio Grande, yet data on the contributing watershed are lacking. Gaining a clearer picture of stream connectivity and rainfall-runoff relationships in this channel will be useful for quantifying flow generation as well as aquifer recharge and transmission loss through the stream bed. These processes affect flow conditions, and thus sediment transport.

Over the past monsoon season seventeen Hobo U20 pressure transducers were installed in the Arroyo de los Piños watershed (Figure 1). These absolute pressure loggers monitored water level at five-minute intervals. Atmospheric pressure loggers allow compensation of barometric pressure, which can very considerably under different atmospheric conditions. To determine the hydrostatic pressure associated with a change in water stage, we subtract the atmospheric pressure from the total (atmospheric and hydrostatic) pressure monitored by the loggers in the channel. In addition, one recording rain gauge was added to the two existing gauges. For this analysis, we focus on the two rain gauges towards the middle of the watershed (Rain Gauge A and B in Figure 1). The placement of the loggers and rain gauges aim to capture geologic heterogeneities within the watershed. Being able to determine the geology that experiences overland flow during a given event likely has implications for the composition of the sediment transported to the monitoring study site (Stonestrom et al., 2007).
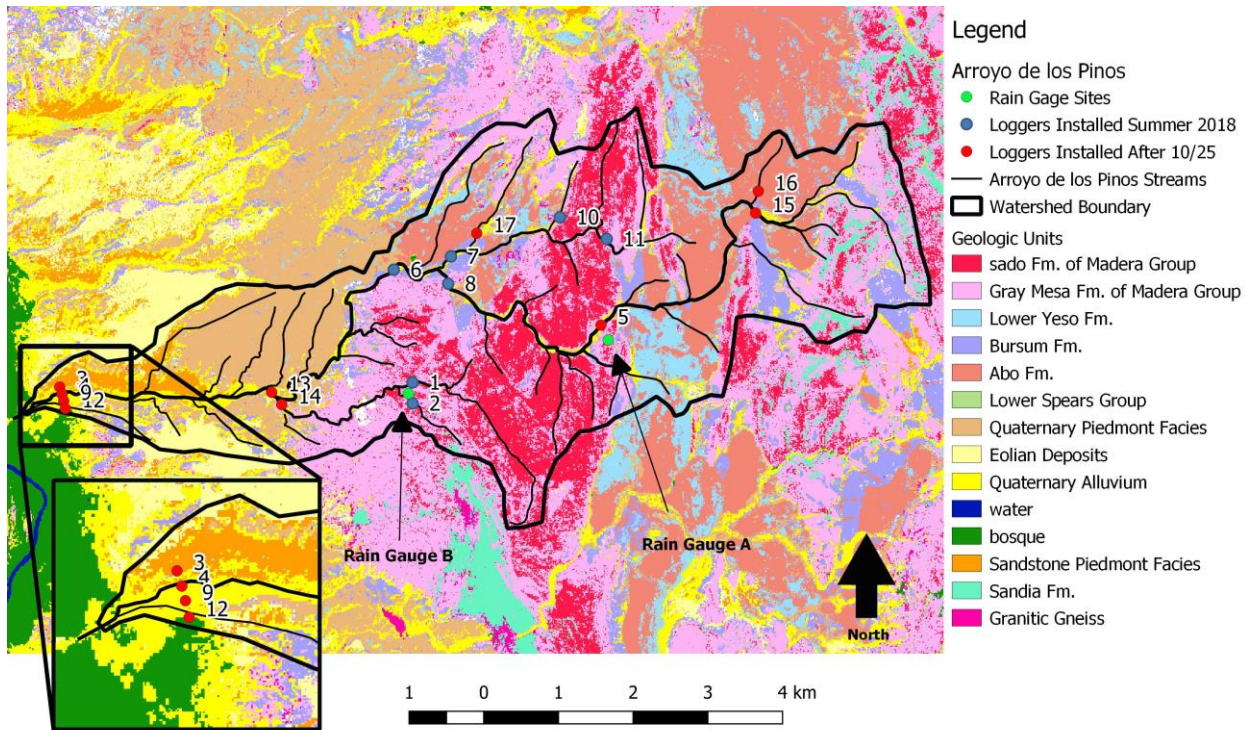
Figure 1: Arroyo de los Piños pressure transducer and rain gauge sites, with inset of closely placed pressure transducers in the lower braided reach. The underlying geologic map is adapted from Cather 2005. Red circles are pressure transducers installed after the two storms looked at in this paper (we do not have flood data at these sites).

Several floods have been recorded in the arroyo tributaries since the loggers have been installed. Here we investigate two flood events (October 2-3 and October 23-25, 2018) to illustrate how flow propagated through the network of tributaries.

Both flood events produced small floods that arrived at the basin outlet to the Rio Grande. The first event took place from the evening of October 2, to the morning of October 3 (Figure 2). Rainfall in this event was most intense in the northern portion of the watershed, and therefore runoff was only registered in tributaries located in this part of the basin.
Water first occurred at sites 10 and 11 (Figure 1, 2), on two small tributaries draining the Madera Group, which is dominated by limestone. Subsequent flow was observed at sites 8, and 7, larger channels farther downstream.
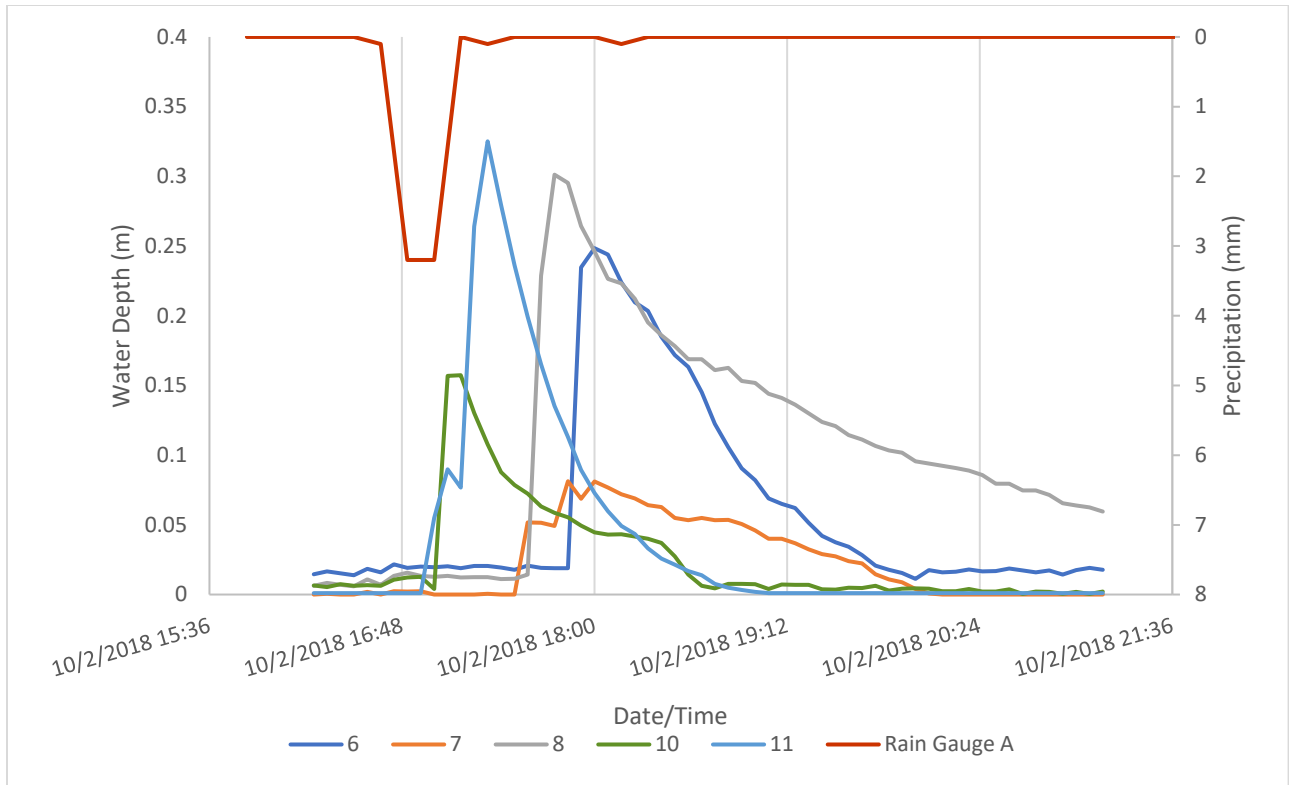
Figure 2: Tributary stage hydrographs as of October 2-3, 2018. Flow was quickly routed downstream from upper tributaries (10 and 11) to the confluence of two main tributaries (7 and 8) and eventually to the basin outlet.

Moderate rainfall over three days (October 22 – 24) caused two distinct flow events on October 22 and on October 24 (Figure 3). Both events were small although recession limbs lasting a few hours are observed. Some water remained in the stilling well after each event and slowly infiltrated into the local aquifer. This is why the graphs of water depth do not return to zero as soon as expected; it is a remnant effect of pooled water. Tributary 6 was first to respond with a small pulse of water, shortly followed in tributaries 2, 8, 11, 10, and 7. From this order and timing it appears that the storm cell was strongest in the center, and weaker towards the eastern and western portions of the watershed.
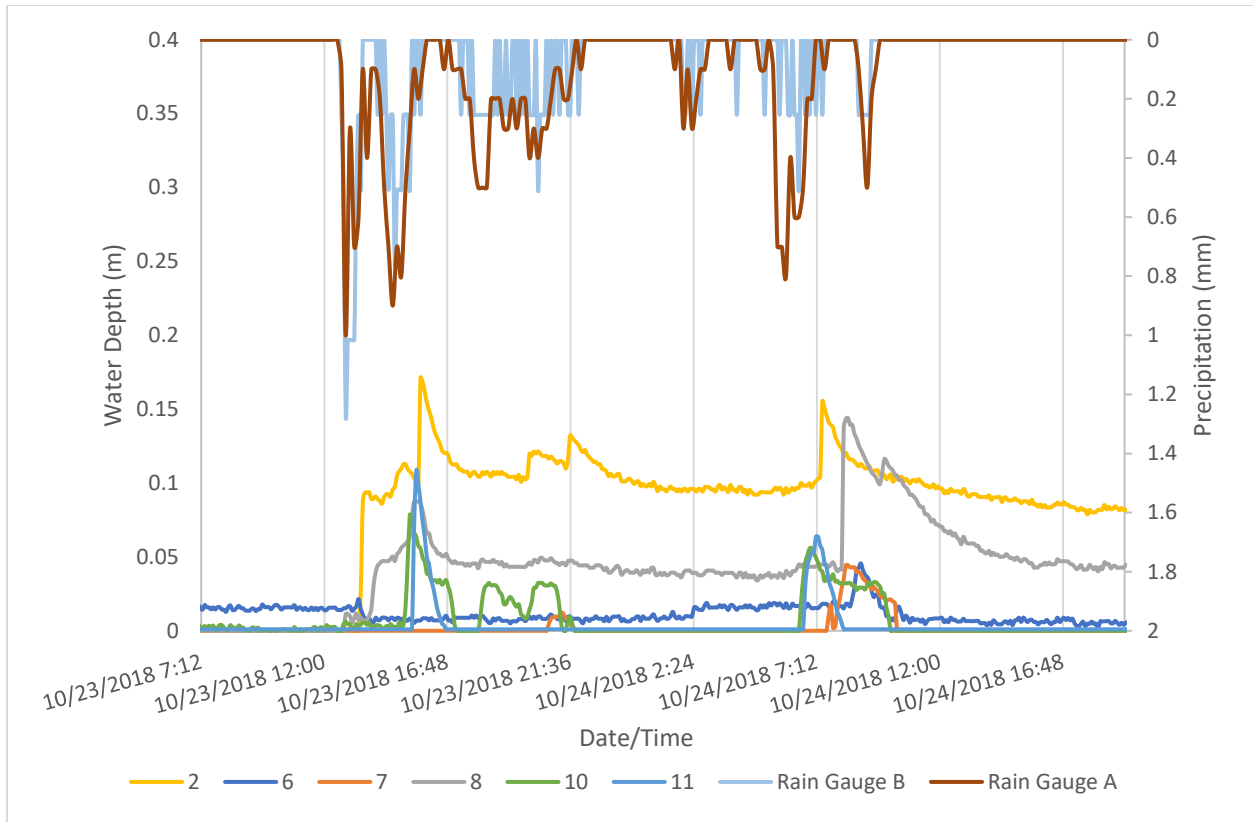
Figure 3: Tributary histograms for October 23. Flow was initiated at pressure transducer 2 in the southern portion of the basin, quickly followed by flow at 8, 10, 11, and 7 in the northern part of the basin.

Through pressure transducer data we can infer the pathway the storm took, and to some degree the intensity of the storm. We can also document which lithologic units produced flow most readily. We have limited rainfall and runoff data from 2018, but now that pressure transducers and rain gauges are installed and fully functional, our instrument coverage for the 2019 monsoon season will allow us to more accurately describe rainfall-runoff relationships in the Piños.

It would be very helpful to have discharge hydrographs instead of stage hydrographs. This would allow us to make better comparisons between the flooding at each cross section, since the cross-sectional area of the channel, channel slope, and roughness vary at each pressure transducer site. Discharge is calculated by multiplying the cross-sectional average water velocity by the cross-sectional area to get a volumetric flux of water. However, at the pressure transducer sites it is not feasible to collect velocity measurements for every flood, and so we will use the Manning's equation to circumvent the velocity measurement. For SI units, the Manning's equation is:

$$V = \frac{1}{n}\left(\frac{A}{P}\right)^{2/3} S^{1/2}$$

Where V is velocity, n is the roughness coefficient, A is the cross-sectional area, P is the wetted perimeter, and S is water surface slope. We make the assumption that water surface slope is essentially equal to bed slope. Figure 4 shows the discharge hydrograph that corresponds with pressure transducer 6 and 8 for the flood on October 2nd. In figure 2, cross section 6 and 8

appear to have similar storm hydrographs. In comparison, in figure 4, cross section 6 and 8 show very different trends. This highlights the importance of comparing discharge at each site instead of stage.
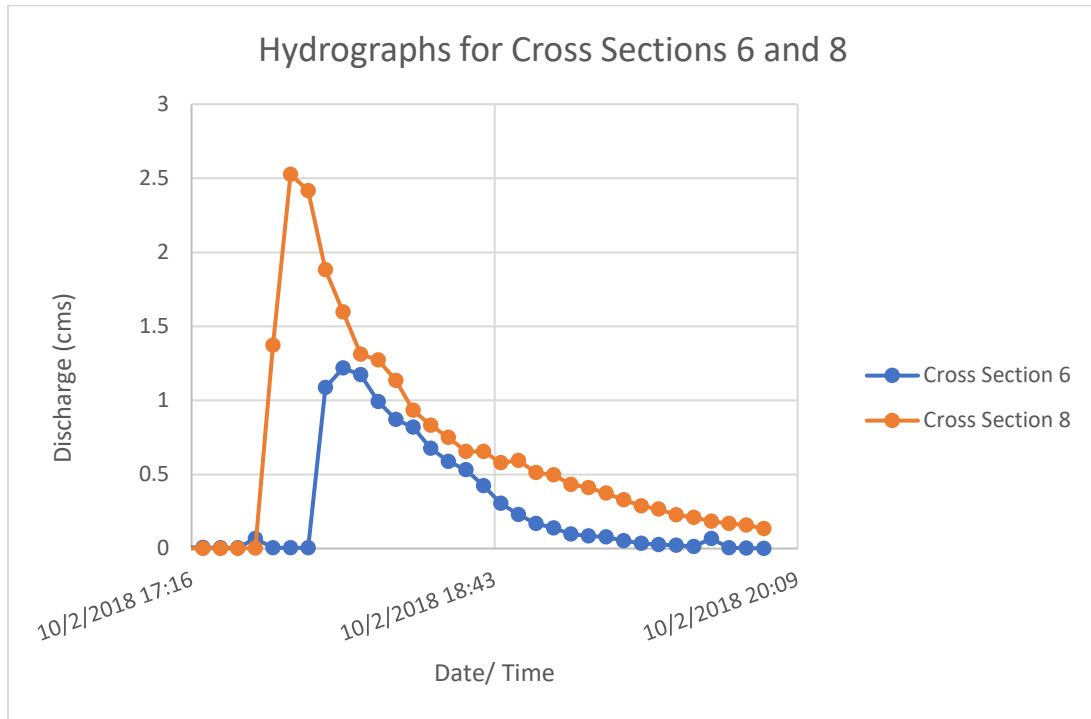
Figure 4: Discharge Hydrograph for cross sections 6 and 8 on October 2.

It is extremely important that we continue to collect more physical precipitation measurements when trying to find a relationship between rainfall and runoff in the Arroyo de los Piños watershed. Radar data available through NEXRAD is not well correated with the precipitation measurements collected using a tipping bucket rain gauge (shown in figure 5). Figure 5 shows precipitation plotted against the NEXRAD reflectivity. Both the reflectivity and rainfall data are taken over 15-minute intervals. The rainfall data is a point source measurement (collected at rain gauge A) while the reflectivity values were averaged over the five raster cells surrounding the rain gauge.
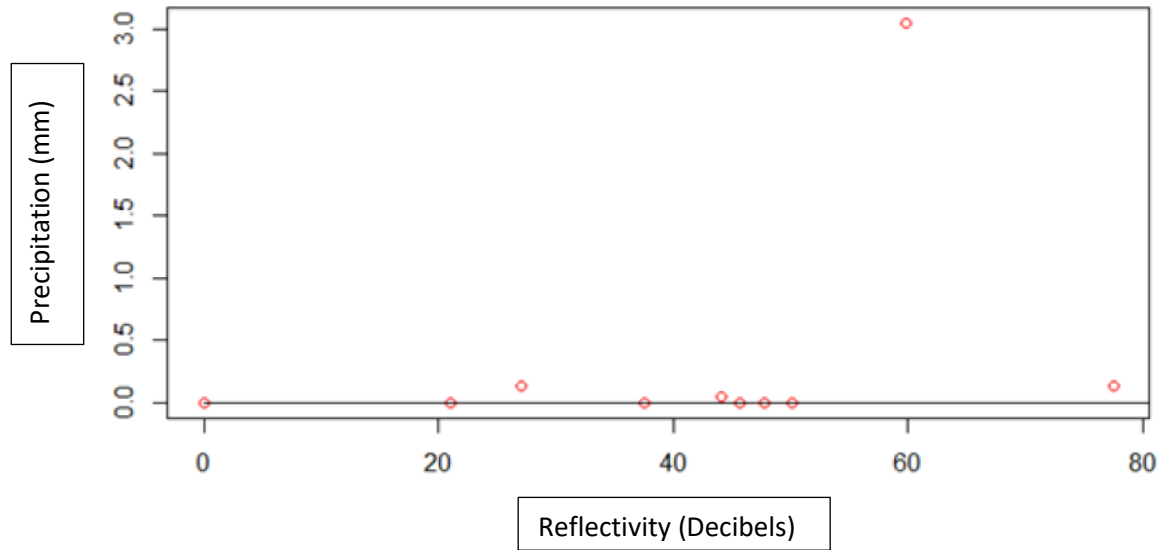
Figure 5: Correlation between NEXRAD reflectivity and tipping bucket precipitation.
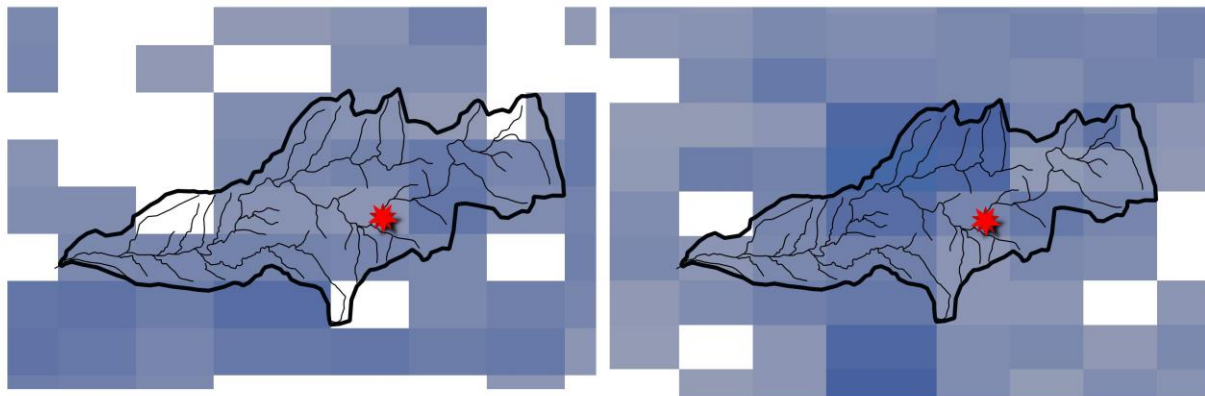
Figure 6: NEXRAD reflectivity raster for October 2nd storm. The left image is from 17:00, and the right is from 18:00. The red star shows the location of the rain gauge used in this analysis.

Figure 6 shows two reflectivity rasters (the left is from 17:00 and the right is from 18:00). Our rain gauge (shown as a red star) measured rain at 17:00, but no rain at 18:00. However, this is the opposite trend shown by the NEXRAD reflectivity raster (figure 6). This highlights the need for a wider array of tipping bucket rain gauges in the watershed to accurately capture the spatial distribution of the storms.

References

Bull, Bill B. (1997). Discontinuous Ephemeral Streams. *Geomorphology 19*. 1-50.

Cather, S. M., & Colpitts, R. M. (2005). *Geologic Map of the Loma de las Cañas Quadrangle, Socorro County, New Mexico*. Socorro, New Mexico.

Stonestrom, David A., Constantz, Jim, Ferre, Ty P.A., Leake, Stanly A., (2007). Ground-Water Recharge in the Arid and Semiarid Southwestern United States. USGS Professional Paper 1703.

Rational Alternative to Linear Excess Shear Stress Formulation for Modeling Fluvial Erosion in Noncohesive Bank Materials Mobilized as Bedload

David M. Waterman, Assistant Professor, Department of Civil and Environmental Engineering, South Dakota School of Mines and Technology, Rapid City, SD, david.waterman@sdsmt.edu

Kory M. Konsoer, Assistant Professor, Department of Geography and Anthropology, Louisiana State University, Baton Rouge, LA, kkonsoer@lsu.edu

Marcelo H. García, Professor, Department of Civil and Environmental Engineering, University of Illinois at Urbana-Champaign, Urbana, IL, mhgarcia@illinois.edu

Realistic numerical modeling of stream morphodynamics requires realistic physical representation of bank erosion. The state-of-the-art bank erosion models that are primarily utilized in practice, BSTEM and CONCEPTS, are being incorporated into a wide range of morphodynamics models. These bank erosion models incorporate the key physical processes of fluvial erosion and mass failure. A knowledge gap has been identified in the research literature regarding the ability to properly parameterize the linear excess shear stress formulation used to quantify fluvial erosion when applied to coarse-grained bank material mobilized as bedload. Such bank materials are commonly encountered in composite river banks containing coarse basal material overlain by fine-grained soil.

In this analysis, the linear excess shear stress formulation is abandoned in favor of the sediment mass conservation equation (Exner equation) with a constitutive relationship for bedload transport rate on a transverse slope. Only the divergence terms in the transverse direction are considered, which allows treatment of individual cross sections in the same modeling framework as BSTEM and CONCEPTS. Simple representations of the boundary shear stress distribution and the modification of the boundary shear stress vector due to secondary flow are implemented. The numerical treatment of the Exner equation is implemented using a finite difference method. If only the bank region is considered rather than the entire cross section, properly establishing the boundary condition at the base of the bank is of critical importance. A flux boundary condition yields realistic results when coupled with a simple bulk depositional model for the point bar region. The bulk depositional model allows the basal boundary to migrate a unit transverse distance when the time-integrated transverse flux of sediment past the thalweg equals the depositional volume required to cause the point bar to shift toward the thalweg by a unit transverse distance.

The current analysis is based on a field site on the lower Wabash River, located on the Illinois-Indiana border, at a bend known as Maier Bend. The river bank contains predominantly coarse sand bank material with only a thin upper layer of fine-grained soil. The data used was from spring 2011 bathymetry obtained during high flows and bank soil data obtained the following summer (Konsoer et al. 2016a; 2016b). A plan view of the site is shown on Fig. 1; cross sections labeled MB148 and MB149 are illustrated on Fig. 2. The cross-section geometry measured during high flow conditions in May 2011 for MB149 is used as the initial condition of the current model. To illustrate the characteristic behavior of bank deformation when comparing BSTEM to the current approach, the noncohesive layer is simplified with a single characteristic grain size equal to 1.0 mm coarse sand. This represents a spatially-averaged mean grain size in Meier bend sampled along the bank at an approximate elevation of 111 m, which corresponds to approximately half the bank height as measured from the high-flow thalweg (elev. ≈ 104 m) to

the top of bank (elev. ≈ 117 m). Flow conditions were set with water surface elevation at bankfull depth throughout the duration of the simulation. The BSTEM simulation was run by implementing the fluvial erosion module in 48-hour time intervals, after which the bank stability module was run to check for potential mass failure before proceeding with the next fluvial erosion interval. The critical shear stress (τ_c) for 1.0-mm sand was set equal to 0.71 Pa; the erodibility coefficient (k) was set equal to 0.119 cm³/Ns. Both the τ_c and k value were calculated by the BSTEM algorithms based on 1.0-mm sand.
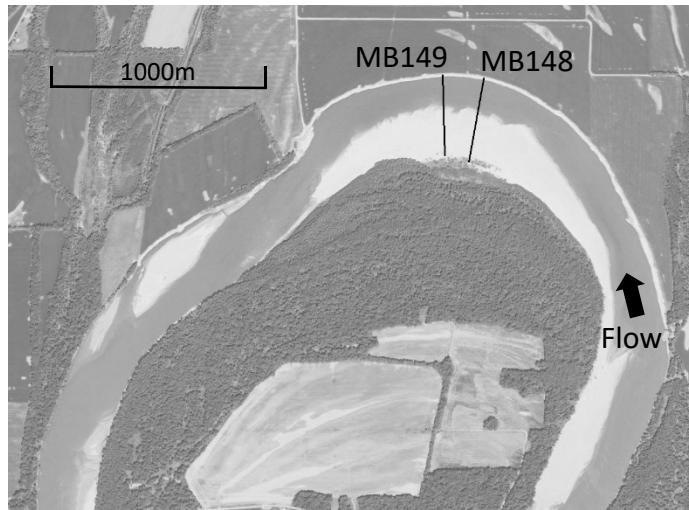
Figure 1. Plan view aerial photograph in fall 2011; source: Google Earth. Note that the field measurements of Konsoer et al. (2016a, 2016b) were from spring 2011.
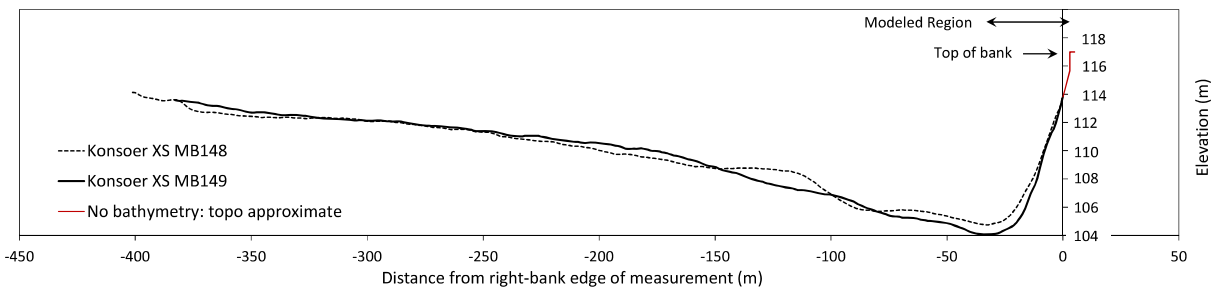
Figure 2. Cross-sections from bathymetric measurements near the bend apex; from the 2011 field measurements of Konsoer et al. (2016a, 2016b). Note that top of bank is at approximate elevation 117 m.

A side-by-side comparison of BSTEM results with the current model results are illustrated in Figures 3 and 4. Because the boundary shear stress increases with depth, the linear excess shear stress formulation for fluvial erosion yields continual steepening of the bank under steady hydrodynamic conditions near the bankfull depth until a mass failure involving nearly the full bank height results. On the other hand, the present model yields development of a concave upward bank shape in the noncohesive bank material that steepens with height above the thalweg; development of steep slopes exceeding the friction angle (imminent failure) only occur fairly high on the bank near the interface where the boundary shear stress drops below the critical value. Continuing evolution of the bank yields a translating bank profile with only modest deviations in profile shape due to shallow mass failures. The net migration of the toe of slope (thalweg) was similar between the two models: BSTEM produced a toe migration equal to 22.4 meters over the 52-day simulation period; the Exner-based model produced toe migration

equal to 18.0 meters over the 52-day simulation period. However, the migration distance for the remainder of the bank was grossly different between the two models. BSTEM yielded very modest top of bank migration (0.9 m) over the first 52-days, followed by a large-scale mass failure resulting in a net bank migration of 5.2 meters over the 52-day simulation period. The Exner-based model resulted in continuous migration of the top of bank, with a net bank migration of 36.6 meters over the 52-day simulation period.
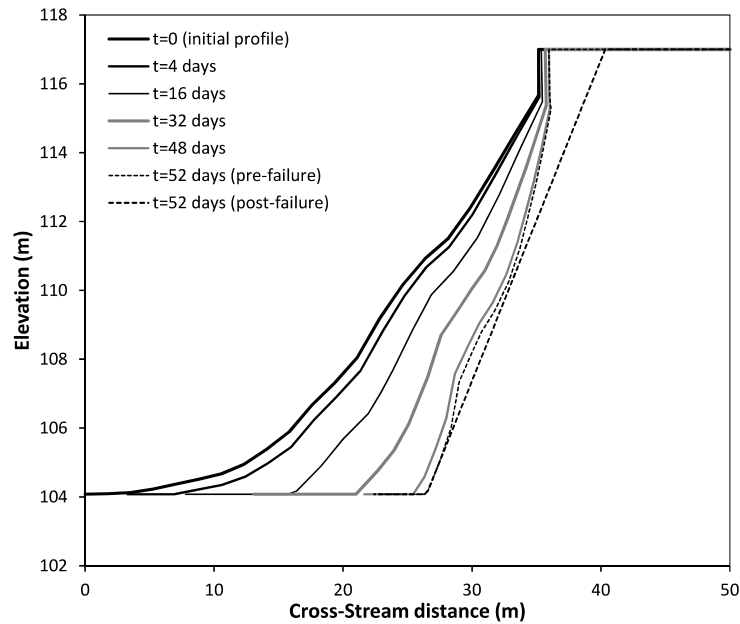
Figure 3. Bank erosion results from BSTEM starting from the initial bank profile of XS MB149, with bank-full flow for 52 consecutive days (first mass failure).
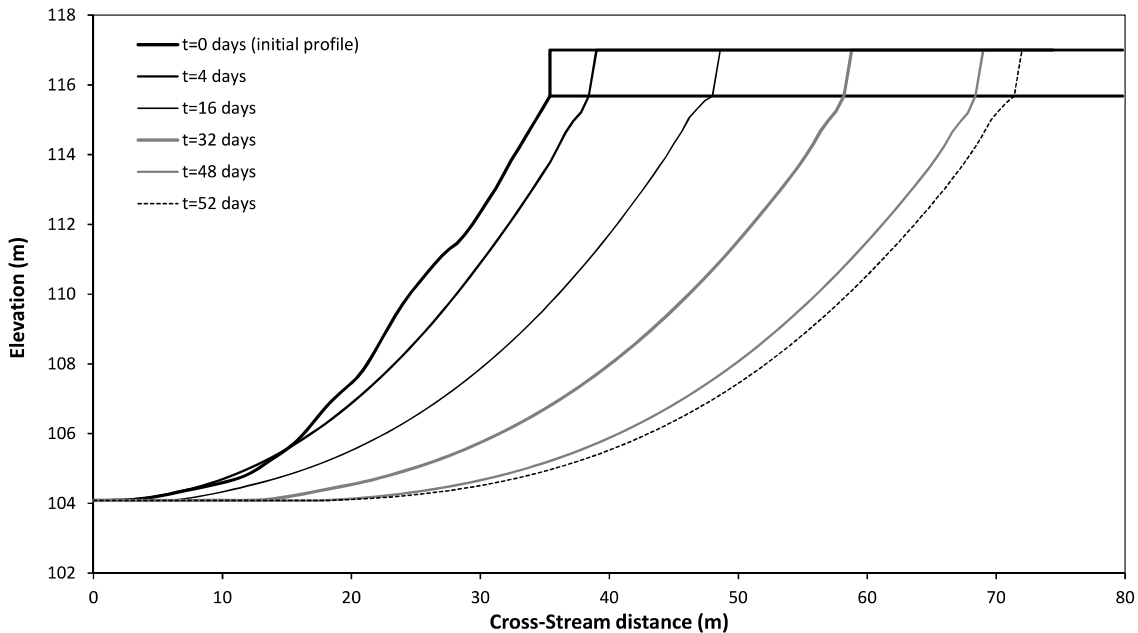
Figure 4. Bank erosion results from the present modeling approach; same initial bank profile and same duration of bankfull flow as Fig 3.

The present model for fluvial erosion of coarse-grained materials is certainly more complex and computationally expensive than the linear excess shear stress formulation used by BSTEM and CONCEPTS; however, the model is more theoretically sound and requires no arbitrary parameterizations. When long simulation time scales are required, the finite-difference scheme can be replaced with a simple migration-rate formula based on an integration of the Exner equation over the bank region.

References

Konsoer, K. M., Rhoads, B. L., Best, J. L., Langendoen, E. J., Abad, J. D., Parsons, D. R., and García, M. H. (2016a). "Three-dimensional flow structure and bed morphology in large elongate meander loops with different outer bank roughness characteristics," Water Resources Research, 52(12), 9621-9641.

Konsoer, K. M., Rhoads, B. L., Langendoen, E. J., Best, J. L., Ursic, M. E., Abad, J. D., and García, M. H. (2016b). "Spatial variability in bank resistance to erosion on a large meandering, mixed bedrock-alluvial river," Geomorphology, 252, 80-97.

Sediment Routing Study and Impact Analysis of USACE Management of the Missouri River, 1994-2014

Miles Yaw, PE, Hydraulic Engineer, Tetra Tech, Ft. Collins, CO, miles.yaw@tetratech.com
Robert Mussetter, PhD, PE, Program Manager, Tetra Tech, Ft. Collins, CO, bob.mussetter@tetratech.com

Abstract

Beginning in 2004, the U.S. Army Corps of Engineers (USACE) implemented a series of habitat restoration actions along the Missouri River between Gavins Point Dam and St. Louis to meet requirements of the 2003 Amended Biological Opinion on the Operation of the Missouri River Reservoir and Navigation Systems. These actions targeted habitat for two endangered or threatened bird species (Interior least tern, Northern Great Plains piping plover), and the endangered pallid sturgeon, and included physical modifications to the river channel and overbanks intended to provide suitable shallow-water and overbank habitat for the species. Severe flooding occurred along the entire system in 2011, and local flooding originating from various tributaries occurred in 2007-2010, 2013 and 2014, causing extensive property damage along the reach. Tetra Tech was retained to evaluate the geomorphic and sediment-transport response of the river to the habitat actions in response to allegations that these actions, coupled with changes in the Master Water Control Manual and river maintenance priorities, were responsible for much, if not all, of the property damages. A key aspect of Tetra Tech's evaluation involved development and application of a comprehensive HEC-RAS-based sediment-transport model of the approximately 400-mile reach of the river between Gavins Point Dam and Leavenworth, KS. The model incorporated the available, extensive physical data, which was then modified to represent what-if conditions that assumed certain actions had not been taken. Comparison of the modeling results for the various scenarios clearly showed that the cumulative effects of the habitat and other management actions did not cause a significant adverse impact, and in some cases, actually increased the flood-carrying capacity of the river. This paper will provide an overview of the methods and challenges associated with development, calibration and application of the model, and will summarize the results obtained for various scenarios, including the effects of the habitat and management actions relative to other factors that are not directly related to those actions.

Background

Historical Context

Prior to implementation of the Pick-Sloan Plan (authorized by the Flood Control Act of 1944) and the BSNP (Bank Stabilization and Navigation Project, authorized by the River and Harbor Act of 1945), the Missouri River was braided, shifted frequently, and contained numerous sandbars, islands and unstable banks (Galat et al. 2005). Historical channel widths between Gavins Point and Kansas City were commonly greater than 1,000 feet and ranged up to 6,000 feet. The river carried an enormous sediment load, hence the nickname "Big Muddy" (Galat et al. 2005), and the main channel was prone to significant lateral migration during high-flow periods. Navigation on the river was hazardous due to the frequent, shifting sandbars and high concentration of log jams and submerged snags (Schenk et al. 2014). Flood peaks ranged from about 160,000 cfs at Yankton to over 210,000 cfs at Rulo in about 1 out of 2 years and peaks ranging from about 240,000 cfs to over 300,000 cfs occurred in 1 out of 10 years, on average. As a result, overbank flooding was common.

Leading up to the Pick-Sloan Plan, the USACE developed a comprehensive basin-wide plan to provide flood protection that consisted of a series of mainstem and tributary reservoirs and protection works for municipalities and agricultural lands. The Bureau of Reclamation (BOR) subsequently recommended a plan for basin-wide development of irrigation, hydropower, and other purposes. The Pick-Sloan Plan

represented the integration of the USACE and BOR plans, and it included the six mainstem dams, numerous tributary reservoirs, levees for protection of agricultural lands and municipalities downstream from Sioux City, irrigation delivery systems, and hydroelectric plants on key mainstem reservoirs.

To achieve the objectives of the BSNP, the USACE created a river planform consisting of a series of smoothly-curved bends of appropriate radii and channel widths by protecting the banks on the outsides of the bends with pile and stone-fill revetments to prevent bank erosion and constructing dikes approximately perpendicular to the flow on the insides of the bends to maintain the target width and promote accretion (USACE 2011). The BSNP, declared complete in 1981 (USACE 1988), resulted in a single-thread, "self-scouring" channel that typically provides sufficient energy around the bends to maintain the desired depth. Shoaling can, however, occur in the crossings between the bends that requires supplemental reservoir releases and periodic dredging.

Congress first authorized construction of the Missouri River Bank Stabilization and Navigation Fish and Wildlife Mitigation Project with the Water Resources Development Act of 1986 (Public Law 99-662) (WRDA 86), based on the recognition that the BSNP and other human activities along the Missouri River had caused extensive losses of fish and wildlife resources in the natural channel and meander belt of the Missouri River from Sioux City, Iowa to its mouth near St. Louis, Missouri. As of September 2003, shallow water habitat (SWH) had been created at nine sites in the reach through dike notching, river structure modifications, excavation and dredging (USACE 2004). The USACE dike-notching program was originally implemented in the mid-1970s (USACE 2013a). Prior to implementation of the 2004 Master Manual Revision (MMR), over 700 dikes had been notched between Sioux City, IA and Leavenworth, KS.

By 2014, 23 shallow-water habitat (SWH) chute channels and 14 SWH backwater projects had been constructed within the reach, in addition to revetment lowering and notching at many locations. Following high flows on the Missouri River that caused overbank flooding between 2004 and 2014, allegations were brought forward that departures from the longstanding management policies and practices of the Corps of Engineers (USACE) were responsible for flooding of land and property. These policies and practices include the habitat restoration activities that made physical changes to the Missouri River channel and overbanks to meet requirements of the 2003 Amended Biological Opinion (2003 Amended BiOp) and application of the Master Water Control Manual for operation of the Missouri River Mainstem System [hereafter referred to as the Master Manual Revision (MMR)]. This paper focuses on the reach-scale sediment transport models that were developed and applied to evaluate the effects of changes in operation of the reservoir system associated with the MMR and related habitat enhancement activities on the sediment-transport balance, and the likely effects of those changes on water-surface elevations and flood carrying capacity, of the Missouri River within the reach from Gavins Point Dam (RM 811) to Leavenworth, KS (RM 397). A map of the reach of interest is shown in **Figure 1.**

Modeling Framework

The modeling was performed using the one-dimensional, reach-scale capabilities of HEC-RAS v5.0 (USACE 2016a).

Model Inputs

Bathymetry Three base hydraulic models were available for the analysis. All three models had nearly identical structure but used different bathymetry to represent (1) conditions prior to implementation of the MMR and associated habitat features (c.1998 bathymetry), (2) conditions after the MMR, but prior to the 2011 flood (c.2008 bathymetry), and (3) conditions after the 2011 flood (c.2012 bathymetry). Because of the length and complexity of the study reach and the computational requirements of such a large model, the base hydraulic models were converted from unsteady to quasi-unsteady mode for the sediment-transport analysis. The conversion required significant changes to the geometry data, including removal of lateral structures and storage areas that were included in the original models to facilitate unsteady-flow routing, and tributary reaches.
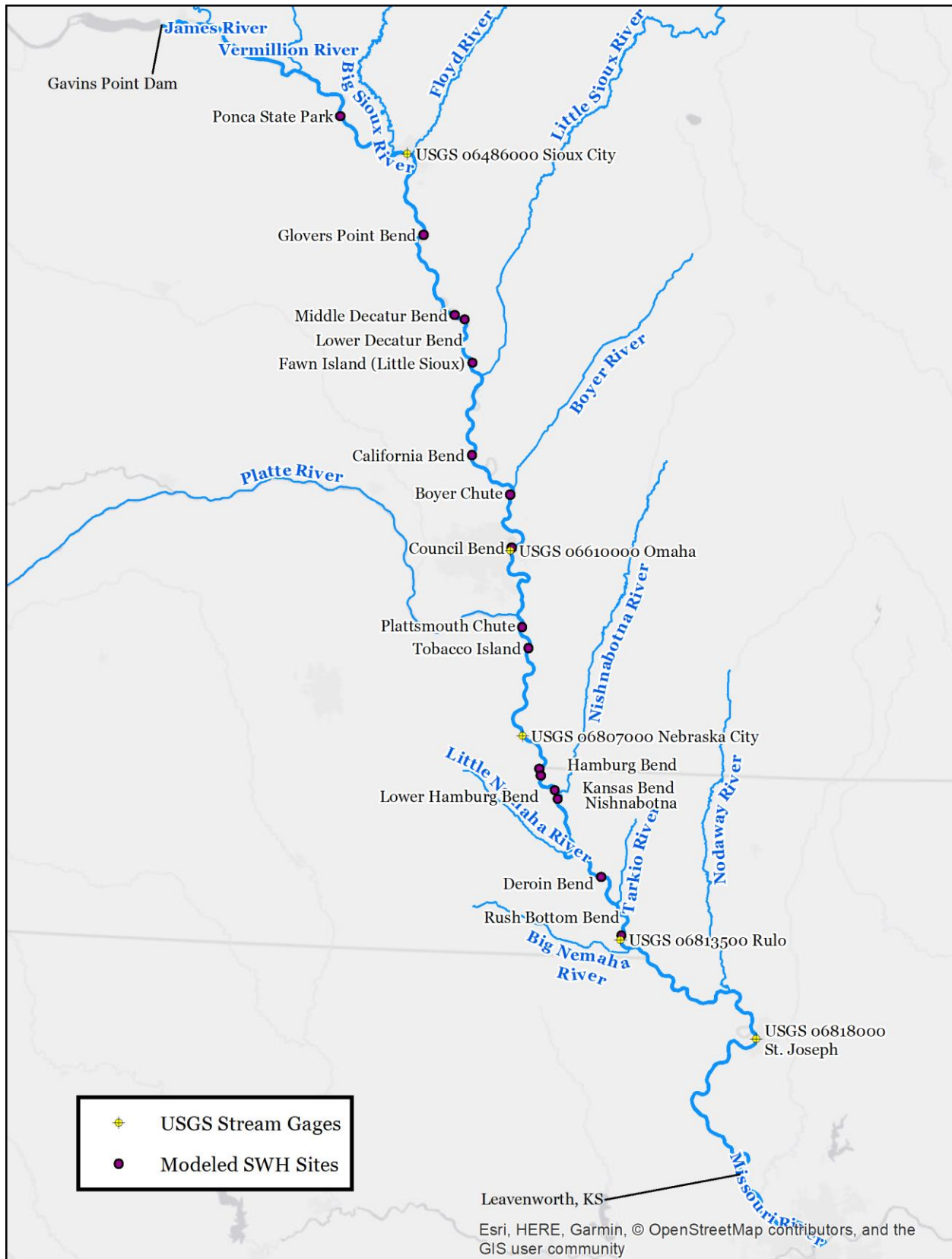
Figure 1. Missouri River, major tributaries, and SWH sites between Gavins Point Dam and Leavenworth, KS.

Hydrology The mobile-boundary model was developed and executed using a quasi-unsteady computational approach with a 14-year flow record extending from WY1999 through WY2012. This period was selected for the analysis because it is bounded by the initial, pre-MMR bathymetric data (c. 1998), and the final, post-flooding bathymetric data (c. 2012). The quasi-unsteady formulation requires hydrologic input records that define the mainstem discharge at key points along the reach and the corresponding tributary inflows for each model scenario. Three hydrologic datasets were used in the modeling:

H1.   Observed conditions, based on the actual releases from Gavins Point Dam and reported flows at the downstream mainstem and tributary gages.

H2.   Simulated Gavins Point releases representing what would have occurred if the MMR had not been implemented over the entire modeled period, with appropriate adjustments to the downstream mainstem flows and with the reported tributary inflows.

H3.   Simulated Gavins Point releases representing what would have occurred with implementation of the MMR over the entire modeled period, with appropriate adjustments to the downstream mainstem flows and with the reported tributary inflows.

The latter two records were developed by others to provide a means of directly assessing the effects of the 2004 and 2006 MMR revisions on the long-term flow characteristics in the study reach. The observed conditions differ from both of the simulated conditions because actual (observed) operations reflect discretionary decisions to balance competing objectives based on real-time information (Riverside, 2016). The reasons for, and implications of, these differences are detailed in Riverside (2016).

Habitat Restoration Activities Two versions of the pre-MMR geometry were developed for purposes of calibration and evaluation of the effects of the SWH. The first version (subsequently referred to as pre-MMR) directly uses the pre-MMR (c.1998) terrain, and thus, includes only the Boyer Bend and Upper Hamburg Bend chute channels that were constructed in 1994 and 1996, respectively (**Table 1**). The second version (pre-MMR, with-SWH) also uses the pre-MMR terrain, but includes all the SWH chute channels that were constructed prior to Summer 2007. All the chute channels that were constructed through WY2012 were included in the post-MMR/pre-2011 flood model, using the post-MMR (c.2008) terrain. The applicable chute channels were included in the initial model geometry for each case, even though many of them were constructed well after the start of the modeling period. This approach was used primarily because the structure of the HEC-RAS software makes it impractical to phase the channels in at the timing at which they were constructed. Inclusion of the channels over the entire model run provides very conservative estimates of the chute-channel effects (i.e., it overestimates their effects compared to what actually happened).

Table 1. Shallow water habitat projects geometrically reflected in the sediment-transport models

Name	River Mile	Year Completed	Model Geometry		
			G1. Pre-MMR	**G2.** Pre-MMR/With-SWH	**G3.** Post-MMR/Pre-2011 Flood
Snyder-Winnebago Complex/Ponca St. Park	753.9	2004		X	X
Glovers Point Bend	713.6	2005		X	X
Middle Decatur Bend	688.22	2009			X
Lower Decatur Bend	685.25	2008			X
Fawn Island	673.88	2009			X
California Bend	649.6	2003		X	X
Boyer Chute	637.7	1994	X	X	X
Council Bend	617.6	2007			X
Plattsmouth Bend	594.5	2005		X	X
Tobacco Island	589.9	2000		X	X

Name	River Mile	Year Completed	Model Geometry		
			G1. Pre-MMR	**G2.** Pre-MMR/With-SWH	**G3.** Post-MMR/Pre-2011 Flood
Upper Hamburg Bend	555.5	1996	X	X	X
Lower Hamburg Bend	553	2005		X	X
Upper Kansas Bend	546	2005		X	X
Nishnabotna/ Lower Kansas Bend	543.6	2005		X	X
Deroin Bend	516.6	2001		X	X
Rush Bottom	501.5	2008			X
Wolf Creek	480.6	2006		X	X
Worthwine Island	458.7	2004		X	X

In general, SWH projects that involved only isolated backwater were not included geometrically in the models because they have minimal effect on the 1-D steady-state hydraulic conditions that affect the sediment-transport balance along the reach. Discrete dike- and bank-notching projects were also not included for the same reason. As part of this impacts analysis, Tetra Tech performed detailed 2-D analysis at several locations indicated that the bank and dike notching had insignificant effect on the main channel hydraulic conditions that control the overall sediment balance.

Sediment Model Input The USACE has collected several sets of core samples from the bed of the Missouri River over the past several decades that provide a basis for determining the bed material gradation. These datasets were compiled into two complete profiles of the riverbed material that represent, as closely as possible, conditions corresponding to implementation of the MMR in 2004 and conditions just prior to the 2011 flood.

Several tributaries along the reach periodically deliver substantial amounts of sediment to the river. Sufficient data were available for the six of the tributaries (James, Big Sioux, Boyer, Platte, Nishnabotna, and Nodaway Rivers) to perform regression analyses on USGS field measurements of suspended bed material using the Maintenance of Variance Unbiased Estimator technique (MVUE) (Cohn and Gilroy 1991) that is recommended by the USGS (1992), to aid in developing the inflowing sediment rating curves. A unit sediment yield analysis for a range of selected discharges was then performed to estimate the load from each of the other eight tributaries based on their drainage area and location along the reach.

There is considerable uncertainty in the tributary relationships for several reasons. Measurements or estimates of the bed load component of the total load are not available for any of the tributaries, and actual bed-material samples that can be used in a sediment-transport equation to estimate the bed load are only available for the Platte River (NE). The available USGS suspended sediment measurements were typically taken at the nearest gage to the Missouri River, but most of the gages are located several tens of miles upstream from the confluence. Given the historic degradation of the Missouri River following closure of Gavins Point Dam, base level in the tributaries has been progressively lowering, and this can cause sediment-transport rates in the lower reaches of the tributaries to be substantially higher than historic measurements at the gages, at least during the early phases of the downcutting. Finally, on all the tributaries except the Platte River, measurements of the gradation of the suspended bed material are too sparse to realistically estimate the variability in gradation of transported material with discharge. Based on these uncertainties, the tributary loadings were used as a calibration parameter by scaling the MVUE and unit sediment yield relationships within physically-reasonable limits to achieve acceptable agreement with the modeled and observed bed changes over the periods for which bathymetry data were available. From a physical-process perspective, the adjustments during the calibration process account for both the missing bed load component and the uncertainty in the overall relationship.

Bank erosion is a key source of sediment to the Missouri River. Bankline mapping indicates that about 1,150 acres of total bank loss occurred in the reach between Gavins Point Dam and RM 750 between 1998

and 2011 (West Consultants, 2013a). Using average bank height calculated from model geometry, this amount of bank erosion equates to about 67.4M tons of sediment. Similarly, West (2013a) concluded that about 914 acres (approximately 56M tons) of material was eroded from the banklines between 1999 and 2011 between Rulo and Ponca State Park. The bank erosion was included in the sediment models using an power-regression estimate for timing of the loads based on the magnitude of streamflow.

In-river disposal of material excavated from the overbanks during construction of some of the SWH features also contributed sediment to the mainstem. USACE records of in-river disposal quantities were used to develop point-source sediment inputs representing construction of the chutes. The USACE data indicate that about 14.5M tons of in-river disposal occurred between 2001 and 2012 within the modeled reach, or about 1.2M tons per year, on average. The largest quantities of in-river disposal during the modeling period occurred in 2009 (~3.4M tons) and 2012 (~4.2M tons). Reported quantities of in-river disposal represent only excavation of the initial channel at the indicated locations. Most of the projects were designed with an initial pilot channel that was expected to scour over time to achieve the final desired cross section. An estimate of the volume of material scoured from the chute channels during the widening phase was made and incorporated into the sediment load inputs. Chute widening was estimated to contribute an additional 13.9M tons of sediment over the period.

Scenario Design

Three categories of models were developed for the analysis: calibration/validation models, baseline models, and SWH and/or MMR scenario models.

The calibration model was run with the pre-MMR/with-SWH bathymetry (G2) for the initial conditions using the observed hydrology (H1) for WY1999 through WY2007. The model was modified with the post-MMR geometry (G3) and the same suite of parameters used for the calibration, and the model was re-run with the observed flows for the period from WY2008 through WY 2012 (H1) to provide independent verification. These parameters were then carried through the remaining scenario models for the actual impact analysis.

Baseline models were then developed to provide a basis of comparison for the scenario runs that represent a range of hypothetical conditions in which the chute channels were not constructed, and/or the MMR was not implemented. Two baseline models were run using the same geometric input as the calibration and validation models, respectively, but using the simulated with-MMR hydrology (H3) for the applicable periods. These models are subsequently referred to as *early-baseline* and *late-baseline*. The third (*long-term*) baseline model covers the entire period from WY1999 through WY2012. This model includes all the chute channels that existed at the end of WY2012 for the entire simulation period.

After completion of the calibration, validation and baseline models, four specific scenarios were evaluated for the impact analysis (**Table 2**). The first three scenarios used the pre-MMR (c. 1998) bathymetry, and only those chute channels that were completed prior to the 1998 bathymetric surveys (G1). The fourth scenario used the post-MMR (c. 2007) geometry (G3). The four scenarios are defined as follows:

S1) *Early period, no MMR or SWH* – Simulated flows for WY1999 through WY2007 using pre-MMR reservoir operating rules.

S2) *Longterm, no MMR or SWH* – Simulated flows for the entire period from WY1999 through WY2012, with pre-MMR reservoir operating rules.

S3) *With-MMR, no SWH* – Simulated flows for WY1999 through WY2007, with reservoir operations reflecting implementation of the MMR.

S4) *MMR Impact Only* – Simulated flows for WY2008 through WY2012, with reservoir operations based on pre-MMR Master Manual.

Comparison of the scenarios to the appropriate baseline scenario thus allows for direct quantification of the impacts of SWH and/or MMR activities.

Table 2. Modeling scenarios used to evaluate claims of adverse flooding impacts due to SWH and MMR activities, and modeling components used in each model

Modeling Scenario	Starting Geometry	SWH Inc.?	Hydrology	Simulation Period	Bed Material
Calibration	Pre-MMR	Y	Observed	WY99-07	Pre-MMR
Validation	Pre-2011 Flood	Y	Observed	WY08-12	Post-MMR
B1. Early Baseline	Pre-MMR	Y	With-MMR	WY99-07	Pre-MMR
B2. Late Baseline	Pre-2011 Flood	Y	With-MMR	WY08-12	Post-MMR
B3. Longterm Baseline	Pre-MMR	Y	With-MMR	WY99-12	Pre-MMR
S1. Early No MMR or SWH	Pre-MMR	N	w/o-MMR	WY99-07	Pre-MMR
S2. Longterm No MMR or SWH	Pre-MMR	N	w/o-MMR	WY99-12	Pre-MMR
S3. With-MMR, No SWH	Pre-MMR	N	With-MMR	WY99-07	Pre-MMR
S4. MMR Impact Only	Pre-2011 Flood	Y	w/o-MMR	WY08-12	Post-MMR

Model Results

Calibration and Validation

Calibration The calibration model was run to ensure that the mobile-boundary model reproduced the observed sediment balance in the primary study reach during the period between the 1998 and 2007 surveys that were used to develop the pre-MMR and pre-2011 flood model geometries. The simulation period for the calibration run was October 1, 1998 through September 30, 2007 (nine water years). The simulation results were compared against the observed change in mean bed elevation (MBE) computed from the coincident HEC-RAS cross sections of the pre-MMR and pre-2011 flood geometries, and the observed cumulative suspended sand loads at the mainstem USGS gages, adjusted for bedload according to estimates by the USACE Engineer Research and Development Center. The modeled bed change trends are in reasonable agreement with the observed changes throughout the primary study reach downstream from RM 750 although the simulation shows slightly less aggradation than is indicated by the surveyed cross sections (average error was -0.5-ft), particularly in the reach downstream from Rulo (**Figure 2**).
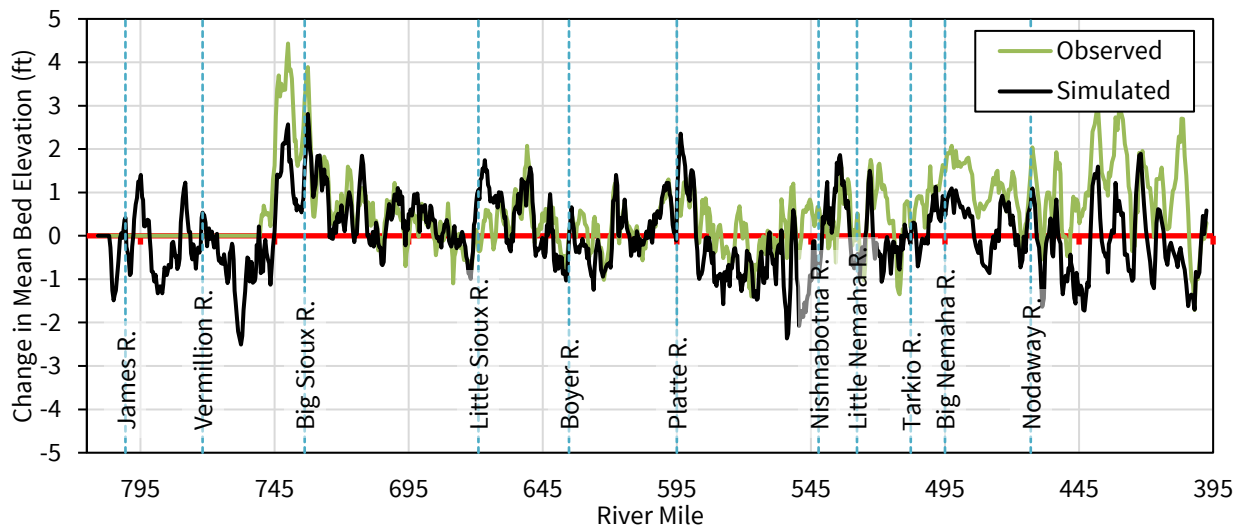
Figure 2. Change in mean bed elevation from the calibration simulation compared to the observed changes between the pre- and post-MMR geometries (five section moving average)

The cumulative suspended mass curves at the four available calibration sites indicate that even though the simulated bed change is slightly lower than the observed, the model has been accurately parameterized for both the supply and the transport capacity. For example, the model predicts about 7-percent less suspended bed-material load over the 9-year simulation period at Sioux City, IA than is indicated by

integration of the rating curve developed from the measured data. At Omaha, the magnitude and amount scatter in the simulated suspended sand-transport rates agree well with the USGS measurements, although the cumulative transport is about 13-percent low. At both Nebraska City and St. Joseph, the simulated suspended bed-material load is within 10 percent of the observed load.

Validation The validation scenario was simulated from October 1, 2007 through September 30, 2012 (five water years). Bed elevation changes predicted by the validation model over the 5-year simulation period are in reasonable agreement with the measured changes (**Figure 3**), with an average error of 0.10-ft. The model tends to over-predict degradation between about RM 620 and RM 640 in the reach upstream from Omaha and between RM 540 and 585, near Nebraska City, and it under-predicts degradation between about RM 415 and RM 465.
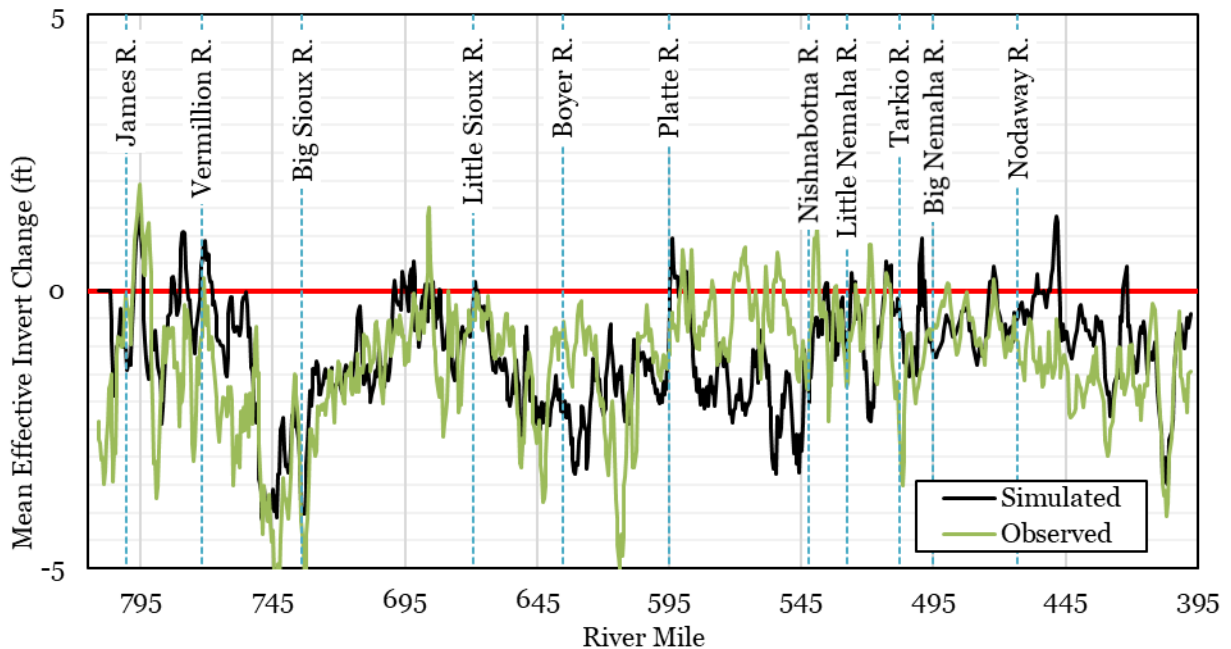
Figure 3. Change in MBE from the validation simulation compared to the observed changes between the pre- and post-MMR geometries (five section moving average)

The scatter in the predicted suspended bed-material loads is well within the scatter of the measured loads at all four of the gages. The simulated cumulative suspended bed-material load passing Sioux City from the validation model is within about 8 percent of the value obtained by integrating the rating curve for the USGS observations, and the suspended load passing the three downstream gages (Omaha, Nebraska City, and St. Joseph) is 15- to 25-percent higher.

Considered together, the simulation results from the calibration and validation runs are in good agreement with the measured data for both sediment loads and bed change during the simulation periods that extend from WY1999 through WY2012.

Baseline Simulations

The baseline simulations provide a basis of comparison for the scenario runs that represent a range of hypothetical conditions in which the chute channels were not constructed, and/or the MMR was not implemented.

Scenario B1 – Early Baseline Scenario B1 differs from the calibration run only in that the hydrologic record has been replaced by the with-MMR record for the applicable simulations. As a result, the flow record represents application of the MMR over the entire period from WY1999 through WY2007 versus actual operations during the period, which included 5 years of operations under the old Water Control

Manual and 4 years of MMR implementation and reflects real-time discretionary decisions made by the system operators. The simulated changes in bed elevation for the calibration run and Scenario B1 are nearly identical, with an average difference of only 0.02 feet and maximum differences of less than 0.2 feet (**Figure 4**), within the uncertainty of the model. These differences are well-within the uncertainty of the model results, and they would have a negligible (within the plausible accuracy of a 1-D sediment model) effect on water-surface elevations, particularly at high flows.
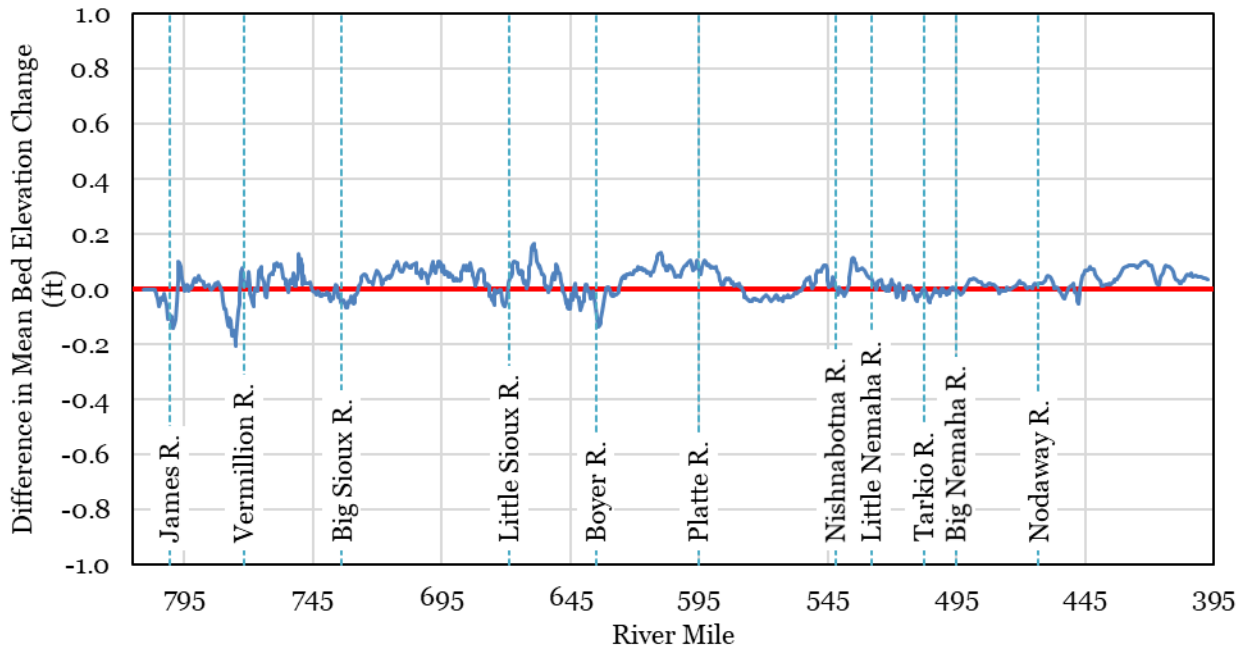
Figure 4. Difference in simulated change in MBE between the calibration run and Scenario B1. Positive values indicate higher final bed profile in the calibration simulation (five section moving average).

Scenario B2 – Late Baseline Scenario B2 is primarily intended to provide a baseline simulation against which without-MMR hydrology scenarios can be compared. Scenario B2 is different from the validation run only in that the hydrologic record has been replaced by the with-MMR record for the applicable simulations. This scenario, therefore, reflects the effects of flow changes resulting from application of the MMR over the period from WY2008 through WY2012 versus actual operations during the period that reflect real-time decisions made under the MMR. This scenario also provides a baseline for isolating the hydrologic effects of MMR implementation from the effects of the SWH projects during this period.

The simulated changes in bed elevation for the Validation run and Scenario B2 are nearly identical, with an average difference of only -0.02 feet and maximum differences about 0.4 feet in isolated locations (**Figure 5**). Like Scenario B1, these differences are well within the uncertainty of the model results, and they would have a negligible effect on water-surface elevations, particularly at high flows.
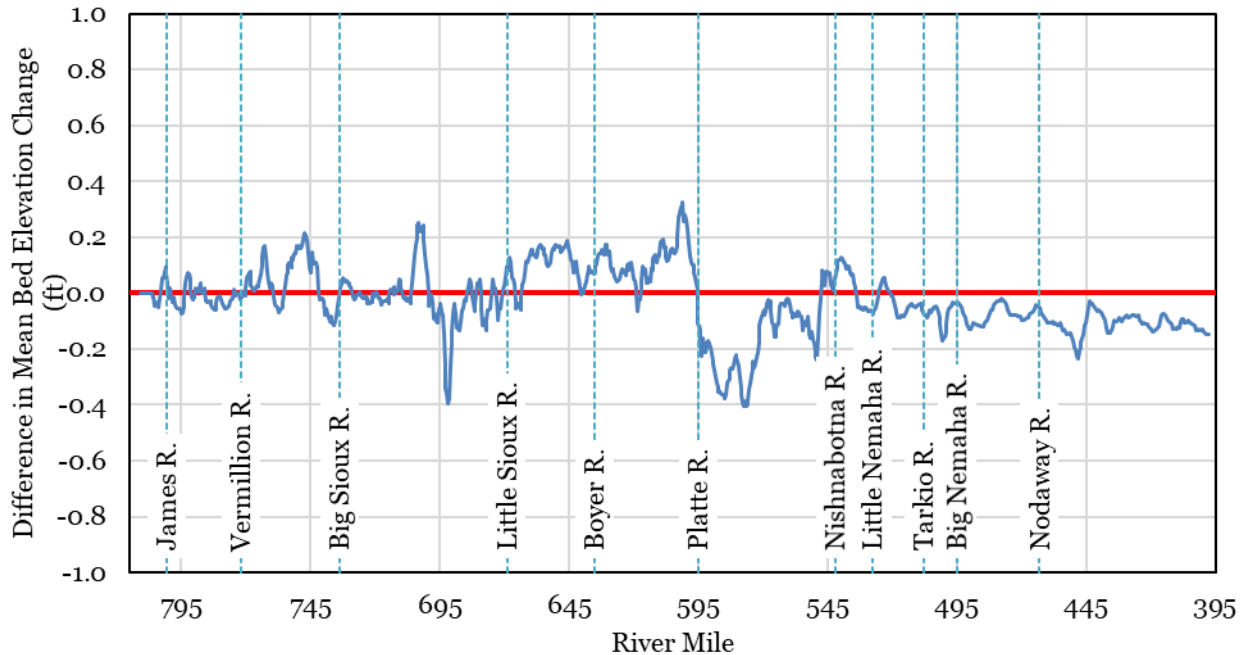
Figure 5. Difference in simulated change in MBE between the valibration run and Scenario B2. Positive values indicate higher final bed profile in the valibration simulation (five section moving average).

Scenario B3 – Longterm Baseline Scenario B3 provides a baseline simulation for evaluating the effects of hydrologic changes associated with the MMR over the entire 14-year period of simulation, and therefore, represents "worst-case effects" because all SWH features that were constructed by the end of WY2012 are included in the initial geometry. The starting conditions for this scenario are the same as Scenario B1. As in the other baseline scenarios, the hydrologic record for Scenario B3 is taken from the simulations of with-MMR operations. Results from the scenario will be discussed in conjunction with Scenario S2 to assess how the aggradation/degradation tendencies along the reach would have changed if the chute channels had not been constructed.

Scenario Simulations

The scenario simulations are intended to quantify the direct impacts of the SWH chute channels and/or MMR hydrology on the sediment balance in the study reach by comparing results from simulations without SWH features and/or MMR hydrology to the baseline scenario results.

Scenario 1 – Early Period without-MMR and without SWH This scenario is intended to show, through a comparison with Scenario B1, the combined effects of hydrologic changes associated with implementation of the MMR and physical changes associated with the SWH chute channel construction prior to 2008 on aggradation/degradation trends along the reach.

In general, simulated changes in bed elevations for this scenario are very similar to those from the Scenario B1, with an average difference of only -0.02 feet over the entire reach. The results show a small decrease in the amount of aggradation in aggradational reaches and small decrease in degradation in the degradational reaches between the Big Sioux River and the Big Nemaha River, a small increase in aggradation between the Big Nemaha River and St. Joseph and a small increase in degradation between St. Joseph and Leavenworth. A modest amount of aggradation occurs in some areas that reflect the local effects of flow diversion into the chute channels, the most notable locations being Glovers Point, California Bend, and Hamburg Bend (**Figure 6**).

The effects of the indicated bed changes on water-surface elevations and flood-carrying capacity were assessed by simulating steady-state water-surface profiles for the 10-percent, 50-percent and 90-percent annual exceedance probability (AEP) flows using the end-of-simulation bed geometry. The profile

comparisons indicate that the water-surface elevations along the reach for Scenario B1 and Scenario 1 at these discharges are very similar, with differences between the two scenarios that are generally less than 0.1 feet (Figure 6). At Glovers Point, where the bed aggraded by about 1.1 feet more with the chute channel in place, the difference in water-surface elevation for the three flows are all less than 0.1 feet because the conveyance in the chute channel compensates for any loss of capacity in the main channel associated with the aggradation. A similar effect occurs at the other two sites, and in fact, the water-surface at Hamburg Bend is about 0.5 feet lower with the chute channel at the 50-percent AEP flow.
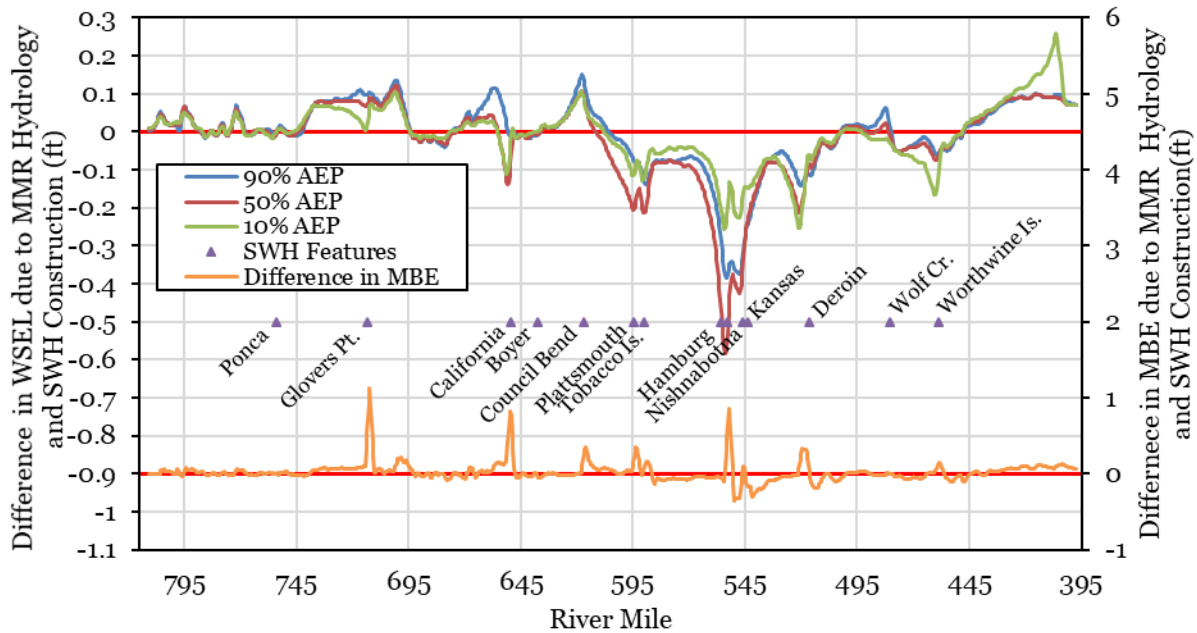
Figure 6. Effects of the MMR hydrology and SWH construction on WSE through WY 2007 for selected discharge profiles. Also shown in the difference in bed elevation between the two scenarios (five section moving average).

Scenario 2 − Longterm without-MMR Scenario 2 is an extension of Scenario 1, designed to evaluate the impact of MMR operations and the chute channels over the entire 14-year simulation period. Differences between the results from Scenario 2 and Scenario B3 (longterm baseline) represent the combined, long-term effects of MMR operations and the presence of all the chute channels that were constructed by the end of WY2012.

The simulated changes in MBE are very similar between Scenario B3 and Scenario 2, with localized areas of higher MBE for Scenario B3 near the head of some of the chute channels. Differences in MBE of 1.0 foot to 1.2 feet occur at four specific locations (Glovers Point, Decatur Bend, Hamburg Bend, and Rush Bottom), and differences of up to 0.5 feet occur at two other locations (Plattsmouth and Deroin) (**Figure 7**).

Based on steady-state water-surface profiles for the 10-, 50- and 90-percent AEP flows using the end-of-run geometry for each scenario, the differences in water-surface elevation between the two scenarios are very small (Figure 7). Where the predicted water surface elevation (WSEL) is higher, the difference is generally less than 0.1 feet, except for limited reaches between Decatur Bend and California Bend where the maximum difference is about 0.4 feet at the 90-percent AEP profile, and Glovers Point, just upstream from Decatur Bend, Boyer Chute, and the portion of the reach downstream from Wolf Creek, where the water-surface is 0.1 to 0.2 feet higher with the chute channels in place. At Glovers Point, where the bed aggraded by about 1.3 feet more with the chute channels in place, the WSEL increased by about 0.15 feet at the 90-percent AEP flow, decreasing to about 0.05 feet at the 10-percent AEP flow. In all cases, the additional conveyance provided by the chute channels compensated for any loss of in-channel capacity

associated a reduction in sediment-transport capacity in the main channel, and the magnitude of the differences decrease with increasing flow.
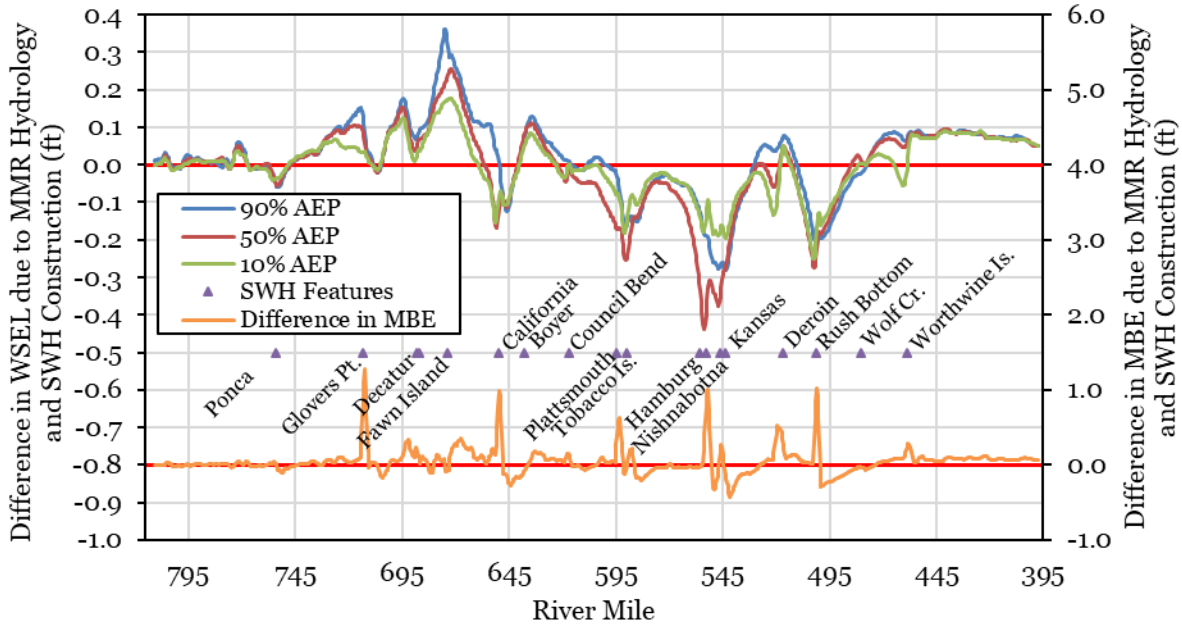
Figure 7. Effects of the MMR hydrology and SWH construction on WSE through WY 2012 for selected discharge profiles. Also shown in the difference in bed elevation between the two scenarios (five section moving average).

Scenario 3 – Early period, no SWH Scenario 3 is designed to isolate the impact of chute channels on the sediment balance in the primary study reach during the period prior to WY2008. The difference in results from Scenario 3 to Scenario B1 represent the direct effects of chute channels constructed between 1998 and WY2008 on the relative sediment balance in the reach.

In general, simulated changes in bed elevations for this scenario are very similar to those from Scenario B1, with an average difference of only 0.02 feet over the entire reach. The chute channels result in a small increase in bed sediment storage in portions of the reach that are net aggradational and a small decrease in bed erosion in degradational portions of the reach. Notable differences in MBE occur in some areas that reflect the local effects of chute channels (**Figure 8**). The MBE is more than 0.5 feet higher with the chute channels in place at three specific locations [Glovers Point (1.1 feet), California Bend (0.8 feet), and Hamburg Bend (0.8 feet)]. As in the previously described scenarios, the increases occur just downstream from the head of the chute channels and are caused by diversion of flow into the chute channels, which reduces the main channel flow and the transport capacity but leaves the bulk of the bed-material load in the main channel. Based on steady-state water-surface profiles for the 10-, 50- and 90-percent AEP flows using the end-of-run geometry for each scenario, the differences in waters-surface elevation between the two scenarios are very small (Figure 8). Where the predicted WSEL is higher, the difference is generally less than 0.1 feet, except for limited reaches near Glovers Point, California Bend and Council Bend where the maximum differences are in the range of 0.1 feet to 0.15 feet at the 90-percent AEP flow and substantially smaller at the higher 10- and 50-percent flows. In all cases, the additional conveyance provided by the chute channels compensated for any loss of in-channel capacity associated with a reduction in sediment-transport capacity in the main channel.
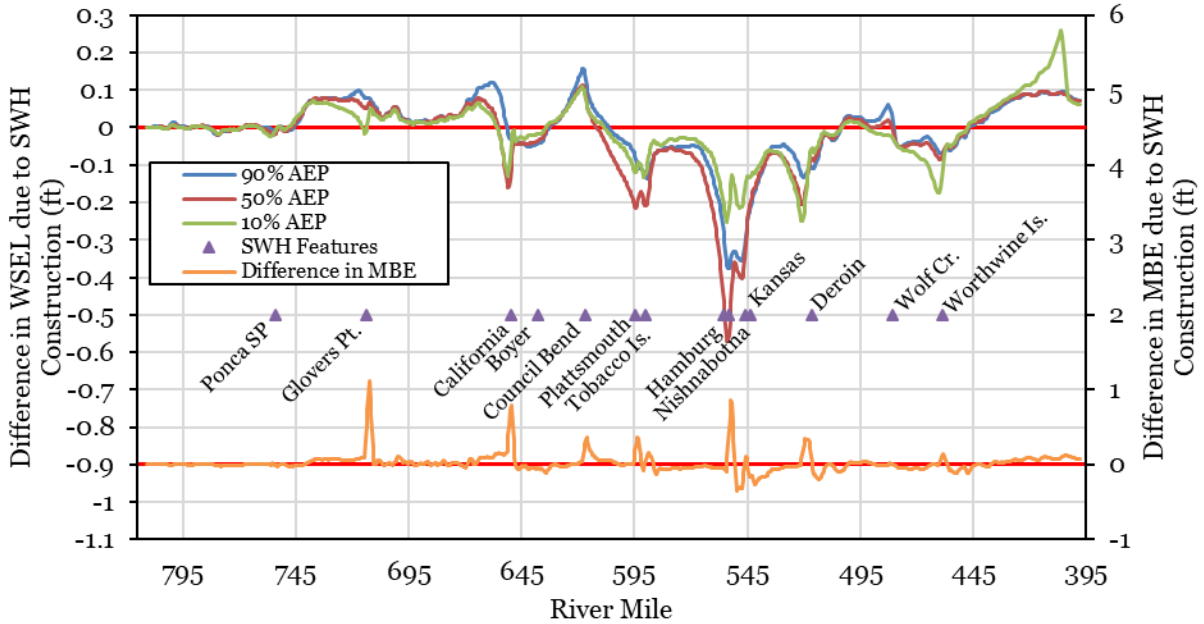
Figure 8. Effects of the SWH construction on WSE through WY 2007 for selected discharge profiles. Also shown is the difference in bed elevation between the two scenarios (five section moving average).

Scenario 4 – Late period, without-MMR hydrology Scenario 4 is designed to evaluate the impact of flow changes associated with implementation of the MMR for the period from WY2008 through WY2012, including the high flows in 2010 and 2011, by comparison with Scenario B2.

The changes in MBE over the 5-year simulation period for this scenario are nearly identical to those for Scenario B2 (**Figure 9**). Water-surface profiles for the 10-, 50- and 90-percent AEP flows indicate differences from Scenario B2 of less than about 0.1 feet throughout the reach.
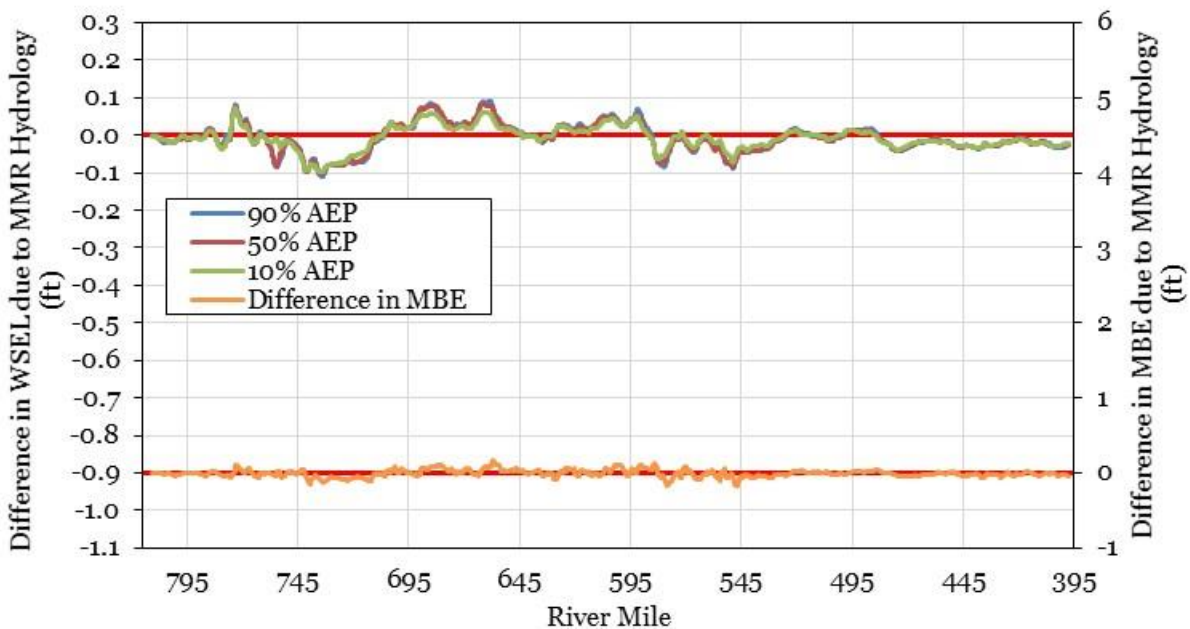
Figure 9. Effects of the MMR hydrology on WSE between WY 2008 and WY2012 for selected discharge profiles. Also shown in the difference in bed elevation between the two scenarios (five section moving average).

Conclusions

The following conclusions were reached based on the modeling and geomorphic analysis that was performed in conjunction with the modeling:

- Based on the available bathymetric data, the river was mildly aggradational throughout most the reach between the late-1990s and 2008, a period of generally low to moderate flows, with the greatest amounts of deposition occurring in the approximately 34-mile reach below Sioux City, and the approximately 97-mile reach between the mouth of the Big Nemaha River and Leavenworth, KS. Between 2008 and 2012, a period that included the large tributary inflows in 2010 and the extremely high, long-duration flows in 2011, essentially the entire reach was degradational.
- Changes in the flows in the primary study reach associated with implementation of the 2004 MMR are minor (Riverside 2016). These changes have had a negligible effect on aggradation/degradation trends, and most importantly, water-surface elevations during flood peak flows.
- Additional sediment was added to the river through in-river disposal and subsequent erosion of the exposed overbank sediments at several of the SWH sites that have been constructed in the reach since implementation of the 2004 MMR. The majority of the sediment introduced to the river at these sites consisted of silt, clay and fine- to very-fine sand that is carried primarily in suspension, with little interaction with the channel bed. As a result, the introduced sediment increased the total sediment load in the river, but had very little, if any, effect on the aggradation/degradation trends in the river.
- Flow diversion into the chute channels that have been constructed to create SWH typically causes a change in the local sediment balance that can induce localized deposition, resulting in minor reductions in the capacity of the main channel; however, in most cases, the reduction in in-channel capacity is more than offset by the increased conveyance provided by the chute channel. As a result, the water-surface elevation at flood flows is at or below the level that would occur in the absence of the chute channel.
  - In cases where the water-surface elevation may increase during high flows as a result of the local in-channel deposition, the increases are very small (typically in the range of 0.1 feet or less). These changes are negligible when considered in relation to the other factors that affect the local water-surface elevations, including wave action, flow accelerations around obstructions, and variability in roughness associated with changes in vegetation, bedforms, and reduced floodplain conveyance from sediment deposition, vegetation, and agricultural berms. As a result, local in-channel deposition associated with this process has had no adverse effect on the flood-carrying capacity of the river.
  - In most cases, the increased conveyance resulting from the chute channels and channel widening projects causes a modest decrease in upstream water-surface elevations that would tend to increase flood carrying capacity and reduce the potential for damages during flood flows.

References

Cohn, T.A. and Gilroy, E.J., 1991. Estimating Loads from Periodic Records. U.S. Geological Survey Branch of Systems Analysis Technical Report 91.01. 81 p.

Galat, D.L., Berry, C.R., Jr, Peters, E.J., and White, R.G., 2005. Missouri River. In A.C. Benke and C.E. Cushing (editors), Rivers of North America, Elsevier, Oxford, pp. 427-480.

Riverside Technologies, Inc., 2016. "Assessment of causes of flooding and impact of the implementation of revised COE master manuals." Prepared for U.S. Department of Justice.

Schenk, E.R., Skalak, K.J., Benthem, A.J., Dietsch, B.J., Woodward, B.K., Wiche, G.J., Galloway, J.M., Nustad, R.A., and Hupp, C.R., 2014. Geomorphic change on the Missouri River during the flood of 2011: U.S. Geological Survey Professional Paper 1798–I, 25 p, http://dx.doi.org/10.3133/pp1798I.

U.S. Army Corps of Engineers, 1988. Missouri River Bank Stabilization and Navigation Project: Structure Maintenance Guidelines. Memorandum for Omaha and Kansas City Districts Commanders, April 5, 14 p.

U.S. Army Corps of Engineers, 2004a. Finding of no significant impact: Hole-in-the-Rock Backwater Restoration Project, Missouri River Bank Stabilization and Navigation, Fish and Wildlife Mitigation Project, Thurston County, NE, 100 p.

U.S. Army Corps of Engineers, 2011. Operation & Maintenance Manual, Missouri River Bank Stabilization & Navigation Project, Sioux City, Iowa to the Mouth, Omaha District, 611 p.

U.S. Army Corps of Engineers E, 2013a. Evaluation of Reported Notch Problem Locations below Rulo, Nebraska, April, 116 p.

United States Army Corps of Engineers (USACE), 2016. HEC-RAS River Analysis System. v. 5.0. USACE Hydrologic Engineering Center. February 2016. Davis, California.

U.S. Geological Survey. 1992. Recommendations for Use of Retransformation Methods in Regression Models Used to Estimate Sediment Loads ["The Bias Correction Problem"]. *Office of Surface Water Technical Memorandum* No. 93.08. December 31.

Sediment Transport Analysis of Missouri River for Red River Valley Water Supply Project McLean County, North Dakota

Chris Bahner, Project Manager, WEST Consultants, Inc., Salem, Oregon, Phone (503) 485-5490, Fax (503) 485-5491, cbahner@westconsultants.com

Abstract

As part of the Red River Valley Water Supply Project (RRVWSP), a new water intake will be constructed on the Missouri River south of Washburn, ND. Because the Missouri River is a sand-bed river and Garrison Dam is upstream, it is important to determine the risk that the new intake could be undermined or buried with sediment as the river naturally migrates. Further, the North Dakota State Water Commission (ND SWC) would be responsible for issuing a Sovereign Lands Permit for the proposed intake. As part of that permit review process, the ND SWC posed two key questions: (1) How would the banks, bed, sandbars, and existing bank protection be affected over the long-term as a result of the proposed intake structure, and how far upstream or downstream would any effects extend?; and (2) How would the banks, bed, sandbars, and existing bank protection be affected during construction because of the (temporary) cofferdam?

A sediment transport study was completed to define the risk of the intake structure being undermined or buried and answer the ND SWC questions. The sediment transport study included development of a one-dimensional (1D) sediment transport HEC-RAS model to evaluate expected elevation changes along the river over the next 50 years and determine whether the Missouri River in the area of the intake be lower or higher on average because of reach-wide riverine processes, and to estimate existing and future water surface profiles for a wide range of flows. The 1D sediment transport model was developed for the reach of the Missouri River between Garrison Dam at the upstream end and Oahe Reservoir at the downstream end. The model was calibrated using range line data collected by the U.S. Army Corps of Engineers, Omaha District for the periods between 1964 and 2012.

The sediment transport study also included the development a three-dimensional (3D) sediment transport model using CCHE3D. The model was developed for the reach in the vicinity of the proposed intake structure. The CCHE3D model was calibrated to observed conditions. The calibration of the CCHE3D model was completed in two phase. The first phase involved the calibration of the model parameters that influence the hydraulic characteristics.   This phase utilized observed flow velocities measured using an Acoustic Doppler Current Profile (ADCP) device and observed water surface elevation obtained during the ADCP measurements and noted during the 2011 flood event. The second phase involved the sediment transport option to consider changes in the channel bed between two bathymetric surveys completed with the reach of interest. The calibrated model was utilized to estimate the scour near the structure and to assess potential impacts from the proposed structure.

Introduction

The Red River Valley Water Supply Project (RRVWSP) will provide a supplemental water supply to eastern and central North Dakota (ND) in the event of drought conditions in the Red River watershed. The RRVWSP, as envisioned by the Garrison Diversion Conservancy District (GDCD) will also supply additional water to support industrial development as well as provide an environmental benefit by augmenting natural stream flows. The source water will be withdrawn from the Missouri River at about 60 feet from the east bank (left side looking downstream) near River Mile (RM) 1350.1 (RM is based on 1960 system), which is about 5.2 miles downstream of Washburn, ND. A map showing the proposed intake structure is provided in Figure 1.

Figure 1. Location Map

Because the Missouri River is a sand-bed river and Garrison Dam is upstream, it is important to determine the risk that the new intake could be undermined during the project life. Further, the North Dakota State Water Commission (ND SWC) would be responsible for issuing a Sovereign Lands Permit for the proposed intake. As part of that permit review process, the ND SWC posed two key questions: (1) How would the banks, bed, sandbars, and existing bank protection be affected over the long-term as a result of the proposed intake structure, and how far upstream or

downstream would any effects extend?; and (2) How would the banks, bed, sandbars, and existing bank protection be affected during construction because of the (temporary) cofferdam?

AE2S and WEST Consultants, Inc. (WEST) was contracted to complete a sediment transport study to define the risk of the intake structure being undermined and to answer the ND SWC questions. AE2S developed a one-dimensional (1D) sediment transport HEC-RAS model to determine expected elevation changes along the river over the next 50 years and to estimate existing and future water surface profiles for a wide range of flows. WEST developed a three-dimensional (3D) sediment transport model using CCHE3D to estimate the scour near the structure and to assess potential impacts from the proposed structure. WEST also defined the geomorphology and hydrology of the site for use in the sediment transport study.

Geomorphology

The present course of the Missouri River was developed in recent geologic time. The course represents the river's adjustment to flow along the farthest southward edge of one of the advances of the Wisconsin ice sheet and forms the dividing line between two physiographic sections (USGS, 2013). The reach of the Missouri River between Garrison Dam and the headwaters of Oahe Reservoir covers a distance of about 80 miles, of which the upper 54 miles is considered the Garrison Degradation Reach. Valley width averages a relatively uniform 2 miles within this reach and is well entrenched in the terrain of the North Dakota prairie. The river channel averages about 2,400 feet in width and is generally divided into several smaller waterways by numerous low sandbars. Occasionally, large wooded islands several miles in length occur, which are separated from the adjacent floodplain by shallow chutes. The channel bed is composed of sand interspersed with silt and clay lenses or gravel pockets. The channel alignment has not changed materially since the Missouri River Commission survey in 1891. Although the Missouri River valley in this reach is considered to be mature with oxbow lakes, cutoffs, and a meandering channel, the river cannot be considered sinuous since the valley is generally too narrow for full meander patterns to develop before being deflected by the adjacent valley bluffs (WEST, 2012).

Information about the geomorphic characteristics of the Missouri River downstream of Garrison Dam is documented in the following references:

- Characteristics of Sediment Transport at Selected Sites along the Missouri River during the High-Flow Conditions of 2011 (USGS, 2013);

- Geomorphic Change on the Missouri River during the Flood of 2011, (USGS, 2014); and

- Missouri River Garrison Project Downstream Channel and Sediment Trends Study (WEST, 2012).

The 2013 USGS report indicates that the bed of the Missouri River degraded in the years following closure of Garrison Dam with reported changes in mean-bed elevation ranging from -10.7 to 0.65 feet in the 54 miles below the dam between 1954 and 1976. The rate of channel bed degradation slowed substantially by 1976 with some (although not definitive) indication that the river bed is approaching a state of dynamic equilibrium.

The 2013 USGS report also includes information about suspended and bedload transport rates measured during the 2011 event. Because of the difficulty in obtaining a high-quality bedload

sample, the 2013 USGS report also included estimated bedload transport rates using the Modified Einstein Procedure (MEP). The measured suspended sediment concentrations ranged from 64 mg/l to 745 mg/l for discharges ranging from 34,500 cfs to 151,000 cfs with about 76 percent of the material being sand-sized material and 24 percent being silt- and clay-sized material. The measured bedload transport rates ranged from 164 to 2,890 tons/day with 94 percent being sand-sized material and 6 percent being gravel-sized material. The estimated bedload transport rate ranges 260 to 58,000 tons/day.

The 2014 USGS report includes a plot showing the percent change in area for the reach downstream of Garrison Dam for the period between 1954 and 2007. The 2014 report also includes information related to changes in the sandbars and islands as a result of the 2011 flood event. Cross-sectional surveys before (2007) and after (2012) the flood indicate that the channel has changed dramatically in some locations in the reach downstream of the dam. The cross-section comparison shows that there was erosion of the mid-channel sandbar and deposition in side channel.

The 2012 WEST study documents changes to historical channel and sediment data on the Missouri River below Garrison Dam, known as the Garrison Degradation Reach for the period from 1954 to 2007. The changes were defined by analyzing cross-section data from numerous field surveys conducted from 1946 to 2007 on forty sediment range lines located in the reach. The data in this report was supplemented with 2012 field survey data provided by the USACE (USACE, 2012). The average bed profiles for the entire main channel at selected years between 1958 and 2012 are shown in Figure 2. This figure also includes the average bed elevation determined using two recent surveys completed by AE2S: (1) August 2016, and (2) October 2017. This figure shows that the average bed elevation at the intake structure has lowered about 8 feet for the period from 1958 and October 2017. The cross-sectional area near the proposed intake structure has increased by about 60 percent.
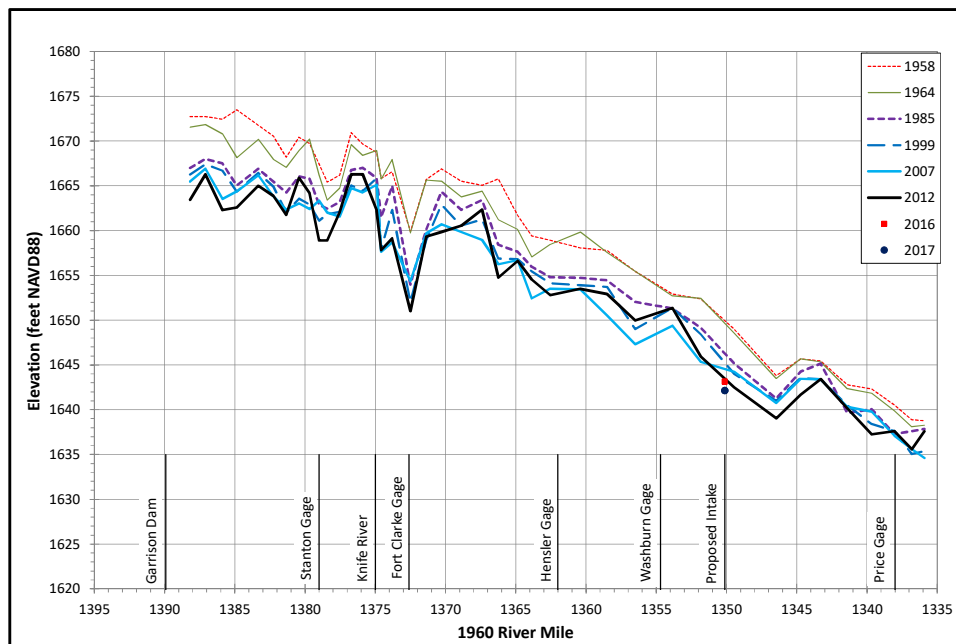
Figure 2. Average Bed Profiles From 1958 to 2007 (USACE, 2012) and the 2016 and 2017 Survey at the Proposed Intake Structure

The comparison of cross sections shows that the Missouri River main channel within the vicinity of the proposed intake structure is highly dynamic with a high level of variability in the side channel bars (elevation changes on the order of 10 feet), and the width has increased during the period between 1958 and 2012. Comparison of sediment samples obtained from 1964 to 1999 shows that the bed material has coarsened over this period. The changes to historical channel and sediment data of the Missouri River estimated at the proposed intake structure are summarized in Table 1.

Table 1. Summary of Change at Proposed Intake Structure from Geomorphic Evaluation

Variable	Source	Period	Change in Value
Average Bed	USACE, 2012	1958 – 2007	-5 ft
	USACE, 2012 and AE2S, 2017	1958 – 2017	-8 ft
Thalweg	USACE, 2012	1958 – 2012	+2 ft (-3 – 5 ft)
Area	USACE, 2012	1958 – 2012	+60%
Width	USACE, 2012	1958 – 2012	+14.3%
d90	WEST, 2012	1964 – 1999	MS to CS
d50	WEST, 2012	1964 – 1999	FS to MS
d10	WEST, 2012	1964 – 1999	VFS to FS

Hydrology

The hydrologic regime of the study reach is controlled largely by upstream Garrison Dam. The Knife River is the only tributary contributing significant flow to the study reach. Garrison Dam discharge releases are available from the U.S. Army Corps of Engineers, Omaha District for the period between 1954 and 2017. The average daily discharge released from Garrison Dam for this period is approximately 20,900 cfs with the minimum release being 0 cfs to the maximum being 150,600 cfs, which occurred during the 2011 flood. The Knife River flows into the Missouri River near Stanton, North Dakota at about 12 miles downstream of Garrison Dam and about 24 miles upstream of the proposed intake location. The average daily discharge for the Knife River is about 200 cfs with the minimum being 10 cfs and the maximum being 26,000 cfs.

Discharge and stage data for stream gages on the Missouri River and Knife River are available from the USGS North Dakota Water Services (USGS, 2018). The gages existing near the proposed intake structure are shown in Figure 2.
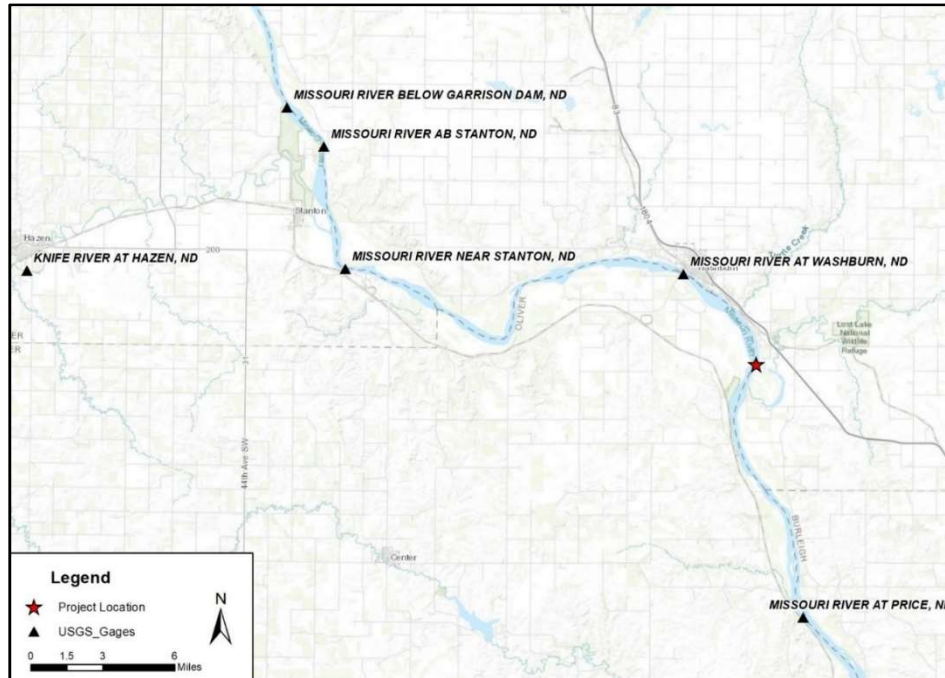
Figure 2. Active USGS gage stations

The daily discharge at the project site for the period between 1954 and 2017 was estimated by combining the releases from Garrison Dam with the adjusted flows for Knife River (adjusted to represent flows at the mouth; adjusted using streamflow data from a USGS gage located at the mouth of Knife River for the period between 2013 and 2016) . This record was analyzed to define the flow duration relationships on an annual and monthly (May through October) basis. The highest flows typically occur for the months of August and July with the lowest being in the months of September and October. The largest flow at the site of about 152,500 cfs occurred during the 2011 flood event. The lowest flow of about 2,860 cfs occurred in March 2009, which corresponds to the year with the lowest average discharge of about 16,000 cfs.

The latest USACE's hydrologic statistics report (USACE, 2013) provides the discharge-frequency relationship for the releases from Garrison Dam. This relationship with the combined daily discharge record was used to estimate the discharge-frequency relationship at the proposed intake structure. The resulting relationship is provided in Table 2.

Table 2. Discharge-frequency relationship for Missouri River at Proposed Intake Structure

Percent Annual Chance of Exceedance	Return Period	Discharge (cfs)
50	2	39,400
20	5	42,400
10	10	48,500
2	50	72,900
1	100	86,000
0.2	500	152,500

Long-Term Sedimentation Modeling (1D Analysis)

A 1D HEC-RAS sediment transport model (Version 5.0.3, which was the latest official release of HEC-RAS at the beginning of the study) was developed for the reach of the Missouri River between Garrison Dam (RM 1381.35) at the upstream end and Oahe Reservoir at the downstream end (RM 1332.71). The model was developed to determine expected elevation changes along the river over the next 50 years and to estimate existing and future water surface profiles for a wide range of flows. Two conditions were considered: (1) Historic to Current Conditions, which is utilized in the calibration of the model parameters; and (2) Current to Future Conditions, which is utilized to determine the future conditions at the proposed intake structure. Information about the model is summarized in Table 3.

Table 3. Summary Information about 1D HEC-RAS Sediment Transport Model

Item	Information
Geometry	For the Historic to Current Conditions, the cross section geometry is based on 1964 range line data. This year was selected as the beginning of the historical conditions simulation because of the prevalence of range line data compared to other years following the construction of Garrison Dam. For the Current Conditions, the cross section geometry is based on the geometry file from the latest USACE model for the Missouri River from Garrison Dam to Oahe reservoir. This model is based on 2012 range line data and was calibrated to the 2011 flood event.
Simulation Period	The simulation period or the Historic to Current Conditions model is from July 22, 1964 to October 21, 2012. The specific days of the year were selected to correspond to the average collection dates for the range line data as documented in the DSS file received from the USACE. The simulation period for the Current to Future Conditions is based on the same hydrology that occurred from 1964 to 2012.
Flow	Quai-unsteady flow hydrology defined using the available flow releases from Garrison Dam provided by the USACE and measured flows on the Knife River available from the USGS.
Time Step	24 hours for flows less than 20,000 cfs and 6 hours for flows greater than 20,000 cfs.
Water Temperature	Limited data on water temperature is available, so the long-term water temperature is based on correlation analysis between river and air temperature available for the Bismarck, ND gage.
Downstream Tailwater	Defined from the daily pool elevation of Oahe Dam obtained from the USACE.
Bed Sediment Distribution	Bed sediment defined using sediment samples obtained near the project site and data available from USACE (WEST, 2012).
Sediment Inflow	Set to zero for the release from Garrison Dam. Knife River sediment discharge and gradation are based on USGS sediment load samples collected by USGS between 1974 and 1993 near Hazen, ND. Relationship defined using the portion of the measured load that represents the bed material load (material finer than 0.062 mm was removed).
Sediment Density	Default densities of 93, 65, and 30 lbs/ft^3 for sand, silt, and clay, respectively.
Movable Bed Limits	Erosion limits were set equal to the bank stations, and deposition was allowed for the entire cross section.
Minimum Bed Elevation	The minimum bed elevation was set to 20 feet below the thalweg elevation.
Sediment Transport Equation	Ackers and White (1973), Yang (1973), and Engelund and Hansen transport functions were considered. Engelund and Hansen transport function was selected from the calibration efforts.
Fall Velocity Method	Toffaleti equation
Sediment Sorting	Copeland (Exner 7) method

The model was calibrated based on a volumetric approach using range line data collected by the U.S. Army Corps of Engineers, Omaha District for the periods between 1964 and 2012. A comparison of the observed and predicted sediment volume change is provided in Figure 2.
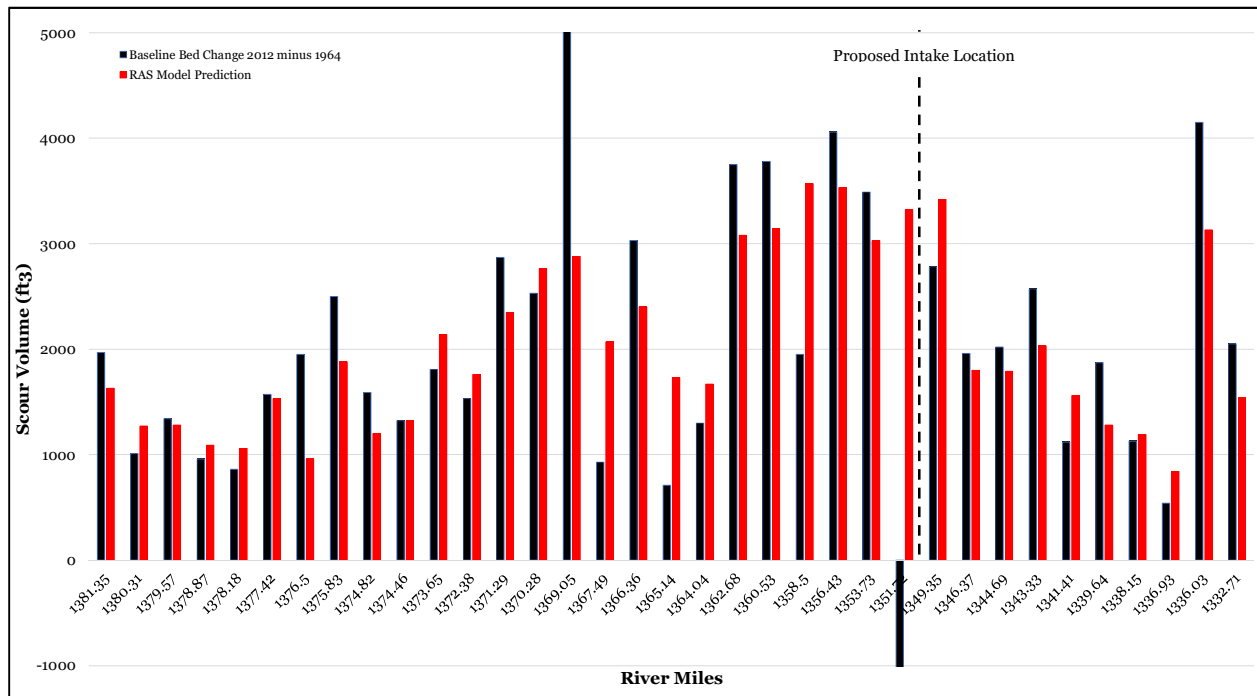
Figure 2. Predicted and observed sediment volume comparison

The Current to Future Conditions results indicate the Missouri River is not expected to reach a new equilibrium within the next 50 years and scour throughout the study reach will continue to be occur, but at a reduced rate. It is anticipated the long-term change in bed elevation will result in a lowering of the water surface elevation at the proposed intake structure of about 4 feet.

Event Sediment Transport Modeling (3D Analysis)

A CCHE3D (NCCHE, 2013) hydraulic and sediment transport software was developed for the reach of the Missouri River between RM 1,349.1 at the downstream end to RM 1,351.6 at the upstream end. CCHE3D (NCCHE, 2013) is a three dimensional (3D) numerical model that can simulate free surface turbulent flows with sediment transport, pollutant transport, and water quality analysis capabilities. Full Reynolds equations are solved using the Efficient Element Method, a collocation approach of the finite element method. Several turbulence closure schemes are available for users to select for their applications. The software can be used for both small scale near field, detailed flows and sediment transport analyses and large-scale engineering applications. The finite element transformation allows the software to be applied to cases with complex natural geometric and topographic domains. Mixed with the finite volume approach, mass conservation is preserved both locally and globally.

The software uses a structured grid to discretize the computational domain, and a partially staggered grid is used for solving the pressure field to eliminate oscillation. Equation systems are solved implicitly with the Strongly Implicit Procedure (SIP) method. Unsteady governing equations are solved for both steady and unsteady flow conditions. A free surface is computed with the free surface kinematic equation. Boussinesq assumptions are used to formulate turbulence stresses, and several turbulence closure schemes are available. A wall function can be applied as boundary conditions for vertical walls as well as for irregular bed surface using a simple slip and partial slip boundary condition. The model has the capability to assess both hydrostatic and dynamic pressures. Dynamic pressure becoming important for pronounced vertical flow acceleration.

The CCHE3D software was developed at the National Center for Computational Hydroscience and Engineering (NCCHE), the University of Mississippi, over the past twenty years. Computational Hydro-engineering Technology Inc. (CHeT) has the exclusive right to sub-lease license the model and provide user support and user services.

The NCCHE has developed two graphical user interface software programs for developing models: (1) CCHE-MESH, and (2) CCHE-GUI. CCHE-MESH is a 2D mesh generator for both structured and unstructured meshes. It allows rapid quality mesh generation from the topography database, topography images or maps, Digital Elevation Model (DEM) data, and GIS shape files. It provides users input and output (I/O) management, algebraic mesh generation, numerical mesh generation, mesh editing, and operations on the topography database. CCHE-MESH generates a geometry file (*.geo) for the computational mesh. The geometry file includes the following information for each of the nodes included in the computational mesh: (1) x-coordinate, (2) y-coordinate, (3) initial water surface elevation, (4) ground elevation, (5) boundary node ID, and (6) hydraulic roughness value (either Manning's n-value or roughness heights for a 2D model and roughness heights for a 3D model).

CCHE-GUI is an integrated software system for file management, simulation management, results visualization, and data reporting for all of the software developed by NCCHE. The CCHE-GUI software is used to create the 3D mesh and run the CCHE3D software. The 3D mesh is developed from the 2D mesh by adding vertical planes as specified by the user in CCHE-GUI. The general steps for developing and running a CCHE3D model is summarized as follows: (1) develop 2D computational mesh, (2) specify boundary conditions, (3) set the model parameters for 2D simulation, (4) run the 2D model using CCHE2D to establish initial flow conditions, (5) create a 3D mesh by defining the number of vertical layers, (6) set the model parameters for 3D simulation, and (7) run the model with CCHE3D. It should be noted that the vertical layers are not at the same elevation. The software distributes the vertical layers based on the flow depth at each of the nodes. The default distribution is to utilize a uniform distribution.

The models for this study were developed using the 64-bit version of the latest version of CCHE-MESH and CCHE-GUI software (Version 4.0), and are based on the metric unit system since it is the only unit system supported by the NCCHE software.

Sediment transport is one of the special features of the CCHE3D software. Transport of sediment could be influenced by vertical motion of fluid flows in addition to horizontal movements, such as within the vicinity of hydraulic structures. If the structures are very large, the water is forced to change its speed and direction near structures in order to pass through

them, resulting in changes in the sediment transport capacity that could cause increased local scouring and deposition over the sediment bed. Sediment transport occurs mostly at a non-equilibrium state related to the exchange between the river bed and flow field.

The CCHE3D software is comprised of general sediment transport capabilities for analyzing typical sedimentation conditions and special sediment transport features to assess local scouring problems near structures. CCHE3D is developed to account for non- equilibrium sediment transport with three different approaches: (1) bed-load type model that simulates bed load only or bed-material load without considering the diffusion of suspended load; (2) suspended load that simulates suspended load only or treats bed-material load as suspended load; and (3) computes bed load and suspended separately. In the case of non-uniform sediment transport, the sediment mixture is divided into several size classes, and the 3-dimensional convection-diffusion equation with a selected bed-transport equation are used to simulate the 3D sediment transport characteristics. More information about the equations and approaches used by CCHE3D are provided in CCHE3D Technical Manual (NCCHE, 2013) and CCHE2D Sediment Transport Model Manual (NCCHE, 2001).

Model Development

Detail Information about the CCHE3D model is summarized in Table 4.

Table 4. Summary Information about CCHE3D Model

Item	Information
Mesh	Mesh development for a CCHE3D model involves developing a 2D structured mesh using CCHE-MESH software. The computational mesh covers a total area of about 1.8 mi^2, and it is comprised of 71 x-direction nodes (j nodes in CCHE-MESH), 54 y-direction (i nodes in CCHE-MESH), and 9 vertical layers (k nodes) for a total of 34,506 nodes (3,834 nodes in each of the 2D layers). The average dimension of 2D grid elements located away from the proposed intake structure is about 25 meters wide by 70 meters long, while near the proposed intake structure they are about a 3.5 meter square. The elevation data for the mesh was based on a DEM developed using bathymetry and LiDAR data (AE2S, 2017) provided by AE2S.
Boundary Conditions	The CCHE3D model requires defined information at the upstream and downstream boundaries (nodestrings) of the mesh. A total discharge was defined at the upstream boundary using the relationship provided in Table 2. A water surface elevation was defined at the downstream boundary using the HEC-RAS model provided by USACE Omaha District.
Initial Water Surface and Flow Velocities	CCHE3D requires that the initial water surface elevation and velocity be defined at all of the mesh nodes. This was accomplished using a two-step process. First, the initial water surface elevations were defined using the HEC-RAS model by incorporating into the geometry (*.geo) file of the computational mesh. The geometry file wan then used in a CCHE2D model to define the initial water surface and flow velocities for the CCHE3D model.
Inflowing Sediment Characteristic and Loading	CCHE3D requires the inflow rate of sediment at the upstream boundary. Separate sediment inflow rating relationships is required for the bed and suspended load due to the method considered for this study. The bed load inflow rating relationship is provided as a unit transport rate (kg/m/s) and the suspended load relationship as a concentration (kg/m3). These relationships are based on sediment data collected at the Missouri River at USGS Washburn gage and information provided the USGS 2013 report (USGS, 2013). This gage has suspended sediment data from Water Year 2000 through Water Year 2012, and some additional samples obtained in Water Year 1988 through 1991.
Hydraulic Roughness Heights	Nine material types were used to define the hydraulic roughness within the study reach. The material type boundaries were defined based on topography, aerial photography, and shapefiles of rock revetment and river training structures. Initially, the Manning's n values for each material were estimated using information documented in Chow's Open-channel

	Hydraulics (Chow, 1959) and the HEC-RAS User's Manual (USACE, 2011). CCHE3D model requires that the bed roughness be defined using the roughness height, ks, and not Manning's n-values. Per the CCHE3D User's Manual, the Strickler's equation was used to estimate the equivalent roughness height based on the estimated Manning's n values. The initial parameters were adjusted as part of the calibration efforts to match the water surface elevation and velocities at various locations within the model reach.
Eddy Viscosity	Per recommendations from NCCHE, the eddy viscosity is represented in the model using the Mixing Length option with a coefficient of 1.
Fall Velocity	The fall velocity reflected in CCHE3D model is based on Zhang's formula (Zhang and Xie, 1993). The resulting fall velocities are similar to the fall velocities computed using Van Rijn's formula. The model uses a kinematic viscosity of 1.007×10^{-6}, which is based on the water have a temperature of 20 ^{0}C (68 ^{0}F).
Adaptable Length	Total load adaptation length quantifies the travel distance required for a packet of sediment to reach a new equilibrium concentration when it moves into a region of higher or lower shear stress (USBR 2013). Two parameters are required as inputs to the total load adaptation length computations. The first parameter is the bedload adaptation length, which characterizes the distance for sediment to adjust from a non-equilibrium state to an equilibrium state and is usually a function of river geometry and the spatial scales of sediment transport, such as bed form and saltation characteristics (NCCHE, 2001). The CCHE3D has three options for the bedload adaptation length: (1) average grid length, (2) 7.3 times the average flow depth (sand dune length defined by Van Rijn), and (3) specified adaptation length. All three options were considered and an adaptation length of 10 was selected from the calibration efforts. The second parameter is the suspended sediment adaptation length coefficients, which characterize how fast suspended sediments may reach the value of the equilibrium transport capacity (NCCHE, 2001). CCHE3D has two options: (1) Armanini and di Silvio method, and (2) specified adaption length. The first option was selected based on the performance of the calibration efforts and how it performed per the evaluation completed by Chen et al (2010).
Active Layer Thickness	The active layer is the top bed surface layer where sediment exchange between the water column and the bed occurs (NCCHE, 2001), which is a required input to CCHE3D. Subsurface layers provide sediments to or receive sediments from the active layer to force the active layer to maintain a specified thickness (NCCHE, 2001). As the active layer thickness increases, the bed and fractions of the active layer thickness will change more slowly, thus decreasing the rate at which armoring of the bed occurs. Conversely, as the active layer thickness decreases, armoring will occur more rapidly (USBR 2012). The active layer thickness was specified to be the default value of 0.05 m based on recommendations by NCCHE.
Bed Sediment Characteristics	CCHE-3D requires that the number of bed layers, number of sediment size classes, sediment size distribution in each bed layer, and the spatial distribution of the sediment be specified. The sediment sampling and USGS data indicates that the channel bed material is comprised of sand size material with some fine gravel material. CCHE-3D recommends a minimum of three layers be specified with each layer having a thickness of 5 meters. The sediment size distribution was also assumed to be the same for each layer. A total of three classes were considered in the model. The distribution and size for each class was based on the results of the bed material data collection effort completed for this study. The percent passing values for each of the samples that contained sand-sized material were averaged to determine the bed sediment size distribution. The bed layers, thicknesses, and sediment distributions were assumed to be uniformly distributed spatially throughout the entire 2D modeling area. CCHE-3D also requires the bed erodibility be defined within the mesh. The overbank and riprap areas were defined as non-erodible that only allows for sediment deposition to occur within the area.
Sediment Transport Approach	CCHE3D is developed to account for non- equilibrium sediment transport with three different approaches: (1) bed-load type model that simulates bed load only or bed-material load without considering the diffusion of suspended load; (2) suspended load that simulates suspended load only or treats bed-material load as suspended load; and (3) computes bed load and suspended separately. The first two options require the user to select a user defined sediment transport function. A total of four transport formula or modules are available: (1) Wu, Wang and Jia formula, (2) Modified Ackers and White formula, (3) Modified Engelund and Hansen formula, and (4) SEDTRA module that used three different transport function depending on the size (Laursen's formula for sediment sizes less than 0.25 mm, Yang's formula for sediment sizes between 0.25 and 2.0 mm, and Meyer-Peter and Mueller's formula sediment sizes greater than 2 mm). The third option was used for the final model.

Model Calibration

The CCHE3D model was calibrated to observed conditions. The calibration of the CCHE3D model was completed in two phase. The first phase involved the calibration of the model parameters that influence the hydraulic characteristics. This phase utilized observed flow velocities measured using an Acoustic Doppler Current Profile (ADCP) device and observed water surface elevation obtained during the ADCP measurements and noted during the 2011 flood event. The second phase involved the sediment transport option to consider changes in the channel bed between two bathymetric surveys completed with the reach of interest.

Phase I Calibration Effort: The first phase involved using the CCHE3D model to calibrate the model parameters that influence the hydrodynamics for observed during the field in early October and water surface elevations observed during the field and during the 2011 flood event. Fixed bed conditions were assumed for this calibration effort due to the short duration of time represented during the ADCP measurements. ADCP velocity data obtained by the River Measurement, which is a division of WEST, and water surface elevations obtained by AE2S was used in the first calibration phase of the CCHE3D model. The measurements consist of two transects that were averaged to provide the representative depth and flow velocity at each measured location. The Phase I calibration effort of the CCHE3D model involved adjusting the roughness height, pressure methodologies, eddy viscosity methods and coefficients, and side wall boundary assumption to minimize the difference between the computed and observed velocity magnitude and direction.

The Phase I calibration model results indicated the following: (1) the CCHE3D model did a good job at representing the water surface elevation and average cross sectional conditions, (2) the results are generally more accurate at the upstream location than for the downstream direction, and (3) the model overpredicts the velocities at the downstream location and underpredicts at the upstream location. A comparison of the velocity magnitude and direction at each measured flow depth for the measurement near the proposed intake structure indicates that the CCHE3D model does a fairly good job at matching observed conditions with the computed velocity being slightly larger than 10% of the observed value and the velocity directions being about 3%. The model overpredicts the velocity in the water column with the difference increasing as the depth increases.

Phase II Calibration Effort: The second phase involved using the CCHE3D model to calibrate the model parameters that influence the bed changes from sediment transport calculations. The elevation data for the mesh was based on a DEM developed using bathymetry obtained in October 2017 (AE2S, 2017). Two other bathymetry data was available: (1) August 2016, and (2) April 2018. A review of the August 2016 bathymetry data indicated that the data is too sparse to use for the Phase II calibration effort. This was not the case for the April 2018 bathymetry data. However, this data set is limited to the area near the proposed intake structure.

The Phase II calibration effort involved changing model parameters to minimize the absolute difference between the computed and observed change of bed elevation. The parameters considered in this phase include the sediment transport method and transport function,

curvature effects, bed thickness, inflowing gradation, bed load adaption lengths, suspended load adaption length, and bed roughness options.

The Phase II calibration results indicate that the absolute difference between the computed and observed change of bed elevation is between 0 and 2 feet for most of the location with some locations being on the order of 5 to 7 feet. The average absolute difference is about 1 feet with the maximum being 7 feet.

Model Conditions

Three model conditions were evaluated with the CCHE3D model: (1) Existing Conditions, (2) Proposed Conditions, and (3) Construction Conditions. The first two conditions were evaluated for flood events ranging from the 50% to 0.2% ACE (2-year to 500-year) events, while the third condition was evaluated only for the 50% and 0.2% ACE events. The Existing Conditions model is based on the calibrated model. The Proposed Conditions model was developed by changing the node elevations of the Existing Conditions model at the proposed intake structure to match the intake structure elevations. The Construction Conditions model was developed eliminating all of the nodes that fall within the cofferdam structure and defining the nodes at the edge of the cofferdam structure as an exterior boundary.

Model Results

Three different types of CCHE3D model results were obtained from the model: (1) velocities on upstream wall of intake structure, (2) scour and deposition pattern near the proposed intake and cofferdam structures; and (3) change in bed elevations and water surface elevations between Proposed\Construction Conditions and Existing Conditions. The average and maximum velocities on the upstream side of the upstream wall of the intake structure ranges from 2.9 to 3.8 ft/s, while the maximum velocity ranges 3.6 to 4.4. ft/s.

The results related to the scour and deposition pattern indicate that the general pattern consist of minor deposition upstream of the structure and scour on the sides of the structure with the deeper scour depths occurring on the west side of the structure. The maximum estimated scour near the proposed structure ranges from 5 to 7 ft on the west side and from 1 ft to 2 ft on the east side. The model indicates deeper scour will occur for the cofferdam in-place with the higher scour occurring near the upstream corners of the structure (and scour on the west side is larger than the east side). The maximum scour for the cofferdam in-place was 17 ft on the west side and about 6 ft on the east side for the 0.2% ACE event.

For the Proposed Conditions, the channel elevation changes are expected to be relatively minor for all flood events evaluated, and most predicted elevation changes and are within the model's resolution (plus or minus a few feet). Further, no upstream effects are expected, and minor elevation changes could occur on the downstream (non-vegetated) sandbar downstream. Minor changes will occur in the bed near the structure, and there will be no adverse impacts to the existing bank protection measures are expected. Changes in the water surface are also considered negligible with only small areas where there is a change greater than 0.1 feet.

The channel elevation changes associated with the cofferdam in-place will be localized and minor changes could occur on the downstream (non-vegetated) sandbar downstream. Cofferdam will

result in a slight increase in the water surface elevation upstream of the structure and a slight decrease in the water surface elevation downstream of the structure.

Scour Estimations using Empirical Equations

Scour near the proposed intake structure was estimated using the equations and methodologies documented in HEC-18 (FHWA, 2012). The total scour for the existing bridge was estimated for discharges ranging from the 50% to 0.2% ACE with the hydraulic characteristics being based on the CCHE3D model results. The total scour is comprised of contraction scour and local scour. The contraction scour was estimated using Laursen's live-bed scour equation (FHWA, 2012). The proposed intake structure will be similar to a pier structure with a complex footing. Therefore, the local scour was estimate using the complex pier procedure and equations presented in HEC-18 (FHWA, 2001). The maximum scour depths using the empirical equation was estimated to be about 18 ft for the 0.2% ACE event (about 17 ft above the top of piles proposed for the structure), and about 22 ft for the cofferdam in-place for the 0.2% ACE event.

Summary

As part of the RRVWSP, a new water intake will be constructed on the Missouri River south of Washburn, ND. Because the Missouri River is a sand-bed river and Garrison Dam is upstream, it is important to determine the risk that the new intake could be undermined during the project life. Further, the ND SWC is responsible for issuing a Sovereign Lands Permit for the proposed intake. A sediment transport study was completed to define the risk of the intake structure being undermined and to address ND SWC key questions. The sediment transport analysis included a geomorphic assessment, 1D model development to assess long-term sedimentation trends, and 3D model development to assess the influences of the proposed structure.

The Missouri River within the vicinity of the proposed intake structure is a highly dynamic sand bed river system that has been degrading due to sediment trapped by the upstream Garrison Dam. Based on the historic sediment range data, the estimated change in the bed elevation over a 50 year period is expected to be about -5 feet, and the change in thalweg elevation over this period will fluctuate between -3 and 5 feet. Results from a 1D HEC-RAS sediment transport model indicate similar trends and magnitude of bed changes over the 50 year period.

The CCHE3D model results indicate that the proposed intake structure will not be undermined by scour, the channel elevation changes associated with the structure are expected to be relatively minor for all flood events evaluated, and most predicted elevation changes and are within the model's resolution (plus or minus a few feet). The CCHE3D model results for the Construction Conditions (cofferdam in-place) indicate the channel elevation changes will be localized with the potential of minor changes on the downstream (non-vegetated) sandbars, and there will be a slight increase in the water surface elevation upstream of the structure and a slight decrease in the water surface elevation downstream of the structure.

References

AE2S. 2016 (August). Hydrographic Survey Data furnished by AE2S.

AE2S. 2017 (October). LiDAR and Hydrographic Survey Data furnished by AE2S.

AE2S. 2018 (April). Hydrographic Survey Data furnished by AE2S.

Chen D., Acharya K., and Stone M. 2010. "Sensitivity Analysis of Nonequilibrium Adaptation Parameters for Modeling Mining-Pit Migration", Journal of Hydraulic Engineering, ASCE, pp 806-810.

Chow, V.T. 1959. Open-Channel Hydraulics. McGraw Hill Publishing Company, Inc., New York.

Federal Highway Administration (FHWA). 2012. "Evaluating Scour at Bridges, FHWA-IP-90-017, Hydraulic Engineering Circular No. 18", Fifth Edition, Washington, D.C.

National Center for Computational Hydroscience and Engineering (NCCHE), School of Engineering, The University of Mississippi. 2001. "CCHE2D Sediment Transport Model (Version 2.1), Technical Report No. NCCHE-TR-2001-3".

National Center for Computational Hydroscience and Engineering (NCCHE), School of Engineering, The University of Mississippi. 2013. "CCHE-GUI – Graphical Users Interface for CCHE Models User's Manual – Version 4.0".

National Center for Computational Hydroscience and Engineering (NCCHE), School of Engineering, The University of Mississippi. 2013. "CCHE-MESH: 2D Mesh Generator for Structured and Unstructured Meshes, Quick Start Guide, Version 4.0".

National Center for Computational Hydroscience and Engineering (NCCHE), School of Engineering, The University of Mississippi. 2013. "Technical Manual of CCHE3D, Version 1.1".

North Dakota Aerial Photography Dissemination Mapservices. 2018. "Historic Aerials". https://aerial.swc.nd.gov/

U.S. Army Corps of Engineers. 2012. "HEC-DSS of Missouri River Range Data", Omaha District.

U.S. Army Corps of Engineers. 2016. "HEC-RAS River Analysis System User's Manual, Version 5.0", Hydrologic Engineering Center, Davis, CA.

U.S. Army Corps of Engineers, Northwestern Division. 2013. "Hydrologic Statistics Technical Report", Missouri River Basin Water Management Division.

U.S. Army Corps of Engineers, Omaha District. 2015. "Missouri River Unsteady HEC-RAS Model Calibration Report, Appendix B: Garrison Dam to Oahe Dam".

U.S. Army Corps of Engineers, Northwestern Division. 2017. "Missouri River Stage Trends Technical Report", Missouri River Basin Water Management Division.

U.S. Geological Survey. 1994. "Nationwide Summary of U.S. Geological Survey Regional Regression Equations for Estimating Magnitude and Frequency of Floods for Ungaged Sites, 1993, Water-Resources Investigations Report 94-4002", https://pubs.usgs.gov/wri/1994/4002/report.pdf

U.S. Geological Survey. 1995. "Transport and Sources of Sediment in the Missouri River and between Garrison Dam and the Headwaters of Lake Oahe, North Dakota, May 1988 through April 1991, U.S. Geological Survey Water-Resources Investigations Report 95-4087", prepared in cooperation with the U.S. Army Corps of Engineers.

U.S. Geological Survey. 2013. "Characteristics of Sediment Transport at Selected Sites along the Missouri River during the High-Flow Conditions of 2011, U.S. Geological Survey Scientific Investigations Report 95-4087", prepared in cooperation with the U.S. Army Corps of Engineers, Omaha District.

U.S. Geological Survey. 2014. "Geomorphic Change on the Missouri River during the Flood of 2011, U.S. Geological Survey Professional Paper 1798-I", http://dx.doi.org/10.3133/pp1798I.

U.S. Geological Survey North Dakota Water Science Center. 2018. "USGS Streamflow Data", https://nd.water.usgs.gov/.

WEST. 2012. "Missouri River Garrison Project Downstream Channel and Sediment Trends Study", prepared for Northwest Division – Omaha District, Sediment and Channel Stabilization Section.

WEST-AE2S. 2015. "Sedimentation Impacts Resulting from the Relocation of the US Highway 85 Bridge", prepared for Western Area Water Supply Authority.

Sediment Transport in the Intake Area of the Cardinal Plant: Field Study and Physical Model

Troy Lyons, Director of Engineering Services, IIHR – Hydroscience & Engineering, The University of Iowa, Iowa City, Iowa, troy-lyons@uiowa.edu

Nathan Young, Research Engineer, IIHR – Hydroscience & Engineering, The University of Iowa, Iowa City, Iowa, nathan-young@uiowa.edu

Marcela Politano, Research Engineer, IIHR – Hydroscience & Engineering, The University of Iowa, Iowa City, Iowa, marcela-politano@uiowa.edu

Abstract

Sedimentation is a chronic problem in many riverside water intakes. As part of US EPA rule 316(b) of the Clean Water Act, American Electrical Power and Buckeye Power Inc. are considering the installation of submerged cylindrical wedge-wire screens in the intake area of the Cardinal Plant. A study was performed to evaluate the sediment transport to the intake area and deposition near the screens. This study was comprised of three primary activities: perform on-site field work, construct and perform tests with a 1/24 reduced-scale laboratory model, and develop and perform simulations with a CFD model. This paper describes the field work and physical model. The model, based on Froude scaling, replicates a range of river flows and intake flows. Sediments were modeled using reduced-scale particles based on field samples. The model was calibrated against velocity data collected in the river upstream and near the intake. Deposition rates and deposition regions predicted with the physical model agree well with the CFD model. According to the models, sediment deposition could negatively affect intake operation with the cylindrical screens for existing conditions. Model results indicate that mitigation measures can be effectively implemented to reduce sedimentation near the intakes. Mitigation measures designed in attempts to mitigate sediment deposition around the screens were evaluated and are discussed.

Introduction

The Cardinal Power Plant (Cardinal) is located on the Ohio River near Brilliant, Ohio and has been in operation since 1967. American Electrical Power and Buckeye Power Inc. (the Owners) are investigating options to comply with U.S. EPA Rule 316(b) for fish impingement and entrainment at their cooling water intakes. Cardinal is unique in that the cooling water intakes are set back from the main bank of the river, in a side pool or forebay, created by excavation at the time of plant construction. Under existing conditions, significant sedimentation occurs in the forebay, requiring dredging every 3 to 5 years. Field measurements, physical modeling, and numerical modeling were utilized in a comprehensive study to help determine the feasibility of replacing the existing traveling water screens (TWS) with a static array of submerged cylindrical wedge-wire screens (screens). Ideally, the screens will be located entirely within the forebay, extending some distance from the intakes, to avoid frequent barge traffic in the main river channel. This paper focuses on the field data collection (Firoozfar et al. 2016a) and physical modeling portions of the work (Firoozfar et al. 2016b). Part 2 of this study is a sister paper and focuses on the numerical portion of the work (Politano et al. 2016).

Field Work

Overview

IIHR collected bathymetric data, velocity data, and sediment samples in the vicinity of the plant during two field programs with special focus on the forebay (Figure 1). The data was used to develop, construct, calibrate, and validate the physical and numerical models used in the study. The data was collected using an 18-ft research vessel, specially outfitted with the appropriate instrumentation and equipment.

Figure 1. Aerial view of the Cardinal Plant forebay (IIHR, September 21, 2015)

Bathymetric Data

An area of the Ohio River and the forebay bed elevations were measured from the research vessel using a single-beam sonar system with GPS tracking. Horizontal and vertical position of the sonar were measured with Real Time Kinematic (RTK) and Global Navigation Satellite System (GNSS) receivers, with correlations from a temporary ground-based reference station. The equipment setup provided riverbed elevation accuracies of approximately +/- 1 inch. Measurements were concentrated within and near the forebay to capture a higher level of detail required for the modeling.

Hydrographic survey software was used to aid in navigation, integrate system components, store measured data, and post-process the data. Elevation points were used to create a triangulated irregular network (TIN) surface model of the surveyed area. Available topographic data of the overbank areas was incorporated to create a final digital elevation model (DEM) of the study area (Figure 2).
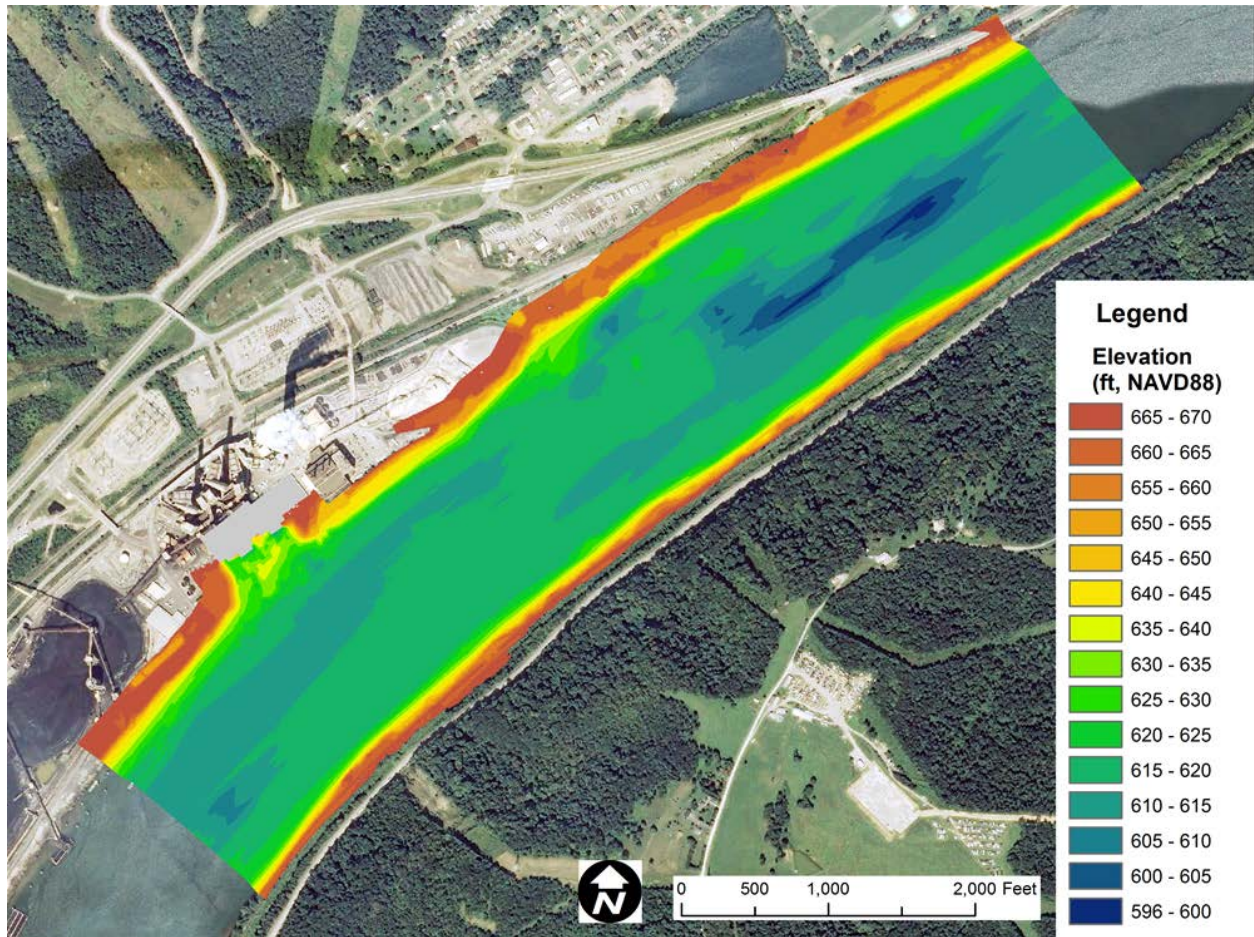
Figure 2. Digital elevation model developed from the bathymetric surface and overbank topographic data

Velocity Data

River discharge and velocity were measured using a vessel-mounted Acoustic Doppler Current Profiler (ADCP). This instrument uses the sound wave reflections generated by four transducers off particles in the water to measure three-dimensional velocities in the water column. The location of each measurement was resolved using the GNSS data streams integrated with the ADCP data collection software, allowing real-time visualization and adjustments for vessel movement.

ADCP measurements were collected along river transects to determine river discharge and at stationary locations to develop accurate vertical velocity profiles at specific locations. Depth-averaged velocity vectors were calculated along each transect over the study reach (Figure 3).
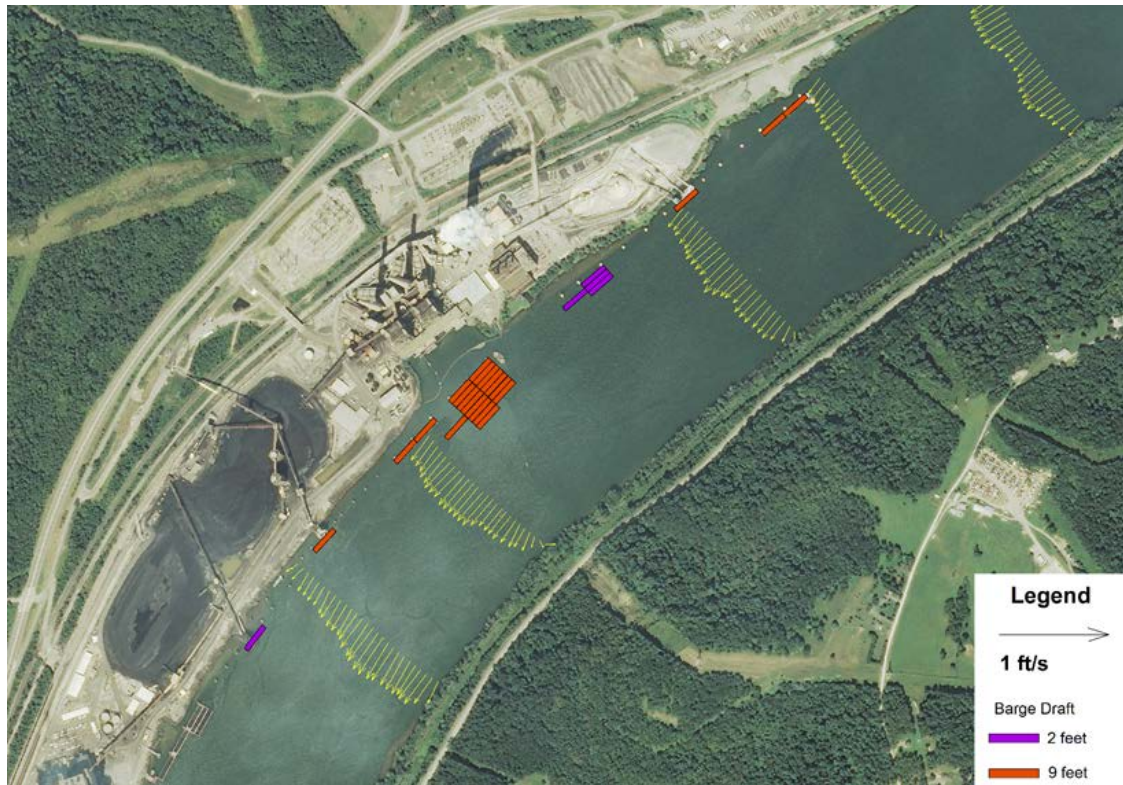
Figure 3. Depth-averaged river velocity data along transects

Sediment Data

River bed sediment samples were collected in the river channel and within the forebay. Samples were collected using a winch-deployed clamshell bucket from the research vessel. Sample locations were measured with the GNSS.

Sediment grain size distribution was determined by sieve and SediGraph analysis of each sample in IIHR's sediment laboratory according to ASTM standards (ASTM, 2006 and ASTM, 2013). Sediment size distribution and characteristic particle sizes D_{10}, D_{50}, and D_{90} were determined, representing the particle sizes in which 10, 50, and 90% of the particles in the sample are smaller in diameter.

Results showed that sediments collected upstream of the forebay ranged from silt to sand along the right bank to gravel and cobble towards the main channel centerline. Sediments collected in front of the forebay ranged from clay and silt to sand near the forebay to gravel and cobble towards the main channel. Sediments collected inside the forebay were finer, ranging from clay to silt and sand. Sediments collected further out in the main channel ranged from sand to cobble. Sediment sample locations were plotted on an aerial view of the project site and colored by the D_{50} sediment particle size (Figure 4).
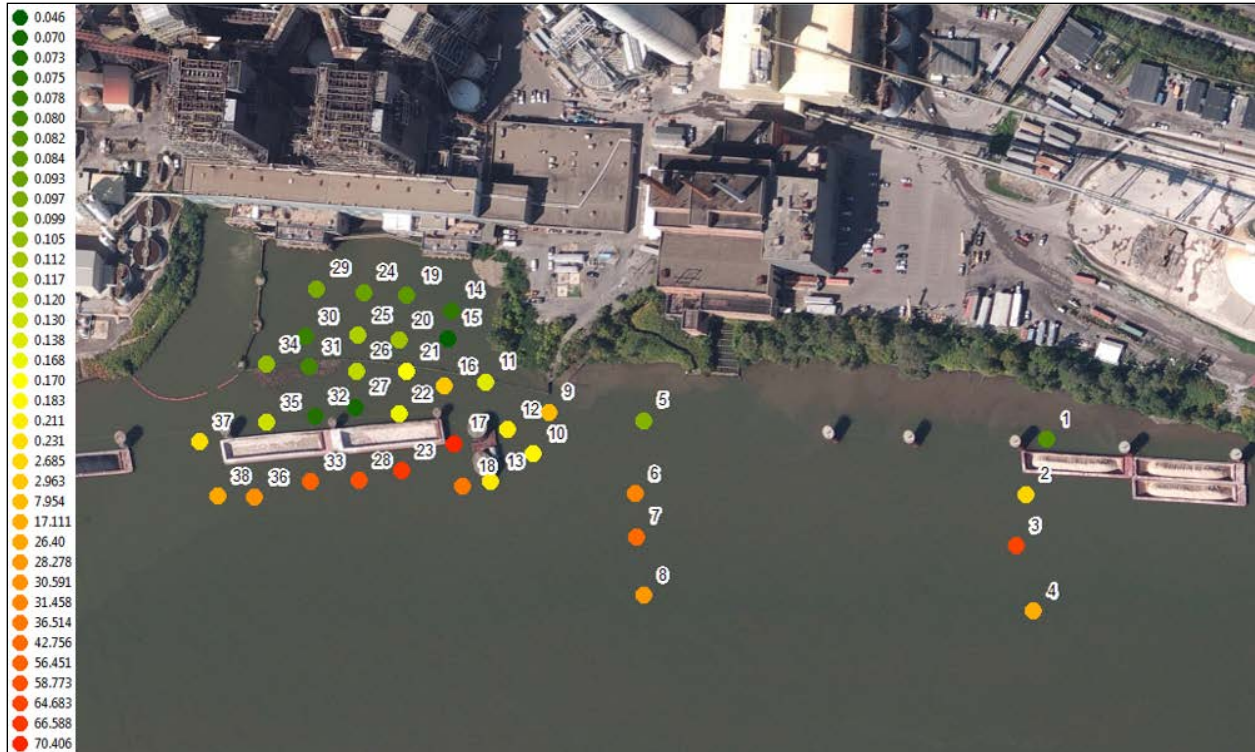
Figure 4. Sediment sample locations colored by the D_{50} characteristic sediment size (mm)

Physical Model

Model Overview

A geometrically undistorted physical model of the cooling water intakes, forebay, and a 2,300-foot portion of the Ohio River channel was constructed at a 1:24 scale (Figure 5). The main river channel was constructed of concrete with an erodible bed in the vicinity of the forebay and intakes. River bathymetry and overbank topography from the field survey were integrated in the model using cross-sectional templates cut with a computer numerically controlled (CNC) gantry router.

The model simulated river flows up to 283,000 cubic feet per second (cfs) and cooling water intake flows up to 800,000 gallons per minute (gpm). The model recirculated river flows from a below-grade sump to the model headbox using pumps. A flow-conditioned headbox distributed flows uniformly across the river width. Flowrates were established with calibrated flow meters. Cooling water intake flows were set with a pump, valves, and flow meters. River water surface elevation was controlled with an adjustable tailgate weir.

Figure 5. Plan view of the 1:24 scale physical model

Model Sediment

In sediment laboratory studies like this one, the sediment sizes measured in the field cannot usually be scaled based on the geometric scale factor due to the effect of gravitational and inter-particle electrostatic forces (i.e., model particles would clump together). Therefore, other scaling relationships must be considered. The two most significant dimensionless parameters of sediment movement in a channel are the Shields parameter and the particle Reynolds number. In order to achieve sediment movement similarity, the values of these parameters must be matched in the model and prototype. However, this strategy usually requires a combination of a geometrically distorted model and/or lightweight particles to achieve a match. Because the use of a geometrically distorted model is not encouraged for complex flow scenarios such as the present study (Ettema, 2000), using lightweight particles in the model was the best way to achieve similarity. Consequently, lightweight Acrylic particles were chosen for the sediment in the model because they provided acceptable movement in the model and matched the Shields parameter and Reynolds number as closely as possible. Acrylic particles have similar specific gravity as coal and walnut shells, which are typically used in mobile bed models (Bettess, 1990; Ho et al., 2010; Frostick et al., 2011; Gorrick and Rodríguez, 2014), but are advantageous since they don't biodegrade and are readily available in specific sizes.

The model sediment was mechanically mixed to the target particle size distribution and artificially fed into the model at a precisely controlled rate to simulate suspended and bed load in the river. This was the same sediment used in the erodible bed portion of the model. The sediment slurry was distributed through a custom fabricated feeder located upstream of the mobile bed area along the right bank. This provided sediment-laden flows in the river for deposition within the forebay and along the right bank.

Figure 6. Model sediment and screens

Velocity Calibration

A series of tests were conducted to assess the capability of the model to replicate the flow velocities and directions measured during the field campaigns. The calibration initially focused on matching the velocity and flow direction in the main channel and then in the forebay. River flowrate, tailwater elevation, barge configuration, and intake flow conditions from the specific dates of the field campaigns were replicated on the model prior to measurement. Over the course of calibration, modification and adjustments to the model headbox and inlet conditions were made to achieve proper flow behavior in the main channel. Field data from the first field campaign was associated with much lower river flows, and therefore had low water velocities, which proved difficult to match within the target range of +/-10% of flow magnitude and +/-10 degrees of flow angle. Field data from the second field campaign was associated with higher river flows, had higher velocities, and was able to be matched more closely on the model. For both conditions, barges were in various configurations and moved throughout the day, adding some uncertainty to the field measurements. However, the comparisons showed that, overall, the flow patterns in the main channel and along the right bank matched well with the field data, with all data points falling within the established criteria. Calibration inside the forebay was more challenging, with factors such as lower velocity magnitudes, influence from physical structures (e.g. moorings and barges), and thermal influences from the discharge canal contributing to uncertainties between model and field data. However, the model forebay flow patterns and velocities were consistent with field measurements and matched reasonably well (Figure 7).
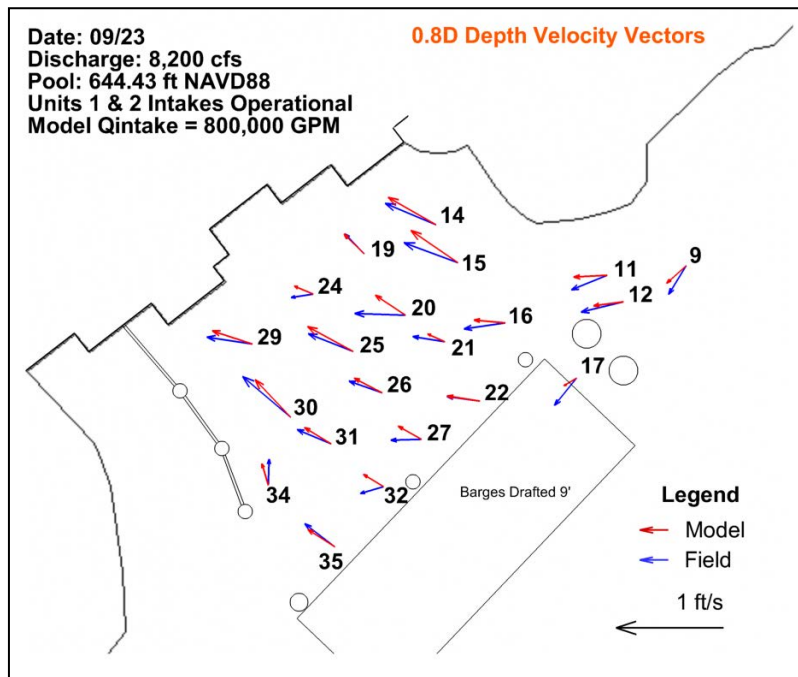
Figure 7. Model and field velocity vectors used for calibration

Sediment Calibration

An additional test was undertaken to determine the models capability of producing a sediment deposit in the forebay similar to what was measured during the field campaign. Prior to the test, the forebay area was flattened to a "dredged" condition. Then an 85-hour model test was run while continually feeding sediment upstream at a known rate. The test resulted in a total volume of sediment deposited in the forebay within 2% of the target known quantity in the field. In the model, the sediment bar deposit was more uniform than observed in the field (Figure 8). This is most likely due to more controlled and constant flow and sediment conditions in the laboratory than experienced in the field. In the field, the sediment deposit was formed over decades, with portions of it dredged out over time to create channels for water to reach the intakes. In addition, the field deposit formed with transient influences from natural hydrologic cycles and highly variable sediment loads that cannot be quantified for comparison. It was concluded that the physical model showed good replication of the overall shape and pattern of the deposition in the forebay based on the existing sediment deposition in the field, given the practical limitations in the laboratory and the unquantifiable field conditions.

(a) Field   (b) Lab
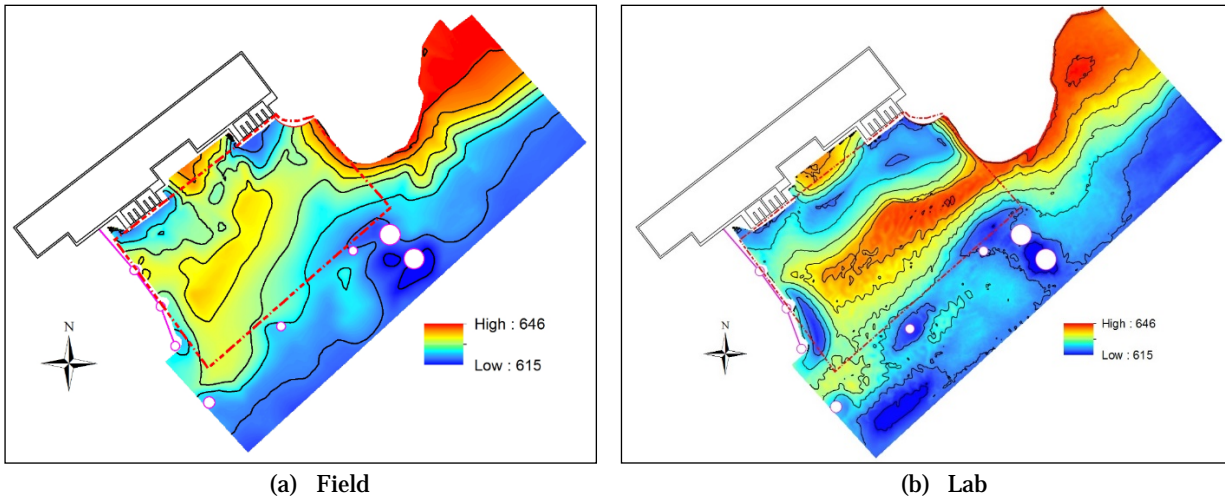
Figure 8. Model and field velocity vectors used for calibration

Sediment Mitigation Testing

To make valid comparisons between each sediment test, the model was run at the same prescribed river flowrates and sediment feed rates for the duration of each test. The model flowrates were selected based on analysis of relationships between the historical river flows and total suspended sediment (TSS) data and observations of sediment transport on the model.

After the completion of each test, the model was slowly drained to minimize sediment disturbance. A terrestrial laser scanner (Plenner et al. 2016) was then used to measure the bed surface in order to quantify the amount of sediment deposited and create elevation maps of the resultant bed (Figure 9) and difference plots of the bed from before and after the test.
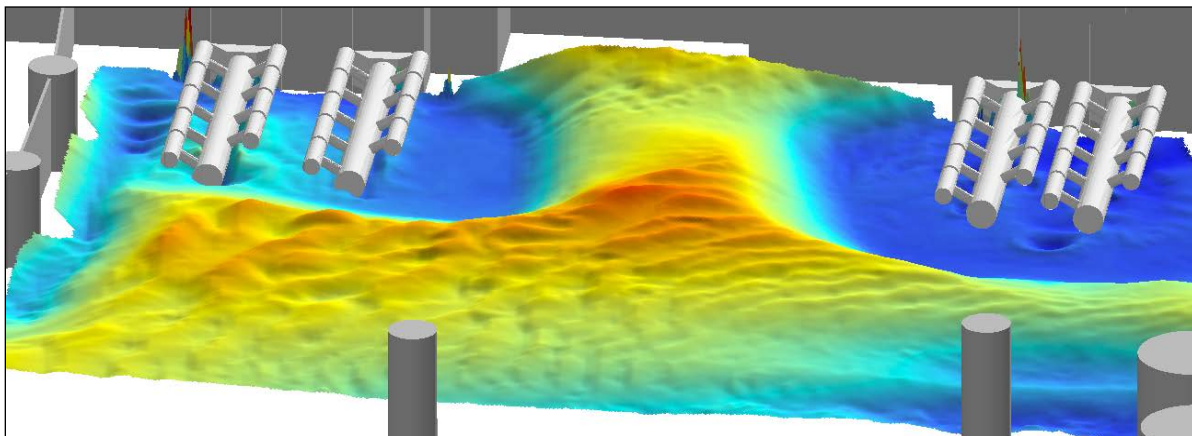
Figure 9. Elevation map of the forebay sediment after a lab test

Several shorter exploratory tests were conducted first with different sediment mitigation approaches in an effort to determine the most effective means to reduce the amount of sediment depositing in the forebay. Several combinations of various structures including submerged

skimmer walls, full height walls, and submerged vanes were tested. Observations revealed that submerged skimmer walls were not effective at reducing sedimentation but rather full height walls and strategic placement of vanes could potentially provide the desired improvements. Based on observations of the initial tests, nineteen preliminary concepts were developed for consideration.

Through further testing, analysis, and discussion with the Owners, nine concepts were selected for full testing. The majority of these scenarios included a full height wall that was used to alter the flow patterns near the entrance forebay and within the forebay. Other scenarios included walls, vane arrays, re-contouring the right bank, or various combinations thereof.

Test results showed that re-contouring of the right bank was effective, but was not pursued due to concerns with handling river debris and higher-than-expected costs to remove the bank material. For the remaining tests, the results showed that deposition from suspended sediments, rather than bedload, was the dominant process for most of the concepts. Therefore, the concepts involving full-height walls rather than skimmer walls or vanes were more effective at reducing sediment deposition within the forebay. The two best performing wall concepts were referred to as option 2B and option 10. Option 2B was an angled wall originating from the right bank at the upstream end of the forebay that directed river flows outward and away from the forebay. Option 10 was an expanded version of option 2B and included the option 2B wall and an additional wall across the forebay face that created a narrow entrance into the forebay (Figure 10). Due to the orientation and extent of the full-height walls, option 10 created a settling region outside of the forebay and downstream of the angled wall in which a significant amount of the sediment particles in the water column deposited. This caused a significant reduction in suspended load entering the forebay and resulted in very little deposition of the total material fed into the model inside the forebay.
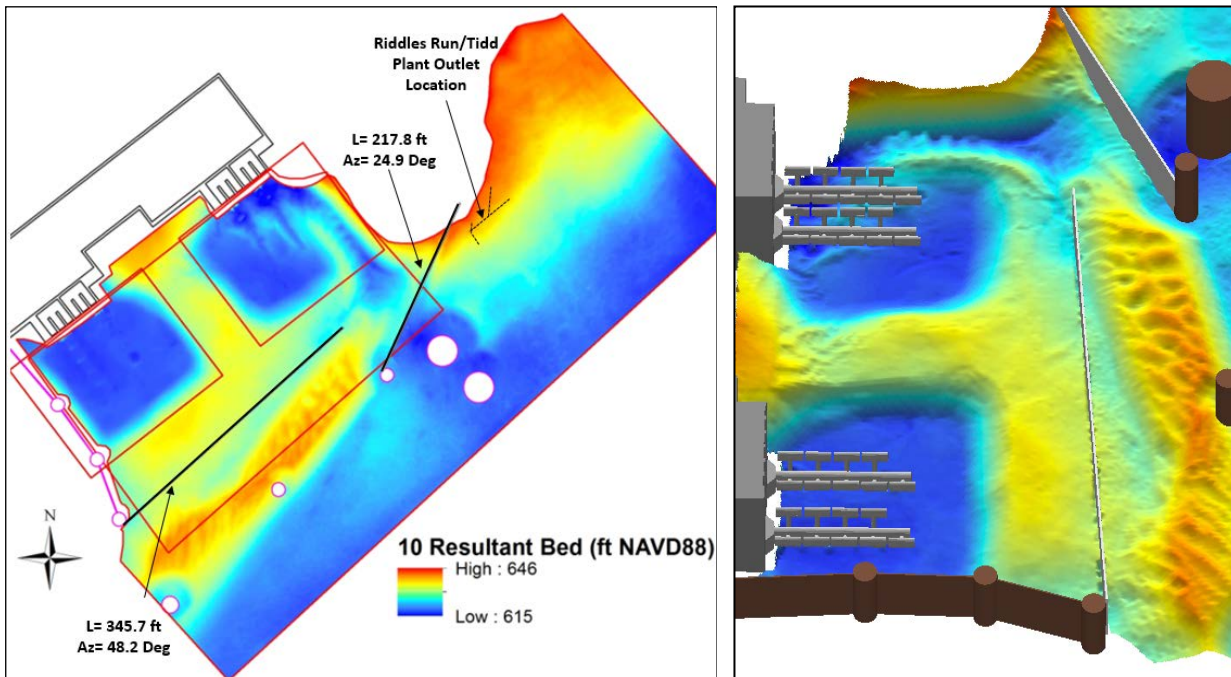
Figure 10. Option 10 test results

Final Testing

Because option 10 would be expensive to implement in the field, the Owner's preferred approach is to install the option 2B wall first and add the additional wall across the forebay to create option 10 at a later date if the option 2B wall alone performs unsatisfactorily. Due to this phased approach, several additional tests were conducted to further explore the performance of the option 2B wall independently. Tests included sensitivity tests on the wall angle, the influence of barges moored across the forebay entrance (as frequently occurs), and operation with unit 1 offline.

The final tests showed that the original wall angle of 25 degrees was optimal. Changing it plus or minus 5 degrees from the original orientation slightly increased the volume of sediment deposited in the forebay, but only by a few percentage points.

Tests to determine the influence of six fully loaded barges (two long and three wide) moored across the forebay entrance showed that the barges increased the amount of sediment deposited in the forebay. Most of the additional sediment was determined to be due to mobilization of the erodible bed beneath the barges, which created locally higher velocities beneath the barges due to the reduced water column from the barge draft. However, even with the barges, the sediment reduction was still better than most other options tested.

Tests with unit 1 offline showed a tendency for more sediment to deposit in front of unit 1 and less to deposit in front of unit 2, with a slight overall increase in deposition over the entire forebay.

Conclusions

The following conclusions were drawn from the study:
- Without mitigation measures, submerged screens in the forebay would encounter significant sedimentation over time, requiring periodic dredging around the screens.
- Sedimentation in the forebay and around the screens can be significantly reduced with implementation of mitigation measures.
- Full-height walls that cause significant changes to the forebay and near-shore river hydraulics are most effective at reducing sedimentation in the forebay.
- Altering the angle of the option 2B wall by five degrees or less does not significantly alter the forebay deposition patterns.
- Mooring barges in front of the forebay with the option 2B wall in place does not significantly alter the forebay deposition patterns.
- Taking unit 1 offline with the option 2B wall in place results in more deposition in front of unit 1 but less deposition in front of unit 2.
- Sediment mitigation option 10 performed most favorably from a flow and sediment perspective. The Owners' plan to implement option 10 incrementally by first installing the option 2B wall and then later installing the wall across the forebay to create option 10 is a reasonable approach. If satisfactory performance is achieved with option 2B, then further improvements provided by the secondary option 10 wall may not be necessary.

References

A.S.T.M. Standard C136-06. 2006. Standard Test Method for Sieve Analysis of Fine and Coarse Aggregates, ASTM International, West Conshohocken, PA.

A.S.T.M.Standard E11-13. 2013. Standard Specification for Woven Wire Test Sieve Cloth and Test Sieves, ASTM International, West Conshohocken, PA, 2013.

Bettess R. 1990. Survey of Lightweight Sediments for Use in Mobile-bed Physical Models. In: Shen, H.W. (Ed.), Movable Bed Physical Models. Kluwer Academic Publishers, Dordrecht, pp. 115e123.

Ettema R. 2000 (ed.). Hydraulic Modeling Concepts and Practice. ASCE Manuals and Reports on Engineering Practice No. 97, ASCE Publications.

Frostick, L.E., McLelland, S.J. and Mercer, T.G., eds. 2011 Users Guide to Physical Modelling and Experimentation: Experience of the HYDRALAB Network. CRC Press.

Firoozfar, A.R., Gilles, D.W., Craig, A.C., and Young, N.C., "Hydraulic Studies for the Cardinal Plant (Units 1 and 2) 316 (B) Cooling Water Intake Fish Impingement/Entrainment Project; Part I: Field Data Collection and Analysis, IIHR Limited Distribution Report No. 406, IIHR-Hydroscience & Engineering, The University of Iowa.

Firoozfar, A.R., Craig, A.J., and Lyons, T.C. 2016. Hydraulic Studies for the Cardinal Plant (Units 1 and 2) 316 (B) Cooling Water Intake Fish Impingement/Entrainment Project; Part II: Physical Modeling, IIHR Limited Distribution Report No. 415, IIHR-Hydroscience & Engineering, The University of Iowa.

Gorrick, S. and Rodríguez J. F., 2014."Scaling of Sediment Dynamics in a Laboratory Model of a Sand-bed Stream". Journal of Hydro-environment Research, 8(2), 77-87.

Ho J., Coonrod J., Gill T., and Mefford B. 2010. Case study: movable bed model scaling for bed load sediment exclusion at intake structure on Rio Grande. Journal of Hydraulic Engineering, 136(4), 247– 250.

Politano, M., Martin, E, and Lyons, T.C. (2016). "Hydraulic Studies for the Cardinal Plant (Units 1 and 2) 316 (B) Cooling Water Intake Fish Impingement/Entrainment Project; Part II: CFD Model", IIHR Limited Distribution Report No. 416, IIHR-Hydroscience & Engineering, The University of Iowa.

Plenner, S., Eichinger, W., and Bettis, E. (2016). "Simple Terrestrial Laser Scanner for Measuring Streambank Retreat." Journal of Hydraulic Engineering, 10.1061/(ASCE)HY.1943-7900.0001184 , 06016015.

Sediment Transport in the Intake Area of the Cardinal Plant: CFD Model

Marcela Politano, Research Engineer, IIHR – Hydroscience & Engineering, The University of Iowa, Iowa City, IA, marcela-politano@uiowa.edu

J. Ezequiel Martin, Asst. Research Engineer, IIHR – Hydroscience & Engineering, The University of Iowa, Iowa City, IA, juan-martin@uiowa.edu

Troy Lyons, Director Engineering Services, IIHR – Hydroscience & Engineering, The University of Iowa, Iowa City, IA, troy-lyons@uiowa.edu

Abstract

Sedimentation is a chronic problem in many riverside water intakes. As part of US EPA rule 316(b) of the Clean Water Act, American Electrical Power and Buckeye Power Inc. are considering the installation of submerged cylindrical wedge-wire screens in the intake area of the Cardinal Plant. A study was performed to evaluate the sediment transport to the intake area and deposition near the screens. This study was comprised of three primary activities: perform on-site field work, construct and perform tests with a 1/24 reduced-scale laboratory model, and develop and perform simulations with a CFD model. This paper describes the CFD model. Sediments are modeled using a particle tracking technique considering that sediment particles can be suspended, deposited or move as bed load depending on the local shear stress. The model was validated against velocity data collected in the river upstream and near the intake and sediment deposition location in the reduced-scale laboratory model. Buoyancy forces, included in the model, originating from temperature differences played an important role in the flow pattern near the intake. According to the model, sediment deposition could negatively affect intake operation with the submerged screens if not properly mitigated. Model results indicated that a wall upstream of the intake minimizes the deposition of sediment near the right bank. However, the wall promotes the entrainment of warm water from the discharge canal into the intake. The inclusion of both a thermal curtain and upstream wall was the best alternative to comply with EPA Rule 316(b) using submerged screens.

Introduction

American Electric Power Corporation (AEP) and Buckeye Power Inc. (the Owners) are investigating options to comply with US EPA Rule 316(b) for fish impingement and entrainment at the water intake for units 1 and 2 of the Cardinal Plant on the Ohio River. One option to reduce cooling water intake velocities below the 316(b) compliance flow rate limit is to install submerged cylindrical wedge-wire screens in the intake forebay. This option, however, raises concerns about sediment accumulation around the screens in the forebay. Under existing conditions, significant sedimentation occurs in the forebay, requiring dredging every 3 to 5 years.

The primary purpose of this study was to assess the feasibility of installing submerged cylindrical screens in the Cardinal forebay. The primary goals of the CFD study were:

- Identify changes in the flow patterns due to installation of the screens
- Evaluate the effect of the screens on sediment deposition rates in the intake forebay

- Analyze possible sediment mitigation measures

This paper presents details of the CFD model, model validation against field data and reduced-scale laboratory model, and discusses changes in the flow pattern and transport of sediments due to installation of the submerged cylindrical screens.

CFD Model

Modeled Domain

The CFD domain comprised approximately 1.3 miles of the Ohio River as shown in Figure 1. Bathymetric data collected by IIHR was used in the model (Firoozfar et al. 2016).
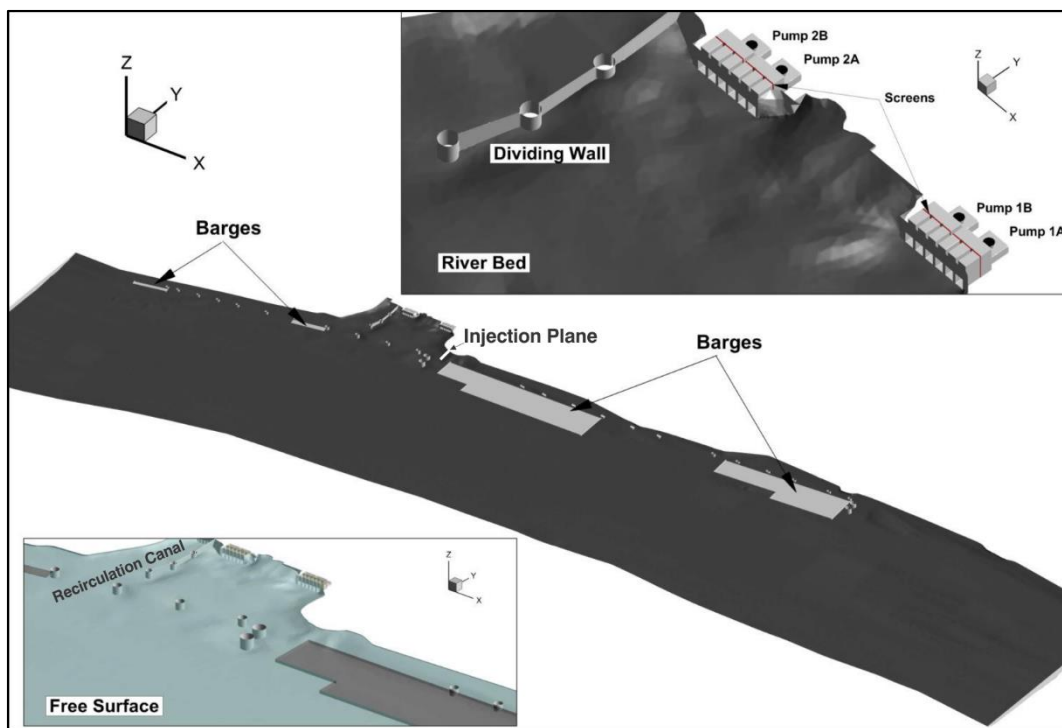
Figure 1. Cardinal CFD model

Numerical Model

Models used in this study are based on the CFD code Fluent, ANSYS. The discrete Reynolds-Averaged Navier-Stokes (RANS) equations were solved to determine the hydrodynamics. A standard $k-\varepsilon$ model with wall functions was used to solve the turbulence. The drawdown caused by the cylindrical screens was simulated using the Volume of Fluid (VOF) approach. Buoyancy forces caused by temperature gradients were included to capture the observed vertical velocity distribution. The temperature was calculated from the energy conservation equation for incompressible flows. Screens were modeled as a homogeneous porous media with an inertial resistance factor. Barges, which were present during the field campaign (Firoozfar et al. 2016),

were modeled as rigid bodies. Once the hydrodynamics were solved, particle tracking simulations were performed to estimate sediment deposition rate. The Fluent 12.0 Theory Guide describes the mathematical and numerical models for the hydrodynamics. The sediment model was developed at IIHR and implemented into Fluent using User Defined Functions (UDF). The discrete RANS equations were solved sequentially. Continuity was enforced using a SIMPLEC algorithm with a skewness correction factor of 2. The discretization scheme selected for momentum was second order. Zero velocity and turbulence were used as initial conditions for the entire domain. Nonlinear iterations were needed to converge all variables to an L2 norm of the error lower than 10^{-4}. The average shear stress at the river bed was monitored to evaluate model convergence.

Sediment Modeling: Sediment transport and deposition rate in the forebay were assessed using a multiple component approach to represent sediments of different grain size, which have distinct critical shear stress and sediment mobility. Sieve and SediGraph analyses indicated that the diameter of most of sediments found in the forebay region ranges from 0.06 mm to 0.21 mm and particle size distribution in that range is approximately uniform (Firoozfar et al. 2016). Particle size distribution at the injection plane is not the same as that measured in the forebay since deposition changes with sediment size. Particle concentration of sediment of size-i at the injection plane was estimated using the particle volume distribution of size-i measured in the forebay and the deposition ratio obtained from a numerical simulation with the existing intake configuration.

Sediment accumulation in the forebay changes the bathymetry and flow pattern over time affecting sediment deposition rates and locations where particles settle on the bed. The Exner equation can be used to compute changes in bed elevation. Deforming the river bed using a UDF to define the position of each node through the divergence of the sediment flux is possible in Fluent. However, this approach was shown to be impractical for this project due to lengthy running times for re-meshing and convergence. Instead, for this study, the deposition rate was calculated assuming a constant river bed and steady state hydrodynamics for a constant river flowrate. Therefore, the computed deposition rate is only valid at the beginning of the sedimentation process (initial deposition rate) and should not be used to estimate time to deposit a given amount of material when significant morphological changes are expected or erosion is one of the main sediment processes.

The prediction of suspended sediment trajectories was predicted by integrating gravity, drag and turbulence forces on a particle:

$$\rho_p \frac{d\vec{u}_p}{dt} = \left(\rho_p - \rho \right) \vec{g} + F_D \tag{1}$$

where $\vec{u}_p$ is the particle velocity and ρ_p the particle density. The first term on the right hand side of Eq. 1 is the buoyant force and the second term represents the drag force. Turbulence dispersion was modeled using a stochastic discrete-particle approach by integrating the trajectory equations for each particle using the instantaneous velocity.

Solids are deposited when the shear stress is smaller than the critical shear τ_c, depending on the sediment material and size. According to Soulsby (1997):

$$\tau_c = \left[\frac{0.3}{1+1.2\,d_*} + 0.055\left(1-e^{-0.02\,d_*}\right)\right] g\,d\left(\rho_p - \rho\right) \tag{2}$$

The dimensionless grain size d_* is $d_* = d\left[g\left(\dfrac{\rho_p - \rho}{\rho}\right)\Big/ v^2\right]^{1/3}$. Bedload transport was calculated

following Meyer-Peter and Muller (1948). The bedload velocity is:

$$\vec{u}_b = B_n\left(\tau - \tau_c\right)^{1.5}\left(g\,d\left(\rho_p - \rho\right)\right)^{1.5}\left(g\left(\frac{\rho_p - \rho}{\rho}\right)d^3\right)^{0.5} \Big/ \left(h_n\,f_b\right) \tag{3}$$

where f_b is the packing fraction of the sediments and B_n is the bedload coefficient, which is between 5 to 5.7 for low transport, 8 for intermediate transport and up to 13 for very high transport. The bedload thickness   is calculated from Van Rijn (1984):

$$h_n = 0.3\,d\,d_*^{0.7}\left(\tau/\tau_c - 1\right)^{0.5} \tag{4}$$

Grid Generation

Numerical grids were generated using the SnappyHexMesh utility supplied with the open source CFD code OpenFoam. SnappyHexMesh creates 3D meshes containing hexahedra and split-hexahedra cells automatically from triangulated surface geometries in Stereolithography format (STL). The mesh conforms to the STL surfaces by iteratively refining a starting Cartesian grid and morphing the resulting split-hex mesh to the surfaces. 3D CAD renderings of the geometry including units 1 and 2, piers, discharge canal outflows, dividing wall, river bed, free surface, and the upstream and downstream end of the model were developed to generate the STL files. Local refinement near boundaries and the river bed was performed to properly capture the geometry and shear stress, respectively. Grid size was selected through a grid sensitivity analysis during the validation of the model. About 30 nodes, with local refinement near the river bed, were needed in the vertical direction to capture turbulent structures and the shear stress near the bed. An aspect ratio of about 2.5 was adopted to achieve proper grid quality. All simulations performed in this study used the grid refinement selected during the grid sensitivity study. The grids used in this study contain approximately 10 million cells.

Model Validation

The model results were compared against field velocity data (Firoozfar et al. 2016) to evaluate the model capability to predict the general flow pattern in the forebay and reproduce vertical and longitudinal velocity profiles in the main channel. The bathymetry measured during the field study was used for model validation of the hydrodynamics. Stationary velocity data measurements from Nov. 3, 2015 were quantitatively compared against model predictions. Velocities in the main channel at three specified water depths were qualitatively compared against transect velocity data. The river flowrate on Nov. 3, 2015 was 34,005 cfs and intake #2 was operating at 400,000 gpm. Temperatures in the river and discharge canal were 53.6 °F and 76.5 °F, respectively. Local refinement using layers near the river bed was applied to satisfy the y+ requirement for proper prediction of the shear stress.

Results

Figure 2 shows velocity data collected at four transects along the moving vessel's path together with model predictions considering water was at a constant temperature. The model properly captured the vertical velocity profile as well as the velocity distribution along the river width. Very good agreement between field and modeled data was observed with exception of the region where water from the discharge canal is released into the river channel.
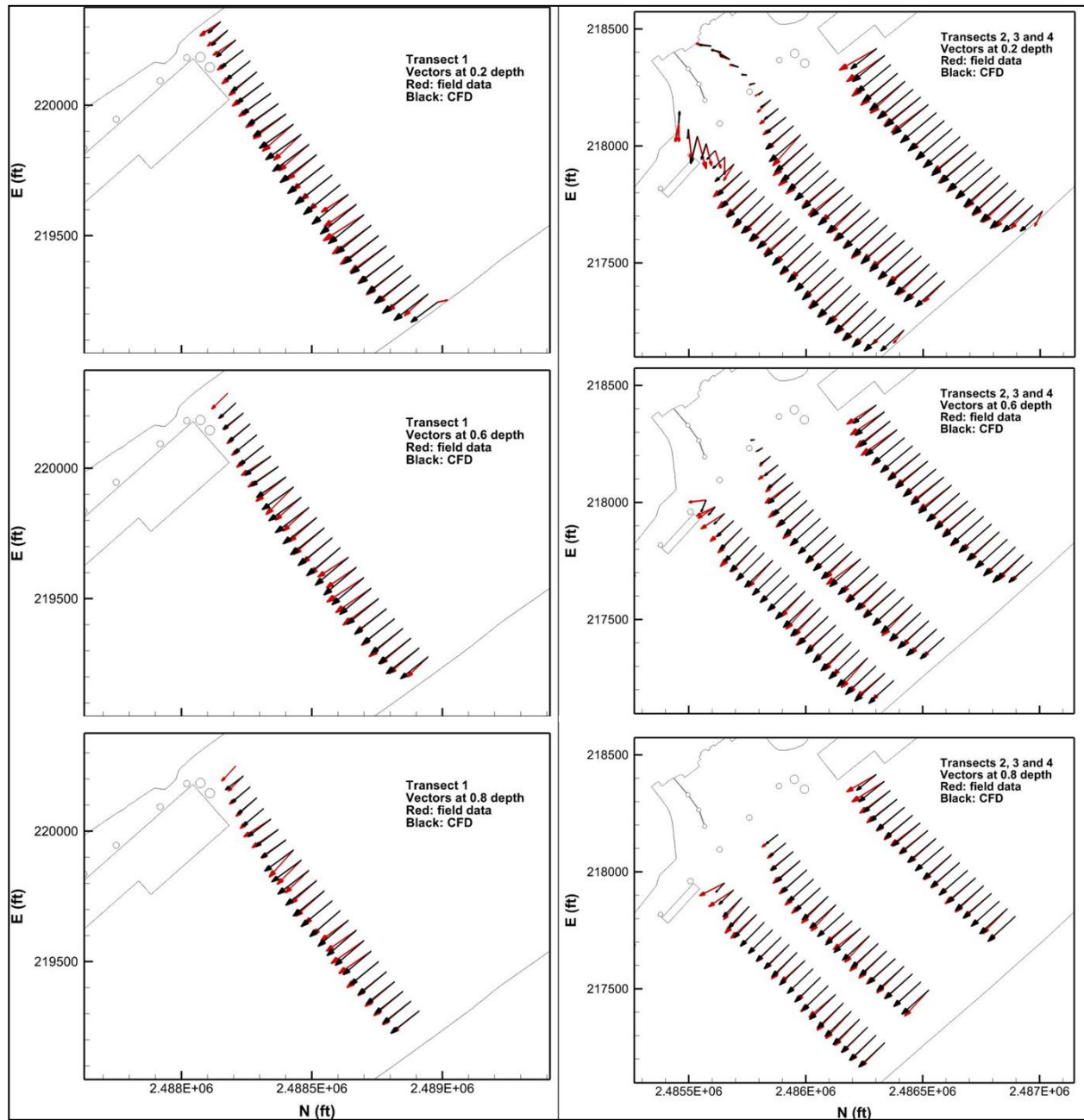
Figure 2. Measured (red) and modeled (black) velocity data at 0.2, 0.6 and 0.8 depth on Nov. 3, 2015

Figure 3 shows stationary collected data and predicted velocity vectors at 0.2, 0.6 and 0.8 depths in the forebay when thermal effects were included. The model captured the observed flow pattern at this location.
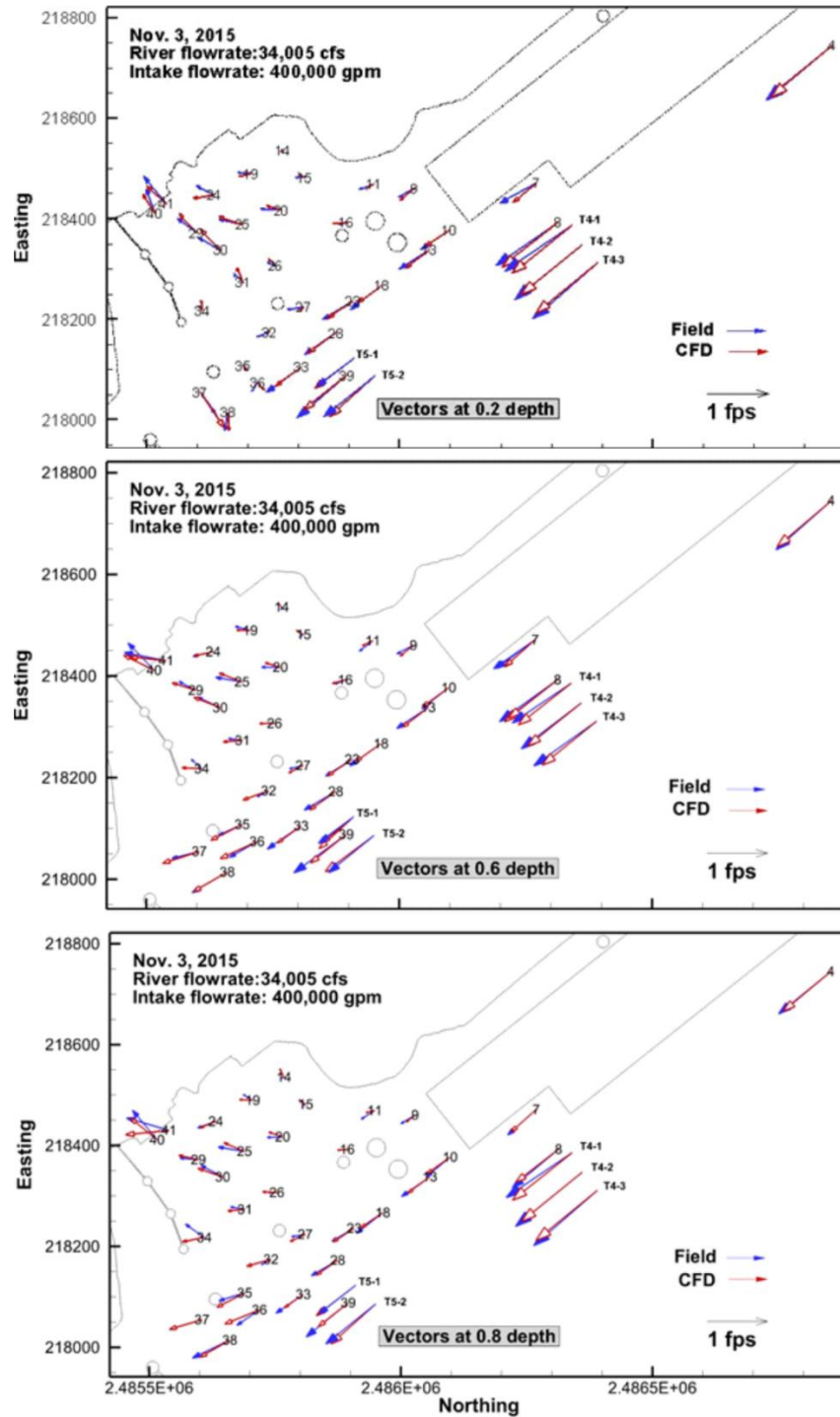
Figure 3. Measured (red) and modeled (black) velocity data at 0.2, 0.6 and 0.8 depth on Nov. 3, 2015

The average error between predicted and measured velocity magnitude at 27 locations with measured velocities larger than 0.33 fps at 0.2, 0.6 and 0.8 depths was 10.7%. The average of the absolute difference in velocity direction at those same locations was 5.5 degrees. The model underpredicted the velocity in the channel near the forebay. The largest average error was 21.2% at location 39 in Figure 3. Note, however, that errors at locations T5-1 and T5-2 near point 39 collected during moving transects were smaller than 5%. This seems to indicate a change in the river flowrate when stationary data was collected or from local unsteadiness due to temperature changes or moving barges.

Sediment Deposition with Existing Intake

A CFD simulation was performed to determine regions in the forebay where sediment deposits and initial deposition rate with the existing intake configuration at a river flow of 150 kilo cubic feet per second (kcfs). This flowrate was identified as a good estimate of the effective flowrate for this location, based on historical sediment and discharge data. General flow pattern and deposition regions were compared against observations in the 1:24 physical model. The forebay area was numerically dredged at constant elevation 618.38 ft (NAVD88) to accommodate an extended screen layout. Figure 4 shows the modeled geometry, bathymetry and grid used for this simulation. Increasing the river flowrate resulted in larger Reynolds numbers in the forebay, which required further refinement in the vertical direction to satisfy the y+ criteria for proper prediction of the bed shear stress. Grid refinement in all directions was performed near the forebay to avoid high aspect ratio elements, which can affect the quality of the solution.
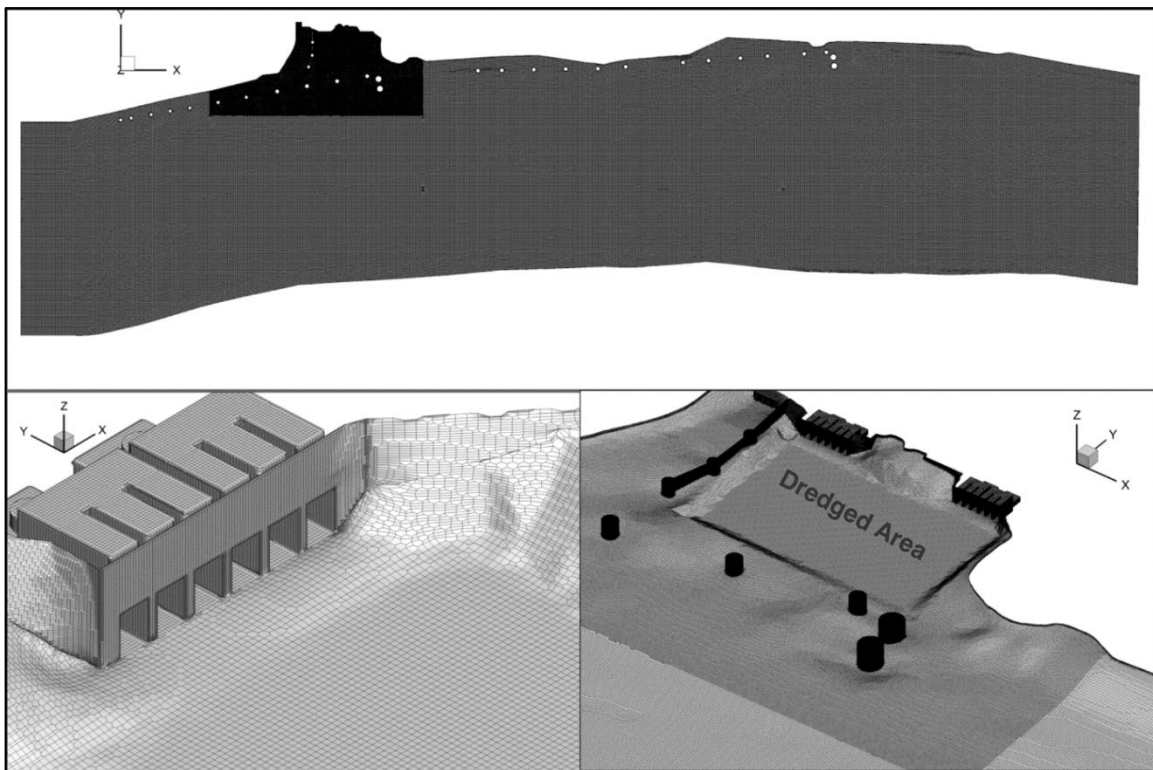
Figure 4. Grid used to evaluate sediment deposition in the existing intake configuration

Results

Figure 5a shows calculated streamlines colored by velocity magnitude for the existing configuration. The length of the dashed lines is proportional to velocity. A large clockwise eddy is present in the forebay region for high river flowrates. At 150 kcfs, water flows to the downstream intake region before moving towards unit 2 first and then unit 1. A similar flow pattern was observed in the laboratory model under equivalent conditions. Figure 5b shows the predicted shear stress. Sediment deposit in regions with shear stress smaller than the critical shear stress. Contours indicate locations in the river bed where coarse silt, very fine sand and fine sand can deposit if sediments are transported by suspension or bed load to that region.
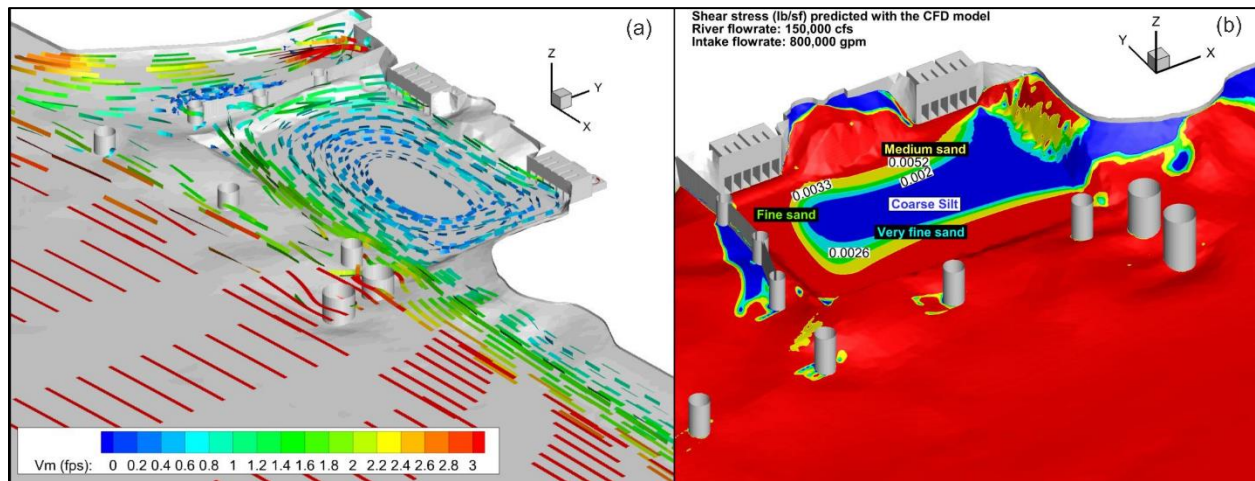
Figure 5. (a) Streamlines colored by velocity magnitude and (b) Bed shear stress

Figure 6 shows the location of the deposited particles together with measured bathymetry in the physical model. Location of particles predicted with the CFD model matches reasonably well with the deposition region observed in the laboratory. Note that measured bathymetry in the physical model was a result of sediment transport and erosion over time at a variable river flowrate, which is expected to produce a different bed than predicted for one particular event. According to the CFD model, 1,438 cubic yards accumulate in the forebay in one month at a constant flowrate of 150 kcfs. This deposition rate was calculated for a specific condition of constant river bed and flowrate and so it is valid only as a reference and for comparative purposes to evaluate the effect of structural modifications or operational conditions on sediment transport. This deposition rate should not be used to represent the accumulation of material in the field under normal river conditions with unsteady flowrates and changing bathymetry.

A rough estimate of material accumulated in the forebay assuming that the retention rate predicted with the CFD model is independent of the flowrate and using the flow exceedance probability by Firoozfar et al. (2016) results in about 1,920 yd^3/year. This value is expected to decrease due to morphological changes as sediment accumulates. As a reference, analysis of bathymetric datasets in 2005 and 2001 indicated that approximately 5,200 yd^3 were deposited in the forebay (Firoozfar et al. 2016). Records of dredging activities during that time period are unavailable. In 2013, 5,200 yd^3 and 6,164 yd^3 were removed in front of unit #1 and unit #2, respectively (Firoozfar et al. 2016).
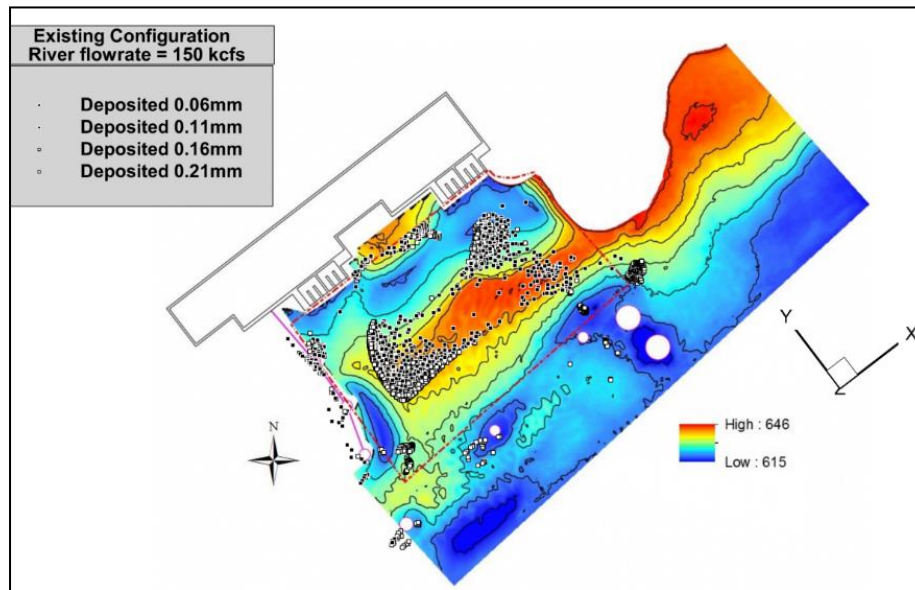
Figure 6. Deposition regions for existing intake configuration predicted with the CFD and physical models. Colors indicate deposit thickness in the hydraulic model

Submerged Cylindrical Screens

Cylindrical screens shown in Figure 7a were incorporated in the forebay. The barges and trash boom were not included in the model. A river flowrate of 150 kcfs with both intakes operating at 400,000 gpm each were used to evaluate the submerged cylindrical screens. The grid was refined near the screens to properly capture the screen geometry (Figure 7b). An additional volume was included at the top of the grid to accommodate the air phase.

Results

An instantaneous free surface is shown in Figure 8; it is clearly seen in this image that the free surface deformation was related to waves refracting from the different semi-submerged structures in the domain and was not significantly affected by the operation of the intakes. According to the model, the drawdown caused by the cylindrical dense screens was insignificant and a rigid-lid model with constant elevation was used to perform all sediment simulations with this screen configuration.

Changes in forebay flow patterns were observed when the screens were included. The large clockwise eddy in the forebay (Figure 9a) persisted with or without the screens. However, some water from the river moved directly into the screen in unit 1 creating several low velocity eddies near the screens. This flow pattern was also observed in the laboratory model. Figure 9b shows the predicted shear stress when submerged screens are included. Adding the dense screens in the forebay and dredging the bathymetry around the screens resulted in a reduction of the shear stress, and thus increased the potential for sediment deposition.
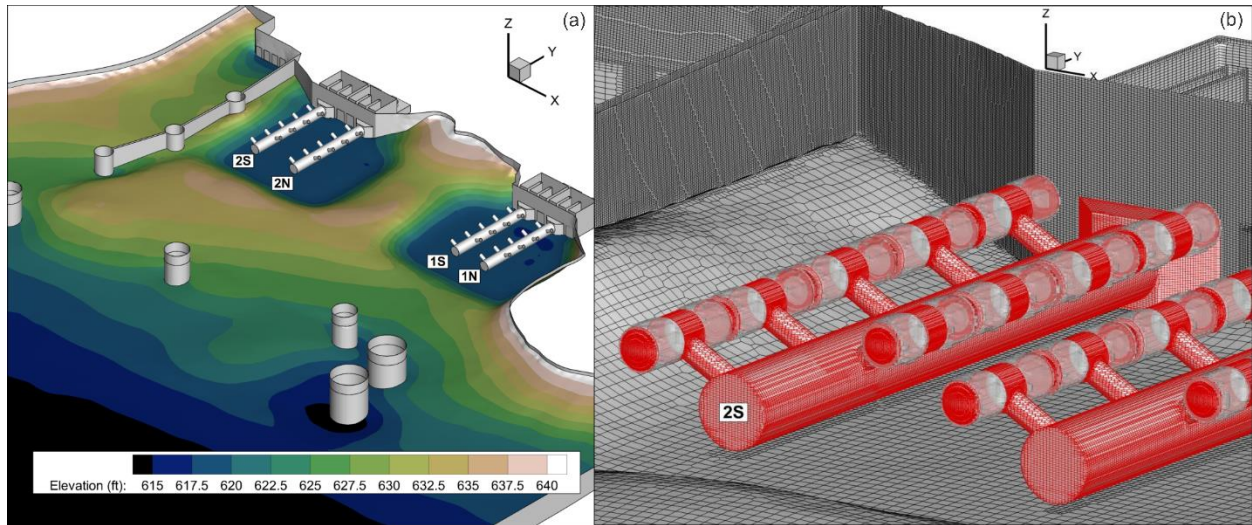
Figure 7. (a) Submerged cylindrical screens and (b) Grid details near the screens
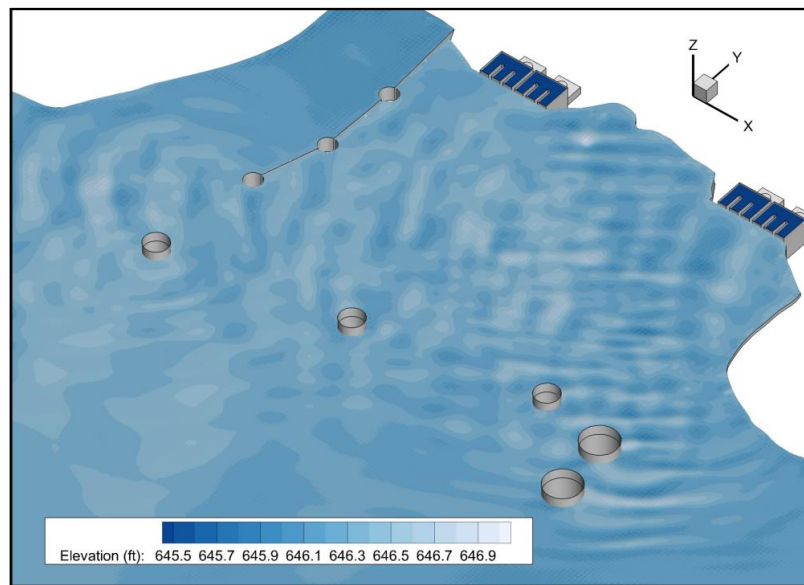
Figure 8. Free surface with submerged cylindrical screens
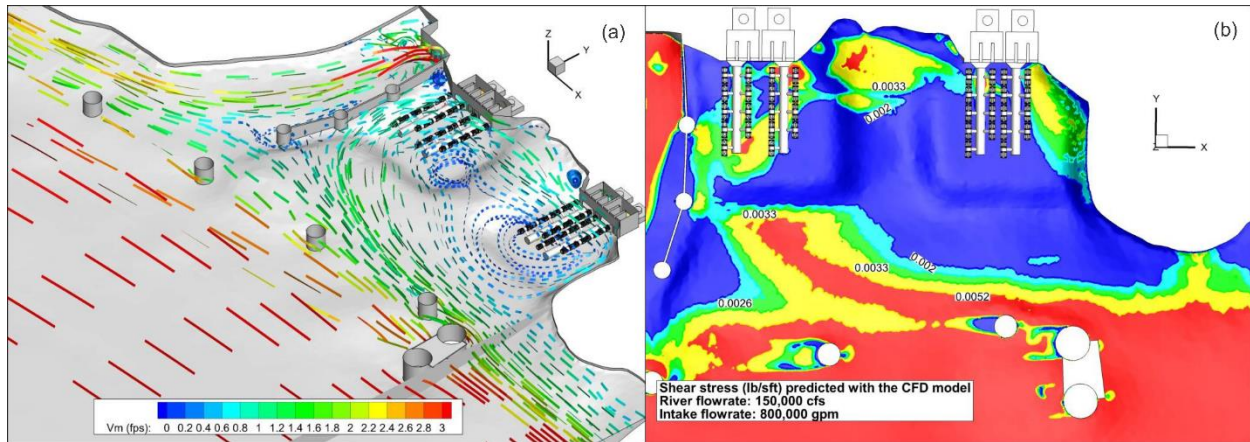
Figure 9. (a) Free surface with submerged cylindrical screens and (b) Shear stress at the river bed for test #6A

More particles deposited when screens were included in the intake. Coarse silt and very fine sand were entrained into the forebay and deposited beneath the dense screens. However, fine sand, which contributes to most of the volume deposited in the forebay, deposited outside of the dredged area. Figure 10 compares deposition regions predicted with the CFD model and measured in the physical model. Blue symbols represent smaller size particles (0.06 and 0.11 mm) while white symbols show deposition of the larger particles (0.16 mm and 0.21 mm). It's important to note that the physical model test was performed with a variable flowrate ranging from 125 to 200 kcfs while the CFD model was run at a constant flowrate of 150 kcfs. Both models predicted that the majority of particles were deposited immediately downstream of the injection region. Note that the shear stress in the forebay downstream of the injection was smaller than the critical shear stress for the smaller particle size (blue region in Figure 9b) indicating that all simulated particles deposited when they reached the river bed at this location. Some of the particles injected closer to the mooring cells were transported downstream by the clockwise eddy and deposited when velocity (and shear stress) was reduced upstream of the dredged area beneath the screen in unit 2. The percentage of small particles (diameter smaller than 0.11 mm) deposited in the forebay significantly increased when screens were included. 87.2% of the largest particles deposited, however most of them settled upstream of the forebay and the percentage of deposited particles in the dredged area was smaller than without the screens. Because the shear stress was reduced when screens were included, the percentage of total deposited particles increased with the dense screen configuration. According to the model, about 1,519 cubic yards accumulate in the forebay region in one month.

The model was run at reduced scale to compare model capability to reproduce the sediment deposition in the forebay observed in the physical model. Sediment feed rate in the physical model was 0.0144 kg/sec of dried material and the same rate was used with the CFD model. The general flow pattern was similar at full and reduced scales. However, since the turbulence is not scaled accurately in the physical model (i.e., water properties do not scale), viscous forces are different and some differences were noticed. Velocity profiles were more uniform in the reduced scale model resulting in larger velocities near the right bank and a stronger clockwise eddy, which is consistent with observations in the physical model. Figure 10b shows locations where particles were deposited in the CFD model overlaid on deposition results from the physical model. White contours indicate regions with the most deposition in the physical model. In both

the CFD and physical models, most of the sediments deposited in the forebay between the dredged area and the river cells. However, sediments were more dispersed in the physical model compared to the numerical results. The CFD model used in this study tracks injected particles in suspension. Some of these particles can be transported as a bed load but the model does not consider the redistribution of particles already found in the river bed, which is an additional process occurring in the physical model with a moving bed. In addition, as stated before, the CFD model does not consider bed changes or particle-particle interactions, which could result in additional dispersive forces. The CFD model predicted that 0.057 cubic yards will accumulate in the forebay in one hour. For the physical model, 0.0688 cubic yards (9,519 cubic yards at full scale) were deposited at a constant flowrate of 150 kcfs during the 12-hour test. According to the CFD model, the same amount of material would be deposited in 12.1 hours, which indicates that sediment mass conservation is correctly enforced in the CFD model. The CFD model does a good job of replicating the physical model sediment deposition volume (to within 1%) and general deposition locations match reasonably well between the models. For the baseline test at a constant 150 kcfs river flow, the physical model predicted 9,519 cubic yards deposited in the forebay in 4.6 months. The full scale CFD model predicted 6.3 months to accumulate the same volume of sediment in the forebay. Another comparison can be made between the physical and CFD models computing capture rates of sediment in the forebay. The capture rate is defined as the volume of sediment deposited in the forebay vs. the volume of sediment released in the river for the model test. For the baseline test at 150 kcfs, the physical model resulted in a capture rate of 58%. The CFD model at 1:24 scale predicted a capture rate of 55% and the CFD model at full scale predicts 47%.
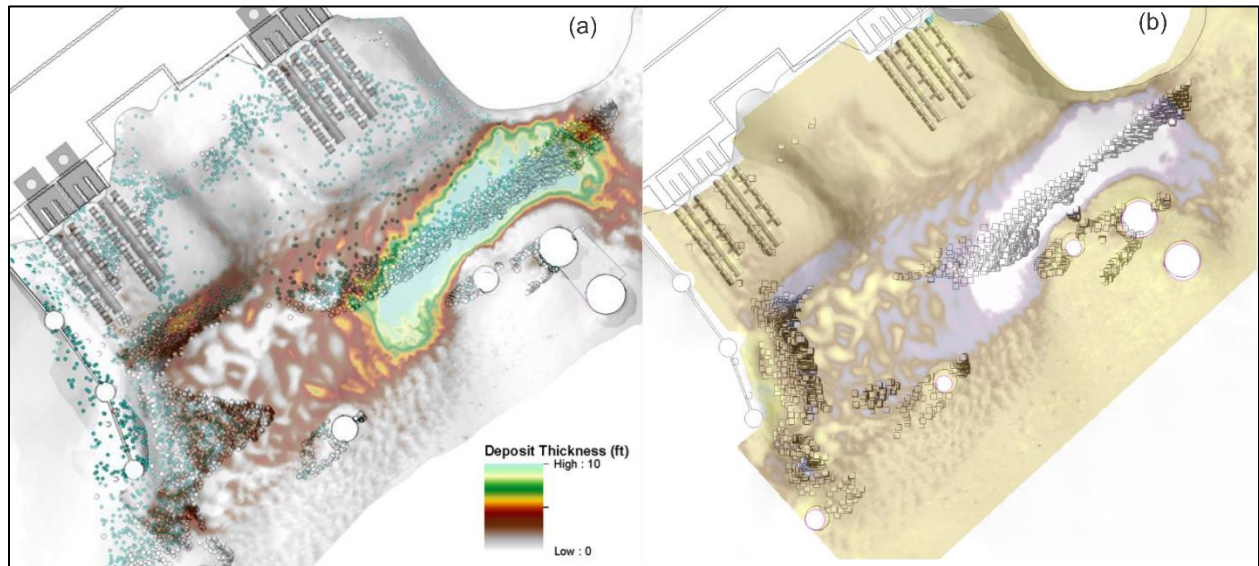
Figure 10. Deposition regions in CFD (particles represented with circles) and physical models. (a) CFD at prototype scale. Colors indicate deposit thickness in the hydraulic model (b) CFD at reduced scale. Deposited sediments in the hydraulic model shown in white.

Sediment Mitigation Measure

Several mitigation measures were considered, but only the final recommended one (option 2B) is presented. A full height wall from the upstream shore to the first small river cell (cylindrical mooring structure) was simulated in an attempt to minimize the transport of sediment near the right bank into the forebay region (Figure 11). Simulation conditions used to evaluate the effect of the submerged screens were used to evaluate the effectiveness of the sediment mitigation measure.

Results

Recirculation of warm water from the discharge canal into the forebay was considerably noticeable when the upstream wall was included. As shown in Figure 11a, a strong clockwise recirculation was predicted in the forebay. The wall prevented transport of water from the right bank into the forebay requiring the screens to draw water at higher velocity downstream of the second small river cell. Figure 11b illustrates the predicted shear stress. Water at relatively high velocity (around 2 fps) from the discharge canal increased the shear upstream and beneath the unit 2 screens. This high shear region can result in erosion, the extent of which cannot be predicted with the sediment model used in this study. Including the upstream wall reduced the velocity and shear stress upstream and downstream of the wall, which is expected to favor sediment deposition in these regions. Most of the material deposited outside of the dredged area, reducing the number of particles deposited in the forebay.
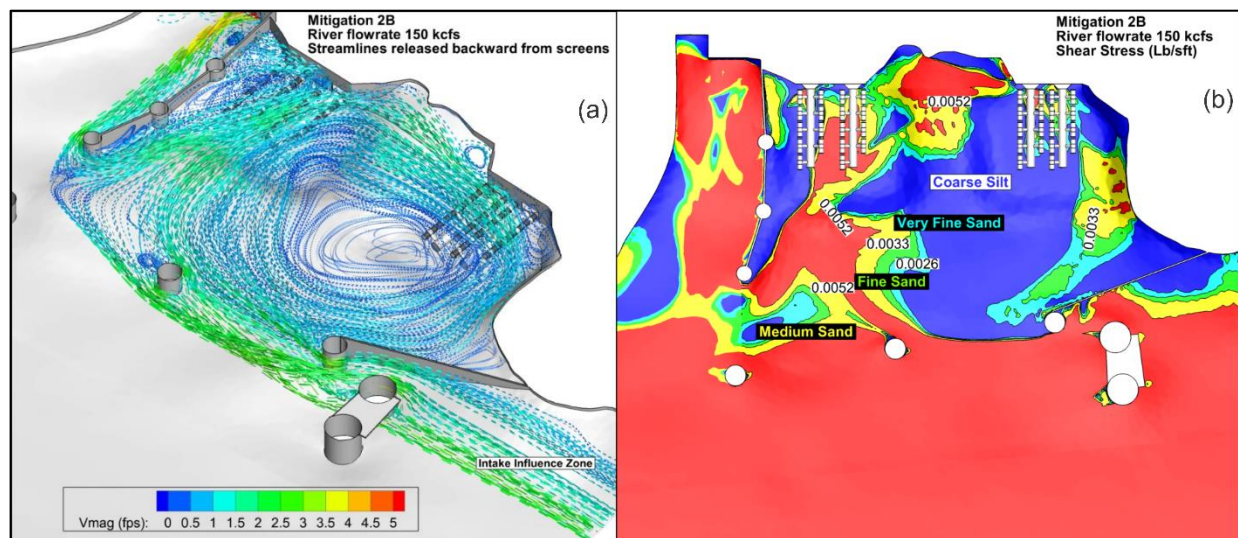
Figure 11. (a) Streamlines colored by velocity magnitude and (b) Shear stress at the river bed

A simulation was performed to assess the effectiveness of a thermal curtain located at the end of the discharge canal wall on preventing the transport of warm water from the discharge canal into the forebay region when the sediment mitigation is included (Figure 12). The river flow was determined based on historical analysis of summer flows (June to September) available from 1986 to 2016. A flow of 15,000 cfs was selected for the simulation to evaluate the thermal curtain. It is expected that summer conditions which can combine high temperatures with

relatively low river flow rates are representative of the worst scenario for transport of warm water back into the forebay region. Average air temperature of 90 °F from 1986 to 2014 was used to compute the heat flux at the free surface. Water temperature data at circulating water pumps provided by the Owners from 2005 to 2015 was used to estimate the river temperature. 73.4 °F was considered representative of the river temperature and was imposed at the model inflow.

Figure 12 shows streamlines colored by temperature when the sediment mitigation and thermal curtain are included. Two eddies are observed in the forebay; water near the right bank is diverted by the upstream wall (mitigation measure) and entrained by the screens in unit 1 creating a clockwise recirculation. Screens in unit 2 draw water from the main channel and from the recirculation canal. A counterclockwise eddy with significant thermal mixing is predicted near the unit 2 submerged screens. At the simulated flowrate, only water from the discharge outlets closer to the dividing wall moves toward the forebay and about half of the curtain length is effective in retaining warm water. the thermal curtain prevents the transport of water warmer than 84 °F toward the forebay. Most of the forebay region near the dividing wall is affected by the recirculation of warm water. The simulation indicates that a deeper curtain could help to further prevent the warming of the forebay since water at temperature of approximately 80 °F moves toward the screens. The impact of warm water from the discharge canal on unit 1 screens is negligible. On the other hand, the temperature at the unit 2 screens is 1 °F higher than the river temperature.
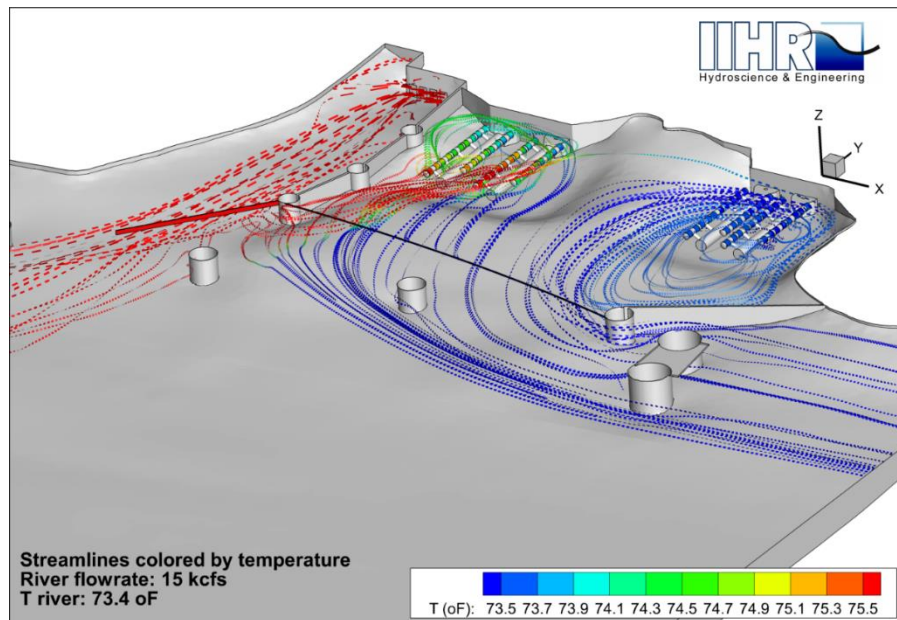
Figure 12. (a) Streamlines colored by temperature with the thermal curtain and sediment mitigation measure

Conclusions

A CFD model was developed to assess the effect of installing submerged cylindrical screens on the intake forebay of units 1 and 2 of the Cardinal Plant. The model includes a reach of the Ohio River upstream and downstream of the Cardinal Plant, the forebay, the intake structure for units 1 and 2, and the discharge canal. Bathymetric data collected during a field study in Sep. 2015

was used to represent the river bed. The model was used to predict the hydrodynamics, temperature distribution and sediment deposition rate considering a fixed river bed. The sediment model takes into account that particles can be suspended, deposited or moved as bed load depending on sediment size, flow turbulence and local shear stress at the river bed. Percentage of the injected particles that are deposited, suspended or moving as a bed load were calculated with the CFD model for each particle size.

The model provides a good replication of measured flow velocities and directions. Buoyancy forces were included in the model for proper prediction of the change of velocity direction with depth caused by temperature gradients in the forebay. Locations of particles deposited in the CFD model with the existing intake condition at 150 kcfs were consistent with deposition patterns observed in the physical model. The difference between the volume of material deposited in the forebay in the reduced 1:24 scale CFD model and the physical model was about 1%. According to the CFD model, sediment deposition rates are strongly dependent on the river flowrate and sediment size. Reducing the river flowrate resulted in decreased deposition in the area of the unit #1 screens but increased sediment deposition either around the unit #2 screens or upstream of the forebay.

Consistent with the physical model, the sediment mitigation wall reduced the deposition rate in the forebay but also resulted in a recirculation of water from the discharge canal into the forebay. The sediment structure increased the water temperature in the screens, particularly in unit #2 screens. A thermal curtain located at the end of the discharge canal wall helped reduce warm water flow from the discharge canal into the forebay region when the sediment mitigation wall was included. Future recommended CFD simulations to further evaluate the effectiveness of the sediment mitigation should include variable flowrates between 60 to 90 kcfs.

References

Firoozfar, A., Gilles, D., Craig, A., Young, N. 2016. "Hydraulic model studies for the Cardinal Plant (Units 1 and 2) 316(B) cooling water intake fish impingement/entrainment project part I: field data collection and analysis," IIHR LDR No 406.

Meyer-Peter, E. and Müller, R. 1948. "Formulas for bed-load transport," Proceedings of the 2nd Meeting of the International Association for Hydraulic Structures Research.

Soulsby, R.L., and Whitehouse, R.J.S.W. 1997. "Threshold of sediment motion in coastal environments," Proc. Combined Australian Coastal Engineering and Port Conference. EA.

Van Rijn, L.C. 1984. "Sediment transport, part I: bed load transport," Journal of Hydraulic Engineering 110(10):1431-1456.

Sedimentation Analysis and Dredging Optimization of Mayo Lake Hydropower Intake Channel

Dragi Stefanovic, Ph.D., P.E., D.WRE, Sr. Technical Program Manager, HDR Inc., San Diego, California, Dragoslav.Stefanovic@hdrinc.com

Goran Sreckovic, Ph.D., P.Eng, Director of Resource Planning and Regulatory Affairs, Yukon Energy Corporation, Whitehorse, Yukon Territory, Canada, Goran.Sreckovic@yec.yk.ca

Abstract

Yukon Energy Corporation (YEC) is proposing to enhance the reservoir storage of the Mayo Lake Hydropower Plant by lowering its current licensed minimum operating level by up to one meter (3.3 feet). However, significant sediment deposition in the hydropower intake channel is caused by wave-induced erosion of glacio-lacustrine soils (mostly fine sands and silt/clay) along the lake shoreline and it hampers the YEC's ability to fully utilize this enhanced storage project. HDR and Northwest Hydraulic Consultants have conducted a comprehensive fluvial sedimentation analysis, by developing a series of sediment transport models (HEC-RAS) of the intake channel, to address the viability of maintaining adequate conveyance through bed mobilization and to evaluate the optimal amount and location of channel dredging that would be required. Twelve (12) dredge alternatives were considered to reduce both the initial cut volume and ongoing maintenance dredging cost. The main goal was to minimize dredge quantities, while maximizing the hydraulic capacity of each alternative, as necessary input parameters for YEC's economic analysis. The potential flow volume increase over the next 30 years was found significant for all the alternatives, between 15 and 20 percent, which would enable a corresponding increase in hydropower generation. Also, all the dredge alternatives allow for a significant increase in the channel through-flows at the current minimum lake elevation, from less than 1 m³/s (in existing conditions) to a minimum of 7 m³/s and a maximum of 15 m³/s for optimized dredge designs. Several alternatives have the ability to lower the current licensed minimum lake level by up to one meter, providing a channel through-flow of minimum 5 m³/s. This increased operating range would allow YEC to take advantage of high flow years where otherwise the excess water would spill over the control structure (in the late summer and fall) and be unusable for energy production in the winter.

Introduction

YEC was established in 1987, as a publicly owned electrical utility that operates separately from the Yukon government. It is the main generator and transmitter of electrical energy in the Yukon, providing almost 15,000 electricity consumers in the territory with a sufficient supply of safe, reliable electricity and related energy services. YEC is currently proposing to enhance the reservoir storage of the Mayo Lake Hydropower Plant by lowering the current licensed minimum lake level by up to one meter (3.3 feet). This would provide additional storage to displace diesel generation. The water would be drawn in the wintertime, but at times there would be a lower level in spring than is currently allowed under the existing water license. The increased operating range would allow YEC to take advantage of occasional high flow years where otherwise the excess water would just spill over the Control Structure (in the late summer and fall) and be unusable for energy production in the winter.

In 2011 observations were made in the Mayo Lake Outlet Channel (which is the hydropower intake channel) that prompted a study to understand if and how sediment deposition in the Outlet Channel may be affecting outflows from the lake. A geomorphic analysis was completed in 2013 and identified that sediment deposition over the last 60+ years was impacting the ability to use stored water in Mayo Lake. Maintenance of this existing Mayo Lake asset, by dredging or flushing of the accumulated sediment, was then proposed in order to provide the full generation capacity of the Mayo Lake Enhanced Storage Project (ESP). These initial analyses in Phase I of the study ultimately led to a hydraulic and sediment transport modeling stage (Phase II) where the key project concerns are whether an efficient and reasonably long-lasting dredging design can be developed and at what cost. Thus, the ultimate goal of this sedimentation project is to determine if there is an economic justification for dredging, and if so, to identify optimal dredge parameters and costs. This paper presents a comprehensive fluvial sedimentation analysis performed in Phase II by HDR, Inc. and Northwest Hydraulic Consultants, Ltd. (NHC) to address the viability of maintaining adequate conveyance through the Outlet Channel and to evaluate the optimal amount and location of channel dredging that would be required.

Project Setting

Mayo Lake, with a surface area of 96.9 km², is one of the largest lakes in the central Yukon Territory (YT), Canada. Mayo Lake is drained by the Mayo River, which flows into the Stewart River near the community of Mayo, YT (Figure 1). During the early 1950's, the Northern Canada Power Commission built hydroelectric facilities on the Mayo River. This included the construction of Wareham Dam, approximately 12 km upstream from the mouth of the Mayo River; a powerhouse approximately 600 m downstream of the dam; and, a control structure at the outlet of Mayo Lake which increased water levels in Mayo Lake by approximately 4.6 m. A second powerhouse (Mayo B) was commissioned in 2011 approximately 4.9 km downstream of the existing plant (Mayo A).
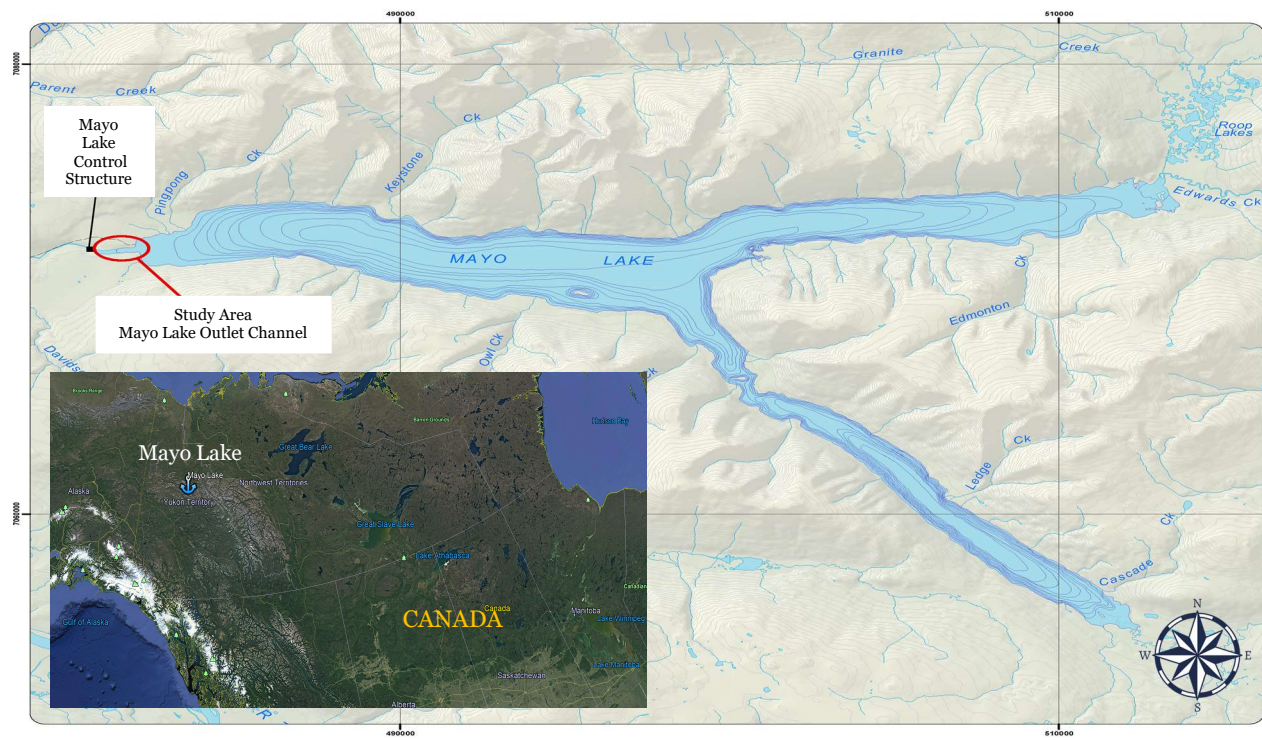
Figure 1. Mayo Lake location in Yukon Territory, Canada (adapted from EDI 2014)

The existing Outlet Channel is an impounded section of the Mayo River which was submerged after the construction of the Control Structure during the 1950's. Over time, the Outlet Channel has gradually infilled with fine sediments and previous studies (Tetra Tech 2016) indicated that this area may limit the water flow out of Mayo Lake, particularly when the lake is at lower elevations (below 663.5 m). YEC is currently investigating the possibility of dredging this shallow portion of Mayo Lake to provide more efficient flow out of the lake and allow for the electricity generation facilities on the lower Mayo River to be utilized to their full potential.

Sediment Inflow Load Analysis

Previous studies in Phase I (Tetra Tech 2016) concluded that the genesis of the surficial geology that forms the eroding escarpment next to the north entrance of the Mayo Lake Outlet Channel is glacio-lacustrine, primarily fine sands, silts and clays. Very limited evidence was found to support either erosion or slumping of the banks within the Mayo Lake Outlet Channel. Based on the available information, a reasonably high level of certainty was placed on identifying the primary sediment sources. However, the level of certainty associated with sedimentation rates in the Outlet Channel was found low without further sediment transport analysis. Given the relative stability of the channel margins along the Outlet Channel, the principal source of fine sediments deposited on top of the historic channel and floodplain/terrace segments to an elevation of about 665 m (i.e. raised lake level) was found to be within the lake, along the eroded shoreline (Figure 2). Phase I also identified that the vast majority of the lake shoreline retreat had occurred in the first decade following impoundment, with an exponential decrease in cliff erosion with time. This suggested that the initial cliff erosion was due to saturation of the cliff face and wave erosion. As the cliff was progressively cut back, the shelf fronting the cliffs widened and shoaled to such an extent that bottom friction and wave breaking dissipated the majority of wave energy before reaching the cliff, hence the reduction in erosion rate. However, without sediment sampling and sediment transport modeling, it was not possible to determine how much material can be transported downstream through the Control Structure. Therefore, within the constraints of information available in Phase I of the study, it was not possible to predict future sedimentation rate within the Outlet Channel or to determine if the system had established an equilibrium state where the sediment inflow is balanced by the outflow.

Figure 2. Mayo Lake eroded shoreline near Outlet Channel entrance

Based on the Phase I understanding of this complex geomorphic system in a harsh climate setting, the fine sediments are being entrained into the Outlet Channel from wave-shoreline erosion by shallow water transport processes, while the transport of sediments through the channel is governed by hydraulic (fluvial) processes. In order to estimate the inflowing sediment load from the lake into the Outlet Channel, an analysis of the wind climate was first completed by Northwest Hydraulic Consultants (NHC 2018), since the wave erosion potential of the cut banks is directly tied to the wind power.

Wind Climate Analysis: YEC installed a wind climate station near the Outlet Channel on the south slope beside the Control Structure (Figure 3). This station has been in operation since August of 2016. The wind station uses a Xlink weather module which integrates a Sutron Xlink Datalogger and a Lambrecht Wind Speed and Direction Sensor. Wind data was continually recorded and the overlapping time frame compared with the wind data from Mayo Airport (to determine if the long-term data from Mayo Airport could be used in the wave analysis). The collected data was manually downloaded from the station during periodic maintenance visits.

Mayo Lake typically experiences ice conditions that would prevent wave formation from approximately November until May each year; therefore, the summer and early-fall represent the 'wave season'. From the wind records obtained at the Mayo Lake climate station, the summer and early fall of 2017 was the only complete wave season available for the analysis. Subsequently, 2017 has been determined to be a reasonably typical year near Mayo Lake (with no outlier wind events occurring) such that the winds from the Mayo Lake climate station were found suitable for use in the wave erosion analysis.

Figure 3. Mayo Lake Climate Station looking westward towards Control Structure and Outlet Channel (NHC 2018)

The winds from 2017 were used in a wave hindcast for Mayo Lake. NHC (2018) utilized the JONSWAP parametric wave hindcasting methodology for a series of input conditions as presented in Kamphuis (2010). This hindcasting method computes fetch and duration limited conditions based upon examination of the wind speed and direction, fetch lengths

corresponding to the wind direction, and duration of the winds. Given that most wind events on the lake last longer than two hours and the lake is not very large, the waves were likely to be mostly fetch limited (maximum fetch for winds from the east was estimated at 20 km). The wave hindcast was successfully validated with field observations. HDR and NHC conducted a field visit from July 20-25th 2018 where an east wind-wave event was observed on July 23rd, with approximately 20-30 cm wave heights observed. A wave hindcast was completed for the same period using the recorded lake climate data and a significant wave height of 25 cm was predicted, which was well within the observed range.

Wave Erosion Analysis: NHC completed a wave erosion analysis for the longshore transport of the eroded material at the east end of the Outlet Channel using the observed wind and wave hindcasted data for the year 2017. All the wave data outside the months of May to November was assumed to be zero due to ice conditions. There was assumed to be no aerial transport of sediments from the wind when the lake is frozen.

Using the hindcasted significant wave height, wave period and wave direction, as well as the beach profile parameters, sediment density, grain size, offshore water depth, and beach orientation, the alongshore erosion rate can be estimated using various bulk sediment transport formulations. Three such formulae were used to explore a range of estimates: the Kamphuis bulk sediment transport equation (2013), the CERC expression (USACE 1984; 2006), and the van Rijn equation (2014).

The most widely used formula for longshore erosion is the CERC equation (USACE 1984; 2006). This method is based on the principle that the rate of longshore sediment transport (including bedload and suspended load) is proportional to the longshore wave power per unit length of beach. The CERC equation had been calibrated using field data from sand beaches. It does not account for particle size and beach slope and is valid only for sandy conditions (note that bed materials in the nearshore environment at Mayo Lake are dominated by sandy silts and fine sands). The van Rijn equation (2014) includes the particle size and bed slope, spanning a larger range of particle sizes from sand to cobble (0.1 – 100 mm). It was validated using field and laboratory conditions.

Using the bulk erosion predictions described above, the longshore transport was summed over the year to estimate the annual sediment load into the Outlet Channel (Table 1). The range of estimates for a typical and extreme year was determined assuming that the shoreline angle is 45 degrees to the wind, which results in higher transport rates than when the shoreline is more perpendicular to the incoming waves.

Table 1. Estimated annual sediment load into Mayo Lake Outlet Channel (NHC 2018)

Method	Typical Load (m³/year)	Maximum Load (m³/year)
Kamphuis (2013)	143	191
CERC (2006)	4,750	4,940
Van Rijn (2014)	509	860

Site observations indicate that wave-induced longshore erosion has the potential to mobilize sediments in the nearshore and transport them towards the Outlet Channel. Figure 4 shows an aerial view of the northern shoreline of Mayo Lake at the approach to the Outlet Channel during a moderate westerly wind event in July 2017 that generated waves between 20 and 30 cm in height. The suspended sediments were clearly observed as increased turbidity in the water, indicating that these waves are entraining and transporting sediments along the shoreline.

Figure 4. Northern side of Outlet Channel entrance; red arrows indicate longshore sediment transport (NHC 2018)

Figure 5. Outlet Channel looking west towards Control Structure; (a) shows the entire Outlet Channel from eastern entrance; (b) is from a position above southern shoreline (NHC 2018)

Field observations suggest that the majority of sediment deposition is occurring near the entrance shorelines of the Outlet Channel, as seen in Figure 4 and Figure 5. On the southern shoreline, a spit has formed beginning about 300 m into the Outlet Channel, and there is an underwater bench of coarser deposition east of this spit. Along the northern shoreline, there is a wide shallow bench of fine sediments extending some distance from the lake entrance (approximately 500 m) into the Outlet Channel. The estimated sediment loads (from Table 1) could generate deposition rates of 2 to 70 mm per year at the eastern end of the Outlet Channel. At the higher limit of this estimate (using CERC load), an aggradation rate of 70 mm per year would result in about 2 m of deposition in 30 years. In reality, it appears that depositional rates vary within the Outlet Channel and the overall deposition is substantially lower.

Sediment Load Verification: The predicted annual sediment loads from wave-induced erosion (NHC 2018) vary in a wide range depending on the methodology used (Table 1). They are also based on only one complete wave season (2017) that was available for the analysis. Therefore, a rough order-of-magnitude analysis was performed by HDR to establish a ballpark validation of the sediment load range.

Phase I investigations (Tetra Tech 2016) identified that the lake shoreline erosion rate between 1966 and 1990 was on the order of 0.7 m/yr, reducing to about 0.4 m/yr between 1990 and 2008 as a result of development of a subaqueous shelf that dissipates wave energy. It was found reasonable to expect the lake shoreline to continue to erode at a rate of about 0.4 m/yr in the future.

Based on field observations and aerial imagery, the maximum length of the eroding escarpment (Figure 2) next to the north entrance of the Outlet Channel is approximately 700 m. If the height of the eroding cliffs is about 5 m (Figure 6), assuming that the entire wetted perimeter of the right bank can be eroded in one wave season, then the total volume of entrained cliff material by waves is ~1,400 m^3. This is the maximum expected annual amount of eroded material from the northern shoreline of Mayo Lake as a dominant source of glacio-lacustrine sediments. It is reasonable to believe that only a portion of this amount will enter the Outlet Channel. If some 50 to 100 percent of the entrained sediment reaches the Outlet Channel, the annual sediment load from wave-induced erosion would be on the order of 700 to 1,400 m^3. This ballpark estimate is matching the van Rijn range in Table 1, while the CERC range appears to be overly conservative.

Based on the order-of-magnitude analysis, it was decided to proceed with using the CERC load estimate as a conservative upper bound that may capture unforeseen sediment sources (e.g. melting permafrost, erosion of southern lake escarpment, etc.), while the van Rijn load should provide more realistic sediment transport results.
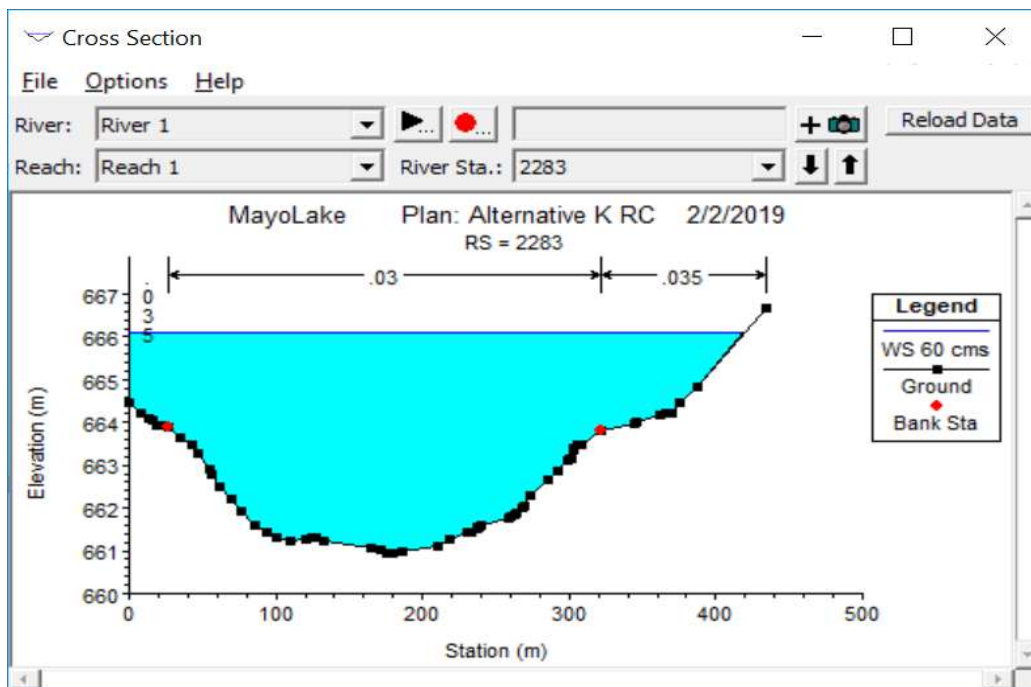
Figure 6. Mayo Lake cross section near Outlet Channel entrance

Fluvial Sediment Transport Modeling

The sediment inflow load analysis by NHC (2018) suggests that there is potential for longshore bulk erosion through wave-induced forcing which drives sediments into the Mayo Lake Outlet Channel. Once the mobilized sediments are entrained into the Outlet Channel, they are primarily transported towards the Control Structure by hydraulic (fluvial) processes governed by gravity forcing.

Hydraulic Modeling of Outlet Channel: HDR developed a one-dimensional (1-D) hydraulic model of the Mayo Lake Outlet Channel in HEC-RAS 5.0.6 based on bathymetric surveying performed by NHC in July 2018. A Digital Elevation Model (DEM) of the Outlet Channel was produced from LAS (LiDAR) point clouds with a fine resolution of 5 cm for accurate representation of bathymetric features. Cross sections for the HEC-RAS model (Figure 7) were cut every 50 m, starting from the channel entrance on the upstream (eastern) side to about 400 m downstream of the Control Structure. The roughness coefficient was estimated at 0.03 for a silty bottom with little vegetation in the main channel and at 0.035 on the more vegetated benches.

The flow Control Structure (also called Mayo Lake Dam) is a stair-stepped lumber decking (20 m long in the streamwise direction) with riprap foundation protection on the downstream side and three bottom outlets (steel culverts) with an inside diameter of 1.35 m (Figure 8 and Figure 9). The structure was coded in HEC-RAS as a regular bridge/culvert at River Station (RS) 734.
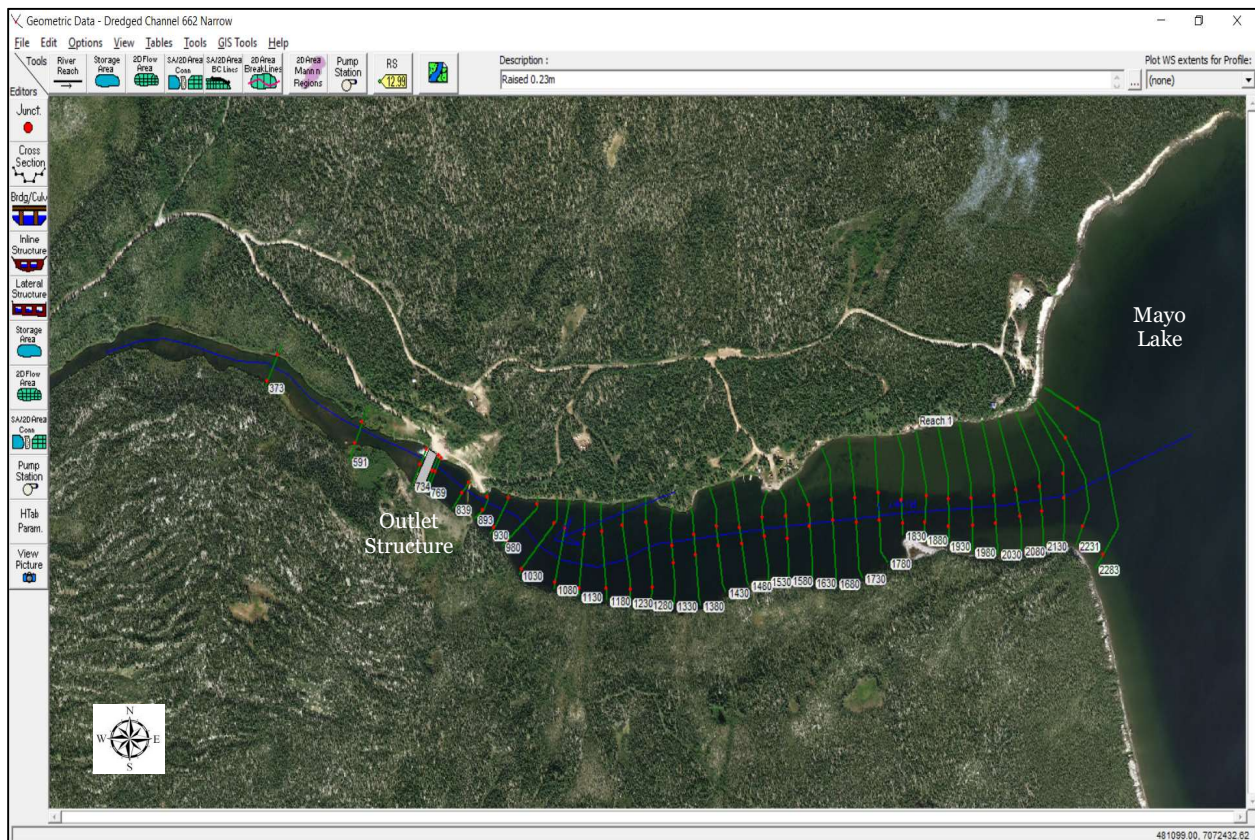
Figure 7. Mayo Lake Outlet Channel HEC-RAS model schematic

Figure 8. Mayo Lake Control Structure

Figure 9. Mayo Lake Control Structure bottom outlets

Sediment Transport Modeling: HDR performed a 1-D mobile-bed sediment transport analysis for the Outlet Channel using HEC-RAS 5.0.6. The sediment transport model requires geometric data (cross sections), flow data, and sediment data. The cross-section geometry was developed in the hydraulic component of the program. A 30-year historical record of daily flows through the Control Structure was provided by YEC and used as a quasi-unsteady flow input. Bed sediment samples (Figure 10) were collected by NHC in July 2018 to define bed material gradation (Figure 11). The majority of sediment samples are in the silt range, except those near the shoreline (Bed 1 and Bed 4) which are coarser (fine sand) due to nearshore wave action.
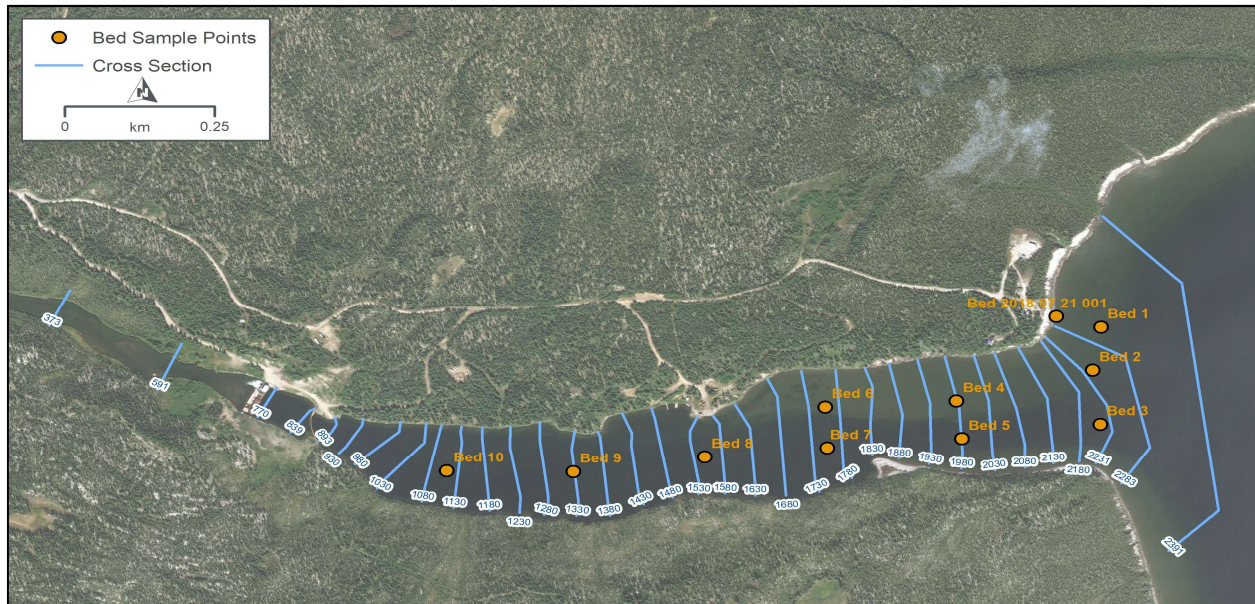
Figure 10. Mayo Lake Outlet Channel sediment sample locations
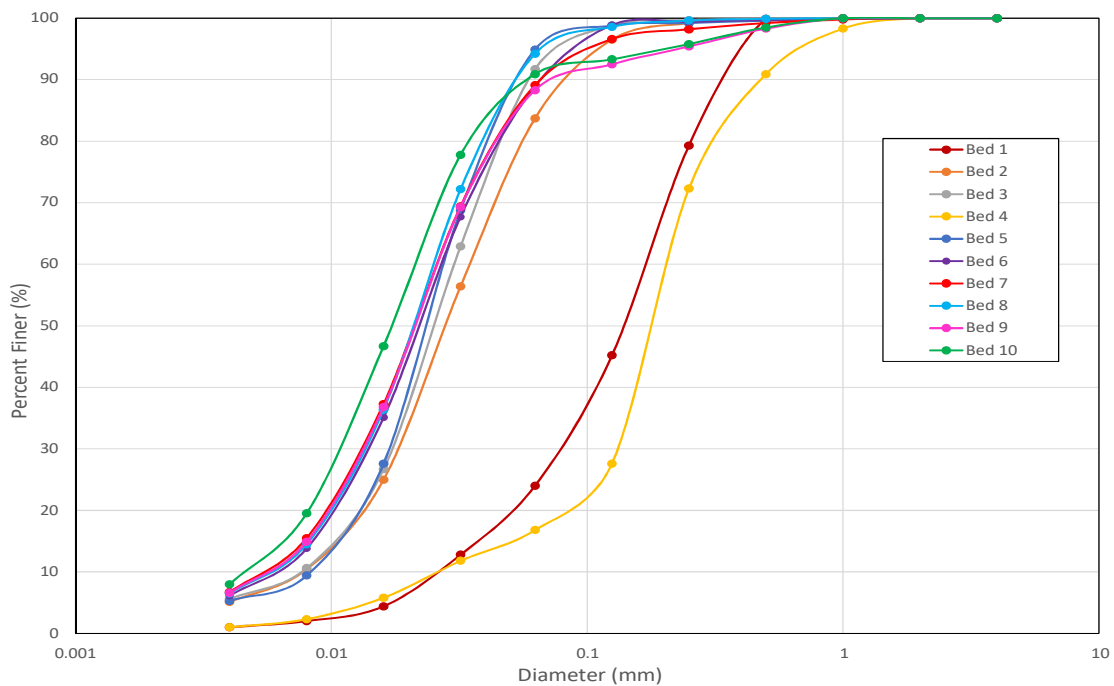
Figure 11. Mayo Lake Outlet Channel bed gradation

The sediment inflow load was varied between the van Rijn and CERC volume estimates (Table 1), resulting in the annual amount between 790 and 7,380 metric tons (based on a measured bulk sediment density of 1,550 kg/m³). It was assumed that the sediment load fractions correspond to sample Bed 1 (predominantly very fine sand to medium sand) located along the northern shoreline of the lake where waves mobilize sediments and transport them towards the Outlet Channel.

Several transport functions were considered for the given range of sediment sizes and hydraulic conditions in the Outlet Channel (Ackers-White, Yang, Toffaleti, Engelund-Hansen and Laursen). The Toffaleti formula was developed for large sand-bed rivers, which is not directly applicable to the study reach. The Engelund-Hansen function was found best for sandy rivers with significant suspended load; however it typically overpredicts transport at low shear values (Williams 1995), which was confirmed in this study with maximum shear stresses ~ 0.1 Pa. Similar conclusion was reached here for the Laursen formula, which was originally developed for silts. The Yang function is good for small rivers and highly applicable to medium-sand range (Williams 1995). The Ackers-White formulation was recommended for fine- to medium-sand range (Williams 1995) and has provided very consistent results in this study.

Sediment Transport Results: The sediment transport models were run with the 30-year daily flow record for existing channel conditions and twelve dredge alternatives. The selected thalweg profiles at the end of the simulation period for the CERC (maximum) load are shown in Figure 12 and Figure 13.
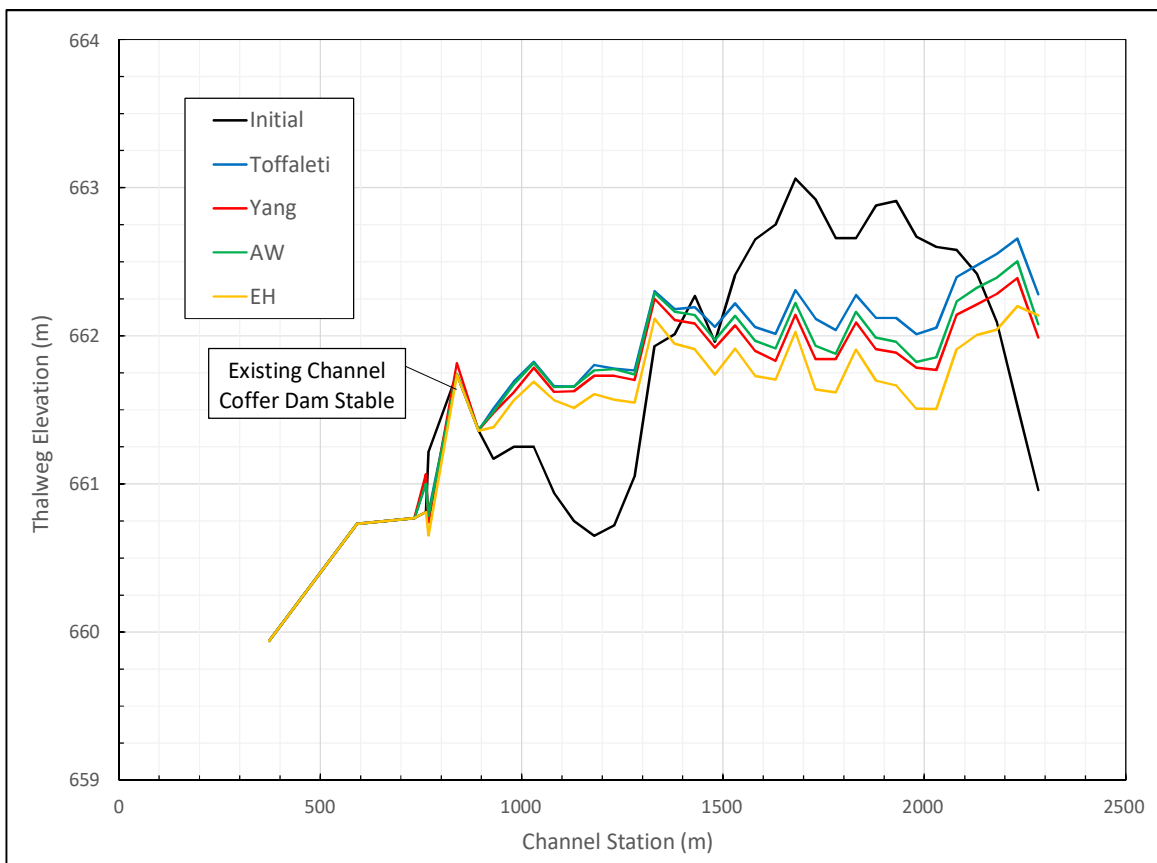
Figure 12. Outlet Channel 30-year simulated thalweg profile for existing conditions and CERC load
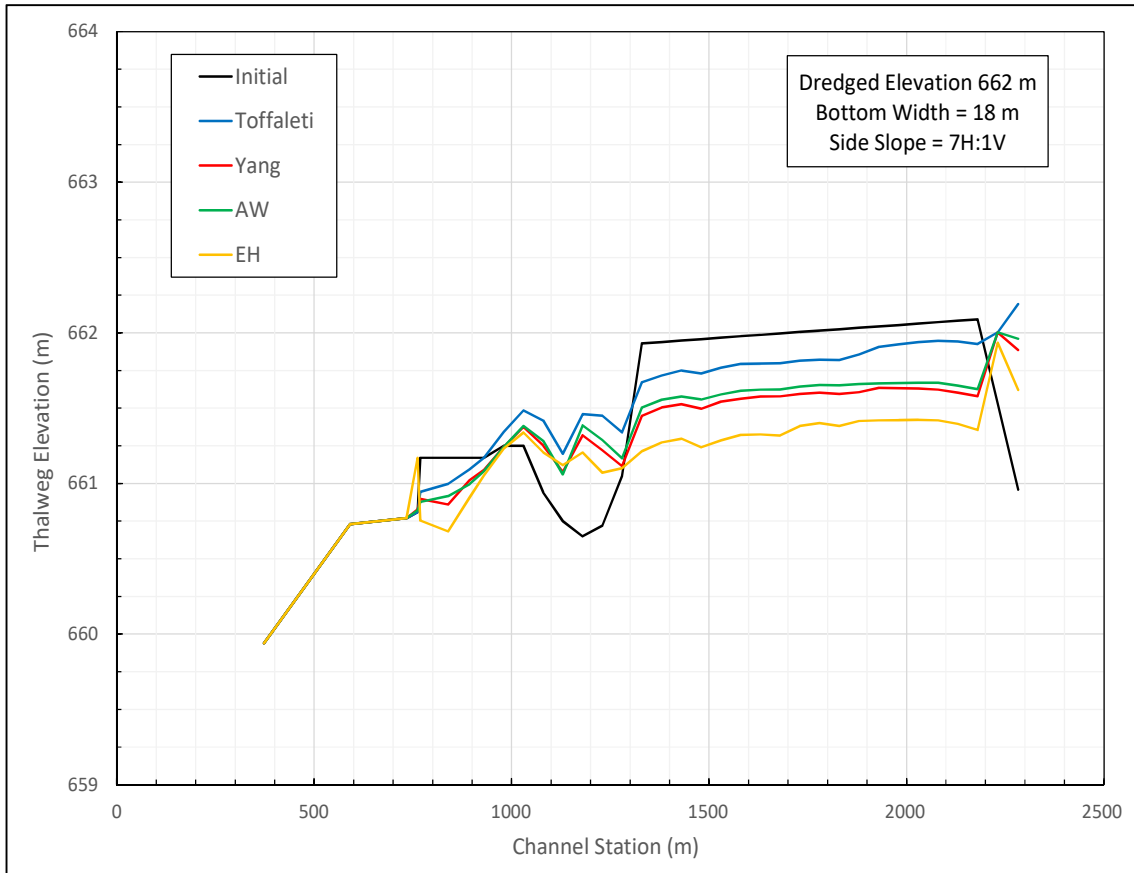
Figure 13. Outlet Channel 30-year simulated thalweg profile for dredge alternatives and CERC load

Figure 12 indicates that the Outlet Channel in current conditions has the potential to initially mobilize bed sediments (self-scour) and transport them towards the Control Structure. However, its entrance portion does not have enough transport capacity to receive all the inflowing load from the lake and continues to build up a steeper equilibrium slope according to Lane's balance. The predicted upstream aggradation in 30 years is on the order of 1.5 m (for this very conservative sediment load scenario) and about 1 m for the more realistic van Rijn load. It should be noted that these estimates are approximate since they are extracted at the model boundary where the results are inherently more uncertain.

The old coffer dam remnants present in the Outlet Channel (between RS 839 and 893) will likely remain stable since the surface bed material in that area is much coarser than silt (predominantly pebbles), based on sample T4 in EDI (2014) report. HDR performed an incipient motion analysis and found that the grain sizes of minimum 6 mm would not be mobilized by the hydraulic conditions in the Outlet Channel. Therefore, the coffer dam was modeled as a grade control (armor layer) in the existing channel conditions (see Figure 12).

Figure 13 shows the 30-year simulated bed profiles for dredging to a bottom elevation of 662 m (Table 2, Alternative C). The channel initially remains in self-scouring mode, while the excessive aggradation at the upstream end is prevented by periodic dredging of the entrance area (dredging is only needed after 20 years for this very conservative sediment load scenario).

Dredging alternatives were based on a trapezoidal template (Figure 14), with stable side slopes for silt (7H:1V), cut in the middle of the channel to stay as clear as possible from existing

depositional areas where it is expected that further deposition will occur during high wind events. The dredging design was optimized in five alternatives (Table 2, Alternatives A-E) to achieve better balance between cut and fill volumes. The remaining seven alternatives were based only on channel bottom cuts to daylight without any side filling (Table 2, Alternatives F-L) to avoid placing the dredgeate back in the channel due to environmental concerns. The channel bottom widths were set between 5 and 35 m, while the dredging elevations varied between 661 m and 663 m.
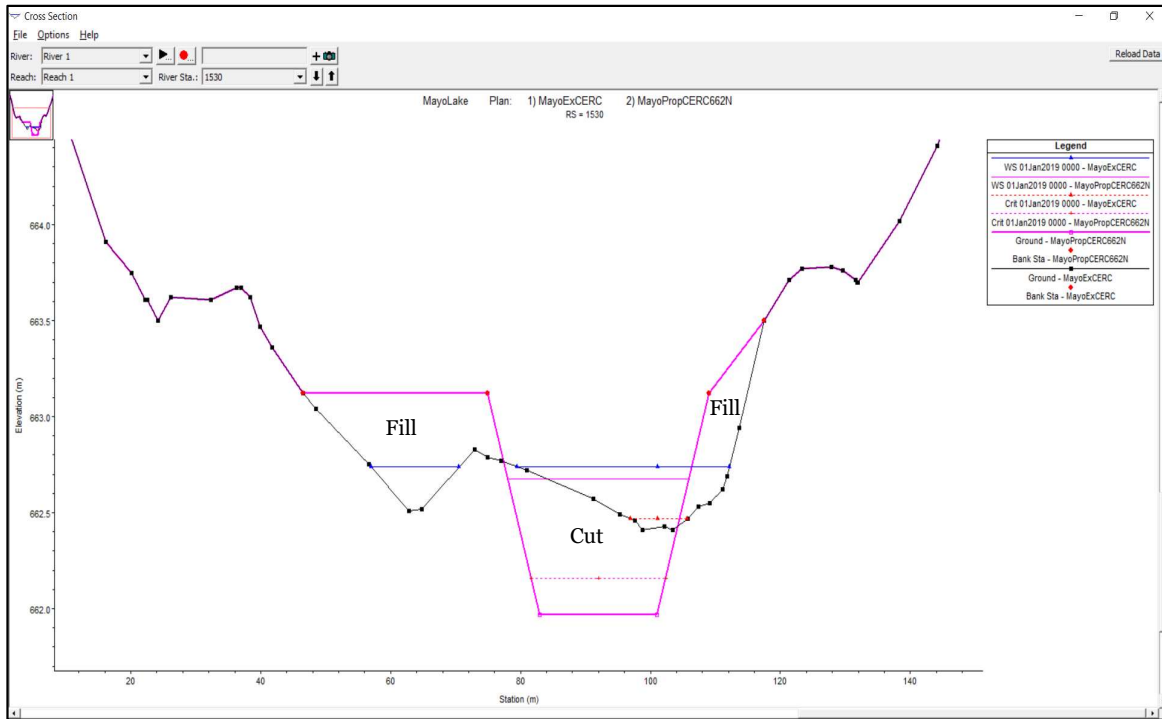
Figure 14. Mayo Lake Outlet Channel typical dredging template with cut and fill (magenta color)

The required volumes of dredge material are presented in Table 2 for each alternative. The benefit of each alternative is expressed by three parameters: (1) Entrance Head Gain, a cumulative lowering of the simulated entrance water surface elevation in 30 years (using the conservative CERC load) with respect to existing conditions, which is a measure of potential increase in the channel through-flows and ultimately enhanced storage capacity of the lake (the higher the Entrance Head Gain, the lower lake elevations can be utilized for power generation); (2) Flow Volume Increase, a potential increase in the channel through-flow volumes in 30 years, due to rating curve lowering at the Outlet Channel entrance (RS 2130) with respect to existing conditions. This parameter is a direct measure of increased hydroelectric energy potential since the hydropower is proportional to discharge (turbine throughput) as it passes through the power plant; and (3) Annual Bed Change, a potential sediment accumulation on the channel bed for the conservative CERC load, as an indicator of long-term channel stability.

Alternative L provides the overall highest entrance head gain and large flow volume increase, similar to Alternative F but at half a dredging cost, which would enable more efficient hydropower production. The top-ranked dredge alternative among cut-and-fill options (Alternative C) would not require excessive initial dredging (with completely balanced cut and fill volumes) and exhibits low maintenance dredging, with moderately high entrance head gain. The alternatives with an entrance head gain less than 5, would generally be more susceptible to future sediment accumulation at the upstream end.

Table 2. Mayo Lake Outlet Channel dredge alternatives

Alternative	Dredge Elevation (m)	Bottom Width (m)	Initial Dredge Volume (m³)		CERC Entrance Dredge Volume (m³)*	Van Rijn Entrance Dredge Volume (m³)*	Entrance Head Gain (m)*	Flow Volume Increase (%)*	Annual Bed Change (tonnes)
			Cut	Fill					
A	661.0	18	51492	23127	7891	3038	4.3	20.0	2388
B	661.5	18	33501	23447	8151	3187	3.6	19.7	1934
C	662.0	18	18541	18739	5330	596	5.6	18.7	1357
D	662.0	35	34283	10072	5469	596	1.2	19.5	1425
E	662.5	18	8241	8305	4940	905	3.9	14.6	1062
F	661.0	18	51492	0	9544	1021	9.8	20.0	2437
G	661.5	18	33501	0	5562	713	6.5	19.8	1948
H	662.0	18	18541	0	5110	713	5.0	18.9	1508
I	662.5	18	8241	0	5319	890	2.7	15.8	1000
J	662.0	5	8595	0	5035	871	4.8	15.7	1038
K	661.5	5	17503	0	5334	712	8.5	18.7	1510
L	661.0	5	28761	0	7187	726	10.8	19.6	2083

*over 30 years

Three alternatives with a minimum bottom elevation of 661 m (A, F, and L) can potentially lower the current licensed minimum lake level by up to one meter, providing a channel through-flow of at least 5 m³/s.

Although the sediment transport model indicates the need for periodic entrance dredging after approximately 20 years of operation, the future sediment accumulation within the main channel would likely be much less in reality than predicted by conservative modeling assumptions. The economic analysis will ultimately determine if there is a cost-effective dredging solution and identify optimal dredging parameters.

Summary and Conclusions

The Outlet Channel sediment transport models for different dredging scenarios were constructed using a dredging design tool within HEC-RAS, which automatically computes the cut and fill volumes. HDR considered twelve (12) dredging design alterations to reduce both the initial dredge quantities and ongoing maintenance dredging, while increasing the channel hydraulic and sediment transport capacity. Dredging was limited to the thalweg of the pre-inundation Mayo River channel, with a bottom elevation between 661 and 663 m. To minimize the overall dredge volume and maximize self-scouring of the dredge cut channel, a minimum channel cross section required to achieve the necessary transport capacity was explored (between 5 m and 30 m). Also to reduce excavation quantities, the dredge cut was specified with as steep a side slope as feasible for muds and fine silts (7H:1V). The old cofferdam remnants were shaved in each alternative to a bottom elevation of ~661 m (below armor layer) to increase the hydraulic capacity of the channel. Starting with initial dredging template for each specified bottom elevation, 30-year sediment transport simulations were performed to predict potential channel evolution for an assumed sediment inflow load and historical lake flows.

The dredging templates were optimized in five alternatives to achieve better balance between cut and fill volumes. The remaining seven alternatives were based only on channel bottom cuts to daylight, without any side filling to avoid placing the dredgeate back in the channel due to environmental concerns. The potential flow volume increase over 30 years was found significant for all the alternatives, between 15 and 20 percent, which would enable a corresponding increase in hydropower generation. Also, all the dredge alternatives allow for a significant increase in channel through-flows at the current minimum lake elevation (663.27 m), from less than 1 m³/s (in existing conditions) to a minimum of 7 m³/s and a maximum of 15 m³/s for the dredge

alternatives. It is important to note that three alternatives (with a minimum dredge elevation of 661 m) can potentially lower the current licensed minimum lake level by up to one meter (to 662.27 m), providing a channel through-flow of minimum 5 m^3/s. This increased operating range would allow YEC to take advantage of high flow years where otherwise the excess water would spill over the Control Structure (in the late summer and fall) and be unusable for energy production in the winter.

Although the sediment transport model indicated the need for periodic entrance cleanup after approximately 20 years of operation, the sediment accumulation within the main channel would likely be much less in reality than predicted by conservative modeling assumptions, thus eliminating the need for regular maintenance dredging. The economic analysis will ultimately determine if there is a cost-effective solution for dredging and identify optimal dredge alternatives based on their benefit-cost ratio.

The top five dredge alternatives (L, K, F, G, and J) were recommended as promising candidates for the economic analysis based on a relatively large flow volume increase, high entrance head gain, and low bottom elevation. Alternative C was also recommended for consideration if the cut-and-fill options were of interest. In general, the narrower alternatives (L, K, and J with a bottom width of 5 m) require less dredging and are more geomorphically stable (i.e. less susceptible to future bed sediment accumulation).

Regardless of the selected alternative, it was recommended that an inspection program be developed to periodically monitor potential sediment accumulation in the Outlet Channel, particularly its inlet area.

References

Environmental Dynamics Inc. (EDI). 2014. "Mayo Lake outlet channel fisheries investigations," prepared for Yukon Energy Corporation, Whitehorse, Yukon, Canada.

Kamphuis, J. W. 2013. Introduction to Coastal Engineering and Management. 2nd edition, World Scientific, Queen's University.

Northwest Hydraulic Consultants (NHC). 2018. "Mayo Lake outlet channel – wave induced sediment transport analysis," prepared for Yukon Energy Corporation, Vancouver, Canada.

Tetra Tech. 2016. "Mayo Lake outlet channel erosion, sedimentation and dredging study – phase I," prepared for Yukon Energy Corporation, Irvine, California.

U.S. Army Corps of Engineers (USACE) and Coastal Engineering Research Center (CERC). 2006. "Shore protection manual," 4th ed. Vicksburg, Dept. of the Army, Waterways Experiment Station, Washington, DC.

van Rijn, L. C. 2014. "A simple general expression for longshore transport of sand, gravel and shingle," Coastal Engineering, 90, 23–39.

Williams, T.D. 1995. "Review of sediment transport formula comparisons," Ph.D. Thesis, Colorado State University, Fort Collins, Colorado.

Simulations of Gully Erosion Using a Physically Based Numerical Model

Yafei Jia, Research Professor, the University of Mississippi, University, MS, jia@ncche.olemiss.edu

Robert R. Wells, Research Engineer, National Sedimentation Laboratory, USDA, Oxford, MS, robert.wells@ars.usda.gov

Henrique G. Momm, Associate Professor, Middle Tennessee State University, Murfreesboro, TN, henrique.momm@mtsu.edu

Sean J. Bennett, Professor, University at Buffalo, Buffalo, NY, seanb@buffalo.edu

Abstract

Gully erosion is detrimental to agricultural lands and threatens agricultural productivity. There are still more questions than answers following several decades of study. Erosions by sheet runoff and concentrated flows are very complex problems related to soil properties, hydrology, human activity, shape of the landscape, climate and their interactions. Understanding rainfall, runoff and erosion processes requires a combined effort of field observations, physical experiments and numerical simulations.

In this paper, a physically based numerical model, CCHE2D, is applied to simulate landscape evolution processes due to raindrop impact and overland flow. CCHE2D solves a set of full hydrodynamic equations for depth-integrated flows. The numerical model is capable of simulating the thin layer of runoff that flows over complex terrains and mixed regimes of sheet and concentrated flow. The sediment transport model includes rain splash erosion and soil surface erosion. Two soil erosion simulations are presented in this study: an experimental landscape and an agricultural field. Experiments in the laboratory created overland flow and soil erosion using simulated rainfall, in which the evolving topographic surface was captured by close-range photogrammetry and sediment-laden runoff was recorded at multiple time periods at the flume outlet. The field data were collected by aerial photogrammetry using an unmanned aerial system (UAS) following planting and approximately one month later. Climate during the period was collected using NexRad radar. Preliminary results were compared to simulated geomorphological and sediment budget changes over time with observed experimental values. Integration of high resolution spatial and temporal topographic measurements with physically-based models supports the development of dynamic geomorphological models needed for accurate quantification and prediction of gully formation, evolution and impact of soil erosion.

Introduction

Soil erosion due to rainfall and overland flow is detrimental to agricultural management: creating rills, gullies, and removal of fertile top soil. It contributes to sediment yield from agricultural lands and pollutes downstream water bodies. Gully erosion is particularly harmful because gullies can accelerate erosion, can yield more sediment than interrill sources, and are more difficult to mitigate. Gully erosion control in agricultural lands is a difficult task due to the limited capabilities and effectiveness of available prediction tools.

Many studies focused on erosion processes using a variety of methods including experimental measurements, field observation, and mathematical modeling. Among these, mathematical modeling is more cost effective and allows a more robust consideration of influencing factors. Hydrological numerical models are often developed based on assumptions and simplifications of the physical processes. If a numerical model introduces too many simplifications and/or idealizations, it would be difficult to capture key physical processes. Physically based models with fewer simplifications should have a higher potential to model the complex hill-slope hydrologic processes more effectively.

Overland soil erosion processes are difficult to parameterize in models. Wei et al. (2009) developed equations relating the sediment discharge to rainfall intensity and runoff rate using field data. Xiao et al. (2017) studied soil erosion rate in concentrated flows and related this to shear stress, stream power, water depth, and flow discharge. Zhang et al. (2003) studied soil detachment using undisturbed soil and found good correlations between soil detachment rate and flow parameters. Zhang et al. (2009) measured sediment transport capacity over relatively steep soil slopes (8.8-46.6%) and found that transport capacity had a close relationship to soil shear stress. Using experimental data, Aksoy et al. (2017) tested sediment transport formulae and found that total sediment transport rate was related to combinations of slope, rainfall intensity, runoff rate, and sediment size. For rills and interrill areas, Liu et al. (2006) applied sediment transport formulae for open channels to rill erosion processes. However, their sediment detachment function for interrill erosion was related to runoff velocity rather than rainfall intensity and no topographic change was computed. These studies often focus on the erosion rate and the flow parameters for a specific soil, area, slope steepness, rainfall, flow rate and are typically one-dimensional models. The results are difficult to apply to other studies in which multiple unsteady processes occurred in a real watersheds.

In this study, a physically-based finite element hydrodynamic and sediment transport model, CCHE2D, is used to simulate watershed hydrological process and sediment transport. The model is first applied to simulate soil erosion processes generated by simulated precipitation in a laboratory experiment conducted at the USDA-ARS National Sedimentation Laboratory. Rain splash erosion, runoff flow erosion, and sediment transport process are simulated. The model is then applied to a small agricultural field located in Shelby County, Iowa. The numerical model and simulation results are briefly presented and discussed.

Numerical Methods

CCHE2D hydrodynamic model

Overland flow, interrill and rill erosion due to rainfall are simulated using CCHE2D, a finite element model, which solves the depth-integrated Reynolds stress equations. The water surface elevation of the runoff flow, η, is calculated by the continuity equation:

$$\frac{\partial h}{\partial t} + \nabla \cdot (\vec{u}h) = R \tag{1}$$

where $h = \eta - \zeta$ is the local water depth, η and ζ are water surface and bed elevation, respectively. $\vec{u} = (u, v)$ is a vector of the depth-averaged velocity components, u and v in x and y directions, respectively, t is time, R is rainfall intensity, which may be a temporal and spatial variable. The depth-averaged 2D momentum equations for turbulent flows are shown below.

$$\frac{\partial u}{\partial t} + u\frac{\partial u}{\partial x} + v\frac{\partial u}{\partial y} = -g\frac{\partial \eta}{\partial x} + (\frac{\partial \tau_{xx}}{\partial x} + \frac{\partial \tau_{xy}}{\partial y}) - \frac{\tau_{\zeta x}}{\rho h} \qquad (2)$$

$$\frac{\partial v}{\partial t} + u\frac{\partial v}{\partial x} + v\frac{\partial v}{\partial y} = -g\frac{\partial \eta}{\partial y} + (\frac{\partial \tau_{yx}}{\partial x} + \frac{\partial \tau_{yy}}{\partial y}) - \frac{\tau_{\zeta y}}{\rho h} \qquad (3)$$

where g is the gravitational acceleration, ρ is water density, τ_{xx}, τ_{xy}, τ_{yx} and τ_{yy} are depth-averaged Reynolds stresses, and $\tau_{\zeta x}$, $\tau_{\zeta y}$ are bed shear stresses. For the interrill areas, the Reynolds stress terms vanish, and Eqs. 2 and 3 become the regular shallow water equations. In many segments of rills and gullies, the Reynolds number in terms of the depth or width of the flow would be quite large.

The bed shear stresses on the soil surface are evaluated in conjunction with the Manning's formula as:

$$\tau_{\zeta x} = \frac{1}{h^{1/3}}\rho g n^2 uU, \qquad \tau_{\zeta y} = \frac{1}{h^{1/3}}\rho g n^2 vU, \qquad (4a, b)$$

where n is the Manning's roughness coefficient, and $U = \sqrt{u^2 + v^2}$ is the total velocity. Manning's n normally is determined by calibrating the numerical model using experimental data. Fraga et al. (2013) found that n varies significantly with the depth of overland flow. Dramatic increases would occur when water depth is less than about 2 mm, and this change would be greater in the presence of vegetation. This is consistent with many runoff simulation results noting that Manning's n for runoff is much larger than those for rivers (Kalyanapu et al. 2009, Singh et al. 2014 and Downer 2008).

Soil erosion and sediment transport model

When numerical models are used to simulate hillslope soil erosion processes, particularly physically-based models, each process involved should be defined discretely. Hairsine and Rose (1991) defined the splash soil erosion rate due to impact of rainfall as

$$E_I = a_0 \min[1, (\frac{h_0}{h})]^b \cdot I^p \qquad (5)$$

where a_o is the soil detachability, I is rainfall intensity, E_I is non-zero when water depth, h, is less than or equal to the break point depth h_o, and b and p are dimensionless exponents. This equation can be is easily applied to general conditions; it produces splash erosion where water depth is very small, and no rain splash erosion occurs in concentrated flow areas.

Morgan et al. (1997) introduced a comprehensive watershed modeling system: EUROSEM. The soil detachment by rainfall impact is calculated by

$$E_I = \frac{a_0}{\rho_s} KEe^{-2h} \qquad (6)$$

where *KE* is the total kinetic energy of the rain drops at the ground surface. The soil detachment rate by runoff is computed by:

$$E_f = \beta\omega(C_c - C) \tag{7}$$

where C_c is the transport capacity, C is the sediment concentration, ω is the sediment fall velocity, and β is a detachment coefficient that equals unity for non-cohesive sediments. The net erosion of a slope plane can be computed by combined splash and flow erosion:

$$E = E_I + E_f \tag{8}$$

Nearing et al. (1989) developed an equation for rainfall induced interrill erosion, defined as:

$$E_I = k_I I^2 \qquad \text{[kg s}^{-1}\text{ m}^{-2}\text{]} \tag{9}$$

where k_I is the interrill erodibility. Sediment transport in rills is dominated by detachment capacity, E_f, and deposition rate, D_r, defined as:

$$E_f = k_r(\tau - \tau_c)(1 - \frac{G}{T_c}) \qquad \text{[kg s}^{-1}\text{ m}^{-2}\text{]} \tag{10}$$

$$D_r = \frac{\omega}{hu}(T_c - G) \qquad \text{[kg s}^{-1}\text{ m}^{-2}\text{]} \tag{11}$$

where erosion will occur when the sediment transport capacity, T_c, estimated using Yalin's equation, at the end of a slope is larger than the computed sediment load (bed load concentration), G, and vice versa, τ_c is the critical shear stress of the soil, and τ is the shear stress at the soil surface. This is the key equation set for the WEPP model, in which the sedimentation process in rills and interrill areas are handled separately. A watershed, therefore, has to be delineated into rill and interrill zones. Rain erosion occurs only in the interrill area, while the flow shear force is used for rill erosion.

In this study, sediment transport and topographic change are simulated by a two-dimensional flow and sediment transport model. Interrill erosion and rill erosion and deposition are handled with unified formulations. Because the model does not differentiate rill and interrill, the rain erosion equation of Hairsine and Rose (1991) was adopted with the depth delay exponent set as *b*=2 and only the soil detachability is used as a calibration parameter:

$$E_I = a_0 \min[1, (\frac{h_0}{h})]^2 \cdot I^2 \tag{12}$$

The size of rain pellets varies generally from a minimum 0.5 mm to a maximum 10.0 mm (https://hypertextbook.com/facts/2001/IgorVolynets.shtml). The median size is about 2.5 mm. In this study, it is assumed that $h_0 \approx 2.0 \, mm$. No canopy and ground cover effects were considered. The rain splash erosion is effective in the interill area, and it vanishes quickly when water depth becomes larger than h_o.

In the CCHE2D model, bed change due to sediment (bed load) transport is computed by:

$$\rho_s (1-p) \frac{dz}{dt} = \frac{(q - q_c)}{L} \tag{13}$$

where q is the sediment load transport rate, q_c is the sediment transport capacity, and L is a case dependent length scale called adaptation length for non-equilibrium sediment transport. When rain splash exists, disturbed soil particles are made available to transport as sediment sources to sheet flow. Equation 13 is modified as

$$\rho_s (1-p) \frac{dz}{dt} = Fq - (Fq_c + E_I) \tag{14}$$

where F is a calibrated parameter for rill erosion and a_o is a calibrated parameter for interrill erosion. Equation 14 unifies both concentrated flow and rain splash erosion processes. In rills, rain splash erosion vanishes and, deposition and erosion are determined by the relative value of sediment load and sediment transport capacity. In interrill areas, sediment transport capacity is less dominant and rain splash erosion contributes more to sediment load and bed change. The sediment load is solved using the unsteady partial differential equation:

$$\frac{1}{U_b} \frac{\partial q}{\partial t} + \nabla \cdot \vec{q} = Fq - (Fq_c + E_I) \tag{15}$$

$$q = |\vec{q}| , \qquad \vec{q} = (q_x \ q_y) \tag{16}$$

where U_b is the bed load velocity. The source term is the same as that of the Equation (14) because sediment load conservation is also the net sediment exchange between the soil surface and the flow. In WEPP (Nearing et al. 1989), the sediment load capacity in the rill is related to the shear stress and a coefficient. In this study, the sediment load capacity is a 2D variable over the interrill and rill areas. It is computed using the sediment transport formula of Wu et al. 2000), and critical shear stress for sediment entrainment is modified to consider the local sediment angle of repose.

Numerical simulation of soil erosion processes in a flume

The modified CCHE2D was used to simulate the rainfall-runoff-soil erosion process in an experimental landscape (Momm et al., 2018). A soil mantled flume (1.8m x 9.3m) was subjected to constant uniform simulated rainfall over a period of 18.5 hours. Homogenous soil was used in the experiment and the overall flume slope was set to 5% (Momm et al., 2018). In the first 360 min of experiment, the applied rainfall was 30 mm/h, which pre-wetted the soil. The rainfall was then increased to 105 mm/h for 735 min for soil erosion simulation.

A Cartesian mesh of 1.674 million nodes was generated for this experimental watershed using 1.0 cm x 1.0 cm uniform mesh size (i.e. the same as that of the collected photogrammetry). Several topographic surfaces were obtained during the laboratory experiment and projected onto the mesh. The tested soil is a mixture of sand (3%), silt (73%) and clay (24%). The bulk density of the compacted soil was 1450 kg/m3.

Soil erosion started after the rainfall intensity was increased from 30 mm/h to 105 mm/h at 400 min, when the downstream boundary was subjected to exogenic forcing through base level lowering (Momm et al., 2018). The observed erosion rate, and thus sediment yield, stabilized after 600 min (Figure 1). This study simulated the erosion process after the sediment load became steady. The measured soil topography at elapsed time 645 min was used in the simulation as the initial condition. The simulated sediment load agreed very well after 800 min to the measured one except in the dramatic increase at the beginning of the simulation (Figure 1).
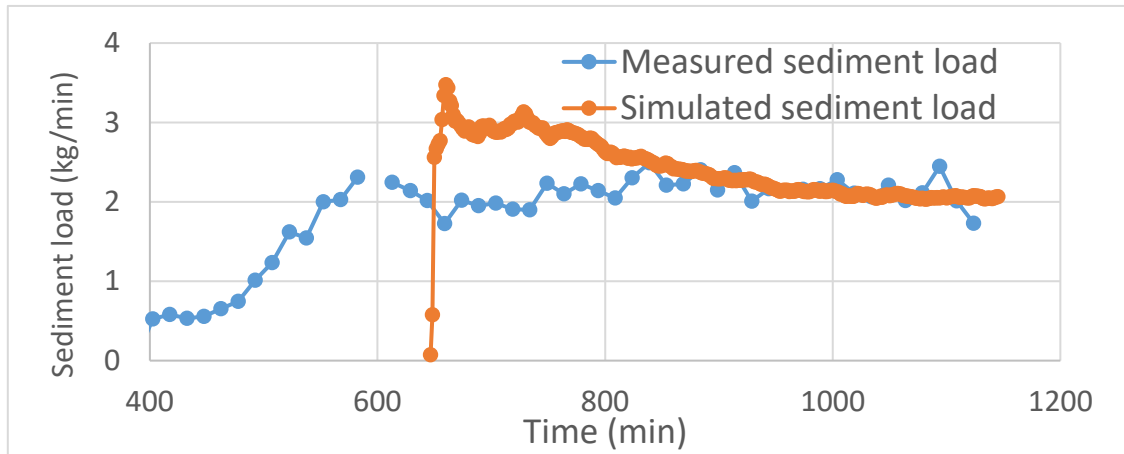
Figure 1. Comparison of simulated and measured rates of sediment yield from the soil erosion flume.

Using the observed topography at elapsed time 645 min as the starting point, the simulated landscape evolved through gully erosion and upstream migration followed by formation and evolution of tributaries gullies/rills (Figure 2). The model captured the formation of multiple channel headcuts (i.e. knickpoints) representing conditions observed during the experiment (discontinuities in contour lines in Figure 2 left-hand side map).
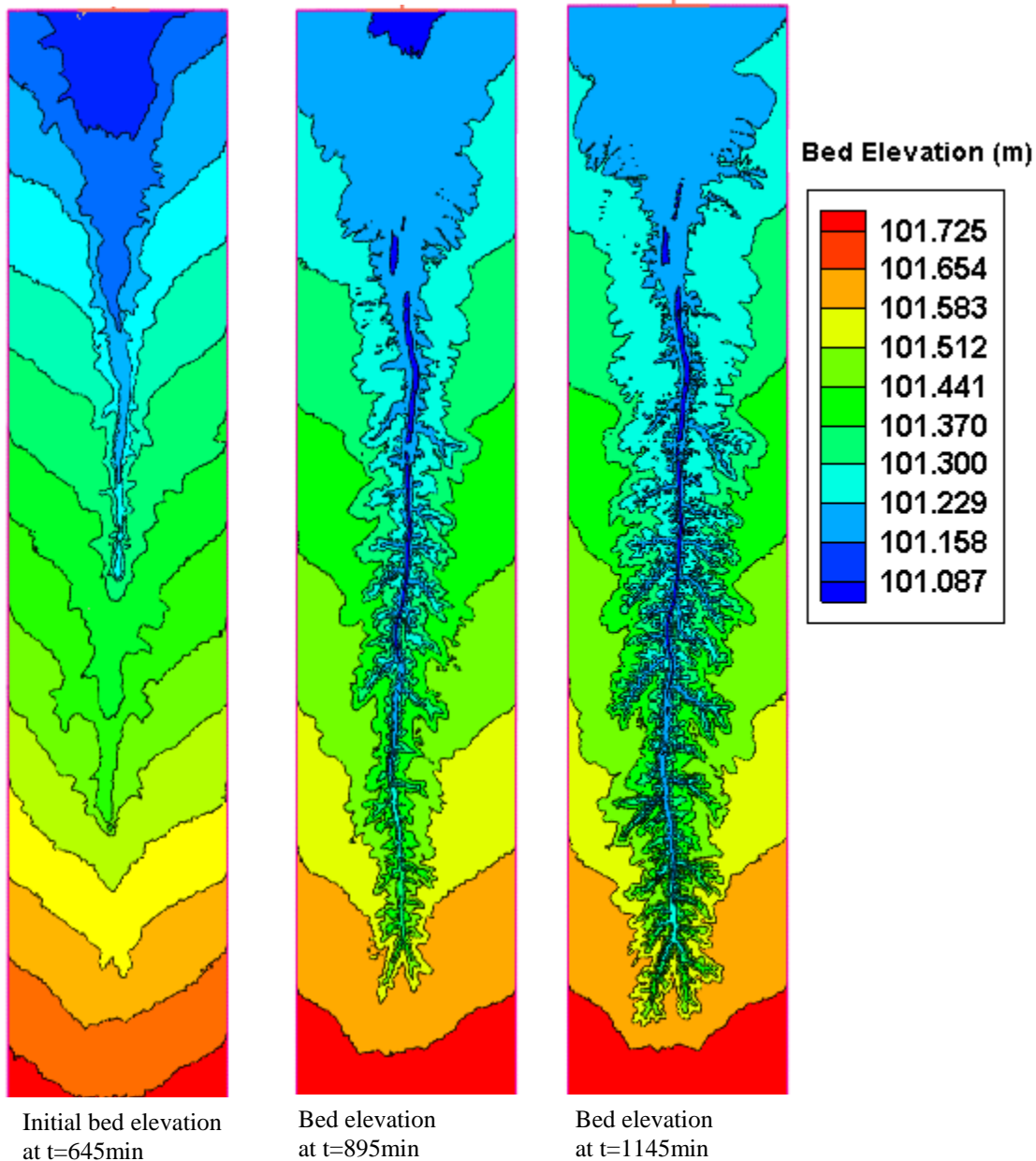
Figure 2. Simulated soil topography at t= 645 min, 895 min, and 1145 min.

Simulated elevation change between two time periods (from 645 min to 895 min, and from 645 min to 1145 min) was used to contrast with lab measured results (from 645 min to 915 min, and from 645 min to 1095 min) (Figure 3). The corresponding time period lengths for the simulation and the measurements are not exact the same but quite close. Similar geomorphological trends of the simulated (left hand side) and measured landscapes (right hand side) are observed. Both results exhibited significant gully head propagation in the upstream portion of the experimental flume. Additional similarities include branching and downstream deposition. The main difference was in the level of incision, where the simulated gully erosion depth reached -36.7 cm while the maximum observed gully erosion depth was about -14.5 cm. This difference may be

attributed to the calibration parameters controlling sediment erosion in the simulation, and future calibration may lead to improved results.

Simulated bed elevation change at t=895min	Simulated bed elevation change at t=1145min

Observed bed change from 645 min to 915 min	Observed bed change from 645 min to 1095 min
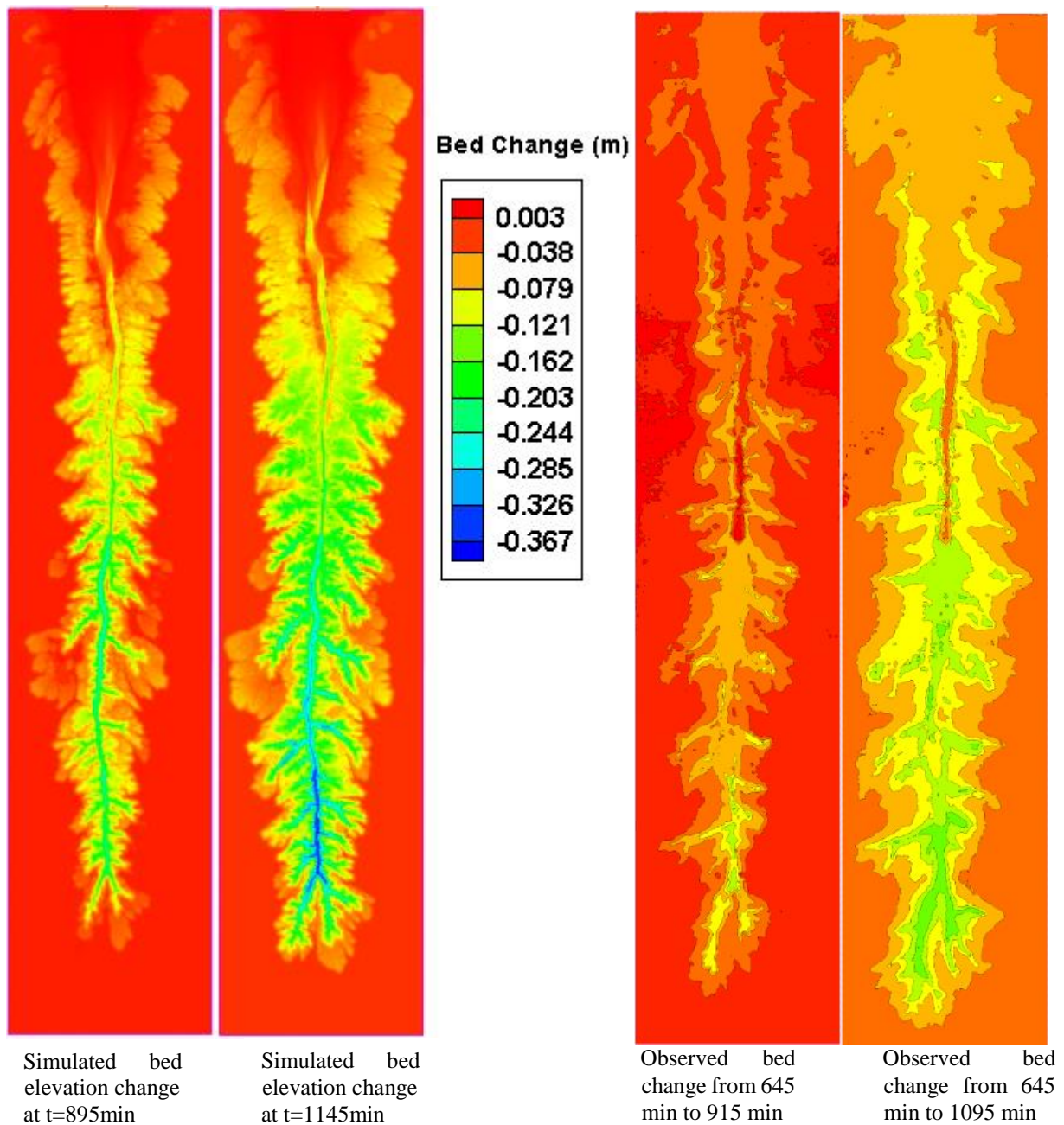
Figure 3. The simulated soil topography change from t=645 min to 895 min and 1145 min (left), and observed topographic change from t=645 min to 915 min and 1095 min. Note the color scheme is for both simulation and observation. The simulated bed change is deeper.

Simulation of soil erosion in field conditions

An agricultural field located in Shelby County, Iowa, U.S.A. with an area of approximately 54,500 m² was surveyed following planting. A novel surveying technique was employed, where

traditional surveying methods were used to establish fixed benchmark points at the edge of the field and multiple ground control points spread throughout the field, to capture very high-resolution UAS survey of the field (Figure 4). The three-dimensional point clouds were then post-processed to assure elevation changes were due to erosional processes rather than survey mis-alignment. The rainfall event of May 20, 2017 in this watershed area was simulated, which was the largest rainfall in the observed period, May 11, 2017 to June 12, 2017.
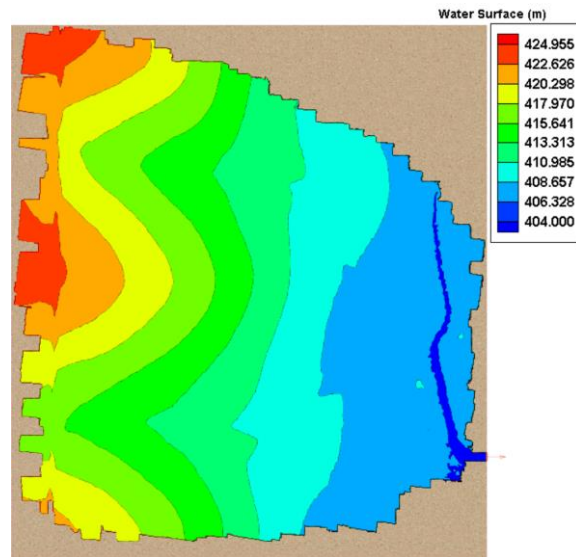
Figure 4 Topographic contour lines of the watershed. The brown areas surround the contours are outside the survey zone.

The landscape relief was less than 20 m. One ditch or small stream was situated at the downslope edge of the watershed, leading to an outlet. Generally, it is not easy to manually divide detailed sub-watersheds based on a contour distribution as shown (Figure 4), because the topography variation is mild and the curvature of the contours is not large. Simulating runoff distribution over the observed terrain provides additional detail to assist in dividing the sub-watersheds. The simulated runoff water depth near the peak rainfall time (Figure 5) was selected from the simulated hydrologic event to delineate sub-watersheds for further analysis. In order to highlight the shallow water depth of the runoffs, the distribution near the rainfall peak time is shown, and the color bar was shifted to show only $h <= 2.5 cm$.

From the runoff pattern, the survey area was separated into four major sub-watersheds, delineated by the highlighted yellow lines (Figure 5). Vectors in black indicate the approximate runoff directions in each sub-watershed. The sheet runoff in the two middle sub-watersheds (W_2, W_3) are convergent, joining the gully channels (in red) at multiple angles. The two side sub-watersheds (W_1, W_4) are only partially surveyed and their main outlets are outside the surveyed study area. The simulated runoff flows sideways toward the simulation boundaries and then flow downstream along the survey boundary. There are tractor trace lines over the landscape. They are not visible in the topographic map (Fig. 4) but can be seen via the runoff water depth distribution: equally spaced and aligned in north-south direction (Fig. 5). These trace lines cross the runoff path lines and interrupt the runoff paths slightly.
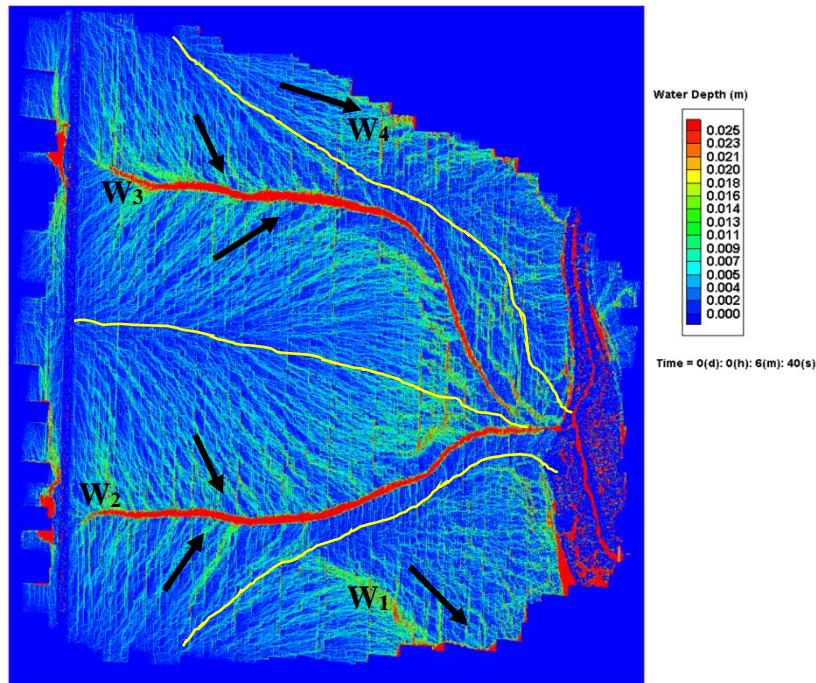
Figure 5 Simulated runoff water depth distribution near the peak of the rainfall. The yellow highlighted lines are divides between the sub-watersheds.

In this modeling study, interrill and rill are not pre-defined, runoff flows along the slope, forming a realistic flow distribution. Without the runoff analysis, it may be difficult to delineate sheet flow zones, sub-watersheds and/or interrill runoff strips prior to numerical simulation.

Rainfall distribution and simulated hydrographs are displayed in Figure 6. The main rainfall lasted about 123.3 min while the runoff simulation covered 405 min. Two Manning's coefficient n=0.1 and n=0.2 were evaluated. In the simulation using n=0.2, the hydrograph peak happens approximately 40 min later than the peak of the rainfall while using n=0.1 the hydrograph peaks approximately 20 min later. Also, when using n=0.1, two separated peaks are observed and they could be attributed to the difference of the arrival time of the two main streams.
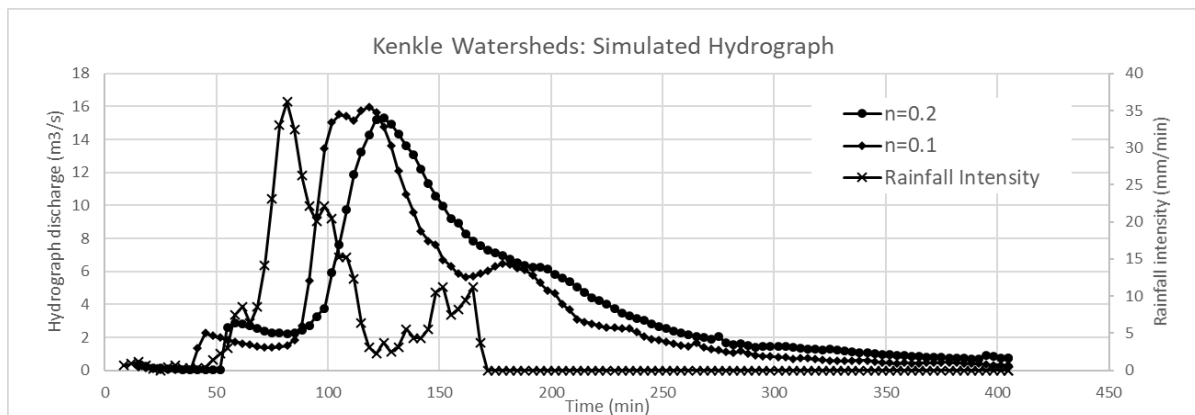
Figure 6 Selected rainfall and simulated runoff hydrographs of the field watershed.

Soil erosion and sediment transport

CCHE2D was then applied to simulate sediment transport and potential topographic change in the watershed. The Manning's coefficient value of n=0.2 was adopted. All other soil erosion parameters were selected based on previous studies without calibration because soil erosion and sediment yield data had not yet been fully processed. Therefore, the simulation results should be considered preliminary and a demonstration of model capability. The largest simulated erosion depths are in the gullies, through incision into pre-existing channels (Figure 7). Feather-like erosion patterns were found over the watershed surface. The pattern of erosion is consistent to that of the runoff shown in Figure 5. The soil erosion pattern seemed to create nearly parallel rills. The erosion depths of these rills are deeper near the watershed gullies, become shallower toward upstream, and vanish near the watershed divides. Figure 8 shows the sediment load distribution in the watershed. It generally increases from the watershed divides to rills and gullies. For the two side-watersheds (W1 and W4), sediment is being transported to and then flows downstream along the boundaries of the computing area.
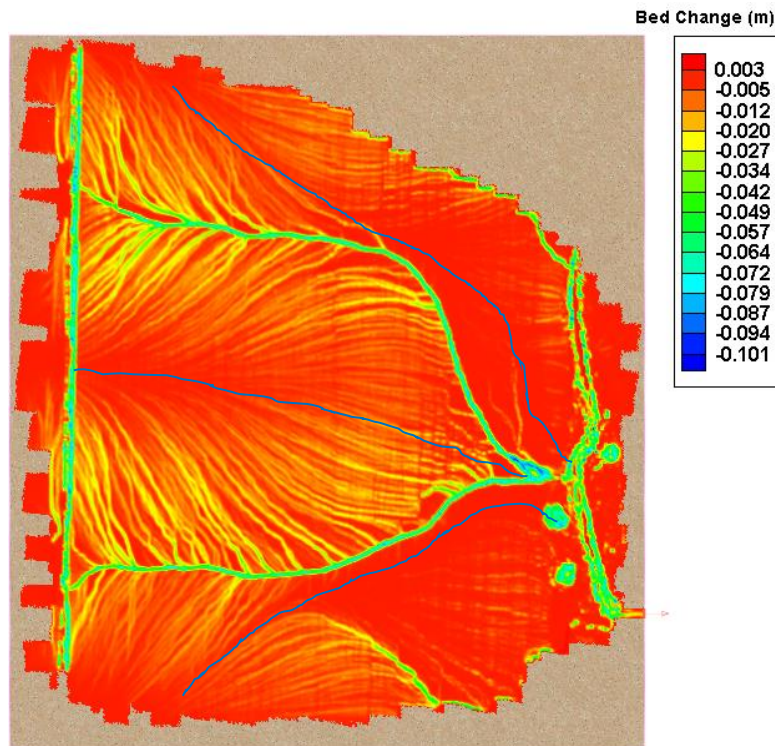
Figure 7 Simulated soil erosion and gully incision in field watershed. Boundaries of sub-watersheds are indicated with fine and blue lines. The external area was not simulated.
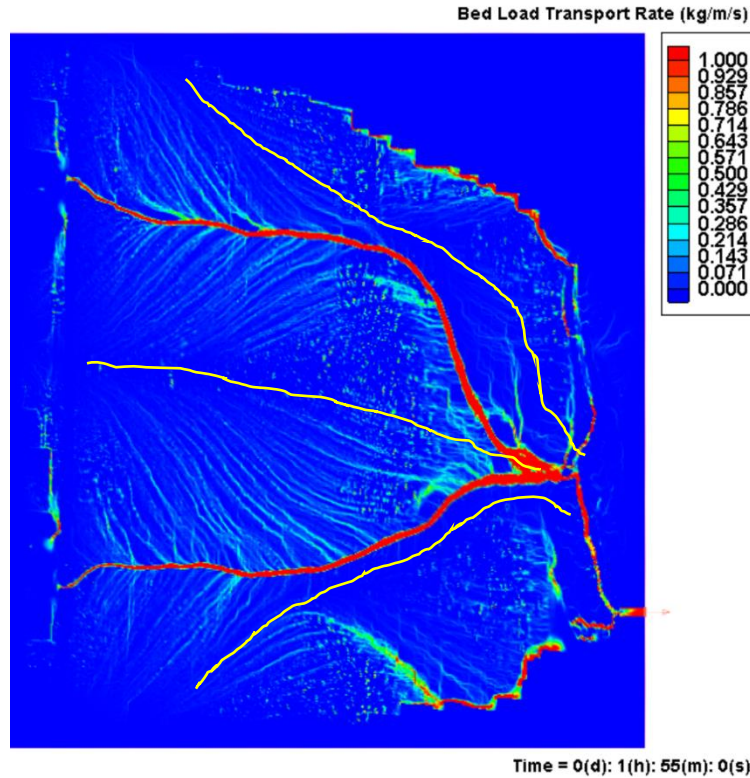
Figure 8 Simulated sediment transport (sediment load) distribution at approximately 2 hours. To make the portion over the rill and interrill area, the range of the color bar was adjusted.

Conclusions

A physically based model CCHE2D was modified and applied to simulate watershed hydrology and soil erosion through interill and gully erosion processes. Rain splash effects were added to the sediment transport and soil erosion equations. Overland flow and soil erosion due to rain splash, sheet flow in interrill areas and concentrated flow in rills and gullies are computed non-discriminatively over the entire watershed, rather than separately in different morphologic zones using different methods.

The model was evaluated using data from a large-scale flume experiment devised to quantify soil erosion and gully development. The simulated morphologic development and sediment yield are consistent to those observed. The model was then applied to simulate soil erosion processes in a field scale agricultural watershed. The topographic map of the watershed was obtained remotely through photogrammetry. Reasonable results were obtained using a strong local rainfall record.

The advantage of this modeling method for soil erosion studies vs. other approaches, is that the physically based hydrodynamic and erosion, sediment transport model do not spatially differentiate these processes. Detailed and continuous spatial and temporal information for the watershed runoff, soil erosion, sediment transport and morphologic change processes were provided. Future research is needed to enhance this method through improved formulations and calibration with measured data.

References

Aksoy, H., Eris, E., and Tayfur, G. (2017). Empirical sediment transport models based on indoor rainfall simulator and erosion flume experimental data. Land Degradation and Development, 28(4), 1320-1328.

Downer, C.W. (2008). "Demonstration of GSSHA hydrology and sediment transport at the Goodwin Creek Experimental Watershed". ERDC TN-SWWRP-08-x, Vicksburg, MS: U.S. Army Engineer Research and Development Center. https://swwrp.usace.army.mil/

Hairsine P.B. and Rose C.W. (1991). Rainfall detachment and deposition: Sediment transport in the absence of flow-driven processes. Soil Science Society of American Journal, 55(2): 320-324.

Kalyanapu A.J., Burian S.J. and McPherson T.N. (2009). Effect of land use-based surface roughness on hydrologic model output. J. Spatial Hydrol., 9(2), Fall 2009.

Liu Q.Q., Xiang H., and Singh V.V. (2006). A simulation model for unified interrill erosion and rill erosion on hillsploes. Hydrol. Process. 20, 469-486.

Momm H.G., Wells R.R., and Bennett S.J. (2017). Disaggregating soil erosion processes within an evolving experimental landscape. Earth Surface Processes and Landforms, Copyright © 2017 John Wiley & Sons Ltd. Published online in Wiley Online Library. DOI:10.1002/esp.4268.

Morgan R.P.C., Quinton, J.N., Smith R.E., Govers G., Poesen J.W.A., Auerswald K., Chisci G., Torri D., and Styczen W.E. (1998). The European soil erosion model (EUROSEM): A dynamic approach for predicting sediment transport from fields and small catchments. Earth Surface Processes and Landforms, 23, 527-544.

Nearing, M., Foster, G., Lane, L., and Finkner, S.C. (1989). A process-based soil erosion model for USDA-Water Erosion Prediction Project technology. Trans. ASAE, 32: 1587–1593.

Singh J., Altinakar, M.S., Ding, Y. (2014). Numerical Modeling of Rainfall-Generated Overland Flow Using Nonlinear Shallow-Water Equations, Journal of Hydrologic Engineering, doi:10. .1061/(ASCE)HE, 1943-5584.

Wei H., Nearing M.A., Stone J.J., Guertin D.P., Spaeth K.E. Pierson F.B., Nichols M.H., and Moffet C.A. (2009). A new splash and sheet erosion equation for rangelands. Soil Science Society of American Journal, 73(4): 1386-1392.

Xiao, H., Liu, G., Liu, P., Zheng, F., Zhang, J., and Hu, F. (2017). Response of soil detachment rate to the hydraulic parameters of concentrated flow on steep loessial slopes on the Loess Plateau of China. Hydrological Processes, 31(14), 2613-2621

Zhang, G.H., Liu, B.Y., Liu, G.B., He, X.W., and Nearing, M.A. (2003). Detachment of undisturbed soil by shallow flow. *Soil Science Society of America Journal.* 67(3): 713-719.

Zhang, G.H., Liu, Y., Han, Y., and Zhang, X.C. (2009). Sediment transport and soil detachment on steep slopes: I. transport capacity estimation. Soil Science Society of America Journal, 73(4), 1291-1297.

Streambank Erosion Assessment in the Catalpa Creek in Mississippi

John Ramirez-Avila, Assistant Professor, Mississippi State University, Starkville, MS, jjr149@msstate.edu

Joby Czarnecky, Assistant Research Professor, Mississippi State University, Starkville, MS, joby@gri.msstate.edu

Tim Schauwecker, Associate Professor, Mississippi State University, Starkville, MS, tschauwecker@lalc.msstate.edu

Sandra Ortega-Achury, Research Associate II, Mississippi State University, Starkville, MS, sandraortega@cee.msstate.edu

Eddy Langendoen, Research Hydraulic Engineer, USDA-ARS, Oxford, MS, Eddy.Langendoen@ars.usda.gov

Extended Abstract

Streambank erosion is an important mechanism driving sediment supply into the streams of the Catalpa Creek Watershed. Headwaters tributaries and main channel stream lengths are visually affected by channel degradation processes. Research is advanced to identify erosion mechanisms, the potential effects of streambank erosion processes, and to quantify and model the magnitude and rates of these processes within the Catalpa Creek Watershed. Identification and assessment of processes and rates are pursued by the combination of field reconnaissance, channel cross section survey and Unmanned Aerial Vehicles monitoring after major stormflow events; weekly grab sampling and sediments and water quality assessments; and laboratory procedures and modeling applications. Preliminary results are helping to determine critical areas to be potentially considered for implementing management and restoration. Modeling would help to optimize a restoration design for a desired outcome and to understand what results might be expected after implementation.

Identifying in-stream process is needed to determine suitable assessment and measurement techniques and appropriate stream restoration designs (Ramirez-Avila et al., 2010). Catalpa Creek is an EPA priority watershed, for which an approved water management plan is in phase of implementation. Around 3-miles of headwater tributaries and 4-miles of main channel stream lengths are visually affected by streambed and streambank processes (Ramirez-Avila et al., 2016). The project involves important collaborative efforts with Mississippi State University faculty members from several colleges, departments and institutes and from state and federal research and education institutions. Training of students with different levels of involvement has been of fundamental support to the performance of the project.

Streambank erosion is an important mechanism driving sediment supply into the streams and an important portion of the sediment budget for the Catalpa Creek Watershed. Research is focused on the identification, assessment, evaluation and prediction of streambank erosion processes within the study watershed. The overall goal of this research is to identify erosion mechanisms, the potential effects of streambank erosion processes, and to quantify and model the magnitude and rates of these processes within the Catalpa Creek Watershed.

This extended abstract summarizes general procedures followed to accomplish project goals and objectives. To accomplish this research, a combination of methods was used, including field reconnaissance and detailed data collection, laboratory analysis, and computational channel modeling.

Weekly data collection was advanced along 40 stations in the main stream and three headwater tributaries, in order to quantify stream hydrologic and hydraulic characteristics (flow velocity and depth), water quality characteristics (pH, turbidity, temperature, total dissolved solids), and collect grab water samples for assessing total suspended concentrations.

Samples were collected at two stations along the main stream, in which an ISCO auto sampler and an area-velocity device were installed.
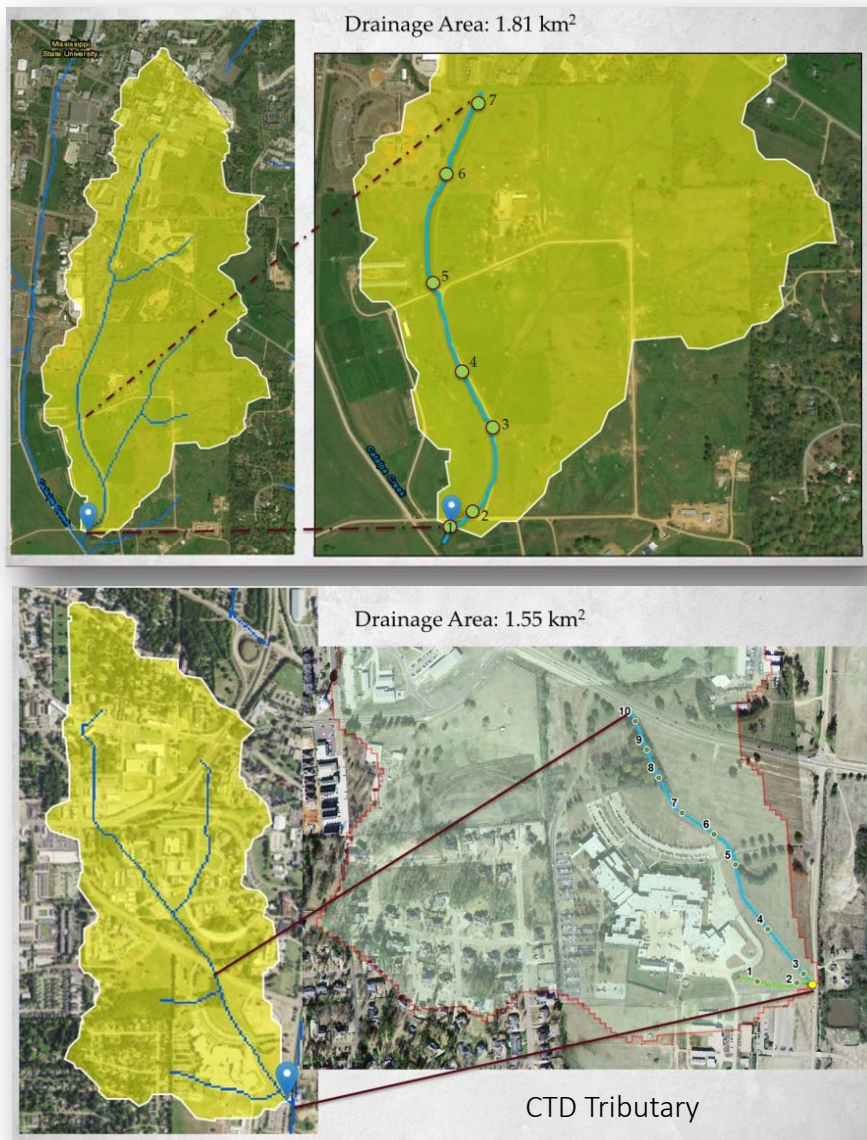
Figure 1. Monitored tributary streams in the Catalpa Creek watershed

Figure 2. Stream monitoring and laboratory analysis

Cross sections along the upper four miles of the main stream and tributaries were periodically surveyed by traditional cross section survey and UAV assessment (Czarnecki et al., 2018) in collaboration with researchers from the Landscape Architecture, the Geosystem Research Institute (GRI) and the Mississippi Agricultural and Forestry Experiment Station (MAFES). Results from experimental procedure advanced by Ramirez-Avila (2011) and Ramirez-Avila et al. (2010) for Town Creek Watershed were taken in consideration to properly compare changes in monitored cross sections. Spatio-temporal changes in channel morphology are evaluated to quantify erosion and sediment deposition rates along streambanks and streambed.

Figure 3. Cross sections and UAV survey.

Research has identified representative streambank erosion processes and channel changes within the entire watershed. Rates of sediment contribution by streambank erosion processes, and the definitive identification of these processes as the driving mechanism of sediment supply within the Catalpa Creek watershed are assessed and determined. Results have also evidenced differences in water quality conditions along stream segments under varying riparian zones (Figure 4 and 5) and significant temporal variability of sediment concentration and loads along the main stream under baseflow and stormflow conditions (Figure 6). Figure 6 shows contrasting differences in relationship between sediment concentrations and loads with stream water turbidity.
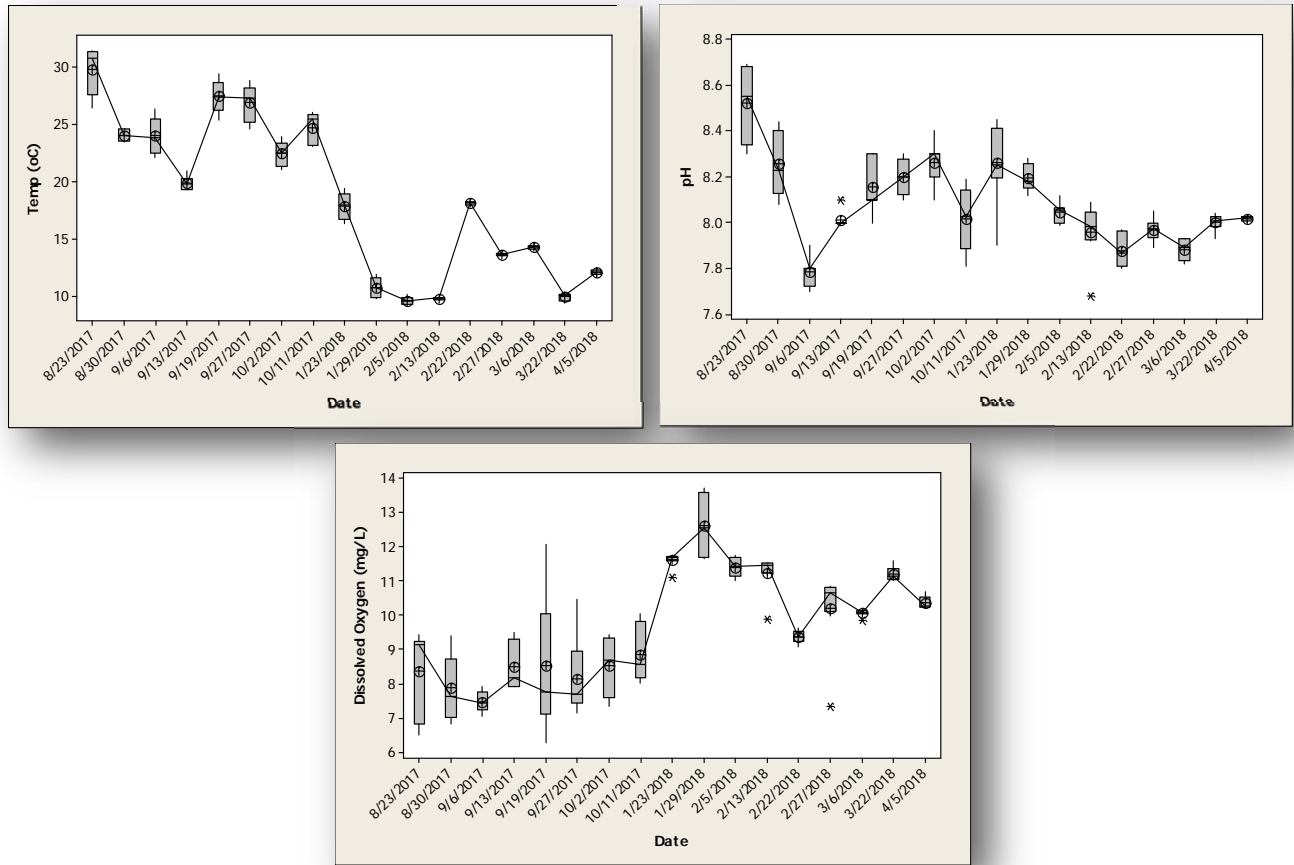
Figure 4. Temporal variability of water quality parameters for the CT tributary of Catalpa Creek
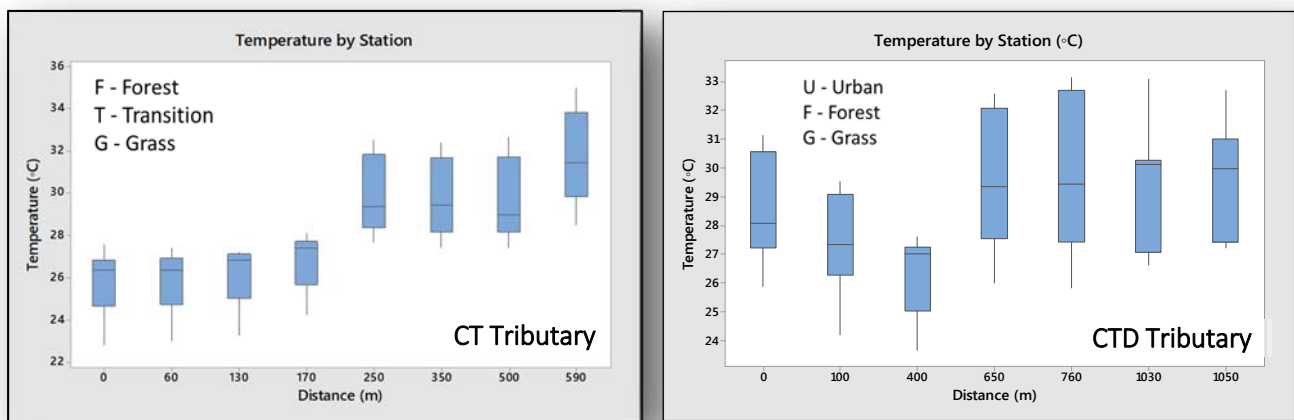
Figure 5. Spatial variability of stream temperature in two tributaries of Catalpa Creek along different riparian zone types (summer 2018)
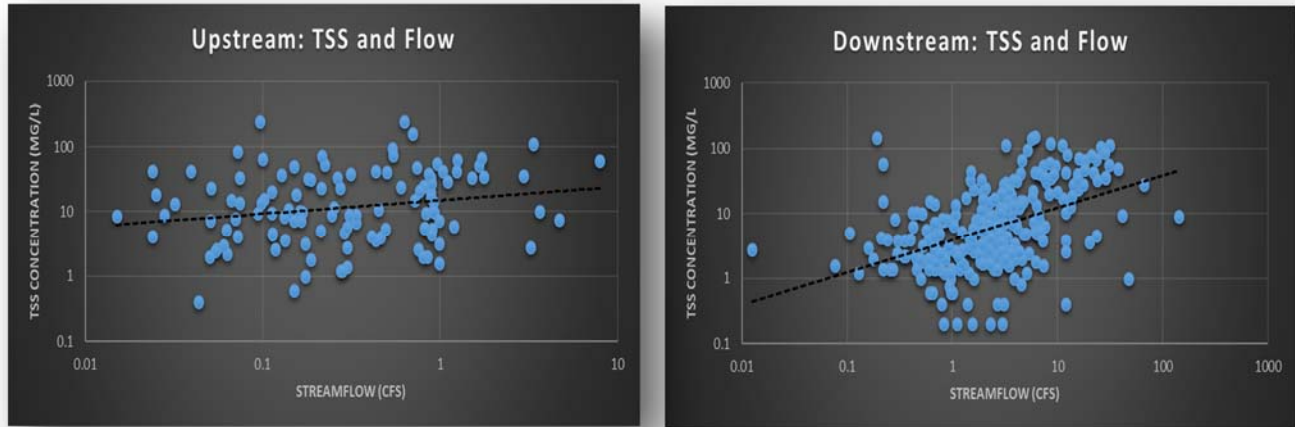
Figure 6. Rating curves for upstream (0.2Km) and downstream (5Km) stations along the main channel of Catalpa Creek

Annual widening and streambank erosion rates on incised channels with limited riparian vegetation are up to 2.8 m and 30 Mg per m^{-1} of streambank, respectively (Fig. 7). Streambank erosion most commonly due to planar failures along main stream and undercutting, cantilever failure and basal clean out along tributaries (Fig. 7).

Figure 7. Temporal variation of in-stream processes along the Catalpa Creek tributary

Modeling results will help to determine critical areas to be potentially considered for future management and restoration activities, as well as to optimize a design for a desired outcome and to understand what results might be expected. Project results will be transferred to a broad group of academic, technical and research stakeholders, supported in collaboration with private, federal and state agencies.

Figure 8. Streambank erosion along main stream and tributaries in the Catalpa Creek watershed

References

Czarnecki, J. M., Ramirez-Avila, J. J., & Hathcock, L. A. (2018). Structure from Motion with Unmanned Aerial Vehicles: A Best Practices Guide for New Users. Mississippi State University: Geosystems Research Institute

Ramirez-Avila, J. J. (2011). Assessment and prediction of streambank erosion rates in a Southeastern Plains Ecoregion watershed in Mississippi. Mississippi State University, ProQuest Dissertations Publishing.

Ramirez-Avila, J., Langendoen, E., McAnally, W., Martin, J., & Ortega-Achury, S. (2010). Assessment and estimation of streambank erosion rates in the Southeastern Plains ecoregion of Mississippi. In 2010 Federal Interagency Sedimentation Conference (FISC) Proceedings.

Ramirez-Avila, J., Schauwecker, T. J., & Czarnecki, J. M. P. (2016). Catalpa Creek Watershed Planning, Restoration, and Protection Project. In Conference: XIX Conferenza Nazionale della Società Italiana degli Urbanisti (SIU). Catania, Italy.

The Movements of Bed and Suspended Sediments and Pollutants by the Stochastic Process Theory

Geraldo Wilson Junior, Docteur d'Etat, COPPE/UFRJ
Federal University of Rio de Janeiro, Rio de Janeiro, Brazil. jrwilsong@gmail.com
Cid da Silva Monteiro, D.Sc., INPI
National Institute of Industrial Property, Rio de Janeiro, RJ, Brazil. csgm25@gmail.com

Abstract

The Stochastic Processes Theory describes the sediment movements, as well as of the pollutants' particles fixed or not by the fine solid grains, either in contact with the bed or in suspension, in open channel flows. Einstein (1937) was pioneer when considering the bed-load movement as Stochastic Processes. Todorović *et al.* (1976) extended the use of this theory for the movement of suspended sediments. Then the liquid and sediment movements: bed and suspended load; wash load; pollutants fixed or not by fine grains, were approached by the same theory. The *2-D* suspension movements were considered at SEDHYD2015, held in Reno, Nevada, USA. They characterize stochastic processes whose elementary events are the two-dimensional trajectories of individual particles *ω (x, z, t)* which result from the combination of two independent chronological series of displacement in the directions *i = 1, 3*; intercalated by periods in which the particle ceases to advance in these directions. These two independent *1-D* series and their combination *2-D* are considered in this paper: longitudinal and vertical series of movements, simultaneously. When they are described by Homogeneous Poissonian Stochastic Processes, the resulting *2-D* model is also Homogeneous Poissonian, defined by four mobility density functions that characterize the motions of the particles. In the SEDHYD2019, we focus on the longitudinal and vertical movements of the sediments with transfers between the bed and the suspension. The objectives of this article are multiple: (i) application of *2-D* stochastic models to describe the suspension movement of cohesive and non-cohesive sediment of different diameters and concentrations; (ii) presentation of experimental equipment and devices that allow recording such sediment movements, with vertical transfers; (iii) description of the probability density functions of the positions of the deposited particles. For the development, calibration and validation of the Stochastic Processes *1-D* (two mobility parameters) and *2-D* (four mobility parameters), experimental results obtained in open channel flows with radioactive and fluorescent tracers have been considered, where the mobile bed layer behaves in four distinct ways: (i) as a reflective barrier of cohesive sediments of varying concentrations and of non-cohesive fine sediments of different size classes of silt and fine sand, (ii) as a source for bed load movements of uniform sand (D_{50} = 0.150 and 1.200 mm) in ripple and dune regimes, (iii) as a barrier of sediment absorption and (iv) as a simultaneous barrier of absorption of fine sediments and, at the same time source of bed sediment movements. To study the *1-D* and *2-D* Poisson Models, a software for stochastic processes with instantaneous and continuous injections, named PAICON-D, was developed. Results obtained with this program are presented in this article.

Introduction

Sediment Movement Mechanism

According to the hydrodynamic properties of the liquid phase, and physicochemical of the solid, the sediment movement in river flows occurs in three distinct modes (Figure 1), (Sayre,1971; Wilson-Jr., 1987):

As a suspension of pelytic sediments and/or pollutants dissolved or in colloidal form. Pelytic sediments are those whose grains are indistinct to unarmed sight. In this case, the particles are transported by the average velocity of the flow. Simultaneously, they are mixed and dispersed transversely and longitudinally, by the combined action of turbulent diffusion, and the differentiated advection due to spatial variations of the fluid velocity field. The solid particles are so small, the coarser in the range of 30 to 40 µm, that the force of gravity is not significant for the sedimentary movement. It is the general case of the movement of type "*wash-load*".

As suspensions of non-pelytic sediments and fixed pollutants. They are sediments such as silt and fine sand, which are transported in suspension by the same mechanism of the "*wash load*", where, however, the gravitational force has a significant performance: the solid grains decant and can be deposited on the river bed. Once deposited, they behave like sediments of the mobile layer of the bed.

As grains of the active or mobile layer of the bed. These grains are also subject to the action of the instantaneous hydrodynamic forces of the turbulent flow, which vary continuously and randomly over time. When these forces overcome the resistance forces, derived from the action of gravity on the grain, i.e., the weight of the submerged grain and its contact with other particles of the bed, the sediment's grain moves. The particle is displaced from the bed and travels a certain distance until it is stopped by other grains, or until the hydrodynamic forces are no longer able to maintain their movement. The grain is again part of the bed until a new displacement occurs. Some grains can get out from the mobile bed and return their movement in suspension, but most of it rolls, jumps and drags on the other grains of the bed.
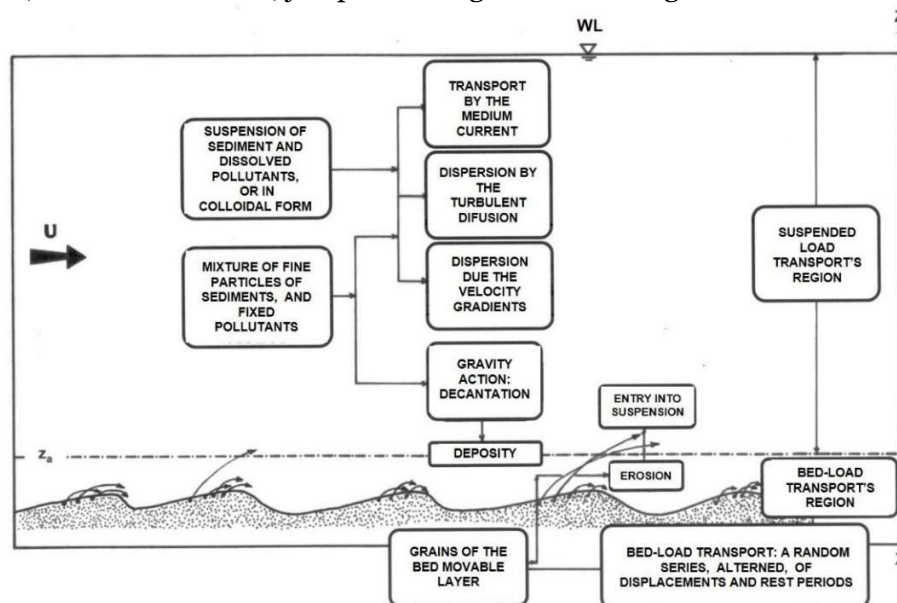
Figure 1. General description of the sediment movement in river flows (Sayre, 1971, Wilson-Jr. 1987)

The Importance of the River Bed

A natural water course carries water, sediment and organic substances. The fluid models the movable bed, at the same time it has its hydrodynamic characteristics modified by the forms it has modeled. Thus, hydrodynamic studies and solid mass transfers should be carried out simultaneously.

For solid particles of the same nature, it is expected that the variables that intervene in the bed-load and suspended-load movements relate to each other, at least in its common frontier: the **mobile bed**, which assumes four important roles:

(i) **Supply source** of grain moving in contact with the bed and/or in suspension.
(ii) **Absorption barrier** of suspended sediments that are deposited in the bottom and behave as sediments of the movable layer of the bed, moving in contact with the bed or which remain motionless, due to its physicochemical properties.
(iii) **Reflection barrier** of suspended sediments that touch the bed under the effect of turbulence and gravity, and return, completely, to the suspension movement.
(iv) **Simultaneous barrier** of absorption and reflection of fine sediments and source of bed sediment movements.

Sediment Movement as Stochastic Processes

The sediment and contaminant particles movements in open channel flows characterize random processes, where the elementary events are the single grains' trajectories. The **Theory of Stochastic Processes** describes these movements, as well as of the pollutants fixed by the grains of fine sediments, either in contact with the mobile bed, either in suspension in the middle of the eddies, either inside reservoirs and lakes, or in estuaries and marine environments. The same theory describes all these movements.

The first studies that considered the random nature of the sedimentary movement were those of Einstein (1937). However, most of the authors who later devoted to this theme did not adopt this type of description. Instead of a probabilistic, kinematic, too theoretical description for the time, they preferred deterministic estimates of the solid discharge in function of the hydrodynamic variables of the flow. However, despite the large number of researchers and several decades of work on the subject, there is still no universal mathematical expression for estimating the solid discharge of the flows with free surface.

It has been necessary to wait for the 60's years to verify a new evolution of the probabilistic theory of the sedimentary movement, thanks to the use of radioactive tracers, as a technique of hydrodynamic and sedimentological measurements.

The tracers proved to be extremely useful in the studies related to the fundamental mechanics of sediment movement, allowing Eulerian and Lagrangean measurements of the simple grain trajectories and/or particle groups (Vukmirović, 1975; Wilson-Jr. 1972, 1987). It was possible to measure the evolution in time, the distribution of sediment positions along a channel or river, and, the passage times of the particles through selected sections of these flows.

For several years, the authors among others (Wilson-Jr., 1972, 1987, 2012; Vukmirović, 1975; Vukmirović & Wilson-Jr. 1976, 1977; Wilson-Jr. & Vukmirović, 1981; Monteiro & Wilson-Jr., 2001, 2002, 2003; Monteiro, 2004; Wilson-Jr. & Monteiro, 2016, 2017, 2018) have been dedicated to the development and applications of random models in laboratory channels with sediments labeled with radioisotopes, in streams and in rivers with fluorescent and radioactive

tracers, simulating pollutants and sediments, respectively. The types of studies performed by these authors are summarized in Figure 2. Its results constitute an important collection of data on transport and dispersion of sediment, fundamental for a better understanding of sediment movement in open channel flows.
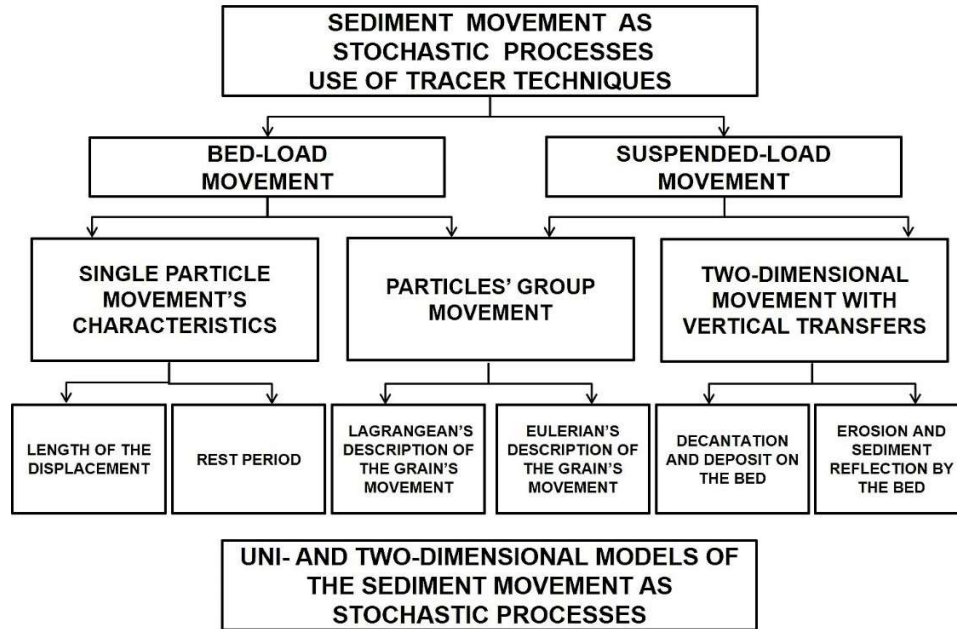
Figure 2. Studies performed with radioactive tracers on the sediment movement by the Theory of Stochastic Processes.

The **Theory of Stochastic Processes** proposes a kinematic analysis of the movements of the liquid and solid phases, while considering the turbulent characteristics of the flow. Thus, problems related to: (i) the nonlinearity of the equations; (ii) the complexity of liquid and solid interactions; and, (iii) the lack of knowledge of the mutual interference of the movements of the two phases; are circumvented.

Objectives

The objectives of this article are multiple:

1. Presentation of a synthesis of the mathematical development of the Lagrangean Description of the 2-D Homogeneous Poissonian' Stochastic Process.

2. Application of 2-D stochastic models to describe the suspension movement of cohesive and non-cohesive sediment of different diameters and concentrations.

3. Presentation of experimental equipment and devices that allow recording such sediment movements, with vertical transfers.

4. Description of the probability density functions of the positions of the deposited particles.

For the application of the Poissonian 1-D and 2-D models, the software called **PAICON-D -** Stochastic Processes with Instant and Continuous Injection (*Processos Aleatórios com Injeções*

Instantâneas e CONtínuas, in Portuguese) was used. Among others, the model calculates the values of the probability density functions of the positions of the sediment particles in suspension as a function of time: <u>Lagrangean Descriptions</u> f_t (x), f_t (z) and f_t (x, z); and its times of passage through transversal and horizontal sections: <u>Eulerian Descriptions</u> q_t (x), q_t (z) and q_t (x, z), for values of the mobility functions $\lambda_{x1}(t, n)$, $\lambda_{z1}(t, n)$, $\lambda_{t2}(x, n)$ and $\lambda_{t2}(z, n)$, obtained experimentally.

Synthesis of Mathematical Development

The basic mathematical development that characterize the sediment movement as stochastic processes can be followed through the works of Wilson-Jr. (1972, 1987), Vukmirović (1975), Hanno (1979) and Monteiro (2004). For Congresses and Symposiums' papers, the authors elaborated a synthesis of this development, periodically updated, for improvements and applications of the theme (Wilson-Jr. & Monteiro, 2015, 2016, 2018).

Intensity of Grain Mobility Functions

The bed and suspended load movements of sediments and contaminant particles in open channels flows characterize stochastic process, where the elementary events are the single grains' trajectories. They are dependent of the turbulent hydrodynamic process. These trajectories or achievements of the single particles or of the group of particles are analyzed by Lagrangean or Spatial, and Eulerian or Temporal Descriptions and by the Stochastic Processes Theory. Two stochastic processes are considered:

$$\vec{R}(t, \omega) = [X(t, \omega), Y(t, \omega), Z(t, \omega)] = X_{ti}(\omega); i = 1, 2, 3 \tag{1}$$

that characterizes the evolution of the particle's position vector as a function of time, which longitudinal, lateral and vertical components are X (t, ω), Y (t, ω) and Z (t, ω), respectively. The second 3D stochastic process:

$$T(x, y, z, \omega) = [T(x, \omega), T(y, \omega), T(z, \omega)] = T_{xi}(\omega); \ i = 1, 2, 3 \tag{2}$$

characterizes the particle's passing time by the point of coordinates (x, y, z).
T (x, ω), T (y, ω) and T (z, ω) represent the times spent by the particle to travel the distances 0x, 0y and 0z, respectively. ω represents the trajectory or the sediment particle achievements.
$X_{ti}(\omega)$ and $T_{xi}(\omega)$ processes can be defined by their <u>Probability Distribution Functions</u>:

$$F_t(x_i) = P\{X_i(t, \omega) \leq x_i\}; \ x_i \geq 0; \ i = 1,2,3 \tag{3}$$

$$Q_{xi}(t) = P\{T(x_i, \omega) \leq t\}; \ t \geq 0; \ i = 1,2,3 \tag{4}$$

which are related to each other by Todorović's Equation (5) (Todorović *et al.*, 1966):

$$F_t(x_i) = 1 - Q_{xi}(t); \ x_i \geq 0; t \geq 0; \ i = 1,2,3 \tag{5}$$

It was shown that the Probability Distribution Function of these random processes can be expressed in terms of two pairs of Approximate Functions F_{t1} (x$_i$) and F_{t2} (x$_i$); $Q_{x1i}(t)$ and Q_{x2i}(t); i = 1,2,3, respectively, such that:

$$0 \leq F_{t1i}(x_i) \leq F_{ti}(x_i) \leq F_{t2i}(x_i) \leq 1; \ t \geq 0; \ i = 1,2,3 \tag{6}$$

$$0 \leq Q_{x2i}(t) \leq Q_{xi}(t) \leq Q_{x1i}(t) \leq 1; \ t \geq 0; \ i = 1,2,3 \tag{7}$$

In each direction, e. g. in the longitudinal direction $Ox_{i=1}$, where $x_i = x_1 = x$, the Approximate Distribution Functions $F_{tj}(x)$ and $Q_{xj}(t)$, $j = 1,2$ can be explained as functions of two new stochastic processes $G_n^{0,x}$ and $E_n^{0,t}$ from the same elementary events ω:

$$G_n^{0,x} = \{\mu_{0,x} = n\} \tag{8}$$

which represents the medium number of grain displacements, $\mu_{0,x}$ over the distance [0, x], and,

$$E_n^{0,t} = \{\eta_{0,t} = n\} \tag{9}$$

the medium number of grain displacements, $\eta_{0,t}$ over the time period [0, t]. $G_n^{0,x}$ and $E_n^{0,t}$ are Markovian Processes with similar properties. So, for the set $G_n^{0,x}$, it has:

$$\begin{cases} P\left\{G_1^{x,x+\Delta x} \middle| G_k^{0,x}\right\} = \lambda_2(x,k)\Delta x + \vartheta(\Delta x) \\ P\left\{G_v^{x,x+\Delta x} \middle| G_k^{0,x}\right\} = \vartheta(\Delta x), v \geq 2 \\ P\left\{G_0^{x,x+\Delta x} \middle| G_k^{0,x}\right\} = 1 - \lambda_2(x,k)\Delta x + \vartheta(\Delta x) \\ P\left\{G_0^{0,0}\right\} = 1 \end{cases} \qquad \text{when } \Delta x \to 0 \tag{10}$$

where $\vartheta(\Delta x)$ is a grain first order infinitesimal displacement distance. The $G_n^{0,x}$ and $E_n^{0,t}$ occurrence probabilities are solutions of the system of equations derived from these properties:

$$\begin{cases} \frac{\partial}{\partial x} P\{G_k^{0,x}\} = \lambda_2(x,k-1)\, P\{G_{k-1}^{0,x}\} - \lambda_2(x,k)\, P\{G_k^{0,x}\} \\ \frac{\partial}{\partial x} P\{G_0^{0,x}\} = -\lambda_2(x,0)\, P\{G_k^{0,x}\} \end{cases} \tag{11}$$

with the following initial conditions:

$$x = 0 \quad \begin{cases} P\{G_0^{0,x}\} = 1 \\ P\{G_k^{0,x}\} = 0; \ k \geq 1 \end{cases} \tag{12}$$

Similar analytical expressions to the Equations (10), (11) and (12) are obtained for the $E_n^{0,t}$ process. The solution of these differential equations yields the probability laws for the numbers of displacements in time and spatial intervals. Two functions $\lambda_1(t, n)$ and $\lambda_2(x, n)$ appear, which describe the sediment particle mobility, in time and in that particular direction $x_{i=1} = x_1 \approx x$. Considering the three directions of the orthogonal axes Ox_i, $i = 1, 2, 3$, three pairs of Mobility Functions $\lambda_{1i}(t, n)$ and $\lambda_{2i}(x_i, n)$ are obtained, which describe the sediment grains 3D movements, in time and space. In each x_i direction it has been:

$$\begin{cases} \lambda_{1i}(t,n) = lim_{\Delta t \to 0} \dfrac{P\left\{E_{1i}^{t,t+\Delta t}\middle|E_{ni}^{0,t}\right\}}{\Delta t} \\ \lambda_{2i}(x_i,n) = lim_{\Delta t \to 0} \dfrac{P\left\{G_{1i}^{x_i,x_i+\Delta x_i}\middle|G_{ni}^{0,x_i}\right\}}{\Delta x_i} \end{cases} \qquad i = 1, 2, 3 \tag{13}$$

Different models can be obtained from the mathematical expressions that define these mobility functions, which should consider the sediment and/or contaminant particle characteristics, as well the hydrodynamic properties. The general expressions for λ_{1i} and λ_{2i}, $i = 1, 2, 3$ were

obtained by Vukmirović (1975) and Wilson-Jr. (1987, 2012) considering the bed load movement of single grains of sediment labeled with radiotracers. They considered the mobility of the particle as a function of time, of the distance traveled in one direction and of its past performance in time (n) and distance (k), in each direction (i):

$$\begin{cases} \lambda_{1i}(t,n) = \lambda_{1i}(t)\,\lambda_{1i}(n) \\ \lambda_{2i}(x,k) = \lambda_{2i}(x)\,\lambda_{2i}(k) \end{cases} \qquad i = 1, 2, 3 \qquad (14)$$

where: λ_{1i} and λ_{2i} are particle mobility factors in a given time t in the direction i, and in a certain position x_i, respectively.

These functions are obtained from experiments performed with liquid and solid particles of tracers: radioactive, dyes and chemicals, in bed-load and/or suspended-load movements. Wilson-Jr. (1987, 2012) classified the Stochastic Models according to their mobility functions in Homogeneous Poissonian Models (constant mobilities), Non-Homogenous and Non-Poissonians, which are indicated in Figures 3 and 4. With the experimental device shown in Figure 5, the movements of suspended sediment and of bed-load, with vertical transfers, were recorded. Thus, we obtained a collection of original data for the study of random movements 1D and 2D of sediments, cohesive and non-cohesive, and analysis of the evolution of a group of particles that moves sometimes suspended in the middle of the liquid phase, sometimes by dragging on the movable bed of a river. Particularly, for the case of suspended movement, the grain mobility functions in the longitudinal and vertical directions assume constant values and the resultant Stochastic Models are Homogeneous Poissonian.
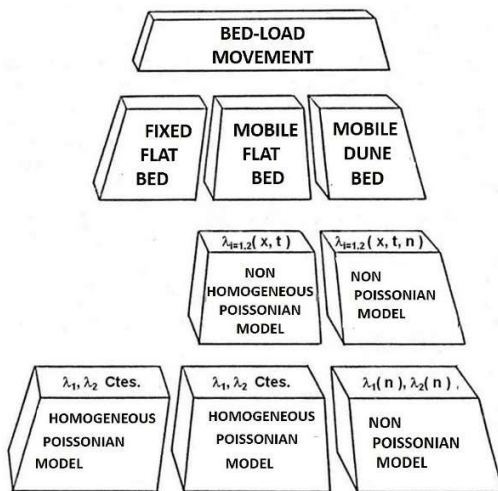
Figure 3. Stochastic models of the bed-load movements (Wilson-Jr. 1987)

$\lambda_1(t, n)$	$\lambda_2(x, m)$	Authors	Date	Movement	Models
$\lambda_1 = $ Cte	$\lambda_2 = $ Cte	Einstein	1937	Bed-load	Homogeneous Poissonian
		Sayre e Hubbell	1965	Bed-load	
		Todorović e Vukmirović	1966	Bed-load	
		Paintal	1971	Bed-load	
		Todorović, Simmons, Li	1976	Suspension	
		Hanno	1980	Bed-load	
		Wilson-Jr.	1987	Bed & Suspension Load	
		Mendes e Wilson-Jr.	1995	Suspension	
		Monteiro e Wilson-Jr.	2005	Suspension	
		Wilson-Jr.	2007	Bed & Suspension Load	
$\lambda_1(t)$	$\lambda_2(x)$	Shen e Todorović	1971	Bed-load	Non Homogeneous Poissonian
		Frickmann e Wilson-Jr.	1996		
$\lambda_1 = $ Cte	$\lambda_2(x, r_2)$ $r_2 > 0$, Cte	Sayre e Yang	1968	Bed-load	
		Grigg	1971		
$\lambda_1(x, r_1)$ $r_1 > 0$, Cte	$\lambda_2(x, r_2)$ $r_2 > 0$, Cte	Wilson-Jr.	1972	Bed-load	
$\lambda_1(t)$ $\lambda_1(n)$	$\lambda_2(t)$ $\lambda_2(m)$	Vukmirović e Wilson-Jr.	1975,77	Bed-load	Non Poissonian
? $\lambda_1(t)$	? $\lambda_2(x)$	Hung e Shen	1976	Bed-load	Causality Functions
$\lambda_1(t)$ $\lambda_1(n)$	$\lambda_2(t)$ $\lambda_2(m)$	Cheong e Shen	1983	Bed-load	Non Poissonian
		Vukmirović e Wilson-Jr.	1985,87		

Figure 4. Models resulting from expressions of λ1 (t, n) and λ2 (x, m) (Wilson-Jr. 2012)

2-D Homogeneous Lagrangean Stochastic Poissonian Process

Over the last few decades, the authors have been dedicated to the development and applications of Homogeneous and Non-Homogeneous Poissonian Models, in laboratory channels with sediment labeled with radiotracers, in streams and in rivers with fluorescent (dyes) and radioactive tracers, simulating contaminated liquid and sediment particles (Figures 5 and 6). For the suspended movement, the grain mobility functions in the longitudinal and vertical directions assume constant values and the resultant models are Homogeneous Poissonian.
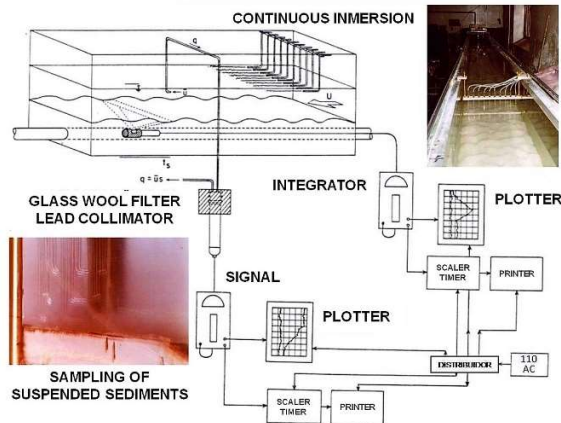
Figure 5. Immersion and detection system of bed and suspended movements of fine sediments in a LCHF's laboratory channel (Wilson-Jr. 1987).
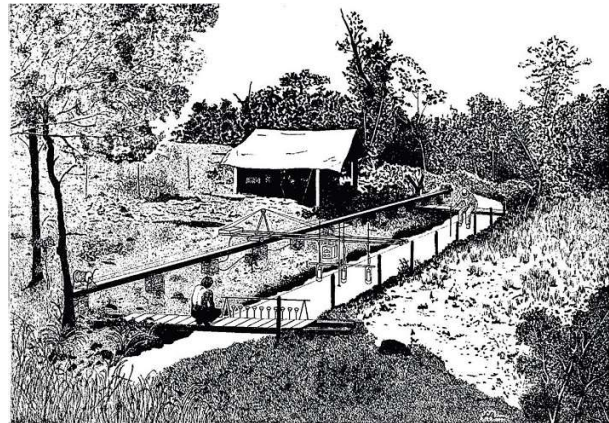
Figure 6. Experiments carried out in streams with sediments labeled with radioisotopes (Wilson-Jr. 1987, 2003)

To illustrate the particles behavior, one adopts the Lagrangean 2-D Homogeneous Poissonian Stochastic Processes $X_{ti}(\omega)$, i = 1, 3, described by:

$$\begin{cases} \lambda_{1i}(t,n) = \lambda_{1i} = const. \\ \lambda_{2i}(x,k) = \lambda_{2i} = const. \end{cases} \quad i = 1,3 \tag{15}$$

which means that the probability of the grains' displacements, in time and distance [t, t+Δt] and [x, x+Δx], Δt and Δx tending to zero, are independent of time, particle position and of previous displacements, i.e., independent of the particle history. This movement is called _out of memory_.

The Density Probability Functions of the particles in time t is given by the following equations which characterize the Homogeneous Poissonian Random Processes (Wilson-Jr., 1987; Wilson-Jr. & Monteiro, 2015):

$$f_t(x,z) = \frac{\partial^2 F_t(x,z)}{\partial x \, \partial z} = f_t(x) \, f_t(z) \tag{16}$$

$$0.0 \leq f_{t1}(x_i) \leq f_t(x_i) \leq f_{t2}(x_i) \leq 1.0 \quad i = 1,3 \tag{17}$$

$$\begin{cases} f_{t1}(x_i) = \lambda_{2i} e^{-\lambda_{1i}t - \lambda_{2i}x_i} \sum_{k=0}^{\infty} \frac{(\lambda_{1i}t)^k}{k!} \frac{(\lambda_{2i}x)^k}{k!} \\ f_{t2}(x_i) = \lambda_{2i} e^{-\lambda_{1i}t - \lambda_{2i}x_i} \sum_{k=0}^{\infty} \frac{(\lambda_{1i}t)^{k+1}}{(k+1)!} \frac{(\lambda_{2i}x)^k}{k!} \end{cases} \quad i = 1,3 \tag{18}$$

Statistical Properties of the 2-D Homogeneous Poissonian Models: Some of the main statistical properties that characterize the 2-D Homogeneous Lagrangean Random Process X_t (x, z), for cases of instantaneous and continuous immersions, are described analytically in this item (Monteiro, 2004; Wilson-Jr. & Monteiro, 2016, 2017). The originality is the substitution of the inferior and superior approximations of the functions probability density f_{tj} (x, z), j = 1,2 and of the other approximate statistical characteristics, by the expressions of

their average values, $f_{tm}(x, z)$, $h_{tm}(x, z)$, $F_{tm}(x, z)$ and $H_{tm}(x, z)$ for example, for cases of instantaneous and continuous immersions, respectively, as shown as following:

Instantaneous Immersion Case:

Mean Probability Density Function $f_{tm}(x, z)$

$$f_{t1}(x,z) \ \leq \ [f_t(x,z) \ = \ f_t(x) \, f_t(z)] \ \leq \ f_{t2}(x,z) \tag{19}$$

$$f_t(x,z) \ \cong \ f_{tm}(x,z) \ \cong \ \frac{1}{2}[f_{t1}(x,z) \ + f_{t2}(x,z)] \tag{20}$$

$$\begin{cases} f_{t1}(x,z) \ = \ \lambda_{21} \, \lambda_{23} \ e^{-\lambda_{11}t \, -\lambda_{21}x} \ e^{-\lambda_{13}t \, -\lambda_{23}z} \ \sum_{n=0}^{\infty} \sum_{k=0}^{\infty} \frac{(\lambda_{11}t)^n}{n!} \frac{(\lambda_{21}x)^n}{n!} \frac{(\lambda_{13}t)^k}{k!} \frac{(\lambda_{23}z)^k}{k!} \\ f_{t2}(x,z) \ = \ \lambda_{21} \, \lambda_{23} \ e^{-\lambda_{11}t \, -\lambda_{21}x} \ e^{-\lambda_{13}t \, -\lambda_{23}z} \sum_{n=0}^{\infty} \sum_{k=0}^{\infty} \frac{(\lambda_{11}t)^{n+1}}{(n+1)!} \frac{(\lambda_{21}x)^n}{n!} \frac{(\lambda_{13}t)^{k+1}}{(k+1)!} \frac{(\lambda_{23}z)^k}{k!} \end{cases} \tag{21}$$

Mean Probability Distribution Function $F_{tm}(x, z)$

$$F_{t1}(x,z) \ \leq \ \left\{ F_t(x,z) \cong F_{tm}(x,z) \cong \frac{1}{2}[F_{t1}(x,z) \ + F_{t2}(x,z)] \right\} \ \leq F_{t2}(x,z) \tag{22}$$

$$\begin{cases} F_{t1}(x,z) = \ e^{-\lambda_{11}t \, -\lambda_{21}x} \ e^{-\lambda_{13}t \, -\lambda_{23}z} \ \sum_{n=0}^{\infty} \sum_{k=n}^{\infty} \frac{(\lambda_{11}t)^n}{n!} \frac{(\lambda_{21}x)^k}{k!} \ \sum_{m=0}^{\infty} \sum_{p=m}^{\infty} \frac{(\lambda_{13}t)^m}{m!} \frac{(\lambda_{23}z)^p}{p!} \\ F_{t2}(x,z) = \ e^{-\lambda_{11}t \, -\lambda_{21}x} \ e^{-\lambda_{13}t \, -\lambda_{23}z} \ \sum_{n=0}^{\infty} \sum_{k=n}^{\infty} \frac{(\lambda_{11}t)^{n+1}}{(n+1)!} \frac{(\lambda_{21}x)^k}{k!} \ \sum_{m=0}^{\infty} \sum_{p=m}^{\infty} \frac{(\lambda_{13}t)^{m+1}}{(m+1)!} \frac{(\lambda_{23}z)^p}{p!} \end{cases} \tag{23}$$

Mean of the Average Particle Positions, $M_{tm}(x, z)$

$$M_{t1}(x,z)_{Inst} \ \leq \ \left\{ [M_t(x,z)_{Inst}] \cong [M_{tm}(x,z)_{Inst}] \cong \frac{1}{2}[M_{t1}(x,z)_{Inst} + M_{t2}(x,z)_{Inst}] \right\} \ \leq \ M_{t2}(x,z)_{Inst} \tag{24}$$

$$\begin{cases} [M_{t1}(x,z)_{Inst}] \ = \ E[F_{t1}(x,z)] \ = \ \frac{1}{2\lambda_{21}\,\lambda_{23}}[2\lambda_{11}\,\lambda_{13}\,t^2 \ + \ (\lambda_{11} \ + \ \lambda_{13})t \ + \ 1] \\ [M_{t2}(x,z)_{Inst}] \ = \ E[F_{t2}(x,z)] \ = \ \frac{\lambda_{11}\,\lambda_{13}}{\lambda_{21}\,\lambda_{23}}\,t^2 \end{cases} \tag{25}$$

Mean of the Particle Position Variances $[S_t^2(x,z)]_{Inst}$

$$[S_{t1}^2(x,z)]_{Inst} \ \leq \ \left\{ [S_t^2(x,z)]_{Inst} \cong [S_{tm}^2(x,z)]_{Inst} \cong \frac{1}{2}[[S_{t1}^2(x,z)]_{Inst} + [S_{t2}^2(x,z)]_{Inst}] \right\} \ \leq \ [S_{t2}^2(x,z)]_{Inst} \tag{26}$$

$$\begin{cases} [S_{t1}^2(x,z)]_{Inst} \ = \ \frac{2\lambda_{11}\lambda_{13}(\lambda_{11}+\lambda_{13})t^3+[(\lambda_{11}+\lambda_{13})^2+10\lambda_{11}\lambda_{13}]t^2+6(\lambda_{11}+\lambda_{13})t+3}{(\lambda_{21})^2\,(\lambda_{23})^2} \\ [S_{t2}^2(x,z)]_{Inst} \ = \ \frac{2\lambda_{11}\lambda_{13}(\lambda_{11}+\lambda_{13})t^3+2\lambda_{11}\lambda_{13}t^2}{(\lambda_{21})^2\,(\lambda_{23})^2} \end{cases} \tag{27}$$

Continuous Immersion Case:

Mean Probability Density Function $h_{tm}(x, z)$

$$h_{t1}(x,z) \leq \left\{ \left[h_t(x,z) = \frac{1}{t_d} \int_0^{t_d} f_{t-\tau}(x) f_{t-\tau}(z) d\tau \right] \cong h_{tm}(x,z) \cong \frac{1}{2}\left[h_{t1}(x,z) + h_{t2}(x,z) \right] \right\} \leq h_{t2}(x,z) \tag{28}$$

$$\begin{cases} h_{t1}(x,z) = \dfrac{1}{t_d}\lambda_{21}\,\lambda_{23}\displaystyle\int_0^{t_d} e^{-\lambda_{21}x-\lambda_{23}z}\,e^{-(\lambda_{11}+\lambda_{13})(t-\tau)}\left\{\sum_{n=0}^{\infty}\dfrac{[\lambda_{11}(t-\tau)]^n}{n!}\dfrac{(\lambda_{21}\,x)^n}{n!}\right\}\left\{\sum_{n=0}^{\infty}\dfrac{[\lambda_{13}(t-\tau)]^n}{n!}\dfrac{(\lambda_{23}\,x)^n}{n!}\right\}d\tau \\[2em] h_{t2}(x,z) = \dfrac{1}{t_d}\lambda_{21}\,\lambda_{23}\displaystyle\int_0^{t_d} e^{-\lambda_{21}x-\lambda_{23}z}\,e^{-(\lambda_{11}+\lambda_{13})(t-\tau)}\left\{\sum_{n=0}^{\infty}\dfrac{[\lambda_{11}(t-\tau)]^{n+1}}{(n+1)!}\dfrac{(\lambda_{21}\,x)^n}{n!}\right\}\left\{\sum_{n=0}^{\infty}\dfrac{[\lambda_{13}(t-\tau)]^{n+1}}{(n+1)!}\dfrac{(\lambda_{23}\,x)^n}{n!}\right\}d\tau \end{cases} \tag{29}$$

Mean Probability Density Function $H_{tm}(x, z)$

$$H_{t1}(x,z) \le \left\{\left[H_t(x,z)=\frac{1}{t_d}\int_0^{t_d} F_{t-\tau}(x)\,F_{t-\tau}(z)\,d\tau\right] \cong H_{tm}(x,z) \cong \frac{1}{2}\big[H_{t1}(x,z)+H_{t2}(x,z)\big]\right\} \le H_{t2}(x,z) \tag{30}$$

The distribution functions $F_{t-\tau}(x)$ and $F_{t-\tau}(z)$ are obtained from the 1-D models' approximate equations in the longitudinal and vertical directions, respectively, that is, from the 1-D Homogeneous Poissonian equations systems with instantaneous immersion (Wilson-Jr. & Monteiro, 2015, 2017).

Knowing the values of the longitudinal and vertical probability density functions of the Lagrangean or Eulerian concentration of sediment or contaminants in suspension: theoretically from Equations (19-30), and experimentally as in Figure 5 and 6, it is easy to determine their statistical moments and then their intensity mobility's values: λ_{1j}, λ_{2j}; j=1,3. For example, the following Equations (31-32) represent the upper approximation of the median position $[M_{t2}(x, z, t)]_{Inst.}$ and variance of particles' positions $[S^2_{t2}(x, z, t)]_{Inst.}$ for the instantaneous immersion case. Similar equations were obtained for the continuous case. The Equation (33) describe the upper approximation of the median position $[M_{t2}(x, z, t)]_{Cont.}$ as function of time for the continuous case. Unhappily the variance equations, $[S^2_{t2}(x, z, t)]_{Cont.}$, are so long to be presented in this paper. Nevertheless, they can be obtained from the moments of $h_t(x, z)$ given by Equations (28) and (29).

Instantaneous Immersion Case:

Upper Median Position of Particles: $[M_{t2}(x, z, t)]$ Inst.

$$\big[M_{t2}(x,z,t)\big]_{Inst.} = \frac{\lambda_{11}}{\lambda_{21}}\frac{\lambda_{13}}{\lambda_{23}}t^2 \tag{31}$$

Upper Variance of the Particles' Positions: $[S^2_{t2}(x, z, t)]$ Inst

$$\left[S^2_{t2}(x,z,t)\right]_{Inst.} = \frac{2\lambda_{11}\lambda_{13}(\lambda_{11}+\lambda_{13})t^3 + 2\lambda_{11}\lambda_{13}\,t^2}{(\lambda_{21})^2(\lambda_{23})^2} \tag{32}$$

<u>Continuous Immersion Case:</u>

Upper Median Position of Particles: $[M_{t2}(x, z, t)]$ Cont.

$$\big[M_{t2}(x,z,t)\big]_{Cont.} = \frac{\lambda_{11}}{\lambda_{21}}\frac{\lambda_{13}}{\lambda_{23}}\left(t^2 - t\,t_d + \frac{t_d^2}{3}\right) \tag{33}$$

2-D Homogeneous Poissonian Models' Applications: Summary of Recent Results

The Mutually Independent 1-D Stochastic Process

The hypothesis that has allowed to successfully apply the Theory of Stochastic Processes is the independence of the longitudinal and vertical movements in turbulent open flows. This property was described by Equation (16). It allows us to analyze the one-dimensional movements independently of each other and determining the values of the grain's mobility by simple equations, which may be adjusted to field surveys, as shown in Figure 7. The independent resulting processes are 1-D Homogeneous Poissonian, with the following main properties:

Longitudinal and vertical mean positions of a group of particles

$$\begin{cases} X_m(t) = \dfrac{\lambda_{1x}}{\lambda_{2x}} t = \dfrac{\lambda_{11}}{\lambda_{21}} t \\[2mm] Z_m(t) = \dfrac{\lambda_{1z}}{\lambda_{2z}} t = \dfrac{\lambda_{13}}{\lambda_{23}} t \end{cases} \tag{34}$$

Variances of the longitudinal and vertical positions of a group of particles

$$S_j^2(t) = 2\,\frac{\lambda_{1j}}{\lambda_{2j}^2}\, t \qquad j = x, z \quad \text{or} \quad j = 1, 3 \tag{35}$$

Longitudinal and vertical mean velocities of a group of particles

$$U_j = \frac{\lambda_{1j}}{\lambda_{2j}} \qquad j = x, z \quad \text{or} \quad j = 1, 3 \tag{36}$$

Each pair of values of the <u>Mobility Functions</u> describes the sediment grain movement in one direction. The results of the evolution in time of their approximate superior probability density functions are shown in Figure 7, for an instantaneous immersion, in which: $\lambda_{1x} = 1.0$ s^{-1}; $\lambda_{1z} = 0.10$ s^{-1}; $\lambda_{2x} = \lambda_{2z} = 10.0$ m^{-1}; $U_x = 0.10$ m s^{-1}; $U_z = 0.01$ m s^{-1}. The Figure 8 illustrates a case of a plume of sediments due to a continuous immersion at the free surface during the time interval [0, 120.0 s]. In this case the mobility values are: $\lambda_{1x} = 2.0$ s^{-1}; $\lambda_{1z} = 0.10$ s^{-1}; $\lambda_{2x} = \lambda_{2z} = 10.0$ m^{-1}; $U_x = 0.20$ m s^{-1} and $U_z = 0.01$ m s^{-1}.

Lagrangean and Eulerian Results

Data obtained in a rectangular prismatic channel of the LCHF (Figure 5) have been used to validate and calibrate the models. Figures 9 and 10 show results of the PAICON-D program, for uniformly distributed lateral injections on the free surface, and continuously during the time interval [0, $t_d = 120$ s]. The plumes in Figure 9 correspond to the 2-D movements of fine sediments depending on the diameter of the grain. Once the particles are small, they are supposed to have the same longitudinal mobility of the liquid. The figure clearly illustrates: (i) the variation of vertical grain mobility according to their diameters, and (ii) how the particles from the watershed are integrated into the river bed. The plume in Figure 10 indicates the 2-D behavior of a sample of sediments of varying diameters and percentages. The graphs represent:

(i) the Lagragean 2-D field of normalized concentration C (x, z, t), in a channel 20.0 m long and 2.0 m deep, in the instant t = 100.0 s; (ii) Lagrangean 1-D vertical profiles of sediment concentration in sections x = 3.0; 10.0 and 17.0 m in the instant t = 100.0 s, and (iii) the Eulerian evolutions of the concentrations, in the levels z = 0.4 and 0.8 m, in the three sections.
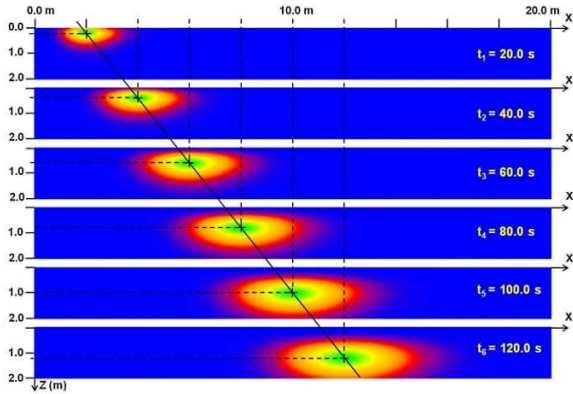
Figure 7. Clouds of sediments due to an instantaneous immersion at the free surface.
(Wilson-Jr. & Monteiro, 2016)
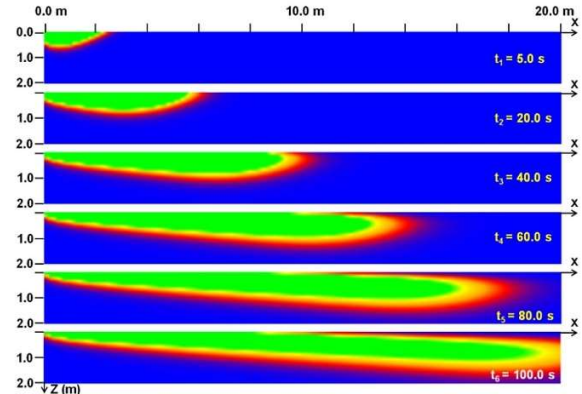
Figure 8. Plumes of sediments due to continuous immersion at the free surface during the [0, t$_d$] interval.
(Wilson-Jr. & Monteiro, 2016)

Figure 9. Bidimensional movements of fine sediment injected continuously over a period, on the watercourse's free surface as a function of the grain diameter (Wilson-Jr. & Monteiro, 2017)

Figure 11 presents the movements of a fine sand plume (D = 0.125 mm), injected on the free surface, at a constant rate, during the interval [0, t$_d$ = 200 s]. The deposit at the bottom is a function of the diameter and of the specific weight of the grain, and of the hydrodynamic properties of the flow, which define the vertical λ_{1z} and λ_{2z}, and longitudinal λ_{1x} and λ_{2x} mobilities. The deposit at the bottom is function of the specific diameter and weight of the grain, and of the hydrodynamic properties of the flow, which define the vertical mobilities λ_{1z} and λ_{2z}; and longitudinal λ_{1x} and λ_{2x}.

In Figure 12, there are weighted deposits, at different depths, of a mixture of sediments of known diameters equally distributed in weight (i_{bd} = 0.25) (Wilson-Jr. & Monteiro, 2018).
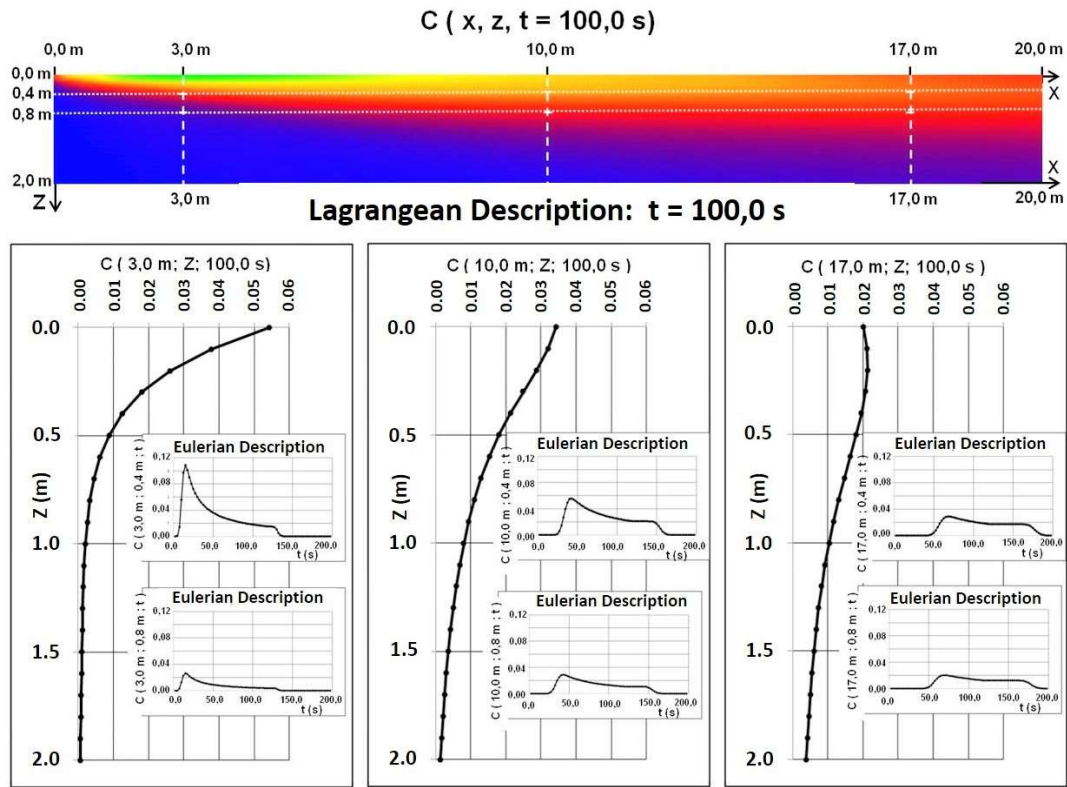
Figure 10. Lagrangean and Eulerian descriptions of the fine sediment's concentration C (x, z, t). Continuous immersion during [0, t_d = 200 s], of grains' sediments 0.040 ≤ D_i ≤0.600 mm. Stationary Regime established in the period 75 s ≤ t ≤ 120 s (Wilson-Jr. & Monteiro, 2016).
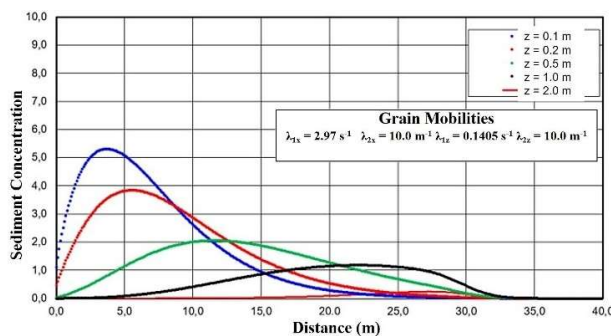
Figure 11. Sediment deposition of D = 0.125 mm in flows of varying depths. Immersion Interval [0, t_d = 200 s] (Wilson-Jr. & Monteiro, 2018)
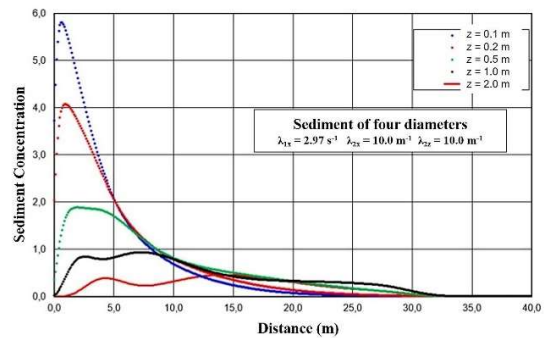
Figure 12. Deposition of a sediment mixture of diameters D = 0.125; 0.200; 0.300; 0.600 mm. λ_{1z} = 0.1405; 0.360; 0.480 and 1.395 s-1. (Wilson-Jr. & Monteiro, 2018)

For the development, calibration and validation of 1-D and 2-D Stochastic Processes of sediment and pollutant which move as bed-load and suspended-load with vertical transfers, there is a set of experimental results obtained in laboratory channels, using tracers where the mobile bed behaves in <u>four distinct ways</u>; as a(n):

i. **Supply source** of sediment grains in contact with the bed and/or in suspension, which can move, for example, as ripples and/or dunes.

ii. **Absorption barrier** of suspended sediments touching the mobile bed. Figure 13 illustrates the longitudinal distribution of sediment deposition of various diameters at the bottom of an open channel flow. The weighted composition of the final deposit of the material injected into the free surface was also presented. They correspond to the case of reflection 0.0 % in Figure 14.

iii. **Simultaneous barrier of absorption and reflection** of sediments.

Figure 14 illustrates cases in which 100.0; 80.0; 60.0; 40.0; 20.0 and 0.00% of fine sediments of D = 0.0125 mm were absorbed by the river bed.

Figure 14. Mobile bed as a barrier of reflection (and/or absorption) of sediment diameter D = 0.0125 mm continuously injected on the free surface during an interval [0, t_d].

Figure 13. Longitudinal profiles of sediment deposits as a function of grain diameter.

iv. **Reflection barrier** of suspended sediments that touch the bed under the effect of turbulence and gravity, and return completely to the suspension, as the case of 100.0% reflection in the Figure 14.

Conclusions

The Stochastic Theory has shown that the 2-D trajectories ω (x, z, t) of suspended sediment particles result from the combination of two chronologic series of movement periods: (i) an alternate series of longitudinal downstream steps intercalated by time periods when the particle does not move in that sense, and (ii) an alternate series of settling vertical steps intercalated by time periods when the grain does not move vertically. These series are defined by the Mobility Functions: λ_{x1} (t, n), λ_{z1} (t, n), λ_{t2} (x, n), λ_{t1} (z, n), which analytical expressions characterize the particles random movements. When they assume constant values, the 1-D and 2-D resultant models are Homogeneous Poissonian, which describe very well the suspension movement but not so well the bed-load movements with dunes and ripples.

Two research lines have been studied: (i) the sediment and/or pollutant movement described by Mobility Functions that vary with time, distance and number of displacements performed in time and space, that is, performed by *particles with memory*; (ii) the sediment movement by 2-D and 3-D processes with different bed behaviors as previously explained. For these researches, a collection of data on sediment and pollutant movement obtained in laboratory channel and in

nature with use of radioactive, dyes and chemical tracers is available for the use of Stochastic Processes.

References

Einstein, H.A., 1937. "Bed-load transport as a probability problem". D.Sc. Thesis. Translated by W.W. Sayre: Sedimentation Symposium. Ed. H.W. Shen, Fort Collins, Colorado, USA.

Hanno, H.A., 1979. "Etude de la dispersion longitudinale de sédiments de fond." Thèse de D.Sc.A. Université de Montréal. Canada.

Monteiro, C.S.G., 2004. "Processos aleatórios com injeções instantânea e contínua, aplicados ao movimento de sedimentos e poluentes em escoamentos com superfície livre". M.Sc. em Ciências em Engenharia Civil. COPPE/UFRJ. Rio de Janeiro, Brasil.

Monteiro, C.S.G.; Wilson-Jr., G., 2001. "PAICON 4.0: Um software descritivo do movimento de sedimentos e poluentes com uso da Teoria dos Processos Aleatórios. *XIV Simp. Bras. Rec. Hídr.,* ABRH. Brasil.

Monteiro, C.S.G.; Wilson-Jr., G., 2002. Descrição do movimento de sedimentos e de poluentes, com uso de microcomputadores e da teoria dos Processos Aleatórios. XIX *Congr. Nac. del Água,* Argentina.

Monteiro, C.S.G.; Wilson-Jr., G., 2003. "Estudo comparativo do movimento de sedimentos em suspensão e de poluentes líquidos no Rio Loire com o uso da Teoria dos Processos Aleatórios". *XV Simp. Bras. Rec. Hídri.,* ABRH. Curitiba, PR, Brasil.

Sayre, W.W. 1971. "Transport and dispersion of fluvial sediments: some mathematical models and their verification by tracer methods," IAEA. Panel on the Uses of Tracers in Sedimentology. Paris, France.

Todorović, P.; Vukmirović, V.; Vukotić, R.; Filip, A., 1966. "A contribution to the kinetic theory of bed material discharge." Symposium of the Use of Isotopes in Hydrology, IAEA, SM-83/19. Vienna.

Todorović, P.; Simons, D.B.; Li, R.M., 1976. "Deterministic and stochastic approaches for modeling of longitudinal dispersion in a turbulent open channel flow". Stochastic Approaches to Water Resources. USA.

Vukmirovic', V., 1975. "Analiza kretanja vucenog nanosa pomucu slucajnih procesa". D.Sc. Thesis. Civil Engineering College. University of Belgrade. Yugoslavia.

Vukmirovic', V., Wilson-Jr., G., 1976. "Mouvement du sédiment charrié – Processus Aléatoire." II International IAHR Symposium on Stochastic Hydraulics. Lund, Sweden.

Vukmirovic', V., Wilson-Jr., G., 1977. "Un modèle aléatoire du sédiment charrié." XVII Congrès de l'AIHR. Baden-Baden, Allemagne.

Wilson-Jr., G. 1972. "Transporte e dispersão de areia em canal de laboratório". Tese de Mestrado em Ciências e Técnicas Nucleares. V. 1,2. UFMG, Belo Horizonte, Brasil.

Wilson-Jr., G. 1987. *Etude du Transport et de la Dispersion des Sédiments en tant que Processus Aléatoires*. Thèse de Doctorat d'État ès Sciences Physiques. Université Pierre et Marie Curie. France.

Wilson-Jr., G. 2012. "Funciones de intensidad de mudanza del estado cinemático del movimiento de los sedimentos en los cursos de agua." XXV Congreso Latinoamericano de Hidráulica Costa Rica.

Wilson-Jr., G.; Monteiro, C.S.G., 2015. "Two-dimensional Poissonian homogeneous model for suspended sediment and pollutant movements in open-channel flow." Sedimentation and Hydrology Conferences – SEDHYD, Reno, Nevada, USA.

Wilson-Jr., G.; Monteiro, C.S.G., 2016. "Homogeneous 2-D Poissonian model applied to the suspended movement of pollutants and non-uniform fine sediments in open-channel flow." River Sedimentation. Stuttgart, Germany.

Wilson-Jr., G.; Monteiro, C.S.G., 2017. "Modelos aleatórios 2-D do movimento de sedimentos em suspensão em cursos de água". 13º SILUSBA. Porto, Portugal.

Wilson-Jr., G.; Monteiro, C.S.G., 2018. "Descrição dos movimentos dos sedimentos em suspensão e por arraste pela teoria dos processos aleatórios". 14º Congresso da Água. Évora, Portugal.

Wilson-Jr., G.; Vukmirović, V., 1981. "Mesures de caractéristiques cinématiques du sédiment charrié." IAHR Workshop on Particle Motion and Sediment Transport, Raperswill, Switzerland.

Acknowledgments

Two-Dimensional Subgrid Sediment Transport Modeling with HEC-RAS

Dr. Alejandro Sánchez, Senior Hydraulic Engineer, Hydrologic Engineering Center, U.S. Army Corps of Engineers, Davis, CA, Alejandro.Sanchez@usace.army.mil
Dr. Stanford Gibson, Senior Hydraulic Engineer, Hydrologic Engineering Center, U.S. Army Corps of Engineers, Davis, CA, Stanford.Gibson@usace.army.mil

Abstract

The Hydrologic Engineering Center's River Analysis System (HEC-RAS) and Hydrologic Modeling System (HEC-HMS) share a two-dimensional (2D) flow solver which utilizes a subgrid modeling approach. The subgrid approach incorporates terrain information from the subgrid scale into the computations and significantly improves the model accuracy when the computational grid cells are larger than terrain resolution (Casulli 2009; Casulli and Stelling 2011). This feature allows the model to use relatively coarse computational grids while reducing computational times and maintaining an accurate solution (Sánchez et al. 2017).

This paper presents recent and ongoing developments in 2D sediment transport modeling within HEC-RAS. The flow is solved with either a shallow water equation or diffusion wave equation solver. Both solvers utilize Finite Volume Methods on an unstructured mesh with subgrid bathymetry. The 2D sediment model solves for total-load sediment transport with a finite volume advection-diffusion solver. Key model features include multi-sized sediment transport, variable particle density, variable bed density, hiding and exposure corrections, bed slope corrections, various transport potential formulas, various subgrid erosion and deposition formulations, sheet and splash erosion, simulation of non-erodible surfaces, and avalanching. HEC-RAS also updates the 2D mesh at subgrid scales based on simulated morphological change. The 2D morphodynamic subgrid modeling approach is similar to that used by HEC-RAS in one-dimensional (1D) simulations, but resolves many 2D specific processes including wetting and drying, bed roughness, erosion, deposition, bed composition and layering, at a subgrid level.

The approach presented here is different from previous 2D morphodynamics approaches developed by Volp et al. (2016) and Volp (2017) in that there is no high-resolution grid utilized and all of the sediment computations are done directly on subgrid property tables. The present approach utilizes both high-resolution and low-resolution property tables for simulating hydrodynamics and morphodynamics, respectively. The presented dual subgrid resolution approach allows for a great deal of flexibility in defining the subgrid resolution for simulating morphodynamics at different locations making the method very efficient computationally. A key feature of the subgrid method is that the subgrid property tables in the sediment model handle partially wet grid cells. This allows for consistent treatment of the wet and dry boundary.

This paper will present a short overview of the modeling features and capabilities. The model performance will be demonstrated with results from example verification and validation test cases as well as example applications.

Approach

The subgrid approach for hydrodynamics is largely based on the methods developed by (Casulli (2009) and Casulli and Stelling (2011). The approach consists of utilizing lookup property tables for various hydraulic variables at cells and faces. Figure 1 shows a schematic of a computational cell in which the bed elevations have been binned into discrete elevations. This produces a piece-wise constant elevation vs. area curve and a piece-wise linear elevation vs volume curve.
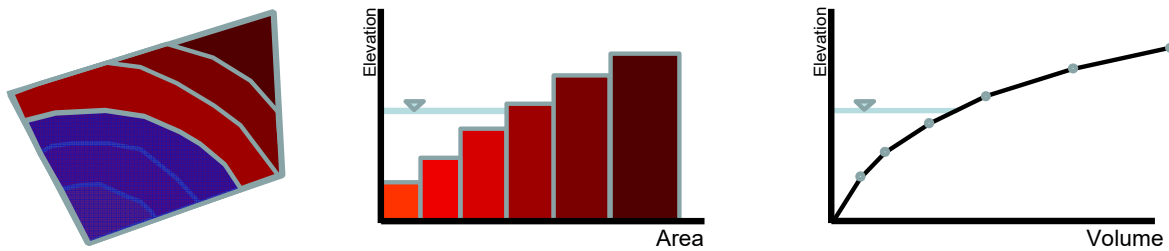
Figure 1. Schematic illustrating the subgrid concept for a computational cell.

Volp et al. (2016) presented a subgrid approach for morphodynamic modeling which utilizes a coarse grid for the hydrodynamics and a fine grid for the morphodynamics. However, since the entirety of the morphodynamic computations are done on the fine grid, it may be actually considered more a dual mesh approach with physics-based interpolation methods from the coarse grid to the fine grid for water levels and current velocities. Volp (2017) presented a subgrid approach in which the suspended-load is solved on the coarse grid but the bed-load transport and bed elevations are still computed on the high-resolution grid. Therefore, this sediment transport approach may be considered as only partially subgrid. The approach presented here is different in that there is no high-resolution grid utilized and all of the sediment computations are done directly on subgrid property tables. This method is very efficient computationally but is obviously is not as spatially explicit as the methods proposed by Volp et al. (2016) and Volp (2017).

In the present approach each computational cell has two sets of curves for the horizontal wetted area and water volume as a function of elevation. In addition, each face also has two sets of curves for the wetted horizontal length and vertical wetted area as a function of elevation. These curves are referred to as the subgrid curves. These sets of curves are relatively high-resolution and are utilized by the flow model in order to capture the effects of the subgrid bathymetry on the water storage and conveyance. The high-resolution (hydraulic) curves are obtained from a detailed terrain model, while the coarse (sediment) curves are derived from the hydraulic curves. In theory it is possible to utilize the same high-resolution curves for both hydraulic and sediment, but this would make the computational time and memory requirements for the sediment transport calculations prohibitively expensive. This is the reason why a second set of relatively coarse curves are utilized by the sediment transport model to compute the subgrid bed change, sorting and bed layering. It also allows for flexibility in defining the subgrid resolution for different parts of the domain depending on the objectives of a project. Figure 2 shows an example of the process of creating the coarse resolution area vs elevation curve utilized for sediment from the high resolution area vs elevation curve utilized for hydrodynamics. The hydraulic model utilizes 6 subareas, whereas the sediment model utilizes only 3. Figure 3 shows the process of modifying

the two sets of curves as a function of bed change. Careful attention is placed to conserving mass and also keeping track of wet and dry bed erosion/deposition rates.
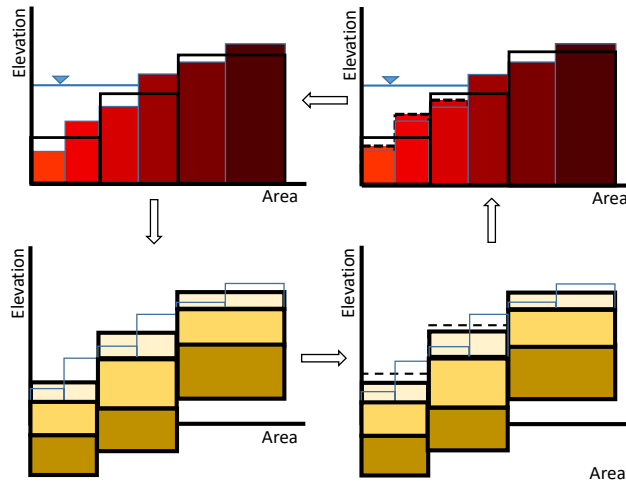
Figure 2. Schematic representing computation of bed change.

Results

The validation case presented is the West Fargo Diversion channel, ND (see Figure 3). The diversion consists of a 6.8-mile channel, which flows north from the City of West Fargo, ND. The bed material consists of mostly fine silts and clays. The 2D sediment transport model was setup for the diversion using only one cell across the channel in order to demonstrate the ability of modifying the subgrid bathymetry and hydraulic property tables. The model was run for approximately 13 years from 1992 (time of construction) to 2005.
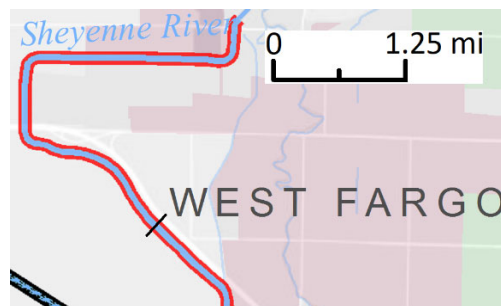
Figure 3. Map of the West Fargo Diversion Channel.

As an example result, Figures 4 shows the computed final subcell bed elevation and bed change at the approximate location indicated by a black line in Figure 3. The left panel shows the computed bed elevations vs horizontal area for the hydrodynamic (red) and sediment (blue) models. A fixed number of 10 subareas was used for the sediment model. Figure 5 shows the computed cross-sectional bed elevations and bed change. The model was able to reproduce the observed erosion in the pilot channel and deposition in the overbanks but under-predicted the bed change in general (Figures 4 and 5).
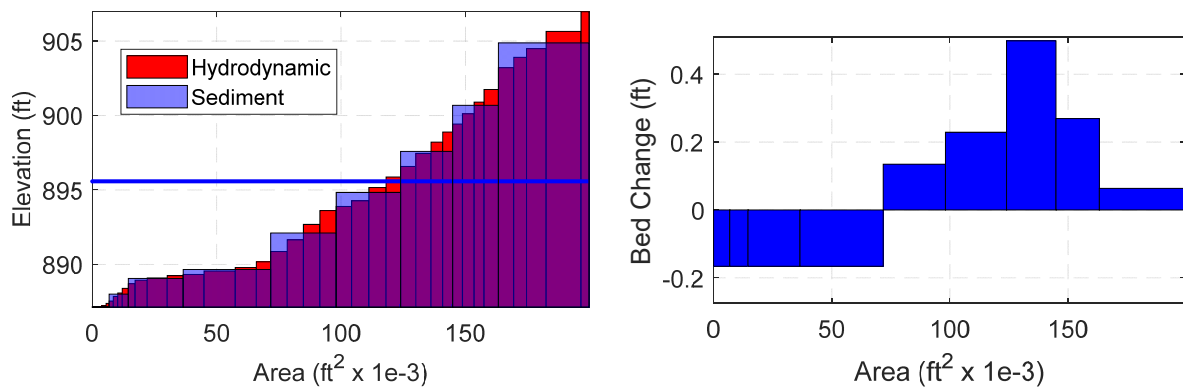
Figure 4. Example subcell bed elevations and bed change after approximately 12.8 years of simulation for the West Fargo Diversion Channel, North Dakota.
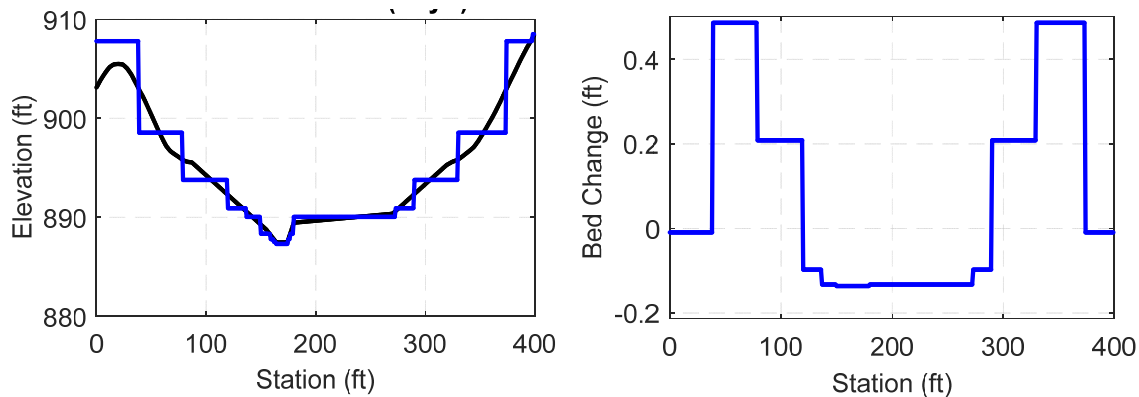
Figure 5. Example subface bed elevations and bed change after approximately 12.8 years of simulation for the West Fargo Diversion Canal, North Dakota.

References

Casulli, V. 2009. A high-resolution wetting and drying algorithm for free- surface hydrodynamics. International Journal of Numerical Methods for Fluids. 60(4):391–408.

Casulli, V., and Stelling, G.S. 2011. Semi-implicit subgrid modelling of three-dimensional free-surface flows. International Journal of Numerical Methods for Fluids. 67(4):441–9.

Sánchez, A., Brunner, G., and Chacon, B. 2017. HEC-RAS Subgrid Modeling: Benefits and Limitations with Example Applications, Environmental & Water Resources Institute Conference, ASCE.

USACE 2019. Sediment Transport Analysis of Diversions in the Red River basin near Far-Moorhead, US Army Corps of Engineers, St. Paul District.

Volp, N.D., van Prooijen, B.C., Pietrzak, J.D., and Stelling, G.S. 2016. A subgrid based approach for morphodynamic modelling. Advanced in Water Resources. 93:105-117.

Volp, N. 2017. Subgrid is Dancing with Sediment: A Full Subgrid Approach for Morphodynamic Modelling. Thesis, Delft University of Technology. 117 p.

Uncertainty in Sediment Transport Balance Estimates using Sediment Load and River Transect Data

Robert A. Mussetter, Program Manager, Tetra Tech, Inc., Fort Collins, CO, bob.mussetter@tetratech.com

Abstract

Two common, data-driven methods for estimating the sediment transport balance in rivers for aggradation/degradation studies rely on: 1) differences in sediment loads from rating curves developed from measured sediment transport data, and 2) differences in field-surveyed transects collected over a defined time-period. Analysis of an extensive data set collected in the central Platte River in Nebraska in 2009 through 2016 indicates that results from these methods are subject to substantial uncertainty, which limits our ability to draw firm conclusions regarding the sediment transport balance in the river. Because of the important role of such conclusions in management decisions, this uncertainty must be clearly understood and methods for limiting uncertainty incorporated into monitoring and analysis programs.

The monitoring data for this study included 8 successive annual surveys at 20 study locations distributed along the approximately 100-mile study reach, each of which consisted of 3 transects, and a series of 15 to 20 individual bed and suspended sediment load measurements at each of 5 locations. Best-estimate aggradation/degradation trends using the field surveyed transect data and the sediment rating transport rating curves were often in conflict. Uncertainty in the sediment transport-based estimates, quantified using the bootstrap method, indicated that the best-estimate trends were not statistically significant in most subreaches. The small size of the data sets was a key factor in the sediment load-based uncertainty. Only limited data were available to perform a rigorous sensitivity analysis on the transect-based estimates. Analysis of green LiDAR data, that penetrates through the water to the bed, that were collected in 2016 and 2017, after the field survey program was complete, suggests that error in the transect-based estimates is also substantial because, in several cases, changes at the clustered transects at each survey site do not adequately reflect changes in the river away from the study sites. As a result, conclusions drawn from the best-estimate values from the transect data are suspect.

Introduction

The sediment transport balance (i.e. the balance between the bed material sediment supply and the transport capacity) is a key factor in driving the dynamic behavior of rivers, including overall river stability, impacts to flood carrying capacity, and the quality of aquatic and riparian habitat. A deficit in bed material sediment supply compared to the transport capacity can lead to degradation (or downcutting) that can further lead to bank instability and damage to infrastructure including bridges, water-supply facilities, and flood protection works (Lagasse, et al. 2012; NTSB, 1988 and 1990). Excess bed material supply can lead to braiding and lateral instability, channel infilling, and reduced flood carrying capacity (Copeland, et al. 1999). Related processes can also affect the quality of instream and riparian habitat (Wohl, et al. 2015 Kondolf, et al. 1996; Gurtz, et al. 1984).

Two common, data-driven methods for estimating the sediment transport balance are based on: 1) differences in sediment loads from rating curves developed from measured sediment transport data, and 2) differences in field-surveyed transects collected over a defined time-period. The rating-curve method has the advantage of providing higher temporal resolution, but the spatial resolution is limited by the locations of the gages. The transect-based method provides high spatial resolution, at least in the area of the survey, but the temporal resolution is limited by the frequency with which the surveys can practically be conducted. Both methods are subject to substantial uncertainty, which limits our ability to draw conclusions regarding the sediment transport balance in the river. Because of the important role of such conclusions in management decisions, this uncertainty must be clearly understood and methods for limiting uncertainty incorporated into monitoring and analysis programs.

Sediment load-based estimates are typically developed by fitting a regression equation to sediment transport data, integrating the resulting curves over the appropriate flow record, and applying mass conservation principals to quantify aggradation/degradation trends. Uncertainty from this method derives from variability in the underlying measurements, uncertainty in the sediment transport rating curve, and lack of information on lateral inputs/sinks from tributaries, bank erosion and diversions between the gage sites. Transect-based estimates of the sediment transport balance are obtained by estimating the change in bed sediment volume based on changes in elevation along the transects between the successive surveys. Properly collected survey data accurately represent the elevation profile along the individual transects at the point in time when the surveys are conducted, but uncertainty in the balance estimates can still be quite large because of uncertainty in how well the changes at the individual transects represent changes in the remainder of the river bed away from the transects.

An extensive set of monitoring data that provides a means of assessing the uncertainty in both types of estimates in a wide, sand-bed river were collected in the central Platte River in Nebraska from 2009 through 2016 for the Platte River Recovery Implementation Program (PRRIP). The dataset includes annual transect surveys at 20 study sites distributed along the approximately 100-mile study reach (Figure 1), each of which consisted of 3 primary transects. The dataset also includes a series of approximately 20 individual bed and suspended load measurements at each of 5 locations distributed along the reach. In addition, a detailed topographic/bathymetric surface of the river bed was developed from LiDAR flights in Fall 2016 and Fall 2017 that integrated the traditional near-infrared spectrum with the green wavelength to sample both the subaerial and subaqueous portions of the river bed (Quantum Spatial, 2017 and 2018). This dataset provides a limited means of assessing the uncertainty in the transect-based estimates.

Figure 1. Central Platte River study reach. Sediment Transport measurements at labelled bridges.

Context for the Platte River Data Collection Program

The PRRIP was initiated in 2007 between Nebraska, Wyoming, Colorado, and the Department of the Interior to rehabilitate habitat in the Platte River for three bird species of concern (whooping crane, piping plover, and interior least tern) by restoring a braided channel morphology with sand bars free of vegetation, increased channel widths, and unobstructed views, while avoiding impacts to pallid sturgeon. Because of uncertainty in how the river will respond to proposed management actions, the Program developed several hypotheses related to the linkage between channel geomorphology, in-channel vegetation, and habitat (PRRIP, 2006). Among other hypotheses, the PRRIP postulated that eliminating the average annual sediment imbalance of approximately 400,000 tons in eroding portions of the reach will reduce net erosion of the river bed, restore and increase the sustainability of a braided planform, contribute to channel widening, and shift the river over time to a more vertically stable condition. Prevailing estimates at inception of the PRRIP indicated that an average annual sediment deficit of approximately 185,000 tons existed in the upper part of the reach between Overton and Kearney (~19 mi).

A channel geomorphology and vegetation monitoring program was carried out from 2009 through 2016 to collect and analyze a suite of data over a multi-year time-frame to test these and other key hypotheses (Tetra Tech, 2017; PRRIP, 2012). As part of this program, transect surveys were conducted once per year during mid- to late-summer at 20 study sites distributed along the approximately 100-mile reach. Each study site included 3 primary transects spaced at approximately 500-foot intervals (Figures 2 and 3), the endpoints of which were marked with permanent monuments to insure consistency in location during repeat surveys. In addition to the annual surveys, a series of 15 to 20 individual bed and suspended load measurements were made at each of 5 bridge crossings distributed along the reach (Figure 4). The data from the surveys and sediment load sampling were used to make independent estimates the sediment transport balance within the reach.
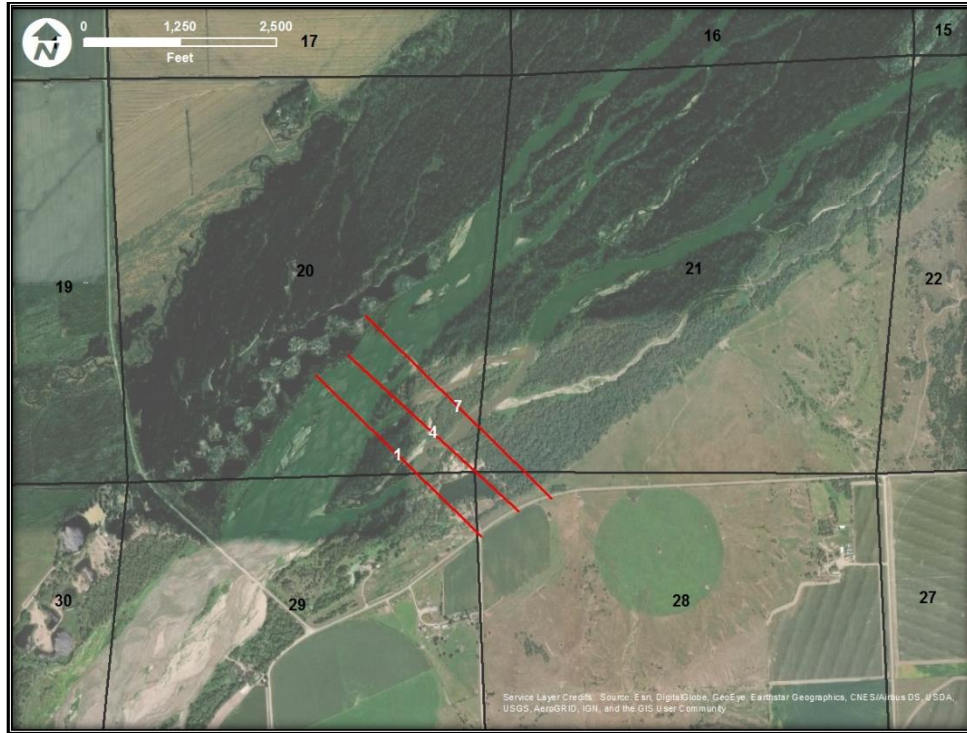
Figure 2. Typical layout of the 20 individual study sites
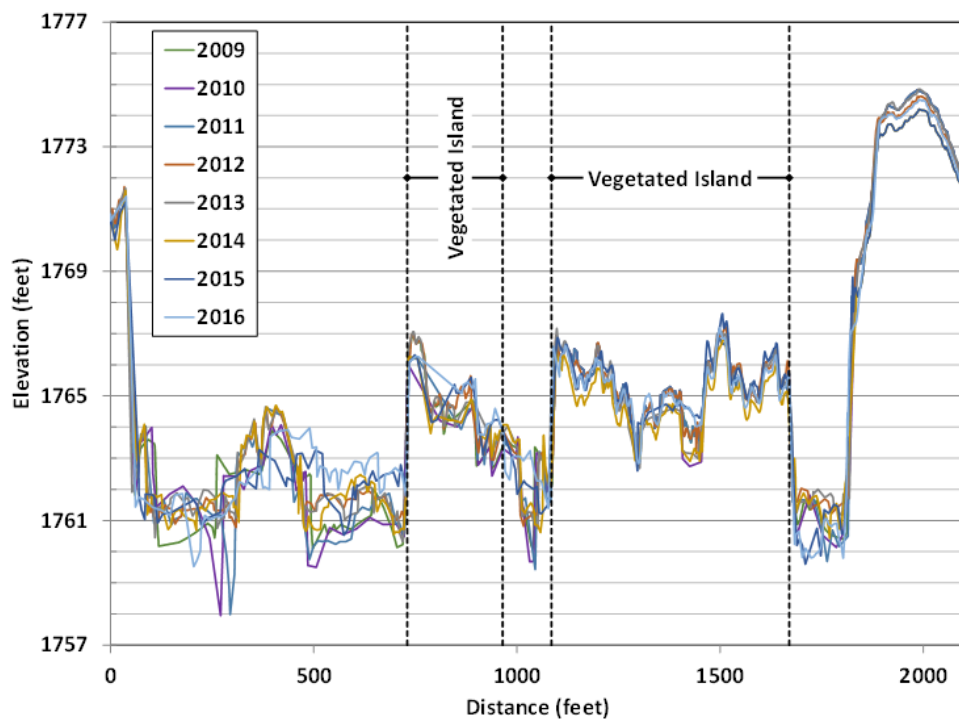
Figure 3. Profiles from repeat surveys of Transect 4 at the site shown in Figure 2.
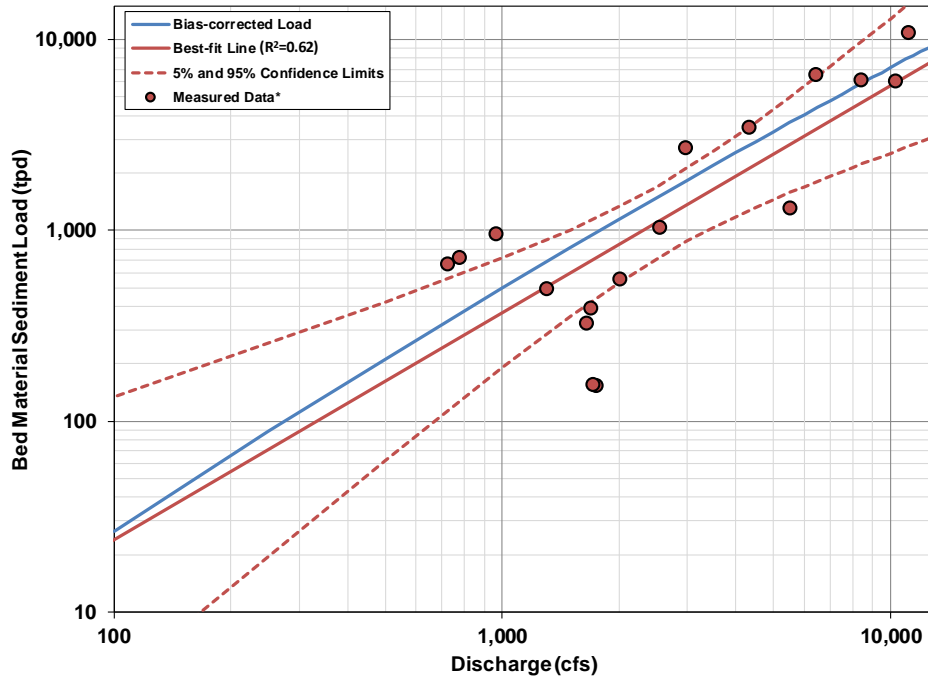
Figure 4. Example results of sediment transport monitoring, bed load measurements and bed load regression curves at Darr

Geomorphic Characteristics of the Central Platte River

An understanding of the current and historical geomorphic characteristics of the study reach are important to put the current condition into the context of anthropogenic activities, and particularly appreciating the challenges in collecting both the sediment load and survey data. Prior to European settlement of the Great Plains, the Platte River had a wide, braided planform that was driven primarily by snowmelt runoff from the mountainous regions of Colorado and Wyoming. In 1889, the journalist and humorist Edgar Nye coined the well-known phrase "a mile wide and an inch deep" to describe the Platte River. The river has undergone major changes in hydrologic regime and morphology since the mid-1860s (Eschner, et al. 1983; Williams, 1978). The changes in morphology primarily result from the changes in flow regime associated with upstream water-development, including construction and operation of storage reservoirs (Figure 5), irrigation diversions and ongoing groundwater development. Islands were a ubiquitous feature in the river, even prior to water development, with many large, timbered islands that were sufficiently high to "...be secure from the annual flood" (Freemont, 1845), and numerous smaller islands, most of which were covered by riparian species such as shrubs, young willows and cottonwoods (Eschner, et al. 1983). The change in flow regime, upstream sediment supply and other factors, including the effects of introduced species such as common reed (Phragmites australis) and encroachment into the river by infrastructure, caused the river to narrow dramatically from the conditions in the mid-1860s, primarily by progressive encroachment of vegetation and consequent vertical and horizontal accretion on sandbars in the channel (Eschner, et al. 1983; Williams, 1978) (Figure 6). As a result, the bed of the Platte River converted from a primarily braided planform characterized by constantly shifting sandbars and numerous braid channels over the bars in the mid-1860s to an island-braided planform with more stable, vegetated bars/islands and less channel shifting by the early- to mid-1900s, and then to an anastomosing planform with stable, vegetated bars/islands and a limited number of

relatively stable channels by the late-1990s (Fotherby, 2008; Eschner, 1983; Williams, 1978). Despite the "relatively stable channels" under current conditions, the primarily sand bed remains highly mobile with active bedforms that present challenges for bathymetric surveying and bed load sampling.
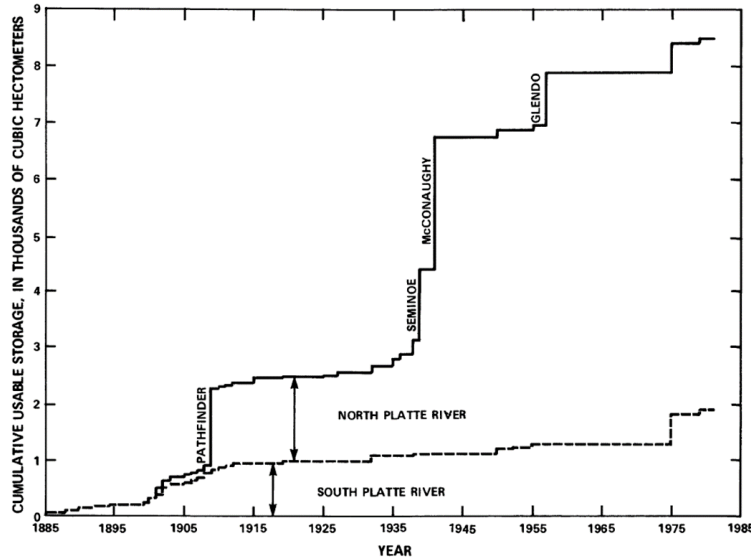
Figure 5. Cumulative usable storage of reservoirs in the Platte River basin (from Eschner, et al. 1983)
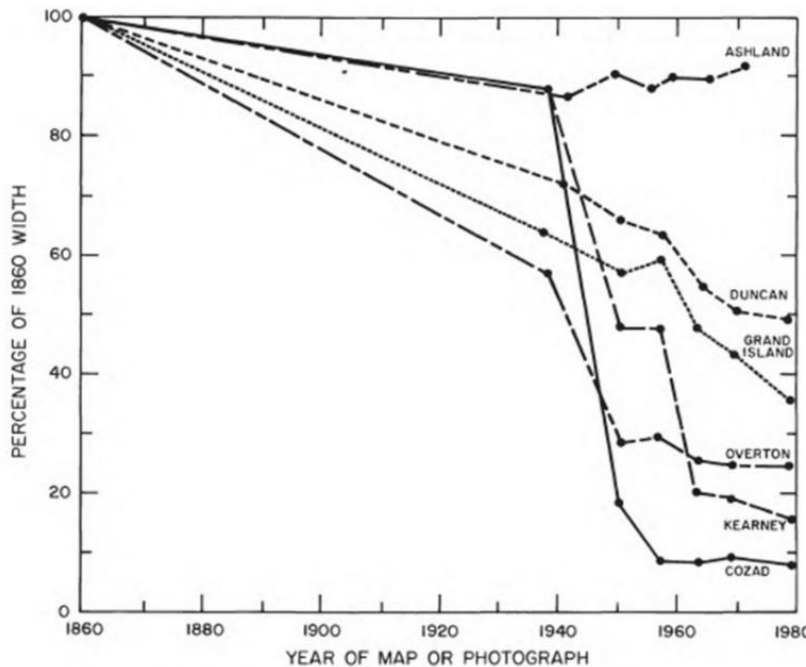
FIGURE 11.—At-a-station changes of channel width of the Platte River, Nebraska, with time.

Figure 6. At-a-station changes of channel width of the Platte River with time (from Eschner, et al. 1983)

Sediment Transport Balance Estimates

Bed and Suspended-Bed Material Load Measurements

The sediment transport measurements were made from the 6 bridges following USGS protocols (Edwards, et al. 1999) using a crane-mounted, 3" Helley-Smith bed load sampler and a crane-mounted D-74 suspended sediment load sampler. The data collection protocol envisioned up to 6 sampling events per year, including 3 samples at flows between 1,000 cfs to 3,000 cfs, 2 samples at flows between 3,000 cfs and 5,000 cfs and 1 sample at a flow greater than 5,000 cfs. Because of limitations caused by the timing and magnitude of the flows that occurred during the data collection period and access issues caused by road and bridge re-construction, 11 to 23 individual samples were ultimately collected at each of the bridges over the 7-year data collection period. As is typical with bed load measurements, in general, and those in a wide, shallow, sand-bed rivers, in particular, there was considerable scatter in the data. Correlation coefficients (R^2) for power-function rating curves for the bed load data ranged from 0.29 to 0.62 at the individual sampling locations. Less, but still substantial, scatter occurred in the suspended sand load measurements, with R^2 values ranging from 0.68 to 0.77.

Annual bed material sediment loads (i.e., sand and larger sizes) passing each bridge were estimated for each year of the data collection period using the above-described datasets and the recorded mean daily flows at each location. The estimates were made by developing bias-corrected rating curves using the Maintenance of Variance Unbiased Estimator (MVUE) method (Cohn and Gilroy, 1991) that is recommended by the U.S. Geological Survey (USGS, 1992), and integrating those rating curves over the mean daily flow records. The bed load and suspended bed material (primarily sand) load were treated separately and added together to provide the total load to maximize the number of data points, since there were some cases where a suspended sediment load sample was not collected in conjunction with a bed load measurement. An example curve for bed load transport resulting from least-squares regression and the corresponding bias-corrected curve are shown in Figure 4. The proportion of the total annual bed material load represented in the bed load ranged from 23% to 68% and averaged about 37% over all sites and years. In general, the percentage of bed load decreases with increasing discharge (Figure 7). The proportion bed load from this data set is consistent with those reported by Turowski, et al (2010) for large sand bed rivers.

Annual flow volume during the survey period varied widely from about 500,000 acre-feet (af) at Overton between the 2012 and 2013 surveys (exceeded in about 90 percent of the years between 1943 and 2017) to nearly 2.5M af during 2011 (exceeded in only about 6 percent of the years) (Figure 8). Maximum discharge also varied widely from about 4,070 cfs in 2013 (exceeded in about 60 percent of the years) to 15,900 cfs in 2015 (exceeded in only 4 percent of the years). Consistent with the flow variability, the estimated annual bed material loads also varied widely from year to year, with the loads in the dry year of 2013 typically in the range of 150,000 tons, increasing to about 1.5M tons during the wet years in 2011 and 2015.

Uncertainty in the annual loads was quantified using the bootstrap method (Efron, 1979; Efron and Tibshirani, 1986; Chernick, 1999). Bootstrap is a technique that involves resampling the original data set to develop empirical distributions of the key regression parameters, and from those distributions, nonparametric, Monte Carlo estimates of the uncertainty parameters (Chernick, 1999). The method is implemented by repeatedly generating new data sets equal in size to the original data set, but consisting of randomly selected values from the original data set.

This is accomplished by resampling with replacement, and then repeating the basic analysis of the parameters of interest for each new data set. The statistical parameters (e.g., mean, median, variance, skewness, etc.) of the resulting bootstrap-derived data sets represent estimates of the population parameters and their uncertainty, free of assumptions regarding the statistical distribution the variability about the mean, as is necessary using most analytical techniques for quantifying uncertainty. For purposes of this analysis, the bootstrap technique was used to generate 1,000 resampled data sets for each component, bed load and suspended bed material load, of the sediment load at each sampling location. The upper and lower 95% confidence limits on the estimates (whiskers in Figure 9) averaged about 34% and 26%, respectively, of the mean values from the Monte Carlo simulations.
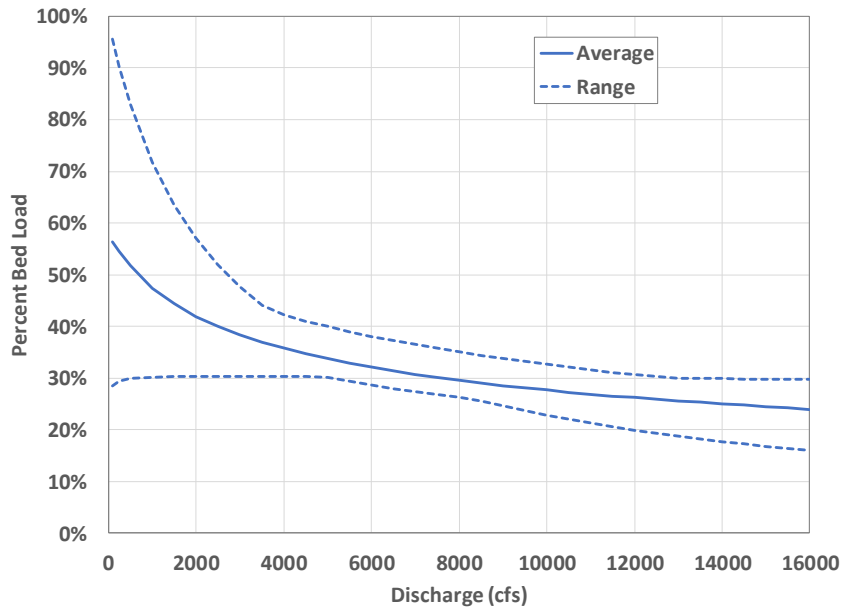
Figure 7. Percent of bed load in the total bed material load.
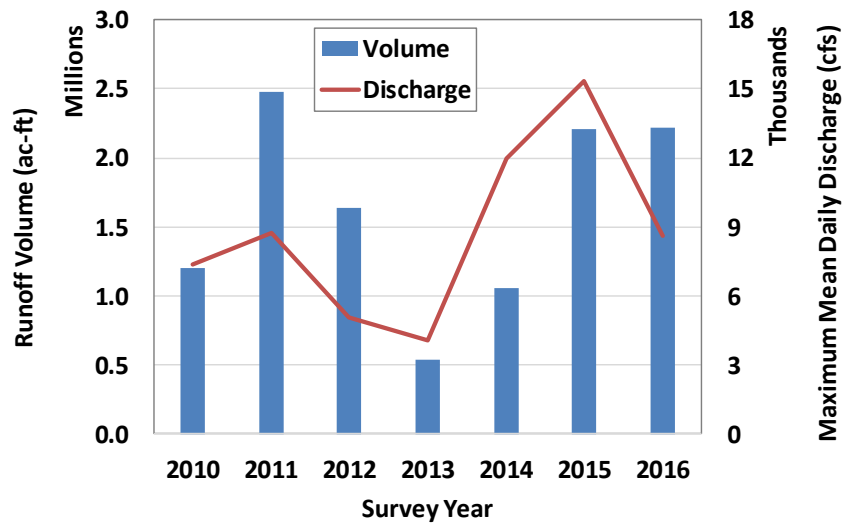
Figure 8. Annual runoff volume and maximum mean daily discharge at Overton during the 7-year survey period (initial survey conducted in 2009)
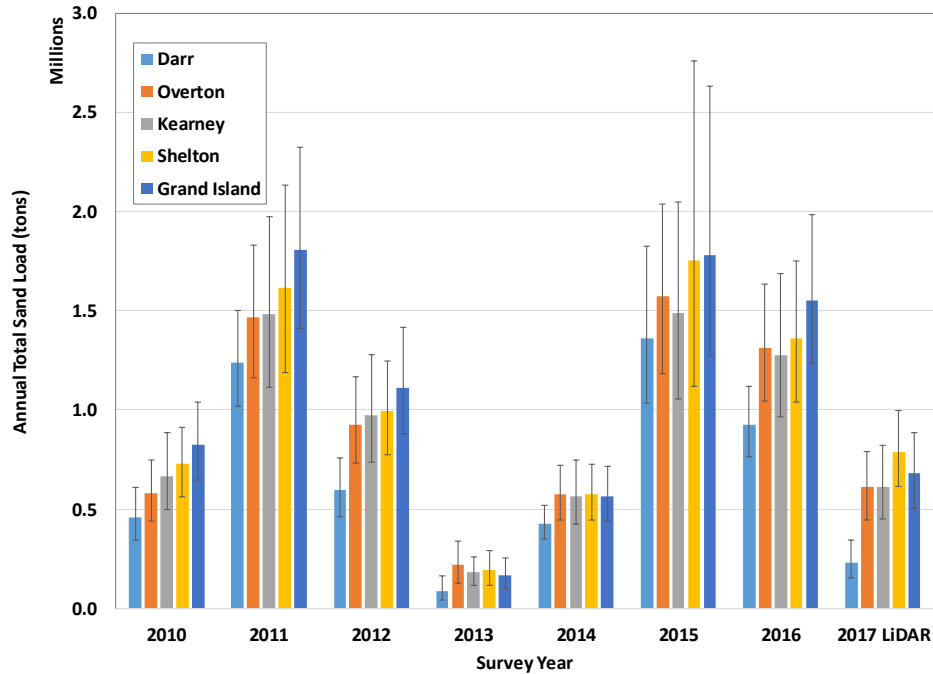
Figure 9. Estimated annual total bed material (sand) load at 5 measurement locations. Whisker represent upper and lower 95% confidence limits on the estimates. Also shown are the values for the period between the 2016 and 2017 LiDAR surveys.

Based on the best-estimate values of the annual loads from the rating curves, the reach from Darr to Overton was degradational in all years, with average deficit of about 215,000 tons per year over the period (Figure 10). The Overton to Kearney reach was mildly degradational during the first 3 years and then mildly aggradational during the last 4 years, with an overall average aggradation for the period of about 8,000 tons. The Kearney to Shelton reach was also degradational in all years, averaging about 89,000 tons per year over the period, and the Shelton to Grand Island reach was degradational during the first 3 years and the last year and aggradational during the 2014 and 2016, with overall average degradation over the 7-year period of 77,000 tons. Based on the error bands from the bootstrap analysis, however, the only result that is statistically significant at the 95% level is 2012, 2013 and 2016 in the Darr to Overton reach. For this analysis, the null hypothesis is that the reach is in sediment-transport balance. Since the error bands (whiskers in Figure 10) cross zero for all other cases, the null hypothesis cannot be rejected at the 5% (one-sided) level, and it must be concluded that the inferred aggradation/degradation trend is not statistically significant. Integration of the bias-corrected rating curves over the recorded flows for all years from 1984 through 2016 indicates that the portion of the overall reach between Overton and Kearney is approximately in-balance with no trend with annual runoff volume, while the portion of the reach from Kearney to Grand Island is net degradational with a strong trend of increasing degradation with increasing flow volume. (Figure 11).
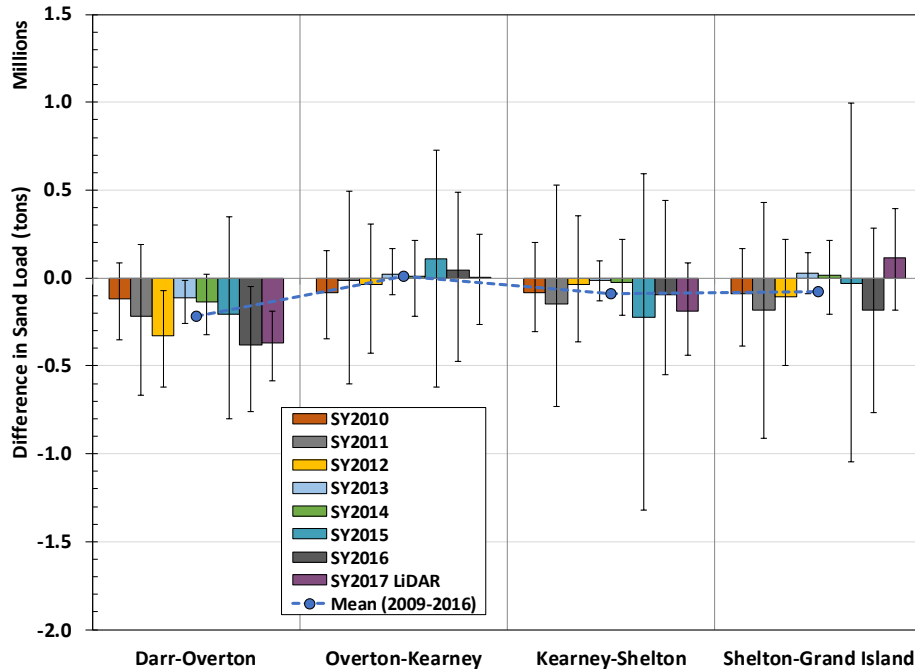
Figure 10. Estimated sediment deficit (-) or excess (+) in 4 reaches of the Platte River between 2009 and 2016, based on integration of the MVUE-based sediment load regression equations. Also shown are the values for the period between the 2016 and 2017 LiDAR surveys. Whiskers represent the upper and lower 95% confidence bands on the estimates.
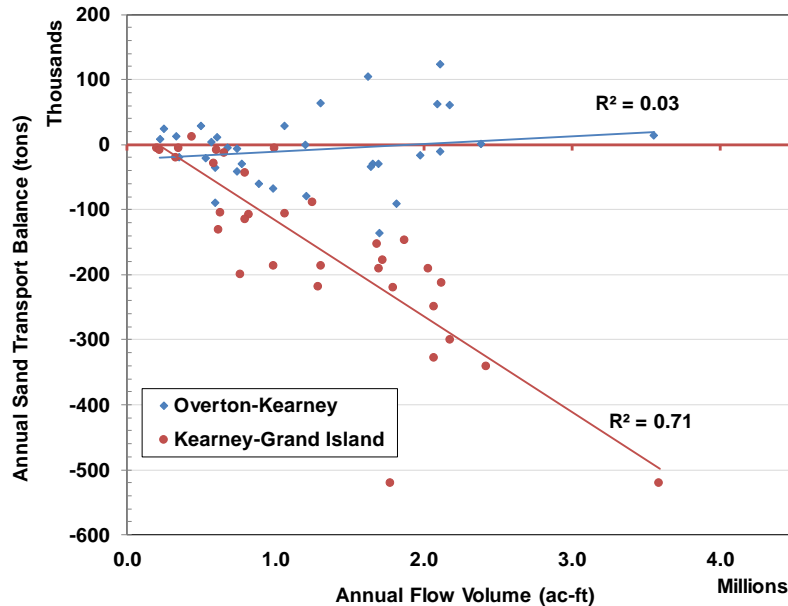
Figure 11. Annual sand transport balance based on integration of the bias-corrected rating curves over the flow record for the period from Water-year (WY) 1984 through WY2016.

Although there is considerable scatter in the data, the large uncertainty in the rating curve-based estimates stems in large part from the small size of the data sets. A reasonable question is, how much data would actually be necessary to reduce the uncertainty sufficiently to allow statistically-valid conclusions to be drawn regarding at least the direction of change (i.e.,

aggradation or degradation tendency) in a system like the Platte River? An approximate answer to this question can be obtained by repeating the bootstrap analysis using larger data sets developed by resampling the original data sets. A key assumption in this approach is that the magnitudes and variability in the data from a longer-term, systematic sampling program would be the same as that obtained from the limited sampling program on which the above analysis was based. This approach will provide the same best-estimate aggradation/degradation values, but the about uncertainty bands will diminish with increasing size of the data set due the reduced variability in the rating curves among the Monte Carlo trials. The upper and lower 95% uncertainty limits on the estimates for the Darr to Overton reach are 1.3 and 1.5 times greater than the best-estimate value for the overall 7-year monitoring period based on the approximately 20-sample dataset; thus, the upper band indicates aggradation while the best-estimate and lower band values indicate degradation (Figure 12). The trend is, therefore, not statistically significant. If the dataset included an additional approximately 30 points (for a total of 50), the upper uncertainty limit indicates slight degradation, and at least the direction of the trend would be statistically significant. Increasing the dataset size to 100 and 200 points results in a substantial reduction in the width of the width of the uncertainty band. However, for the other 3 reaches considered in this evaluation, even 200 data points would not reduce the uncertainty bands sufficiently to make the best-estimate trend statistically significant.
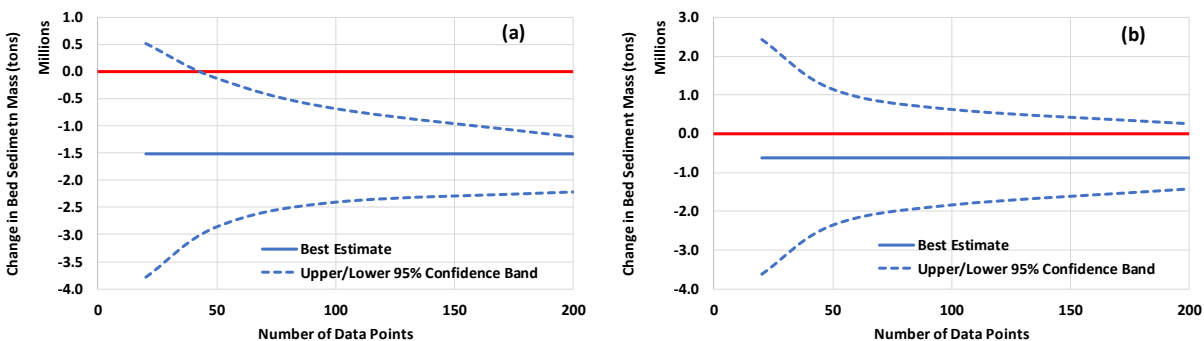
Figure 12. Effects of the size of the sediment transport data set on uncertainty bands on the estimated change in bed sediment mass over the 7-year monitoring period: (a) Darr to Overton (b) Kearney to Shelton. Curves for Overton to Kearney and Shelton to Grand Island similar to (b).

Transect Surveys

The transect data indicated considerable variability from year-to-year at the individual survey sites, in terms of both the magnitude and direction of changes, and this translated to large variability in the estimates for the reaches encompassed by the sediment transport measurement sites (Figure 13). The total bed sediment mass lost or gained in some of the reaches exceeded the rating-curve based estimates by an order of magnitude or more in some cases (compare equivalent bars in Figure 10 and 13 – note difference in scale). In addition, the direction of changes was different. For example, net aggradation occurred at the transects in the Darr to Overton reach during 3 of the years and significant aggradation occurred in the Kearney to Shelton reach during one of the years, while estimates based on the sediment transport data showed a net sediment deficit (i.e., degradation) in all years in both reaches. The rating-curve based result also showed degradation in 4 of the 6 years in the Kearney to Shelton reach, with net degradation over the 7-year period, while the transects indicated aggradation in 4 of the 6 years, with net aggradation over the period.
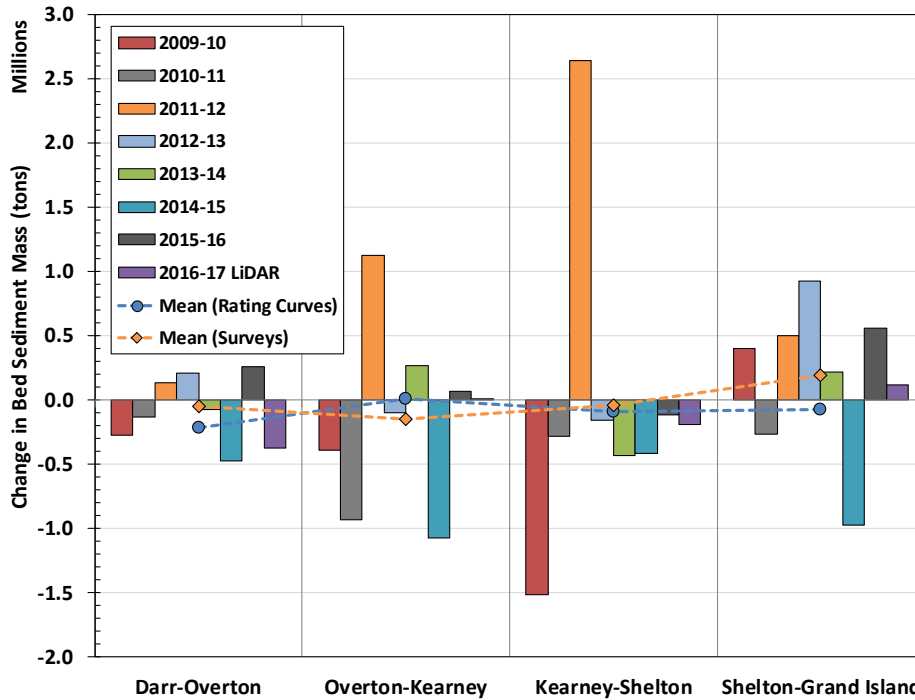
Figure 13. Estimate sediment deficit (-) or excess (+) in 4 reaches of the Platte River between 2009 and 2016, based on the transect data. Also shown are the values for the period between the 2016 and 2017 LiDAR surveys.

Unfortunately, data with which to directly quantify the uncertainty in the transect-based estimates over the 7-year monitoring period are not available. The detailed topo/bathymetric surfaces from the 2016 and 2017 LiDAR data do, however, provide a limited means of evaluating the uncertainty. The analysis was performed by cutting transects from the 2 LiDAR surfaces at the same locations at which the transect surveys were performed, and the aggradation/degradations volumes estimated using the same procedure that was used for the transect surveys. These results should be equivalent to those from the transect surveys. The surfaces were also used to develop volume estimates for each of the survey sites that consisted of 3 transects spaced at approximately 500-foot intervals to evaluate how well the transects represent the changes at the individual sites. The estimates were then repeated using the entire surface within each reach to evaluate how well the both transect- and rating-curve based estimates represent the actual bed changes that occurred between the two LiDAR surveys.

The correlation coefficient (R^2) between the estimates from the transect lines and the LiDAR surfaces at the individual study sites was 0.97, indicating excellent agreement (Figure 14). The estimates for this single year of data obtained by extrapolating the transect- and local LiDAR-based estimates to the longer reaches between the sediment transport measurement sites show the same aggradation/degradation trends as both the complete LiDAR- and the sediment transport rating curve-based estimates, however, the magnitudes of change are quite different (Figure 15). In general, the estimates from the rating curves suggest the smallest amount of change in bed sediment mass, the local estimates from the transects and local LiDAR surfaces indicate the largest overall changes, and the values from the complete LiDAR surface fall about midway between the two for all but the most downstream part of the study reach between helton and Grand Island. In that reach, the complete LiDAR surface actually shows the largest change.
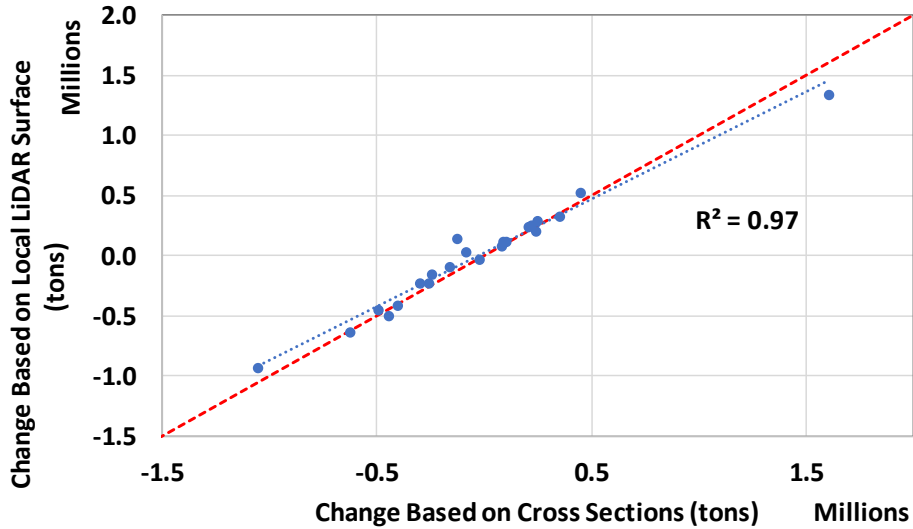
Figure 14. Comparison of change in bed sediment mass between the Fall 2016 and Fall 2017 LiDAR surveys based on the individual transects and the local LiDAR surfaces
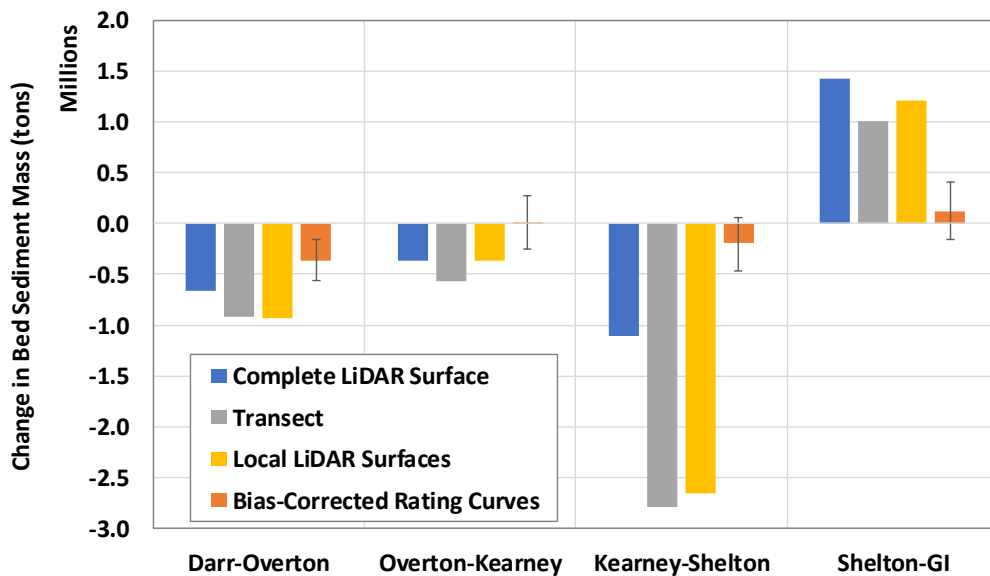
Figure 15. Change in bed sediment mass between the Fall 2016 and Fall 2017 LiDAR surveys based on 4 estimation methods

Error statistics from the LiDAR mapping contractor indicate that the Root Mean Square Error (RMSE) for the two flights in the range of 0.08 feet for dry areas and about 0.15 feet for subaqueous areas. A bootstrap test of the potential error in the LiDAR surfaces in an approximately 0.8-mile segment within the Overton to Kearney reach using these values statistics indicates that the potential error in the estimates from the LiDAR surface is less than 1%. Since the complete LiDAR surface represents the overall bed surface along the reach, and the error in the volume estimates from the surface are quite small, the estimates based on the complete LiDAR surface should accurately represent the changes that occurred in the reach over the year between the flights. The fact that the estimates from the complete LiDAR surface fall

outside the 95% confidence bands on the rating curve-based estimates in Figure 14 suggests that the rating curve-based estimates may be in error, probably because of the limited size of the data sets. To put these changes into perspective, however, the total bed elevation change, averaged over the length and width of the channel, over the 7-year survey period associated with the estimated volumes is only about -0.6 feet foot in the Darr to Overton reach, and the total changes in the other reaches are in the range of +/-0.1 foot. Except in the Darr to Overton reach, the indicated changes from either method is probably not statistically significant.

Conclusions

Data from an 8-year monitoring program on the Central Platte River in Nebraska provides a means of assessing the uncertainty in estimates of the sediment transport balance in a wide, sand-bed river based on sediment transport measurements and transect surveys, both methods of which are commonly used in geomorphic studies. Analysis of the sediment transport data, that included a relatively limited set of bed and suspended sediment samples (~20 samples at each location), indicates that the uncertainty in annual aggradation/degradation estimates from these data are quite large, and in most cases, even the direction of change (i.e., aggradation or degradation) is not statistically significant. For one of the reaches analyzed, increasing the size of the dataset to 50 samples would reduce the uncertainty sufficiently to make at least the direction of change statistically significant. In the other 3 reaches between the measurement locations, increasing the dataset to even 200 samples would not be sufficient to provide statistically significant estimates of the trends. For these reaches, the magnitudes of the annual differences are actually quite small compared to the total bed material load passing through the system; thus, the lack of statistical-significance is likely an indication that these reaches are approximately in sediment-transport balance.

Data from transect surveys collected over a 7-year period at 20 locations, each of which consisted of 3 transects spaced at approximately 500-foot intervals resulted in estimated aggradation/degradation trends that, in many cases, were quite different from those indicated by the sediment transport-based estimates. LiDAR surface created from a combination of the near-infrared and green wavelengths, and thus capable of sampling the bed through the shallow water, indicates that the transect-based estimates represent the magnitude and direction of the changes at the local study sites very well, but significant error is introduced when these values are extrapolated to the overall reach between the study sites. Since uncertainty in estimates from the complete LiDAR surfaces are probably quite small, LiDAR mapping is probably the most effective means of making accurate aggradation estimates. This is especially true in systems like the Platte River where the data can be collected during periods when the water is relatively clear and shallow, and the green LiDAR can penetrate to the river bed.

References

Chernick, M.R., 1999. Bootstrap Methods: A Practitioner's Guide, John Wiley & Sons, Inc., New York, NY, Wiley Series in Probability and Statistics, 264 pp.

Cohn, T.A., and Gilroy, E.J., 1991. Estimating Loads from Periodic Records. U.S. Geological Survey Branch of Systems Analysis Technical Report 91.01. 81 p.

Copeland, R.R., C.R. Thorne, and P.J. Soar, 1999. "Continuity of Sediment in Channel Restoration Design," ASCE, Proceedings of the International Water Resource Engineering Conference, Seattle, WA.

Edwards, T.K., and G.D. Glysson, 1999. Techniques of Water-Resources Investigations of the U.S. Geological Survey, Book 3, Applications of Hydraulics, Chapter C2, Field Methods for Measurement of Fluvial Sediment. U.S. Department of the Interior, U.S. Geological Survey. Reston, VA. 89 p.

Efron, B., 1979. Bootstrap methods: another look at the jackknife. Ann. Statist. 7, 1-26.

Efron, B. and R. Tibshirani, 1986. Bootstrap methods for standard errors: confidence intervals and other measures of statistical accuracy. Statist. Sci. 1, 54-77.

Eschner, T.R., Hadley, R.F., and Crowley, K.D., 1983. Hydrologic and Morphologic Changes in Channels of the Platte River Basin in Colorado, Wyoming, and Nebraska: A Historical Perspective. U.S. Geological Survey Professional Paper 1277-A, 39 pp.

Fotherby, L.M., 2008. Valley Confinement as a Factor of Braided River Pattern for the Platte River, Geomorphology, 103(4), 15 pp.

Gurtz, E.G and J.B. Wallace, 1984. Substrate-Mediated Response of Stream Invertebrates to Disturbance, Ecology, 65(5):1556-1569.

Kondolf, G.M. and P.R. Wilcock, 1996. The Flushing Flow Problem: Defining and Evaluating Objectives, Water Resources Research, AGU, 32(8):2589-2599.

Lagasse, P.F., L.W. Zevenbergen, W.J. Spitz and L.A. Arenson, 2012. Stream Stability at Highway Structures, Fourth Edition, Hydraulic Engineering Circular No. 20, Publication No. FHWA-HIF-12-004, 328 pp.

National Transportation Safety Board, 1988. "Collapse of the New York Thruway (I-90) Bridge Over Schoharie Creek, near Amsterdam, New York, April 5, 1987," Highway Accident Report No. NTSB/HAR-88/02, Washington, D.C.

National Transportation Safety Board, 1990. "Collapse of the Northbound U.S. Route 51 Bridge Spans over the Hatchie River near Covington, TN, April 1, 1989," Highway Accident Report No. NTSB/HAR-90/01, Washington, D.C.

Platte River Recovery Implementation Program, 2006. Attachment 3, Adaptive Management Plan, 254 ppp.

Platte River Recovery Implementation Program, 2010. PRRIP Channel Geomorphology and In-Channel Vegetation Monitoring, 24 pp.

Quantum Spatial, 2017. Platte River, Nebraska – Fall 2016, Topobathymetric LiDAR Technical Data Report, prepared for Headwaters Corporation, February 2, 37 pp

Quantum Spatial, 2018. Platte River, Nebraska – Fall 2017, Topobathymetric LiDAR Technical Data Report, prepared for Headwaters Corporation, February 17, 35 pp

Tetra Tech, 2016. 2016 Platte River Final Data Analysis Report, Channel Geomorphology and In-Channel Vegetation Report. Prepared for Platte River Recovery Implementation Program, October, 305 pp.

Turowski, J.M., D. Rickenmann, and S.J.Dadson, 2010. The partitioning of the total sediment load of a river into suspended load and bedload: a review of empirical data. Sedimentology 57, 1126–1146, doi: 10.1111/j.1365-3091.2009.01140.x.

U.S. Geological Survey. 1992. Recommendations for Use of Retransformation Methods in Regression Models Used to Estimate Sediment Loads ["The Bias Correction Problem"]. Office of Surface Water Technical Memorandum No. 93.08. December 31.

Williams, G.P., 1978. The case of the shrinking channels–the North Platte and Platte Rivers in Nebraska. USGS Geological Survey Circular 781, 48 pp.

Wohl, E., S.N. Lane and A.C. Wilcock, 2015. The science and practice of river restoration. Water Resources Research, AGU, 51(8):5974-5997.

Use of a Gridded Runoff Flow Routing Model to Estimate Sedimentation and Dredging Burdens

Elissa Yeates, Research Hydraulic Engineer, United States Army Corps of Engineers (USACE), Engineer Research and Development Center (ERDC), Coastal and Hydraulics Laboratory (CHL), Vicksburg, Mississippi, Elissa.M.Yeates@erdc.dren.mil

Ahmad Tavakoly, Research Hydraulic Engineer, United States Army Corps of Engineers (USACE), Engineer Research and Development Center (ERDC), Coastal and Hydraulics Laboratory (CHL), Silver Springs, Maryland, Ahmad.A.Tavakoly@erdc.dren.mil

Shahab Afshari, Postdoctoral Research Associate, Climate System Research Center Laboratory, Department of Geosciences, University of Massachusetts, Amherst, Massachusetts, Sha17hab.Afshari@gmail.com

Gregory Dreaper, Research Physical Scientist, United States Army Corps of Engineers (USACE), Engineer Research and Development Center (ERDC), Coastal and Hydraulics Laboratory (CHL), Vicksburg, Mississippi, Gregory.W.Dreaper@erdc.dren.mil

Kenneth Mitchell, Research Program Manager, United States Army Corps of Engineers(USACE), Engineer Research and Development Center (ERDC), Coastal and Hydraulics Laboratory (CHL), Oxford, Mississippi, Kenneth.N.Mitchell@erdc.dren.mil

Abstract

The United States Army Corps of Engineers (USACE) mission includes the maintenance of about 25,000 miles of waterways critical to national commerce and security. Operations and Maintenance budgets for these waterways have to be planned in advance of two-year budget cycles, which challenges managers to estimate future sediment loads and channel dredging burdens. Inland hydrologic activity can drastically impact sedimentation in channels and harbors, often with a timing lag after major hydrologic events in the upstream watershed. The Coastal and Hydraulics Laboratory (CHL) at the United States Army Engineer Research and Development Center (ERDC) has developed the Streamflow Prediction Tool (SPT), which employs a watershed-scale gridded runoff routing flow model to forecast flows within a fine-scaled stream network using ensemble precipitation forecasts. Here, the 30-year hindcast flow records produced within the Streamflow Prediction Tool are applied to the watersheds feeding the Sabine and Port Arthur Harbor systems in Texas to evaluate whether watershed-level modeling of inland streamflow in response to precipitation can be appropriately used to improve estimations of future dredging burdens at maintained waterways. Several modeled relationships are explored between base flow volumes, peak flow volumes, and dredging event volumes from 1980 through 2014 for stream reaches in these navigation systems. Results indicate that for maintained channels some distance from the coast, inland hydrologic activity is correlated with subsequent dredged sediment loads. Established numerical relationships between flows and resulting dredging burdens could potentially enable managers of channel dredging to better estimate future needs by accounting for inland hydrologic activity.

Introduction

The purpose of this study is to leverage existing USACE models and datasets for potential insights useful in the channel management process for USACE Operations and Maintenance budget development. We investigated correlations between precipitation-driven, inland riverine flow rates calculated using the USACE-developed Streamflow Prediction Tool (SPT) (Snow et al. 2016) and historical dredged volume records from 1980 through 2014 for the Sabine and Port Arthur harbor channel system in Texas. Regression relationships between precipitation-driven riverine flows and subsequent channel dredging burdens could provide channel managers with additional tools to plan for likely future operations and maintenance needs, and lead to better optimization of channel dredging resources.

Methodology

For this analysis, we processed historic dredging records (reported in total cubic yards dredged per event) and reconstructed stream flow hydrographs (reported in three-hourly average flow in cubic feet per second) to connect these spatially by stream reach. Then dredged volumes were analyzed as a function of the cumulative flow volumes in the same reach using eight different regression models to evaluate relationships between precipitation-driven riverine flow and subsequent dredging at the channel reach level. This is similar to methods applied by Dahl, et al. (2018) in assessing the potential impact of climate-varying future precipitation on dredging burdens. In this section we detail the study area, datasets and models used, and data processing methodology for this analysis.

Study Area

The study the link between cumulative streamflow and dredging volumes, we selected three study areas in Texas Gulf Coast Regions (Figure 1): Sabine and Port Arthur Harbor (Sabine-Neches river system), the Houston, Galveston, and Texas City Harbor system (Houston Ship Channel), and Corpus Christi Harbor (Nueces River). We selected these test sites to represent a full range of Texas coastal riverine systems, and to take advantage of available historic dredging records. This report covers the results of the analysis in the Sabine and Port Arthur Harbor. Within this study area, specific channels were used in the analysis based on the availability of dredging records. Detailed maps of the selected channels in this system are presented in the Results section.
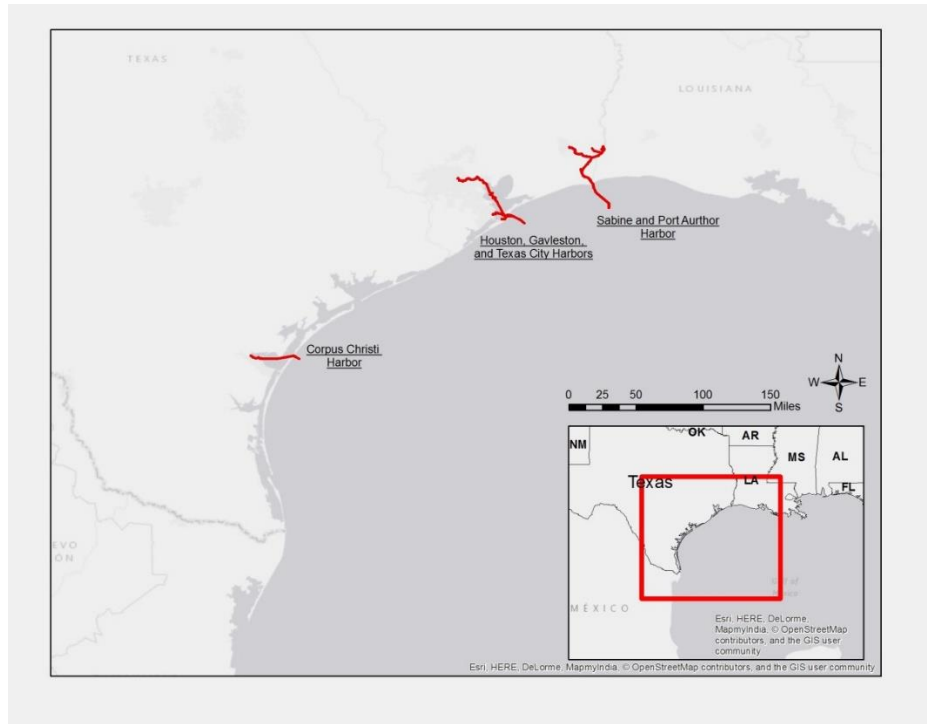
Figure 1. Study area of interest: three harbors in the Texas Gulf Hydrologic Region

Watershed-Scale Hydrologic Routing Model and Input Data

To simulate historical watershed-scale hydrology for this analysis, we used hindcast streamflow simulation results from the Streamflow Prediction Tool (SPT). The SPT was used to produce three-hourly flow rates from 1980 through 2014 for every stream reach in the Texas Gulf Region by routing historical atmospheric data from the European Centre for Medium Range Weather Forecasts (ECMWF, Balsamo et al., 2009) through the river routing model Routing Application for Parallel computatIon of Discharge (RAPID, David et al., 2011b). This framework takes advantage of over 30 years of runoff estimates available globally to reconstruct flows at ungauged locations. The benefit of this framework is to calculate streamflow anywhere in a river network without a dependency on rainfall or streamflow gages. Hence, the estimated historical and forecast streamflow can be obtained for the locations of dredging projects in any watershed of interest.

The RAPID model is an open source river network routing model. Notable features of RAPID include the use of the "blue lines" on the map and a grid network for river networks with an automated parameter estimation procedure (RAPID, David et al., 2011b). RAPID uses a matrix-based version of the Muskingum flow-routing method (Overton, 1966, and Gill, 1978) to compute the flows in river networks containing many thousands of reaches. Inputs to RAPID are runoff time series (in this case, ECMWF historical atmospheric data), K and X Muskingum parameter files (produced within the SPT), and catchment ID files. The output file of RAPID is a time series of flow rates for all river reaches in the river network.

The NHDPlus dataset, available for the continental United States, was used in this study to determine the locations of river reaches in the watershed as a "blue line" and to derive required parameter attributes for RAPID input file preparation. This dataset is a horizontal integration of the medium-resolution (1:100,000 scale) National Hydrography Dataset (NHD, McKay 2012),

the National 3D Elevation Program dataset (NED, Sugarbaker 2015), and the National Watershed Boundary Dataset (WBD, U.S. Geological Survey, 2013).

The performance of the RAPID model and application of the NHD data for river routing were described in detail by several authors: David et al., 2011a, 2011b and 2013; Follum et al., 2016; Tavakoly et al., 2016 and 2017. David et al. (2013) found the RAPID model to perform similarly to observed gage data in the Texas Gulf Hydrologic Region, which is the domain to which we apply the RAPID model output in this study.

Data Processing Work Flow

A number of steps were taken to connect the stream flow time series data with the historical dredging datasets for analysis. The streamflow time series for reaches in the study area were downloaded from the SPT online portal interface (accessible at https://umip.erdc.dren.mil/apps/streamflow-prediction-tool/ with a Common Access Card authentication). The historic dredging data came from the USACE Galveston District records, and was plotted spatially using the USACE National Channel Framework GIS database. This enabled spatial matching of channel dredging records with the Common IDs (COMIDS) used to identify river reaches within the SPT results. The National Channel Framework (NCF) is a set of enterprise Geographic Information System (eGIS) feature classes providing geospatial locations of the congressionally authorized navigation channels maintained by USACE. Galveston District dredge history database includes channel reaches, stations, quantities, and project date end for each dredging event in the last forty years of dredging.

Two spatial relationships were needed for this analysis. First, we related the NHDPlusV2 to the channel reaches from the National Channel Framework. Typically, there were several stream links for each reach and we noted the most downstream link. Next, we linked the local dredge history records to that of the NCF. These relationships provide the ability to pull all dredging events and amounts and relate those events to the COMID stream flows. These connections were all performed spatially in ArcGIS software version 10.3 (ESRI, 2011). Several further data manipulations and assumptions were required to correlate dredged amounts in each reach with the reconstructed stream flows produced be the SPT:

1. Dredging events were coded as occurring on the date recorded as "Work Complete." Dredging records with work completion dates before 1980 were discarded, to ensure sufficient overlap with the SPT time series output. Dredging records with multiple project volumes reported for the same reach location and same day were aggregated into a single project volume for that day.

2. Return period analyses were performed on the flow time history for each reach to determine the magnitude of the 1.5-year, or bankfull, flow, at that reach. All streamflow values in the time history for that reach were then coded as being either less than or greater than this bankfull flow value. This was done to enable analyses of base flows (considered here to be below bankfull, 1.5-year flow) and peak flows (considered here as flows above bankfull, 1.5-year flow), further discussed in the "Methodology for Analysis of Results" section below.

3. Streamflow data were partitioned into time history sets separated by the dredging events for each reach to enable the computation of cumulative flow between dredging events.

Methodology for Analysis of Results

We selected nine stream channel COMIDs in the Sabine and Port Arthur Harbor for analysis to represent a variety of reach conditions in the regions of interest: closer to inland riverine systems, closer to the outlet to bay areas, man-made channelized areas, and before and after various stream confluences in each region. Furthermore, stream reaches with spatially matched robust historical dredging records were chosen.

We then performed single and multivariate regression analyses of dredged volumes as a function of precipitation-driven streamflow at the matched stream reach and region level. As mentioned in the Data Processing Work Flow section above, stream flow rates were categorized as above or below the average 1.5-year stream flow rate by reach to approximately disaggregate base flows and peak flows. Flow rates were multiplied by the three-hour time step to approximate channel flow volumes for the time series. The flow volumes were summed for the time periods between dredging events to obtain cumulative flow volume in a channel between dredging events. Table *1* describes the variables used in analysis. Note that flow volumes are in cubic meters and dredged sediment volumes are in cubic yards, following convention.

Table 1. Description of regression model variables

Variable	Description (units)
Vol_d	Total dredged volume from one dredging event (cubic yards)
Q_{tot}	Total cumulative flow since the last dredging event (cubic meters)
Q_{base}	Cumulative base flow (flow rate less than the 1.5 year flow rate for that reach) since the last dredging event (cubic meters)
Q_i	Cumulative peak flow (flow rate less than the 1.5 year flow rate for that reach) since the last dredging event (cubic meters)
k	Regression intercept (cubic yards)
a, b, c, d	Regression coefficients

Four different models were tested with the dredging data for the Sabine Neches cases. These are described in Table 2 below. The simplest is a single-variate model to predict the next dredged volume as a linear function of the total cumulative flow in the reach since the last time the channel was dredged (Model 1). Model 2 is a multi-variate function which disaggregates that cumulative flow since the last dredging into base flow and peak flow. Models 3 and 4 mirror the variables tested in 1 and 2 but are nonlinear.

Results by reach were visualized in two ways: First, the cumulative streamflow volume in cubic meters between dredging events was plotted as a time series, with the subsequent dredged volumes in cubic yards plotted on a secondary axis. This provides an intuitive way to relate cumulative flow volumes to corresponding subsequent dredged sediment volumes. It also represents both flow and dredged volumes as time series, allowing for visualization of changes in the dredging practices in each stream reach over time. Second, the plot for Model 1 was presented with the observed dredging data to illustrate how skillfully the single-variate model

describes the relationship between cumulative flow rates and dredged volumes. These plots are shown for selected reaches in the Results section.

Table 2. Equations for tested regression models

Model	Equation
Linear models using the total cumulative flows immediately prior to the dredging event:	
1	$Vol_d = k + aQ_{tot}$
2	$Vol_d = k + aQ_{base} + bQ_i$
Exponential models using the total cumulative flows immediately prior to the dredging event:	
3	$Vol_d = k(Q_{tot}{}^a)$
4	$Vol_d = k(Q_{base}{}^a)(Q_i{}^b)$

Results

Coefficients of determination (R-squared) values for many of the tested models were sufficiently high to indicate that the incorporation of precipitation-driven inland hydrology into forecasts of future dredging burdens can improve these estimates. In general, the models performed best in channelized reaches upstream of coastal outlets, and worse in the reaches connected to coasts and bays where coastal sedimentation processes would likely dominate over sediment delivered by the upstream watershed. Results by model type are further presented below.

Single-Variate Linear Model Results

For this model, Model 1, up to 63% of the variance in dredging amounts in the Sabine-Neches system from the 1980-2014 period can be explained using the total cumulative flow since the last dredging event as the predictive variable. For reaches closer to the bays or coasts, this falls to 0%.

Table 3 shows goodness of fit results for the single-variable linear regression model comparing dredged volumes to cumulative streamflow prior to each dredged event for nine stream reaches in the Sabine Neches Waterway. Reported P-values are for confidence in the null hypothesis that dredging burdens are not correlated with the cumulative flow volumes between dredging events. For this model, Model 1, up to 63% of the variance in dredging amounts in the Sabine-Neches system in the 1980-2014 period can be explained with a simple linear model using the total cumulative flow since the last dredging event as the predictive variable. For reaches closer to the bays or coasts, this falls to 0% with low confidence in the estimate.

Table 3. Summary of single variable linear regression Model 1 fit

Stream ID	Drainage Area, square km	Number of dredging events since 1980	R-squared value	P-value
1112455	25,931	11	0.38	0.03
1115825	26,058	9	0.30	0.10
1477515	26,064	15	0.04	0.50
1477595	26,220	15	0.16	0.10
1477713	26,204	12	0.48	0.04
1477589	26,215	16	0.16	0.10
1477725	26,201	11	0.63	0.01
1481563	27,705	23	0.20	0.02
24719331	53,730	12	0.00	0.89

For the Sabine-Neches study area, we selected reaches upstream, along the canal, and close to the outlet (Figure 2). Stream reaches are highlighted in light blue in the figure, with the corresponding COMID displayed along the stream reach. Streams were filtered for analysis to include only those with more than five dredging event records from 1980 to 2014. This accounts for the gaps in the streams analyzed in the figure.
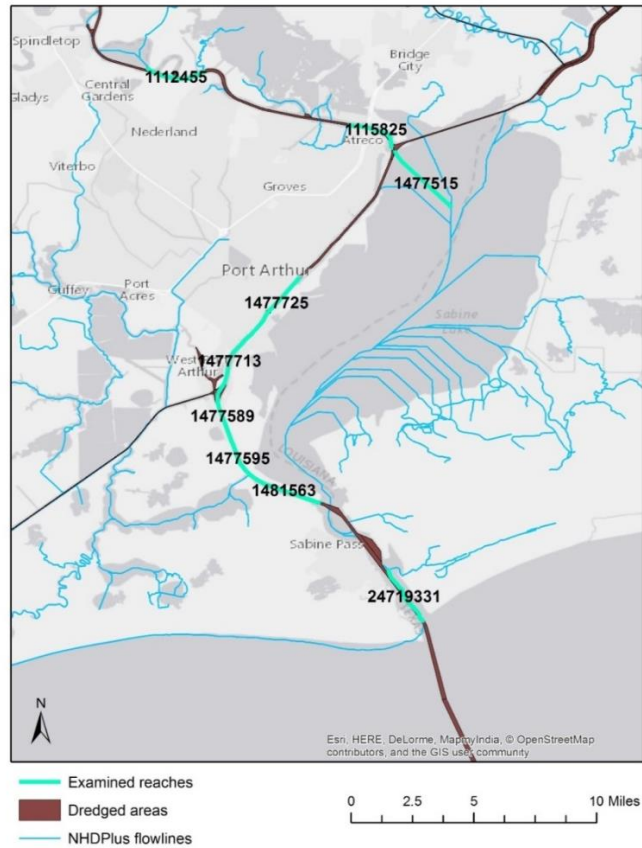
Figure 2. Examined COMIDs and dredged channel areas in the Sabine Neches Waterway

Stronger linear relationships were found in inland stream reaches, such as the most upstream COMID 1112455 (R-squared of 0.37 with a p-value of 0.03), and channelized reaches, such as COMID 1477725 (R-squared of 0.62 with a p-value of 0.01). R-squared values close to 0, indicating no correlation between streamflow and dredging burden, and high p-values indicating low confidence in the validity of the model were found in stream reaches that directly connected to bay and coastal outlets, including 1477515 (R-squared of 0.04 with a p-value of 0.47) and 247719331 (R-squared of 0.00 with a p-value of 0.89). COMID 1477515 is actually in Sabine Lake – the NHDPlus Streamlines dataset automatically represents lake bodies as series of streamlines. Although the lake is dredged often, the dredged volumes are not well correlated with the associated streamline cumulative flow. This demonstrates the failure of the SPT to accurately represent flows in areas like lakes, and the pitfall of using this association in an area like Sabine Lake.

Visualizations of stream reach Model 1 results for the reaches in the Sabine Neches Waterway with the highest model skill are presented below in Figure 3. These streamflow and Figures were produced using Rstudio (Rstudio Team, 2015).
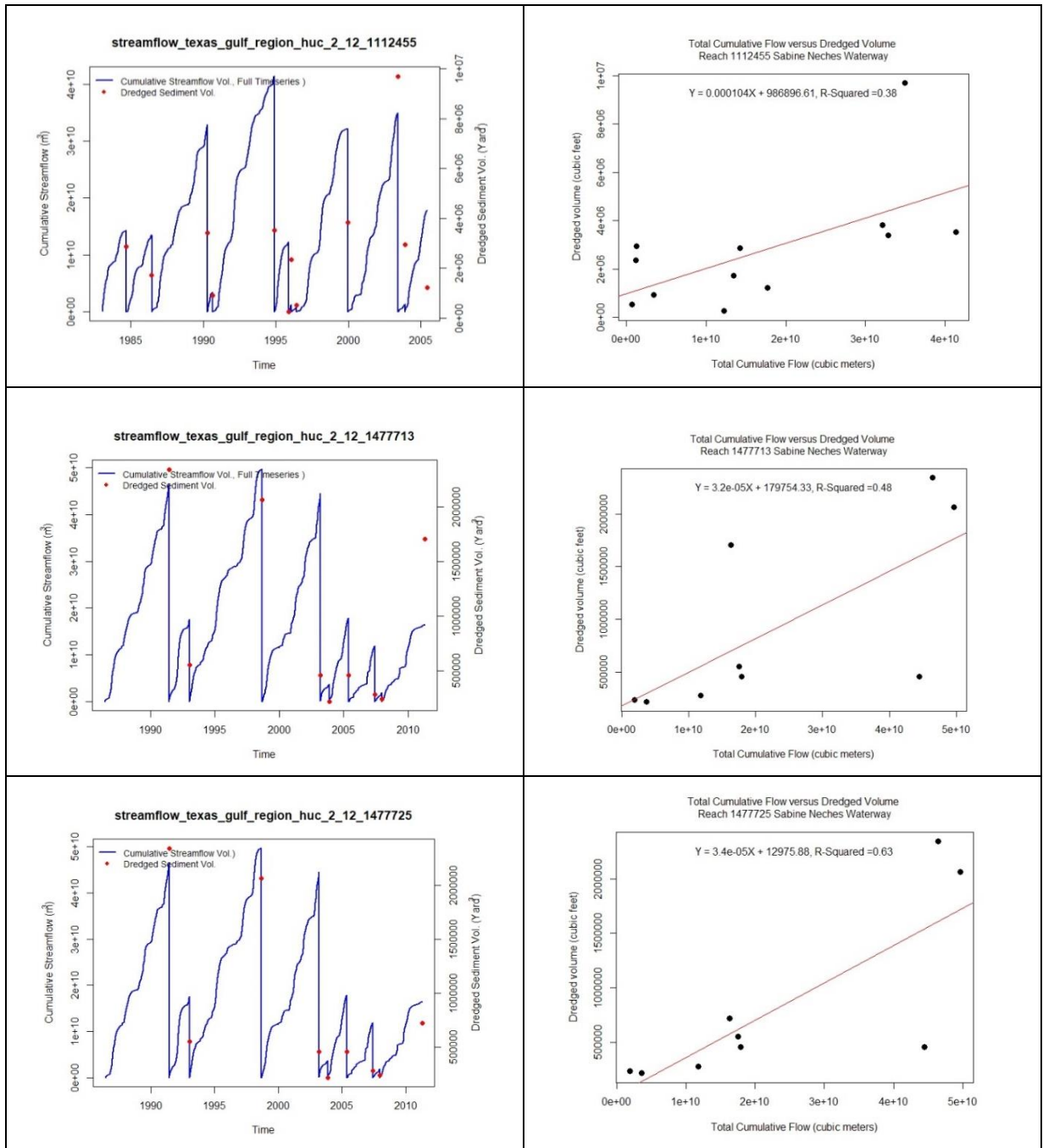
Figure 3. Visualization of selected stream reach results in the Sabine Neches Waterway

Nonlinear and Multivariate Model Analyses

Seven additional models were tested, as outlined in Table 2 in the Methodology section. These models disaggregated the cumulative flow into base flow (below the 1.5 year flow rate) and peak flow (above the 1.5 year flow rate) (models 2, 4, 6, and 8); applied non-linear frameworks (models 3, 4, 7, and 8); and incorporated prior event flow volumes to account for system lag (models 5, 6, 7, and 8). Model performance varied widely across model, harbor system, and river

COMID. Most of the time, the percentage error in the predicted volumes was within one order of magnitude. In the Sabine-Neches system, 50% of the model estimates were within 40% error of the actual magnitude of sediment dredged. Model estimates became more accurate as the dredged sediment volumes increased. Figure 4 shows the percentage error of prediction by event for each model for the reaches in the Sabine Neches system. Errors were predominantly positive – the models tended to over-predict dredging loads at lower volumes and under-predict loads at higher volumes.
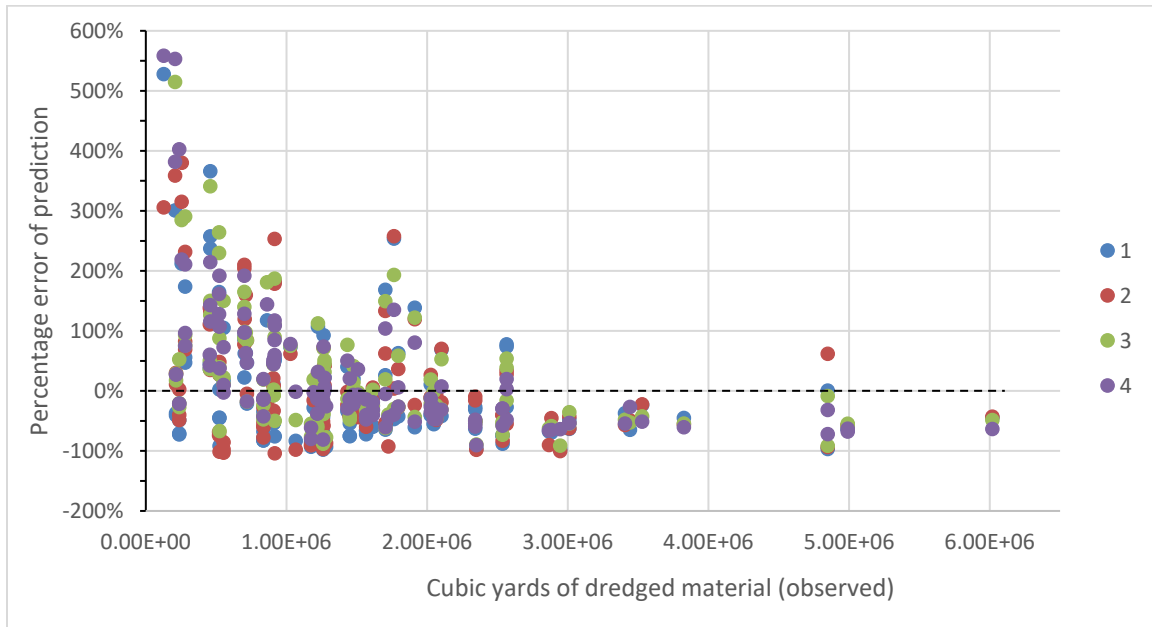
Figure 4. Percentage error of predictions by model, Sabine Neches

Table 4 shows the R-squared and p-values by model for two of the reaches for which inland precipitation-driven flow demonstrated the most skill in predicting dredged sediment loads. Generally, these models had the high associated levels of confidence. The models which disaggregated flow volumes into base flow and peak flow, 2 and 4, tended to outperform the models which treated all cumulative flow as a single variable, 1 and 3. Interestingly, for most reaches the coefficient of the peak flow term was negative, indicating that peak flows may reduce total sediment loads, and subsequent dredging burdens, and base flows may contribute more in terms of deposition.

Table 4. R-squared and p-value by model for best performing reaches

COMID	Sabine-Neches			
	1477725		1477713	
Model	R^2	p-val	R^2	p-val
1	0.63	**0.01**	0.48	**0.04**
2	0.77	**0.01**	0.66	**0.04**
3	0.62	**0.01**	0.54	**0.02**
4	0.68	**0.03**	0.57	0.08

Discussion

This approach demonstrates enough skill to be considered as potentially useful in estimating downstream dredging burdens. For the river system examined, inland riverine flow seems highly correlated with subsequent dredging loads at reaches inland of bays and coasts. The dredging history datasets used made no distinction between maintenance channel dredging and special channel widening or deepening projects, which would not be well-correlated with inland precipitation. Additionally, channel maintenance is strongly tied to budget availability, which is not captured in these models. Recognizing those limitations, it does seem that using flow volumes can provide additional information about channel maintenance needs without necessarily deploying data-intensive, high-fidelity sedimentation models.

As streamflow forecasting improves to give longer lead times on flow variability, techniques like this can alert channel managers to the need for upcoming maintenance. The development of regional model equations and additional model validation would improve the approach.

References

Balsamo, G., A. Beljaars, K. Scipal, P. Viterbo, B. van den Hurk, M. Hirschi, and A.K. Betts, (2009), A Revised Hydrology for the ECMWF Model: Verification from Field Site to Terrestrial Water Storage and Impact in the Integrated Forecast System. Journal of Hydrometeorology 10(3):623-643.

Coe, L. A., L. Dunkin, and A. A. Tavakoly, (2017), Dredging Tools White Paper.

Dahl et al. 2017. Impacts of projected climate change on sediment yield and dredging costs. DOI: 10.1002/hyp.11486

David, C. H., F. Habets, D. R. Maidment and Z.-L. Yang (2011a), RAPID applied to the SIM-France model, Hydrological Processes, 25(22), 3412-3425. DOI: 10.1002/hyp.8070.

David, C. H., D. R. Maidment, G.-Y. Niu, Z.- L. Yang, F. Habets and V. Eijkhout (2011b), River network routing on the NHDPlus dataset, Journal of Hydrometeorology, 12(5), 913-934. DOI: 10.1175/2011JHM1345.

David, C. H., Z.-L. Yang and J. S. Famiglietti (2013), Quantification of the upstream-to-downstream influence in the Muskingum method, and implications for speedup in parallel computations of river flow, Water Resources Research, 49(5), 1-18, DOI: 10.1002/wrcr.20250.

ESRI 2011. ArcGIS Desktop: Release 10.1. Redlands, CA: Environmental Systems Research Institute.

Follum, M. L., A. A. Tavakoly, J. D. Niemann, and A. D. Snow (2016), AutoRAPID: A Model for Prompt Streamflow Estimation and Flood Inundation Mapping over Regional to Continental Extents, Journal of the American Water Resources Association, 1-20. DOI: 10.1111/1752-1688.12476.

Gill, Mohammad Akram. "Flood Routing by the Muskingum Method." Journal of Hydrology 36, no. 3 (February 1, 1978): 353–63. https://doi.org/10.1016/0022-1694(78)90153-1.

McKay, L., Bondelid, T., Dewald, T., Johnston, J., Moore, R., and Rea, A., "NHDPlus Version 2: User Guide", 2012

Overton, D. E. "Muskingum Flood Routing of Upland Streamflow." Journal of Hydrology 4 (January 1, 1966): 185–200. https://doi.org/10.1016/0022-1694(66)90079-5.

RStudio Team (2015). RStudio: Integrated Development for R. RStudio, Inc., Boston, MA URL http://www.rstudio.com/

Snow, Alan D., S. D. Christensen, N. R. Swain, E. J. Nelson, D. P. Ames, N. L. Jones, D. Ding, N. S. Noman, C. H. David, F. Pappenberger, and E. Zsoter, (2016), A High-Resolution National-Scale Hydrologic Forecast System from a Global Ensemble Land Surface Model, Journal of the American Water Resources Association (JAWRA) 52(4):950–964, DOI: 10.1111/1752-1688.12434

Sugarbaker, L.J., Eldridge, D.F., Jason, A.L., Lukas, Vicki, Saghy, D.L., Stoker, J.M., and Thunen, D.R., 2017, Status of the 3D Elevation Program, 2015: U.S. Geological Survey Open-File Report 2016–1196, 13 p., http://dx.doi.org/10.3133/ofr20161196.

Tavakoly, A. A., D. R. Maidment, J. McClelland, T. Whiteaker, Z.-L. Yang, C. Griffin, C. H. David, and L. Meyer (2016a), A GIS Framework for Regional Modeling of Riverine Nitrogen Transport: Case Study, San Antonio and Guadalupe Basins, Journal of the American Water Resources Association, 52(1), 1-15. DOI: 10.1111/1752-1688.12355.

Tavakoly, A. A., A. D. Snow, C. H. David, M. L. Follum, D. R. Maidment, Z.-L. Yang (2016b), Continental Scale River Flow Modeling of the Mississippi River Basin Using High-Resolution NHDPlus Dataset, Journal of the American Water Resources Association, 1-22 DOI: 10.1111/1752-1688.12456.

U.S. Geological Survey and U.S. Department of Agriculture, Natural Resources Conservation Service, 2013, Federal Standards and Procedures for the National Watershed Boundary Dataset (WBD) (4 ed.): U.S. Geological Survey Techniques and Methods 11–A3, 63 p. Available on the World Wide Web at http://pubs.usgs.gov/tm/tm11a3/

Using HEC-WAT and HEC-RAS-Sediment to Evaluate the Effect of Hydrologic Uncertainty on Bed Evolution

Stanford Gibson, Senior Hydraulic Engineer, Hydrologic Engineering Center, US Army Corps
of Engineers, Davis, CA, stanford.gibson@usace.army.mil
William Lehman, Senior Economist, Hydrologic Engineering Center, US Army Corps of
Engineers, Davis, CA, william.p.lehman@usace.army.mil
Michael Koohafkan, California Department of Water Resources, Sacramento CA/University
of California – Davis, koohafkan@ucdavis.edu
Dan Pridal, Omaha District, US Army Corps of Engineers, Omaha, NE
Daniel.B.Pridal@usace.army.mil

Introduction

Long term river aggradation or degradation can compromise flood risk management measures like levees, reservoirs, diversions, and conveyance channels. Deposition can reduce channel conveyance or reservoir capacity over time, reducing future project benefits. Channel incision and migration can affect levee fragility, increasing risk of failure. Therefore, project benefit calculations, in morphologically active systems, must account for deposition or erosion.

Additionally, sediment transport has a non-linear relationship to flow. Large flows carry a disproportionate fraction of the sediment load. This makes sediment impacts on flood risk management projects very sensitive to the projected future hydrology, including both the frequency and timing of peak flows. The Hydrologic Engineering Center (HEC) has developed new stochastic tools to investigate the impact of morphological responses to natural variability (i.e. uncertain future flows) on project benefits and future flood risk. This paper introduces two main sources of morphological uncertainty on flood risk (magnitude and timing) and demonstrates how the connection between HEC's stochastic hydrology and sediment transport modeling tools help quantify these uncertainties.

Morphological Flood Risk: Magnitude

Non-linear morphological processes amplify the effects of flow variability. Rivers commonly transport most of their sediment during a relatively limited time period, the 1 to 10% of the year with the highest flows. Rivers with significant year-to-year hydrologic variability can transport most of the system sediment in a few high flow years.

Morphological amplification of flow variability can complicate flood risk studies. For example, Figure 1 includes fifty, synthetic, 50-year time series, that sample of a hypothetical, non-linear depositional distribution. The final bed elevation depends on the frequency and magnitude of the largest flows. Because deposition reduces channel capacity and increases water surface elevations, each potential hydrologic future will not only expose a project to different hydrologic risks but will also degrade the level of protection at different rates. If this project began losing befits after 2.5 meters of deposition, project performance would vary dramatically over these different hydrologic futures. Additionally, the non-linearity of the flow-transport relationship can skew the bed change distribution (see the histogram summarizing the final bed change distribution in Figure 1), introducing some low probability-high deposition events.
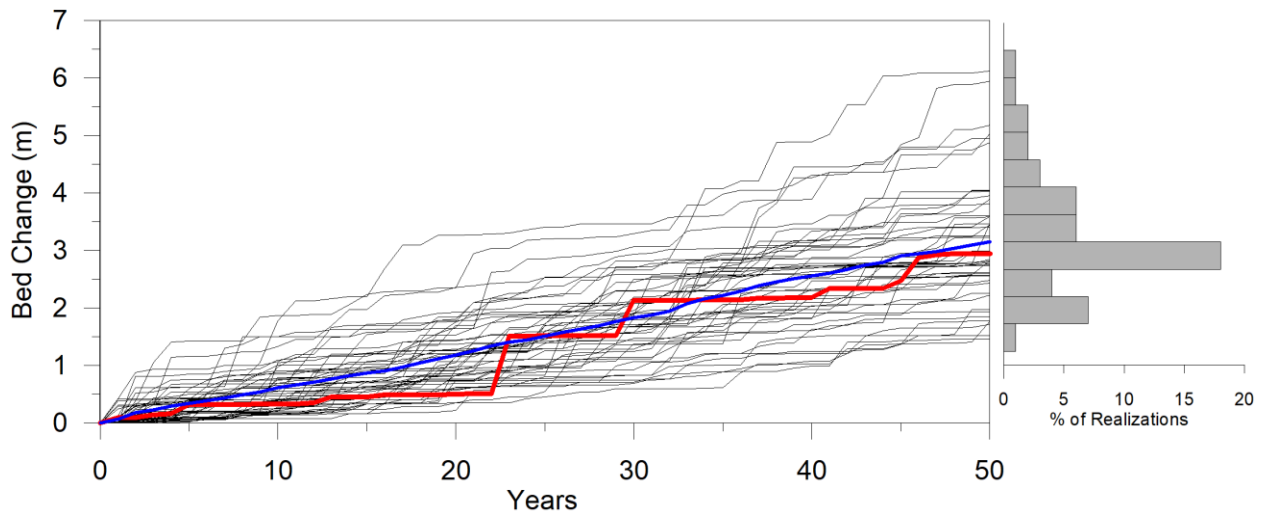
Figure 1. Fifty Realizations sampling a non-linear, annual, bed change distribution and a histogram of final bed change (right). The median final bed change realization is red and the mean is blue.

Morphological Flood Risk: Timing

Morphological, flood-risk impacts are not limited to the magnitude and frequency of large events. The non-linearity of sediment processes makes the flood risk benefits sensitive to the *timing* of these events. Figure 2 illustrates the importance of event timing on morphological benefit impacts.
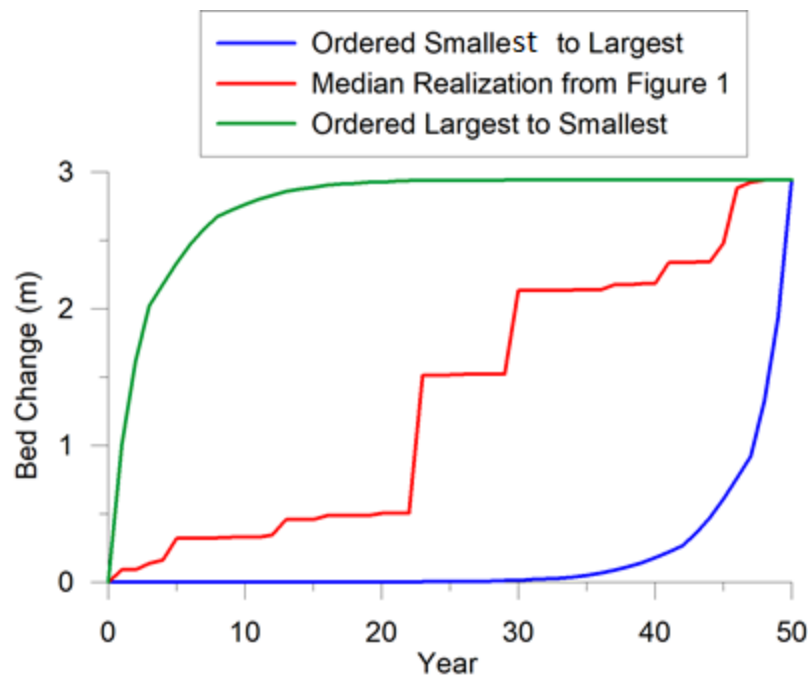
Figure 2. Median bed change time series from previous plot (red), reordered from max-to-min bed change (green) and min-to-max bed change (blue) to demonstrate the morphological impact of event timing on flood risks. If the larger events occur earlier project benefits are likely negatively impacted or project O&M expenses may be significantly increased.

Figure 2 includes the median, total, bed-change time series from Figure 1 (red curve). Figure 2 also re-orders these events in worst- and best-case-scenarios, front loading and back loading the large events respectively. Because the system deposits almost 70% of the total material in three events, the timing of these events affects the subsequent level of protection and the overall project benefits. Early deposition reduces benefits for most of the project life while hydrologic time series that backload the large flows retain benefits for most of the project life, for example the timing of large capital improvement costs (e.g. dredging, lowering water intakes that are necessary to accommodate degradation). USACE costs estimates of O&M during the project life may also be impacted by timing.

Even with just one future hydrologic realization, a hypothetical project that starts to lose benefits at 2.5 meters will perform better if the large events are later than if they are earlier or evenly distributed. For example, engineers sometimes assume constant deposition rates (e.g. historic bed change divided by years between surveys) when computing the benefits raising a levee in a depositional system. However, early events can reduce the level of protection and reduce the benefits throughout the project life. This makes morphologically active reaches sensitive to not only the magnitude and frequency of future events but also the timing.

Sediment feedbacks also affect the flow-stage relationship in a reach. Channel deposition in each event is not independent. Deposition tends to increase the slope of the reach and decrease subsequent deposition. So the magnitude, frequency, and timing of the morphologically significant events not only affects the project performance, but also the impact of future events on project performance. For example, **Error! Reference source not found.** simply re-orders depositional events without year-to-year feedbacks, yielding identical final conditions. In reality (and in a high quality model) the event order will also affect subsequent bed change, potentially driving divergent final conditions.

Continuous Simulation in HEC-WAT

Flood risk management benefits can be very sensitive to the magnitude, frequency and timing of future flows on morphologically dynamic reaches. Therefore, project teams must quantify the impact of natural variability on project performance in these systems. The Hydrologic Engineering Center's Watershed Analysis Tool (HEC-WAT) can quantify the impact of natural variability by sampling historic and synthetic flow records and run other HEC software with multiple, stochastic, future time series.

Previous versions of HEC-WAT combined flood risk computations by feeding the HEC's River Analysis System (HEC-RAS) multiple, independent, sampled, water years and compiling the results. Simulating independent, annual events is appropriate if the channel is static and the relationship between flow and river stage is stationary. However, HEC-WAT required a new approach to support serial impacts of continuously simulated events to account for morphological change.

HEC-RAS has a mobile-bed, sediment-transport model (Brunner and Gibson, 2006, Gibson et al., 2006, Gibson et al., 2017a) that can simulate deposition and erosion and the water surface response in morphologically dynamic systems (Shelley and Gibson, 2015, Gibson et al., 2017b). However, if the channel is dynamic, water-surface elevations in each year are contingent on the previous flood history. The assumption of year-to-year temporal independence breaks down.

Therefore, the HEC-WAT could no longer run independent water years through HEC-RAS and compile the results. Computing the morphological impacts on flood stage with HEC-RAS required a new, continuous-simulation module in the HEC-WAT. HEC added functionality to the Hydrologic Sampler plugin to generate continuous simulations. Through that plugin HEC-WAT can now generate long term, multi-year, stochastic time series. The study team then used this tool to investigate the impact of natural variability on HEC-RAS mobile bed results.

Simulating the Impact of Natural Variability on Reservoir Deposition with HEC-WAT and HEC-RAS

The study team applied the continuous-simulation plugin in HEC-WAT with the mobile-bed mode in HEC-RAS to investigate the role of natural variability on reservoir sedimentation. The study team used Gibson and Boyd's (2014) calibrated, unsteady, sediment transport model of the Lewis and Clark reservoir. The Lewis and Clark reservoir is the downstream pool of the Missouri Cascade, impounded by Gavins Point Dam (Boyd and Gibson, 2015). While the Missouri River delivers most of the flow in this system, the Missouri Reservoirs (including Fort Randall, just upstream) are an efficient sediment trap. Therefore, the Niobrara River - a mid-reservoir tributary – delivers most of the sediment load to this reservoir. The study team set up HEC-WAT to sample both the upstream Missouri flows out of Fort Randall and the Niobrara flows that deliver most of the sediment. HEC-RAS computed Niobrara sediment loads with a flow-load rating curve.

HEC-WAT ran 350, 50-year, mobile-bed, HEC-RAS, sediment transport simulations of this reservoir with sampled, future, hydrologies. Figure 3 includes time-series results of bed change for two cross sections. The final (50 year) longitudinal cumulative volume change profiles for all 300, 50-year realizations are plotted in Figure 4. The reservoir bed and volume change included more uncertainty in the reservoir pool and along the foreset bed of the delta (approximately downstream of river mile 830) than upstream, along the topset bed of the delta.
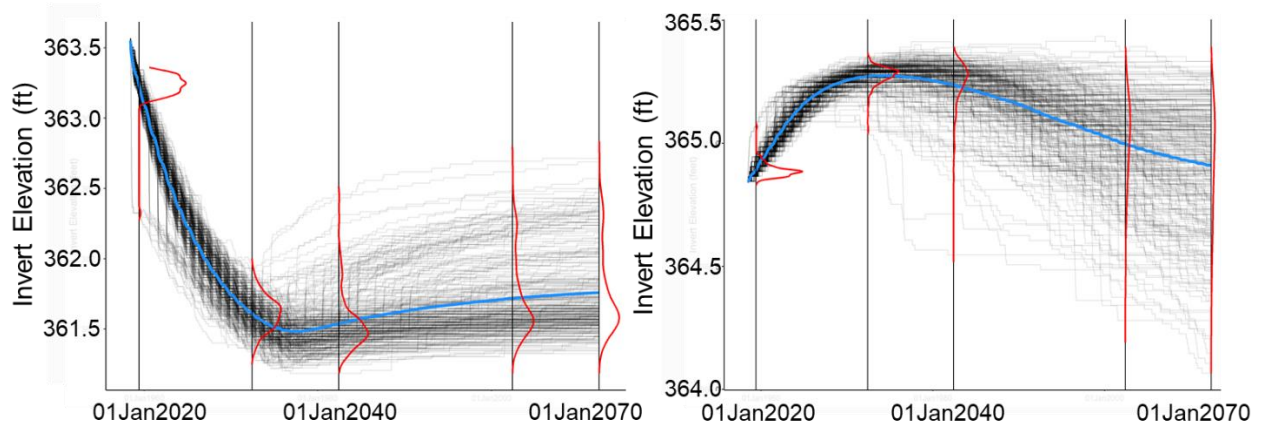
Figure 3. HEC-RAS bed change time series traces at two cross section on the Missouri River. Plots include 350 realizations based on stochastic 50-year future hydrologies provided by HEC-WAT. Blue line is mean and red lines are proportional distributions.
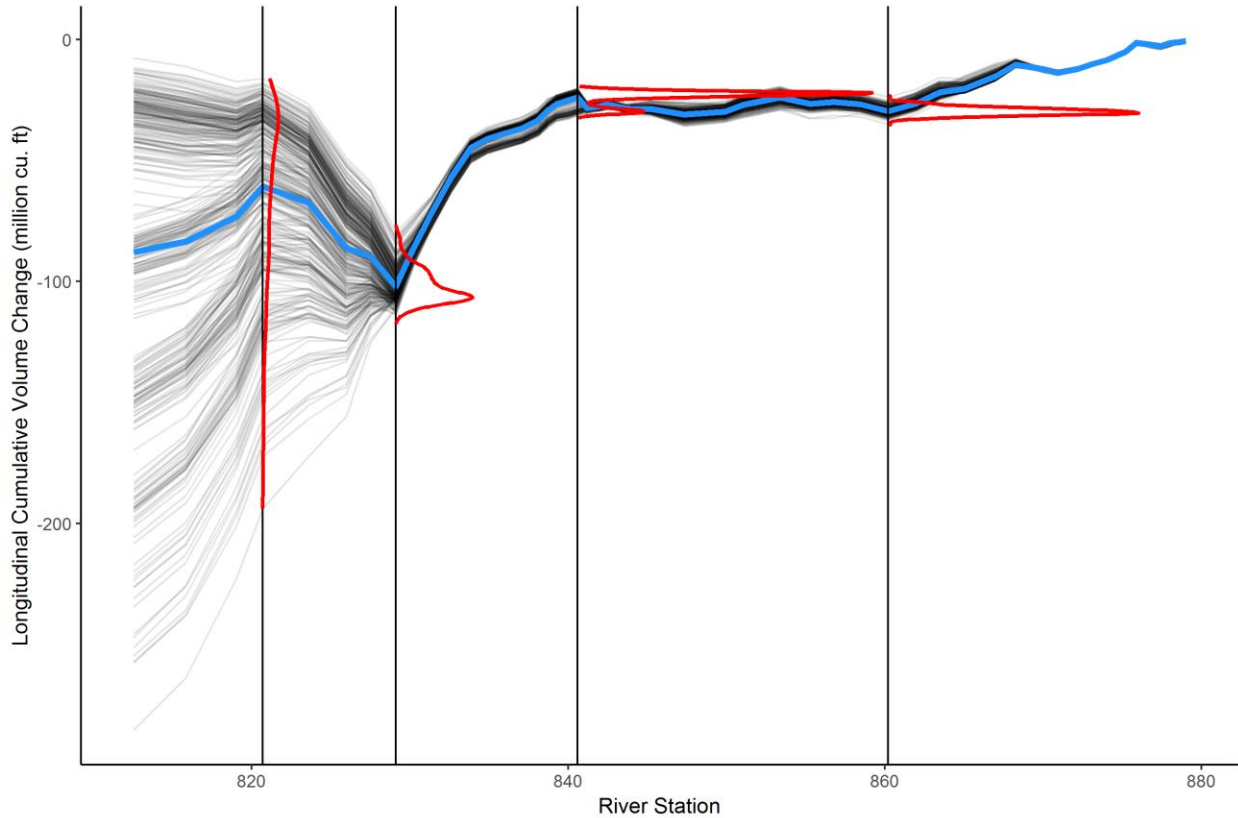
Figure 4. Longitudinal cumulative volume profile for 300, 50-year, mobile-bed, sediment-transport simulations with different hydrologic realizations from HEC-WAT. The blue line is the mean and the red lines are distributions at differnt locations.

Limitations and Development

HEC-WAT generates continuous, future, flow series in HEC's Data Storage System (HEC-DSS) through the Hydrologic Sampler plugin. Therefore, an HEC-RAS project must use HEC-DSS flow boundary conditions to leverage the continuous, natural-variability features of HEC-WAT. In version 5.0.7, only unsteady sediment transport can use HEC-DSS flow boundary conditions. Therefore, in the 5.0.x versions of HEC-RAS, these features are available for unsteady sediment transport models, not the more common quasi-unsteady models. Developmental versions of HEC-RAS 5.1 now include quasi-unsteady, HEC-DSS boundary conditions, making these tools applicable for quasi-unsteady models in future releases. Additionally, sampled boundary conditions are sampled together (e.g. the upstream and tributary flows represent the same sampled year). Future versions should include options to sample these boundary conditions independently or with correlation assumptions.

Conclusion

Sediment processes are non-linear, and can amplify the uncertainty associated with natural hydrologic variability (future flows). The magnitude, frequency, and timing of future flows can introduce uncertainty in the future stage-flow curve and project benefits. HEC added continuous simulation capabilities to the HEC-WAT's Hydrologic Sampler plugin that feeds

multi-year flow series to mobile-bed, sediment-transport simulations in HEC-RAS. This connection helps project-delivery teams quantify the influence of natural variability and future flow assumptions on future-with-project, flow-stage uncertainty. Quantifying this uncertainty is critical to understand risk to project benefits in morphologically active systems.
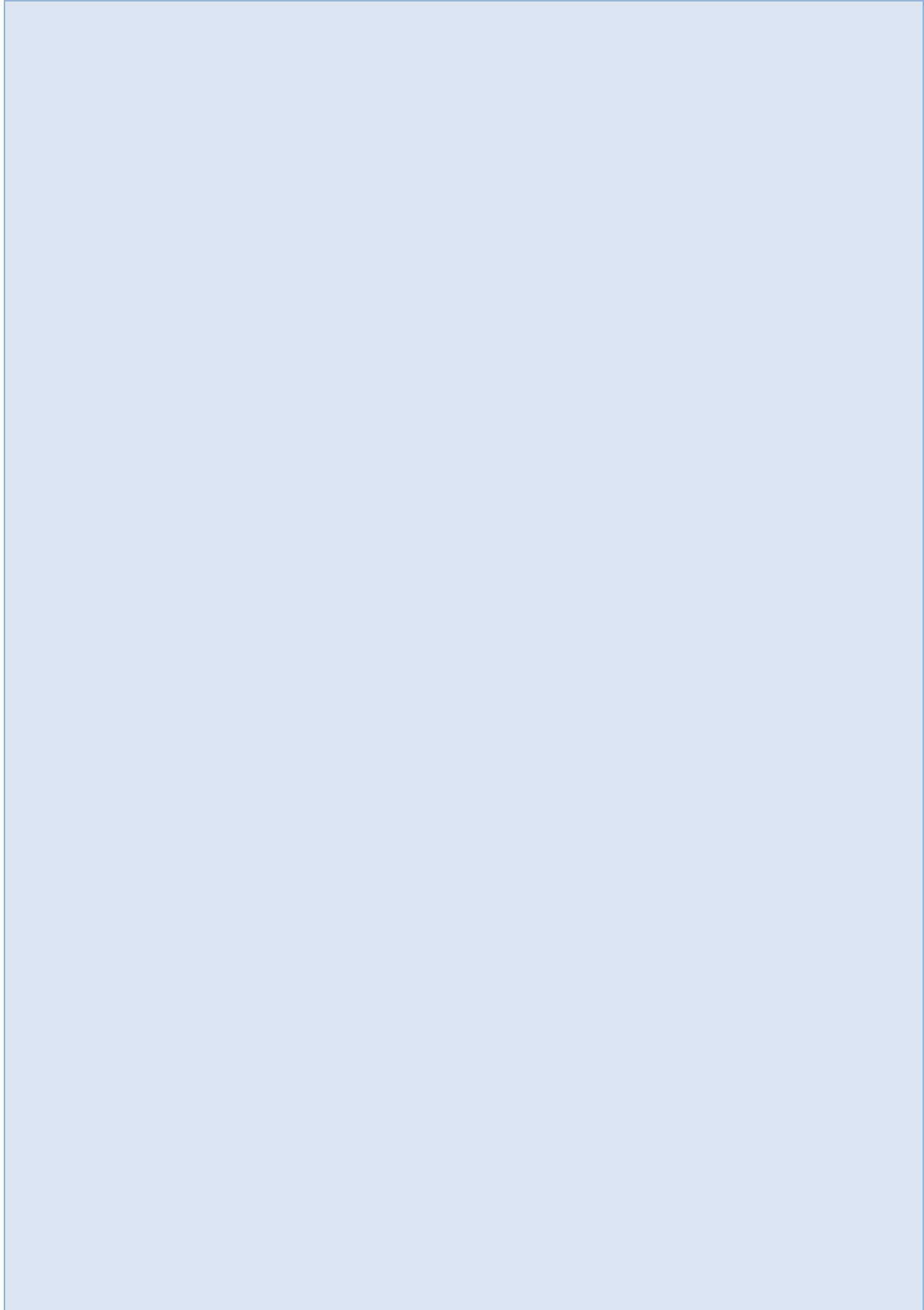
Acknowledgments

References

Boyd, P. and Gibson, S. (2015) "Evaluating Sustainable Sediment Management Alternatives for Lewis and Clark Lake," Federal Interagency Sediment Conference, SedHyd Proceedings.

Bruner, G., and Gibson, S., (2005) "Sediment Transport Modeling in HEC-RAS" *Proceedings World Water and Environmental Resources Congress 2005*, Editor: Raymond Walton, May 15–19, 2005, Anchorage, Alaska, American Society of Civil Engineers.

Gibson, S., A. Sánchez, S. Piper, and G. Brunner, (2017a) "New One-Dimensional Sediment Features in HEC-RAS 5.0 and 5.1," Proceedings, ASCE EWRI World Environmental & Water Resource Congress.

Gibson, S., B. Comport, and Z. Corum. (2017b) "Calibrating a Sediment Transport Model through a Gravel-Sand Transition: Avoiding Equifinality Errors in HEC-RAS Models of the Puyallup and White Rivers," Proceedings, ASCE EWRI World Environmental & Water Resource Congress.

Gibson, S. and Boyd, P. (2016) "Designing Reservoir Sediment Management Alternatives with Automated Concentration Constraints in a 1D Sediment Model," Proceedings International Symposium on River Sedimentation.

Gibson, S. and Boyd, P. (2014) "Modeling Long Term Alternatives for Sustainable Sediment Management Using Operational Sediment Transport Rules," *Reservoir Sedimentation* –Scheiss et al. (eds), 229-236.

Gibson, S., Brunner, G., Piper, S., and Jensen, M. (2006) "Sediment Transport Computations in HEC-RAS." *Eighth Federal Interagency Sedimentation Conference* (8thFISC), Reno, NV, 57-64.

Shelley, J. and Gibson, S. (2015) "Modeling Bed Degradation of a Large, Sand-Bed River with In-Channel Mining with HEC-RAS," Federal Interagency Sediment Conference, SedHyd Proceedings.

Hydroecological Modeling

A Method for Partitioning Total Leaf Area Index into Overstory and Understory Strata for Distributed Hydrologic Modeling Based on Forest Inventory, Remote Sensing, and Biophysical Data

Sara A. Goeking, Biological Scientist, USDA Forest Service, Ogden, UT, sgoeking@fs.fed.us
David G. Tarboton, Professor, Dept. of Civil and Environmental Engineering, Utah State University, Logan, UT, dtarb@usu.edu

Extended Abstract

Recent tree mortality across the western US has led to numerous investigations of the relationship between forest disturbance, snow accumulation and ablation, and runoff. Although historical studies suggested that recent forest disturbances would lead to increased runoff (Andréassian 2004; Bosch and Hewlett 1982; Troendle 1983), in recent studies on the effects of insect-caused tree mortality on runoff, this expectation was not met (Biederman et al. 2015; Slinski et al. 2016). Further, several studies have found that forest density and structure can affect snow accumulation and melt rates either positively or negatively (Ellis et al. 2011; Harpold et al. 2014; Lundquist et al. 2013). To better understand the mechanisms that determine whether forest disturbance will lead to increased snowpack and runoff, distributed hydrologic models require accurate representations of forest density and structure at sufficiently fine resolution to detect disturbances (Andréassian 2004). Several existing distributed hydrologic models, such as the Regional Hydro-Ecological Simulation System (RHESSys; Tague and Band 204) and the Distributed Hydrology-Soil-Vegetation Model (DHSVM; WIgmosta et al. 1994), are capable of representing overstory versus understory canopy strata in terms of leaf area index. Leaf area index, or LAI, is a dimensionless quantity that represents the one-sided surface area of all leaves within a given ground area divided by that ground area. However, most existing LAI datasets are based on remote sensing (e.g., Xiao et al. 2013), and do not distinguish overstory from understory LAI. Thus, most applications of distributed hydrologic models represent vegetation in terms of total LAI rather than separate overstory versus understory layers. The ability to use distributed hydrologic models to enhance our understanding of the link between forest disturbance and water resources requires distinction of overstory versus understory LAI.

This paper describes the development of a new spatially explicit dataset of overstory and understory LAI. We used forest inventory data to estimate overstory and understory LAI at the plot scale, and then applied a statistical learning algorithm to produce spatially gridded overstory and understory LAI by combining the plot-level LAI estimates, remote sensing, and biophysical predictors. Forest inventory data were collected by the USDA Forest Service's Forest Inventory and Analysis (FIA) program (Burrill et al. 2017; USDA 2013), which measures permanent plots with a mean spacing of about 5 km and a re-measurement period of 10 years or less, throughout all ownerships and forest types of the United States. Although FIA

measurements do not include LAI, they do include the depth and density of understory and overstory vegetation. Using this information, we partitioned remote sensing-based estimates of LAI into overstory versus understory components. Remote sensing LAI data were obtained from Moderate Resolution Imaging Spectrometer (MODIS) satellite data at 500 m resolution; see Xiao et al. (2013) for more information on MODIS and the LAI dataset. The plot-based estimates of overstory LAI were entered into a random forests model (Breiman 2001), with remote sensing, climate, and topographic data as predictors (Table 1).

Table 1. Predictor variables, as well as their sources and citations, that were included in the random forests models for producing spatially gridded overstory and understory leaf area index (LAI)

Predictor variables	Source	Citation
Elevation (DEM)	The National Map	NA
Slope	DEM/ArcGIS Pro function	NA
Folded aspect	DEM/ArcGIS Raster Calculator	McCune and Keon (2002)
Solar radiation index	DEM/ArcGIS Raster Calculator	McCune and Keon (2002)
Topographic wetness index	DEM/TauDEM	http://hydrology.usu.edu/taudem/
Slope:area ratio	DEM/TauDEM	http://hydrology.usu.edu/taudem/
Distance up to ridge	DEM/TauDEM	Tesfa et al. (2011)
Distance down to stream	DEM/TauDEM	Tesfa et al. (2011)
Mean annual precipitation[1]	http://www.prism.oregonstate.edu	Daly et al. (2000)
Maximum annual temperature[1]	http://www.prism.oregonstate.edu	Daly et al. (2000)
Minimum annual temperature[1]	http://www.prism.oregonstate.edu	Daly et al. (2000)
STATSGO soil map units	http://websoilsurvey.nrcs.usda.gov	NA
NLCD cover classes	http://viewer.nationalmap.gov/viewer/	Homer et al. (2015)
NLCD tree canopy cover	http://geoinfo.msl.mt.gov/	Homer et al. (2015)
Mean NDVI of snow-free dates	http://www.ntsg.umt.edu/project/landsat/	Robinson et al. (2017)

[1]PRISM normals are based on the period 1981-2010 at 800 m resolution.

We developed and tested the model in the South Fork Flathead watershed of Montana (Figure 1). This watershed experience extensive tree mortality in recent decades due to a combination of insects, drought, wildfire, and disease. Therefore, we produced separate models for two time periods that represent pre- (2003-2009) and post-disturbance (2010-2016). We used package randomForests (Liaw and Wiener 2001) in the open-source statistical analysis program R (R Core Team 2018) to produce separate maps of overstory and understory LAI for the two time

periods (Figure 2). The out-of-bag error rates for the two time periods were 0.13 and 0.10, respectively, where out-of-bag error is calculated as the mean error among multiple iterations of bootstrap aggregated (bagged) subsets of the data being sampled with replacement, withheld from model calibration, and then used for validation (Breiman 2001). Model R^2 values were 0.463 and 0.615, respectively, for the two time periods. Comparisons of overstory, understory, and total LAI for the two time periods indicated an overall decrease in LAI, which was expected given the recent disturbances in this watershed (Figure 3). Note that the locations of the greatest decrease in overstory LAI correspond to areas burned between the two periods (Figure 1).
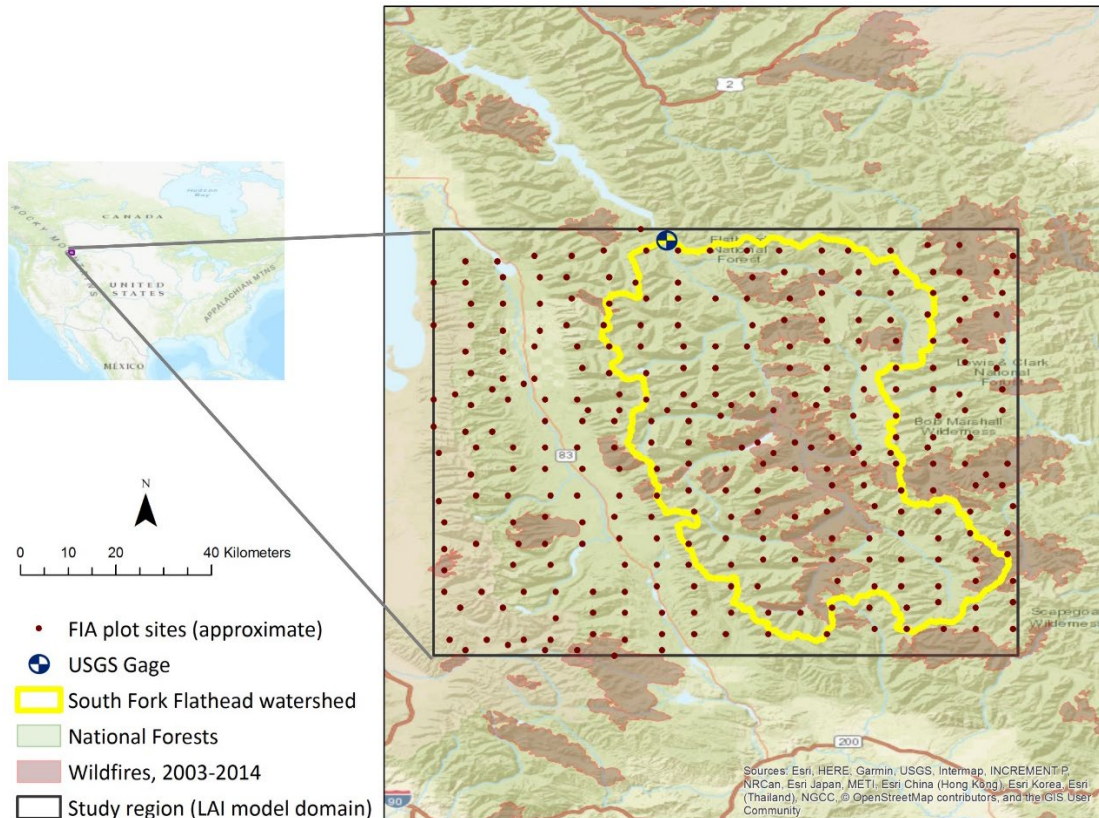
Figure 1. The South Fork Flathead watershed of northwestern Montana. Wildfire polygons were mapped by the Monitoring Trends in Burn Severity program (Eidenshink et al.2007).

The importance of this work is that it provides separate overstory versus understory LAI datasets and thus enables more precise assessment of the effects of widespread tree mortality and forest disturbance on hydrologic processes and water availability. The distinction of LAI strata capitalizes on the ability of existing distributed hydrologic models, several of which represent separate overstory and understory strata, to accurately represent the effects of forest disturbance. This capability will enable more accurate simulation of the various process-level responses, such as interception, radiation transmission, sublimation, and evapotranspiration, following forest disturbance. Therefore, it may lead to more accurate predictions of the net effect of forest disturbance on the partitioning of precipitation into runoff versus evapotranspiration.
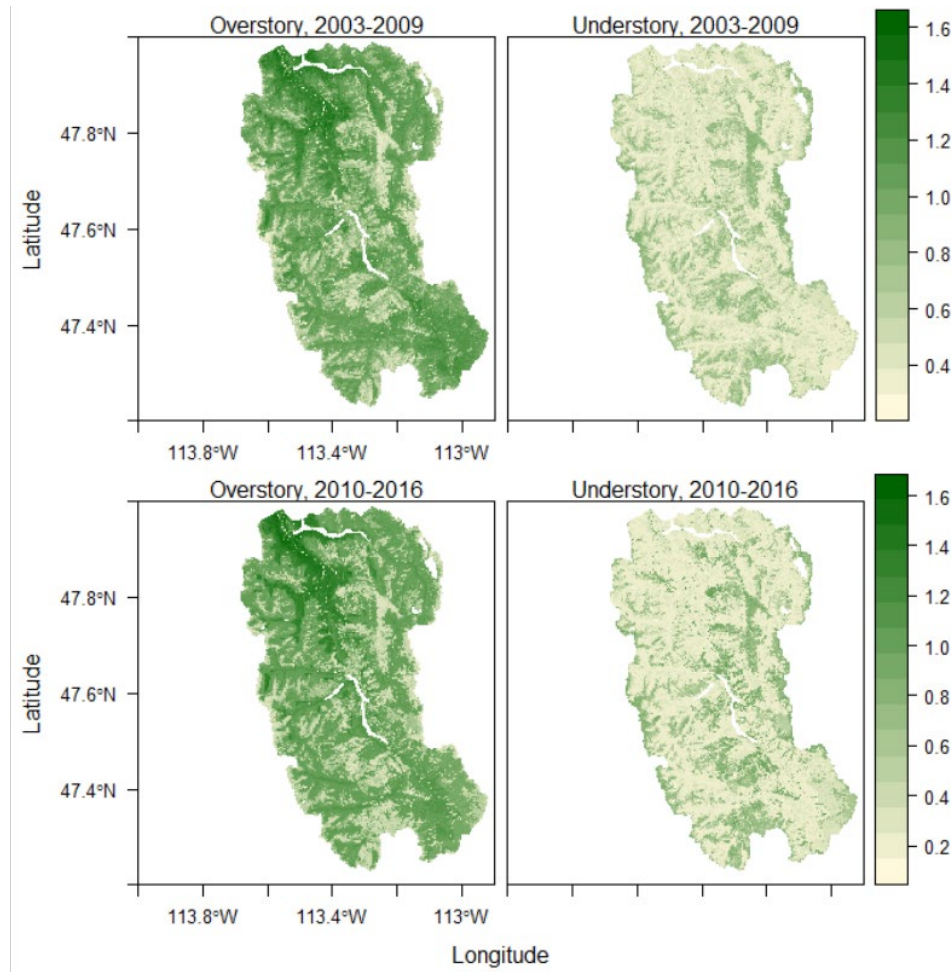
Figure 2. Overstory and understory leaf area index in the South Fork Flathead watershed, Montana, for two time periods: 2003-2009 and 2010-2016
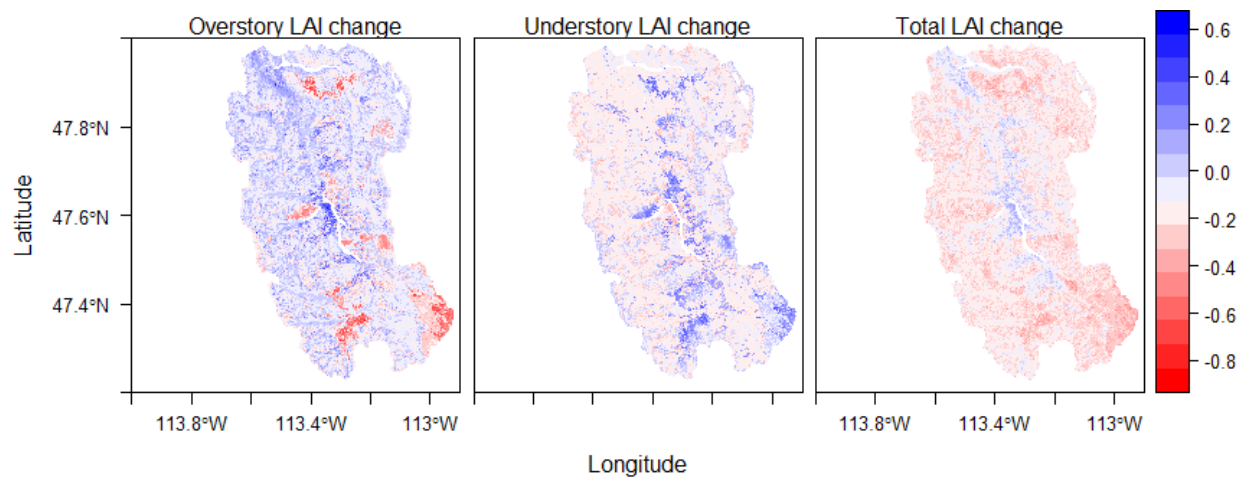
Figure 3. Change in overstory, understory, and total LAI between two time periods (2003-2009 and 2010-2016)

References

Andréassian, V. 2004. "Waters and forests: from historical controversy to scientific debate," Journal of Hydrology, 291:1-27.

Biederman, J. Somor, A.J., Harpold, A.A., Gutmann, E.D., Breshears, D.D., Troch, P.A., Gochis, D.J., Scott, R.L., Meddens, A.J. and Brooks, P.D. 2015. "Recent tree die-off has little effect on streamflow in contrast to expected increases from historical studies," Water Resources Research, 51(12):9775-9789.

Bosch, J. and Hewlett, J. 1982. "A review of catchment experiments to determine the effect of vegetation changes on water yield and evapotranspiration," Journal of Hydrology, 55:3-23.

Breiman, L. 2001. "Random forests," Machine Learning, 45(1):5-32.

Burrill, E.A.; Wilson, A.M.; Turner, J.A.; Pugh, S.A.; Menlove, J.; Christiansen, G.; Conkling, B.L.; David, W. 2017. The Forest Inventory and Analysis Database: Database description and user guide version 7.2 for Phase 2. U.S. Dept. of Agriculture, Forest Service. 946 p. [Online]. Available at web address: http://www.fia.fs.fed.us/library/database-documentation/. Last accessed 23 April 2019.

Daly, C., Taylor, G.H., Gibson, W.P., Parzybok, T.W., Johnson, G.L., and Pasteris, P.P. 2001. "High-quality spatial climate data sets for the United States and beyond," Transactions of the American Society of Agricultural Engineers, 43: 1957-1962.

Eidenshink J., Schwind B., Brewer K., Zhu Z., Quayle B., and Howard S. 2007. "A project for monitoring trends in burn severity," Fire Ecology, 3(1):3–21.

Ellis, C., Pomeroy, J., Essery, R. and Link, T. 2011. "Effects of needleleaf forest cover on radiation and snowmelt dynamics in the Canadian Rocky Mountains," Canadian Journal of Forest Research, 41(3):608-620.

Harpold, A.A., Biederman, J.A., Condon, K., Merino, M., Korgaonkar, Y., Nan, T., Sloat, L.L., Ross, M. and Brooks, P.D. "Changes in snow accumulation and ablation following the Las Conchas Forest Fire, New Mexico, USA," Ecohydrology, 7(2):440-452.

Homer, C.G., Dewitz, J.A., Yang, L., Jin, S., Danielson, P., Xian, G., Coulston, J., Herold, N.D., Wickham, J.D., and Megown, K. 2015. "Completion of the 2011 National Land Cover Database for the conterminous United States-Representing a decade of land cover change information," PERS, 81: 345-354.

Liaw, A., and M. Wiener. 2002. "Classification and regression by randomForest," R News, 2(3):18–22.

Lundquist, J., Dickerson-Lange, S., Lutz, J. and Cristea, N. 2013. "Lower forest density enhances snow retention in regions with warmer winters: A global framework developed from plot-scale observations and modeling," Water Resources Research, 49(10):6356-6370.

McCune, B. and Keon, D. 2002. "Equations for potential annual direct incident radiation and heat load," Journal of Vegetation Science, 13:603-606.

R Core Team. 2018. R: A language and environment for statistical computing. R Foundation for Statistical Computing, Vienna, Austria. Available online: http://www.R-project.org/[Accessed 15 February 2019].

Robinson, N.P., Allred, B.W., Jones, M.O., Moreno, A., Kimball, J.S., Naugle, D.E., Erickson, T.A., and Richardson, A.D. 2017. "A dynamic Landsat derived normalized difference vegetation index (NDVI) product for the conterminous United States," Remote Sensing, 9(8): 863.

Slinski, K., Hogue, T., Porter, A. and McCray, J. 2016. "Recent bark beetle outbreaks have little impact on streamflow in the Western United States," Environmental Research Letters, 11(7):074010.

Tague, C. and Band, L. 2004. "RHESSys: Regional Hydro-Ecologic Simulation System—An object-oriented approach to spatially distributed modeling of carbon, water, and nutrient cycling," Earth Interactions, 8:1-42.

Tesfa, T.K., Tarboton, D.G., Watson, D.W., Schreuders, K.A.T., Baker, M.E., and Wallace, R.M. 2011. "Extraction of hydrological proximity measures from DEMs using parallel processing," Environmental Modelling & Software, 26: 1696-1709.

Troendle, C. 1983. "The potential for water yield augmentation from forest management in the Rocky Mountain region," Journal of the American Water Resources Association, 19:359-373.

U.S. Department of Agriculture, Forest Service. 2013. Interior West Forest Inventory and Analysis Forest Survey field procedures, Ver. 5.0. Available online: http://www.fs.fed.us/rm/ogden/data-collection/pdf/iwfia_p2_60.pdf [Accessed 18 December 2018].

Wigmosta, M., Vail, L. and Lettenmaier, D. 1994. "A distributed hydrology-vegetation model for complex terrain," Water Resources Research, 30:1665-1679.

Xiao Z., Liang, S., Wang, J. Wang, Chen, P., Yin, X., Zhang, L., and Song, J. 2014 "Use of general regression neural networks for generating the GLASS leaf area index product from time series MODIS surface reflectance," IEEE Transactions on Geoscience and Remote Sensing, 52(1):209-223.

Application Program Interfaces (APIs) for Modularized and Flexible Engineering Software Deployment

Drew Allan Loney, PhD PE USACE ERDC, Vicksburg, MS drew.a.loney@usace.army.mil
Kimberly Pevey, PhD USACE ERDC, Vicksburg, MS kimberly.c.pevey@usace.army.mil
Scott Christensen, PhD USACE ERDC, Vicksburg, MS
scott.d.christensen@usace.army.mil
Kevin Winters, USACE ERDC, Vicksburg, MS kevin.d.winters@usace.army.mil

Abstract

Engineering software platforms are increasingly asked to be more flexible, adaptable, and robust to handle modern engineering problems. Common challenges include spanning multiple computer architectures, adapting to differing user skill levels, and performing multiple types of analyses all while maintaining performance and ensuring accurate results. Development of next generation federal engineering software must focus on these challenges to maintain relevance and be broadly applicable.

The US Army Corps of Engineers (USACE) Engineer Research and Development Center (ERDC) is at the forefront of engineering software development. With mandates in both civil infrastructure and military programs, the ERDC has focused on developing engineering software platforms with broad applicability and flexible deployment. Efforts of the ERDC have centered around the creation of Application Program Interfaces (APIs) that provide a standard means of exposing and accessing functionality as well as eliminating much of the complexity in using high-fidelity numerical models. These API platforms aim to create a system of modularized, open-source code that can be easily interchanged without major architectural modifications. This provides others with a foundation from which to develop and helps to maintain the codebase.

Recent efforts have focused on creating API platforms to support data acquisition and archival, hydrodynamic/hydrologic modeling, and waterborne logistics within the Military Engineering and Engineered Resilient Systems (ERS) programs.

Quest is a Python library that includes an API to search, publish and download data (both geographical and non-geographical) across multiple data sources including both local repositories and web-based services. Quest also provides tools in order to manipulate and manage user data, using a hierarchical structure to organize and manage datasets and data sources.

The Rapid Operational, Access, and Maneuver Support (ROAMS) platform integrates hydrodynamics, wave, hydrology, and vessel routing capabilities across six component toolboxes: roamsADH (shallow-water hydrodynamics); roamsSTWAVE (surface waves); roamsGSSHA (hydrology and sedimentation); roamsROUTE (vessel route prediction); roamsCOUPLING (inter-model iterative solutions); and roamsUTIL (supporting capabilities such as meshing and projection handling). These toolboxes wrap more high-fidelity numerical models to minimize complexity while maintaining functionality.

Benefits of using Quest and ROAMS include:

- API based model access for simple model manipulation
- Platform independent model calls, allowing the same code to execute across multiple compute resources
- Automated workflows to reduce model generation time and accelerate time to solution
- Web-oriented interfaces to increase model accessibility

This presentation introduces the Quest and ROAMS APIs. The capabilities of each API are presented, along with ERDC use cases. Future development of the API platforms is also discussed.

Introduction

The design of scientific software has historically centered on code customized and optimized to specific applications. While this provided the end user with the desired functionality for a specific case, maintenance of the software often required supporting the same functionality across multiple programs increasing software complexity and the extending the development cycle. Program specific software design also limits the flexibility of the end user, requiring the developer to continue to create customized code for new application cases or to expand existing functionality. Application Program Interfaces (APIs) within scientific software development change the architecture underlying scientific computing.

API architectures expose individual tasks as callable functions, allowing the assembly of a customized program by linking together a series of preconstructed operations. This change in structure yields multiple benefits to the user and developer. By inherently including flexibility, APIs enable significantly faster application development times and reduce the maintenance burden from redundant functionality across platforms. APIs also improve the ability to isolate issues within the code, debug individual tasks, and distribute any fixes without concern for impacting other sections of a program. New functionality can also be developed in isolation and merged into the API when completed. Cross-platform deployment is often facilitated as well through the ability to reuse code among computing platforms. Development of scientific software as APIs produces more flexible, adaptable, and customizable software with more broad application than traditional customized programs.

The US Army Corps of Engineers (USACE) Engineer Research and Development Center (ERDC) exists at the forefront of scientific software development to support the Nation's civil infrastructure and its Warfighters. Software development at the USACE ERDC recognizes its hybrid mission, building in flexibility to be broadly applied across both use areas. These missions often require rapid, customized applications to solve specific one-off problems. Similarly, these missions can require many thousands of computational runs, each customized according to a specific need by following the same overall logic. These use cases, combined with the USACE ERDC access High Performance Computing (HPC) resources and cross-platform deployment requirements, allow for software developed by USACE ERDC to be ideally suited for implementation as APIs. Two API platforms have been of principle development focus: Quest for data acquisition and the Rapid Operational, Access, and Maneuver Support (ROAMS) for hydrodynamics and waterborne logistics.

Quest is an open source Python library that automates many steps in the data management process including searching, downloading, organizing, processing (filtering), and publishing. Quest accomplishes these operations by managing key metadata and through the use of three

types of plugins: (1) provider plugins, (2) tool plugins, and (3) I/O plugins. The plugin architecture makes it easy to expand the capabilities of Quest to include additional data sources, data manipulations, and to be compatible with additional file formats. This flexibility is needed to meet the diversity of data needs, to support the many different storage formats, and to communicate with APIs of external data providers for the various projects at the USACE ERDC.

ROAMS is a Python library intended for interactions with hydraulic, hydrology, and waterborne logistics software developed by the USACE ERDC. The roamsAPI is composed of five independent but related packages that are each tasked with a separate portion of the analysis. The four principal packages are roamsADH to model hydrodynamics using the Adaptive Hydraulics (AdH) model, roamsSTWAVE to model the wave environment using the STeady-state spectral WAVE (STWAVE) model, roamsROUTE to calculate waterborne logistics parameters using hydrodynamic information, roamsCOUPLE which allows for iterative solutions between models, and roamsUTIL which contains supporting functionality such as meshing and projection. For the AdH and STWAVE packages, as these include standalone modeling engines used by USACE, the packages serve as Pythonic wrappers with which one can interact with the engines. An additional package, roamsGSSHA, is currently in development to facilitate hydrology modeling.

This paper highlights and describes the Quest and ROAMS APIs. It begins by highlighting the functionality and architecture of each API, and then outlines specific use cases. Demonstrations are provided of several use cases. It then concludes with the future development plans for the Quest and ROAMS APIs as well as information to obtain access to each API.

Quest

Background

Improvements in environmental modeling have been driven by increased spatial domain extents, finer input resolutions, and better characterization of the underlying physical processes. These mechanisms require large amounts of input data to yield the desired improvements. (Michener et al., 2012; Tolle, Tansley, & Hey, 2011) The amount of input data required for environmental modeling is only expected to increase as new acquisition methods improve the fidelity of input datasets. This is combined with a similar problem regarding model output data which has grown in lockstep with the input requirements. While the size of the environmental model data products has grown, tools to facilitate user interaction with the datasets has not kept pace. The result is often a barrier to deployment of these higher-fidelity models and increased deployment times.

Quest was development to overcome these data management issues for the USACE ERDC. Quest provides automation of the data management cycle, as shown in Figure 1. Using a series of provider plugins, tool plugins, and I/O plugins, the user can create workflows to manipulate data as necessary for their application. The data management cycle consists of several phases that include (1) data discovery, (2) data retrieval, (3) local data management and organization, (4) data processing or manipulation, and (5) data publishing and archival. The final phase of publishing and archival should complete the cycle by permitting the data to be discoverable for future use.
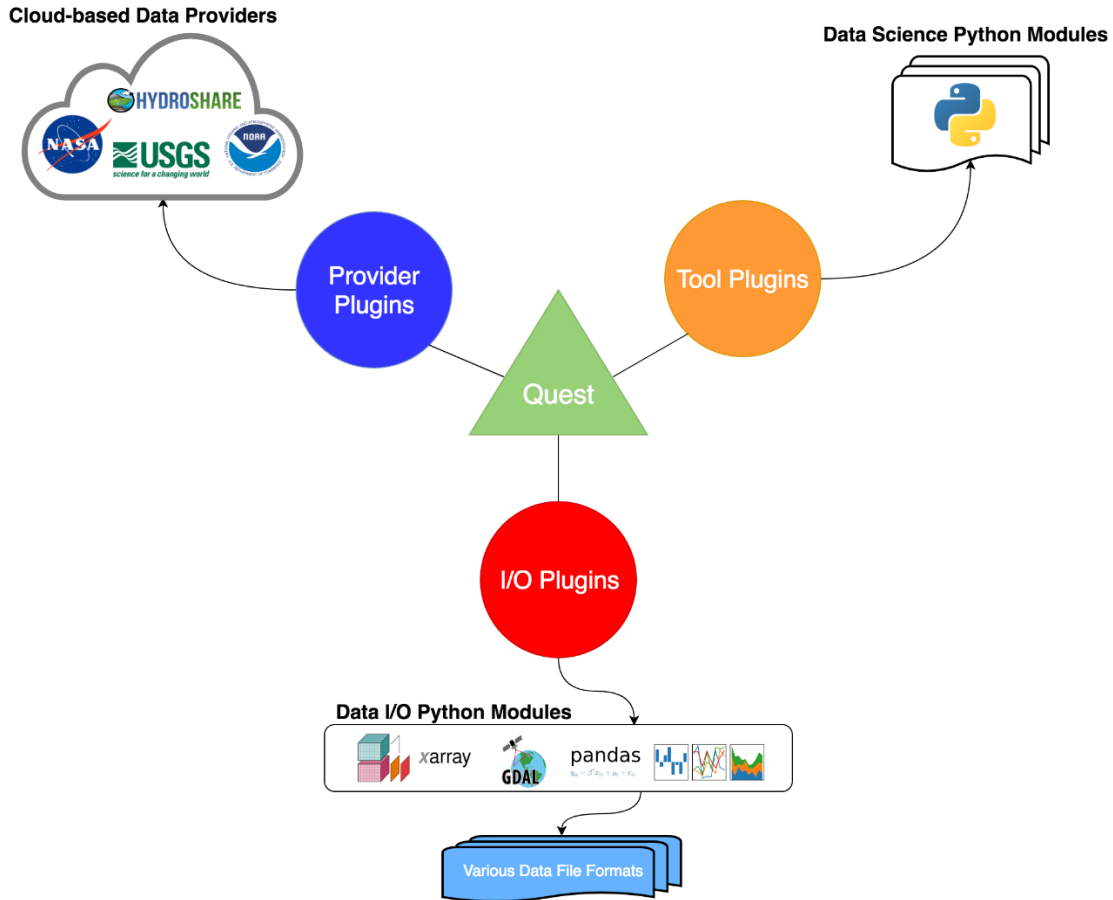
Figure 1: Structure of Quest and its plugins. Quest utilizes Provider, Tool, and I/O plugins to acquire, manage, and publish data for users.

Searching: Quest is able to search for data from data providers that are described by provider plugins. A data provider is any academic, governmental, public or private organization that provides data accessible to a consumer through a web-based service such as the USGS National Water Information System (NWIS). Provider plugins are written as an interface between the Quest internal API and the API or data organization of the specific data provider. In the search process, Quest downloads and caches metadata from each provider to create a knowledge base of available data. It can then quickly perform queries on the metadata based on location (for geographic data), parameter, or other metadata tags.

To quickly support data produced within the USACE ERDC or data procured from other U.S. governmental agencies that is not accessible through automated means, a special data provider, known as a user provider, can be described to interact with a simple file server (file system listing). All Quest requires to access these local repositories is a description of the data and its parameters and hierarchical organization written in a YAML file which accompanies the data. Users can then dynamically add these data sources to Quest at runtime by simply providing the link or path to the YAML file describing the data.

Downloading: The provider plugins also handle retrieving downloading data. Downloaded data is saved to disk in a standardized directory hierarchy created by Quest. Each provider plugin defines a set of download options that the user must specify when downloading data. The

download options are customized for each service plugin and are based on what input the service provider's API requires, which often includes options such as the parameter name, the start date, and the end date. The download options are one of several instances of user specified options in Quest. In each of these cases the definition of the options is specified using the Python library Param. Param allows a description and the validation of the options to be coded into the option definition and also provides an easy way to map the options to graphical user interface (GUI) widgets when working with Quest through browser-based interfaces.

Organization: Quest provides a simple organization structure consisting of projects and collections. A project corresponds to a directory on disk and contains a SQLite database that stores metadata about the project and its collections and data. Collections are subdirectories to the project and are containers for the actual data files. A project must have at least one collection and all data must belong to a collection. By default, the project directories are all stored in a standard location in a user's home directory. This simple organization method provides a consistent and predictable structure for storing the data and metadata.

Processing: Quest provides a mechanism for performing data transformations or manipulations through the use of tools. Tools are enabled by tool plugins and can consist of any operation or set of operations that can be done via Python. For example, the resampling tool will operate on time series data and aggregate the data based on a specified time frame (e.g. daily, weekly, monthly) using a specified method (e.g. sum, average, max, min, etc.). Similarly, the raster-merge tool takes several raster datasets and merges them to create a new dataset. A tool plugin must define a set of options, following the same pattern as download options, which serve as the input to the tool. Tools can accept one or several datasets as input; however, these input datasets are not modified directly. Rather, a new dataset or datasets are created as a result of the running the tool. The tool name and options are stored in the metadata of each new dataset so that the provenance of the data can be tracked.

Tool plugins rely on the I/O plugins to access the data from disk. The I/O plugins enable datasets of various file formats to be read in as Python data structures. Python libraries such as xarray, and Pandas, provide standard data structures with the capability of reading many different file formats. Quest uses the metadata stored for each dataset to determine which I/O plugin to use to read the data in. Once the data is in memory the tool plugin can use other Python libraries to operate on the data.

Publishing: Quest enables data publishing through the provider plugins. A provider plugin, therefore, can have two purposes: (1) finding and retrieving data from a data repository, and (2) publishing data to a repository. Not all service plugins meet both purposes. In fact, most service plugins only serve as sources for retrieving data. However, the HydroShare plugin is an example of a service plugin that has the ability to both retrieve and publish data is since HydroShare serves as both a data repository and a data archival service. Similar to other processes in Quest, a publisher in a provider plugin must define options that allow the user to specify what datasets to publish and any other required metadata that is needed for the publishing process on the specified publisher.

Examples

Map Management: Quest can serve maps that be utilized to both illustrate data and perform analyses. This workflow, illustrated using EarthSim tools in Figure 2, uses the GrabCut algorithm in OpenCV to extract coastlines. ("OpenCV," 2019) Quest presents users with an

interactive world map from which the user the selects a region of interest and a tile service. Quest then operates to request the image from the tile service and download it locally as a georeferenced tiff file. The user then specifies which regions are land and which are water. The GrabCut algorithm is run on the image and the result is a polygon of the extracted coastline. There are also options to filter out coastlines based on size constraints (e.g. for small lakes of no interest) and options to redistribute or down sample the number of vertices along the coastline polygons.
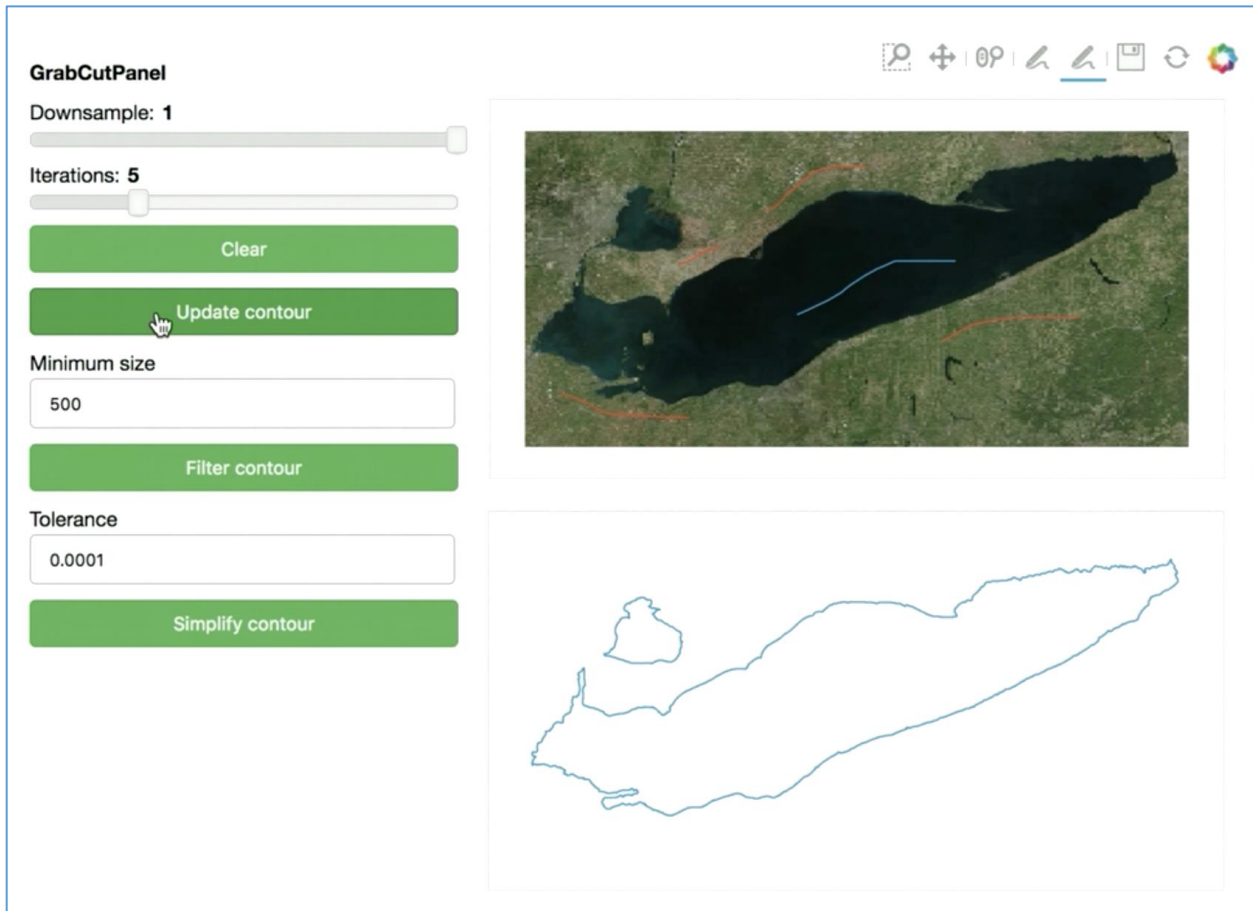
Figure 2: Quest serving map tiles to the GrabCut workflow to determine coastlines.

Data Visualization: Quest can be incorporated as the data management backend for use in GUI data visualization/management tools. Figure 3 demonstrates a web-based tool that uses Tethys. (Swain et al., 2016) Web-based interfaces allow users to interact with data without downloading or installing any software locally on their machines. It also facilitates determining which data is necessary for a particular use case prior to downloading the data and simplifies workflows where automation is not possible.
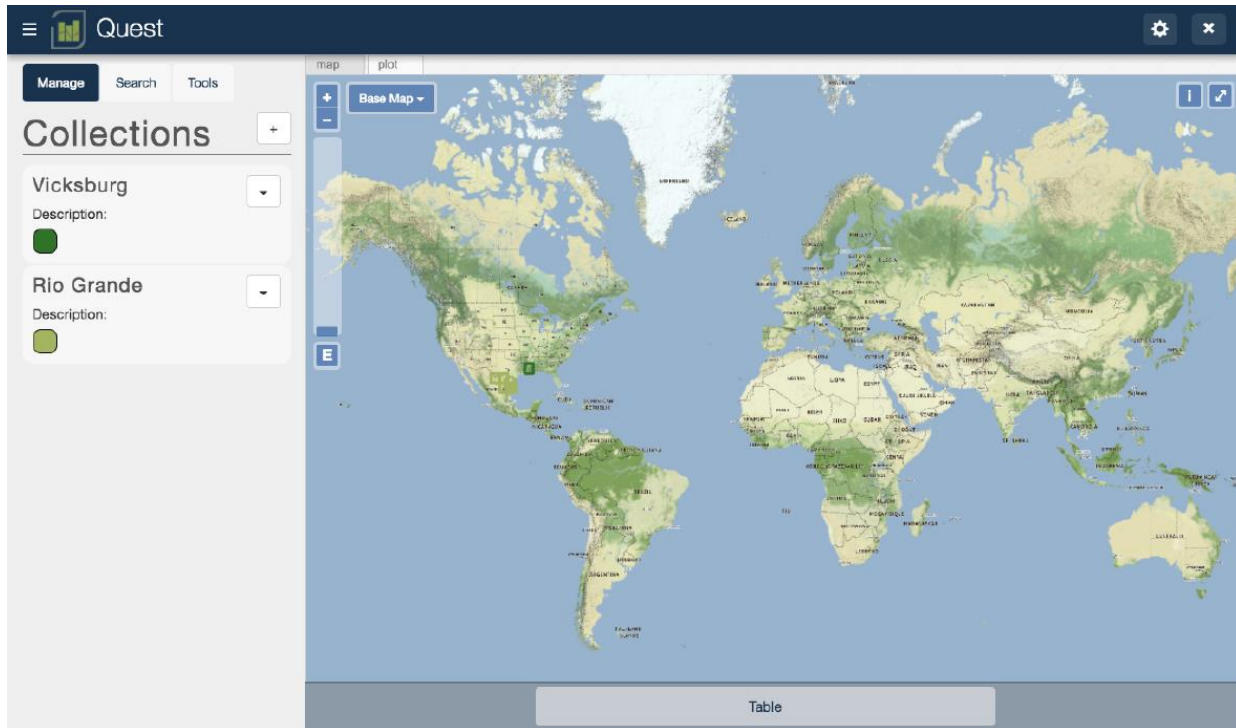
Figure 3: Quest implemented as a web-interface to visualize data

Data Management: Quest is broadly applicable to any script or workflow that requires data acquisition, processing, and publishing. These cases can incorporate Quest to simplify their data workflows, reducing the need to create custom code to support a single use case and improving performance through simple access to optimized data processing methods.

Rapid Operational, Access, and Maneuver Support (ROAMS)

Background

Manual deployment of environmental models is a labor-intensive task. Once the input data is obtained and preprocessed, the most common workflow calls for utilization of a graphical interface to perform any additional preprocessing, apply boundary/initial conditions, and generate the computational mesh. While model runs are often separate from a graphical interface, users often will return to the graphical interface to post-process and explore the results. This workflow functions well for labor-intensive models that have the required functionality bundled into the user interface. However, it lacks the flexibility to quickly adapt when changing functionality is necessary, to reduce the human burden when a workflow can be automated, or extend readily across different platforms. Moreover, the most convenient means to overcome these limitations is to modify the model source code directly, an option not available to many model users who may lack the coding or technical expertise to do so. ROAMS provides an API framework that sits between graphical tools and model source code to overcome these limitations. (Loney, Pevey, McAlpin, Nelsen, & Hargis, 2018)

ROAMS provides expanded analysis, model automation, and enhanced visualization tools to hydraulic, hydrology, and waterborne logistics by providing a Python-based API for the USACE computational engines using an object-oriented architecture. The full structure of ROAMS is shown in Figure 4. (Loney, Pevey, McAlpin, Nelsen, & Hargis, 2017) This permits the complex computational models to be readily setup, manipulated, and post-processed with the same interactive Python prompts and scripting workflows on local workstations (PC, Mac or Linux), the supercomputing environment, and web-oriented architectures. Particular emphasis has been placed on code modularity and performance. The independent package structure allows use of only the minimal subset of ROAMS codebase necessary to complete a task which helps to maintain code performance and quality. Modularity in this form also ensures that the components of ROAMS are widely applicable throughout USACE operations.

roamsAdH: AdH is a finite element engine capable of solving the two-dimensional (2D) and three-dimensional (3D) shallow water equations, the 3D Navier-Stokes equations, and the 3D groundwater equations(Coastal and Hydraulics Laboratory, 2015). Source code for the AdH engine is actively developed and maintained by the ERDC Coastal and Hydraulics Lab (CHL). roamsADH provides a means by which to create, run, and post-process an AdH model. The toolbox functionality is accessed by means of an AdH model object that contains all of the parameters specific to a single AdH model. These parameters include all of the associated input cards, domain meshes, initial conditions, boundary conditions, and results. All functionality of the AdH engine is accessed through setting the object parameters or calls to the AdH model object functions. Generated AdH simulations can be solved independently or coupled to STWAVE model instances to account for wave setup effects using the roamsCOUPLE package.

roamsSTWAVE: STWAVE is a finite difference engine for solving the steady state wave actions balance equation to determine wave height, period, direction, and spectral shape between the offshore and near shore in less than 40 meters (m) of water. (Coastal and Hydraulics Laboratory, 2019) The capabilities of the STWAVE engine including solving for wave refraction, shoaling, current induced effects, and wind/wave growth. roamsSTWAVE estimates the wave height and period in order to anticipate when and where the water surface becomes energetic. The STWAVE model can be solved on its own or iteratively with an AdH model to fully account for the changing hydrodynamics due to wave run-up. When solved iteratively, an STWAVE snapshot is periodically produced using the AdH result as the initial condition.

roamsROUTE: The roamsROUTE package utilizes environmental information produced by roamsADH and roamsSTWAVE to determine waterborne logistics quantities that may be of interest, including vessel operating paths and accessible times. This allows military planners to rapidly conduct course-of-action analysis to respond to changing threat and environmental conditions. The package implements a distributed penalty/barrier optimization methodology to compare real world vessel maneuverability constraints against the environmental domain to forecast accurate routes though a given region.

roamsCOUPLE: The roamsCOUPLE package contains functionality to map data between different computational engines as well as to iteratively solve models. Mapping data between computational engines is necessary because solutions are often calculated on different meshes and may require different reference frames. roamsCOUPLE simplifies this mapping by automating the conversion between model objects. Iterative solvers are implemented to support high accuracy hydrodynamics, such as wave run-up, which requires alternating solutions of the wave state with the hydraulics.

roamsUTIL: The roamsUTIL package contains much of the supporting functionality that is shared between the other packages. As such, it is a necessary dependency from ROAMS for any of the other packages to function correctly. roamsUTIL contains automated meshing, projection, geometry, and statistical tools to simplify model generation and post-processing. (Loney, Yeates, & Hargis, 2018) Significant attention has been given to ensuring computational performance of the implemented routines.

roamsGSSHA: The Gridded Surface/Subsurface Hydrologic Analysis (GSSHA) model is a physics-based, distributed model intended to perform high-fidelity hydrology modeling. It implements multiple types of physics, ranging from overland flow and stream routing to groundwater, snow melt, and sediment transport, that can be enabled for particular cases. roamsGSSHA is currently under development, leveraging the open source package GSSHApy. When completed, it will provide an object-oriented platform in which to create, manipulate, and post-process GSSHA models. Additionally, it will facilitate communication with shallow water physics through the roamsCOUPLE package. ("GsshaPy Documentation — GSSHAPY 2.3.7 documentation," 2019)
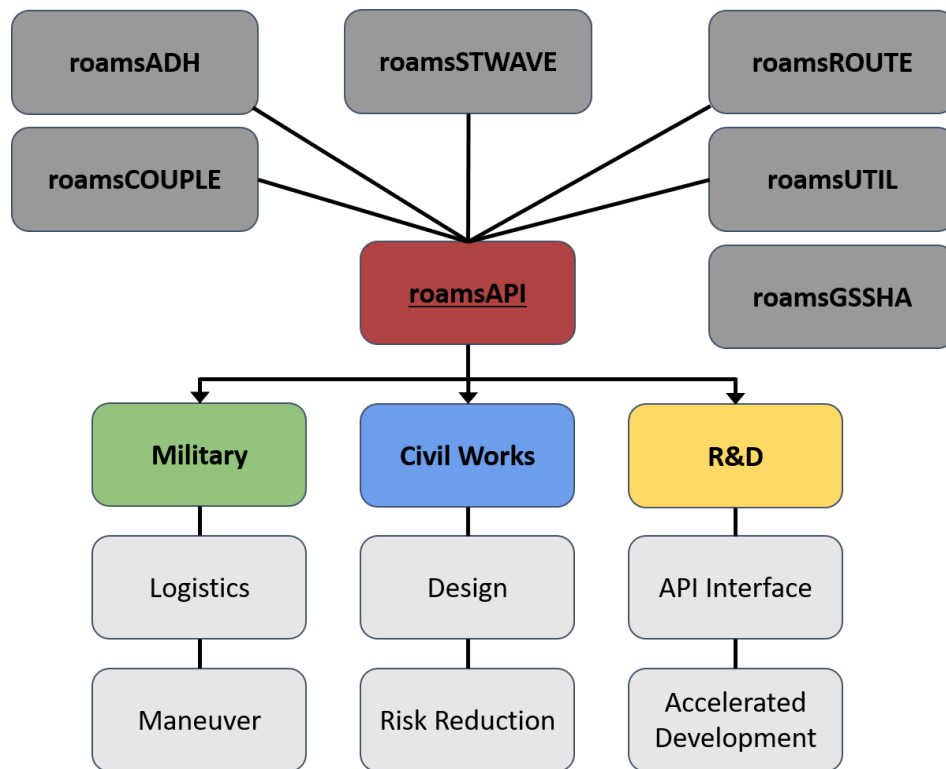
Figure 4: Structure of ROAMS and its component APIs. The ability to use ROAMS across various business areas is illustrated with use cases within each area.

Examples

AutoMesh: roamsUTIL contains the AutoMesh tool that automatically creates triangular finite-element meshes without human interaction. The procedure detects the boundary of a point cloud to filter the elements of a Delaunay triangulation and refines the output to maintain element size constraints. AutoMesh greatly accelerates mesh creation, producing near manual quality meshes, as shown in Figure 5. More information about the performance of AutoMesh

compared to other programs, such as Aquaveo Surface Modeling System (SMS), is available in Loney et al. (Loney, Yeates, & Hargis, 2018)
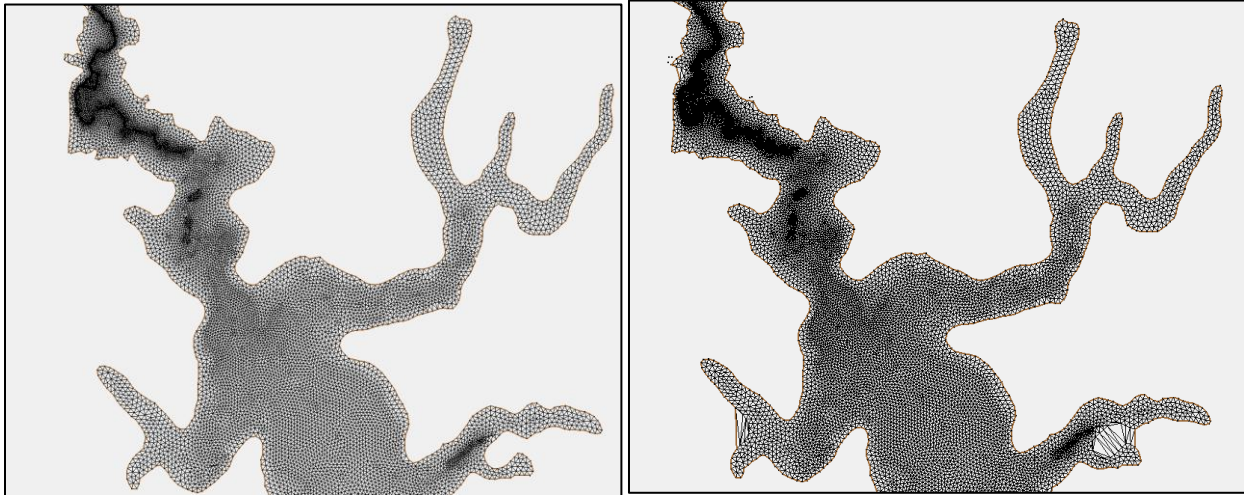
Figure 5: Demonstration of AutoMesh to create computation finite-element meshes with minimum user interaction. Left: User generated mesh created by hand. Total development time of approximately three days. Right: AutoMesh generated mesh without user interaction. Total development time of approximately ten minutes.

AdH Models: roamsADH provides a means to script the process of creating AdH models. This allows models to be generated following a fixed workflow for arbitrary domains. The capability has been broadly applied for such cases as parametric runs. The example below, Figure 6, leverages the use of roamsADH for handling of the model data along with an additional package, EarthSim which provides visualization tools. ("EarthSim — EarthSim 0.0.1 documentation," 2019) This workflows illustrates use of roamsADH for automated dam break modeling, allowing watersheds to be selection, boundary conditions to be calculated, and inundation to be forecast for multiple pool elevations with minimal user input.

Vessel Routing: roamsRoute gives the capability to forecast vessel movements through a region based on the hydraulic and vessel properties. This allows military planners to forecast accessible regions and determine vessel transit times. This is particularly helpful in regions with rapidly changing conditions or in areas unfamiliar to vessel pilots. Figure 7 demonstrates an example maneuverability analysis conducted in a coastal metropolitan area. (Loney et al., 2018)
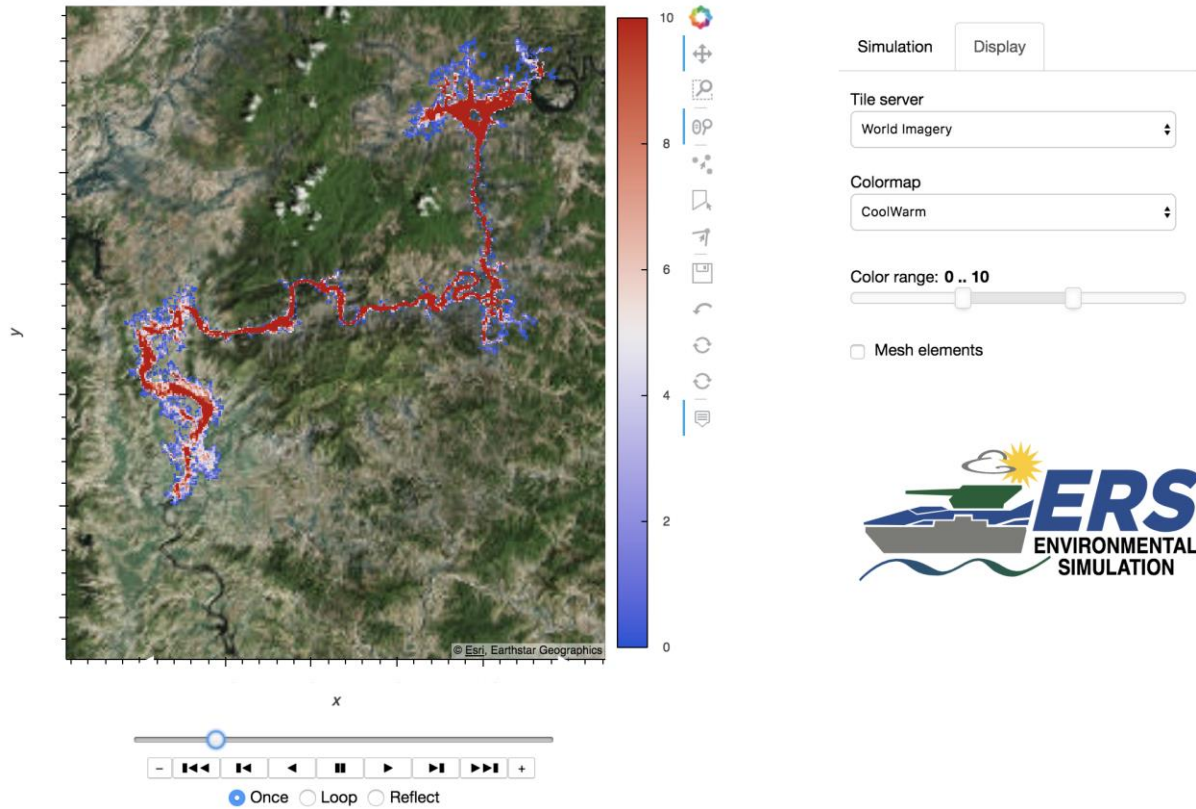
Figure 6: Web-based visualization tool for rapid dam break analysis. This workflow utilizes roamsADH for model creation combined with EarthSim visualization tools to display model output.
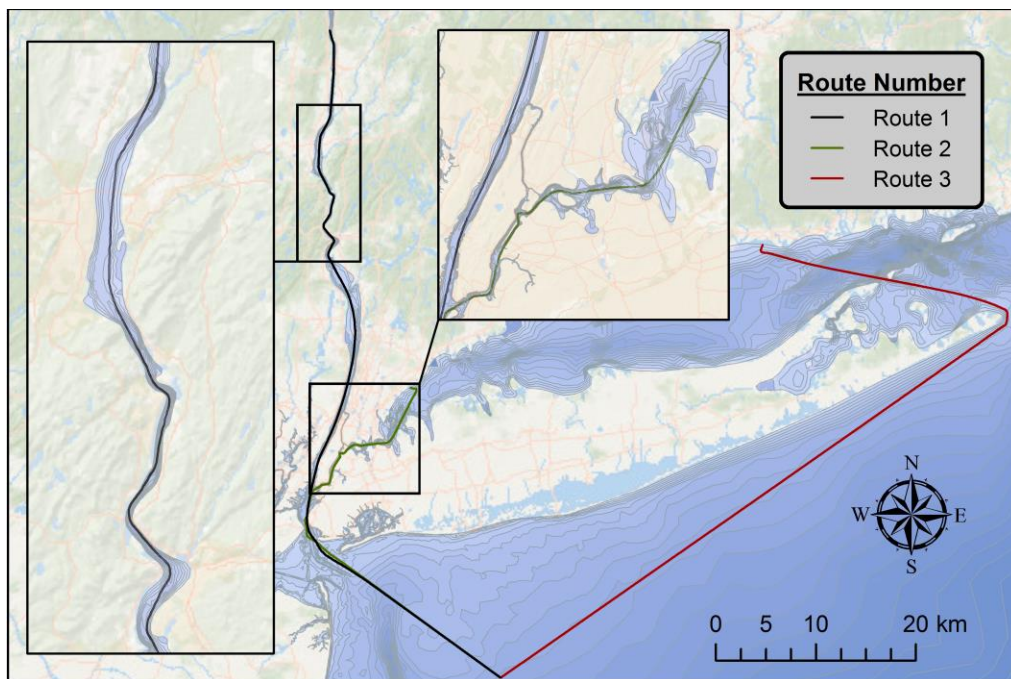
Figure 7: Output of roamsROUTE for a vessel routing analysis. The user specifies the desired entry and landing positions, with roamsROUTE determining whether a route between the locations exists and, if so, the best route between locations based on vessel characteristics.

Conclusion

This paper highlighted ongoing development of scientific APIs by the USACE ERDC for environmental modeling. It highlighted two API platforms, Quest and ROAMS, which facilitate data acquisition and management as well as environmental model creation. The components of each platform were given and example use cases discussed.

The USACE ERDC intends to maintain and expand the Quest and ROAMS APIs. Future development of Quest will focus increasing the number of data sources available through the platform. Additional improvements will also be made to the data preprocessing operations to further reduce user effort. Future ROAMS development will focus on complete incorporation of roamsGSSHA as a stand-alone package and within roamsCOUPLE. Attention will also be given to automating boundary condition specification to facilitate common workflows.

It is anticipated that both Quest and ROAMS will be developed in combination with the EarthSim platform also being developed by the USACE ERDC. EarthSim is a set of Python based tools for specifying, launching, visualizing, and analyzing computational models. EarthSim has developed capabilities within the SciPy and PyViz projects for working with large datasets using open source tools. Quest and ROAMS both currently utilize EarthSim for data visualization and workflow generation. It is anticipated that the dependencies will become stronger among these three projects as they grow together into a robust open source modeling platform.

References

Coastal and Hydraulics Laboratory. (2015, December 7). The Adaptive Hydraulics (AdH) Modeling System. Retrieved December 7, 2015, from Coastal and Hydraulics Laboratory, US Army Corps of Engineers website: http://adh.usace.army.mil/new_webpage/main/main_page.htm

Coastal and Hydraulics Laboratory. (2019, January 15). Steady State Spectral Wave. Retrieved July 17, 2016, from Engineer Research and Development Center website: https://www.erdc.usace.army.mil/Media/Fact-Sheets/Fact-Sheet-Article-View/Article/476716/steady-state-spectral-wave/

EarthSim — EarthSim 0.0.1 documentation. (2019, January 15). Retrieved January 15, 2019, from http://earthsim.pyviz.org/

GsshaPy Documentation — GSSHAPY 2.3.7 documentation. (2019, January 15). Retrieved January 15, 2019, from https://gsshapy.readthedocs.io/en/latest/

Loney, Drew A., Yeates, E. M., & Hargis, B. H. (2018). *Automatic mesh generation and element filtering : the AutoMesh tool* (REPORT No. ERDC/CHL CHETN-VI-47). http://dx.doi.org/10.21079/11681/26530

Loney, Drew Allan, Pevey, K. C., McAlpin, J. T., Nelsen, B. W., & Hargis, B. H. (2018). Rapid Operational Access and Maneuver Support platform for military logistics and operation planning in water environments. *Journal of Defense Modeling and Simulation: Applications, Methodology, and Technology*, 11. https://doi.org/10.1177/1548512918772028

Loney, Drew Allan, Pevey, K., McAlpin, J., Nelsen, B., & Hargis, B. (2017). *Rapid Operational Access and Maneuver Support (ROAMS) platform for improved Military logistics lines of communication and operational vessel routing* (No. ERDC/CHL CHETN-IX-45). https://doi.org/10.21079/11681/22642

Michener, W. K., Allard, S., Budden, A., Cook, R. B., Douglass, K., Frame, M., … Vieglais, D. A. (2012). Participatory design of DataONE—Enabling cyberinfrastructure for the biological and environmental sciences. *Ecological Informatics*, *11*, 5–15. https://doi.org/10.1016/j.ecoinf.2011.08.007

OpenCV. (2019, January 15). Retrieved January 15, 2019, from OpenCV website: https://opencv.org/

Swain, N. R., Christensen, S. D., Snow, A. D., Dolder, H., Espinoza-Dávalos, G., Goharian, E., … Burian, S. J. (2016). A new open source platform for lowering the barrier for environmental web app development. *Environmental Modelling & Software*, *85*, 11–26. https://doi.org/10.1016/j.envsoft.2016.08.003

Tolle, K. M., Tansley, D. S. W., & Hey, A. J. G. (2011). The Fourth Paradigm: Data-Intensive Scientific Discovery [Point of View]. *Proceedings of the IEEE*, *99*(8), 1334–1337. https://doi.org/10.1109/JPROC.2011.2155130

Development of a Physically-Based Distributed Watershed Scale Model

Yong G. Lai, **Hydraulic** Engineer, Bureau of Reclamation, Denver, CO, ylai@usbr.gov
Blair P. Greimann, **Hydraulic** Engineer, Bureau of Reclamation, Denver, CO,
bgreimann@usbr.gov

Abstract

This talk presents the conceptual design, numerical methodology, and progress of a new watershed model named SRH-W. It is developed to simulate event-based runoff and soil erosion processes in order to predict sediment erosion and delivery to rivers and reservoirs. It is physically-based, process-oriented, and mesh-distributed. The model mesh can be Cartesian or polygonal; the mesh may be very coarse while fine-scale features may be represented through local mesh refinement. Terrain resolution can be finer than the mesh and is taken into account in the water storage and budget computation. The overland soil-erosion module incorporates the recent developments in sheet and rill erosion research. The presentation will focus on the methodologies of the model along with the preliminary results of a case study.

Introduction

Waterways are facing crises worldwide due to frequent occurrence of extreme weather (drought or flood), increased population (demand of water consumption), and worsening water quality (in particular, nutrient and contaminant). Many do not meet the safe water standard established for streams. In the United States, for example, over 40% of the assessed waters did not meet the water quality standard established under the 1977 Clean Water Act (NRC, 2001). This occurred even though the required level of pollution control technology was installed at point source pollution locations. The polluted waterways represented over 20,000 river segments, lakes, and estuaries, covering about 300,000 miles of rivers and shorelines and 5 million acres of lakes. The data in 2010 did not show significant improvement. The US Environmental Protection Agency (EPA) estimated that 53% of the assessed rivers and streams and 69% of the assessed lakes, ponds, and reservoirs were impaired (USEPA, 2010). The EPA Total Maximum Daily Load (TMDL) program, as a result, has become a foundation for the nation's efforts to meet the water quality standards by the states. The federal law requires that states should establish priority rankings for waters on the impaired list and develop TMDLs for them. A TMDL specifies the maximum amount of point and non-point source pollutant a water body can receive and still meet the water quality standard. By law, EPA must approve or disapprove the state lists and TMDLs. Point source loads, such as loading from sewage treatment plants, have received much attention over the years and significant reductions have been achieved. Major violations of TMDL today come primarily from non-point sources. In fact, the non-point source pollution was the primary reason that 40% of the assessed water bodies in the United States were unsafe for basic uses such as fishing or swimming (NRC, 2001). For non-point source pollution, sediment has been identified as the number one pollutant that impairs water (NRC, 2001). Most sediments in rivers, lakes, reservoirs, wetlands, and estuaries come from two sources: soil erosion from watersheds and bank erosion from streams. This shows the need to understand the sediment detachment and movement processes at the watershed scale and along the stream banks.

In addition to TMDLs, sediment supply and management are also critical to many infrastructures on the watersheds or streams. For example, sediment directly impacts the sustainable use of reservoirs due to increased sedimentation, required release for water quality reason, and aquatic and riparian habitat for endangered species. With a large number of man-made facilities and structures on the rivers in the world, the sediment supply, movement and storage can only be measured at limited locations and over a limited time period. Few feasible ways are available to obtain the sediment delivery information in ungauged, non-point source areas. Further, the future impacts of manmade projects are difficult to estimate as historical data are limited. Therefore, there is a wide range of needs for the use of numerical models that are becoming important alternatives. Numerical models may provide additional watershed scale data for assessment and predict future trends and impacts due to implemented projects. Hydrological watershed models have been routinely used by project managers and engineers to assess and evaluate the impact of watershed management and mitigation strategies as well as the impact of floods on facilities. There is little disagreement regarding the usefulness of watershed scale numerical models for understanding hydrologic systems and erosion and sediment transport issues (Sharika et al., 2000). Numerical modeling is widely utilized as a complementary research methodology to theory and experiment (Post and Votta, 2005).

Another potential use of watershed models is for flood prediction. Due to climate change, extreme hydrologic events will likely be more frequent than before. An estimate by the European Environment Agency (EEA, 2010) found that floods have led to 1,126 deaths and 60 billion Euro economic loss in Europe alone between 1998 and 2009. This category of watershed model usage is gaining attention in recent years as the interest in developing flood forecasting and warning systems has increased. For example, the European Commission launched the development of a pan-European Flood Awareness System to improve disaster risk management through early warning (Bartholmes et al., 2009).

Many watershed models have been developed in the past and a large body of literature exists. Reviews have been reported by, e.g., Ewen et al. (2000), Daniel et al. (2010), Devi et al. (2015), Mello et al. (2016), and Lai et al. (2019). Review and discussion of existing models are omitted herein. Despite continuing advances in watershed modeling, however, the ability to predict multi-year hydrologic responses in large-scale watersheds is still limited as most models are primarily developed for agricultural uses. In this study, a new watershed model, SRH-W, will be developed which is an extension of the river simulation model of SRH-2D (Lai, 2010). The model will incorporate the current runoff and soil erosion research results and address some limitations of the existing models. Key SRH-W features are as follows:

- An event-based, process-oriented, and mesh-distributed watershed model for runoff and soil erosion simulation;
- Initial application targets are for flood prediction and sediment delivery to streams and reservoirs owing to a relatively large precipitation event although the model theory is generally applicable to many other applications;
- Applicable to both small and large watersheds;
- Use of special meshing technology allowing both coarse and refined mesh simulations;
- Finite-volume discretization method, explicit and implicit schemes, and diffusive wave routing equation;
- Flexibility to use different erosion models: both empirical and processes-based soil erosion models.

The Numerical Model

The spatial representation of a watershed needs to be specified first with a watershed model. SRH-W adopts the meshed approach so that model parameters, variables and governing equations of the underlying physical processes may be represented on the mesh. The meshed approach is most flexible in watershed model applications. Almost all model parameters and state variables may represented and stored in the Geographical Information System (GIS), and they may be easily mapped onto the mesh for modeling. The meshed model, however, needs to solve more sophisticated process-based governing equations which may potentially increase the computing time.

SRH-W is designed to simulate a wide range of watershed sizes, from small (<10 km²) to large (>1,000 km²). For small watersheds, a fine-resolution mesh may be used; detailed local process features may be represented using the first principle governing equations. For large watersheds, a coarse-resolution mesh may be used; parameterized relationships from large-area-averaged data may be used for selected processes. This dual-scale model capability means that appropriate mathematical equations should be selected for the relevant spatial scale of the watershed, along with the associated model parameters. SRH-W consists of the following modules: terrain, atmospheric forcing, land use (vegetation), soil type, infiltration, overland runoff, overland erosion, and channel network. Only selected overland processes are discussed below.

The terrain module reads and processes the watershed terrain information for the spatial representation of a watershed. Terrain data of the finest possible resolution is used by SRH-W. First, a mesh is generated to represent the spatial features such as terrain, land use, soil type, etc. Two meshing options are offered: the polygonal mesh and the Cartesian mesh. The polygonal mesh adopts the method of SRH-2D (Lai, 2010). The benefit of the polygonal mesh is that different spatial resolution may be used in different zones; a primary drawback is that the solution algorithm is complex leading to increased computing time. The Cartesian mesh adopts the rectangular or square mesh cells. This mesh is generated automatically based on the user inputs of the watershed boundary, breaklines, hard points, and the mesh cell size. The Cartesian mesh has the benefit of increased computing efficiency; but the drawback is the difficulty of varied spatial resolution. Local mesh refinement will be developed to overcome this drawback. A locally refined storage (LRS) procedure is to be developed that may offer an increased accuracy when the mesh resolution is coarser than the terrain. LRS uses locally refined computation of volumes and areas of mesh cells based on the terrain data. The objective is to maintain the local volumes and flow areas even when the 2D mesh is progressively coarsened.

The mathematical equations presented below follow the same ones reported by Sanchez (2002) and details are documented in Lai et al. (2019). The overland runoff module resorts to the first principle governing equations for overland routing that transforms rainfall excess into overland flow depth. The diffusive wave equation is solved as follows:

$$\frac{\partial h}{\partial t} = \frac{\partial}{\partial x}\left(\frac{h^{\beta}}{n\sqrt{S}} \frac{\partial z}{\partial x} \right) + \frac{\partial}{\partial y}\left(\frac{h^{\beta}}{n\sqrt{S}} \frac{\partial z}{\partial y} \right) + e \tag{1}$$

In the above, h is overland flow depth (m); x, y are the Cartesian coordinates (m) projected onto the horizontal plane; t is time (s); e is rainfall excess rate (m/s) (rainfall minus the intercept,

storage and infiltration), z is water surface elevation, n is Manning's roughness coefficient, $\beta = 5/3$ is a constant, and S is computed by:

$$S = \sqrt{S_{fx}^2 + S_{fy}^2} \tag{2a}$$

$$S_{fx} = \frac{\partial z}{\partial x}; \qquad S_{fy} = \frac{\partial z}{\partial y} \tag{2b}$$

Soil eroded from an overland may come from sheet, rill erosion, and gully erosions. Only the sheet and rill erosions are considered. The detachment and sediment transport are treated as separable and independent processes. A number of sediment size classes may be used to represent the soil particles such as clay, silt, sand, and aggregates. Each soil size class is described by its density, fall velocity and percentage of presence (composition). The non-equilibrium sediment routing is adopted: sediment concentration does not equal the sediment transport capacity in transport. This is in contrast to the commonly used Exner equation method - an equilibrium model that assumes instant exchange between the transported sediment and the bed sediment. The non-equilibrium sediment routing equation is expressed on an overland as:

$$\frac{\partial AC}{\partial t} + \frac{\partial UAC}{\partial x} + \frac{\partial VAC}{\partial y} = \frac{\partial}{\partial x}\left(AD\frac{\partial C}{\partial x}\right) + \frac{\partial}{\partial y}\left(AD\frac{\partial C}{\partial y}\right) + S_C \tag{3}$$

In the above, C is volume concentration of a size class, A is the flow area per unit width (m), U and V are the flow velocity components (m/s) in x and y directions, respectively, D is dispersion coefficient, and S_C is the sediment exchange between the sediment in water and that on the bed (m/s). The sediment exchange rate is computed by:

$$S_C = E_C - D_C \tag{4}$$

where E_C is the detachment rate (m s^{-1}) and D_C is the deposition rate (m s^{-1}). The deposition rate for loose sediments in suspension is computed by:

$$D_C = ahC \tag{5a}$$

$$a = \frac{\omega}{\zeta h} \tag{5b}$$

where ω is the sediment fall velocity and ζ is the adaptation constant ranging from 0.1 to 1.0.

The detachment rate is computed by:

$$E_C = E_{Cr} + E_{Cf}$$

where E_{cr} and E_{cf} are the rates due to splash and flow runoff, respectively. Such a bi-linear relation was used by, e.g., KINEROS and CATFLOW-SED (Scherer and Zehe, 2015). The detachment rate due to rainfall and leaf drip (E_{Cr}) may be computed by the empirical equation of Wicks and Bathurst (1996) that was adopted by SHETRAN.

The flow runoff rate (E_{Cf}) may adopt several approaches. The first is the shear stress based method that uses the rate equation of Ariathurai and Arulanandan (1978). The second is the

velocity based method adopting the modified Kilinc-Richardson equation (Julien, 1998; Velleux et al., 2005). And the third is the unit stream power based method (Yang, 1996).

Results and Discussion

SRH-W is still under development to achieve its full capabilities. At present, only a preliminary version has been completed with a number of test cases. In this paper, model verification is reported using a set of measured data at the Goodwin Creek Experimental Watershed located in Panola County, Mississippi. The model domain for this watershed has a size of 21.3 km², and is situated in the bluff hills of the Yazoo River basin of northern Mississippi. The watershed is under research management by the National Sedimentation Laboratory, Agricultural Research Service. The current preliminary SRH-W can solve the diffusive wave equation on a Cartesian or hybrid quadrilateral-triangle mesh with explicit or explicit time discretization scheme. Capabilities such as the local mesh refinement and LRS (locally refined storage) are yet to be developed.

The digital elevation model (DEM) at the 30-meter resolution was used and processed to obtain a depressionless DEM by Sanchez (2002). The channel network was delimited from the smoothed 30-meter DEM as shown in Figure 1a. These data were made available to us in the model testing of the present study. Note that the channel network routing is carried independent of the 2D overland runoff and the coupling between the two is achieved with a one-way approach as described in Sanchez (2002). The water runoff simulation is carried out first and is discussed next.

The storm event that occurred on October 17, 1981 is simulated. The storm started at 9:19pm and lasted for 4.8 hours. Precipitation data were recorded by rain gages distributed within the watershed and the rain data from a total of sixteen gages are used (the locations of the sixteen rain gages are plotted in Figure 1a). Input data include DEM, channel network geometry and hydraulic properties, rainfall intensity at sixteen gages, soil type and land use class maps and the associated infiltration, Manning's roughness coefficients and rainfall interception parameters. For a more detailed description of the input data, the reader is referred to Sanchez (2002) who simulated the same event using the CASC2D model. No attempt has been made in this study to calibrate the input parameters to fit the measured data. Comparisons between the model results and the measured data are mostly at the six outlet locations shown in Figure 1b.

(a) Model domain, channel network and rain gages

(b) Six outlet locations
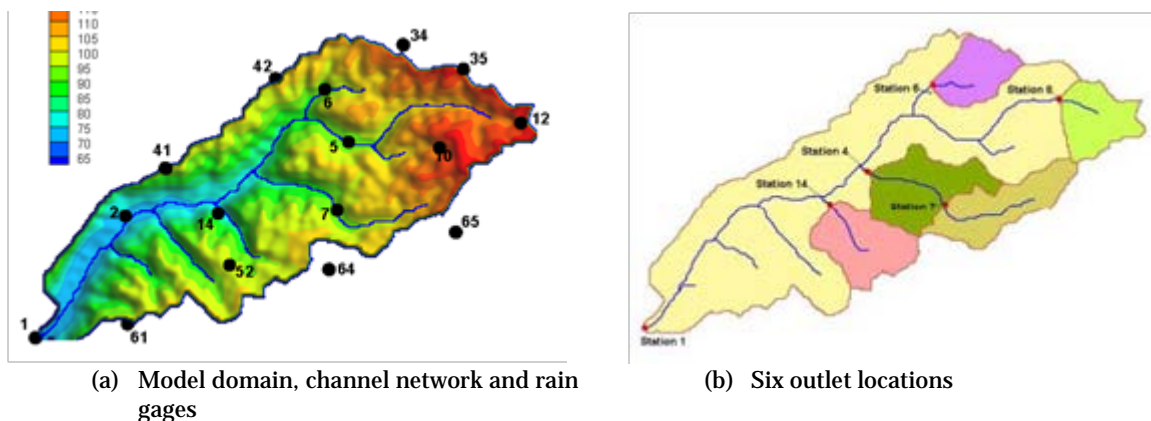
Figure 1. General information of the Goodwin Creek Watershed

Four model options are used to simulate the runoff event; they are the Cartesian mesh with a spatial resolution of 30 meters with both the explicit and implicit schemes and the hybrid quadrilateral-triangle mesh with both the explicit and implicit methods. The results of CASC2D by Sanchez (2002) are also reproduced for comparison with the SRH-W results. Note that CASC2D model is limited to the Cartesian square mesh and the explicit solver only.

The flow hygrograph results from the Cartesian mesh are compared with the measured outlet data in Figure 2. The SRH-W explicit and implicit model results are found to be almost the same (so only one curve plotted in Figure 2.), which demonstrates that the discretized equations are solved correctly by both solvers. It is noted that a significant under-prediction of the peak runoff occurs at outlet 6 and 14. The two are the smallest sub-watersheds (see Figure 1b) and the under-prediction may be attributed to the inaccuracy of the precipitation input and the delineated channel network.

(a) Outlet 1

(b) Outlet 14
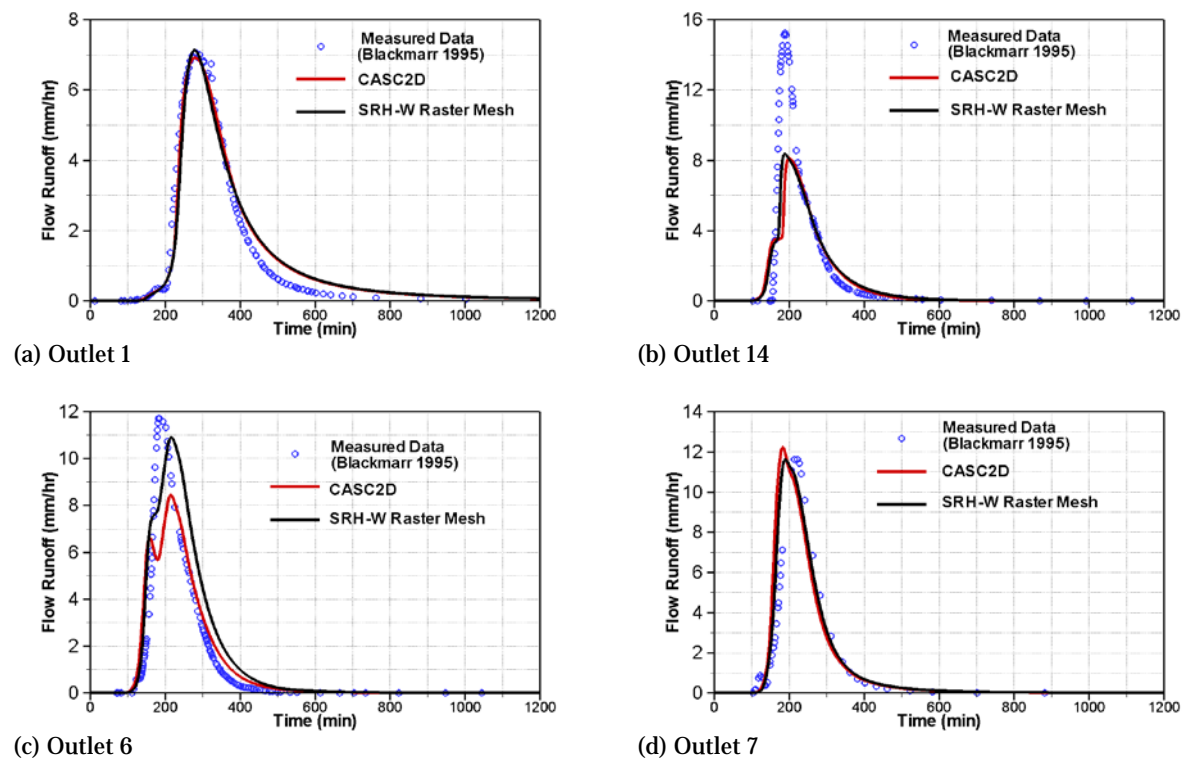
(c) Outlet 6

(d) Outlet 7

Figure 2. Comparison of results with the Cartesian mesh

Next, the flow runoff results from the hybrid mesh are compared (Figure 3). The predicted runoff hydrograph at the watershed exit (Outlet 1) deviates significantly from the measured data although the comparisons at other outlets are good. This discrepancy is not the failure of the model; it is caused by the difference in channel representation. The channel network is represented with the overland mesh cells by CASC2D. The channel is thus represented by a zigzag 2D cells which artificially lengthens the channel length. The hybrid mesh, however, follows the natural channel network longitudinally without distortion. If the channel network longitudinal length of the hybrid mesh is arbitrarily increased to match the length used by CASC2D, it is confirmed that the runoff at Outlet 1 is almost the same between the two meshes. This shows that the channel representation of the Cartesian mesh needs to be modified. In addition, it suggests that the calibrated channel Manning's coefficient used with the CASC2D modeling is based on the longer channel length, which is incorrect. The Manning's coefficient

should be re-calibrated with the hybrid mesh modeling. This would show that the coefficient should be 0.06 instead of 0.035. New SRH-2D hybrid mesh results are shown in Figure 4 with the new Manning's coefficient. It is seen that the agreement between the two meshes is much closer. The difference at Outlet 6 may be due to the difference of mesh size and resolution within that sub-watershed. The roughness coefficient of 0.06 is probably a realistic value as the same roughness coefficient was calibrated and used by Langendoen (2000) in applying the 1D CONCEPTS model to the channels of the Goodwin Creek watershed.

(a) Outlet 1

(b) Outlet 14
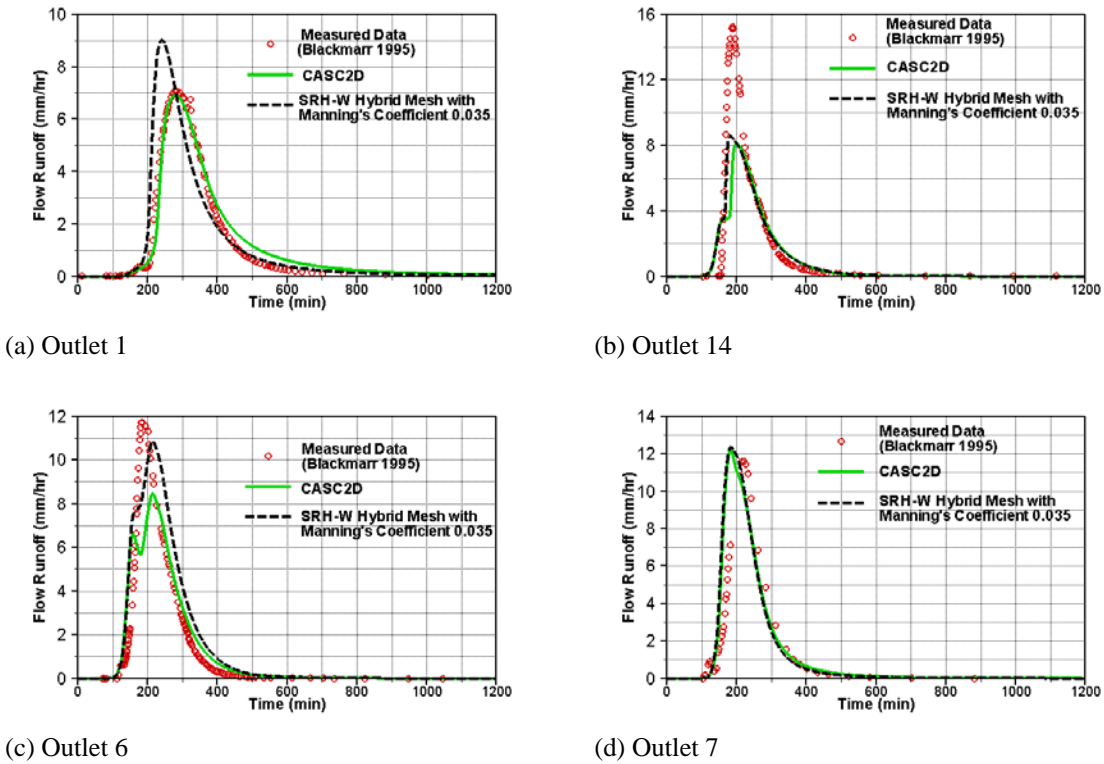
(c) Outlet 6

(d) Outlet 7

Figure 3. Comparison of results with the hybrid mesh (n=0.035).

(a) Outlet 1

(b) Outlet 14
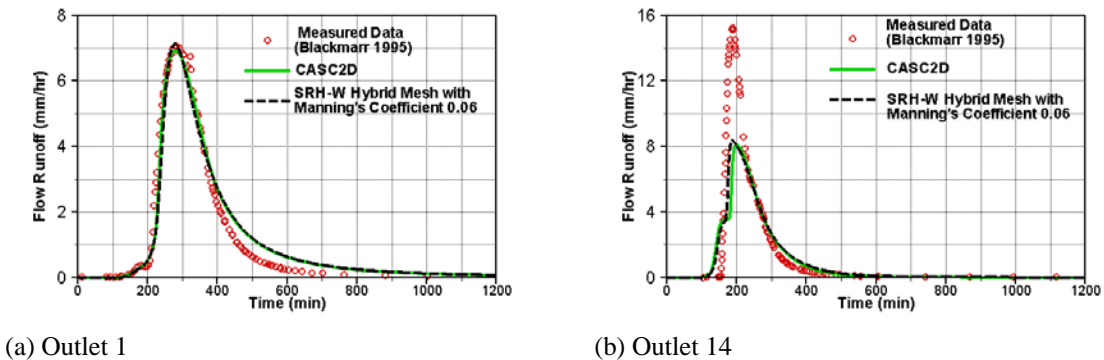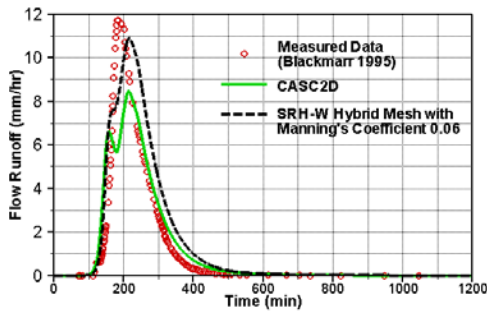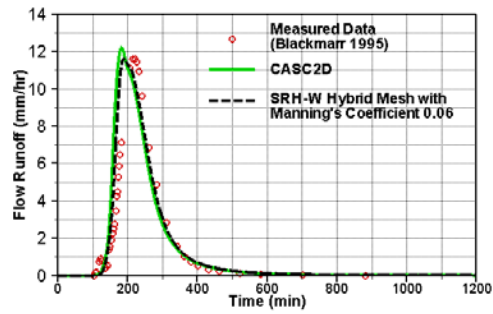
(c) Outlet 6   (d) Outlet 7

Figure 4. Comparison of results with the hybrid mesh (n=0.060).

Finally, soil erosion and sediment transport are also simulated. The simulated and measured sediment discharge rates are compared in Figure 5. The simulated sediment transport rates by SRH-W are similar to CASC2D, as essentially the same input parameters and the same transport capacity equations have been used. In comparison with the measured data, it is noted that significant under-prediction at outlets 7 and 14 is observed. The reason is unclear and possibilities may be various. One reason may be that bank erosion and mass failure in the channel or gully erosion on the sub-watershed may have occurred that are not simulated by the model.
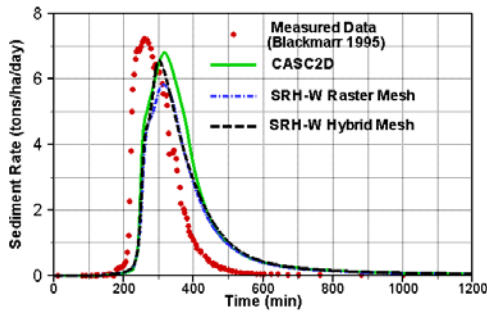
(a) Outlet 1   (b) Outlet 14
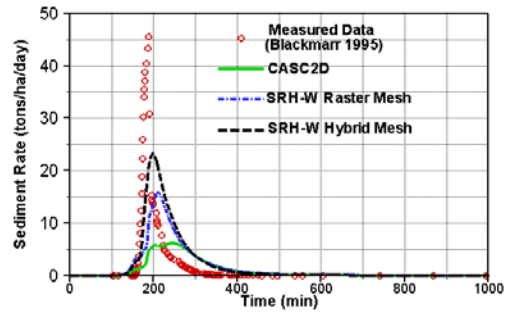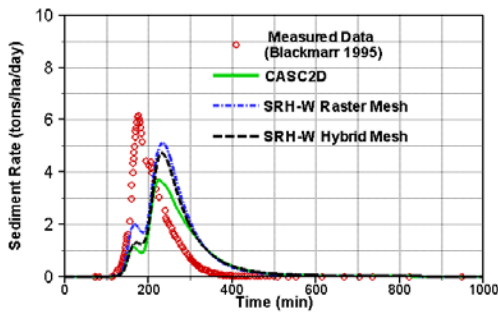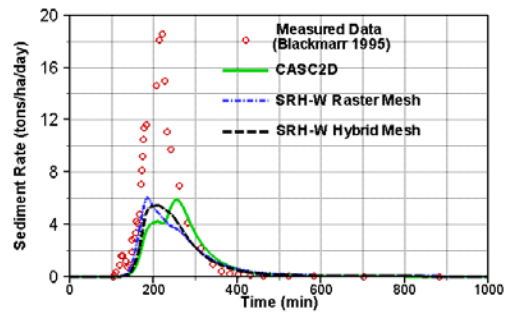
(c) Outlet 6   (d) Outlet 7

Figure 5. Comparisons of sediment rates at four outlets.

Conclusion

An event-based, processes-oriented, mesh-distributed runoff and soil erosion watershed model is developed. The preliminary results show that the model works well as intended. The Cartesian mesh may potentially be efficient but the channel network representation has to be redesigned for modeling accuracy. The hybrid mesh is accurate and robust but the simulation time is larger than the Cartesian mesh. In future, new capabilities will be developed. Primary developments include the use of the local mesh refinement with the Cartesian mesh, local refined storage technique by which the finer terrain data may be used even when the model mesh is coarse, and the development of a new channel network solver that is based on the dynamic wave equation.

References

Ariathurai, R. and Arulanandan K. 1978. "Erosion Rates of Cohesive Soils," *J. Hydraulics Division*, **104** (2), 279-283.

Bartholmes, J.C., Thielen, J., Ramos, M.H., Gentilini, S. 2009. "The European flood alert system EFAS - part 2: statistical skill assessment of probabilistic and deterministic operational forecasts," *Hydrology and Earth System Sciences*, **13**(2), 141-153.

Blackmarr, W. A. 1995. Documentation of Hydrologic, Geomorphic, and Sediment transport Measurements on the Goodwin Creek Experimental Watershed, Northern Mississippi, for the Period 1982-1993 - Preliminary Release, *Research Report No.3 (CD-ROM),* U.S, Dept. of Agriculture. Agricultural Research Service.

Daniel, E.B., Camp, J.V., LeBoeuf, E.J., Penrod, J.R., Abkowitz, M.D., and Dobbins, J.P. 2010. "Watershed Modeling Using GIS Technology: A Critical Review," *Journal of Spatial Hydrology*, **10**(2), 13-28.

Devi, G.K., Ganasri, B.P. and Dwarakish G.S. 2015. "A review on hydrological models," *Aquatic Procedia*, **4**, 1001-1007.

EEA. 2010. Mapping the Impacts of Natural Hazards and Technological Accidents in Europe: an Overview of the Last Decade. EEA Technical Report. European Environment Agency, Copenhagen, 144.

Ewen, J., Parkin, G. and O'Connell, P.E. 2000. "SHETRAN: Distributed river basin flow and transport modeling system," *J. Hydrologic Engineering*, **5**(3), 250-258.

Julien, P.Y. 1998. *Erosion and Sedimentation* (First Paperback Edition). Cambridge University Press, Cambridge, UK, pp.280.

Lai, Y.G. 2010. "Two-dimensional depth-averaged flow modeling with an unstructured hybrid mesh," J. Hydraulic Engineering, 136(1), 12-23.

Lai, Y.G., Greimann, B.P., and Politano, M. 2019. Watershed Erosion Modeling: Literature Review and SRH-W Design, Project Report ENV-2019-034, Technical Service Center, U.S. Bureau of Reclamation.

Langendoen, E. J. 2000. CONCEPTS – Conservational channel evolution and pollutant transport system: Stream corridor version 1.0. Research Report No. 16, US Department of Agriculture, Agricultural Research Service, National Sedimentation Laboratory, Oxford, MS.

Mello, C.R., Norton, L.D., Pinto, L.C., Beskow, S. and Curi, N. 2016. "Agricultural watershed modeling: a review for hydrology and soil erosion processes," Ciência e Agrotecnologia, 40(1), 7-25.

NRC, National Research Council. 2001. Assessing the TMDL Approach to Water Quality Management. Committee to Assess the Scientific Basis of the TMDL Approach to Water Pollution Reduction. National Academy Press, Washington, D.C.

Post, D.E. and Votta, L.G. 2005. "Computational science demands a new paradigm," *Phys. Today*, **58**(1), 35−41.

Sanchez, R. R. 2002. GIS-based Upland Erosion Modeling, Geovisualization and Grid Size Effects on Erosion Simulations with CASC2D-SED, Ph.D. Thesis, Civil Engineering, Colorado State University, Fort Collins, CO.

Sharika, U., Senarath, S. Ogden, F.L., Downer, C.W. and Sharif, H.O. 2000. "On the Calibration and Verification of Two-Dimensional, Distributed, Hortonian, Continuous Watershed Models," *Water Resources Research*, **36**(6), 1495-1510.

Scherer, U. and Zehe, E. 2015. "Predicting land use and soil controls on erosion and sediment redistribution in agricultural loess areas: model development and cross scale verification," *Hydrology and Earth System Sciences*, **12**, 3527−3592, doi:10.5194/hessd-12-3527-2015.

USEPA. 2010. National summary of impaired waters and TMDL information. U.S. Environmental Protection Agency. Washington, D.C.. Report available at: http://iaspub.epa.gov/waters10/attains_nation_cy.control?p_report_type=T

Velleux, M.L., England, J.F. and Julien, P.Y. 2005. *TREX Watershed Modeling Framework User's Manual: Model Theory and Description*. Colorado State University, Dept. Civil and Environmental Engineering, Fort Collins, CO.

Wicks, J. M., and Bathurst, J.C. 1996. "SHESED: A Physically Based, Distributed Erosion and Sediment Yield Component for the SHE Hydrological Modeling System," *J. Hydrology*, **175**, 213-238.

Yang, C.T. 1996. Sediment Transport: Theory and Practice. McGraw-Hill Book Company, New York.

Evaluating Riparian Vegetation Roughness Computations in the One-Dimensional HEC-RAS–RVSM Model

Zhonglong Zhang, PhD, PE, PH, Research Professor, Department of Civil and Environmental Engineering, Portland State University, Portland, OR 97207, e-mail: zz3@pdx.edu

Abstract

From the immense body of vegetative roughness literature, eleven computation equations have emerged with generic applicability and incorporated into the riparian vegetation module (RVSM) coupled with the one-dimensional HEC-RAS model. To evaluate the performance and applicability of eleven vegetation roughness equations, the HEC-RAS-RVSM model was applied to predict river stages of the San Joaquin River reach with dense and diverse riparian vegetation. Among eleven roughness equations, the Freeman et al. clearly overestimates the Manning's n values for the flow depth greater than its original experimental flow depth (1.5m). Whittaker et al. (2015) considers the reconfiguration of flexible vegetation and uses measured vegetation projected area, resulting in slightly more accurate prediction of river stage than all of the other equations. The equations of Baptist et al. (2007), Huthoff et al. (2007), and Cheng (2011), which modeled vegetation as rigid cylinders, produce identical and reasonable prediction of the river stage. Järvelä (2004) includes the impact of velocity on vegetation roughness and uses an indirect metric leaf area index to represent vegetation projected area, producing similar river stage prediction as the other equations based on a rigid cylinder analogy. Compared with manually calibrated Manning's n, the HEC-RAS–RVSM model with vegetation roughness equations is able to predict observed river stage, and performs particularly better for the flows exceeding the maximum calibration flow. The present study also demonstrates that the equations modeled vegetation as rigid cylinders are applicable for computing dynamic n values in 1D hydraulic simulation for the areas where most of the riparian vegetation is not fully submerged and dominated by trees and shrubs.

Introduction

Riparian vegetation on the floodplains has significant ecological functions in providing critical habitat, stabilizing the river bank and improving water quality through intercepting nutrients and contaminants (Naiman, 2005). On the other hand, vegetation increases local hydraulic roughness, exert additional drag force and thus may intensify flooding (Augustijn et al., 2008; Luhar and Nepf, 2013; Stone et al., 2013). The trade-off between flood and ecological management underlines a need to predict dynamic channel resistance and vegetation Manning's roughness coefficient (n) values in river hydraulic modeling studies. Vegetation roughness is generally spatially and temporally dynamic and is highly dependent on the distribution and physical properties of vegetation as well as hydraulic conditions such as flow depth and velocity (Acrement and Schneider, 1989; De Doncker, 2009). In river hydraulic modeling, it has always been a challenge to calibrate and determine hydraulic roughness resulting from riparian vegetation (Stone et al., 2013).

A large number of numerical equations have been developed to estimate hydraulic roughness of vegetated rivers in terms of Manning's n. Hession and Curran (2013) provide a comprehensive

literature review of trends and research in the topic of vegetation-induced roughness in fluvial systems. From the immense body of vegetative roughness literature, eleven roughness quantitative equations listed in Table 1 have emerged with generic applicability. Some of these equations are developed based on laboratory or field experiments (Wu et al., 1999; Freeman et al., 2000). Most equations (Fischenich, 2000; Järvelä, 2004; Baptist et al., 2007; Huthoff et al., 2007; Cheng, 2011; Luhar and Nepf, 2013; Whittaker et al., 2015) are theoretically derived from the force balance of a control volume of water in which gravitational force in the flow direction is equal to the drag force of vegetation and of the bed. For simplicity, Baptist et al. (2007), Huthoff et al. (2007), and Cheng (2011) modeled vegetation plants as uniformly distributed rigid cylinders. The flow resistance of leaves and branches is neglected and only resistance of stems is taken into account in their equations. Theoretically, these equations are applicable for trees and shrubs with few leaves and branches or for leaves and branches that are not submerged. Järvelä (2004) introduced a stream ordering scheme into trees to estimate the frontal area of stems and branches for leafless trees and shrubs. Fischenich (2000) and Whittaker et al. (2015) included a measured frontal projected area of the vegetation. Järvelä (2004) and Jalonen et al. (2013) used leaf area index (LAI) as an alternative to the frontal projected area. Järvelä (2004) and Whittaker et al. (2015) introduced the Vogel exponent, ψ, of velocity into their drag force equations. Additional mechanical properties of vegetation were included into equations of Freeman et al. (2000), Kouwen and Fathi-Moghadam (2000), Whittaker et al. (2015), and Kouwen and Li (1980).

Table 1. Vegetation roughness equations and associated parameters

Roughness equation	Suitability	Physical property of vegetation						Hydraulic metrics			Parameters	
		Plant density	Plant height	Stem diameter	Canopy height & width	Stiffness	LAI	Depth	Velocity	Energy slope	Drag coeff	Vogel exp
Huthoff et al., 2007	Tree, shrub	√	√	√				√			√	
Cheng, 2011	Tree, shrub	√	√	√				√			√	
Baptist et al., 2007	Tree, shrub	√	√	√				√			√	
Järvelä, 2004 (leafy)	Emergent tree, shrub		√				√	√	√		√	√
Järvelä, 2004 (leafless)	Emergent tree, shrub	√	√	√				√				
Freeman et al., 2000	Tree, shrub	√	√		√	√ (E_s)		√		√		
Fischenich, 2000	Tree, shrub	√	√	√	√			√			√	
Kouwen and Fathi-Moghadam, 2000	Emergent conifer trees		√			√ (ξE)		√	√			
Luhar and Nepf, 2013	Emergent tree, shrub	√	√	√	√			√			√	
Whittaker et al., 2015	Emergent tree, shrub	√	√	√	√	√ (EI)		√	√		√	√
Kouwen and Li, 1980	Submerged grass		√			√ (MEI)		√		√		
n-UR	Submerged grass		√					√	√			

The vegetation roughness qualitative equations listed in Table 1 were integrated into HEC-RAS – RVSM model to compute spatially and temporally varying Manning's n values in hydraulic simulations. The applicability and performance of these equations in HEC-RAS – RVSM model was evaluated through the San Joaquin River case study.

Methodology

HEC-RAS–RVSM Model

The eleven vegetation roughness equations were incorporated in HEC-RAS–RVSM for computing varying Manning's *n* values in hydraulic simulations (Zhang et al. 2019). Given that the Manning's *n* values are defined at the river cross section in the 1D hydraulic model, the hydraulic model domain is first discretized into rows of slice polygons that are centered on cross sections. The number of slice polygons along the cross section is defined according to the spatial heterogeneity of local vegetation and cross-section geometry. A high-resolution polygon mesh is necessary where either river bottom is steep or vegetation distribution changes. Initial riparian vegetation information is mapped to the cross-section slice polygons through the overlay of cross-section slice polygons and vegetation mapping. The 1D HEC-RAS model computes flow depth, velocity, and energy slope for the cross section slice polygon, which are directly used in above roughness equations to estimate Manning's *n* values. In turn dynamically computed Manning's *n* values are fed back into the 1D HEC-RAS model. In HEC-RAS, computed Manning's *n* can be updated at the user defined time step during the simulation.

Riparian vegetation along the river is often diverse, probably with grass or forest on the upland and willow or cottonwood at the water's edges. Flow depth and velocity along the river cross section are also varying. The diverse vegetation distribution and flow conditions can result in highly varying Manning's *n* values within a cross section. If multiple vegetation types coexist within the cross-section slice polygon, Manning's *n* values are first computed for each vegetation type. After Manning's *n* for riparian vegetation is computed, it is added to the user-defined Manning's *n* value for bare river bed to obtain the total Manning's *n* value of the cross-section using the equation given by Acrement and Schneider (1989) and Wu (2007):

$$n = \sqrt{n_v^2 + n_b^2} , \quad n_v = \sqrt{\sum_{i=1}^{k} n_i^2}$$

where *n* is the total Manning's *n* value for a cross-section; and n_b is the Manning's *n* value for the bare river bed, n_v is the combined Manning's *n* value of all the vegetation types within the cross-section slice polygon; *i* is the *i*th vegetation type; n_i is Manning's *n* value of the *i*th type; and *k* is the total number of vegetation types.

Application and Evaluation of HEC-RAS–RVSM

Study Site:

A reach of the San Joaquin River below Friant Dam from Highway 99 to Gravelly Ford near Fresno, California (Figure 1) was chosen to evaluate the feasibility of computing dynamic Manning's *n* values in modeling vegetated channels. This reach extends 25.7 km with dense and diverse native riparian vegetation. Typical riparian vegetation communities of the southwest USA such as cottonwood forest, willow forest, oak forest, riparian scrub are distributed along this river reach (Moise and Hendrickson, 2002). As a portion of the San Joaquin River restoration program, this reach has abundant hydraulic and vegetation data available for studying riparian vegetation's impact on river hydraulics. Three hydrologic stations have been installed and operated from the early 2000s, namely Donny Bridge (DNB), Skaggs Bridge (SKB), Gravelly Ford (GRF). USGS gage station No. 11251000 (below Friant Dam) is located approximately 40 km upstream of this reach. The flows of the study reach were observed to be low and stable due to the regulation of the upstream Friant Dam. Large flood events (above 200

m³/s) occurred only in 2005, 2006, 2011 and 2017 since the establishment of the first hydrological station GRF in 2002. Water losses due to infiltration, evaporation and diversion were observed for the reach (Tetra Tech, 2013).
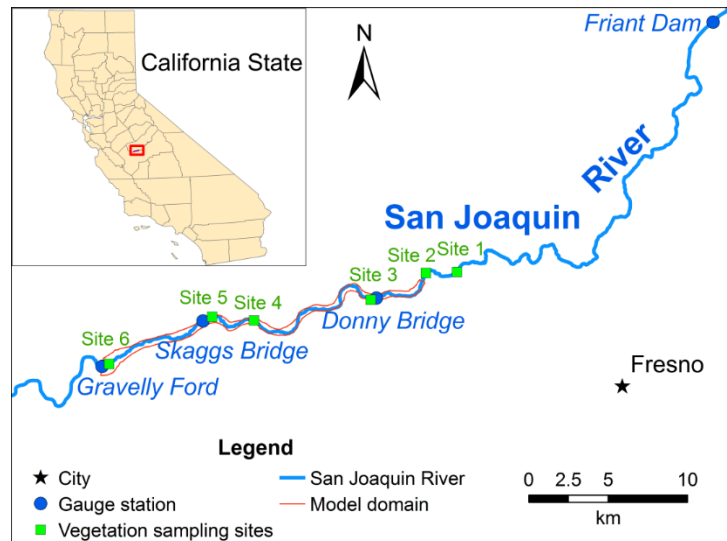
Figure 1. Study reach of the San Joaquin River

2002's vegetation map was used to represent initial spatial distribution of the vegetation communities. Previous research (Moise and Hendrickson, 2002) classified the riparian vegetation of the study reach into 28 vegetation communities based on a modified Holland system (Holland, 1986) and the work of Hink and Ohmart (1984). Six vegetation types, e.g. cottonwood riparian, mixed riparian, willow riparian/scrub, riparian scrub, invasive giant reed and herbaceous were identified from these vegetation communities. Physical properties of each vegetation community were surveyed at six sites in 2013. The measured parameters included vegetation height, stem diameter, density, and LAI. Other vegetation parameters including modulus of plant stiffness, *E,* flexural rigidity, *EI,* were not measured in the field study, their values were obtained from the literature.

Model Development and Calibration:

In the San Joaquin River HEC-RAS–RVSM model, the *n-UR* curve was used to compute Manning's *n* values for herbaceous. Seven equations for trees and shrubs were used to compute the *n* values for cottonwood, mixed riparian, willow riparian, riparian scrub and giant reed. The parameters used in the seven roughness equations were calibrated against observed river stage profiles under six flow scenarios of 2011. The six flow scenarios cover a wide range of flow rates from 16.03 to 201.62 m³/s. Each scenario was run as an independent unsteady flow simulation using a constant discharge as upstream boundary. Uniform lateral flow was included to take account of the observed water loss of the reach.

The species-dependent parameters in each vegetation roughness equation were calibrated to obtain the *best match* possible between modeled and observed profiles under all of the six flow scenarios. During the model calibration, the vegetation parameter values provided in the original roughness equation were always used as a starting point, drag coefficents were generally the primary calibration parameters while the values of Vogel exponent and reference velocity were mostly kept consistent with the original studies. The final calibration values of species-dependent parameters used in the vegetation roughness equations are given in Table 2. In addition, Manning's *n* value of the bare river bed was set to 0.035 s/m$^{1/3}$ for the entire reach

except a portion of the upper reach with 0.05 s/m$^{1/3}$. Since the vegetation field survey did not include agricultural land, river wash and disturbed, constant Manning's n values were applied: n = 0.045 s/m$^{1/3}$ for agricultural land, n = 0.03 s/m$^{1/3}$ for river wash, and disturbed, which is based on the calibration study of Gillihan (2013).

Table 2. Species-dependent parameter values in six vegetation roughness equations

Roughness equations	Vegetation type	Drag coefficient C_d	Vogel exponent ψ	Reference velocity U_χ (m/s)
Baptist et al., 2007;	cottonwood	0.5	-	-
Huthoff et al., 2007;	mixed riparian	0.7	-	-
Cheng, 2011;	willow riparian	0.5	-	-
Luhar and Nepf, 2013	riparian scrub	0.5	-	-
	arunda donax	0.5	-	-
Järvelä, 2004 (leafy)	cottonwood	0.1	-1	0.1
	mixed riparian	0.24	-0.5	0.1
	willow riparian	0.2	-1	0.1
	riparian scrub	0.2	-1	0.1
	arunda donax	0.2	-1	0.1
Whittaker et al., 2015	cottonwood	0.76	-0.8	-
	mixed riparian	0.99	-0.6	-
	willow riparian	0.88	-0.81	-
	riparian scrub	0.88	-0.81	-
	arunda donax	0.88	-0.81	-

Note: C_b in the equation of Baptist et al. (2007) was set to a large value i.e. 1000 to eliminate the contribution of river bed resistance to vegetation roughness.

Figure 2 compares river stage profiles predicted by the San Joaquin River HEC-RAS model with dynamically computed Manning's n values and observed data under the six calibration flow scenarios. The model with Manning's n computed by Freeman et al. (2000) clearly overestimates the river stages with the flows greater than 68.81 m^3/s. Nevertheless, the modeled river stage profiles from Freeman et al. (2000) as well as Järvelä (2004), Baptist et al. (2007) and Whittaker et al. (2015) match the observations under the low flow conditions (Figure 2a-b). When the discharge is low, the roughness of bare river bed is the major contributor of flow resistance because only a small fraction of riparian vegetation is submerged. Therefore, no significant difference is found among these vegetation roughness equations when they are used for simulating low flow conditions.

Besides of the overestimation of Freeman et al. (2000), the river stage profiles predicted by the model with Järvelä (2004), Baptist et al. (2007) and Whittaker et al. (2015) are remarkably similar and match the observations fairly well. The model with other three vegetation roughness equations based on a rigid cylinder analogy, e.g. Huthoff et al. (2007), Cheng (2011) and Luhar and Nepf (2013) also predicts the river profiles as good as Baptist et al. (2007), but these profiles are not necessarily presented in Figure 2. The modeled river stages are slightly lower than the observed data when the upstream flow reached 169.33 m^3/s in January 2011 (Figure 2e). According to the study of Tetra Tech (2013), the high river stage of this flow resulted from a great amount of debris captured during its initial rising limb, given that the study reach had not

experienced flows of this magnitude for years. In addition, modeled river stages deviate from the observations at few locations, for example, the most upper and lower portion of the study reach for Q = 201.62 m³/s (Figure 2f), this is presumably because spatial distribution of vegetation at these locations in 2011 changed greatly from the 2002's vegetation map used in this study.
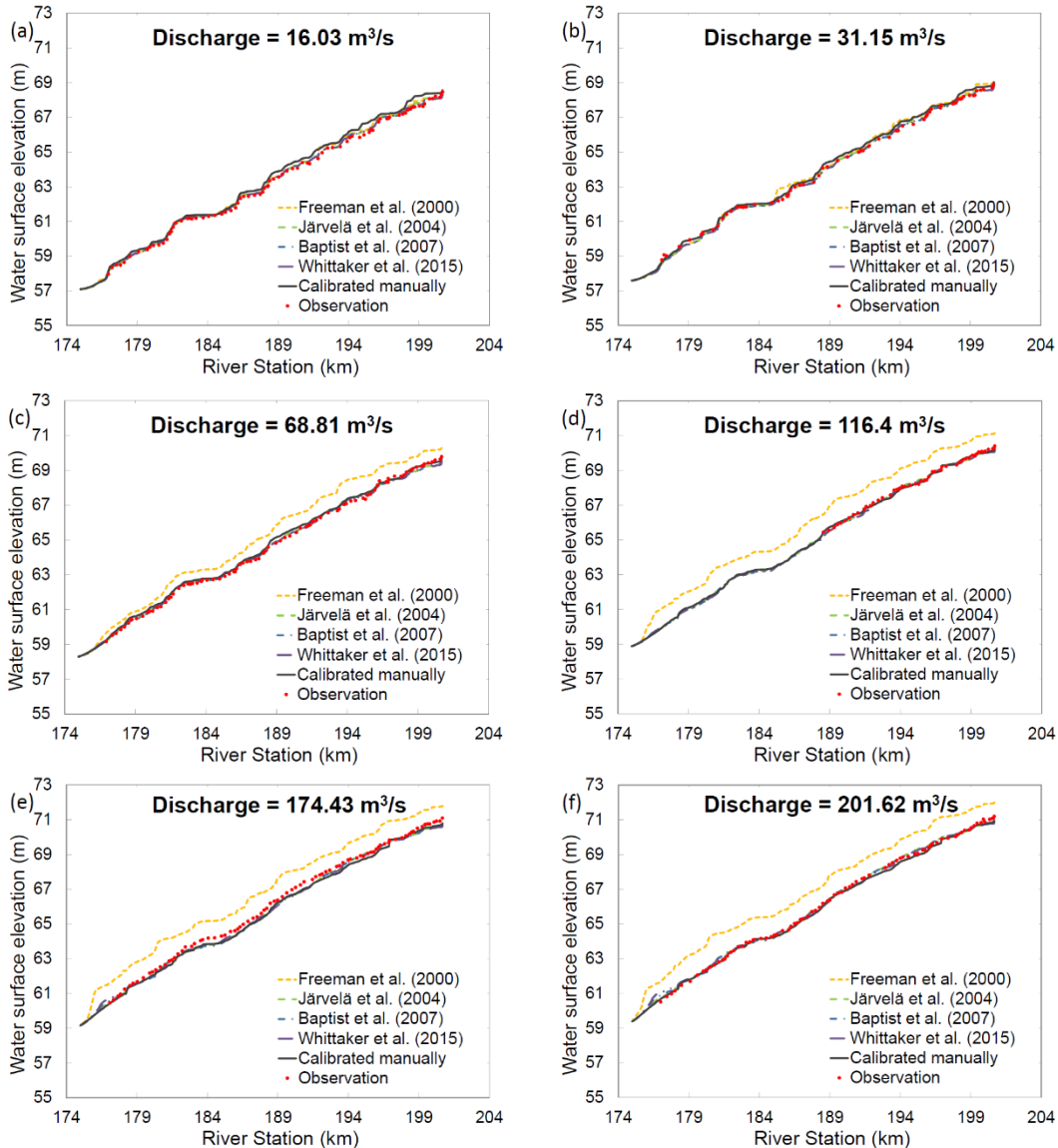
Figure 2. Observed and modeled river stage profiles by using Manning's n under six flow scenarios

Compared to the river stage profiles predicted by the HEC-RAS model with manually calibrated n values (Tetra Tech, 2013), the models integrated with vegetation roughness computation equations predict river stage profiles more accurately against observed data, particularly for the flows lower than 31.15 m³/s (Figure 2a-b). The manually calibrated model was able to reproduce observed river stage profiles for high flow conditions, but overestimated river stages under the low flow conditions. The manually calibrated Manning's n values were set too high for open water (0.035−0.056), which resulted in the larger error for the low flow conditions. This result demonstrates that the constant Manning's n values defined through the model calibration do

not work well for a wide range of flow conditions. The HEC-RAS – RVSM model has the advantage of automatically computing dynamic Manning's n values based on the varying flow conditions and vegetation dynamics.

The root mean square errors (RMSEs) between observed and modeled river stages calculated for the seven roughness equations and six flow scenarios are presented in Table 3. The first four equations modeled vegetation as evenly distributed rigid cylinders have almost the same RMSE values. That is because that most trees in the study reach were only partially submerged even under the largest flow rate, these four equations are equivalent for partially submerged trees and shrubs. The water depth increased by 2.44~3.05 m when the river flow rate increased from 16.03 m³/s to 201.62 m³/s (Figure 2). This magnitude of flows could only completely submerge the short vegetation at low elevation such as riparian scrub, willow scrub and few mixed riparian low density. Except for the equation of Freeman et al. (2000), the two equations of Järvelä (2004) and Whittaker et al. (2015) that consider vegetation flexibility, have similar RMSE values with these four equations (e.g. Baptist et al., 2007; Huthoff et al., 2007; Cheng, 2011; Luhar and Nepf, 2013) based on a rigid cylinder analogy.

Table 3. RMSEs between observed and modeled river stage profiles by using computed Manning's n

Q	16.03m³/s	31.15m³/s	68.81m³/s	116.40m³/s	174.43m³/s	201.62m³/s
Roughness equations	RMSE (m)					
Baptist et al. (2007)	0.106	0.106	0.125	0.113	0.242	0.142
Huthoff et al. (2007)	0.106	0.106	0.125	0.112	0.241	0.141
Cheng (2011)	0.106	0.106	0.125	0.112	0.237	0.139
Luhar and Nepf (2013)	0.106	0.106	0.125	0.112	0.239	0.139
Freeman et al. (2000)	0.194	0.272	0.855	1.106	1.051	1.208
Järvelä (2004) leafy	0.121	0.106	0.137	0.121	0.225	0.126
Whittaker et al. (2015)	0.113	0.110	0.126	0.121	0.231	0.148
Calibrated manually	0.322	0.199	0.164	0.094	0.251	0.207

Model Validation:

The calibrated HEC-RAS –RVSM model was validated using observed river stage hydrographs at DNB in 2011 and SKB in 2017. The RMSE between modeled and observed river stage was used to evaluate the performance of different vegetation roughness equations in hydraulic simulations. Furthermore, a HEC-RAS model originally developed by Tetra Tech (2013) with manually calibrated Manning's n values was also used to compare against the HEC-RAS – RVSM model with dynamically computed n values. Figure 3 compares HEC-RAS modeled and the observed river stage hydrograph at Donny Bridge gauge (river station 196.9 km) in 2011 and at Skaggs Bridge gauge (river station 182.6 km) in 2017. For both locations, the modeled river stage hydrographs using computed Manning's n values by Freeman et al. (2000) are approximately 1 m higher than the observations for the flows greater than 50 m³/s. The other vegetation roughness equations, in contrast, compute more reasonable Manning's n values and produce reasonable river stage predictions under most flow conditions.

The HEC-RAS model performs similarly for the validation period as it does for the calibration period at Donny Bridge gauge in 2011. Compared with manually calibrated Manning's n, the model with computed vegetation roughness predicts river stages better matching observed data under the low flow conditions. The two models predict similar river stages under the high flow conditions. Nevertheless, all the vegetation roughness equations except for Freeman et al.

(2000) under-predict Manning's *n* values for the middle flow range, 50-80 m³/s, resulting in the modeled river stage lower than the observation. The prediction error is probably caused by the fact that the channel contracted sharply at the Donny Bridge gauge and raised the local river stage. The 1D hydraulic model is not able to accurately simulate the river stage change around the complex channel geometry with bridges.
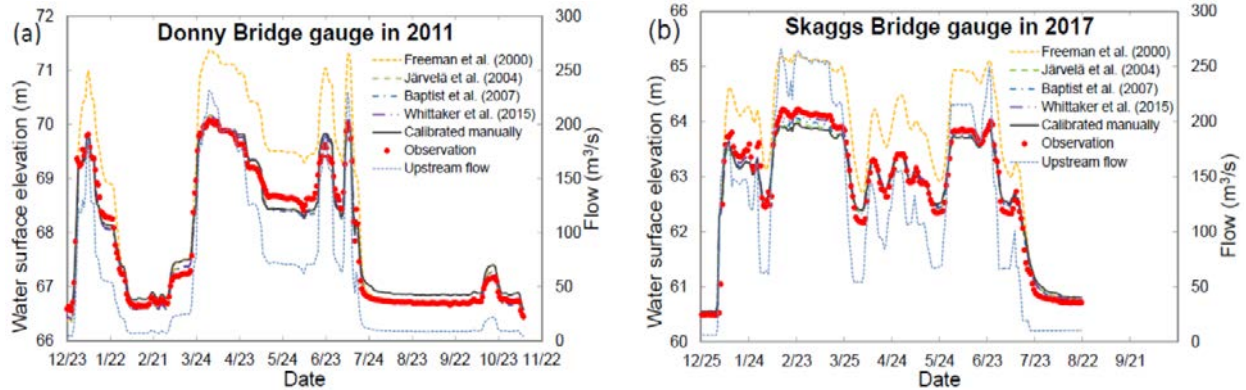
Figure 3. Observed and modeled river stage hydrographs by using computed Manning's *n* at Donny Bridge gauge (a) and Skaggs Bridge gauge (b)

The model validation result at Skaggs Bridge gauge in 2017 reveals that the HEC-RAS –RVSM model is able to predict river stages more accurately for flows higher than the maximum calibration flow (Figure 3b). The simulation of the high flood event (*Q* = 266 m³/s) in 2017 demonstrates that as river flow and water level increase, vegetation roughness also increases when most riparian vegetation has not been completely submerged yet. The manually calibrated Manning's *n* values in HEC-RAS can be spatially varying, but usually are constant, therefore, the dynamic change of vegetation roughness with flow conditions cannot be reflected in the hydraulic simulation. The constant Manning's *n* values used for the HEC-RAS model are attributed to too low river stage prediction for the high flood event in 2017. It is worth noting that although the models with dynamically computed Manning's *n* performed better, the predicted river stage for the large flood is still slightly lower than the observation (Figure 3b). This is probably because the flow resistance of leaves and branches was not considered in this study as a result of no survey data about their projected area being available. As the river stage rises to a certain level, plenty of leaves and branches of trees and shrubs start to be submerged, flow resistance caused by the submerged leaves and branches should be taken into account (Västilä and Järvelä, 2014).

According to the above validation results of the two gauges, the HEC-RAS–RVSM model with Whittaker et al. (2015) performed best among the seven roughness equations for trees and shrubs. The RMSE values of the modeled river stage hydrographs at Donny Bridge in 2011 and Skaggs Bridge in 2017 are 0.17 m and 0.19 m, respectively.

Concluding Remarks

Eleven vegetation roughness equations were integrated into the 1D HEC-RAS - RVSM model to compute dynamic roughness coefficients for hydraulic simulations. The model was then applied to a reach of the San Joaquin River for evaluating the performance and applicability of different vegetation roughness equations in 1D hydraulic modeling. The model results demonstrate that the equation of Freeman et al. (2000) clearly overestimates the Manning's *n* values for the flow depth greater than its original experimental flow (1.5m) as a result of the approximately linear

relationship of n versus R used for emergent vegetation. The equation of Whittaker et al. (2015) considers the reconfiguration of flexible vegetation and uses measured vegetation projected area and is able to predict Manning's n values and river stage more accurately than all of the other roughness equations. The four roughness equations modeled vegetation as rigid cylinders produce almost the same results and perform reasonably well in computing Manning's n values under the river flows not large enough to completely submerge most riparian vegetation. The equation of Järvelä (2004) includes the impact of velocity on vegetation roughness but uses an indirect metric LAI to represent vegetation projected area, resulting in the similar simulation accuracy with the four equations based on a rigid cylinder analogy.

Compared with manually calibrated Manning's n values, the HEC-RAS–RVSM model is able to predict river stage more accurately, particularly under the river flows larger than the maximum calibration flow. The Manning's n values computed from these equations reflect their spatial and temporal variations with vegetation distribution and flow conditions. In the study area with the same vegetation type, the vegetation closer to river centerline induces relatively higher Manning's n values due to the greater flow depth. Under the similar flow conditions the n values of mixed and willow riparian are generally larger than those of cottonwood and riparian scrub because of the higher vegetation density and stiffness. The grassland with shallow flow and low velocity can produce very large n values and result in only little conveyance. As flow and river stage increase, the model computed n values continuously increases until most riparian vegetation is fully submerged.

Through the application to the San Joaquin River reach, the following suggestions in applying these vegetation roughness equations are given. The equation of Freeman et al. (2000) might be used only for the flow depth within the range of its original experiments. The four rigid vegetation equations can be used to compute dynamic Manning's n values for 1D hydraulic modeling when most riparian vegetation is not fully submerged and dominated by trees and shrubs. The projected area of each vegetation community in the foliated and defoliated state needs to be estimated appropriately in order to get the best hydraulic simulation when applying the relatively accurate roughness equation, Whittaker et al. (2015). If vegetation field property data is not available, the equation of Järvelä (2004) that uses the LAI data from remote sensing is a feasible option to compute dynamic Manning's n values. Finally, additional data is needed to further evaluate the performance and applicability of the vegetation roughness equations in determining Manning's n values for both emergent and submerged vegetation.

Acknowledgments

References

Augustijn, D. C. M., F. Huthoff, and E. H. v. Velzen. 2008. "Comparison of vegetation roughness descriptions." *Proceedings of River Flow 2008 - Fourth International Conference on Fluvial Hydraulics*, M. S. Altinakar, M. A. Kokpinar, I. Aydin, S. Cokgor, and S. Kirkgoz, eds., Kubaba Congress Department and Travel Services, Çe¿me, Turkey, 343-350.

Baptist, M., V. Babovic, J. U. Rodríguez, M. Keijzer, R. Uittenbogaard, A. Mynett, and A. Verwey. 2007. "On inducing equations for vegetation resistance." *J. Hydraul. Res.*, 45(4),

435-450.

Cheng, N. S. 2011. "Representative roughness height of submerged vegetation." *Water Resear. Res.*, 47(8).

De Doncker, L., P. Troch, R. Verhoeven, K. Bal, P. Meire, and J. Quintelier. 2009. "Determination of the Manning roughness coefficient influenced by vegetation in the river Aa and Biebrza river." *Environ. Fluid Mech.*, 9(5), 549-567.

Fischenich, J. C. 2000. "Resistance due to vegetation." *ERDC TN-EMRRP-SR-07,* US Army Engineer Research and Development Center, Environmental Laboratory, Vicksburg, MS.

Freeman, G. E., W. J. Rahmeyer, and R. R. Copeland. 2000. "Determination of Resistance Due to Shrubs and Woody Vegetation." *ERDC/CHL TR-00-25*, Vicksburg, MS.

Gillihan, T. 2013. "Dynamic Vegetation Roughness in the Riparian Zone." Master of Science, University of New Mexico, Albuquerque, NM.

Hession, W.C., and J.C. Curran. 2013. "The impacts of vegetation on roughness in fluvial systems." In Schroder, J.F., D.R. Butler, and C.R. Hupp (Eds.), *Treatise on Geomorphology,* Vol. 12, 75-93. San Diego, CA: Academic Press.

Hink, V., and R. Ohmart. 1984. "Middle Rio Grande biological survey. Final report to the US Army Corps of Engineers No. DACW47-81-C-0015." Center for Environmental Studies, Arizona State University Tempe, AZ.

Holland, R. F. 1986. "Preliminary descriptions of the terrestrial natural communities of CA."

Huthoff, F., D. Augustijn, and S. J. Hulscher. 2007. "Analytical solution of the depth-averaged flow velocity in case of submerged rigid cylindrical vegetation." *Water Resear. Res.*, 43(6).

Järvelä, J. 2004. "Determination of flow resistance caused by non-submerged woody vegetation." *Int. J. River Basin Manage.*, 2(1), 61-70.

Jalonen, J., J. Järvelä, and J. Aberle. 2013. "Leaf area index as vegetation density measure for hydraulic analyses." *J. Hydraul. Eng.*, 139(5), 461-469.

Kouwen, N. 1988. "Field estimation of the biomechanical properties of grass." *J. Hydraul. Res.*, 26(5), 559-568.

Kouwen, N., and M. Fathi-Moghadam. 2000. "Friction factors for coniferous trees along rivers." *J. Hydraul. Eng.*, 126(10), 732-740.

Kouwen, N., and R. M. Li. 1980. "Biomechanics of vegetative channel linings." *J. Hydraul. Div.*, 106(HY6), 1085-1103.

Luhar, M., and H. M. Nepf. 2013. "From the blade scale to the reach scale: A characterization of aquatic vegetative drag." *Adv. Water Resour.*, 51, 305-316.

Moise, G. W., and B. Hendrickson. 2002. "Riparian vegetation of the San Joaquin River." Department of Water Resources, San Joaquin District, Environmental Services Section, Fresno, CA.

Naiman, R. J., H. Decamps, and M. E. McClain. 2005. *Riparia: ecology, conservation, and management of streamside communities*, Academic Press.

Stone, M. C., L. Chen, K. S. McKay, J. Goreham, K. Acharya, J. C. Fischenich, and A. B. Stone. 2013. "Bending of submerged woody riparian vegetation as a function of hydraulic flow conditions." *River Res. Appl.*, 29(2), 195-205.

Tetra Tech. 2013. "San Joaquin River and Bypass System 1-D Steady State HEC-RAS Model Documentation." Fort Collins, CO.

Västilä, K., and J. Järvelä. 2014. "Modeling the flow resistance of woody vegetation using physically based properties of the foliage and stem." *Water Resear. Res.*, 50(1), 229-245.

Whittaker, P., C. A. Wilson, and J. Aberle. 2015. "An improved Cauchy number approach for predicting the drag and reconfiguration of flexible vegetation." *Adv. Water Resour.*, 83, 28-35.

Wu, W. 2007. *Computational river dynamics*, CRC Press.

Zhang, Z., B.E. Johnson, and B.P. Greimann. 2019. HEC-RAS–RVSM (riparian vegetation simulation module), *ERDC TN-EMRRP-SR-X.* Vicksburg, MS.

Pond Inundation and Timing Model (Pond-IT) for Management of Habitat for Hydroperiod-Dependent Species

Kealie Pretzlav, PhD, Balance Hydrologics, Berkeley, CA, kpretzlav@balancehydro.com **Zan Rubin**, PhD, Balance Hydrologics, Berkeley, CA, zrubin@balancehydro.com
Eric Donaldson, PG, Balance Hydrologics, Berkeley, CA, edonaldson@balancehydro.com
Barry Hecht, Sr Principal, Balance Hydrologics, Berkeley, CA, bhecht@balancehydro.com

Abstract

In Mediterranean and arid climates, seasonal ponds play important roles for native species, whose life cycles are often timed with the annual wet-up and dry-down period, or hydroperiod. With anticipated changes in climate, existing habitat may be affected by changing air temperature or precipitation patterns. Throughout much of California, properly managed anthropogenically-formed cattle ponds have the potential to be valuable aquatic habitat for endangered and target native species. To effectively manage these resources and prioritize conservation efforts, we ask ourselves two main questions: 1) Can the aquatic feature sustain habitat for a target species in the existing configuration? and 2) Can proposed modifications or enhancements create additional habitat that is resilient to changing climates? To answer these questions, we have developed a flexible, robust, and cost-effective Pond Inundation and Timing (Pond-IT) model to quantify relative importance of hydrologic drivers of hydroperiod in ponds which could serve as valuable habitat for many species, such as native frogs, salamanders, and turtles. The water balance model infers the monthly balance between hydrologic fluxes of runoff, evapotranspiration, and groundwater, to develop a record of pond water-surface elevation. While this technique is not novel, most water-balance models require many years of monitoring data, which is expensive to acquire, especially in remote environments. In contrast, Pond-IT leverages increasingly available aerial photographs to collect model calibration remotely, which is cost-effective and can span multiple decades. Development of a hydroperiod model requires only one field visit to obtain a bathymetric survey; the remaining model inputs use publicly available datasets. POND-IT was developed using Python, an open-source programming language known for being both readable and customizable. Here we present POND-IT results for two ponds in Santa Clara County Parks. Management scenarios are simulated optimizing hydroperiod for the federally listed (threatened) California red-legged frog (CRLF), which requires pond persistence through September. Pond drying in August or September discourages predatory Bullfrog breeding, which require year-round ponding. Results quantify hydroperiod response of the ponds from 1980 to present, which includes multiple wet periods and droughts. The historical model is easily extended to model projections of climate change to understand impacts to habitat resilience in the future. Pond modifications (e.g. spillway elevation changes, re-grading pond, clay-lining, etc) are optimized and presented for the target species, in this case CRLF. The flexibility of this model means the potential for application to a wide range of global environments and target species that are hydroperiod-dependent.

Introduction

Vernal pools, stock ponds, and seasonal wetlands (generically referred to as ponds herein) offer a wide range of habitat for both plant and animal communities across California and beyond. The natural hydrologic cycles of many of these ponds has been altered by increased urbanization and changing climates, often with detrimental impacts to the associated ecosystems. In Santa Clara County, historical ranching and agricultural practices have created and preserved

perennially-wetted stock ponds which can provide ideal habitat for non-native bullfrog (*Rana catesbeiana*), a key predator of native and federally listed California Red-Legged Frog (*Rana draytonii*, CRLF). In the central valley of California, conversion of vernal pool complexes to other uses has endangered vernal macroinvertebrates (e.g. vernal pool fairy shrimp, *Branchinecta lynchi*) and rare vernal pool vegetation. The success of these specialized ecosystems is heavily dependent upon the duration of pool inundation, or hydroperiod, which is typically determined by the balance of rainfall, runoff, evapotranspiration, and groundwater fluxes.

Quantifying hydrology of a pool typically requires time-intensive monitoring to develop a model balancing these hydrologic fluxes. Effective calibration of such models is difficult to do well, as long-term monitoring is expensive, time-consuming, and acquisition of the data is rarely considered sufficiently in advance of the construction of the model. Scaled across landscapes with many pools, costs of collecting site-specific calibration data can become prohibitive.

Here, we present the Pond Inundation and Timing (Pond-IT) model which was developed to optimize hydroperiod for CRLF in stock ponds in Santa Teresa, Almaden Quicksilver, Calero, and Coyote Harvey Bear Lake Ranch, Santa Clara County, California (Donaldson et al., 2018) and has since been applied to 13 more ponds in Joseph D. Grant County Park. POND-IT reconstructs the historical water-surface elevation across a range of hydrologic conditions and can be extended past the calibration period and into the future with climate change projection data. At its core, POND-IT is a numerically straight-forward water balance model, but with a novel method for model calibration. With only a bathymetric map of the pond, historical aerial imagery can be leveraged to compile historical model calibration data when water depth monitoring data are not available. Each historical image is converted into a single calibration data point and repeat pond area measurements form the historical calibration record. This calibration data can be supplemented with available pond monitoring data, while not strictly necessary, even a few months of continuous pond depth monitoring can improve the model performance.

The goal of a POND-IT model is to understand the range of potential hydroperiods under existing conditions, and with a calibrated model, to efficiently explore a range of possible mitigation or restoration activities with the goal of creating or improving habitat for the target species. In this paper, we examine the hydroperiod of two ponds in Joseph D. Grant county park under historical and projected climatic conditions for the optimization of CRLF habitat. The ponds examined are 1) Eagle pond, which is typically perennially wetted and would likely support predatory bullfrogs, and 2) Hotel pond, which dries in July in more than half of years and therefore may not be inundated long enough to support a full range of early to late metamorphs of the CRLF lifecycle. Design alternatives include changes to pond spillway elevation, pond capacity (e.g. stage-storage relationship), clay lining to limit seepage losses, or drain infrastructure and take into account long-term viability of infrastructure under changing climate.

Hydrologic and Geologic Setting

POND-IT has been investigated and refined in the two Grant Park ponds about 10 miles to the east and southeast of the city of San Jose, California, where mean annual rainfall averages 23 to

24 inches. Total annual precipitation varies widely from year to year, ranging from 11 to 45 inches in one year. The floor of Santa Clara Valley was formed by a large graben, or down-dropped block between major fault boundaries on either side of the valley. The two pools are on the eastern side of the valley, at elevations of 1,950 and 2,073 feet, or about half-way between the valley floor and Mt. Hamilton (4,381 feet). Bedrock geology is Franciscan and Great Valley consolidated sandstones, mudstones and shales; unconsolidated surficial deposits are widespread, particularly deep-seated landslides. Soils are primarily well-drained loams, with moderate to high shrink-swell properties which tend to recharge rapidly during the first storms of the year until the soil cracks seal. In contrast with many other settings in western North America, strike-slip (lateral) and dip-slip (vertical) faulting form conduits and barriers which strongly affect soil water and shallow groundwater movement to the ponds, particularly in late winter.

Methods

Pond Monitoring

We conducted topographic surveys with a total station in August and September 2017 to develop an empirical relationship between water level, pond storage, and pond area at each water level. Surveys prioritized key points that enabled us to define the bathymetry of each pond, including staff plate, spillway, berm, high-water marks, and current water surface elevation. We established benchmarks at each pond, so surveys could be repeated and to relate water-surface elevations during future site visits. Contour lines were constructed based on the elevation relative to the deepest point recorded during the survey to create a stage-storage relationship (i.e., depth-capacity curve) for each pond. Although not required to build the model, both of the ponds were instrumented with Solinst Leveloggers©, which measured hourly water depth and temperature from December 2016 through June 2018. Both ponds were visited at least six times throughout the monitoring period to field-verify recorded water levels. The staff plates and stilling wells were protected with barbed-wire 'teepees' to discourage cuddling by cattle and by wild boars. Water temperatures are not used directly in the model computations but were tracked to assess whether actual water temperatures were within known acceptable ranges for individual species or for particular life stages.

Pond Inundation and Timing (Pond-IT) Model

Model Framework: The main purpose of the Pond Inundation and Timing (Pond-IT) model is to infer the dry-down timing across a range of hydrologic years and to credibly extend the model into the future using climate projections. To meet this objective, a monthly timestep is sufficient compared to a daily timestep, which required more data and more computation time. In addition, many climate projection datasets are available at the monthly timestep. For the model to be integrated seamlessly from historical through projected time periods, we used the same (monthly) timestep for historical and projected climate datasets. The model uses Python, an interpreted high-level programming language with many general-purpose programming tools. Open-source Python libraries are used for this model (e.g., numpy, pandas) to take advantage of data analysis tools which can readily manipulate numerical tables and time-series datasets. All Python packages used in this model are open source and free to use.

Model Input Data: The primary time-dependent input variables used in the model are air temperature, used in the Blaney-Criddle equation to estimate evapotranspiration (ET), and total monthly precipitation. Historical air temperature and monthly precipitation are sourced from PRISM Climate Group (PRISM, 2017). Air temperature and precipitation are interpolated for each 4-km grid cell through a DEM-based interpolation between publicly available gaging datasets (e.g., sourced from California Irrigation Management Information System, US Geological Survey, California Department of Water Resources, etc.). For this analysis, the historical data were downloaded from the PRISM website on July 25, 2018. Downloaded historical data begin with water year 1975, (beginning October 1, 1974 and ending September 30, 1975, WY1975). Because each pond model begins with an empty pond at the beginning of WY1975, results are presented beginning in water year 1980 to allow 5 years of model spin-up to allow for interannual hydrologic carryover to equalize.

Soils data for contributing watershed were sourced from the National Resources Conservation Service (NRCS) Soil Survey Geographic Database (SSURGO). A depth-weighted water capacity is calculated across the soil profile thickness. If multiple soil types are located in a single watershed, the water capacity is area-averaged in addition to depth-averaged. The watersheds were initially delineated using the 2006 Santa Clara County LiDAR dataset, using an automatic routine in ArcGIS and then refined based on field observations of flow paths around roads, berms and other structures. Watershed size was used to calculate soil moisture storage and runoff, further explained below.

Projected climate change data were sourced from the Intergovernmental Panel on Climate Change (IPCC) fifth phase of the Coupled Model Intercomparison Project (CMIP5). Data were retrieved from the University of California's Lawrence Livermore National Lab repository of bias-corrected, spatially-downscaled (BCSD) datasets which have a spatial resolution of 1/8 degree. Over 50 Global Circulation Models (GCMs) are available from various sources, but Cal-Adapt has recommended 10 GCMs as the most applicable for climate change projections in the state of California. Our analysis is limited to these 10 GCMs, some of which have multiple model builds, resulting in a total of 25 projected timeseries of mean monthly air temperature and monthly precipitation. Climate projections indicate that annual average air temperatures may increase up to 6.5 degrees Fahrenheit by 2100, with the standard deviation taken amongst the 25 GCMs increasing from 0.8 to 1.7 degrees Fahrenheit indicating an increase in the temperature variability. Average annual precipitation is projected to increase only marginally, but precipitation patterns are expected to shift, with more frequent, higher magnitude storm events in the winter months. This is observed in the projected data by an increase in the standard deviation of total annual precipitation, from 7.5 inches to 11 inches.

Model Calibration Data: The ponds were calibrated using the water depth gaging data and historical aerial imagery available in Google Earth®. Google Earth® historical imagery was available starting in the mid-2000s (2004 – 2009, pond dependent), with images sourced from various planes and satellites. Ponded area was measured in each aerial image where the wetted boundary is clearly defined and observable. When drawing pond boundaries, some judgment was used to define pond water surface through emergent vegetation, or with interpretations of floating aquatic vegetation or algae around the pond edges. Examples of four calibration images for a pond in Coyote Harvey Bear Lake Ranch County Park in Santa Clara County, California is in Figure 1.

The stage-storage relationship was then used to convert pond area to a water surface elevation for use in the model calibration. The use of Google Earth® historical imagery proved to be a powerful and cost-effective approach to calibrate and validate modeled long-term historical pond

hydroperiod records. Images were available up to several times per year from 2004 to present, providing calibration data for a wide range of hydrologic years and sequences of years, such as extended droughts or very wet years.

Figure 1. Sample calibration images for a pond in Coyote Harvey Bear Lake Ranch Park, Santa Clara County
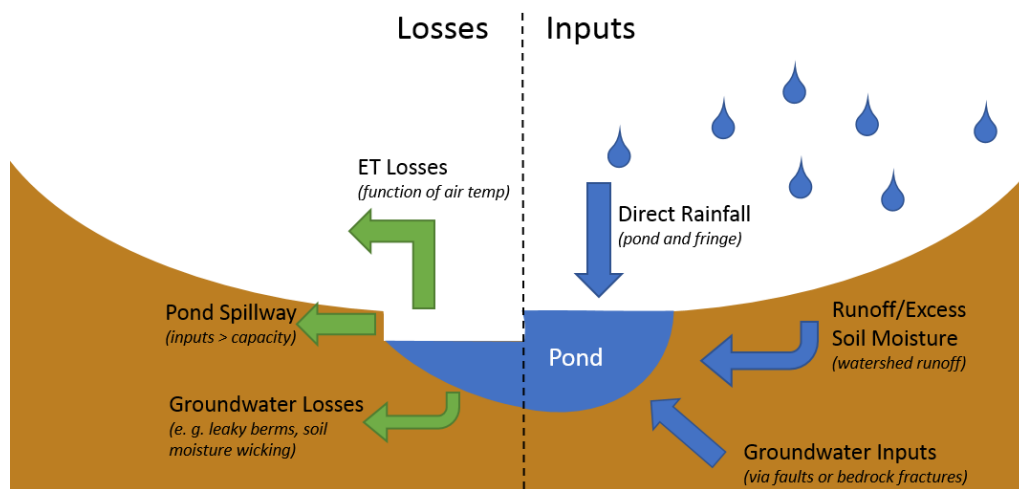
Figure 2. Schematic diagram of the model inputs and outputs.

Pond Inundation and Timing (Pond-IT) model. POND-IT was constructed using the above input and calibration data using twelve model-fit parameters (named and underlined below). A cartoon schematic of the modeled hydrologic fluxes is in Figure 2. Model parameters can be optimized using a numerical solver to minimize the sum of the mean squared error between the model results and calibration data.

Model input modules are:

1. **Direct Rainfall.** Precipitation that falls directly on the pond surface plus an additional pond fringe area that directly contributes water to the pond. Pond fringe area was suggested to be up to 2 to 4 times the pond surface area by Hecht and Napolitano (1991), who demonstrated that bank-exchange zones in surrounding hollows and swales contribute directly to runoff into the ponds once the near-pool watershed has reached watershed saturation. The area of the pond fringe is specified by the <u>rainfall fringe area</u>

parameter and is represented as a percentage of total pond area. Fringe area depends largely on local topography and soil properties.

2. **Watershed Runoff.** A soil-moisture accounting routine calculates the monthly soil moisture. Maximum soil water capacity is calculated using soil properties of the contributing watershed. When precipitation exceeds available soil-water capacity plus ET, the excess precipitation is routed into the pond as runoff. To adjust for local variation in the ability of a soil to store water, regional soil properties can be adjusted as needed to account for local soil properties based on field observations and expertise.

3. **Groundwater Inputs.** Groundwater input delivery mechanism and timing varies widely based on soil types, underlying geology, and pond construction and so three types of groundwater inputs have been implemented in POND-IT. They are listed below in increasing order of lag from incident rainfall to appearance in the pond.

   a. **Pond Fringe Groundwater Input.** Ponds are typically in local topographic depressions, so soil moisture from the surrounding area can infiltrate into the pond fringe area over short timescales. To model this, the direct rainfall (module 1, above) is lagged 1 month, and scaled by the model parameter, <u>pond fringe groundwater</u>. Modeling results tended to over-predict pond water surface elevations in years following very wet years and under-predict pond water surface elevations following very dry years. To address this long-term effect of precipitation, a memory scaling factor was applied to this variable, represented by the ratio between the previous year's annual precipitation and the historical average annual precipitation. For example, after WY2014, which was very dry, the memory scaling factor would reduce the pond fringe groundwater input during WY2015, because the dry conditions of WY2014 over-taxed shallow aquifers, which needed to be re-filled prior to resuming contributing groundwater into a pond.

   b. **Shallow Bedrock Fracture Groundwater Input.** In watersheds with shallow, fractured bedrock, additional groundwater discharge can be sourced from these fractures with a medium-term time lag. For the pond models presented here, this <u>shallow fracture time lag</u> ranges from two to five months. Model results and calibration data have shown that this medium-term groundwater discharge is typically only active in wet years, when precipitation is above a certain <u>shallow fracture threshold</u>, which is specified in the model using the annual precipitation. The amount of water reaching the pond is based on the total volume of water stored in the soil column below the root zone, which is assumed to be 18 inches for this study. This volume of water is released more quickly when the soil column is saturated, and more slowly when the soil is drier. The total volume of water is calculated over a <u>shallow fracture contributing watershed area</u>, which can sometimes be different than the contributing surface watershed area, depending on topography, deep weathering and geology.

Shallow bedrock fracture groundwater seeps are modeled so that either the seep is active and contributing water to the pond, or the seep has run dry. The threshold for when the seep is active and contributing varies by pond, with some seeps active every year and other active during only the wettest years.

   c. **Deep Fault Groundwater Input.** Groundwater that flows through deeper bedrock fractures and faults is often slower than shallow bedrock fracture ground water flow.

The total amount of deep fault groundwater input is the <u>deep fault percentage</u> of precipitation over the contributing watershed. The <u>deep fault time lag</u> is parameterized at seven to eight months. The lag may not represent actual groundwater flow velocities through the inferred faults, but instead may represent the timescale at which groundwater elevations in the basin have adjusted for discharge into the pond to be numerically significant. Ultimately, deep fault groundwater input is best monitored rather than estimated based on soil properties, as water levels beneath the pools can (a) also originate from delayed drainage of landslide scarps, and (b) may be largest during the second or third year of above-average rainfall, based on our experience elsewhere. A very similar effect is observed following a fire, especially where plant roots are shallow relative to the depth to water in the deeply-weathered zone (Hecht and Richmond, 2011). However, for this application, groundwater inputs characterized as sourced from deep fault are inferred based on model calibration results, pond characteristics, specific conductance of the water in the pond, and knowledge of the geology, soils, and topography.

Model output modules are:

1. **Evapotranspiration (ET).** ET is calculated using the Blaney-Criddle Equation, represented by

$$ET_o = p \, (a \, T_{mean} + b) \tag{1}$$

   where ET_o is the ET of the reference crop, irrigated turf, which is published by CIMIS as a function of CIMIS zones (CIMIS 1999), T_{mean} is the mean monthly temperature, and p is the mean daily percentage of annual daytime hours as a function of site latitude, and a and b are fitting parameters estimated using least squares fit to the historical mean monthly air temperature. The Blaney-Criddle Equation is a simplified method for deriving ET, only using air temperature and zonal reference ET as input parameters. Our choice to use a monthly model timestep reduces the likelihood that the more complex Penman-Monteith equation would improve model results. At a minimum, the Penman-Monteith formula requires daily timeseries data for solar radiation, wind speed, relative humidity, in addition to air temperature, which can vary significantly between pond locations and even with a single watershed. Use of the Blaney-Criddle Equation assumes that ET_o for the reference crop, is approximately equal to ET from a standing body of water (Allen et al., 1998).

2. **Spillway.** In wet months, the pond may spill, with water surface elevations exceeding the spillway elevation during these times. However, these spill events do not need to be explicitly modeled for the purposes of hydroperiod modeling and are therefore removed from the model, with water surface elevation limited to the spillway elevation.

3. **Groundwater Outputs.** Groundwater discharge varies as a function of pond soil permeability and connectivity and water use on the pond fringe, so two types of groundwater outputs have been used in POND-IT. These are:

   a. **Soil Moisture or ET Groundwater Output.** As seasonally increasing air temperatures places more demand on water supplies in the pond fringe, ponded water is lost through additional vegetation uptake or the wicking of dry soils not captured in the calculated ET from the water surface. Active grazing in the pond area may also increase this type of groundwater loss as cattle are likely to drink

more water in summer months compared with cooler, wetter months. Water lost in this way is parameterized as a percent of ET to groundwater over the pond fringe area. The magnitude of this parameter sets the shape of the draw-down curve in the summer months when ET is high; the higher the percentage loss, the steeper the drawdown curve.

b. **Leaky Pond Groundwater Output.** The soils underlying each pond have a range of soil permeability and connectivity to shallow groundwater. Clayey soils prevent water from infiltrating into the shallow subsurface as quickly as loamy or sandy soils. Except for some Pedogenic ponds, we expect most ponds to consistently loose some amount of water to the shallow subsurface, as a function of the volume of water in the pond. A fuller pond loses a larger volume of water over the larger wetted pond bottom area and with higher head pressure exerted on the underlying soils, compared with pond that is less full. Therefore, groundwater output is specified as a function of total pond volume as a percent pond volume to groundwater. Each month, the pond loses the specified volume of water to the shallow subsurface, which typically ranges from 2 to 40 percent. The higher the value, the "leakier" the pond, which may relate to the composition of the underlying soils, the proximity to faults and fractures, or the construction of the berm. The rate at which a pond loses water because it is "leaky" (i.e. the percent pond volume to groundwater is larger) defines the shape and slope of the draw-down curve.

Results and Discussion

Historical and Projected Hydroperiod

In this paper we present results from two of the 13 ponds monitored and modeled for this study. The first is Eagle pond (Figure 3), which has a watershed that is 12.9 acres, holds approximately 13.9 acre-feet, and has a maximum ponding depth of 11.7 feet. The second pond is Hotel pond (Figure 4), which has a relatively small watershed, approximately 3.9 acres and smaller storage capacity of approximately 2.0 acre-feet and a maximum depth of 7.9 feet.

Figure 3. Eagle Pond

Figure 4. Hotel Pond

Figure 5 and 6 illustrate model results in comparison to calibration data collected on site and via historical aerial imagery for Eagle and Hotel ponds, respectively. Despite a numerically straight-forward approach to model development, and the rather coarse monthly model timestep, results show surprisingly close agreement with model calibration data (Hotel pond $RMSE = 1.25$, Eagle pond $RMSE = 0.66$), illustrating the success of using historical imagery and limited monitoring data for model calibration. Modeled deviation from observed water-surface elevation varies seasonally and is pond-dependent.

Model results also show that Eagle pond is perennially wetted in all but the most extreme droughts (e.g. 2014). Despite having a large berm, model results also show that Eagle pond is not very leaky and is not connected to active groundwater supplies. The main fluxes in and out of Eagle pond are direct rainfall and runoff, and ET. Conversely, Hotel pond completely dries in all but the wettest years. Water year 2017 was extremely wet and was the only year in which Hotel did not dry completely during the calibration period. The best-fit model parameters suggest that Hotel pond is very leaky, with groundwater losses exceeding ET in most modeled months, suggesting high permeability in the shallow soils underlain by the fractured bedrock typical of this area.
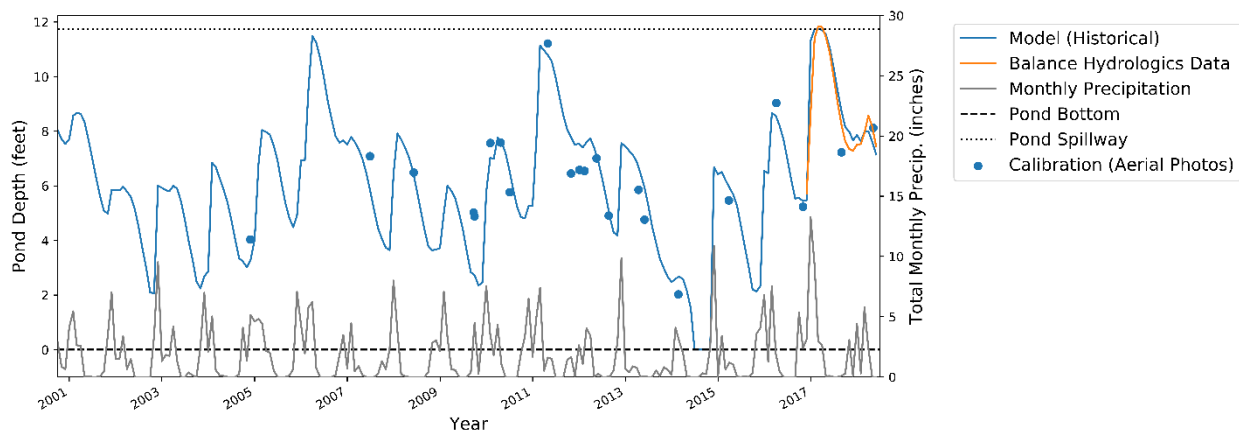
Figure 5. Historical model results for Eagle pond
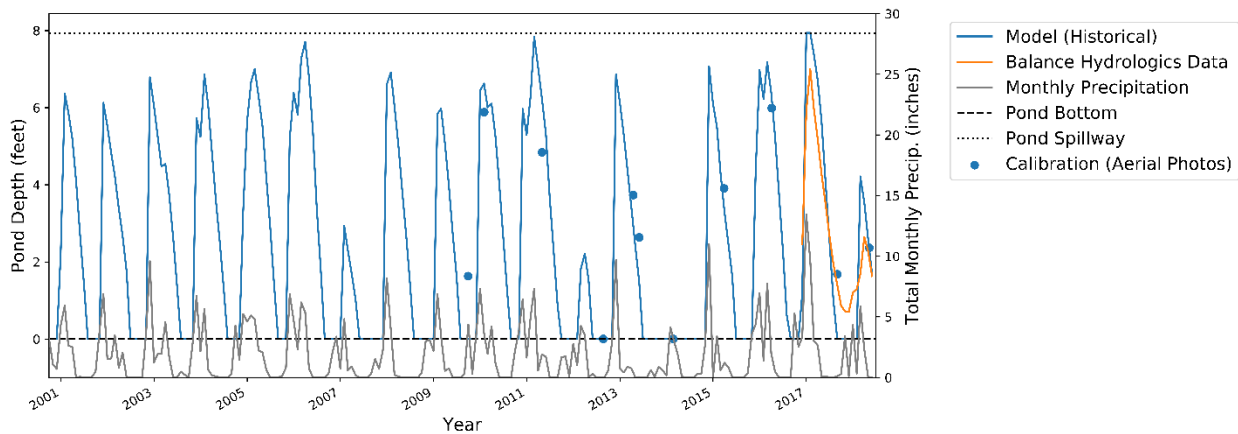
Figure 6. Historical model results for Hotel pond

Hydroperiod model results are also presented visually for each pond in Figure 7 and Figure 8 using historical and projected climate datasets. Each hydroperiod plot has the month, starting with October, plotted versus the year, which visually depicts when each pond dries each year. The colorbar indicates the inundation probability of each decade, with the darkest color indicating a higher probability of inundation. The decade 2010 – 2020 is a mix of historical climate data through 2017 and projected climate data beginning 2018. Inundation probabilities are based on the 10 historical model runs in that decade or the 25 GCMs modeled for each year in the projected time period (250 total scenarios for each month).

Although Eagle pond has rarely dried up historically, model results indicate that the expected warming will have a significant impact of the hydroperiod of Eagle pond, with the pond drying in 15-20% of years after 2050. Similarly, Hotel pond is expected to get drier sooner in the year and remain inundated year-round less frequently.
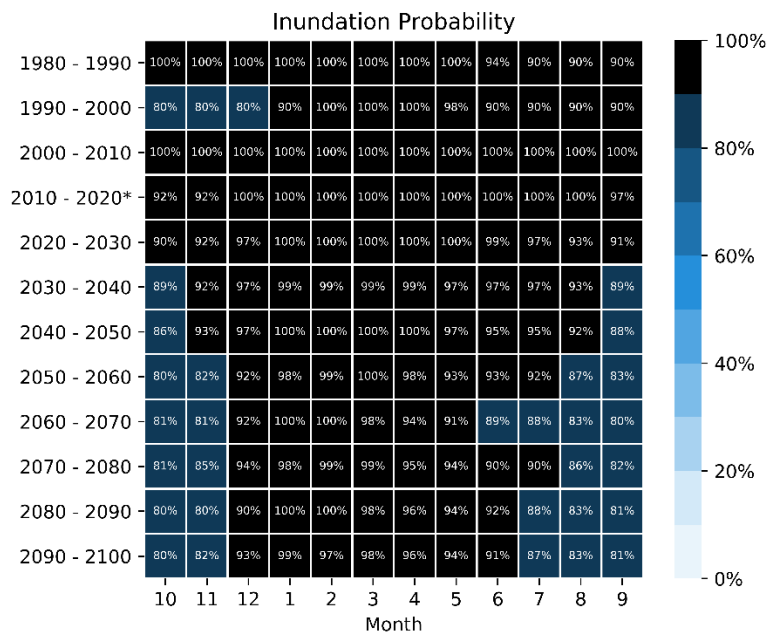
Figure 7. Historical and Projected inundation probability for Eagle pond, existing conditions.
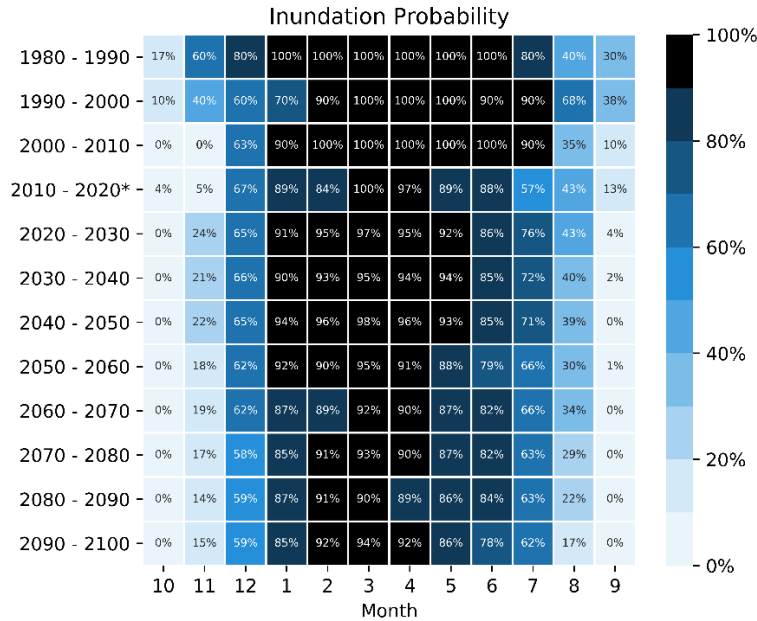
Figure 8. Historical and Projected inundation probability for Hotel pond, existing conditions.

Optimization of CRLF Habitat

With a clearer understanding of the hydroperiod in Eagle and Hotel ponds, and a calibrated water-surface elevation model, we next examined possible pond reconfigurations that may help reach target hydroperiod for CRLF. Current thinking amongst biologists in the region is that ponds should dry up each year to inhibit bullfrog colonization, but that ponding into late August or early September is ideal for the CRLF lifecycle. An easily-implemented approach to improving habitat for CRLF is to install a drain in perennially-wetted ponds, draining them completely in September. However, drains require reliable ongoing maintenance and present logistical challenges in remote sites. The act of completely draining the pond may also have adverse effects on other target species.

Modifying functional ponds inhabited by listed or sensitive species is seldom sought. Hence, restoration criteria are perhaps most usefully considered as guidelines for repairing damaged or degraded ponds or providing enhancement for existing, but under-utilized ponds. Bauder et al. (2009) note the importance of having guidelines for pond or pool repair to be an important aspect of conservation management. The use of Pond-IT for the characterization pond hydroperiod offers both understanding of historical and projected conditions, but also is a useful tool for the exploration of pond restoration alternatives. Pond-IT can be leveraged to evaluate the following habitat improvements on pond inundation:

- **Spillway modifications.** Raise or lower the spillway to change the total volume each pond can accommodate. Ponds with year-round hydroperiods may reach target seasonal hydroperiod if the spillway is lowered and less runoff is captured each year. If water supply is adequate, raising the spillway may extend the hydroperiod. The model can easily simulate many different spillway elevations to explore a range of possible hydroperiods.

- **Pond hypsometry modifications.** Like spillway elevation, the stage-storage relationship also dictates the pond capacity. In some cases, altering the hydroperiod to the desired length could include re-grading the pond to alter hypsometry (e.g. deepen or widen the pond). This may have the added benefit of creating heterogeneous pond depths which may suit different species throughout their lifecycles.

- **Clay-lining pond bottom.** Lining a pond with a low-permeability clay layer will likely cut-off or reduce groundwater inputs and outputs, significantly altering the pond hydroperiod. Introduction of a clay liner may decrease the 'leakiness' of the pond, prolonging the hydroperiod.

- **Engineering infrastructure.** With the model as a decision-making tool, we can establish a target maximum water-surface elevation for the spring months that will most likely result in a dry pond by the target desiccation date. As an actively managed alternative, a spillway or drain can be installed at this pre-determined elevation, which can be opened in the spring or early summer when the pond elevation is higher than needed to achieve the desired hydroperiod. This has the benefit of minimizing direct impacts to target species compared to completely draining the pond in the fall. By comparison, a typical pond drain that is operated in September to completely drain a pond would likely be decanting relatively cold water, and may also desiccate overwintering CRLF tadpoles (Fellers et al. 2001) In some situations, the water supplies in a pond with an existing year-round hydroperiod may be held over year-to-year and completely draining the pond each year may not maintain sufficient water supply to achieve the desired maximum water-surface elevation. Because the POND-IT model is custom-built, engineered water-surface elevations management programs can easily be incorporated into the existing model to understand year-over-year water supplies.

We have simulated three possible restoration design scenarios, two for Eagle pond and one for Hotel pond. The first scenario seeks to reduce the total water losses from ET in Hotel pond, to increase the hydroperiod duration. In this scenario (Figure 9), Hotel pond would be re-graded so that a central portion of the pond is 2 feet deeper, holding the same volume of water, but with less surface area, thus resulting in a reduced ET. The second scenario decreases the Eagle pond spillway by 2 feet, from 11.7 feet to 9.7 feet which decreases the total pond capacity by 56% (Figure 10). Results show that decreasing the spillway crest elevation by 2 feet does result in fewer years with year-round inundation. However, with the projected increase of inter-annual variability (i.e. larger and more frequent flood events and droughts), few years projected years would result in the ideal September drawdown. The third scenario introduces an adaptive management approach (Figure 11). In this scenario, if by April 1st, the pond depth is greater than 4 feet, a valve could be opened to slowly drain the pond to 4 feet deep. Beginning around 2050, projected temperatures are expected to increase ET so that the drawdown period is shortened. Therefore, this scenario changes the valve opening date; after 2050, if the pond depth is greater than 4 feet by May 1st, the valve should be opened. The intake for the drain could be mounted on a floating structure to allow the warmer surface water to be removed from the pond, and preserving the cooler temperatures preferred by CRLF. Although this management strategy requires ongoing maintenance of engineering infrastructure, given the uncertainly of the extent of climate change, this adaptable method also allows greater flexibility in resource management.
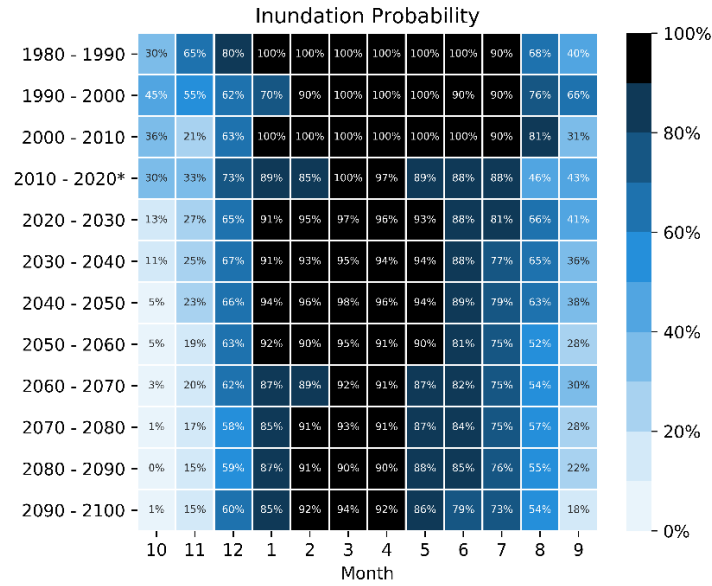
Figure 9. Historical and projected inundation probability for Hotel pond, re-graded to be 2 feet deeper. Historical climate data ends in 2017 with projected climate data beginning in 2018.
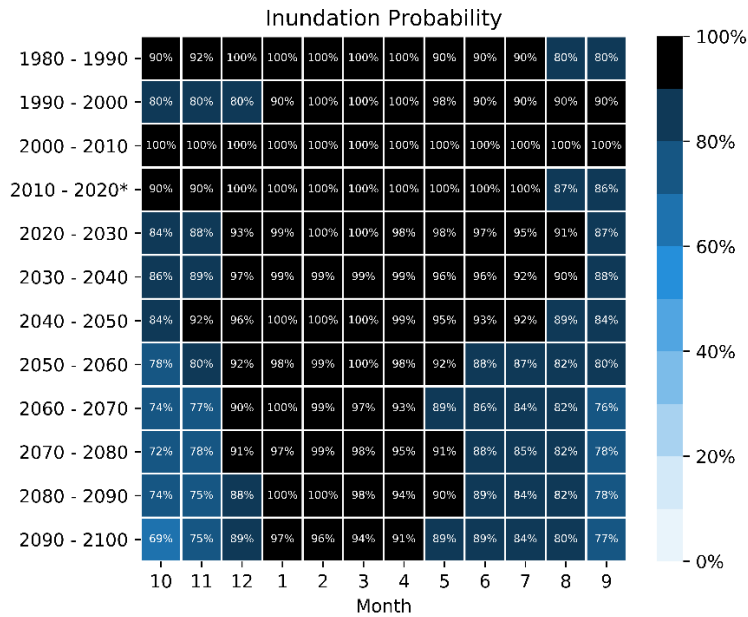
Figure 10. Historical and projected inundation probability for Eagle pond, spillway lowered 2 feet. Historical climate data ends in 2017 with projected climate data beginning in 2018.
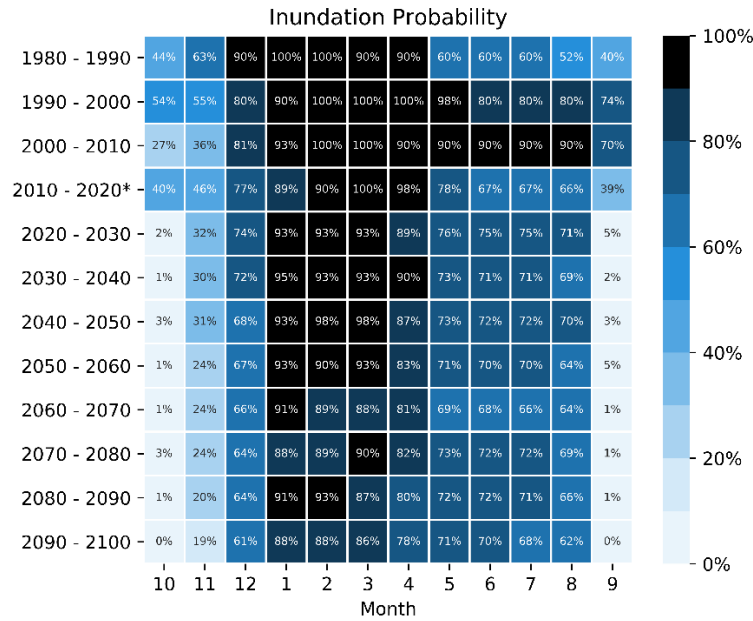
Figure 11. Historical and projected inundation probability for Eagle pond, pond drained to 4 feet in April until 2050 and in May after 2050. Historical climate data ends in 2017 with projected climate data beginning in 2018.

Closing

POND-IT has been developed to be a flexible, robust, and cost-effective decision-making tool to improve understanding of the hydrologic drivers of hydroperiod in ponds which have the potential to serve as valuable habitat for native frogs, salamanders, and turtles, an understanding that is particularly relevant for climate change adaptation and strategy development. The goal of this model was to develop a pond hydroperiod tool that can be used across a variety of scales and environments by planners, land use managers and scientists with a variety of skillsets. The model was developed using Python, an open-source programming language with simple and easy-to-learn syntax to emphasize readability and reduce the cost of program maintenance for its users. The model framework is an excellent and cost-efficient way to assess potential changes in hydroperiod resulting from different pond configurations (e.g. spillway or grading changes) for habitat restoration design. Initial demonstrations indicate this model is an efficient way to simulate the hydroperiod of a large and diverse population of ponds. POND-IT was built to infer pond hydroperiod in a range of climate conditions and can therefore be used in a range of environments and covered species across California and beyond, not limited to the Santa Clara Valley. Although POND-IT has currently been applied to salamander, frog, and turtle habitat, it can be similarly applied to most communities sensitive to hydroperiod such as vernal pool fairy shrimp, various vegetation associations, and general wetland communities. The pond model can be used anywhere to forecast changes in the water balance (and therefore the timing and frequency of pond-drying events) under future climate scenarios.

References

Allen, R.G., Pereira, L.S., Raes, D. and Smith, M. 1998. Crop Evapotranspiration: Guidelines for Computing Crop Water Requirements. Irrig. and Drain. Paper No. 56, United Nations Food and Agriculture Organization, Rome, Italy

Bauder, E., Bohonak, A., Hecht, B., Simovich, M., Shaw, D., Jenkins, D. and Rains, M., 2009, A draft regional guidebook for applying the Hydrogeomorphic Approach to assessing wetland functions of vernal pool depressional wetlands in Southern California: Prepared by San Diego State University for the U.S. Environmental Protection Agency. 118 p. + 7 apps.

California Irrigation Management Information Systems (CIMIS). 1999. Reference Evaporation Map.

Donaldson, E., Pretzlav, K., and Hecht, B. 2018. A new framework for modeling pond habitat in a changing climate: Observed and modeled pond hydroperiods in central Santa Clara County. Balance Hydrologics Inc. consulting report prepared for Guadalupe-Coyote Resource Conservation District, 79p.

Fellers, Gary M., et al. "Overwintering tadpoles in the California red-legged frog (Rana aurora draytonii)." Herpetological Review 32.3 (2001): 156-157.

Hecht, B. and Richmond, S. 2011. Post-fire flow premium: Increased summer flows promoting salmonid survival following large wildfires in Monterey County. Salmonid Restoration Federation 45th annual conference, San Luis Obispo, California. 24p.

Hecht, B., and Napolitano, M.B. 1991. Hydrologic processes affecting vernal pools at Ellwood Beach, California, and suggested approaches to mitigation, Balance Hydrologics Inc. consulting report prepared for LSA Associates, 67p.

PRISM, 2017, data download from http://prism.oregonstate.edu/, accessed on July 25th, 2018.

Rains, M. C., Dahlgren, R.A., Fogg. G. E., Harter, T., and Williamson, R.J. 2008. Geological control of physical and chemical hydrology in California vernal pools. Wetlands 28: 347-362

Acknowledgments

Modeling Infiltration In Constructed Micro-Catchments

Michael Founds, Research Hydrologist, Desert Research Institute, Reno, Nevada, USA, mfounds@dri.edu

Kenneth McGwire, Associate Research Professor, Desert Research Institute, Reno, Nevada, USA, kenm@dri.edu

Mark Weltz, Research Leader, USDA Agricultural Research Service, Reno, Nevada, USA, mark.weltz@ars.usda.gov

Sayjro Nouwakpo, Research Assistant Professor, University of Nevada, Reno, Nevada, USA, snouwakpo@cabnr.unr.edu

Abstract

Micro-catchments (MCs) have successfully been used in arid regions to promote infiltration of rainfall and water availability for plants (e.g. Malagnoux, 2008; Oweis, 2017). In addition to these beneficial outcomes, MCs also have the ability to reduce soil erosion and sedimentation in arid and semiarid rangelands. The Vallerani® System was developed in 1988 to efficiently harvest runoff by creating a series crescent-shaped MCs with oscillating ripper and plow blades (Oweis et al. 2011). The Vallerani System has been used in degraded rangeland settings in numerous countries (Malagnoux, 2008, Oweis, 2017). Like any engineered structure, MCs need to be sized and spaced adequately for optimal function and cost effectiveness, and better understanding of the infiltration capacity of MCs would allow better engineering of these structures. The research described here tests the ability of a numerical infiltration model to emulate field measurements for a set of constructed MCs.

Field work for this study was performed at a Bureau of Land Management (BLM) experimental research site at Bedell Flat that is located north of Reno, Nevada. The soil at the study area is a coarse-loamy aridic argixeroll with underlying bedrock at approximately 1-2 m depth. Eight MCs were created on two transects along the hillslope contour. One transect was located at the hillslope toe where the slope was 5-8%. The second transect was located 50 m uphill where the slope was 10-15%. MCs were constructed using a small tractor with two offset plow shovels. MCs were then manually shaped to approximate the width, depth and berm of pits created by a Vallerani Plow. Each MC was approximately 350 cm long, 150 cm wide, and 30 cm deep. A digging bar was used to break up soil along the centerline of the pit down to an additional 10-15 cm in order to approximate the ripper of the Vallerani system.

Three dimensional models of each MC were created using handheld photography and Agisoft Photoscan software. Eight control targets around the pit were surveyed with a Nikon NPR 352 total station to accurately project the 3-D models in space. The Photoscan software created digital elevation models (DEMs) that were accurate to within 0.5 cm, and these DEMs were imported to ArcMap GIS software where the surface volume tool was used to capture the 3-D surface area and volume across a range of depths. Polynomial relationships were then developed to relate water stage in each MC to the corresponding wetted surface area (4th order polynomial) and volume (2nd order polynomial) of the pit.

Multiple soil samples around the pits were measured for bulk density and soil particle size distribution (PSD) at five 10-cm depth intervals, as well as from the soil berm and the bottom of the pit. A Guelph permeameter (GP) was used to measure soil conductivity (K_s) at depths of 15 cm, 25 cm, 35 cm, 45 cm, 55 cm on each side of an MC, as well as 15 cm within the MC berm. GP measurements were obtained using a single ponded height, since vertical heterogeneity of the soil profile can cause erroneous results with two ponded heights (Elrick et al., 1989). Measurements were taken with the GP set to 10 cm of water pressure, and the water level was recorded at minute intervals until three recordings of a steady rate of infiltration were observed (10-25 minutes).

A Walnut Gulch Rainfall Simulator (WGRS) was used to simulate two rainfall events over each MC. The rainfall simulator applied water with two events of variable intensity and duration, delivering 3-5 cm of water at an intensity of 10-15 cm/hr. A rill simulator then simulated concentrated flow from upslope. Flow from the rill simulator was maintained for at least 15 minutes after water overtopped the MC. When the rill simulator was shut off, the level of water in the MC was continuously measured using both an ISCO bubbler and a vented KPSI 700 level transducer. The polynomial relationship between depth and volume allowed the calculation of the infiltration rates and volumes with time. One MC (upper site #2) was removed from the study, since the water opened up an animal burrow and the pit drained.

The MC field experiments were simulated using the Hydrus 2D/3D software package. A representative cross-section was derived from each of the two hillslope positions by overlapping the multiple 3D models of pit geometries for low versus high slopes. A model domain was created that characterized the soil profile based on soil measurements made in the field. The model domain for upper and lower sites was approximately 500 cm wide by 500 cm tall. Seven soil layers were specified: 0-5 cm, 5-15 cm, 15-25 cm, 25-35 cm, 35-45 cm, >45 cm, and the unconsolidated berm material (Fig. 1). The properties that were assigned to the berm were also specified for a wedge of soil at the bottom of the pit to represent the 10 cm of unconsolidated soil created with the digging bar.
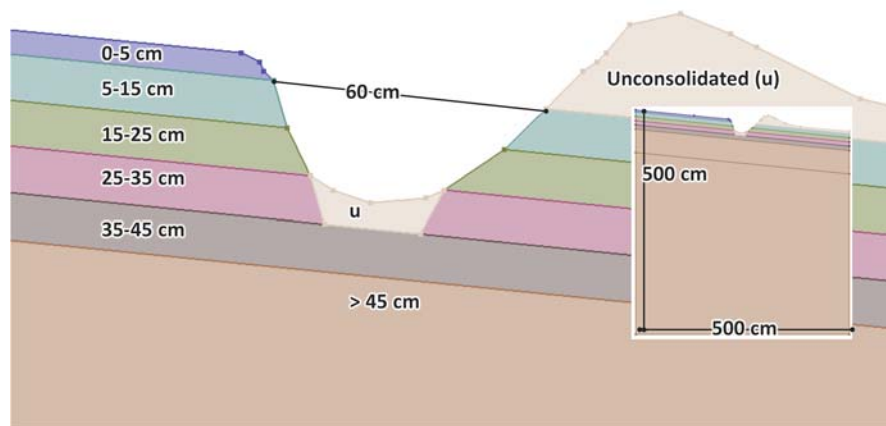
Figure 1. Hydrus model geometry.

The Hydrus 2D model was set up in the vertical plane with a simplified soil profile based on field measurements. The profile was converted to a finite element (FE) mesh using the MESHGEN software in Hydrus, with a targeted element size of 10 cm that was refined to 1 cm at the soil surface. The shape of the water retention curve was defined by the van Genuchten – Mualem hydraulic model with no hysteresis, and water flow parameters were originally specified based on measured PSD data for each depth interval. Water retention parameters (Q_r, Q_s, Alpha, n, I)

were held constant for each simulation and were based on predictions from PSD data. The saturated conductivity (K_s) at each soil layer was specified based on the maximum K_s measurement at each depth interval measured in the field and averaged between upper and lower hillslope positions. A time-varying head boundary at the soil surface was used to simulate the height of ponded water within each MC, based on changes in the measured height of ponded water for each pit. The simulation was run for 400 minutes with a one-minute time step.

Water velocity estimates around the pit boundary from the Hydrus model (Fig. 2) were averaged for each 1 cm depth interval in the pit and multiplied against the corresponding surface area for that interval to provide a volumetric flow rate for infiltration. A summation of all depth intervals provided a total flow rate at each time step of the model. Differences between the modeled volumetric flow rates and field measured values were calculated for each pit for 6 time steps of the Hydrus simulation that were separated by 5 minutes after the rill simulator was shut off and the water level receded.
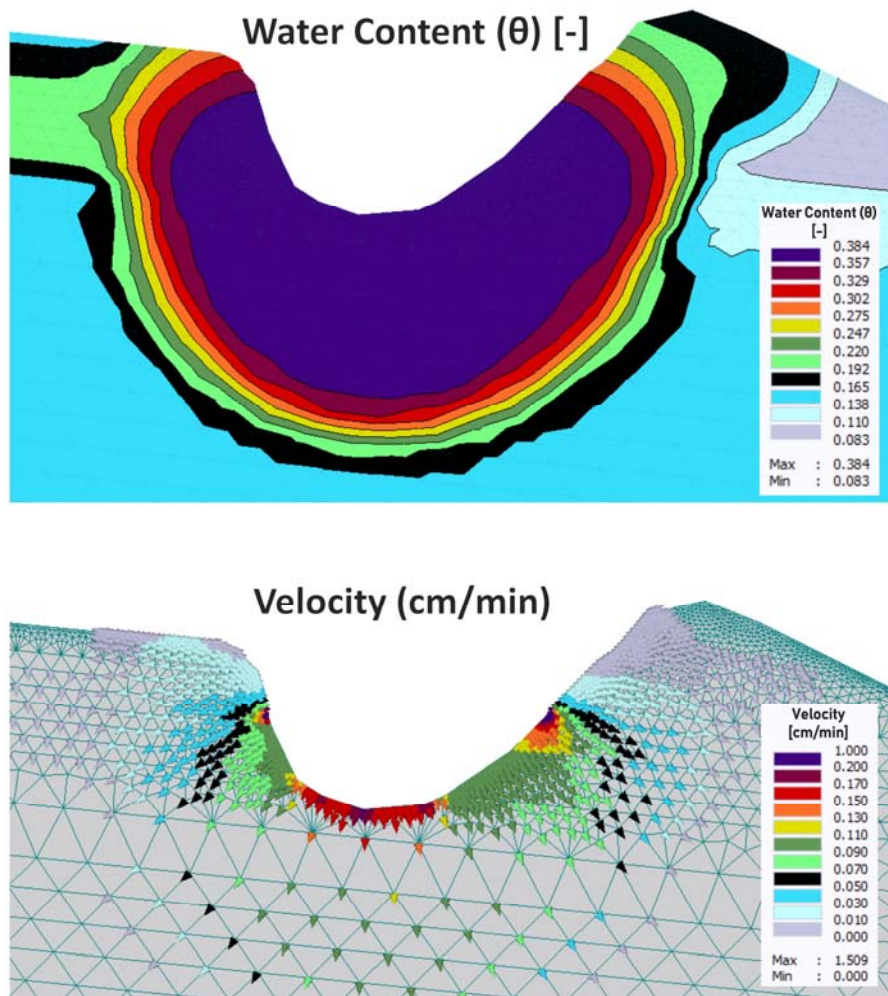
Figure 2. Hydrus output for lower site 1 at 255 minutes displaying water content and velocity.

On a MC-by-MC basis, disagreement between field measured and modeled rates of infiltration was as high as 90%. As a group, the Hydrus model underestimated infiltration at lower sites by 20% and overestimated upper sites by 30%. However, without any direct calibration of the Hydrus model, average error across all MCs on the hillslope was less than 1% (Fig. 3).
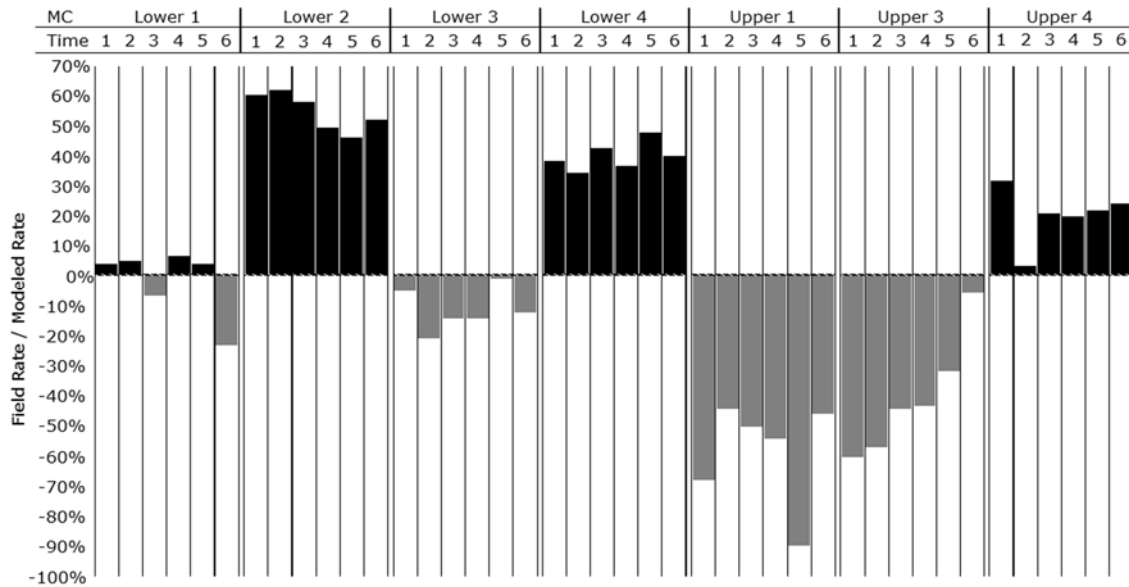
Figure 3. Relative error of Hydrus model estimates compared to field measures for six time steps.

Given the innately high level of heterogeneity in soil properties and the generalization of a single model domain for each hillslope position, it is not surprising that individual MCs would perform differently. The results of the modeling effort were encouraging, and point to a number of topics that should be studied to improve results. These include determination of the required density of PSD and GP measurements for model parameterization, and determination of whether the different biases of upper and lower slopes were an artifact of small sample size or a factor that might be addressed in the model. Future work could adapt such simulations to represent weather patterns over a seasonal time scale in order to develop a flow budget for the MCs, including quantification of total water stored in the soil profile or simulation of plant growth. The Hydrus model could also be used in conjunction with physically-based erosion models to simulate how different configurations on the hillslope might reduce erosion and to predict how quickly the MCs would fill with sediment.

References

Elrick, D. E., Reynolds, W. D. and Tan, K. A..1989. Hydraulic conductivity measurements in the unsaturated zone using improved well analyses. Ground Water Monitoring and Remediation, 9(3):184-193.

Malagnoux, M. 2008. Degraded Arid Land Restoration for Afforestation and Agro-Silvo-Pastoral Production through New Water Harvesting Mechanized Technology. In: Lee C., Schaaf T. (eds) The Future of Drylands. Springer, Dordrecht, pp: 269-282.

Oweis, T. Y. 2017. Rainwater harvesting for restoring degraded dry agro-pastoral ecosystems: a conceptual review of opportunities and constraints in a changing climate. Environmental Reviews, 25(2):135-162.

Oweis, T. Y., Karrou, M., Ziadat, F. and Awawdeh. F., 2011. Rehabilitation and integrated management of dry rangelands environments with water harvesting. International Center for Agricultural Research in the Dry Areas (ICARDA), Report no. 9, Alepo, Syria, 208 pp.

Reynolds, W. D., and Elrick, D., 1985. Insitu measurement of field-saturated hydraulic conductivity, sorptivity, and the alpha-parameter using the Guelph Permeameter. Soil Science, 140(4):292-302.

Representation of Large Wood Structures Using a Numerical Two-Dimensional Model

Michael Sixta, Hydraulic Engineer, Bureau of Reclamation, Denver, CO, msixta@usbr.gov
Caroline Ubing, Hydraulic Engineer, Bureau of Reclamation, Denver, CO, cubing@usbr.gov

Abstract

An understanding of the importance and need of large wood in river systems has gained significant strength in the research and applied studies of eco-hydraulics in recent history. Large wood structures are being incorporated into habitat restoration project designs at a more frequent rate today than ever before. There is usually a significant impact to the local hydraulics with the addition of these types of structures that drives their geomorphic influence. Successful restoration projects require an understanding of the relationship between the structure, resultant hydraulic processes, and eventual geomorphic forms. Having greater confidence in how to best represent these features numerically will aid in their design helping drive down inflated safety factors resulting in better, faster, cheaper installations as well as ensure feature effectiveness, stability, and longevity.

The Bureau of Reclamation has partnered with the Sonoma County Water Agency to research how to best represent large wood structures in a depth-averaged two-dimensional numerical hydraulic model (SRH-2D) by using a selection of methodologies through a matrix of varying model parameters and techniques. Applying the results of this sensitivity analysis to a field data set the best overall methodology was selected and it was determined just how applicable two-dimensional hydraulics modeling can be in representing large wood structures.

Introduction

Large Wood Structures (LWS) are widely used in stream and watershed restoration projects due to the many ecological benefits it offers. They have been shown to provide excellent fish habitat for a variety of life stages and species by developing deep scour pools with associated tailout spawning areas as well as complex cover (Saldi-Caromile et al., 2004). They also add much needed organic carbon into the system (Wohl et al., 2016). However, its use in streams has unresolved challenges regarding its impact to stream morphology, safety and risk, as well as, design and modeling uncertainties. Large wood structures are being incorporated into project designs at a more frequent rate today than ever before. Hydraulic model results are instrumental in choosing structure type, placement, design parameters, and overall benefit. There is usually a significant impact to the local hydraulics with the addition of these types of structures that drives their geomorphic influence. Successful restoration projects require an understanding of the relationship between the structure, resultant hydraulic processes, and eventual geomorphic forms. However, accurately representing the large wood geometry and structural evolution through hydro-dynamics modeling can be challenging.

There are several ways to incorporate these structures into a hydraulics model, and although the resultant patterns are inherently sensible to what would be expected, the validation between what the model outputs and what is observed in the field is still being resolved through collaborative research. Having a better understanding of the model limitations along with the effects of implementing these types of structures through improved numerical model representation will aid in ensuring the design and effectiveness of stable wood structures. Increasing our confidence in how we numerically represent the hydraulic effects of large wood structures will help project managers and designers alike by driving down inflated factors of safety resulting in better, faster, and cheaper installations.

Modeling Large Wood Structures

Two-dimensional numerical hydraulics modeling is becoming more conventional than ever before and is far superior to one-dimensional models in examining large wood effects. The advantage of using two-dimensional models in habitat restoration studies is their capability of reproducing the detailed flow features, such as transverse flows, eddies, velocity gradients, and other complex flow patterns found within streams (He et al., 2009). Modeling these structures in two dimensions allows for a more detailed analysis of the flow stages, depth-averaged velocity magnitudes and vector directions, shear stresses, and bed scour, all of which are common parameters when evaluating habitat suitability and structure stability.

Model Selection

This research used SRH-2D as its modeling platform. SRH-2D is a model that is developed and maintained by the Bureau of Reclamation's (Reclamation) Sedimentation and River Hydraulics Group in Denver, Colorado. SRH-2D is a two-dimensional (2D) fixed or mobile-bed hydraulics and sediment transport model for river systems (Lai, 2008). This research made use of only the fixed bed hydraulics module. SRH-2D solves the depth-averaged dynamic wave equations with a depth-averaged parabolic turbulence model using a finite-volume numerical scheme. The model adopts a zonal approach for coupled modeling of channels and floodplains; a river system is broken down into modeling zones (delineated based on natural features such as topography, vegetation, and bed roughness), each with unique parameters such as flow resistance. SRH-2D adopts an unstructured hybrid mixed element mesh, which is based on the arbitrarily shaped element method of Lai (2000) for geometric representation. This meshing strategy is flexible enough to facilitate the implementation of the zonal modeling concept, allowing for greater modeling detail in areas of interest that ultimately leads to increased modeling efficiency through a compromise between solution accuracy and computing demand.

Study Approach

Reclamation partnered with the Sonoma County Water Agency in Santa Rosa, California to research how to best represent large wood structures with a two-dimensional numerical hydraulics model using a two-phased approach. Phase I employed a sensitivity analysis through utilizing numerous methodologies with a matrix of varying model parameters and geometric representation techniques. Phase II applied the results of the sensitivity analysis that yielded the most reasonable foreseen modeling approaches to a field data set to determine the best overall methodology and see how applicable two-dimensional hydraulics modeling can be in representing large wood structure effects.

Phase I — Sensitivity Analysis

Site Selection: The sensitivity analysis (phase I) utilized a habitat restoration site on the upper Entiat River in north-central Washington. The reach of river selected, locally known as the Stormy Reach, can be characterized as being a slightly-to-moderately sinuous single thread channel with a relatively low gradient, gravel-dominated bed, and active unconfined floodplain (average floodplain width much greater than average active channel width) with high in-channel complexity and lateral controls consisting of alluvial fans, bedrock, and levees that constrain the channel position.

The small subset area focused on for the sensitivity analysis features two large wood structures. The upstream structure is intended to deflect flow away from the bank, while the downstream structure splits the flow in the active channel. Two non-uniform, unstructured meshes were generated using Aquaveo's SMS software. Rectangular elements were used within the active channel with transverse spacing ranging from 5 ft near the structures to 15 ft at the upstream and downstream edges of the model. A combination of triangular and rectangular elements was used to mesh the large wood structures and overbank areas. Six material types were identified within the project area (Figure 1) with Manning's roughness (*n*) values based on previous model calibration efforts (Sixta, 2018) and published literature values (Chow, 1959).
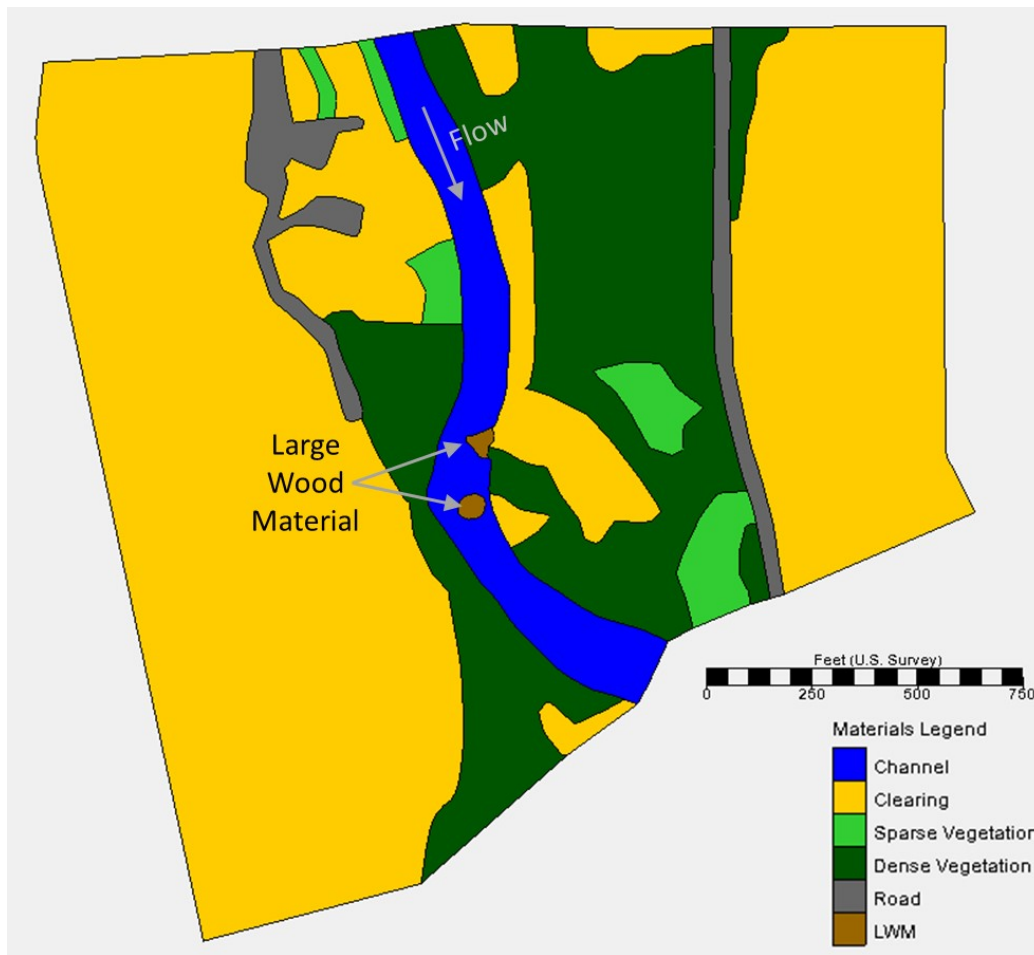
Figure 1. Sensitivity analysis model domain and material delineations.

Modeling Methodology: For the sensitivity analysis, large wood structures were modeled utilizing four methods: adding obstructions (fully or partially blocked), increasing the Manning's roughness value (n), increasing the drag coefficient (C_D), or a combination. A total of 15 model scenarios were executed, including baseline conditions, Table 1.

Table 1. Sensitivity analysis matrix.

Scenario No.	Method	Variation
1	Baseline Conditions	$n = 0.03$; $C_D = 0$
2	Full Obstruction	$n = 0.03$
3	Full Obstruction + increase roughness	$n = 0.1$
4	Full Obstruction + increase roughness	$n = 0.2$
5	Full Obstruction + increase roughness	$n = 1.0$
6	Increase drag coefficient	$C_D = 1.3$
7	Increase drag coefficient	$C_D = 10$
8	Increase drag coefficient	$C_D = 25$
9	Increase roughness	$n = 0.1$
10	Increase roughness	$n = 0.2$
11	Increase roughness	$n = 1.0$
12	Partial obstruction	$n = 0.03$
13	Partial obstruction + increase roughness	$n = 0.1$
14	Partial obstruction + increase roughness	$n = 0.2$
15	Partial obstruction + increase roughness	$n = 1.0$

Fully blocked obstructions were created by raising the model mesh elevations to the design elevation of the top of the large wood structure. While adding a fully blocked obstruction is a fairly simple way to add LWS to the model mesh, it does not account for structure permeability and may prove to produce overly conservative results. Assuming the structures are not porous can result in a 10-20% overestimation of drag force (Manners et al., 2007). Furthermore, a fully blocked obstruction will result in a dry (assuming no overtopping) structure footprint, which affects habitat suitability analysis results. Therefore, representing a LWS as a partially blocked obstruction through three, 10 ft-by-5 ft elevated rectangles spaced 14 ft apart (center-to-center), was another employed method to try and better simulate the permeable nature of LWS.

A third method solely increased the Manning's roughness value within the LWS footprint. Selection of roughness values for complex natural channels with debris is an art based on judgement and experience (Fasken, 1963). Three arbitrary values (0.1, 0.2, and 1.0) were selected based on previous studies and literature value recommendations (Sixta, 2018; Shields and Gippel, 1995).

Finally, increasing the drag coefficient within the LWS footprint was another tested approach. An initial drag coefficient of 1.3 is the upper bound recommended for circular cylinders over the range of Reynolds number typical of natural streams (Hoerner, 1958). The subsequent drag coefficient values were arbitrarily assigned based on the results using $C_D = 1.3$. It's important to note that commonly cited drag coefficients (e.g. Engineering ToolBox, 2004) are not applicable for 2D depth-averaged processes that are being modeled; the drag coefficient was really used as a calibration parameter when used for representing LWS.

Model response to each method was evaluated based on changes from baseline conditions for water depth, velocity magnitude, and shear stress, which were evaluated through monitoring points at seven locations (Figure 2).

Figure 2. Sensitivity analysis model response evaluation areas.

Sensitivity Analysis Results: Hydraulically, LWS's act as large roughness elements that provide a scale-dependent varied flow environment, reduce average velocity, and locally elevate the water surface profile (Gippel, 1995). More specifically, and based on field observations and hydraulic principles, model results should show an increase in flow depth upstream of the structure and decreased velocity through the structure and in its wake. Meanwhile the velocity magnitude through the main channel and adjacent to the structure should increase. Baseline conditions, in which structures were not represented, established a control for the sensitivity analysis.

The fully blocked obstructions were not overtopped during the evaluated flow event. Therefore, the cells with varying roughness values were not activated and no differences were observed amongst scenarios 2 through 5. Full obstructions altered flow depth and velocity magnitude surrounding the structures; an overall increase in depth was observed; velocities decreased upstream and in-between the two structures and increased in the channel adjacent to and downstream of the structures.

Velocity magnitudes through the partially blocked obstructions varied significantly depending on the assigned roughness value, while velocities were seen to increase in the channel adjacent to the structures likely due to the flow contraction. The flow depth increased at all monitoring point locations except for in the channel downstream of each structure.

Only increasing the Manning's roughness value within the footprint of each structure resulted in what were deemed appropriate trends in flow depth and velocity; however, shear stress is dependent on the roughness value and do not yield realistic results when using artificially high roughness values and should be cautioned against using in design. Three different roughness values were evaluated, and while the trends were consistent throughout, the location most influenced by the change in roughness depended on its value.

The relationship between LWS and hydraulic function is quantified through drag force (F_D), which is the difference in pressure the water exerts on the structure from upstream to downstream (Abbe and Montgomery, 1996). LWS can be a significant source of form drag in a river, accounting for 50 percent of the total drag in the channel (Curran and Wohl, 2003). One of the main (and user defined) variables in computing F_D is the drag coefficient (C_D). Increasing the drag coefficient resulted in an increase in flow depth at six of the seven monitoring points, an increase in flow velocity adjacent to each LWS, a decrease in velocity within and upstream of the structures, and a decrease in shear stress within the structures. The magnitude of change in these three hydraulic parameters increased as the drag coefficient increased.

Phase II – Field Verification

The methods that yielded what were deemed as being the most realistic results from the sensitivity analysis are being used to evaluate the overall representation effectiveness on a set of field installations. The only method not utilized in the field case modeling was the partial blocked obstruction based on its arbitrary nature and inconsistencies with repeat application. The field verification phase of the research is still ongoing.

Site Selection: The field sites being utilized for effectiveness modeling are located on Dry Creek below Lake Sonoma near Healdsburg, California. Numerous wood installations on three distinct project sites, all on the order of one river mile in length, were recently installed for the purposes of habitat restoration. Included with each of these projects is an extensive monitoring program that includes the collection of ground surface topography, depth, water surface elevation, and velocity measurements using a combination of total station, an unmanned aircraft system, and velocity flow meter mounted on a wading rod.

Methodology Verification: The tested modeling methodologies are currently being utilized to see how closely the model can represent what was measured in the field. Field data was utilized to calibrate a 'baseline' conditions model by modifying the channel roughness value

(Manning's n) until the observed water surface elevations were matched in a part of the project reach that was deemed unaffected by the presence of LWS. The various modeling methodologies were then employed to the baseline conditions and validation was performed by spatially comparing the field measured discharge flux and water depths to the modeled values. Given the sporadic and instantaneous nature of velocity, this data was only qualitatively used, ensuring consistent trends between the observed and predicted values were being represented.

Conclusion

The overall goal of this research is to evaluate the representation effectiveness of modeling LWS with a two-dimensional hydraulics model to aid in the design of these features as well as gain a better understanding of the model limitations and uncertainty. The intent behind using a two-dimensional model was to make the results applicable to large scale restoration projects with potentially hundreds of wood installations. Therefore, each structure was represented through idealized simplifications of actual geometries. A sensitivity analysis of various modeling methodologies was utilized to gain a better understanding of the range of hydraulics impact that can be registered by varying different model input parameters. These modeling methodologies are currently being used to evaluate the representation effectiveness on a series of field installations; this phase of research is still in progress. A preferred method, at least with respect to absolute accuracy, may not surface from this effort considering each method will be individually calibrated to field data. However, it is hopeful that a greater confidence in model results forecasting structure effects for whichever method is chosen will be gained that ultimately leads to better design and consequently greater structure stability as well as a clearer picture of the particular project benefits that are being sought in the goals and objectives.

References

Abbe, T., and D.A. Montgomery. 1996. Large woody debris jams, channel hydraulics and habitat formation in large rivers. Regulated Rivers Research and Management, 12, 201-221.

Chow, V.T. 1959. Open-channel hydraulics (Vol. 1). New York: McGraw-Hill.

Curran, J.H., and Wohl, E.E. 2003. Large woody debris and flow resistance in step-pool channels, Cascade Range, Washington. Geomorphology, 51(1-3), 141.

Engineering ToolBox. 2004. *Drag Coefficient*. [online] Available at: https://www.engineeringtoolbox.com/drag-coefficient-d_627.html [Accessed May 3, 2019].

Fasken, G.B. 1963. Guide for selecting roughness coefficient "n" values for channels. USDA Soil Conservation Service, Lincoln, Neb.

Gippel, C.J. 1995. Environmental Hydraulics of Large Woody Debris in Stream and Rivers. Journal of Environmental Engineering, 121(5): 388-395.

He, Z., W. Wu, and F.D. Shields. 2009. Numerical analysis of effects of large wood structures on channel morphology and fish habitat suitability in a Southern US sandy creek. Ecohydrology. John Wiley & Sons, Ltd.

Hoerner, S.F. 1958. *Fluid dynamic drag*. Hoerner, New Jersey.

Lai, Y.G. 2000. "Unstructured grid arbitrarily shaped element method for fluid flow simulation," AIAA Journal, 38(12), 2246-2252.

Lai, Y.G. 2008. SRH-2D version 2: Theory and User's Manual. Sedimentation and River Hydraulics–Two-Dimensional River Flow Modeling, US Department of Interior, Bureau of Reclamation, November.

Manners, R. B., Doyle, M. W., & Small, M. J. 2007. Structure and hydraulics of natural woody debris jams. Water Resources Research, 43(6).

Saldi-Caromile, K.K., K. Bates, P. Skidmore, J. Barenti, and D. Pineo. 2004. Stream Habitat Restoration Guidelines: Final Draft. Co-published by the Washington Departments of Fish and Wildlife and Ecology and the U.S. Fish and Wildlife Service. Olympia, Washington.

Shields, F.D. and Gippel, C.J. 1995. Prediction of Effects of Woody Debris Removal on Flow Resistance. Journal of Hydraulic Engineering, 121(4): 341-354.

Sixta, M. 2018. Hydraulics Modeling of the Gray and Stormy Reaches, Entiat River, WA, Pacific Northwest Region. U.S. Department of Interior, Bureau of Reclamation, Technical Service Center, Denver, Colorado. September 2018.

Wohl, E., B.P. Bledsoe, K.D. Fausch, N. Kramer, K.R. Bestgen, and M.N. Gooseff. 2016. Management of large wood in streams: An overview and proposed framework for hazard evaluation. Journal of American Water Resources Association (JAWRA), 52(2): 315-335.

The KINEROS2-AGWA Suite of Modeling Tools

David Goodrich, Research Hydraulic Engineer, USDA-ARS, Tucson, Arizona, dave.goodrich@ars.usda.gov

D. Phillip Guertin, Professor, Univ. of Arizona, Tucson, AZ, dpg@email.arizona.edu

Shea Burns, Senior Research Specialist, Univ. of Arizona, Tucson, Arizona shea.burns@ars.usda.gov

Carl Unkrich, Hydrologist, USDA-ARS, Tucson, AZ, carl.unkrich@ars.usda.gov

Lainie Levick, Principal Research Specialist, Univ. of Arizona, Tucson, Arizona, llevick@email.arizona.edu

Yoganand Korgaonkar, Graduate Student, University of Arizona, Tucson, AZ, yoganandk@email.arizona.edu

Phil Heilman, Research Leader, USDA-ARS, Tucson, AZ, phil.heilman@ars.usda.gov

Mariano Hernandez, Hydrologist, USDA-ARS, Tucson, AZ, mariano.hernandez@ars.usda.gov

Ben Olimpio, Graduate Student, University of Arizona, Tucson, AZ, bolimpio@email.arizona.edu

Haiyan Wei, Assistant Research Specialist, University of Arizona, Tucson, AZ, haiyan.wei@ars.usda.gov

Jane Patel, GIS Analyst, Tucson Water, Tucson, AZ, jane.patel@tucsonaz.gov

Mark Kautz, Hydrologist, USDA-ARS, Tucson, AZ, mark.kautz@ars.usda.gov

Abstract

KINEROS2 (K2) is a spatially distributed rainfall-runoff erosion model dating back to the 1960's. Development and improvement of K2 has continued for a variety of projects and purposes resulting in an informal suite of K2-based modeling tools. Like any detailed, distributed watershed modeling tool, the K2 suite of tools can require considerable time to delineate watersheds, discretize them into modeling elements and then parameterize these elements. These requirements motivated the development of the Automated Geospatial Watershed Assessment (AGWA) tool (see: www.tucson.ars.ag.gov/agwa or https://www.epa.gov/water-research/automated-geospatial-watershed-assessment-agwa-tool-hydrologic-modeling-and-watershed). AGWA is a GIS interface jointly developed by the USDA-Agricultural Research Service, the U.S. Environmental Protection Agency, the University of Arizona, and the University of Wyoming to automate the parameterization, execution, and visualization of simulation results of a suite of hydrologic and erosion models (RHEM, KINEROS2, and SWAT) using nationally available data or user provided input. The objectives of this paper are to: 1) Provide background on K2 and AGWA; 2) Provide an overview of the main features of K2 and AGWA tools; 3) Describe new features and tools; and, 4) Discuss plans for future model improvements.

Introduction

The KINEROS2 (K2) and AGWA suite of modeling tools have been discussed in prior Joint Federal Interagency and SEDHYD conference papers (Goodrich et al. 2010; 2015). Therefore, abbreviated information on the background and development of K2 and AGWA will be

presented herein. Greater emphasis will be given to describing features (historic and new) of K2 and AGWA.

KINEROS2 - KINematic Runoff and EROSion Model

Development of KINEROS and subsequently KINEROS2, by the USDA-Agricultural Research Service dates back to the 1960s. KINEROS was formally released in 1990 (Woolhiser et al. 1990; Smith et al. 1995). The model simulates runoff, erosion, and sediment transport. The kinematic equations used for flow routing are coupled interactively with the Smith-Parlange infiltration equation. KINEROS and K2 represent a watershed as a collection of overland flow elements (planar or curvilinear) contributing to channels as depicted in Figure 1. Representation of the watershed in this form enables solution of the flow-routing partial differential equations in one dimension that substantially reduces simulation time. KINEROS2, released in 2002 (Goodrich et al. 2002) includes an updated overall computational structure and additional model element types compared to KINEROS.

In addition to the overland flow and trapezoidal channel model element depicted in Figure 1, KINEROS2 includes the following additional model elements:

- Compound trapezoidal channel: Includes an overbank channel section with the capability of having different infiltration and roughness characteristics
- Irregular channel cross-section: As might be derived from a ground survey or extracted from LIDAR-derived topography (more details provided below)
- Ponds/Detention Structures: Arbitrary shape, controlled outlet – discharge as a f(stage)
- Urban: Mixed infiltrating/impervious surfaces with various runoff-runon combinations
- Culverts/Pipes: Circular with free surface flow
- Injection: Hydrographs and sedigraphs injected from outside the modeled system, or from a point discharge (e.g. pipe, drain)
- Diversion: Divert water and sediment from a single upstream element to as many as 10 downstream elements
- Adder: Summing the outflow from more than two upstream elements

A relatively thorough overview of the theoretical background of K2, including several applications, is presented by Semmens et al. (2008). Goodrich et al. (2012) provided further details on K2 and included a discussion of model limitations, expectations, and strategies and approaches for K2 calibration and validation. Both of these publications are available at https://www.tucson.ars.ag.gov/unit/Publications/Search.html. K2 is public domain software that is distributed freely, along with associated model documentation and example input files (www.tucson.ars.ag.gov/kineros). Additional versions of KINEROS2 have been developed for specialized applications. They include the KINEROS2-Opus2 (K2-O2) continuous model that can simulate biogeochemical nutrient cycling and plant growth under various types of management (Massart et al. 2010). The documentation and user manual for K2-O2 are available at http://www.tucson.ars.ag.gov/k2o2/doku.php. A flash flood forecasting version of K2 for a rapidly responding basin that ingests National Weather Service (NWS) Digital Hybrid Reflectivity (DHR) or Digital Precipitation Rate (DPR) radar products has also been developed (Unkrich et al. 2010). It has undergone testing on 40+ watersheds in over a dozen NWS Weather Forecasting Offices (Schaffner et al. 2014; 2016; 2017) and is operational in 10+ watersheds in the southwest. Guber et al. (2010) used K2 as the runoff and routing tool to simulate the transport of indicators for organisms and manure-borne pathogens by coupling K2 to the Simulator of Transport With Infiltration and Runoff (STWIR).

Watershed topography discretized into areas of predominately overland flow and a channel network

Model elements:
Overland Flow Planes
Trapezoidal Open Channels

Upland Plane - concentrated flow into upstream end of channel element

Lateral Plane - distributed inflow along channel element

Overland Flow Plane

rainfall, r

infiltration, f

$$\frac{\partial h}{\partial t} + \alpha m h^{m-1} \frac{\partial h}{\partial x} = r - f$$

Trapezoidal Open Channel

q_1 q_2

A = cross sectional area of flow
Q = discharge

$$\frac{\partial A}{\partial t} + \frac{\partial Q}{\partial A} \frac{\partial A}{\partial x} = q_1 + q_2 - f$$

infiltration, f

Figure 1. Abstraction of watershed discretized into KINEROS2 model elements (Goodrich et al. 2012)

The Automated Geospatial Watershed Assessment (AGWA) Tool

AGWA (Miller et al. 2002; 2007) was developed to support the parameterization, execution, and visualization of simulation results of K2 and the Soil Water Assessment Tool (SWAT; Arnold and Fohrer 2005) using GIS tools and geospatial data. AGWA was developed jointly by the USDA-ARS Southwest Watershed Research Center, US EPA Landscape Ecology Branch, University of Arizona, and University of Wyoming. The development of AGWA was undertaken with the following objectives: 1) that it provides simple, direct, transparent, and repeatable parameterization routines through an automated, intuitive interface; 2) that it is applicable to ungauged watersheds at multiple scales; 3) that it evaluates the impacts of management and be useful for scenario development; and 4) that it uses free and commonly available GIS data layers. Like K2, AGWA is public domain software available from the AGWA website (Miller et al. 2007; www.tucson.ars.ag.gov/agwa). The current version of AGWA is for ArcGIS/ArcMap 10.x. The AGWA web site also contains documentation, supporting references, tutorials, and a user forum. Support for K2 and AGWA is typically accomplished via the user forum, e-mail, or phone communication.

To derive watershed model parameters with AGWA, descriptive geospatial data layers over the watershed of interest are required. These include raster based digital elevation model (DEM)

data, polygon soils data, and a raster based land cover/land use data. In addition to relatively common DEM data from the USGS, LIDAR data can also be used if interpolated into a raster format. Soils data that are supported include NRCS SSURGO and STATSGO as well as FAO data. Land cover and land use data that are supported by AGWA include NLCD, NALC, and GAP. Precipitation data are required to drive the model and can be input in several different formats.

The primary steps for conducting watershed modeling and analysis with AGWA are depicted in Figure 2 and include:

- Selection of a watershed outlet and delineation of the contributing watershed area
- Model selection and watershed discretization into model elements
- Watershed model element parameterization
- Precipitation input
- Model execution
- Change Analysis
- Results visualization.

AGWA intuitively guides the user through these steps. In addition to analyzing a single watershed, AGWA has an area of interest tool for multi-watershed analysis. During the delineation step AGWA will automatically fill the DEM if necessary and compute associated flow direction and flow accumulation rasters.

There are several options for *discretizing* the watershed into spatially distributed model elements. At this stage the user selects whether K2 or SWAT will be used, as the two models conceptualize stream contributing areas differently. Commonly used is the contributing source area (CSA). At this area, the head of a first order channel is initiated. The CSA can be input as an area or a percentage of the total drainage of the watershed being analyzed. The second option is selecting a maximum hillslope flow length before stream initiation, and third, importation of a pre-existing stream network. A fourth case uses a point theme to define channel initiation points. In the third and fourth case the most upstream points of the existing stream network and the initiation points, respectively, are snapped to the stream network defined by DEM flow accumulation.

In the *parameterization* step the model element polygons are intersected with soil polygons and the land use/land cover raster. AGWA contains lookup tables (editable) that relate the land cover, soils, and topographic properties to necessary hydrologic parameters for each model element. These tables were developed based on prior studies (Woolhiser et al. 1990; Rawls et al. 1982, etc.), experimental data, and expert opinion. AGWA uses regional empirical hydraulic geometry relationships (Bieger et al. 2015) to estimate trapezoidal channel geometry if that option is selected. It should be stressed that model parameters derived from the look-up tables and channel geometry regressions should only be viewed as initial estimates. An interface is provided to input multipliers to a subset of the more sensitive parameters that are applied uniformly across all model elements to facilitate simple manual calibration. As AGWA generates input files for K2 and SWAT it is relatively straightforward to link to external parameter estimation software (Hernandez et al. 2000) if model calibration is desired.
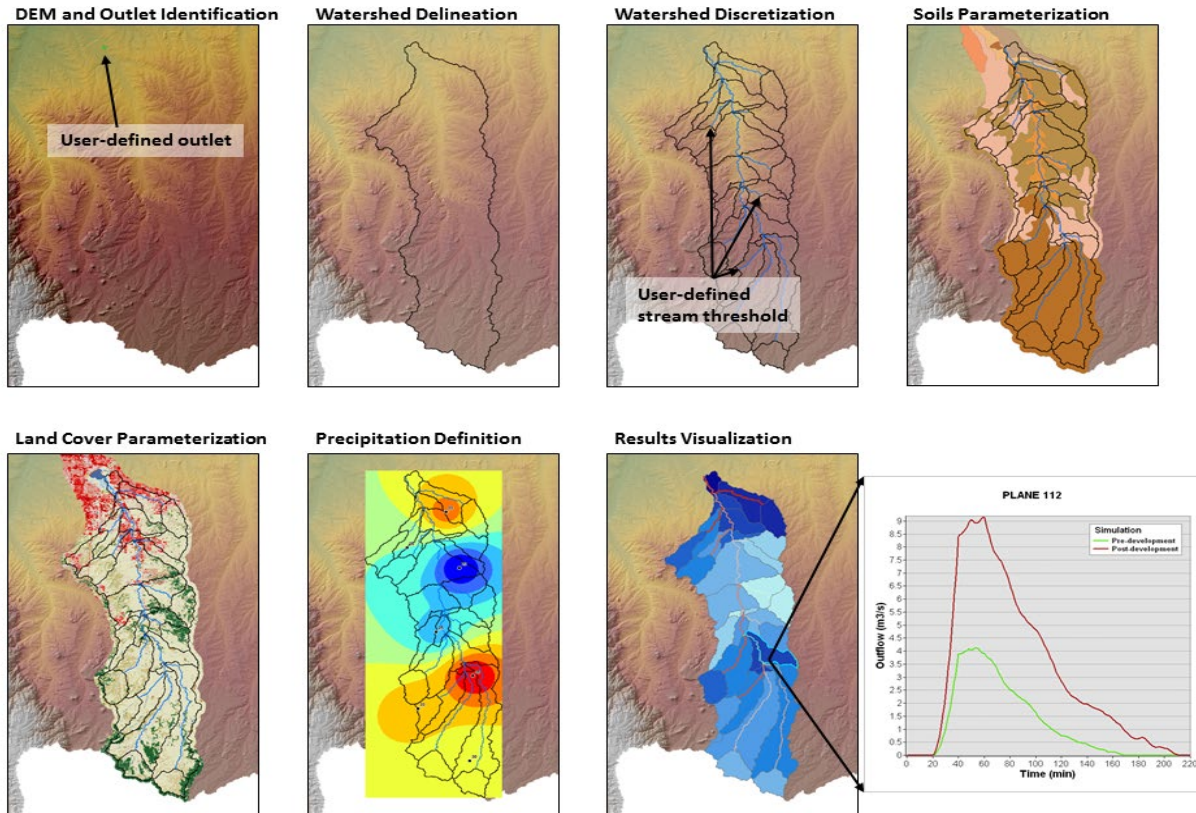
Figure 2. Primary steps in a watershed assessment using AGWA. Watershed delineation and subdivision into model elements is done using a DEM. Model elements are parameterized with soils, topography and land cover layers. Precipitation drives the model and spatially distributed results for each model element are imported and visualized in the GIS. Hydrographs and sedigraphs for any model element selected can also be displayed (lower right) (Goodrich et al. 2015).

To drive either K2 or SWAT, *precipitation inputs* must be defined. As SWAT is a continuous model, daily rainfall from one or more rain gauges is required. Daily precipitation and temperature files can also be generated from a nearby, user-selected weather station (weather stations are included in AGWA for the US). In the case of more than one gauge, AGWA will create Thiessen polygons that are intersected with watershed elements to create area-weighted precipitation inputs. The current release version of K2 is event-based but a continuous version is undergoing testing (see below). For the event-based version the user can input observed or user-defined hyetographs, design storms, or raster based precipitation surfaces representing return period-durations depths. For NOAA design storms, intensity distributions defined by SCS regional types can be selected.

Model execution also encompasses model simulation file creation. Simulation creation entails selection of the files created in the prior steps. Between creation and execution the user may select parameter multipliers for K2. In SWAT, the user can define other aspects of the simulation not defined by AGWA in the steps above, such as subbasin adjustment factors, crop types, simulation start and stop dates, groundwater parameters and the output time step. By separating creation and execution, the user can edit input files and apply the adjustments noted above and rerun the simulation without having to repeat the prior processing steps in AGWA.

Change analysis is facilitated in AGWA by storing simulation results for all the model elements in flat files associated with the simulation. AGWA has the capability to difference results from multiple simulations and save the result in terms of absolute change or percent change for a variety of model outputs for each model element. This capability is especially useful for scenario analysis where the user can explore the hydrologic impacts of land cover change resulting from things like development or wildfires, changes in storm inputs, or the addition of ponds or constructed channel features.

Model *results visualization* maps the simulation results back into the GIS environment for selected output variables and for differences of output variables (absolute or percent change) between two simulations. A variety of outputs can be displayed for any upland or channel model element including major water balance components and fluxes (e.g. peak runoff rate, runoff volume, sediment yield, etc. – for a full list see the AGWA documentation). This function enables the user to visualize the spatial variability of model results and readily identify problem areas where conservation or mitigation efforts might be focused (e.g. application of post-fire mulch to reduce erosion). For K2 simulations, hydrographs and sedigraphs can also be displayed.

Specialized Tools Within AGWA: A number of tools within AGWA have been developed for various users to enable scenario analysis. These tools have been available for some time and include:

- Land Cover Modification Tool
- Multi-Point and Multi-Watershed Tool
- Riparian Buffer Tool
- Post Fire Assessment Tool
- Urban Tool (add-in to ArcMap)
- Channel Diversion – Artificial Wetlands Tool

New tools and features are described in the following section.

The *Land Cover Modification Tool* (LCMT) has proven to be one of the more widely used tools and its implementation within AGWA is the basis for several of the other tools. The LCMT allows users to modify a land cover map and run AGWA to simulate the hydrologic effects of the land cover change. Land cover modifications can account for fire, urbanization, or other natural or anthropogenic changes. The tool can be used with the supported AGWA datasets (MRLC, NALC, etc.) or with custom defined land covers. The classification choices for the modified surface are limited to those classifications found in the selected land cover look-up table.

The Land Cover Modification Tool offers four modification options. They allow the user to modify the land cover within an interactively drawn polygon, or within an existing polygon map.
- Single Change: Change all of the land cover in an area to a new land cover type
- Single Change: Change one land cover type in an area to a new land cover type
- Random Distribution: Change all of the land cover in an area to up to 3 new land cover types in a spatially distributed random pattern
- Random Distribution: Change all of the land cover in an area to up to 3 new land cover types in a patchy fractal distribution pattern

The multifractal surface generator was implemented to create more realistic land cover surfaces for multiple land cover classifications than those created with the spatially random surface

generator. It is based on a two-dimensional midpoint displacement algorithm (Saupe and Peitgen 1988) and allows users to specify multiple land cover classifications, the proportion of each class to be found in the new surface, the degree of clustering, and the boundary of the modification area. The modified surface contains land cover patches whose size is determined by the degree of clustering within the boundary area. A variant of the patchy fractal distribution pattern allows the user to specify the success level of a best management practice (e.g. brush management). For example, if herbicide application and reseeding in an area is 70% percent successful, then the final surface is created with a combination of 70% of the new land cover class (grass) and 30% of the current class (brush). This feature enables the simulation of various vegetation changes associated with management actions for U.S. Natural Resources Conservation Service's ecological sites and their state and transition models (Scott 2005).

The *Multi-Point and Multi-Watershed Tool* has two functions. The multipoint tool forces the watershed discretization to create the downstream location of channel element at specified locations or points of interest from a user input point shape file (e.g. campground, road crossing) so model simulation output is available at that point of interest. If point locations of downstream channel elements are not specified, their location is controlled by the discretization and flow accumulation process where channels converge. The multi-watershed tool was implemented so users could more efficiently perform AGWA analyses over an area of interest that includes multiple watersheds. A polygon defining the area of interest (e.g. property boundary, allotment boundary, parks) is input as well as an analysis extent region to limit the search area for the potential watershed outlets. AGWA will automatically delineate all watersheds within the boundary of interest and carry out the additional steps noted above (discretization, parameterization, etc.).
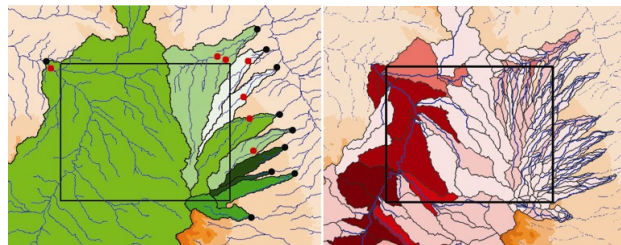
Figure 3. (left) Area of Interest outlet identification and delineation for the boundary. Red points indicate a potential outlet; black points are final watershed outlets that ensure watershed coverage of the area of interest. (right) Area of Interest watershed discretization

The *Riparian Buffer Tool* allows users to identify a section of a channel reach to insert a riparian buffer strip, one of the most commonly used best management practices, and simulate its effects using K2 (Scott 2005). Scenarios of buffer location, buffer geometry, and buffer land cover composition can be explored with the tool. If the selected reach does not fall along the entire length of a channel derived from AGWA discretization, the tool will further discretize the channel segment and the upland areas contributing to the buffer (Figure 4). A separate overland flow model element representing the buffer (No. 35 in Figure 4) is inserted between the upland area (No. 33) and the stream segment as K2 can simulate runoff-runon from one overland flow element to another with different characteristics. Geometry and cover characteristics for the element are entered by users via an AGWA input interface.
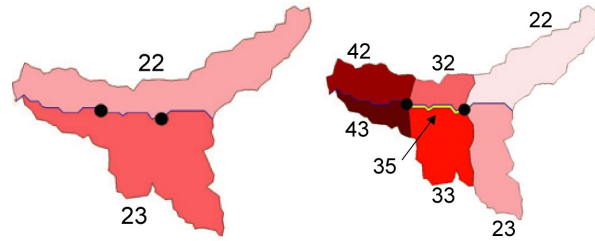
Figure 4. KINEROS2 Buffer discretization. (left) The unbuffered overland flow elements with buffer location and length defined by points. (right) The buffered overland elements (Goodrich et al. 2006)

AGWA/K2 and the _Post Fire Assessment Tool_ has gained relatively widespread use with the increasing size and frequency of wildfires. It has been adopted by the U.S. Department of Interior (DOI) National Burned Area Emergency Response (BAER) Team for post-fire watershed assessments following large wildfires. Its use by the DOI BAER team has greatly streamlined the hydrologic analysis component of the comprehensive, interdisciplinary BAER process (limited to 14 days) to develop a post-fire treatment plan. As part of the BAER process, a soil burn severity map is produced from a field verified remotely sensed Burned Area Reflectance Classification (BARC) map of the wildfire area. Burn severity is classified as high, medium, or low. With analysis from a limited number of watersheds where good rainfall-runoff data were available (Canfield et al. 2005; Sheppard 2016) look up tables were developed to adjust the saturated hydraulic conductivity and hydraulic roughness as a function of burn severity and pre-burn land cover. AGWA imports the soil burn severity map and automatically makes the parameter adjustments, with appropriate spatial weighting, to burn affected modeling elements. Pre- and Post-fire simulations driven by the same design storm can be done and using the AGWA simulation differencing the BAER teams can easily identify at-risk areas for high runoff and erosion potential to focus post-fire mitigation efforts. AGWA also has the ability to assess common post-fire treatments, such as the application of straw mulch. AGWA/K2 has been used on over 52 wildfires on over 3.8 million acres since 2011, and the AGWA team and a number of users were the recipients of the 2018 Federal Laboratory Consortium's Interagency Partnership Award. Further details on the Post-Fire Assessment and its application can be found in Guertin et al. (2019a; 2019b), Sidman et al. (2016a; 2016b), Natural Resources Conservation Service (2016), and Chen et al. (2013).

The AGWA _Urban Tool_ was developed with the intent of using K2 within AGWA to conduct relatively rapid green infrastructure (GI) planning and assessments from the lot-to-subdivision-to-watershed level (Korgaonkar et al. 2015). K2 provides the capability to model the built environment using its urban component by representing various flow-on and flow-off areas at the scale of a single housing lot or parcel. The AGWA Urban tool can model urban hydrology by representing different roof, driveway, yard, and street characteristics using the KINEROS2 urban element. The AGWA Urban tool is also capable of representing green infrastructure (GI) practices such as retention/detention basins, permeable driveways and streets, and rainwater harvesting off the roofs (Figure 5). The AGWA Urban tool can be utilized to model urban watersheds at various scales (parcel, subdivision, neighborhood, or city). Additionally, it can be used to assess the effect of GI practices on peak flows, volumes, and on water availability for domestic use. Korgaonkar et al. (2018) demonstrates these capabilities by modeling a small subdivision in Sierra Vista, Arizona.
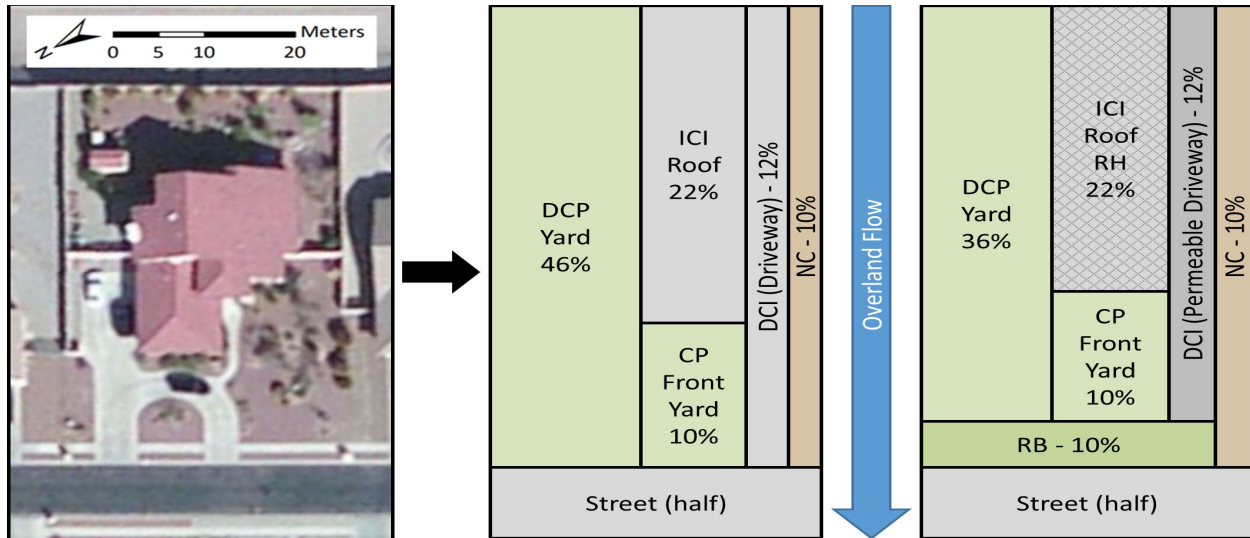
Figure 5: Representing a typical housing lot (Left) using the KINEROS2 Urban Element without GI practices (Center), and with retention basin (RB), permeable driveway (PD), and rainwater harvesting (RH) GI practices (Right). Percent values of each of the overland flow areas are indicative of the percent of the total parcel area. DCP: directly connected pervious; ICI: indirectly connected impervious; CP: connecting pervious; DCI: directly connected impervious; NC: noncontributing area. (Source: Korgaonkar et al. 2018)

Most natural watersheds are morphologically analogous to a tree structure where upstream elements can only contribute to a single downstream element. The basic structure of K2 mimics this concept. The AGWA *Channel Diversion – Artificial Wetlands Tool* was developed to address partial diversion of flow such as for irrigation, into constructed wetlands, etc. It consists of a K2 diversion element and input interface describing diversion functions. This element can divert water and sediment from a single upstream element to as many as 10 downstream elements. Diversion rates are determined from a user-supplied tabular relationship between the inflow rate from the upstream element and the rates diverted into each downstream element.

New Tools and Features

AGWA

The following tools have recently been developed for AGWA:

- Military Disturbance Tool
- Storage/Pond Characterization Toolbox
- Inundation Tool
- Facilitator Export Tool.

The AGWA *Military Disturbance Tool* (MDT) is used to simulate on-site and downstream effects on runoff and erosion resulting from military training activities. It is an optional tool in AGWA's parameterization step, and includes three general disturbance levels: light, moderate, and heavy. It modifies key input parameters for AGWA's embedded hydrologic models based on the disturbance level. Reductions to soil porosity, surface roughness (Manning's n), and canopy cover for each level are applied in K2, with hydraulic conductivity adjusted according to porosity. Reductions are also applied to canopy cover, litter cover, and basal cover for RHEM. Curve numbers in SWAT are modified for each disturbance level based on land cover type

condition and hydrologic soil group according to published data (i.e., USDA-NRCS 2004). The MDT is currently implemented only for K2 within AGWA, but will be available in the near term for RHEM. The MDT is discussed in more detail in another paper being presented at this conference (Levick et al. 2019).

The *Storage Characterization Toolkit* (SCT) has recently been developed and is currently available for AGWA. The SCT uses high-resolution topographic data (typically LIDAR) to characterize existing stocks ponds and link those with K2 discretizations created in AGWA. Using a user-defined threshold and an unfilled DEM, it can automatically identify features with a minimum area in the landscape/topography that detain or retain water. Once storage features are identified, the SCT determines their stage-volume-surface area relationship. Following this characterization and using additional user-defined outflow properties, the SCT can calculate and add discharge to the stage-volume-surface area relationship. The final step in the SCT associates the previously derived stage-volume-surface area-discharge relationship with a KINEROS2 discretization for use in AGWA. This tool has been developed as a separate toolkit and is in the process of being implemented in AGWA. The SCT is discussed in more detail in another paper being presented at this conference (Guertin et al. 2019b).

The *Inundation Tool* was developed to aid BAER teams to quickly estimate and map inundated areas at values at risk (VAR - e.g. visitor center) in post-fire situations. The AGWA Post-Fire Assessment tool discussed above can estimate post-fire peak discharge (Qp) rates from design storm input at any location in the watershed being modeled. The inundation tool was developed by Barlow (2017) as Python scripts accessed through an ArcGIS Toolbox that can use the AGWA/KINEROS2 Qp estimate with algorithms from the U.S. Army Corps of Engineers Hydrologic Engineering Center HEC-2 model (CEIWR-HEC 1990). It requires inputs related to channel properties that can be collected at specified channel cross sections in the field or estimated using high-resolution elevation data (e.g. LIDAR) in addition to hydraulic roughness values. It computes surface water elevations that are then compared to the channel cross section ground elevations to come up with **the** wetted area and mapped to estimate the inundated area. The tool is limited to relatively simple channel geometry and downstream conditions (without major constriction and backwater). This tool has been developed and is in the process of being implemented in AGWA.

The *Facilitator Export Tool* was developed to ingest K2 outputs for peak flow and sediment yield into the Facilitator Decision Support System. The Facilitator software helps individuals and groups of people in making decisions by encouraging participation by all stakeholders. It uses decision rules, a hierarchical system for ranking criteria, score functions and linear programming to identify preferred management options consistent with the ranking of criteria. It can accommodate measured data, simulation results from models like K2 and expert opinions in the decision making process (Yakowitz and Weltz 1998; Lawrence et al. 1997; (https://sourceforge.net/projects/facilitator/files/). It is also useful for documenting the decision making process.

Several new features have also been included to take advantages of new land cover data, more generalized channel geometry, more regionally specific storm distribution type curves, as well as tutorials. In the first case, AGWA has incorporated *Regional Hydraulic Geometry Relationships* from the United States compiled by Bieger et al. (2015) to improve initial channel geometry estimates nationally. The user can elect to have AGWA automatically select a relationship associated with the Physiographic Division, Province, or Section that intersects or is closest to the watershed, but also has the option of overriding that selection. These additional

relationships may provide better initial channel widths, which is important to channel infiltration dynamics and flow timing, because the relationships are based on physiographic regions, which are more representative of the climate and weather, geomorphology, soils, and land use patterns that influence channel geometries.

The ability to ingest and use the _LANDFIRE Existing Vegetation Cover_ (EVC; www.landfire.gov) dataset natively in AGWA has been added and offers the opportunity for improved land cover parameterizations. The EVC dataset has canopy cover information at the pixel level for tree, shrub, and herbaceous lifeforms, which is an improvement over the standard practice in AGWA where canopy cover is static and set to the average condition of each land cover type used. For K2, this addition invokes spatially varying saturated hydraulic conductivity (Ks) within a soil type given that soil-based Ks is adjusted by cover using the following equation:

$$Ks_{adjusted} = Ks_{soils} * (2.71828^{(canopy\ cover\ *\ 0.0105)}) * (1 - percent\ impervious) \qquad (1)$$

Note that this improvement will only be observed for the tree, shrub, and herbaceous lifeforms with canopy cover information in the dataset; the other land cover types will default to their average condition value from the AGWA land cover look-up table.

Regional Rainfall Distribution Curves: The use of 23 NRCS and Northeast Regional Climate Center (NRCC) rainfall distribution curves for K2 precipitation input has been added to AGWA to improve regional rainfall distribution of design storms. These additional curves cover 29 states, and offer an alternative to the SCS Type II rainfall distribution curve previously used in AGWA. In addition to the regional/state-based NRCS and NRCC distribution curves, the Type I, IA, and III curves were also added to AGWA to establish complete coverage of the United States. The AGWA website has an assortment of step-by-step _tutorials_ highlighting different functionality available in the tool. Currently there are 11 tutorials, and the requisite data to run them, available on the AGWA website, with plans to add more as new features and tools are released. Additionally, a series of YouTube video tutorials have been requested by users and are currently being developed and will be released as they are completed.

K2

For the overland flow elements, K2 now allows unequal widths at the upstream and downstream ends of the element. This essentially generalizes the plan form shape of the element from a rectangle to a trapezoid, and effectively creates a convergent/divergent flow condition depending on the relative widths at the upstream and downstream ends of the element. For channels, a new efficient method has been developed to carry out channel routing in a natural cross-section without having to approximate the channel with a trapezoidal shape. The hydraulic properties and their derivatives are obtained during routing by interpolation using piecewise cubic Hermite interpolating polynomials (Fritsch and Butland 1984), which have desirable shape and monotonicity properties for this application. Using components adapted from the model Opus (Smith 1992), K2 can also track the evolution of soil moisture between events, allowing continuous simulation. The soil water model is a finite difference solution to Richards' equation, and potential evapotranspiration is estimated using a method developed by Ritchie (1972).

Future Plans and Model Development

The flash flood forecasting (FFF) version of K2 is currently a standalone tool. This version utilizes input from NOAA National Weather Service radar products. Weighting coefficients relating the radar grid to the K2 model elements are currently computed via an external GIS operation. Incorporating the FFF version of K2 into AGWA will require a few additions: 1) distributing the FFF version of K2 with AGWA; 2) distributing the polar-centric radar grids for all available radars in the US; and, 3) adding and automating the GIS functionality that intersects the radar grid and watershed discretization to derive the weighting coefficients that associate radar grids cells to K2 model elements.

With the greater availability of LIDAR derived topographic data and the new functionality in K2 to do routing in an irregular channel cross-section, initial development of an AWGA channel cross-section extraction tool has been carried out. It will segment existing stream reaches identified by AGWA in the discretization into user defined intervals and extract channel cross sections perpendicular to the stream at the defined interval. Once the cross sections are extracted the tool will perform calculations to develop a table of stage, wetted area, and wetted perimeter that can be input into K2. Further refinement is required to treat cases where more than one channel section is identified near channel junctions. In addition, the K2 web site and documentation will be updated and efforts will be initiated to incorporate the continuous version of K2 into AGWA.

Future Releases of AGWA

Anticipating preliminary releases in the second half of 2019, the next major releases of AGWA will include dotAGWA, featuring a transition to the internet with a fully-featured, rich web-application, and AGWA for ArcGIS Pro, featuring a transition to ESRI's latest professional desktop GIS application. Although major ESRI ArcMap releases beyond 10.6 are not anticipated, support for AGWA 3.x for ArcMap 10.x versions will continue indefinitely. Additionally, support for AGWA 2.x for ArcMap 9.x and AGWA 1.x for ArcView 3.x can be provided for users who are unable to transition to current ESRI desktop GIS applications.

The transition to dotAGWA and AGWA for ArcGIS Pro will feature a shared Python codebase of core functionality. This will allow both versions to maintain parity such that output between the two is indistinguishable given the same input. This may also offer the opportunity to import/export input and output between the applications. The transition will also more completely leverage the geoprocessing tools in ArcToolbox, improving robustness and reliability, and allowing for improved troubleshooting of unexpected behavior.

Acknowledgements

References

Arnold, J.G., and Fohrer, N. 2005. SWAT2000: current capabilities and research opportunities in applied watershed modeling. Hydrological Processes 19(3): 563-572.

Barlow, J.E. 2017. Python Tools to Aid and Improve Rapid Hydrologic and Hydraulic Modeling with the Automated Geospatial Watershed Assessment Tool (AGWA). Unpublished M.S. Thesis, University of Arizona.

Bieger, K., Rathjens, H., Allen, P.M., and Arnold, J.G. 2015. Development and Evaluation of Bankfull Hydraulic Geometry Relationships for the Physiographic Regions of the United States, Journal of the American Water Resources Association (JAWRA), 51(3): 842-858. DOI: 10.1111/jawr.12282

Canfield, H.E., Goodrich, D.C., and Burns, I.S. 2005. Selection of Parameter Values to Model Post-Fire Runoff and Sediment Transport at the Watershed Scale in Southwestern Forests. In: Proceedings for the 2005 ASEC Watershed Management Conference, Managing Watersheds for Human and Natural Impacts: Engineering, Ecological, and Economic Challenges, Williamsburg, VA, July 19-22, 2005. http://dx.doi.org/10.1061/40763(178)48.

CEIWR – HEC (Corps of Engineers - Institute for Water Resources – Hydrologic Engineering Center). 1990. Hec-2 Water Surface Profiles User's Manual. U.S. Army Corps of Engineers, Institute for Water Resources, Hydrologic Engineering Center, Davis, CA

Chen, L., Berli, M., and Chief, K. 2013. Examining Modeling Approaches for the Rainfall-Runoff Process in Wildfire-Affected Watersheds: Using San Dimas Experimental Forest. Journal of the American Water Resources Association, 49(4): 851-866.

Fritsch, F., and Butland, J. 1984. A Method for Constructing Local Monotone Piecewise Cubic Interpolants. SIAM Journal on Scientific and Statistical Computing, Volume 5, Number 2, pages 300-304.

Goodrich, D.C., Unkrich, C.L., Smith, R.E., and Woolhiser, D.A. 2002. KINEROS2 - A distributed kinematic runoff and erosion model. in Proceeding of the Second Federal Interagency Hydrologic Modeling Conference, July 28 - August 1, 2002, Las Vegas NV, CD-ROM, 12 p.

Goodrich, D.C., Scott, S., Hernandez, M., Burns, I.S., Levick, L.R., Cate, A., Kepner, W., Semmens, D.J., Miller, S.N., and Guertin, D.P. 2006. Automated geospatial watershed assessment (AGWA) - A GIS-based hydrologic modeling tool for watershed management and landscape assessment. Proc. 3rd Fed. Interagency Hydrologic Modeling Conf., April 2-6, 2006. Reno, Nevada. https://www.gcmrc.gov/library/reports/physical/Fine_Sed/8thFISC2006/3rdFIHMC/1D _Goodrich.pdf.

Goodrich, D.C., Unkrich, C.L., Smith, R.E., Woolhiser, D.A., Guertin, D.P., Hernandez, M., Burns, S., Massart, J., Levick, L., Miller, S., Semmens, D., Keefer, T., Kepner, W., Nearing, M., Heilman, P., Wei, H., Paige, G., Schaffner, M., Yatheendradas, S., Gupta, H., Wagener, T., Troch, P., Brookshire, D., Guber, A.K., Pachepsky, Y.A., Boyd, J. 2010. The AGWA-KINEROS2 suite of modeling tools in the context of watershed services valuation. Proc. 2nd Joint Federal Interagency Conference, Las Vegas, NV, June 27 - July 1, 2010, 12 p. http://acwi.gov/sos/pubs/2ndJFIC/.

Goodrich, D.C., Unkrich, C.L., Korgaonkar, Y., Burns, S., Kennedy, J., Sidman, G., Sheppard, B.S., Hernandez, M., Guertin, D.P., Miller, S.N., Kepner, W., Heilman, P., Nearing, M. 2015. The KINEROS2-AGWA suite of modeling tools, Proc. of the 3rd Joint Federal Interagency Conference on Sedimentation and Hydrologic Modeling, April 19-23, 2015, Reno, Nevada, USA, p. 1759-1770. https://acwi.gov/sos/pubs/3rdJFIC/Proceedings.pdf

Guertin, D.P., Goodrich, D.C., Burns, I.S. Sheppard, B.S., Patel, J., Clifford, T.J., Unkrich, C., Kepner, W.P, and Levick, L. 2018. Assessing the impact of wildland fire on runoff and erosion using the Automated Geospatial Watershed Assessment tool. Proc. of the 6th Interagency Conference on Research in the Watersheds, July 23-26, 2018 at the National Conservation Training Center (NCTC) in Shepherdstown, West Virginia (in press).

Guertin, D.P. Goodrich, D.C., I.S. Burns, Sidman, G., Sheppard, B.S., Patel, J., Clifford, T.J. Unkrich, C., and Levick, L. 2019. Assessing the Hydrological and Erosional Effects of Wildland Fire. Proc. 2019 SEDHYD Conf., Reno, Nevada, June 24-28, 2019.

Guertin, D.P., Patel, J., Levick, L., Wei, H., Goodrich, D.C., Burns, I.S., and Unkrich, C. 2019. The Impact of Small Ponds on Streamflow Response and Sediment Yield. Proc. 2019 SEDHYD Conf., Reno, Nevada, June 24-28, 2019.

Hernandez, M., Miller, S.N., Goodrich, D.C., Goff, B.F., Kepner, W.G., Edmonds, C.M., and Jones, K.B. 2000. Modeling runoff response to landcover and rainfall spatial variability in semi-arid watersheds. Environmental Monitoring and Assessment 64: 285-298.

Korgaonkar, Y., Burns, I., Barlow, J., Guertin, D., Unkrich, C., Goodrich, D., and Kepner, W. 2015. Representing Green Infrastructure Management Techniques in Arid and Semi-arid Regions: Software Implementation and Demonstration using the AGWA/KINEROS2 Watershed Model. Proc. of the 3rd Joint Federal Interagency Conference on Sedimentation and Hydrologic Modeling, April 19-23, 2015, Reno, Nevada, USA, p. 1771-1782. https://acwi.gov/sos/pubs/3rdJFIC/Proceedings.pdf

Korgaonkar Y., Guertin D.P., Goodrich D.C., Unkrich C., Kepner W.G., and Burns I.S. 2018. Modeling Urban Hydrology and Green Infrastructure Using the AGWA Urban Tool and the KINEROS2 Model. Frontiers in Built Environment. 4:58. doi: 10.3389/fbuil.2018.00058

LANDFIRE, 2014, Existing Vegetation Type Layer, LANDFIRE 1.4.0, U.S. Department of the Interior, Geological Survey. Accessed 2016 at http://landfire.cr.usgs.gov/viewer/.

Lawrence, PA., J.J. Stone, P. Heilman, and L.J. Lane. 1997. Using measured data and expert opinion in a Multiple Objective Decision Support System for semiarid rangelands. Transactions of the ASAE. 40(6):1589–1597.

Levick, L.R., Wei, H., Burns, I.S., Guertin, D.P., and Goodrich, D.C. 2019. Military disturbance tool in the Automated Geospatial Watershed Assessment (AGWA) tool for management of military lands. Proc. 2019 SEDHYD Conf., Reno, Nevada, June 24-28, 2019.

Massart, J., Guertin, D.P., Smith, R.E., Goodrich, D.C., Unkrich, C.L., and Levick, L. 2010. K2-O2 (KINEROS-Opus) spatially based watershed hydrologic and biogeochemical model. Proc. 2nd Joint Federal Interagency Conference, Las Vegas, NV, June 27 - July 1, 2010, 12 p. http://acwi.gov/sos/pubs/2ndJFIC/

Miller, S.N., Semmens, D.J., Miller, R.C., Hernandez, M., Goodrich, D.C., Miller, W.P., Kepner, W.G., and Ebert, D.W. 2002. GIS-based Hydrologic Modeling: The Automated Geospatial Watershed Assessment Tool. In: Proceedings, Second Federal Interagency Hydrologic Modeling Conference, Las Vegas, Nevada, July 28 - August 1, 2002.

Miller, S.N., Semmens, D.J., Goodrich, D.C., Hernandez, M., Miller, R.C., Kepner, W.G., and Guertin, D.P. 2007. The Automated Geospatial Watershed Assessment Tool. J. Environmental Modeling and Software. 22:365-377.

Natural Resources Conservation Service. 2016. Hydrologic analysis of post-wildfire conditions. Hydrology Technical Note No. 4.

Rawls, W.J., Brakensiek, D.L., and Saxton, K.E. 1982. Estimation of soil water properties. Transactions of the American Society of Agricultural Engineers 25 (5): 1316-1320, 1328.

Ritchie, J.T. 1972. A Model for Predicting Evaporation from a Row Crop with Incomplete Cover. Water Resources Research, 8:1204-1213.

Saupe, D. and Peitgen, H. eds. 1988. The Science of Fractal Images. Springer, NewYork.

Schaffner, M., Unkrich, C., Goodrich, D., Tardy, A., and Laber, J. 2014. Modeling Flash Flood Events in an Ungaged Semi-Arid Basin using a Real-Time Distributed Model: Fish Creek near Anza Borrego, California. NOAA Western Regional Technical Attachment 14-02, 42 p. (https://www.weather.gov/media/wrh/online_publications/TAs/TA1402.pdf).

Schaffner, M., Unkrich, C., Goodrich, D., Lericos, T., Czyzyk S., and Pierce, B. 2016. Modeling Hydrologic Events in a Semi-Arid Basin of Complex Terrain using a Real Time Distributed Model: Short Creek at Colorado City, Arizona. NOAA Western Regional Technical Attachment 16-03, 42 p.
(https://www.weather.gov/media/wrh/online_publications/TAs/TA1603.pdf).

Schaffner, M., Tardy A., Dandrea, J. Unkrich, C., and Goodrich, D. 2017. Operational Success with Distributed Modeling to inform Flash Flood Warning Operations at Weather Forecast Office San Diego. NOAA Western Regional Technical Attachment 17-02, https://www.weather.gov/media/wrh/online_publications/TAs/TA1702.pdf

Scott, S. 2005. Implementing best management practices in hydrologic modeling using KINEROS2 and the Automated Geospatial Watershed Assessment (AGWA) Tool. Master's Thesis, School of Natural Resources, University of Arizona, Tucson, AZ

Semmens, D.J., Goodrich, D.C., Unkrich, C.L., Smith, R.E., Woolhiser, D.A., and Miller, S.N. 2008. KINEROS2 and the AGWA modeling framework. Chapter 5: In: Hydrological Modelling in Arid and Semi-Arid Areas (H. Wheater, S. Sorooshian, and K. D. Sharma, Eds.). Cambridge University Press, London. pp. 49-69.

Sidman, G., Guertin, D.P., Goodrich, D.C., Unkrich, C.L., and Burns, I.S. 2016a. Risk assessment of post-wildfire hydrological response in semiarid basins: the effects of varying rainfall representations in the KINEROS2/AGWA model. International Journal of Wildland Fire, 25(3): 268-278.

Sidman, G., Guertin, D.P., Goodrich, D.C., Thoma, D., Falk, D., and Burns, I.S. 2016b. A coupled modelling approach to assess the effect of fuel treatments on post-wildfire runoff and erosion. International Journal of Wildland Fire, 25(3): 351-362.

Smith, R.E. 1992. Opus, An Integrated Simulation Model for Transport of Nonpoint-Source Pollutants at the Field Scale: Volume I, Documentation. U.S. Department of Agriculture, Agricultural Research Service, ARS-98.

Smith, R.E., Goodrich, D.C., Woolhiser, D.A., and Unkrich, C.L. 1995. KINEROS - A kinematic runoff and erosion model, Chap. 20 of Computer Models of Watershed Hydrology, (Ed. by Singh, V. J.) Water Resour. Pub., Highlands Ranch, Colo., pp. 697-732.

Unkrich, C.L., Schaffner, M., Kahler, C., Goodrich, D., Troch, P., Gupta, H., Wagener, T., and Yatheendradas, S. 2010. Real-time flash flood forecasting using weather radar and a distributed rainfall-runoff model. Proceedings, Federal Interagency Hydrologic Modeling Conf., Las Vegas, NV, June 27 - July 1, 2010, 11 p. http://acwi.gov/sos/pubs/2ndJFIC/.

USDA-NRCS. 2004. National Engineering Handbook (NEH), Part 630, Hydrology, Chapter 9, Hydrologic Soil-Cover Complexes. Washington, DC.

Woolhiser, D.A., Smith, R.E., and Goodrich, D.C. 1990. KINEROS, A Kinematic Runoff and Erosion Model: Documentation and User Manual. ARS-77. Tucson, Ariz.: USDA-ARS Southwest Watershed Research Center. Available at: www.tucson.ars.ag.gov/kineros.

Yakowitz, D.S. and Weltz, M. 1998. An algorithm for computing multiple attribute additive value measurement ranges under a hierarchy of the criteria: application to farm or rangeland management decisions. In: Multicriteria analysis for land-use management, pp. 163-177, Springer, Dordrecht.

Two-Dimensional Hydraulic, Vegetation, and Sediment Modeling in Support of River Restoration Projects

Daniel Dombroski, Hydraulic Engineer, Bureau of Reclamation, Denver, CO, ddombroski@usbr.gov
Blair Greimann, Hydraulic Engineer, Bureau of Reclamation, Denver, CO, bgreimann@usbr.gov

Abstract

Predicting the effects of riparian vegetation on hydraulics and sediment transport within managed riverine systems is a growing challenge due to the increasing priority of maintaining ecosystem function while sustaining water conveyance. Quantitative predictive tools are needed to aid the science, economics, and policy of establishing environmental flows by addressing questions regarding the physical interaction of flow, vegetation, and sediment in rivers and floodplains. A quantitative two-dimensional model (Dombroski D. E., 2014) is in active development at the Bureau of Reclamation Technical Service Center for simulating the effect of vegetation characteristics on river and floodplain hydraulics. The model is based upon the SRH-2D package (Lai, 2010), which contains a two-dimensional flow and mobile bed sediment transport model. The vegetation-hydraulic solver uses measured vegetation parameters and calculated hydraulic variables to estimate a spatially-distributed, dynamic roughness coefficient that is coupled to the simulated hydrodynamics and sediment transport through the bed shear stress. Updates to the model are presented, including enhanced ability to predict effects of partitioned roughness and implementation of algorithms to estimate roughness based on remotely-sensed vegetation characteristics. Results are presented from a case study on the San Joaquin River in California. Further testing, validation, and refinement of the model will continue as it is applied at the project level with support from the San Joaquin River Restoration Program.

Introduction

Theoretical Background: Predicting the effects of riparian vegetation on hydraulics and sediment transport within managed riverine systems is a growing challenge due to the increasing priority of maintaining ecosystem function while sustaining water conveyance. Quantitative predictive tools are needed to aid the science, economics, and policy of establishing environmental flows by addressing questions regarding the physical interaction of flow, vegetation, and sediment in rivers and floodplains. These tools are especially critical for regions of the Western U.S. like Central California, in which multi-benefit water projects (e.g., projects that enhance flood safety, wildlife habitat, and public recreation) are legally mandated components of regional and State-wide planning and funding efforts. These multi-benefit projects can be critically dependent on accurate estimates and modeling of vegetation effects on hydraulic conveyance, due to concerns over increases in roughness resulting from vegetation establishment and growth.

The new SRH-2D package features the addition of a hydraulic roughness module for computing dynamic, spatially-distributed Manning's *n* values based on vegetation characteristics

(Dombroski D. E., 2014). The computed Manning's n roughness values incorporate resistance due to form drag of flow through the vegetation. The vegetation module receives spatially-distributed input data via a user-generated ArcGIS shapefile that is automatically mapped to the computational grid of the hydraulic solver at runtime. The computational time step for the hydraulic solver is generally limited by numerical instability, whereas the computational time step for the vegetation module is limited by ecologically-relevant scales (e.g., growth, dessication), and can generally be significantly larger. A larger time step between vegetation updates offers the benefit of decreased computational overhead.

The vegetated flow formulas of Baptist et al. (2007) and Järvelä (2004) for calculating roughness were implemented in the model during initial phase of development; the algorithms depend on parameters that are correlated to measured vegetation characteristics. Two primary challenges associated with the new capability were identified:

1. Direct measurement of vegetation characteristics becomes unfeasible for large riparian corridors
2. Increased roughness to account for hydraulic resistance may cause gross over-predictions of sediment transport capacity

The work documented herein addresses two primary challenges associated with the vegetation-hydraulic solver by (a) implementing algorithms to estimate roughness based on remotely-sensed vegetation characteristics and (b) introducing a partitioned roughness that separates grain roughness used to compute sediment transport capacity from the total hydraulic roughness. The developments represent important improvements to the model that increase the usability and accuracy in simulating vegetation effects on hydraulics and sediment transport.

Ongoing Development: Numerical modeling tools (e.g., SRH-1D, SRH-2D, U2RANS) developed at Reclamation (Lai, Weber, & Patel, 2003; Lai Y. G., 2010; Huang & Greimann, 2012) are commonly used to simulate flow and sediment transport in order to predict effects of management changes on sedimentation in rivers and reservoirs. These quantitative predictive tools have been valuable in understanding and comparing outcomes of management alternatives; however, the complexity of issues that Reclamation faces is growing with increasing priority of maintaining ecosystem function while sustaining water supply and providing flood protection. Growing challenges call for continued development of tools that can better predict the effects of complex ecohydraulic processes related to sediment transport in the riparian environment. The models currently simulate unsteady sediment transport by solving total sediment load equations (Greimann & Huang, 2008). The formulation, derived from the advection-diffusion equation, is generally coupled to the flow through ensemble and depth-averaged flow velocities. Although the total sediment load equations perform well in simulating transport under uniform flow conditions, the lack of direct linkage to some important flow characteristics (e.g., turbulence production due to interaction with objects and complex geometries) limits the practical applicability to conditions under which the effects are small. In order to be able to address the increasingly common sedimentation issues associated with more complex flow geometries and vegetated conditions, further development of the theoretical framework upon which the sediment transport models are based is necessary.

Sediment transport under complex flow conditions has been studied in the laboratory setting in order to develop better understanding of the interactions and important parameters governing transport rates and distributions. Active areas of research include how vegetation characteristics within a flow determine the trapping and redistribution of sediment (Nepf H. , 2012; Nepf H. M., 2012). Controlled experiments have been conducted in outdoor (Rominger, Lightbody, & Nepf, 2010) and indoor (Yang, Kerger, & Nepf, 2015) laboratories in order to

measure flow and vegetation characteristics with the intent of developing relationships to physical mechanisms governing sediment transport.

Future work is aimed at improving predictions of sediment mobility related to stem-generated turbulence. Incorporating unsteady flow, vegetation, and sediment characteristics, quantitative dependencies are being formulated between turbulent flow models and sediment transport models under vegetated flow conditions.

Methods

San Joaquin River Hydraulic Model

Domain: The model domain of study (Figure 1) extends from the Chowchilla Bifurcation Structure at the top of Reach 2B to the head of the proposed Mendota bypass where a new control structure will be built to distribute flow for meeting restoration project goals and deliveries to exchange contractors through the Mendota Pool (Greimann B. P., SRH-2015-26, 2015). Although the stage will likely vary greatly at the downstream extent based on the operational mode of the proposed Mendota control structure (restoration flows vs. water deliveries), the model described herein was developed to model only the mode of restoration flow operation. The nodal elevations of the computational mesh were derived from a digital elevation model updated with 2015 LiDAR data and modified by proposed side-channel cuts (Greimann B. P., SRH-2015-26, 2015) as part of the restoration design.

Hydrograph: A 40-day high-flow hydrograph was designed to drive the simulated sediment effects of a hydrologic season, representative of the period of time necessary for meeting restoration goals. Because the baseline flow through the remainder of the year is not expected to move significant sediment, the modeled hydrograph is comprised of five iterations of the high-flow period. The 40-day high-flow hydrograph was developed from the results of RiverWare operational software (Vandegrift, 2015), extracted for the period April 1, 2003 to May 12, 2003 at the location labeled "SJR Below Chowchilla Bifurcation."

San Joaquin River Riparian Vegetation Model

The vegetation model is dependent on input of spatially-distributed vegetation characteristics that are used in quantifying the dynamic roughness at each cell within the computational domain. The vegetation delineations were derived by adapting and simplifying the product of the riparian mapping study that was performed by Moise & Hendrickson (2002) along the San Joaquin River corridor from Friant Dam to the confluence with the Merced River. A product of this study was a shapefile containing delineated polygons with attributes specific to each riparian classification.

Side-channel cuts, as proposed in the draft design, to benefit habitat restoration were incorporated into the land-use polygon areas and digital elevation model. Due to the preliminary nature of the Reach 2B design, additional steps were taken to reduce the delineation of land-use regions into a conceptually very simple configuration (Figure 1). As design alternatives and revegetation plans evolve, the land-use delineations and attributes can be refined to better inform the hydraulic and sediment modeling effort.

Herbaceous vegetation classification and parameters were used for the channel cut out areas and all other areas where vegetation is present (not main channel and disturbed areas). It is important to note that the design vegetation conditions post-construction will likely be very different than the riparian conditions mapped in the Moise & Hendrickson (2002) study.
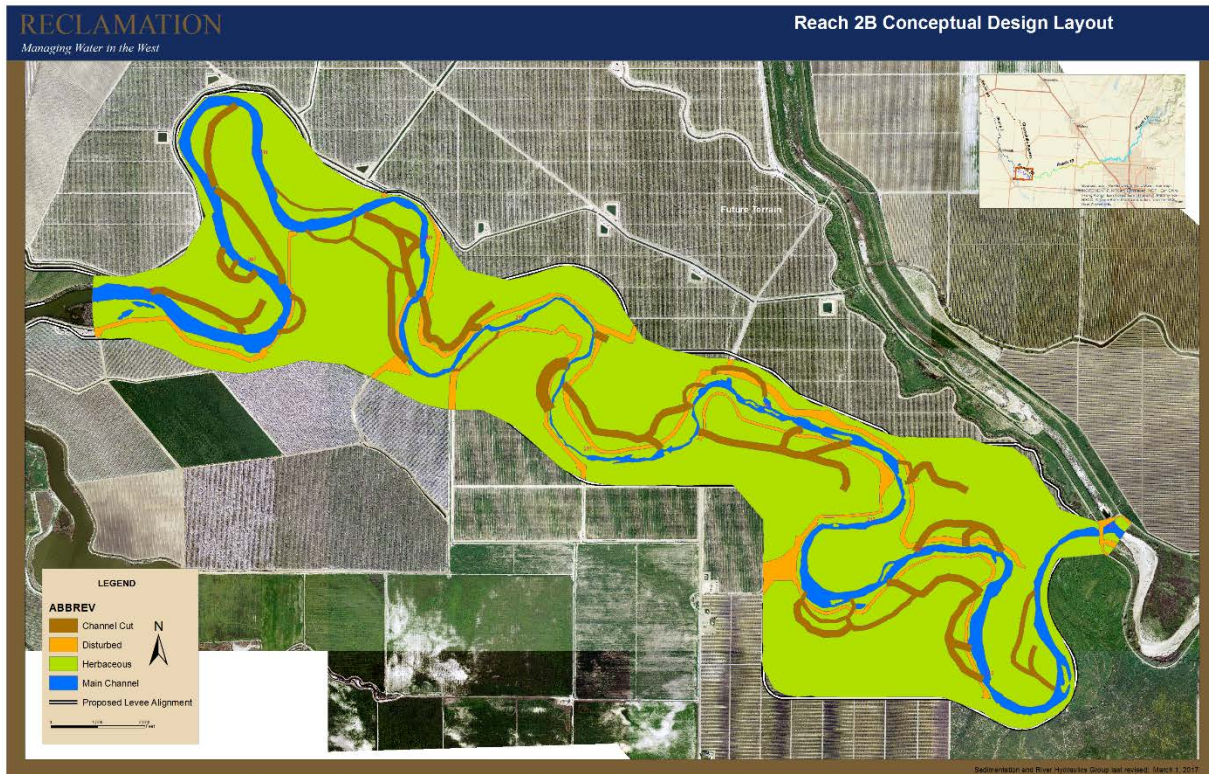
Figure 1. Delineation of land-use areas and associated vegetation mapping used in the hydraulic and sediment model to represent a simple scenario of proposed Reach 2B improvements.

San Joaquin River Sediment Model

Reach 2B is a sand bed dominated system downstream of the Chowchilla Bifurcation structure. Of the monitoring sites documented in the 2010-2012 Sediment Budget Analysis (Greimann B. , 2015) site SJB is identified as being most closely correlated spatially to Reach 2B. Therefore, sediment classifications and parameters for the mobile bed model were based on the analysis for site SJB. In order to reduce computational overhead, the material gradations for site SJB were simplified to six sediment classes. The cumulative size fractions specified in the model are shown in Table 1.

The Engelund-Hansen (1972) total load formulation was chosen to calculate sediment capacity in the reach, a generally accepted approach to predicting transport in sand-dominated systems. Exchange between the bed material and bed load in transport is determined partially by the active layer. Exchange between the active layer and subsurface layer(s) is determined in part by the depth and gradations in each layer. It is assumed that all layers involved in exchange processes in Reach 2B are predominantly sand and that no significant variation in the gradation is likely to occur with erosional, depositional, and exchange processes (Table 1). Active layer thickness is uncertain (assumed 30 mm), especially considering that processes may be determined more by dune height than grain size.

The incoming sediment supply specified as part of the "Inlet-Q" upper boundary condition of the mobile bed model was taken from the fit to measured gravel and sand bed load transport rate at site SJB on pg. 64 of the sediment budget analysis (Greimann B. , 2015). The majority of the material transported at this site is transported as bed load. The sediment rating curve for total sand bed load was partitioned according to the distribution in Table 1, although the size

classes in the range $0.0625 - 2$ mm were renormalized according to a maximum sand size of 2 mm. The entire sediment rating curve predicted for gravel bed load was assumed to apply to the largest sediment size class, $2 - 4$ mm. The input sediment supply to the model is specified for each of the six size classes as specified in Table 2.

Table 1. Sediment grain size distributions as specified in the SRH-2D mobile bed sediment model for Reach 2B. The distribution was derived from a simplification of the material gradations measured at site SJB in the 2010-2012 Sediment Budget Analysis (Greimann B. , 2015).

	Model Sediment Grain Size Distributions						
Size class (mm)	0.0625	0.125	0.25	0.5	1	2	4
Cumulative % finer	0	3.1	9.1	23.6	57.3	83.7	100

Table 2. Input sediment supply to the model for each of six size classes specified as rating curve

	Sand (ft³/s)					Gravel (ft³/s)
Q (cfs)	0.0625-0.125 mm	0.125-0.25 mm	0.25-0.5 mm	0.5-1 mm	1-2 mm	2-4 mm
0	0	0	0	0	0	0
500	2.2E-05	4.2E-05	1.0E-04	2.4E-04	1.8E-04	7.2E-06
1000	7.2E-05	1.4E-04	3.3E-04	7.8E-04	6.1E-04	3.6E-05
1500	1.4E-04	2.8E-04	6.7E-04	1.6E-03	1.2E-03	9.2E-05
2000	2.4E-04	4.6E-04	1.1E-03	2.6E-03	2.0E-03	1.8E-04
2500	3.5E-04	6.7E-04	1.6E-03	3.8E-03	3.0E-03	3.0E-04
3000	4.7E-04	9.2E-04	2.2E-03	5.2E-03	4.0E-03	4.6E-04
3500	6.2E-04	1.2E-03	2.9E-03	6.7E-03	5.3E-03	6.5E-04
4000	7.8E-04	1.5E-03	3.6E-03	8.5E-03	6.6E-03	8.9E-04
4500	9.5E-04	1.8E-03	4.5E-03	1.0E-02	8.1E-03	1.2E-03
5000	1.1E-03	2.2E-03	5.4E-03	1.2E-02	9.7E-03	1.5E-03

Simulation Cases

A set of six simulations were performed to test the effect of varying vegetation characteristics on simulated sediment dynamics within the reach. The simulations applied roughness classifications based on land-use types. For all simulation cases below (except for Case 1 in which no vegetation was simulated), roughness was partitioned into a grain roughness component associated with the sand substrate and a drag roughness component associated with the vegetation (Dombroski D. E., 2017). Vegetation height was assumed uniform $H_p = 2$ ft in channel cut areas and uniform $H_p = 1$ ft in overbank areas. Areas classified as in-channel and disturbed were assumed to be void of vegetation (total roughness equal to grain roughness).

Case 1, No Vegetation: A baseline simulation (Case 1) was performed to establish predicted conditions under the case of no revegetation in Reach 2B. The simulation assumed sand throughout the system and a static, uniform roughness value $n = 0.03$ was applied to all regions within the mesh.

Case 2, Baptist 2007 High-Density: For Case 2, a grain roughness value of $n_o = 0.03$ was assumed throughout the mesh. Vegetation roughness n_v was computed using the Baptist et

al. (2007) methodology with a high-density value of the parameter mD = 10. The parameter mD represents the areal density m multiplied by the stem diameter D.

Case 3, Baptist 2007 Low-Density: For Case 3, a grain roughness value of n_o = 0.03 was assumed throughout the mesh. Vegetation roughness n_v was computed using the Baptist et al. (2007) methodology with a low-density value of the parameter mD = 1, an order of magnitude smaller than in Case 2.

Case 4, Kouwen 1980: For Case 4, a grain roughness value of n_o = 0.03 was assumed throughout the mesh. Vegetation roughness n_v was computed using the Kouwen & Li (1980) methodology. The implementation follows the approach of Mason et al. (2003), except that the future vegetation height was assumed instead of derived from LiDAR estimates.

Case 5, Static Veg High Roughness: For Case 5, a grain roughness value of n_o = 0.03 was assumed throughout the mesh. Vegetation roughness was statically-assigned according to n_v = 0.07 and n_v = 0.05 in channel cut and overbank areas, respectively.

Case 6, Static Veg Low Roughness: For Case 6, a grain roughness value of n_o = 0.03 was assumed throughout the mesh. Vegetation roughness was statically-assigned according to n_v = 0.04 and n_v = 0.025 in channel cut and overbank areas, respectively.

Results

Figure 2 and Figure 3 show the spatial pattern of erosion and deposition through the reach for Case 1 (no vegetation) and Case 2 (Baptist 2007 High Density) as driven by the wet hydrograph. The Case 1 simulation results show extensive patterns of erosion and deposition through both the main channel and channel cut zones. In comparison, the vegetated flow results predict very little erosion and deposition in the channel cut zones. Although the fine-scale patterns vary among the different vegetative cases, the overall trend is consistent relative to the non-vegetated case.

A significant concern regarding the design of side-channels for habitat restoration is maintaining connectivity through the channels and floodplain at times critical to the rearing of juvenile salmonids. Erosion and deposition of sediment poses a risk to maintaining connectivity. Distributions of simulated water depth were calculated mid-way through the rising limb of the fifth high-flow peak in the hydrograph at an approximate discharge of 1500 cfs. The depth maps (not shown) indicate that simulations with vegetation growth in the channel cut and overbank areas predict better maintenance of flow connectivity than the simulation without vegetation growth. Isolated patches of inundation, both on the floodplain and in the channel cut areas, indicate regions that were hydraulically connected at higher flow rates but did not drain as the water surface declined. While floodplain connectivity is generally considered a favorable attribute from a habitat perspective, disconnected regions of inundation as the hydrograph declines pose a stranding risk and should be considered for further floodplain grading in order to promote drainage.

One possible explanation for the difference in predicted erosional and depositional patterns between the vegetated and non-vegetated conditions is that the inflow to the channel cut areas is getting cut off by sediment deposits. Figure 4 shows water depth plotted over the distribution of erosion at the end of the hydrograph. The simulated flow in Figure 4 corresponds to a discharge of approximately 150 cfs. It is evident that there is a strong backwater effect in the lower extent of the reach due to the downstream boundary condition. This may be due to the fact that the lower boundary condition is specified as a rating curve that is constant in time despite the erosion evident in the lower portion of the reach. In the portion of the reach upstream of the

backwater, localized depositional areas can be observed amongst inundated patches at the head of some channel cuts. Figure 5 and Figure 6 present closeup images of erosion and deposition maps in the vicinity of several of the channel cuts. The images contrast the Case 1 (no vegetation) simulation case with that of Case 2 (Baptist 2007, High-Density). The non-vegetated Case 1 generally shows dramatically more patterning of erosion and deposition, although deposition is dominant near channel inlets.

To quantify differences in predicted erosion and deposition of sediment in the channel cut areas, the summation of deposition and erosion was computed for the channel cut areas as a function of simulation time:

$$W_s(t) = \varphi \rho_s \sum_i^{n_c} E_i(t) A_i$$

In the above equation, $W_s(t)$ is the total mass weight of sediment within the channel cut areas, φ = 0.4 is the assumed solid fraction, ρ_s is the sediment density, $E_i(t)$ is the erosion at cell i and time t, A_i is the projected area of cell i, and n_c is the total number of cells in the channel cut area. The computations were performed by finding the erosion depth (negative values of erosion indicate deposition) at each mesh cell within the delineated channel cut polygons. The erosion depth was multiplied by the projected area of the mesh cell to obtain an erosion volume at each cell. A summation is performed over all grid cells within the channel cut areas and multiplied by the estimated solid fraction and density to obtain a total cumulative sediment weight mobilized as a function of time. Figure 7 presents a comparison of total erosion in channel cut areas $W_s(t)$ as a function of simulation time for Case 1 (no vegetation) and Case 2-6 under vegetated conditions. The comparison indicates that the sediment in channel cut areas is significantly more dynamic under non-vegetated conditions than for vegetated conditions.
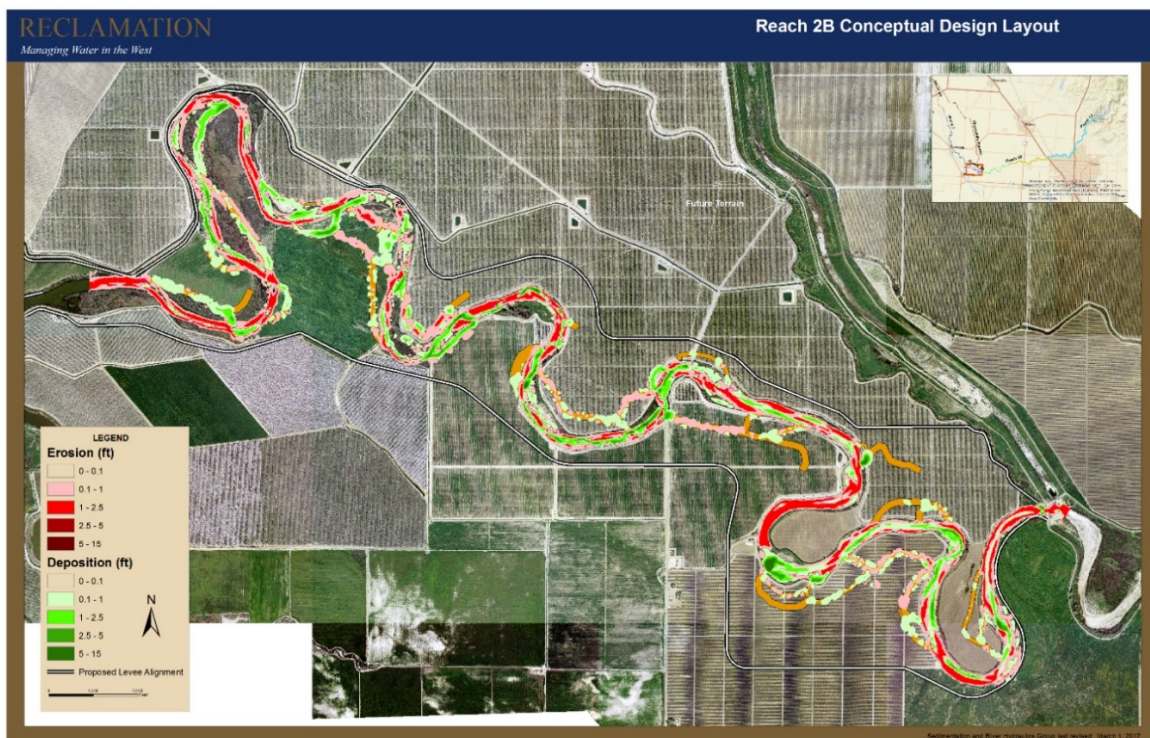
Figure 2. Spatial distribution of erosion (red) and deposition (green) for Case 1 (no vegetation) simulation at completion of five-season wet hydrograph.
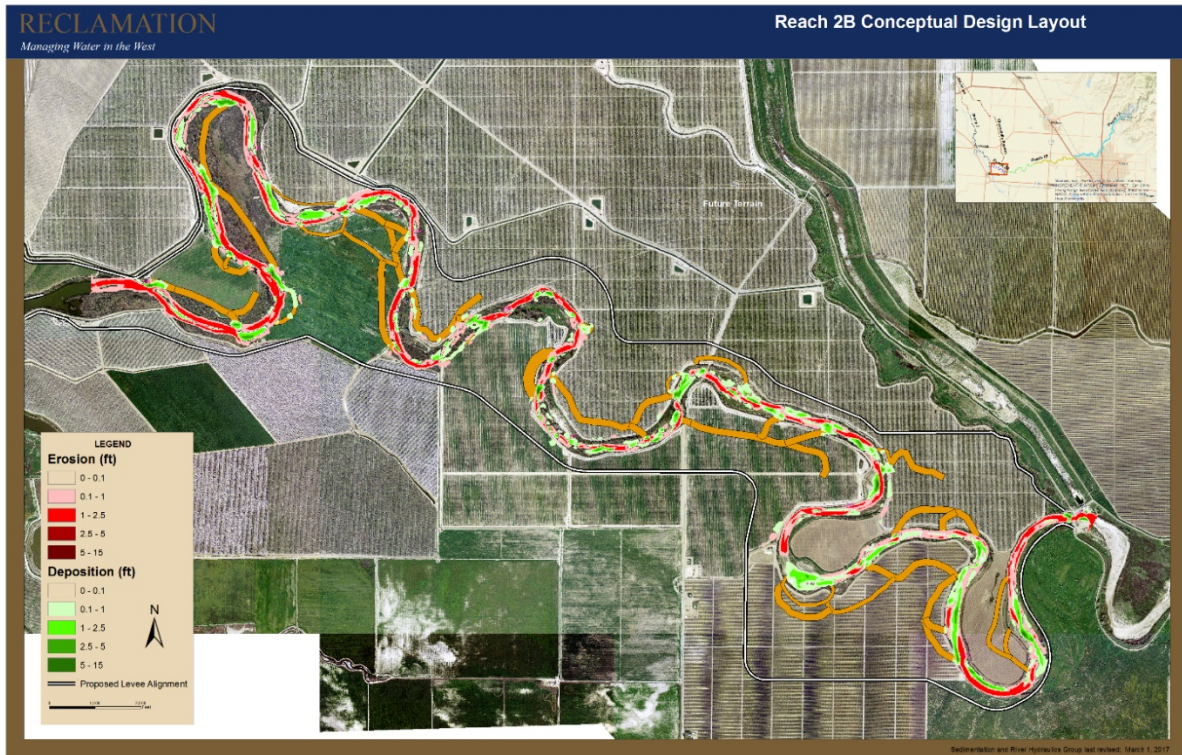
Figure 3. Spatial distribution of erosion (red) and deposition (green) for Case 2 (Baptist 2007, High-Density) simulation at completion of five-season wet hydrograph.
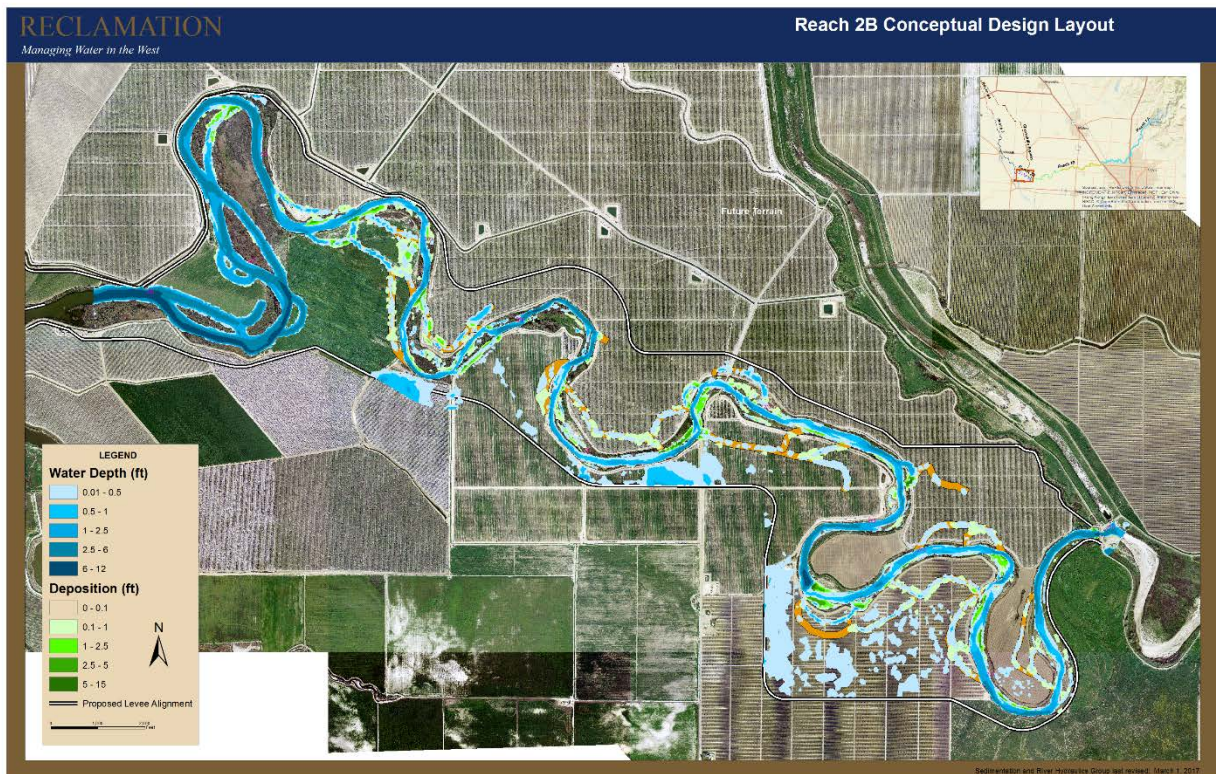
Figure 4. Water depth (blue) plotted over deposition (green) for Case 1 (no vegetation). It appears that deposition of sediments in and at the mouth of channel cut areas may be choking off flow and reducing hydraulic connectivity.
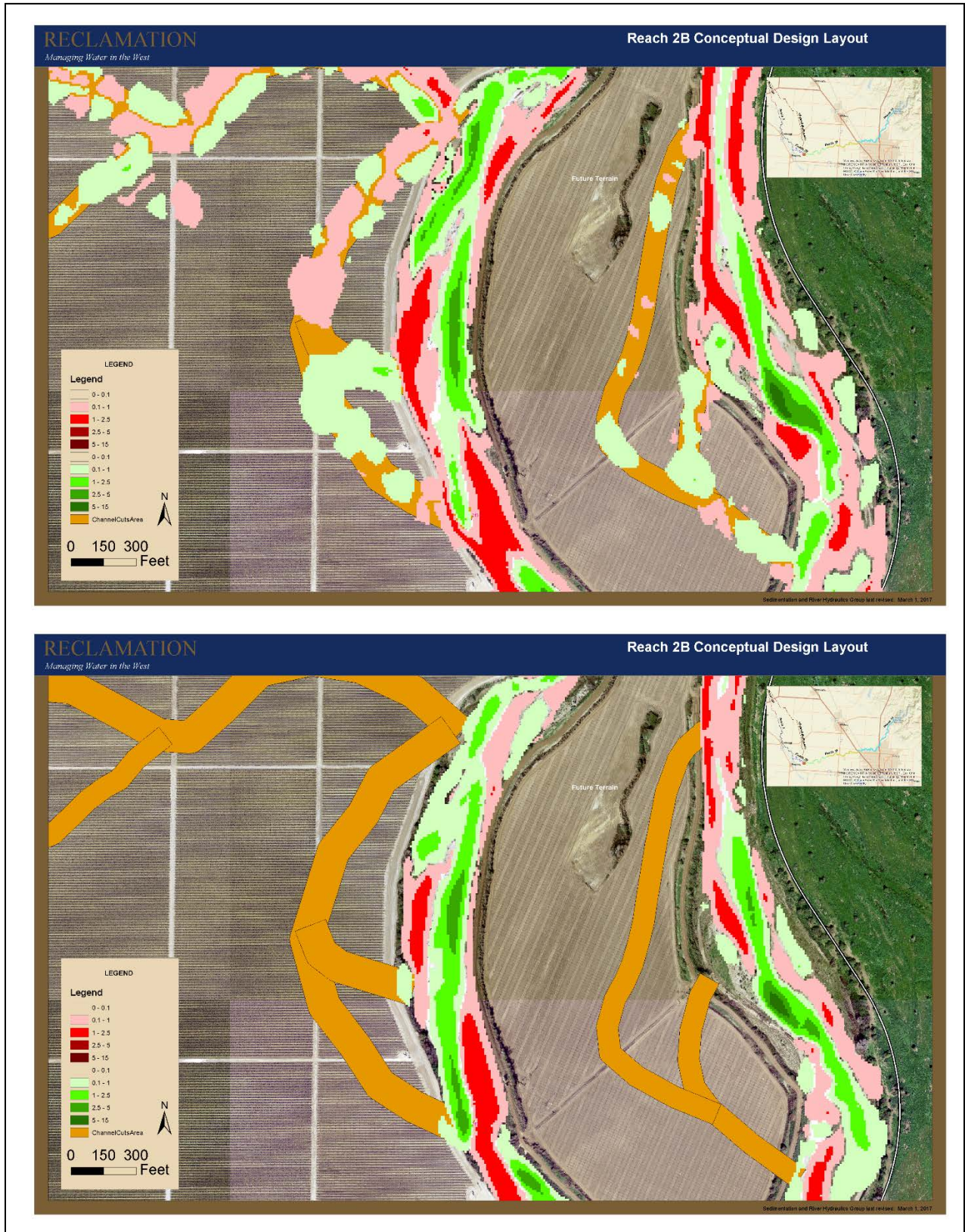
Figure 5. Closeup comparison of erosion (red) and deposition (green) patterns for Case 1 (non-vegetated; top) and Case 2 (Baptist 2007, High-Density; bottom) in the vicinity of channel cut areas for wet hydrograph.
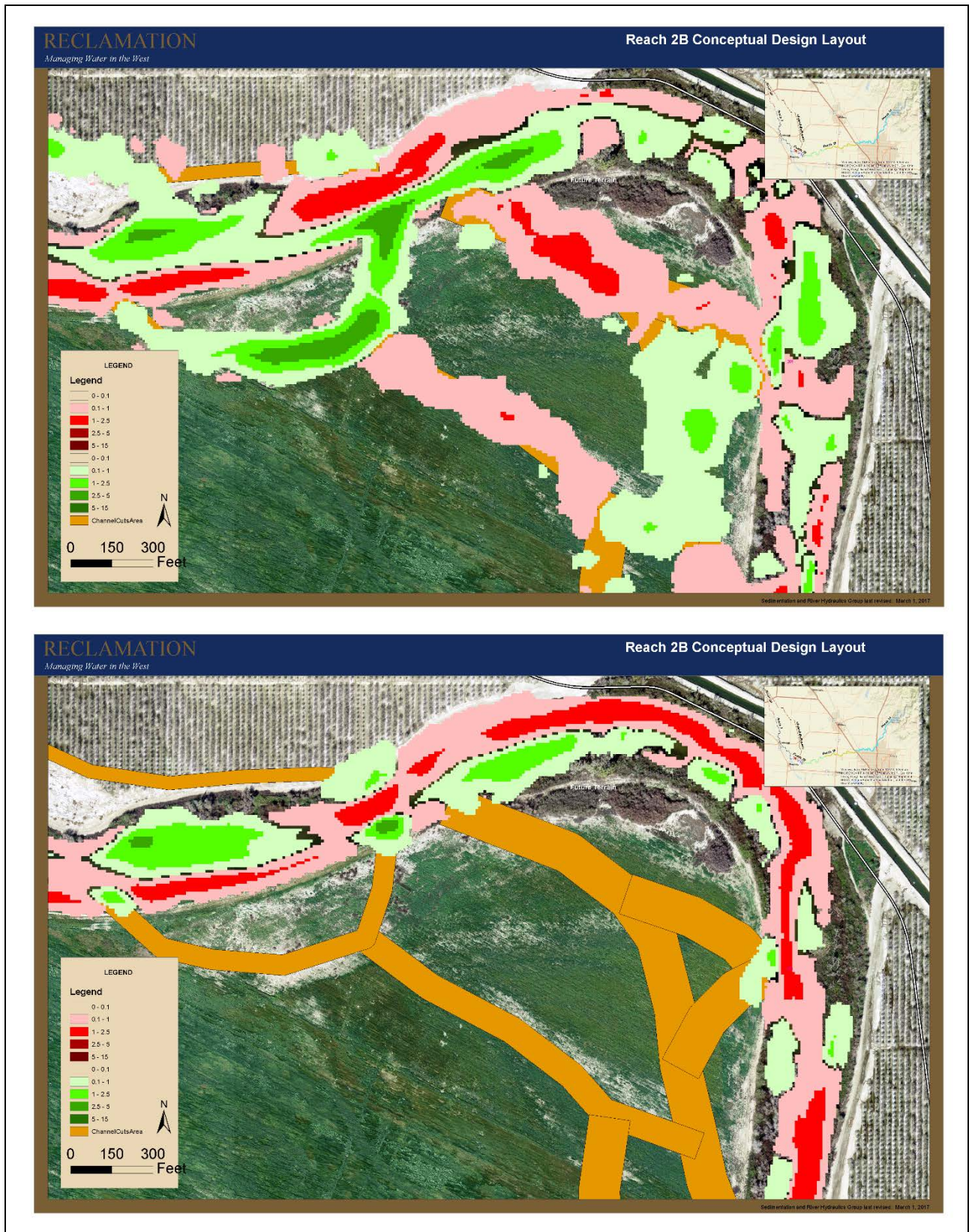
Figure 6. Closeup comparison of erosion (red) and deposition (green) patterns for Case 1 (non-vegetated; top) and Case 2 (Baptist 2007, High-Density; bottom) in the vicinity of channel cut areas.
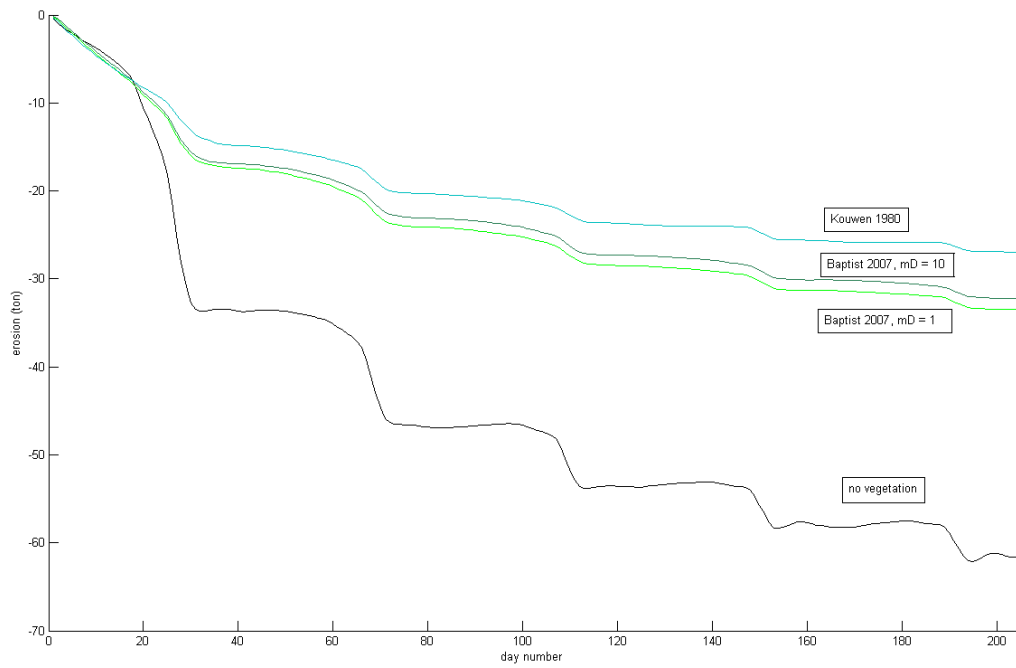
Figure 7. Total computed erosion (negative values indicate deposition) in the channel cut areas as a function of wet hydrograph simulation time for Case 1 (no vegetation) and comparison of simulated vegetated conditions.
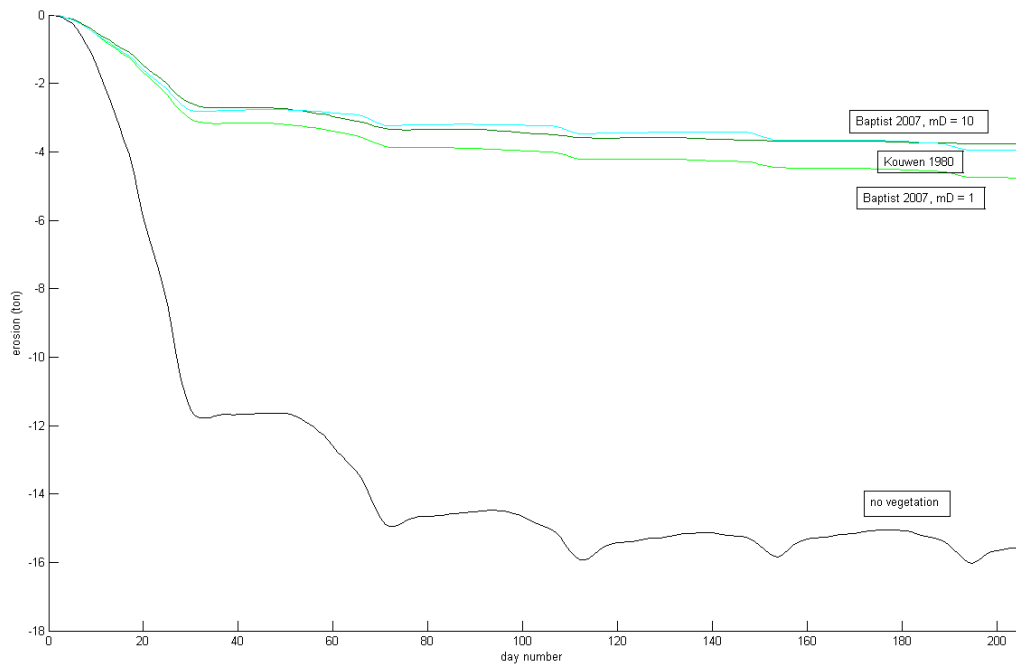
Figure 8. Total computed erosion (negative values indicate deposition) in the vicinity of channel cut inlet areas (Figure 19) as a function of wet hydrograph simulation time for Case 1 (no vegetation) and comparison of simulated vegetated conditions.

In order to test the hypothesis that sediment was being deposited at the mouth of the channel cut areas and therefore limiting hydraulic connectivity, the analysis was further refined by focusing the delineated area of interest on the inlet of the channel cut areas. Figure 8 presents a comparison of total erosion in the vicinity of channel cut inlet areas as a function of simulation time for Case 1 (no vegetation) and Case 2-6 under vegetated conditions. In comparing Figure 7 and Figure 8, it appears that a significant portion of the overall erosion and deposition volume (relative to area of analysis) is predicted to occur in the vicinity of the channel cut inlet areas. This trend is particularly evident for the Case 1 (no vegetation) simulation. In some cases, it appeared that the inlet to the channel cut areas was actually erosional, but the sediment was then deposited in an area within the channel cut immediately downstream. Therefore, some regions of interest were delineated both at the channel cut mouth and just downstream of the mouth. Figure 9 presents a map of erosion and deposition in the vicinity of a channel cut inlet with delineated regions of interest at the mouth and immediately downstream. Figure 10 and Figure 11 show the computed erosion and deposition $W_s(t)$ in the regions of interest, respectively, for Case 1 (no vegetation) and Case 2 (Baptist 2007, High-Density). For the non-vegetated case, the mouth of the channel cut area is erosional, however sediment is deposited immediately downstream. This can be visualized in the map (Figure 9) by observing the erosional and depositional zones resulting from the Case 1 simulation within the delineated polygons; the inclusion of vegetation within the channel cut areas dramatically changes the predictions. The simulation results suggest that vegetation in the channel cut and overbank areas may stabilize sediment dynamics, help maintain hydraulic connectivity, and that the effects may be most significant in the vicinity of the channel cut inlet areas.
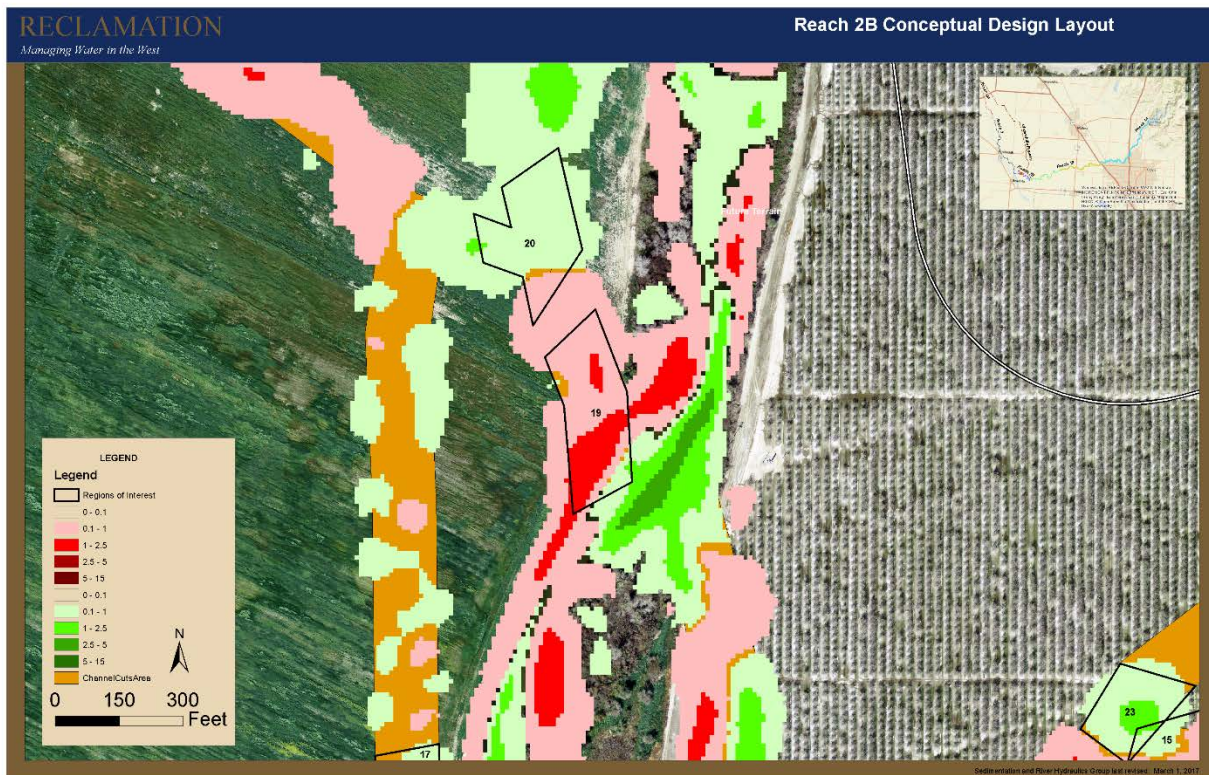
Figure 9. Erosion (red) and deposition (green) in the vicinity of channel cut inlet area for Case 1 (no vegetation). The delineated polygons (black outline) denote regions of interest at the mouth and immediately downstream of the mouth.
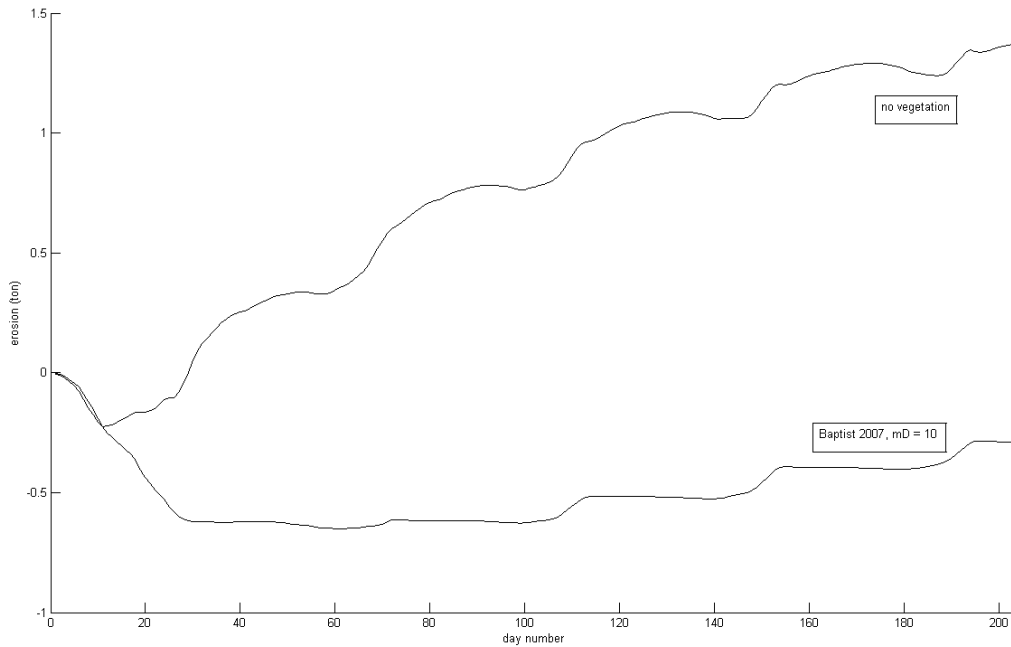
Figure 10. Total computed erosion (negative values indicate deposition) at the mouth of channel cut area (Figure 9; polygon #19) as a function of wet hydrograph simulation time for Case 1 (no vegetation) and Case 2 (Baptist 2007, High Density). The comparison suggests that the presence of vegetation at the mouth of the channel cut (e.g., in Case 2) stabilizes the sediment from erosion.
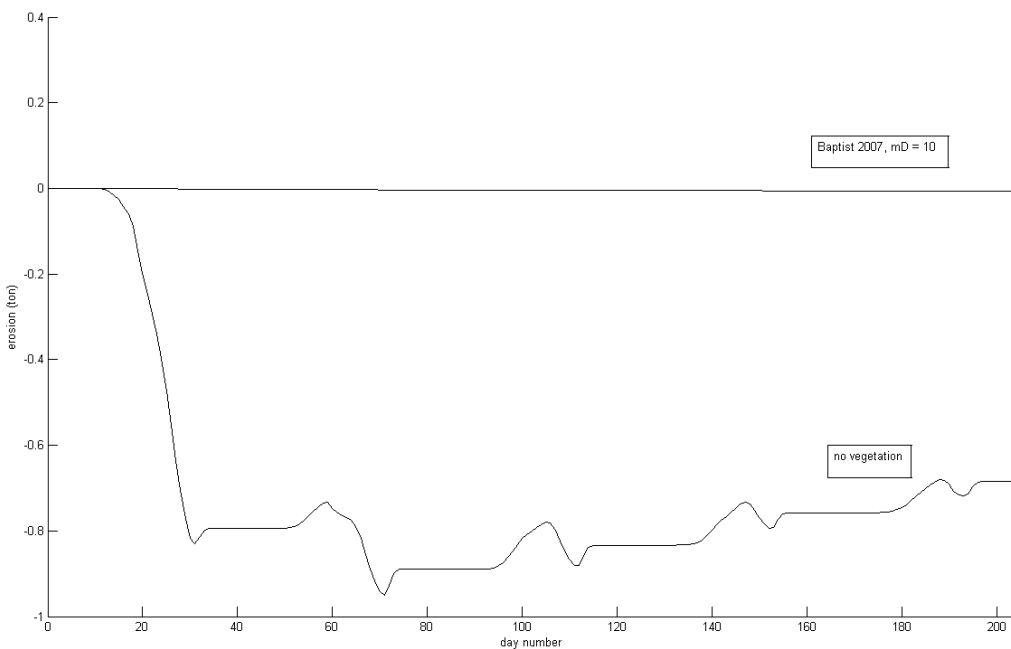
Figure 11. Total computed erosion (negative values indicate deposition) just downstream of the mouth of channel cut area (Figure 9; polygon #20) as a function of wet hydrograph simulation time for Case 1 (no vegetation) and Case 2 (Baptist 2007, High Density). The comparison suggests that the presence of vegetation (e.g., in Case 2) stabilizes the sediment from erosion and deposition.

Discussion

Presented are results from numerical simulations of hydraulics and sediment transport within a proposed restoration design for Reach 2B of the San Joaquin River. The study focused on comparing and contrasting the predicted effects of revegetation actions in the channel cut and overbank areas. Flows simulated represent projections of multiple "wet" seasons through the system; simulations of more moderate conditions may also be performed.

The revegetation design modeled in the study is simple and subject to thorough refinement; likewise, the channel cut areas are preliminary. A goal of this study is to focus on gross aspects of the Reach 2B design in order to provide general guidance regarding conceptual design directions. As more refined restoration design alternatives are proposed, the modeling may also be refined to provide strategic analysis and optimization.

The results of the modeling generally demonstrate that the presence of vegetation in the channel cut and overbank areas is expected to decrease the local mobility of sediment, stabilizing the bed topography relative to the non-vegetated case.

From this analysis, a general recommendation may be made regarding revegetation efforts as part of side-channel design and routing. Due to the constraints imposed by the levee alignment, most of the channel cuts are located at the inner bends. Overall, the channel cut areas are depositional for the Case 1 (no vegetation) simulation, although there are exceptions where erosion dominates. In observing the patterns of erosion and deposition, it is not clear that a specific design attribute is predicted to stabilize the sediment in the channel cuts. The simulation results suggest that without significant revegetation actions in the channel cut areas, there is risk that the constructed side channel habitat will partially fill in with sediment (potentially reducing hydraulic connectivity) within the course of a single high flow hydrograph.

There is some concern regarding the downstream water surface elevation boundary condition used in the model, specifically related to the amount of erosion predicted to occur in the vicinity of the model outlet. The simulations predict approximately $1 - 2$ ft of erosion at the downstream extent of the model, however the rating curve developed for the model is not adjusted to reflect that erosion. This may lead to an artificial backwater condition in the simulations. Since the majority of the erosion occurs early in the simulation time, one potential remedy would be to restart the simulation with an adjusted rating curve after some initial erosion has occurred in order to observe how the hydraulics and sediment respond.

In an attempt to quantify the gross flow characteristics, the averaged bed slope, velocity, and water depth were computed for the channel cut and main channel areas, respectively (Table 3). The computations were performed at a simulated flow of about 1500 cfs on the rising limb of the hydrograph. On average, the channel cut areas have a higher slope but lower velocity and depth than the main channel. However, SVD, a metric of the unit stream power, is similar for both regions. The stream power is commonly used as one measure of capacity to move sediment within a river. Designing channel cut areas to specified ranges of bed slope and hydraulic conditions may be useful in future alternative scenarios.

Table 3. Average bed slope, velocity, and water depth for the channel cut and main channel areas, respectively. Also computed is a metric of stream power, SVD, the product of slope, velocity, and depth. Conditions were computed at a flow of approximately 1500 cfs.

	Bed Slope S	Ave Vel (ft/s) V	Ave Depth (ft) D	Stream Power SVD
Channel Cut	0.095%	1.1	2.0	0.0021
Main Channel	0.031%	1.8	3.4	0.0019

References

Baptist, M., Babovic, V., Rodriguez Uthurburu, J., Keijzer, M., Uittenbogaard, R., Mynett, A., & Verwey, A. (2007). On Inducing Equations for Vegetation Resistance. *Journal of Hydraulic Research, 45*(4), 435-450.

Dombroski, D. E. (2014). *A Deterministic Spatially-Distributed Ecohydraulic Model for Improved Riverine System Management.* Denver: USBR.

Dombroski, D. E. (2017). *Remote Sensing of Vegetation Characteristics for Estimation of Partitioned Roughness in Hydraulic and Sediment Transport Modeling Applications.* Denver TSC: Bureau of Reclamation Research and Development Office, Science and Technology Program.

Greimann, B. (2015). *Technical Report No. SRH-2015-18 Sediment Budget Analysis of the San Joaquin River for Water Years 2010 through 2012.* Denver: Bureau of Reclamation Technical Service Center.

Greimann, B. P. (2015). *Technical Report No. SRH-2015-26 Conceptual Hydraulic Design of the Mendota Bypass.* Denver: Bureau of Reclamation Technical Service Center.

Greimann, B. P., & Huang, J. V. (2008). Two-Dimensional Total Sediment Load Model Equations. *ASCE, 134*(8), 1142-1146.

Huang, V. H., & Greimann, B. P. (2012). *SRH-1D, Version 3.0.* Denver Technical Service Center: Bureau of Reclamation.

Jarvela, J. (2004). Determination of Flow Resistance Caused by Non-Submerged Woody Vegetation. *International Journal of River Basin Management, 2*(1), 61-70.

Kouwen, N., & Li, R.-M. (1980, June). Biomechanics of Vegetative Channel Linings. *Journal of the Hydraulics Division, Proceedings of the ASCE, 106*(HY6), 1085-1103.

Lai, Y. G. (2010). Two-Dimensional Depth-Averaged Flow Modeling with an Unstructured Hybrid Mesh. *Journal of Hydraulic Engineering, 136*(1), 12-23.

Lai, Y. G., Weber, L. J., & Patel, V. C. (2003). Nonhydrostatic Three-Dimensional Model for Hydraulic Flow Simulation. I: Formulation and Verification. *ASCE, 129*(3), 206-2014.

Mason, D. C., Cobby, D. M., Horritt, M. S., & Bates, P. D. (2003). Floodplain friction parameterization in two-dimensional river flood models using vegetation heights derived from airborne scanning laser altimetry. *Hydrological Processes, 17*, 1711-1732.

Moise, G. H., & Hendrickson, B. (2002). *Riparian Vegetation of the San Joaquin River.* State of California Department of Water Resources.

Nepf, H. (2012). Flow and transport in regions with aquatic vegetation. *Ann. Rev. of Fluid Mech., 44*, 123-142.

Nepf, H. M. (2012). Hydrodynamics of Vegetated Channels. *Journal of Hydraulic Research*, 262-279.

Rominger, J., Lightbody, A., & Nepf, H. (2010). The effects of vegetation on sand bar stability and stream hydrodynamics. *ASCE, 136*(12), 994-1002.

Vandegrift, T. (2015). *TAC Template Hydrograph Simulations: RiverWare Daily Flow Model.* Denver: Bureau of Reclmation, Technical Service Center.

Yang, J., Kerger, F., & Nepf, H. (2015). Estimation of bed shear stress in vegetated and bare channels with smooth beds. *Water Res. Res., 51*(5), 3647-3663.

Vegetation Modeling of the Trinity River between Lewiston Dam and the North Fork Trinity River

Jianchun Victor Huang, Ph.D., P.E., Hydraulic Engineer, Sedimentation and River Hydraulics Group, Technical Service Center, Bureau of Reclamation, Denver, CO, vhuang@usbr.gov

Blair P. Greimann, Ph.D., P.E., Hydraulic Engineer, Sedimentation and River Hydraulics Group, Technical Service Center, Bureau of Reclamation, Denver, CO, bgreimann@usbr.gov

Abstract

SRH-1DV, developed by the Sedimentation and River Hydraulics Group of Bureau of Reclamation, was selected to simulate the vegetation establishment, growth, and desiccation in a 40-mile reach of the Trinity River between Lewiston Dam and the North Fork Trinity River. Upon the completions of the Trinity and Lewiston Dams in the early 1960s, the dams stored and transferred water resources of the Trinity to the Sacramento River and the Central Valley. These dams regulated the flows and reduced the flow peaks. Historic flows ranging from 100 to 100,000 cfs were regulated to nearly constant flows between 100 to 300 cfs. The elimination of the high flow regime reduced the channel dynamics of the river and changed the river into a narrow, single channel in most areas, and thus reduced salmonid habitat. A combination of active revegetation (plantings) and natural regeneration and recruitment processes are applied to address the vegetative restoration component of Trinity River Restoration Program (TRRP). Application of our numerical model aids in understanding the river processes and supports predictions of future physical conditions.

In this application of SRH-1DV, four basic vegetation communities are simulated: cottonwood, white alder, narrowleaf willow, and shiny willow. The numerical model covers 10 years from 2001 to 2011. Vegetation map 2001 is used to provide initial vegetation conditions regarding vegetation density and age. Vegetation establishment, growth, and desiccation are modeled and results are compared with the 2011 vegetation map. The goal of this study is for us to understand how well SRH-1DV can be used to replicate vegetation growth and mortality on the Trinity River, demonstrate the potential and limitations of the model on Trinity River vegetation, and identify future study directions.

Introduction

The Bureau of Reclamation's (BOR) Trinity River Restoration Program (TRRP) is actively rehabilitating the Trinity River between Lewiston Dam and the North Fork Trinity River. Upon the completions of the Trinity and Lewiston Dams in the early 1960s, the dams stored and transferred water resources of the Trinity to the Sacramento River and the Central Valley. Trinity Dam was completed in 1962. Lewiston Dam, about 8 miles downstream from Trinity Dam, was completed in 1963.

Up to 90% of the annual water yield of the Trinity was diverted for agricultural and urban uses (Bair, 2001). These dams regulated the flows and reduced the flow peaks. Historic flows ranging from 100 to 100,000 cfs were regulated to nearly constant flows between 100 to 300 cfs.

The elimination of the high flow regime reduced the channel dynamics of the river and changed the river into a single channel in most areas, and thus reduced salmonid habitat.

A combination of active revegetation (plantings) and natural regeneration and recruitment processes are applied to address the vegetative restoration component of TRRP. Active planting is accomplished by planting and initially irrigating willow and cottonwood species in the floodplains and river banks. Natural regeneration and recruitment processes are being accomplished by restoring some of the high flow regime and by construction of side channels and floodplains. The long-term goal is to restrict vegetation encroachment along the low water edge while encouraging establishment on floodplains.

SRH-1DV, developed by the Sedimentation and River Hydraulics Group of Bureau of Reclamation, was selected to simulate the vegetation establishment, growth, and desiccation in a 40-mile reach of the Trinity River between Lewiston Dam and the North Fork Trinity River. The vegetation model uses the 2001 vegetation map, developed by McBain and Trush and USDA Forest Service Redwood Science Laboratory (RSL) (Mcbain and RSL, 2004). The vegetation map was based on low altitude ortho-rectified air photos (1:1,200 scale) from Lewiston Dam (RM 112.0) to the North Fork Trinity River (RM 72.4), taken in November 2001, with a Lewiston Dam release of 300 cfs. The vegetation map was then verified with field surveys during July and October 2003. The mapping boundary was defined as 820 ft (250m) from the channel centerline and 82 ft (25m) vertically above the water surface, whichever occurred first. Forty-one different cover types were mapped and field verified along the Trinity River mainstem. Most cover types were synonymous with a plant stand. However, four non-plant dominated cover types were also mapped: (1) human disturbance, (2) open ground, (3) open water, and (4) roads. The remaining 37 cover types were all dominated by a single plant species or co-dominated by two or more plant species.

In this application of SRH-1DV, four basic vegetation communities are simulated, which include cottonwood, white alder, narrowleaf willow, and shiny willow. Vegetation establishment, growth, and desiccation are modeled, and results are compared with the 2011 vegetation map (Hoopa Valley Tribe and McBain Associates, 2015). The goal of this study is to understand how well SRH-1DV can be used to replicate vegetation growth and mortality on the Trinity River and demonstrate the potential and limitations of the model on Trinity River vegetation.

Model Description

SRH-1DV is an extension of the Sedimentation and River Hydraulics - One Dimensional (SRH-1D), a 1D flow and sediment transport model developed by the Technical Service Center (TSC) (Huang and Greimann, 2007). The model is capable of simulating steady and unsteady flows, internal boundary conditions, cohesive and non-cohesive sediment transport, and lateral inflows in natural rivers and constructed canals with or without mobile boundaries. SRH-1DV was developed to include ground water and vegetation simulation (Fotherby, 2013; Greimann et al., 2011).

Groundwater Module

Groundwater elevation is a critical factor in the survival of riparian vegetation and is predicted in the model from the computed water surface in the river. The ground water module within

SRH-1DV is a cross-section based saturated flow model. Ground water levels are a function of the river water elevation and a soil permeability coefficient. The module solves for the ground water levels, and assumes no ground water interaction between cross sections. Therefore, the ground water solutions obtained from SRH-1DV will only be applicable near the river, i.e., generally within the alluvial soils of the floodplain.

Vegetation Establishment Module

The Establishment Module simulates germination due to air dispersal assuming an unlimited supply of seed. If air dispersal is being simulated, a plant is assumed to germinate if there is available space, available seeds and moist soil. Established plants can also expand to adjacent points through lateral spread of roots. Narrow leaf willow and similar plants are able to expand through lateral growth of roots. These plants can colonize closely spaced adjacent points in the cross section or even closely spaced adjacent cross sections.

Vegetation Growth Module

The Growth Module calculates vertical growth of the root (depth), stalk (height), and canopy (width). User-specified growth rates for the roots, stalks, and canopy are based upon the month and age of the plant; that is, a growth rate can be assigned for each month of the first year, and then different growth rates can be assigned for each subsequent year of plant life. Root growth is computed at the specified rates until reaching a user-specified depth with respect to the ground water table. Stalk growth and canopy width are also computed and tracked in the Growth Module until the plant reaches an assigned maximum height or width for the vegetation type.

Vegetation Mortality Module

The Mortality Module calculates whether the plant survives each time step. There are multiple ways a plant may die in this study, and thus be removed from the module:
- Desiccation, if a plant experiences too much stress due to lack of water;
- Scour, if the local flow velocity at the plant becomes larger than a user-specified value;
- Inundation, if flows exceed the root crown by an assigned depth and flow duration;
- Competition, where assigned rules define the dominant plants; and
- Shading, when a susceptible plant is under the canopy of another plant.

Flow Model Input

In this study, only the flow and vegetation parts of SRH-1DV are used.

Hydrology

Five stream gages in the Trinity River and three gages in the tributaries are operated and maintained by the U.S. Geological Survey (USGS) in the study reach. The numerical model uses flow at the Trinity R A Lewiston CA Gage (USGS 11525500) as the upstream boundary conditions, and adjusts the flow in the river according to the downstream gages in the river or tributaries. Flows from the tributaries are simulated as point sources. The difference between a

downstream gage and the combination of upstream gage and tributaries between these two gages is treated either as point source or non-point source.

Cross Section Geometry

Cross section geometry was obtained from a separate study performed by the Northern Region Office of the California Department of Water Resources (CDWR, 2014). CDWR performed the hydraulic computations from Lewiston Dam to just downstream of the North Fork Trinity River (River Mile 112.16 to 72.23). The geometry data were based on a 2009 terrain developed from a compilation of ground control, bathymetry, and LiDAR (Light Detection and Ranging) data acquired during the month of April 2009. The terrain was converted to a Triangulated Irregular Network (TIN) and then interpolated into SRH-1DV cross section geometry.

Other Parameters

Downstream boundary conditions were determined based on a rating curve of water surface elevation and discharge at the downstream most cross section (RM 72.23). Channel and overbank roughness values (Manning's n values) were kept the same based on previous HEC-RAS numerical simulations (CDWR, 2014). The overbank roughness was set as 0.08 and the channel roughness was set as 0.045. In the groundwater module, the hydraulic conductivity of the soil was set as 100,000 ft/day and the capillary fringe height is set as 0.8 ft. The time steps were set as one hour for river flow and ground water simulations and 1 day for vegetation simulation.

Vegetation Input

Vegetation data required as input to the model include germination, growth, and mortality parameters for each modeled vegetation type along with an initial vegetation conditions map. This study used the 2001 vegetation inventory as the initial conditions map and initially adopted vegetation parameters from other research. The model was run for approximately 10 years, and the vegetation parameters were calibrated such that final vegetation map matched the 2011 vegetation inventory as closely as possible.

Vegetation Alliances

Four vegetation types or alliances were selected to represent species or communities of interest in the Trinity River (Table 1). Black cottonwood (*Populus balsamifera ssp. Trichocarpa*) and Fremont cottonwood (*Populus fremontii*) are combined into a single type. Two vegetation types are used to represent willows. One is used for shrub-type willows, including narrowleaf willow (*Salix exigua*) and dusky willow (*Salix melanopsis*), and another is used for large shrub or small tree-type willows, including arroy willow (*Salix lasiolepis*), shiny willow (*Salix lucida* ssp. *Lasiandra*), and red willow (*Salix laevigata*). White alder (*Alnus rhombifolia*) is also simulated in the model. One alliance, referred to as the Other Alliance was used to represent all the other vegetation, where no vegetation establishment, growth, and desiccation are modeled. Some are upland species that are not influenced by the flows in the river channel. Some of the species in the Others category are riparian plants which can be simulated in future studies. The last alliance, referred to as the No Grow alliance was used to represent roads, agriculture area, and

other distributed areas, where none of the other alliances are permitted to grow. Agricultural lands are designated as a no-grow surface to distinguish between plant growth on cultivated and uncultivated lands.

Table 1. Vegetation alliances modeled in SRH-1DV.

Modeled Vegetation Alliance	Latin Name	Abbreviation
Black Cottonwood Fremont Cottonwood	*Populus balsamifera* ssp. *Trichocarpa* *Populus fremontii*	BKCW
White Alder	*Alnus rhombifolia*	WHAD
Narrowleaf Willow Dusky Willow	*Salix exigua* *Salix melanopsis*	NLWL
Arroyo Willow Shiny Willow Red Willow	*Salix lasiolepis* *Salix lucida* ssp. *Lasiandra* *Salix laevigata*	OTWL
Others	NA	OTER
No Grow (ag and roads)	NA	NOGR

Germination, Growth and Mortality Parameters

The model requires germination, growth, and mortality parameters for each vegetation alliance being simulated. Information including root growth rates, stem growth rates, canopy spread rates, capillary fringe height, germination seasons, germination time, longevity of seeds, basal sprouting, and days for desiccation mortality were based primarily on values from Mahoney and Rood (1998), McBride and Strahan (1983), Shafroth et al. (1998), and Stella et al. (2006). Values were also selected from USDA plant guide information and from previous flow-sediment-vegetation modeling by Reclamation's Sedimentation and River Hydraulics Group (Fotherby, 2013; Gordon, 2011; Greimann et al., 2011; Greimann et al., 2007; and Murphy et al., 2006) and calibrated in this study. When no other information was available regarding a particular species, values were assigned based on similar vegetation types or general field observations of physical attributes. No previous germination, growth, and mortality parameters are available for white alder, and therefore values were estimated from USDA plant guide information and Bair (2001).

Initial Vegetation Conditions

SRH-1DV allows the user to input initial vegetation conditions for each point in each cross section. Identification of the vegetation present at the beginning of the simulation for each point is accomplished through a polygon shapefile containing areas assigned with a specific vegetation type.

The vegetation model uses the 2001 vegetation inventory map, developed by Mcbain And Trush and USDA Forest Service Redwood Sciences Laboratory (Mcbain and RSL, 2004). The vegetation map was based on low altitude ortho-rectified air photos (1:1,200 scale) from Lewiston Dam (RM 112.0) to the North Fork Trinity River (RM 72.4), taken in November 2001, with a Lewiston Dam release of 300 cfs. The vegetation map was then verified with field surveys during July and October 2003. The mapping boundary was defined as 820 ft (250m) from the channel centerline and 82 ft (25m) vertically above the water surface, whichever occurred first.

Five vegetation types or alliances were selected to represent species or communities of interest in this Trinity River study: cottonwood (BKCW); white alder (WHAD); narrowleaf willow (NLWL) including narrowleaf willow and dusky willow; other willows (OTWL) including arroyo willow, shiny willow, and red willow; and all other vegetation. No Grow alliance was used to represent roads, agriculture area, and other distributed areas.

Each mapped community of vegetation was assigned an age and density for at least one of the six vegetation alliances including No Grow. The age and density for the initial conditions were estimated from descriptions provided in the vegetation inventory and mapping. Vegetation density represents the percentage of the area occupied by the vegetation type. In SRH-1D, a vegetation type only exists in a fraction of stations in a cross section. For example, if cottonwood has a density of 0.8 (80%) in polygons with vegetation code BC and 10 points of cross section stations are located in polygons BC, 8 points will be assigned as cottonwood, and 2 points will be assigned as no vegetation.

Results

Numerical simulation was performed from November 15 2001 through April 15 2011 with historical flow rates as discussed in Section 2.1. The extent of the 2001 and 2011 vegetation inventory maps is different. The 2001 vegetation inventory map covers a larger area than the 2011 map, and some areas in the 2011 map are not covered by 2001 map. For comparison, both maps were clipped in GIS to keep the same overlapped area, and the numerical model was calibrated only in the remaining area.

Vegetation Area with Density Considered

SRH-1DV simulates vegetation density by initially assigning vegetation on a percentage of station points in a cross section. After the simulation, all station points in a cross section were counted to estimate the area changes in each vegetation polygon.

Initial and final vegetation areas for each vegetation alliance are summarized in Table 2. The mortality areas for each vegetation alliance were also listed. The model represented both the correct magnitude and direction of change for each simulated vegetation alliance.

Table 2. Initial and final vegetation areas and removed vegetation areas due to different mortality mechanism.

			Vegetation Area (Acres)			
			BKCW	WHAD	NLWL	OTWL
Living	2001 Mapping		36.8	246.6	254.1	129.3
	2011 Mapping		31.6	177.0	262.4	154.5
	2011 Simulated	Total	30.0	185.4	259.3	153.9
		Old	30.0	185.4	136.2	110.6
		New Growth	0	0	123.1	43.3
	Field Change		**-14%**	**-28%**	**3%**	**19%**
	Modeled Change		**-19%**	**-25%**	**2%**	**19%**
	Competition		0	0	12.6	1.6

Mortality cause	Desiccation	1.9	39.3	68.6	6.9
	Drowning	0	20.9	3.1	4.2
	Scour	5.0	1.0	33.6	6.0

Vegetation Calibrated with Visual Inspection

2011 aerial photographs were used to visually check the vegetation modelling results regarding vegetation establishment, survival, and different types of mortality. In areas where 2011 aerial photographs were not available, 2010 and 2014 aerial photos were used. Currently, SRH-1DV simulates vegetation mortalities due to competition, inundation, desiccation, and scour. Inundation mortality was predicted to occur most inside the channel or in the side channel, where water covers the vegetation even during a low flow stage. Desiccation mortality was predicted mostly on highlands where the vegetation roots could not reach the ground water. Predictions of scour mortality were most frequently in shallow channel areas, where the water velocity exceeds the critical velocity.

Figure 1 and Figure 2 show the initial and simulated final vegetation status for cottonwood at Station 94.35, on aerial photos 2001 and 2010, respectively. Because the 2011 aerial photograph was unavailable at this site, the 2010 aerial photo was used. At this station cottonwoods did not survive due to scour on the left side of the channel near the left bank (right bottom of the channel), and did survive on the right floodplain. In the figures, larger size dot represents initial condition and smaller final condition. The color of a dot represents the vegetation status (green: alive; white: no vegetation; brown: mortality due to shade and competition; black: mortality due to drown; red: mortality due to desiccation; and purple: mortality due to scour).

Figure 1. Initial and final cottonwood existence and mortality illustrated at Station 94.35 on 2001 aerial photo.

Figure 2. Initial and final cottonwood existence and mortality illustrated at Station 94.35 on 2010 aerial.

Figure 3 through Figure 5 show the initial and simulated final status of shrub-type willows (NLWL) at Station 92.25. The primary cause of mortality for the shrub-type willows was desiccation and drowning. The numerical model shows that shrub-type willows (narrowleaf and dusky willows) were killed by scour at two locations; the one on the right side of the channel (at the center of the figure) is not supported by the 2010 aerial photo, but is clear in the 2014 aerial photo, and the one near the left bank (left side of the figure) is not supported by either the 2010 or 2014 aerial photos. New narrowleaf willows were established on right floodplain.
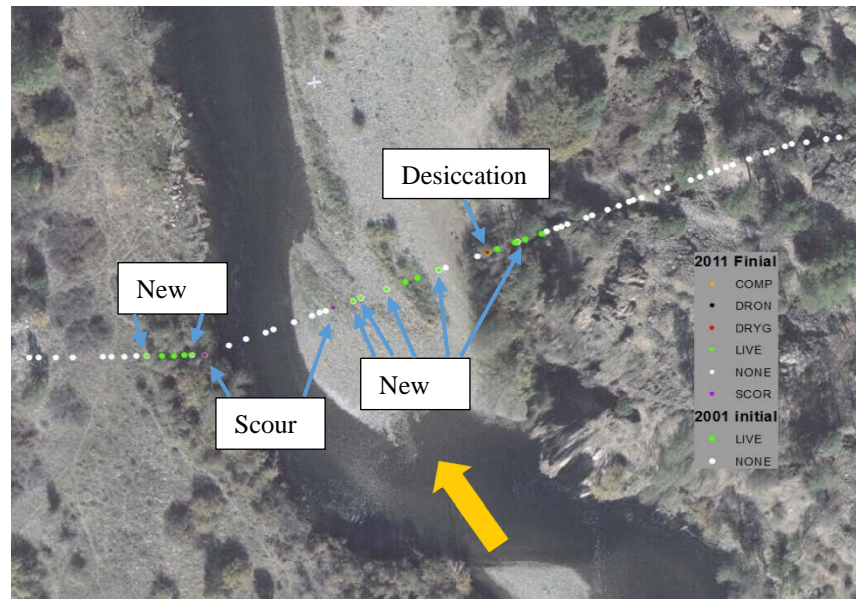
Figure 3. Initial and final narrowleaf willow existence and mortality illustrated at Station 92.25 on 2001 aerial photo.

Figure 4. Initial and final narrowleaf willow existence and mortality illustrated at Station 92.25 on 2010 aerial photo.

Figure 5. Initial and final narrowleaf willow existence and mortality illustrated at Station 92.25 on 2014 aerial photo.

Summary

SRH-1DV is used to simulate the vegetation germination, growth, and desiccation in a 40-mile reach of the Trinity River between Lewiston Dam and the North Fork Trinity River. Four vegetation types or alliances were selected to represent species or communities in this study, which include cottonwood, white alder, shrub-type willow, and large brush and tree-type willows. Two additional types were used in the model, one for all the other riparian vegetation alliances and one to represent roads, agriculture area, and other distributed areas. The numerical model spanned a 10-year period from November 2001 to April 2011. A vegetation inventory from 2001 was used to provide initial vegetation conditions regarding vegetation density and age. A vegetation inventory from 2011 was used to calibrate the model regarding each vegetation parameter.

The numerical model roughly reproduced the survival rate of cottonwood, white alder, shrub-type willow, and other large brush and tree willows based on the predicted area covered by each vegetation types. A qualitative comparison of model results and field conditions was used to examine the existence and mortality of each vegetation type.

While it may not be realistic to expect a 1D numerical model to quantitatively predict the specific locations of vegetation survival, mortality, and establishment, the calibrated numerical model can be used to compare the general vegetation response under different river restoration flow and management alternatives.

Acknowledgments

References

Bair, J. H. (2001). Riparian woody plant initiation, establishment, and mortality on rehabilitated banks of the Trinity River, California. Master Thesis, Humboldt State University.

CDWR. (2014). Trinity River Flood Insurance Study Hydraulic Analysis. California Department of Water Resources, Northern Region Office.

Fotherby, L. (2013). Vegetation Modeling with SRH-1DV. Technical Report SRH-2013-09, Sedimentation and River Hydraulics Group, Technical Service Center, Bureau of Reclamation, Denver, CO.

Gordon, E. H. (2011). Sediment Transport and Vegetation Modeling of Reach 2B Alternatives for the San Joaquin River Restoration Program. Technical Report SRH-2011-33, Sedimentation and River Hydraulics Group, Technical Service Center, Bureau of Reclamation, Denver, CO.

Greimann, B.P., Fotherby, L., Lai, Y., Varyu, D., Tansey, M.K., Young, C., and Huang, J. (2011). Calibration of numerical models for the simulation of sediment transport, river migration, and vegetation growth on the Sacramento River, California. NODOS investigation Report.

Prepared by Bureau of Reclamation, Stockholm Environmental Institute, and Colorado State University.

Greimann, B.P., Mooney, D., Varyu, D., Lai, Y., Randle, T., Bountry, J., and Huang, J. (2007). Development and calibration of the models for the physical river processes and riparian habitat on Sacramento River, CA. NODOS project report. Bureau of Reclamation, Technical Service Center, Denver, CO.

Hoopa Valley Tribe and McBain Associates. (2015). Trinity River Project Area Riparian Mapping. Prepared for: Trinity River Restoration Program

Huang, J., and Greimann, B.P. (2007). User's Manual for SRH-1D 2.0 (Sedimentation and River Hydraulics – One Dimension Version 2.0). Sedimentation and River Hydraulics Group, Technical Service Center, Bureau of Reclamation, Denver, CO. (www.usbr.gov/pmts/sediment).

Mahoney, J.M., and Rood, S.B. (1998). "Streamflow requirements for cottonwood seedling recruitment- an integrative model." Wetlands, Vol.18(4), 634-645.

Mcbain and RSL. (2004). Biannual Report, Final Riparian Habitat Inventory and Mapping of the Mainstem Trinity River. Prepared For: Trinity River Restoration Program, Technical Modeling And Analysis Group

McBride, J.R., and Strahan, J. (1983). "Establishment and survival of woody riparian species on gravel bars of an intermittent stream." The American Midland Naturalist, Vol.112(2), 235-245.

Murphy, P.J., Fotherby, L., Randle, T., and Simons, R. (2006). Platte River sediment transport and riparian vegetation model. Bureau of Reclamation, Technical Service Center, Denver, CO. www.usbr.gov/pmts/sediment.

Roberts, M.D., Peterson, D.R., Jukkola, D.E., and Snowden, V.L. (2002). A Pilot Investigation of Cottonwood Recruitment on the Sacramento River. The Nature Conservancy, Sacramento River Project. http://www.aquaveo.com/pdf/SMS_10.1.pdf

Shafroth, P.B., Auble, G.T., Stromberg, J.C., and Patten, D.T. (1998). "Establishment of woody riparian vegetation in relation to annual patterns of streamflow, Bill Williams River, Arizona." Wetlands, Vol.18(4), 577-590.

Stella, J.C., Battles, J.J., Orr, B.K., and McBride, J.R. (2006). "Synchrony of Seed Dispersal, Hydrology and Local Climate in a Semi-arid River Reach in California." Ecosystems, Vol.6(9), 1-15. DOIL 10.1007/s10021-005-0138-y.

Infrastructure in the Stream Environment

Advancements in Bridge Scour Evaluation with Two-Dimensional Hydraulic Modeling using SRH-2D/SMS

Scott Hogan, Senior Hydraulic Engineer, Federal Highway Administration, Fort Collins, Colorado, scott.hogan@dot.gov

Abstract

The US Federal Highway Administration (FHWA) has promoted the use of two-dimensional hydraulic modeling for bridge hydraulic analysis for many years, and in recent years adopted the US Bureau of Reclamation (Reclamation) SRH-2D model. Reclamation and FHWA have since worked in partnership to incorporate new hydraulic structure features into SRH-2D and have facilitated a custom graphical user interface in the Surface Water Modeling System (SMS, by Aquaveo) that includes powerful tools for analyzing and communicating results to others. Most recently, FHWA developed a bridge scour tool to extract hydraulic parameters needed for bridge scour analysis and transfer them into the FHWA's Hydraulic Toolbox, where users can compute each of the scour components, generate a total scour summary table, and plot the resulting scour profiles at the bridge cross section. This paper provides a brief background of the FHWA bridge scour program and how technology has advanced to support improved bridge scour evaluations.

Introduction

In September 1988, the United States Department of Transportation's (USDOT) Federal Highway Administration (FHWA) established a national scour evaluation program. A major impetus for establishing the FHWA scour program was the April 1987 I-87 Schoharie Creek bridge failure in New York. After the failure, FHWA had immediately directed that each State should evaluate the risk of its bridges being subjected to similar damage during floods on the order of a 100 to 500-year return period or more. Where vulnerable, bridges should be evaluated for the need for additional riprap or channel protection, spur dikes, groins or other river training devices and in some cases strengthening of the foundation through addition of piles, sheeting, or other appropriate measures (FHWA, 1987). However, subsequent investigations led to recommendations of a formal and structured FHWA oversight process and associated guidance.

This resulted in the September 1988 issue of Technical Advisory (TA) T 5140.20 (FHWA, 1988) to provide guidance for program development and implementation. TA T 5140.20 included interim guidelines for evaluating scour at bridges. The TA provided scour mitigation recommendations for both new and existing bridges. TA T 5140.20 also described FHWA's intent to develop and publish a new FHWA publication Hydraulic Engineering Circular (HEC) No. 18, "Evaluating Scour at Bridges" (HEC-18).

FHWA established the scour program and issued TA T 5140.20 under its authorities associated with the National Bridge Inspection Standards (NBIS) and associated regulation (US Code of Federal Regulations (CFR), Title 23 CFR 650 Subpart C "National Bridge Inspection Standards.") All bridges in the National Bridge Inventory (NBI) were subject to the guidance of TA T 5140.20. Additionally, FHWA added a scour focused data collection item to the NBI to provide a data driven component of the

scour program. The April 1989 failure of the Route 51 Hatchie River bridge illustrated how stream instability and lateral migration were also important elements that the fledging scour program needed to address.

In February 1991, FHWA published the first edition of HEC-18. At the same time, FHWA also published a companion technical reference (1991a), HEC-20 "Stream Stability at Highway Structures." These two documents provide guidance on the development and implementation of procedures for evaluating bridge scour and stream stability processes.

In October 1991, FHWA issued TA T 5140.23, that updated and superseded TA T 5140.20 (FHWA, 1991b). TA T 5140.23 specifically cited HEC-18 as FHWA's recommended procedures for addressing scour at both new and existing bridges. In turn, HEC-18 refers to HEC-20 for additional aspects of the stream stability issues and components.

In conjunction with on-going bridge scour research and significance advances in the state-of-practice over the years, HEC-18 and HEC-20 have gone through several major revisions, with the current versions being HEC-18 Fifth Edition (FHWA 2012a) and HEC-20 (FHWA 2012b) Fourth Edition. Recognizing the need for guidance in scour countermeasures, in July 1997, FHWA issued HEC-23 "Bridge Scour and Stream Instability Countermeasures" (HEC-23) (the September 2009, third edition is the latest release of HEC-23).

Currently, the FHWA scour program involves more than 509,000 bridges over water in the U.S. (NBI, 2017), or about 80 percent of U.S. bridges. The original 1988 technical advisory and subsequent documents launched a massive scour screening and evaluation program that effectively continues to this day. Scour vulnerability evaluation (evaluation) is required for all new bridges over waterways, and bridges are required to withstand the effects of scour from a "superflood," on the order of a 500-year flood, without failing (FHWA 1995).

Evolution of Bridge Scour Evaluation Technology

Bridge scour evaluations require an engineering analysis to evaluate hydraulic variables (including flow depths, velocity magnitudes, and directions) through the bridge reach and use them to compute each of the components that contribute to total scour, which include long-term degradation, contraction scour, and local scour (pier scour and abutment scour), as described in HEC-18 (FHWA 2012b). Engineers who perform infrequent scour evaluations typically follow the steps in HEC-18 by performing manual calculations; however, most who perform multiple scour evaluation, have integrated the equations into spreadsheets for efficient and consistent calculations.

Other computer programs have also been developed over the years and supported by FHWA. For example, FHWA developed the program "HY-9: Scour" in 1992, drawing upon the second edition of HEC-18 (1993) for solving numerous scour equations and documenting the results. The transportation community used HY-9 through the 1990s. In the mid-1990's, the U.S. Geological Survey (USGS) and FHWA integrated HEC-18 scour procedures into the one-dimensional (1D) hydraulic model Water-Surface PROfile computations (WSPRO) software (FHWA 1990). In 2001, the U.S. Army Corps of Engineers (USACE) Hydrologic Engineering Center's River Analysis System (HEC-RAS) version 3.0.1 included bridge scour evaluation options that followed the Fourth Edition of HEC-18 (FHWA 2001), and has been used widely since 2001, but the scour options in HEC-RAS (through current version 5.0.3) have not been updated to reflect the fifth edition of HEC-18 (FHWA 2012a). Consequently, in 2013, FHWA added HEC-18, fifth edition based scour calculators for the individual scour components to the FHWA Hydraulic Toolbox (HTB) (Version 4.2) software program. Subsequently, in HTB version

4.4, FHWA added additional scour tools that allow computation of total scour, generation of scour summary tables, and plotting scour profiles.

Scour Evaluation with One-dimensional Hydraulic Modeling

Prior to 2012, most bridge scour evaluations were based on hydraulic variables that were determined from a 1D hydraulic model, such as HEC-RAS 1D (HEC 2002) and WSPRO software (FHWA 1990). The variables needed for scour evaluations include, velocity, depth, discharge, unit discharge, and flow direction, for the main channel and overbank sections at an "approach section", located upstream of the influence of the bridge, and at the "contracted section" located at the maximum contraction beneath the bridge. The quality and accuracy of these hydraulic variables directly impact the accuracy of the scour calculations, and the variables are also dependent on the suitability of the hydraulic model to define the flow distribution (FHWA 2012c).

For 1D models, it is important to understand that the computed flow distribution is an approximation based on several assumptions, which include: flow direction, flow path, effective flow area, cross section averaged properties for water surface elevation and velocity, and flow distribution at each cross section that is based on the available incremental conveyance (FHWA 2012c). Furthermore, 1D models assume the flow distribution at each cross section is completely independent of the adjacent cross sections, up- and downstream, and continuity within the channel and overbank sections is not implicitly preserved. Bridge crossings where these assumptions are reasonable and acceptable warrant the use of 1D model results. However, many bridge crossings exhibit complex flow conditions that are overly simplified in a 1D model, resulting in the potential to incorrectly predict.

Examples of complex flow conditions include: bridges and/or road embankments that are skewed to flood flows, wide flood plains with a meandering river channel, braided channels, river crossings with multiple bridge openings, roadway overtopping, bridges with highly contracted flows, abrupt changes in channel geometry or roughness, etc. (FHWA 2012a). For bridge, hydraulic and scour analyses, these conditions would be better represented with a two-dimensional (2D) hydraulic model. However, until recent years 1D modeling has been the most practical tool available to most engineers.

Scour Evaluation with Two-dimensional Hydraulic Modeling

FHWA has been involved with 2D modeling since at least 1977, sponsoring workshops that investigated potential and actual 2D modeling application to transportation projects (FHWA 1977). However, such use typically focused on research aspects of such modeling. For project delivery, FHWA began using 2D hydraulic modeling in 1988, on a limited basis for select complex bridge design projects. FHWA recognized the many benefits of utilizing a 2D model, and has since envisioned widespread use and application of 2D hydraulic modeling within the U.S.

It has taken many years, however, for computer hardware and software to develop to a point where 2D modeling technology can be practically integrated into hydraulic engineering practice. By the early 2000s, FHWA was promoting the use of the Finite-Element Surface-Water Modeling System (FESWMS) 2D hydraulic model (FHWA 2003) for analyzing complex bridge hydraulics. Although FESWMS was successfully used by many for complex bridge hydraulics projects, it did not become

integrated as a standard practice for bridge hydraulic modeling, primarily because of the difficulty in use and extended time it took to create and run a model. In the late 2000s, FHWA began supporting the development of custom graphical user interface features in the Surface Water Modeling System (SMS, 2018). SMS is a pre- and post-data processor that is used to evaluate results from hydraulic models. It also includes several powerful graphical visualization tools that are helpful in communicating modeling results to others.

After an extensive search for a new 2D hydraulic model to replace FESWMS, FHWA selected the U.S. Department of Interior's Bureau of Reclamation's (Reclamation) Sedimentation and River Hydraulics – Two-Dimensional (SRH-2D) model (Reclamation 2006). FHWA selected SRH-2D because of its advanced modeling capabilities and proven stability for riverine applications and Reclamation's interest in partnering for further development of transportation related hydraulic structures (Reclamation 2016). SRH-2D had been thoroughly tested and verified by Reclamation since their initial 2004 model creation and development. FHWA's partnership with Reclamation began in 2013 and funded the development of a custom graphical user interface in SMS (version 12). Most recently, FHWA has been promoting 2D hydraulic modeling technology through its Every Day Counts (EDC) program that seeks to identify and deploy proven but underutilized technology to improve the project delivery process and the safety and resiliency of transportation infrastructure.

Given the significant development of 2D hydraulic models and resources, and recognition that 2D hydraulic models provide more accurate representations of the flow field and flow distribution, the 2012, fifth edition of HEC-18 included FHWA's recommendation to use 2D hydraulic analysis for all bridges with complex flow characteristics. Complex flow distributions produced by channels and/or bridges skewed to the floodplain simply cannot be accurately predicted with a 1D hydraulic model. FHWA further noted, in Hydraulic Design Series (HDS)-7 "Hydraulic Design of Safe Bridges," that "Two-dimensional models should be used on all but the simplest bridge crossings as a matter of course," (2012c).

Two-dimensional hydraulic models overcome the significant assumptions required for 1D hydraulic modeling, and they improve the estimation of bridge scour by helping to identify correct locations of the "approach section" and "contracted section" that are used in scour evaluation (Figure 1). They also provide more accurate evaluation of the hydraulic variables at these locations. Flow magnitude, direction, and depth are computed for every element in a 2D hydraulic model, allowing a more accurate depiction of flow distribution. The best location for the "approach section" is often noted by the point at which the computed flow direction (noted by velocity vectors) in the overbank areas takes a marked turn toward the channel, indicating the upstream limit of the bridge encroachment influence on flow distribution. Correctly identifying the location of this section is critical in determining whether contraction and abutment scour are governed by "live-bed" or "clear-water" conditions. Furthermore, if "live-bed" conditions exist, accurate flow distribution in the main channel at the "approach section" is important in quantifying the volume of sediment that is effectively transported to the bridge (contracted) section. Subsequently, the location of the "contracted section" at the bridge opening determines the sediment transport capacity through the contraction and potential for scour, when compared to hydraulic conditions at the approach section. Without the additional insights and information offered by a 2D hydraulic model, assessing the location and orientation for the approach and contracted sections with 1D hydraulic model results can be challenging, and is much more subjective, especially for complex flow conditions.

New Scour Evaluation Tools

New features have been developed in the SMS graphical user interface, through FHWA, which may be used to conveniently and efficiently extract the hydraulic variables needed for bridge scour computations. Within the SMS software package, users create a bridge scour specific coverage (layer) and draw arcs along the "approach section" and "contracted section" locations, as shown in Figure 1.
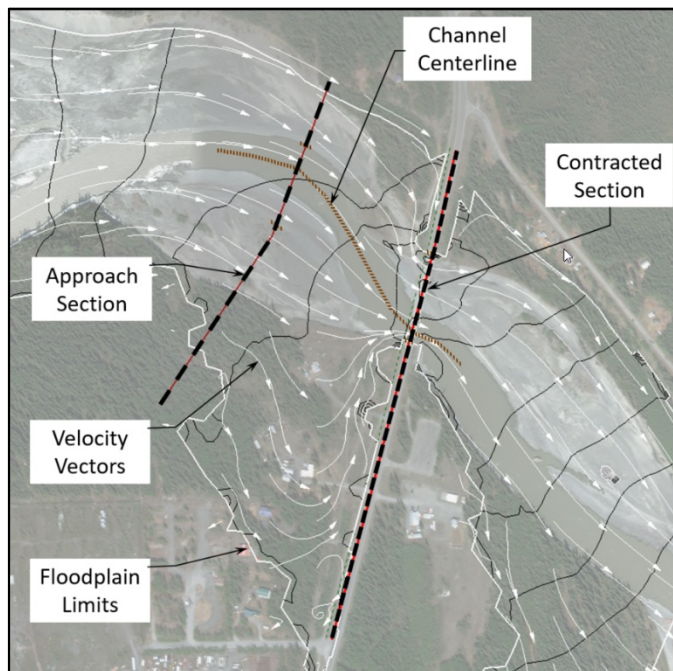
Figure 1. Example of the approach and contracted section arcs drawn in an SMS bridge scour coverage (Image source: ESRI World Imagery)

Additional shorter arcs are also drawn to note channel bank locations, pier locations and alignment, and the locations of the toe of slope at the bridge abutments. After the user specifies a gradation for the channel bed material and selects the model results for a specific flood simulation (e.g., 100-year), the hydraulic variables, along with bridge cross section geometry, are extracted and copied into a Hydraulic Toolbox (HTB) input file. In the Hydraulic Toolbox, users select the appropriate scour calculators for contraction scour, pier scour, and abutment scour, and the HTB computes each of the
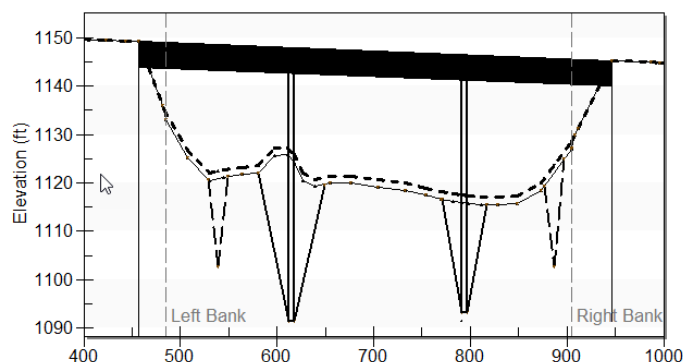
Figure 2. Example bridge scour plot from the Hydraulic Toolbox. (Image source: FHWA)

scour components. With the bridge contracted section geometry as reference, the total scour elevations can be computed and displayed in a summary table and bridge cross section plot, as shown in Figure 2.

An additional benefit of using 2D hydraulic modeling, is that users can gain better insights into the hydraulic flow patterns by viewing continuous lateral coverage of the results (scalar and vector) through the model limits, in contrast to viewing results only at cross section locations in a 1D hydraulic model. The SRH-2D standard output variables include velocity, depth, water surface elevation, Froude number, and shear stress, but additional parameters may also be computed using a data calculator tool in the SMS package. The energy grade line (EGL) and the "critical velocity index" are two example parameters that can be beneficial to hydraulic analysis. The 'critical velocity index' is a ratio of the computed flow velocity to the critical velocity for a specific sediment size, as computed using Equation 6.1 in HEC-18 (2012a). With a known material gradation and model results for depth and velocity, users can develop a critical velocity index coverage that can show whether the material in transport at the "approach section" is maintained in transport through the bridge section. In the example provided in Figure 3, the critical velocity index (CVI) shows that the velocity in the main channel exceeds the critical velocity (CVI>1) from the "approach section", through the "contracted section" at the bridge, therefore confirming a "live-bed" scour condition for the specified flow.

Conclusion – Future Developments

These bridge scour tools were developed to take advantage of the improved information available with 2D hydraulic models and to help reduce the subjective judgement needed by engineers when assessing hydraulic variables for bridge scour calculations, and ultimately to improve the consistency of calculations between different engineers. FHWA plans continue to improve and enhance these tools in the years to come.
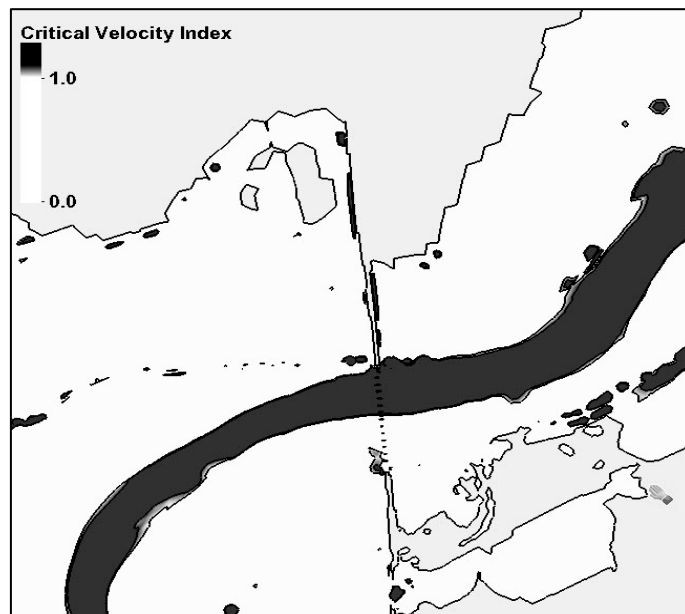
Figure 3. Example of critical velocity index plot confirming "live-bed" conditions in the channel through the bridge. (Image source: FHWA)

References

Aquaveo, Inc. (Aquaveo). 2018. Surface Water Modeling System v12.3, graphical user interface for SRH-2D and other hydraulic models, available in a free community version (www.aquaveo.com/down-loads).

FHWA. 1977. "Summary Report from Workshop on Two-Dimensional Mathematical Models for Use In Hydraulic Problems," Report No. FHWA-RD-77-55.

FHWA. 1987. "Assessing the Vulnerability of Bridges to Damage From Floods," Office of Engineering internal FHWA memorandum. US Department of Transportation.

FHWA. 1988. Technical Advisory T 5140.20 "Scour at Bridges."

FHWA. 1990. "HY-7 - User's manual for WSPRO - A computer model for water surface profile computations," Report No. FHWA-IP-89-027 (Shearman, J.O.).

FHWA. 1991a. "Stream Stability at Highway Structures," HEC-20, Report No. FHWA-IP-90-014 (P.F. Lagasse, J.D. Schall, F. Johnson, E.V. Richardson, J.R. Richardson, F. Chang).

FHWA. 1991b. Technical Advisory T 5140.23 "Evaluating Scour at Bridges."

FHWA. 1993. "Evaluating Scour at Bridges," HEC-18, Second Edition, Report No. FHWA-NHI-01-001 (Dr. E.V. Richardson, L.J. Harrison, Dr. J.R. Richardson & S.R. Davis).

FHWA. 1995. "Evaluating Scour at Bridges," HEC-18, Third Edition, Report No. FHWA-NHI-01-001 (E.V. Richardson and S.R. Davis).

FHWA. 2001. "Evaluating Scour at Bridges," HEC-18, Fourth Edition, Report No. FHWA-NHI-01-001 (E.V. Richardson and S.R. Davis).

FHWA. 2003. "User's Manual for FESWMS FST2DH, Two-dimensional Depth-averaged Flow and Sediment Transport Model," Release 3, Publication No. FHWA-RD-03-053 (David C. Froehlich).

FHWA. 2009. "Bridge Scour and Stream Instability Countermeasures: Experience, Selection, and Design Guidance – Third Edition," Hydraulic Engineering Circular No. 23, Volume 1, Report No. FHWA-NHI-09-111.

FHWA. 2012a. "Evaluating Scour at Bridges," HEC-18, Fifth Edition, Report No. HIF-FHWA-12-003 (Arneson, L.A, L.W. Zevenbergen, P.F. Lagasse, P.E. Clopper).

FHWA. 2012b. "Stream Stability at Highway Structures," HEC-20 Fourth Edition, Report No. HIF-FHWA-12-004 (Lagasse, P.F., L.W. Zevenbergen, W.J. Spitz, L.A. Arneson). Federal Highway Administration (FHWA), 2012c, "Hydraulic Design of Safe Bridges," HDS-7, Report No. FHWA-HIF-12-018 (L.W. Zevenbergen, L.A. Arneson, J.H. Hunt, A.C. Miller).

U.S. Army Corps of Engineers, Hydrologic Engineering Center (HEC). 2002. "HEC-RAS River Analysis System User's Manual Version 3.1"

U.S. Army Corps of Engineers, Hydrologic Engineering Center (HEC). 2016. "HEC-RAS River Analysis System User's Manual Version 5.0"

U.S. Department of the Interior, Bureau of Reclamation, Technical Service Center (Reclamation). 2008. "SRH-2D version 2: Theory and User's Manual, Sedimentation and River Hydraulics – Two-Dimensional River Flow Modeling," (Lai, Y.G.).

U.S. Department of the Interior, Bureau of Reclamation, Technical Service Center (Reclamation). 2016. "Modeling In-Stream Structures and Internal Features with SRH-2D," Technical Report: SRH-2016-09, (Lai, Y.G.).

CFD Analysis of Local Scour at Bridge Piers

Brian Fox, Senior Applications Engineer,
Flow Science Inc., Denver, CO, brian.fox@flow3d.com

Robert Feurich, CFD Engineer,
Flow Science Deutschland, Innsbruck, Austria, robert.feurich@flow3d.de

Abstract

Conventional methods for predicting local scour at bridge piers rely on predictive equations developed from physical modeling. These methods may have limited applicability in situations with unique pier shapes or configurations since the complex hydraulic conditions driving the scour processes around piers are inherently three dimensional. This uncertainty may result in excessive conservatism and may even require additional physical modeling to accurately define the local scour depths for unique pier geometry and shapes. Recent advances in computational fluid dynamics (CFD) and computer performance have made 3D modeling a practical approach to evaluate the complex hydraulic conditions driving the local scour processes. Additional progress in sediment transport modeling, has now made it possible for engineers to directly simulate the fully coupled 3D hydraulic and scour processes at complex structures, including bridge piers.

In this study we evaluate the use of a CFD numerical model for predicting the local equilibrium scour depth and deposition around two different pier geometries using a mobile bed 3D sediment transport model. A sensitivity analysis evaluates the range of results based on likely user inputs, and the final numerical predictions are compared to experimental results. This study demonstrates that the results obtained by the numerical model are in good agreement with the results of the physical model.

Introduction

Flood induced scour at bridge abutments and piers is the most common cause of bridge failure in the USA (Ameson et. al, 2012), and underscores the importance of reliable methods for evaluating bridges or other infrastructure at risk for such failure. The hydraulic mechanisms driving scour at bridges are characterized by a complex, 3D horseshoe vortex structure (HSVS) (Ameson et. al, 2012). The HSVS develops as water flows into the leading edge of the pier, which initiates localized erosion at its base. The intensity of the HSVS is diminished as the scour hole grows and an equilibrium scour depth is achieved (Richardson and Richardson, 2008). Factors affecting the scour process include the pier size/shape, approach flow velocity/angle, material size and bed configuration. The most common approaches for evaluating scour potential use empirically derived equations that require inputs derived from 1D/2D hydraulic models. The strong 3D nature of the HSVS means that these common methods for evaluating scour may be insufficient to reliably predict the physical processes that are forming scour holes at bridges (Spasojevic and Holly, 2008). In these cases, fully 3D non-hydrostatic simulations may be required to accurately resolve the local detail of the flow field.

Computational Fluid Dynamics (CFD) is a powerful tool for simulating complex hydraulic environments, such as those found near existing bridge infrastructure, and provides a viable

option for addressing some of the uncertainty associated with the standard scour analysis techniques. Coupling the 3D hydraulic simulation results with scour models provides exciting potential for improved methods of predicting scour and deposition processes near critical infrastructure such as bridge piers and abutments.

Several previous studies have been completed to evaluate the use of CFD to analyze bridge hydraulics and fully coupled CFD/sediment transport models. Olsen and Melaan (1993) were some of the first researchers to use a fully coupled sediment transport model within a 3D CFD code to evaluate pier scour. Richardson and Panchang (1998) used FLOW-3D to evaluate hydraulic patterns within an already developed equilibrium scour hole at the base of a bridge pier. Khosranejad (2012) tested a fully coupled 3D CFD and sediment transport model for evaluating scour at three different pier shapes. More recently, Omara et al. (2018) and Zhang et al. (2017) evaluated the sediment transport model in FLOW-3D to predict the equilibrium scour hole development at different shaped bridge piers. They found that FLOW-3D accurately predicted the maximum scour depth and shape for cylindrical pier configurations.

The current study seeks to validate the latest updates to the FLOW-3D sediment transport model for predicting the scour and deposition patterns at bridge piers. Specifically, we will be validating the results of FLOW-3D simulations against physical model measurements of scour at cylindrical and diamond shaped piers reported in Khosranejad (2012). We also test a range of user defined input parameters to determine the sensitivity of the final scour and deposition patterns to common input variables.

Model Description

Hydrodynamic Model

FLOW-3D is a commonly used general purpose CFD software that solves the fully 3D non-hydrostatic Reynolds-averaged Navier-Stokes equations. Additional capabilities include linkages with other physical phenomena such as air entrainment, chemical reactions, multi-species flows, ect. A full derivation of the governing equations and model capabilities can be found in Flow Science (2019). In all subsequent sections FLOW-3D will be referred to as the "numerical model".

A key feature of the numerical model is the implementation of the Volume of Fluid (VOF) method for simulating free surfaces (Hirt and Nichols, 1981). The VOF method is a numerical technique used to track the location and movement of complex free surfaces and apply proper dynamic boundary conditions to those free surfaces. The current version of the numerical model incorporates major improvements beyond the original (VOF) method to increase the accuracy of the boundary conditions and interface tracking (Barkhudarov, 2004). The numerical model has been used and validated extensively for a wide range of free surface hydraulic engineering applications (Burnham, 2011).

Another important feature of the numerical model is the use of a structured computational mesh that is composed of rectangular elements defined by a set of planes perpendicular to each of the coordinate axes. The numerical model uses a method called Fractional Area Volume Obstacle Representation (FAVOR) to incorporate the effects of geometry into the conservation equations (Hirt and Sicilian, 1985). This approach calculates the open volume fraction and open area fractions to define obstacles in each cell and offers a simple and accurate method to represent complex surfaces without requiring a body fitted mesh.

Sediment Transport Model

A sediment model was first introduced to the numerical model by Brethour (2003) and has since been updated as described in Wei et al. (2014). The numerical model's sediment transport module simulates a 3D transient mobile bed. It is fully coupled with the 3D hydrodynamic solver to simulate the morphological changes to an erodible solid boundary composed of non-cohesive sediments. The model is capable of simulating both bedload transport and suspended sediment transport; and allows for the exchange of material between the two transport mechanisms. The model includes the capability to simulate up to 10 different sediment species, where each species defines a unique combination of grain size and material density. A non-uniform grain size distribution or variable sediment density can be simulated by defining multiple sediment species.

In the numerical model, sediment can exist as either a packed bed or as a suspended sediment concentration. A packed bed is an erodible solid object that is represented using FAVOR, the same method used to represent solid objects in the hydrodynamic solver. The morphological change in the packed bed is governed by the conservation of sediment mass, or Exner equation.

$$\phi \frac{\partial z}{\partial t} = \left(\frac{\partial q_{bx}}{\partial x} + \frac{\partial q_{by}}{\partial y} + D - E \right) \qquad \text{(eq. 1)}$$

z, Bed elevation
q_b, Volumetric bedload transport rate per unit width
ϕ, Maximum packing fraction
D, Downward sediment deposition flux
E, Upward entrainment flux

The physical processes governing the morphological changes are represented numerically on the right side of Equation 1 and illustrated below in Figure 1.
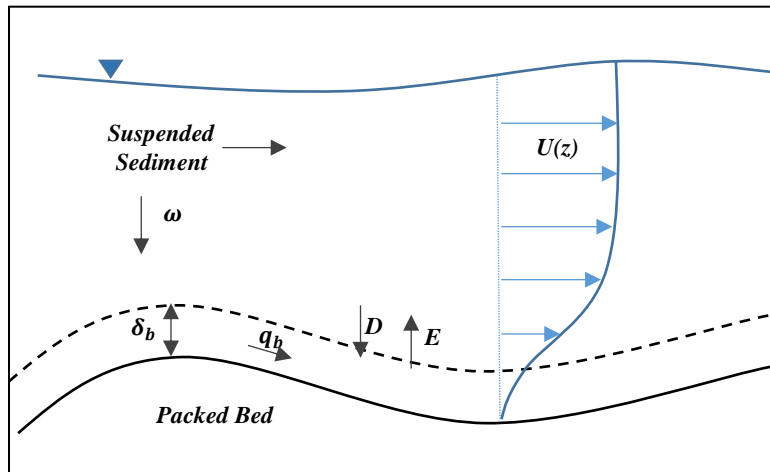
Figure 1. Schematic of physical processes included in the **FLOW-3D** sediment transport model

Bedload transport represents the physical process of sediment moving laterally along the channel without being carried into suspension. Entrainment represents the erosion of the packed bed into suspension; and deposition represents suspended grains settling out of suspension onto the packed bed. Together the difference in the entrainment and deposition

rates define the exchange between the packed bed and suspended sediment. Additionally, an angle of repose defines the maximum angle of a stable slope before failure.

The suspended sediment is represented as a scalar concentration in the fluid filled cells. The concentration is assumed to be uniform in a given cell and is coupled with the fluid cell density and viscosity. For each species, the suspended sediment concentration is calculated by solving its own transport equation.

$$\frac{\partial C_i}{\partial t} + \nabla \cdot (u_{s,i} C_i) = \nabla \cdot \nabla(\varepsilon C_i)$$ (eq. 2)

C_i, Suspended sediment concentration, species i
$u_{s,i}$, Suspended sediment velocity, species i
ε, Diffusivity

Bedload Transport: The bedload transport rate is computed separately for each sediment species. The dimensionless transport rate, $\Phi_{B,i}$, can be defined by choosing between three available bedload transport functions: Meyer-Peter Müller (1948), Nielsen (1992) and Van Rijn (1984), though additional bedload functions can be added by customizing the source code.

$$q_{b,i} = \Phi_{B,i} \sqrt{\|g\| \left(\frac{\rho_{s,i} - \rho_f}{\rho_f} \right) d_i^3}$$ (eq. 3)

$q_{b,i}$, Volumetric bedload transport rate per unit width, species i
$\Phi_{B,i}$, Dimensionless bedload transport rate, species i
$\rho_{s,i}$, Density of sediment, species i
ρ_f, Density of fluid
g, Gravitational acceleration
d_i, Grain size, species i

To compute the motion of bedload transport in each computational cell, we calculate a bedload layer thickness (eq.4; Van Rijn, 1984) and convert the volumetric bedload transport rate, $q_{b,i}$, into a bedload velocity (eq. 5):

$$\frac{\delta_i}{d_i} = 0.3 d_*^{0.7} \left(\frac{\tau_{*,i}}{\tau_{*c,i}} - 1 \right)^{0.5}$$ (eq. 4)

δ_i, Bedload layer thickness
d_i, Grain size, species i
$d_{*,i}$, Dimensionless grain size, species i
$\tau_{*,i}$, Dimensionless shear stress, species i
$\tau_{*c,i}$, Critical dimensionless shear stress, species i

$$u_{bedload,i} = \frac{q_{b,i}}{\delta_i \, c_{b,i} \, f_b}$$ (eq. 5)

$u_{bedload,i}$, Bedload velocity, species, i
$c_{b,i}$, Volume fraction of species, i
f_b, Critical packing fraction

Entrainment and Deposition: Entrainment and deposition are treated as two opposing micro-processes that take place at the same time. They are combined to determine the net rate of exchange between packed and suspended sediments. For entrainment, the velocity at which the grains leave the packed bed is the lifting velocity and is defined in the numerical model based on Mastbergen and Van Den Berg (2003):

$$E = \alpha_i \boldsymbol{n}_b d_{*,i}^{0.3} \left(\tau_{*,i} - \tau_{*c,i}\right)^{1.5} \sqrt{g d_i (s_i - 1)} \qquad \text{(eq. 6)}$$

E, Entrainment rate
α_i, Entrainment rate coefficient, species i (default value is 0.018),
$\boldsymbol{n}_b$, Surface normal vector
$d_{*,i}$, Dimensionless grain size, species i
d_i, Grain size, species i
s_i, Specific gravity, species i
$\tau_{*,i}$, Dimensionless shear stress, species i
$\tau_{*c,i}$, Critical dimensionless shear stress, species i

The deposition or packing rate is defined as the product of the effective settling velocity and near bed suspended sediment concentration. This is the rate at which sediment moves from suspension to the packed bed at the solid boundary:

$$D = \omega_i \, c_i \qquad \text{(eq.7)}$$

D, Downward sediment deposition flux
ω_i, Settling velocity, species, i
c_i, Near bed suspended sediment concentration, species i

The vertical settling rate is defined from Soulsby (1997), where the settling motion is assumed to be in the direction of gravity:

$$\omega_i = \frac{\nu_f}{d_i}\left[\left(10.36^2 + 1.049 d_{*,i}^{0.5}\right) - 10.36\right] \qquad \text{(eq. 8)}$$

ω_i, Settling velocity, species i
ν_f, Kinematic viscosity of fluid
d_i, Grain size, species i
$d_{*,i}$, Dimensionless grain size, species i

The settling equation accounts for the relative motion of sediment in the fluid. The total vertical velocity of the suspended sediment will be the sum of the settling velocity and the vertical component of the mean fluid-sediment mixture velocity. The settling velocity can be further modified using the Richardson-Zaki correlation to account for concentration effects (Richardson, 1954). Note that additional settling and entrainment equations can be defined through source code customization.

Shear Stress Calculation: Both the bedload transport and entrainment rates are driven by the selected turbulence model. Near-wall boundary conditions are defined for 2-equation turbulence models using the logarithmic law (eq. 9), which provides the shear velocity (and consequently the shear stress) without requiring cells small enough to fully capture the velocity profile in the laminar sub-layer:

$$\frac{u}{u^*} = \frac{1}{\kappa} ln\left(\frac{y}{c_s d_{50}}\right) + 8.5 \qquad \text{(eq. 9)}$$

u, Near bed fluid velocity
u^*, Shear velocity
y, distance from wall
c_s, Roughness multiplier
κ, Von Karmen constant = 0.41
d_{50}, Median particle diameter

For hydraulically rough surfaces the form of the wall function is modified to include a variable for the roughness height that defines the Nikuradse sand grain equivilant roughness. The roughness height accounts for additonal turbulence at hydraulically rough surfaces and is calculated in the numerical model as $c_s d_{50}$. The d_{50} is calculated from the current composition of the sediment species in the packed bed, and c_s is a multipler to define the roughness height as a function of the d_{50}. The computed bed shear stress is converted to the dimensionless shear stress value that is used in both the bedload and entrainment equations.

The incipient motion conditions are defined using a critical dimensionless shear stress value (τ_{*c}) for each sediment species. Additionally, the τ_{*c} value can be modified to account for slope effects (eq. 10; Soulsby, 1997). This modification increases the τ_{*c} value for fluid moving upslope and decreases τ_{*c} for sediment movement in the downslope direction:

$$\frac{\tau'_{*c,i}}{\tau_{*c,i}} = \frac{cos\psi sin\beta + \sqrt{cos^2\beta tan^2\phi_i - sin^2\psi sin^2\beta}}{tan\phi_i} \qquad \text{(eq. 10)}$$

$\tau'_{*c,i}$, Critical dimensionless shear stress with slope adjustment, species i
$\tau_{*c,i}$, Critical dimensionless shear stress, species i
ψ, Angle between flow and slope
β, Angle of packed bed
ϕ_i, Angle of repose, species i

Methods

Experimental Data

Experimental data from the physical model reported in Khosranejad (2012) was used to validate the numerical model for predictions of equilibrium scour depth and deposition patterns for cylindrical and diamond shaped piers. The experimental flume has a 10 m length; 1.21 m width; and 0.45 m depth. The flume contained a 20 cm depth of uniformly graded, non-cohesive sand with a d_{50} = 0.85 mm. For a 16.51 cm diameter cylindrical pier, the experimental setup included an inflow average velocity of 0.25 m/s and a uniform flow depth of 18.6 cm. The diamond pier had a width of 23.35 cm; average inflow velocity of 0.21 m/s; and a uniform flow depth of 15.7 cm. For both cases, physical model results were reported as the maximum scour depth and deposition height; the maximum scour depth over time; and a contour plot of the final equilibrium bed elevation. Results from Khosranejad (2012) will be referenced below as the "physical model".

Numerical Model Setup

Both pier configurations were set up in the numerical model to replicate the conditions described for the physical model. Simulations were first performed by completing steady-state solutions for the hydraulics only, which were used as the initial condition for the sediment transport simulations. The sediment model was activated with a single sediment species with a diameter of 0.85 mm and density of 2650 kg/m³. The computational mesh was defined using a uniform cell size of 1.25 cm, and the extents of the domain were reduced to 2 m upstream and downstream of the pier, thus affording a finer resolution in the area of interest. The upstream boundary was defined by transferring the velocity profile from the steady state solution, and the downstream boundary was defined with a fixed sub-critical water surface elevation. Other important model setup inputs include the selection of the RNG turbulence model; 2nd order momentum advection; the Nielsen (1992) bedload transport equation; $\tau_{*c} = 0.03$; and a surface roughness of $6*d_{50}$. Simulations were run until achieving an equilibrium scour depth, and results were then compared against physical model measurements. All simulations were completed using FLOW-3D/MP on a single compute node with two Intel Skylake processors. The approximate run time on 40 cores for 4000 seconds of simulation time was 24 hours.

One of the major challenges of 3D sediment modeling is the need to define empirical relationships to quantify the sediment transport processes – bedload, entrainment, and settling. The selection of the appropriate transport coefficients can be difficult and may introduce a high degree of uncertainty into the analysis. The predicted changes in bed elevations will be a function of a complex set of interactions between the hydraulic solution and the transport processes that occur simultaneously at each simulation timestep. In these cases, parameter sensitivity testing can be used to evaluate the range of influence for how possible inputs affect the solution. In this study, sensitivity testing was performed for cell size, the bedload transport equation, τ_{*c} and the surface roughness height to determine the extent of their effect on simulation results.

Results and Discussion

Results for the diamond pier case are shown in Figures 2 and 3. The results from the numerical model are in excellent agreement with the physical model. The predicted maximum scour depth of 8.5 cm is within 3% of the measured value of 8.3 cm. Further, we see good overall agreement with the deposition pattern downstream of the pier, and the predicted maximum deposition height of 6.0 cm is within 9% of the measured value of 5.5 cm. The general shape and pattern of the deposition is consistent with those found in the physical model; however, the location of the maximum deposition is shifted slightly downstream relative to the observed data. We also observe excellent comparison in the predicted maximum scour depth over time as illustrated in Figure 3. Note that a slight discontinuity in the contour lines can be observed in plots presented in this section. This discontinuity is a rendering artifact and does not reflect the actual predicted scour patterns at these locations.
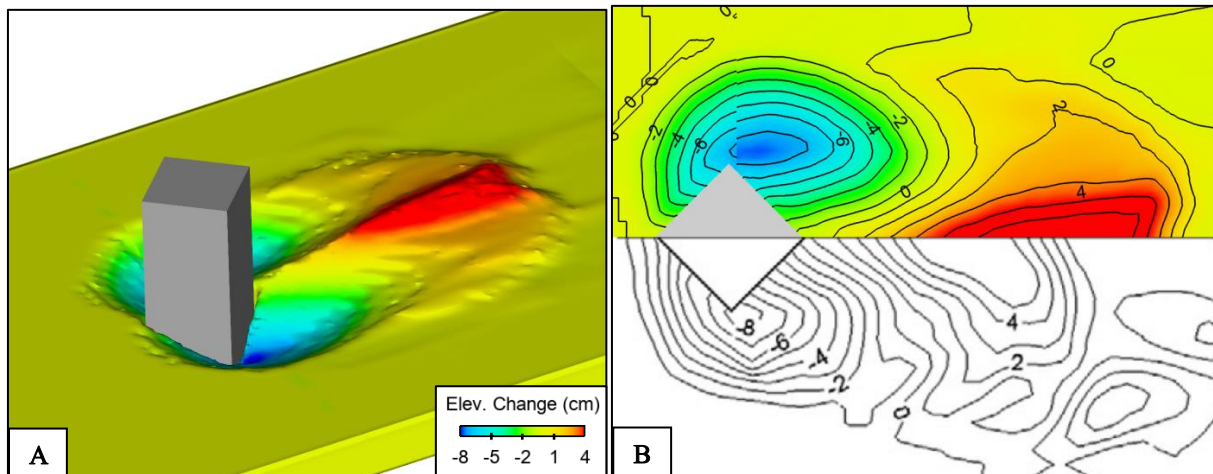
Figure 2. Equilibrium bed elevation changes predicted by the numerical model for the diamond pier. (A) Isometric view of scour and deposition adjacent to the pier. (B) Comparison between numerical results (top) vs physical model measurements (bottom).

Figure 3. Comparison of numerical model results of maximum scour depth and deposition height with physical model measurements (circles) for the diamond pier case.

Results for the cylindrical pier case are shown in Figures 4 and 5, and these also show excellent agreement between the numerical and physical model. The overall deposition and scour patterns compare favorably with those observed by the physical model, but the overall size and shape of the scour region is slightly larger in the numerical model. The predicted average depth of the scour hole is approximately 7.5 cm deep, is observed near a 60 degree angle from the front of the pier, and is within 12% of the maximum measured scour depth of 6.7 cm. The predicted maximum deposition height of 2.9 cm is within 30% of the physical model measurement of 4.1 cm. Additionally, we can observe the location of the deposition in the numerical model is shifted downstream in relation to the measured data.

Note that the scour at the nose of the pier is underpredicted when compared against measured data. This is consistent with other 3D numerical simulations of scour at blunt shaped piers, and it has been proposed that that this is caused by the inability of RANS turbulence models to fully resolve the complex HSVS (Khosranejad, 2012). This effect is less pronounced for the diamond shaped pier where the sharp leading edge on the upstream side of the pier is likely inhibiting the formation of the HSVS.
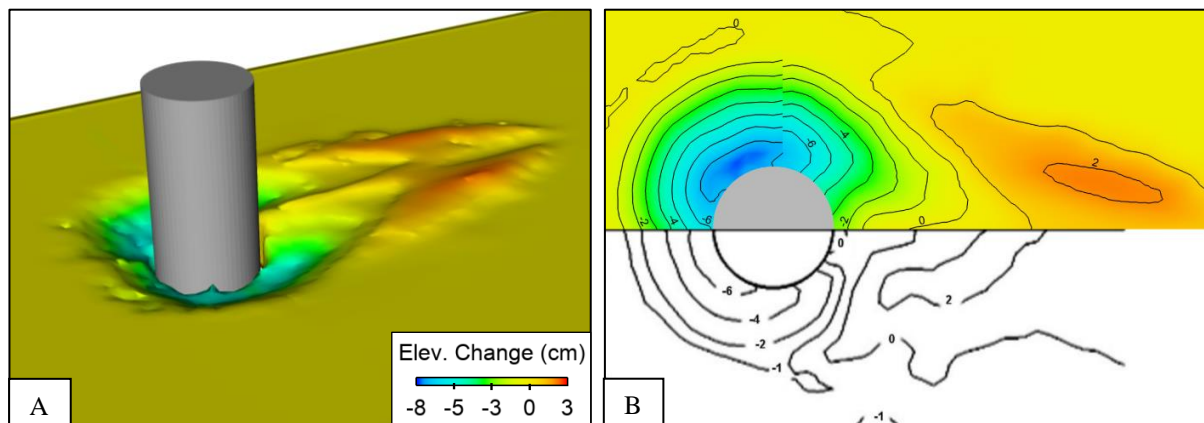
Figure 4. Equilibrium bed elevation changes predicted by the numerical model for the cylindrical pier. (A) Isometric view of scour and deposition adjacent to the pier. (B) Comparison between numerical results (top) vs physical model measurements (bottom).
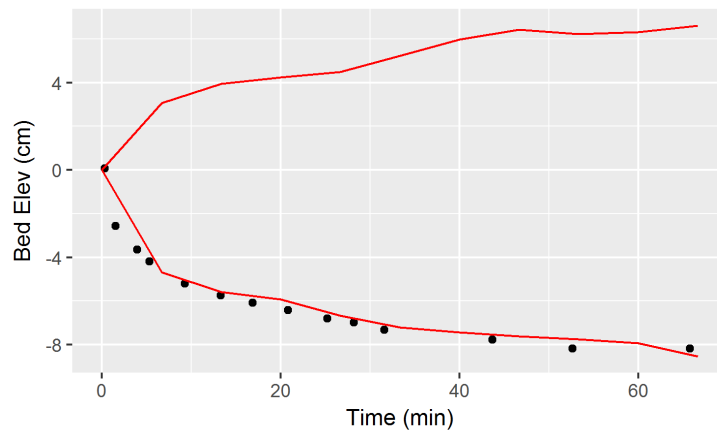

Figure 5. Comparison of numerical model results of maximum scour depth and deposition height with physical model measurements (circles) for the cylindrical pier case.

Sensitivity Testing

The parameter sensitivity tests evaluated the effects of mesh cell size, bedload equation, τ_{*c} , and roughness height on predicted scour and deposition for the diamond shaped pier. The mesh sensitivity tests evaluate the results of three different cell sizes on simulation results (Figures 6 and 7). These results indicate that the general scour and deposition patterns are consistent for all cell sizes. However, we can clearly observe a dependency of scour and deposition magnitude on mesh size. Compared with the results for the smallest cell size (1.25 cm), increasing the cell size to 1.75 cm and 2.5 cm decreased the predicted scour magnitudes by 25% and 30%, respectively. We can also observe a reduction in deposition height for the larger mesh sizes. Since shear stress is the primary mechanism for bed erosion, accurately predicting it in the numerical model is of primary importance. Any model setup input affecting shear stress can directly affect scour rates at the packed bed. The size of the mesh cells can directly affect the resolution of the spatially varying flow features and thus the calculated shear stresses near the base of the pier. This is especially important considering the complexity of the flow and turbulent boundary layers near the pier. Additionally, smoothing of the packed bed elevation may result from the surface reconstruction occurring at each timestep.

Figure 6. (Above) Mesh size sensitivity results comparing numerical model results of maximum scour depth and deposition height with physical model measurements (circles).

Figure 7. (Left). Equilibrium scour and deposition predicted with different mesh cell sizes. All mesh elements are defined with uniform aspect ratios and dimensions. (A) 1.25 cm (initial settings); (C) 1.75 cm; (D) 2.5 cm.

Results for the bedload equation sensitivity tests are illustrated in Figures 8 and 9. Simulations were completed using the Van Rijn and Meyer-Peter Müller bedload equations and compared against results for the Nielsen equation. These results show the Nielsen and Meyer-Peter Müller equations generally produce a consistent pattern and shape for both scour and deposition, though the Meyer-Peter Müller equation predicts scour magnitudes that are 14% less than Nielsen. The Van Rijn bedload equation resulted in maximum scour predictions 30% less those

predicted by Nielsen. The results of bedload sensitivity are interesting in that the Nielsen equation is predominantly used in coastal applications for uniform gravel and sands (Garcia, 2008), but provided the closest match with measured data in the current test case. The form of the Nielsen equation is very similar to Meyer-Peter Müller, therefore it is reasonable to expect similarity between the two results, as was observed in the general patterns of scour and deposition. Additionally, given the Van Rijn equation was derived for fine particles (0.2 - 2.0 mm), it was somewhat surprising that it performed the worst of the three available bedload equations. We suspect these results may actually be indicating an underprediction of erosion due to entrainment, which is being compensated with bedload equations that result in higher transport rates. In this study, sensitivity testing on the entrainment equation parameters were not performed, but these results may indicate the need for further evaluation of the interaction between bedload transport and entrainment processes for this case.

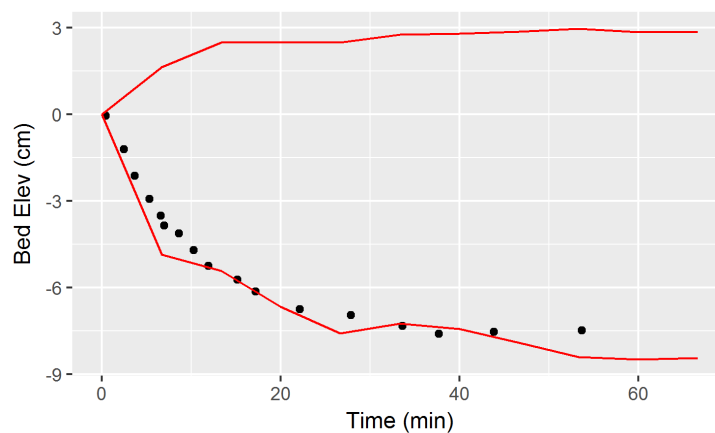**Figure 8.** (Above) Bedload equation sensitivity results comparing numerical model results of maximum scour depth and deposition height with physical model measurements (circles).

Figure 9. (Left). Equilibrium scour and deposition predicted from the numerical model for different bedload transport equations: (A) Nielsen (initial setting); (B) Meyer-Peter Mueller; (C) Van Rijn.

Results for the sensitivity tests of τ_{*c} are shown in Figures 10 and 11. We tested values of $\tau_{*c} = 0.027$ and $\tau_{*c} = 0.033$, and compared the results with the initial simulation value of $\tau_{*c} = 0.030$. Decreasing the value of τ_{*c} decreases the threshold of particle motion and results in larger computed bedload and entrainment transport rates. Increasing τ_{*c} has the opposite effect, increasing the threshold for motion and decreasing transport rates. The simulation results were consistent with this expected behavior. Setting $\tau_{*c} = 0.033$ resulted in a 14% decrease in the scour magnitude prediction. Setting $\tau_{*c} = 0.027$ resulted in only a slight increase in the predicted maximum scour depth, but we can qualitatively observe the spatial extent of the scour region has significantly increased. Regardless of the chosen τ_{*c} values, scour and deposition patterns are largely consistent between the numerical and physical models.

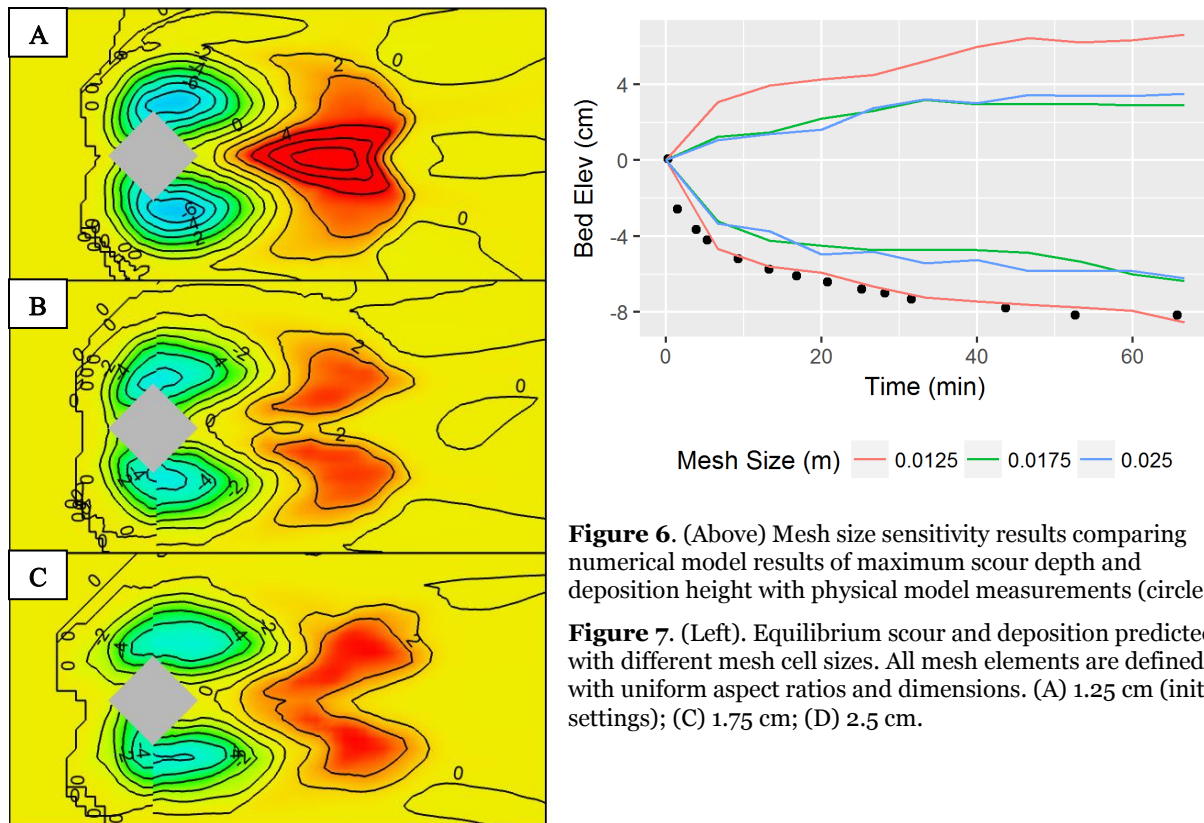**Figure 10**. (Above) Critical dimensionless shear stress sensitivity results comparing numerical model results of maximum scour depth and deposition height with physical model measurements (circles).

Figure 11. (Left). Equilibrium scour and deposition results from the numerical model for different values of critical dimensionless shear stress: (A) $\tau_{*c} = 0.027$; (B) $\tau_{*c} = 0.030$ (initial setting); (C) $\tau_{*c} = 0.033$.

Results for the sensitivity test of the roughness height are shown in Figures 12 and 13. For riverine applications, the roughness height is often calculated as a function of a representative grain size diameter, and a wide range of literature is available that proposes values for the roughness height multiplier. Garcia (2008) summarizes these studies and reports values for roughness height that range from 1 - 6.6 * d_{50}. Van Rijn (1982) also reviewed studies of roughness height and reported a range of effective roughness height between 1 - 10 * d_{90} for plane beds. These reviews indicate a considerable degree of uncertainty for defining the roughness height as a function of grain size. To understand the effect of this input, we tested roughness height values of 2.5 * d_{50} and 9 * d_{50} to compare with the initial parameter set value of 6*d_{50}. Modifying the roughness height directly affects the computed dimensionless shear stress values that drive both the bedload and entrainment functions. Increasing the roughness height will have the expected effect of increasing shear stress and scour magnitudes. Alternatively, decreasing roughness height should result in decreased scour magnitudes. From the results, we observe differences in the magnitude of both deposition and scour are consistent with the expected outcomes of increasing or decreasing bed shear stress. Increasing the value of roughness height to 9 * d_{50} resulted in a 15% increase in predicted scour depth, while decreasing the roughness height to 2.5 * d_{50} resulted in a 36% decrease in predicted scour depth.
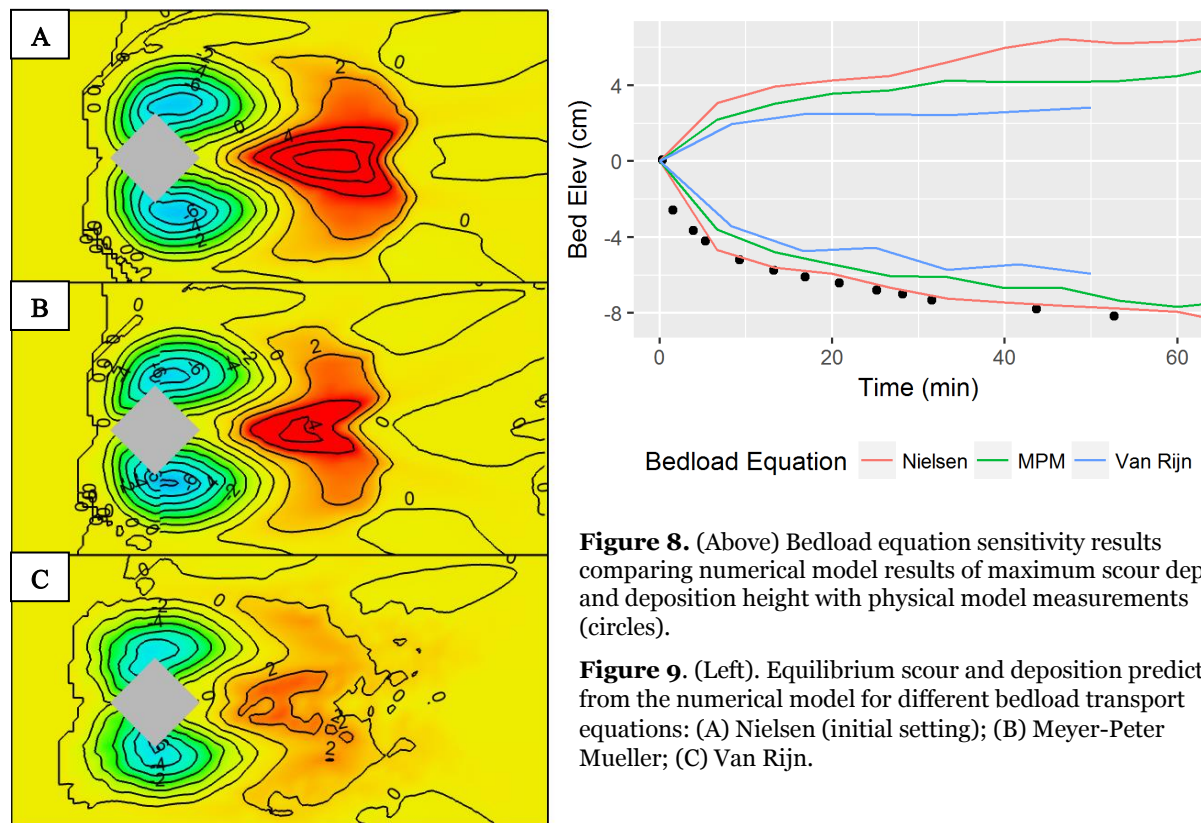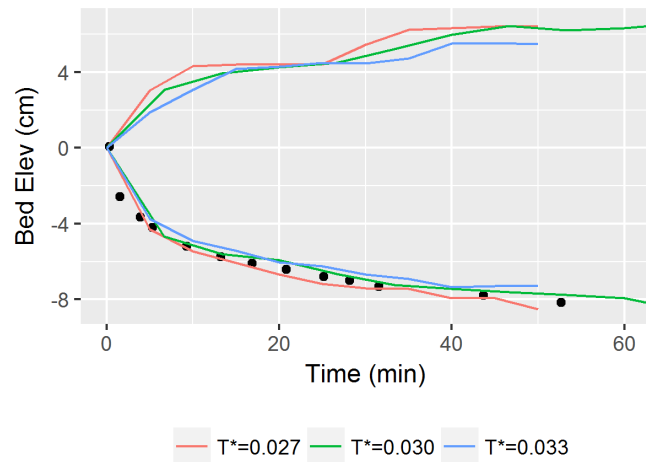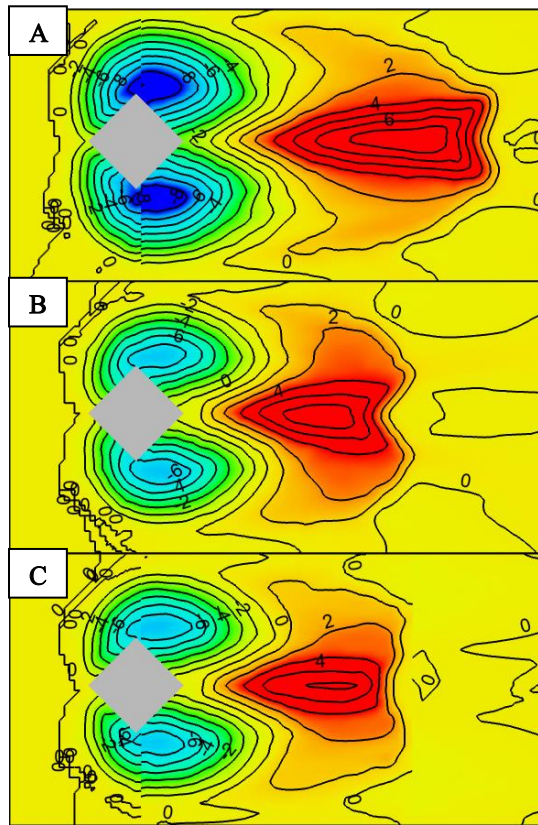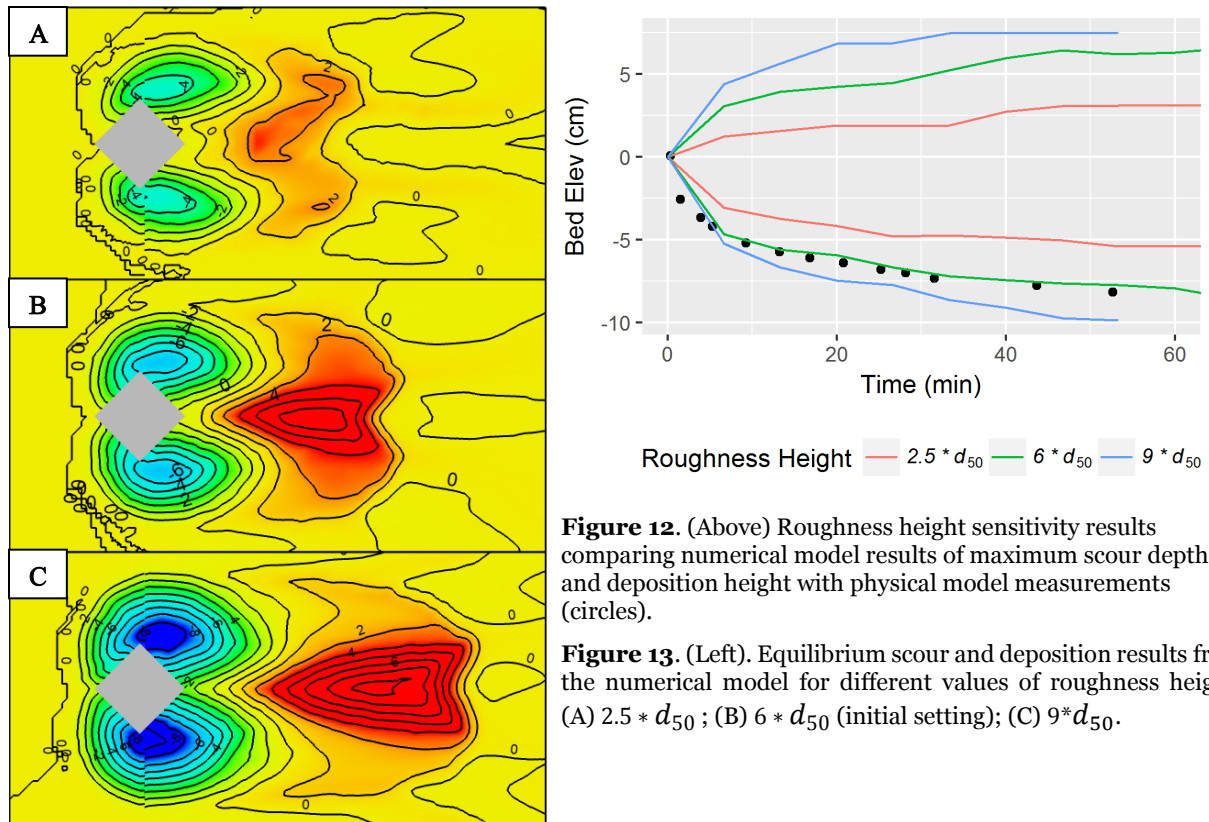
Figure 12. (Above) Roughness height sensitivity results comparing numerical model results of maximum scour depth and deposition height with physical model measurements (circles).

Figure 13. (Left). Equilibrium scour and deposition results from the numerical model for different values of roughness height: (A) $2.5 * d_{50}$; (B) $6 * d_{50}$ (initial setting); (C) $9 * d_{50}$.

Conclusions

We tested the implementation of a fully mobile bed 3D sediment transport within the commercial CFD software, FLOW-3D. The model has the capability for simulating morphological changes due to bedload transport, entrainment, settling, advection and slope failure. Numerical model results were validated against measured physical model data for cylindrical and diamond shaped piers. Simulation results show that the numerical model was in close agreement with the physical model for general scour and deposition patterns of both pier shapes. The model also showed close agreement with predictions of maximum scour depth, and compared within 3% and 12% for the diamond and cylindrical shaped piers, respectively. Predictions for the maximum deposition height showed a higher degree of variation and compared to predicted values within 9% and 30% for the diamond and cylindrical piers, respectively.

Overall, the use of 3D CFD numerical models coupled with sediment transport models shows excellent promise as a tool for evaluating complex scouring events where conventional methods may result in a high degree of uncertainty. The model shows to be a useful tool for predicting general deposition and scour patterns. However, the challenges for successful 3D sediment transport simulations should not be understated. One of the most immediate challenges is the computational expense for simulations at a practical scale. This limits the current range of applications to small spatial and temporal scales. However, with the increasing availability of HPC, improving computer processing speeds, and increases in numerical code efficiency, this limitation will continue to diminish. Computational resource limitations directly affect accuracy by limiting the possible size of mesh cells. As observed in the current study, the cell size can

affect the magnitude of scour and deposition. Reducing mesh cell size can improve the resolution of the hydraulic conditions that are driving the scour processes, and the resulting predictions of scour magnitudes. However, the reduction in cell size also come at the cost of increased simulation run times. Future developments and improvements to the numerical model are planned to improve run time efficiency and reduce mesh dependency. Regardless, mesh dependency studies are always recommended to understand the effects of cell size on the solution.

The selection of model inputs to define the sediment transport parameters also poses significant challenges. These transport equations may only be valid under a limited range of grain sizes and hydraulic conditions, and using them outside of these prescribed ranges many introduce additional uncertainty into the analysis. Additionally, these inputs may have a complex set of interactions that can be difficult to evaluate. Sensitivity testing allows modelers to identify critical input parameters, evaluate interacting variables, and validate known influences. Sensitivity testing was performed in the current study and found variation of scour depths up to 36% for the range of variables tested. It is also important to mention that any conclusions drawn from the current study are limited to the range of inputs and boundary conditions that were tested. Extrapolating these results to other applications or ranges of hydraulic conditions should be treated with caution. Moving forward, we plan to continue further validation and sensitivity testing of the numerical model for a range of other common sediment transport applications.

References

Arneson, L. A., Zevenbergen, L. W., Lagasse, P. F., & Clopper, P. E. 2012. "Evaluating scour at bridges".

Barkhudarov, M. R. 2004. "Lagrangian VOF Advection method for FLOW-3D". *Flow Science Inc*, *1*(10).

Burnham, J. 2011, "Modeling Dams with Computational Fluid Dynamics-Past Success and New Directions", Dam Safety 2011, National Harbor, MD.

Brethour J., 2003, "Modeling Sediment Scour", Technical note FSI-03-TN-62, Flow Science.

Brethour, J. and Burnham, J., 2010, "Modeling Sediment Erosion and Deposition with the *FLOW-3D* Sedimentation & Scour Model", Technical note FSI-09-TN-85, Flow Science.

Flow Science. 2018. *FLOW-3D®* Version 11.2 Users Manual. Santa Fe, NM: Flow Science, Inc. https://www.flow3d.com

Flow Science. 2019. *FLOW-3D®* Version 12.0 Users Manual. Santa Fe, NM: Flow Science, Inc. https://www.flow3d.com

Garcia, M. H. 2008. Sediment Transport and Morphodynamics. *Sedimentation engineering: processes, measurements, modeling, and practice*, 683-761.

Hirt, C. W., & Nichols, B. D. 1981. "Volume of fluid (VOF) method for the dynamics of free boundaries. *Journal of computational physics*", *39*(1), 201-225.

Hirt, C.W. and Sicilian, J.M., 1985, September. "A porosity technique for the definition of obstacles in rectangular cell meshes". *International Conference on Numerical Ship Hydrodynamics, 4th*.

Julien, P. Y. 2010. Erosion and sedimentation. Cambridge University Press.

Khosronejad, A., Kang, S., & Sotiropoulos, F. 2012. "Experimental and computational investigation of local scour around bridge piers". *Advances in Water Resources*, *37*, 73-85.

Mastbergen, D. R., & Van Den Berg, J. H. 2003. "Breaching in fine sands and the generation of sustained turbidity currents in submarine canyons". *Sedimentology*, *50*(4), 625-637.

Meyer-Peter, E. and Müller, R., 1948, "Formulas for bed-load transport". Proceedings of the 2nd Meeting of the International Association for Hydraulic Structures Research. pp. 39–64.

Nielsen, P. 1992. "*Coastal bottom boundary layers and sediment transport* (Vol. 4)". World scientific.

Olsen, N.R.B. and Melaan, M.C. 1993. "Three dimensional calculation of scour around cylinders". J. Hyd. Eng., ASCE, 119(9),1048-1054.

Omara, H., Elsayed, S. M., Abdeelaal, G. M., Abd-Elhamid, H. F., & Tawfik, A. 2018. "Hydromorphological Numerical Model of the Local Scour Process Around Bridge Piers". *Arabian Journal for Science and Engineering*, 1-17.

Richardson, J. E., & Panchang, V. G. 1998. "Three-dimensional simulation of scour-inducing flow at bridge piers". *Journal of Hydraulic Engineering*, *124*(5), 530-540.

Richardson, J.R. & Richardson E.V. 2008. Bridge Scour Evaluation. *Sedimentation engineering: processes, measurements, modeling, and practice*, 683-761.

Richardson, J. T. 1954. "Sedimentation and fluidisation: Part I". *Transactions of the Institution of Chemical Engineers*, *32*, 35-53.

Soulsby, R., 1997, Dynamics of Marine Sands, Thomas Telford Publications, London.

Soulsby, R. L. and Whitehouse, R. J. S. W., 1997. "Threshold of sediment motion in Coastal Environments". Proc. Combined Australian Coastal Engineering and Port Conference, EA, pp. 149-154.

Spasojevic, M., & Holly, F. M. (2008). Two-and three-dimensional numerical simulation of mobile-bed hydrodynamics and sedimentation. *Sedimentation engineering: processes, measurements, modeling, and practice*, 683-761.

Van Rijn, L. C. 1982. "Equivalent roughness of alluvial bed". *Journal of the Hydraulics Division*, *108*(10), 1215-1218.

Van Rijn, L. C., 1984, "Sediment Transport, Part I: Bed load transport", Journal of Hydraulic Engineering 110(10), pp 1431-1456.

Wei, G., Brethour, J., Grünzner, M., & Burnham, J. 2014. "Sedimentation scour model". *Flow Science Report*, *7*, 1-29.

Zhang, Q., Zhou, X. L., & Wang, J. H. 2017. "Numerical investigation of local scour around three adjacent piles with different arrangements under current". *Ocean Engineering*, *142*, 625-638.

Design and Analysis of Ecosystem Features in Urban Flood Control Channels

Nathan Holste, Hydraulic Engineer, Bureau of Reclamation, Denver, CO,
nholste@usbr.gov

Jennifer Bountry, Hydraulic Engineer, Bureau of Reclamation, Denver, CO,
jbountry@usbr.gov

Extended Abstract

Rivers and streams have been severely impacted by anthropogenic development and urbanization. Degraded ecological conditions have resulted from alterations to watershed hydrology and sediment yield, along with imposed constraints that limit natural channel adjustment and floodplain access. In some urban corridors, such as the Los Angeles (LA) River, streams have been completely channelized and lined with concrete to efficiently convey floods and minimize erosion (Figure 1). These original goals have largely been accomplished but have resulted in limited ecosystem services. Flow depths are uniform across the channel and velocities are increased with no refugia for aquatic species. Rivers that have been converted to urban flood control channels have also suffered from a disconnect between communities and their waterways, which has economic and social consequences. Revitalization can be accomplished by considering channel functions over a range of low to high flows, thereby transforming a single purpose (flood conveyance) waterway to a multi-purpose (flood control, habitat, aesthetics, and recreation) feature of the urban landscape.

Figure 1. Los Angeles River looking downstream from 1st Street, annotated with approximate dimensions and base flow rate

This conceptual design study addresses the question: How can ecosystem features be designed within urban flood control channels to increase habitat values without significantly raising flood stage? A two-mile reach of the LA River near downtown Los Angeles, from 1st Street to Washington Blvd, was selected as the pilot site. The LA River provides an excellent pilot site for the study because of the extreme urbanization of the watershed and channel, and the interest

and momentum that is being generated towards improving the ecosystem and aesthetic qualities of the river (e.g., City of Los Angles 2007, U.S. Army Corps of Engineers 2015, lariver.org).

A series of large floods in the early 1900s caused loss of life and extensive property damage, leading to construction of a concrete-lined channelized river in 1938. The channel was designed to contain a discharge of 104,000 cfs, plus freeboard, which is similar to the 100-year flow of 109,000 cfs from later hydrologic analysis (U.S. Army Corps of Engineers 2015). The design discharge is orders of magnitude larger than the current base flow (~100 cfs) throughout most of the year. About 80% of dry weather base flow is contributed from effluent discharge of three water reclamation plants (The Nature Conservancy 2016). Recycled water has been identified as an important resource that can be used to improve urban streams by providing reliable flow augmentation (Bischel et al. 2013). Although these effluent discharges have high treatment standards, there are water quality concerns because summer temperatures in the LA River may be too warm for native fish, which include steelhead, arroyo chub, and Santa Ana sucker (Mongolo et al. 2017). However, warm summer temperatures should not preclude restoration efforts because the mainstem LA River historically served as an important migration corridor during winter months.

The purpose of the 1938 design was to create a non-erodible channel that would quickly convey flood events from the watershed to the ocean. Therefore, it is not surprising that the low to medium flows that occur during more than 95% of the year provide no habitat for aquatic species. These flows are either confined to a small notch or spread out at shallow depths across the concrete bed. Owing to the smooth concrete boundary and relatively steep channel slope (0.45%), flows in the LA River are generally supercritical. Even low flows have a velocity of 5 to 6 ft/s, which is above the cruising speed of steelhead trout (Caltrans 2007). The depth and velocity of the LA River serve as a hydraulic fish passage barrier, regardless of the presence of other physical obstructions. Therefore, the general objectives for LA River channel designs are to: reduce velocity, provide sufficient depth at low flows, provide refugia for native fish, and not significantly increase flood stage. Increasing the channel and floodplain width would help meet these objectives but are cost prohibitive and not feasible to implement due to adjacent railways and extensive infrastructure, so the scope of the current study is confined to the existing channel footprint.

This study primarily considers how to rework the channel bed and banks, or add features such as flow deflectors and pools-riffles, to provide increased flow complexity and habitat heterogeneity. As resources devoted to urban restoration, and the LA River in particular, increase, it is important to have performance data on various ecosystem features. Design concepts are tested and evaluated with a two-dimensional (2D) numerical model and a physical model. Habitat suitability and effect on flood stage are assessed for each of the proposed ecological enhancement methods. The study is ongoing, but the design concepts developed so far include the following: (Geometry 1) existing channel, (Geometry 2) existing channel with increased roughness in low-flow notch, (Geometry 3) increased width, depth, and roughness for low-flow channel, (Geometry 4) meandering low-flow channel with increased width, depth, and roughness, (Geometry 5) variable width low-flow channel with increased width, depth, and roughness, (Geometry 6) pool-riffle low-flow channel with increased width, depth, and roughness, (Geometry 7) meandering, variable width, pool-riffle low-flow channel with increased width, depth, and roughness. Figure 2 illustrates the design for Geometry 7. Each

successive design adjusts one component at a time to better compare and isolate effects of the unique features. Additional designs continue to be developed and analyzed.
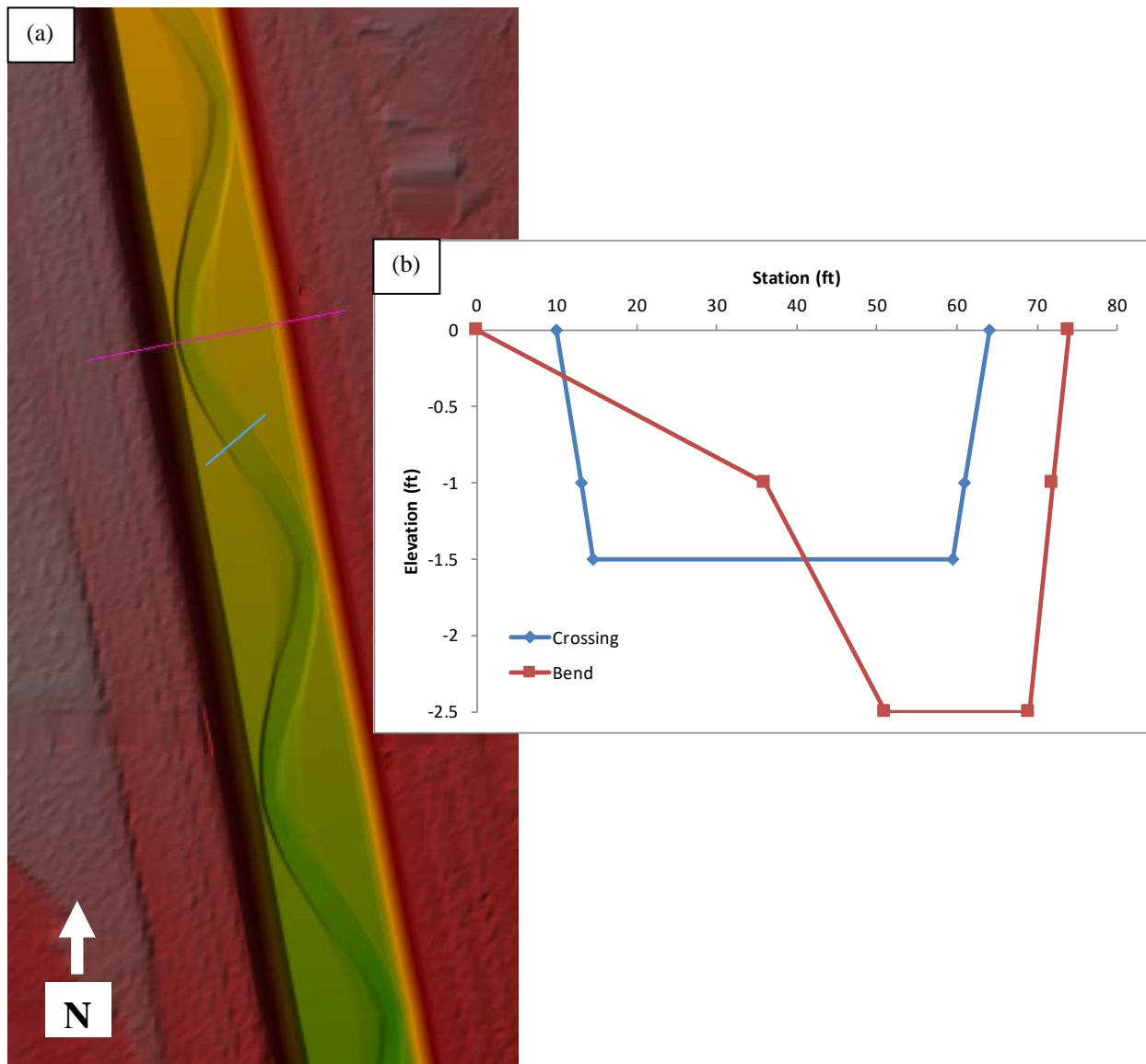
Figure 2. Conceptual design geometry for a meandering low-flow channel with pools and riffles: (a) plan view of channel layout (b) cross section view at channel bend (looking downstream from plan view pink line location) and crossing (blue line) showing depth below existing concrete bed. Low-flow channel dimensions were designed to contain about 300 cfs. For reference, the straight and uniform existing low-flow channel has a top width of 20 ft and a depth of about 0.5 ft, which contains about 75 cfs.

A habitat suitability index (HSI) for depth and velocity was applied to hydraulic results from the 2D model over a range of flows. Southern steelhead was selected as the indicator species with HSI values from Allen (2015). A location was classified as hydraulically suitable if the geometric mean of depth and velocity HSI was greater than 0.4. Figure 3 presents these results, where the hydraulically suitable area is normalized by wetted area to calculate percent suitable habitat. Simply adding roughness to the existing low-flow notch (Geometry 2) provides some limited

benefit. Increasing width and depth of the low-flow channel, with added roughness, substantially increases the hydraulic suitability (Geometry 3 – Geometry 7). There is not much difference between the HSI scores for these five alternatives that modify the low-flow channel dimensions. HSI is a generalized analysis method that does not necessarily reflect nuances between designs. For example, closer inspection of velocity maps reveals lower velocity zones over the point bars of Geometry 7, and increased variability compared to Geometry 3.
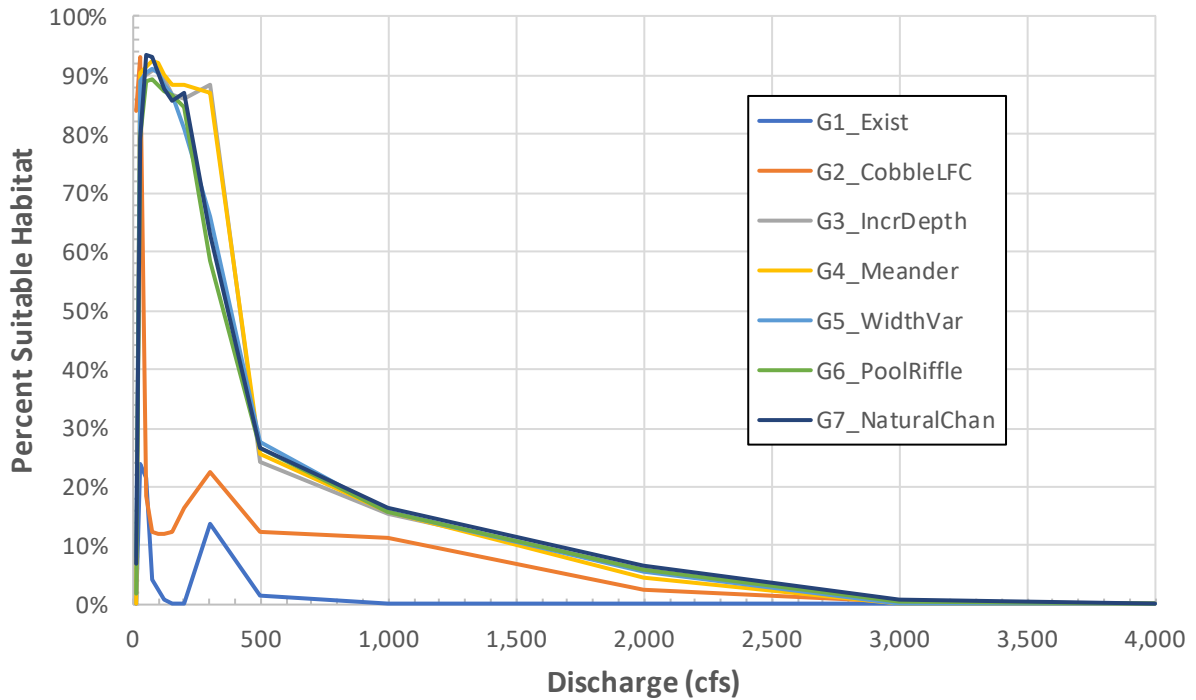
Figure 3. Habitat suitability results for various low-flow channel design configurations

Further design concepts will work with an interdisciplinary team including local biologists to explore the benefits of adding features such as flow deflectors and boulder clusters. These would provide additional low velocity areas when habitat decreases at flows above 1,000 cfs. Other concepts will investigate a multi-thread or anastomosing low-flow channel rather than a single thread channel. For additional evaluation methods, fish passage criteria will be applied to spatially map velocity "patches" that indicate where fish may be able to swim for a limited time at higher flows. These areas may be usable during migration even if the HSI score is low. Hydraulic suitability results for initial design concepts show that, despite constraints and limitations, there is value in designing a low-flow channel and other ecosystem features within confined urban channels. Aquatic species habitat, particularly at low flows, is improved by creating areas of reduced velocity and adding diversity and complexity to the flow field. Results from this study will provide design and analysis tools for transforming urban flood control channels to multi-function streams with increased ecological and aesthetic values.

References

Allen, M.A. 2015. Steelhead Population and Habitat Assessment in the Ventura River/Matilija Creek Basin 2006-2012. Normandeau Associates, Inc. Arcata, CA.

Bischel, H.N., Lawrence, J.E., Halaburka, B.J., Plumlee, M.H., Bawazir, A.S., King, J.P., McCray, J.E., Resh, V.H., and Luthy, R.G. 2012. "Renewing Urban Streams with Recycled Water for Streamflow Augmentation: Hydrologic, Water Quality, and Ecosystem Services Management," Environmental Engineering Science, 30(8):455–479.

Caltrans. 2007. Fish Passage Design for Road Crossings.

City of Los Angeles. 2007. Los Angeles River Revitalization Master Plan.

Mongolo, J., Trusso, N., Dagit, R., Aguilar, A., and Drill, S. 2017. "A longitudinal temperature profile of the Los Angeles River from June through October 2016," Bulletin of the Southern California Academy of Sciences, 116(3):174–192.

The Nature Conservancy. 2016. Water Supply and Habitat Resiliency for a Future Los Angeles River: Site-Specific Natural Enhancement Opportunities Informed by River Flow and Watershed-Wide Action, Los Feliz to Taylor Yard.

U.S. Army Corps of Engineers. 2015. Los Angeles River Ecosystem Restoration Integrated Feasibility Report.

Effects of Dike Fields on Channel Characteristics of the Lower Mississippi River

Andrew Simon, Senior Principal, Cardno, Oxford, MS, andrew.simon@cardno.com

Kimberly Artita, Senior Civil Engineer, Sci-Tek Consultants, Inc., Clemson, SC, kartita@scitekanswers.com

Jennifer Hammond, Senior Engineer, Cardno, Fayston, VT, jennifer.hammond@cardno.com

David S. Biedenharn, U. S. Army Engineer Research and Development Center Coastal and Hydraulics Laboratory, Vicksburg, MS, David.S.Biedenharn@erdc.dren.mil

Charles D. Little Jr., Mendrop Engineering, Vicksburg, MS, clittle@mendrop.net

Abstract

Dike fields were initially constructed along the Lower Mississippi River (LMR: Cairo, IL to below Natchez, MS) in the late-1950s through the early-1970s to control channel alignment and to maintain a 9-ft deep low-flow navigation channel. Dike construction and extension continue to the present day. This study combines an empirical analysis of 35 dike fields along the Lower Mississippi River (LMR) with 2D numerical-modeling experiments of a single dike system (three adjacent dike fields) to evaluate the role of dikes on channel characteristics and water-surface elevations. Using time-series surveys at 21 dike systems, as well as stage and discharge observations, this study shows that the dikes function as intended, and that is to maintain a navigable low-flow channel that exceeds the minimum 9-ft depth requirement at low flow. We find no evidence that the dike fields alone increase flood discharges and bank-full elevations, as proposed by other researchers. The marginal increases in water-surface elevations at the highest modeled flow, 1,275,000 cfs (approximating bankfull) in 1973 and 2013 indicate that the impact of the dikes themselves on water-surface elevations are minimal, if not within survey and model error. The spatial and temporal trends of channel adjustments along LMR are largely attributed to the meander-cutoff program (1929-1942), which shortened the reach by about 45%, leading to upstream incision and downstream aggradation. Other engineering activities such as levees, revetments, and dam construction have contributed to long-term, broad adjustment processes on the LMR. Adjustments to main-channel depth at +0 Low Water Reference Plane (LWRP), and total channel depths and cross-sectional areas at +35 LWRP (at or near bankfull) indicate that dikes assist with maintenance of a uniformly deep, navigable channel. On average, bankfull discharges today are about 20% greater than before the cutoff program and roughly equivalent to the post-cutoff values of the late 1950s when dike construction began. Results of 2D numerical modeling of a dike system between Vicksburg and Natchez show marginal differences in water-surface elevations with and without dikes.

Discussion of Study and Results

This paper is an abridged version of a much larger report by the same authors produced for the U.S. Army Corp's Engineer Research and Development Center (Simon et al., in press). That study provides copious details of the empirical and numerical-modeling aspects of the research to determine the role of dike fields on channel characteristics and flood stage on the Lower Mississippi River (LMR) (Figure 1).

Figure 1. General location map of the Lower Mississippi River (LMR), considered to extend below Cairo, IL.

The LMR is a dynamic alluvial river that has been subjected to a range of environmental and anthropogenic factors that have resulted in spatial and temporal adjustments to its channel characteristics. These include, but are not limited to, floods and sustained high flows, the meander-cutoff program, installation of revetments, maintenance dredging, construction of levees, and the closing of dams on the Missouri River and other major tributaries. Dikes represent still another anthropogenic factor imposed on the river. These structures were designed to increase and maintain main-channel depths by constricting or contracting flow and thereby increasing the ability of the river to entrain and transport sediment in the main-channel section of the river. The primary purpose was to maintain a navigation channel 300-ft wide by 9-ft deep, therefore, reducing the need for maintenance dredging.

This study focused on the effects of the 21 dike systems (composed of 35 individual dike fields) constructed along the LMR. Morphologic data were available from the late-1950s through the mid-2010s. Results pertain to changes over this period and only to in-channel conditions, excluding floodplain characteristics and any imposed changes there.

Empirical Analysis of the 21 Dike Systems:

As an alluvial river, the Mississippi, like any other responds to changes in the balance between the amount and character of the hydraulically-controlled sediment (sand-sized material and coarser) delivered from upstream, and the transport capacity of the flow in a given reach. Because of the myriad of imposed in-channel factors and the river's subsequent responses, it is often difficult to isolate the effects of a single factor. Such is the case with the dike fields and dike systems. Interpretation of morphologic data in these reaches was placed in the context of broader adjustments operating along the river. Winkley (1977), Biedenharn et al. (2015), and others clearly describe the far-reaching effects of the meander-cutoff program on temporal and spatial trends of aggradation and degradation in the LMR. Thus, recorded changes in the total conveyance (at the +35 Low-Water Reference Plane Elevation, approximately bankfull; LWRP) in the dike-system reaches likely reflect the broader adjustment trends described by specific-gage analysis (Biedenharn et al. 2015).

Conveyance at a fixed reference elevation such as the +35 LWRP is indicative of the ability of the river to transmit water at that water-surface elevation. Changes in conveyance with time thus reflect the influence of anthropogenic changes imposed on the LMR as well as any adjustments to those changes (e.g. responses to the cutoff program, etc.). Not surprisingly then, total conveyance was shown to decrease by about 20% from pre-dike conditions to the mid 2010's in those downstream reaches characterized by deposition and aggradation (between about RM 375 to RM 450). With distance upstream in the adjacent, reaches (RM 490 to RM 546), changes in total conveyance shift from small decreases (-4% to -7%) to small increases (+7%) in the equilibrium reach, and then show up to 10% increases further upstream in the erosional reach. From the qualitative interpretation of the longitudinal trends in total conveyance with documented changes in specific-gage elevations, the dike systems appear to have little effect on total conveyance at +35 LWRP. Today, the greatest conveyance along the LMR occurs in the transitional zone and not at the furthest point downstream.

Changes in main-channel depth and main-channel boundary shear stress, however, provide a more useful metric in determining the effect of the dike systems on channel characteristics. Measures of main-channel depth, which are primary metrics to evaluate the effectiveness of the dike fields, show significant increases at both +0 and +35 LWRP. Compared to pre-dike and base conditions at +0 LWRP, the average increase in main-channel depth for all of the studied dike systems was 32.5% and 35.3%, respectively. Results show general increases in main-channel depth even in the downstream depositional areas. This is an indication that the dike systems are having their intended effect on deepening of the main channel. There are indications of greater increases in depth in some sub-reaches of the erosional zone compared to the aggradational and transitional reaches. This suggests that the effects of the dike fields may be being enhanced by the larger-scale erosional conditions within these reaches.

Based on the most recent surveys conducted in the mid-2010s, main-channel depths at +0 LWRP range from a maximum of 40.5 ft at the Catfish dike system (RM 568) to a minimum of 21.1 ft in the Above Loosahatchie dike system (RM 742). On average, the main-channel at +0 LWRP for the surveyed dike systems was 27.6 feet, indicating that main-channel depths in the dike-system reaches have been maintained well above the minimum 9-ft value required. This result, in combination with general indications of significant increases in main-channel depth, support the premise that the dike systems have been largely effective at increasing and

maintaining main-channel depths above the 9-ft requirement that is stipulated for the navigation channel along the LMR.

Similar to changes in main-channel depths, changes in average boundary shear stress reflect the increases in depth, resulting in average increases from base conditions of about 9 and 17% for the whole channel and main channel at +35 LWRP, respectively. These changes indicate that transport capacity has increased in both the whole-channel cross section and within the main channel over the survey periods. This provides further evidence that overall, sediment-transport capacity in the main-channel sections have increased since the dike systems were constructed.

Summaries of how specific channel characteristics have changed throughout the LMR are provided for general reference. Here, we bring together data on how characteristics of the entire channel have changed relative to pre-dike (Table 1) and to base-year conditions (Table 2). Data on changes relative to pre-dike conditions are not available for several dike systems and, therefore, these cells are left blank in Table 1.

Table 1. Summary of changes in total-channel characteristics at +35 LWRP relative to pre-dike conditions.

Dike System	Location (RM)	Change in Depth	Change in Cross-Sectional Area	Change in $AD^{2/3}$	Change in Discharge	Change in Slope	Change in Conveyance	Change in Shear Stress
		(%)	(%)	(%)	(%)	(%)	(%)	(%)
Waterproof	377	-2.5	6.4	7.6	-16.0	9.6	-21.8	9.7
Bondurant	392	-6.4	1.5	-1.1	-9.4	15.8	-20.7	0.4
Marshall Cutoff / Forest Home	448							
Baleshed	490	-7.5	-13.4	-15.2	-2.2	4.4	-4.1	-15.2
Wilson Point	498	3.3	-6.7	-12.1	-4.4	2.4	-5.4	-4.6
Lower Cracraft	507	5.7	-34.7	-26.9	-6.1	1.0	-6.6	-3.3
Island 86	518	13.4	-14.9	-4.4	-2.4	3.2	-3.6	3.8
Ashbrook	546	21.3	-1.4	8.1	-10.5	-12.6	-6.5	7.5
Chicot	560	20.3	-5.2	13.0	-5.0	-22.3	6.8	29.6
Catfish	568	14.7	3.3	13.4	-5.9	-22.8	7.3	-14.4
Island 70	607	0.4	-35.6	-30.2	4.6	3.2	4.8	10.1
Island 62/63	638							
Cat Island	708	18.1	-2.5	12.8	11.2	3.5	5.8	39.8
Dismal	721							
Above Loosahatchie	742	22.6	-5.3	10.4	14.6	2.8	9.9	28.5
Randolph	747	9.7	10.7	21.2	11.4	3.0	6.9	6.9
Densford	755	8.6	1.7	12.3	7.9	1.8	7.1	12.9
Forked Deer	798	4.3	-0.6	7.7	6.2	2.7	0.2	6.3
Island 25	803	-8.0	9.2	9.0	3.9	1.6	-2.1	11.6
Wrights Point	819	1.8	-7.8	-1.3	7.7	3.3	1.9	4.5
Pritchard / Island 1	944							
Average		**7.0**	**-5.6**	**1.4**	**0.3**	**0.0**	**-1.2**	**7.9**
Standard deviation		**10.2**	**-2.5**	**14.8**	**8.8**	**10.1**	**9.3**	**14.5**

Table 2. Summary of changes in total-channel characteristics at +35 LWRP relative to base-year conditions.

Dike System	Location (RM)	Change in Depth	Change in Cross-Sectional Area	Change in AD$^{2/3}$	Change in Discharge	Change in Slope	Change in Conveyance	Change in Shear Stress
		(%)	(%)	(%)	(%)	(%)	(%)	(%)
Waterproof	377	-2.4	6.3	7.4	-15.8	9.4	-21.4	9.5
Bondurant	392	-6.3	1.4	-1.0	-9.2	15.3	-21.0	0.4
Marshall Cutoff / Forest Home	448	-14.1	-38.3	-42.3	-9.6	-6.9	-7.8	-19.5
Baleshed	490	-7.3	-12.9	-14.6	-2.1	4.2	-3.9	-14.6
Wilson Point	498	3.3	-6.6	-11.9	-4.3	2.4	-5.3	-4.5
Lower Cracraft	507	5.5	-34.1	-26.4	-6.0	1.0	-6.4	-3.2
Island 86	518	12.4	-13.5	-4.1	-2.3	2.9	-3.4	3.7
Ashbrook	546	19.5	-1.3	7.5	-9.8	-11.8	-6.1	6.9
Chicot	560	19.8	-5.1	12.7	-4.9	-22.0	6.6	28.7
Catfish	568	14.3	3.2	13.0	-5.8	-22.4	7.1	-14.1
Island 70	607	0.4	-33.7	-32.0	4.7	3.2	4.9	9.2
Island 62/63	638	24.9	-24.0	-6.4	6.4	0.4	9.4	24.9
Cat Island	708	17.3	-2.4	12.3	11.0	3.5	5.7	37.9
Dismal	721	17.2	18.6	35.0	6.3	3.4	1.8	17.2
Above Loosahatchie	742	21.3	-5.0	9.8	13.8	2.7	9.3	26.6
Randolph	747	9.1	10.0	19.9	10.8	2.8	6.6	6.5
Densford	755	8.1	1.6	11.7	7.5	1.7	6.7	12.2
Forked Deer	798	4.1	-0.5	7.4	5.9	2.6	0.2	6.0
Island 25	803	-7.7	8.6	8.8	3.7	1.6	-2.0	11.1
Wrights Point	819	1.7	-7.5	-1.3	7.3	3.1	1.8	4.3
Pritchard / Island 1	944	20.4	18.3	36.7	2.3	1.7	7.6	31.7
Average		7.7	-5.6	2.0	0.5	0.0	-0.5	8.6
Standard deviation		11.2	-2.4	19.7	8.2	8.9	8.9	15.4

The effectiveness of the dike fields and dike systems in maintaining main-channel depths and reducing the need for maintenance dredging is supported by the inverse relation between the amount of dredging and the cumulative length of constructed dikes along the LMR (Figure 2). Maintenance dredging which peaked in the late-1960s at more than 60 million yd³ in the Memphis, Vicksburg and New Orleans Districts, has decreased to about 10 million yd³ in the 2000s. This coincides with the ever-increasing length of dikes starting in the late-1950s and continuing through to the present day.

In summary, it can then be concluded that the dike systems are functioning as intended to provide for greater sediment-transport capacity, main-channel flow depths, and reduce the need for maintenance dredging. Longitudinal trends in total channel depths and cross-sectional areas at +35 LWRP (at or near bankfull) indicate that dikes assist with maintenance of a uniformly deep, navigable channel. Cases where total conveyance has decreased appears to be the result of longer-termed, broad adjustment processes related to other factors along LMR. Finally, to quantify the specific hydraulic and sediment-transport effects of the dike systems independent of the broader responses of the LMR, two-dimensional hydraulic modeling should be conducted. This deterministic approach, combined with data on bed-material composition would provide compelling evidence of the effects of the dike systems on channel characteristics of the LMR.
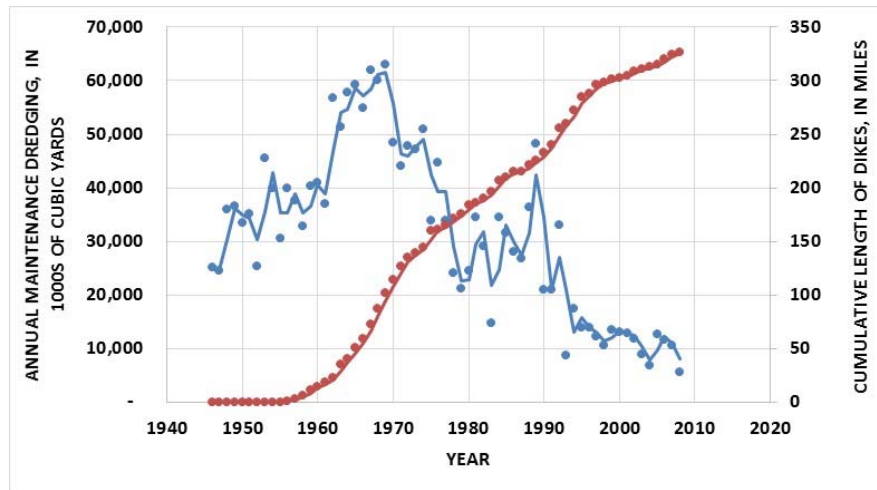
Figure 2. General inverse relation between annual maintenance dredging and the cumulative length of dike fields (in red) along the LMR. Trend lines are two-point moving averages. Data from Biedenharn, written comm. (2018).

Role of Dike Fields on Water-Surface Elevations via Two-Dimensional Numerical Modeling:

One of the central questions of this part of the work was to ascertain the direct role of dikes on water-surface elevations, particularly at the higher flows. This was critical because in much of the empirical analysis reported earlier in this report, it was very difficult to separate channel adjustments that could be attributed exclusively to the dikes due to all of the things imposed on the LMR. Here however, two-dimensional numerical experiments using AdH provided a framework for separating out these causes. The 13-mile model reach is aggradational, situated about halfway between Natchez and Vicksburg, MS (RM 393 to RM 406). Starting in the mid 1970's and continuing over a span of about 26 years, eleven dikes (three dike fields) were installed in the model reach (Figure 3). Following calibration for the *No Dike* and *With Dikes* conditions, simulations were conducted for five years where surveys were available: 1973 (Pre-Dike), 1977, 1988, 2004 and 2013.

Results show marginal increases (0.6 to 0.8 ft) in water-surface elevations between 1973 and 2013 at the highest modeled flow, 1,275,000 cfs (approximating bankfull), indicating that the impact of the dikes themselves on water-surface elevations are limited, if not within survey or model error. This conclusion can be clearly seen in viewing the difference in water-surface profiles at 1,275,000 cfs that show (Figure 4):

- Marginal differences between the 1973 *No Dike* and the 1973 *With Dikes* (hypothetical) scenarios, without and associated channel adjustment (Figure 4, Top);
- Marginal differences between the 2013 *No Dike* (hypothetical) and 2013 *With Dikes*, using channel geometry after 40 years of adjustment on the LMR (Figure 4, Middle); and

- Relatively small differences (< 1 ft) between the 1973 *No Dike* and the 2013 *With Dikes* condition, representing channel adjustments due to both the dike fields (which are shown to be marginal) and overall channel adjustment (aggradation) in this part of the LMR (Figure 4, Bottom).
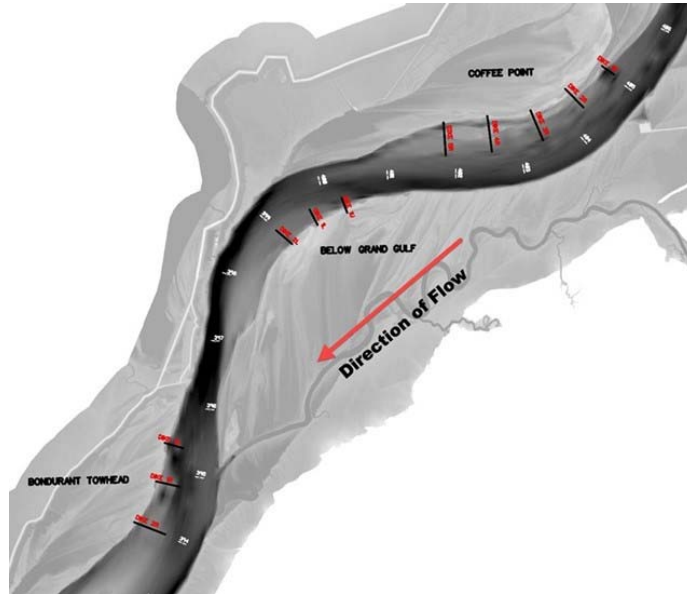
Figure 3. Overview of model reach showing the three dike fields after installation of all dikes by 2001.

The increases in peak water-surface elevations over the 40 years represented by the 2D simulations can be mostly attributed to broad, systematic channel-adjustment processes active in this section of the LMR. The impact of the dike fields at 1,275,000 cfs is quite small in comparison. The influence of the dike fields on increasing water-surface elevations does increase with decreasing discharge (and flow depth). These results are applicable to this dike system in an aggradational reach of the LMR. Additional research in a degradational reach of the river is merited to test whether these conclusions are applicable under those circumstances as well.
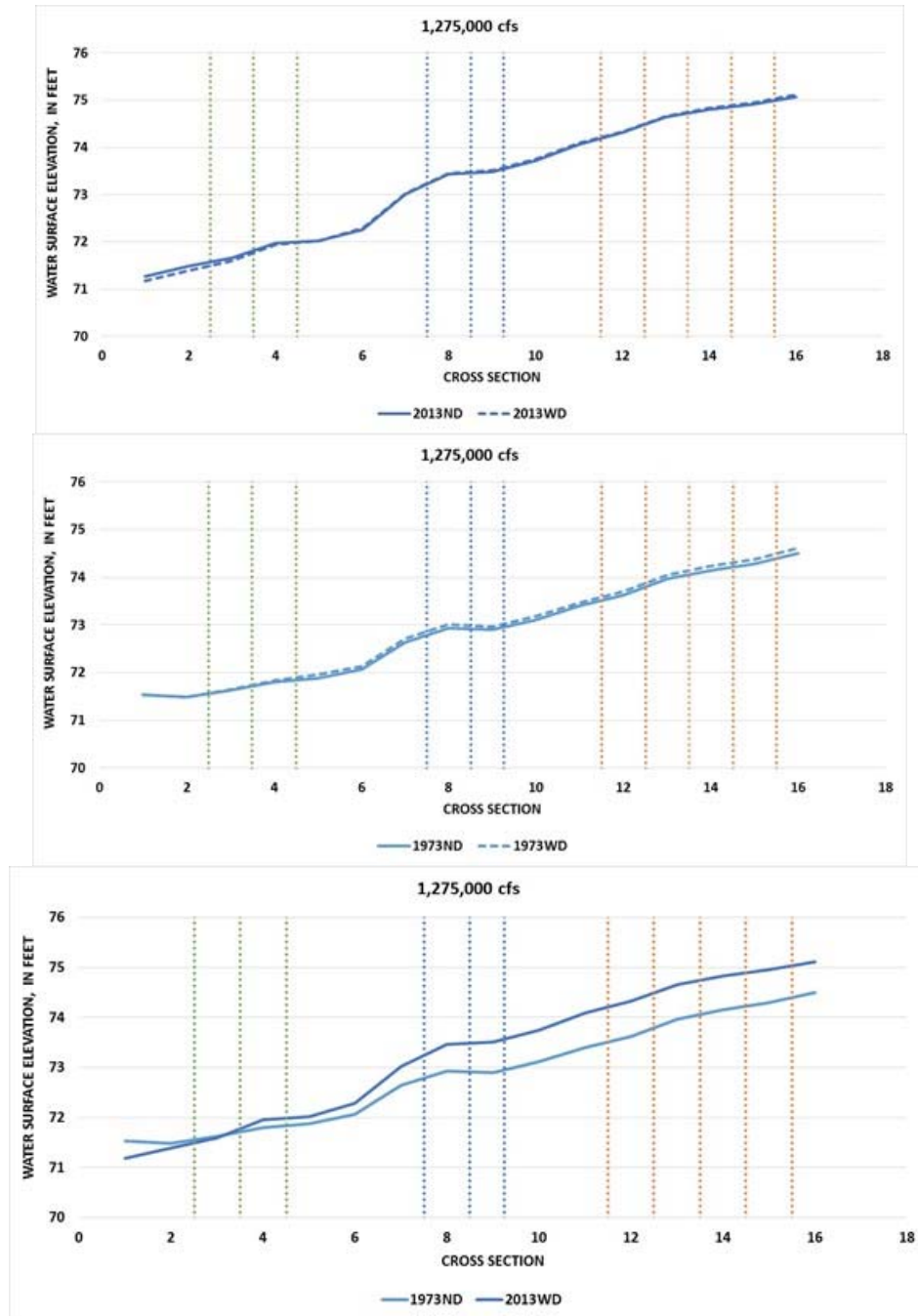
Figure 4. Marginal differences in water-surface profiles between 1973 *No Dike* and 1973 *With Dikes* scenarios (Top) and between 2013 *No Dike* and 2013 *With Dikes* scenarios (Middle); and Small differences between 1973 *No Dike* and 2013 *With Dikes* (Bottom). The upper two plots show differences due solely to the dike fields while the Bottom plot shows difference due to the dike fields and overall channel adjustment (aggradation) in this part of the LMR.

References

Alexander, J.S., R.C. Wilson, and W.R. Green. 2012. A brief history and summary of the effects of river engineering and dams on the Mississippi River system and delta. U.S. Geological Survey Circular 1375, 43 p.

Azinfar, H., and J.A. Kells, 2007. Backwater effect due to a single spur dike. Canadian Journal of Civil Engineering, 34, p. 107-115.

Baker, J. A., R. L. Kasul, L. E. Winfield, C. R. Bingham, C. H. Pennington, and R. E. Coleman. 1988a. An ecological investigation of the Baleshed Landing-Ben Lomond and Ajax Bar dike systems in the Lower Mississippi River, River Mile 481 to 494 AHP. Lower Mississippi River Environmental Program, Report 12, April, 104 p.; Vicksburg, MS: U. S. Army Corps of Engineers, Mississippi River Commission.

Baker, J. A., R. L. Kasul, L. E. Winfield, C. R. Bingham, C. H. Pennington, and R. E. Coleman. 1988b. An ecological investigation of revetted and natural bank habitats in the lower Mississippi River. Lower Mississippi River Environmental Program, Report 9, March, 123 p.; Vicksburg, MS: U. S. Army Corps of Engineers, Mississippi River Commission.

Biedenharn, D. S., L. Hubbard, and P. H. Hofman. 2000. Historical analysis of dike systems on the Lower Mississippi River. Draft Report to the U. S. Army Engineer Research and Development Center, Coastal and Hydraulics Laboratory, 172 p.; Vicksburg, MS: U. S. Army Corps of Engineers.

Biedenharn, D. S., M. A. Allison, C. D. Little, Jr., C. R. Thorne, and C. C. Watson. 2015. Large-scale geomorphic change in the Mississippi River from St. Louis, MO, to Donaldsonville, LA, as revealed by specific gage records. MRG&P Technical Report (in press), 50 p.; Vicksburg, MS: U. S. Army Corps of Engineers, Mississippi Valley Division.

Brauer, E. 2013. The Effect of Dikes on Water Surfaces in a Mobile Bed. MS Thesis. University of Illinois, Urbana-Champaign.

Brauer, E., and D.L. Duncan Jr. 2014. Discussion: Theoretical analysis of wing dike impact on river flood stages. Journal of Hydraulic Engineering, 140(11).

Cobb, S. P., and A. D. Magoun. 1985. Physical and hydrologic characteristics of aquatic habitat associated with dike systems in the Lower Mississippi River, River Mile 320 to 610, AHP. Lower Mississippi River Environmental Program, Report 5, December, 176 p.; Vicksburg, MS: U. S. Army Corps of Engineers, Mississippi River Commission.

Criss, R. E., and E.L. Shock. 2001. Flood enhancement through flood control. Geology, 29(10), p. 875-878.

Elliott, C. M., R. R. Rentschler, and J. H. Brooks. 1991. Response of the Lower Mississippi River low-flow stages. Pages 4-16 – 4-23, Volume 1 (Section 4), S.-S. Fan and Y.-H. Kuo (Eds.) in: Proceedings of the Fifth Federal Interagency Sedimentation Conference (5th FISC), Las Vegas, NV, March 18-21; Washington, DC: Federal Energy Regulatory Commission.

Huizinga, R.J. 2009. Examination of Direct Discharge Measurement Data and Historic Daily Data for Selected Gages on the Middle Mississippi River, 1861-2008. U.S. Geological Survey Scientific Investigations Report 2009-5232, 60 p.

Huthoff, F., N. Pinter, and J.W.F. Remo. 2013. Theoretical analysis of wing dike impact on river flood stages. Journal of Hydraulic Engineering, ASCE, 139(5): 550-556.

Jemberie, A.A., N. Pinter, and J. W. F. Remo.2008. Hydrologic history of the Mississippi and Lower Missouri Rivers based upon a refined specific-gauge approach. Hydrological Processes, 22, p. 4436-4447.

Kesel, R.H., E.G. Yodis, and D.J.McCraw. 1992. An approximation of the sediment budget of the lower Mississippi River prior to human modification. Earth Surface Processes and Landforms, 17, p. 711-722.

Keown, M. P., E. A. Dardeau, Jr., and E. M. Causey. 1981. Characterization of the suspended sediment regime and bed-material gradation of the Mississippi River basin. Potamology Program (P-1) Report 1, Accession No. ADA111236; Vicksburg, MS: U. S. Army Waterways Experiment Station.

Lamb, M. S., and L. T. Etheridge. 1991. Sediment management on the Mississippi. Pages 1-1 – 1-8, Volume 1 (Section 1), S.-S. Fan and Y.-H. Kuo (Eds.) in: Proceedings of the Fifth Federal Interagency Sedimentation Conference (5th FISC), Las Vegas, NV, March 18-21; Washington, DC: Federal Energy Regulatory Commission.

Piotrowski, J.A., Young, N.C., Weber, L.J. 2012. Supplemental Investigation of the Influence of River Training Structures on Flood Stages from River Mile 179.5 to 190.0 of the Middle Mississippi River. Submitted to the U.S. Army Corps of Engineers, St. Louis, Missouri.

Pinter, N., and R.A. Heine. 2005. Hydrodynamic and morphodynamic response to river engineering documented by fixed-discharge analysis, Lower Missouri River, USA. Journal of Hydrology, 302, p. 70-91.

Pinter, N., A.A. Jemberie, J.W.F. Remo, R.A. Heine, and B.S. Ickes. 2010. Cumulative impacts of river engineering, Mississippi and Lower Missouri Rivers. River Research and Applications, 26, p. 546-571.

Pinter, N., and R. Thomas, 2003. Engineering modifications and changes in flood behavior of the Middle Mississippi River. In R. Criss and D. Wilson, (eds.), At The Confluence: Rivers, Floods, and Water Quality in the St. Louis Region, pp. 96-114

Pinter, N., R. Thomas, and J.H. Wlosinski. 2001. Flood-hazard assessment on dynamic rivers. Eos: Transactions of the American Geophysical Union, 82(31), p. 333-339.

Remo, J.W.F., and N. Pinter, 2007. Retro-modeling of the Middle Mississippi River. Journal of Hydrology. doi: 10.1016/j.hydrol.2007.02.008.

Robbins, C. H., and A. Simon. 1983. Man-induced channel adjustment in Tennessee streams. U. S. Geological Survey Water-Resources Investigations 82-4098, 129 p.; Washington, DC: Government Printing Office.

Simon, A. 1994. Gradation processes and channel evolution in modified West Tennessee streams: process, response, and form. U. S. Geological Survey Professional Paper 1470, 84 p.; Washington, DC: Government Printing Office.

Simon, A., K. Artita, and G. L. Simon. 2019. Changes in hydrology and suspended-sediment transport in the Mississippi River Basin over the past century. Report to the U. S. Army Engineer Research and Development Center, Coastal and Hydraulics Laboratory, 412 p.; Vicksburg, MS, in press.

Simon, A., K. Artita, J. Hammond, D.S. Biedenharn, and C.D. Little Jr. (in press). Effects of dike fields on channel characteristics of the Lower Mississippi River. Report to the U. S. Army Engineer Research and Development Center, Coastal and Hydraulics Laboratory, 234 p.; Vicksburg, MS.

Smith, L.M., and B.R. Winkley. 1996. The response of the Lower Mississippi River to river engineering. Engineering Geology, 45(1-4), p. 433-455.

Sukhodolov, A.N. 2014. Hydrodynamics of groyne fields in a straight river reach: insight from field experiments. Journal of Hydraulic Research. 52:1, 105-120. DOI:10.1080/00221686.2014.880859.

Sutron Corporation. 1987. Effects of dike systems on sedimentation in the Lower Mississippi River – Project Report. Work Order Number 586.7, 11 p.

U.S. Army Corps of Engineers (USACE). 1982. Analysis of major parameters affecting the behavior of the Mississippi River. Potamology Program (P-1), Report 4, J. R. Tuttle and W. Pinner (Eds.), December, 67 p.; Vicksburg, MS: U. S. Army Engineer Division, Lower Mississippi Valley, Potamology Branch.

U. S. Army Corps of Engineers, Mississippi River Commission (USACE, MRC). 1977. Channel improvement feature, flood control, Mississippi River and tributaries. 63 p.; Vicksburg, MS: U. S. Army Corps of Engineers, Mississippi River Commission.

U. S. Army Corps of Engineers, Mississippi Valley Division (USACE, MVD). 1997. Biological assessment, interior population of the least tern, sterna antillarum, Regulating Works Project, Upper Mississippi River (River Miles 0-195) and Mississippi River and Tributaries Project, channel improvement feature, Lower Mississippi River (River Miles 0-954.5, AHP). Draft, December; Vicksburg, MS: U. S. Army Corps of Engineers, Mississippi Valley Division / Mississippi River Commission.

USACE 2016. Hydrodynamic Study of Vancill Towhead Reach on the Middle Mississippi River. U.S. Army Corps of Engineers, St. Louis District.

U.S. Government Accounting Office (USGAO). 2011. Mississippi River: Actions needed to help resolve environmental and flooding concerns about the use of river training structures. Report to Congressional Requesters. GAO12-41, 64 p.

Wang, B., and Y. J. Xu. 2018. Dynamics of 30 large channel bars in the lower Mississippi River in response to river engineering from 1985-2015. Geomorphology, 300, p. 31-44.

Watson, C. C., and D. S. Biedenharn., 2010. Specific gage analysis of stage trends of the Middle Mississippi River. Proceedings of the 2nd Joint Federal Interagency Conference, Las Vegas, June 27- July 1, 12 p.

Winkley, B. R. 1977. Man-made cutoffs on the Lower Mississippi River, conception, construction, and river response. Potamology Investigations Report 300-2, March, 219 p.; Vicksburg, MS: U.S. Army Waterways Experiment Station.

Yossef, M. F. M. 2004. The effect of the submergence level on the resistance of groynes: An experimental investigation. The 6th International Conference on Hydroscience and Engineering (ICHE-2004), May 30-June 3, Brisbane Australia, 9 p.

Effects of Elwha River Dam Removals on the US 101 Bridge

Casey Kramer, Principal Hydraulic Engineer, NHC, 711 Capitol Way S., #607
Olympia, WA, 98501, ckramer@nhcweb.com, 206-241-6000
Jennifer Bountry, Hydraulic Engineer, Bureau of Reclamation, 6th and Kipling, Building 67
Denver, CO, 80225, jbountry@usbr.gov, 303-445-3614
Timothy Randle, Supervisory Hydraulic Engineer, Bureau of Reclamation, 6th and Kipling,
Building 67 Denver, CO, 80225, trandle@usbr.gov, 303-445-2557
Andy Ritchie, Geomorphologist, U.S. Geological Survey, 2885 Mission St, Santa Cruz, CA,
95060, aritchie@usgs.gov, 831-460-7454

Introduction

Northwest Hydraulic Consultants (NHC), working for the Washington State Department of Transportation (WSDOT), collaborated with the United States Bureau of Reclamation (USBR) and United States Geological Survey (USGS) with assessing the effects of the removal of the Elwha River Dams on the existing and proposed US 101 Elwha River Bridges (Figure 1). The effects to-date, along with the estimated effects to occur in the future, were used to assess the vulnerability of the existing US 101 Bridge and aid in the design of the proposed bridge.

Background

The US 101 Elwha River Bridge was constructed in 1926 and consists of a three-span concrete arch structure with two in-water intermediate piers, Piers 6 and 7 (Figure 2). The bridge was originally constructed between two dams, which were removed between 2011 and 2012, namely the former Elwha Dam (located downstream) and the Glines Canyon Dam (located upstream). Both dams had influences on the Elwha River reach from above Glines Canyon Dam, through the US 101 crossing and downstream to the Strait of Juan de Fuca. The Elwha Dam was built first, with construction completed in 1913, followed by the Glines Canyon Dam in 1927. The Elwha and Glines Canyon Dams influenced the hydraulics through the US 101 crossing and thus impacted sediment transport through the US 101 Bridge reach. Due to the influence of the Elwha Dam (Lake Aldwell), sediment was deposited at the US 101 crossing from the time of construction in 1913 until 1926 when the US 101 Bridge was constructed. As such, the US 101 Bridge had never seen a free-flowing river and was most likely founded on sediment deposited due to the Elwha Dam construction (although as-builts indicated the bridge foundations were founded on bedrock). In October 2016, the WSDOT Geotechnical Office conducted a subsurface investigation to determine types and thicknesses of soil/rock below the in-water piers (Allen 2016). The geotechnical borings assisted in determining that the US 101 in-water intermediate piers were founded on lake sediment deposits. Pier 6 has approximately 4 to 8 feet of sand/gravel (lake deposit), underlain by approximately 6 to 11 feet of cobbles/boulders (pre-dam river alluvium) below the foundation seal. Basalt was observed approximately 11 to 20 feet below the foundation seal. Pier 7 has approximately 3 to 4 feet of sand/gravel (lake deposit) below the foundation seal, until basalt was observed. Based on this assessment, and changes post dam removal, the US 101 Elwha River Bridge was rated scour critical and an emergency was declared to protect the bridge from scour.
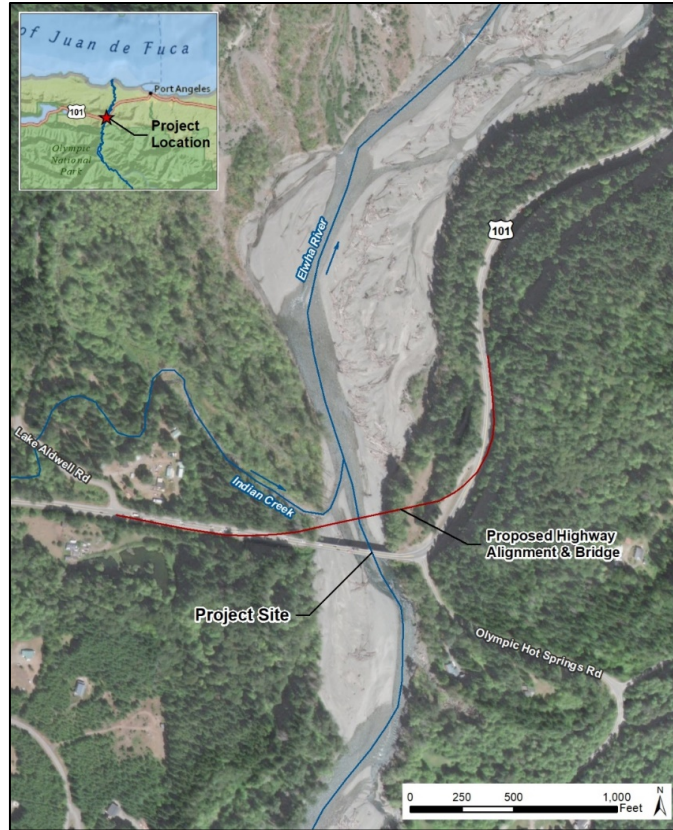
Figure 1. Vicinity Map
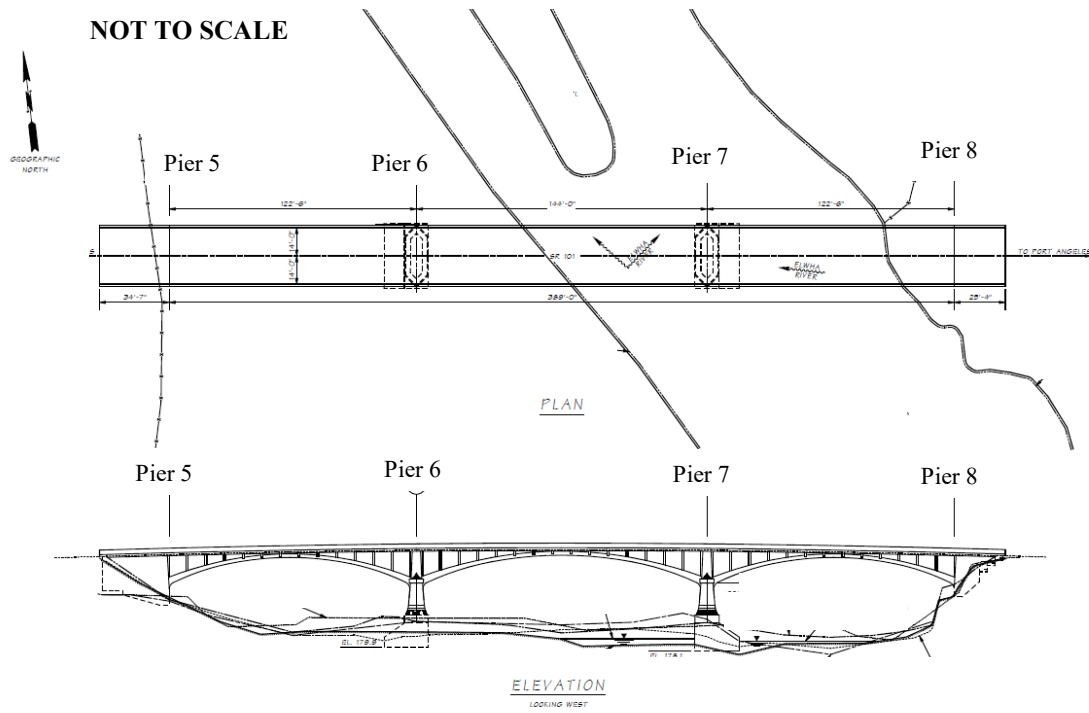
Figure 2. Existing Bridge Layout

Watershed Assessment

Watershed and Landcover

At the US 101 Bridge (project site), the Elwha River drains approximately 293 square miles from the central portion of the northern slope of the Olympic Mountains. The contributing basin ranges in elevation from about 190 feet to 7,300 feet (Figure 3). The basin is essentially undeveloped as it lies mostly within the boundaries of the Olympic National Park and a Federally protected Wilderness Area upstream from Lake Mills. More than 70% of the basin's area is covered by lowland and sub-alpine forest landcover. The remaining area is mostly above the elevation of 4,500 feet and is dominated by alpine landcover including meadows, perennial snow cover, and bare rock and talus. Only Lake Mills and Lake Aldwell interrupted sediment connectivity between the alpine peaks and the valley bottom.
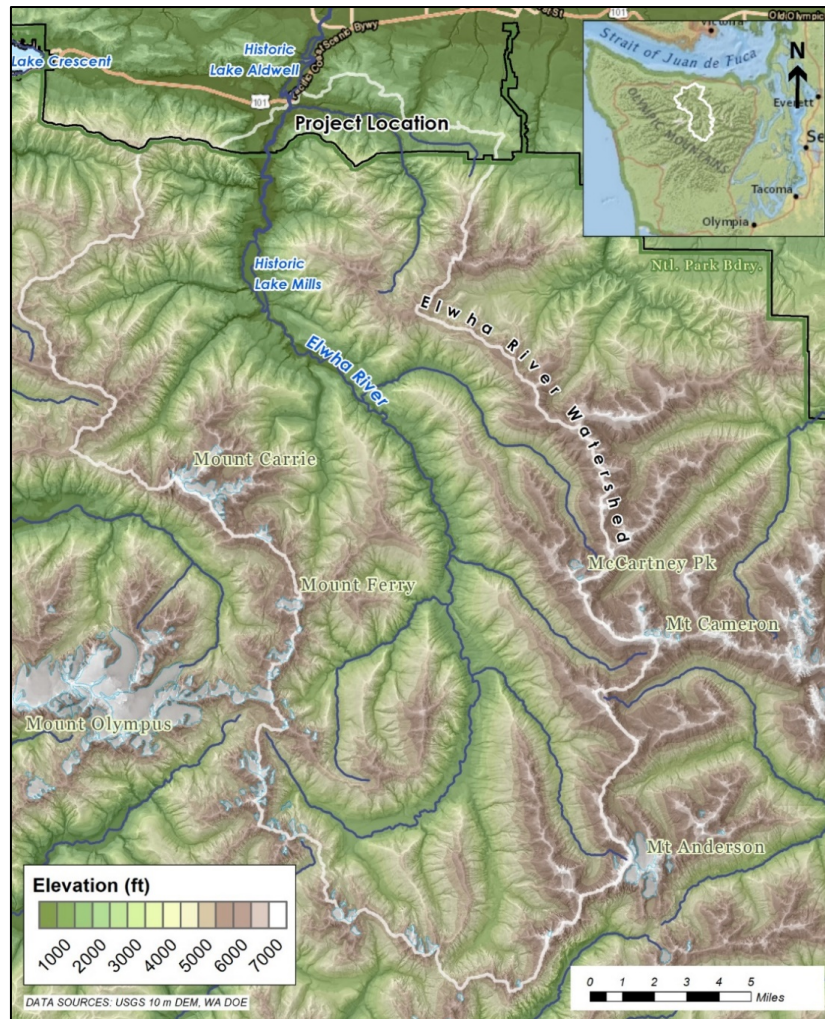
Figure 3. Overview of Elwha River Basin Topography

Peak Flow Analysis

The USGS operates a streamflow gage on the Elwha River that is located approximately 0.9 river miles upstream of the US 101 crossing (Elwha River at McDonald Bridge near Port Angeles, WA, USGS Gage 12045500). This gage has operated from 1898 to present and thus includes over 100 years of peak flow data. The USGS 12045500 gage was utilized to develop estimates of peak flows at the US 101 crossing as it has essentially the same basin characteristics, and nearly the same drainage area, as the US 101 crossing. Little River is the only named tributary entering the Elwha River, between the stream gage and the US 101 crossing.

To determine peak flows at the US 101 crossing, data from the USGS 12045500 gage was evaluated utilizing the methods provided by the USGS's *Magnitude, Frequency, and Trends of Floods at Gaged and Ungaged Sites in Washington* (Mastin et al., 2016). The USGS PeakFQ statistical software was used to conduct a flow frequency analysis on the gage data (Veilleux et al., 2014).

Peak flow estimates were then scaled following USGS guidelines (Mastin et al., 2016) to obtain flows at the US 101 Bridge crossing. Flows were analyzed utilizing both the weighted and unweighted flood frequency analysis. In general, the weighted flow values provide benefit for sites with smaller records of data; however, the USGS gage #12045500 has over 100 years of recorded data and thus provides an adequate record for analysis. Flows calculated from the unweighted gage analysis was therefore determined to be the most accurate to assess hydraulic and scour conditions at the bridge. Table 1 depicts the peak flows utilized for the project site.

Table 1. Peak Flows for Elwha River

Mean Recurrence Interval (MRI)	Gage Analysis from USGS Gage #12045500	Gage Analysis from USGS Gage #12045500 at the US 101 Crossing
2	14,300 cfs	15,500 cfs
5	21,400 cfs	23,100 cfs
10	26,200 cfs	28,400 cfs
25	32,400 cfs	35,100 cfs
50	37,100 cfs	40,200 cfs
100	41,900 cfs	45,300 cfs
200	46,600 cfs	50,500 cfs
500	53,100 cfs	57,400 cfs

Geomorphology

The project site is located on the Middle Reach of the Elwha River, which lies between the historic locations of Lake Mills and Lake Aldwell. This reach is highly dynamic and continues to respond to changed geomorphic controls from the removal of the Elwha Dam in 2012 and the removal of the Glines Canyon Dam in 2014 (with the Lake Mills being drained in 2012). The Elwha Dam impounded Lake Aldwell just downstream of the project location since 1913 and the Glines Canyon Dam impounded Lake Mills upstream of the project location since 1927. Substantial work has been completed which aimed to predict the expected channel responses prior to removal of

the dams and actual responses post removal. Key publications documenting channel geomorphology impacts include East et al. (2015), Magirl et al. (2015), and Warrick et al. (2015). This work summarizes channel changes between the Elwha Dam removal in 2012 and in the Spring of 2013, which occurred during relatively modest flows following the dam removals. This however does not include details of response to larger flood flows in water years 2015, 2016, or 2018 (Figure 4). A report, recently produced by a U.S. Department of the Interior (DOI) technical team, analyzed sediment management and channel response along the Elwha River (DOI, 2018). This report includes the more recent large flood flows, specifically investigating sediment transport from 2011 through 2017.
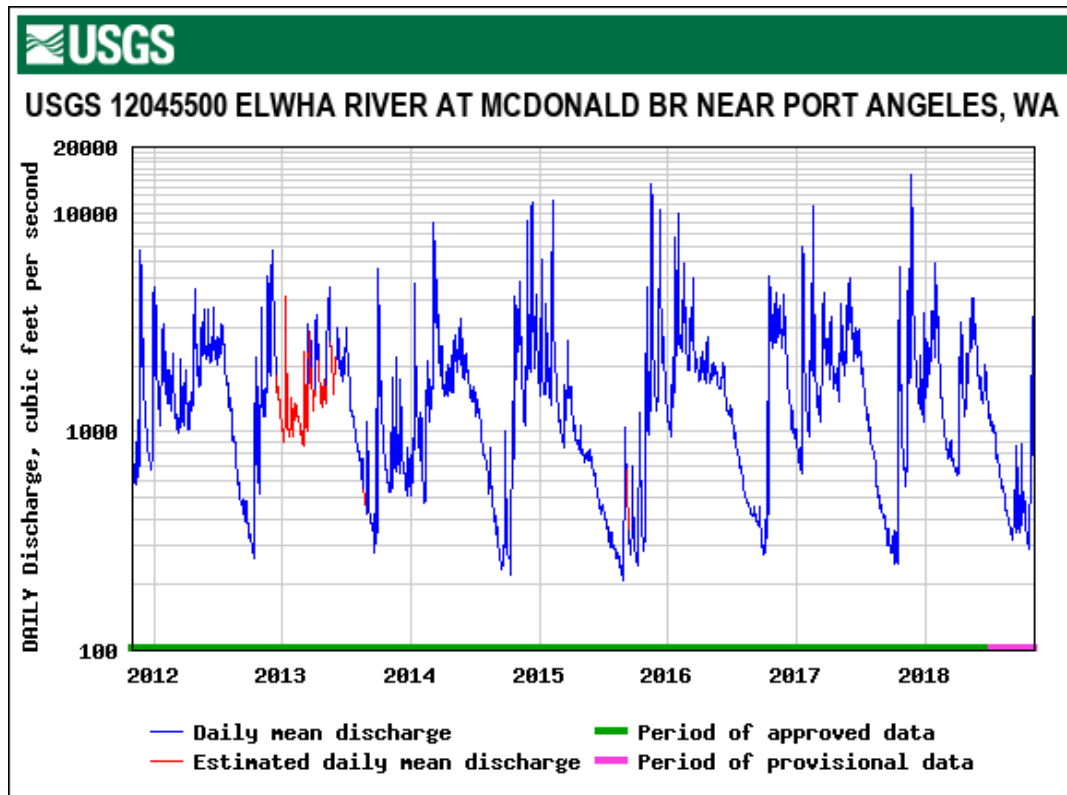
Figure 4. Elwha River Flows Following Dam Removal

The US 101 Bridge spans the location where the Elwha River formed the Lake Aldwell delta. Removal of the Elwha Dam, therefore, lowered the geomorphic base level for the channel at the bridge location, leading to incision and channel profile steepening (East et al., 2015), possibly leading to the scour that threatened the existing structures' foundations (Figure 5).

Removal of the Glines Canyon Dam upstream, in contrast, released a large and relatively coarse sediment pulse into the river channel. Between October 2012 and September 2013, roughly 9.1 metric tons (Mt) of the 23 Mt (plus or minus 6 Mt) of stored sediment had eroded from reservoir deposits in Lake Mills, increasing sediment transport rates through the Middle Reach by a factor of more than 100, compared to the incoming load (Warrick et al., 2015). This resulted in about 5 feet of channel aggradation in alluvial portions of the middle reach not affected by incision into the Lake Aldwell delta (East et al., 2015). A substantial fining of the bed material was caused by the transport of smaller sediment stored behind the Glines Canyon Dam. This resulted in an

increase in bed material transport rates in the Middle Reach as the bed shifted from a range of small boulders to pebble sized sediment to cobble to medium sand sized sediment.
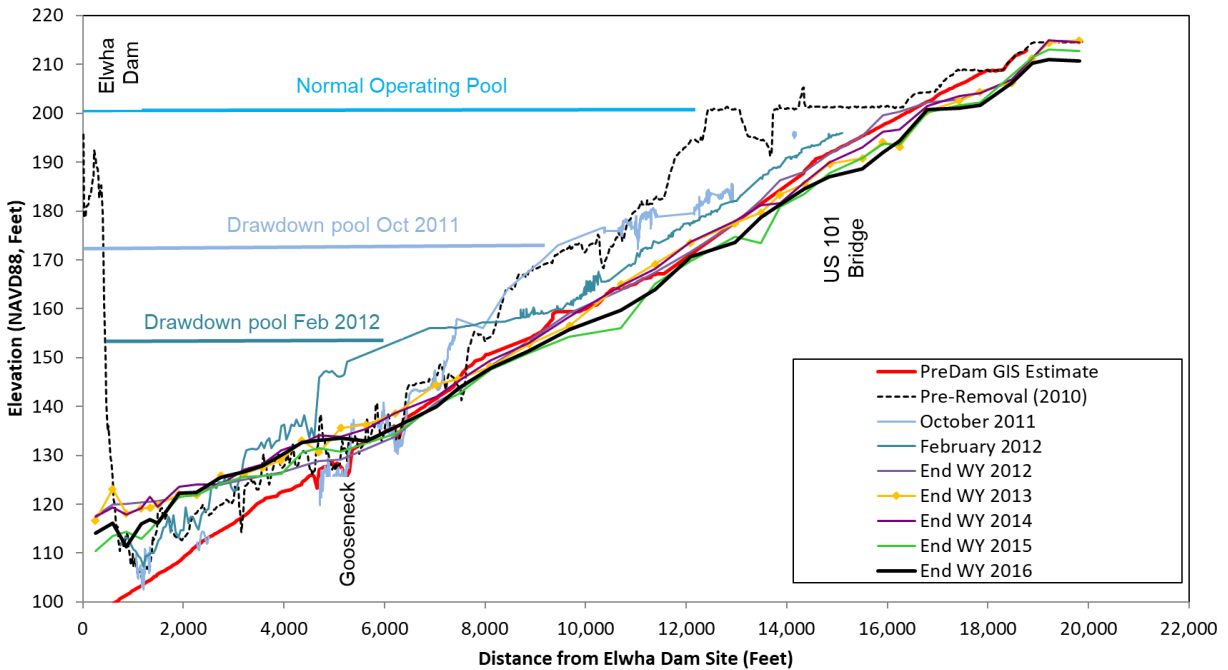
Figure 5. Lake Aldwell Longitudinal Profile

Aggressive channel migration and substantial channel widening are occurring through the project reach, as the channel is responding to perturbations in its base level and sediment supply due to removal of the upstream and downstream dams. Figures 6 and 7 show erosion patterns through the project reach, following removal of the dam near the US 101 Bridge, in plan and cross section, respectively.

Cross Section 1 (XS 1), shown in Figure 6, is located approximately 400 feet upstream of the US 101 Bridge. As can be seen in Figures 6 and 7, the main channel has incised by several feet and has, in general, moved to the east. Significant erosion occurred during the months of November and December, 2014 just upstream of the bridge (shown with yellow and orange polygons in Figure 6 and the groundlines between Station ~175 and ~350 in Figure 7). The groundline between stations ~175 and ~350 dropped upwards of 8 feet, when the channel meander translated upwards of 350 feet in the downstream and westerly direction.

Cross Section 2 (XS 2), shown in Figure 6, is located approximately 1,350 feet downstream of the US 101 Bridge. As can be seen in Figures 6 and 7, the main channel has incised by a couple of feet, however has more dominantly moved to the west. Significant erosion has progressively occurred from Water Year (WY) 2013 to WY 2018 (blue and red polygons in Figure 6 and grey line to green line in Figure 7). Overall, the river's left bank has migrated from approximately station 900 to station 250 (650 feet) between WY 2013 and WY 2017, for an average rate of 130 feet/year. Notably, there was no indication of changes at the left bank between WY 2013 and WY 2014.

Cross Section 3 (XS 3), shown in Figure 6, is located approximately 3,300 feet downstream of the US 101 Bridge. As can be seen in Figures 6 and 7, the main channel has incised by a couple feet, however more evident is the widening and movement to the west. Significant erosion has progressively occurred from WY 2013 to WY 2018 (blue and red polygons in Figure 6 and grey line to green line in Figure 7). Overall, the river's left bank has migrated from approximately station 1025 to station 400 (625 feet) between WY 2013 and WY 2017, for an average rate of approximately 125 feet/year. Notably, there was no indication of changes at the left bank between WY 2016 and WY 2017.

These rates suggest migration on the order of hundreds to a thousand feet are possible, even during relatively low to moderate flood flows that occurred during this period (Figure 4). It is expected that the channel will continue to be highly dynamic in both vertical and horizontal dimensions until oversupply of bed material from upstream ceases and a new equilibrium profile is established through the historic extent of Lake Aldwell.
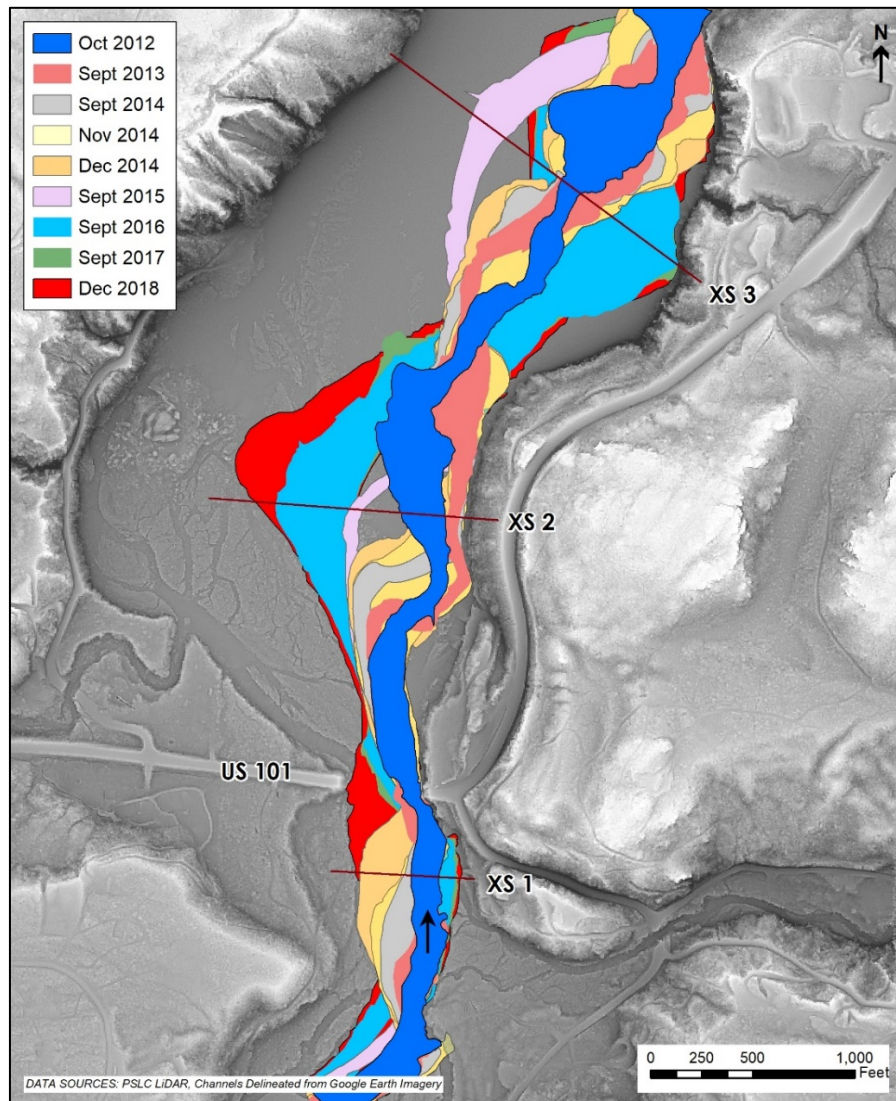

Figure 6. Active Channel Positions Following Removal of the Elwha Dam. Channels are Stacked with the Most Recent on the Bottom to Highlight Meander Growth Patterns

Figure 7. Cross Sections at Locations Shown in Figure 6

Figure 8 shows photos taken from a remote camera looking towards the left bank of cross section 3 (XS3), shown in Figures 6 and 7, during the November 2014 flow event (Figure 4). The red polygon highlighted in yellow is depicting erosion that happened between November 27th and December 15th, 2014.

Figure 8. Photos Taken November 27th, 2014 (Left) and December 12th, 2014 (Right)

Long-term Aggradation/Degradation of the River Bed: Channel response has been highly dynamic at the US 101 Bridge crossing due to the interplay of changing bed material sediment supply from the removal of Glines Canyon Dam and base level control at the Elwha Dam. As describe above, this has caused substantial bed elevation volatility at the US 101 Bridge, but the overall trend has been degradational following the Elwha Dam removal. This suggests the dominant controlling factor at the bridge has been both erosion and downcutting, following the removal of the Elwha Dam. It is expected that the channel will continue to degrade, but the presence of bedrock near the surface should limit long-term degradation.

The DOI technical team (which included the USGS, National Park Service and Bureau of Reclamation (Reclamation)) recently analyzed sediment management along the Elwha River (DOI, 2018). Their report indicates that portions of the Elwha Dam foundation, which are still exposed, may influence channel responses upstream (DOI, 2018). Figure 9 depicts this portion of the remaining Elwha dam and caisson compared to historic and more recent water surface and groundline data. Once these exposed portions are removed, the channel will likely experience additional degradation which will likely extend upstream to the US 101 Bridge and contribute to the expected eventual exposure of bedrock near the proposed bridge.

The DOI technical team believes it is unlikely that the bedrock would become exposed during all flow durations at the US 101 Bridge, rather it may become exposed during large floods which may mobilize larger material covering the bedrock.

It is possible that the bed material pulse from the removal of the Glines Canyon Dam may drive some future aggradation at the project site, but bridge sounding data (Figure 10) do not suggest this impact has, to date, overwhelmed the degradational response from the removal of the two dams.
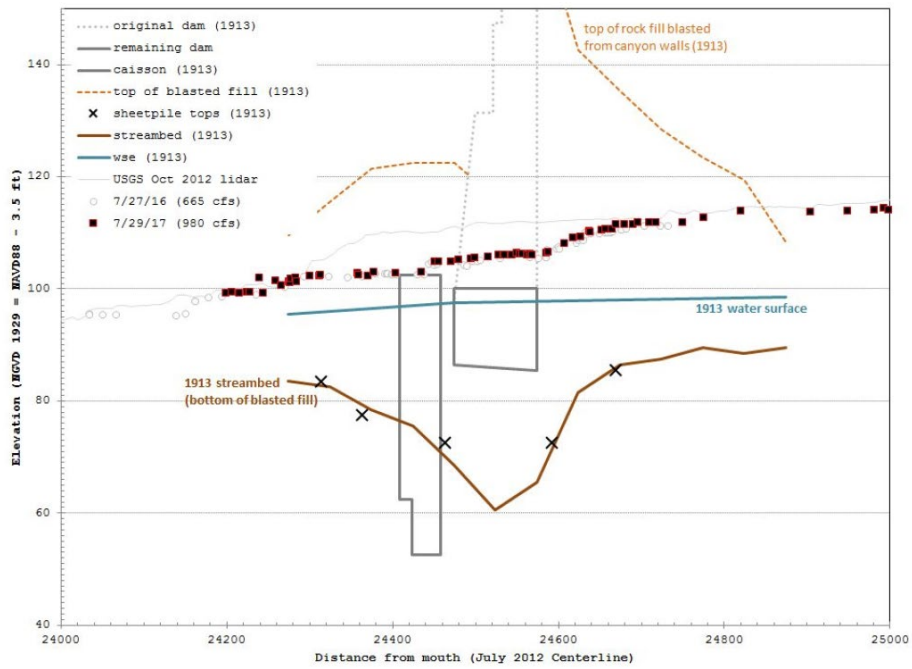
Figure 9. Longitudinal Profile at Elwha Dam (Figure 72 from DOI, 2018)
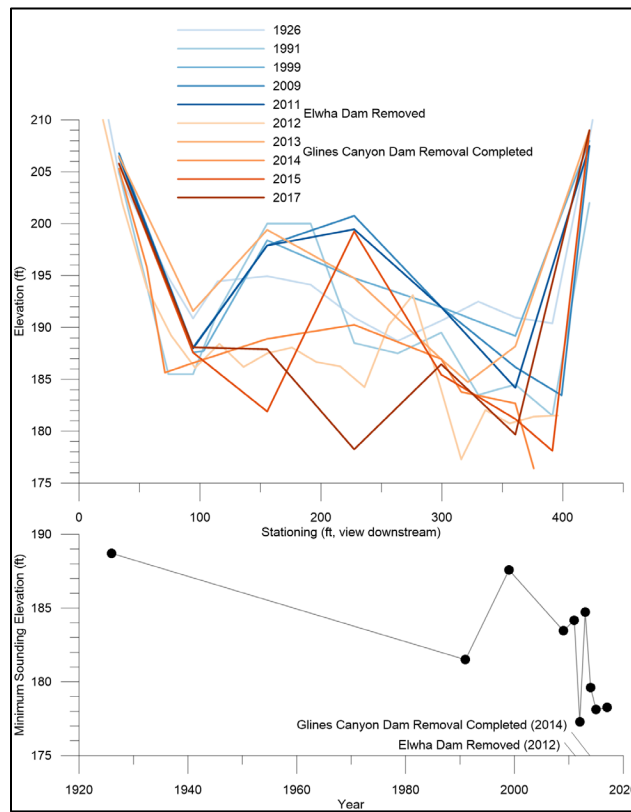
Figure 10. Plot of Bridge Sounding Data

Hydraulic Analysis

The hydraulic analyses of the existing and proposed US 101 Elwha River Bridge crossings were performed utilizing SRH-2D (U.S. Bureau of Reclamation, 2016), a two-dimensional, depth-averaged hydraulic model. The SRH-2D model allowed for a detailed understanding of the hydraulics through the existing and proposed bridge crossing near the abutments, piers, and along the banks to be utilized for the scour analysis.

Proposed Conditions

Figure 11 depicts the water surface elevations (WSE) determined by the 2D model for the 100-year peak flow on the Elwha River under proposed conditions. The model results indicate that the proposed bridge crossing reduces the 100-year backwater condition that is caused by the existing bridge. Figure 12 shows an average reduction in WSE of 0.8 feet along the cross section labeled XS1, in Figure 11, located at the upstream face of the existing bridge. Throughout the right side of the channel, the localized reduction in WSE is approximately 3 to 4 feet (Figure 12).
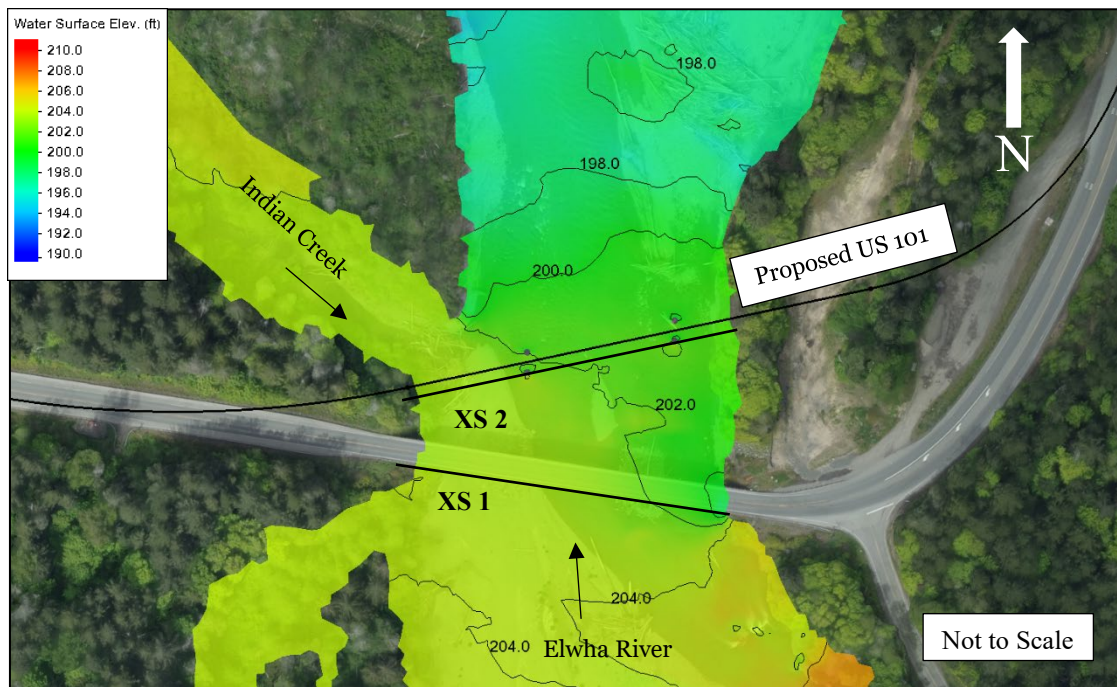
Figure 11. Proposed Conditions Water Surface Elevations Near Proposed US 101 Crossing at 100-year flood
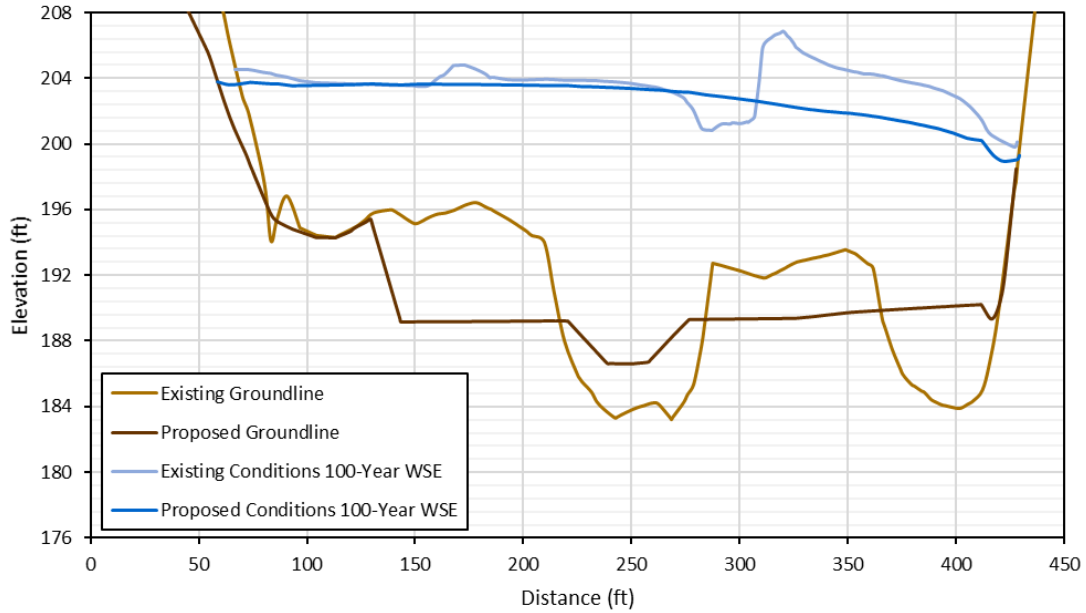
Figure 12. Water Surface Elevations Comparison at Upstream Face of Existing Bridge

Figure 13 depicts velocity magnitudes and vectors for the proposed conditions during the 100-year event. The blue and smaller arrows show areas of low velocity, whereas the red and longer arrows show areas of high velocities.
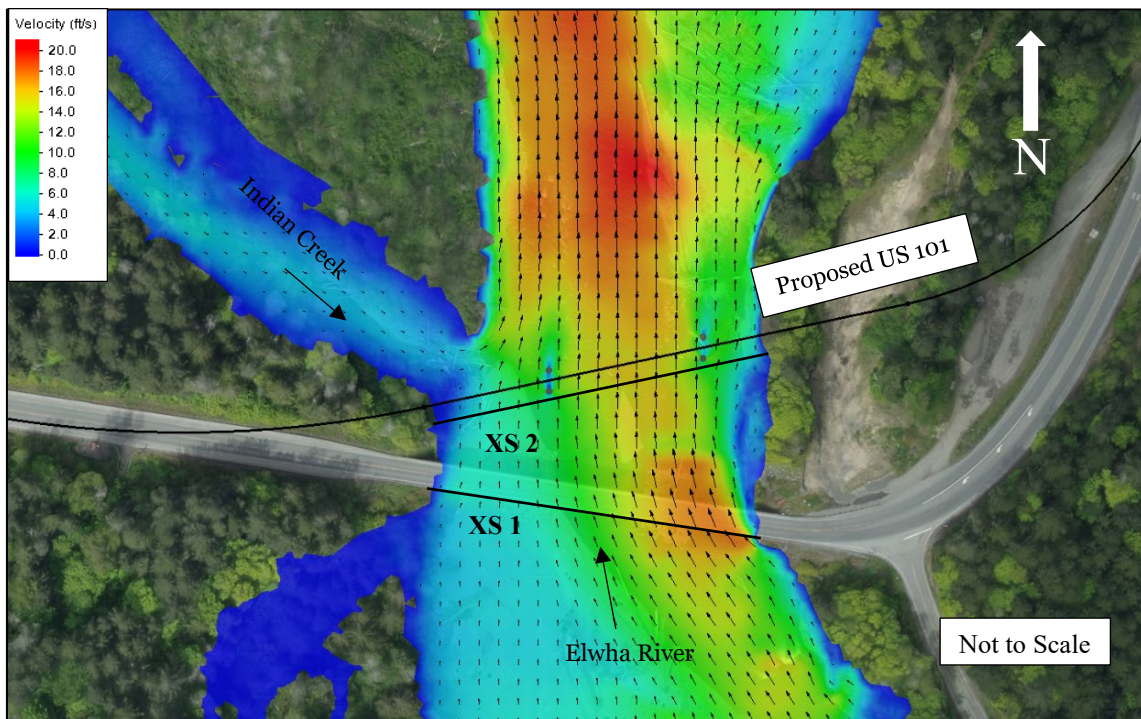
Figure 13. Proposed Conditions Velocity Magnitudes Near Proposed US 101 Crossing

Figure 14 provides velocity values for existing and proposed conditions plotted along cross section XS2 from Figure 13, to illustrate the velocity shadows caused by the wakes of the existing Piers 6 and 7. The proposed conditions velocity magnitude values are typically lower than the existing conditions throughout most of the channel, except where there are large dips where the existing Pier 6 (~Station 130) and Pier 7 (~Station 260) had significant effects on the velocity distribution. The averaged velocity magnitude for both existing (10 feet/sec) and proposed conditions (9.4 feet/sec) are also displayed on this figure as pink and red lines, respectively. The proposed conditions average velocity magnitude is also lower than the existing conditions value, likely due to providing a larger bridge span and minimizing widths of in-water piers. Consequently, the proposed conditions velocity distribution is more natural, therefore, the proposed bridge will better allow for the natural movement of water, wood, and sediment.
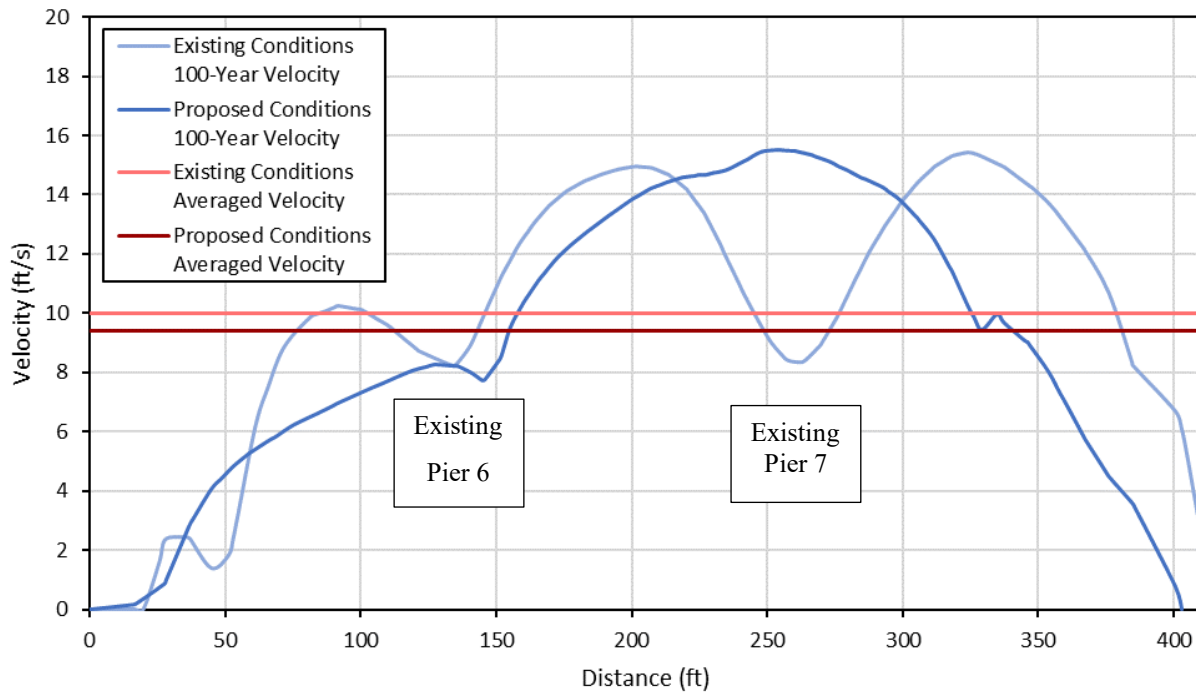
Figure 14. Velocity Magnitude Comparison at Upstream Face of Proposed Bridge

Conclusion

Practitioners should assess hydrology, hydraulics, and geomorphology (e.g. potential channel responses) when designing bridges and other infrastructure, especially in highly dynamic fluvial systems. The existing US 101 Bridge was constructed on lake sediment deposits, which likely became mobilized following the removal of the Elwha River Dam. Impacts from depositional deltas may extend well upstream from the normal reservoir water surface elevations. Consequently, dam removals can result in channel incision through the entire length of the reservoir delta, including the river channel upstream of the delta. Any infrastructure built after reservoir sedimentation may be threatened by the channel incision, resulting from dam removal, and therefore should be evaluated when designing new infrastructure and when analyzing existing infrastructure. These considerations will allow for more sustainable structures to be designed and maintained.

References

Allen, T.A. and Hegge, W. 2016. SR 101, MP 239.42, Elwha River Bridge Scour Repair, Geotechnical Subsurface Investigation.

East, A.E., Pess, G.R., Bountry, J.A., Magirl, C.S., Ritchie, A.C., Logan, J.B., Randle, T.J., Mastin, M.C., Minear, J.T., Duda, J.J., and others. 2015. Large-scale dam removal on the Elwha River, Washington, USA: River channel and floodplain geomorphic change. *Geomorphology*, 228, pp 765–786.

Magirl, C.S., Hilldale, R.C., Curran, C.A., Duda, J.J., Straub, T.D., Domanski, M., and Foreman, J.R. 2015. Large-scale dam removal on the Elwha River, Washington, USA: Fluvial sediment load. *Geomorphology*, 246. doi:10.1016/j.geomorph.2014.12.032. pp 669–686.

Mastin, Mark C., Christopher P. Konrad, Andrea G. Veilleux, and Alison E. Tecca 2016. *Magnitude, Frequency, and Trends of Floods at Gaged and Ungaged Sites in Washington, Based on Data through Water Year 2014: Scientific Investigations Report 2016-5118*. United States Geological Survey. Reston, VA.

United States Bureau of Reclamation. 2016. Sedimentation and River Hydraulics – Two-Dimensional (SRH-2D) Model v3.

United States Department of the Interior. 2018. *Adaptive Sediment Management Program Final Report for the Elwha River Restoration Project, Prepare for National Park Service. Technical Report SRH-2018-13.*

Veilleux, A.G., Cohn, T.A., Flynn, K.M., Mason, R.R., Jr., and Hummel, P.R. 2014. Estimating magnitude and frequency of floods using the PeakFQ 7.0 program: U.S. Geological Survey Fact Sheet 2013-3108, 2 p., https://dx.doi.org/10.3133/fs20133108.

Warrick, J.A., Bountry, J.A., East, A.E., Magirl, C.S., Randle, T.J., Gelfenbaum,G., Ritchie, A.C., Pess, G.R., Leung, V., and Duda, J.J. 2015. Large-scale dam removal on the Elwha River, Washington, USA: Source-to-sink sediment budget and synthesis. Geomorphology, 246. doi:10.1016/j.geomorph.2015.01.010. pp 727-750.

Hydraulic Design of Sustainable River Abstraction Works on alluvial rivers with Sediment Management Features for Potable Water Supply

Gerrit Basson, Professor, Department of Civil Engineering, Stellenbosch University, Stellenbosch, South Africa, grbasson@sun.ac.za

Claudia McLeod, MEng student, Department of Civil Engineering, Stellenbosch University, Stellenbosch, South Africa

Abstract

Regional potable water supply schemes require a high assurance of supply and the river abstraction works (pump station) has often been found to be the most critical component in the scheme. River abstraction works are hydraulic systems which consist of different components, such as a weir, boulder trap, gravel traps and pump canals, and is used to abstract raw water from rivers. Abstraction works on alluvial rivers are susceptible to coarse sediment abstraction which damages the duty pumps in the long term and cause sediment deposition at the intakes. Abstraction works are also prone to floating debris which blocks the intakes, insufficient pump submergence during low flow periods, low flows that do not reach the intakes during droughts, and extreme floods which could damage the works. If the abstraction works are not designed with sediment management features, they are often not sustainable. Following many years of careful research with physical model testing and validation by field measurements, a suitable river abstraction works design was found. This paper discusses this hydraulic design of a relatively large potable use abstraction works adopted in Southern Africa for sustainable operation of regional water supply schemes. The case study under discussion is the Lower Thukela River abstraction works. The abstraction works is located at the outside of a bend in the river and the best hydraulic location to divert coarse sediment away from the intakes was found by physical hydraulic model tests. The abstraction works and weir was constructed at a cost of $32000 and was commissioned during September 2017. The paper also discusses field sediment flushing tests carried out at the abstraction works during January 2018. In general, the hydraulic design of the abstraction works is robust, with limited maintenance requirements and is suggested to be used for future designs.

Introduction

The goal of the paper is to explain the design of a suitable river abstraction works to deal with sediment, with physical model testing and validation by field measurements. The case study under discussion is the Lower Thukela River abstraction works in South Africa which was commissioned during September 2017. The Thukela River is one of the larger rivers in South Africa with a catchment area of about 30000 km², a mean annual flow of 3200 million m³/annum and is highly sediment laden with a mean annual sediment load of 18 million t/annum. The river is alluvial with mainly fine sand and some gravel in the bed, with 0.4 mm median particle diameter in the river bed. During floods the transported sediment load (washload) consists mainly of silt and clay. The abstraction works is the first of a new type of works designed in South Africa to deal specifically with sediment for potable water use which requires a high assurance of supply. The SA Water Research Commission (2002) proposed the conceptual design of the abstraction works with a weir, which was later refined in guidelines for

the SA Water Research Commission (Basson, 2006) and the Lower Thukela design (Basson, 2012), the latter with physical model testing. Figure 1 shows the abstraction works location on the river.
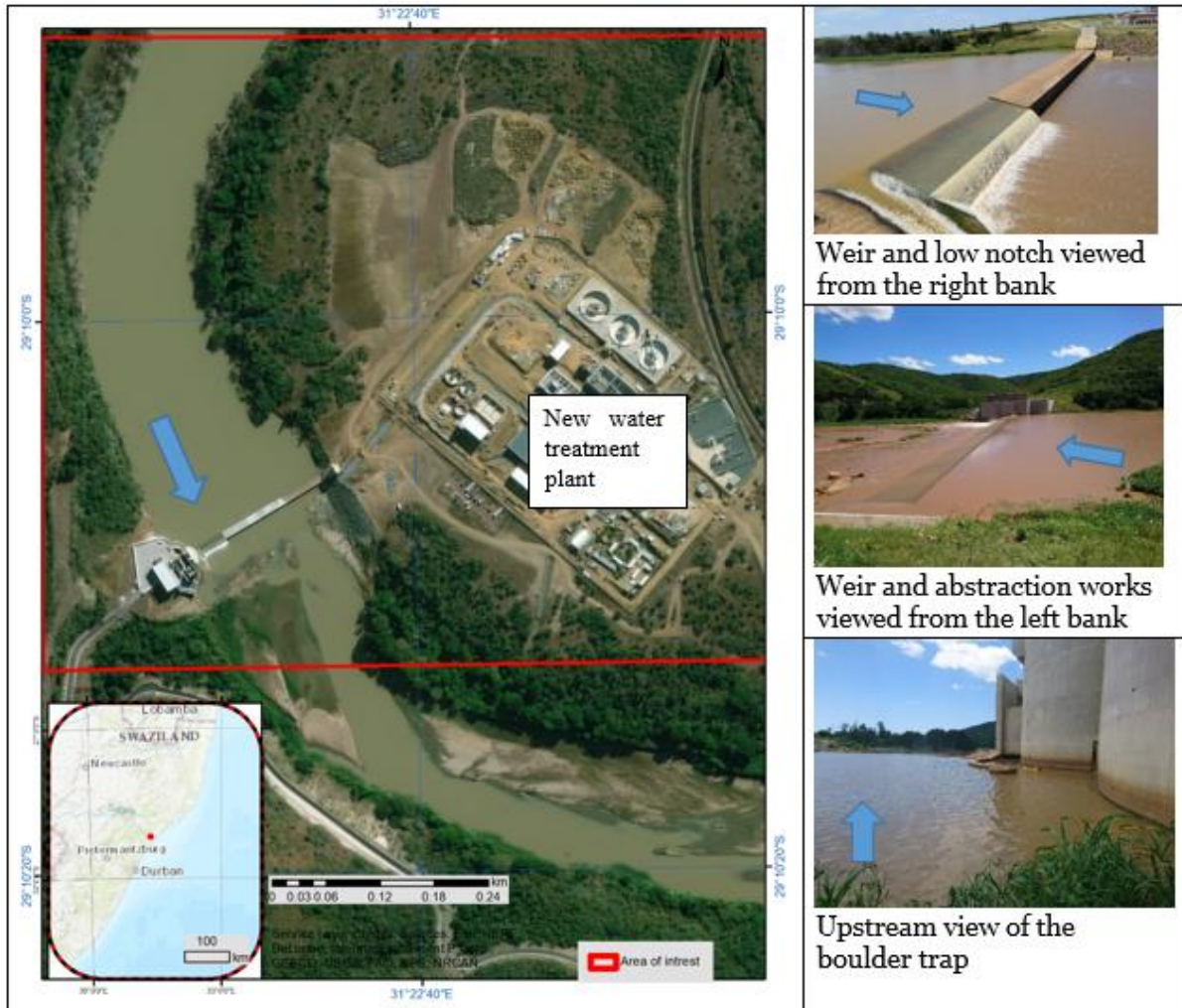
Figure 1. General location of Lower Thukela River abstraction works

The Lower Thukela River abstraction works consists of the following components: a boulder trap with a radial gate near the right bank, located next to a weir extending to the left bank of the river, with a high intake wall above the 100 year flood level, submerged intake slots on the intake wall to limit floating debris abstraction, two gravel traps with a submerged dividing wall between them, intakes with trashracks, and four pump canals fitted with fine screens downstream of the intakes to allow sand deposition and uniform flow towards the pumps bells. The high intake wall which is shaped as large halve pier, improves the secondary currents and local scour at the intakes during floods, and the intakes are self-scouring without opening any of the gates at the works during medium and large floods. The gates need to be operated infrequently under small flood conditions. The weir is 5.3 m high and has no gates to save capital and maintenance costs, and to limit the risk of gate failure due to poor maintenance. The abstraction works is therefore designed to flush sediment near the intake, but silt is assumed to accumulate to the weir crest in the upstream reservoir. The abstraction works also has a fishway (vertical slotted), and a low notch on the right bank side of the weir acts as an eelway.

Conceptual Hydraulic Design of the Abstraction Works and Weir

The Lower Thukela River abstraction works (110 Ml/d) completed during 2017 is located on the right bank of the river bend with the water treatment plant on the left bank, as seen in Figure 1. The WRC (2002) guidelines for abstraction works with a weir's general layout is shown in Figure 2. This design is the basis for the abstraction works design. The lower Thukela abstraction works components that are of interest to this paper are summarized below: weir, high intake walls with submerged slots, boulder trap, 2 gravel traps with a dividing wall, 4 sand traps/pumps canals, fish ladder, trash racks, fine screens and pumps.

The Lower Thukela abstraction works hydraulic design modified the Figure 2 basic design as follows:

a) A boulder trap with a large gate was added on the river side of F to ensure the submerged intake at C can be flushed during small floods

b) F in Figure 2 is a gravel trap consisting of 2 canals controlled by two radial gates which are opened at the same time. There are two canals because during flushing a dividing wall acts as a deflector to ensure the sediment is not washed into the pump canals at G (Figure 2).

c) The trashracks at J were moved to location D

d) Location K consists of several pump canals to act as settlers and to achieve uniform flow conditions during pumping. They are flushed one after the other by gate control.

e) The pumps at L could be a wet well design (immersible pumps) or a dry well design. The latter was selected for the Thukela design. The pump intake bells for the dry well pumps had to be raised above the floor (more than in a standard design), and detailed physical model tests indicated the safe submergence required. The raised bells are required for free flow flushing of sediments underneath the bell.
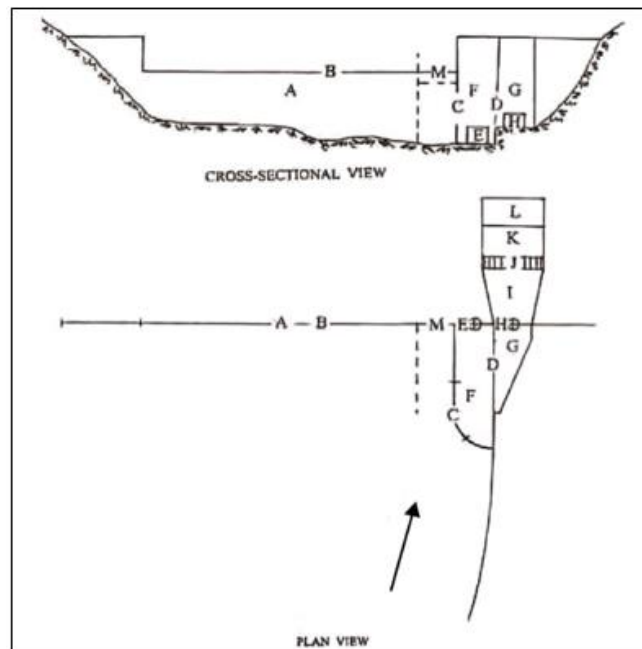
Where: A: Weir, B: Spillway, C: Open intake, D: Screen intake, E: Scour gates, F: Scour chamber, G: Collection channel, H: Control gate(s), I: Transition channel(s), J: Vortex suppressor, K: Settling basin, L: Pumps, M: Low notch weir.

Figure 2. Typical conceptual layout of abstraction work for South Africa (WRC, 2002)

Detailed Hydraulic Design of the Abstraction Works and Weir

The final detailed layout of the abstraction works is shown in Figures 3 and 4. The basic dimensions of the abstraction works is about 50 m x 50 m in plan. The hydraulic/sediment design aspects considered were as follows:

Location of the abstraction works:
The abstraction works is located on the outside of a river bend where the secondary current ensures that the bedload is transported away from the intake near the river bank. The optimum location of the abstraction works on the river bend was found by physical model testing.

Hydraulic design of the abstraction works:
- The intake wall is about 20 m high and designed for the 100 year flood of 13500 m^3/s with freeboard. The intake without a trashrack is submerged at the high intake wall at the boulder trap, to limit floating debris reaching the trashracks. The curved high concrete wall creates secondary flow patterns which causes local scour upstream of the intake slot during floods. This scour is required during floods when the tailwater levels are too high to flush this intake area under gravity. The wall should be designed not to be overtopped during the 100 year flood.
- The slot (orifice) in the curved wall is designed for 0.4 m/s flow velocity at peak pumping rate of 1.4 m^3/s. The slot height is 0.4 m. The soffit of the slot is at the Minimum Operating Level (MOL), which is at the low notch crest of the weir. With the IFR passing over the weir under normal flow conditions and during floods, the slot will be under water. This is to prevent floating debris from entering the abstraction works and is the best way of protecting the trashracks.
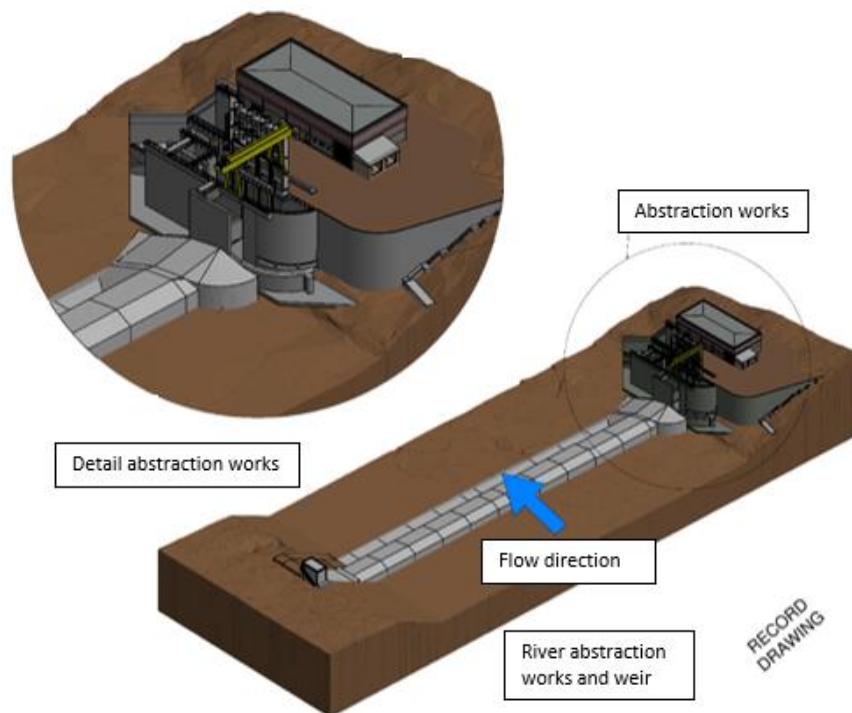
Figure 3. Three dimensional views of the Lower Thukela abstraction works and weir
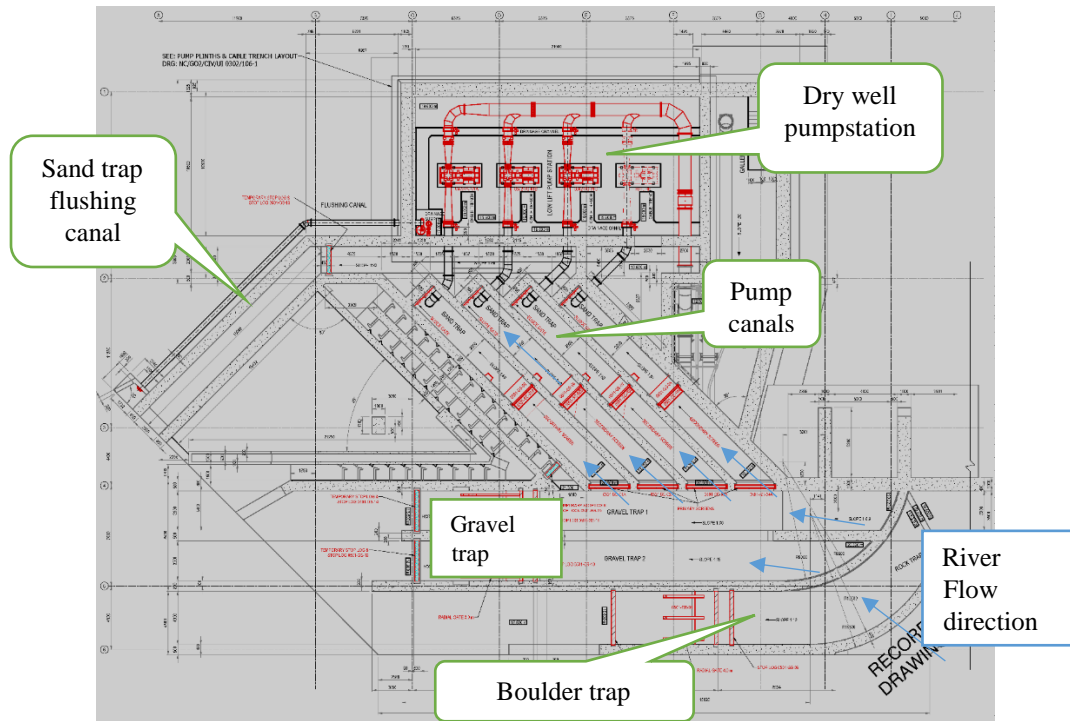
Figure 4. Plan layout of the final detail designed abstraction works

- Due to the weir, scour by secondary currents during small floods could be limited at the intake slot. A flushing canal has been provided upstream of the high wall and slot, called a "boulder trap". The boulder trap is 4 m wide and has a steep bed slope of 1:12. At the upstream end of the boulder trap a low weir accelerates the flow to be supercritical during flushing. It is required to flush sediment from this trap following a small flood which did not scour the area upstream of the intakes. At its downstream end a radial gate controls the flushing. The left wall of the boulder trap has a negative slope to ensure effective flushing of the boulder trap. The flow velocities in the boulder trap are high due to the 1:12 steep bed slope and therefore the flow is supercritical in the boulder trap even for relatively large river flows. At higher river discharges when the flow becomes subcritical in the upper part of the boulder trap, the flow velocities are still high enough for effective flushing.

- The gravel trap with dividing partially submerged wall during normal operation, has bed slopes varying from 1:15 to 1:20 to remove sand and gravel quickly during flushing when both gates are opened. The ideal flow velocity during flushing is above 4 m/s in the boulder and gravel traps. The gravel trap, situated behind the high wall and its slots, is 6.8 m wide, and consists of two 3 m wide canals. The two canals have a dividing wall between them which is partially submerged at MOL when pumping. The role of the dividing wall is to deflect the water from the slots during flushing, which act as an orifice, to improve flushing of the gravel trap. The two canals of the gravel trap have different slopes. At the downstream end of the trap two 3 m wide by 3 m high radial gates allow flushing of the gravel trap.

- The trashracks are on the right bank side of the gravel trap. A trashrack at a 15 degree angle to the vertical was considered, but the final design has vertical racks which can be raised for cleaning. The invert level of the trashrack is high enough to allow flushing of the gravel trap. The trashrack was constructed from vertical flat bars 50 x 10 mm, with

40 mm openings between bars. The trashrack could also be cleaned by a mechanical rake. 50% blockage of the openings of the trashrack has been allowed for in the design. The flow velocity through the trashrack at 1.4 m³/s and at MOL, with an unblocked scenario is 0.3 m/s.

- Four concrete sand trap canals have been designed based on a maximum discharge of 0.47 m³/s in each canal. The required length of the sand trap is 20 m. The sand trap canals have bed slopes of 1:80 to allow flushing of sand and gravel under gravity. The flow velocities in the sand trap are less than 0.2 m/s at MOL to trap sediment larger than 0.3 mm in diameter. Each sand trap canal is 2.0 m wide. Concrete benching is required at the bottom corners of the canals to improve flushing at low river flows. Fine screens are located in each pump canal with vertical and horizontal bars and 40 mm openings.

Hydraulic design of the weir:

- The weir is a truncated Crump weir, with a proposed upstream sloped section (1:2) having a length of 4 m, and the downstream sloped section (1:5), with a length of 8 m in the flow direction.
- The weir is about 5.3 m high and about 160 m long across the river. At the abstraction works at the right bank side the low notch also acts as structure for eels. The weir is designed to measure flow during small floods. The weir is relatively high specifically to ensure the sediment traps can be flushed effectively during small floods by opening gates. Note that it is not a design requirement for the flushing to flush sediments from upstream of the weir, but rather only the immediate zone at the intake need to be flushed. The sedimentation of the weir will therefore reach equilibrium within the first flood season and the bed level will typically build up as high as 0.5 m from the crest of the Crump weir.
- The low notch of the weir is next to the boulder trap. The crest of the low notch determines the minimum operating level at 21.33 masl. The low notch length was planned to be 10 m, with a step up to the next notch of 0.5 m (later modified to incorporate the eelway). The weir has 3 notches (from left bank to right bank): 120 m long at 22.38 masl; 30 m long at 21.88 masl; 10 m long at 21.33 masl. The bed level at the weir is at 16 masl, at the river bend.
- The weir is 5.3 m high in the main channel, but much lower on the floodplain. Outside the main channel the weir is relatively lower and less than 4.4 m high above the floodplain. The weir height is required due to the minimum pump operating head and sand trap flushing requirements.
- The weir site is located on solid rock. Since the bedrock is of good quality, no energy dissipation structure was required.

Sediment flushing durations and sequence:

- Expected flushing duration of the components: boulder trap, gravel trap and each sand trap canal should be less than 20 minutes each. The sediment is flushed back to the river from time to time as required and not continuously. The impact on the river downstream is therefore limited and the relative sediment volume that could be flushed small. The sand trap is therefore actually a "settler". During pumping operations clear water from the sand trap is abstracted at the downstream ends of the sand trap canals.
- In general the sequence of sediment flushing during small floods should be as follows: boulder trap, then gravel trap, then pump canals one at a time, from downstream to upstream. This is to ensure that no sediment is transported from one trap into another during flushing.

- Both gates of the gravel trap should be opened during flushing.
- None of the boulder, gravel or pump canal gates are opened during medium to large floods due to the high tailwater levels, which will make flushing less effective. These traps can however be flushed during small floods typically when the river flow is less than say 1100 m³/s. During floods larger than 3000 m³/s the secondary currents make the intake zone at the boulder trap self-scouring.

Mechanical equipment within the abstraction works:
- Vertical gates were installed upstream of each sand trap canal to control flushing flow and to shut off a canal for maintenance if required. Fine screens were installed at the gate positions as a second line of defense when the trashrack is cleaned. The fine screens are placed vertically and can be raised to clean. These screens must be raised prior to flushing of the pump canals. A trash basket was added at the bottom and upstream end of the fine screen to trap debris when the screen is raised. The fine screens have openings of 40 mm x 40 mm, and height of 2.62 m.
- The pumps, in this case a dry well design, were selected to be robust to deal with coarse sediment from time to time, to remove particles that can pass through the fine screen. The abstraction works was designed for a maximum pump discharge of 1.4 m³/s. There are three normal duty and one standby pump. Based on the typical hydraulic design requirements as specified by Sulzer, the pump intake design would be as indicated in Figure 5. The minimum water depth at the intake is 2.25 m for a total pump discharge of 1.4 m³/s. This specific design is for a dry well configuration. The intake design was later optimized in the laboratory with the bell located 0.9 m above the floor to allow free flow flushing. The pumps should be able to handle coarse sediment up to 40 mm in diameter if required, but a sand trap upstream of the pumps should remove the sand and gravel (d > 0.3 mm) most of the time.
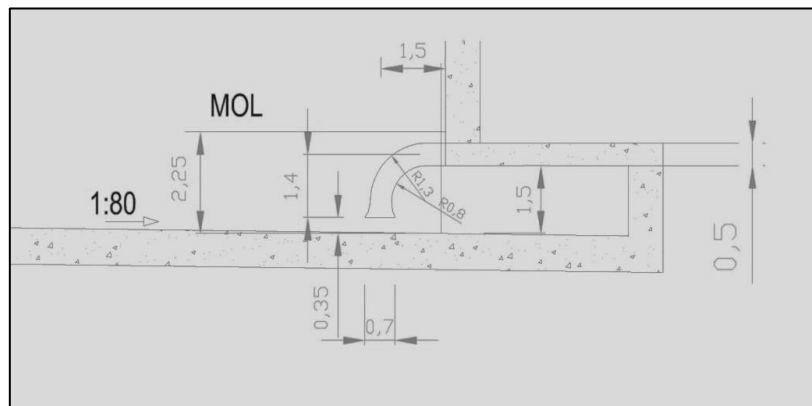
Figure 5. Elevation of typical pump intake to pump 1.4 m³/s (with 3 pumps)

Accessibility for operation:
- Access for operators on foot from the left bank to right bank of the river is made possible by gallery through the concrete weir. The gallery also contains the low lift pipeline to the water treatment plant. In practice it was found that black mamba snakes which are highly venomous, enter the gallery and for safety 5 people are needed to walk through the gallery at any one time, for in case one is bitten, 4 colleagues have to carry him/her out.
- There is a right bank access road 5 km in length with a bridge across the river which links the abstraction works with the water treatment plant.

A fishway (vertical slots) was designed with downstream entrance on the right bank side of the gravel trap, and upstream entrance in the gravel trap. An eelway was designed on the low notch of the weir by making the concrete rougher (Figure 6).

Figure 6. Eelway viewed from downstream

Physical model tests

The optimum location of the abstraction works on the river bend was found by physical model testing. The specific river bend was selected because of the secondary currents at the outside of the bend which would limit coarse sediment abstraction and the bend sites were close to the proposed water treatment plant on the inside of the bend. A distorted scale model was constructed to evaluate 3 possible sites. Model scales of 1:120 (H) and 1:40 (V) were selected for a 4.2 km reach of the river to identify the most suitable site (Figure 7). Movable bed conditions were simulated in the laboratory to evaluate local scour at the possible intakes (Figure 7). These tests were carried out for a range of annual recurrence interval floods from the 2 year to the 100 year flood of 1400 to 13500 m³/s respectively. From the physical model test results and a cost analysis the bend site resulted in the least expensive site, mainly due to the much shorter weir length required. The physical model tests also indicated that the bend site with a weir, gravel trap with a high wall and sand trap would abstract the least coarse sediment. This is the preferred site and design scenario, therefore it was tested further in an undistorted model.
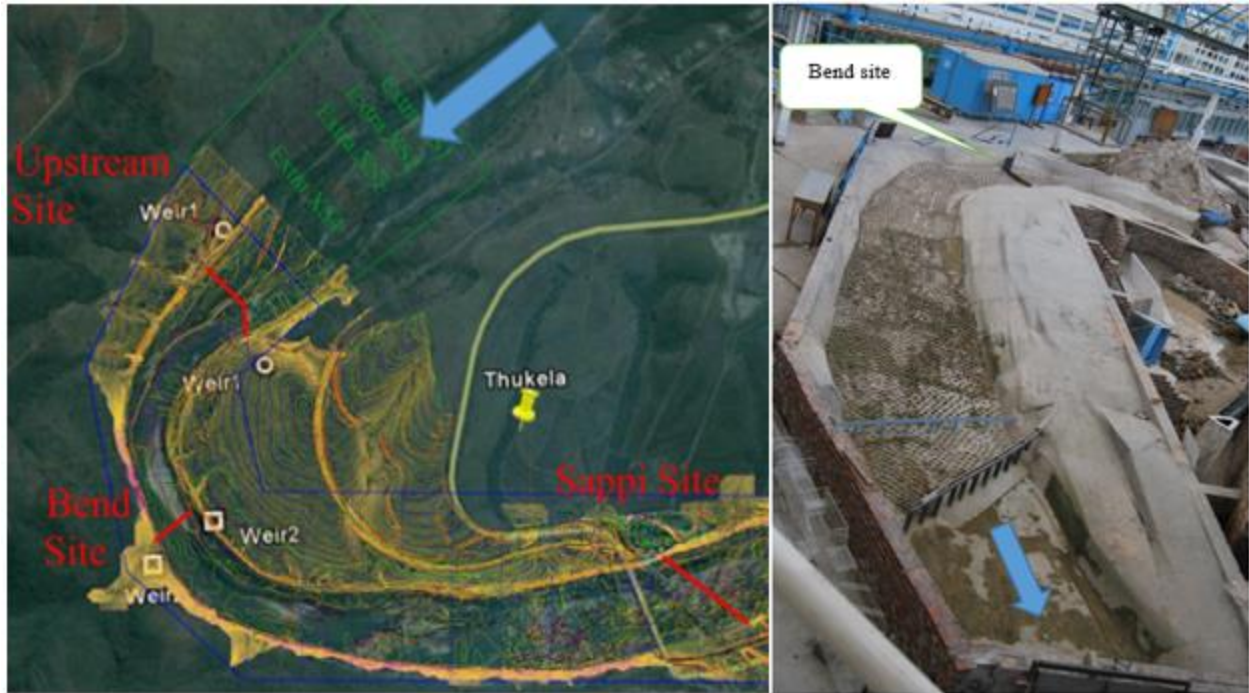
Figure 7. Plan layout of physical model area (distorted scale model) (left) and a view of the distorted scale model looking upstream (right)

The final selection of the bend site was based on calculations of the estimated sediment abstraction, especially what the pumps will have to deal with (Table 1). The bend site was found to be the best site as less sediment was pumped at this site. More detailed physical model testing was carried at this site by using a 1:40 undistorted model scale (Figure 8). Low flows of 25 m³/s to the 5 year flood of 3000 m³/s were tested. These tests with movable bed conditions investigated firstly the self-scour of the intake during floods with all the trap gates closed, followed by sediment flushing tests during smaller flows/floods of each sediment trap.

Table 1. Thukela abstraction works scenario and sediment abstraction: mean annual sediment abstraction at pump rate of 3x0.467=1.4 m³/s

Design scenario	Upstream site	Bend site	SAPPI site
• River abstraction works with gravel trap and high intake wall as well as trash racks which are protected. • The abstractions works' pump canals can be flushed. • A weir is required.	Total sediment pumped: (t/annum)		
	36481	34534	37844
	Sand and gravel pumped: (t/annum)		
	644	155	2144
	Flood total sediment pumped: (t/day)		
	596	528	643
	Flood total sand pumped: (t/day)		
	121	53	168

Figure 8. Plan layout of the undistorted model of the abstraction works and weir

Physical model tests were carried out to find the discharge at which the tailwater levels surpasses the low notch elevation at the weir. This was to evaluate possible submergence of the outflow conditions of the sediment traps when they are flushed. When these traps are submerged due to high tailwater levels a hydraulic jump forms in the trap with slower flow velocities and less efficient flushing of the sediments from the traps. The discharge and corresponding tailwater water level graph can be seen in Figure 9. The water level reaches the low notch level (minimum operating level) at the weir at a river discharge of about 1200 m³/s. From the historical flow records of the river this discharge has been exceeded for a maximum period of 8 consecutive days in the past, but on average the exceedance duration is less than 1 day, so the potential risk of not being able to flush the sediment traps efficiently during flood flow conditions is small.
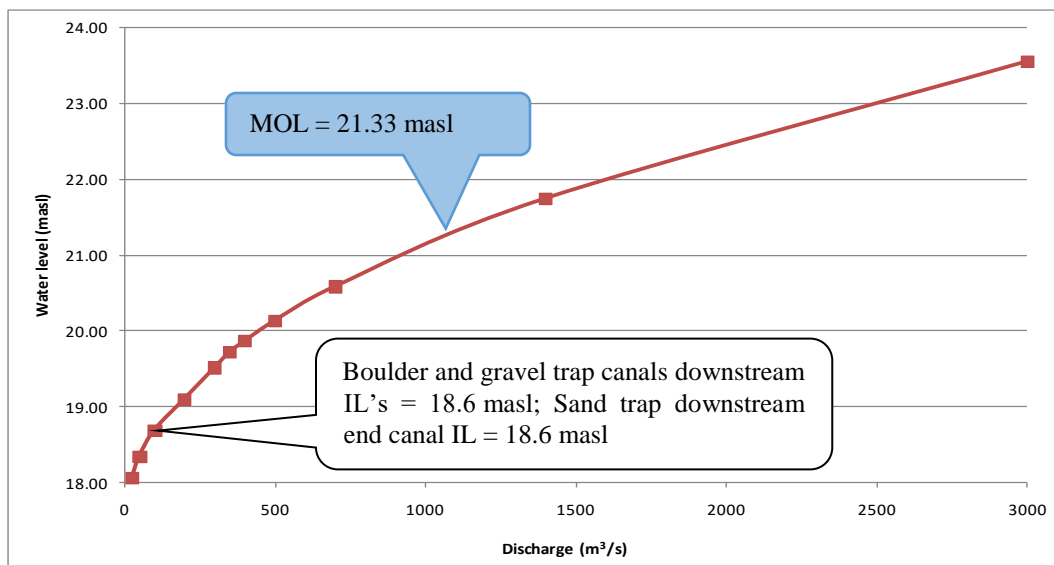
Figure 9. Weir tailwater levels

Local Scour at the Intake and Sediment Flushing Tests

Local scour of the boulder trap: Bakelite was used as movable bed to simulate sediment in the field, which is more representative of sand in the field. The boulder trap was filled with sediment at the start of the tests level with the invert level of the submerged slot, which is 0.4 m below the low notch crest of the weir. The scour patterns for different flows measured from upstream to downstream along the curved wall where the slot is located, is shown in Figure 10 (without opening the gate). As seen in Figure 10, deeper scour develops at river flows above 350 m³/s and the boulder trap area upstream of the slot would be self-cleaning at river discharges exceeding this discharge (with all gates closed). From the physical model tests it was found that at a river discharge of 3000 m³/s, a 5-year annual recurrence interval flood, all the sediment was scoured in the boulder trap. At the downstream end of the slot some sediment was deposited during larger floods, but this would not affect the functioning of the submerged slot. The radial gates at the gravel trap could also be used to remove this sediment.

Flushing of the boulder trap: Flushing of the boulder trap was carried out for different river flows by opening the gate. It was found that up to 3000 m³/s river flow, the boulder trap could be flushed effectively. At larger floods the secondary currents would scour the sediment even with the boulder trap gate closed. The boulder trap design was optimized for flushing by considering a negative slope on the left side wall of the boulder trap, and a weir at the upstream end of the boulder trap. The low weir ensures super critical flow at low flow flushing.
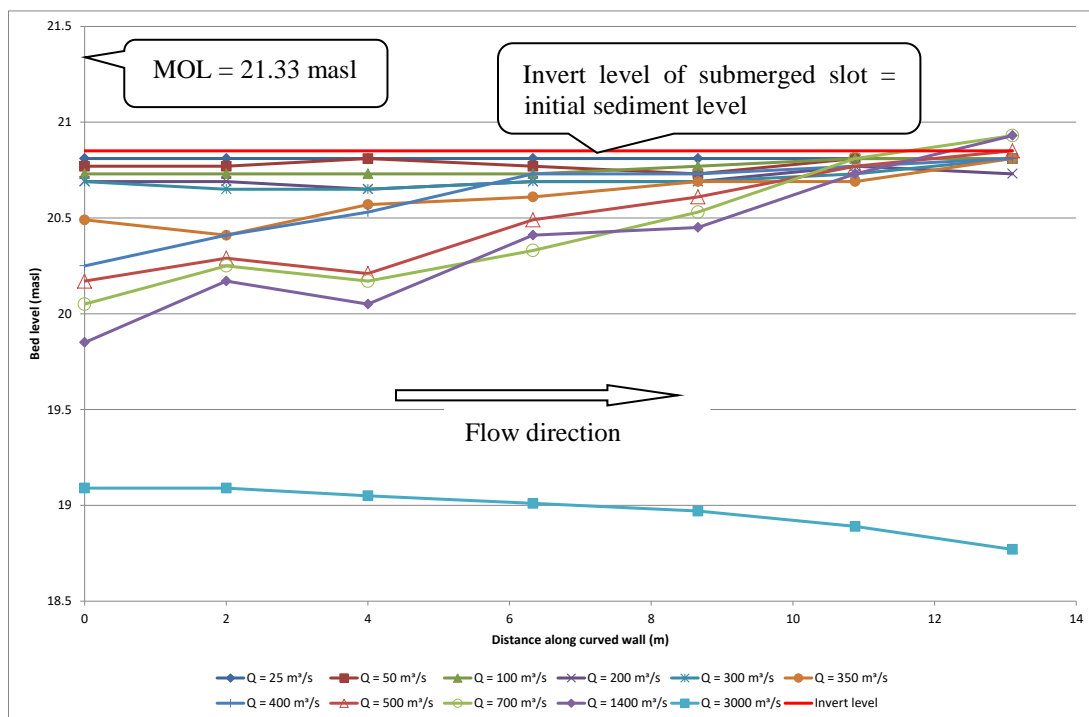
Figure 10. Scour pattern with sediment recorded along the submerged slot at the boulder trap (all gates closed)

Flushing of the gravel trap: Flushing of the gravel trap was tested by using Bakelite to evaluate whether the proposed design is effective. Both gravel trap gates were opened together during each test and the correct tailwater level was set corresponding to the river flow. The trashrack invert level is exceeded when flushing at a river discharge of about 1100 m³/s. Free

outflow at the gravel trap gates is possible at smaller river flows than 1400 m³/s. Flushing of the gravel trap at higher river flows was however found effective. The flushing of the gravel trap is shown in Figure 11.

Flushing of the pump canals: The maximum discharge per sand trap canal with a flow depth of less than 1.5 m, equal to the gate opening height downstream of the pump intakes, is 15 m³/s, but a sand trap canal can be flushed at river flows as low as 1 m³/s. The sand trap canals can be flushed from time to time, one at a time, up to a river discharge of 700 m³/s with supercritical free outflow conditions. During higher river flows the tailwater could cause subcritical flow conditions in the sand trap which would decrease flushing efficiency.

Figure 11. Flushing of the gravel trap at a river discharge of 300 m³/s

Abstracted Sediment Load

The proposed abstraction flow rate at the Thukela pumpstation is 100 Ml/d (average 1.157 m³/s; peak 1.4 m³/s), which was phased with 50 Ml/d installed initially (average 0.579 m³/s; peak 0.7 m³/s). During the period 1971 to 1984 suspended sediment data was collected from the Thukela River at flow gauging station V5H002, which is located a short distance upstream of the abstraction works site. By plotting the data as sediment load (concentration times discharge), versus discharge in the river at the time of sampling, the sediment load rating curve shown in Figure 12 was obtained. To account for bed load and non-uniformity in the suspended sediment concentrations across the river, the observed suspended sediment grab sample concentrations were increased by 25%, based on historical sediment transport measurements during floods in South Africa.

The highest sediment concentration recorded over this period occurred in 1972, with a concentration of 42600 mg/l at a relatively low river discharge of 507 m³/s. The scatter in sediment concentrations (and loads) is large as shown in Figure 12. This is due to sediment availability limitations from the catchment. A line was fitted to the data which represents the first half of the flood season (red) which is slightly higher than the blue data of the second half of

the season data, when sediment from the catchment is less available. The fitted line based on the red data was used throughout the year in this assessment of abstracted sediment loads due to the changes in land use which occurred since the river sediment data of Figure 12 was obtained (1971 to 1984).
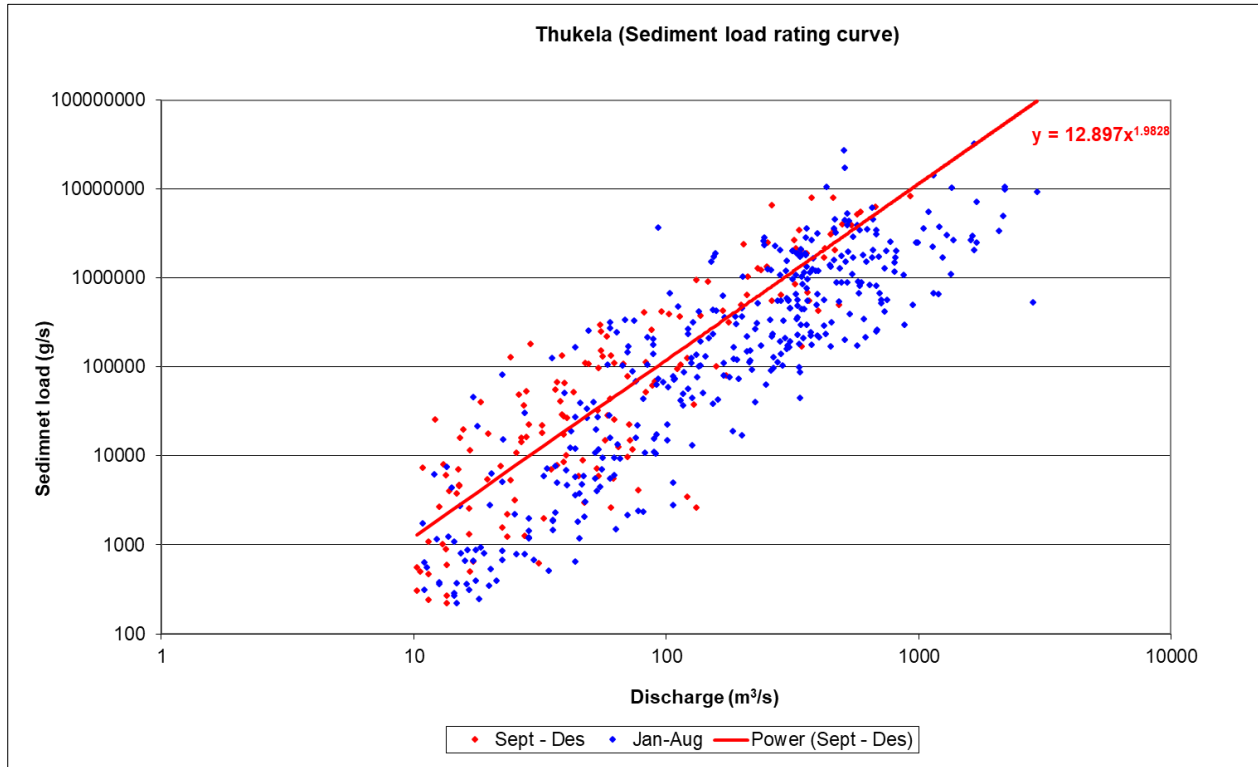
Figure 12. Observed sediment load-discharge rating curve on the Thukela River at the upstream gauging station (V5H002)

At an average abstraction rate of 100 Ml/d at the river abstraction works located at the bend site, the sediment loads abstracted are as shown in Table 2.

Table 2. Abstracted sediment loads at river pump station

Description	Sediment loads abstracted from the river
Total sediment pumped (clay, silt, sand and coarser)	34534 t/annum on average
Sand and gravel pumped	< 155 t/annum on average
1:10 year flood total sediment pumped	528 t/d on average during flood; sand pumped 53 t/d

Field Measurements during Flushing of the Sediment Traps

The boulder trap, one gravel trap and one pump canal were flushed during field work in January 2018 shortly after commissioning of the works. At the time of the field work the flood season has not started and the river flow was about 40 m^3/s. Pre-flush bed grab sampling indicated 5 micron median size deposited sediment (cohesive) in the boulder trap and 1.6 micron at the pump intakes. Suspended sediment samples were taken every 2 minutes for a total of 10 minutes during flushing at a location immediately downstream of the trap gates. The observed sediment

concentration results are shown in Figures 13 to 15 for the boulder trap, gravel trap and pump canal respectively. It was observed that the boulder trap and gravel trap flushing took approximately 5 minutes, and 4 minutes was needed for the pump canal. The highest sediment concentration was recorded at the pump canal at 10,800 mg/l. The sediment volumes flushed were not large because the traps had limited sediment deposition at the start of the flood season and the sediment particles were mainly clay and silt. In general the flushing of the traps was found to be highly effective as designed.
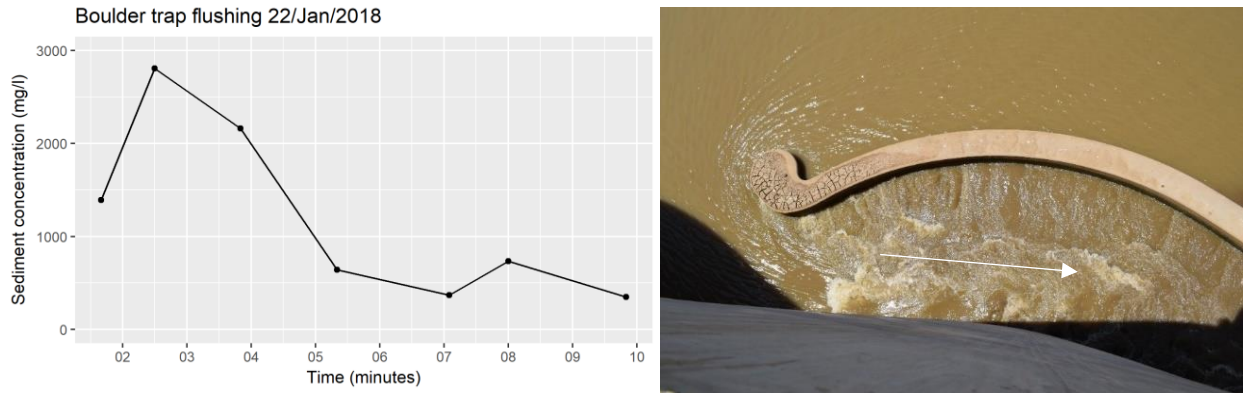
Figure 13. Observed outflow sediment concentrations for the boulder trap flushing
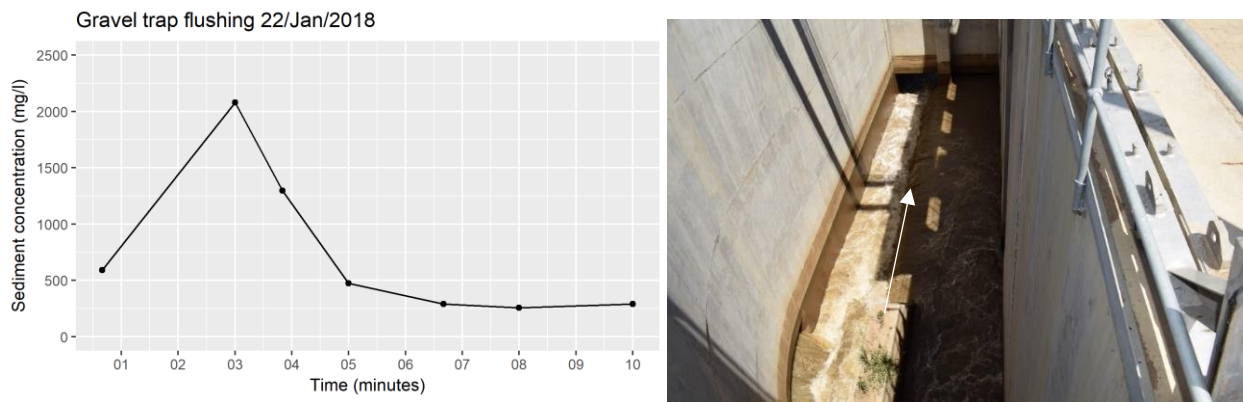
Figure 14. Observed outflow sediment concentrations for the gravel trap flushing
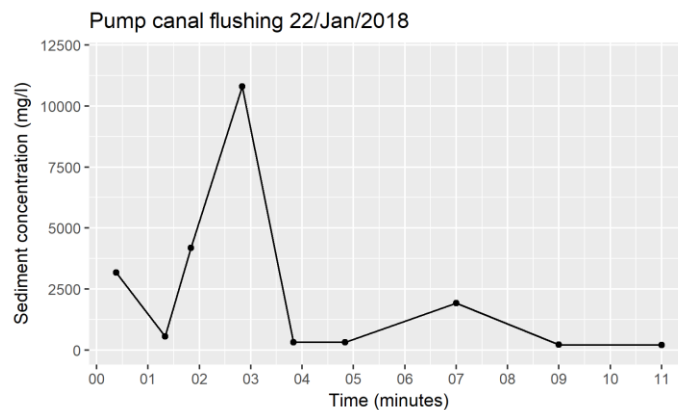
Figure 15. Observed outflow sediment concentrations at pump canal flushing

Conclusions

Regional potable water supply schemes require a high assurance of supply and the river abstraction works has often been found to be the most critical component. This paper discusses a case study on the Lower Thukela River in South Africa. Following many years of careful research with physical model testing and validation by field measurements, a suitable river abstraction works hydraulic design was found. Key characteristics of the hydraulic design are:

- Identification of a suitable site at a river bend where the secondary currents ensure local scour of the intake zone and bedload is transported away from the intake
- A high intake wall curved to improve local secondary currents during floods and protruding into the river away from the river bank. The high wall is typically designed to provide access during a 100-year recurrence interval flood.
- Sediment flushing traps such as boulder, gravel and sand traps and pump canals, which can be flushed from time to time as required during small floods. Flushing durations of each trap are less than 20 minutes each. Average downtime due to flushing operation is estimated at 0.3 % or 1 day per year.
- Self-scour of the intake zone without opening any gates during medium to larger floods.
- No need for a barrage design with gates across the river; instead an uncontrolled low weir design is used and flushing gates only at the abstraction works to flush locally. A barrage with many flushing gates has maintenance and operational issues and has caused fish kills due to flushing of anaerobic sediments in the past.
- A fishway/eelway can be integrated with the abstraction works design.

In general, the hydraulic design of the abstraction works is robust, with limited maintenance requirements. Umgeni Water has decided to standardize the design for all its future regional schemes so that operators and spare parts are easily interchangeable between plants.

Acknowledgements

References

Basson, G. R. (2006). Considerations for the design of river abstraction works in South Africa (Vol. II). WRC Report NO TT 260/06.

Basson, G.R. (2012). Lower Thukela Bulk Water Supply Scheme. Hydraulic Design and Modelling of the Proposed Lower Thukela River Abstraction Works. Umgeni Water.

WRC. (2002). The extraction of water from sediment-laden streams in Southern Africa. WRC Report NO: 691 /2/02.

Managing Infrastructure in the Stream Environment

Joel Sholtes, Instructor, CMU/CU Boulder Civil Engineering, Grand Junction, CO, jsholtes@gmail.com

Caroline Ubing, Hydraulic Engineer, Bureau of Reclamation, Denver, CO, cubing@usbr.gov

Timothy Randle, Hydraulic Engineer, Bureau of Reclamation, Denver, CO, trandle@usbr.gov

Jon Fripp, Civil Engineer, USDA-Natural Resource Conservation Service, Fort Worth, TX, jon.fripp@ftw.usda.gov

Dan Cenderelli, Hydrologist, U.S. Forest Service, Fort Collins, CO, dcenderelli@fs.fed.us

Drew Baird, Hydraulic Engineer, Bureau of Reclamation, Denver, CO dbaird@usbr.gov

Introduction

Infrastructure in the stream environment provides indispensable services required for the development and operation of our nation's economy. However, much of the infrastructure in the U.S. was built when fluvial processes and stream ecology were not well understood, putting it in conflict with the stream environment. High maintenance costs are often required to operate such infrastructure. Some of it has led to degradation of fluvial ecosystems. The information presented in this extended abstract has been published as a comprehensive guidance by the Advisory Committee on Water Information, Subcommittee on Sedimentation, Infrastructure and Environment working group (Sholtes et al., 2017, https://acwi.gov/sos/pubs/managing_infrastructure%20_in_the_stream_environment.pdf) and as an article by the Journal of the American Water Resources Association (Sholtes et al., 2018). The intention of these publications is to educate infrastructure designers and managers on how to build and manage infrastructure that is more immune to riverine hazards and is less damaging to the local ecosystem. We intend to accomplish this goal by introducing well-studied concepts on physical and ecological stream processes, discussing common problems and proposing solutions associated with eleven types of riverine infrastructure, and introducing a decision-tool, which outlines steps to replace, repair, remove old infrastructure and to build new infrastructure. Finally, the papers conclude with a discussion on best practices for managing infrastructure under hydrologic uncertainty and rebuilding after a natural disaster. "We provide managers and designers with the knowledge and tools to begin the conversation about how to best manage riverine infrastructure, increase their resiliency, and improve stream ecosystems." (Sholtes et al., 2018).

Management Options and Decision Tools

Management Options: Management challenges and solutions associated with 11 types of riverine infrastructure and channel or floodplain modification were presented in both published papers. Riverine infrastructure is defined broadly in these publications "[...] to include a spectrum of human activities in the stream corridor that fall under the umbrella of public works, stream engineering, and stream management" (Sholtes et al., 2018). These types can be separated into

three categories: channel and floodplain modification (e.g., stream channelization, weirs), stream crossing infrastructure (e.g., bridges, culverts, pipelines), and streamside infrastructure (e.g., streambank protection, dikes, levees).

Decision Tool: Both papers published a decision tool flowchart to provide a framework for considering sustainable and resilient approaches to infrastructure design and management (Sholtes et al., 2017 and Sholtes et al., 2018). The first stage includes project planning where the following topics should be explicitly addressed: project purpose, goals, and scale. Social, economic, and ecological values should be identified by speaking with local stakeholders and consulting existing watershed studies. Regulatory requirements should also be identified. Watershed plans can provide context for infrastructure operation and management within the existing ecological system to prioritize capital improvement and restoration work (USFS, 2011).

The second stage recommends evaluating the project based on its exposure to fluvial and ecological impacts. A hazard assessment, performed by an experienced fluvial geomorphologist, can identify how flooding and potential stream migration may put the project at risk. The evaluation may consider the prevalence of protected species along with existing recreational, economic, and cultural values associated with a stream corridor.

Alternative designs are formulated in the third stage, focusing on new and existing infrastructure. Environmental impacts to the river system should be avoided or minimized during the development of new infrastructure (ex. widening a bridge span to accommodate meander migration and flood flows). Where hazards cannot be avoided, alternatives should include a maintenance plan and budget. Opportunities to restore upstream or downstream riverine corridor should be explored to mitigate hydrologic and ecological impact. Damaged or aged infrastructure may be rehabilitated, replaced, relocated, or removed. In conjunction with these efforts, an opportunity for restoring stream or riparian habitat may exist.

The final stage of the flowchart recommends evaluating alternatives in terms of feasibility, costs, benefits, hazards, and risks. We recommend final decisions are reached by stakeholder consensus with the aid of decision-making tools (Martin et al., 2016). Sholtes et al., 2018 provides an example of how watershed master planning aided the flood recovery efforts after the devastating 2013 Colorado Front Range flood.

1. Identify Project Goals and Scope

Identify the issue(s)

Determine:
- purpose,
- scale,
- goals,
- constraints, &
- values
- permitting

Is the project part of a larger infrastructure **master plan**?

— yes → Does the master plan include **stream processes**? — yes →

no ↓

no ↓

Consider developing a master plan incorporating stream processes
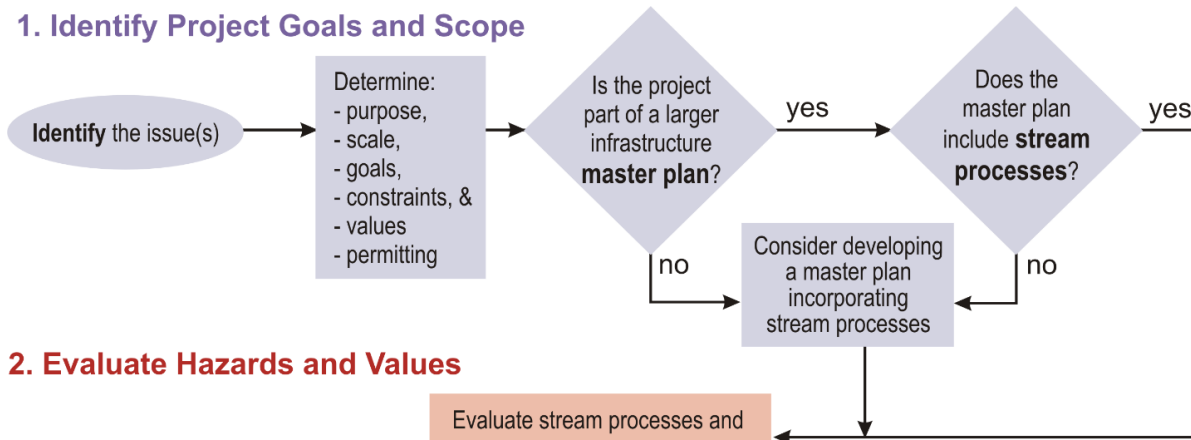
2. Evaluate Hazards and Values

Evaluate stream processes and Perform **Hazard Assessment**

Avoid Hazard / Waterway?

— yes → **Avoid** Stream Impacts

no ↓

3. Formulate Alternatives

Formulate Alternatives

New Infrastructure

Existing Infrastructure

New Infrastructure?

yes ← | → no

Mitigate impact with **Off-Site Rehabilitation**

Minimize impact

Relocate & rebuild

Replace existing infrastructure

Improve existing design and repair

Remove infrastructure & rehabilitate

4. Evaluate Alternatives, Decide, Implement

Identify:
- risks,
- benefits, and
- opportunities

Evaluate:
- engineering feasibility,
- economic benefit,
- environmental benefits

Decide & Implement
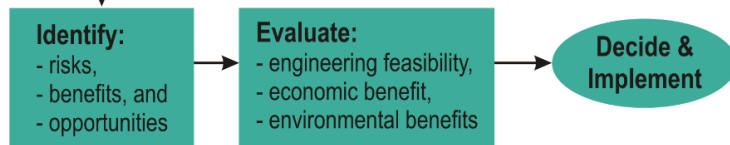
Figure 1. Decision tool flowchart for managing river infrastructure (Sholtes et al., 2017).

Managing Riverine Infrastructure Under Uncertainty

"Infrastructure design in stream environments often relies on estimates of design flows and sediment yield. These estimates are subject to uncertainty due to an imperfect or relatively short data record, uncertainty in deterministic modelling, as well as changing hydrology under climate and land-use change." (Sholtes et al., 2018). Engineers often apply safety factors to ensure the longevity of their design and safety of its users. While some factors of safety decrease hazard exposure (taller and/or wider bridges, larger floodplain setbacks for a project footprint). Other approaches may conflict with natural stream systems (larger riprap), which can result in higher maintenance costs in the long term. Sholtes et al. (2017 and 2018) presents a risk management approach which includes: incorporating tolerances into the design, designing for a range of projected conditions, analyzing future climate and hydrologic conditions in the area of interest, and employing adaptive management.

Flood Disaster Response and Recovery

When large floods compromise infrastructure and surrounding communities, it provides an opportunity to replace the damaged infrastructure with that which is more compatible with natural stream processes to better survive future floods. Sholtes et al., 2018 suggests that permitting and funding agencies be more flexible with post-disaster recovery efforts. "Providing incentives and funding to incorporate resiliency into the reconstruction process will enhance public safety and reduce reconstruction costs for the next flood. An overall lack of literature on regulatory limitations to "building back better" (Kim and Olshansky, 2015) post-disaster indicates this is a ripe area for research and action." (Sholtes et al., 2018).

Summary and Conclusions

This extended abstract is based on two previous publications: a comprehensive guidance (Sholtes et al., 2017) and a journal article (Sholtes et al., 2018). We present information to better understand the stream environment along with advice to better build and manage infrastructure that is economically, socially, and environmentally sustainable. We suggest a decision tool for managing riverine infrastructure that "integrates it into a watershed-scale master plan considering physical and ecological stream processes, ecological restoration goals, and hazards" (Sholtes et al., 2018). As infrastructure ages and is damaged during large events, it is an opportune time to build infrastructure that is more resilient to riverine hazards, decrease maintenance costs and preserve valuable riparian ecosystems.

References

Kim K. and Olshansky, R. B. 2014. "The theory and practice of building back better." Journal of the American Planning Association 80(4): 289-292.

Martin, D. M., Hermoso, V., Pantus, F., Olley, J., Linke, S., & Poff, N. L. 2016. "A Proposed Framework to Systematically Design and Objectively Evaluate Non-Dominated Restoration Tradeoffs for Watershed Planning and Management." *Ecological Economics* 127:146-155.

Sholtes, J. S., Ubing, C.U., Randle, T. J., Fripp, J., Cenderelli, D., and Baird, D.C. 2017. "Managing Infrastructure in the Stream Environment." Advisory Committee on Water Information,

Subcommittee on Sedimentation, Environment and Infrastructure Working Group. 65p. https://acwi.gov/sos/pubs/managing_infrastructure%20_in_the_stream_environment .pdf

Sholtes, J. S., Ubing, C.U., Randle, T. J., Fripp, J., Cenderelli, D., and Baird, D.C. 2018. "Managing infrastructure in the stream environment," Journal of the American Water Resources Association, 54(6):1172-1184.

U.S. Forest Service (USFS). 2011. "Watershed Condition Framework." FS-977. Washington, DC. 34p. https://www.fs.fed.us/biology/watershed/condition_framework.html

Pipeline Ephemeral Channel Crossing Fluvial Hazard Analysis

Drew C. Baird, Hydraulic Engineer, Technical Service Center, U.S. Bureau of Reclamation, Denver, CO, dbaird@usbr.gov,

Michael Sixta, Hydraulic Engineer, Technical Service Center, U.S. Bureau of Reclamation, Denver, CO, msixta@usbr.gov, ,

Melissa Foster, Geomorphologist, Technical Service Center, U.S. Bureau of Reclamation, Denver, CO, mfoster@usbr.gov,

Joel Sholtes, Instructor, CMU/CU Boulder Civil Engineering, Grand Junction, CO, jsholtes@gmail.com,

Caroline Ubing, Hydraulic Engineer, Technical Service Center, U.S. Bureau of Reclamation, Denver, CO, cubing@usbr.gov

Abstract

Underground pipelines containing water, crude oil and other petroleum products cross underneath channels with perennial, continuous and ephemeral, intermittent, flow. Ephemeral channels that experience runoff from episodic, intense rainfall can become dynamic during floods, resulting in channel bed and bank erosion. Associated fluvial hazards may include short-term general scour with potential re-deposition and long-term channel degradation, bank erosion, and lateral migration. Additional pipe burial depth extending some lateral distance underneath ephemeral channels is needed to prevent pipe exposure and the potential for pipeline failure. Determining general scour, long-term degradation and lateral migration for dynamic, ephemeral channels is difficult to accomplish and highly uncertain due to a lack of widely applicable models. Evaluating these fluvial hazards requires the application of geomorphic field assessments, empirical scour depth estimates and historical aerial photography inspection. We compiled procedures from multiple projects evaluating fluvial hazards where pipelines cross ephemeral channels. A risk-based approach is presented, and best practices outlined to estimate pipeline burial depth and lateral extent and reduce risk of pipeline exposure and failure at stream crossings.

Introduction

The most efficient way to transport and deliver potable water, gas and oil is through pipelines; burial is the most common installation method for such pipelines. There are more than 2.5 million miles of pipeline across the U.S. and approximately 18,000 locations where these pipelines cross under rivers, streams and lakes (American Rivers, 2017). Potential hazards to pipelines from erosion exist at the intersection between waterways and pipelines (here referred to as a crossing). To mitigate these hazards, we have developed guidelines to help determine the appropriate depth and lateral extent of burial to protect pipelines from stream-related hazards, with a focus on ephemeral stream systems. These guidelines are being adapted from existing published methodology (ASCE, 2005) by compiling and modifying methods for the application to ephemeral channels. ASCE (2005) guidelines added together bend, general, bedform, long term degradation, and multiplied the total by a safety factor ranging from 1.1 to 1.5. Here we present the preliminary steps and assessments that are included in these guidelines, but caution that these are subject to change. One key modification from the ASCE (2005) methodology is that either general or bend scour calculations are applied, not both because general scour in bends is included in bend scour methdologies. In addition, a new degradation-analysis

methodology was developed because threshold channel methods found in Pemberton and Lara (1984) aren't typically applicable to alluvial ephemeral channel crossings. Historic channel morphology, anthropogenic alterations to the channel and local geology are also investigated to offer insight into past and potential channel incision and migration.

Ephemeral channels are common in arid regions. They flow intermittently but are often dynamic during floods, resulting in channel bed and bank erosion. There are few stream gages installed on such systems. Therefore, the link between hydrology and stream erosion is not well understood. The main stream-related hazards to pipeline alignments are scour, degradation and lateral migration. If pipelines are not buried deeply enough, each of these hazards can expose a pipeline, subjecting it to direct attack from hydraulic forces or debris during high flow events. Pipelines should be installed below the total scour depth; this burial depth should laterally extend along the pipeline alignment to cover potential channel widening or migration of the crossing. We compiled procedures from multiple projects evaluating fluvial hazards where pipelines cross ephemeral channels. A risk-based approach is presented, and best practices outlined to estimate pipeline burial depth and lateral extent and reduce risk of pipeline exposure/failure at stream crossings. In this paper we include a description of: 1) channel-related hazards to pipelines, 2) methods and analysis of scour and lateral migration 3) how to determine total pipeline cover depths and 4) lateral burial lengths.

Channel-Related Hazards to Pipelines

Scour is defined as the removal of sediment from the bed and banks of a channel by the flow of water (Warren, 2011; FHWA, 2012) and may occur as general scour or bend scour, or channel bedform scour. General scour is sediment removal generated by peak discharges, not associated with bridge piers or abutments, bank stabilization or cross channel structure scour. Dunes and anti-dunes (NRCS 2007) can result in additional bedform scour since they have a process of erosion and deposition. The passage of dunes may increase local scour depths by as much as 30% (NRCS 2007). Bedform is estimated as the dune or anti-dune height (ASCE 2005, PBS&J 2008). Scour may occur on the streambed during the rising limb of a flood hydrograph, continuing until the erosive capacity of the water is lower than the ability of the earth material to resist it. At that stage the maximum extent of scour has been reached (Annandale, 2006). Following the flood peak, sediments in transport may be deposited on the streambed, potentially infilling portions of the scoured bed. Therefore, a comparison of pre-and post-flood channel cross sections may not reveal the maximum extent of general scour. Consequently, the maximum extent of scour, rather than the net change in stream bed elevation, poses the greatest risk to pipelines. Recent pipeline impacts from scour include the 2015 failure of the Poplar gas pipeline underneath the Yellowstone River near Glendive, Montana. Scour unearthed the pipeline, releasing roughly 40,000 gallons of oil which contaminated local water supplies and harmed valuable fish and wildlife habitat (American Rivers, 2017). The Pipeline and Hazardous Material Safety Administration (PHMSA) has regulations for minimum pipe cover (PHMSA, 2019) in some situations. These guidelines contain methods to determine pipe cover or burial depth based on watershed characteristics, and channel properties. For water pipelines, there are most often local regulations defining minimum burial depth to prevent freezing. Pipelines crossing ephemeral channels most often need burial depth to protect against total scour than for freezing prevention.

Degradation is a long-term lowering of the channel bed due to erosion, over a relatively long channel length. It is typically caused by a lowering of the stream's downstream bed elevation, a reduction in upstream sediment supply, or an increase in surface runoff (FHWA, 2012). The

stream degrades because it is adjusting its bed slope toward a new equilibrium to match the changing sediment, runoff, or bed elevation control. Degradation can occur as an overall lowering in elevation that is applied to a large portion of the stream's longitudinal profile. Alternatively, degradation can occur due to the upstream propagation of a knickpoint (headcut), which is an abrupt vertical drop in the streambed profile. As the streambed erodes and lowers the knickpoint, channel incision propagates upstream (Wilcox et al., 2001). The channel profile downstream of the knickpoint is incised while the channel profile upstream of the knickpoint is not yet affected.

Channel degradation exposed a series of gas lines at an arroyo crossing in west-central New Mexico, leaving the gas lines suspended above the channel (Figure 1). This pipeline was likely originally buried about 5 ft. below the bed prior to the degradation shown in Figure 1. Degradation from propagating headcuts along ephemeral channels in the arid southwest are especially common.

Figure 1. Exposed gas lines as a result of channel degradation in New Mexico

Lateral migration, shifts in channel planform) and widening can also threaten pipelines, causing scour at pipeline locations that were previously outside the limits of erosion during the original design. As a generalization, bank erosion is low on straight and anastomosing channels, moderate on meandering channels and high on braided channels (Knighton and Nanson, 1993). However, sediment supply, water discharge and the erodibility of the bed and banks are key factors which control the lateral and vertical incision of channels and their subsequent channel patterns. For the ephemeral streams in the western United States that were the focus of this study, highly erodible bank material coupled with modifications to stream channels often resulted in the lateral movement of channels over the past few decades. Natural meander migration was also noted on several channels. To protect pipelines, it is important to consider

channel planform, historic channel movement and anthropogenic modifications to the channel to forecast the potential extent of a channel's lateral movement.

Figure 2. Active headcut creating an ephemeral drainage channel below it in New Mexico

Methods and Analysis

A preliminary assessment of the pipeline alignment can identify channel crossings and related hazards. Aerial imagery and coarse topography can provide preliminary determination of the channel morphology and geometry, which can indicate the types of analyses and data needed to determine vertical incision and lateral migration potential.

The next steps are to conduct a detailed analysis of the site to determine appropriate pipeline cover depths and lateral burial length to mitigate the risk of exposing the pipeline via lateral migration or general scour. Once the topographic data and aerial imagery have been reviewed, a field evaluation is recommended to confirm the channel's geomorphic form and provide sedimentary evidence. The results will inform the suite of hydrologic and hydraulic analyses that need to occur at each site. Finally, key variables from the hydraulic assessment serve as input data for empirical equations used to estimate event-based local scour and channel degradation.

Required data commonly include: (1) finalized pipeline alignment, (2) detailed topography (surveyed cross sections and longitudinal profiles or high-quality digital elevation models derived from LiDAR or photogrammetry), (3) geologic and historic topographic maps, (4)

historical aerial photographs or satellite imagery, (5) exploratory drill logs detailing subsurface material type and depth to bedrock and (6) surface and subsurface sampling and size gradation analysis for alluvial channel sediment. It is important to identify data gaps early in the process, as it may take time to acquire these data. Following are sections describing analysis methods: 1) analysis of maps, imagery and topography, 2) field assessment, 3) hydrology assessment, 4) hydraulics assessment, 5) event-based scour assessment and long-term degradation analysis.

Analysis of maps, imagery and topography: After preliminary site identification, stream channels should be cross-referenced with existing and historic aerial imagery, topographic maps and geologic maps.

Historic channel planform and lateral migration may also be assessed using the historical aerial imagery, where available. Satellite imagery from the 1990s through present is available from Google Earth, while earlier imagery may be downloaded from the USGS Earth Explorer (earthexplorer.usgs.gov). Digital imagery pre-dating the 1990s must often be georeferenced for use in GIS software. Channel morphology may be digitally mapped and compared through decades. Features which should be mapped include: the active channel morphology, areas of past erosion which may be re-vegetated in more modern imagery, the presence or absence of terraces, lateral channel migration, movement of channel meanders, locations of alluvial fans, and up- and downstream infrastructure which affects the channel alignment (including culverts or drainage ditches). Vertical incision and bank erosion are often visible in imagery and can often be useful to identify downstream headcuts that may propagate upstream to the pipeline. The imagery analysis should be used to identify how the channel has migrated in the past and features (such as small terraces) which are susceptible to erosion. Modern mapping should be confirmed through a field visit and from high-quality topography detailed in digital elevation models or survey data.

Recent detailed topography is used to extract longitudinal profiles along a channel, demonstrating how streambed elevation changes with distance downstream. These data can be used to identify or confirm headcut locations; longitudinal profile data are also used for subsequent degradation and scour analyses. Topographic data analysis should also indicate the width of in-stream terraces, width of any instream channels (along a cross section), the bottom channel width (across the channel, between the base of the right and left banks) and top channel width (between the tops of the right and left banks, above inset terraces or floodplains). These widths and features are used to help delineate the lateral extent of increased pipeline burial depths.

Geologic and maps available from the USGS (http://ngmdb.usgs.gov/maps/mapview/) should be used to determine if Geologic data and rock type are used to inform the depth of alluvial cover and resistance to erosion at crossing locations.

Field Assessment: The field assessment is used to confirm identified features, note the channel's geomorphic form (straight, anastomosing, meandering, braided) and collect field data. Stream channels should be investigated up and downstream of the pipeline alignment. In many cases, road crossings or grade control structures can limit the scope of the investigation. For example, if the pipeline alignment is located immediately downstream from a large highway crossing, there is likely little risk of lateral migration (assuming the highway crossing is properly

aligned and not at risk of failure). Alternatively, other features such as a native (dirt fill) road crossing can pose additional degradation risk; if the crossing were to wash out or be removed in the future, it could result in scour and degradation that may propagate upstream.

During the field assessment it is important to note the channel's current geomorphic form and any sedimentary evidence that the channel is approaching a threshold which could change its channel pattern, such as the initiation of meanders or braid development. Field mapping should note any areas with active erosion or deposition. Many sites that appear erosive on aerial imagery may actually be depositional and thus not pose a risk to the pipeline. Mapping should also include the location and measurements (height) of headcuts which may propagate upstream and affect the pipeline alignment. Bedrock outcrops and characteristics (i.e., erodibility) should be noted as related to lateral migration and degradation potential. Active springs, gullies through channel banks and other signs of erosion and sediment transport should also be noted. Field samples of alluvial material should be collected at sites that require scour assessments.

Hydrology Assessment: Basic criteria for evaluating pipeline hazards is the selection of structure design life and design flows and the required burial depth to prevent pipeline exposure during floods. The Federal Highway Administration (FHWA) recommends a risk-based approach for selecting the return period interval for scour determination. A 50-year design life can be used for many pipelines and a 100-year peak discharge recurrence interval is usually selected for the analysis of scour depth (ASCE, 2005). A 50-year peak discharge would have a 63.4% chance of exceedance during the design life of the pipeline, while there is a 39.5% chance that a flood will exceed a 100-year peak discharge during the 50-year period following construction of the pipeline (FHWA, 2012).

The National Resources Conservation Service (NRCS) method TR-55 (USDA, 1986) for determining peak flow hydrology for ungagged ephemeral channels provides the peak discharge associated with a return period of 100 years. Stream gage data is rarely available for these sites. Where gage data of sufficient length (eg. 50 to 100 yr) of record is available standard Log-Pearson Type III peak flow analysis (Viessman et. el., 1989) can be used.

Hydraulics Assessment: With peak discharge estimates from the design floods and a topographic survey of the crossing channel, hydraulic parameters for scour estimation can be computed. Cross sections and a longitudinal profile of the channel may be acquired utilizing both field survey data and high-resolution topographic data such as that collected from a LiDAR or photogrammetric survey. The 10-meter resolution National Elevation Model topography data are too coarse to be used in hydraulic analysis. A suitable channel roughness value should be determined from bed material size and channel properties to represent bed roughness.

Hydraulic methods include at-a-station analysis, one-dimensional (1D) hydraulic modeling such as HEC-RAS (USACE, 2016), or two-dimensional (2D) hydraulic model such as SRH-2D (Lai, 2008). For ephemeral channels that are sand bedded or with some gravel, using at-a-station analysis is usually sufficient because the bed slope tends to be relatively constant during high flows events. For gravel bedded channels with more defined riffles and pools, a 1D gradually varied flow model is more suitable given the longitudinal changes in slope and channel width associated with this morphology. A 1D model is also needed when there are downstream culverts that create backwater at high flows, downstream bridge crossings or other in channel structures. For more complex channel geometries with side channels, or complex contraction or expansion at bridges, a 2D model provides the most accurate representation of the flow field.

An at-a-station hydraulics or normal depth calculation requires a single cross section of the channel at or near the crossing and average bed slope through that cross section. This can be accomplished using a spreadsheet tool or commercial software, such as Bentley's FlowMaster® (2009). The current version of HEC-RAS (USACE, 2016) for at a station hydraulics, does not provide all of the hydraulic variables necessary for scour calculations. Using a single cross section to compute local hydraulics does not represent the backwater downstream of crossing sites or secondary flow paths. This simplification results in an overestimate of velocity and scour depth because backwater effects in the downstream channel are not accounted for. However, the uniform flow assumption would tend to underestimate the stream velocity and scour depth at locations downstream from road culverts due to flow concentration by these features. A backwater model such as HEC-RAS would be more appropriate in this situation.

1D, gradually-varied flow modeling generally requires a minimum of four cross sections spaced to represent channel conditions or at least four channels widths apart, downstream of the crossing site. These cross sections provide the model more distance and nodes to converge on a solution downstream of the crossing thereby reducing the influence of using a reach averaged slope as the downstream boundary condition for normal depth calculation. 2D models require the development of a topographic surface and use a downstream boundary water surface elevation generally from either an at-a-station or 1D analysis.

The calculated hydraulic variables are used as input variables in scour calculations. Key hydraulic variables include flow depth, cross sectional average velocity, unit discharge and Froude number. Scour equations use hydraulic depth as an input value defined as the flow cross sectional area divided by the wetted top width. Some equations provide a more conservative estimate when using the normal depth from the at a station hydraulics. For many ephemeral channels, using the 100-year return period peak flow with simplified hydraulics not influenced by the backwater effect of downstream infrastructure results in conservative scour estimates.

Event-Based General Scour Assessment: Empirical scour depth equations determine the potential depth of event-based scour in a channel bed because of general scour, bend scour, and scour from passing bedforms. These guidelines do not consider local scour associated with structures such as expansion, contraction, bridge abutments and piers; refer to the Federal Highway Administration's HEC-18 (2012) for guidelines on evaluating these types of scour if the pipeline is buried near a stream crossing structure.

Event-based general scour typically affects all or most of the channel width, may be uniform or non-uniform in depth over a cross-section and occurs over relatively short time periods associated with a passing flood event. Sediment transported from upstream may refill scour zones after the peak of the flood has passed (Colby, 1964). Channels may scour over the course of one flood then fill with sediment as a result of a subsequent flood as sediment waves move through a stream system (Colby, 1964). Bend scour occurs along channel bends where transverse or "secondary" currents are induced that scour sediment from the outside of a bend and deposit it along the inside of the bend (i.e., a point bars) and downstream. Bend scour is a function of bend radius of curvature and is not computed on channels with negligible curvature, which may be common in 1st order streams. Table 1 provides a summary and references of available general and bend scour equations. Professional judgement should be used in selecting appropriate empirical general and bend scour equations. Each equation has a range of hydraulic, channel dimension and bed sediment size conditions within which it is valid. The equation producing maximum calculated scour depth may be used as a conservative estimate of

general and bend scour depth. Because bend scour equations include all of the scour associated with a bend, general scour is not added to bend scour rather, and the maximum of two is selected.

For channels with sand beds there is a need to evaluate the height of migrating bedforms, such as dunes, which are common on sand bed channels. Transient scour below the bed surface may result from migrating bedforms; however, this is typically a fraction of the general and bend scour depths as bedform heights are limited by the flow depth. Bedform scour is computed using two different methodologies (Table 1) with the maximum value being used as part of the total scour depth calculation.

Total event-based scour depth, Z_{event} is calculated as the summation of the maximum of the general and bend scour ($Z_{general}$, Z_{bend}) and the bedform scour, $Z_{bedform}$:

$$Z_{event} = MAX(Z_{general}, Z_{bend}) + Z_{bedform} \qquad (1)$$

Table 1. Equations used to evaluate various scour types along channels distant from structures

Scour Form	Equation	Source
General Scour	Zeller General Scour	Simons Li & Associates (1985)
	Neill Incised	Neill (1973)
	Neill Competent Velocity	Pemberton & Lara (1984)
	Blench Zero Bed Factor	Pemberton & Lara (1984)
	Lacey	ASCE, Predicting Bed Scour (2005)
	USBR Mean Velocity Method	Pemberton & Lara (1984)
	USBR Envelope Curve	Pemberton & Lara (1984)
Bend Scour	Zeller Bend Scour	Simons Li & Associates (1985)
	Maynord Bend Scour	Maynord (1996)
	Thorne Bend Scour	Thorne et al. (1995)
	USACE Bend Scour Design Curves – sand	EM 1110-2-1601, Plate B41, in USACE (1994)
Bedform Scour	Simons Li & Associates	Simons Li & Associates (1985)
	Dune Scour Equation	Flood Control District of Maricopa County (2003), as presented in the PBS&J Scour Spreadsheet (PBS&J, 2008)
Confluence Scour	Confluence in sands & gravels	Ashmore and Parker (1983), as presented in Melville and Coleman (2000)

Several scour analysis methodologies and assessments rely on bed sediment gradation estimates. Composite bed sediment samples are collected on the bed surface as well as through the potential depth of scour as much as is practical (1-3 feet). Samples are analyzed to determine their grain size distribution following standard procedures (ASTM D6913, Bunte and Abt, 2001). Resultant median grain size values of both bed samples at each sampled site are utilized in the scour analyses.

Degradation Analysis: Long-term degradation refers to the depth to which a channel bed may degrade as a result of net export of sediment (incision). Alteration and concentration of runoff flow paths from infrastructure, such as culverts, as well as runoff augmentation from land use change can de-stabilize a channel and result in long-term degradation. Sand and mixed sand-gravel bed streams common the U.S. Southwest are typically alluvial channels and an estimate of sediment supply is required to calculate a stable slope.

Long-term degradation in mostly sand bedded ephemeral channels is determined by direct or indirect observations of channel degradation.. Direct observations include measurement of the height of downstream headcuts, which may migrate upstream to the crossing. Acute reductions in channel slope downstream may indicate that the channel at the crossing has the potential to reduce its slope by degradation. Here, the bed profile can be extended from the milder slope reach through a gravel roadway to the location of the crossing (Figure 3). Long-term bed degradation is then estimated from the difference in bed elevations at the crossing as an indirect approach. Where crossings occur upstream of and proximal to controls on grade, such as engineered culverts at major roads, long-term degradation may be considered negligible as long as the grade control remains functional. Evaluating the potential longevity of various grade control structures is beyond the scope of this paper. The expected rate of long-term degradation (i.e., rate of upstream progression of gullies or headcuts) will inform how much degradation depth to expect over the design life of the pipeline.
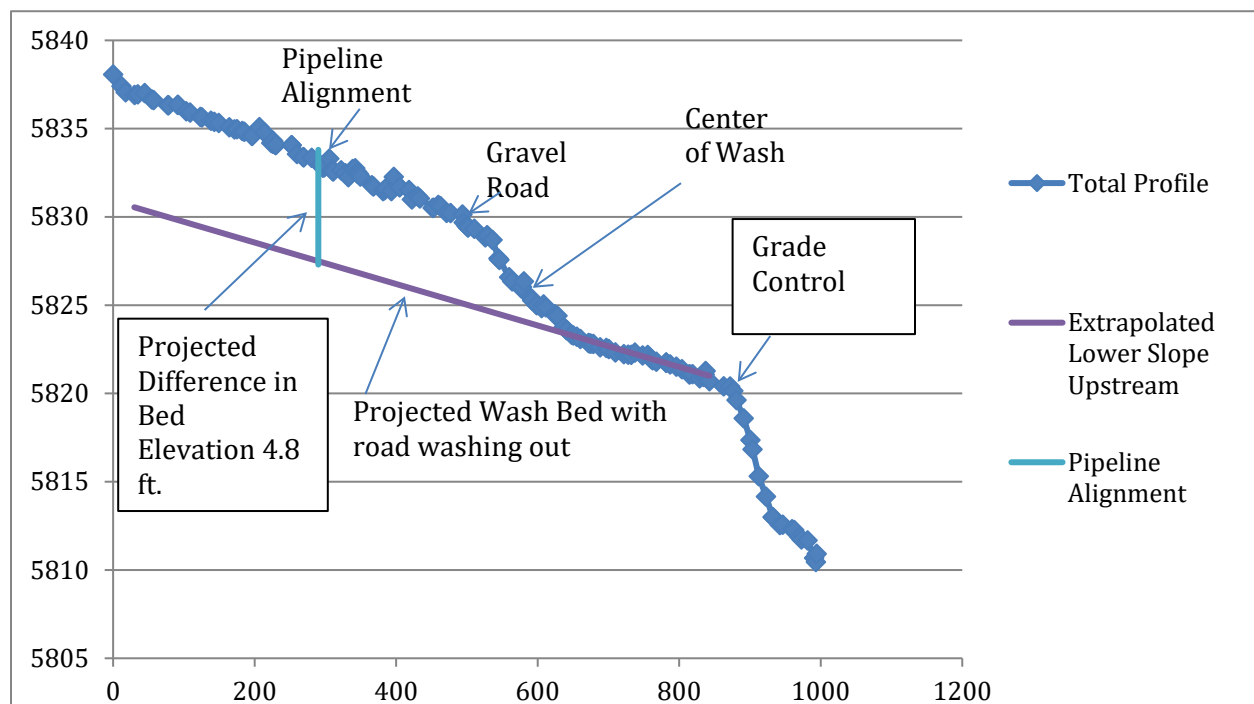
Figure 3. Shows how the downstream flatter slope is projected up to pipe crossing location to estimated potential long-term degradation.

Total Pipeline Cover Depths And Lateral Burial Extent: Total recommended pipeline cover depth is estimated as the summation of the maximum of general scour or bend scour, Z_{event}, along with bedform scour, $Z_{bedform}$, long-term degradation depth, $Z_{degradation}$ and the application of a safety factor, *SF*. Event-based scour estimates utilize the peak design discharge (typically 100-yr event), which is based on the design life of the system. Equation 3 summarizes:

$$Z_{total} = (Z_{event} + Z_{degr})SF \qquad\qquad (2)$$

Safety factors usually range from 1.1 to 1.5 (ASCE, 2005) depending upon the uncertainty of scour estimates. Channels showing potential for future degradation or have migrating headcuts downstream of the alignment crossing would receive a larger safety factor. Total scour depth

from equation 2 is subtracted from the channel thalweg elevation to determine the elevation of the top of the pipe. Total burial extend is the total of the channel top width plus estimated long-term lateral migration plus a safety factor. Checking local, state or federal regulations such as PHMSA (2019) is recommended to ensure all cover depth requirements are met. The maximum burial depth is calculated along the bottom width of the active stream channel; however, this maximum burial elevation must extend for some length on either side of the channel to accommodation the potential for channel migration (burial extent). For sites without a significant probability of lateral migration or channel widening, using the top channel width plus an additional safety factor extending from both channel margins may be used for this burial extent. This approach may cover any inset terraces or floodplain features that may be more prone to erosion.

Channels at risk for widening or migration should be given additional consideration; in these cases, professional judgement should be used to determine the burial extent by incorporating analysis from map, aerial imagery and field assessments. Historic rates of lateral migration may be applied to help predict future rates of migration over the design life of the pipeline (e.g., Lagasse et al., 2004). Rates of bank retreat may also be applied to predict channel widening. However, this assumes uniform movement of the stream channel when many channels experience periods of stasis punctuated by periods of channel movement; in addition, channels cannot widen indefinitely under the same flow regime. For channels that appear to be widening or initiating braiding, nearby channels with similar flow regimes and geologic settings could inform potential future channel width.

The proposed burial extent (at maximum burial depth) should extend to cover the current channel's top width, $L_{top\,width}$ and any potential movement of the channel due to migration or widening, $L_{movement}$, plus a factor of safety, SF (Eqn. 4).

$$L_{total} = L_{top\,width} + L_{movement} + SF \ (3)$$

The factor of safety in equation 3 is determined from the review of historical migration rates.

Conclusion

Buried pipelines encounter scour, long-term degradation and lateral migration hazards when crossing underneath ephemeral channels. Ephemeral channels flow intermittently and often dynamically experience bed and bank erosion during peak flows. Without sufficient burial depth and additional burial length on each channel bank, pipelines can be exposed to hydraulic forces during high flow events often leading to pipeline failure. Analysis of maps, historical imagery and topography can be used to estimate future lateral migration. Using NRCS method of estimating peak flows for ungaged watersheds (USDA, 1986) and based on a risk-based approach (FHWA, 2012), peak discharges associated with a return period of 100 years can be determined. A hydraulic assessment provides parameters used for scour computations. Long-term degradation based on field assessment and downstream channel bed slope change can be used to determine long term degradation potential. Total vertical scour to determine burial depth to the top of the pipe is the sum of the larger of general or bend scour, bedform scour, long-term degradation with the total being multiplied by a safety factor.

References

ASTM D6913 / D6913M-17, Standard Test Methods for Particle-Size Distribution (Gradation) of Soils Using Sieve Analysis, ASTM International, West Conshohocken, PA, 2017, www.astm.org

American Rivers, 2017. Pipeline Failures and Our Water Supplies. Online post. https://www.americanrivers.org/threats-solutions/energy-development/pipeline-failures/

Annandale, G.W., 2006. "Scour Technology, Mechanics and Engineering Practice", McGrawHill, New York, NY.

ASCE, 2005. "*Predicting Bed Scour for Toe Protection Design for Bank Stabilization Projects.*" American Society of Civil Engineers, Continuing Education Seminar Course Workbook.

Bunte, K. and S.R. Abt, 2001. Sampling Surface and Subsurface Particle-Size Distributions in Wadable Gravel- and Cobble-bed Streams for Analyses in Sediment Transport, Hydraulics and Streambed Monitoring. USD A-Rocky Mountain Research Station, General Technical Report RMRS-GTR-74. 74.

Bentley Systems, Inc., 2009. Flowmaster V8i SELECT series 1 software.

Colby, B.R., 1964, *Scour and Fill in Sand-Bed Streams.* Geological Survey Professional Paper 462-D, United States Department of the Interior, Geological Survey.

FHWA, 2012. *Evaluating Scour at Bridges.* Fifth Edition. FHWA-HIF-12-003 HEC-18, Federal Highway Administration, Hydraulic Engineering Circular 18, Washington, DC.

Flood Control District of Maricopa County, 2003. Draft Drainage Design Manual, Hydraulics. September.

Knighton, A.D. and G.C. Nanson, 1993. Anastomosis and the continuum of channel pattern. Earth Surface Processes Landforms, 18, 613-625.

Lagasse, P.F., Spitz, W.J., Zevenbergen, L.W. and Zachmann, D.W., 2004. Owen Ayres & Associates, Fort Collins, CO. Handbook for predicting stream meander migration. NCHRP Report 533.

Lai, Y.G. 2008. SRH-2D version 2: Theory and User's Manual. Sedimentation and River Hydraulics – Two-Dimensional River Flow Modeling. U.S. Department of the Interior, Bureau of Reclamation, Technical Service Center, Denver, CO.

Maynord, S.T., 1996. "Toe-Scour Estimation in Stabilized Bendways," *ASCE Journal of Hydraulic Engineering,* Technical Note, p. 460-464.

Melville, B.W. and S.E. Coleman, 2000. *Bridge Scour.* Water Resources Publications, LLC, Highlands Ranch, Colorado.

Natural Resources Conservation Service (NRCS), 2007. "Scour Calculations" Technical Supplement 14B, Part 654 National Engineering Handbook, Department of Agriculture, Washington, DC.

Neill, C.R., 1973. *Guide to Bridge Hydraulics.* Published for Road and Transportation Association of Canada.

Pemberton, E.L., and Lara, J.M., 1984. "Computing Degradation and Local Scour" United States Bureau of Reclamation, Technical Service Center, Denver, Colorado.

PBS&J, 2008. Scour Spreadsheet, version 1.2, May 28, 2008. Presented by David Williams at Stream Stabilization Short Courses: http://www.dnrc.mt.gov/wrd/water_op/floodplain/streambank_course/.

PHMSA, 2019, Part 1912—*Transportation of Natural and Other Gas by Pipeline: Minimum Federal Safety Standards.* https://www.phmsa.dot.gov/regulations/title49/section/192.327 *accessed on 2-9-2019.* Pemberton, E.L. and J.M. Lara, 1984. *Computing Degradation and Local Scour.* Technical Guideline for Bureau of Reclamation, Denver, CO.

Simons Li & Associates, 1985. *Design Manual for Engineering Analysis of Fluvial Systems.* Prepared for Arizona Department of Water Resources.

Thorne, C.R., S.R. Abt and S.T. Maynord, 1995. "Prediction of Near-Bank Velocity and Scour Depth in Meander Bends for Design of Riprap Revetments," *River, Coastal and Shoreline Protection: Erosion Control Using Riprap and Armourstone.* Edited by C.R. Thomas, S.R. Abt, F.B.J. Barends, S.T. Maynord and K.W. Pilarczyk, John Wiley and Sons, New York, NY.

Viessman, W., Lewis, G.L., and Knapp, J.W., 1989, *Introduction to Hydrology, 3rd Edition,* Harper and Row Publishers, New York, NY.

Warren, L.P., 2011. "Scour at Bridges: Steam Stability and Scour Assessment at Bridges in Massachusetts, U.S. Geological Survey, 2011.

Wilcox, J. et al., 2001. "Evaluation of Geomorphic Restoration Techniques Applied to Fluvial Systems," Feather River Coordinated Resource Management Group, Dec. 2001.

USACE, 1994. *Hydraulic Design of Flood Control Channels.* EM 1110-2-1601, U.S. Army Corps of Engineers, Waterways Experiment Station, Vicksburg, MS, Platte B41.

USACE, 2016. *HEC-RAS River Analysis System, Hydraulic Reference Manual, U.S. Army* U.S. Army Corps of Engineers, Hydrologic Engineering Center, Davis CA.

USDA, 1986. Urban Hydrology for Small Watersheds, TR-55. 164 pp.

USGS, 2015. The National Map Viewer and Download Platform Web site: http://viewer.nationalmap.gov, accessed 2015. United States Geological Survey.

Revising the Basis of Sediment Management in Rivers: Incorporating Real-Time Sonar, Hydroacoustic and Hydrodynamic Field Data

Andre Zimmermann, Principal Geomorphologist, Northwest Hydraulic Consultants, Vancouver, BC, azimmermann@nhcweb.com

Jose Vasquez, Principal, Northwest Hydraulic Consultants, Vancouver, BC, jvasquez@nhcweb.com

Dan Haught, Fluvial Geomorphologist, Northwest Hydraulic Consultants, Sacramento, CA, dhaught@nhcweb.com

Achilleas Tsakiris, Hydraulic Specialist, Northwest Hydraulic Consultants, Olympia, WA, atsakiris@nhcweb.com

Ashley Dudill, Project Engineer, Northwest Hydraulic Consultants, Vancouver, BC, adudill@nhcweb.com

Introduction

Sediment transport and accumulation can cause serious problems for the operation of run-of-river hydroelectric developments. In general, sediment-related problems can increase maintenance and operation costs, while simultaneously reducing revenue from power generation. Sediment passing through a powerhouse can cause abrasion damage that reduces the efficiency and life of turbines, increasing the frequency of shutdowns and repairs. Sediment buildup at an intake can block flow paths and reduce the amount of water available for power generation. Consequently, there is a strong economic incentive to effectively manage the accumulation of sediment in front of intake structures and the passage of sediment through turbines. These actions maximize power generation, which increases revenue. However, the practical challenge with developing an effective sediment management strategy is the inability to physically see how sediment behaves underwater and how effective changes in plant operations are in minimizing sediment accumulation and transport.

Sediment transport processes at intakes of run-of-the-river hydroelectric plants therefore provide both a management challenge and an opportunity to examine the applicability of existing sediment management approaches and tools, and to evaluate the utility of novel monitoring techniques.

The relatively modern tools considered in this paper include continuous sonar scanning of the river bed using Dual Axis Scanning (DAS) sonars, hydrophones and acoustic backscatter sensors (ABS) that are integrated directly into the plant control network. All three of these technologies utilize hydroacoustic sensors that are less easily fouled in high sediment environments and can operate continuously to collect information when sediment is moving. Hydroacoustic methods of monitoring sediment load with an Acoustic Doppler Current Profiler (ADCP) and hydrophones have also been around for several decades; however, we are unaware of sites where these have been integrated into the plant controls and utilized for real-time sediment monitoring.

More traditional approaches to monitoring sediment transport include bedload and suspended load transport measurements, which provide an estimate of the load at a single point in time, as

well as sounding surveys with a boat or raft that collect data over a limited duration in time. Traditionally these data are often used to calibrate numerical and/or physical models and the results from the numerical and physical models are used to adjust how the facility is designed and operated. The traditional approach follows a typical 'study' design where a question is posed, an approach is developed, results are compiled, and a report is written describing the results and how things can be changed to address the original problem. In contrast, the approach presented here is one of ongoing data monitoring and real-time adjustments based on the observations at site during operations.

This paper will present a case study, the Forrest Kerr Hydroelectric Project, which illustrates how modern real-time field monitoring tools including a hydrophone, ABS sediment concentration sensor, ultrasonic flow meter and dual axis scanning sonars, can be used to improve sediment management strategies. We discuss how the available tools and approaches for working with real-time operating facilities are changing, and how as a community we should be responding to these changes in order to further our understanding of sediment dynamics at hydroelectric facilities and improve their operation.

Background

The 195-MW Forrest Kerr Hydroelectric Project has a large run-of-river intake with capacity to divert 250 m³/s for hydropower generation. The project is located in Northwest British Columbia at the confluence of the Iskut River and Forrest Kerr Creek. Both watersheds are glaciated and the reaches of both rivers upstream of the facility feature extensive gravel bed braided reaches. The hydrology at the Project is dominated by a substantial snowmelt/glacial melt freshet. Rainfall and rain-on-snow events result in the highest annual floods.

Based on field measurements of suspended sediment transport, it is estimated that 6.4 M tonnes of suspended sediment moves past the intake per year. Bedload transport modeling conducted in the 1980's suggest there is 0.8 M tonnes of bedload moving past the intake per year (DPJ&A and HGPD, 1984). Observations from site show that bedload is readily mobilized during flows that are approximately the mean annual discharge and the river remains turbid when flows are approximately half the mean annual discharge or greater. The braided reaches upstream of the intake are very mobile and not armored; they are the major source of bedload that is directly transported past the intake.

Over a two year period, which included the first year of operations, 0.75 M tonnes of sediment were deposited in the reach of Forrest Kerr Creek upstream of the project. This creek is estimated to only produce 12 to 17 % of all the sediment coming past the intake (NHC, 2014), which suggests that the total bedload may be as much as 2.5 to 5 M tonnes per year. All in all, there is a substantial amount of sediment transported past the intake each year. The grain size of the material includes the full range of sand, gravel and cobbles that are typical of braided rivers at transport capacity.

Prior to the construction of the facility, NHC undertook both physical and numerical modeling to assess intake hydraulics. Both models proved useful in helping define hydrodynamic conditions during different scenarios, including during flood conditions. However, both the numerical and, to a lesser extent, the physical model could not realistically simulate the extremely complex and stochastic nature of sediment transport processes observed in the field that have subsequently become increasingly apparent with the current field program. Furthermore, the questions that need to be answered now only became apparent once the facility was operating.

Sediment Management and Monitoring Technology

The Forrest Kerr project includes a number of unique structures for handling sediment transport with the goal of minimizing sediment entering the intake, which are shown in Figure 1 through Figure 4. The sediment management structures include:

1. **A submerged box culvert** located at the base of the sluiceway channel (see **Figure 2**). The submerged box culvert acts as a tunnel bedload excluder by passing bedload arriving at the sluiceway channel into the river reach downstream of the dam rather than into the intake. Flow through the box culvert is controlled by a radial gate and the box culvert can transport the entire transport capacity of the river for small and moderate floods depending on how it is operated.

2. **A desander** at the intake entrance that includes 8 sediment collection bays with sediment removal pipes at their base which cycle over time. Depending on the river flows, when the desander is operating, one or two of the pipes draining the sediment out of desander are opened for a few minutes and then the pipe is closed and the next pipe is opened. This cycle continues continuously. If these sediment removal pipes become blocked, there is an air purge system which clears debris and sand off the pipe openings. A photograph showing the installation of the air purge system can be seen in Figure 3. In general gravel should not enter the desander; although it has happened when the box culvert inlet becomes overwhelmed by bedload.
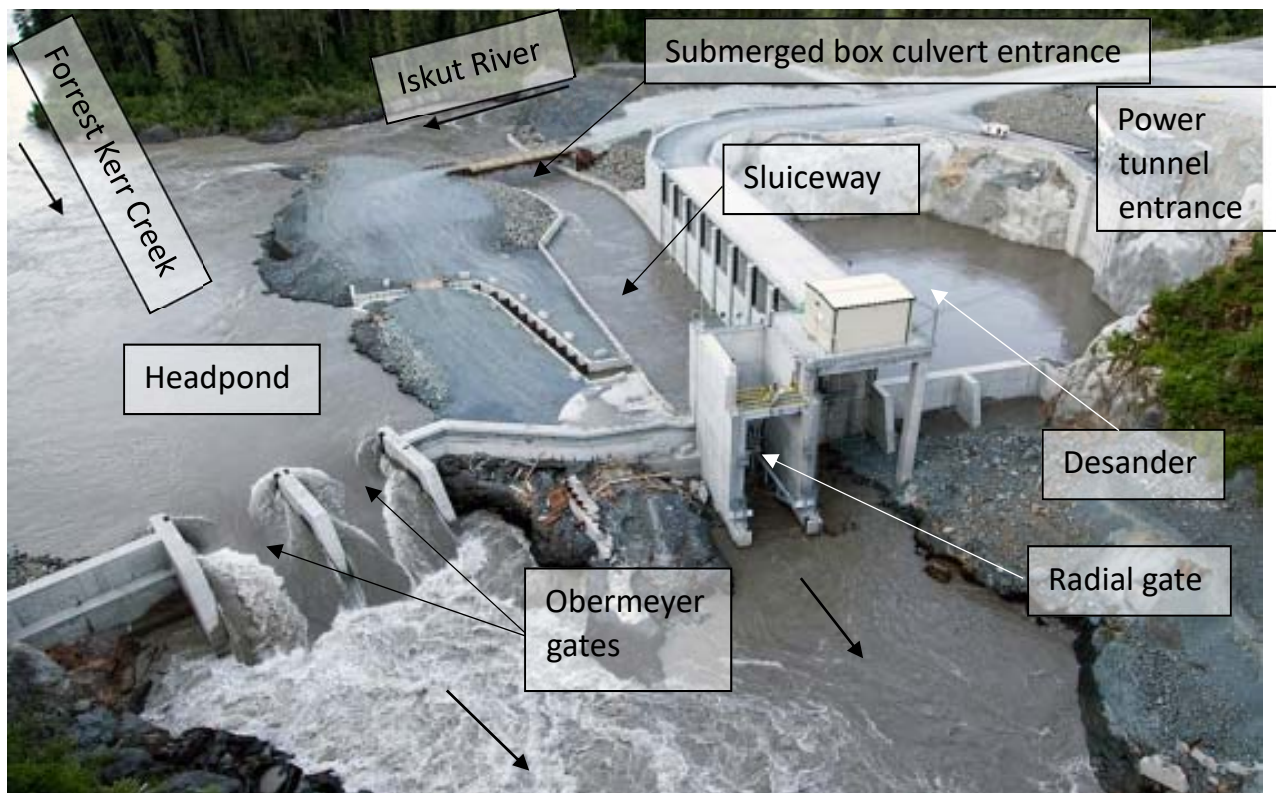

Figure 1. Aerial view of Forest Kerr run-of-river facility (box culvert on the bottom of the sluiceway is fully submerged and not visible).
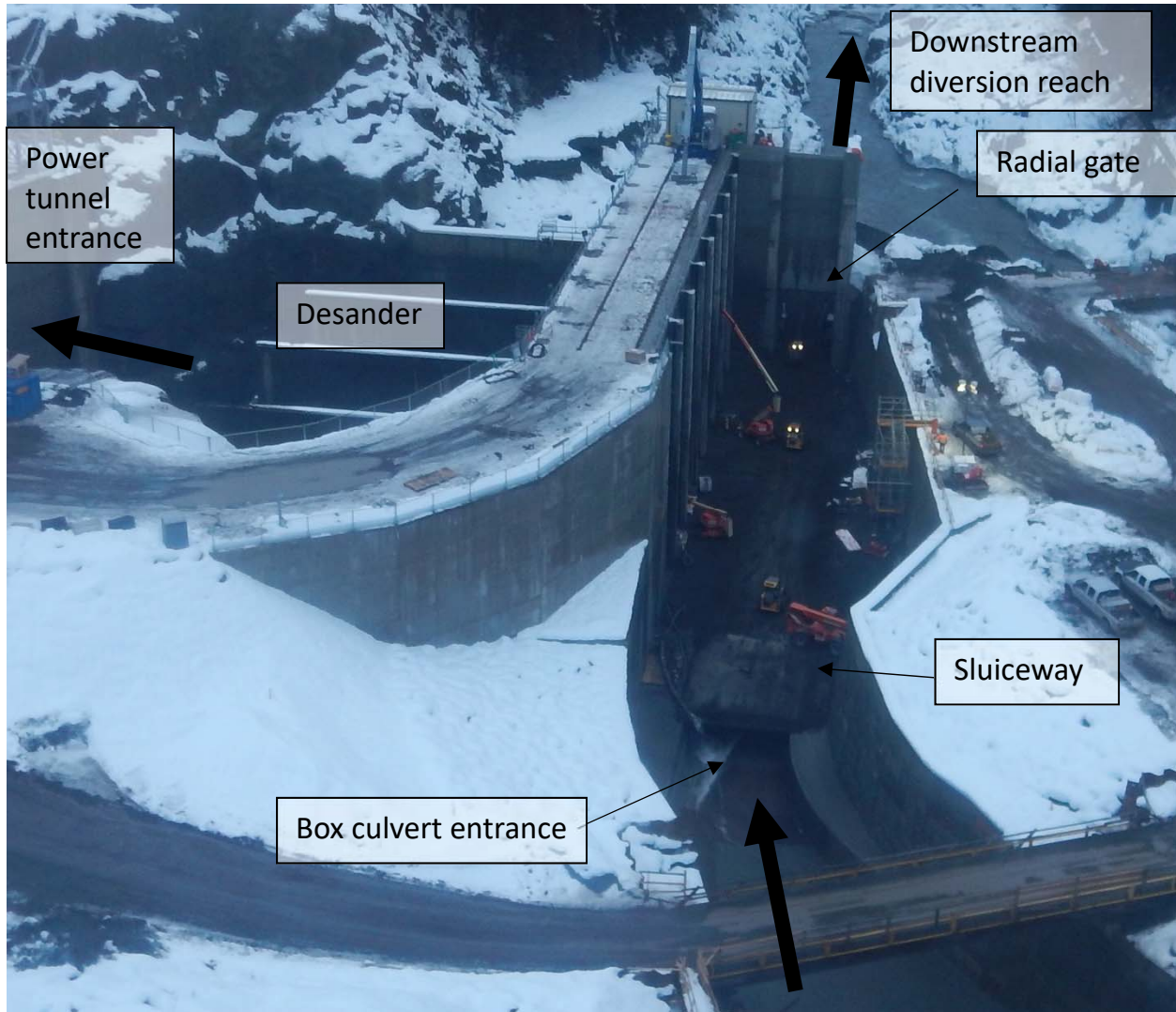
Figure 2. Intake during maintenance when the headpond has been drained. Box culvert and sluiceway are clearly visible. Large black arrows indicate direction of flow.

Figure 3. Air purge system being installed along desander sediment collection pipes. Each slot in the larger pipe is equipped with an air nozzle that blasts material off the sediment collector pipe.

To optimize sediment sluicing at the intake and monitor the desander bays to ensure they are functional, several modern real-time field monitoring instruments have been employed at the Forrest Kerr intake. These instruments are illustrated in the schematic shown in Figure 4 and include:

1. **Three Dual Axis Scanning (DAS) sonars** have been installed at the intake for real-time bathymetric monitoring (Haught and Zimmermann, 2019). The DAS sonars inform the operator on sedimentation levels at the intake every 30 minutes and enables the elevation of the bed to be tracked nearly continuously.
2. **A hydrophone** installed at the sluiceway entrance for detecting sediment motion (Tsakiris et al. 2019). The hydrophone is used to monitor bedload sediment moving into the box culvert, and consequently informs the operator whether the radial gate opening is sufficient to mobilize and transport sediment.
3. **An ABS and turbidity sensor and flow meter** have been installed in the desander to infer how much sediment is being flushed out of the desander sediment collection pipes. The ABS uses backscattered sound while the turbidity sensor uses backscattered light to infer sediment concentration. In general the ABS is most sensitive to the full range of sand sizes and coarse silt, while the turbidity sensor is most sensitive to the silt load (https://www.sequoiasci.com/article/response-of-lisst-abs-and-obs-to-log-normal-size-distributions). The flow meter uses the transit time of sound to infer flow, which indicates that sufficient water is moving through the system, or the ports along the pipes are clogged. For the purposes of this study none of the sensors have been calibrated and the relative change in the signal is used to infer changes in sediment transport. After a few years of use the sensors continue to zero well during low flow conditions when no transport is occurring.
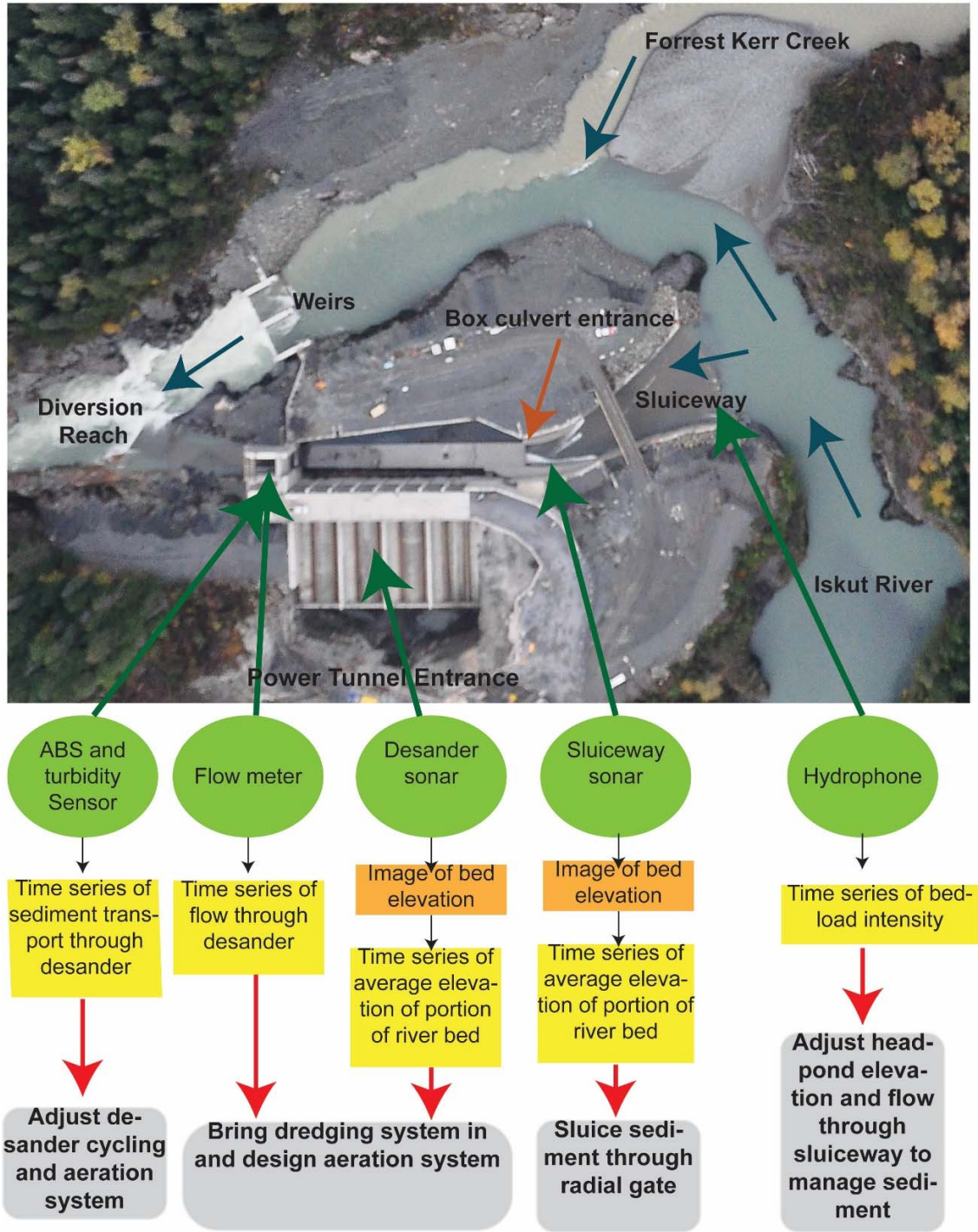
Figure 4. Schematic showing the location of the various sensors (green ovals). Orange boxes represent data plots illustrating the elevation of the entire bed surface in a single image while yellow boxes illustrate time series that can be reviewed by scientists, engineers and operators on the HMI. Grey boxes illustrate some of the changes that can occur in response to the data. Black arrows represent automatic data processing that is done to create the time series while red arrows represent interpretation by operators and scientist to make an informed decision using the data in the yellow boxes, plus information on plant flows, river flows and water levels at the intake. Blue arrows indicate the direction of river flow.

These data are supplemented by a continuous record of gate positions, flow values and water levels upstream and downstream of each flow control structure that is maintained as part of the facility. The systems that have been installed enable measurements of bed elevations, sediment transport and flow conditions which update every minute to every half an hour, depending on the parameter being monitored.

Monitoring Outcomes

Based on our experience with the system over the last few years, we have concluded that the most effective approach for managing sediment at these facilities is to work closely with operators and advise them on the optimal facility operation at a given time, based on collected field data in real-time. This approach has radically changed how sediment is managed at the Forrest Kerr facility and could have comparable benefits for other, similar facilities. Some key changes are as follows:

- During times when the river flow is sufficiently low that only the instream flow requirement (IFR) of 10 m³/s needs to be released through the diversion reach, the box culvert is flushed with 1 to 2-minute duration bursts of 40 m³/s every few hours to clear sediment that can be seen from the sonar to have accumulated in front of the entrance. The real-time monitoring during trials with different flow conditions revealed that continuously releasing 20 or 30 m³/s is ineffective at moving bedload and results in substantially less energy production.
- During flood events the entrance to the box culvert is tracked closely to ensure sediment isn't building up and passing over the box culvert entrance. Monitoring is particularly challenging in large events as the water column can be 0.1 % sediment and the energy from the sonar is largely absorbed by the water.
- The hydrophone can be used to track the intensity of the sediment transport; see Figure 5. Figure 5 illustrates the period from July 8th to 10th, 2018 when the hydrophone shows that sediment has been mobilized and is being transported following a drop in the sluiceway water level that resulted in an increase in local water velocities. Burial of the hydrophone is used to indicate that sediment has accumulated at the entrance to the sluiceway. This is particularly valuable in very high sediment transport conditions, when the sonar cannot penetrate the water column.
- The ABS, turbidity sensors and flow meter on the sediment extraction pipes in the desander can indicate that a desander bay is not removing sediment and the air purge system that clears debris off the extraction pipe openings needs to be adjusted.
- The desander bays can be inspected using the sonar to see if any of the pipes are clogged and if so, where they are clogged. This can then guide dredging works, determine which air purge zone needs to be run, or for planning additional improvements to the system. Earlier scans of the desander showed sediment filled the desanders as a wave of bedload with Gilbert type deltas and were instrumental in getting the air purge system installed, which has proven to be very effective.
- The sonar has revealed that gravel sediment accumulation at the intake is more of an issue during the falling limb of the freshet than at the beginning of the freshet when flows are roughly similar. This enables more energy production in the spring when sediment inputs are lower. The sonar has also revealed that at high flows the box culvert may become overwhelmed by bedload and shutting down the intake entirely so the box culvert entrance doesn't get buried may be the best course of action.

- Data acquired from the ABS were utilized to optimize the cycle duration for the desander flushing valves and if they needed to be operated at all. This determination was based on whether a change in the transport rate through the sediment collection pipes could be detected when the desander valves were cycled.
- The sonar at the box culvert can be used to track when sediment transport is occurring past the intake. This information is critical as the stage-discharge rating curve at the downstream hydrometric gauge is likely to shift as a result of sediment deposition.

Following all aforementioned changes in the facility operation, the productivity of the plant has seen a substantial increase. The addition of the air purge system and a better understanding of sediment transport in the desander has greatly reduced the flow of sediment through the powerhouse and wear on the turbine infrastructure.
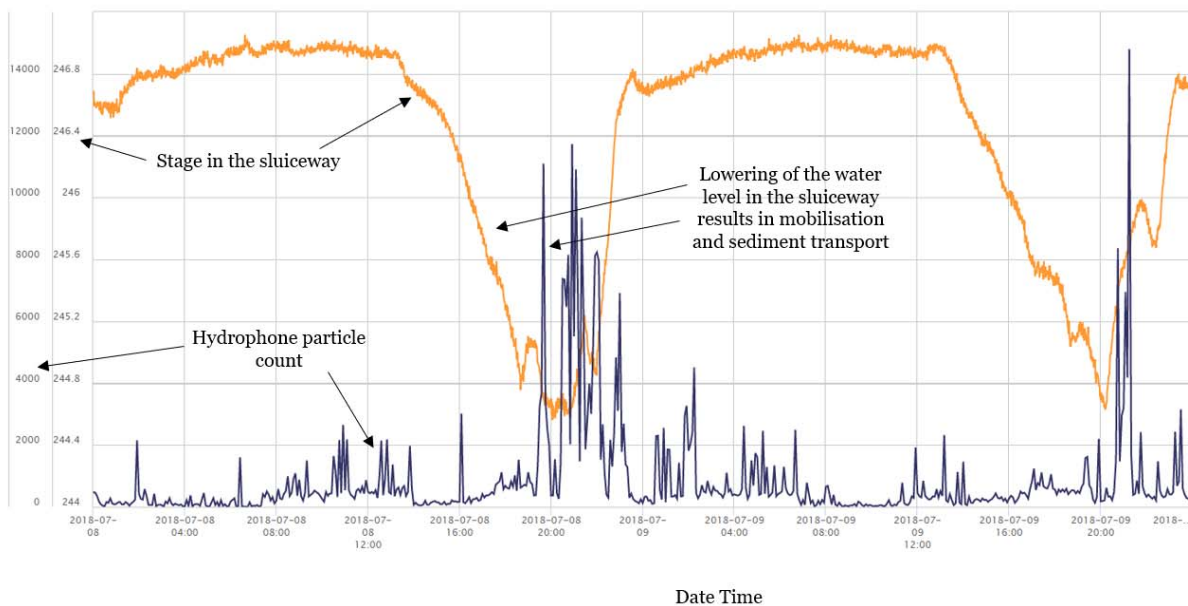
Figure 5. Sluiceway stage and hydrophone particle count between July 8th and 10th, 2018.

Excitement and Challenges of Ongoing Monitoring

The ability to monitor sediment transport in real time as described with the Forrest Kerr case study has fundamentally changed the approach to sediment management at many facilities. Historically, the approach to addressing sediment transport problems at hydropower, and particularly at existing facilities, involves some basic investigations on site, building a numerical or physical model and performing a series of simulations to assess how the problem might be addressed. At the end of the project, a report summarizing the findings and providing operational guidance is compiled.

Significant challenges with the traditional approach include:

- Bed elevation is often based on little-to-no, and often outdated, survey data. As a result, the variability of the bed elevation, especially during flood events is not captured or

known, which creates a substantial issue when defining an initial bed condition. This uncertainty has an impact upon water levels and discharges.

- The grain size of the bed and amount of sediment supplied to the reach is estimated, or assumed. Further, it requires simplification of the complex and stochastic nature of sediment supply for use in a model.
- The numerical models have a range of sediment transport formulae, which incorporate a range of simplifying assumptions. Furthermore, most sediment transport formulae have been developed and are applicable on a uniform river reach scale and generally employ cross section average flow conditions, but most numerical models apply them at much smaller scale, i.e., from node to node.
- Models often require a substantial amount of time to run to steady state, causing them to lag behind real-time observations. The long model run time makes real time decision making and solving impossible, as models will likely require longer time to run than the actual event.

To overcome some of these challenges today, the work at the Forrest Kerr facility demonstrates that it is possible to instrument a facility and 'see' what is happening and how the conditions change in real time, allowing for faster response to changes in flow conditions and sediment buildup. Predicting conditions outside of normal operating conditions or evaluating a potential change in design or operational approaches, could still employ numerical or physical models, but would be better done if site data are used to understand when the bed elevations are changing, by how much they are changing and when sediment transport starts and stops. Current computational fluid dynamics (CFD) modeling for the FK facility makes use of the data from the field program to assess the possible range in bed levels during different flood events. The model is then used to test different operating scenarios (e.g. variations in Obermeyer levels and radial gate openings) to help determine the most effective strategy to minimize sedimentation at the intake during flood events.

Major challenges during the transition to direct observation of sediment transport, and in particular real-time support for sediment monitoring, include:

- Large datasets - there is a substantial amount of data to manage and sort through. To do this effectively one needs a good means of managing the data or the data will be unworkable and not useful.
- Trained operators and continuous coverage – for whatever reason the most interesting flood events seem to happen when the operators who know the site the best are on holiday. In general, you need a few people to know each site and they need to be able to pull up and review the data with minimal effort. This is hard to finance as storm events typically only last a few days, so the amount of time to on-board multiple people for the scenario of one or two key people being away is substantial.
- Complex hydraulics - the hydraulics at most of the sites are complicated and often controlled by a downstream control that can vary with time such as a sluicegate, the Obermeyer gates in the Forrest Kerr facility, as well as with the discharge through a power plant. As these factors change the sediment transport rates, having a solid knowledge of hydraulics and how they will change the flow pattern is very important for interpreting real time information from the sensors.
- Knowledge of sediment transport - a knowledge of bed forms is useful when interpreting noisy data to help assess if a feature that is possibly visible in the scans is present or if it is a signal artifact.

- Strong communication skills - the engineers and scientists need to have good communication with the operators at the facility and learn from what the operators are seeing and what the operators interpret to be going on.
- Data interpretation for informed decision making - for real time operations there is a need to train operators on how to interpret the data so they can make informed decisions on how to change operations.

To address the challenges discussed above a series of standard documentation protocols have been put in place so a wider number of individuals can understand the data flow. Automatic reports that run hourly have also been configured to summarize the key data and this enables easy data review when professionals are out of the office. Furthermore, notifications on key variables, such as the bed elevation in front of an intake have been enabled.

NHC has also started to use the data to train professionals on the pattern and processes of sediment transport at river intakes. While the data are complex, they are also extremely insightful, and can provide young professionals a chance to work with data that is not readily available elsewhere.

Conclusions

Overall, the introduction of the new technology has enabled much more information on the movement of sediment in rivers to be tracked in real time. At some locations this enables sediment to be tracked minute by minute and inform operations in real time on how much sediment is moving and where it is building up or being scoured from. The availability of such comprehensive, real-time data has fundamentally transformed how we approach the field of sediment management at these projects. From a passive consulting role of writing technical reports and static operational protocols, we have moved to a more active role that involves ongoing communications, dynamic data management and analysis, which ultimately benefits hydropower generation thorough an increase in efficiency and improved management techniques.

References

DPJ&A and HGPD. 1984, "Stikine-Iskut development: Environmental hydrology report volume 1: Hydrology, sediment transport and morphology of the Stikine and Iskut Rivers," Prepared by David P. Jones & Associates and Hydroelectric Generation Projects Division.

Haught, D., and Zimmermann, A.E. 2019. "Continuous River Bed Monitoring at Hydroelectric Intakes Using Dual-Axis Sonar Scanners," Proc. of the 2019 Federal Interagency Sedimentation and Hydrologic Modeling Conference, Reno, Nevada.

NHC. 2014. "Forrest Kerr Hydroelectric Project, Geomorphology Monitoring Plan," Prepared by Northwest Hydraulic Consultants Ltd. for AltaGas Ltd., North Vancouver, BC. 36 pp.

Tsakiris, A., Zimmermann, A.E., Meier, D., and Reynolds, A. 2019. "Optimizing Hydropower Facility Operations Via Acoustic Sediment Monitoring," Proc. of the 2019 Federal Interagency Sedimentation and Hydrologic Modeling Conference, Reno, Nevada.

Techniques for Fish-Passage Evaluation through Instream Structures

S. Michael Scurlock, Hydraulic Engineer, RiverRestoration.org, Carbondale, Colorado, Michael.scurlock@riverrestoration.org

J. Marty Holtgren, Fisheries Biologist, Encompass Socio-ecological Consulting, Manistee, Michigan, mholtgren@encompassLLC.org

The quantitative evaluation of fish passage at instream structures has continued to be elusive, even with advances in computational resources, numerical hydraulic modeling capabilities, and biological science. There is yet to be a formally accepted methodology for passage evaluation readily implemented during the hydraulic design process to increase comfort and reliability of structure performance, both for passage and blockage. Specifically, the evaluation of hydraulic structure velocities for fish passage or blockage is examined herein.

Common practice for structure evaluation and design for fish passage follows one of two tenants: 1) structure geometric parameters and channel characteristics are compared with those found with anecdotal success and literature recommendations (e.g. Mooney *et al.* 2007, Turek *et al.* 2016); or 2) binary thresholds are established, typically based on literature, which are readily applied to hydraulic model output or measurements (e.g. Parsons *et al.* 2016; Castro-Santos *et al.*, 2013, Stephens *et al.*, 2015; Hardee, 2017).

The first evaluation methodology has largely have arisen from previous difficulties in realization of hydraulic distributions within open-channel natural, passage, and barrier-type structures. Rapid assessment of these structure types is now possible with numerical modeling, capable of generating velocity distributions throughout the full flow field and capture complex flow dynamics.

The second method follows from the difficulty of application of complex fish swimming behaviors to hydraulic data, both field-collected or numerically modeled. Swimming energetics functions ubiquitous to the fisheries biology literature are typically distilled to either a binary sustained swimming threshold (in the case of passage evaluation) or burst threshold (in the case of barrier evaluation). Therefore, spatial hydraulics distributions and biological energetic budgets are compressed into instantaneous criteria and fish swim-speed criteria maybe misapplied.

This study investigates the application of energetics functions from the fisheries biology literature over space throughout flow fields through instream structures in the Great Lakes Region. Katopodis and Gervais (2016) compiled data from approximately 2,000 literature sources and present a series of swim-speed and endurance time curves for a variety of species types and body lengths in graphical (e.g. Figure 1) and formulaic versions. Reported methods are empirically derived and have associated prediction confidence intervals. Of particular interest in this study is the evaluation of the grouped Salmon and Walleye species and the grouped Eel species. Walleye (*Sander vitreus*) are of particular interest in the Great Lakes Region as a sport fish with successful passage highly desirable, while sea lamprey (*Petromyzon marinus*) have been targeted for migration barriers.

Three structures or structure fields are evaluated herein using two-dimensional numerical modeling output coupled with the robust endurance functions compiled by Katopodis and Gervais (2016). One instream structure system analyzed is an as-built rock-weir and constructed-riffle matrix in Dexter, MI. This structure system was designed according to the

first tenant of adhering to geometric guidelines associated with naturalized features which pass fish. The second and third structures investigated are currently in the design phase for the Grand River, MI. One of the structure types encourages walleye passage, while the other functions as a sea lamprey barrier.

Hydraulics are extracted from two-dimensional model results of the structures where depth-averaged velocities are corrected by a factor for near-boundary values. Endurance-time curves are interpolated along velocity-space distributions to assess barrier presence across varying body lengths and confidence limits. Figure 2 illustrates an example swimpath extracted from a velocity distribution within a structure field. It represents one of many possibilities for a fish to pass the structure field. Figure 3 provides analysis of the swimpath velocity distribution for the Katopodis and Gervais (2016) salmon and walleye group, where red lines indicate initiation of sustained swimming for a given fish size. The associated table in Figure 3 indicates where a fish of a given size has a percentage chance per passage, with red indicating a predicted barrier.
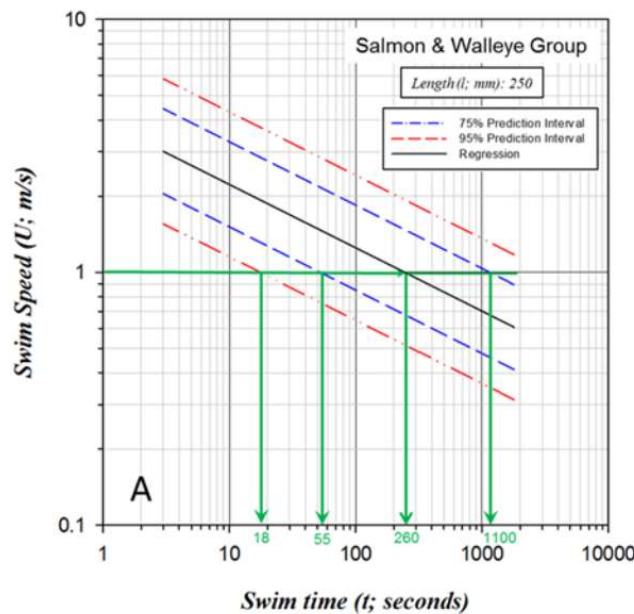
Figure 1. Example Katopodis and Gervais (2016) endurance-time curve
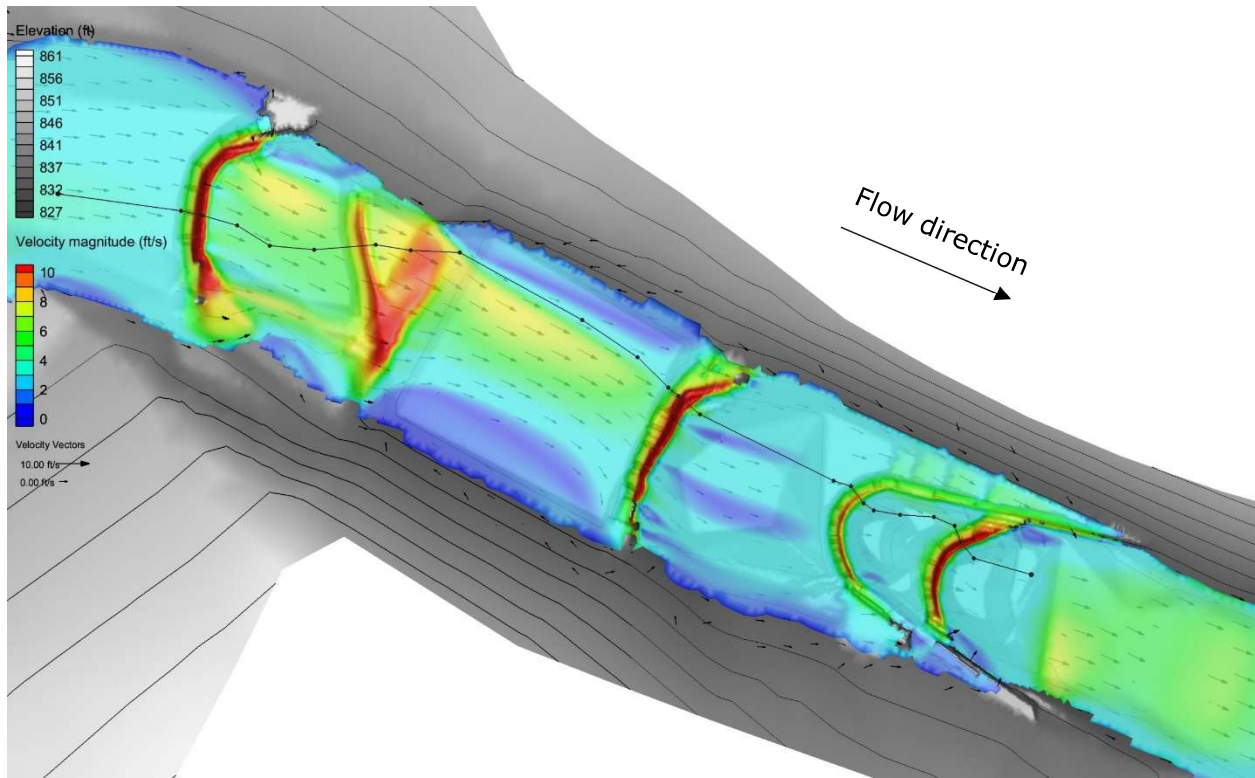
Figure 2. Example velocity distribution and extracted swim path (black)
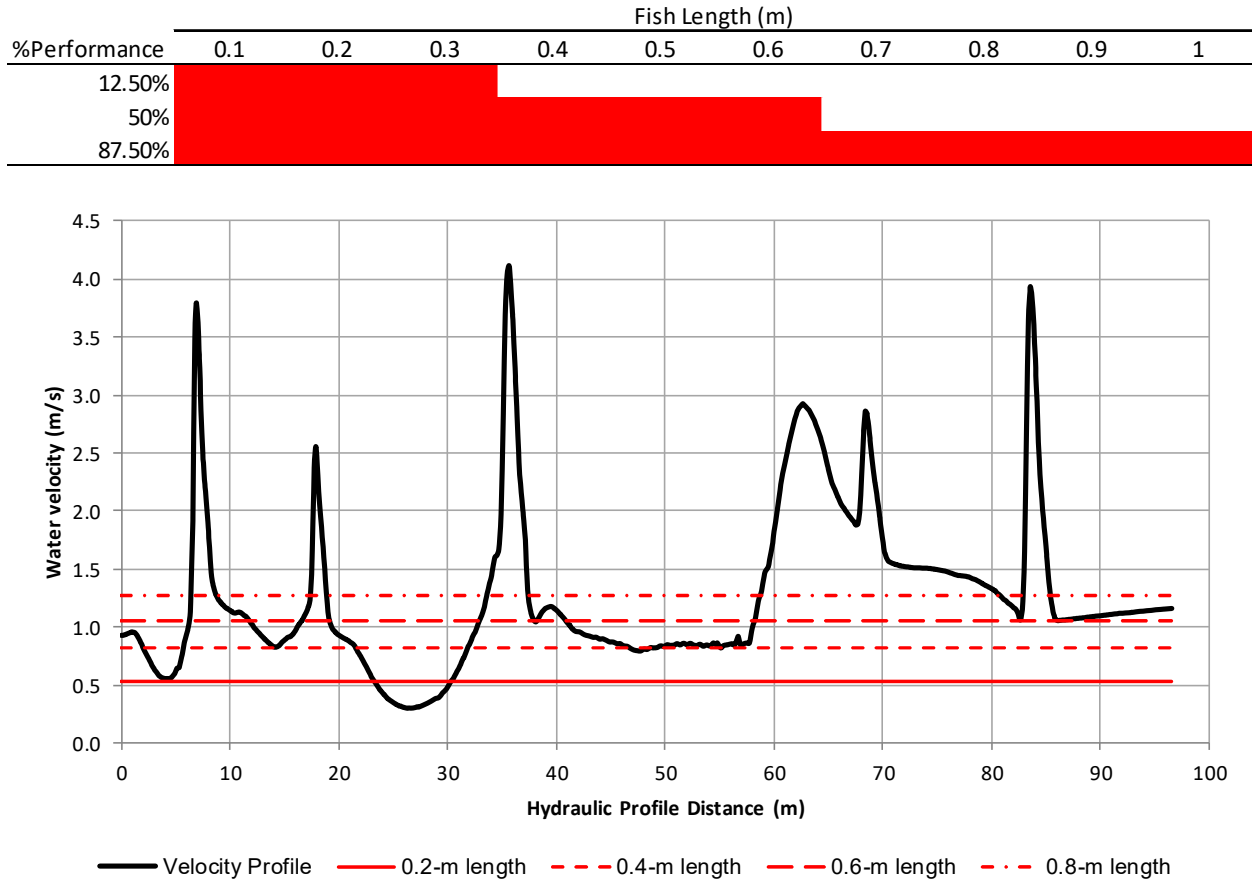
Figure 3. Analysis of example swim-path velocity distribution with endurance-time function and barrier identification

References

Castro-Santos, T., Sanz-Ronda, F.J., and Ruiz-Legazpi, J. (2013). "Breaking the speed limit – comparative sprinting performance of brook trout (*Salvelinus fontinalis*) and brown trout (*Salmo trutta*)). *Can. J. Fish. Aquat. Sci.* 70: 280-293.

Hardee, T.L. (2017). "Evaluating fish passage at whitewater parks using a spatially explicit 2D hydraulic modeling approach." M.S. Thesis. Colorado State University. Dept. of Civil and Environmental Engineering.

Katopodis, C. and Gervais, R. (2016). "Fish swimming performance database and analyses." Canadian Science Advisory Secretariat Research Document 2016/002.

Mooney, D.M. Holmquist-Johnson, C.L. and Broderick, S. (2007). "Rock ramp design guidelines." US Bureau of Reclamation. Department of Interior. Denver, CO.

Parsons, G.R., Stell, E., and Hoover, J.J. (2016). "Estimating burst swim speeds and jumping characteristics of silver carp (*Hypophthalmichthys molitrix*) using video analyses and principles of projectile physics." USACE-ERDC ANSRP-16-2.

Stephens, T.A., Bledsoe, B.P., Fox, B.D., Kolden, E., and Kondratieff, M.C. (2015). "Effects of whitewater parks on fish passage: a spatially explicit hydraulic analysis." *Ecological Engineering*, 83: 305-318.

Turek, J., Haro, A., and Towler, B. (2016). "Federal Interagency Nature-like Fishway Passage Design Guidelines for Atlantic Coast Diadromous Fishes."

The Sacramento River Levee Setback: Floodplain Rehabilitation Design to Enhance Ecologic Function with Consideration of Geomorphic Processes

John Stofleth, M.S., P.E., cbec Inc., Wadesville, IN, j.stofleth@cbecoeng.com
Sam Diaz, P.E,. cbec Inc., W. Sacramento, CA, s.diaz@cbecoeng.com
Chris Bowles, Ph.D. P.E., cbec Inc., W. Sacramento, CA, c.bowles@cbecoeng.com
Doug Shields, Ph.D. P.E. D.WRE, cbec Inc., University, MS, d.shields@cbecoeng.com
Kenric Jameson, West Sacramento Area Flood Control Agency, W. Sacramento, CA

Abstract

The focus of this study is on a 4-mile reach of the Sacramento River downstream of the City of Sacramento (Figure 1) where a major levee setback is currently under construction as a part of a multi-objective flood control and habitat restoration effort. This project lies in the heart of a relatively unique and heavily regulated portion of the flood-control system surrounding the greater Sacramento area. This system is comprised of regulated levees, a large flood bypass system (Yolo Bypass) as well as large flood control reservoirs; however, many of the levees within this system are not constructed to modern engineering standards, which presents a significant risk to surrounding communities and prompts the need to improve the levee infrastructure. In addition, levees along many of the rivers within the California Central Valley, including the Sacramento River, are tightly confined along the river, which significantly limits the available habitat for native aquatic species, such as salmonids, whose spawning and rearing habitat have also been significantly reduced by the construction of dams. Given these constraints, this levee setback project represents an important step towards combining better flood management with significant increases in high quality aquatic habitat.

In our presentation, we will provide an update on the multi-disciplinary approach employed by cbec to integrate hydrodynamic modeling with interpretation of geomorphic response to maximize the restoration benefits that were incorporated into the design of this levee setback project. Our approach utilized the 2-dimensional hydrodynamic and sediment transport model, MIKE21C, along with HEC-EFM (Hydrologic Engineering Center – Ecosystems Functions Model) as analytical tools for characterizing the dynamics of floodplain inundation at ecologically significant flows that correspond to the timing, duration and frequency of inundation essential to specific life cycles (i.e. rearing) of target species. The MIKE 21C model was also used to characterize the overall sediment regime (morphological change and sediment transport) for specific flood events under both existing and design conditions for a 12-mile reach of the Sacramento River. Our assessment was used to support recommendations for restoration actions that optimized both geomorphic and ecologic function. Our analysis provided insight into the geomorphic evolution of the study reach under the design condition and this insight was used to develop strategies for long-term floodplain management.

The physical design criteria for this project includes various functions and processes related to the sustainability of the setback area and are broadly defined as follows:

- Maximize the sustainability of inlet and outlet configurations to the setback area. In this context, sustainability refers to minimizing sediment deposition or scour at the inlet or outlet, thus maintaining an open passage for floodplain inundation in the proposed setback.

- Minimize the potential for fish stranding by maximizing draining of floodplain depressional areas, where reasonably practical.

- Minimize hydraulic and sediment transport impacts to the river corridor, the setback levee, and setback area through consideration of the setback physical design, planting types and habitat mosaics.

- Minimize impacts to existing land uses and other infrastructure adjacent to, or in the vicinity of, habitat enhancement and mitigation areas.

- Consider USACE levee vegetation policy to balance habitat with flood management objectives.

- Maximize compatibility with potential recreation features.

- Apply habitat features where they provide a flood management benefit, such as for erosion control or hydraulic influence.

The restoration design considered and adhered to the overall design criteria of the entire flood control project. An effort was made to ensure the proposed restoration design fell within the constraints of the flood impact analysis with special consideration for design features, such as, instream wood material (IWM) and variation in floodplain topography (topographic heterogeneity).

Hydrodynamic model results from this study generally indicated minor dampening of the natural erosional and depositional trends within the project reach after implementation of the project setback levees, with virtually no changes to the channel morphology (bed forms) beyond the project reach following simulated flood events (Figure 2). However, there are concerns surrounding the relatively small quantities of sediment deposition predicted for the setback area. The sustainability of the setback is key to realizing the project's environmental benefits. Due to the manner in which flow is conveyed through the setback areas, three-dimensional processes are likely to influence the division of sediment between the channel and setback area. Although the MIKE 21C sediment transport module includes quasi-three-dimensional algorithms, such as a vertical profile gradient for suspended sediment concentration and helical flow, fully three-dimensional sediment transport simulations of setback inlets would be useful to verify these results.

Results from the hydrodynamic sediment transport modeling conducted in this study served as an essential tool for quantifying how the proposed project may affect geomorphic processes and how geomorphic processes may influence the performance of the project. However, there are inherently large uncertainties in sediment transport computations due to the episodic nature of the processes that drive the transport of sediment in rivers. We recommend a post-construction monitoring program to assess changing conditions, to inform adaptive management actions (including maintenance activities), and to refine data for subsequent modeling efforts. The development of a plan to monitor sedimentation and erosion would be informed by modeling results and should be developed in later phases of the project.

These types of levee setbacks represent of a significant opportunity for the future; as means of achieving both increased flood protection and habitat restoration and in turn, providing multiple benefits to society. This floodplain management approach is illustrative of one of the most promising solutions to the current levee integrity / flood management crisis in California.
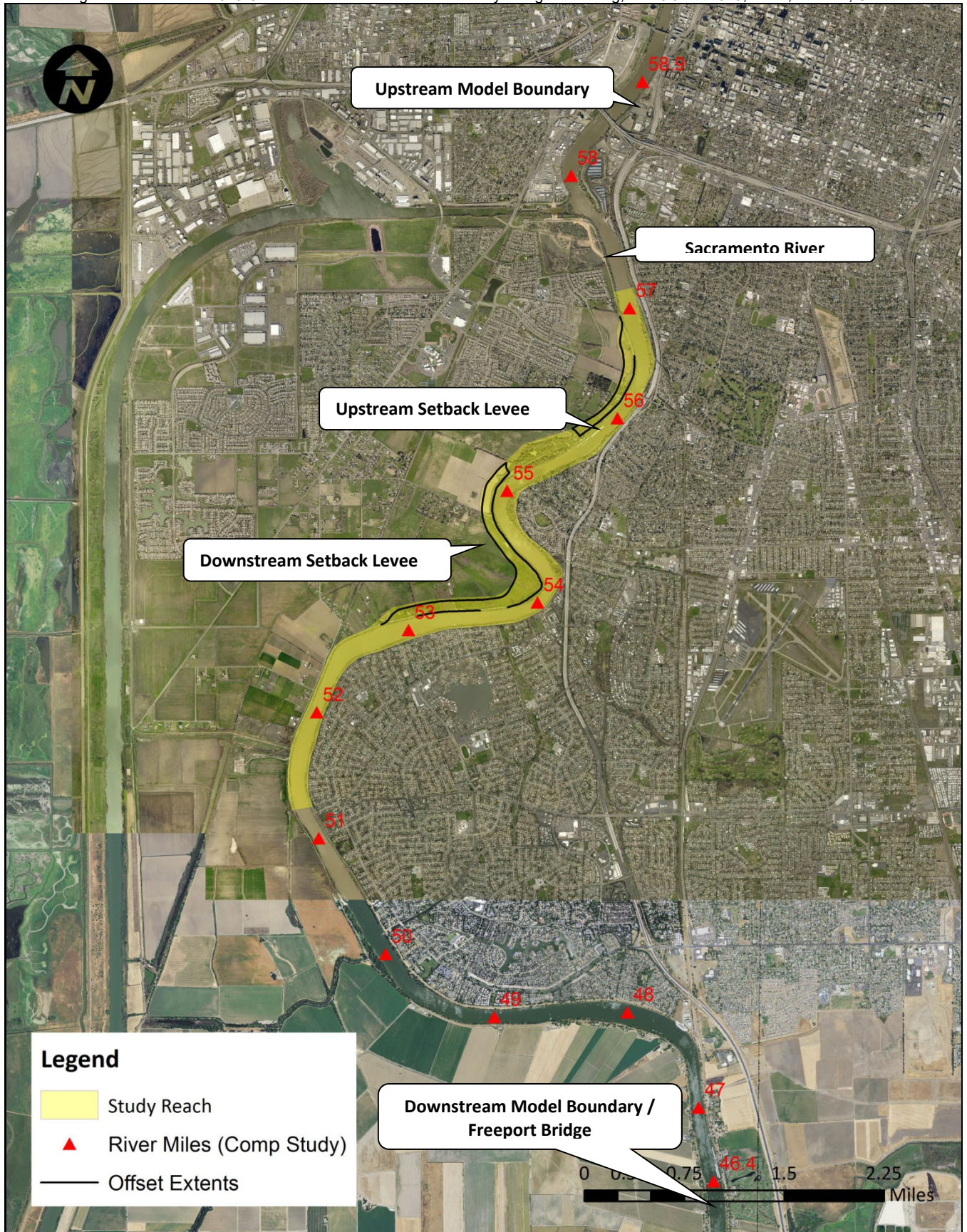
Study reach / MIKE 21C model domain

Figure 1

Notes: Figure illustrates the difference between bed elevations subsequent to the modeled 100-year flood event for existing and setback conditions.

Source: 2010 Aerial Photo. MIKE 21C model output, cbec

SEDHYD 2019

Change Bed in Level – Proposed Compared to Existing Conditions; 100-year Flood Event

Figure 2

International Opportunities - Brazil
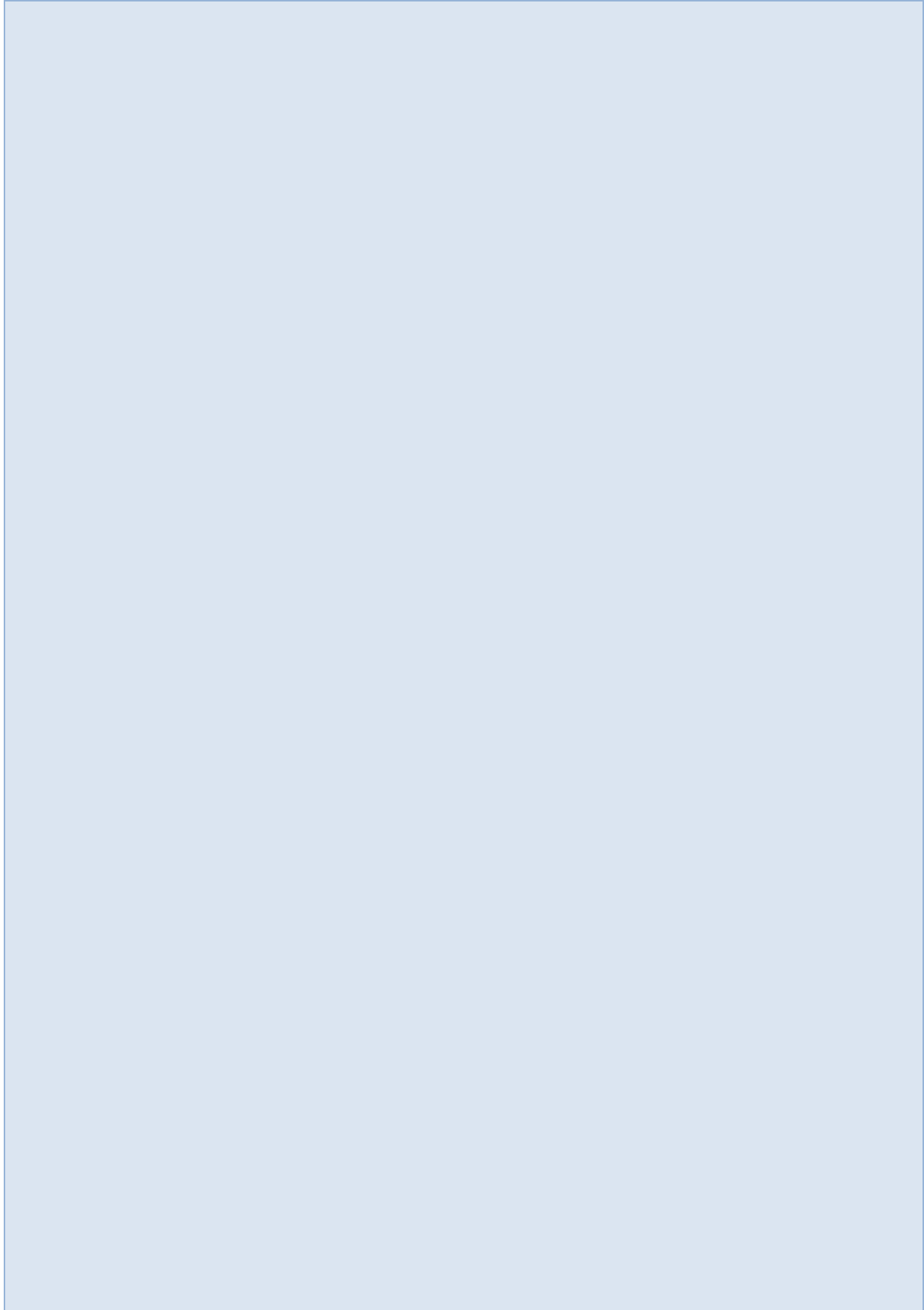
Combined Fluvial Geomorphology, Sediment Transport and Hydrodynamic Model of Navigation Improvement Designs on the Madeira River, Brazil

Calvin Creech, PhD, PE, Lead Interdisciplinary Engineer, USACE, Brasília, Brazil, Calvin.T.Creech@usace.army.mil

Stanford Gibson, PhD, Research Hydraulic Engineer, Hydrologic Engineering Center USACE, Davis, CA, Stanford.Gibson@usace.army.mil

Ana Luisa Osorio, Engineer, DNIT, Brasília, Brazil, ana.nunes@dnit.gov.br

John Hazelton, PE, Hydraulic Engineer, USACE, Wilmington, NC, John.M.Hazelton@usace.army.mil

Renato Amorim, Engineer, DNIT, Brasília, Brazil, renato.amorim@dnit.gov.br

Abstract

The Madeira River is the largest tributary of the Amazon River with average annual discharges (approximately 25,000 cms) greater than the Mississippi River. The Madeira River is also an important waterway for the transport of agricultural commodities produced in central west Brazil to the deep draft ports on the Amazon River. However, navigation reliability is impacted by the low water levels during the dry season (August through October). Three approaches were combined within a planning and engineering study to analyze proposed navigation improvement designs on the Madeira River. These methods include: 1) a fluvial geomorphology study to determine constriction widths and long-term stability of proposed alternatives; 2) a sediment transport model used to analyze effectiveness of navigation alternatives, including river training structures and dredging; and 3) a 2-D hydrodynamic model of proposed alternatives used to optimize river training structure designs.

The fluvial geomorphology study aided navigation design by identifying the necessary constriction width to achieve a self-scouring channel condition. A constriction width of 900 m was used to establish layouts of proposed river training structures. These structures were designed to reduce the effective hydraulic width to the constriction width and were analyzed in the sediment transport and hydrodynamic models. The one-dimensional movable bed sediment transport model was developed in HEC-RAS, and results were compared to sediment loads collected for environmental monitoring of a recently constructed dam. Credibility tests were performed at a decadal, reach scale to validate dynamic equilibrium conditions, and the model was then used to predict the system response associated with the proposed navigation alternatives. Simulations resulted in self-scouring depths of over 2 meters, which is sufficient to meet required navigation reliability. Finally, a 2-D HEC-RAS hydrodynamic model was developed and used to optimize the design of the river training structure alternatives. The hydrodynamic model demonstrated that increases in local velocities due to the proposed structures would not cause impacts to navigation maneuverability within the navigation channel. Mapping shear stress changes for the proposed design identified locations of self-scouring conditions, as well as deposition (primarily between structures). During design optimization, the volume of rock required for improving navigation reliability at one of the critical navigation shoals (Tamanduá) was reduced from approximately 496,000 cubic meters to 332,000 cubic meters while simulating the same level of improvement to navigation.

Introduction

Background

The Madeira River is an important waterway in western Brazil for the transport of agricultural commodities (downbound), petroleum (primarily upbound), and other cargo. Currently, approximately 8 million tonnes of commercial goods are transported along the waterway between the city of Porto Velho, Rondônia and Itacoatiara, Amazonas. However, navigation on the Madeira River is limited by natural morphologic and sediment processes in the river, which include localized shoaling and rock outcrops. These conditions force navigators to light-load and break-up tows during the dry season.

In 2016, the Brazilian National Department of Transportation Infrastructure (in Portuguese, Departamento Nacional de Infraestrutura de Transportes – DNIT) and the US Army Corps of Engineers (USACE) began an intergovernmental agreement to jointly develop designs for waterway improvements throughout Brazil. One objective of this agreement consists of improving navigation reliability of the Madeira River Waterway. The USACE planning processes were leveraged throughout the study to develop alternative plans that optimized design solutions to meet navigation objectives.

Site Conditions

The Madeira River is the largest tributary of the Amazon River. The 1,400,000 km² drainage area of the Madeira River basin constitutes 19% of the total Amazon basin (see Figure 1). Average annual discharges of the Madeira River at the confluence with the Amazon River are approximately 25,000 cms, which are larger than average annual discharges of the Mississippi River at Tarbert Landing (15,000 cms). The Madeira's navigable reach is approximately 1,086 km, from its confluence with the Amazon River (downstream) to Porto Velho, Rondônia (upstream).

Figure 1. Madeira River Watershed location within the Amazon Basin (a); and Study Area along the Madeira (b) from Gibson et al., 2019.

The land use within the Madeira River watershed is dominated by forest, although agriculture is significantly increasing, particularly within the state of Rondônia and in the headwaters in Bolivia. According to the GlobCover 2009 database (European Space Agency, 2010) 76% of the land use within the Madeira River Watershed is classified as forest, and 11% is classified as agricultural (Figure 2a). Outside the watershed, there is significant agriculture, especially to the east in the state of Mato Grosso (Figure 2b). Most of the agricultural commodities that are transported on the Madeira River are produced outside of the watershed. All agricultural commodities shipped on the Madeira River use the Federal Highway BR-361 to arrive in Porto Velho for transfer to the shallow draft waterway.
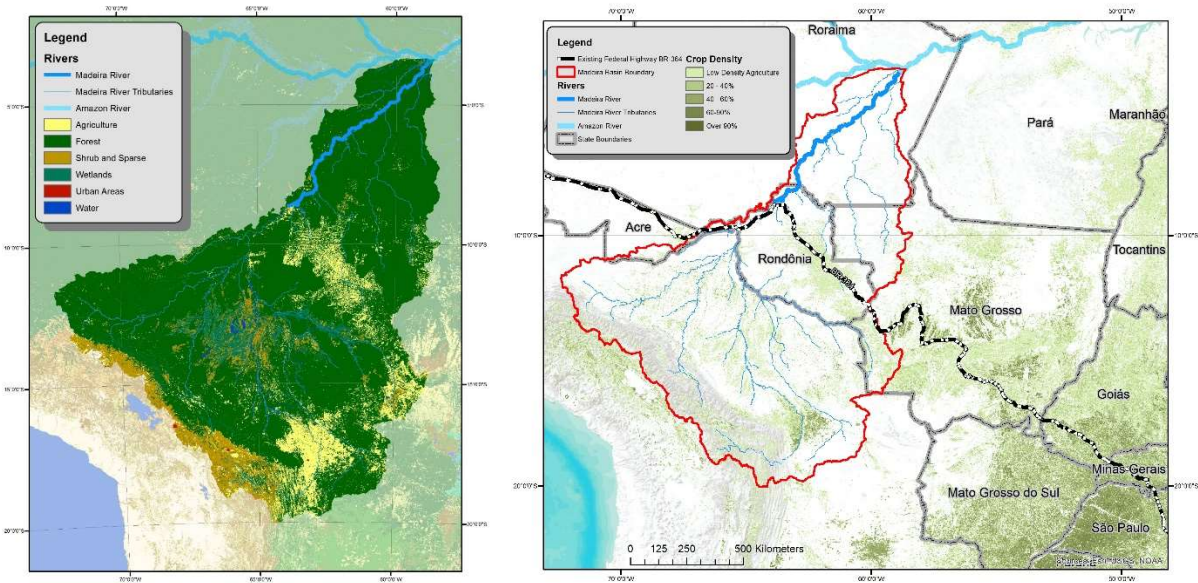
Figure 2. Landuse within the Madeira River Basin (left) and agricultural intensity in surrounding region (right)

Methods

Navigation Reliability and Low Water Reference Plane (LWRP)

The Brazilian government has established the required level of navigation reliability, navigation channel depth, and design barge convoy dimensions. In Brazil, the Madeira River between Porto Velho and the Amazon River has been established as a Brazilian Class II-A River (DNIT, 2016). A Class II-A Waterway includes the following parameters:

- A waterway depth of 3.5 m shall be available 90% of the time. This is to allow a navigation draft of 3.0 m with a 0.5 m overdraft.
- Barge convoys of 33 meters wide by 210 meters long shall be able to navigate 90% of the time. This corresponds to a required waterway width of 145.2 meters (4.4 times the design barge tow width for two-way traffic) for the navigators in straight reaches.
- Waterway widths shall be increased in bends using a formula of $B = L^2/2R$ (where B is the additional waterway width in the bend, L is the length of the barge tow, and R is the bend radius). This applies when the radius is less than 10 x L.

The navigation reliability is influence by hydrologic conditions. Discharges on the Madeira are very consistent from year to year. The average hydrograph is smooth and symmetrical (Figure 3). The wet season runs from February to May, with peak discharges generally in March or April. Discharges decrease from May to September, with the lowest discharges (and the critical navigational condition) in September and October. Stage and discharge data were downloaded from the ANA (Agência Nacional de Águas, National Water Agency) HidroWeb website (ANA, 2017) for this study.

Figure 3. Average Discharge at Porto Velho (blue) with Daily Maximum (red) and Minimum (green) Discharge for each Calendar Day. Data from 1967 through 2018.

A total of twelve (12) navigation shoals have been identified by navigators and have been confirmed with recently collected bathymetric data (by the Brazilian Navy). All of the permanent navigation shoals and the majority of the rock outcrops exist on the upper 620 km of the Madeira River between Manicoré, Amazonas and Porto Velho, Rondônia (which is the focus of this study). The Brazilian Navy uses three gages (Porto Velho, Humaitá, and Manicoré) to establish a 90% exceedance stage (these gages are shown in Figure 1b). To establish a Low Water Reference Plane (LWRP) between gages, a one-dimensional HEC-RAS model was developed. The stages at the Brazilian Navy gages were converted to a discharge at each gage by developing a rating curve and were used for both boundary conditions (Manicoré) as well as calibration points (Humaitá and Porto Velho) in the hydraulic model.

The open channel steady-state hydraulic model HEC-RAS (version 5.0.4) was used to model the Madeira River between Porto Velho and Manicoré. Bathymetric data was commissioned by DNIT and collected by the Brazilian Navy in February and March 2016 (during high water conditions). This is the primary data used for in-channel elevations in this study. This survey consists of bank to bank single beam depth readings with cross sections spaced approximately 150-175 meters apart (or 6-7 cross sections per km) for the 1,086 km navigation channel.

The downstream boundary of the model was located at Manicoré, Amazonas. A rating curve boundary condition was supplied to the model representing the discharge-stage relationship associated with the most recent rating curve (using stage-discharge data collected since 2010).

The stage data was converted to elevations (EGM08 datum, using a "zero of the gage" of 6.81m). These data were used to establish the LWRP at the 90% exceedance level.

Fluvial Geomorphology

The Madeira River can be categorized into two morphologically distinct reaches: Segment I is downstream of Manicoré and Segment II is upstream of Manicoré (Teixeira and Maia, 2009). The upstream reach between Manicoré, Amazonas and Porto Velho, Rondônia is the focus of this study and is characterized by a wider alluvial valley where the river makes occasional contact with the Pleistocene bluffs. This segment is more sinuous (sinuosity = 1.4) and more morphologically active, eroding and building islands and bars more frequently. Downstream of Manicoré, the sinuosity decreases to 1.18 and the alluvial valley narrows. As the valley narrows, the river has more contact with the Pleistocene terraces (see Figure 4).

Most of the navigation impedances are located in Segment II (upstream 620 km of the waterway). Therefore, this reach was the focus of the modeling efforts performed for the study. This segment was investigated to establish constriction widths at locations of limited navigation reliability.
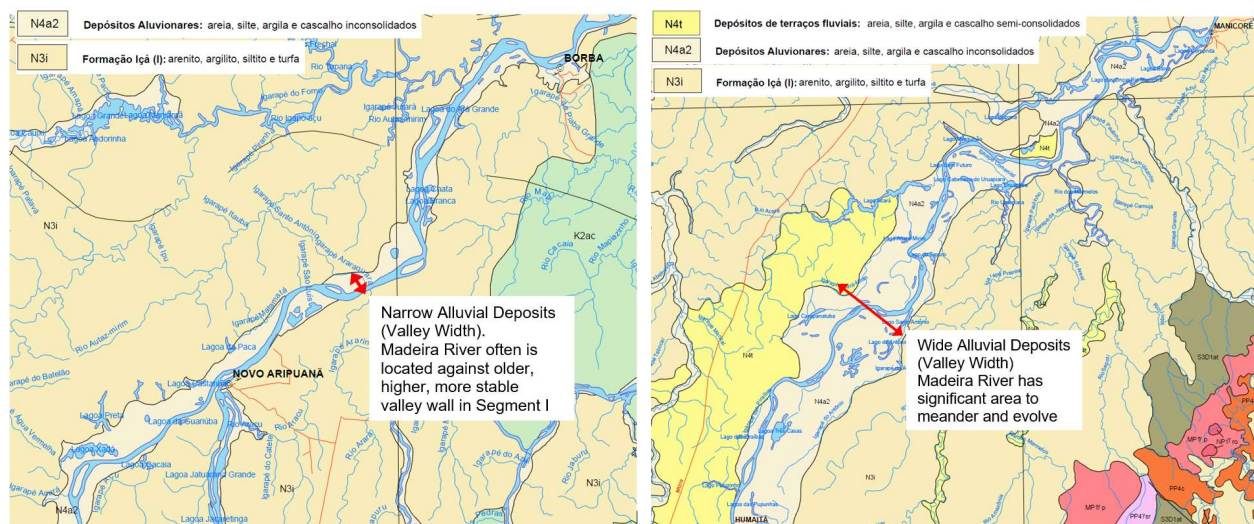
Figure 4. Typical Holocene Valley Widths of Segment I between the Amazon River and Manicoré (left) and Segment II between Manicoré and Porto Velho (right)

Sediment Transport Modeling and Sediment Data

A sediment transport model was used to assess the existing conditions of the sediment dynamics and was the primary tool to address long-term impacts to the navigation channel depths based on the proposed alternatives. The sediment transport functionality in HEC-RAS was applied, which used the Lausen (Copeland) sediment transport function with the Exner 7 sorting method. This model also used data primarily from the hydraulic model as well as recent studies on sediment conditions (sediment gradations, sediment load estimates, boundary conditions, etc) collected by the Santo Antônio Energy Company (PCE, 2015a and PCE, 2015b).

Bed Gradations: Bed gradation data were estimated from about 268 bed gradation samples collected at three sites (PCE, 2015a). Sand bed rivers generally fine downstream (though Gibson et al.,2016, reported downstream coarsening on the Missouri River). Rosseto (2013) recorded 12 channel bar gradations along the Madeira River but the data did not demonstrate reliable longitudinal trends (e.g. fining or coarsening). Therefore, the bed material for the entire reach was initially represented with a single average bed gradation. Very fine sand was the most prevalent grain class, and about 75% of the bed material was fine and very fine sand (Figure 5, left).

Boundary Loads (Discharge-Load Curve): Model objectives drove the decision to limit the mobile bed model to the sand fraction of the Madeira sediment load. Turbidity analysis, overbank deposition, or total sediment budget computations could benefit from a total load model; however, navigation alternatives are influenced almost entirely by bed material load, which is limited to the sand fraction of the total load. HEC-RAS sediment modelers have used this approach on other large sand bed rivers (Shelley and Gibson, 2015). The modeling team used the best estimate of historic sand loads, crafting a discharge load curve from collected data (Figure 5, right). An initial discharge load curve for the HEC-RAS model used pre-dam (earliest data) to validate a pre-dam sediment condition of dynamic equilibrium along the study reach.
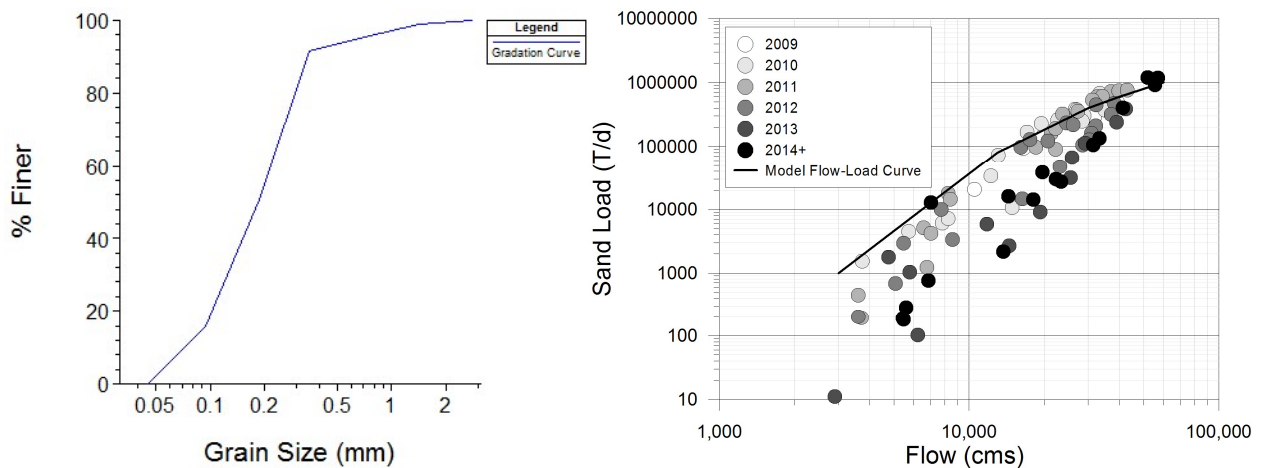
Figure 5. Bed Gradation used in the Sediment Transport Model (left) and Upstream Boundary Condition Discharge-Load Curve (right)

Boundary Load Gradations (Discharge-Gradation): The Madeira River coarsens with discharge; however, this coarsening tends to be the result of wash load exhaustion, as the highest discharges occur after the wash load peak. PCE (2015b) data included sub-sand resolution data on the sediment loads. Up to the maximum measured discharge, most of the sand load is fine sand (FS). These data do not distinguish between FS (0.125-0.25 mm) and VFS (0.0625-0.125 mm). Initial assumptions that split the boundary load evenly between these grain classes resulted in a model run that failed the equilibrium credibility test, depositing too much sediment in the test time period. However, most bed samples included more very fine sand than fine sand, suggesting that more of the "Fine Sand" in the PCE (2015a) measurements should be attributed to the VFS grain class in HEC-RAS. As a result, a 70%-30%, VFS-FS, base discharge partition was adopted in the model.

Hydrodynamic Modeling in HEC-RAS

A multi-dimensional hydrodynamic model of structural alternatives (dikes, cutoffs, etc.) was developed at site-specific locations to analyze designs aimed to improve navigation reliability. These locations were identified as candidate locations for river training structures in both a planning Charette in March 2018 and the sediment transport modeling task. This model was used to refine alternatives by optimizing structure layouts. Boundary conditions were provided by the Hydraulic and Sediment Modeling tasks.

The modeling was conducted using the two-dimensional capabilities in HEC-RAS (version 5.0.4). The model was primarily used to evaluate hydrodynamic impacts associated with the proposed river training structures. In addition to the structural alternatives, a without-projects condition hydrodynamic simulation was made for use in comparison of the results of the structural alternatives.

The discharge area boundaries were matched to the upstream and downstream 1D model cross sections and also served as the boundary condition lines. A DX, DY spacing of 20 m x 20 m was used for the 2D discharge area mesh. Breaklines were created at 5 m minimum spacing along the river banks, islands and significant changes in elevation. The Manning's n layers were created as Map Layers within RAS Mapper. The calibrated 1D Manning's n values were used for the main channel layer (n = 0.028) and the overbanks (n=0.08).

Results

Navigation Reliability

Low Water Reference Plane (LWRP): A combination of the hydrology and hydraulic studies were used to develop the Low Water Reference Plane (based on a 90% exceedance condition). A LWRP had not previously been available for the Madeira River, and this plane was required to determine dredging volumes or project success associated with proposed river training structure measures. The results of the LWRP are shown in Figure 6.

Dredging Requirements: Using bathymetry data from the 2016 Navy survey, the team analyzed the amount of material that is impacting navigation and requires interventions (rock removal, dredging, self-scouring structures, etc.) for achieving specific levels of reliability. The depths collected by the Brazilian Navy were subtracted from the calculated LWRP, and volumes of material that are greater than specified navigation depths (of 3.0m, 3.5m, and 4.0m) were calculated (see Figure 7). The planning study has determined that a desired navigation channel shall be a minimum of 3.5 meters deep with a 90% level of reliability. Based on the analysis performed on the current reliability, a 3.5 meter channel is only available approximately 75% of the time, which does not meet the objective defined in the planning study. To achieve 90% reliability, minimum dredging of 500,000 m^3 per year is required.
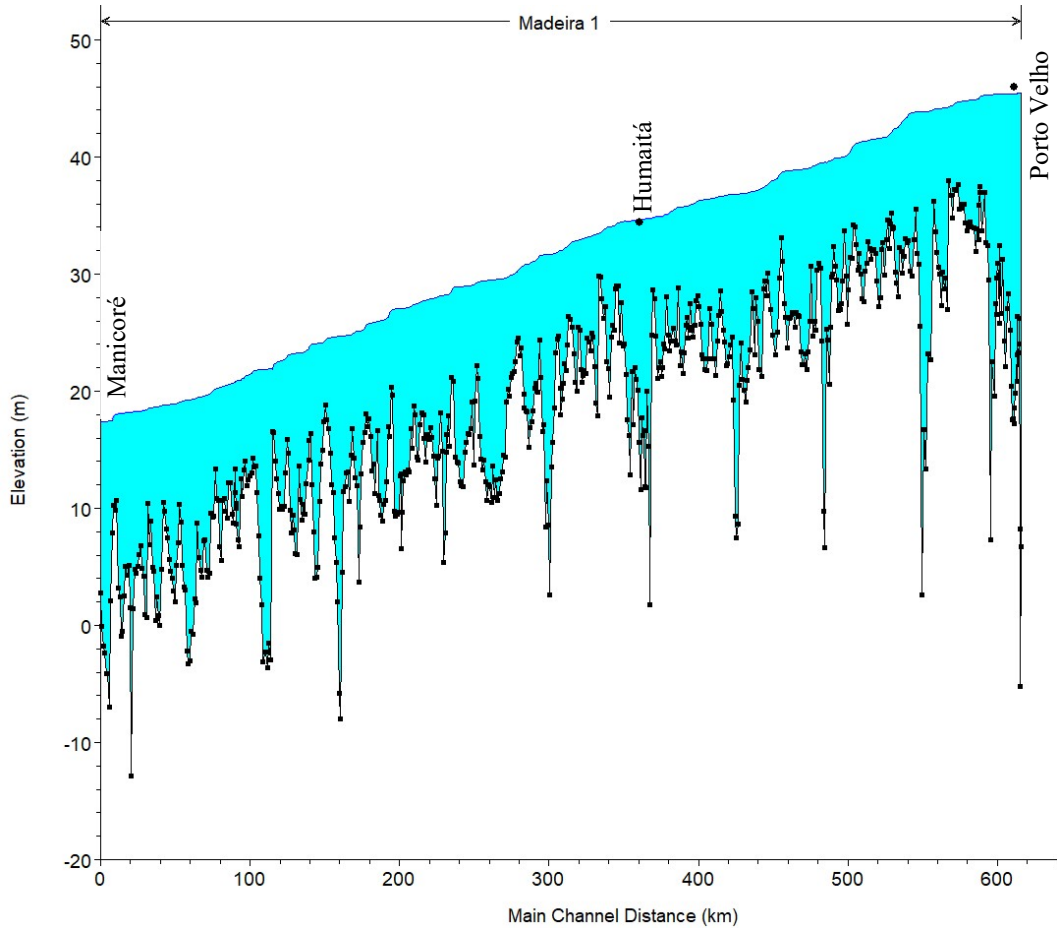
Figure 6. HEC-RAS Low Water Condition Calculated Reference Level
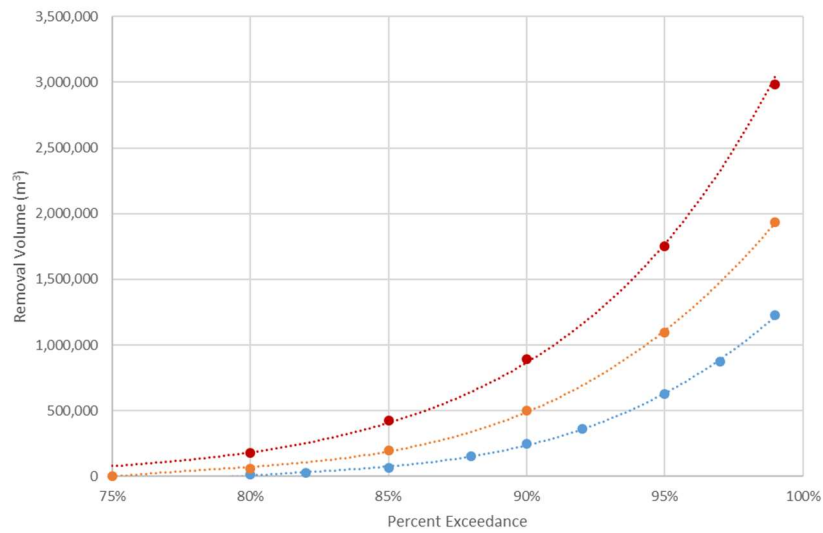
Figure 7. Calculated Dredging Volumes and Reliability for 3m Depth (blue), 3.5m Depth (orange), and 4m Depth (red) Two-Way Traffic on the Madeira River Navigation Channel

Fluvial Geomorphology Conditions

When designing river training structures, the goal is often to approximate the natural width of a self-maintaining (or limited-dredging) channel. This width is referred to as the channel stabilization width or constriction width. An estimate for the channel stabilization width was developed for the Madeira River between Porto Velho, Rondônia and Manicoré, Amazonas. The width of contiguous sufficient depth was measured every 10 kilometers. Measurements were not taken in areas where split flows existed in the channel, or where shoaling prevented contiguous sufficient depth. In total, 39 width measurements were taken which represent locations of reliable sufficient navigation depths along the channel. The constriction width does not significantly increase in the downstream direction (see Figure 8), and therefore a single constriction width was applied to the entire reach between Manicoré and Porto Velho. The median width was approximately 630 m; the maximum and minimum were approximately 1070 m and 450 m, respectively. The 75th and 25th percentiles were approximately 810 meters and 570 meters. Based on this analysis an initial constriction width of 800 meters was applied to the river training structures (although this was subsequently increased to 900 meters during the sediment transport modeling task).
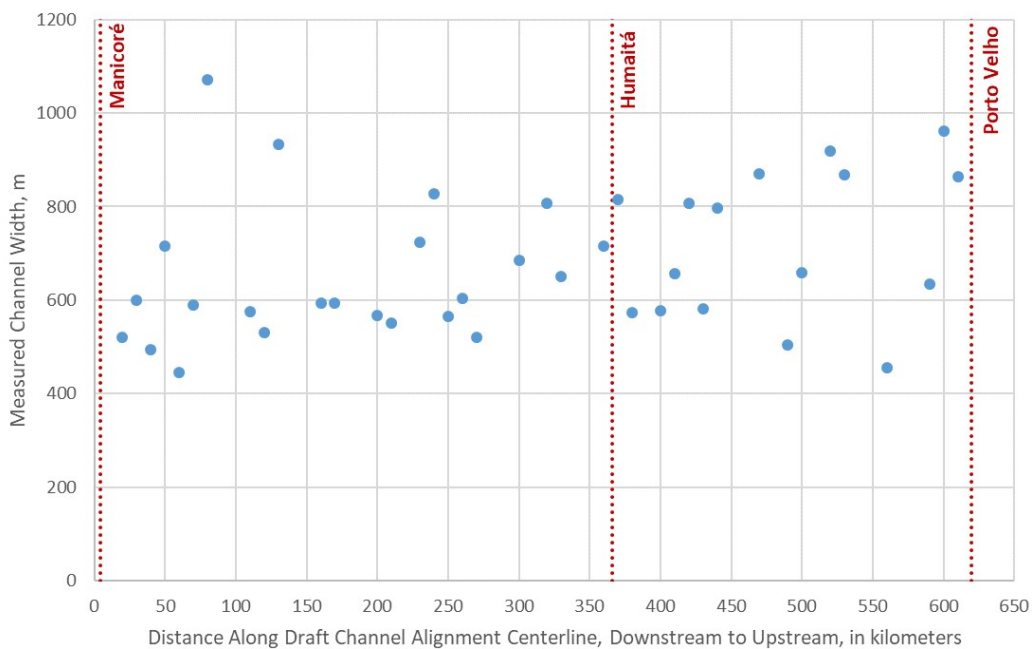
Figure 8. Measured width of the Madeira River in locations without navigation impedances

Sediment Transport Modeling

Based on the fluvial geomorphology study, the Madeira River was determined to be in a general state of dynamic equilibrium prior to dam construction (except near Manicoré, which has been aggrading due to a large natural meander cutoff that occurred in the 1980s). Therefore, the sediment transport model was first used to conduct a quasi-equilibrium credibility test. The

model ran the 1967-2014 discharge time series with the best estimate algorithms and historic sediment boundary conditions (e.g. the rating curve in Figure 5b). To test model credibility, the study team evaluated the period of record mass change along the reach against the assumption that the Madeira was in a long term, decadal scale, equilibrium before the dams. This assumption was tested with the Longitudinal Cumulative Mass Curve (LCMC), which sums the mass change from upstream to downstream. The LCMC for the period of record, mobile bed, sediment transport analysis of the 620 km study reach on the Madeira is included in Figure 9. These results show a general state of dynamic equilibrium and an aggradation trend near Manicoré, Amazonas.
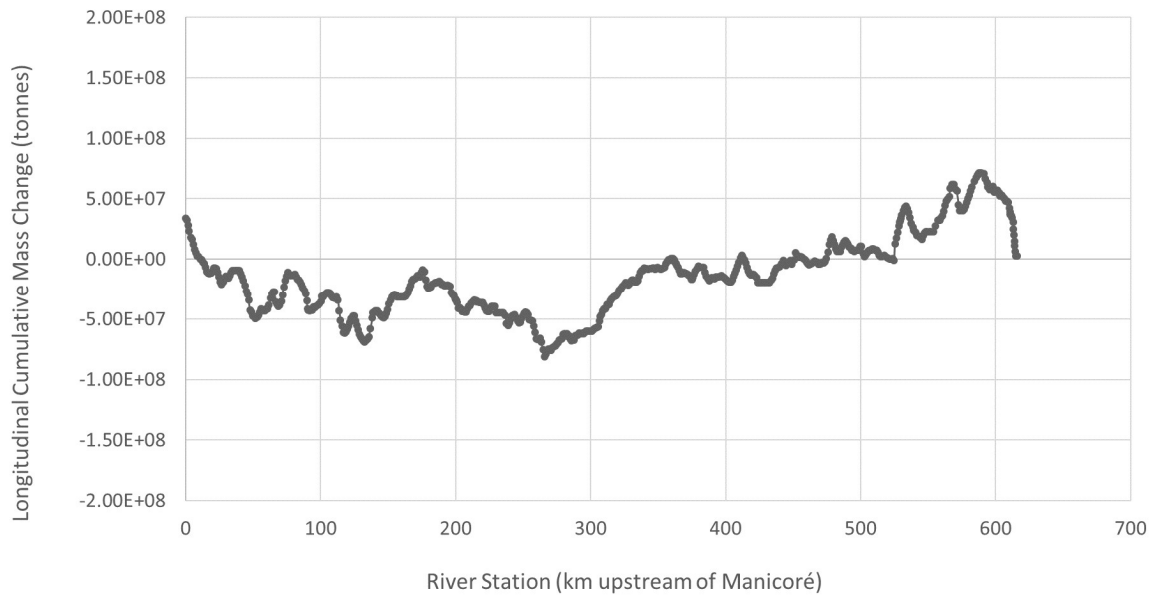
Figure 9. Longitudinal Cumulative Mass Curve for the sediment transport model of the Madeira River

A mid-reach concentration calibration of the sand fraction of the total load was performed using PCE (2015b) data at Humaitá. The model sand flux at Humaitá was slightly higher than the observed data (particularly for low discharges) but the observed data was within the variability of the computed results. The monthly sand flux that HEC-RAS computed over the 47-year historic period of record (in tonnes per day) is plotted against discharge in Figure 10 (left). In addition, the observed data were compared to only the fluxes computed during the measurement window (2009-2014) in Figure 10 (right) to test if this is a non-stationary effect, but the time-window specific trend is similar to the entire period of record.

The twelve (12) navigation critical sites were each evaluated to determine whether the site could be viably improved using river training structures. Of the twelve (12) sites, seven (7) were identified to be candidate locations for river training structures based on morphological stability and the permanence and scale of the navigation shoal. A channel stabilization width of 900 meters was applied to these sites and an example of the channel layout for the Tamanduá site (located approximately 30 km downstream of Porto Velho) is shown in Figure 11. The sediment transport model was then applied to the sites to demonstrate the self-scouring potential associated with the proposed alternative. A 10-year simulation was performed to investigate the system response to these designs. A plot of the initial conditions, final without-project

conditions, and final with-project conditions is shown in Figure 12, which demonstrates the proposed alternative at Tamanduá results in over 2 m of self-scour. This would sufficiently address the navigation shoal without the need for significant future maintenance dredging.
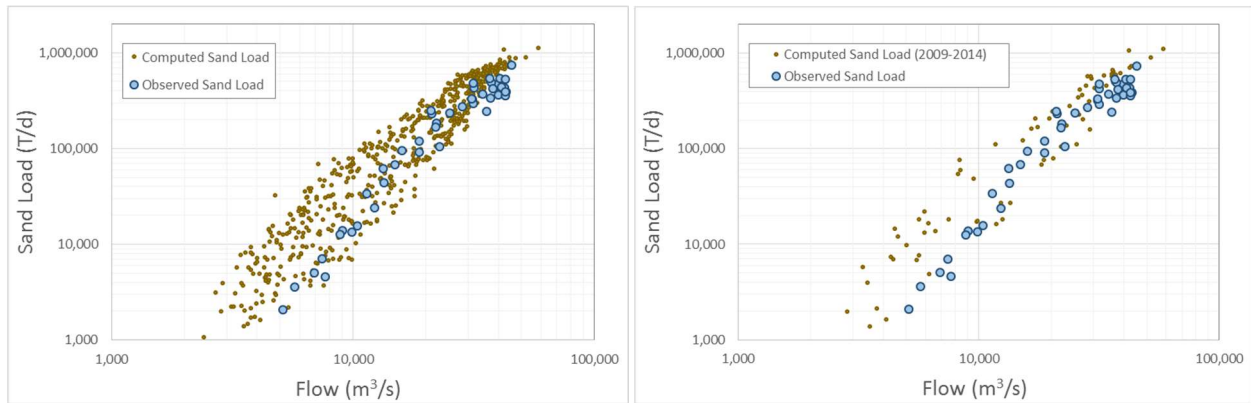
Figure 10. Sand load corresponding to discharge, computed during HEC-RAS period of record simulation (left) and limited to the period of observed data (2009-2014, right)
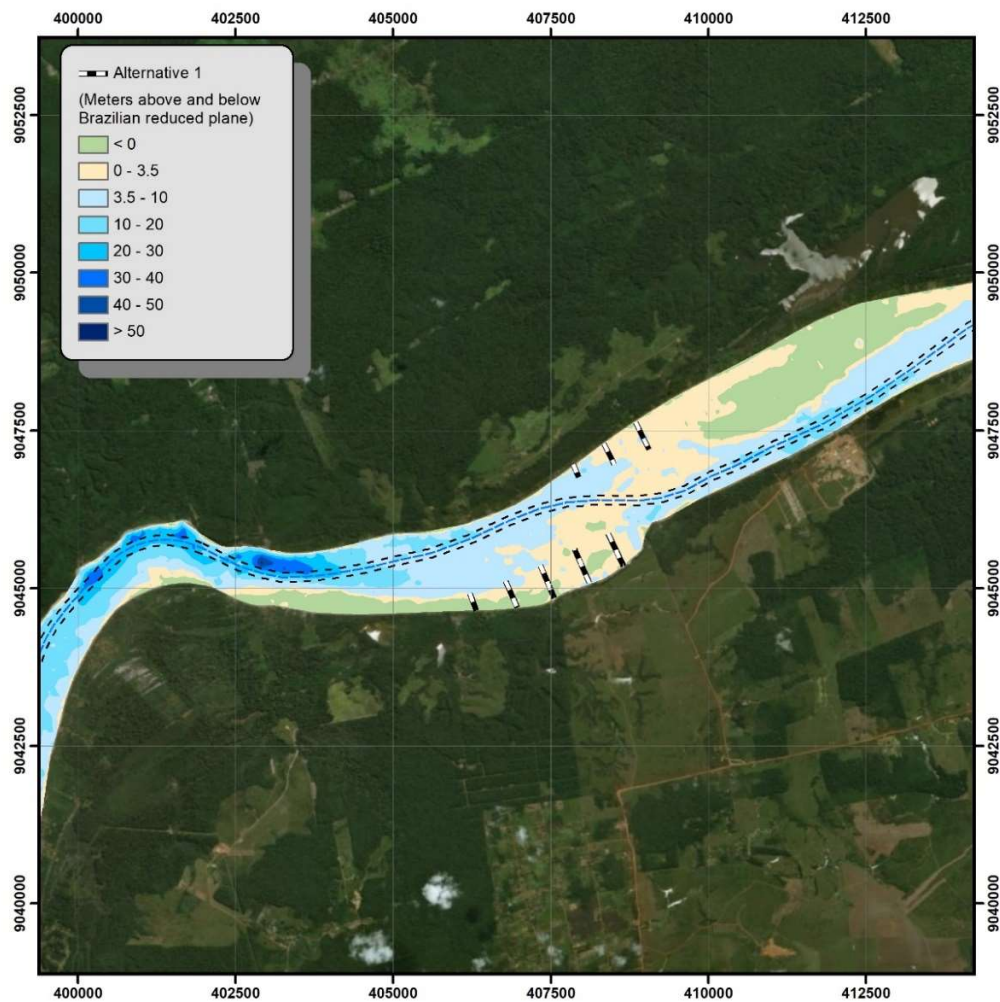
Figure 11. Example River Training Structure Alternative at Tamanduá
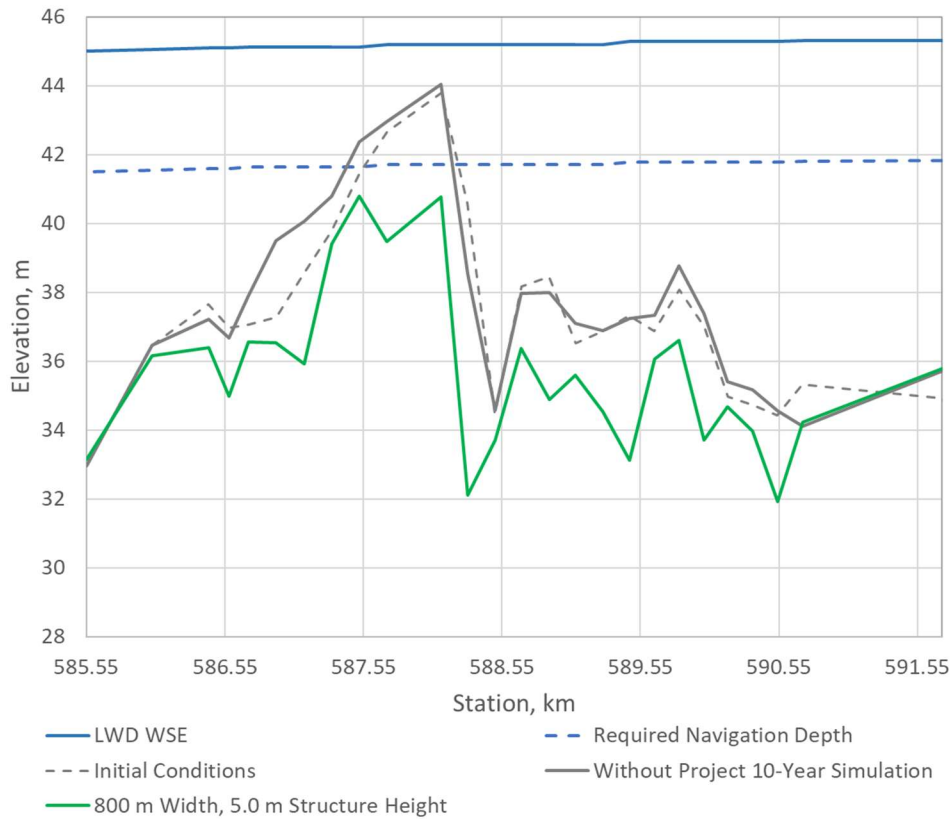
Figure 12. Evaluated impacts resulting from proposed river training structures at Tamanduá

Hydrodynamic Modeling

The effectiveness of the alternatives was evaluated by comparing the change in shear stress along the channel bottom between existing conditions and with the structure alternative in place. HEC-RAS Mapper was used to create a raster of the shear stress in Pascals for existing conditions and with structural alternatives in place. The existing condition raster was subtracted from the alternative raster to estimate the change in shear stress associated with the proposed alternative. Color shaded maps were prepared, indicating areas of increased shear stress with the potential for increased scour of the channel bottom. Areas of decreased shear indicate areas of potential sediment deposition. Changes in velocity patterns were also used to evaluate the alternatives.

As an example, eight alternatives with varying structure type and dike configuration were evaluated at Tamanduá. The top elevation of the structures was set to 5.0 m above the 90% exceedance stage. The evaluation used the shear stress parameter results from the 2D HEC-RAS model to determine the effectiveness of the alternative to encourage scour in the shoaling areas. Various derivations of the dike field design and constriction widths were generated and analyzed, but all designs are similar in nature with a dike field on the upper right bank and a second dike field on the lower left bank.

The number of dikes, location and lengths were modified within the 2D HEC-RAS model to determine the optimal configuration. Constriction widths of 650 m, 800 m, 900 m and 1000 m were modeled to evaluate the change in shear stress when compared to existing conditions. The 650 m width between training structures produced excessive velocities. During the 50% exceedance discharge of 16,000 cms, the velocity in the navigation channel increased from 1.2 m/s to 2.8 m/s compared to existing conditions and no structures. The high velocities could become a hazard to barge traffic given the close proximity of the rock structures. The narrow 650 m width also increased scour potential along the right river bank downstream of the structures leading to possible bank erosion. The 800 m width exhibited some of the same negative high velocity issues but to a lesser degree than the 650 m. Balancing the self-scouring potential, limiting increases in velocities, and limiting construction volumes, an iterative approach (with revised sediment transport modeling) yielded a constriction width of 900m for the Tamanduá site. This corresponds to a volume of 332,000 m^3 to construct the structures, which reduced volumes from the initial design of 496,000 m^3 (associated with a constriction width of 800m). The impacts to shear stress for the proposed design are shown in Figure 13, and the velocity fields are shown in Figure 14.
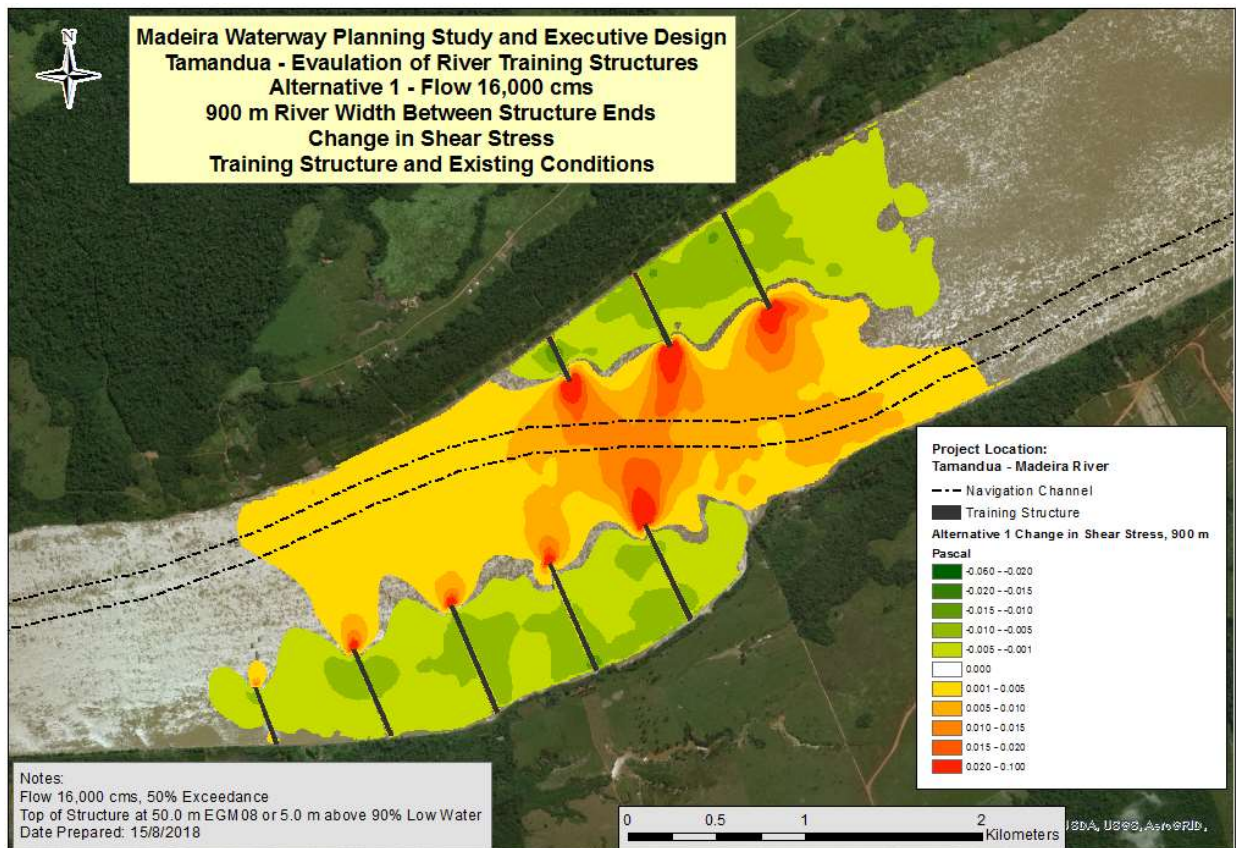
Figure 13. Change in shear stress at Tamanduá (medium discharge)
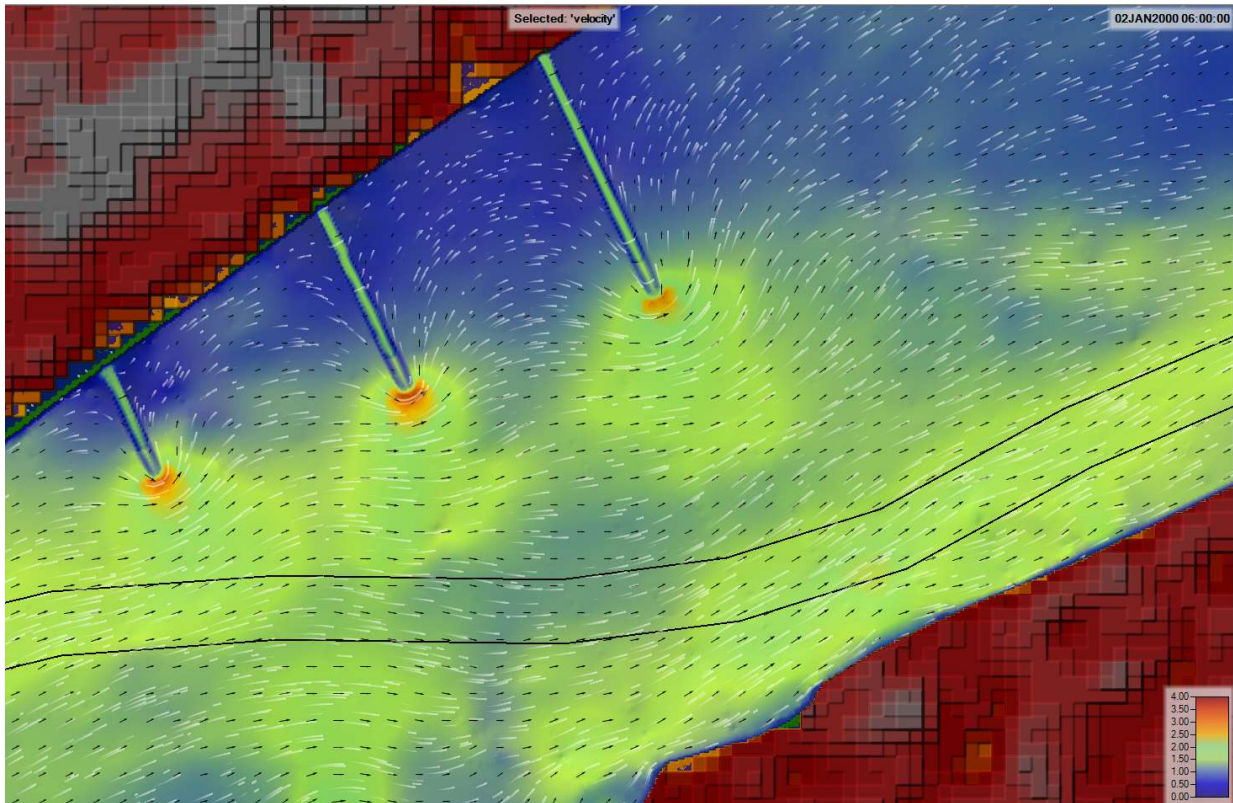
Figure 14. Velocity vectors associated with Tamanduá proposed design

Summary and Conclusions

The Madeira River in Brazil has not undergone significant development to improve navigation reliability. Only recently, dredging has begun during the dry season to improve navigation depths at some critical shoals. Currently, USACE and DNIT are developing alternative plans aimed to improve the navigation reliability, with measures to include river training structures as well as dredging and rock excavation.

The design of the river improvement required several studies including the development of a Low Water Reference Plane (LWRP), hydraulic models, fluvial geomorphology study, a sediment transport model, and hydrodynamic modeling to optimize structure design. The LWRP was based on a 90% exceedance stage, and a steady state HEC-RAS model simulated LWRP between calibration points. A fluvial geomorphology study identified candidate locations for river training structures and the necessary constriction width associated with the structure design (initially 800m). The sediment transport model then was used to evaluate system response to the proposed design and, together with a hydrodynamic model, was iteratively run to optimize results and minimize construction volumes. While the model should not predict absolute responses to management alternatives, it should credibly predict relative differences between with- and without-project conditions, at the reach scale. In addition to developing tools that were used to optimize navigation improvement design, the approaches used and tools developed also met the capacity building objectives of the intergovernmental partnership between USACE and DNIT.

References

ANA. 2017. Hidroweb.http://hidroweb.ana.gov.br/. Accessed February 2017.

DNIT. 2016. Boletim Administrativo, N°. 172, 13 September 2016.

European Space Agency. 2010. GlobCover 2009. http://due.esrin.esa.int/globcover/. Accessed on 23 June 2016.

Gibson, S., Osorio, A., Creech, C., Amorim, R., Dircksen, M., Dahl, T., and Koohafkan, M. 2019 Two pool-to-pool spacing periods on large sand-bed rivers: Mega-pools on the Madeira and Mississippi. Geomorphology 328, 196-210.

Gibson, S.A., Shelley, J., and Cai, C. 2016. Downstream Coarsening on the Missouri River. Proceedings of the 2016 River Flow Conference, St. Louis, MO.

PCE. 2015a. Levantamento Topobatimétrico do Rio Madeira para Acompanhamento da Evolução do Leitoa Jusante da UHE Santo Antônio (Topo-Bathymetric Survey of the Rio Madeira to Evaluate the Evolution of the Bed Downstream of the Santo Antônio Hydroelectric Power Facility). PJ0955-X-H41-GR-RL-0002-0A.

PCE. 2015b. Consolidação e Análise dos Dados Hidrossedimentológicos do Rio Madeira – Janeiro de 2008 a Dezembro de 2014 (Consolidation and Analysis of the Hydrologic and Sediment Data of the Madeira River – January 2008 through December 2014). PJ0955-X-H41-GR-RL-0004-0A.

Rosseto, M. 2013. Proveniência sedimentar das areias holocênicas do rio Madeira, Amazonas, Brasil. 71 p.: il & mapas. Dissertação (Mestrado): IGc/USP.

Shelley, J., and Gibson, S.A. 2015. Modeling bed degradation of a large, sand-bed river with in-channel mining with HEC-RAS. Proceedings of the 2015 Federal Interagency Sediment Conference, SedHyd, Reno, NV.

Teixeira, S.G., and Maia, M.A.M. 2009. "Análise da Dinâmica das Marges do Rio Madeira (AM) no Período de 1987 à 2007, A Partir de Imagens de Sensores Remotos Òpticos," XIV Simpósio Brasileiro de Sensoriamento Remoto, Natal, Brasil, 25-30 abril 2009, INPE, p. 1559-1566.

Development and Use of Hydraulic Modeling for a Navigation Project in a Reservoir Backwater Influenced River

Matthew Dircksen, Hydraulic Engineer, US Army Corps of Engineers Chicago District, Chicago, Illinois, Matthew.S.Dircksen@usace.army.mil

Calvin Creech, Lead Interdisciplinary Engineer, US Army Corps of Engineers Mobile District, Mobile, Alabama, Calvin.T.Creech@usace.army.mil

Renato Amorim, Civil Engineer, DNIT, Brasilia, DF, Brazil, renato.amorim@dnit.gov.br

William Veatch, Hydrologist, US Army Corps of Engineers New Orleans District, New Orleans, Louisiana, William.C.Veatch@usace.army.mil

Ana Luisa N.A.O. Castañon, Civil Engineer, DNIT, Brasilia, DF, Brazil, ana.nunes@dnit.gov.br

Abstract

One and two dimensional hydraulic modeling was used to evaluate approaches for determining a project design reference plane for a navigation project in a reservoir-backwater-influenced reach in the Tocantins River in the Northern region of Brazil. A proposed rock excavation project in the Pedral do Lourenco reach is intended to provide adequate depths and conditions for safe navigation during the dry season. Numerical models were developed using HEC-RAS software to determine water levels throughout a 35 kilometer section of river with significant rock outcrops. Recent high-resolution bathymetric surveys were used to adequately capture the rapid changes in depth and width of the main channel of the river. Calibration was completed using a temporally-rich and spatially-rich dataset of records from staff gauges located throughout the project area. Profiles - and in turn project design reference planes - were modeled for boundary conditions based on separate statistical analyses of upstream flow and downstream reservoir levels. One dimensional and two dimensional models were developed and compared. A period a record simulation was completed to establish historical time exceeded water levels at each station along the navigation channel throughout the project reach. A coincident frequency analysis was completed using the total probability method to incorporate the appropriate influence of the flow from upstream and the Tucuruí Reservoir level downstream. With-project conditions were modeled to determine the hydrodynamic response for each of the aforementioned approaches. An analysis of past hydrologic conditions on the system, revised to include the proposed navigation channel, determined the relative effectiveness of each approach. As necessary, iterations of modeling with-project conditions were completed until desired navigational criteria were met or desired probability levels were met. Modeling tools and results were used to hindcast navigation reliability had the project been in place, estimate rock removal quantities for the project, and estimate the probability of desired navigation conditions if the project is completed.

Introduction

Background

The Tocantins River runs through the northern Brazilian states of Tocantins and Pará and discharges to the Atlantic Ocean near Belém, in Northeast Brazil, as shown in Figure 1. Navigation on the Tocantins River is impeded by shallow depths and sharp bends in the river planform geometry. One major impedance is known as the Pedral do Lourenço, located in the State of Pará, Brazil, approximately 150 kilometers north of the city of Marabá. A rock removal project has been proposed at the Pedral do Lourenço site. The project consists of the removal of approximately 1.3 million cubic meters of rock (primarily basalt and granite) from the river, based on a preliminary estimate, to improve conditions for navigation through a 35-km-long rock outcrop reach. The Pedral do Lourenço rock site is located just upstream (south) of the reservoir impounded by the Tucuruí hydroelectric dam.

Figure 1. Location Map

Two factors can contribute to low (or high) water levels through the project area. First, the controlled Tucuruí dam, whose reservoir delta backs up into the project area, can induce a low downstream level, minimizing backwater effects seen when the reservoir is high. Second, the river flow is a function of precipitation in the basin. The dry season causes low flows each year, and a recent multi-year drought has caused even lower flows.

The Brazilian federal department of transportation infrastructure known as DNIT (in Portuguese: Departamento Nacional de Infraestrutura de Transportes) is responsible for the planning, design, and construction of transportation infrastructure in Brazil including federal roads, federal railways, and federal waterways. The US Army Corps of Engineers (USACE) and DNIT entered into an agreement to support DNIT waterway projects. USACE provides engineering support as needed on the Tocantins River waterway development project.

DNIT contracted a design-build project using preliminary bathymetry and design reference plane criteria. Further analysis has been completed to better understand site conditions and to design the project to meet intended reliability standards.

Objectives

A large rock removal project was planned for the Pedral do Lourenço reach in order to remove an impediment to navigation in the Tocantins River. An analytical and iterative process was applied to collect information and develop tools to achieve a greater understanding of the project area and design a project reference plane for identifying the locations and bottom elevations for rock removal. The development of one-dimensional (1-D) and two-dimensional (2-D) hydraulic models was chosen as the means to achieve these general objectives.

Hydraulic modeling was completed to achieve several specific objectives: (1) to identify the rock removal locations needed to meet the navigation criteria (depth, turning radius), (2) to better understand flow patterns under different river and reservoir conditions, (3) to calculate duration exceedance statistics and annual chance of exceedance statistics of water levels throughout the project area, (4) to develop a cost-effective plan and profile of a design reference plane for the navigation channel, (5) to evaluate the stage response to a post-project condition after rock has been removed from the navigation channel.

Methods

1-D Hydraulic Modeling

A 1-D hydraulic model was developed using HEC-RAS software. This 1-D model enables short runtimes and the ability to perform multi-year simulations. Water level profiles were computed using the steady flow option in HEC-RAS. A spatially- and temporally-rich data set of water levels was available to analyze the project area and calibrate hydraulic models to represent the project area accurately. Fifteen staff gauges were installed to monitor water levels throughout the project area before and during project construction. Figure 2 shows the locations of the staff gauges that were installed. Not all of the installed gauges were recorded on a regular basis. Each staff gauge has a code in the format of two letters followed by two numbers, which increase in the downstream direction, e.g. RN06.
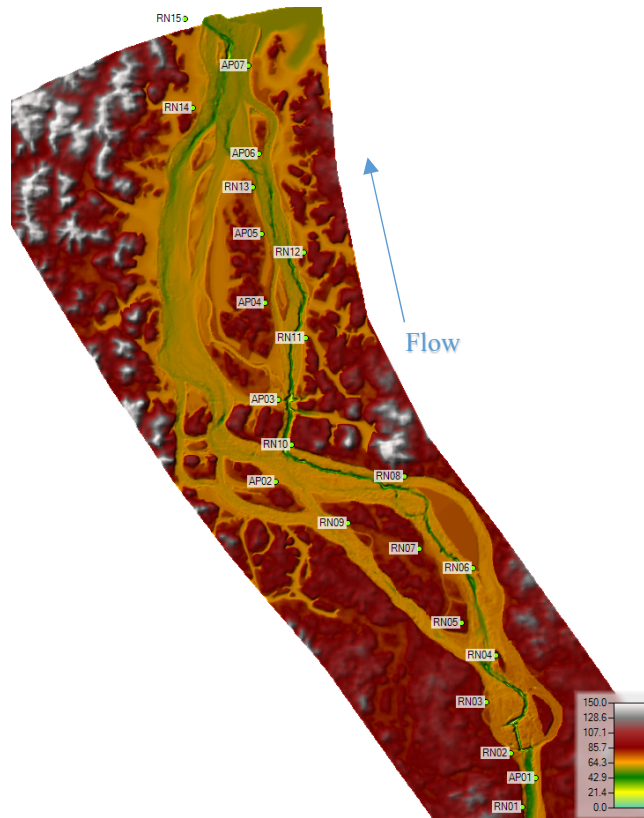
Figure 2. Terrain and Staff Gauge Locations

Model Inputs: A digital terrain model (DTM) was developed using the elevations considered to be the most accurate available in all locations throughout the model domain. This was derived from three sources: bathymetry collected in 2017 from multibeam and singlebeam surveys and compiled into a 1-meter resolution raster; a combined elevation dataset consisting of the previous bathymetric survey mixed with other survey efforts compiled into a 25-m resolution raster; and topographic elevations from the Shuttle Radar Topography Mission (SRTM) dataset compiled into a 1-arc-second (approximately 30 meters) resolution raster.

Cross sections were laid out to include the main channel, the seasonally inundated side channels, and floodplains. Preliminary simulations with the 2-D model (described later in the text) showed flow directions at various locations across the channel and floodplain. The direction vectors were utilized to align cross sections perpendicular to the direction of flow. The downstream extent of the geometry is the downstream end of the detailed bathymetry survey, which is also near the downstream-most staff gauge. The upstream extent of the geometry is the location of the stream gauge upstream of the project, called Itupiranga.

Boundary conditions were applied to the model in two locations: the upstream and downstream ends. A flow hydrograph was applied at the upstream-most cross section using computed or measured flows. A stage hydrograph was applied at the downstream-most cross section and populated with observed daily water levels from a staff gauge, or an estimate of the water level based on the published level of the Tucuruí reservoir. There is a small tributary of the West side of the river. Flow from this basin was not included in the modeling as there was not flow data available and the drainage basin is small compared to the Tocantins River.

Manning's n values, ineffective flow areas, and contraction and expansion coefficients were initially estimated and later utilized to refine model parameters to match observed stages.

Energy losses from the strong eddies observed in the river were estimated by raising the contraction and expansion coefficients to 0.6 and 0.8, respectively, in the areas where these observations were made. The default values are 0.1 and 0.3 for contraction and expansion, respectively. The HEC-RAS Hydraulic Reference Manual [HEC, 2016] includes guidance on maximum contraction and expansion coefficients to use, as shown in Table 1.

Table 1. Subcritical Flow Contraction and Expansion Coefficients

	Contraction	Expansion
No transition loss computed	0.0	0.0
Gradual transitions	0.1	0.3
Typical Bridge sections	0.3	0.5
Abrupt transitions	0.6	0.8

2-D Hydraulic Modeling

A 2-D hydraulic model was developed using HEC-RAS software and the 2-D capabilities available in versions 5.0 and later. The objectives of the 2-D model were to simulate flow patterns, assess channel velocities and directions, and determine flow directions for the 1-D model cross section layout.

Model Inputs: The digital terrain model used for the 1-D model was also used for the 2-D model. The 2D mesh in HEC-RAS uses an unstructured format with cells of up to eight sides. The mesh uses cells of varying sizes to allow for higher resolution in critical areas and lower resolution in more uniform areas further from the areas of interest. Breaklines were used to control the higher resolution areas in the 2D area. Normally aligned on ridges or elevation changes, breaklines were used in an innovative manner by placing a breakline along the center of the channel, allowing the cell size to be controlled in the most dynamic portion of the channel. Cell spacing was set to 10 meters along the breaklines, transitioning to a spacing of 50 meters throughout the rest of the 2D area. Table 2 shows summary statistics for the 2D mesh.

Table 2. 2-D Area Summary Statistics

Number of Cells	120,252
Average Cell Area, m²	2,248.51
Maximum Cell Area, m²	4,664.75
Square root, m (if l=w)	68.30
Minimum Cell Area, m²	55.70
Square root, m (if l=w)	7.46

The model domain, shown in Figure 3, includes the upstream and downstream extents of the 2017 bathymetric survey with additional overbank and island areas included to allow for accurate simulation of flood periods. These extents also match the downstream-most stage staff gauge and the upstream flow measurement transect.

Figure 3. 2-D Area Extents

Boundary conditions were applied in two locations: at the upstream and downstream ends. A flow hydrograph was applied across the channel at the upstream end of the 2-D area, populated with ADCP-measured flows from a series of measurement campaigns. A stage hydrograph was applied across the downstream end of the 2-D area and set to the water levels observed daily at RN-15, the furthest downstream staff gauge.

2-D Equations Used: The full momentum equations were used in the computations. The acceleration term included in the full momentum equation set is critical to account for the losses through rapidly deepening and narrowing canyon-like structure of the channel. The eddy viscosity mixing coefficient is a user-inputted parameter and was set based on observed stages and other research of the project area (Tomas, 2018).

Manning's n values were also refined to better match observed stages. A single value was used for the entire 2-D area for modeling, although this is recognized as a matter where the model can be improved. A recently-added HEC-RAS feature allows for spatially-varied Manning's n values in 2D areas. In the Tocantins River application, different n values could be set for rock-bottom areas, sand-bottom areas, and vegetated areas. The single n value used was 0.035. A separate detailed 2-D modeling study completed by Gustavo Pacheco Tomas of Universidade Federal do Paraná (UFPR) resulted in the use of a Manning's roughness coefficient of 0.035 upon calibration to observed stages (Tomas, 2018).

The full momentum equations include the acceleration term in computations. This equation set uses an eddy viscosity coefficient to account for turbulent motion. A value of 1.0 was used for the eddy viscosity coefficient. Table 3 presents values from the HEC-RAS 2D Modeling User's Manual for the eddy viscosity mixing coefficient that have been found to be appropriate in certain conditions [USACE, 2016]. The value used is within the range of appropriate values.

Table 3. Eddy Viscosity Mixing Coefficients

D_T	Mixing Intensity	Geometry and surface
0.11 to 0.26	Little transversal mixing	Straight channel Smooth surface
0.3 to 0.77	Moderate transversal mixing	Gentle meanders Moderate surface irregularities
2.0 to 5.0	Strong transversal mixing	Strong meanders Rough surface

Velocity and directional patterns: Several site visits were made to gain an understanding of site conditions, identify barriers to side channel access, and identify high turbulence areas. The most upstream rock outcrops mark a particularly difficult-to-navigate section where the deep channel make two sharp turns within a short distance. Velocity and cross currents are important to model in this location as alignments for a post-rock-removal navigation channel are evaluated. Information gained regarding barriers to side channel access was applied to the 1-D model as normal ineffective areas up to the elevation of the barrier. Observed high turbulence areas justified the use of a higher eddy viscosity mixing coefficient in the 2-D modeling.

Results

Water Level Calibration

Fifteen staff gauges were installed to monitor water levels throughout the project area before and during project construction. Locations can be found on Figure 2. Daily readings were recorded for more than one year, sufficient to capture the three combinations of interest for

designing the navigation project: low reservoir with low flow, high reservoir with low flow, and low reservoir with high flow.

1-D Model: The primary means of calibration were adjusting Manning's "n" roughness values, adjusting contraction and expansion coefficients, and setting ineffective flow areas to define conveyance areas within the cross section and also control main channel/side channel flow distribution.

A total of seven days were simulated in the 1-D model calibration process. While there were hundreds of days for which water level measurements were available, there were many fewer when flow measurements were available and still fewer for which the prior day's flow was close to the current day's flow. Simulation of multiple days was completed to build confidence in the model when simulating extreme low water levels, no matter the cause.

While there were several days simulated in the model, one day – 29 November 2017 – was used as the primary calibration event. Of all the days when flow measurements at the upstream end were available, this day had the lowest stages throughout the project area. Additionally, this day was more than one year into the period when water levels were being recorded, and after reporting reliability had improved. The profile view of the computed profile compared to measured levels is shown in Figure 4.
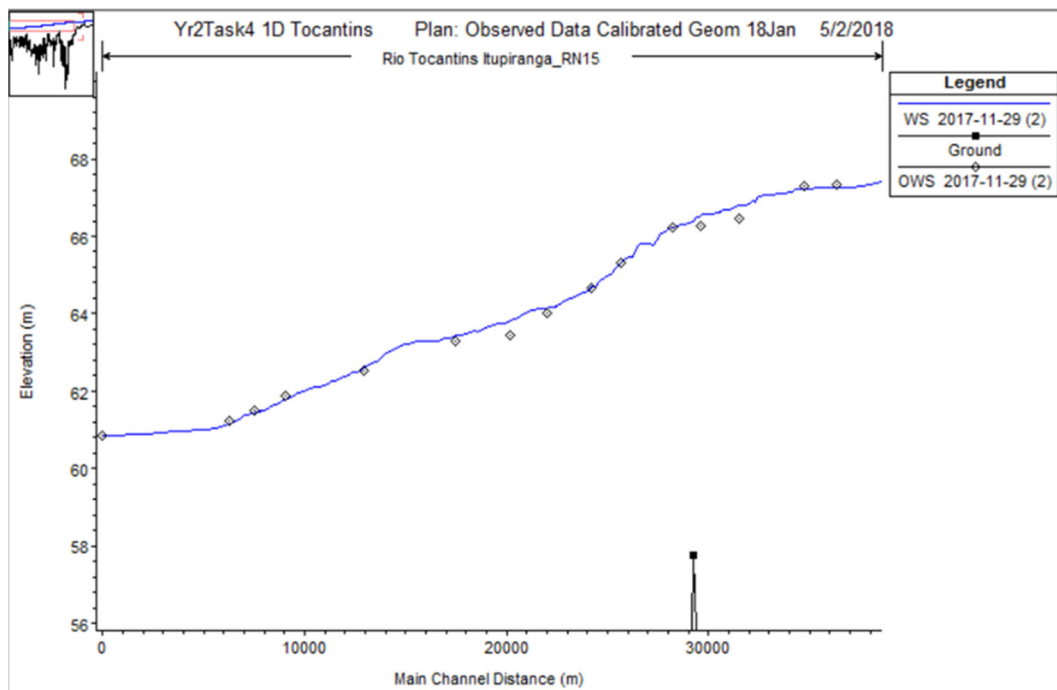
Figure 4. 29 November 2017 Computed Profile with Observed Values

The root-mean-square error (RMSE) was used to measure the accuracy of the model in matching the observed water levels. The simulation in Figure 4 has an RMSE of 0.17 meters.

Comparisons of model results to observed stages for each of the seven days simulated are shown in Table 4. A visual dashboard was designed to easily identify locations or days where the modeled stages did not closely match observed stages. Values in the table are differences

between modeled and observed water levels. Green shading represents locations where the modeled stage is higher than the observed stage. Red shading represents locations where the modeled stage is lower than the observed stage. The shading intensity is a function of the absolute value of the difference.

Table 4. 1-D Model Calibration and Validation Results

		ADCP Measured Flows						
	Q (m³/s):	3,354.2	3,817.0	3,586.5	3,326.0	1,770.0	6,243.9	2,863.1
	RN15 el.	62.56	62.41	62.27	61.95	71.74	74.12	60.85
	Date:	12/1/2016	12/5/2016	12/6/2016	12/8/2016	9/1/2017	5/24/2017	11/29/2017
Upstream	1	0.45	0.32	0.14	0.30	-0.01	-0.02	-0.09
	2	0.47		0.17	0.33	-0.01	0.00	-0.08
	3					-0.04	-0.03	0.36
	4	0.17	0.11	-0.04	0.07	-0.06	-0.06	0.27
	5	0.45	0.37	0.21	0.37	-0.05	-0.12	0.02
	6	0.16	0.34	0.14	0.14	-0.06	-0.07	0.00
	7	-0.21	-0.11	-0.23	-0.14	-0.04	-0.06	0.05
RN	8		-0.01	-0.08	0.03	-0.05	-0.09	0.13
	9	-0.04	0.21	0.14	0.30	0.00	-0.05	0.37
	10	0.02	0.07	0.05	0.25	-0.01	-0.07	0.12
	11	0.07	0.22	-0.39	-0.22	-0.04	-0.07	0.08
	12	-0.46	-0.20	-0.18	-0.07	-0.05	-0.08	-0.09
Downstream	13	-0.17	-0.05	-0.07	-0.06	-0.05	-0.08	-0.04
	14	-0.25	0.13	0.12	0.10	-0.04	-0.02	-0.08
	15							

2-D Model: The primary means of calibration in the 2-D model were Manning's n values and the eddy viscosity mixing factor, as described in the Methods section.

The 2-D model results for the day when the lowest water levels were measured are presented in Table 5.

Table 5. 2-D Model Calibration Results

Date of Measurements: 30 November 2017. Q=2,863 m³/s. RN15 elevation: 60.85 m.				
		Measured Water Level, m	Modeled Water Level, m	Difference, Modeled-Measured, m
Upstream	1	67.35	67.21	-0.14
	2	67.31	67.21	-0.10
	3	66.44	66.53	0.09
	4	66.27	66.37	0.10
	5	66.22	66.15	-0.07
	6	65.33	65.40	0.07
	7	64.66	64.82	0.16
RN	8	64.01	64.14	0.13
	9	63.46	64.00	0.54
	10	63.31	63.24	-0.07
	11	62.53	62.39	-0.14
	12	61.87	61.59	-0.28
Downstream	13	61.48	61.35	-0.13
	AP06	61.25	61.19	-0.06
	15	60.85	60.85	0.00
			RMS Error	0.19

The differences between modeled and observed stages were computed, resulting in a RMSE of 0.19 meters for this simulation.

A longer period of 13 days in November and December 2016 was simulated in the 2-D model. This allowed for comparison of multiple days of observed stages to modeled stages at each staff gauge, and evaluation of how the model tracked the temporal changes in water level. Figure 5 shows this comparison at staff gauge RN06, which is near the middle of the model. In Figure 5, the blue line shows the modeled water levels, while the red asterisks show daily observed water levels. The figure shows modeled water levels higher than observed levels, a pattern that was seen in a majority of gauges in this November-December 2016 event. This event occurred soon after the deployment of the staff gauge network, and it is noted that the observed data appear questionable. In the weeks and months after the initial deployment, datum errors were found and corrected. Observation and reporting also improved as evidenced by gage-to-gage trends and day-to-day trends in the records.
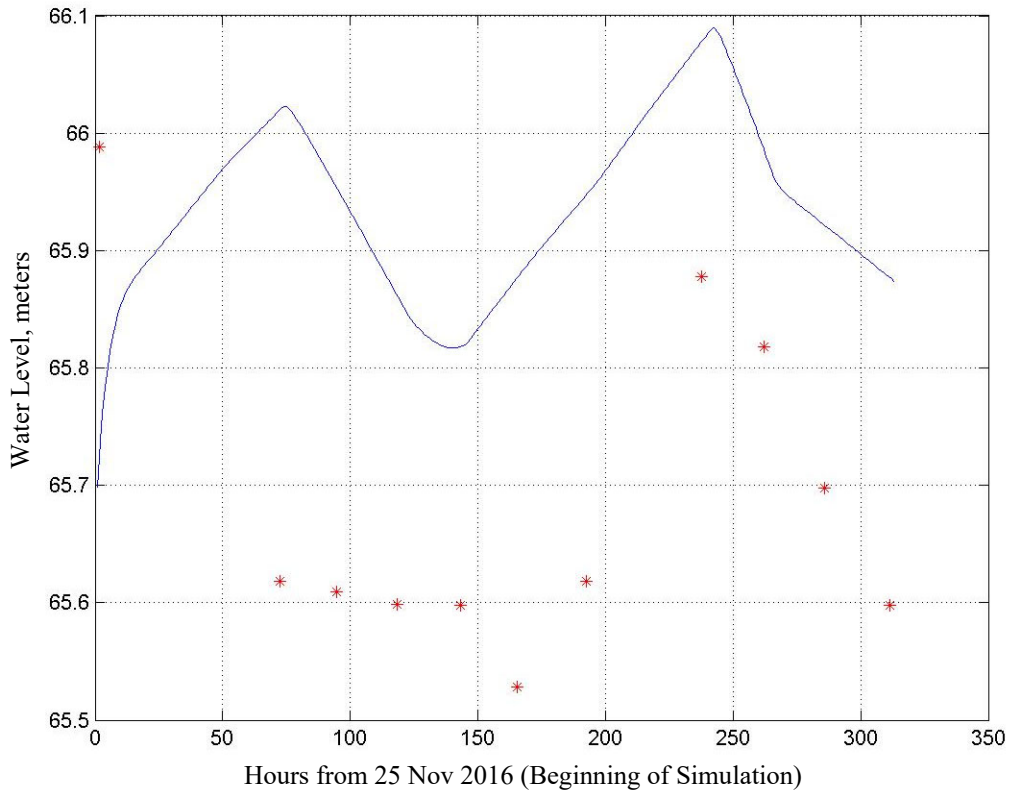
Figure 5. RN06 Calibration

Flow Calibration

Flow measurements were completed in numerous locations throughout the project area during the measurement campaigns that occurred four times throughout one year. The measurements were utilized to determine the flow splits between the main channel and side channels under different flow and reservoir stage conditions. In the downstream half of the model, the river splits around a large island that is approximately 10 kilometers in length, which is shown in Figure 6. Initially, the 1-D model over-predicted flow to the left side of the island, in the secondary channel. Ineffective flow areas were added to the secondary channel portion of the cross sections to reduce the active conveyance area and keep more of the flow in the main channel on the right side of the island.
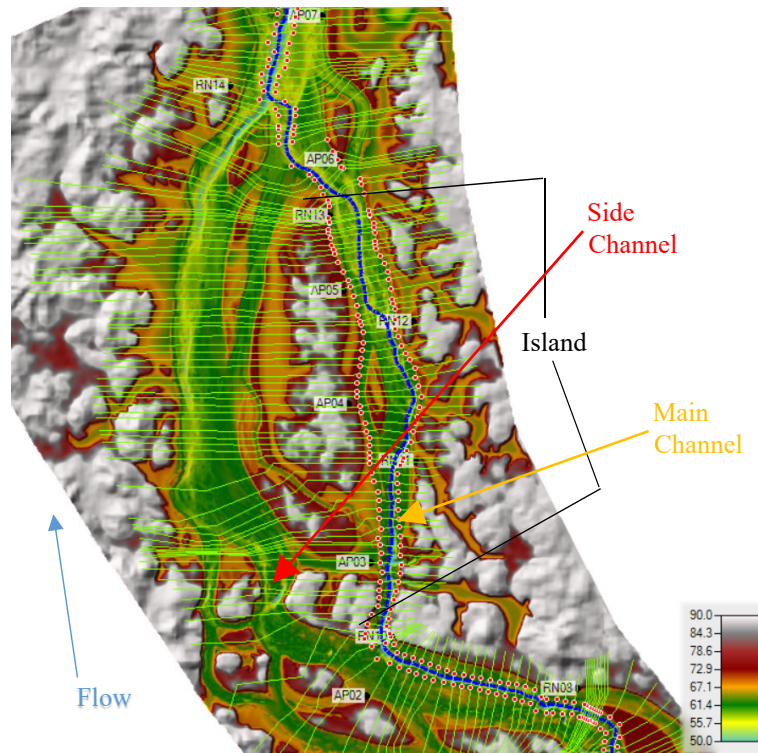
Figure 6. Main Channel and Side Channel

Model Uses

The calibration process built confidence in the model to predict water levels accurately throughout the model domain. With that step completed, the models could then be used to perform simulations of extreme conditions, long-term period-of-record simulations, and simulations of index values of flow and downstream reservoir stage for a coincident frequency analysis. The 1-D model was utilized to answer specific questions about the project area.

The calibrated 1-D model was used to compare the project design reference plane profile and estimated rock removal volume to the preliminary estimates developed previously. Boundary conditions of an extreme low flow and an extreme low stage were simulated in the 1-D model using the recently-collected high-resolution bathymetry.

Long-term simulations of 15 years and longer were completed to develop a water surface profile that has historically been exceeded 96% of the time. Model results were post-processed to calculate stage-duration relationships at each cross section in the model.

The 1-D model was also utilized to populate a "response surface" at selected locations throughout the project area, which is simply a collection of modeled stages for a range of possible upstream flow and downstream reservoir stage combinations. This response surface was queried in a coincident frequency analysis that was completed to determine annual probabilities of water levels less than a threshold value.

Conclusions

The development and calibration of the 1-D and 2-D models achieved the objectives of the effort. An analytical and iterative process was applied to improve the performance of the models. A 1-D model was developed and refined after observing results from the 2-D model.

The 1-D model was preferable for multi-year simulations to determine water level duration and annual exceedance values throughout the project area. Further, it was used to analyze the effect of the rock removal on stages and currents throughout the project area. The contraction and expansion coefficients were used to model the significant energy losses in the system.

The 2-D model was preferable for localized evaluation of currents, velocity magnitudes, determining thresholds for access to side channels, and to aid in development of the 1-D model in an iterative manner. The eddy viscosity coefficient was utilized to account for the turbulence in certain areas in the project area.

Model development and simulations provided high-quality hydraulic information to support the rock removal project in the Tocantins River.

References

Tomas, Gustavo Pacheco. April 2018. Mapeamento 3D da Variacao da Viscosidade Turbulenta em Canions Sumbersos e sua Aplicacao Modelagem Numerica. Universidade Federal do Parana.

USACE, (2016). HEC-RAS River Analysis System, Version 5.0, Hydrologic Engineering Center 2D Modeling User's Manual. U.S. Army Corps of Engineers. February 2016.

USACE, (2016). HEC-RAS River Analysis System, Version 5.0, Hydrologic Engineering Center Hydraulic Reference Manual. U.S. Army Corps of Engineers. February 2016.

Development of a Navigation Channel Coincident Probability Method for Improving Navigation Reliability in a Reservoir Backwater Influenced River, Tocantins, Brazil

Will Veatch, Hydrologist, US Army Corps of Engineers, New Orleans, LA, William.C.Veatch@usace.army.mil

Matt Dircksen, Civil Engineer, US Army Corps of Engineers, Chicago, IL, Matthew.S.Dircksen@usace.army.mil

Ana Luisa Osorio, Engineer, DNIT, Brasília, Brazil, ana.nunes@dnit.gov.br

Renato Amorim, Engineer, DNIT, Brasília, Brazil, renato.amorim@dnit.gov.br

Calvin Creech, PhD, PE, Lead Interdisciplinary Engineer, USACE, Brasília, Brazil, Calvin.T.Creech@usace.army.mil

Abstract

A spatially distributed coincident frequency analysis was developed and applied to determine a project reference plane at a 96% level of navigational reliability for a proposed navigation project on the Tocantins River in Northern Brazil. A rock outcrop navigation impedance, known as the Pedral do Lourenço, is located approximately 50 km downstream of the city of Marabá, in the state of Pará, and 110 km upstream of the Tucuruí Dam. The study reach is a 35 kilometer long section of river influenced by reservoir backwater. Water levels are influenced by the flow from upstream and the reservoir level downstream. Temporal coincidence of low reservoir levels and low river flow result in shallow depths throughout the study reach. The reach of the river where rock outcrops impede navigation includes a subsection where the flow is the dominant variable and reservoir stage is a clear secondary variable, and a subsection where the reservoir level is the dominant variable and the flow is a clear secondary variable. The total probability method and calibrated numerical hydraulic models were used to determine longitudinal water surface profiles for several stage duration targets, e.g. 1%, 4%, 10% of the days exceeded in a year. Then, various recurrence intervals were computed for these duration series, including a 2-year, 10-year, and 25-year recurrence intervals using the normal and Gumbel distributions. Daily reservoir stage records and daily river flow records were used for the corresponding duration and frequency analyses. A calibrated hydraulic model was used to determine the response at selected locations throughout the study area to changing flows and reservoir levels. The coincident frequency analysis determined the water surface profile and required rock removal volumes for desired levels of exceedance and probabilities. The analysis informed decision makers of the relationships between rock removal volumes and probability of desired navigation conditions being met during a year. The method developed and demonstrated here offers a design approach for situations where the relative importance of two coincident variables reverses over the project domain. This is believed to be the first application of this method to a navigation (i.e., low-flow) project design.

Introduction

Project Setting and Context

The Tocantins River originates in the Pireneus Mountains of Brazil, in the state of Goiás near the national capital city of Brasília, and discharges to the Atlantic Ocean near the mouth of the Amazon River. At over 2,600 km of length and an average discharge of over 13,000 m³/s, the Tocantins is among the world's largest rivers. The Tocantins is navigable over much of its length during high water periods, but during low water, exposed rock outcrops impede navigation in several areas. One of these areas, a 35 kilometer outcrop of basalt and granite known as the Pedral do Lourenço (roughly "Lawrence's rocky place"), is a critical impediment because when impassable, it establishes the upstream limit of navigability on the Tocantins. The Pedral do Lourenço is in the state of Pará, approximately 150 km north of the city of Marabá between river kilometers 350 and 393 (Figure 1). The Pedral do Lourenço is located just upstream (south) of the upper reaches of the Tucuruí Reservoir, one of the world's largest with a volume of over 45 km³. Therefore, the water surface at this site is not a function of river flow alone, but of river flow along with the downstream boundary condition of the stage in the reservoir.
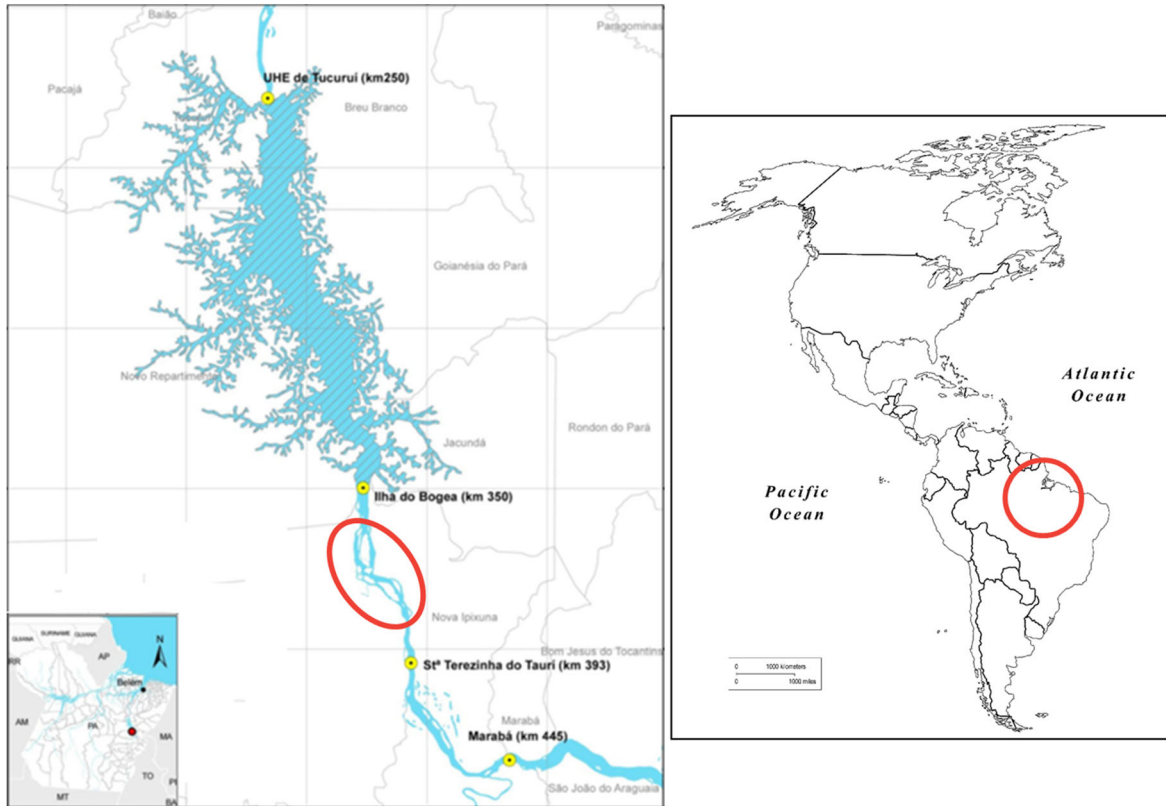
Figure 1. Project site location in State of Pará, Brazil.

The Brazilian National Department of Transportation Infrastructure (*Departamento Nacional de Infraestrutura de Transportes*, or DNIT) has identified the Tocantins River as a priority waterway for navigational improvement. A DNIT feasibility study concluded that improvement of navigational reliability is technically feasible, and a conceptual design for a navigation channel through the Pedral do Lourenço site was completed in 2015 by the Federal University of

Paraná (UFPR). The US Army Corps of Engineers and DNIT entered into an agreement in 2016 to support DNIT objectives in the areas of river engineering and river navigation services. DNIT is responsible for planning, design, and construction of transportation infrastructure in Brazil, including waterways. USACE supports this mission by providing capacity building and knowledge transfer using subject matter experts embedded at DNIT headquarters in Brasília and support from USACE districts in the United States.

The stated goal of the Tocantins navigation project is to achieve 96% navigational reliability along the river, but the complex interactions between the reservoir and river at the Pedral do Lourenço mean that various combinations of conditions can cause this standard to go unmet in this location. A 2013 study by engineering firm CB&I (originally known as Chicago Bridge and Iron Works, now part of McDermott International) recommended using a design flow of 1,898 m^3/s (said to be the 4% annual non-exceedance low flow) with a reservoir stage of 58.0 m, the minimum stage for operation of the navigational lock at the downstream end of the reservoir. USACE and DNIT engineers sought to reassess these design assumptions in the context of navigational reliability and determine the required volume of rock removal necessary to achieve a reliable channel.

Conceptual Background

The total probability of a continuous outcome y (e.g. river stage) that results from two continuous underlying conditions q and h (e.g. river flow and downstream stage) is given by

$$F(y) = \int \int F(y|q,h)f(q,h) \, dq \, dh \tag{1}$$

The first term $F(y|q,h)$ describes the likelihood of observing a particular river stage given a particular combination of flow rate and downstream reservoir stage, while the second term $f(q,h)$ is the joint probability of that particular pair of conditions being exceeded (Need et al. 2008). If the exceedance probabilities of the two underlying conditions are independent of each other, then the probability of exceeding both at once is simply the product of the two marginal probabilities,

$$f(q,h) = f(q)f(h) \tag{2}$$

If the two events are not independent, then other formulations such as copulas may be used to address this dependence, though in many practical hydrological contexts the period of available data is too short to establish the nature of this dependence with confidence. The $F(y|q,h)$ term may be determined from a hydraulic model such as HEC-RAS (USACE Hydrologic Engineering Center's River Analysis System; Brunner, 2010). However, inserting an HEC-RAS model into equation (1) does make it rather harder to compute the total probability integral. Therefore, it is common to rely again on the law of total probability, constructing a series of conditional probability curves for the response as a function of one of the two underlying variables, each for a specific "index" value of the other variable. These conditional curves are then summed together into a total probability curve by multiplying the probability from each conditional curve by the probability of each index value, estimated by the proportion of time that index value is exceeded.

$$F(y) = \Sigma f(y|h)f(h) \tag{3}$$

Here, $f(y|h)$ is the probability of observing the stage y, as a function of the variable q, given a fixed index value of variable h. This is the method recommended by USACE Engineering Manual 1110-2-1415 (USACE, 1993) and implemented in HEC-SSP (HEC Statistical Software Package; Brunner and Fleming, 2010).

Alternative methods to the one described above exist. Need et al. (2008) recommended fitting a Gumbel copula to model the flood risk along a tidal river, when the downstream ocean boundary and the river discharge are somewhat, but not perfectly, correlated. Kilgore et al. (2013) explored several methods for computing coincident design flows for areas near the confluence of two streams, including bivariate probability distributions, copulas, the total probability approach, regression approaches, and synthetic storms. Finally, one could simply posit that the two underlying variables are perfectly correlated, so that the river stage with a given coincident probability is simply the result of the river flow and downstream boundary conditions that each have that marginal probability. While this is a conservative assumption, it is not as conservative as it might initially appear. Over most of the project domain the overall stage response is largely a function of only one of the two variables, so this conservatism significantly overestimates risk only in the transitional region where both variables are highly influential on the response (Need et al. 2008).

Methods

For the analysis of the Pedral do Lourenço, the team selected the total probability approach for the computation of the design water surface profile. However, the method described above presented two challenges. First, it had been developed for analysis of floods, not droughts, and to the team's knowledge had not been applied previously to a navigational design project. Indeed, HEC-SSP software was unable to perform a coincident probability analysis using a flow frequency non-exceedance curve (though it performs perfectly well for a frequency exceedance curve). Second, the implementation of the total probability approach using conditional exceedance curves requires that one of the two underlying variables be deemed the "more influential" variable and the other the "less influential" of the two. The more influential variable determines the probability of the response for the conditional curves, each of which is indexed to a fixed value of the less influential variable. For the Pedral do Lourenço, this creates an issue because the choice of which variable is more influential varies along the project reach. At the downstream end of the project near the Tucuruí reservoir delta, the reservoir stage is much more influential than the river flow, while at the upstream end the opposite is true (Figure 2).
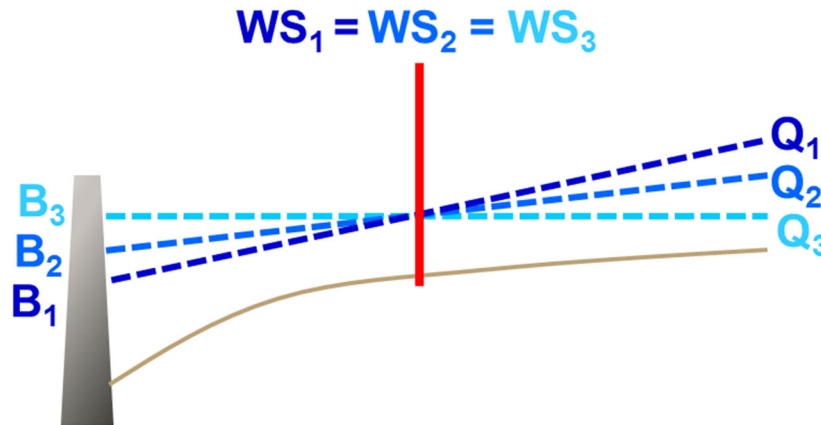
Figure 2. At the downstream end of the reach, the reservoir stage "B" is the more influential variable, while at the upstream end the river discharge "Q" is more influential. There is therefore no single correct choice of index variable to use in construction of the coincident frequency exceedance curves.

Before the coincident frequency analysis could begin, exploratory data analyses were performed to assess the stability of the stage-discharge rating curve and the assumption of independence between river flow and reservoir stage. Discharge data for the Itupiranga gage near river kilometer 393 were downloaded from the Hidroweb database operated by the Brazilian National Water Agency (*Agência Nacional de Águas*, or ANA) for the period of record, January 1977 through May 2016. Quality-assured data were available through 2006 and were prioritized over raw data when available, and obvious errors such as zeroes were deleted. A specific-gage analysis was used to assess the stability of the discharge rating at Itupiranga. While it would have been preferable to use the direct-step method for this analysis (assessing changes in the observed discharge measurements themselves), data availability was insufficient for that approach. Therefore, the observed data were used to generate a moving-window five year rating curve, allowing the stage associated with a given flow to be extracted from each curve and plotted as shown in Figure 3. While periods of missing data complicate the task of computing the statistical significance of any change in stage over time, visual inspection does not show an obvious trend. The rating was deemed to be sufficiently stable, and a single-value rating curve was used to generate a daily record of river flows.
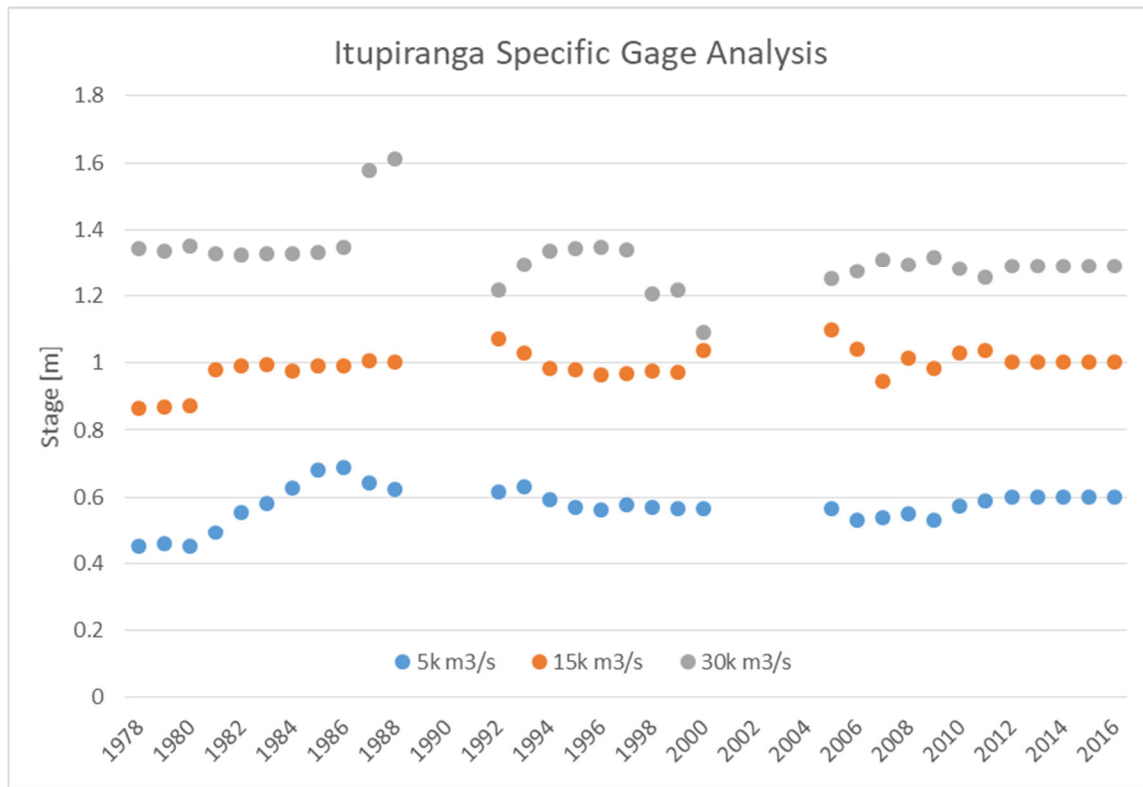
Figure 3. Specific gage analysis for Itupiranga gage. The stage-discharge rating was found to be sufficiently stable to use for generating the daily flow record.

As mentioned in the previous section, the coincident frequency approach is limited in most practical applications to situations where the two controlling variables can be assumed to be independent. The Tucuruí reservoir is so large that minimum stage in the reservoir tends to lag minimum flow in the river by several months, so a strong correlation between the two was not expected. To check this assumption, the annual minimum flows for the Tocantins at Marabá were plotted against the coincident stages in the reservoir as shown in Figure 4. With an r² of just 0.0034 and a p-value of 0.85 for the slope of the regression line, there was insufficient evidence to reject the null hypothesis of no significant correlation between the two variables, so the assumption of independence was adopted.
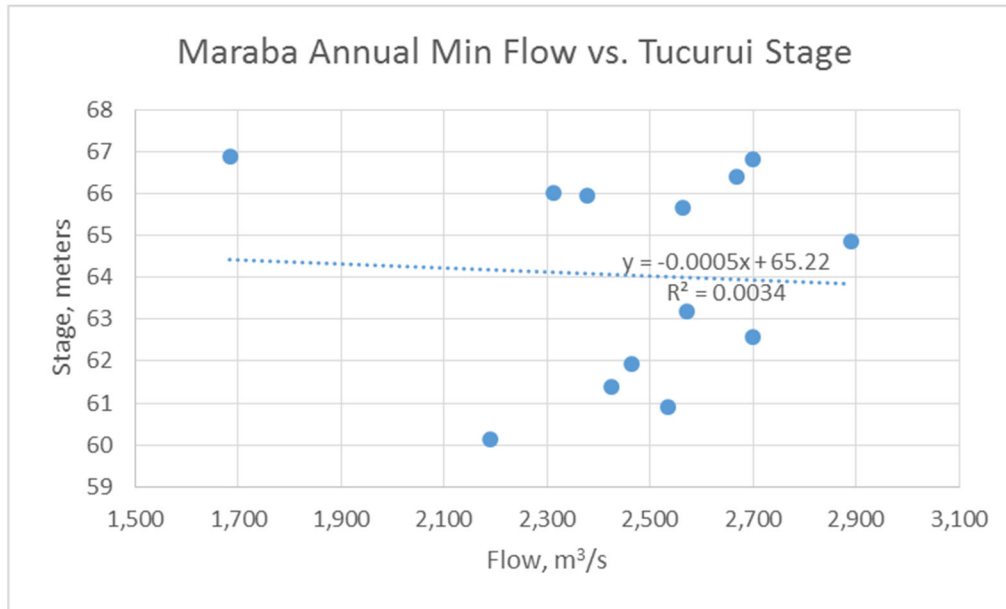
Figure 4. No significant correlation was found between annual minimum flow on the Tocantins River and the simultaneous stage in the Tucuruí reservoir, allowing the two variables to be considered independent.

To address the issue of the dominant variable switching from one to the other over the project domain, the team decided to develop two low-water profiles, the first using downstream stage as the more influential variable and the second considering river flow to be more influential. The two profiles would then be compared, with the final profile being governed by whichever of the two is lowest at any given point along the reach. This "envelope" approach is implied (for estimating flood elevations) though not specifically recommended by both EM 1110-2-1415 and Kilgore et al. (2013).

Results

Low-Water Profiles and Design Condition Envelope

Two low-water profiles were computed in Microsoft Excel software via the total probability approach, by generating sets of conditional probability curves and summing them together in a weighted sum according to the likelihood of each index value of the less influential variable. The response surface defining the river stage for various combinations of river flow and reservoir stage was extracted from a one-dimensional HEC-RAS model developed jointly by USACE and DNIT. The total probability approach allows an exceedance curve to be computed for any probability of exceedance and for any confidence interval around the curve. The team decided that the best match to the project intent of 96% navigational reliability would be achieved by first generating an annual series of 4% stage duration values, then computing the 2-year recurrence interval (i.e. best estimate) of this series for each location of interest using a Gumbel distribution. Other recurrence intervals were also computed, though ultimately not used for this design. The coincident frequency analysis was repeated for nine locations along the reach, with locations between these points interpolated using a water surface profile from the hydraulic model. The two resulting profiles are shown in Figure 5, with the design profile being governed at every point by whichever of the two profiles is lowest.
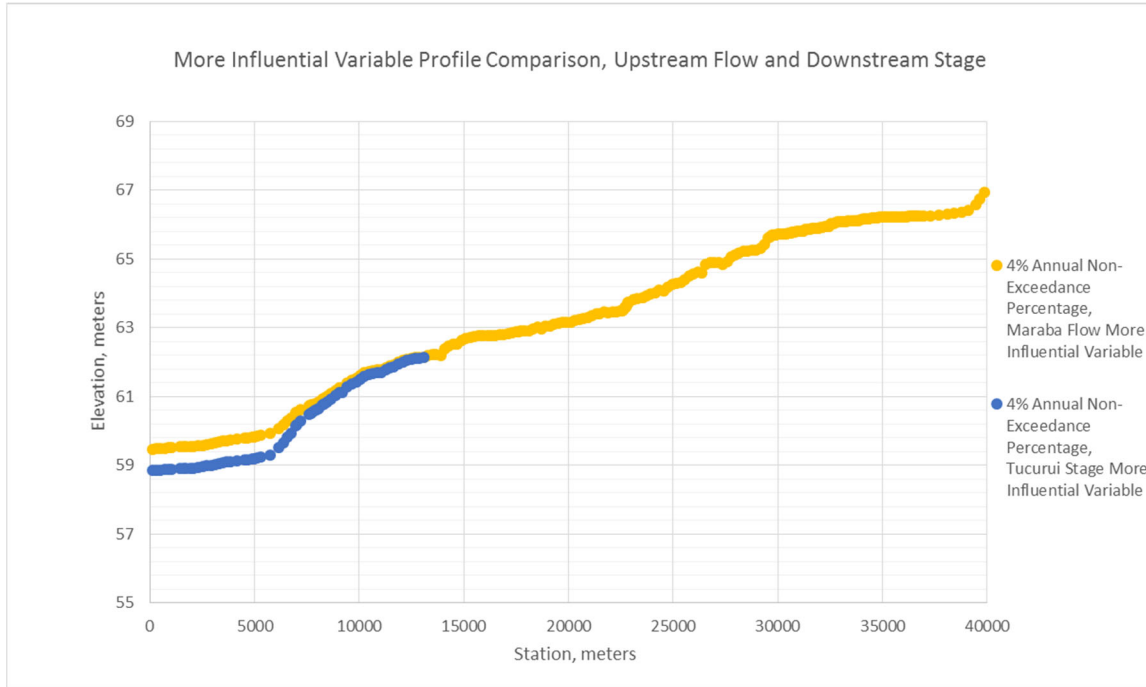
Figure 5. The two profiles resulting from two applications of the total probability approach. At every point along the profile, the design is governed by whichever profile is lowest.

Having computed the design profile, the team then computed the corresponding required volume of rock removal and the actual resulting navigational reliability based on historical data. Transit of the Pedral do Lourenço in a towboat requires approximately one day, so the profile was compared to observed data from 2003-2015 to determine how many days of that time the channel would have been safely navigable if the specific volume of rock had been removed. If any part of the channel did not meet the Brazilian minimum criteria for safe draft, channel width, turning radius, or length between curves, the entire channel was deemed to be impassable for that day. Results are shown in Table 1, with the without project alternative and two other design approaches shown for comparison.

Table 1. Required rock volume excavation and navigational reliability for the coincident frequency design as compared to two alternative designs and the without project alternative

Condition	Approximate Rock Volume Removed, million m³	Estimated Historic (2003-2015) Reliability
No navigation channel project	0	15-20%
Coincident Frequency [a]	1.78	76%
Duration Exceedance [b]	1.95	90%
Established boundary conditions [c]	4.23	98.9%

[a] 50% confidence estimate of 96% annual chance of exceedance

[b] 96% duration exceedance

[c] Q=1,898 m³/s Tucuruí=58.0 m

Discussion

As shown in Table 1, a coincident probability based navigational channel design, using a 50% annual total probability of non-exceeding a 96% duration stage, results in a channel that is navigable on approximately 76% of days based on historic data from 2003-2015. This apparently paradoxical finding is explained by three observations. First, the coincident frequency-based 96% reliability stage applies to each specific location along the profile where it is calculated. In other words, a 96% duration stage at a given location corresponds to a water surface elevation that is not exceeded approximately 15 days per year. However, at a different location along the profile, where either the reservoir stage or flow becomes more influential, the calendar days where water surface elevations are below this threshold may be non-simultaneous. This results in a profile for which more than 15 days of navigation may be impacted, meaning the 96% duration profile corresponds to an actual level of reliability closer to 76% along the entire 35 km reach (or 88 days of impacted navigation). Second, because the entire channel is considered impassable if any part of it is impassable, there may be days when the river flow or the downstream reservoir stage are too low to allow for navigation, even if the overall conditions, considered together, are less extreme than those represented by the profile. And finally, uncertainty (irreducible error) exists around the profile, which is unaddressed when the profile is considered at the 50% confidence interval.

Three other approaches for profile design are also shown in Table 1 for comparison. The first is the without-project condition. It should be noted that there is no commercial navigation at present in the proposed channel through the Pedral do Lourenço; rock pinnacles are visible above the water surface even during high water conditions. An alternate route around these pinnacles exists that is potentially navigable during high water conditions, and this is route referred to in Table 1. The "duration exceedance" design refers to a profile such that each point along the route is exceeded by 96% of the data, evaluated using the HEC-RAS hydraulic model and historical data. Again this design does not yield 96% navigational availability because the entire channel is considered impassable if any part of it does have sufficient draft. Finally, the last design is the one based on the boundary conditions from the CB&I (2013) study. It delivers very high reliability but requires an extremely large amount of rock excavation. The optimal design is still to be determined. Due to the strong seasonality of river conditions in the Amazon Basin, year-round availability may be less essential than navigability during the agricultural harvest and shipping season. This is an area for further study.

The envelope approach used here may be considered most accurate as the profile approaches the two extremes of the project reach. In these areas, the choice of which variable is most influential is clear, and the lower of the two profiles is the more accurate estimate of the true 50% annual coincident non-exceedance curve. In the transition region between the two, the choice is less clear, and the design profile here may be considered less certain. There is no precise definition for where this transition zone begins and ends, so engineering judgment may be used to determine whether areas of concern exist based on the incidence of rock pinnacles in parts of the channel where the two coincident frequency profiles are near to each other. In accordance with risk-based design, this part of the reach may be an appropriate area to use a greater degree of confidence (beyond 50%) or, equivalently, a less frequent non-exceedance event (than 2-year recurrence) to define the design profile in recognition of this increased uncertainty.

Conclusion

A total probability approach was used to develop a low-water profile for a navigational channel through a rocky outcrop on the Tocantins River in northern Brazil. Coincident frequency analysis was required because the river stage in this area is a function of both river flow and the stage in the downstream reservoir. Which of these two variables is most influential on river stage changes over the course of the project area, so two coincident frequency analyses were performed, with the lower of the two governing the design at all points. This design results in a profile corresponding to conditions that can be expected to have a 50% annual chance of being non-exceeded during 4% of the year. Historical data indicate that the proposed channel with approximately 1.8 million cubic meters of rock removed would have been completely passable without the need for light loading on about 76% of days from 2003-2015. This level of reliability is not as high as the stated project goal of 96%, but it also requires a dramatically smaller volume of rock removal than the boundary conditions approach defined in a previous study. To the authors' knowledge, this is the first application of a coincident frequency envelope design to a navigation channel (i.e. low-water) project.

References

Agência Nacional de Águas. 2016. Hidroweb. http://hidroweb.ana.gov.br/. Accessed January 2018.

Brunner, G.W. 2010. HEC-RAS river analysis system: hydraulic reference manual. US Army Corps of Engineers, Institute for Water Resources, Hydrologic Engineering Center, Davis, CA.

Brunner, G.W., and Fleming, M.J. 2010. "HEC-SSP Statistical Software Package." US Army Corps of Engineers, Institute for Water Resources, Hydrologic Engineering Center, Davis, CA.

CB&I. 2013. Relatórios Técnicos – Projeto de Navegação do Rio Tocantins.

Kilgore, R.T., Thompson, D.B., and Ford, D.T. 2013. Estimating Joint Probabilities of Design Coincident Flows at Stream Confluences. National Cooperative Highway Research Program, Transportation Research Board of the National Academies.

Need, S.F., Lambert, M.F., and Metcalfe, A.V. 2008. "A total probability approach to flood frequency analysis in tidal river reaches." *World Environmental and Water Resources Congress 2008: Ahupua'A.*

US Army Corps of Engineers. 1993. Engineer Manual 1110-2-1415: Hydrologic Frequency Analysis. US Army Corps of Engineers, Department of the Army, Washington, DC.

Navigation & Ecological Implications for Management of Large Wood on the Madeira "Wood" River, Amazonas Basin, Brazil

Zachary P. Corum, PE Hydraulic Engineer, USACE Seattle District, Seattle, WA U.S.A. Zachary.P.Corum@usace.army.mil
Calvin Creech, PhD, PE, LEED AP Hydraulic Engineer, USACE Mobile District, Brasília, Brazil Office, Calvin.T.Creech@usace.army.mil
Renato Sousa Amorim, Hydraulic Engineer, DNIT, Brasilia, Brazil, Renato.Amorim@dnit.gov.br

Abstract

This paper documents findings from a high flow reconnaissance along two reaches of the Madeira River, the largest tributary to the Amazon River, in the Amazonas and Rondônia states of Brazil. The study purpose was to understand the likely causes of recent damage to public port infrastructure caused by large wood (LW) during the annual high flow pulse, and recommend strategies to mitigate these impacts. A secondary objective was to better understand the quantity of LW and primary geomorphic processes associated with LW fluxes. The team determined that a new hydropower dam near Porto-Velho has modified the timing of LW transport, concentrating it into the high flow season when river flows exceed powerhouse capacity. This has reduced the response time for downstream ports to manage the unnaturally large pulses of LW, which has resulted in raft jams forming at ports, contributing to failure of cable anchors, closure of facilities, costly repairs, and fatalities. The project team identified several strategies for reducing LW impacts at ports including: use of self-adjusting anchor cable winches, log deflector booms, log pusher and snag removal boats, better coordination with the dam managers, and switching to concrete ramp port designs. LW passing through the dam is the primary source of LW in the study reaches, however the banks are significant sources as well. Many modes of LW input, transport and storage were observed and classified. Natural LW accumulations are generally small and LW is transported readily through the reach, however trees and wood are ubiquitous features during all phases of the annual Amazonian flood pulse throughout the aquatic terrestrial transition zone (termed by Dr. Wolfgang Junk) to describe the zone of seasonal inundation along the wetted edge of the river. Anecdotal observations during high flow provided many examples of submerged trees and logs trapping organic material and sediment, and creating complex hydraulic conditions heavily used by the biotic community. These channel margins are reported by others to be vital for the biodiversity of the Madeira. Infrastructure and development projects that fail to consider the importance of these "aquatic-terrestrial transition zones" and role of trees and LW may have profound implications of ecological health of this mega river.

Background

Overview

U.S. Army Corps of Engineers (USACE) is assisting the Brazilian Department of Transportation Infrastructure (DNIT) with development of a plan to improve navigation on the Madeira River

between Porto Velho, Rondônia and the confluence with the Amazon River near Itacoatiara, Amazonas. The primary objective is to improve the reliability of the Madeira River Waterway between these two port cities.

This paper presents a summary of the findings from field investigations on Madeira River during the annual low and high flow periods as they relate to large wood (LW) loading and associated problems on the river. The Madeira River investigations presented in this paper consisted of the following activities: Literature review; in person interviews with longtime residents (local boat operators), dam managers, port managers, a grain terminal manager, and federal hydrologists studying the river; a port, dam and river reconnaissance at low flow and high flow; and a limited GIS analysis of locations of LW accumulation to better understand the amount of LW present in the system and the primary processes associated with LW fluxes.

Low and High Flow Reconnaissance

The DNIT-USACE team performed a reconnaissance trip to the Madeira River under both low and high flow conditions. The first site visit was performed in August and September of 2016, when a team from DNIT and USACE navigated the length of the navigation channel of the Madeira River under low flow conditions (DNIT/USACE 2016). On April 24-28, 2017 a second reconnaissance trip was performed by DNIT and USACE during high flows (DNIT/USACE 2017). This paper summarizes the observations made during this second site visit with a focus on frequency and conditions of LW in the study reach, observations of the hydraulic and geomorphic effects of LW, and local and federal efforts to manage LW. The location of the high flow reconnaissance was centered on a 35 km reach of the Madeira near Porto Velho, Rondônia and a 32 km reach Humaitá, Amazonas, where the public port operators have experienced significant challenges keeping the ports open due to damage caused by LW accumulations. The reconnaissance included detailed physical inspections (laser range finder measurements, photos, video) of public and private port facilities and a nearly complete photographic record of the streambanks including LW encountered in these reaches.

Setting

River Basin and Hydrology

The Rio Madeira ("Wood River" in English), is the largest tributary of Amazon River (Figure 1) and has major ecological, cultural and economic significance within Brazil and internationally, being one of the ten largest rivers in the world (a "mega river"). The Madeira drains the eastern flanks of the Andes Mountains in Peru and Bolivia, flows a distance of approximately 3,250 km (2,020 mi) and supplies about 15% of annual flow but more than half the sediment load (Gibson et al. 2019). Basin average annual precipitation is 1.7 m and can approach 7 m in the upper basin (CPRM). The equatorial climate is tropical, hot and humid with distinct, predictable seasonality that results in "monomodal" hydrology. The annual wet season typically occurs between November and March, and the dry season typically occurs between April and October. Flows on the Madeira predictably peak in March or April and reach base flow between August and October. Recorded streamflow during the period of record at Porto Velho, which is the upstream end of the study area, ranged from a minimum of 2,500 m^3/s (88,000 cfs) to a maximum of 58,000 m^3/s (2,050,000 cfs) during the March 2014 flood (Figure 2). For context the 2014 peak flow rate on the Madeira is comparable to the historic 1927 and 1937 floods on the Mississippi river measured at Vicksburg MS, for a basin area of roughly half the size (Latrubesse 2008, see

also Figure 1). The mean annual discharge exceeds 1,000,000 cfs near the confluence with the Amazon. The Madeira has a fine to medium sand bed and supplies about 450 Mt of sediment to the Amazon River mainstem annually, which is about three times more sediment than that transported by the Mississippi (Latrubesse 2008) for a basin half the size.
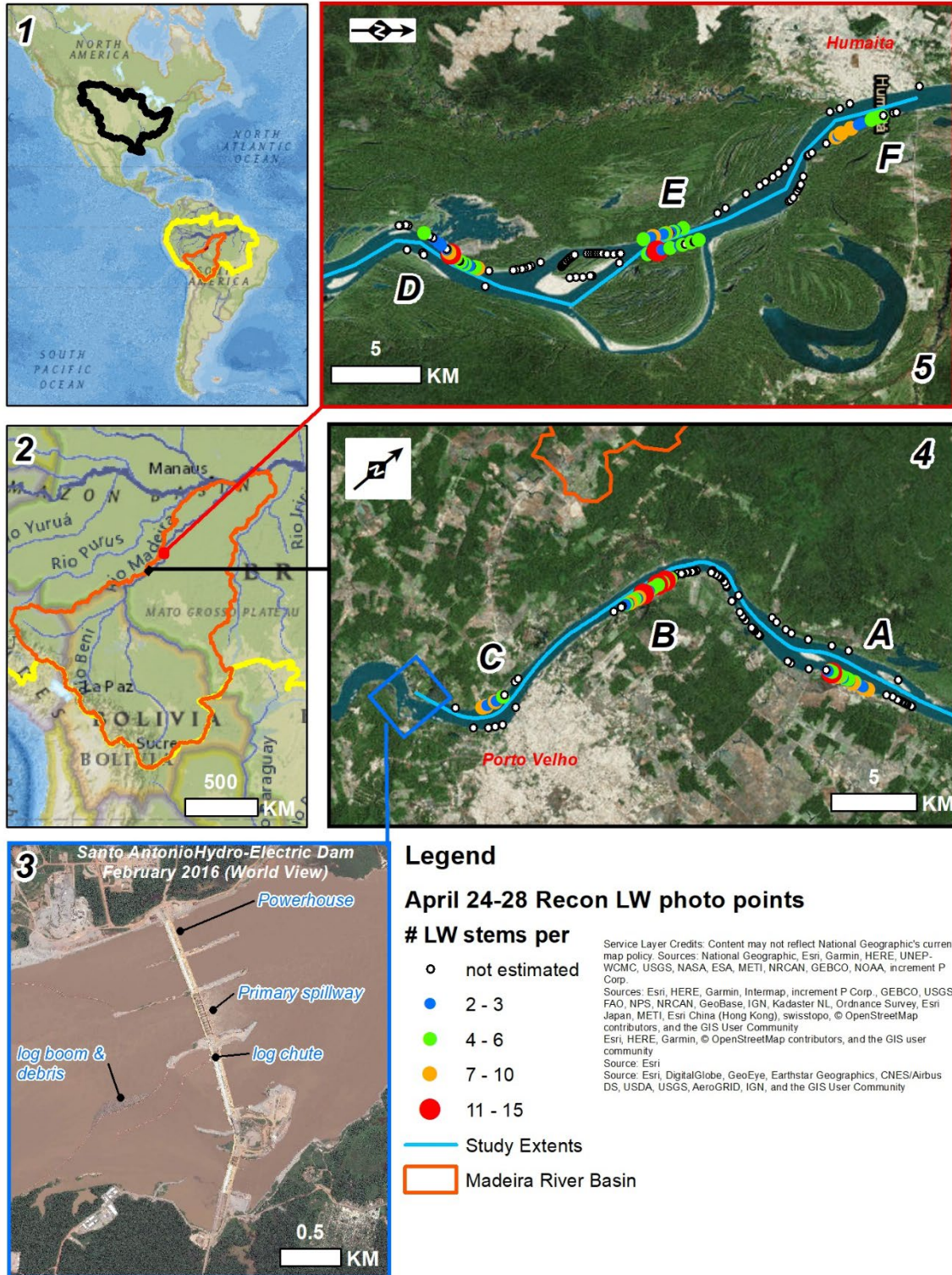
Figure 1. (1) Amazon River basin (outlined in yellow) and Madeira River basin (outlined in red), compared with Mississippi River basin (outlined in black). (2) Madeira River sub-basin boundaries. Rio Beni is the primary wood source for the Madeira River. (3) Santo Antonio hydroelectric dam, completed in 2012, located 5 km upstream from Porto Velho. High flow recon reach LW photo points and stem densities (within wetted edge of channel during 2017 high flow), Porto Velho reach with hot-spots A, B, C (4), Humaitá reach with hot-spots D, E, F (5)

Madeira River Geomorphic Conditions and Várzea Floodplain Forest

The Amazon River basin includes three main river types, distinguished by the color of the water and nutrient levels: whitewater, blackwater and clearwater. The Madeira River is a nutrient rich "whitewater" river with an average width of 1.4 km that occupies a 3.5-47 km wide floodplain estimated to be less than 12,000 years old, bounded by Pleistocene terraces (Gibson et al. 2019). Late Pleistocene and Holocene era climate change (120 m sea level rise, Irion et al. 2010), ongoing tectonics (Rosetti et al. 2014) are considered to be the primary factors responsible for the abrupt (25-35 m) vertical separation between the modern whitewater high *várzea* forest floodplain and the bounding Pleistocene age *terra-firma* or paleo *várzea* forests (which often have the same species composition, Junk et al. 2012). The river slope, like the Amazon mainstem, is very flat (approximately 4cm per km). The river is relatively straight, with a single thread to anabranching planform (Latrubesse, 2008). Lateral migration rates are low (10-20 m/yr) however the islands within the active channel limits are dynamic features, emerging and eroding over the course of a few decades (Gibson et al. 2019). The frequently flooded forests occupying the active floodplain in side channels and large islands areas are referred to as *várzea* forests, whereas the forests occupying both the Holocene terraces (15 meters above Low Water Reference Plane) and Pleistocene terraces (10-30 meters above the Holocene terraces) are referred to as high *várzea* or *terre-firme* forests. Despite having many of the same species, high *várzea* forests are infrequently flooded, while *terre-firme* forests are no longer flooded by the mainstem river.

In contrast with rivers in the northern latitudes and Australia, tropical "mega" or "great" rivers remain poorly studied from the standpoint of the geomorphic and hydraulic effects of LW (Kramer and Wohl 2017, Wohl 2017). The discussion below summarizes some of the literature we found most valuable in explaining and interpreting our field observations during the high flow reconnaissance. The unique flood pulse hydrology of the Amazon Basin including the Madeira River and its influence on geomorphic and biological conditions is discussed by Junk et al (1989), Wittmann et al. (2004) and is critical to understanding the origin and dynamics of this tropical forested river ecosystem. The annual flood pulse creates distinct vegetation communities of increasing age and biodiversity with distance from the river along a well-defined elevation gradient that accords with the annual duration and depth of inundation (Wittmann et al. 2004, Junk et al 2012). Junk describes the portion of the river that is periodically flooded by the annual flood pulse as the aquatic terrestrial transition zone (ATTZ). The ATTZ has very high biological productivity and ecological importance and spans from sand dunes exposed at base flow into the infrequently flooded mature forested floodplain (high *várzea*). It also represents the portion of the river channel that our reconnaissance team spent the most time investigating and is most familiar with. The ATTZ is the primary location for LW to enter or deposit within the river channel.

Sedimentation and erosion along the river channel are directly related to the types and amount of vegetation present, which in turn are dependent on the ground elevation relative to the annual flood pulse peak. Similarly, the ubiquitous fine and course grained alluvial deposit sequences (sand and clay) found along the banks are related to the same phenomena. Thus,

geomorphic conditions of the Madeira, including the anabranched planform must be partly governed by conditions of the adjacent floodplain forest. The anabranched planform of the Madeira is consistent with other world mega rivers with forested floodplains (Latrubesse 2008, Junior et al. 2016, Rozo et al. 2012).

Research by Latrubesse (2012), Junk et al (2012), Rozo et al (2012), Wittmann et al (2004) and others indicates that the vegetation community of the Amazonian (varzea) floodplain forest, annual flood pulse and geomorphic conditions are strongly interrelated. Wittmann (2004) found that alluvial patches and ridges (bars, proto-islands, scroll bars, levees) nearest the channel were quickly colonized by pioneering vegetation that can tolerate inundation depths of up to 7 meters, and inundation periods averaging 230 days per year. Sedimentation rates in these locations are high, about 20 cm per year. The portions of the channel with the highest inundation and sedimentation rates experienced the lowest species diversity and lowest clay content. These ridges are locations where emergent woody vegetation that can survive more than half the year under water create roughness that amplifies sediment deposition, which in turn creates elevated surfaces for less water tolerant species to establish. In contrast the slack water conditions that develop landward of the flooded, heavily vegetated scroll bars (within flooded swales, lakes and side channels) promote rapid deposition of clays and silts. Near vertical streambanks are common along the river, due to the cohesion provided by the clayey soils.

Work in the Pacific Northwest temperate rainforest rivers (Collins et al. 2012) provides a conceptual model based on field research that links the presence of riparian forests, LW accumulations in the channel, stable vegetated alluvial patches (islands and floodplains) with a self-reinforcing anastomosing (anabranched) channel pattern. Rozo et al (2012), Latrubesse (2008) and Eaton (2010) observed that the anastomosed and anabranched channel patterns likely emerge in sediment laden environments as they more efficiently convey sediment for a given flow, by reducing channel width and maximizing depth. Brooks (2003) documented the stabilizing role tropical forests play in regulating riverbank erosion, hydraulics, morphologic and habitat conditions in Australia. This literature suggests that the *várzea* forest and geomorphic conditions are not independent of each other, and further research is needed to explain the interlinkages. Estimation of a wood budget for our study reach would assist with such research, following a study design similar to those suggested in Wohl (2017) and Kramer and Wohl (2017).

Study Findings

Site Visits and Public Interviews Regarding Recent River Conditions

Overview: The USACE/DNIT high flow recon team inspected the Port of Porto Velho and talked with port managers and local residents (boatmen) during the first day of our reconnaissance, and, on the second day, met with staff of Santo Antônio Energia who operate the hydroelectric dam to discuss how they manage the supply of LW and debris at the reservoir. On the last day of our reconnaissance, the team drove to Humaitá (250 km downstream) to inspect the geomorphically dynamic reach upstream of the port that has had severe challenges with LW and floating debris in recent years.

Management of large wood at Santo Antônio hydroelectric dam: The Santo Antônio dam is a single-purpose run-of-the-river dam built for hydroelectric power generation.

Construction of the dam was completed in 2014. Our team toured the powerhouses, control room, spillways, log-boom maintenance areas and interviewed key staff to develop a comprehensive understanding of the studies undertaken before and during dam construction and current operations. Staff were forthcoming and candid about their roles and experiences which was very helpful to our investigation. Photos and slides of the dam debris management system are shown below in Figure 2. The primary method of managing debris and LW consists of floating log booms composed of stainless steel grating and plastic barrels for buoyancy, connected to concrete pillars placed in the reservoir prior to filling. More than 6 km of booms are used for temporary storage of wood and floating organic material. A full time crew of boat and equipment operators collect wood from the booms and discharge it through the dam via a log chute or compartment next to the powerhouse and primary spillway (see figure 1.3 above for locations). From our interviews we learned that the dam operators are required to discharge all wood through the dam. No wood is burned or mulched as is common in U.S. reservoirs. Wood is collected for months at a time when flows are too low to operate the spillways. Most wood is released when flows exceed powerhouse capacity, often in December or January.

Figure 2. Examples of equipment and methods used to prevent debris and LW from damaging hydroelectric facilities at Santo Antônio dam. Upper left: "Wood pusher" tug boat, log boom, and log chute. Upper right: Tug, barge and excavators to remove logs that get through/under/around booms. Lower left: log chute spillway; lower right: typical floating log boom unit in reservoir

River navigation and ports: Our discussions in the field with locals conducted during this study as well as media reports viewed for context indicate that the dam has been polarizing for the community. Most people we encountered who were unaffiliated with the dam expressed negative viewpoints about the dam, often based on personal experiences and observations of changes that occurred in their community. For example, recent bank erosion in Porto Velho experienced following the 2014 flood of record (which occurred shortly after dam construction), and damage to ports caused by high concentrations of LW originating from the dam, have

caused many local people to blame the dam managers for these changes/impacts. Data provided by CPRM (Brazilian Geologic Survey) staff from their repeated hydrographic surveys indicated up to 20 meters of degradation indeed occurred downstream within 5 km of the dam in the Porto Velho vicinity, consistent with our field observations and local reports of severe bank caving and channel widening (CPRM 2016). While the dam itself remains highly controversial (Latrubesse et al. 2017), the dam managers and operators we interviewed expressed enthusiasm about the benefits provided by the dam and were forthcoming about the challenges faced by the community, their role in mitigating the impacts and the limitations of their mission. The dam managers have a robust system in place to manage a very high annual supply of floating debris and LW within the confines of the reservoir that provides a local example to draw from for management of wood in the river downstream.

Challenges experienced by Public Ports related to large wood accumulations: Interviews with Port Managers indicated that that they are much more constrained than dam managers in their ability to manage periodic accumulations of wood at their facilities. The constraints are dictated by the degree of exposure to the river, limited operating budgets for the ports, design of the facilities (that inadvertently promote trapping of wood), and varying levels of pro-activeness of the staff managing the ports. While the port designs and exposure to the river varied, stark differences in staff pro-activeness were observed in the two ports we inspected. Both of the recently constructed small public ports (IP-4 ports) we visited (Porto Velho, Humaitá) were closed at the time due to damage to mooring winches used to anchor the ports to the riverbed. Figure 3 shows the massive amounts of woody debris that can accumulate at the Humaitá Port.

Figure 3. A. Major debris accumulation at Humaitá IP-4 port; B. Porto Velho IP-4 port facility damage: Mooring winch upstream side, with frayed cable under load; C. failed mooring winch cable, and damaged barge, downstream side

The primary indicators for this failure mode are: debris accumulations on the bow, listing pontoons, frayed cables, broken cables and grooves cut into the edges of the pontoons by the cables. The management measures being used to prevent cable failure are frequent manual adjustments of the winches; ample greasing of the cables; and break-up of raft jams that form on the port facilities with boats, people in skiffs and ropes, and occasionally with barges and tugs with excavators. These debris operations are hazardous, and fatalities during removal operations were reported by port managers. Within an hour of beginning our inspections of the Port Velho facilities, the team found widespread evidence of over-stressing and abrasion of

mooring winch cables which is caused by LW becoming trapped by the anchor cables on the upstream side of the structure (Figure 3B, above). We observed that the floating debris (and rising stages) increases the tension force on the upstream facing mooring winches that, if not offset by manually releasing tension on the winches, forces the bow of the structures down and pushes the port downstream. These movements are counteracted by the mooring winches placed on the stern, which if not adjusted in concert with those on the bow, results in the anchor cables becoming more vertically inclined, until they begin to bite down on the edges of the metal pontoon. This causes abrasion of the cable strands, resulting in loss of the lubricant, rusting, and premature cable breakage. See Figure 4 for an illustration of the failure mode.
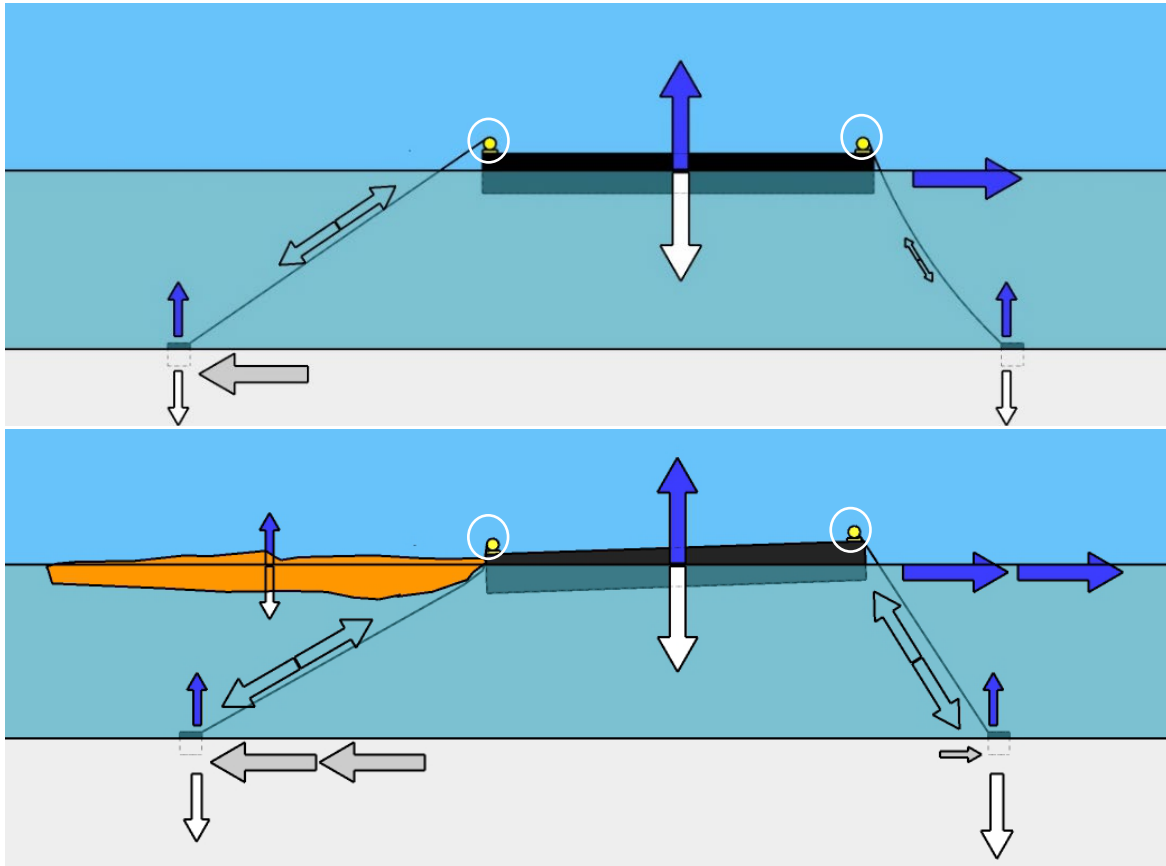

Figure 4. Illustration of barge mooring cable LW loading and failure modes. White circles represent mooring winch cables under wear/stress. Blue arrows represent hydrodynamic loading direction and magnitude (buoyant or drag force), white and grey arrows represent resisting forces (weight, lateral earth pressure), and hollow arrows represent tensile forces in cables. Primary effect of LW (orange blob) is increase in drag load on barge, which causes upstream cable to bow downstream. The tensile force created by this motion, if resisted by the anchors, pulls the bow of the barge into the water and causes the stern to rise. The downstream anchor cables which normally lie slack over the edge of the barge, resist the upwards movement by pulling taught. If the cables are worn due to repeated contact with the barge, they easily rust, and the outer strands begin to fail from abrasion. Once the frayed cable is loaded beyond its critical limit, the entire cable fails. We saw evidence of this failure mode on both upstream and downstream facing mooring winch anchors in Porto Velho and Humaitá ports.

Impact of large wood on Madeira River infrastructure: From our riverbank reconnaissance, interviews, and literature reviews, we learned that where concrete ramps are used to provide ingress/egress from the river to the shoreline, large logjams are not observed, and wood accumulations do not appear to have an influence on port operations. Concrete ramps

were common at private port facilities handling commodities at an industrial scale (petroleum, natural gas, corn, soybeans, and containerized freight) and in Humaitá where a large boat ramp is cut through a Pleistocene terrace. Where reinforced concrete piers are used to attach floating or rigid structures to the shoreline, debris accumulations are observed; however, based on interviews, these accumulations do not pose significant threats and are readily managed. Boatmen we interviewed were not forthcoming with concerns but were cognizant of the risks posed by floating wood as this is the background condition of the river.

Recommendations for Mitigating Large Wood Impacts at Ports

Switching the port designs to reinforced concrete ramps set back from the flow or oriented to shed debris would eliminate many of the issues we observed; however, we understand that unique site conditions and high water level fluctuations and strong currents make these designs costly and difficult to implement. Fortunately the team identified several options to address damage by LW and floating organic material at the IP-4 ports that rely on the pontoon design and do not require major modifications of existing infrastructure. These include:

1) Improve communication between port managers, Brazilian Navy and dam managers to alert them prior to opening the log compartment. This will increase reaction time for adjusting anchor cables and breaking up raft jams. 2) Invest in a log snag removal boat and crew that has adequate horsepower to navigate the river, remain stationary in strong currents, and has suitable hydraulic equipment, such as a hydraulic grapple, to remove and break up log accumulations. 3) Invest in log booms similar to those at Santo Antônio dam or use other measures to deflect wood away from port facilities to prevent accumulations from forming. 4) Replace the manually operated mooring winches to self-tensioning systems to minimize frequency of over stressing cables.

Observations and Analysis of Madeira River Large Wood Loading

Riverbank large wood inputs in the Porto Velho and Humaitá reaches in 2016-2017: The high flow conditions obscured geomorphic conditions along the bank toe; however, the low flow reconnaissance reports (DNIT/USACE, 2016) provides representative conditions for the same reaches along the toe.

All LW visible along the banks or in the river channel between the Santo Antônio Dam and 27 km downstream from Porto Velho (reach length of 35 km) was recorded with digital cameras on 4-26-17. On 4-28-17 the team inspected a 32 km long portion of the Madeira upstream of Humaitá. Geotagged photos were taken wherever LW was visible.

Continuous photos of the shoreline were analyzed in six hotspots to estimate the quantity and size of LW present in contact with the river along the edge, in the process of being recruited to the channel. The density of LW present in and along the edge of the channel in hotspots ranged from 12 pieces per km in disturbed areas near Porto Velho to 58 pieces per km for forested/ pasture reach near Humaitá. Undisturbed forested patches A and D had lower quantities of wood entering the river than the partially forested patches B and E, suggesting bank disturbance may increase wood loading. Average loading for all hot spots was about 30 pieces per km in both reaches, however geomorphic conditions in the Humaitá reach were more dynamic, with a lower degree of human disturbance. Generally loading densities in disturbed areas were one fifth to one third that of highly vegetated areas. By multiplying these densities by reach lengths,

and assuming the wood present along the edge was recruited to the river, we estimated the annual loading (Table 1).

Table 1. Madeira River large wood loading (to channel) estimates from high flow recon photo points, Porto-Velho and Humaitá Reaches, 2017

Hot spot	Distance from dam	Bank	Condition	Number of photo points	Avg. # LW pieces per photo point (1)	Large Wood Loading (#/km) (2)	Annual loading in reach (#/yr) (3)	% of annual debris load at dam (4)
A	29.8-33.6 km	right	forested	31	4.4	36	2513	4.0%
B	14.7-18.1 km	right	disturbed forest and pasture	36	4.9	52	3632	5.8%
C	2.4-5.9 km	left	disturbed forest and pasture	10	4.3	12	860	1.4%
D	229.3-225.8 km	left	forested	37	3	32	2093	3.4%
E	239.8 - 242.9 km	both	forest and pasture	39	4.6	58	1910	3.1%
F	252.4 - 255.6 km	right	disturbed forest and pasture	11	4.6	16	1044	1.7%

(1) Visual estimate of stems larger than 1 m in length and 0.1 m in diam. In or entering channel
(2) = (1) / hot spot length
(3) = (2) x 2 x reach length (Porto Velho = 35 km, Humaitá = 33 km),
(4) = (3)/ avg. annual number of LW pieces released from dam (in 2016)

Watershed floating organic debris volumetric loading at Santo-Antônio dam:
During our interviews with Santo Antônio Dam managers, they presented baseline data from when the dam was being constructed, showing how many pieces of LW (referred to as the Brazilian Portuguese word "troncos" in Figure 5) entered the reservoir site (prior to
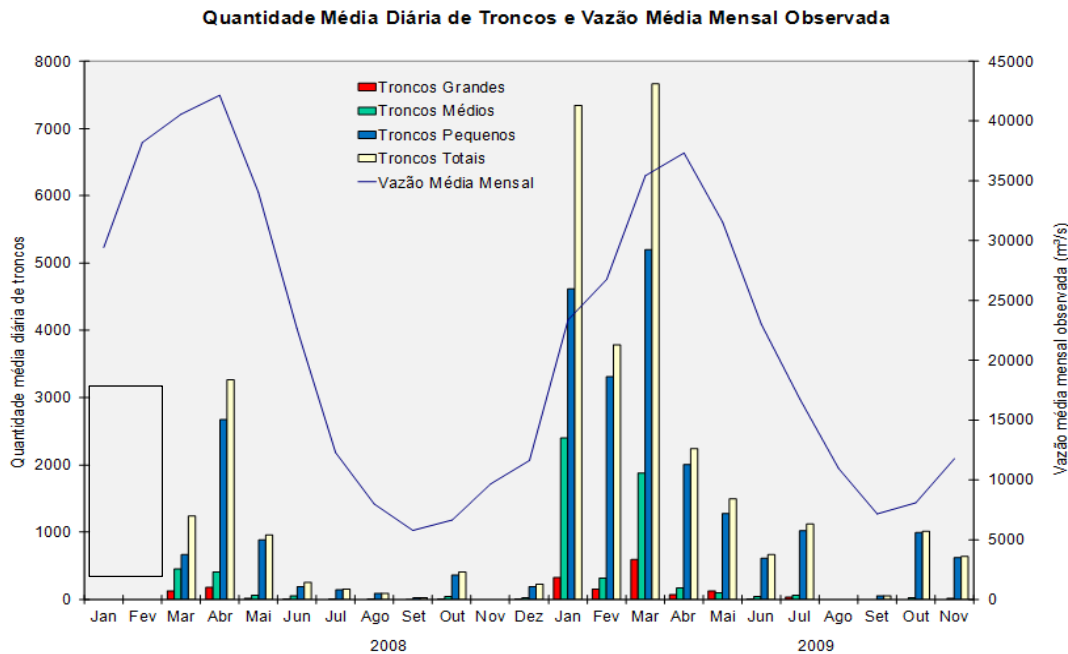

Figure 5. Historical monthly average streamflows (blue line) measured at Porto Velho Brazil and large wood pieces (troncos) entering reservoir site in 2008 and 2009 (source: Santo Antônio Energia). Red bars are large logs, green bars are medium sized logs, blue bars are small logs, and yellow bars are total logs.

impoundment) each month, between 2008 and 2009 (Figure 5). The total number of inflowing wood pieces in 2008 (approximately 6,440) was much smaller than the total in 2009 (26,050) despite the peak monthly average streamflow being higher in 2008 than 2009 by approximately 5,000 m^3/s. Wood inflows were minimal in September and November 2008 and August and September 2009. Peak monthly wood inflows in 2008 occurred in April (a total of 3,200 pieces) coincident with peak monthly streamflows. In 2009, peak wood inflows occurred in March, prior to the April peak in streamflow. No additional information was provided by managers to explain differences between the two years. Additionally, small (blue bars) and medium (green bars) pieces far outnumber large (red bars) pieces in both years. No dimensions were provided to allow for volumetric loading estimates.

Following the site visit to the dam, we reviewed Google Earth™ imagery (February, June, and October 2016) to see how much debris was present behind log booms. The aerial imagery was acquired during the low flow period when the spillways are not frequently operated (June and October) and wood is accumulating behind log booms) and during the high flow period when the spillways are in operation and wood is being routinely discharged (February). Using the rate of change in debris area during the low and high flow periods with assumed debris depth and porosity, we estimated the volume of material that entered the reservoir in 2016 through integration. The volume of debris estimated to have entered the reservoir in 2016 (which consists of floating vegetation, trees, branches, logs of all shapes and sizes) depending on assumptions used, varies by a factor of 2 (Table 2). Our average estimate of debris accumulated, prior to onset of spillway discharge, was 44,000 m^3, which is equivalent in surface area to nearly a square kilometer. An additional 60,000 m^3 may have been discharged when the spillways were open. The proportion of the debris that consists of LW is unknown but if we assume 100% of the debris was composed of 10 m long, 0.3 m diameter logs, this would equate to passage of 155,000 logs from the upper watershed annually.

Table 2. Santo Antônio Reservoir debris inflow estimate from Google Earth™ imagery, 2016-2017

Time period	Minimum			Average			Maximum		
	vol. (m³)	area (km²) (2)	logs (1)	vol. (m³)	area (km²) (2)	logs (1)	vol. (m³)	area (km²) (2)	logs (1)
June-Dec.	48,515	0.7	44,000	62,212	0.9	62,000	87,494	1.2	34,000
Annual	118,250	1.7	110,000	155,138	2.2	161,000	227,371	3.2	84,000

(1) equivalent number of 10 m long, 0.3 m diameter logs
(2) equivalent surface area, assuming 90% porosity and 0.5 m thickness

Total floating organic material (debris) loading between Santo Antônio dam and Humaitá: Multiplying the photo-point derived densities of LW loaded from the banks of the river in the study reach by the 256 km total reach length and assuming (crudely) all of this wood is eroded to the river and replaced by wood from the adjacent forest stands, results in an annual loading of 8,800 to 14,800 pieces of LW from the banks of the Madeira River between Santo Antônio Dam and Humaitá. By adding this quantity to the average number of pieces that were counted in 2008 and 2009 at the Santo Antônio dam site (16,250), a total annual loading of 25,000 to 31,000 pieces of LW is obtained at Humaitá. Thus the river banks are a significant source of LW entering the river downstream of Porto Velho and have become an increasingly important component of the annual load with distance from the dam. The

equivalent volume of floating organic material (aquatic plants, branches, leaves, LW, etc.) entering the reservoir estimated from satellite imagery is likely several times greater than the volume of LW and trees entering the river from the banks downstream of the dam. Thus floating debris accumulations at ports are likely dominated by material passing through the dam, especially at Porto Velho. At Humaitá the proportion of LW in the river that passed through the dam is likely to represent at least half of the annual supply of LW, but if all organic material is considered, the LW originating from the banks may represent less than 10% of the accumulation volume. This suggests proper design of debris countermeasures in this setting needs to take into account both the considerable volume of LW present and the vastly greater volume of smaller organic material. Much of the wood passing through the dam goes downstream and does not impact port facilities or navigation. A wood budget would be needed to estimate the fate of wood in the river and the proportion that is likely to interact with port operations.

Classification of Large Wood Recruitment Patterns Observed in the Porto Velho and Humaitá Reaches in 2017: Patterns of wood recruitment (delivery of wood to the channel) and wood deposition or storage were observed and classified from inspection of shoreline photographs. The primary input (recruitment) mechanisms we observed along the Madeira between Porto Velho and Humaitá include: riparian forest inputs from breakup (due to senescence, fire, wind); human activity (land clearing, etc.); watershed inputs from upstream (wood floating in the channel); remobilized flood deposits (from islands, bars, banks); isolated river bank geotechnical failure that recruits live standing trees; exhumation of dead logs from the bed of the river; rapid bank erosion over considerable distances that recruits a large volume of sediment and wood (toe scour/cupping failure/bank migration) acting gradually over much longer time scales (ongoing channel migration).

Although many processes contribute to the recruitment and mobilization of large wood, based on field observations during the low and high flow recons, our team proposes the following hypothesis: 1. Flood flows from December through April are present in the Madeira system; 2. On the falling limb of the hydrograph (when there is a high water table and positive pore water pressure), bank erosion rates are at a maximum; 3. LW is "recruited" in this process, but remains primarily at the bank location; 4. LW remains along the eroded bank during the low water; 5. The LW is mobilized on the rising limb of the following flood event; 6. Most of this wood is washed into the main channel, and either flows to the Amazon River or jams at the recently constructed public ports, until maintenance activities remove the jams. The remainder is stored closer to where it was recruited, buried under sediment or deposited into the floodplain forest; 7. This process is repeated each year.

Classification of large wood depositional patterns observed in the Porto Velho and Humaitá reaches in 2017: The primary types of LW accumulations along the channel that we identified include: Floating /rafted wood jam racked or trapped against vegetation or LW; 2. Floating wood jam racked or trapped against infrastructure; 3. Mobile Floating Raft jam; 4. Dead wood buried in bed of channel; 5. Live trees rooted into bed of channel; 6. Ramped trees or logs on banks; 7. Flood deposited LW; 8. Flood deposited LW jam.

Notable processes observed include trapping of mobile wood by larger trees in the channel or falling into the river, which created low velocity hydraulic shadows in the lee of the accumulation and fairly extensive separation zones along and downstream of the riverward margin of the accumulation (Figure 6). We also frequently observed floating wood being restrained by emergent woody vegetation usually along scroll bar levees. The largest logs we observed were either standing submerged trees, massive (>2 m diameter) logs cabled to the

bank or used as pontoons for house boats, or logs and trees floating in raft jams on the upstream face of the dam, against the highway bridge piers or public ports.

Figure 6. Common recruitment mechanism for large wood (left) and common deposition mechanism (raft jam on obstruction –pioneering cecropia trees - creating slack water area). Note that the largest visible LW accumulations were encountered at the upstream dam, port infrastructure, and the federal highway bridge near Porto Velho.

Discussion

Navigation concerns at public ports: With the exception of fully armored shorelines, LW was present and plentiful along the river. Our field data from six locations suggest that higher amounts of ground disturbing activity (development, land clearing) are associated with a reduced quantity of LW along the channel edges. LW entering the river in our 70 km (combined) study reach spanning a distance from the dam to Humaitá of 256 km likely represents less than 10% of the annual estimated inflow of floating organic material to the upstream dam (for the previous year). A lack of wood loading data for previous years, other Amazon tributaries, or other mega rivers prevents conclusions about whether the volume of wood in these reaches is "typical" or "atypical" or significantly different from previous years. Discussions with people who live and work along the river suggests that the local community believes that wood loading has increased since the dam became operational. We attribute these reports, based on our conversation with dam managers, to an alteration in the timing and concentration of LW present in the river downstream of the dam. The trapping of wood over several months while flows are below powerhouse capacity and subsequent release when the spillways are opened results in rapid releases of large volumes of floating debris and LW that are likely in excess of naturally-occurring concentrations.

Geomorphic and ecological considerations: While little evidence was found for LW accumulations exerting reach scale control on planform and gradient (as is common for smaller rivers), it was clear that near bank erosion and depositional patterns, hydraulic complexity and vegetative communities are strongly inter-related with the presence or absence of LW (living and dead). Channel segments along the inside of bends were strongly depositional with intact vegetation at all elevations of the flood pulse and zonation, which is typical of pioneering riparian plant communities. Channel segments with marginally stable banks experienced isolated cupping failures caused by toe undercutting that were responsible for entraining entire trees and dropping them down vertically several meters, often upright, such that the tree tops with leaves attached were emerging from the flow, creating complex slow water refuge areas

which were strongly associated with wildlife usage (birds, dolphins) and from their presence we infer large concentrations of fishes as well. These areas were more frequent in calmer, quasi stable reaches downstream of Porto Velho and upstream of Humaitá, but were infrequent near Santo Antônio dam, where bank heights, flow energy, bank erosion and vertical bed degradation were maximal, and similarly along the outer bends of bank segments experiencing ongoing and rapid bank erosion. Natural logjams are most frequent along the banks of the channel and were generally small even when very large stable key pieces are present and floating wood is a persistent feature in the center of the very wide river channel. The wide channel is likely responsible for this as indicated by the fact that the largest logjams encountered were created by man-made obstructions projecting into the channel such as the piers supporting the highway bridge at Porto Velho and the IP-4 ports.

While deepest pools are often associated with wood jams on smaller rivers with coarse beds (Buffington et al. 2002), alluvial forcing and geologic outcrops are the dominant pool forming features on sand bedded sediment laden mega rivers like the Madeira (Gibson et al. 2019). Madeira River flood depths in mega pools and alluvial forced pools were estimated by Gibson and others (2019) to be about 40 m and 25 m respectively, and the shallowest crossing was a depth of 18 m. The largest *ceiba* trees we encountered near the river in comparison had heights and crown widths in excess of 40 m. Thus a freshly recruited mature *ceiba* tree floating down river would have half of its massive canopy limbs resting safely above water if it encountered the shallowest part of the channel. Such a condition would create ample opportunity for some of the massive limbs to become snagged into the bed. In a sediment rich environment, a single snag of this size would rapidly begin trapping sediment and wood, likely resulting in rapid burial of the tree and amplification of bar growth. Thus island formation could foreseeably be initiated by the size of trees that presently exist in the floodplain. Trees of this size are very rare in the reaches we visited and we suspect most trees entering the channel are unable to initiate island formation during flood conditions. Subsurface investigations of mid-channel islands would provide better insights on the role of LW and the island building process on the Madeira.

Scientific literature indicates *várzea* forested floodplains are ecologically rich which is consistent with our anecdotal observations along the Madeira River where the forest/river edge (ATTZ) is heavily used by fish and wildlife. Trees and LW, locally recruited and from upstream sources, are fundamental components of the ATTZ and play a role in the bank erosion, island and floodplain building processes. River management projects that seek to limit the amount of LW in the river or the river's ability to migrate over long reaches would likely be cost prohibitive in addition to having incalculable ecological impacts.

References

Brooks, A.P., Brierley, G.J., and Millar, R.G. 2003. The long-term control of vegetation and woody debris on channel and flood-plain evolution: insights from a paired catchment study in southeastern Australia. Geomorphology 51, 7–29.

Buffington, J.M., Lisle, T.E., Woodsmith, R.D., and Hilton, S. 2002. Controls on the size and occurrence of pools in coarse-grained forest rivers. River Res. Appl. 18, 507–531.

Collins, B.D., Montgomery, D.R., Fetherston, K.L., and Abbe, T.B. 2012. The floodplain large wood cycle hypothesis: a mechanism for the physical and biotic structuring of temperate forested alluvial valleys in the North Pacific coastal ecoregion. Geomorphology 139-140, 460–470.

CPRM. (Serviço Geológico do Brasil) 2016. Deslizamento em Talude Fluvial no Porto JP,Bairro Triângulo, Porto Velho-RO (August, 2016).

DNIT/USACE 2016. Madeira Waterway Planning Study and Executive Design Sub-task 4: Madeira River Reconnaissance, Rio Madeira, Amazonas and Rondônia, Brazil 30 August – 8 September, 2016. Prepared by USACE Mobile District and DNIT, Brasilia. September 2016.

DNIT/USACE 2017. Madeira Waterway Planning Study and Executive Design Sub-task 4: Madeira River Reconnaissance, Rio Madeira, Amazonas and Rondônia, Brazil 24 April – 28 April, 2017. Prepared by USACE Mobile District and DNIT, Brasilia. June 2017.

Eaton, B.C., Millar, R.G., and Davidson, S. 2010. Channel patterns: Braided, anabranching, and single-thread, Geomorphology, Volume 120, Issues 3–4, 2010, Pages 353-364.

Gibson, S., Osorio, A., Creech, C., Amorim, R., Dircksen, M., Dahl, T., and Koohafkan, M. 2017. Two pool-to-pool spacing periods on large sand-bed rivers: Mega-pools on the Madeira and Mississippi, Geomorphology, Volume 328, 2019, Pages 196-210.

Irion, G., de Mello, J.A.S.N., Morais, J., Piedade, M.T.F., Junk, W.J., and Garming, L. 2011. V W.J. Junk et al. (eds.), Amazonian Floodplain Forests: Ecophysiology, Biodiversity and Sustainable Management, Ecological Studies 210, pages 27-41.

Júnior, E.S.G., Soares, E.A.A., Tatumi, S.H., Yee, M., and Mittani, J.C.R. 2016. Pleistocene-Holocene sedimentation of Solimões-Amazon fluvial system between the tributaries Negro and Madeira, Central Amazon. Braz. J. Geol., 46 (2) (2016), pp. 167-180.

Junk, W.J. 1997. General aspects of floodplain ecology with special reference to Amazonian floodplains. In: Junk, W. (Ed.), The Central Amazon Floodplain: Ecology of a Pulsating System. Ecological Studies, vol. 126. Springer-Verlag, Berlin, pp. 3–22.

Junk, W.J., Piedade, M.T., Schöngart, J., and Wittmann, F. 2012. A classification of major natural habitats of Amazonian white-water river floodplains (várzeas). Wetlands Ecology and Management. 20. 10.1007/s11273-012-9268-0.

Kramer, N. and Wohl, E. 2017. Rules of the road: A qualitative and quantitative synthesis of large wood transport through drainage networks, Geomorphology, Volume 279, 15 February 2017, Pages 74-97, ISSN 0169-555X.

Latrubesse, E.M., 2008. Patterns of anabranching channels: the ultimate end-member adjustment of mega rivers. Geomorphology 101, 130–145.

Latrubesse, E. 2012. Amazon Lakes. In Lakes and Reservoirs. Bengtsson, L., Herschy,R. and Fairbridge, R. (Eds). Springer Verlag, 13-26.

Latrubesse, E., Arima, E., Dunne, T., Park, E., Baker, V., Horta, F., Wight, C., Wittmann, F., Zuanon, J., Baker, P., Ribas, C., Norgaard, R., Filizola, N., Ansar, A., Flyvbjerg, B., and Stevaux, J. 2017. Damming the rivers of the Amazon basin. Nature 546, 363–369.

Rossetti, D.F., Cohen, M.C.L., Bertani, T.C., Hayakawa, E.H., Paz, J.D.S., Castro, D.F., and Friaes, Y. 2014. Later Quaternary fluvial terrace evolution in the main southern Amazonian tributary. Catena 116, 19–37.

Rozo, M.G., Nogueira, A.C.R., and Truckenbrodt, W. 2012. The anastomosing pattern and the extensively distributed scroll bars in the middle Amazon River. Earth Surf. Process. Landf. 37, 1471–1488.

Wittmann, F., Junk, W.J., and Piedade, M.T.F. 2004 The várzea forests in Amazonia: flooding and the highly dynamic geomorphology interact with natural forest succession. Forest Ecology and Management 196:199–212.

Wohl, E., 2017. Bridging the gaps: an overview of wood across time and space in diverse rivers. Geomorphology 279, 3–26.